XVII International Conference on Chemical Reactors

CHEMREACTOR-17

ABSTRACTS

May 15-19, 2006 Athens-Crete, Greece

Boreskov Institute of Catalysis of the Siberian Branch of Russian Academy of Sciences, Novosibirsk, Russia

Russian Scientific and Cultural Center in Athens

Russian Center of International Scientific and Cultural Cooperation under RF Government

Ministry of Education and Science of the Russian Federation

European Federation on Chemical Engineering

Scientific Council on Theoretical Bases of Chemical Technology RAS

Scientific Council on Catalysis RAS

With assistance of the General Secretariat for Research and Technology of the Ministry of Development, Greece

XVII International Conference on Chemical Reactors CHEMREACTOR-17
Post-Symposium "Catalytic Processing of Renewable Sources: Fuel, Energy, Chemicals"

Athens-Crete, Greece
May 15-19, 2006

ABSTRACTS

Novosibirsk, 2006

INTERNATIONAL SCIENTIFIC COMMITTEE

Mikhail G. Slinko, **Honour Chairman**	State Research Center "Karpov NIPCI", Moscow, Russia
Valentin N. Parmon, **Chairman**	Boreskov Institute of Catalysis SB RAS, Novosibirsk, Russia
David Agar	University of Dortmund, Germany
Alex Bell	University of California, Berkeley, CA, USA
Anthony Bridgwater	Bio-Energy Research Group, Aston University, Birmingham, UK
Jiří Hanika	Institute of Chemical Process Fundamentals, Prague, Czech Republic
Raghunath Chaudhari	National Chemical Laboratory, Pune, India
Mike P. Duduković	Washington University, St. Louis, USA
Gerhardt Eigenberger	Stuttgart University, Germany
Pio Forzatti	Technical University of Milan, Italy
Sergei S. Ivanchev	St. Petersburg Department of the Boreskov Institute of Catalysis SB RAS, Russia
Boris V. Gidaspov	RSC "Applied Chemistry", St. Petersburg, Russia
John Gleaves	Washington University, USA
Guiliano Grassi	European Biomass Industry Association – EUBIA, Brussels, Belgium
Valerii A. Kirillov	Boreskov Institute of Catalysis SB RAS, Novosibirsk, Russia
Guy Marin	Ghent University, Belgium
Dmitrii Yu. Murzin	Åbo Akademi University, Turku, Finland
Stylianos Neophytides	Institute of Chemical Engineering and High Temperature Chemical Processes, Patras, Greece
Alexander V. Putilov	Federal Agency for Atomic Energy of the Russian Federation, Moscow, Russia
Pavel D. Sarkisov	Mendeleyev University of Chemical Technology of Russia, Moscow, Russia
Vladimir G. Sister	Moscow Government, Russia
Vladimir A. Sobyanin	Boreskov Institute of Catalysis SB RAS, Novosibirsk, Russia
Gennadii F. Tereschenko	Russian Academy of Science, St. Petersburg, Russia
Constantinos G. Vayenas	University of Patras, Greece

ORGANIZING COMMITTEE

Alexander S. Noskov, **Chairman**	Boreskov Institute of Catalysis SB RAS, Novosibirsk, Russia
Victor A. Chumachenko	JSC «Katalizator», Novosibirsk, Russia
Sergei M. Foshkin	Russian Scientific and Cultural Center, Athens, Greece
Arthur Iordanidis	ABB Switzerland Ltd, Baden-Dattwil, Switzerland
Vitalii N. Kashkin	Boreskov Institute of Catalysis SB RAS, Novosibirsk, Russia
Tatiana B. Khlebnikova	Boreskov Institute of Catalysis SB RAS, Novosibirsk, Russia
Sergei I. Reshetnikov	Boreskov Institute of Catalysis SB RAS, Novosibirsk, Russia
Norbert Vasen	ETA Renewable Energies, Florence, Italy
Vadim A. Yakovlev	Boreskov Institute of Catalysis SB RAS, Novosibirsk, Russia
Ilya A. Zolotarskii	Boreskov Institute of Catalysis SB RAS, Novosibirsk, Russia
Tatiana V. Zamulina, **Secretary**	Boreskov Institute of Catalysis SB RAS, Novosibirsk, Russia

PLENARY LECTURES

XVII International Conference on Chemical Reactors

FUNDAMENTAL KINETIC MODELING FOR REACTOR DESIGN AND SIMULATION

G.F. Froment

Artie Mc Ferrin Department of Chemical Engineering

Texas A & M University, Texas, USA

The necessity and the potential of a more fundamental approach to the kinetic modeling of catalytic processes is illustrated by means of a few examples in which special attention is given to the role of the catalyst.

The first example deals with phthalic anhydride synthesis in which the catalyst itself provides the oxygen inserted into the reacting species.

A second example deals with solid-acid alkylation and with the conversion of methanol into olefins on zeolites. In these processes the catalyst is progressively deactivated through irreversible site coverage or channel blockage by heavy reaction products, but the latter are not inert towards the reacting species and also contribute to the evolution of conversion and selectivities.

Finally, the transformation of heavy oil fractions into more valuable and clean transportation fuels is considered. A realistic representation of the overwhelming product distribution of these processes requires the decomposition of the reaction scheme in terms of elementary steps of carbocation chemistry. The fundamental modeling based upon the single event concept, in combination with the Evans-Polanyi relationship, permits a drastic reduction of the number of independent rate parameters, accessible through judicious experimentation. The potential of such an approach in the simulation of the commercial hydrocracking of vacuum gas oil is illustrated.

References:
1. Papageorgiou, J.N. and G.F. Froment. "Phthalic Anhydride Synthesis-Reactor Optimization Aspects." Chem. Eng. Sci. Vol. 51, 10, 2091-2098 (1996).
2. Park T.Y. and Froment G.F., "Reaction Rates in the Methanol-to-Olefins Process and their Role in Reactor Design and Operation" Ind. Eng. Chem. Res. (2004), 43(3)682-689
3. Saeed M. Alwahabi and Gilbert F. Froment, "Single Event Kinetic Modeling of the Methanol-to-Olefins Process on SAPO-34" Ind. Eng. Chem. Res, (2004), 43, 5098-5111
   Saeed M. Alwahabi and Gilbert F. Froment, "Conceptual Reactor Design for the Methanol-to-Olefins Process on SAPO-34" Ind. Eng. Chem. Res, (2004), 43, 5112-5122.
   Jorge.M.Martinis and Gilbert F Froment, "Solid Acid Alkylation. Part I. Experimental Investigation of Catalyst Deactivation" Ind.Eng.Chem.Res,(2006),45, 940-953.
4. Jorge.M. Martinis and Gilbert F Froment, "Solid Acid Alkylation. Part II Single-Event Kinetic Modeling", Ind. Eng. Chem. Res ,(2006), 45,954-967.
5. Gilbert F. Froment; "Single Event Kinetic Modeling of Complex Catalytic Processes", Catalysis Reviews (2005)1, 83-124.

WOVEN FIBER GLASS MATERIALS AS A
NEW GENERATION OF STRUCTURED CATALYSTS

Bair S. Bal'zhinimaev

Boreskov Institute of Catalysis SB RAS,

Prospect Akademika Lavrentieva, 5, 630090, Novosibirsk, Russia

fax: 7 383 330 80 56 e-mail: balzh@catalysis.ru

Abstract

The potentiality of silicate glass fiber materials modified with Zr and REM (Rare Earth Metal) oxides as a new catalysts for application in reactions of oxidative and environmental catalysis is evaluated. The questions related to study of molecular structure of glass, formation and stabilization of highly dispersed metal (mostly, Pt and Pd) species in the bulk of glassmatrix are elucidated. The glass fiber based catalysts showed high performance in number reactions (deNOx, VOC removal, selective hydrogenation of acetylene/ethylene feedstock, $_{CH4}$ conversion to C_2H_4 via intermediate selective halogenation of methane to methylchloride, etc). The effect of heat/mass transfer on catalyst performance, the results of pilot testings, as well as the main advantages of these catalysts in comparison with traditional ones are also considered.

The silicate glass fiber materials are produced in the industry and widely used as perfect heat and electric insulators. At the same time these materials are practically unknown to people from catalysis despite of obvious advantages such as high thermostability (up to 1200°C), mechanical strength, improved hydrodynamic properties, as well as possibility to make catalytic reactors with new flexible design and to move from traditional packed catalysts beds to structural ones.

The lecture is devoted to study of glass fiber materials modified with Zr and REM (Rare Earth Metals) oxides in order to reveal their potential properties in catalysis. These materials comprise of elemental fibers of 7 - 9 μm in diameter, twisted into separate yarns of 0,2 - 1 mm in size which are used for manufacturing of different shape textiles. The glass fibers are nonporous and surface area is equal to geometrical one (*ca*. 1 m^2/g). The average chemical composition of leached materials is a following (% wt.): 80-90 SiO_2, 10% ZrO_2 or REM + 0,5-3 Al_2O_3. By means of IRS and NMR the layered model of glass structure, when 2-3 rows of SiO_4 tetrahedra are altered by hydroxyl groups, was proposed. The presence of OH-groups is important because the introduction of active metal cations via ion exchange mechanism with

protons takes place. The effective procedure for introduction of metal (mostly, Pt, Pd) complexes into the bulk of glassmatrix, their further reduction into highly dispersed metal species (clusters) or unusual low-valent states at elevated temperatures was developed and characterized by UV-Vis DRS in combination with TPO and TPR. The size of metal clusters was too small to be observed by high resolution electron microscopy. These species (up to 10 Å in size) appeared under heating by electron beam only, possibly due to partial sintering of smaller metal particles. Pt or Pd clusters are located in the bulk of glass matrix up to hundred angstroms of depth which is confirmed by XPS data combining with ion etching.

Despite of very low noble metal content (~0,01% wt.) the glass fiber catalysts exhibited high performance in many reactions (deNOx, VOC removal, SO_2 oxidation, destruction of chlorinated wastes etc.). The main reason is a capability of the materials to stabilize highly dispersed metal clusters in upper layers of glass fibers. It was found that REM cations can significantly modify the charge of Pd clusters resulting in substantial improvement of catalyst performance. Another feature of glass materials is a capability to absorb predominantly the polar or polarizable molecules from gas or liquid. Because of active sites are located in the bulk of fibers it allows to involve into reaction the polar substances with extremely low concentration. It was demonstrated clearly by the example of selective hydrogenation of acetylene (polarizable molecule) in ethylene feedstock when very high selectivity and purification level (less than 0,1 ppm of acetylene) were achieved.

Due to specific geometry and structure of glass fiber textiles, as well as high reaction rate the heat- and mass transfer limitations related to mostly, external and intra-yarn diffusion were revealed. It was shown these phenomena lead to decreasing of activity in oxidation of methane and CO, catalytic reduction of NO with CH_4 and may cause some operation unstability like overheating, oscillations of thermokinetic origin. In case of selective hydrogenation of acetylene/ethylene feedstock the intra-yarn diffusion limitation leads to deacreasing not only activity, but selectivity as well. Special isotopic studies showed that diffusion of reacting molecules inside of glassmatrix doesn't control the reaction rate and limiting step is mass transfer on the gas (liquid) – glass interface.

In conclusion, the results of glass fiber based catalysts testing in various reactions, including 2-step conversion of methane to ethylene via intermediate halogenation of methane to methylchloride, the results of pilot testing in SO_2 oxidation, treatment of diesel exhausts, as well as the main advantages of these catalysts in comparison with traditional ones are listed.

IS IT WORTH DOING KINETIC MODELLING IN ASSYMETRIC HETEROGENEOUS CATALYSIS OF FINE CHEMICALS?

Dmitry Yu. Murzin

Åbo Akademi University, Biskopsgatan 8, 20500, Åbo/ Turku, Finland, dmurzin@abo.fi

Proper reactor modeling requires physico-chemical understanding of catalytic processes. Catalysis is a kinetic process according to its definition, therefore reliable kinetic models are needed for design and intensification of catalytic processes. Kinetic and engineering studies of heterogeneous catalytic reactions are widespread, especially in connection with oil refining or production of bulk and specialty chemicals. However, in the filed of fine chemicals and pharmaceuticals, kinetic studies are rather sparse, although application of heterogeneous catalysis is growing. Interestingly a great number of various mechanisms are advanced in the literature for many organic catalytic reactions on rather rare being supported by kinetic studies.

Analysis of experimental data in complex reaction networks typical for synthesis of fine chemicals is not trivial, requiring laborious experimentation. Moreover, often only data for the major products and some by-products are available; while other components are lumped into pseudo- components.

Therefore many researchers neglect kinetic studies, presuming that kinetic analysis of complex catalytic reactions has no scientific value at all being "just a mathematical exercise and not really chemistry at all" [*]

In the presentation modeling of kinetics, stereo-, regio- and enantioselectivity of reactions representing different typical cases of multiphase organic catalysis will be discussed. Challenges in establishing kinetic regularities and subsequent modeling will be illustrated by experimental data on liquid-phase hydrogenation of α,β unsaturated aldehydes (citral, cinnamaldehyde, crotonaldehyde), alkylaromatics and alkylphenols, sitosterol, various sugars, asymmetric hydrogenation of diketones, one-pot synthesis of menthol, hydrogenolysis of hydroxymatairesinol, oxidation of lactose, α-pinene isomerization and synthesis of conjugated linoleic acid, performed with participation of the author [1-19]. Among others the following items will be addressed: the rate determining steps, the adsorption mode of organic

---

[*] One of the reviewers comment on the manuscript of H. Lineweaver and D. Burk, [*J. Am. Chem. Soc., 56*, 658, **1934**] on enzymatic kinetics, which eventually became the most cited *JACS* paper in XXth century [*C&EN, 81* (24), 27, **2003**]

compounds, type of gas (hydrogen or oxygen) adsorption, the competitiveness between small molecules and large organic molecules, changes of adsorption mode with coverage, catalyst deactivation to name a few. Special emphasis will be put on selectivity, analysis of which (Figure 1) allows for instance discrimination of rival models.

Despite the obvious difficulties in doing kinetic modeling of heterogeneous catalytic reactions in fine chemicals, kinetic analysis of selectivity, which in broad sense is understood as chemo-, regio- and enantioselectivity, is a very powerful tool in establishing reaction mechanisms as well as in process development.
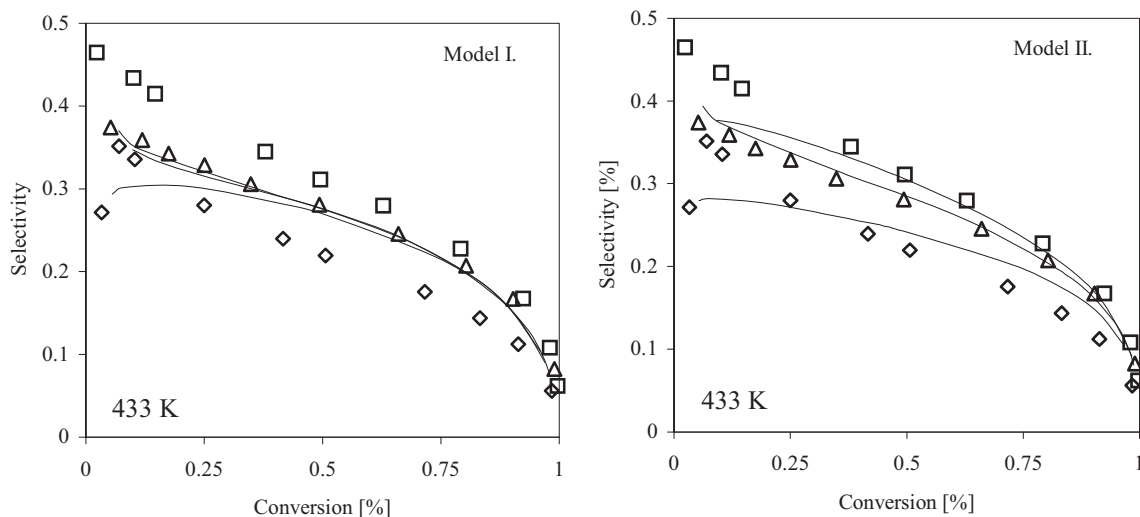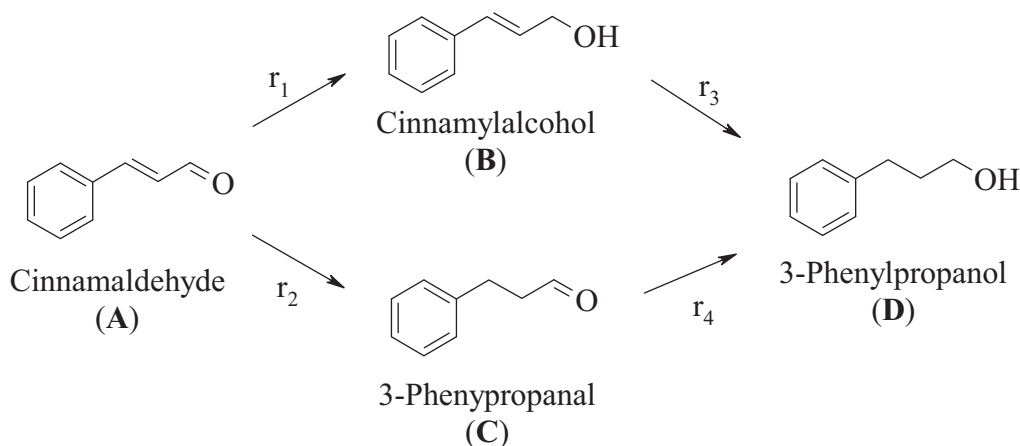
Figure 1. Selectivity to 3-phenylpropanal in cinnamaldehyde hydrogenation as a function of conversion: experimental vs. estimated (Δ - 59, □ - 37, ◊ - 14 bar) [6]

11

PL-3

References

1. A. Allahverdiev, S. Irandoust, B.Andersson, D.Yu.Murzin, Kinetics of α-pinene enantiomeric isomerization over clinoptilolite, *Applied Catal. A.Gen.* **2000**, *198*, 197.

2. J. Aumo, J. Wärnå, T. Salmi, D.Yu. Murzin, Interaction of kinetics and internal diffusion in complex catalytic three-phase reactions: activity and selectivity in citral hydrogenation, *Chemical Engineering Science,* **2006**, *61*, 814.

3. H. Backman, A.Kalantar Neyestanaki, D.Yu. Murzin, Mathematical modeling of o-xylene hydrogenation kinetics over Pd/Al$_2$O$_3$, *Journal of Catalysis,* **2005***, 233,* 109.

4. A. Bernas, D.Yu. Murzin, Linoleic acid isomerization on Ru/Al$_2$O$_3$ catalyst. 1. Conjugation and hydrogenation, *Chemical Engineering Journal,* **2005***, 115*, 13.

5. A. Bernas, D.Yu. Murzin, Linoleic acid isomerization on Ru/Al$_2$O$_3$ catalyst. 2. Elementary step mechanism and data fitting, *Chemical Engineering Journal*, **2005***, 115*, 23.

6. J. Hájek, J. Wärnå, D.Yu. Murzin, Liquid-phase hydrogenation of cinnamaldehyde over Ru-Sn sol-gel catalyst. Part II Kinetic modeling, *Industrial & Engineering Chemistry Research*, **2004**, *43*, 2039.

7. A. Kalantar, H. Backman, J.H. Carucci, T. Salmi, D.Yu. Murzin, Gas-phase hydrogenation of 4-tert-butylphenol over Pt/SiO$_2$, *J. Catalysis,* **2004**, *227*, 60.

8. K. Liberkova, R. Touroude, D. Yu. Murzin, Analysis of deactivation and selectivity pattern in catalytic reduction of a molecule with different functional groups: Crotonaldehyde hydrogenation on Pt/SnO$_2$, *Chem. Eng. Sci.*, **2002**, 57, 2519.

9. M.Lindroos, P. Mäki-Arvela, N. Kumar, T. Salmi, D.Yu. Murzin, Catalyst deactivation in selective hydrogenation of β-sitosterol to β-sitostanol over palladium, *Catalysis in Organic Reactions,* **2002,** 587.

10. H. Markus, P.Mäki-Arvela, N.Kumar, N.V. Kul'kova, P. Eklund, R. Sjöholm, B. Holmbom, T. Salmi, D.Yu. Murzin, Hydrogenolysis of hydroxymatairesionol over carbon supported palladium catalysts, *Catalysis Letters*, **2005**, *103*, 125.

11. D. Yu. Murzin, P. Mäki-Arvela, E. Toukoniitty, T. Salmi, Asymmetric heterogeneous catalysis: science and engineering, *Catalysis Reviews, Science and Engineering,* **2005***, 47,* 175.

12. P.Mäki-Arvela, N.Kumar, A.Nasir, T.Salmi, D.Yu.Murzin, Selectivity enhancement by catalyst deactivation in three phase hydrogenation of nerol, *Industrial & Engineering Chemistry Research* **2005**, *44*, 9376.

13. P.Mäki-Arvela, N.Kumar, D. Kubicka, A.Nasir, T.Heikkilä, V.-P.Lehto, R. Sjöholm, T.Salmi, D.Yu.Murzin, One-pot citral transformation to menthol over bifunctional micro- and mesoporous metal modified catalysts: effect of catalyst support and metal, *Journal of Molecular Catalysis A. Chemical*, **2005**, *240*, 72.

14. P.Mäki-Arvela, J. Hajek, T.Salmi, D.Yu.Murzin, Chemoselective hydrogenation of carbonyl compounds over heterogeneous catalysts, *Applied Catalysis A. General*, **2005**, 292, 1.

15. P. Mäki-Arvela, N.Kumar, V. Nieminen, R. Sjöholm, T.Salmi, D.Yu.Murzin, Cyclization of citronellal over zeolites and mesoporous materials for production of isopulegol, *J. Catal.* **2004**, *225*, 155.

16. V. Nieminen, A. Taskinen, E. Toukoniitty, M. Hotokka, D.Yu.Murzin, One-to-one reactant-modifier interactions in enantio- and diastereoselective hydrogenation of chiral a -hydroxyketones on Pt(111), *Journal of Catalysis,* **2006**, *237*, 131.

17. M.L. Toebes, T. A. Nijhuis, J. Hajek, J.H. Bitter, A.J. van Dilen, D.Yu.Murzin, K.P. de Jong, Support effects in hydrogenation of cinnamaldehyde over carbon nanofiber-supported platinum catalysts: kinetic modeling, *Chemical Engineering Science,* **2005***, 60,* 5682.

18. B. Toukoniitty, J. Kuusisto, J.-P.Mikkola, T. Salmi, D.Yu. Murzin, Effect of ultrasound on catalytic hydrogenation of D-fructose to D-mannitol, *Industrial & Engineering Chemistry Research,* **2005**, *44*, 9370.

19. E.Toukoniitty, B. Sevcikova, P. Mäki-Arvela, J. Wärnå, T.Salmi, D.Yu. Murzin, Kinetics and modeling of 1-phenyl-1,2-propanedione hydrogenation, *Journal of Catalysis*, **2003**, *213*, 7

TRICKLE BED REACTOR OPERATION UNDER FORCED LIQUID FEED RATE MODULATION

J. Hanika[a,b], **V. Jiricny**[a], **J. Kolena**[c], **J. Lederer**[c], **V. Stanek**[a], **V. Tukac**[b]

[a]*Institute of Chemical Process Fundamentals, Czech Academy of Sciences, Rozvojová 135, 165 02 Prague 6, Czech Republic, fax +420 220 390 286, hanika@icpf.cas.cz*

[b]*Institute of Chemical Technology, Technická 5, 166 28, Prague 6, Czech Republic, vratislav.tukac@vscht.cz*

[c]*Unipetrol, a.s., div. VUANCH, 436 70, Litvinov, Czech Republic, jaromir.lederer@vuanch.cz*

Trickle bed operations are well spread, especially in the base chemical industry[1], biochemical industry and also in toxic gas purification and waste water treatment. Trickle bed reactors are used in the chemical and biochemical industry for heterogeneously catalysed reactions, e.g. for hydrogenation, oxidation and hydrotreating processes. In the trickle beds gas and liquid percolate continuously through a fixed bed of solid particles and they are flowing in the downward direction. The particles contain at their surface solid catalyst on which components from the gas- and liquid phase react. The reaction product is then transported out of the bed by the flowing liquid.

Two phase flow of reaction mixture through catalyst bed is complicated by mal-distribution of both phases in a void space between individual neighbouring catalyst pellets on cross section and along the bed[2]. Mal-distribution of volatile reaction mixture in catalyst bed can also initiate hot spot formation in imperfect or partially wetted zones in the bed[3] where both reaction rate and rate of heat production (in case of exothermal reaction) are higher. The diffusion resistance of gaseous component in flowing liquid film is lower there and simultaneously there is lower thermal conductivity.

Out of nature this type of reactor is very non-linear in performance. This fact is very important from the point of view of its safe operation[4]. There are several reasons: high concentration of reactants (high adiabatic temperature rise and low heat capacity of the system), high activation energy of reaction (its value strongly depends on catalyst nature), change of reaction system selectivity with temperature (substrate decomposition by undesirable reaction like methanization on nickel catalysts at temperature above 200 °C) decrease of mass transfer resistance (partial evaporation of liquid phase, exceeding of critical

point of reaction mixture). As an extreme, in exothermic reactions (most of those mentioned) temperature excursions can and do sometimes lead to severe runaways and accidents[3].

Trickle bed reactors can operate in a number of flow regimes. Hydrodynamic regime of reaction mixture flow in reactor can be characterised by so called "flow map". For industrial design the flow regime with a gas continuous phase and a liquid trickle regime is usually chosen. Nevertheless, high interaction pulsing regime for waste water treatment is conveniently applied. Therefore, at certain gas and liquid rates during reactor control or after some parameter disturbance, pulses develop in the bed, whereby dense slugs of liquid form. These pulses are in fact waves of liquid that move downward, take up the liquid at their front and leave liquid at the back. The pulses can be promoted also by forced feed rate modulation. The influence of pulses is very beneficial for the following reasons[5-8]:

- Pulses drown any temperature deviation, suppress hot spot formation in the bed and improve the safety operation of the reactor.
- Mass transfer of reaction components between gas, liquid and solid phases is enhanced in pulsing flow regime and thus process intensification can be reached.
- During pulsed flow regime the radial concentration gradients are mixed out and better plug flow performance of the reactor is expected.
- Forced feed oscillations can produced pulses with frequencies reached in order several hundredths Hertz and because of the non-linearity of the process better reaction conversion can be made.

The paper reports results of the project *"New operation methods of industrial trickle bed reactors - intensification and safe control"* granted by the Ministry of Industry and Trade of the Czech Republic, *project No. FT-TA/039*. Scope and motivation for the research was a need for improvement of selective hydrogenation of dienes in light pyrolysis gasoline. This process is installed e.g. in CHEMOPETROL Co. Litvínov.

Using model reactions - unsaturated hydrocarbons hydrogenation on palladium supported catalyst - an effect of periodic feed rate modulation on trickle bed reactor performance has been investigated. It was confirmed that under specific conditions the feed rate modulation enables enhancement of the mean reaction rate in catalyst bed as a result of lower mean thickness of liquid film covering external surface of catalyst pellets. Moreover, higher gas-liquid mass transfer interaction during the liquid rich part of period is possible. An

enhancement of reactor throughput depends at feed rate modulation conditions on both the hydrodynamics in the catalyst bed and the feed rate modulation parameters, i.e. period length and its split value.

The research was aimed to investigate possible improvement of safe operation and throughput of trickle bed reactor by periodic modulation of reaction mixture feed rate which brings total wetting of catalyst and improves interaction and mass transfer rate between gas and liquid in liquid rich part of the period. The application of periodically modulated liquid feed rate brings smaller mean thickness of the liquid film flowing down along the external surface of catalyst pellets (lower diffusion resistance to gas component transfer to catalyst surface) and tubulisation of potential stagnant zones in the reactor. Period length, split to liquid rich and poor parts, and/or feed rate amplitude are important parameters of the feed rate modulation mode. It is evident that modulated feed rate of liquid reaction mixture affected liquid hold-up, concentration and temperature fields in the reactor.

Pilot plant unit built by Institute of Inorganic Chemistry Usti n.L. in Research Centre of CHEMOPETROL Co. Litvinov was used for feasibility tests of dynamic operation and control of trickle bed reactor. Adiabatic trickle bed reactor of diameter 0.1 m, length 2 m was made for operation till temperature 200 °C and pressure 2.5 MPa. The unit was equipped by two pumps (maximum feed rate 120 and 600 lt/h resp.), two tanks of 1.1 m^3 volume, phase separator of 40 lt volume and data logger and control system ControlWeb 2000 SP9 (Moravské přístroje Zlín).

The model reactions used in this study represent many of similar transformations of dienes and other unsaturated hydrocarbons during selective hydrogenation of pyrolysis gasoline. The reactor performance at continuous feed rate was compared with that one observed during feed rate modulation at the same operation conditions, i.e. at the same mean throughput of catalyst, identical temperature, pressure and feed composition.

Experiments confirmed the possible way for increase of throughput of trickle bed reactor by periodic modulation of reaction mixture feed rate[9]. Under optimal conditions transfer improvement of gaseous component across flowing liquid film represents approx. 6% relatively. The similar effect in case of exothermal reaction like unsaturated hydrocarbons hydrogenation is based on the higher mean temperature of the catalyst bed which was confirmed by reactor dynamic model solution. The gain in reactor throughput by the higher interaction between gaseous and liquid phases in the vicinity of change of the system hydrodynamics between film and pulsing flows (which is periodically overcame at feed rate modulation) represents additional intensification of the trickle bed reactor (approx. 12%rel).

PL-4

Conclusion

Induced pulsing flow of the reaction mixture in the trickle bed reactor is a promised way for the improvement the time-average reaction conversion with respect to that observed under the steady-state trickle bed reactor operation. The better catalyst wetting, improved mixing of reaction mixture in the stagnant pockets in the catalyst bed, uniformity in radial temperature profile were reached during the induced pulse operation regime.

Periodic operation of trickle bed reactor by application of the feed rate modulation can reasonably improve reaction conversion in comparison to the steady state operation mode. It was confirmed that temperature effects of exothermic reaction can contribute to the enhancement factor of the system in the order of several percents. There are of course the other effects such as periodic renewal of external catalyst surface accelerating gas component transfer to the poorly wetted catalyst pellets, stronger interaction of gas and liquid flowing co-currently through bed of catalyst close to the frontier between trickle and pulsing flow regimes, etc. The simulation results were compared with experimental data.

References

1. Hanika J., Lederer J.: *Simultaneous hydrogenation of dienes and olefines using palladium catalyst in plant trickle bed reactor*, Congress EUROPACAT-1, Montpellier, September 1993.

2. Staněk V.: *Fixed bed operations – flow distribution and efficiency*, Ellis Horwood Ltd. Chichester & Academia Prague, 1994.

3. Gossens E., Donker R., van den Brink F.: *Reactor runaway in pyrolysis gasoline hydrogenation*, 1st Internat Symp. on Proc. Safety, Oostende, Feb. 17-19, 1997.

4. Hanika J.: *Safe operation and control of trickle bed reactor*, Chem. Eng. Sci. 54, 4653-4659 (1999).

5. Boelhouver J.G., Piepers H.W., Drinkenburg A.A.H.: *Liquid induced pulsing flow in trickle bed reactors*, Chem. Eng. Sci. 57, 3387-3399 (2002).

6. Silveston P.L., Hanika J.: *Challenges for the periodic operation of trickle bed catalytic reactors*, Chem. Eng. Sci. 57, 3373-3385 (2002).

7. Silveston P.L., Hanika J.: *Periodic operation of three-phase catalytic Reactors*, Canad. J. Chem. Eng. 82, 1105-1142 (2004).

8. Giakoumakis D., Kostoglou M., Karabelas A.J.: *Induced pulsing in trickle beds - characteristics and attenuation of pulses,* Chem. Eng. Sci. 60, 5183-5197 (2005).

9. Tukač V., Šimícková M., Chyba V., Lederer J., Kolena J., Hanika J.: *Dynamic behaviour of trickle bed reactor,* CAMURE-05 & ISMR-4 Symposium, Portorož 15.-18.6.2005, Book of Extended Abstracts 87-88 (2005).

MONOLITHIC ELECTROPROMOTED REACTORS:
FROM FUNDAMENTALS TO PRACTICAL DEVICES

Costas G. Vayenas

Department of Chemical Engineering, University of Patras, Patras, Greece

A Monolithic electropromoted reactor (MEPR) is a new type of high-throughput reactor which permits the in situ use of the phenomenon of electrochemical promotion of Catalysis (EPOC or NEMCA effect) to enhance the rate and selectivity of catalytic reactions. The concept, design and construction of the first MEPR units is discussed, together with the first performance results in high space velocity laboratory and car exhaust environments.

1. Electrochemical promotion of catalytic reactions

The phenomenon of Electrochemical Promotion of Catalysis (EPOC) or Non-Faradaic electrochemical promotion of catalytic activity (NEMCA effect) and its close relationship with classical promotion and with metal-support interaction has been discussed and analyzed in numerous publications [1-15]. Work in this area has been reviewed recently [14,16]. The metal or conductive metal oxide catalyst is deposited on a solid electrolyte component and electrical current or potential is applied between the catalyst and a second electrode (termed counter electrode) also deposited on the solid electrolyte component (Figure 1). This electrical current or potential applications causes pronounced and usually reversible changes in the catalytic activity and selectivity of the catalyst electrode. The induced change in catalytic rate is up to 6 orders of magnitude larger than the rate, I/nF, of electrochemical supply or removal of ions (of charge n) to or from the catalyst-electrode through the solid electrolyte, where I is the applied current and F is the Faraday constant. The induced change in catalytic rate can be up to 300 times larger than the catalytic rate before current or potential application. The counter electrode may be exposed to a separate gas compartment (fuel cell-type design) or may by exposed to the same reactive gas mixture as the catalyst-electrode (single chamber design). The solid electrolyte component (e.g. plate or tube) may be either gas impervious, but can also be porous (Vayenas et al, European Patent 0480116 (1996)). The phenomenon of electrochemical promotion has been studied already for more than seventy catalytic reactions (Vayenas et al, "Electrochemical Activation of Catalysis: Promotion, Electrochemical Promotion and Metal-Support Interactions" Kluwer/ Academic Publishers (2001)) but so far there has been no practical reactor configuration designed, constructed and tested in order to utilize it in industrial practice or in automotive exhaust catalysis.

We discuss here a new reactor and method for utilizing the effect of electrochemical promotion of catalysis to enhance the rate and selectivity of catalytic reactions. The new reactor has all the geometric characteristics of a monolithic honeycomb reactor but, due to its special design, can be dismantled and assembled at will and can be used to electrochemically promote

the catalyst-electrodes deposited on its plate components with only two external electrical connections. Therefore both electrical manifolding and also gas manifolding is extremely simplified in the new monolithic electrochemically promoted reactor (MEPR) [16-19].

2. Description and operation of the MEPR

Figure 2 shows the monolithic electrochemical promoted reactor (MEPR) concept. The plate and reactor dimensions are quite flexible and those shown in Figure 2 are indicative and corresponding to those of the prototype units tested [16-19].

The ceramic reactor walls (casing) must be insulating and can be made, for example, by Machinable Ceramic (MACOR) material. It is enclosed in a suitably designed metal (or ceramic) gas manifolding casing with insulating material (e.g. vermiculite) placed, if desirable, between the ceramic reactor walls and the metal (or ceramic) gas manifolding casing in order to reduce mechanical stresses when the unit is used in an automotive exhaust (Figure 3).

The internal side of the two opposing reactor walls has appropriately machined parallel grooves (typically 1-5 mm deep, thickness a few μm larger than the plate thickness (typically 500 μm).

The distance between the parallel grooves dictates the reactor channel height and is typically 0.5 to 2 mm, depending on the desired reactor surface to volume ratio.

The grooves can be made to terminate before the reactor exit in order to ensure that the plates cannot be entrained by the flowing gas stream.

The solid electrolyte plates can be flat, in which case the resulting reactor channels are rectangular, or can be ribbed in which case the resulting reactor channels are rectangular or square. The rib height can be adjusted to either make contact with the next plate or to leave a small (e.g. 5 μm) margin between the rib top and the next plate. The plates can be gas-impervious or porous.

Two different catalysts, based on the rate vs potential behaviour of the catalytic reaction of interest (electrophobic, electrophilic, volcano or inverted volcano type [14-16,20,21].

The first catalyst is coated (e.g. via metal evaporation or sputtering) or using organometallic metal pastes followed by sintering on one side of the plates in such a way as to ensure electrical contact on one side of the plate with the electronic current collector deposited on one side of the inner reactor wall [16-19].

The second catalyst is coated on the other side of the plate in such a way as (a) to avoid short-circuiting with current collector 1 (e.g. by leaving 4-6 mm of the plate surface uncoated, Fig. 2) and (b) to ensure electrical contact with the current collector 2 deposited on the opposite inner reactor wall (Fig. 2).

The thickness of the catalysts 1 and 2 can be as low as 10 nm or as high as 10 μm. The catalysts can be porous. The current collectors 1 and 2 are connected via insulated metal sheets or wires to the external power supply or galvanostat or potentiostat.

Figure 3 shows a prototype MEPR reactor with 24 8%Y_2O_3-stabilized-ZrO_2 (YSZ) plates and Rh (catalyst 1) and Pt (catalyst 2) catalyst-electrodes.

Experimental details and performance data have been discussed elsewhere [16-19]. Here we discuss some results obtained with a MEPR loaded with 22 Rh/YSZ/Pt plates.

The reaction studied was the reduction of NO by ethylene in presence of gaseous O_2. Under mildly reducing conditions at 320°C (Fig. 4) electropromotion with an anodic current (+30mA) increases the conversion of C_2H_4 from 49% to 59%, the conversion of O_2 from 68% to 81% and the conversion of NO from 72% to 93%.The shape (flat leveling) of the rate transients suggests that under these conditions the conversions of C_2H_4, O_2 and NO reach a saturation level which is limited by gas bypass.

The reactor was operated at much higher flowrates (1.8 l/min), (more recent studies have utilized flowrates up to 20 l/min), hourly space velocities (1200 h^{-1}) and conversions (~90%) than all previous electropromoted units and shows significant promise for practical applications. More important is the successful electropromotion of its thin (40 nm) Rh and Pt elements, with metal dispersions of at least 10%, i.e. comparable with metal dispersions of supported commercial catalysts. This appears to eliminate the major economic obstacle for the practical utilization of electrochemical promotion. It will be necessary to develop suitable reactor-electrochemical reactor models and scale-up or scale-down strategies for potential practical applications.

References

[1]   C.G. Vayenas, S. Bebelis, S. Ladas, Nature 343 (1990) 625.
[2]   J. Pritchard, Nature 343 (1990) 592.
[3]   R.M. Lambert, F. Williams, A. Palermo, M.S. Tikhov, Top. Catal. 13 (2000) 91.
[4]   G. Foti, S. Wodiunig, C. Comninellis, Cur. Top. Electrochem. 7 (2001) 1.
[5]   C.A. Cavalca, G.L. Haller, J. Catal. 177 (1998) 389.
[6]   L. Ploense, M. Salazar, B. Gurau, E.S. Smotkin, JACS 119 (1997) 11550.
[7]   P. Vernoux, F. Gaillard, L. Bultel, E. Siebert, M. Primet, J. Catal. 208 (2002) 412.
[8]   I. Metcalfe, J. Catal. 199 (2001) 247; J. Catal. 199 (2001) 259.
[9]   C. Sanchez, E. Leiva, in Handbook of Fuel Cells: Fundamentals, Technology and Applications, Vol. 2 (W. Vielstich,H. Gasteiger and A. Lamm, eds.), John Wiley & Sons Ltd., England, 2003.
[10]   G.-Q. Lu, A. Wieckowski, Current opinion in Colloid and Interface Science 5 (2000) 95.
[11]   B. Grzybowska-Swierkosz, J. Haber, *Annual Reports on the Progress of Chemistry*, The Royal Society of Chemistry, Cambridge, 1994.
[12]   J.O.M. Bockris, Z.S. Minevski, Electrochim. Acta 39 (1994) 1471.
[13]   C.G. Vayenas, M.M. Jaksic, S. Bebelis, S.G. Neophytides, in Modern Aspects of Electrochemistry, Vol. 29 (J.O.M. Bockris,B.E. Conway and R.E. White, eds.), Kluwer Academic/Plenum Publishers, New York, 1996, p. 57.
[14]   C.G. Vayenas, S. Bebelis, C. Pliangos, S. Brosda, D. Tsiplakides, *Electrochemical Activation of Catalysis: Promotion, Electrochemical Promotion and Metal-Support Interactions*, Kluwer Academic/Plenum Publishers, New York, 2001; references therein.
[15]   A. Wieckowski, E. Savinova, C.G. Vayenas, eds., Catalysis and Electrocatalysis at Nanoparticles, Marcel Dekker, Inc, New York, 2003.
[16]   D. Tsiplakides, S. Balomenou, A. Katsaounis, D. Archonta, C. Koutsodontis and C.G. Vayenas, Catal. Tod. 100 (2005) 133-144.
[17]   S. Balomenou, D. Tsiplakides, A. Katsaounis, S. Thiemann-Handler, B. Cramer, G. Foti, Ch. Comninellis and C.G. Vayenas, Appl. Cat. B-Envir. 52 (2004) 181-196.
[18]   S.P. Balomenou, D. Tsiplakides, A. Katsaounis, S. Brosda, G. Fóti, Ch. Comninellis, S. Thiemann-Handler, B. Cramer and C.G. Vayenas, *Solid State Ionics*, in press (2006).
[19]   PCT/GR2004/000006 "Method and Apparatus for carrying out electrochemically promoted reactions" C.G. Vayenas, S. Balomenou, D. Tsiplakides, A. Katsaounis, S. Brosda, G. Foti, C. Comninellis, S. Thieman-Handler, B. Cramer (2004).
[20]   C.G. Vayenas, S. Brosda and C. Pliangos, J. Catal. 203 (2001) 329-350.
[21]   S. Brosda and C.G. Vayenas, J. Catal. 208 (2002) 38-53.
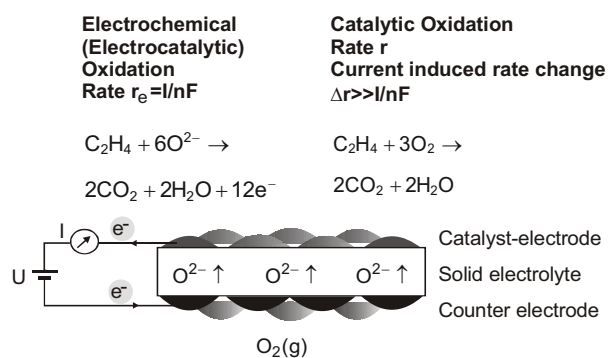
Fig. 1. Principle and basic experimental setup used in electrochemical promotion (NEMCA) experiments.

Fig. 2. Schematic of the monolithic electropromoted reactor (MEPR) with ribbed plates.


Fig. 3. Photographs of the MEP reactor-sensor tested showing: (a) the machinable ceramic reactor walls, one of the Ag current collectors on the wall, the plate location for two-plate operation (top plate was used as sensor element) and part of the metal casing. (b) the twenty-two plate unit (c) the assembled reactor with metal casing in the furnace. Also shown are the two thermocouple housings and the four shielded electrical connections for sensing and electropromotion.

Fig. 4. Transient effect of a constant applied current (+30mA) on the catalytic rates of CO_2 production (r_{CO_2}) and NO reduction (r_{NO}), on the NO conversion (x_{NO}) and on the Rh-Pt potential difference (U). T=320°C.

HYDROGEN PRODUCTION FOR FUEL CELLS

V.A. Kirillov and **V.A. Sobyanin**

Boreskov Institute of Catalysis SB RAS, Novosibirsk, Russia
pr. Akademika Lavrentieva, 5, 630090 Novosibirsk, Russia,
E-mail: vak@catalysis.ru

Hydrogen production from hydrocarbon fuels is a key problem of hydrogen energy. Technologies relying on utilization of catalysts at all stages of fuel conversion are wide spread for this purpose: (i) conversion of hydrocarbon feedstock into synthesis gas; (ii) steam reforming of CO; (iii) preferential CO oxidation. Conversion of fuel into hydrogen is performed in fuel processors (FP) designed as compact heat-and-function integrated devices comprising of catalytic reactors, heat exchangers, feed systems and operation regime controllers. Because of specific requirements for FP, the existing commercial catalysts cannot be used in fuel processors for a number of reasons. This necessitates the development of novel catalysts oriented for utilization in FP. These catalysts should meet the following requirements: high thermal stability and scale resistance of the support and catalyst; catalyst heat conductivity at a level about 1-5 W/m·K; catalyst life not less than 6000 hours; possible application of catalysts as structural units for the reactor construction; low cost; equal coefficients of thermal expansion of catalyst layer and support; good adhesion between the catalyst layer and the metal wall. The structured metal porous catalysts supported on metal nets are most completely met the above requirements. In given work there are analyzed variants of possible application of these catalysts at the synthesis gas production by means of partial oxidation and steam reforming of natural gas, steam reforming of methanol and bio-ethanol, auto-thermal reforming of diesel fuel. These catalysts were tested during short-term and life-timing tests in the abovementioned reactions. There was developed a number of catalytic reactors on a base of coupling by heat of endothermic and exothermal reactions for natural gas steam conversion.

Experimental data on the specific productivity and temperature and concentration profiles within the exo- and endothermic channels are presented. Numerical analysis of the developed mathematic model proved good agreement between the calculated data and experiment. A radial-type reactor for partial oxidation of natural gas has been developed and studied. The reactor includes a perforated gas-distributing tube with a structured net-supported catalyst

PL-6

sintered on the outer surface of the tube. Mathematical model for the reactor has been developed. The results of mathematical modeling agreed well with the experiment. The reactor modifications for water-gas shift and preferential CO oxidation in hydrogen-rich gas have been designed and tested successfully. Current state of hydrogen generation by fuel processors has been analyzed that proved high promises of a heat-integrated fuel processor, in which heat losses are minimized due to efficient arrangement of reactors, heat exchangers and other constituent parts. Particular example of that type processor has been considered and results of experimental studies of its heat regimes and specific productivity presented.

ALTERNATIVE CATALYTIC PROCESSES FOR LIGHT OLEFINS PRODUCTION: FROM LAB TO PRACTICE

Angeliki A. Lemonidou

Department of Chemical Engineering, Aristotle University of Thessaloniki,

P.O.Box 1517, University Campus, GR-54006, Thessaloniki, Greece

Light olefins, ethylene and propylene, are the major building blocks of the petrochemical industry with annual production exceeding 75.000 kt and 45.000 kt respectively for 2004. Ethylene and propylene are used in the production of diverse products, ranging from solvents to plastics. The established process for their production is steam cracking of various hydrocarbon feedstocks (ethane, LPG, naphtha, gas oils), a process that operates under severe conditions. Steam cracking is the most energy-consuming route in the petrochemical industry with energy requirements exceeding 26 GJ/ton of ethylene. Ethylene is exclusively produced via steam cracking while a significant part of propylene (around 30%) is additionally produced as by-product of fluid catalytic cracking process. With lower olefins market growing at 3-4% per year and fuel costs constantly rising, research efforts have been focussed on the development of less-energy intensive, environmental processes for their production.

The availability and the low cost of lower paraffins have spurred the industrial interest for paraffin transformation to high value products, namely olefins. Successful development of this approach is the catalytic dehydrogenation of propane to propene. Indeed, nowadays about 2 % of propene is produced via this route. The thermodynamic limitations combined with the high endothermicity of the reaction and the coke tendency are the major drawbacks limiting the large exploitation of the process.

The catalytic oxidative dehydrogenation of light alkanes is an appealing alternative route, which due to the mild exothermicity may allow developing an energetically well-balanced process. A highly active and selective catalytic system, able to efficiently transform the alkanes to alkenes and not to oxidation products in the presence of an oxidant, is the key for the successful realization of the new method. Oxidative dehydrogenation of ethane and propane has been studied over a wide range of catalytic materials. Supported early transition

metal oxides (V, Mo, Cr) operate at low temperature (<550°C) and exhibit high initial olefin selectivity. However, high activity can only be achieved at the expense of olefin production, since these catalysts are as a rule more reactive towards olefins. High olefins yields have been reported over chlorine-promoted non-reducible oxides (e.g. LiCl/MgO), where the reaction proceeds at high temperature (>600°C) via a homogeneous-heterogeneous reaction scheme. Still, serious problems, such as the low catalyst stability and the release of chlorine, are associated with the use of these catalysts.

Multicomponent mixed oxides seem to be the most promising class of materials, especially for the ethane oxidative dehydrogenation reaction. Research on multicomponent catalysts has been mainly focused on Mo/V/Nb formulations, promoted with various metal combinations. A recent breakthrough has been achieved with the development of hydrothermally prepared Mo/V/Nb/Te multi-oxides, where the key component has been related to the crystalline structures formed in the materials. These materials appear active in both oxidative dehydrogenation of ethane and propane to olefins and oxygenates, respectively. Another recent appealing alternative to the traditional early transition metal-based oxides, with all the associated disadvantages, is nickel oxide-based catalysts. Although NiO exhibits well-known total hydrocarbon oxidation properties, it was surprisingly observed that when the oxide is supported on a suitable oxidic carrier it demonstrates significant ethane selective oxidation abilities. The same effect can be also realized by promoting the unsupported NiO phase with a suitable transition metal. Recently developed Nb-promoted NiO mixed oxide exhibit very good potential as catalysts for ethylene production. The Ni-Nb mixed oxides combine both high activity at low temperature and high ethene selectivity at high conversion level resulting in an overall ethene yield of 46% at 400°C. Variation of the Nb/Ni ratio indicates that the key component for this excellent catalytic behavior is the Ni-Nb solid solution formed upon doping of NiO with Nb, since small amounts of niobium effectively convert NiO from a total oxidation catalyst to an effective ODH catalytic material. Optimum incorporation of Nb ions in the NiO lattice is achieved for intermediate Nb/Ni ratios ($Ni_{0.85}Nb_{0.15}$ catalyst), since higher Nb concentrations lead to the saturation of the bulk sites and segregation of the nickel and niobium phases. Correlation of the surface properties of the materials with their catalytic behavior shows that nickel sites are the active sites responsible for the activation of the parafinic substrate, with niobium affecting mainly the selectivity to the olefin by modifying the oxygen species on the catalytic surface.

Significant information on the functionality of the materials is deduced via isotopic-labelling studies. Transient and SSITKA experiments with isotopic $^{18}O_2$ show that on both NiO, a typical total oxidation catalyst, and the Ni-Nb-O mixed oxide catalysts, the reaction proceeds via a Mars and van Krevelen type mechanism, with participation of lattice oxygen anions. The prevalent formation of cross-labelled oxygen species on NiO indicates that dissociation of oxygen is the fast step of the exchange process, leading to large concentration of intermediate electrophilic oxygen species on the surface, active for the total oxidation of ethane. Larger amounts of doubly-exchanged species observed on the Ni-Nb-O catalyst indicate that doping with Nb renders diffusion the fast step of the process and suppresses the formation of the oxidizing species. The performance of the $Ni_{0.85}Nb_{0.15}$ catalyst is kinetically described by a model based on a redox parallel-consecutive reaction network with the participation of two types of active sites, sites I responsible for the ethane ODH and ethene overoxidation reaction and sites II active for the direct oxidation of ethane to CO_2.

The perspectives for industrial application of the Ni-Nb-O mixed oxide catalysts are very good given that the catalyst is stable under reaction conditions for extended TOS. A further advantage of these catalysts is that the only byproduct detected is CO_2 making these materials attractive from engineering point of view because of the greatly reduced separation cost downstream from the reactor. Reactor designs, which allow high alkene selectivity with effective heat management of the exothermic oxidative dehydrogenation is a real challenge. Multitubular fixed bed or fluidised bed with staged oxidant feed or decoupled operation in alkane and oxidant feeding, are possible reactor configurations and mode of operations.

In the frame of globalization and sustainability: some tracks for the future of chemical and catalytic process engineering (molecules into money)

Jean-Claude CHARPENTIER
ipPresident of the European Federation of Chemical Engineers
Laboratoire des Sciences du Génie Chimique CNRS/ENSIC/INPL Nancy
and Ecole Supérieure de Chimie Physique Electronique de Lyon – France
e-mail: jean-claude.charpentier@ensic.inpl-nancy.fr and charpentier@cpe.fr

In today's economy, chemical engineering must respond to the changing needs of the chemical process industry in order to meet market demands involving a move away from materials sold according to their purity, to "structured" materials sold for their performance (powders, emulsions, colloids, catalysts, soft solids…). These materials have to be formulated and designed and their properties are determined primarly, not by their overall composition, but rather by their nano and microstructure. Concurrent product and process design is especially critical for structured products as processing conditions during manufacture will greatly influence their nano and microstructure and, hence, their end-use properties.

The ability of chemical engineering to cope with managing such complex systems together with the scientific and technological problems encountered is addressed in this lecture. To satisfy both the market requirements for specific end-use properties of formulated products and the social and environmental constraints of the industrial-scale processes, it is shown that an integrated system approach of complex multidisciplinary, non-linear, non equilibrium processes and phenomena occurring on different length and time scale of the supply chain (see figure 1)
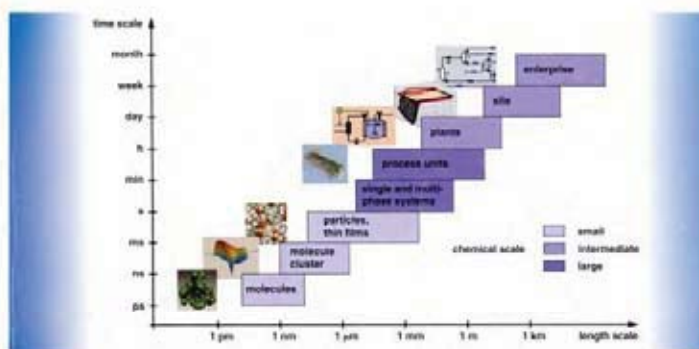
Figure 1: The chemical supply chain

from molecular-scale to industrial-scale is required. This will be obtained due to breakthroughs in molecular modelling, scientific instrumentation and related signal and image processing, and powerful computational tools.

The evolution of chemical engineering, especially involved with the product and (catalytic) process design for structured product formulation can be summarized by four main tracks:

(1) **Increase productivity and selectivity through intensification of intelligent operations and a multi length scale approach to process control** by supplying the process with **a local "informed" flux of energy or materials**; or by **nano or microtailoring** of materials with controlled structure. Indeed synthetic materials with targeted properties are now conceived and designed to a successful catalytic process with such development of an effective catalyst, i.e, the ability to better control its microstructure and chemistry allows for the systematic manipulation of the catalyst's activity, selectivity, and stability.

(2) Design novel equipment based on scientific principles and new production methods, i.e., **process intensification** using **multifunctional reactors** (i.e, catalytic distillation, or monoliths applied either as catalysts or as a functional reactor internal), or using **new operating modes** (i.e, induced pulsing liquid or periodic operations in trickle bed reactors to improve liquid-solid contacting at low liquid mass velocities, or membrane contactors in phase transfer catalysis for developing cleaner processes and increasing productivity and quality and enhancing safety), or using **microengineering** and **microtechnology** for **high throughput and formulation screening**. Microengineered reactors have some unique characteristics that create the potential for high performance chemicals and information processing on complex system. Moreover it is clear that there exists today a current trend which can be called **"from microreactor design to microreactor process design"**.

So process intensification refers to complex technologies that replace large, expensive, energy-intensive equipment or processes with ones that are smaller, less costly, more efficient, or that combine multiple operations into a single apparatus or into fewer devices. So many technologies are thus being developed in chemical industries motivated by improved chemistry, low inventories, capital cost reduction, enhance corporate image, novel or enhanced products and values to customers, enhanced safety, and improved processing energy and environments benefits (see figure 2a which presents a vision of how a future plant employing process intensification may look versus a conventional plant and this is already obtained today in certain cases for petroleum plant processing-see figure 2b).

Figure 2a: One vision of how a future plant employing process intensification may look (right) vs a conventional plant (left)

Figure 2b: the example of a modern plant

(3) Extend chemical engineering methodology to **product focussed design and engineering**, using an integrated system approach of complex pluridisciplinary non linear, non-equilibrium processes phenomena occurring on different length and time scales (see figure 3)
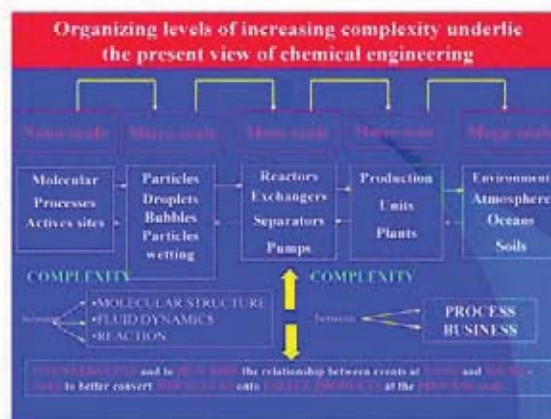

Figure 3: Levels of increasing complexity

which is defined as the "triplet molecular Processes - Product-Process Engineering (3PE)" approach, i.e., organizing levels complexity, by translating molecular processes into phenomenological macroscopic laws to create and control the required end-use properties and functionality of structured products such as complex fluids and solids manufactured by a continuous or batch process;

(4) **Implement multiscale application of computational chemical engineering modelling** and simulation to real-life situations from the molecular scale to the production scale in order **to understand how phenomena at a smaller length scale relate to properties and behaviour at a longer length scale.** The long term challenge is to combine the thermodynamics and physics of local structure-forming processes like network formation, catalytic phase separation, agglomeration, nucleation, emulsion, crystallization, mixing, sintering etc… with multiphase computer fluid dynamics (CFD).

In conclusion chemical product design has historically been the domain of chemists, material scientists, and food and pharmaceutical technologists while most chemical engineers focused on process design.

However it is shown now that there are new opportunities for chemical engineering in product and process design for structured product formulation, both in process analysis of product end use and in concurrent product / process design, the last one can offer strategic competitive advantage in speed-to-market, cost, and product innovation.

In such a framework and with the help of the multidisciplinary and multi-scale approach, chemical and process engineering are totally involved in the theme **"Molecules into Money"** which is based on the premise that chemical engineering drives today economic development and is fundamental to wealth creation in the frame of globalization and sustainability (i.e, catalytic processing of renewable sources). It addresses the generation of new opportunities through product formulation and/or process and equipment innovation, discusses techno-economic analysis taking into account the protection of environment considerations, business decision making, the role of entrepreneurship in chemical and process engineering, and the strategies and methodologies for technical innovation and sustainable technologies for efficient mass and energy utilisation in process industries. And chemical engineers and researchers are uniquely positioned **to play a pivotal role in this technological revolution** with their broad training in chemistry, physical chemistry, catalysis, life sciences, multi scale modelling and simulation, processing, system engineering and product design.

ORAL PRESENTATIONS

Section 1. Kinetics of catalytic reactions

KINETIC MODELLING OF ETHANE OXIDATIVE DEHYDROGENATION OVER Ni-Nb-O MIXED OXIDE CATALYSTS

E. Heracleous, A.A. Lemonidou, I.A. Vasalos

Department of Chemical Engineering, Aristotle University of Thessaloniki and Chemical Process Engineering Research Institute (CERTH/CPERI), POBox 1517, University Campus, GR-54006 Thessaloniki, Greece Tel. +30-2310-996199, Fax. +30-2310-996184, e-mail: eheracle@cperi.certh.gr

1. Introduction

The oxidative dehydrogenation (ODH) of ethane to ethylene has been studied over a wide range of materials [1-4], however most catalysts suffer from low yields at high conversion levels due to the thermodynamically favored oxidation of both reactant and product to carbon oxides. We have recently reported [5] the high potential of a new class of catalytic materials based on nickel for the oxidative dehydrogenation of ethane to ethylene. The developed bulk Ni-Nb-O mixed nano-oxides exhibit high activity in ethane ODH at low reaction temperature and very high selectivity (~90% ethene selectivity), resulting in an overall ethene yield of 46% at 400°C. Varying the Nb/Ni atomic ratio led to an optimum catalytic performance for the catalyst with a Nb/Ni ratio equal to 0.176. Detailed characterization of the as-synthesized materials with several techniques [5] showed that the key component for the excellent catalytic behavior is the Ni-Nb solid solution formed upon the introduction of niobium in NiO. The incorporation of Nb in the NiO lattice, by either substitution of nickel atoms and/or filling of the cationic vacancies in the defective non-stoichiometric NiO surface structure, led to a reduction of the electrophilic oxygen species (O^-), abundant on NiO and responsible for the total oxidation of ethane to carbon dioxide. Mechanistic studies, performed by employing various isotopic $^{18}O_2$ exchange techniques on Nb-doped NiO [6], showed that the reaction proceeds via a Mars and van Krevelen type mechanism, with participation of lattice oxygen anions. Based on the obtained mechanistic information, we performed and present in this work kinetic studies which led to the development of a macroscopic kinetic model, describing the catalytic behavior of the $Ni_{0.85}Nb_{0.15}$ catalyst in the ethane ODH reaction.

2. Experimental part

The kinetic studies were conducted at atmospheric pressure in a continuous fixed bed flow reactor. The reaction products were analyzed on line by a Perkin Elmer gas chromatograph in a series-bypass configuration equipped with a thermal conductivity detector (TCD). The main

reaction products were C_2H_4, CO_2 and H_2O. The kinetic experiments were conducted at four different temperatures (240, 260, 280 and 300°C) with varying inlet partial pressures of ethane (1.01-9.12 kPa), oxygen (1.01-20.26 kPa) and balance helium. In order to assess the secondary reactions of ethene oxidation, the same experiments were repeated using ethene as feed instead of ethane. Catalyst weight was adjusted accordingly in each set of conditions in order to keep the reactants conversion lower than 6% and maintain differential conditions in the reactor. The total flow rate was 150cm^3/min in all cases. The absence of heat and mass transfer limitations were confirmed theoretically and experimentally.

3. General considerations for kinetic modelling

The kinetic parameters were determined by modelling the quartz tubular reactor as an isothermal axial plug flow reactor. Assuming steady-state operation, the material balance for each gas phase component was expressed by the PFR equation, resulting in a first-order differential equation system. Surface coverage values were calculated by numerically solving a system of algebraic equations describing the mass balance of each species and the global balance of the normalized surface coverages for each centre. The system of differential equations was numerically integrated over the catalyst mass for each set of initial experimental conditions, using an explicit Runge-Kutta (2,3) pair method. In the parameter search procedure, the minimization was performed by first obtaining initial estimates of the kinetic constants by employing a genetic algorithm, which were then used as starting values for non-linear regression analysis, using a Gauss-Newton algorithm with Levenberg-Marquardt modifications. All computational calculations were performed with MATLAB software.

4. Results and Discussion

The product distribution in ethane ODH over the $Ni_{0.85}Nb_{0.15}$ catalyst [5] allowed the construction of a very simple reaction network consisting of the oxydehydrogenation of ethane to ethylene ($C_2H_6 + 0.5O_2 \rightarrow C_2H_4 + H_2O$), the primary oxidation of ethane to carbon dioxide ($C_2H_6 + 3.5O_2 \rightarrow 2CO_2 + 3H_2O$) and the secondary oxidation of produced ethene to CO_2 ($C_2H_4 + 3O_2 \rightarrow 2CO_2 + 2H_2O$. The influence of the reactants partial pressure on the ethane oxidative dehydrogenation reaction was studied by maintaining the partial pressure of the one reactant constant and varying that of the other, while keeping the total inlet flow constant by balancing with He. Increasing the ethane concentration in the feed stream proved beneficial for the ODH reaction, increasing similarly the consumption rate of ethane and oxygen and formation rate of ethylene and carbon dioxide. Concerning the oxygen concentration, at low oxygen pressures all rates increased almost linearly up to a C_2H_6/O_2 ratio of 1. Further increase reduced the influence of O_2 on the ethane consumption and ethene

formation rate, while that of O_2 and CO_2 kept increasing, showing that high oxygen concentrations promote total oxidation in expense to the oxydehydrogenation reaction.

The kinetic data obtained from the experiments described above were then used in order to develop the kinetic model and estimate the corresponding parameters. Based on the mechanistic indications derived from isotopic and transient experiments presented elsewhere [6], which confirmed the participation of catalyst oxygen in both the selective and unselective steps of the reaction sequence, we formulated four basic models of the Mars-van Krevelen (MVK) mechanism assuming the presence of one or two types of active sites with several variants. The kinetic parameters for ethylene oxidation were obtained separately by fitting data with ethylene/oxygen as feed and were then considered constant for the estimation of the rest of the model parameters. For brevity reasons, we present here the reactions, rate equations and estimated kinetic parameters, with the 95% confidence intervals for the dominant kinetic model (R-square value 0.99978) in Table 1. The dominant kinetic model considers the presence of two types of active sites, sites [M-O] responsible for the ethane ODH and ethene overoxidation reaction and sites [T-O] active for the direct oxidation of ethane to CO_2. Based on the indications derived from the $^{18}O_2$ isotopic experiments [6], sites [M-O] correspond to strongly bonded lattice O^{2-} species, whereas sites [T-O] to the limited amount of non-stoichiometric O^- species which remain on the surface after incorporation of Nb.

Table 1. *Reactions, rate equations and estimated kinetic parameters for the proposed model*

REACTION	RATE EQUATION	KINETIC PARAMETERS	
		k_o or K_o	E or ΔH (kJ/mol)
$C_2H_6 + [M\text{-}O] \rightarrow C_2H_4 + H_2O + [M]$	$r_1 = k_1 p_{C_2H_6} \theta_{[M\text{-}O]}^2$	12.523 ± 0.295	98.43 ± 2.40
$C_2H_6 + [T\text{-}O] + 3O_2 \rightarrow 2CO_2 + 3H_2O + [T]$	$r_2 = k_2 p_{C_2H_6} \theta_{[T\text{-}O]}^2$	2.040 ± 0.089	88.82 ± 4.25
$C_2H_4 + [M\text{-}O] + 2.5O_2 \rightarrow 2CO_2 + 2H_2O + [M]$	$r_3 = k_3 p_{C_2H_4} \theta_{[M\text{-}O]}^2$	3.868 ± 0.389	105.66 ± 7.60
$H_2O + [M] + [M\text{-}O] \leftrightarrow 2[M\text{-}OH]$	$r_4 = k_4 p_{H_2O} \theta_{[M\text{-}O]} \theta_{[M]} - (k_4/K_4) \theta_{[M\text{-}OH]}^2$	383.53 ± 71.60	-206.88 ± 9.36
$0.5O_2 + [M] \rightarrow [M\text{-}O]$	$r_5 = k_5 p_{O_2}^{1/2} \theta_{[M]}$	4.284 ± 0.171	52.49 ± 2.06
$0.5O_2 + [T] \rightarrow [T\text{-}O]$	$r_6 = k_6 p_{O_2}^{1} \theta_{[T]}$	0.981 ± 0.031	90.84 ± 2.86

A comparison between experimental and simulated data is shown in Figure 1 for all data points included in the parameter estimation. The parity plots do not show any systematic deviations, with all points equally spread around the diagonal line, indicating that the deviations are due to experimental and not model-based error.

In a further step, the developed kinetic model was employed in order to predict the catalytic performance data of the $Ni_{0.85}Nb_{0.15}$ catalyst reported in [5], which were realized in considerably different conditions than the kinetic experiments. The results of the model simulation (represented by full lines) and the experimental data (represented by symbols) for
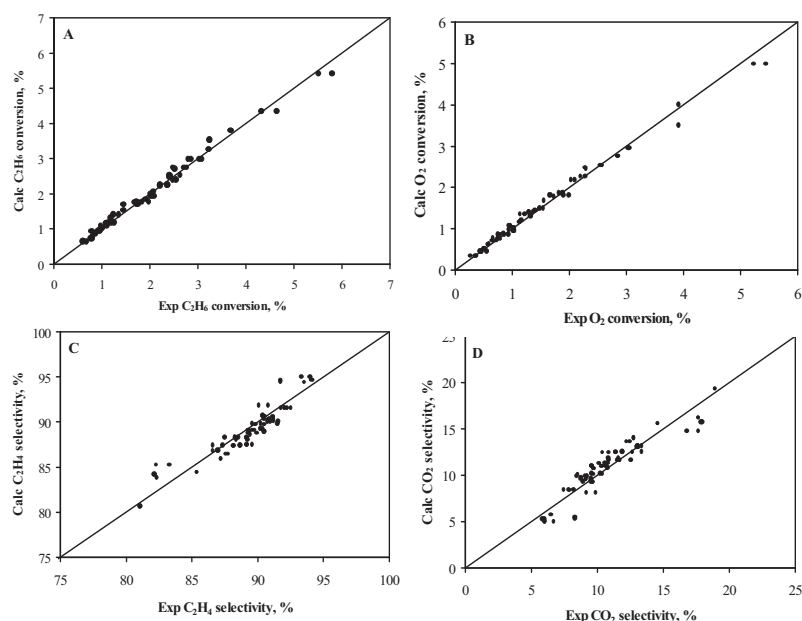
Figure 1. *Parity plots of measured and calculated values for dominant kinetic model including all data used in parameter estimation. (a) C_2H_6 conversion; (b) O_2 conversion; (c) C_2H_4 selectivity; (d) CO_2 selectivity.*

ethane and oxygen conversion and ethylene and CO_2 selectivity versus temperature are illustrated in Fig. 2. The excellent ability of the model to predict the catalytic data is apparent. The successful application of the kinetic model proves the physicochemical sense of the kinetic parameters and ensures that the underlying mechanistic assumptions are correct.

5. Conclusions

A mechanistic kinetic model, able to successfully predict the catalytic performance of the $Ni_{0.85}Nb_{0.15}$ catalyst in ethane ODH over a wide range of experimental conditions, was developed.

Figure 2. Comparison of experimental and simulated results

The kinetic modelling showed that the ethane oxidative dehydrogenation reaction on Ni-Nb-O occurs via a redox parallel-consecutive reaction network, with the participation of two types of active sites, strongly bonded lattice O^{2-} species responsible for the ethane ODH and ethene overoxidation reaction and non-stoichiometric O^- species, active for the direct oxidation of ethane to CO_2.

References

1. G. Centi, F. Cavani, F. Trifiro, Selective Oxidation by Heterogeneous Catalysis, Kluwer Academic Publishers/Plenum Press, New York, 2001.

2. M.A. Banares, Catal. Today 51 (1999) 319.

3. T. Blasco and J.M. Lopez-Nieto, Appl. Catal. A 157 (1997) 117.

4. H.X. Dai, C.T. Au, Current Topics in Catal. 3 (2002) 33.

5. E. Heracleous, A.A. Lemonidou, J. Catal. 237 (2006) 162.

6. E. Heracleous, A.A. Lemonidou, J. Catal. 237 (2006) 175.

KINETICS OF ENZYMATIC TRANS-ESTERIFICATION OF LOW QUALITY OLIVE OIL FOR THE PRODUCTION OF BIODIESEL

V. Calabrò, M. G. De Paola, S. Curcio, G. Iorio

Dipartimento di Ingegneria Chimica a dei Materiali, Università della Calabria

Via P. Bucci Cubo 45/A, Arcavacata di Rende (CS) – ITALY

Tel. +39 0984 496703 -+39 0984 496672 Fax: +39 0984 496655

E-mail: vincenza.calabro@unical.it, stefano.curcio@unical.it, gabriele.iorio@unical.it

Summary

In this paper the enzyme trans-esterification of low purity (60%) triolein or low quality olive oil with ethanol has been studied in a reaction medium containing hexane as solvent at temperature of 37 °C finalised to the production of biodiesel from vegetable oil.

As enzyme the Lipase from Mucor Miehei has been used, immobilized on ionic exchange resin, with the aim to achieve high catalytic specific surface and to recovery, regenerate and reuse the biocatalyst to improve the performance of enzyme trans-esterification in the biodiesel production. A kinetic analysis has been carried out to define the reaction path and the rate equation whose kinetic parameters have been also calculated. The kinetic model has been validated with experimental data. The yield of the reaction with different reactor configurations has been also predicted.

Introduction

Biodiesel is a mixture of alkyl esters of fatty acids from biological source. It that can be obtained by means of trans-esterfication (catalytic or bio-catalytic) of glycerides of fatty acids of vegetal oils with short chain alchools. Compared with other vegetable oils, biodiesel shows a lower viscosity and it's less polluting with respect to the production of CO_2, (saving 2.4 – 3.2 kg of CO_2 per kg of fuel). Furthermore, it is biodegradable and, during the combustion, a reduced level of particulate, carbon monoxide and nitrogen oxides is produced.

The research of an alternative fuel for diesel motor has acquired great importance because of both the reduction of oil stocks and of the environmental pollution due to the emissions of greenhouse gases from the combustion of oil products.

It seems very interesting to use low quality olive oil as substrate for the trans-esterification to produce biodiesel, since it not usable for food industry, should be in this way revalued and recovered.

Enzyme trans-esterification is the most expensive technique but it offers some advantages such as:

 – the presence of free fatty acids in the reaction mixture doesn't imply the production of saponification products;

 – a higher yield and a better glycerol recovery can be obtained

Materials and methods

Triolein pure at 60% (same composition of olive oil) and olive oil from husk have been tested as reactants, with Ethanol as alcohol and Hexane as solvent.

Lipase from Mucor Miehei, immobilyzed on ionic exchange resin (Lypozyme) has been used as biocatalyst, after a preliminary screening based on the optimization of costs and performances of lipases from different sources.

The concentrations of reactants and products have been measured by HPLC (JASCO) under the following conditions: RI detector, eluent phase acetone/acetonitrile 70/30 vol., flux 1 ml/min, internal normalization as integration method. Before the analysis the lipase has been removed with centrifugation and the hexane with evaporation.

Experiments have been carried out using a batch reactor. The operating parameters that have been investigated are the feed Enzyme/Substrate ratio, the reaction medium (anhydrous or not), the reactants molar ratio (in particular the feed Ethanol/Substrate ratio).

All the experimental reactions have been carried out at Temperature $T = 37\ °C$ and $pH = 7$.

Experimental Results

Experimental results permit to estimate the effect of reaction medium on instantenous yield of reaction, the effect of feed Enzyme/Substrate mass ratio, and Ethanol/Substrate as on the reaction behaviour and on the kinetic rate.

To verify the possibility to recovery and reuse the enzyme, after the reaction, the Lipase has been recovered by filtration, washed three times with acetone, then dried at room temperature and reused for the new reaction. More reaction cycles have been carried out with good yield with both triolein and olive oil the reaction yield was higher then 75%.

OP-1-2

Kinetic Analysis

Experimental data have been elaborated to evaluate the kinetic rate behaviour as function of triolein concentration and as function of triglycerides concentration when using olive oil.

The reaction pattern can be predicted as a sequence of three reactios in series, with the production of one mole of esther for step and the production of glycerol only at the third step, when also the monoglycerides are converted. But the lipase that has been used shows a 1-3 regio-specificity, consequently, the glycerol production is strongly limited

A ping-pong mechanism with inhibition of ethanol has been preliminarly hyphotesized to describe the kinetics of the reaction with triolein, and the kinetic rate **v** has been formulated as function of concentration of triolein (A), ethanol (B), mixture of glycerides (P) and Ethyl Oleate (Q), as following:

$$\frac{v}{E} = \frac{\alpha \cdot [A] \cdot [B] - \beta \cdot [P] \cdot [Q]}{[A]^2 + \delta \cdot [A] + \varepsilon}$$

where δ and ε are functions of initial ethanol concentration B_0:

$$\delta = \delta_{B0} \cdot B_0 + \delta_0 \qquad \varepsilon = \varepsilon_{B0}^2 \cdot B_0^2 + \varepsilon_{B0} \cdot B_0 + \varepsilon_0$$

All the parameters δ_0, δ_{B0} and ε_0, ε_{B0} have been estimated.

When using olive oil, all triglycerides have been calculated and time evolution of total tryglicerides during all the experiments seems to show a pseudo first order kinetic behaviour.

In the literature it is reported that the reactions catalysed from free or immobilised lipase follow a ping-pong bi-bi mechanism in which either acylation or deacylation of the enzyme, first order reaction, is the rate-controlling step. Consequently a simplified kinetic equation rate has been hypothized and integrated to give the instantaneous concentration of total triglycerides Y according to the following equation:

$$Y = c_{tl} + (c_0 - c_{tl}) \cdot e^{-k \cdot t}$$

where C_{tl} and (C_0-C_{tl}) are the coefficients that depend on the operating conditions, C_{tl} being the concentration of triglycerdes at long time (t > 24 hr) and C_0 the initial concentration of triglycerides; k is a kinetic parameter also depending from operating conditions.

All these parameters have been estimated with their functionality with operating conditions.

Both kinetic models showed a good agreement with experimental data.

It was possible to estimate the operating optimal conditions, as reported in the figure 1.

Conclusions

The trans-esterification carried out with low purity triolein (60%) and low quality olive oil gave the same results. The immobilized enzyme can be successfully used for the trans-estheryfication, confirming the possibility to be recovered and reused. Furthermore, a good stability of the enzyme when reused for further reaction cycles has been observed.

The kinetic mechanism and the kinetic models with the evaluation of kinetic parameters have been defined and the optimal operating conditions have been calculated too, both with triolein and with olive oil from husk.
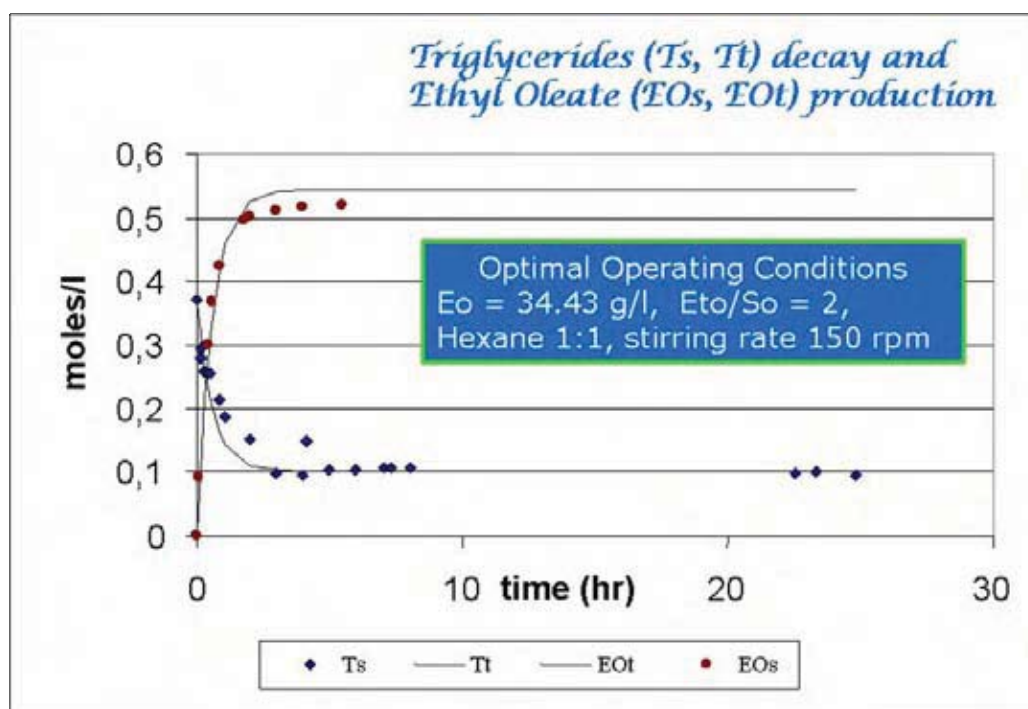
Figure 1 Optimal Operative Conditions for enzymatic trans-estherification of oil; comparison from theoretical predictions (t) and experimental data (s).

References

1. H.Fukuda, A.Kondo, H.Noda, (2001), REVIEW Biodiesel Fuel Production by Transesterification of Oils, Journal of Bioscience and Bioengineering, Vol 92, No 5, 405-416
2. F.Ma, M.A.Hanna, (1999), Biodiesel production: a review, Bioresource Technology, 70, 1-15.
3. G. Knothe, (2005), Dependence of biodiesel fuel properties on the structure of fatty acid alkyl esters, Fuel Processing Technology, 86, 1059-1070.
4. M.Iso, B.Chen, Masashi Eguchi, T.Kudo, S.Shrestha, (2001), Production of Biodiesel fuel from triglycerides and alcohol using immobilized lipase, J.of Molecular Catalysis B:Enzymatic, 16,53-58.
5. A.V.L.Pizarro, E.Y.Park, (2003), Lipasi-catalyzed production of biodiesel fuel from vegetable oils container in waste activated bleaching earth, Process Biochemistry, 38, 1077-1082.
6. C.J.Shieh, H.F.Liao, C.C.Lee, (2003), Optimization of lipasi-catalyzed biodiesel by response surface methodology, Bioresource Technology , 88, 103-106
7. M. M. Soumanou, U.T.Bornscheuer, (2003), Improvement in lipase-catalyzed synthesis of fatty acid methyl esters from sunflower oil, Enzyme and microbial technology, 33, 97-103.

REACTION RATE EQUATION OF COMPLEX CATALYTIC REACTION IN TERMS OF HYPERGEOMETRIC SERIES

Mark Lazman

Aspen Technology Inc. 900 – 125 - 9th Avenue SE, Calgary, Alberta CANADA T2G OP6

e-mail: Mark.Lazman@aspentech.com, tel: (403) 303-1000, fax: (403) 303-0927

Introduction The Quasi Steady State Approximation is a common method for generation of kinetic models of complex catalytic reactions. This is a zero-order approximation of original (singularly perturbed) system of differential equations corresponding to the reaction mechanism. We are simply replacing differential equations corresponding to the "fast" intermediates with algebraic equations. This algebraic system defines the chemical source function (i.e. rate of generation or consumption of reagents) for the rest of our model (for instance, the model of catalytic reactor). An explicit reaction rate equation is most effective for the applications form of source function.

Steady state reaction rate Assuming Mass Action Law (MAL), our algebraic system consists of polynomial equations. Models, corresponding to the linear reaction mechanisms, allow the explicit formula for reaction rate. These expressions were interpreted in terms of reaction graph in enzyme kinetics and, later, in heterogeneous catalysis. Additional assumptions make possible in some cases the explicit reaction rate expressions for models corresponding to the non-linear reaction mechanisms. There are two classic approximations, hypothesis of rate-limiting step (i), and vicinity of thermodynamic equilibrium (ii). Hypothesis of the single rate-limiting step was a key assumption in the theory of reaction rate of heterogeneous catalysis founded independently by J. Horiuti and by G.K. Boreskov in 1940s. Approximations (i) and (ii), as well as theory of linear mechanisms produce the following reaction rate equation for single-route reaction mechanism

$$r = r_+ \{ 1 - [\frac{f_-(\mathbf{c})}{K_{eq} f_+(\mathbf{c})}]^M \} , \tag{1}$$

where r is the steady-state reactiond rate, r_+ is the reaction rate in forward direction, K_{eq} is the equilibrium constant of the overall reaction, $f_+(\mathbf{c})$ and $f_-(\mathbf{c})$ are the products of concentrations written according to the MAL for the net stoichiometric equation (forward and

reverse), and $\mathbf{c}$ is the vector of concentrations of reactants and products of the net reaction. The degree M is 1 for linear mechanism as well as for approximation (ii) and $M = \nu_L^{-1}$ in the case of single rate-limiting step (ν_L is the stoichiometric number of the rate-limiting step). While this equation and its particular forms like the Hougen-Watson kinetic equation play a fundamental role in the kinetics of heterogeneous catalytic reactions, there are open problems. For instance, what is the form of kinetic equation corresponding to the expression (1) in the general case? What is the domain of applicability of equation (1)? What is the general expression for r_+?

Kinetic polynomial To some extent these questions were answered in the theory of non-linear MAL kinetic models [1]. We have proved that the system of polynomial equations corresponding to the single-route mechanism of heterogeneous catalytic reaction has the resultant with respect to reaction rate, i.e. the polynomial

$$R(r) = B_L r^L + ... + B_1 r + B_0, \tag{2}$$

vanishing iff r corresponds to the zero of this system. This resultant, named *kinetic polynomial*, is the general form of kinetic equation corresponding to the single-route reaction mechanism. Coefficients $B_0,..., B_L$ are polynomials in terms of reaction weights of elementary steps. The fundamental property of polynomial (2) is

$$B_0 \sim C = k_+ f_+(\mathbf{c}) - k_- f_-(\mathbf{c}) \ , \tag{3}$$

where $k_\pm = \prod_{i=1}^{n} k_{\pm i}^{\nu_i}$ is the net reaction constant, $k_{\pm i}$ are the kinetic constants (forward and reverse) of ith reaction stage, ν_i is the stoichiometric number, and n is the number of reaction stages. Property (3) provides the thermodynamic correctness of kinetic polynomial; it guarantees that there is a zero of polynomial (2) vanishing at the thermodynamic equilibrium. This zero belongs to the branch of multivalued algebraic function $r(B_0,..., B_L)$. The latter (i.e. the *thermodynamic branch*) is defined in the vicinity of thermodynamic equilibrium by the lower order terms of polynomial (2). Expression

$$r \approx -B_0 / B_1 \tag{4}$$

gives in many cases a reasonable approximation of the exact reaction rate dependence in the vicinity of thermodynamic equilibrium [1]. Expression (4) corresponds to the expression (1) for $M = 1$. Thus, kinetic polynomial theory predicts expression (1) in the vicinity of thermodynamic equilibrium. As a byproduct of this theory, we found the explicit r_+ expression for the case of single rate-limiting step [1].

OP-1-3

Reaction rate in terms of hypergeometric series General algebraic equation cannot be solved in terms of radicals if $L > 4$ (Galois). It is possible, however, to find the analytic (not necessarily algebraic) expression for zero of general polynomial. For instance, F.Klein (late XIX century) showed that zero of quintic ($L = 5$) can be found from solution of some differential equation in terms of hypergeometric functions. In modern times, Sturmfels [2] expressed zeros of algebraic equation in terms of A-hypergeometric series. Applying this result to the thermodynamic branch, we can write the following reaction rate equation in terms of multidimensional hypergeometric series

$$r = -\frac{B_0}{B_1} \cdot D, \quad D = \sum_{i_2=0,\dots,i_n=0}^{\infty} \frac{(-1)^{i_1}}{i_0+1} \binom{i_1}{i_2,\dots,i_n} \cdot \frac{B_0^{i_0} \prod_{k=2}^{n} B_k^{i_k}}{B_1^{i_1}} , \quad i_1 = \sum_{k=2}^{n} k i_k, i_0 = \sum_{k=2}^{n} (k-1)i_k . \quad (5)$$

It follows from property (3) and other properties of kinetic polynomial that we can represent the equation (5) as a *four-term reaction rate equation*

$$r = \frac{k_+(f_+(c) - K_{eq}^{-1} f_-(c))}{-B_1'} \left(1 + \sum_{i=1}^{\infty} t_i C^{d_i}\right), \quad (6)$$

where B_1' is either coefficient B_1 or its multiplier (see [1]) , t_i $i = 1,2,\dots$ are rational functions in $k_{\pm i}, \mathbf{c}$, and integer degree d_i is non-negative.

The latter property guarantees vanishing of reaction rate at the thermodynamic equilibrium. Equation (6) corresponds to the equation (1) with $M = 1$. Also, similar to the Hougen-Watson equation, we have the kinetic term k_+, the potential term $f_+(c) - K_{eq}^{-1} f_-(c)$ as well as the term $-B_1'$ which can be interpreted as the adsorption resistance term.

However, unlike the known approximations, our exact expression has the fourth term $(1 + \sum_{i=1}^{\infty} t_i C^{d_i})$ that represents the infinite series. It is important to know the convergence domain of this series. It is intuitively clear that reaction rate series (6) may converge near equilibrium. We have found that series (6) could provide an excellent fit to the exact reaction rate not only in the vicinity of thermodynamic equilibrium but also *far from thermodynamic equilibrium*. For the model, corresponding to the non-linear Eley-Rideal mechanism, series (6) converges for any set of feasible values of kinetic parameters. For the case of Langmuir-Hinshelwood mechanism, we found a certain convergence domain. The region of non-

convergence for the LH model looks similar to the domain of steady state multiplicity (see Fig. 1).
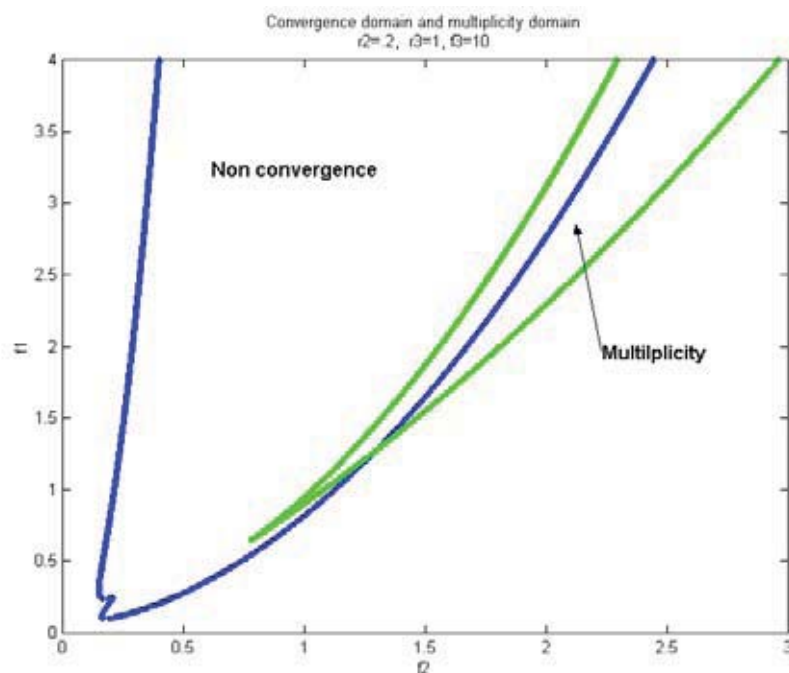
Fig.1 Convergence and steady-state multiplicity domains for Langmuir-Hinshelwood mechanism on the plane f1, f2 at r1 = 0; f1,f2,f3 and r1,r2,r3 are reaction weights of forward and reverse reactions of corresponding stage

Our case study shows that even the first term (4) provides satisfactory approximation of exact reaction rate value. Unlike classical approximations, the approximation with truncated series (6) has non-local features. We may think of the domain of convergence of series (6) as a domain where reaction rate is relatively small.

Conclusions We have presented a new form of quasi-steady-state model of complex catalytic reaction corresponding to the single-route reaction mechanism in terms of multidimensional hypergeometric series in coefficients of kinetic polynomial. This form generalizes known explicit reaction rate equations and provides the exact solution of kinetic model for non-linear reaction mechanism.

References

[1] M.Z. LAZMAN, G.S YABLONSKII. *Kinetic Polynomial: A New Concept of Chemical Kinetics* // In: The IMA Volumes In Mathematics And Its Applications, V. 37: Patterns and Dynamics in Reactive Media. R. Aris, D.G. Aronson, H.L. Swinney Eds. Springer-Verlag, New York, (1991), P. 117-150.

[2] B. STURMFELS *Solving algebraic equations in terms of A-hypergeometric series*, Discrete mathematics, v, 210,1-3, (2000), P.171-181.

KINETICS FOR THERMAL OXIDATION OF LEAN METHANE – AIR MIXTURES IN REVERSE FLOW REACTORS

K. Gosiewski[1], K. Warmuzinski[2], M. Jaschik[2], M. Tanczyk[2]

[1]*Institute of Chemistry and Environmental Protection, Jan Dlugosz University in Czestochowa, ul. Armii Krajowej 13/15, 42-201 Czestochowa, Poland,*

E-mail: k.gosiewski@ajd.czest.pl;

[2]*Institute of Chemical Engineering, Polish Academy of Sciences, ul. Baltycka 5, 44-100 Gliwice, Poland.*

Large amounts of methane are discharged into the atmosphere with mine ventilation air. A single ventilation shaft can emit over 500 000 m^3(STP)/h of ventilation air in which methane content can be as high as 1 vol.% The abatement of this emission is therefore important from both economic and environmental point of view, as the gaseous fuel is inadvertently lost, simultaneously contributing to greenhouse effect. A number of studies have been carried out to utilize this methane via combustion and to recover the energy thus produced. Due to very low CH_4 concentrations the most promising solution seems to be autothermal combustion in reverse flow reactors. So far, most of the studies have focused on catalytic combustion in CFRRs (catalytic flow reversal reactors) - cf., among others, the work done by CANMET in Canada [1]. Simulations and experimental studies performed within a European project [2] show that CFRRs are characterized by high operating temperatures (up to 800 ^{o}C for the 0.5 % Pd / γ-Al_2O_3 catalyst), leading to the deactivation or even destruction of the relatively expensive catalyst. Therefore, non-catalytic oxidation in TFRRs (thermal flow-reversal reactors) is now frequently regarded as an attractive alternative. Such reactors have long been used, e.g. for the homogeneous (thermal) combustion of volatile organic compounds (VOCs). However, obvious differences exist between the combustion of VOCs and the oxidation of mine ventilation methane in flow-reversal reactors. In the former case no heat is withdrawn from the system (sometimes the reactor has even to be heated in order to sustain autothermicity), whereas during the combustion of lean methane-air mixtures it is estimated that some 7 MW_t can be produced per 100 000 m^3(STP)/h of the gaseous feed. Thus, an installation connected to an average ventilation shaft can produce several dozen MW_ts. The thermal combustion in a TFRR should be carried out under conditions that do not promote excessive formation of NO_x, i.e. at maximum temperatures in the reactor below

1 300 $^{\circ}$C. With the combustion of methane such temperatures are quite possible. The use of a TFRR for the combustion of lean methane mixtures requires therefore detailed studies to determine the reasonable operating conditions. While for the CFRR thermal combustion occurs in parallel to catalytic oxidation, for the TFRR overall conversion and other parameters are much more dependent on kinetic parameters that describe thermal combustion. Therefore if simulation is to be used in process analysis, then the reliability of kinetic equations used becomes by far more important than for the CFRR. Unfortunately, kinetic data for such combustion, taken from various sources, differ significantly. Moreover, the combustion in the TFRR takes place in voids of the reactor bed. Therefore, the first order kinetic equations of

the type
$$r_{hom} = k_0 \exp\left(-\frac{E}{RT}\right) \times C_{CH_4}$$

exhibit dependence of the experimentally obtained kinetic parameters (k_0 and E) on the geometry of the bed used in the experiments (e.g. diameter of the combustor or the particle size for pelletized beds). This, obviously, is difficult to explain theoretically. Such dependence was included in the kinetic equation developed by the Boreskov Institute of Catalysis SB RAS (BIC) for [2].

This paper presents results for the TFRR computer simulations based on various kinetic equations of the foregoing type taken from [3], [4], on the kinetics developed in the Institute of Chemical Kinetics and Combustion SB RAS (ICKC) in [] and, additionally, on our own kinetic data measured in the Institute of Chemical Engineering, Polish Academy of Sciences (ICE) [5]. Simulations were carried out for a 30 000 m^3(STP)/h pilot plant (similar to the CFRR analyzed in [2]). The computations reveal that the results differ significantly for the different kinetic equations used in the simulations. The maximum temperature varied from 827 to 1190 $^{\circ}$C, while the reactor starting temperature (i.e. the initial preheating), necessary to heat up the reactor to an autothermal cyclic steady state had to be assumed case by case within a range of 660 to 950 $^{\circ}$C.

These simulations are summarized in the Table:

Kinetic Equation	k_o [1/sec]	E [J/mol]	Effective conversion	Starting temperature	Maximum temperature
ICKC [2]	1.2×10^{10}	209 340	0.937	1063 K (790 $^{\circ}$C)	1310 K (1037 $^{\circ}$C)
Coekelbergs & Mathieu [3] [*]	1.1×10^{11}	263 768	0.9999	1223 K (950 $^{\circ}$C)	1256 K (983 $^{\circ}$C)
Boshoff-Mosert & Viljoen [4]	1.8×10^{8}	130 000	0.9999	933 K (660 $^{\circ}$C)	1100 K (827 $^{\circ}$C)
ICE [5]	1.15×10^{7}	138 650	0.997	1223 K (950 $^{\circ}$C)	1463 (1190 $^{\circ}$C)
[*] For this case kinetic equation of the form: $r_{hom} = k_0 \exp\left(-E/RT\right) \times C_{CH_4}^{0.5} \times C_{O_2}^{0.5}$ was used.					

OP-1-4

On the other hand, for all the kinetic equations employed in the simulations (except for that given by the ICKC in []) a very high methane conversion (close to 100%) is easily achieved in the cyclic steady state. Only in case [2] conversion is lower, but still exceeds 90%.

Conclusion

Large differences in simulation results are due to the fact that experimental conditions of homogeneous combustion in a packed bed or in an empty space can produce substantial differences in the parameters of the estimated kinetic equations. It was assumed by BIC in [2] that combustion in such an environment follows a two-step consecutive scheme $CH_4 \rightarrow CO$ and $CO \rightarrow CO_2$. It cannot be expected that a universal kinetic equation for the TFRR can readily be obtained. On the other hand, simulations for various kinetic equations reveal that either temperature range or conversion in such a reactor is acceptable from the practical standpoint. Since the operating temperature range of the TFRR is very important in the process design, one should rely upon experiments on a reasonable scale rather than on purely numerical simulations.

1. Sapoundjiev H., Trottier R., Aube F. (1999). *Greenhouse Gas Control Technologies, Elsevier Science* 805 – 810.

2 . European Union Grant (Contract No. ICA2-CT-2000-10035) – Final Report (2003).

3 . Coekelbergs & Mathieu: Genie Chemique June 1963 p. 183

4 . Boshoff-Mosert & Viljoen: Chem. Eng. Sci. 1996 p. 1107

5 . Gosiewski K., Matros Yu., Warmuzinski K., Jaschik M., Tanczyk M. (2006) – to be presented at USPC-5, Osaka, Japan

CHOICE OF A REACTOR TO STUDY KINETICS OF HYDROGEN RELEASE FROM METHYLCYCLOHEXANE

G.V. Santa Cruz B.[a], Ph. Kerleau[a], I. Pitault[a], <u>V. Meille</u>[a], F. Heurtaux[b]

[a]*Laboratoire de Génie des Procédés Catalytiques – CNRS/CPE – BP 2077 –*
69616 Villeurbanne Cedex – France –
00 33 (0) 4 72 43 17 55 – Fax : 00 33 (0) 4 72 43 16 73 – vme@lgpc.cpe.fr
[b]*Renault – Direction of research – 1 Avenue du golf – 78288 Guyancourt – France –*
00 33 (0)1 30 02 89 05 - Fax : 00 33 (0)1 30 02 83 05 - fabien.heurtaux@renault.com

Introduction

To feed an on-board fuel cell, hydrogen can either be produced in situ by a chemical reaction or chemically or physically stored. The process we are studying can be either seen as a production or a storage one. It consists in releasing hydrogen from naphthenic molecules. The by-products of the dehydrogenation reaction, aromatic compounds, can be recycled ex situ in a hydrogenation plant to restore the hydrogen-rich reactants.

The hydrogen-rich reactant chosen was methylcyclohexane (MCH) because of its high capacity in hydrogen (6 wt-%) and the lower toxicity of the produced toluene compared to benzene. Its dehydrogenation is very endothermic (204kJ/mol) and thus requires a particular attention with regard to the reactor. A previous published study on the same reaction by Touzani et al. [1] showed that a 6cm-diameter reactor filled with 1.6mm-diameter catalyst induces thermal gradient between the core and the reactor wall of about 160K [Tw = 610K – Tc = 450K]. To increase the efficiency of an on-board engine, and thus avoid heat transfer limitations, a solution consists in washcoating the wall of a plate-reactor with the catalyst.

However, to design car engine, published kinetics [2, 3] can not be used, firstly, due to the different catalyst natures and, secondly, due to the omission of thermodynamics of this reversible reaction. To determine the kinetics of the reaction, two solutions can be envisaged: either a laboratory reactor implementing a thin catalyst layer coated on tube wall or the same scrapped catalyst in a classical micro packed bed.

In this work, the first alternative has been chosen. Firstly, we have determined the kinetics using the washcoated catalyst and we have shown the pertinence of our choice comparing its performance with that of a classical reactor (packed bed).

OP-1-5

Kinetics

An annular reactor composed of one catalytic wall has been used. The catalyst was obtained by coating the external surface of a 6mm stainless steel tube with γ-Al$_2$O$_3$ (around 50μm thick) and impregnating the alumina layer with Pt(acac)$_2$. This tube was placed in another tube (8mm I.D.). The reactor was heated by 5 independent copper shells. The isothermicity of the reactor was checked by comparing the temperatures of both sides of the annular space. Methylcyclohexane flow rate (0.05 to 2mL/min liquid flow rate), the temperature (598 to 658K), the total pressure (2 to 5.5 bar), the hydrogen flow rate (0 to 40NmL/min) and the inlet molar MCH/toluene ratio (100/0 to 30/70) were varied. The MCH conversion was calculated from the GC analysis of the condensed phase and confirmed from the produced hydrogen flow rate.

Under kinetic control, the conversion was found to be independent on the MCH pressure and on the hydrogen pressure. Nevertheless, the presence of hydrogen stabilises the catalyst activity and avoids deactivation.

Considering an ideal and isothermal plug flow model of reactor (Pe > 100) and a Langmuir-type kinetic law, the kinetic parameters have been estimated using a Levenberg-Marquardt routine in Matlab.

$$r = \frac{k_0 \exp\left(\frac{-E_a}{RT}\right) K_{MCH} P_{MCH}}{1 + K_{MCH} P_{MCH} + K_{TOL} P_{TOL}} \left(1 - \frac{P_{H_2}^3 P_{TOL}}{P_{MCH}}\right) \qquad [mol.s^{-1}.g_{Pt}^{-1}]$$

with $k_0 = 13.34 \pm 6.54$ mol.s^{-1}.g$_{Pt}^{-1}$

$K_{MCH, 0} = 1.34 \cdot 10^{-2} \pm 0.32 \cdot 10^{-2}$ bar^{-1}

$K_{TOL, 0} = 2.09 \cdot 10^{-5} \pm 0.74 \cdot 10^{-5}$ bar^{-1}

$E_a = 28.46 \pm 2.56$ kJ.mol^{-1}

$H_{MCH} = 31.2$ kJ.mol^{-1} [4]

$H_{TOL} = 60.3$ kJ.mol^{-1} [4]

Comparison of reactor performance - simulation

A series of simulations was carried out to justify the choice of our reactor instead of more traditional fixed bed reactors. Our annular reactor was compared to packed beds containing the same amount of catalyst (0.82g of 0.1wt-% Pt/Al$_2$O$_3$). The reactor diameters vary between 5.29mm and 15mm with particle diameters varying between 10μm and 200μm.

The simulation was performed using a pseudo-homogeneous bidimensional plug flow model taking into account variations of physical properties of gas and heat transfer coefficients with composition and temperature.

(a)   **(b)**
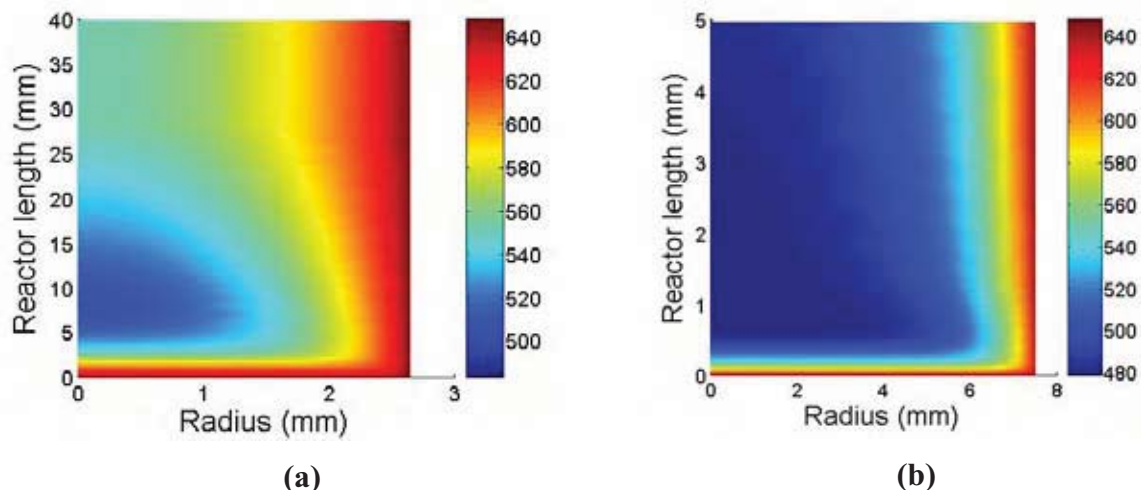
Figure: *Simulated temperature profiles in a) a fixed bed of 5.3mm I.D. filled with particles of 10µm diameter b) a fixed bed of 1.5cm I.D filled with particles of 200µm diameter. Conditions: 648K, 2 bar, 0.4mL/min liquid MCH.*

As the figure shows, the temperature can drop from 648 to 530 K in the reactor corresponding to the scrapped catalyst and even to 480 K in the centre of the bigger packed bed. At the centre of the reactors, the temperatures are so low that they lead to the reverse reaction, and thus to decrease the conversion. In this case, assuming the isothermicity of the reactor leads to overestimate the apparent reaction rate.

Conclusion

The wall-coated reactor was shown to be optimal to estimate methylcyclohexane dehydrogenation kinetics. Moreover the low temperature gradients make this kind of reactor attractive in terms of hydrogen productivity.

This encouraging result has made us hope that the configuration could also be suitable to study the combustion kinetics since we have planed to replace the electric furnace by a combustion reaction (for example, the combustion of a few part of the produced toluene) providing the calories required by the dehydrogenation reaction. However, the combustion experiments have shown important temperature gap between the wall and the gas (150K) and large temperature gradients all along the reactor that can not reasonably be compensated by heating shells.

OP-1-5

This kind of reactor can thus find some limitations due to too large local power production or supply. The nature of the material should be studied to demonstrate the effect of heat conductivity.

Another limitation concerns the catalyst. Its preparation at the reactor wall is not easy to make reproducible and moreover, its characterisation requires the scrapping of the wall and can thus be only achieved at the end of all experiments.

Perspectives

This process could provide an intermediate efficiency between pure hydrogen supply and reforming. Less than 40 grams CO_2 per km should be produced. Nevertheless, more knowledge of the combustion reaction is still required to design a heat-exchange reactor coupling dehydrogenation and combustion reactions.

References

[1] : A. Touzani et al., Int. J. of Hyd. Energy 9 (1984) 929-936.

[2]: A. Touzani et al., Studies in Surface Science and Catalysis 19 (1984) 357-364.

[3]: J. H. Sinfelt, J. Mol. Catal. 163 (2000) 123-128.

[4]: Z.S. Gonenc et al., Recent advances in Chem. Eng. (1990) 266-271.

KINETICS OF AMMONIA OXIDATION OVER PLATINUM FOIL STUDIED IN A NOVEL MICRO-STRUCTURED QUARTZ REACTOR

R. Kraehnert

Leibniz-Institut für Katalyse e. V. an der Universität Rostock, Außenstelle Berlin

Richard-Willstaetter-Str. 12, D-12489 Berlin, Germany

fax: +49 30 6392 4454   e-mail: kraehnert@aca-berlin.de

Introduction

The selective oxidation of ammonia to NO over Pt-containing alloy gauzes is widely applied in the industrial production of nitric acid. The reaction has been studied repeatedly, but a common understanding of the reaction mechanism and kinetics has not been reached yet, due to high exothermicity and reaction rate, reaction-induced changes of Pt morphology, and structure sensitivity of ammonia oxidation on Pt. Since the exothermicity results in ignition, i.e. loss of temperature control in the reactor, the ammonia oxidation on Pt has so far been investigated either at low pressures (reduced heat generation: [1, 2]) or on wall-coated supported catalyst (improved heat removal: [3]), but not on the unsupported polycrystalline Pt that is relevant for the industrial application.

The aim of the present work was to overcome the experimental difficulties related to temperature control during catalytic tests on polycrystalline Pt in the kPa pressure range, and to elucidate the kinetics of Pt-catalyzed ammonia oxidation under such conditions. For this purpose, kinetic data were measured applying a novel micro-structured quartz-reactor. The obtained kinetic data were used to develop the first micro-kinetic model of ammonia oxidation on polycrystalline Pt for reactant partial pressures as high as 6 kPa. Extrapolation of the kinetic model beyond the conditions of the actual experiments shows that the trends observed in low-pressure experiments and also at nearly industrial conditions are reasonably well described.

Methodology

The kinetics of ammonia oxidation over a Pt-foil catalyst was investigated in steady-state experiments applying the novel micro-structured quartz reactor described before [4]. The influence of temperature (286-385°C), feed composition (p_{NH3}=1-6 kPa, p_{O2}=1-6 kPa, p_{NO}=0-0.4 kPa, p_{N2O}=0-0.4 kPa) and time-on-stream on the rate of product formation (N_2,

OP-1-6

N$_2$O, NO) was assessed following an experimental design with 108 different experimental conditions and 16 replicate runs. Additional tests concerned the proof of differential reactor operation and the absence of mass transfer limitations. The surface morphology of selected catalyst samples was studied by electron microscopy prior and after catalytic tests.

Different kinetic models were developed based on available mechanistic information for single-crystal Pt systems and already published models [1, 3]. The kinetic models were fitted to experimental data applying an optimization strategy that employs genetic and Nelder-Mead algorithm. The best-fitting model was identified via model discrimination based on statistic criteria.

Results

Catalysts were equilibrated to reaction conditions prior to kinetic measurements. During this equilibration period the catalysts became more active with time on stream, accompanied by a temperature-dependent faceting of the Pt surface as observed by SEM. Ongoing catalyst activation and mass-transfer limitation imposed the upper temperature limit of the kinetic study.

Nitrogen was the major product at all temperatures, NO was only formed above 374°C. N$_2$ formation increased with partial pressure of ammonia as well as oxygen, but without marked inhibition in excess of either NH$_3$ or O$_2$. In contrast, NO and N$_2$O formation occurred preferably in oxygen excess. Adding NO to a mixture of NH$_3$ and O$_2$ increased the rate of N$_2$O formation, but decreased N$_2$ production at low temperatures. In contrast, adding N$_2$O had no influence on the product distribution.

Three kinetic models were used to describe the measured rate data, two of them being based on published kinetic models (models A, Pt(533) [1] and B, Pt/Al$_2$O$_3$ [3]). All models including C were derived from mechanistic and kinetic information of possible elementary reaction steps, and simplified to reduce the number of parameters. Surface species were assigned to either one type of adsorption site ("model A"), or to two energetically different types of sites assuming either a Pt(100) ("B") or a Pt(111) ("C") model surface. Reactions and adsorption sites included in model C are shown schematically in Fig. 1.

For all models only moderate agreement was obtained between experimental and simulated temperature dependences. The inadequate description of the temperature influence could be overcome by including a term for temperature-dependent roughening of the catalyst surface, derived from SEM images of the catalyst surface taken after reaction.

Models B and C described the influence of ammonia and oxygen partial pressures on rates of product formation well. Model C achieved a smaller lack-of-fit than model B, although the difference in model quality is significant only for the rates of formation of NO and N$_2$O (F-test: $(1-\alpha) = 99$ %). Moreover, only model C describes the experimentally observed increase in N$_2$O formation when NO was added to a feed mixture containing ammonia and oxygen. The kinetic model C containing one lumped reaction (NH$_3$-s + O-s → …..) and 9 elementary reaction steps, and an assignment of two energetically different adsorption sites assuming a Pt(111) model surface is concluded to provide the best description of the experimental data.
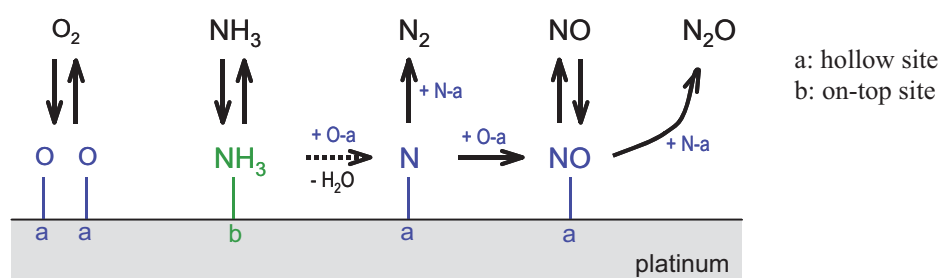
Fig. 1 Reactions on which the kinetic model C for ammonia oxidation on Pt is based
         solid lines: elementary reaction steps
         dashed line: lumped reaction

To test its predictive qualities, the best kinetic model was extrapolated beyond the range of experimental conditions towards lower and higher temperatures (50 - 900 °C) as well as pressures (p$_{NH3}$ = 10 Pa … 40 kPa), and compared to available experimental data. For previously published pulse experiments at lower pressures (TAP reactor, p$_{NH3,max}$~10 Pa) [4] the model describes the observed trends in product formation as a function of temperature and NH$_3$/O$_2$ ratio reasonably well. At higher pressures, the typical condition for a mid-pressure ammonia oxidation plant (p$_{total}$ = 4 bar, 10.5 % NH$_3$ in air, 900 °C) computed selectivity's are S$_{NO}$ = 50 % and S$_{N2O}$ = 0.5 %. The values are reasonable, considering the simplifications of the simulation that assumed a differential reactor and a catalyst different from the industrially applied PtRh.

Conclusions

The applied novel micro-structured reactor allows to study ammonia oxidation over polycrystalline Pt foil with partial pressures of reactants up to 6 kPa in a temperature-controlled way and in kinetic regime. The experimental data is described well by a micro

OP-1-6

kinetic model (Fig. 1) containing 9 elementary steps, as well as one lumped reaction for oxidative activation of adsorbed ammonia, assuming two energetically different adsorption sites consistent with known adsorption site preferences on Pt(111). Finally, the model reproduces reasonably well the trends observed in low-pressure experiments and also near industrial conditions.

References

[1] A. Scheibe, M. Hinz, and R. Imbihl, Surface Science, 576 (2005) 131.

[2] V. Kondratenko, doctoral thesis, *Mechanistic aspects of the platinum-catalysed ammonia oxidation*, Humboldt Universitaet Berlin, Berlin, 2005.

[3] E.V. Rebrov, M.H.J.M.d. Croon, and J.C.Schouten, Chemical Engineering Research and Design, 81 (2003) 744.

[4] M. Baerns, R. Imbihl, V.A. Kondratenko, R. Kraehnert, W.K. Offermans, R.A. van Santen, and A. Scheibe, Journal of Catalysis, 232 (2005) 226.

VAPOUR PHASE EPOXIDATION OF PROPENE USING N_2O AS AN OXIDANT: REACTION NETWORK, KINETICS AND CATALYST DEACTIVATION

T. Thömmes, <u>A. Reitzmann</u>, B. Kraushaar-Czarnetzki

Institute of Chemical Process Engineering (CVT), University of Karlsruhe (TH),

Kaiserstr. 12, 76131 Karlsruhe, Germany

fax: +49 - 721 - 608 61 18; e-mail: Kraushaar@cvt.uka.de

The present study focuses on the kinetics of the direct epoxidation of propene to propylene oxide (PO) in the vapour phase using nitrous oxide (N_2O) as an oxidant. Addition of intermediates to the feed provided information to derive a detailed reaction network. A mathematic model was developed which describes the kinetics satisfactorily. Carbonaceous deposits (coke) were identified as major by-products. The formation of coke leads to a rapid deactivation of the catalyst.

Background and objective

Several approaches to the vapour phase epoxidation of propene are under investigation today. The objective is to replace current processes for the production of PO, which are featured by multiple reaction steps in liquid phase. A promising route comprises the use of N_2O as an oxidant – firstly applied in propene epoxidation by Duma and Hönicke [1] – and a $CsO_x/FeO_y/SiO_2$ catalyst that provides selectivities to PO of up to 70 % among the vapour phase products at propene conversions of about 10 % [2]. However, a rapid deactivation of the catalyst was observed, which was supposed to be caused by coking [3].

Experimental

Experiments were carried out in a fixed bed reactor with plugflow characteristics. Reactants and products were analysed by on line gas-chromatography. Unit and catalyst preparation are described in [2]. The unit allows for measurements both in reactor and by-pass mode. A total oxidation reactor downflow, equipped with NDIR for CO_2-detection, was used for on-line monitoring of the carbon balance. Coke on the spent catalysts was measured by thermogravimetry. Varied parameters in the kinetic measurements were reaction temperature (350-400 °C), residence time, and feed composition. Not only propene and N_2O were fed into the reactor in varying concentrations, but also the products PO and propion aldehyde (PA).

Results

In all experiments, a deficiency in the carbon balance of the vapour phase was revealed. After determining the amount of coke deposited on the catalysts, the carbon balance could be completely closed. The selectivity to coke was between approx. 40 % and approx. 60 % at propene conversions between 10 % and 30 %, respectively. Thus, the formation of coke is an important side reaction of the epoxidation of propene and should not be neglected. As a result, the over-all selectivity to PO was limited to 40 % at the conditions under investigation. Besides propene, the $C_2 - C_4$ olefins formed through PA conversion were identified as coke precursors. The addition of PO and PA to the reactor feed gave a deep insight into the reaction network which is presented in the figure.
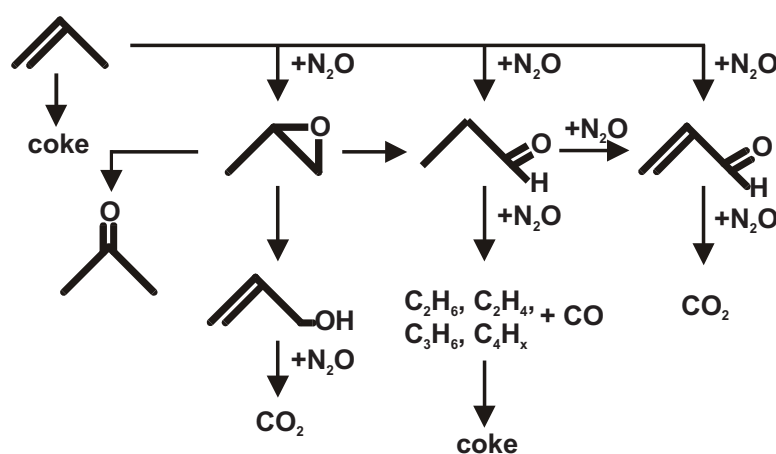
Figure: Reaction network of propene epoxidation

To model the kinetics, a simplified reaction network was used, containing only propene, PO, PA, acetone and coke lumped together with other by-products. All reaction rates had to be described via rate laws in the form of rational functions containing inhibition terms in concordance with experimental findings [3]:

$$r_i = \frac{k_i \cdot c_j}{1 + \sum_k b_k c_k}$$

Herein k and b_k are the model parameters and c is the respective concentration. The rate laws for propene conversion to PO, PA and coke contain inhibition terms for propene; the laws for PO conversion to PA, acetone and coke contain inhibition terms for propene, PO, PA and N_2O. The PA consumption was only inhibited by PA itself. A set of 11 parameters in the model was fitted to 160 experimental data points. The resulting average error was below 10 %.
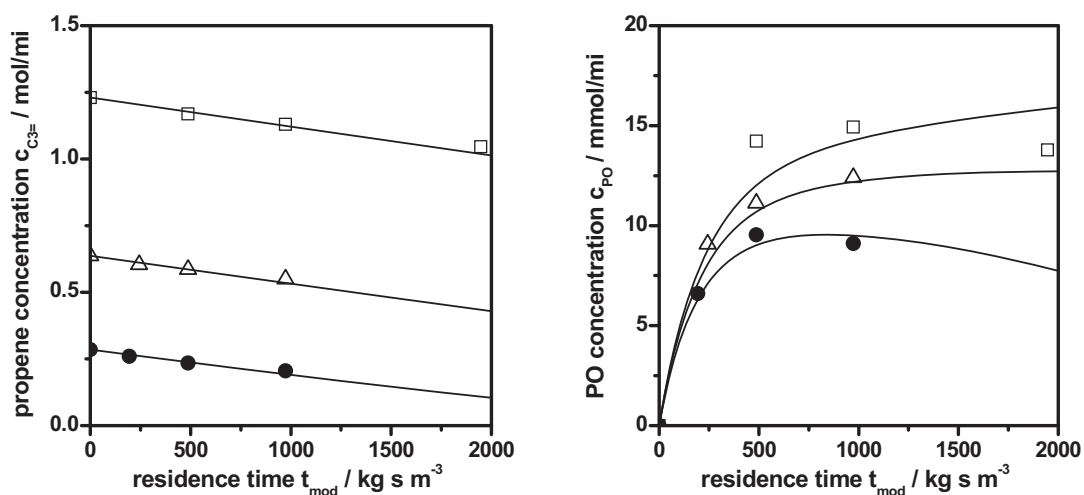
Figure: **Selected measured (symbols) and calculated (lines) concentration profiles of propene (left) and propylene oxide (right) along the modified residence time ($t_{mod} = m_{cat.}/\dot{V}$) at different inlet concentrations of propene ($c_{0,N2O} = 3.6$ mol/m³, T=375°C)**

Conclusions

The kinetic analysis showed that the values of the rate coefficients in PO-consuming reactions are about one magnitude larger than those in the formation of PO. Furthermore, the formation of carbonaceous deposits on the catalyst is the most important side reaction. Our current investigations focus on this deactivation phenomenon and its kinetics. As coke deposition also consumes valuable propene and limits the selectivity to PO, it is our aim to identify suitable measures to suppress those reactions yielding coke.

[1] V. Duma, D. Hönicke, J. Catal. 191 (2000) 93.

[2] E. Ananieva, A. Reitzmann, Chem. Eng. Sci. 59 (2004) 5509.

[3] A. Reitzmann, T. Thömmes, A.Wix, B. Kraushaar-Czarnetzki, Proceedings of the DGMK/SCI-Conference Milan, Italy, DGMK-Tagungsbericht 2005-2 (2005) 231.

OP-1-8

KINETIC MODELLING OF AN INDUSTRIAL FLUIDIZED CATALYTIC CRACKING (FCC) PROCESS

Joana L. Fernandes[a], **Carla I.C. Pinheiro**[a], **Nuno Oliveira**[b], **F. Ramôa Ribeiro**[a], **José Inverno**[c], **Maria A. Santos**[c]

[a]*CEBQ, Department of Chemical Engineering, Instituto Superior Técnico, Av. Rovisco Pais, 1, 1049 – 001 Lisboa, Portugal*

[b]*GEPSI-PSE Group, Department of Chemical Engineering, University of Coimbra, Pinhal de Marrocos, 3030-290 Coimbra, Portugal*

[c] *Galpenergia, Tecnologia e Controlo Processual, Refinaria de Sines, Portugal*

Abstract

This work describes an improved 6-lumped kinetic model for a fluidized catalytic cracking industrial process. The model represents a progress in the simulation of the kinetic behavior of an industrial FCC unit because the kinetic constants are correlated to the industrial routinely available feedstock API gravity parameter. The results presented show good agreement with industrial data.

Introduction

Fluidized Catalytic Cracking (FCC) is one of the most important processes in a refinery, and is therefore sometimes referred to as the heart of the refinery.

The development of efficient and reliable kinetic models for FCC processes is normally a difficult task because it involves a variety of components and also a high number of possible reactions. In a general way there are two types of kinetic models: the fundamental models and the lumped models. In the particular case of cracking kinetics for an industrial feed what is found in the literature are lumped models since the fundamental models are more demanding at the analytical and computational level.

The initial attempts to model FCC units where primarily oriented towards the kinetics of cracking. The first and most widely used kinetic models are the three lump model proposed by Weekman et al. (1970), which mainly focused on feedstock conversion and gasoline selectivity, and a ten lump model that introduced a more chemical description of the heavier fractions, also proposed by Weekman and coworkers a few years later (Jacob et al., 1976). In more recent studies, detailed kinetic models for the catalytic cracking of industrial Vacuum Gas Oil (VGO) feeds have been developed based on the single events approach (Moustafa and Froment, 2003). This modeling technique aims at retaining the full detail of the reaction pathways of all individual feed components and reaction intermediates by describing the

reaction network in terms of elementary steps. It therefore requires a very detailed characterization of feeds and products, which is generally not available in industry, and is computationally more demanding than lumped models. Semi-lumped models that consider the different types of elementary reactions occurring in catalytic cracking have also been proposed, in which the reaction scheme is detailed to the level of the carbon atom number (Carabineiro et al., 2004). Unfortunately, studies concerning this type of models have been made mainly for model molecules and like the single events models they require good characterization of the reactants and products.

The choice of the kinetic model to be used should be supported by the desired level of detail, which normally depends on the type of usage that the FCC model will have.

Kinetic Model

The proposed kinetic model will be subsequently used in studies of real time optimization in an industrial FCC unit, so the major classes of economical valuable cracking products were considered. The cracking kinetics will then be described by a modified 6-lumped model, based on the model presented by Takatsuka et al. (1987). The lumps considered are: VGO/DO – Vacuum Gas Oil+Decanted Oil ($>360°C$); LCO – Light Cycle Oil ($220 – 360°C$); GLN – Gasoline ($C_5 – 220°C$); LPG – Light Petroleum Gas (C_3 and C_4); FG – Fuel Gas (H_2, C_1, C_2 and H_2S) and Coke (Figure 1).
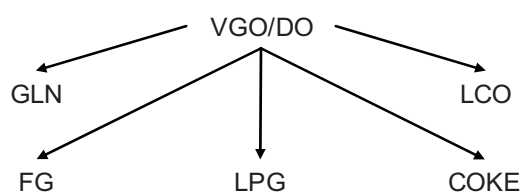
Figure 1. Kinetic scheme of the cracking reactions.

It is well known that cracking products distribution is strongly affected by feedstock properties and composition. Usually, in simplified lumped models found in literature, this dependence is usually disregarded, since a detailed feedstock characterization would lead to a more complicated model with an increasing number of estimated parameters. On the other hand, if the model is being developed for the purpose of being used in real time optimization, it is important that all the information required by the kinetic model can be available every time the optimizer runs. In our modified 6-lumps kinetic model the kinetic constants were then correlated to the API gravity parameter, which is an important feedstock property routinely available in the refineries.

According to this kinetic model the rate of the reaction of lump i towards lump j is given by:

OP-1-8

$$r_{ij} = \Phi A_{ij} \ \exp\left(-\frac{E_{ij}}{RT_{RS}}\right) C_i^{n_{ij}} \tag{1}$$

In the rate expression above, Φ accounts for the catalyst deactivation along the riser due to coke deposition on the catalyst:

$$\Phi = \exp\left(-\alpha Y_{ck}^{cat}\right) \tag{2}$$

The pre-exponential factors, A_{ij}, for VGO$\rightarrow$Products are correlated with the feedstock property API gravity parameter:

$$A_{i\rightarrow j} = a_{i\rightarrow j} \times APIe^{b_{i\rightarrow j}} \tag{3}$$

Results and Discussion

Figure 2 shows some validation results for products distribution of catalytic cracking of industrial feedstocks. The model of the riser used for simulating the industrial cases has been presented in previous works (Fernandes et al. 2005a and 2005b) and assumes that both gas and catalyst are in plug flow along the riser.

In this modified model new orders of reaction, n_{ij}, were estimated for each lump i$\rightarrow$ lump j reaction, as also the parameters $a_{i\rightarrow j}$ and $b_{i\rightarrow j}$ in equation 3.

Predicted results showed that the feed VGO reacts to give products (FG, LPG, GLN, LCO and Coke) with orders higher than 1 and lower than 3.
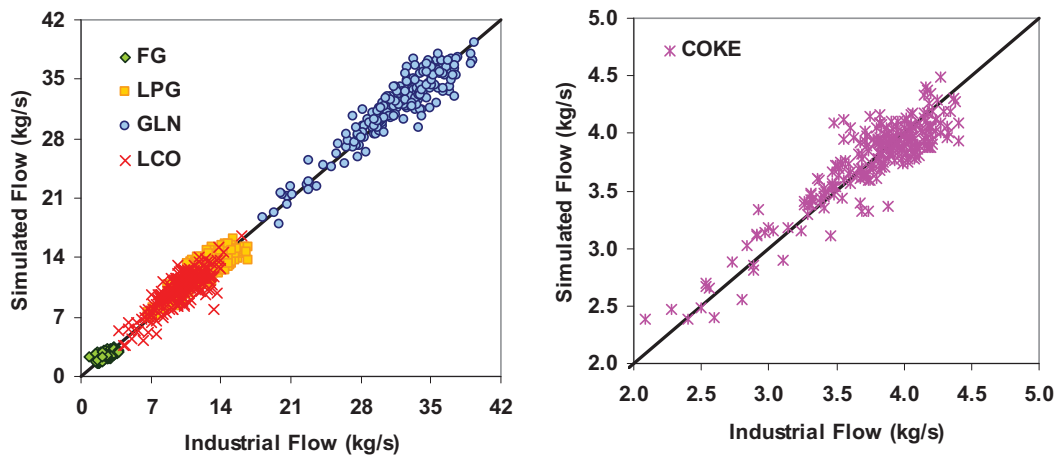
Figure 2. Products and coke flows predicted by the model vs. industrial data from Galpenergia for a 5 year period (May 2000 until May 2005).

Considering the large period of time used for parameters estimation, the model shows a very good agreement with industrial data.

Conclusions

This work shows that the simplified 6-lumped kinetic model is capable of predicting the major classes of cracking products in a large period of operation of an industrial FCC unit.

The influence of a characteristic property of the feedstock in products distribution was included in the model by taking into account the refinery routinely available API gravity parameter in the kinetic constants calculation.

Nomenclature

A_{ij}: Pre-exponential factor of the reaction i→j (s^{-1} or m^{3}s^{-1}kg^{-1}); a_{ij} and b_{ij}: kinetic parameters for A_{ij} calculation; E_{ij}: Activation energy (J/mol); $\hat{C}_i$: Mass concentration of lump i (kg/m^3); n_{ij}: Order of reaction; R: Universal gas constant (Jmol^{-1}K^{-1}) r_{ij} : Rate of reaction i→j (kgm^{-3}s^{-1}); T_{RS}: Riser Temperature (K); Y_{ck}^{cat}: catalytic coke content on catalyst (kg/kg); α: deactivation constant; Φ: Deactivation function

References

1. Fernandes, J.L., Verstraete, J., Pinheiro, C.I.C., Oliveira, N., & Ribeiro, F.R. (2005a). Mechanistic Dynamic Modelling of an Industrial FCC Unit, in: Book and CD of Proceedings of the 15th European Symposium on Computer-Aided Process Engineering – ESCAPE 15, 589-594, Barcelona.

2. Fernandes, J.L., Pinheiro, C.I.C., Oliveira, N., & Ribeiro, F.R. (2005b). Modelling and Simulation of an Operating Industrial Fluidized Catalytic Cracking (FCC) Riser, in: Full Papers CD of the 4th Mercosur Congress on Process Systems Engineering – ENPROMER 2005, 38, Rio de Janeiro.

3. Jacob, S., Gross, B., Voltz, S. E., & Weekman, V. W. Jr. (1976). A Lumping and Reaction Scheme for Catalytic Cracking. AIChE Journal, 22(4), 701-713.

4. Moustafa, T. M., Froment, G. F.(2003). Kinetic Modelling of Coke Formation and Deactivation in the Catalytic Cracking of Vacuum Gas Oil. Industrial Engineering & Chemical Research, 42, 14-25.

5. Carabineiro, H., Pinheiro, C.I.C., Lemos, F., & Ramôa Ribeiro, F. (2004). Transient microkinetic modelling of n-heptane catalytic cracking over H-USY zeolite. Chemical Engineering Science, 59, 1221-1232.

6. Takatsuka, T., Sato, S., Morimoto, Y., & Hashimoto, H. (1987). A Reaction Model for Fluidized-Bed Catalytic Cracking of Residual Oil. International Chemical Engineering, 27, 107-115.

7. Weekman, V. W. Jr., Nace, D. M. (1970). Kinetics of Catalytic Cracking Selectivity in Fixed, Moving, and Fluid Bed Reactors. AIChE Journal, 16(3), 397-404.

Acknowledgments

EMULSION POLYMERIZATION SYSTEMS
AS INTERCONNECTED CONTROLLABLE MICROREACTORS

S.S. Ivanchev, V.N. Pavlyuchenko, V.P. Tyulmankov, S.V. Myakin

St-Petersburg Department of the Boreskov Institute of Catalysis SB RAS
14, prospect Dobrolubova, 197198, St-Petersburg, Russia
fax: +7 812 2330002, e-mail: ivanchev@SM2270.spb.edu

Emulsion polymerization as a method for the preparation of polymer systems is attractive for researchers within a long time since the capabilities of the relating versatile approaches are far from exhaustion. Important advantages of emulsion polymerization technologies include their safety, environment friendly nature and possibilities for obtaining products in industrially applicable forms of latexes or water dispersed polymeric materials. For the recent two decades processes for obtaining such promising systems as latexes with a radial gradient of the chemical composition in the polymer particle, hollow particle latexes and latexes for the production of coatings with special properties have been developed and commercially implemented.

This report presents a consideration of the emulsion polymerization peculiarities in respect of the formation and functioning of the system of microreactors where the processes of polymerization initiation, proceeding and yielding of the resulting product take place. These microreactors are represented by growing polymer-monomer particles arising on the basis of micellar structures or microdroplets.

The main approaches to the selection of emulsion polymerization system recipes providing the change or control of the size and size distribution of the particles acting as microreactors during the process are discussed. Different variants of the distribution of the polymerization system components responsible for the possibility of the polymerization elementary reactions (initiation, propagation, termination) localization in microreactor areas are considered. These factors afford the control over the emulsion polymerization kinetic behavior and processes taking place in the system of microreactors.

The possibilities and conditions for obtaining monodispersed latexes or polymer dispersions are also discussed. The process providing core-shell latex systems with adjustable radial gradient of the copolymer composition inside the particle and conditions for the preparation of hollow particle latexes are analyzed.

The suggested microreactor concept is considered in comparison with the theoretic notions conventionally used in the study of emulsion polymerization.

CARRY OUT CATALYTIC EPOXIDATION IN REACTION CALORIMETER: KINETICS AND MECHANISM STUDIES

Chee Wee Quah, <u>Jie Bu</u>

Institute of Chemical and Engineering Sciences, 1, Pesek Road, Jurong Island, Singapore 627833, DID: +65 67963951, Fax: +65-63166185, bu_jie@ices.a-star.edu.sg

Epoxides are known to be valuable, versatile building blocks in organic syntheses and significant attention has been given to developing efficient catalysts for epoxidation of olefins[1-3]. Aside from dioxygen, hydrogen peroxide is probably the terminal oxidant of choice with respect to environmental and economic considerations. Recently, Burgess' group reported the epoxidation of alkenes with H_2O_2, using manganese salt and bicarbonate as catalysts[4]. The system for epoxidation that uses hydrogen peroxide in conjunction with ligand free and cheap catalyst, relatively nontoxic metals, therefore, have the potential to be viable for the large scale production of inexpensive products, as well as for more specialized applications in development, process, and research. In this study, the catalytic epoxidation of styrene using $MnSO_4$, bicarbonate and H_2O_2 (30%) oxidant was carried out in the reaction calorimeter (RC1e as shown in Fig.1). RC1e is a well-designed, precise jacketed calorimeter equipped with accurate control of temperature, pH sensor, on line FT-IR and a digital gas flow meter. This reactor is best suited for the study of exothermic release of heat energy in manganese-catalyzed epoxidation and H_2O_2-buffer feeding to the reactor can be carefully controlled to prevent reaction runaway.
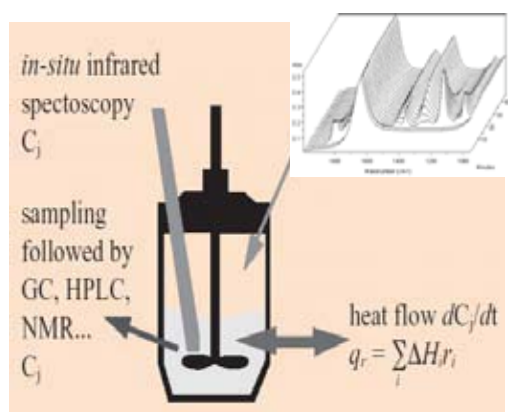
Figure 1. RC1e equipped with on-line analyzers
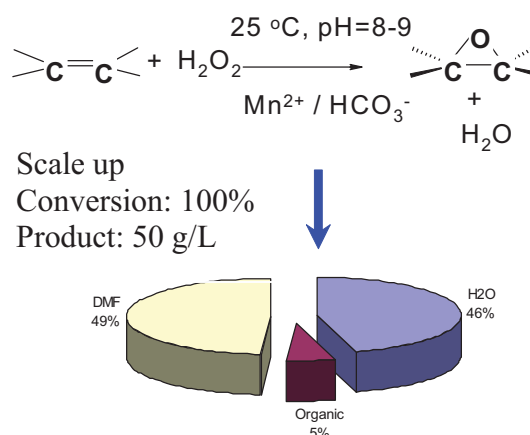
Scheme 1. Scale up of epoxidation process

With the safety controls design in RC1e, the study on the mechanism and kinetics of catalytic epoxidation was carried out by in-situ FT-IR, 13-C NMR analysis and calorimetric

data. Epoxidation in RC1 shows that scale-up can be potentially achievable up to 50 g/litres and 100% conversion with optimization of the DMF: H_2O ratio as shown in Scheme 1. For mechanistic studies aided by on-line analyses, experiments indicate that the catalytic reactions consist of 2 steps – (1) Formation of catalyst phase and (2) Epoxidation reaction. A possible oxomanganese complex (Phase A, Mn-Cpx) is formed. By feeding styrene and H_2O_2 into the mixture, containing phase A, a high conversion of epoxide (up to 90%) was observed, which implies that phase A plays the role as catalyst for epoxidation. Figure 2 shows the changes of heat flow and the conversion of epoxide during the reaction. Three distinctive peaks were observed. The first peak indicates the formation of catalyst agent (phase A) and the second peak shows the heat generation for the formation of epoxide.
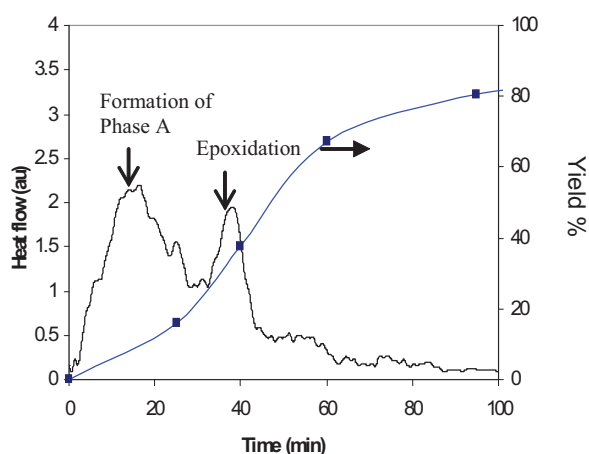
Figure 2. Reaction carried out in RC1e
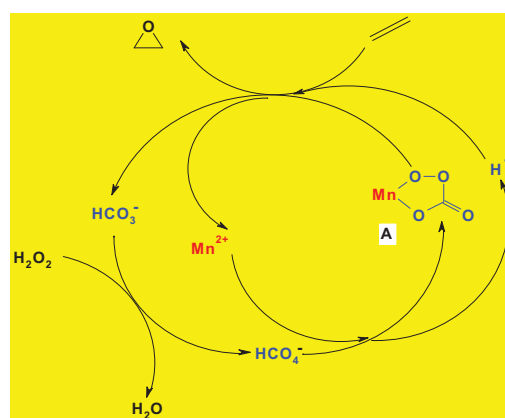
Scheme 2. Proposed mechanism

Calorimetric experiments confirmed that bicarbonate (HCO_3^-) plays an important role in transferring an oxygen atom (from H_2O_2) to C=C, i.e., bicarbonate reacting with H_2O_2 generates peroxymonocarbonate (HCO_4^-)[4-5], which then reacts with Mn^{2+} to form manganese-peroxycarbonate complex (phase A), acting as catalyst agent to donate the oxygen to the olefin. The proposed reaction mechanism is fully shown in scheme 2. Evidence for the presence of this HCO_4^- species and the Mn-complex was shown in the NMR spectrum in Figure 3.
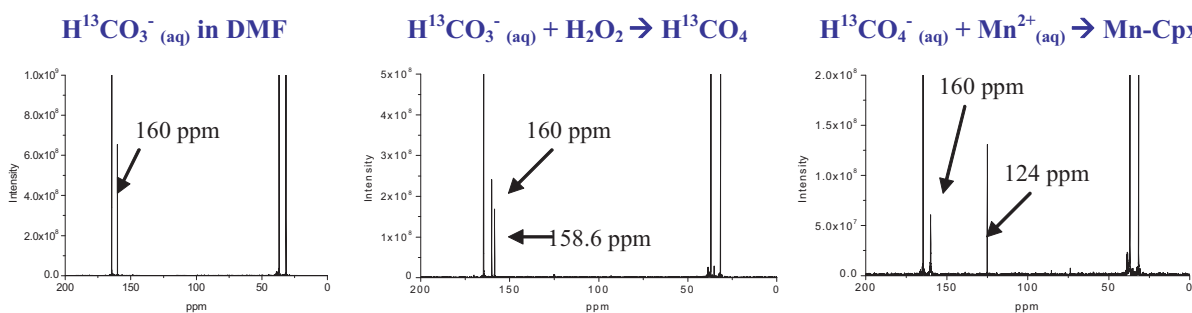
Figure 3. 13-C NMR spectrum

Based on this proposed reaction mechanism in Scheme 2, the reaction kinetics was studied and monitored using FT-IR spectroscopy as shown in Figure 4.

Rate Expressions

$$HCO_3^- + H_2O_2 \underset{k_{-1}}{\overset{k_1}{\rightleftharpoons}} HCO_4^- + H_2O$$

$$HCO_4^- + Mn^{2+} \underset{k_{-2}}{\overset{k_2}{\rightleftharpoons}} MnCO_4 + H^+$$

$$\diagup\!\!\!= + MnCO_4 + H^+ \overset{k_3}{\longrightarrow} \triangle\!\!O + Mn^{2+} + HCO_3^-$$

Overall Rate

$$\diagup\!\!\!= + H_2O_2 \overset{k}{\longrightarrow} \triangle\!\!O + OH_2$$
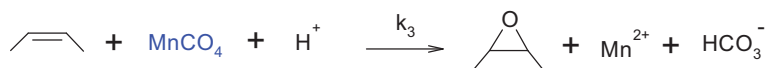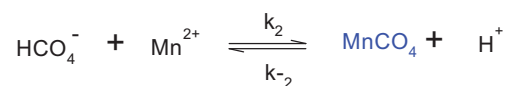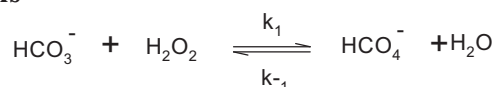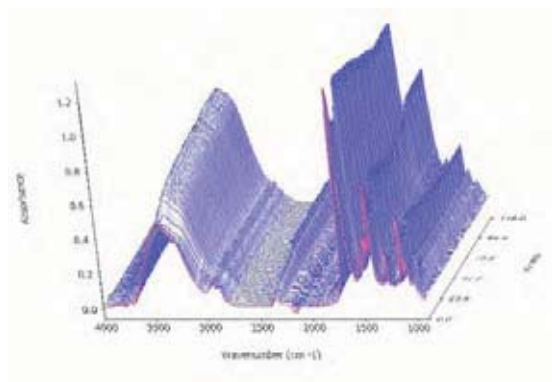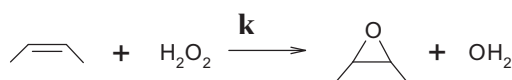
Figure 4. FTIR Spectrum (3-D)
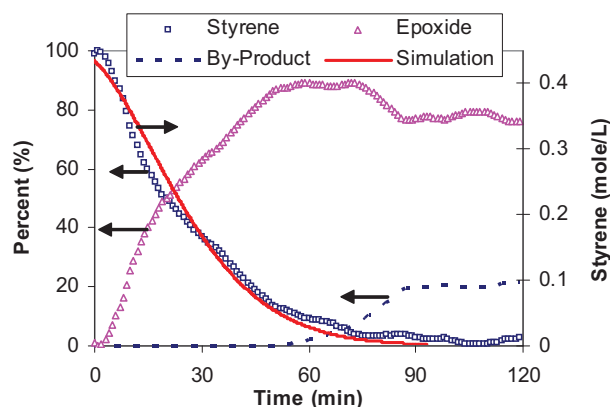
Figure 5. Reaction concentration profile

Chemometrics method was applied to convert the FT-IR spectrum (Fig.4) to the concentration profile of styrene, epoxide and by-product (Fig.5). Subsequently, the overall reaction rate constant, k, could be calculated as 1.4 L/mole.hr. The simulated curve of styrene concentration matches well with the experimental data as illustrated in Figure 5. The kinetic study of this cheap and efficient catalytic epoxidation enables reactor design and sizing for future potential scale-up operations.

References

1. B. S. Lane and K. Burgess, *Chem. Rev.*, **2003**, *103*, 2458.
2. E.N. Jacobsen, in: *Catalytic Asymmetric Synthesis*, ed. I. Ojima, ch. 4.2, VCH, New York, 1993.
3. J. Bu and H.-K. Rhee, *Catal. Lett.*, **2000**, *65*, 141.
4. B. S. Lane, M. Vogt, V. J. DeRose, and K. Burgess, *J. Am. Chem. Soc,* **2002124** ,11946 (2002).
5. D. E. Richardson, H. Yao, K. M. Frank, and D. A. Bennett, *J. Am. Chem. Soc.* **2000,** *122,* 1729.

CATALYST DEACTIVATION WITH RESIDUAL ACTIVITY
History, models, mechanisms and examples

N.M. Ostrovskii

AD Chemical Industry – HIPOL, Odžaci, Serbia & Montenegro

Fax: 381-25-743-452, E-mail: ostrovski @ hipol.com

The nature of catalyst deactivation with residual activity is analyzed, several models and mechanisms are proposed, and examples of industrial processes are presented

Scope of problem

It is observed in many processes that the catalyst is not completely deactivated, but reaches a "stationary" or "residual" activity (fig. 1,2).
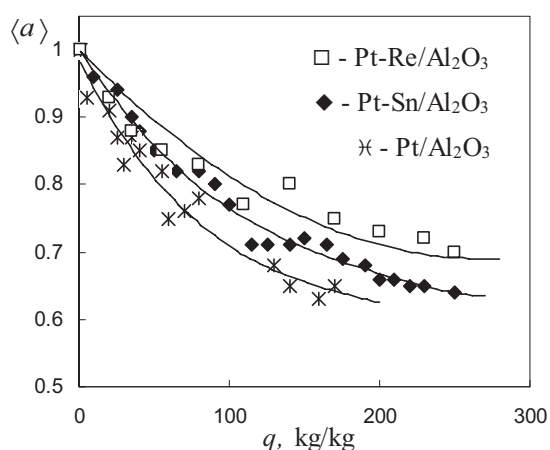
Fig. 1. Relative activity in heptane reforming vs. feed loading. From [1].
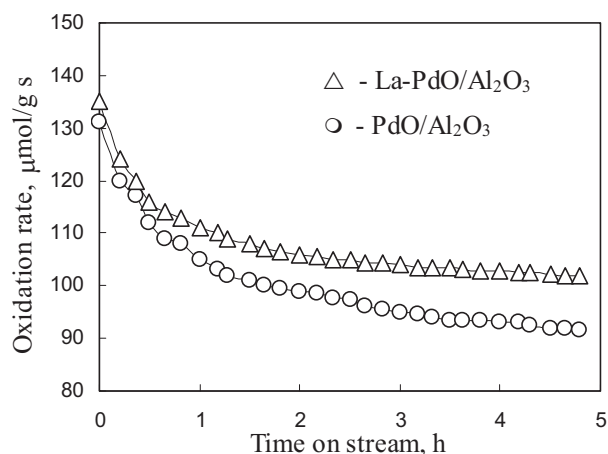
Fig. 2. Oxidation rate of CH_4 over Pd catalysts at 1123 K vs. time. From [2].

The existence of a residual activity was mentioned as yet in the fifties, but the suitable models and explanations were published only in eighties [3-6].

There are two explanations of residual activity: 1 – the presence of active centers that are not deactivated, which is wrong in most cases; 2 – the presence of reversible deactivation. This reversibility of deactivation is not the catalyst ability to be regenerated. It means that along with catalyst deactivation a certain process of recovery of active centers takes place during the reaction. That is the process of "self-regeneration" [1,6] because it is provided by the catalyst itself and with the assistance of some reagents taking part in the main reaction.

For example, in almost all hydrogenation processes the catalyst deactivation by surface oligomers is accompanied by self-regeneration due to the saturation of oligomeric precursors by hydrogen that is activated on the catalyst.

The same mechanism of self-regeneration takes place in processes of naphtha reforming, hydrotreating of distillates, paraffins isomerization and others, where the hydrogen exceeds in circulating gas. Here the hydrogenation of coke precursors causes the self-regeneration [8].

Another agent is water steam that provides the catalyst self-regeneration in methane steam reforming and in some dehydrogenation processes due to the coke gasification. Finally, in many deep and partial oxidation processes, the oxygen is not only the main reagent, but also the agent of catalyst self-regeneration.

In all these processes the "stationary" or "residual" activity (a_S) is achieved when the rate of deactivation (r_D) becomes equal to the rate of self-regeneration (r_R):
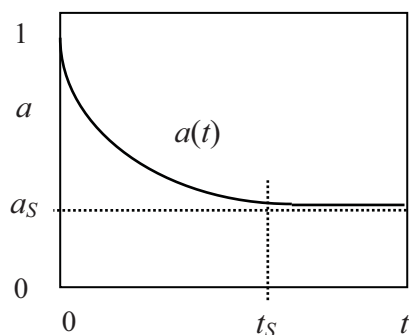
Fig. 3.
The illustration of stationary (residual) activity.
$a(t) = r(t)/r^o$ – relative activity;
$a_S \approx a(t \geq t_S); \quad t \geq t_S: r_D \approx r_R$.

Several problems of catalyst deactivation kinetics can be solved easily using term of residual activity: (i) the treating of experiments become convenient and more descriptive; (ii) deactivation models become simpler for interpretation and for estimation of parameters; (iii) the border between catalyst deactivation and ageing gains in physical meaning.

Mathematical model

A general equation applicable to any linear mechanisms has been derived in [5,6]:

$$- \frac{da}{dt} = \frac{r^o}{w_j} w_D \frac{a - a_S}{1 - a_S}, \qquad a_S = \left(1 + \frac{r^o w_D}{w_j w_R} \right)^{-1}. \tag{1}$$

In the case of any linear mechanism of main reaction and nonlinear binary deactivation step $r_D = w_D \Theta_i \Theta_j$ the equation has the following form [1]:

$$- \frac{da}{dt} = \frac{(r^o)^2}{w_i w_j} w_D \left(a^2 - a_S^2 \frac{1 - a}{1 - a_S} \right). \tag{2}$$

There is no general equation if the mechanism of main reaction is nonlinear. However, if adsorption steps are in equilibrium, the same binary deactivation step $r_D = w_D \Theta_i \Theta_j$ yields:

67

$$-\frac{da}{dt} = \frac{(r^o)^2}{w_i w_j} w_D \sqrt{a} \left(a - a_S \frac{1-\sqrt{a}}{1-\sqrt{a_S}} \right). \tag{3}$$

It is more convenient for practice to express the relative activity (a) in terms of some measured parameter, for example conversion at the reactor exit (X). The relation $a = f(X)$ depends on reaction kinetics and the type of reactor [1,7]. In the case of single first order reaction $r = k\, C_A^{\,o}\,(1\text{-}X)\,a$:

in gradientless reactor $k\,\tau = X_o/(1-X_o)$, and

$$a = \frac{1-X_o}{X_o}\frac{X}{1-X}, \qquad a_S = \frac{1-X_o}{X_o}\frac{X_S}{1-X_S}; \tag{4}$$

in plug flow reactor $k\,\tau = -\ln(1-X_o)$, and

$$\langle a \rangle = \frac{\ln(1-X)}{\ln(1-X_o)}, \qquad \langle a_S \rangle = \frac{\ln(1-X_S)}{\ln(1-X_o)}. \tag{5}$$

Then the deactivation equation in term of conversion takes the following form:

in gradientless reactor: $\qquad -\dfrac{dX}{dt} = X_o(1-X)\,r_D(X)\,\dfrac{X-X_S}{X_o-X_S}, \tag{6}$

where $r_D(X) = k_D\, C_A^{\,o}$ – independent deactivation; $r_D(X) = k_D\, C_A^{\,o}\, X$ – deactivation by product; $r_D(X) = k_D\, C_A^{\,o}\,(1\text{-}X)$ – deactivation by reagent.

in plug flow reactor: $\qquad \dfrac{dX}{dt} = \psi_D(X)\left(\ln\dfrac{1-X}{1-X_S} \middle/ \ln\dfrac{1-X_o}{1-X_S} \right) \dfrac{\ln(1-X_o)}{\ln(1-X)}, \tag{7}$

where $\psi_D(X) = k_D\, C_A^{\,o}\,(1\text{-}X)\ln(1\text{-}X)$ – independent deactivation; $\psi_D(X) = -k_D\, C_A^{\,o}\, X\,(1\text{-}X)$ – deactivation by reagent; $\psi_D(X) = k_D\, C_A^{\,o}\,(1\text{-}X)\,[X + \ln(1\text{-}X)]$ – deactivation by product.

Note that in (7)

$$\left(\ln\frac{1-X}{1-X_S} \middle/ \ln\frac{1-X_o}{1-X_S} \right) = \frac{\langle a \rangle - \langle a_S \rangle}{1 - \langle a_S \rangle}, \quad \text{and} \quad \frac{\ln(1-X_o)}{\ln(1-X)} = \frac{1}{\langle a \rangle}.$$

Residual activity

According to (1) the residual activity depends on the ratio of deactivation and self-regeneration rates w_D/w_R, and also on the reaction rate r^o/w_j. In most cases the j-th step coincides with the rate-limiting step, then $r^o/w_j = 1$.

For example, in the case of heptane reforming (fig. 1) [1,6]:

$$a_S = \frac{1}{1 + k_D Y_{N5}/k_R Y_{H2}}, \tag{8}$$

where Y_{N5}, Y_{H2} are mole fractions of N_5-naphthenes and of hydrogen. Hydrogasification of coke in heptane reforming has been studied in [8], and the effect of Y_{H2} was examined.

Similar approach was proposed in [9,10] for the deactivation of supported metals by sintering, using the term of residual metal dispersion (D_{SS}):

$$-\frac{dD}{dt} = \psi_G \left(D - D_{SS}\right), \qquad D_{SS} = D_T \frac{1}{1 + \psi_S / \psi_R} ; \qquad (9)$$

where ψ_S, ψ_R are functions of sintering and redispersion rates.

When the activity falls due to reversible deactivation and irreversible ageing, the residual activity will also change slowly (like in fig. 2). It is possible (using term a_S) to split the complex model of such a phenomenon in two independent equations [1]:

deactivation period ($t < t_S$): $\qquad -\frac{da}{dt} \approx \frac{r^o}{w_j} \left(w_D + w_A\right) \frac{a - a_S}{1 - a_S} ; \qquad (10)$

ageing period ($t > t_S$): $\qquad -\frac{da}{dt} \approx \frac{r^o}{w_j} w_A \frac{a_S}{1 - a_S} a . \qquad (11)$

It means that the reaction is quasi-steady state with respect to deactivation ($r_D \approx r_R \ll r$) and similarly deactivation is quasi-steady state with respect to ageing ($r_A \ll r_D \approx r_R$).

Models like (10,11) are applicable to many industrial processes in which "quick" deactivation is caused by poisoning, coking, surface or subsurface phase transitions, and "slow" ageing is caused by sintering, bulk phase transitions, pores plugging, etc.

Several examples of application will be presented in the report.

Nomenclature

$a = r/r^o$ – relative activity of the catalyst; r, r^o – current and initial reaction rate; $w_j = r/\Theta_j$ – weight of key step in reaction mechanism; r_D , r_R – rates of deactivation and self-regeneration; Θ_j – intermediate (coverage) taking part in deactivation; $w_D = r_D /\Theta_j$, $w_R = r_R /\Theta_D$ – corresponding weights; k , k_D – constants of reaction rate and deactivation; τ – contact time; X, X_o, X_S – current, initial and residual conversion at the reactor exit; $\langle a \rangle$ – mean integral activity of catalyst bed; w_A – weight of ageing step.

References

1. N.M Ostrovskii, Catalyst Deactivation Kinetics, Nauka, Moscow, 2001 (in Russian).
2. Y. Ozawa, Y. Tochihara, M. Nagai, S. Omi – Chem. Eng. Sci., 2003, 58, 671- 677.
3. G.A. Fuentes – Appl. Catal., 1985, 15, 33-40.
4. J.M. Arandes, M.J. Azkoiti, J. Bilbao – Chem. Eng. Journ., 1985, 31, 137-143.
5. N.M. Ostrovskii, In "Chemical Kinetics and Catalysis. Theoretical Problems", Chernogolovka, 1985, p. 143-150 (in Russian).
6. N.M. Ostrovskii, G.S. Yablonskii – React. Kinet. Catal. Lett., 1989 39, 287-292.
7. N.M. Ostrovskii – Kinetics and Catalysis, 2005, 46, No. 5, 693-704.
8. K. Liu, S.C. Fung, T.C. Ho, D.S. Rumschitzki – Ind. Eng. Chem. Res. 2003, 42, 1543-1550.
9. G.A. Fuentes, F.A. Ruiz-Trevino – Proc. AIChE Meeting, New York, Nov. 1987.
10. A. Monzón, T.F. Garetto, A. Borgna – Applied Catalysis A: General, 2003, 248, 279-289.

Section 2.

Physico-chemical and mathematical bases
of the processes in chemical reactors

OSCILLATIONS IN CATALYST PORES:
FROM THEORY TO PRACTICE

B. Blümich[1], L.B. Datsevich[2], A. Jess[2],
T. Oehmichen[2], X. Ren[1], S. Stapf[1]

[1] *Technical University of Aachen (RWTH-Aachen), Worringer Weg 1,*
D-52056 Aachen, Germany
[2] *University of Bayreuth, Universitaetsstr. 30, D-95447, Bayreuth, Germany*
Fax: ++49 921 55 74 35. Email: datsevich@gmail.com, datsevich@uni-bayreuth.de

The oscillation theory predicts that in multiphase reactions on a porous catalyst with gas and/or heat evolution, the alternating motion of liquid with velocities of 10-100 m/s at frequencies more than 1 Hz can occur in pores, caused by periodical formation of gas/gas-vapor bubbles. Such behaviour differs very much from the conventional models and fundamentals used for description of chemical processes inside and outside the catalyst particles (e.g. the Thiele/Zeldovich model (TZM) and the approaches to external and internal mass transfer correlations).

In opposition to TZM where the delivery of reacting species to active centres is carried out by comparatively slow molecular diffusion, the oscillatory motion of liquid in the parts of pores alongside the particle shell (in the distance of oscillation penetration) leads to a significant acceleration of internal mass transfer. That results in a change of the macrokinetic mechanism and increases the overall reaction rate. The theoretical predictions concerning internal mass transfer have been confirmed by the *in-situ* NMR observations and by the experiments with the deuterium oxide exchange.

Fig. 1 shows an extremely chaotic pattern inside the catalyst particle in the reaction of hydrogen peroxide decomposition; the distance of oscillation penetration can also be distinguished (during the presentation, the movie will be demonstrated). The experimental results of the deuterium oxide exchange are presented in Fig. 2. As can be seen, the more the reaction rate (more intensive oscillations), the higher the values of the effective diffusivity are observed.

Oscillations in pores not only affect the mechanism of internal mass transfer, but also have a strong impact on external mass transfer. Because of liquid motion in pore mouths, the flow around the particle is severely disturbed. That causes a vigorous turbulence in the

boundary layer, which, in turn, leads to a tremendous increase in mass transfer coefficients. The dispersion coefficient (effective diffusivity) outside the catalyst pellet alongside its shell is measured by the NMR technique. Depending on the reaction rate, the oscillations can produce up to a 500-fold increase in external mass transfer (Fig. 3). It is noteworthy that the influence of hydrodynamic properties in a reactor on external mass transfer can completely be overwhelmed by the impact of oscillations (Fig. 4).

From a scientific point of view, the importance of the oscillation theory is not only that it explains the phenomena related to mass transfer, but also that this theory explicates some other physicochemical features observed in practice (e.g. catalyst destruction due to cavitations, macrokinetic dependences, etc.).

The most important issue for practice is that the oscillation theory indicates the distinct ways for process intensification by a special pore design (Table 1) or by induction of oscillations (even if a reaction runs without them) with the help of some physical methods.

Table 1. Reaction rates of original and modified particles.

Reaction: hydrogenation of 1-octene to n-octane.

Catalyst: NISAT (Süd-Chemie) 6 mm×6 mm

Experiment	$R_{original}$ (mol/s)	$R_{modified}$ (mol/s)	Intensification factor $R_{modified}/R_{original}$
P1	2.93×10^{-6}	4.35×10^{-6}	1.48
P2	2.5×10^{-6}	7.75×10^{-6}	3.1
P3	4.53×10^{-6}	7.49×10^{-6}	1.65
P4	6.82×10^{-6}	8.39×10^{-6}	1.23
P5	5.11×10^{-6}	10.57×10^{-6}	2.07
P6	6.06×10^{-6}	10.23×10^{-6}	1.69
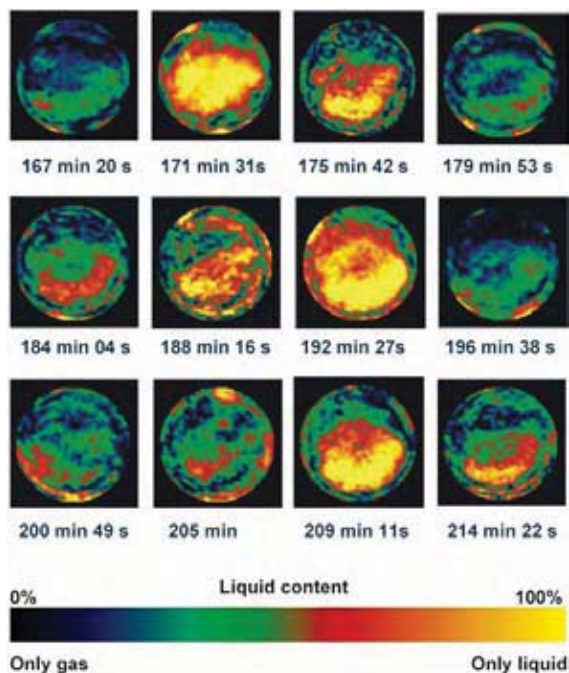
Fig. 1. Spatial distribution of liquid in the catalyst pellet (Fe/Al$_2$O$_3$, 4 mm×4 mm) in the course of hydrogen peroxide decomposition.

Fig. 2. Dependence of the effective diffusion coefficient of deuterium oxide D$_{eff, osc}$ on the reaction rate (D$_{eff,0}$ - diffusivity without oscillations). Reaktion: hydrogen peroxide decomposition. Catalyst: NISAT (Süd-Chemie) 6mm×6 mm.
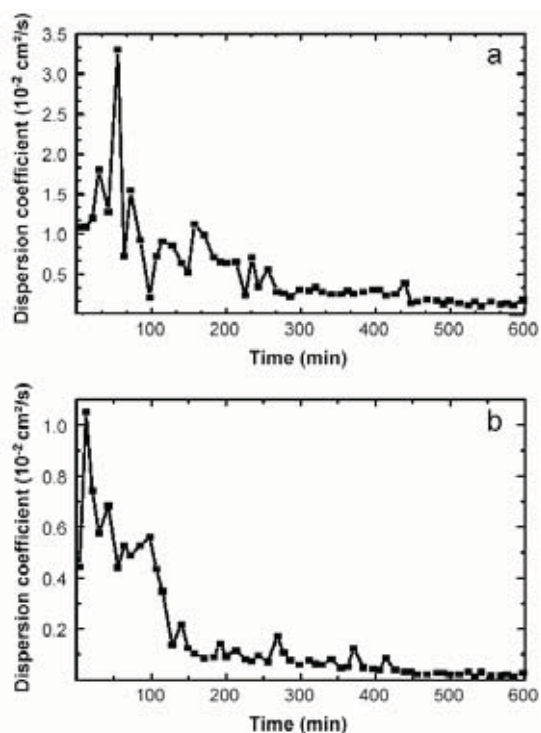
Fig. 3. Dispersion coefficient (effective diffusivity) outside the catalyst pellet (Fe/Al$_2$O$_3$, 4 mm×4 mm) alongside its shell. Initial concentration of H$_2$O$_2$ is (a) 22.5 % mass, (b) 7.5 % mass. (For comparison: the diffusion coefficient of H$_2$O$_2$ is 1.92×10^{-5} cm^2/s.).
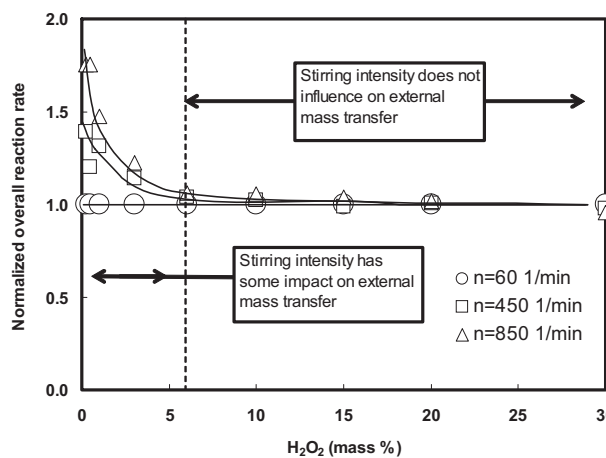
Fig. 4. Overall reaction rate normalized to the reaction rate at the stirring of n=60 min^{-1}. Reaction: hydrogen peroxide decomposition. Catalyst: NISAT (Süd-Chemie) 6mm×6 mm.

MATHEMATICAL MODELING OF SPATIO-TEMPORAL PATTERN FORMATION IN THE NO+CO/Pt(100) REACTION

Kurkina E.S.

Lomonosov Moscow State University, Moscow, Russia

The present work is aimed at modeling of spatiotemporal concentrations patterns arising on the Pt(100) single crystal surface in the NO+CO reaction. Recent investigations with the photo-emission electron microscope (PEEM) have revealed a rich variety of wave trains, spiral waves, fronts, chemical turbulence and others structures during this reaction [1]. A four-variable mathematical model of the reaction-diffusion type was studied to describe the self-organization phenomena [2]. This model is based on the previously developed space-independent model, which provides very good agreement between simulation results and various experimental facts measured on a macroscopic level. The point model successfully reproduces temperature programmed desorption (TPD) spectra, hysteresis phenomena, oscillatory behavior, the dependence of period of oscillations upon temperature and reactant partial pressures, the explosive development of the reaction etc. The nonlinearities of the mathematical model associated with lateral interactions play a crucial role in an adequate description of complex dynamical behavior of the system.

To study the spatial behavior of the system, the diffusion terms which take into account the influence of site-blocking on the diffusion rates, were included in the model. Under certain condition the distributed model demonstrates an excitable dynamics. Solitary pulses, fronts, wave trains, spatiotemporal chaos (STC) and other spatiotemporal patterns were detected. Travelling pulses, their domain of existence, instabilities and bifurcations were investigated in the present work. Pulses are considered as solutions of the system of four second order differential equations with the Neiman boundary conditions in large domains in a moving frame. The evolution of the traveling pulse solution with the changing of a parameter was investigated by means of path-following algorithm for the travelling wave ODEs and direct simulations in the full partial differential equations (PDE) frame with periodic boundary condition on the large domains. Several bifurcations of pulse solutions were revealed and examined: a saddle-node bifurcation leading to the coalescence of stable and unstable pulses, a bifurcation in which a traveling-pulse solution ceases to exist as it

merges with an unstable spatially uniform steady-state solution, a bifurcation through transformation of a traveling pulse into a traveling front, etc. In particular two scenarios of transition to spatiotemporal chaos were examined. In the first case chaos observed in the domain of multiple spatially uniform steady states. At the bifurcation point, a branch of stable solitary pulses collides with a branch of unstable fixed points, and a double heteroclinic connection appears in the phase space. After the critical value of the parameter is passed, pulse solution disappear and chaos develops in the system.

In the second scenario of transition to spatiotemporal chaos stable solitary pulses transforms to modulated traveling pulses (MTP), due to a supercritical Hopf bifurcation. The further changing of parameter leads to a cascade of period-doubling bifurcations of the MTP and chaotic MTP is appeared. Finally, at some value of parameter the chaotic MTP begins to split and as a result the complicated dynamics corresponding to spatiotemporal chaos is observed. The spatio-temporal evolution of the system in the chaotic regime was examined. The bifurcation analysis revealed all participants of this process such as stable and unstable homogeneous states and pulses which are the driving forces of STC dynamics. It was revealed self-replicated processes (SRP) and front emitting waves (FEW). Also an annihilation of two pulses and so called 'backfiring' phenomenon there were detected in the model. The considered model usually demonstrates STC dynamics of traveling type with annihilation.

2D computations revealed a variety of spatiotemporal patterns in the considered model. They are the one-hand and two-hand spiral waves in a self-oscillating medium connected with the self-oscillation region in the point model of the reaction, and spiral and spot chaos in an excitable medium.

It was shown that the new reaction-diffusion model actually describes the some main features of the experimental PEEM observations. In addition the simulation predicts various interesting phenomena such as formation of localized pulses (stationary, oscillating and chaotic) which probably can be discovered during experimental studies in future.

References

1. Veser G., Imbihl R. // J. Chem. Phys. V. 100. № 11. P. 8483-8491. 1994.

2. E.S. Kurkina, A.V. Malykh. //Computational Mathematics and Mathematical Physics, Vol.41, No.10, 2001, pp. 1519-1531.

TRANSIENT AND PROFILE MEASUREMENTS IN SYNGAS FORMATION BY AUTOTHERMAL CATALYTIC PARTIAL OXIDATION OF CH$_4$ ON Rh FOAMS

R. Horn, N.J. Degenstein, K.A.Williams, L.D. Schmidt

Department of Chemical Engineering and Materials Science, University of Minnesota

432 Amundson Hall, 421 Washington Ave. SE, Minneapolis MN 55455, USA

e-mail: horn@cems.umn.edu

1.   Introduction

The production of synthesis gas from methane by **C**atalytic **P**artial **O**xidation (**CPO**) is a process of growing importance because of the role of natural gas as an energy carrier and chemical feedstock. In contrast to steam reforming (CH$_4$ + H$_2$O $\rightarrow$ CO + 3H$_2$ ($\Delta_r H^\circ$ = +206 kJ/mol)), the CPO reaction is exothermic (CH$_4$ + ½ O$_2$ $\rightarrow$ CO + 2H$_2$ ($\Delta_r H^\circ$ = -36 kJ/mol)). Steam reforming on Ni requires contact times in the range of 1s to achieve sufficient conversions. For the CPO reaction on Rh, CH$_4$ conversion close to 100 % and selectivities to H$_2$ and CO, both > 90 %, can be achieved in a few ms [1] so that CPO reactors can operate autothermally and are much smaller than steam reformers.

There is still a debate about the mechanism of the CPO reaction. A direct (partial oxidation) mechanism and an indirect (combustion-reforming) mechanism are discussed in the literature [2]. The direct mechanism assumes that H$_2$ and CO are primary reaction products formed in the hot oxidation zone at the catalyst entrance. The combustion-reforming mechanism postulates total oxidation of CH$_4$ at the catalyst entrance to CO$_2$ and H$_2$O, followed by steam and CO$_2$ reforming to H$_2$ and CO. Here, H$_2$ and CO are secondary reaction products. This paper presents spatial profile and transient measurements on autothermally operated Rh coated foam catalysts. The goal of these measurements is to obtain insight into the reaction mechanism under conditions as close to a practical application as possible.

2.   Experiments

To verify the presence of different reaction zones in the catalyst, temperature and species profiles have been measured. These profiles are, to our knowledge, the first measured on foam catalysts. A fine quartz capillary (o.d.=0.8mm) enclosing a type K thermocouple is moved with sub - mm resolution through a slightly larger channel drilled through the monolith.

The quartz capillary is connected to a capillary sampling quadrupole mass spectrometer.

Figure 1 shows the experimental setup. The transient measurements shown here have been done in an integral mode, i.e. the composition at the reactor outlet was measured. Figure 2 shows the reactor configuration. Transient measurements at different positions in the catalyst by combination of both experiments are currently being performed. The C/O ratio has been changed stepwise by switching the CH_4 mass flow controller, keeping the other flows constant. The transient data shown in Figures 4 and 5 were measured with a response time of ~1s. For the newly developed capillary system (Fig. 1) MS response times of 50 to 100 ms were measured. Thus transient experiments with capillary sampling will give one order of magnitude better time resolution. Rh coated α-alumina foams of 16 mm diameter with 80 pores per linear inch (pore diameter ~ 0.3 mm) have been used for all experiments. The metal loading was typically 5 wt-%. The foams were 5 mm long for transient experiments and 10 mm long for profile measurements.
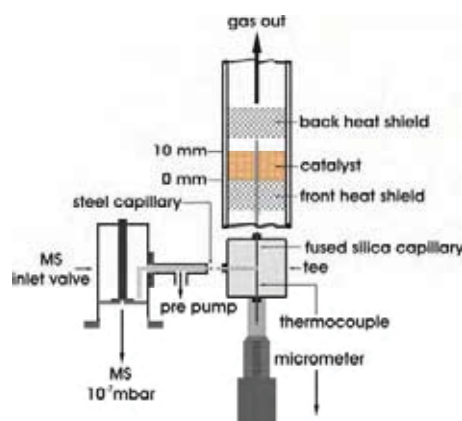
Fig. 1 setup for profile measurements
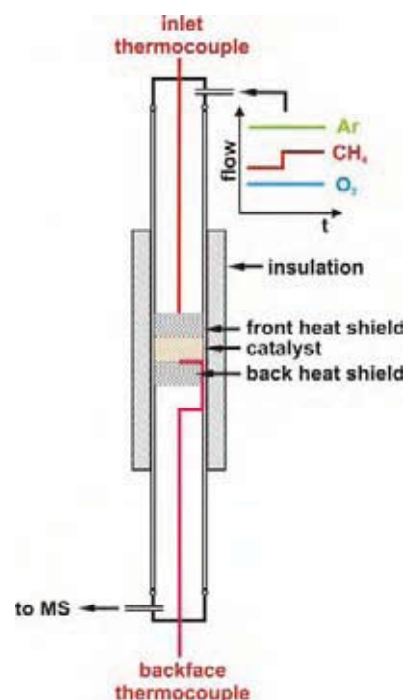
Fig. 2 setup for transient measurements

3.   Results & Discussion

a.   Temperature and Species Profiles

Figure 3 shows a typical profile along the catalyst axis, measured for a total flow of 5 l/min and a C/O ratio of 1.0 . Argon is used as internal standard. The Ar to O_2 ratio of 3.76 simulates air. The profiles reveal interesting details. Oxygen is fully converted within 0.5 mm of the catalyst entrance. CO_2 is formed in the oxidation zone and remains constant afterwards. Thus there is no indication of CO_2 reforming and water gas shift. CO and H_2 are formed in the oxidation zone and also after total O_2 conversion by steam reforming. The H_2O profile

(calculated from the O balance) shows a net formation of H_2O in the oxidation zone followed by its consumption in the reforming zone. Approximately 1/3 of H_2 and ½ of CO are formed in the oxidation zone. At the point of total O_2 conversion (0.5 mm) the CO profile shows a pronounced change in slope whereas H_2 does not. The CO slope decrease indicates that CO is partly a direct oxidation product and partly formed by steam reforming. When direct formation ceases due to absence of O_2, the

Fig. 3 species and temperature profiles, C/O=1, 5 l/min

CO formation rate is reduced to the reforming contribution. The H_2 formation pathway can not be concluded directly from the data. H_2 may be formed as a direct product by immediate recombination of two H atoms or indirect by steam reforming after a kinetically faster intermediate H_2O formation.

The conclusion from the profiles is that the methane CPO proceeds via a mixed mechanism of direct oxidation and steam reforming at these temperatures. An oxidation zone ~0.5 mm thick and a steam reforming zone ~4 mm thick can be identified. H_2 and CO are formed in both zones, but in different molar ratios. The H_2/CO ratio in the oxidation zone is about 1 but increases in the reforming zone up to a final value of about 2. A clear separation between a total oxidation zone with H_2O and CO_2 formation followed by a reforming zone with H_2 and CO formation as suggested by the combustion-reforming mechanism is not observed.

b.　　**Transient Experiments**

The transient data support the result of the profile measurements, that steam reforming has a contribution to synthesis gas formation, but also reveals new aspects of the reaction. Figure 4 shows a transient experiment with a C/O switch from 0.6 – 1.0. Fig. 5 shows the H_2 signal for switches up to 1.4. O_2 consumption is 100 % for all experiments. Diffusion, adsorption reaction and desorption processes proceed on a ms time scale or faster and are not resolved by the measurements shown here.

What is resolved are thermal processes ($\tau\sim10$ s) and probably the buildup and removal of multilayer surface species (e.g. C_xH_y). Also physical and chemical changes of the catalyst may proceed in a time scale that is reflected in these experiments. As shown in Fig. 4, methane and water increase exponentially after the switch from C/O 0.6 – 1.0.
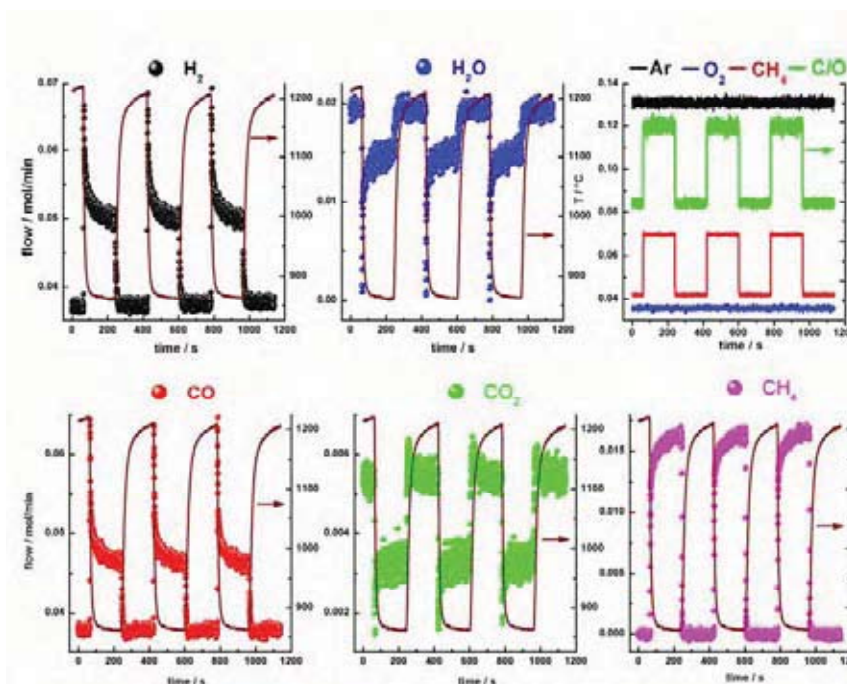
Fig. 4 transient experiment C/O switch 0.6 – 1.0
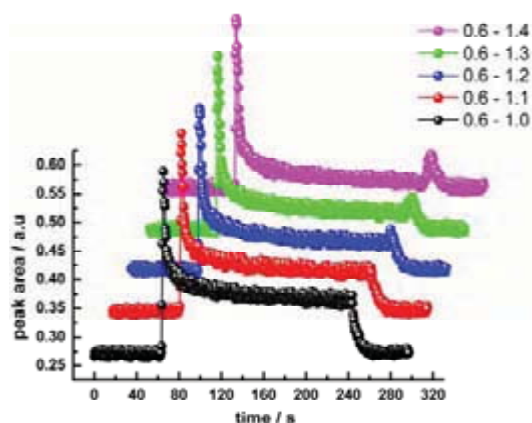
Fig. 5 H_2 signal for high C/O switches

H_2O shows a sharp undershoot and then increases, CH_4 rises from zero. H_2 and CO fall in the same manner after a pronounced overshoot. The curves are parallel (H_2, CO) or anti-parallel (CH_4, H_2O) to the measured back-face temperature. These transients reflect the contribution of the highly endothermic steam reforming to the syngas production, because the temperature dependence of this reaction is strongest. New and surprising are the H_2 (Fig. 5) and CO overshoots (not shown) after switching back from high C/O ratios (≥1.2) to 0.6. One possible explanation is that C_xH_y species build up at the high C/O ratio which are removed as CO and H_2 after switching back to excess oxygen at C/O = 0.6.

The spatial and transient experiments reveal each on its own interesting details about the reaction. Coupled spatially resolved transient experiments will supply even more information.

[1] D. A. Hickman, L. D. Schmidt, *Science*, 1993, **259**, 343.

[2] A. P. E. Yorck, T. Xiao, M. L. H. Green *Top. Catal.*, 2003, **22**(3-4), 345.

MATHEMATICAL MODELLING OF THE NONLINEAR BEHAVIOUR DURING METHANE OXIDATION OVER Ni CATALYSTS

N.V. Peskov, M.M. Slinko*, V.N. Korchak*

Department of Computational Mathematics & Cybernetics, Moscow State University,
119899, Moscow, Russian Federation
*Institute of Chemical Physics, Russian Academy of Science, Kosygina Str. 4,
119334, Moscow, Russian Federation

In the last years the oscillatory behaviour during methane oxidation was discovered by different groups of experimentalists over variety of Ni catalysts including wires, foils, foams and the review of experimental results can be found in the paper of Zhang et. al [1]. Although the properties of oscillations described by various groups were different in all studies it was generally suggested that oscillatory behaviour over Ni catalysts originates due to the repetitive cycles of oxidation and reduction of the metal surface. However no any mathematical model of this process producing the oscillatory behaviour has been developed and the detailed mechanism of oscillations has not been understood. The goal of this study is to develop the mathematical model, which can produce the oscillatory behaviour during methane oxidation over Ni catalysts at realistic values of parameters and to explain the possible origin and the mechanism of the observed reaction rate oscillations.

Recently Bychkov *et al.* [2] have studied the oscillatory behaviour during methane oxidation over Ni foam using thermogravimetric analysis combined with on-line mass-spectrometry analysis of the gas phase. It was shown that oscillatory behaviour of the weight was defined mainly by the amount of oxygen associated with the nickel oxide in the catalyst. It was also discovered that the maxima in temperature oscillations corresponded to the maxima in weight oscillations, i.e. to the oxidised state of the Ni catalyst. Mass-spectrometric analysis of the obtained products revealed that maxima in the rates of CO_2 and H_2O coincides with the maxima of weight and temperature (oxidised state), while maxima in CO and H_2 production rates correspond to the minimum weight and temperature oscillations (reduced state). Basing on these experimental and literature data it was suggested that nickel catalyst contains both oxidised and reduced surfaces (Ni^0/NiO surface). On the reduced surface steps 1-6 proceed including CH_4 and O_2 adsorption, step 7 describes the transformation of the adsorbed oxygen into the nickel oxide and finally steps 8-10 correspond to the reduction of the nickel oxide.

1. $CH_4 + 5[Ni^0] \rightarrow [Ni^0\text{-}C] + 4[Ni^0\text{-}H]$
2. $O_2 + 2[Ni^0] \rightarrow 2[Ni^0\text{-}O]$
2r. $2[Ni^0\text{-}O] \rightarrow O_2 + 2[Ni^0]$
3. $[Ni^0\text{-}C] + [Ni^0\text{-}O] \rightarrow [Ni^0\text{-}CO] + [Ni^0]$
4. $[Ni^0\text{-}CO] \rightarrow [Ni^0] + CO$
5. $2[Ni^0\text{-}H] \rightarrow H_2 + 2[Ni^0]$ (1)
6. $[Ni^0\text{-}O] + 2[Ni^0\text{-}H] \rightarrow 3[Ni^0] + H_2O$
7. $[Ni^0\text{-}O] \rightarrow NiO$
8. $4[NiO] + CH_4 \rightarrow CO_2 + 2H_2O + 4[Ni^0]$
9. $2[NiO] + [Ni^0\text{-}C] \rightarrow CO_2 + 3[Ni^0]$
10. $[NiO] + 2[Ni^0\text{-}H] \rightarrow 3[Ni^0] + H_2O$
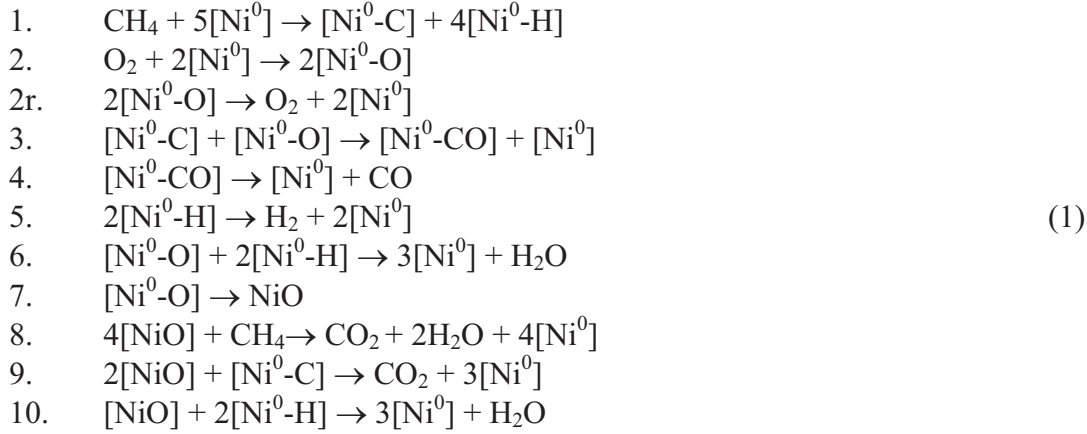
To simulate the surface phase transitions the variable s, $0 \leq s \leq 1$, indicating the fraction of the reduced surface was introduced. Correspondingly, $s_o = 1-s$ denotes the fraction of the oxidized surface. The variables x_1, x_2, x_3, x_4, indicate the average coverages of C, O, CO, and H on the reduced surface. The relation with respecting coverage on the whole surface X_i is the following: $X_i = x_i s$. The equations for the evolution of x_i consider the fact that x_i can change not only due to the surface reactions, but also due to the variation of the area of the reduced surface. In this case the mathematical model, corresponding to the mechanism (1) and describing the dynamic behaviour of the surface coverages, catalyst temperature, partial pressures of reactants can be formulated as follows:

$$
\begin{aligned}
s' &= -R_7 + 4R_8 + 2R_9 + R_{10} \equiv f_s, \\
x_1' &= R_1 - R_3 - R_9/s - x_1(f_s/s), \\
x_2' &= 2R_2 - 2R_{-2} - R_3 - R_6 - R_7/s - x_2(f_s/s), \\
x_3' &= R_3 - R_4 - x_3(f_s/s), \\
x_4' &= 4R_1 - 2R_5 - 2R_6 - 2R_{10}/s - x_4(f_s/s); \\
T' &= \alpha(T_0 - T) + \beta s \sum_{i=1}^{6} q_i R_i + \beta \sum_{7}^{10} q_i R_i. \\
p_1' &= \tau^{-1}(P_{CH4} - p_1) - \gamma s R_1 - \gamma R_8, \\
p_2' &= \tau^{-1}(P_{O2} - p_2) - \gamma s(R_2 - R_{-2}).
\end{aligned}
$$

(2)

Here P_{CH4}, P_{O2}, and T_0, indicate the partial pressures of CH_4 and O_2 in the inlet gas mixture and initial gas phase temperature. p_1 and p_2 denote the partial pressures of CH_4 and O_2 in reactor, and T – the catalyst surface temperature. $\alpha = (hS)/(WC_p)$; $\beta = (SN)/(WC_p)$; $\gamma = (SNRT_0)/V$; $\tau = V/F$, where: h is the heat transfer coefficient, S – the catalyst surface area, W – the catalyst weight, C_p – the catalyst heat capacity; N – the adsorption capacity of Ni; R – the universal gas constant, V – the reactor volume; F – the flow rate of the reactant mixture, q_i – the heat effects of the corresponding studies of the reaction mechanism.

The results of mathematic modelling are demonstrated in Figures 1a, 1b. The model produces oscillatory behaviour at realistic experimental conditions and values of parameters.
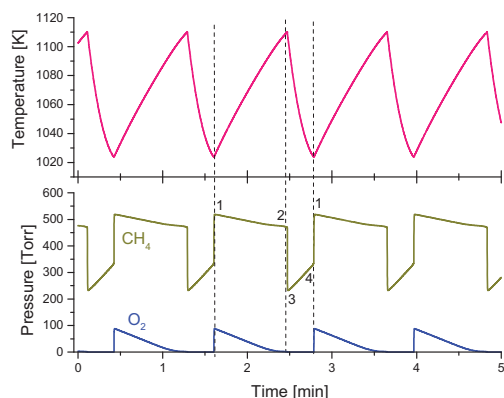
a)   b)
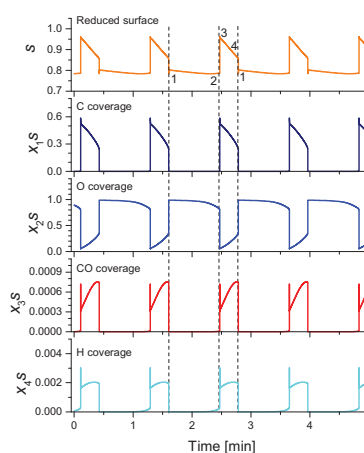
Figure 1. a) Calculated variations of temperature and partial pressures of reactants at P_{CH4} = 570 Torr, P_{O2} = 190 Torr, T_0 = 1023 K. b) Simulated oscillations of reduced surface s and surface species coverages $x_i s$.

The mechanism of oscillations may be presented as follows: during the period of time 1-2, the system is in the so-called "oxidised state". Here the temperature increases due to the exothermic reactions, proceeding on the NiO and the oxygen concentration in the gas phase decreases. At some temperature the rate of the catalyst reduction becomes larger than the rate of the catalyst oxidation and the system moves to the so-called "reduced state" indicated as 3-4. At this point the temperature decreases, because less exothermic reactions producing CO and H_2 occur on the reduced Ni surface. Although CH_4 is in the excess in the gas phase, the concentration of O surface atoms increases, while the concentration of C atoms decreases. This is the result of the competition of CH_4 and O_2 for the free sites. As O_2 adsorption needs less free active sites, at some temperature the surface is covered by oxygen and the system moves to the oxidised state.

The results of mathematical modelling showed that the thermokinetic oscillations during methane oxidation originate on the "reactor level". This means that the pressure variation in the reactor is the essential condition for the appearance of the oscillatory behaviour and parameters of the reactor play the important role in the generating of the oscillatory behaviour.

Acknowledgment

References

[1] X.L. Zhang, C.S-M. Lee, D.M.P. Mingos, and D.O. Hayward, Catal.Today, 105 (2005) 283-294.

[2]. V.Yu. Bychkov, Yu.P. Tulenin, V.N. Korchak, and E.L. Aptekar, Appl. Catal. A, *to be published*

MODELLING OF PARTICLE GROWTH: APPLICATION TO WATER TREATMENT IN A FLUIDIZED BED REACTOR

R. Aldaco, A. Garea, <u>A. Irabien</u>

Deportamento Ingeniería Química y Química Inorgánica, Universidad de Cantabria
ETSIIyT. Avda. de los Castros s/n. 39005 Santander, SPAIN
Tel: +34942201597, Fax: +34942201591, Email: irabienj@unican.es

Introduction

Crystallization in a fluidized bed reactor (FBR) has been used in different water and wastewater treatment plants, including water softening of drinking water, phosphate and fluoride removal, and heavy metal recovery from wastewaters. When it is compared with the chemical precipitation process, the major advantage of this technology is the decrease of sludge formation, the simplification of the materials recovery procedures and the reduction of solid wastes.

In the modeling, design and control of a FBR for water treatment it is necessary to study the particle growth kinetics. The properties of the particles in a crystallization process depend mainly on the crystal growth rate and nucleation kinetics, which control the final properties of the solid product. The crystal growth is a complex mechanism that includes many factors depending on different variables: dispersion, supersaturation, crystal size, solution velocity, admixtures, magnetic field, temperature, and pH. The model allowing the mathematical description of the variables is still very complex and a general expression of crystal growth is difficult to establish, especially for sparingly soluble systems.

This work summarizes the experimental study of crystal growth of calcium fluoride on granular calcite as seed material in a FBR. It has been studied the influence of the main variables on the crystal growth and a mechanism of crystal growth has been suggested.

Materials and methods

The Fluidized Bed Reactor (FBR) is based on the crystallization of CaF_2 upon seed material instead of mass precipitation in the liquid phase [1,2].

The laboratory FBR consists of a methyl methacrylate cylindrical vessel partially filled with granular calcite as the seed material. The fluoride water and calcium reagent solution are pumped upward through the reactor at a velocity that ensures the fluidization of the pellets so that cementing of grains is prevented [2].

A typical run consists of adding about 70g of sieved granular calcite as seed material and controlling the solution velocity so that the solids are uniformly suspended in the FBR. In order to determine the influence of the variables on the calcium fluoride growth, the superficial velocity (SV) in the reactor was changed in the range 21-45 m·h^{-1}, the initial particle size (L_0) of granular calcite was between 260-580 μm, and the supersaturation (S) was between 6.4 and 38.5.

During the operation, the grains increase in diameter and fluoride-coated calcite grains (pellets) were removed from the bottom of the reactor at different times. The pellets were air dried and the particle size was determined by Laser-Ray Diffraction (Mastersizer S, Malvern Instruments).

Results and discussion
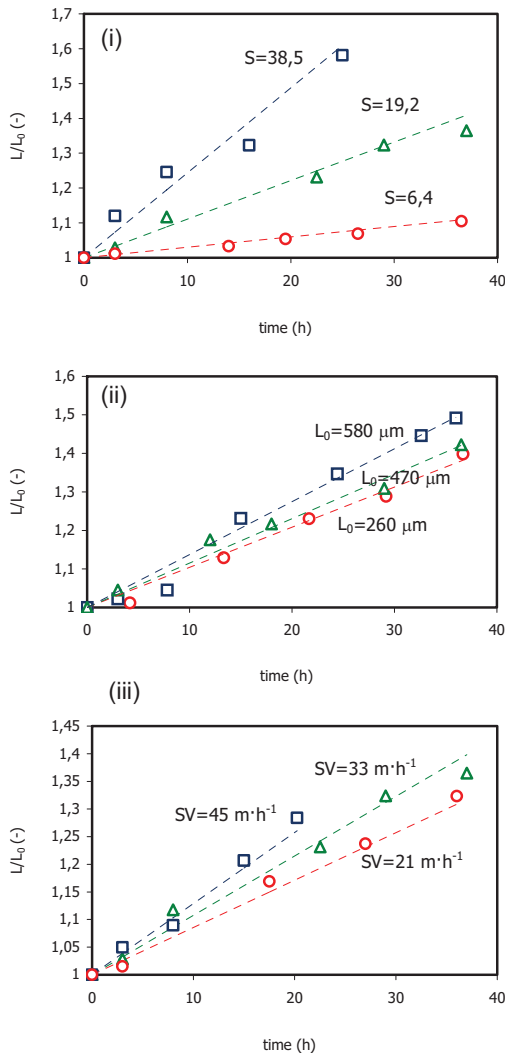
Figure 1. Influence of the (i) supersaturation, particle size (ii) and superficial velocity (iii) on the crystal growth of CaF$_2$ as a function of time.

Figure 1 shows the dimensionless particle size of the pellets as a function of time when the supersaturation, the particle size of the seed material and the superficial velocity change. The superficial velocity in the reactor, the supersaturation and the initial particle size of the seed material show an influence in the growth rate of the calcium fluoride pellets in a FBR.

A general model from the growth has been fitted according to the following equation:

$$G = \frac{dL}{dt} = K_g \; L_0^m \; SV^n \; S^j \tag{1}$$

where G is the overall linear growth rate (m·s^{-1}), L is the size of the particle (m), K_g is an overall crystal growth coefficient , and m, n and j are the crystal growth orders referred to the initial particle size, superficial velocity and supersaturation respectively.

The experimental results have been fitted to the model by the following equation:

$$G = 2.96 \cdot 10^{-5} \; L_0^{1.37} \; SV^{0.49} \; S^{1.01} \quad R^2 = 0.969 \tag{2}$$

From Figure 2 it is possible to deduce that the growth rate increases linearly with the supersaturation. The reason of this influence can be explained in terms of the concentration driving force for crystallization [3].

Figure 3 shows that at a given supersaturation and particle size of seed material, the growth rate increases with the superficial velocity in terms of the particle Reynolds number. Mass transfer between fluidized solid particles and liquid has been studied extensively over a wide range of Reynolds numbers [4].

It appears that most of the reported experimental data can be adequately described by the following correlation:

$$Sh = B_1 \, Re^{1/2} \, Sc^{1/3} \tag{3}$$

where Sh is the Sherwood number, B_1 is a constant, Re is the particle Reynolds number and Sc is the Schmidt number.

The experimental results agree well with the correlations proposed in the literature. Therefore, the influence of the superficial velocity on the growth rate is related to the convective mass transfer.

Results of linear growth rate for different sizes of granular calcite are depicted in figure 4. The particles with larger size have higher growth rate than, those with smaller sizes. The overall linear growth rate may be the addition of two mechanisms:

$$G = K_1 \, SV^{0.5} \, S + K_2 \, SV^{0.5} \, S \, L_0^2 \tag{4}$$

Figure 2. Influence of the supersaturation (S) on the overall linear growth rate.
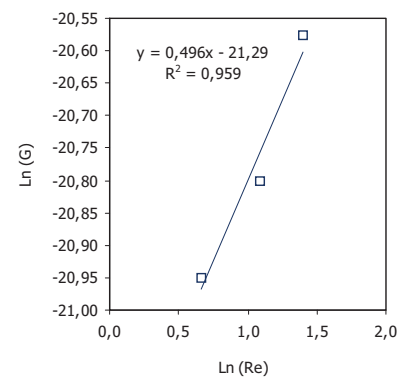
Figure 3. Linear fitting of the overall linear growth rate and the particle Reynolds number (Re).
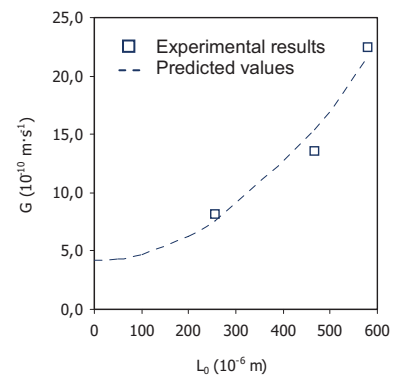
Figure 4. Influence of the particle size of the seed material (L_0) on the overall linear growth rate.

where the first term on the right hand side of the equation arises from aggregation of fines formed by homogenous nucleation in the liquid phase, and the second from molecular growth upon the surface of the seed material. Thus, the crystal growth by aggregation is a function of the superficial velocity and the supersaturation, and the crystal growth by molecular growth is a function of the superficial velocity, the supersaturation and the particle size of the seed material. Therefore, the overall linear growth calcium fluoride pellets in a FBR may be

described according to the flowing equation:

$$G = (K_1 + K_2 \, L_0^2) \, SV^{0.5} \, S \qquad (5)$$

where K_1, the crystal growth rate coefficient by aggregation, and K_2, the crystal growth rate coefficient by molecular growth, are $2.26 \cdot 10^{-10}$ and $2.82 \cdot 10^{-3}$ respectively.

The correlation between the experimental and predicted values of G is shown in Figure 5. The correlation coefficient of the fitting was 0.980, which agrees well with the experimental data.
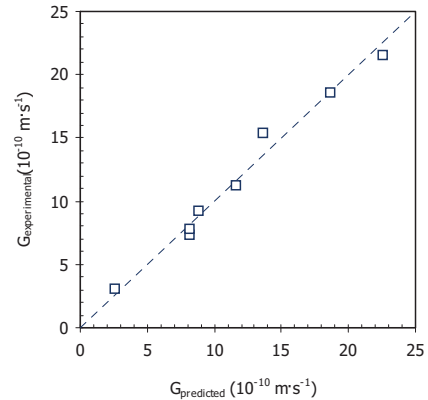
Figure 5. Parity graph for predicted values of overall linear growth rate by the proposed model of crystal growth of calcium fluoride in a FBR.

Conclusions

Based on the results of this work, it can be concluded:

(i) The increase of the superficial velocity in the reactor, the supersaturation and the particle size of the seed material leads to an increase of the linear growth rate of the calcium fluoride in a FBR. The pellets growth in a FBR takes place by aggregation of fines and molecular growth onto seed material.

(ii) It has been applied a crystallization model based on the aggregation and molecular growth mechanisms, which allows the introduction in the mass balances of the industrial process after calculation of the parameters K_1 and K_2. The model is useful in the design, operation and control of Fluidized Bed Reactors for water treatment.

Acknowledgements

References

[1] Aldaco, R., Irabien, A., Luis, P. 2005.Fluidized bed reactor for fluoride removal. Chem.Eng.J., 107,113-117.

[2] Aldaco, R., Garea, A. Irabien, A. 2006. Fluoride Recovery in a Fluidized Bed: Crystallization of Calcium Fluoride on Silica Sand. Ind. Eng. Chem. Res. 45(2), 796-802.

[3] Tai, C.Y., Chien, W.C., Chen, C.Y. 1999. Crystal growth kinetics of calcite in a dense fluidized-bed crystallizer. AIChE J., 45(8), 1605-1614.

[4] Yang, J., Renken, A. 1998. Intensification of mass transfer in liquid fluidized beds with inert particles. Chem. Eng. Process, 37(6), 537-544.

ANALYSIS, MODELING AND SIMULATION OF CATALYTIC PROCESS OF HIGH PURITY ETHYLENE PRODUCTION

E.V. Pisarenko[1], V.N. Pisarenko[1] and A.Sh. Ziyatdinov[2]

[1]*D. Mendeleyev University of Chemical Technology of Russia, Moscow, Russia*
[2]*JSC "Nizhnekamskneftehim", Nizhnekamsk, Russia*

In present century, there is a tendency of stable growth of low olefins production capacities, in particular, ethylene in the Russian Federation. Prices for these products go up as well. The main industrial process of ethylene production is thermal pyrolysis of hydrocarbons of gasoline fraction of crude oil. Gaseous pyrolysis products are separated in ethane-ethylene fraction, propane-propylene fraction and butane-butylene fraction.

Ethane-ethylene fraction usually contains up to 1 % mass. of acetylene. The purification of ethane-ethylene fraction from acetylene is performed by catalytic hydrogenation reactions. However, the technology of catalytic hydrogenation of acetylene in ethane-ethylene fraction needs some improvements due to significant loses of ethylene.

The aim of given research was to develop new catalytic system and improved technology of the process of ethylene purification from acetylene in ethane-ethylene fraction of pyrolysis gases without any ethylene loses and even slight increase in ethylene in the reaction products.

First, efficient catalyst composition has been selected. The composition of active centers among classes of palladium-oxide catalysts, active centers distribution over inner and outer surface of the catalyst grain, pore distribution, grain size and geometry have been selected.

As a result of this research work, new catalyst sample with 0.04 % mass. of Pd was synthesized. Micro quantities of metals of I and II group of the Periodic Table served as promoters in this reaction. α - Alumina oxide was used as a catalyst support. For new catalyst "CPNM-45" technological production documentation was developed. According to this documentation 4 tons of new catalyst was manufactured at JSC "Niznekamskneftekhim".

Second, the detailed mechanism of ethylene and acetylene hydrogenation reactions over "CPNM-45" catalyst was determined. Kinetic model was derived for the mechanism proposed. Kinetic parameters were estimated by the results of 48 experiments carried out in flow circulating reactor operating under pressure. Bartlett and Hagao criteria were used to prove the adequacy of the model to experimental data.

OP-2-6

Third, efficiency factors of the catalyst grain operation with respect to all reactants and reaction routes corresponding to final reaction equations were estimated. The pilot plant reactor with catalyst volume of 4 liters was designed and built. Based on the results of pilot plant experiments, reactor model macrokinetic parameters were estimated and the model adequacy to experimental results was demonstrated.

While carrying out pilot plant experiments, the appearance of some periodic oscillation regimes of the reactor performance was noticed. The reactor model allowed one to determine physical - chemical nature of the appearance of periodic oscillations in certain reaction zones.

Industrial two sectional reactor of ethylene purification from acetylene with ethylene productivity of 70000 tons per year was loaded with new catalyst. Reactor start and optimal regimes of its operation were carried out according to the results calculated due to the model.

Within first 8000 hours of the reactor operation, ethylene increase reached 0.2 % mass, then for next 8000 hours – ethylene increase was 0.1 % mass. Volumetric flow rate was kept at 2700 inverse hours. The results of industrial run of CPNM-45 catalyst showed its high selectivity, activity and the possibility of long and stable service life without deactivation. Overall run of pilot plant was 35000 hours.

DIMENSIONAL ANALYSIS AS A TOOL FOR SCALING UP AND DOWN STEAM CRACKING COILS

K.M. Van Geem, R. Žajdlík, M.-F. Reyniers, G.B. Marin

Laboratorium voor Petrochemische Techniek, Ghent University, Gent, Belgium

Abstract

Steam cracking is an endothermic process and is operated at high temperatures. Next to the intrinsic chemical kinetics, heat and mass transport processes, which are scale dependent, affect the product yields. Product yields obtained in small and large scale reactors will only be identical provided that mass and heat transfer processes are similar and the "chemistry" remains the same. Two different approaches are commonly applied in scale-up and scale-down: direct experimental scale-up and mathematical modeling. Mathematical modeling is the most attractive solution because it has the advantage that once the model is developed, results can be gathered easily and computer simulations take only a limited time.[1] One of the major challenges in this method consists of developing a fundamental reaction network. Moreover fundamental kinetic models work with a detailed feedstock composition and obtaining this information for naphtha's, gas oils and VGO's is not straightforward. Therefore, direct experimental scale-up remains an interesting option and developing a pilot plant set-up, although expensive, is still done quite often.[2]

Table 1: Typical dimensions and operating conditions used in steam cracking reactors of different scale

	Laboratory scale reactor	Pilot Plant reactor	Industrial reactor
Reactor length (m)	1 - 2	10 - 25	10 - 100
Tube diameter (m)	$5.10^{-3} – 1.10^{-2}$	$5.10^{-3} – 2.5\ 10^{-2}$	$3.10^{-2} – 1.5\ 10^{-1}$
Flow rate (kg s^{-1})	$5.10^{-5} – 5.10^{-4}$	$5.10^{-4} – 1.10^{-2}$	10^{-2} - 1
Pressure drop (MPa)	< 0.01	0.02 – 0.06	0.07 – 0.15
COT (K)	850 – 1100	900 – 1200	1000 – 1200
Residence time (s)	0.1 – 8	0.1 – 1	0.1 – 1
Re	10^2	4.10^3 - 1.10^4	1.10^5 - 5.10^5

Direct experimental scale-up requires little or no mathematical treatment and is based upon a large experimental data set. A problem is that the differences in dimensions and in typical operating conditions between industrial reactors, pilot plant reactors and laboratory scale reactors are significant, see Table 1, and evidently this will result in differences between

conversions and product yields obtained at different reactor scales. Basically, the direct experimental scale-up consists in the construction of a small scale unit similar to an industrial one and operating it under conditions of complete or partial similarity. According to the theory of similarity, two processes can be defined as similar if they take place in a similar geometrical space, and if all the dimensionless numbers necessary to describe the process, have the same numerical value.[3] The dimensionless numbers can be determined based on a detailed mathematical description of the steam cracking process.[4] If a 2-dimensional reactor model is used and back mixing is neglected, then the dimensionless energy and continuity equation for a component j are given by:

$$\frac{\partial}{\partial z'}(v'_a \, C'_j) + -\frac{1}{Pe}\frac{1}{\xi}\frac{\partial}{\partial \xi}\left(\xi \, D'\frac{\partial C'_j}{\partial \xi}\right) = Da_I \sum_i \nu_{i,j} r'_{V\,i}$$

[1]

$$\frac{\partial}{\partial z'}(v'_a \, \theta) - Fo\frac{1}{\xi}\frac{\partial}{\partial \xi}\left(\xi \, \lambda'\frac{\partial \theta}{\partial \xi}\right) = Da_{II} \sum_i (-\Delta_r H_i')r'_{V\,i}$$

[2]

with: $Pe = \dfrac{d_t^2}{4\,D_e^0}\dfrac{v_a^0}{L}$; $\quad Da_I = \dfrac{L}{v_a^0}\dfrac{r_V^0}{C^0}$; $\quad Fo = \dfrac{L}{v_a^0}\dfrac{4\,\lambda^0}{c_p\,\rho_g\,d_t^2}$ and $\quad Da_{II} = \dfrac{L\,r_V^0}{v_a^0}\dfrac{|\Delta_r H|}{c_P\,\rho_g\,T^0}$

If only friction with the wall is taken into account and radial pressure gradients are neglected, the momentum equation can be transformed into the following dimensionless form:

$$\frac{dp'_t}{dz'} = \frac{1}{Eu}\left(v'_a\right)^2$$
[3]

with: $Eu = \dfrac{d_t p_t^0}{2f\,\rho_g\left(v_a^0\right)^2\,L}$

Analysis of these dimensionless model equations reveals that complete similarity of 2 different tubular reactors is impossible.[3,5] All the dimensionless numbers defined in equations [1-3] correspond with criteria of process-related similarity. Complete similarity requires geometrical, material, and process-related similarity.[3] However the criteria corresponding to process-related similarity, geometrical similarity [equal L/d_t-ratio] and hydrodynamic similarity [equal Re-number] cannot be met simultaneously[3,5] and therefore both geometrical similarity and hydrodynamic similarity are usually abandoned. Scale-up is thus only possible under partial similarity and inevitably this leads to differences. However, careful relaxation of

the similarity criteria limits differences between units of different scale. Further analysis of the dimensionless model equations shows that, even when allowing for hydrodynamic and geometrical dissimilarities, problems with realizing a similar temperature and pressure profile remain. Similarity of the radial temperature profile, i.e. equal Pe and Fo numbers, and of the pressure profile, i.e. equal Eu number, in two tubular reactors for steam cracking implies that these reactors need to be identical. Hence, two different relaxation strategies are available: the first one aims at realizing similarity of the pressure profile and neglecting radial non-uniformities [equal Eu; different Pe and Fo]; the second focuses on similarity of the radial temperature profile [equal Pe and Fo; different Eu]. Neglecting the similarity of the radial temperature profile leads to more important differences compared to the differences resulting from neglecting the similarity of the axial pressure profile. The radial temperature drop in an industrial reactor differs significantly from the one observed in a pilot plant reactor under similar operation conditions.[6] In the case of ethane cracking, differences between units of different scale resulting from relaxation of the similarity of the radial temperature profile can be up to 4.0 % (rel.) for the conversion and up to 1.2 % (rel.) for the ethylene yield. Similar conclusions are found for n-butane cracking. The preceding insights can be applied to design a so-called ideal pilot plant reactor for a given industrial reactor, i.e. a pilot reactor with a similar radial temperature profile as the reference industrial scale reactor. Creating a unit with a similar radial temperature profile requires that the different reactors have identical diameters. The length of the reactor can be chosen freely, as long as the pilot plant reactor is operated under an average pressure identical to that of the industrial unit. However, practical considerations also affect the design of the pilot plant reactor. The minimum diameter of the pilot reactor tube is limited by the need to measure process variables, such as gas phase temperature. As the dimensions of the furnace are limited, the reactor length should not be more than 20 m long. The recommended range of dimensions and operating conditions of the ideal pilot reactor are specified in Table 1. Taking into account these practical limitations result in a recommended length of 20 m and a diameter of 2.5×10^{-2} m for the ideal pilot plant reactor for scale-down of a Lummus SRT-I reactor or a Millisecond reactor. The total flow rate (hydrocarbons + steam) should be higher than 2.0×10^{-3} kg s^{-1} to guarantee turbulent flow in the pilot reactor (Re>4000). Note that, although "ideal", imperfections remain and some differences between product yields obtained in the pilot plant reactor and the industrial reactor will always remain as the radial temperature drop is still significantly lower in the ideal pilot reactor under similar conditions. This pilot plant reactor is also ideal for studying coke formation but is not perfectly suited to study intrinsic kinetics because in practice it is not

possible to accurately measure the radial temperature profile at a given axial position. To study intrinsic kinetics, the radial temperature drop should be kept as small as possible, and hence, the diameter of the reactor should be as small as possible.

Acknowledgments

References

1. Dente, M., Ranzi, E., Goossens, A.G., (1979). Detailed prediction of olefin yields from hydrocarbon pyrolysis through a fundamental simulation model (SPYRO). Comp. & Chem. Eng., 3, 61-75.

2. Pinter, A., Tungler, A., Nagy, L., Vida, L., Kovacs, I., Kerezsi, J., (2004). A laboratory steam cracking reactor to characterize raw materials. International Journal of Chemical Reactor Engineering, 2, A15.

3. Zlokarnik, M., (2002). Scale-up in chemical engineering. Wiley-VCH, Weinheim.

4. Himmelblau, D.M., Bishoff, K.B., (1968). Process analysis and simulation. J. Wiley, New York.

5. Van Geem, K.M., Heynderickx, G.J., Marin, G.B., 2004. A comparison of one and two-dimensional reactor models for steam cracking: effect on yields and coking rate. AIChE Journal, 50, 173–183.

6. Damköhler, G.Z., (1936). Einflüsse der Strömung, Dffusion und des Wärmeübergenges auf die Leistung von Reactionsöfen. Electrochemie, 42, 846-862.

List of Symbols

C	concentration	kmol m^{-3}	c_p	heat capacity	kJ kmol^{-1} K^{-1}
D	Diffusion coefficient	m² s^{-1}	Da	Damköhler number	-
d_t	internal tube diameter	m	Eu	Euler number	-
f	Fanning friction factor	-	$\Delta_r H_k$	standard reaction enthalpy	kJ kmol^{-1}
L	reactor length	m	p_t	total pressure	MPa
Pe	Peclet number	-	r_V	reaction rate	kmol m^{-3} s^{-1}
Re	Reynolds number	-	T	process gas temperature	K
v	velocity	m s^{-1}	z	axial coordinate	m

Greek symbols

θ	dimensionless temperature	-	λ	thermal conduction coeff.	kJ m^{-1} s^{-1}
ρ_g	density	kg m^{-3}	ξ	normalized radial position	-
ν	stoechiometric coefficient	-	μ	dynamic viscosity	MPa s

Sub- and superscripts

0	initial		a	axial
r	radial		'	dimensionless

SPATIOTEMPORAL PHENOMENA IN CATALYTIC CO OXIDATION: SIMULATION RESULTS

V.V. Volkovskii, <u>N.L. Semendyaeva</u>, E.S. Kurkina

Moscow Lomonosov State University, Faculty of Computational Mathematics & Cybernetics

Leninskie Gory, Moscow, 119992, GSP-2, Russia, E-mail: NatalyS@cs.msu.su

The catalytic CO oxidation is an important reaction of ecological catalysis demonstrating complex behavior. Real time observations of supported catalysts, metal tips, nanostructured composite surfaces, single crystals of Pt-group metals by means of different microscopic techniques have detected propagating fronts, target patterns, rotating spirals, standing waves, solitary pulses, chemical turbulence [1]. In order to understand the origin and driving forces of these non-linear phenomena a new strategy for research of heterogeneous reactions has been applied [2]. Namely, a system of consistent mathematical models of various space scales has been constructed and investigated, and a comparative analysis of the reaction dynamics produced by different mathematical models has been performed. The system includes Monte Carlo (MC) simulations of a lattice gas (LG) reaction model, mean-field (MF) ordinary differential equations (ODEs) and reaction-diffusion equations (RDEs).
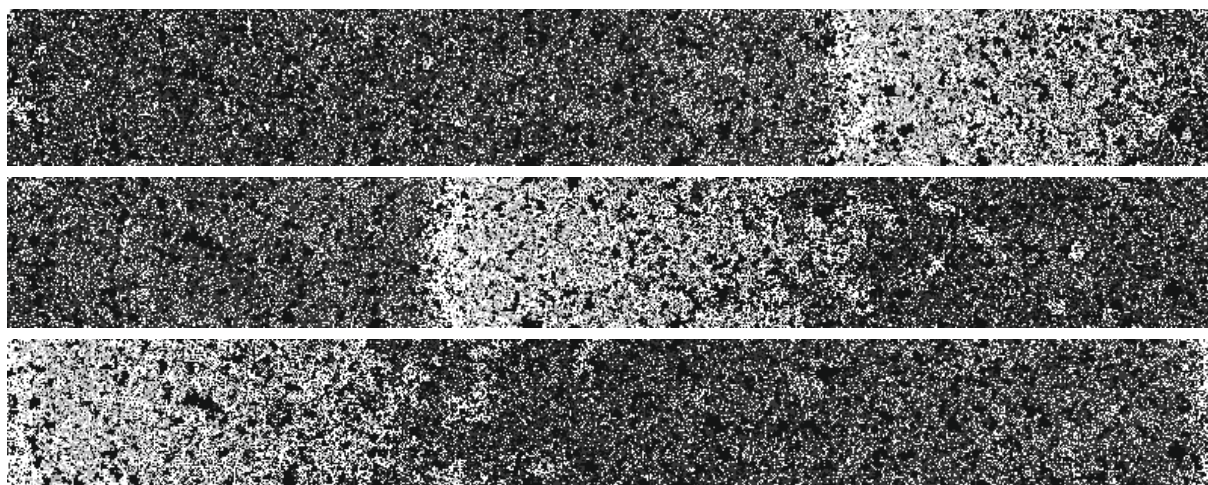
Fig. 1.

Our investigations revealed three types of oscillatory-like behaviour of the $CO+O_2$ reaction on an atomic scale. In the first case oscillations are caused by chemical kinetics. They exist both in small scale LG and MF models in the oscillation region of the latter. RDEs and large scale LG model under the same conditions can reproduce experimentally observed spatio-temporal structures formation on the micrometer and millimetre scales – travelling pulses (fig.1, MC data) and spiral waves (fig. 2, MC data).
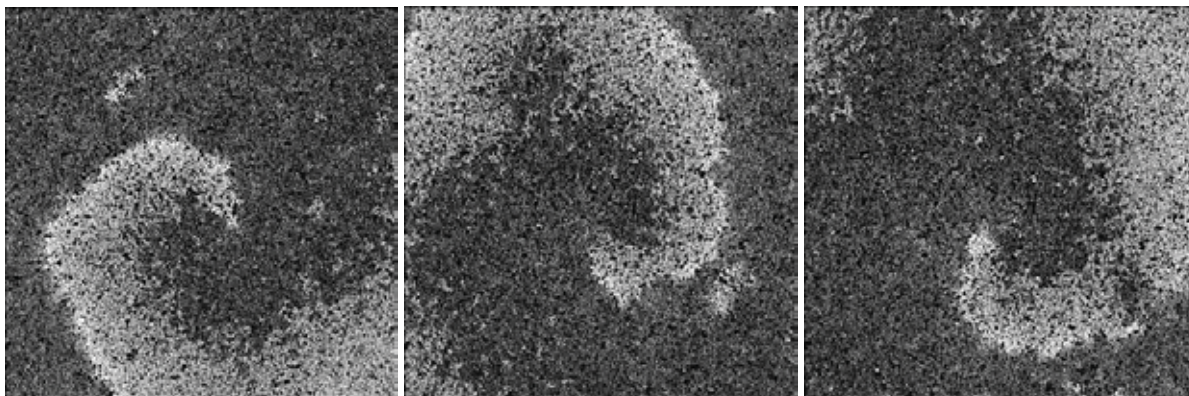
Fig. 2.

Two other types of oscillatory-like behaviour on microscopic level are conditioned by internal fluctuations. Fluctuation-driven transitions from high-reactive stable steady state to low-reactive one (the second type) occur in the region of bistability of the MF model. Transitions take place in an immobile adsorption layer and are induced by internal fluctuations. In the numerical experiments based on RDEs or large scale LG models one can obtain propagating reaction fronts under the same conditions (fig. 3, MC data).

Fluctuation-induced oscillations of the third type take place in the monostable region of the MF model in consequence of the excitable nature of the stable steady state. Atomic scale stochastic models demonstrate excitable dynamics due to internal noise. Excitable dynamics of deterministic systems must be maintained by external conditions. In reaction-diffusion systems and large scale LG models the excitation region can expand forming a travelling pulse (in 1D) or a spiral wave (in 2D).

The presented results allow one to predict, understand and explain the complex nonlinear dynamic behavior of the $CO+O_2$ reaction system over Pt-group catalysts.
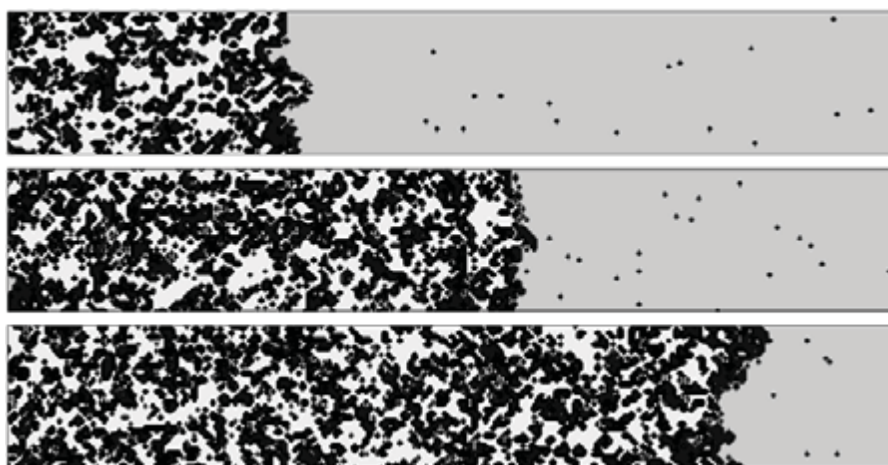
Fig. 3.

References

[1] R. Imbihl, G. Ertl // Chem. Rev. 95(1995) 697.

[2] E.S. Kurkina, N.L. Semendyaeva // Surf. Sci. 558 (2004) 122.

INVESTIGATION OF N$_2$O DECOMPOSITION AND SURFACE OXYGEN FORMATION ON Fe-MFI WITH TRANSIENT RESPONSE METHODS

Ayten Ates[a] and Andreas Reitzmann[b]

[a]*Department of Chemical Engineering, Engineering Faculty, Cumhuriyet University, 58140 Sivas, Turkey. Email: ates@cumhuriyet.edu.tr, Fax:+9003462191179*

[b]*Institut für Chemische Verfahrenstechnik, Universität Karlsruhe, Kaiserstraße 12 76128 Karlsruhe, Germany, andreas.reitzmann@cvt.uni-karlsruhe.de, Fax: +497216086118*

The general aim of this work is to study the elementary steps of the N$_2$O decomposition on iron containing MFI zeolites with transient response methods, namely multi-pulse and step techniques combined with temperature programmed desorption. Both methods should be compared due to their applicability to determine the formation and amount of an surface bound oxygen species. In addition, the global kinetics was determined from steady state experiments at different residence times and temperatures. The formation of an atomic surface oxygen should be linked to the global rate of N$_2$O decomposition.

Introduction

In general, investigations under steady-state conditions give information on global kinetics of reactions, but are not very informative about the reaction mechanisms and the surface species involved. Therefore, regarding these aspects transient studies are believed to give an further insight in the proceeding of a reaction. The decomposition of nitrous oxide is a well known and important example where these techniques have been applied. The following mechanism is generally accepted when different catalysts are applied:

$$Z + N_2O \quad \rightarrow \quad N_2 + Z–O \tag{1}$$

$$2\ Z–O \quad \rightarrow \quad O_2 + 2\ Z \tag{2}$$

$$Z–O + N_2O \rightarrow N_2 + O_2 + Z \tag{3}$$
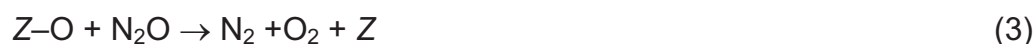
Iron containing zeolites of MFI type are particularly interesting, because they have been successfully applied in the abatement of N$_2$O in waste gases as well as in partial oxidations of aromatic hydrocarbons with N$_2$O. Since for both applications the first step of the mechanism (Eq. 1) is important where an atomic surface bound oxygen species is formed, many investigations in the literature focus on it. Besides of experiments in a static vacuum set-up

combined with [18]O isotope exchange reactions and step-experiments, we proposed recently a multi-pulse method which allows a quantitative tracing of the surface bound oxygen formation [1,2]. Temperature programmed desorption and the CO reduction with the oxygen loaded zeolites revealed that several oxygen species with different stability and reactivity exist. Particularly, the role of molecularly adsorbed N_2O cannot be neglected, on MFI zeolites with high iron content.

Experimental

Iron containing MFI samples were prepared by a solid - state ion exchange with $FeCl_2 \cdot 4 H_2O$ as described in [1,2]. The standard sample (Fe-MFI-A) has a Si/Al ratio of 11.5 and an Fe/Al ratio of 0.75 (5.66 % (wt./wt.) Fe). Prior to all experiments, catalysts were pretreated with Helium at 500 °C. Temperature-programmed and transient studies of N_2O decomposition were performed in a set-up for catalyst characterisation (Autochem 2910, Micromeritics) containing a quartz glass reactor (i.d. 9 mm). The reaction products were monitored in an on-line mode using a quadruple mass spectrometer (QMS 422; Pfeiffer Vacuum). Multi-pulse experiments were performed as described in [1,2] in a temperature range of 150- 500 °C by injecting 0.31 μmol N_2O via a sample loop into a helium flow and over the catalyst, respectively. Step experiments were carried out according to the procedure proposed by Kiwi-Minsker et al [3] and Wood et al. [4] at 150 – 300 °C (1 % (v/v) N_2O / 1 % (v/v) Ar / 98 (v/v) % He). Steady-state kinetics were studied in the temperature range 150 to 500 °C and under different residence times with N_2O inlet concentrations of 1000 ppm (v/v) and 1 % (v/v) in a quartz fixed bed reactor (i.d= 11.5 mm; L= and 250 mm). N_2O concentrations were determined by the non-dispersive infrared spectroscopy (Binos, Leybold Heraeus).

Results and Discussion

Multipulse technique

Figure 1 shows an exemplary result of the multi pulse studies at 250 °C for different amounts of Fe-MFI-A. No molecular oxygen was detected during the pulse sequence. The amount of surface oxygen calculated by summarizing the formed N_2 was in each case 40 - 41 μmol/g. The shape of the curves is determined by the residence time of the pulses in the catalyst bed, which was also found for different flow rates. Therefore this technique provides a suitable method to determine the surface oxygen content. It has been successfully applied to other zeolites with different Si/Al ratio and Fe content (not shown).

Subsequent temperature programmed desorption experiments revealed that oxygen desorbed in two steps up to 900 °C, but only about 1/3 up to 500 °C. Moreover, N_2O also

desorbed up to 600 °C which was surprising, but explained the difference between consumed N_2O and formed N_2 during the pulse sequence.
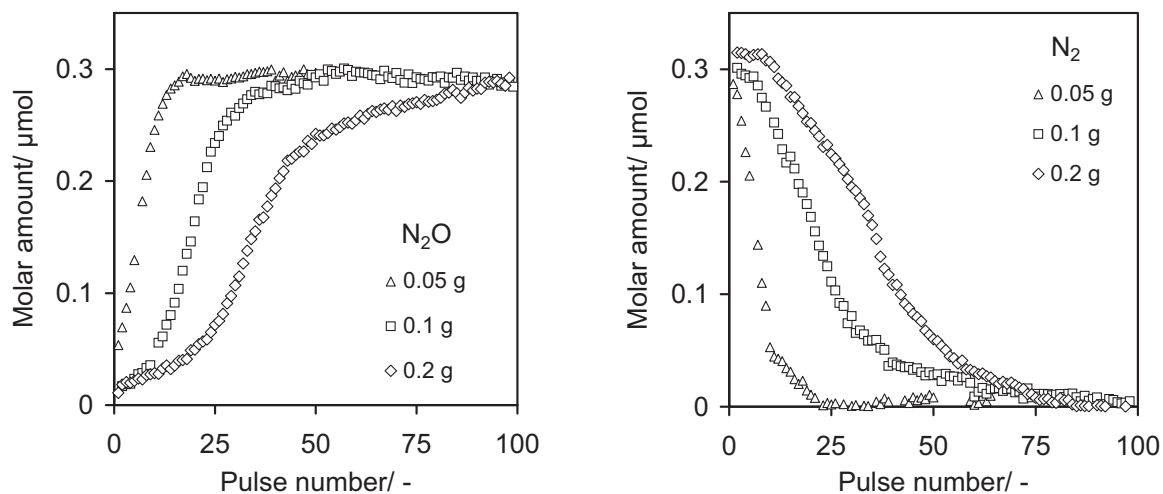
Fig. 1. Influence of Fe-MFI-A amount on the N_2O multi pulse sequence at 250 °C:
N_2O (left), N_2 (right)

Other experiments with this catalyst showed that the surface oxygen formation depends on the reaction temperature: The amount increases from 16 µmol/g (150 °C) to 62 µmol (300 °C) demonstrating that this kind of N_2O activation is an activated process of N_2O with increasing of temperature. This is an important fact if catalyst activity and the amount of surface oxygen formation wanted to be correlated. Although the method is suitable to determine the catalyst storage capacity for oxygen formed during N_2O activation, a study of its formation kinetics is rather difficult. An appropriate model for the reactor must be developed not to falsify the kinetic data. This is in progress at the moment.

Step technique

Applying the step technique proposed by Kiwi-Minsker et al [3] and Wood et al. [4] to Fe-MFI-A sample showed that molecular oxygen was formed during the step experiment already at 200 °C. This was probably due to the higher average concentration of N_2O, so that it was already reacting with surface bound oxygen. After correcting the formed N_2 amount corresponding to the formed O_2 amount, the amount of surface oxygen was still higher than obtained with the multi-pulse method. Therefore the step method is only limited applicable for active zeolites in N_2O decomposition. Nevertheless, the kinetic analysis of Wood et al. [4] has been applied to the corrected rate of N_2 formation:

$$r_{N_2} = k \cdot \theta(t) \cdot c_{N_2O} \text{ with } \theta(t) = \theta_0 \cdot e^{(-k \cdot c_{N2O} \cdot t)}$$

OP-2-9

An activation energy of ~ 24 kJ/ mol and a pre-exponential factor of $3.6 \cdot 10^7$ ml/(g_{cat}·s) was found. Activation energy is lower than in literature reported for zeolites with low iron content (0.38 % (wt) Fe) and can therefore be explained with the high iron content of the sample. However, it is still an open question up to which extent this result is falsified by the O_2 formation during the step. It is investigated at the moment and the method should be applied to zeolites with lower iron contents.

Temperature programmed desorption after the step experiments revealed the same results than after the multi-pulse sequence: Oxygen desorbed in two temperature ranges up to 900 °C and the N_2O desorption took place up to stable up to 600 °C

Steady state measurements

The steady state measurements with 1000 ppm (v/v) and 1 % (v/v) N_2O can each be fitted with a first order rate law commonly proposed in literature. However, activation energy and pre-exponential factor were significantly different in both cases, for 1000 ppm (v/v) $2.41 \cdot 10^{13}$ ml/(g_{cat}·s) and 162 kJ/ mol, for 1 % (v/v) inlet concentrations $9.2 \cdot 10^{14}$ ml/(g_{cat}·s) and 185 kJ/ mol. In order to fit all results, the following model with an inhibition factor for N_2O was developed: $r_{N_2O} = \dfrac{k \cdot C_{N_2O}}{1 + b \cdot C_{N_2O}}$. The rate constant k can be calculated via an

Arrhenius equation with an pre-exponential factor of $4.5 \cdot 10^{12}$ ml/(g_{cat}·s) and an activation energy 152 kJ/ mol. Results for the parameter b obtained from the best fit lead to the assumption that it has the nature of an sorption constant for N_2O at each temperature. Its temperature dependency can be described with exponential law containing a positive exponent. If this is consistent with the sorption constant must be proven by further investigations.

Nevertheless, if the global rate determined under steady state conditions is compared to the rate of the surface oxygen formation, it becomes clear that the latter one is much faster and therefore not the rate limiting step for N_2O decomposition.

This study shows that transient studies are suitable to get further insight to the elementary steps and reaction mechanism of the N_2O decomposition. However, kinetics of elementary steps can only be obtained under the prerequisite of an appropriate model for the reactor operating under unsteady state conditions.

References

[1] A. Ates, A. Reitzmann, J. Catal., 235(1)(2005)164.
[2] A. Ates, A.Reitzmann, Chem. Kinet. Catal. Lett. 86 (1) (2005) 11.
[3] L. Kiwi-Minsker, D.A. Bulushev and A. Renken, J Catal., 219(2003) 273.
[4] B.J. Wood, J.A Reimer, A. T.Bell, M.T. Janicke and K.C.Ott, J.Catal., 224 (2004)148.

SIMULATION OF THE REACTOR'S UNIT FOR CATALYTIC ETHYLENE OXIDE HYDRATION

V.F. Shvets, <u>R.A. Kozlovskiy</u>, I.A. Kozlovskiy, M.G. Makarov, J.P. Suchkov, A.V. Koustov, D.E. Zavelev

D.I.Mendeleev University of Chemical Technology of Russia, Chair of Basic Organic and Petrochemical Synthesis, 9 Miusskaya Square, Moscow, 125047, Russia

e-mail: kra@muctr.edu.ru

Abstract

The model of a tube fixed bed catalytic reactor for ethylene glycol production was used for simulation of the various reactor's units. The model includes equations describing catalyst's deactivation. The catalyst is a cross-linked styrene-divinylbenzene anion-exchange resin in carbonate/bicarbonate form. Various process conditions (temperature, substance's concentrations), heating regimes (isothermal, adiabatic) and reactor combinations were simulated. The optimal conditions for minimum of catalyst consumption were determined.

Introduction

Hydration of ethylene oxide is an industrial approach to glycols in general, and ethylene glycol in particular. Ethylene glycol is one of the major large-scale products of industrial organic synthesis, with the world annual production of about 15,3 million ton/y. Today ethylene glycol is produced in industry only by a noncatalyzed reaction. As it follows from numerous investigations [1-3] hydration of ethylene oxide catalyzed by anion-exchange resin is one of the most promising methods for ethylene glycol production as alternative for conventional industrial noncatalytic process. Catalytic method provides significant energy saving in comparison with noncatalytic one due to much higher selectivity. But the main disadvantage of such a catalyst is it's deactivation that consists of two undesirable processes: loss of catalytically active sites and catalyst's swelling. In our previous works the models of the tube fixed bed catalytic reactor [4] and of catalyst deactivation [5] were elaborated.

In the present work above mentioned models were used for analysis how process conditions influence on catalyst life time.

Results

The main parameters influencing on of the catalyst and its activity are temperature and concentrations of ethylene oxide and glycol. The first series of calculations were made for two types of reactor – isothermal and adiabatic. Process conditions were varied in the following ranges: temperature 80-100°C; initial concentration of ethylene oxide 3-10 % mass.; initial concentration of glycol 0-29 % mass. In each case selectivity, catalyst's capacity, catalyst's volume, catalyst productivity (kmole of glycol per m^3 of catalyst per h) and catalyst consumption (m^3 of catalyst per kmole of glycol) were calculated. Results of simulation showed that adiabatic reactor is more favorable than isothermal. It was found that most profitable conditions for production of outlet stream containing 35% mass of glycol are follows: installation consisting of several (up to 5) consecutive adiabatic tube reactor with distributed ethylene oxide input in each reactor and intermediate heat exchangers; initial concentration of ethylene oxide in each reactor is 6 % mass. These conditions provide selectivity about 95 %, catalyst productivity about 2,4 (kmole of glycol per m^3 of catalyst per h) and catalyst consumption about 7×10^{-5} (m^3 of catalyst per kmole of glycol) and catalyst life time up to 6000 h.

The final simulation was made in order to optimize the installation for glycol production by means of variation of combinations of catalytic and noncatalytic consecutive adiabatic reactors. The optimal scheme allowing minimum of catalyst consumption was found.

References

1. Shvets V.F., Makarov M.G., Koustov A.V., et al. Method for obtaining alkylene glycols. RU Patent 2149864, 2000.

2. Van Kruchten E. M. G. Process for the preparation of alkylene glycols. US Patent 5874653, 1999.

3. Iwakura T., Miyagi H. Production of alkylene glycol. JP Patent 11012206, 1999.

4. Shvets V.F., Kozlovskiy R.A., Makarov M.G., Koustov A.V., Selective catalytic hydration of ethylene and propylene oxides. XV International Conference on Chemical Reactors Chemreactor-15, Helsinki, Finland, June 5-8, 2001, c 102.

5. Shvets V.F., Kozlovskiy R.A., Kozlovskiy I.A., Makarov M.G., Suchkov Y.P., Koustov A.V., The Model of Catalytic Reactor of Ethylene Glycol Production. Organic Process Research & Development (2005), 9(6), 768-773.

REACTION MECHANISM OF TAME SYNTHESIS FROM DIFFUSE-REFLECTANCE FTIR ANALYSIS

Nezahat Boz[1] and Timur Dogu[2]

[1]*Department of Chemical Engineering, Kocaeli University, 41040, Kocaeli, Turkey*

[2]*Department of Chemical Engineering, Middle East Technical University,*

06531, Ankara, Turkey

E-mail: nezahatboz@kou.edu.tr, Tel: +90-262-3351148, Fax: +90-262-3355241

Inroduction

Oxygenated additives, such as MTBE (methyl tert-butyl ether), ETBE (Ethyl tert-butyl ether), TAEE (tert-amyl-ethyl-ether), and TAME (tert-amyl-methyl-ether), are found to be good substitutes for the aromatics, both in accomplishing the desired octane levels and in reducing the hydrocarbon and carbon monoxide emissions. Due to their high octane numbers and low volatilities, tert-amyl-ethyl-ether (TAEE) and tert-amyl-metyhl-ether (TAME) are considered as attractive alternatives to MTBE as gasoline blending oxygenates. The recent problems related to MTBE detection in groundwater, even at very low concentrations in the drinking water, interest in heavier ethers (e.g. TAME and TAEE) has grown steadily. Our earlier adsorption and diffuse reflectance FTIR spectrum (DRIFTS) results obtained for MTBE and ETBE synthesis supported a Langmuir-Hinshelwood type reaction mechanism [1]. Significance of diffusional resistances on the production rate of these ethers using Amberlyst-15 was also reported in our earlier work [2-4]. DRIFTS results obtained with methanol, 2-methyl 1-butene (2M1B) and tert-amyl-methyl-ether (TAME) in adsorption and reaction experiments, supported a Langmuir-Hinshelwood type reaction mechanism involving adsorbed 2M1B molecules, which form a bridged structure between the adsorbed alcohols and the $-SO_3H$ sites of Amberlyst-15. The reaction rate model, which was proposed basing on the DRIFTS results, was shown to give good agreement with the published initial rate data for TAEE synthesis [5].

In the present presentation, DRIFTS results obtained for isoamylenes, isoamylenes-methanol mixtures and the reaction rate model, which was proposed basing on the DRIFTS results in our recent publication [5], for the published initial rate data for TAME synthesis will be presented.

Experimental

DRIFTS experiments were carried out batchwise by injecting a pulse of tracer into the reaction chamber of DRIFTS cell of FTIR instrument (MIDAC) which was filled with nitrogen gas.

Results and Discussions

DRIFT spectra of 2M1B and an equimolar mixture of 2M1B-methanol obtained at 353 K are shown once again here (Figure 1). The IR absorbtion band observed between 930 cm^{-1} and 1170 cm^{-1} with the 2M1B-methanol mixture (reaction experiments) is due to the contributions of CO stretching of methanol (which was expected at 1030 cm^{-1}) and C-O-C IR absorbtion band of reaction product TAME (at around 1085 cm^{-1}).
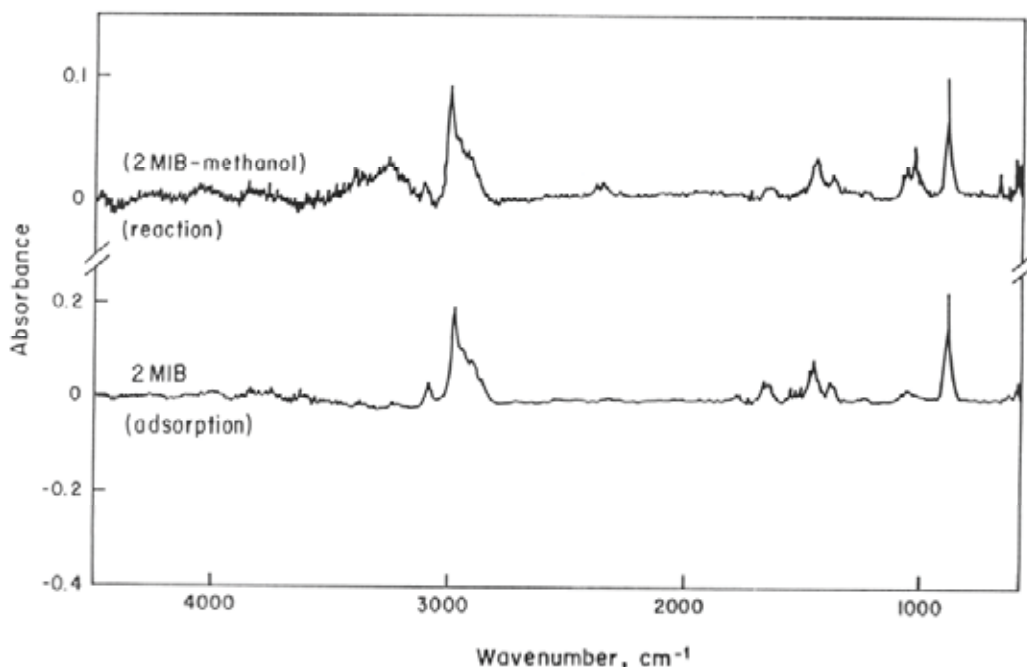
Figure 1. DRIFTS results of 2M1B, methanol and equimolar 2M1B-methanol mixture obtained at 353 K on Amberlyst-15.

Basing on these observations a reaction mechanism was proposed, which involved adsorbed isoamylenes forming bridges structures between adsorbed alcohols and –SO$_3$H sites of the catalyst. The rate expression derived basing on the proposed reaction mechanism was reported in our previous publications [5].

$$r = k\left(a_A a_B - \frac{a_E}{K}\right)\left[\frac{\left[(1 + K_A a_A)^2 + k''\left(a_A a_B + \frac{K_E}{K_A K_B}a_E\right)\right]^{1/2} - (1 + K_A a_A)}{(K_A K_B a_A a_B + K_E a_E)}\right]^2 \quad \text{(Eq.1)}$$

Considering the non-idealities of the alcohol–isoamylene–tert-ether mixtures, activities are used in Eq.1.

For the synthesis of TAME, initial rate data were reported in our previous publications [2-4] and also in other published work was used. In the analysis of the initial rate data, the terms containing activity of ether (a_E) become negligible in Eq.1 and the rate expression reduces to

$$r = k'\left(\frac{a_A}{a_B}\right)\left\{\left[\left(\frac{1}{a_A} + K_A\right)^2 + k''\left(\frac{a_B}{a_A}\right)\right]^{1/2} - \left(\frac{1}{a_A} + K_A\right)\right\}^2 \qquad \text{(initial rate)} \quad \text{Eq.2}$$

Here, the combined rate constants k' and k'' are

$$k' = (kS_o)/(16K_A(K_BS_o)); \qquad k'' = 8(K_BS_o)K_A,$$

where S_o is the total number of sites per unit mass of catalyst (mol/g).

The initial rate data obtained in our studies and also published in the literature at different temperatures were analyzed using Eq.2 and the rate parameters (k', k'') were determined using a Quasi-Newton regression procedure. The adsorption equilibrium constants of methanol (K_A) obtained from independent adsorption experiments were reported in our earlier publication [1]. The agreement of the proposed rate expression with the data published in the literature was found to be quite good.

Typical experimental results and model predictions of the initial rate of TAME formation from 2M1B and 2M2B at 353 K are illustrated in Figures 2 and 3. As it is seen in these figures the rate values pass through a sharp maximum. The predicted rate values are plotted as a function of activity of methanol (a_A) (activity of i-amylene (a_B) being the parameter). In the presence of alcohols, most of the surface is expected to be covered by alcohol molecules. As a result of this, number of available sites involved in the adsorption of i-olefins is drastically decreased with an increase in alcohol concentration. At sufficiently high alcohol activities, reaction rate becomes almost zero order with respect to alcohol activity. However, reaction order with respect to i-olefins is close to one. These observations are also in good agreement with our earlier study of TAEE synthesis [5].
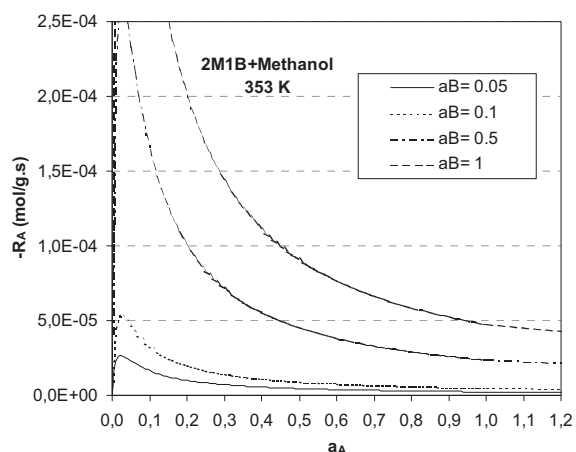
Figure 2. Dependence of initial rate of TAME formation on activities of methanol (a_A) and isoamylenes (2M1B) (a_B) at 353 K.
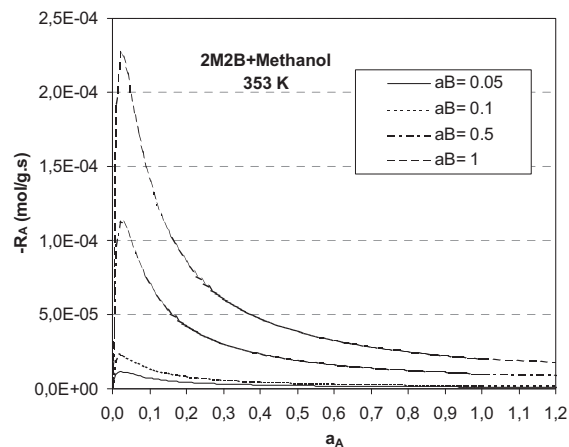
Figure 3. Dependence of initial rate of TAME formation on activities of methanol (a_A) and isoamylenes (2M2B) (a_B) at 353 K.

Acknowledgements

References

1. Dogu, T., Boz, N., Aydin, E., Oktar, N., Murtezaoglu, K., Dogu, G., 2001, "DRIFT Studies for the Reaction and Adsorption of Alcohols and Isobutylene on Acidic Resin Catalysts and the Mechanism of ETBE and MTBE Synthesis", Ind. Eng. Chem. Res., 40, 5044-5051.
2. Dogu, T., Boz, N., Aydin, E., Murtezaoglu, K., Dogu, G., 2003, "Diffusion Studies for Ethanol, Methanol and Isoamylene in a Macroreticular Resin Catalyst by Batch adsorption Moment Analysis ", Int. J. Chem. Reac. Eng., 1, Article A6. (Available online at http://www.bepress.com/ijcre/vol1/A6).
3. Oktar, N., Murtezaoglu, K.,Dogu, T., Dogu, G., 1999a, "Dynamic Analysis of Adsorption Equilibrium and Rate Parameters of Reactants and Products in MTBE, ETBE, and TAME Production", Can. J. Chem. Eng., Vol. 77, 406-412.
4. Oktar N., Murtezaoglu K., Dogu G., Gonderten I., Dogu T., 1999b, "Etherification rates of 2M2B and 2M1B with ethanol for environmentally clean gasoline production", J. Chem. Technol. Biotechnol., 74, 155.
5. Boz, N., Dogu, T., Murtezaoglu, K., Dogu, G., 2005, "Mechanism of TAME and TAEE Synthesis From Diffuse Reflectance FTIR Analysis", Cataly. Today., 100, 419-424.

SYNGAS FORMATION FROM GASOLINE IN ADIABATIC REACTOR: THERMODYNAMIC APROACH AND EXPERIMENTAL OBSERVATIONS

L. Bobrova, I. Zolotarsky, V. Sobyanin, V. Parmon

Boreskov Institute of Catalysis SB RAS

5, Pr. Ak. Lavrentieva, Novosibirsk, 630090, Russia, lbobrova@catalysis.nsk.su

Hydrogen is considered as an important energy carrier for sustained power consumption with reduced impact on the environment. To avoid a hydrogen-supply infrastructure, reforming conventional fuels (natural gas, gasoline, diesel, and jet) to the hydrogen-rich gas in a small scale, near the point of usage may be a good solution [1]. The objective of the present work is centered on the hydrogen-rich gas production from reformulated gasoline. The process performance was studied theoretically by means of calculation of thermodynamic equilibria, as well as experimentally by carrying out of the gasoline partial oxidation reaction with formation of H_2 and CO as main products (syngas) in a nearly adiabatic reactor with the monolith catalyst under short residence times, in the order of milliseconds.

Thermodynamic approach is used to enable describing the process in terms of its input qualities. A correlation between the product composition, temperature, overall energy conversion efficiency, maximum hydrogen yield, adiabatic temperature rise available for the different operating conditions such as the oxygen-to-carbon ratio, the steam-to-carbon ratio and input temperature are established on the base of thermodynamic consideration. For this purpose gasoline containing 191 types of hydrocarbons is represented as a surrogate mixture of 29 organic compounds with well defined properties that can be calculated and compared with the existing thermodynamic database. The model mixture is being formed as a set of the equilibrium distribution of the close-cut fractions C3-C10 (see Table 1). Comparable characteristics of the fuels, base gasoline and their surrogate model used in thermodynamic calculations are summarized in Table 2. The main criteria of the conformity, as to sum of C and H atoms, fractional distillation diagrams, and low heating values, are observed to have very close values for the both fuels. A generic formula for the averaged composition corresponds to $C_{7.2}H_{13.36}$.

Thermodynamic calculations of the gasoline reforming process have been performed with a HYSYS software package (HyproTech. HYSYS.Process.v2.2 AEA.Technology).

OP-2-12

Table 1. The model composition of gasoline.

N	Component	C	H	Mass fraction, w/w %
1	Isobutane	4	10	0.434
2	n-Butane	4	10	0.966
3	Isopentane	5	12	1.540
4	n-pentane	5	12	1.260
5	2.2Dimethylbutane	6	14	0.322
6	2.3Dimethylbutane	6	14	0.322
7	2Methylpentane	6	14	1.127
8	3Methylpentane	6	14	4.828
9	Hexane	6	14	3.702
10	Methylcyclopentane	6	12	0.820
11	cyclogexane	6	12	1.180
12	2.2Methylpentane	7	16	6.322
13	2.3Methylpentane	7	16	4.142
14	2.3 Metylhexane	7	16	7.194
15	Heptane	7	16	4.142
16	Isooctahe	8	18	0.263
17	2,3+2,2 Dimethylhexane	8	18	1.578
18	2,3,4 Trimethylpentane	8	18	0.263
19	2,3,3 Trimethylpentane	8	18	0.263
20	2Methylheptane	8	18	22.092
21	Octane	8	18	1.841
22	Benzene	6	6	10.266
23	Toluene	7	8	14.514
24	m-Xylene	8	10	4.248
25	p- Xylene	8	10	1.770
26	o- Xylene	8	10	1.770
27	Ethylbenzene	8	10	0.708
28	p+o+m-Diethylbenzene	10	14	1.062
29	1,2,4 Trimethylbenzene -	9	12	1.062

Table 2. Characteristics of gasoline and its model mixture

Fuel characteristic	Base gasoline	Model gasoline
C/H ratio	0.539	0.539
Low heating value, MJ/kg	44.5	43.1
Data of fractional distillation, ^{o}C :		
Beginning	42	38
10 w/w %	73	71
50 w/w %	112	110
90 w/w %	165	170
End	185	182
Density, g/ml(20°C)	0.78	0.8

Some results of thermodynamic calculations of equilibrium in processing the surrogate model of gasoline with air and water are shown in Fig.1. At the fixed values of the input temperature and O_2/C ratio in the feed, there is an equilibrium limit for the relative content of hydrogen in syngas. Water addition increases the hydrogen percentage in the product stream up to the value of H_2O/C ~1. This value corresponds to the maximum reformer efficiency, because further increasing in the hydrogen yield would require an additional energy input to dry the reformate gas.
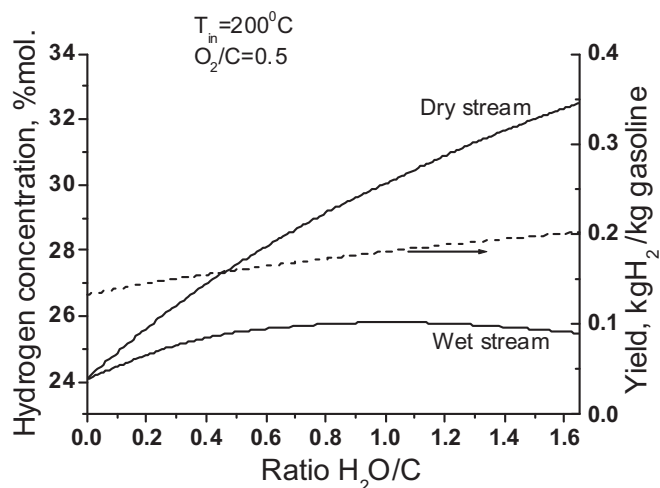
Figure 1. Thermodynamic predictions of equilibrium in adiabatic reactor for the surrogate gasoline: hydrogen concentration in the product gas (left axis) and hydrogen yield (right axis) versus H_2O/C molar ratio in the feed with the temperature of $200^{\circ}C$ (air/gasoline ratio is expressed as O_2/C molar ratio).

Experimental observations. Experimental study of the process has been carried out in the reactor specially designed to operate with a maximum of 90 % adiabaticity.
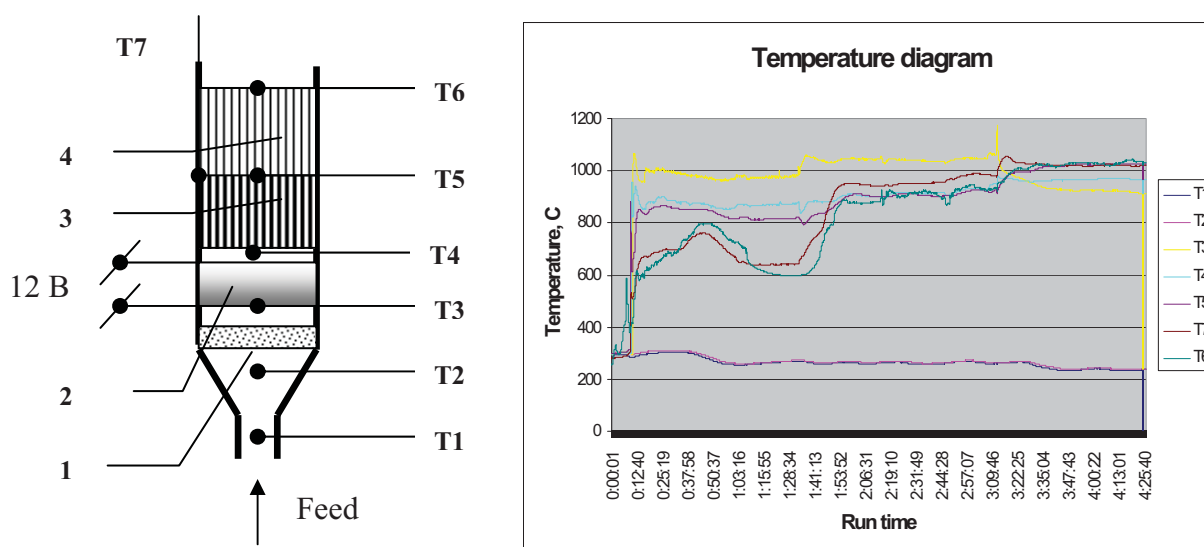
Figure 2. Schematic representation of the experimental short contact time reactor (left) and an experimental temperature diagram (right).

Catalytic monoliths with the metallic supports [2, 3] were loaded into the reactor. A pilot-plant-scale set up was comprised of a feed supply system, vaporization system, the reactor, and GC analysis system. Main electrical equipment (the balances, pumps, flow-mass controller, pressure transducers, GC analysis unit, and the temperature measurement system) was connected to the Pentium-III 700 MHz PC running under Windows XP Professional OS. Special software was created to control the setup operation regimes according to the required

experimental program. Schematic representation of the experimental short contact time reactor (left) and an experimental temperature diagram (right) are shown in Fig.2
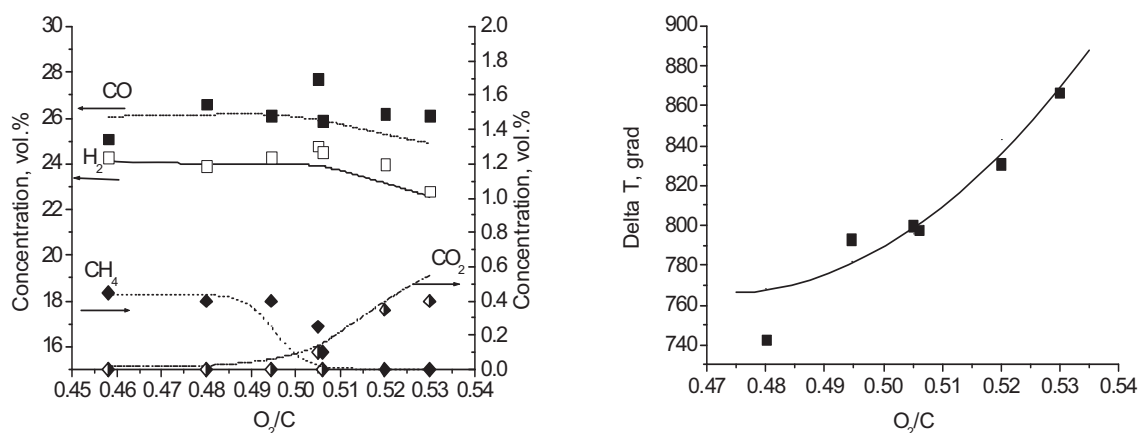
Figure 3. Experimentally measured values (symbols) and thermodynamic predictions (curves) for the process parameters versus O_2/C ratio in the feed stream.

Experimental data obtained in the study of gasoline partial oxidation over metallic monoliths in the short contact time reactor (Figure 3) are compared with thermodynamically predicted one. The operational temperature in the adiabatic reactor is defined by the adiabatic temperature rise at the given inlet conditions. It can be seen that both the product gas composition and the adiabatic temperature rise in the experiments are very close to the calculated values for the surrogate mixture proposed as a model for reformulated gasoline.

References
1. C. Song, Fuel processing for low-temperature and high-temperature fuel cells. Challenges and opportunities for sustainable development in the 21 st century. *Catal. Today,* 77 (2002) 17-49.
2. L. Bobrova, I. Zolotarskii, V. Sadykov, S. Pavlova, O. Snegurenko, S. Tikhov, V. Korotkich, T. Kuznetsova, V. Sobyanin, V. Parmon, Syngas formation by selective catalytic oxidation of liquid hydrocarbons in a short contact time adiabatic reactor. *Chem. Eng. Journal.* (2005) 171-179.
3. V. A. Sadykov et al., Selective Oxidation of Hydrocarbons into Synthesis gas at Short Contact Times: Design of Monolith Catalysts and Main Process Parameters, *Kinetics and Catalysis,* 46, (2005), 227–250.

SYNTHETIC FUEL FROM CATALYTIC DEGRADATION OF WASTE POLYMERS OVER SOLID ACID ZEOLITES

M. Elgarni, S. Debbah, <u>J. Saidan</u>, S. I. Mustafa

Petroleum Research Center, Tripoli, Libya
E-mail: jmsaidan@prclibya.org

The catalytic degradation of polyethylene (PE) into synthetic fuel over H-ZSM-5 catalysts was studied using a SS-tubular batch reactor. The effect of reaction temperature, reaction time and catalyst weight were investigated. Processing under these conditions allowed for a higher conversion into condensable liquid reaction product. Different analytical tools such as GC-FID, IR and NMR have been used to analyze the reaction products. The products were of a narrow range of carbon distribution (C5 to C15). The result showed that the average liquid fraction obtained in the reaction product was 75 by weight. It has been found that the reaction product contains mainly alkane, alkene and aromatics.

SELF-SUSTAINED OSCILLATIONS FOR LANGMUIR-HINSHELWOOD MECHANISM

[a,b] **Alexander V. Myshlyavtsev,** [a] **Marta D. Myshlyavtseva**

[a] *Omsk State Technical University, Omsk, Russia, e-mail: myshl@omgtu.ru*

[b] *Institute of Hydrocarbons Processing SB RAS, Omsk, Russia*

1. Introduction.

The simplest model for CO oxidation on platinum surface is the well known three steps Langmuir-Hinshelwood mechanism

$$A_2 + 2Z \leftrightarrow 2AZ; \qquad B + Z \leftrightarrow BZ; \qquad AZ + BZ \rightarrow AB + 2Z, \tag{1}$$

where AZ and BZ are the adsorbed species on the catalyst Z, and A_2, B and AB the gas phase substances. The conventional mean-field (MF) kinetic equations can be written as [1]

$$\begin{cases} dx/dt = 2k_1 P_{A_2}(1 - x - y)^2 - 2k_{-1}x^2 - k_3 xy \\ dy/dt = k_2 P_B(1 - x - y) - k_{-2}y - k_3 xy \end{cases}, \tag{2}$$

where x and y are the adsorbate concentrations, P_{A_2} and P_B the reactant pressures, and $k_1, k_2, k_{-1}, k_{-2}, k_3$ the rate constants for adsorption, desorption and reaction, respectively; t is time. For some parameter sets there exist the domain of a multiplicity of steady states in the plane $\left(\lg P_{A_2}, \lg P_B \right)$. This domain contains only two internal steady states. The effect of monomolecular adsorption reversibility $(k_{-1} = 0, k_{-2} \neq 0)$ on the domain of the multiplicity of the steady states is very strong. At rather large values of parameter k_{-2}/k_3 for all other parameter values there are the one internal steady state and the one boundary steady state.

The simplest MF equations (2) ignore the non-ideality of surface rate processes. We consider the MF equations incorporating the adsorbate-adsorbate lateral interactions via the coverage dependence of the rate constants. Usually, the coverage dependence of the rate constants is introduced "by hands" [2,3]. However, in the frameworks of the lattice gas model and transition state theory there are exact expressions for the rate constants [4].

The goal of the present work is the study of lateral interactions and monomolecular adsorption reversibility effect on the possibility of self-sustained oscillations appearance for Langmuir-Hinshelwood mechanism.

2. Model and method.

We will consider a lattice gas model as a model of adsorbed overlayer. Two kind of adsorbed species can occupy lattice sites of a square lattice. We take into account only

nearest-neighbor lateral interactions. The thermodynamic Hamiltonian for this lattice gas model can be written as

$$H_{eff} = \varepsilon_{AA} \sum_{\langle nn \rangle} n_{A,i} n_{A,j} + \varepsilon_{AB} \sum_{\langle nn \rangle} n_{A,i} n_{B,j} + \varepsilon_{BB} \sum_{\langle nn \rangle} n_{B,i} n_{B,j} - \mu_A \sum_i n_{A,i} - \mu_B \sum_i n_{B,i} , \quad (3)$$

where $\varepsilon_{AA}, \varepsilon_{AB}, \varepsilon_{BB}$ are the nearest-neighbor interactions energies, $n_{A,i}$ and $n_{B,i}$ the occupation numbers, and μ_A and μ_B the chemical potentials for AZ and BZ adsorbed species, respectively. $\langle nn \rangle$ means summation over all pairs of nearest lattice sites.

As it was emphasized the exact expressions for the adsorption, desorption and reaction rate constants were obtained within the frameworks of the lattice gas model and transition state theory [4]. Let us assume that activated complexes for adsorption, desorption and reaction do not interact with its environment.

Let us introduce the following notations $u = 2k_1 P_{A_2} / k_3$, $v = k_2 P_B / k_3$, $s = k_{-2} / k_3$, $\overline{\mu}_A = \mu_A / RT$, $\overline{\mu}_B = \mu_B / RT$ and $\tau = k_3 t$, where R is the universal gas constant, T absolute temperature in K. Then kinetic equations corresponding to mechanism (1) are as follows:

$$\begin{cases} dx / d\tau = p_{00} \left(u - \exp\left(\overline{\mu}_A + \overline{\mu}_B \right) \right) \\ dy / d\tau = \left(v - s \exp\left(\overline{\mu}_B \right) \right)(1 - x - y) - p_{00} \exp\left(\overline{\mu}_A + \overline{\mu}_B \right), \end{cases} \quad (4)$$

where p_{00} is the probability to find an empty couple of the nearest lattice sites.

Within the framework of our model the exact analytical expressions for p_{00}, x, y are absent [5] and hence we should use an approximate technique. It is well known, that the one of the most effective approach is the transfer matrix method [6-8]. Using the latter approach one can solve the problem of deriving expressions for the rate constants as functions of concentration. Experience shows that the transfer matrix technique yields very good results already for small M, such as $M = 4$ [8,9], where M is the number of the sites belonging to the ring. This ring is used for transfer matrix numerical algorithm.

Taking into account the features of the transfer matrix method we should to move from the (x, y) variables to the $(\overline{\mu}_A, \overline{\mu}_B)$ ones. Then the system (4) can be rewritten as

$$\begin{cases} \dfrac{d\overline{\mu}_A}{d\tau} = \left[\dfrac{\partial y}{\partial \mu_B} \left(u - \exp\left(\overline{\mu}_A + \overline{\mu}_B \right) \right) p_{00} - \dfrac{\partial x}{\partial \mu_B} \left(v(1 - x - y) - p_{00} \exp\left(\overline{\mu}_A + \overline{\mu}_B \right) \right) \right] \Big/ \Delta \\ \dfrac{d\overline{\mu}_B}{d\tau} = \left[- \dfrac{\partial y}{\partial \mu_A} \left(u - \exp\left(\overline{\mu}_A + \overline{\mu}_B \right) \right) p_{00} + \dfrac{\partial x}{\partial \mu_A} \left(v(1 - x - y) - p_{00} \exp\left(\overline{\mu}_A + \overline{\mu}_B \right) \right) \right] \Big/ \Delta, \end{cases} \quad (5)$$

where Δ is the Jacobian.

It was shown that the number of the internal steady states can be equal to arbitrary integer number. We have studied numerically twenty seven models with lateral interaction energies $\varepsilon_{AA}, \varepsilon_{AB}, \varepsilon_{BB}$ which possess the values 10; -10; 0 kJ/mol. All calculations were carried out at $T = 500$ K and $M = 4$. For these interaction energies sets the total number of the steady states was found to come up to twelve.

We have done the systematical analysis of the lateral interactions effect on the possibility of self-sustained oscillations appearance for Langmuir-Hinshelwood mechanism.

3. Results and discussion.

Self-sustained oscillations for the reaction rate were found only for the lateral interaction sets with A-B attraction. It seems the reason of this phenomenon under observation is the increase of the reaction activation energy with surface coverage increasing. This increasing results in nonmonotonous dependence of the reaction rate on the surface coverages and in self-sustained oscillations appearance. From mathematical point of view the self-sustained oscillations for the studied model are the result of Hopf's bifurcation.
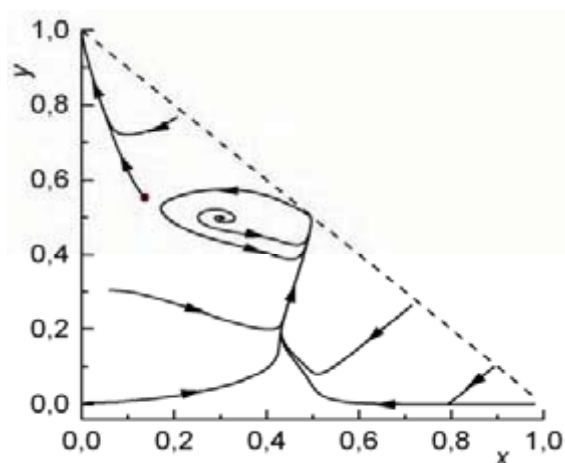
Fig. 1.

Let us consider some results obtained for the model with the lateral interaction energies $\varepsilon_{AA} = 10, \varepsilon_{AB} = -10, \varepsilon_{BB} = 0$ kJ/mol. For irreversible adsorption the multiplicity diagram has domain with eight internal steady states. We chose the point (-3,93;-4,342) in the parameter plane $(\lg u; \lg v)$. It belongs to the domain with two internal steady states. The phase portrait at given parameter values is shown in Fig. 1. The reaction rate for the phase trajectory beginning from the unstable focus located into the limit cycle is shown in Fig. 2. The reaction rate varies by a factor of 10^2 during the oscillations.
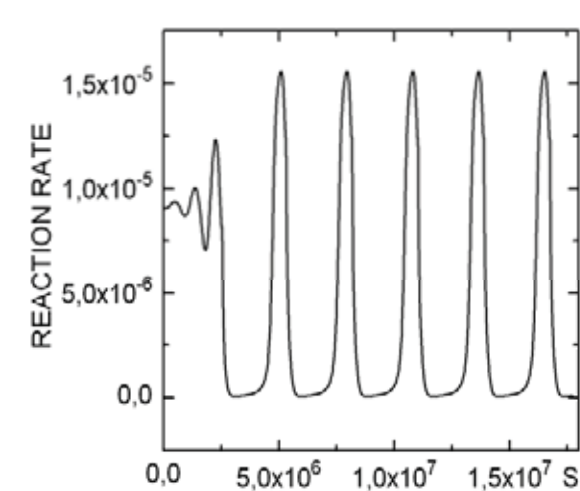
Fig. 2.

When the parameter s increases the multiplicity diagram becomes simpler and after that the multiplicity domain disappears. Self-sustained oscillations disappear as well.

Fig. 3.

We have found that for two sets of the lateral interactions energies (0;-10;-10) and (10;-10;-10) self-sustained oscillations were absent at $s = 0$, but at $s = 10^{-2}$ these ones appeared. We chose the point (-4,065;-4,3825) in the parameter plane $(\lg u; \lg v)$ for the former set. It belongs to the domain with three internal steady states. The phase portrait at given parameter values is shown in Fig. 3. There is the unstable focus into the stable limit cycle. The filled circle exhibits the second unstable steady state. The third internal steady state is a stable focus.

4. Conclusion.

In the framework of the microscopic model of a non-ideal adsorbed overlayer the kinetic behavior of the Langmuir-Hinshelwood mechanism was shown to become essentially more complex than for an ideal overlayer. The self-sustained oscillations of the reaction rate have been found for some sets of lateral interactions. From mathematical point of view the self-sustained oscillations for the studied models are the result of Hopf's bifurcation. It was also shown when the parameter s increases self-sustained oscillations disappear. However, the adsorption reversibility at moderate values of parameter s can be the reason of self-sustained oscillations.

References

1. V.I. Bykov, V.I. Elokhin, A.N. Gorban, G.S. Yablonskii: *Comprehensive chemical kinetics*, Vol. 32. Kinetic models of catalytic reactions (Ed. R.G. Compton). Elsevier, Amsterdam 1991.

2. M.M. Slinko, N.I. Jaeger: *Oscillatory Heterogeneous Catalytic Systems*, Elsevier, Amsterdam, 1994.

3. V.P. Zhdanov: *Surf. Sci. Rep.*, **45**, 231 (2002).

4. V.P. Zhdanov: *Physicochemical Processes on Solid Surfaces,* Plenum Press, New York, 1991.

5. R.J. Baxter: *Exactly Solved Models in Statistical Mechanics*, Academic Press, London, 1982.

6. A.V. Myshlyavtsev, V.P. Zhdanov: *Chem. Phys. Lett.*, **162**, 43 (1989).

7. A.V. Myshlyavtsev, M.D. Dongak: *J. Stat. Phys.*, **87**, 593 (1997)

8. V.I. Bykov, A.V. Myshlyavtsev, M.G. Slin'ko: *Doklady Chemistry*, **384**, 170 (2002)

9. A.V. Myshlyavtsev, J.L. Sales, G. Zgrablich, V.P. Zhdanov: *J. Stat. Phys.*, **58**, 1029 (1990)

Section 3.

Catalytic processes and reactors development: modeling, optimization and catalyst design

STRUCTURED REACTORS PACKED WITH CERAMIC FOAMS FOR THE PARTIAL OXIDATION OF o-XYLENE TO PHTHALIC ANHYDRIDE

A. Bareiss, <u>A. Reitzmann</u>, B. Kraushaar-Czarnetzki, B. Schimmöller*, H. Schulz*, S.E. Pratsinis*

Institut für Chemische Verfahrenstechnik, Universität Karlsruhe (TH), Karlsruhe, Germany
*Particle Technology Laboratory, Swiss Federal Institute of Technology Zürich, Switzerland
e-mail: anika.bareiss@cvt.uni-karlsruhe.de

The objective of this study is to evaluate the applicability of ceramic foams as structured catalyst supports in the partial oxidation of o-xylene to phthalic anhydride (PA). In simulations, the performance of fixed bed reactors packed with foams or filled with catalyst particles have been compared. A new technique to deposit nano-sized V_2O_5/TiO_2 catalysts on foams has been developed (Fig. 1). These foam catalysts have shown a considerably higher catalytic activity than conventionally prepared catalysts.
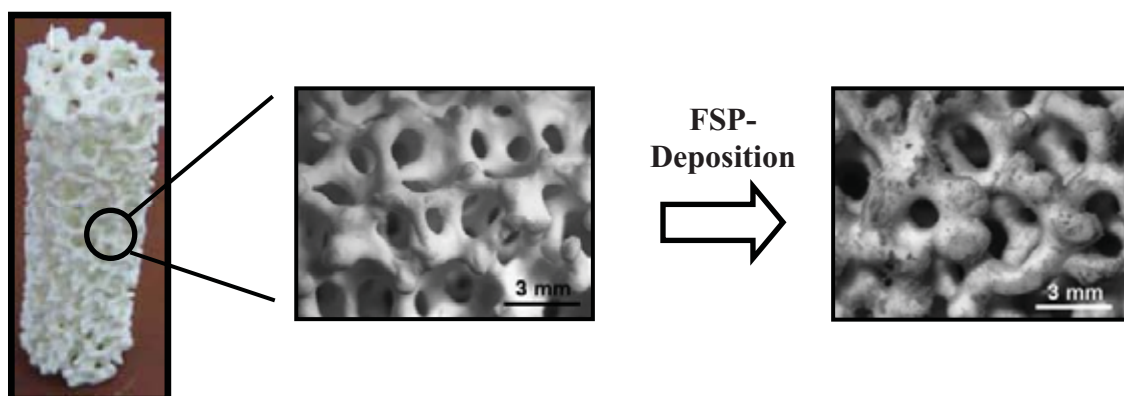
Fig. 1: Structure of foams and FSP-Deposition of foams

Background and motivation

The partial oxidation of o-xylene to PA is a fast and highly exothermic reaction. Although cooled multi-tubular reactors are commonly applied to remove the heat efficiently out of the reactor bed, pronounced radial and axial temperature gradients across the catalyst bed are observed. The risk of catalyst deactivation due to overheating and of thermal reactor runaways is given. Commercial catalysts are usually eggshell type containing an inert, shaped

body (e.g. cylinders, spheres) coated with a thin layer of promoted V_2O_5/TiO_2. Fixed beds of these catalyst bodies lead to a significant pressure drop. This aspect together with the pronounced heat evolution limit the performances of both catalyst and reactor in terms of activity, PA selectivity and space time yield. One opportunity to improve the performance of PA reactors could be the application of ceramic foams as structured carriers for the V_2O_5/TiO_2 catalysts. Literature data indicate that these open cell materials with high porosities and high surface areas improve heat and mass transfer and decrease the pressure drop compared to fixed beds containing conventional catalyst bodies.

Reactor simulations

In order to estimate the potential of ceramic foams, pseudo homogeneous reactor models were developed in the software MATLAB. The kinetic model as well as heat transfer parameters of fixed beds consisting of catalyst bodies and ceramic foams were taken from the literature and applied to the operational conditions of an industrial scale PA reactor.

Simulations and sensitivity studies showed that under certain circumstances a reduction of the temperature gradients and an increase of reactor's thermal stability can be achieved. Therefore, the application of foams principally allows changes in reactor conditions to obtain considerably higher space time yields compared to fixed beds containing catalyst particles [1] (Fig. 2 and Tab. 1).
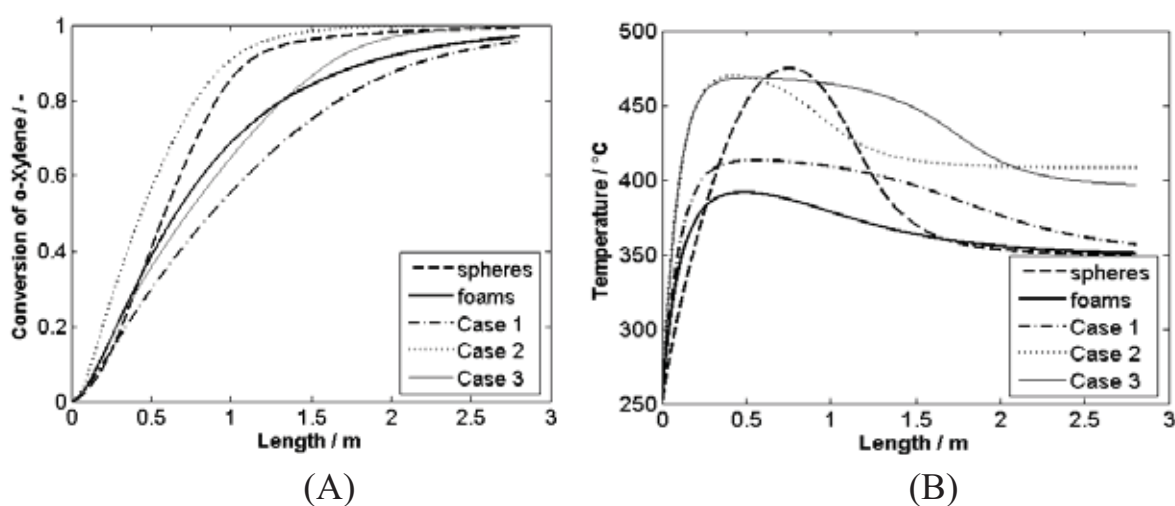
Fig. 2: Influence of reactor operation on the conversion of o-xylene (A) and temperature profile (B) for foams and spheres, conditions and results in Table 1.

Tab. 1: Quantitative results comparing spheres and foams under different operational conditions.

Case	T_{wall}/ (°C)	$T_{HotSpot}$/ (°C)	$C_{0, o-xylene}$/ (g/Nm^3)	STY/ (kg$_{PA}$/(m^3·h))	S_{PA}/ (mol/mol)	Y_{PA}/ (mol/mol)
Spheres	348	475	80	245	0.73	0.730
Foams	348	392	80	229	0.70	0.682
Case 1	348	413	175	496	0.71	0.679
Case 2	408	469	80	249	0.74	0.740
Case 3	395	468	175	542	0.75	0.740

Experimental investigations

In the first step, two types of V_2O_5/TiO_2 catalysts were synthesized, one via impregnating titania (anatase) with vanadia in the wet phase (WP), another one via flame spray pyrolysis (FSP) [2]. Isothermal kinetic measurements were performed in a plug flow reactor to show the impact of mass transfer limitations on activity and product selectivities. Different size fractions of pelletised catalyst particles were used. An significant effect of mass transfer limitation was observed for the pellets from FSP made nano-particles due to their higher intrinsic activity as compared to the wet phase made catalyst.

The next step focused on the coating of catalyst carriers. A method for the direct foam deposition of V_2O_5/TiO_2 nano-particles made by flame spray pyrolysis was developed. The influence of several operational parameters in this technique (duration, particle size, pressure drop) on the quality of the coating was investigated [3]. Foams coated with FSP made particles were twice as active as the smallest fraction of FSP pellets and even 25-30 times more active than WP pellets (Fig. 3+4).
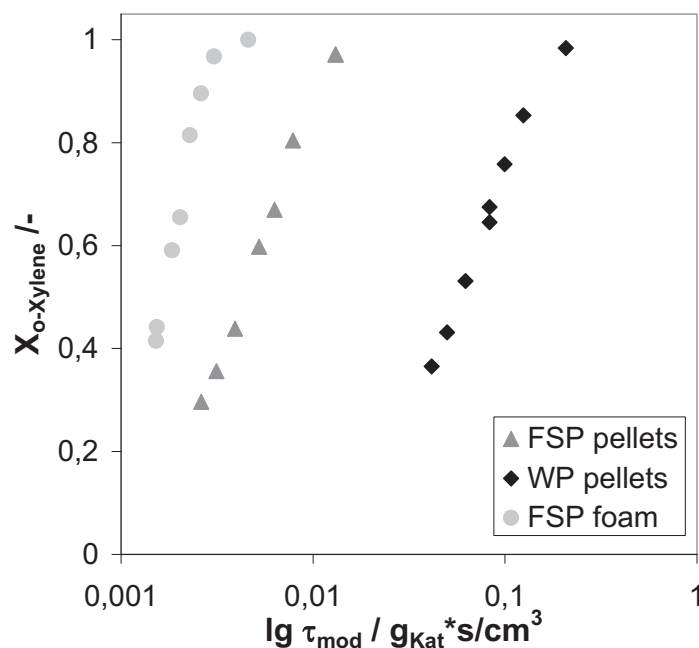
Fig. 3: Activity of FSP pellets, WP pellets and FSP foam.
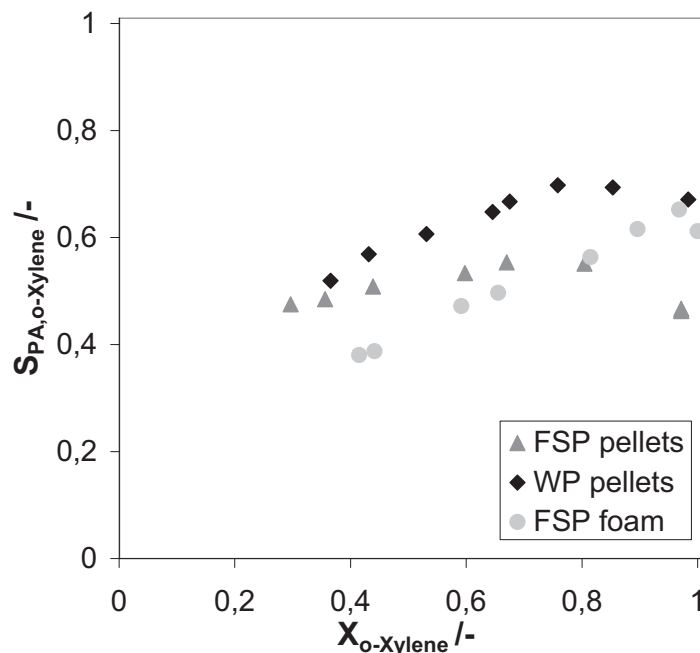
Fig. 4: Selectivity of phthalic anhydride of FSP pellets, WP pellets and FSP foam

FSP nano-particles, in general, exhibit higher surface areas than WP particles. When deposited on a foam rather than compressed to a pellet, the active layer additionally exhibits a very high porosity, enabling a maximum suppression of mass transfer restrictions. Among the materials under investigation, the PA productivity of coated foams was found to be by far the highest.

Conclusions

The simulations of a cooled PA reactor have shown that ceramic foams as catalyst packings allow for much better heat removal as compared to fixed beds of particles and enable a strong increase in PA space time yields under certain circumstances. The experimental data obtained so far at isothermal conditions cannot be compared with the simulation results. They show, however, that the novel coating technique of foams using flame made nano-particles of V_2O_5/TiO_2, produces catalysts with an extraordinary activity and high PA selectivity.

References

[1] A. Reitzmann et al., Proc. of the DGMK/SCI-Conf., Milan, 2005-2 (2005) 107.

[2] L. Maedler et al., Aerosol Science 33 (2002) 369.

[3] B. Schimmöller et al., J. Catal. (2005) submitted for publication.

DESORPTIVE COOLING OF FIXED- BED CHEMICAL REACTORS: A PRACTICAL ALTERNATIVE TO MICROREACTORS

M. Nau, M. Richrath, M. Gruenewald, D.W. Agar

Chair of Reaction Engineering, Departament of Biochemical and Chemical Engineering, University of Dortmund, Germany

Strongly exothermic heterogeneously catalysed gas phase reactions are commonly carried out in multitubular reactors. The inherent limitations of recuperative heat removal lead to hot-spot formation and can even cause reactor runaway. Apart from recuperative cooling *via* the reactor walls, convective, reactive or regenerative cooling principles may be exploited. The last, somewhat neglected, concept entails heat removal through the regenerative heating of the fixed-bed followed by a subsequent cooling phase.

Desorptive cooling represents a new hybrid reactive-regenerative process, with desorption of an inert providing the 'reactive' contribution. Initial studies on a test reactor using CO-Oxidation as a strongly exothermic test system demonstrated the principle feasibility of integrating the desorption process into the catalytic fixed-bed. The heat of reaction liberated from the catalyst pellet is locally dissipated by the desorption of an inert component from adjacent adsorbent particles (see fig. 1), thus leading to quasi-isothermal conditions within the bed. This concept permits operation in a simple adiabatic reactor without internal cooling surfaces. As a result, cycle times in a technically relevant range and much longer than those for simple regenerative processes were attained. Further work has identified
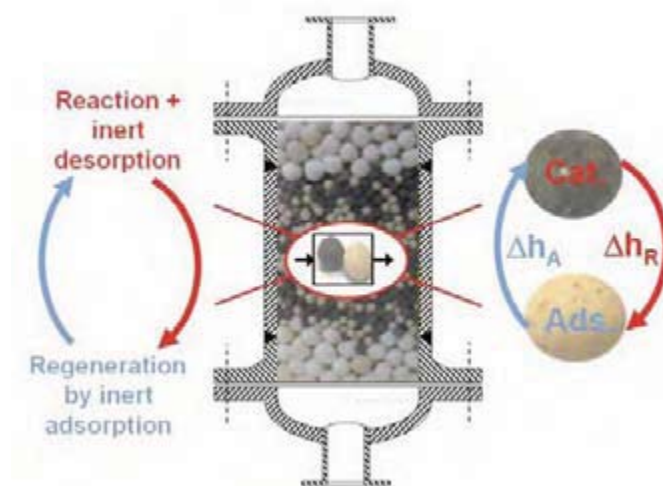
Figure 1: Concept of Desorptive Cooling Process

considerable potential for extending cycle times up to an hour or more: bed structuring and adsorptive profiling in the inlet to achieve more uniform utilisation of cooling capacity. In particular the latter proved to be an effective and feasible strategy for exploiting the concept to its full. While thermal desorption alone provides inadequate cooling capacity, ramping

adsorptive partial pressure avoids initial subcooling and leads to an isothermal temperature profile (see fig.2). Furthermore, the regeneration procedure was modelled in order to establish overall process parameters for a full cycle and the importance of the reaction kinetics for the breakthrough behaviour and the self-regulating character of the process were identified. Present work is focussing on scale-up to pilot plant dimensions and the application of desorptive cooling to the industrial relevant selective hydrogenation of acetylene to ethylene. The presentation focuses on the most recent results from a research programme supported by the German Research Foundation (DFG). Following an introduction to the desorptive cooling process with all the relevant design parameters, a flexible dynamic mathematical model, which is able to simulate various reactor configurations will be described. Two-dimensional simulations were found to be necessary to achieve reasonable agreement with bench-scale experimental results. The degrees of freedom available in the design of desorptive cooling systems will be discussed. In addition, the

Figure 2: Manipulation of Cycle Time by Desorption Driving Force

optimisation of key process parameters, such as the distribution of catalyst and adsorbent along the bed, the regulation of operating parameters, such as the inert level in the feed and the partial pressure ramping for effective cooling with maximum cycle times and acceptable conversion rates and selectivities will be addressed.

[1] M. Richrath, M. Grünewald, D. W. Agar
     Gezielte Temperaturregelung auf partikulärer Ebene durch Kopplung von Reaktion und Desorption - Teil I
     Chem.-Ing.-Tech 77 (1-2): 94-101, 2005

[2] M. Richrath, M. Grünewald, D. W. Agar
     Gezielte Temperaturregelung auf partikulärer Ebene durch Kopplung von Reaktion und Desorption - Teil II
     Chem.-Ing.-Tech 77 (3): 252-256, 2005

[3] M. Grünewald, D. W. Agar
     Intensification of regenerative heat exchange in chemical reactors using desorptive cooling
     Ind. Eng. Chem. Res. 43 (2004), S. 4773-4779

BENZENE HYDROGENATION IN THE THIOPHENE PRESENCE OVER THE SULFIDE Ni-Mo/γ-Al$_2$O$_3$ CATALYST UNDER PERIODIC OPERATION: KINETICS AND PROCESS MODELING

Reshetnikov S.I., Ivanov E.A. and Startsev A.N.

Boreskov Institute of Catalysis SB RAS, Pr. Lavrentieva, 5, 630090, Novosibirsk, Russia

E-mail: reshet@catalysis.ru

Introduction

One of an important subject of environmental catalysis is clean fuels research [1, 2]. In the past decade clean fuels research including hydrodearomatization (HDA) and hydrodesulfurization (HDS) processes. This processes are realizing on the sulfide (Ni, Mo) and (Ni, W) catalysts. The difficult problem of the HAD-HDS processes on sulfide catalysts is the mutual inhibition of hydrogenation reactions by sulfur-organic compounds and hydroginolysis reactions by aromatics. In our paper [3] we have considered the unsteady-state kinetic scheme of a simultaneous performance of the benzene hydrogenation and thiophene hydrogenolysis on the sulfide (Ni, Mo) and (Ni,W) catalysts. However, the scheme did not take into account the HDA activity decreasing when thiophene is absent in the reaction mixture for a long period of time.

The goal of this work is to develop a kinetic model for simulating the transient regime of catalyst taking into account influence of thiophene in feed gas and process modeling under periodic of reactor operation.

Experimental

The benzene hydrogenation reaction was studied in an isothermal reactor with a fixed catalyst bed [4]. Hydrogen was passed through a saturator filled either with pure benzene or a mixture with benzene and thiophene molar ratio 9:1. After being loaded into the reactor, the catalyst was treated with a benzene + thiophene mixture until the benzene conversion becomes permanent. Then the hydrogen+benzene+thiophene flow was changed by a flow of hydrogen+benzene or hydrogen+benzene+thiophene where molar ratio of benzene/thiophene was varied from 20:1 up to 140:1. Conversion of benzene into cyclohexane at the reactor outlet were monitored by chromatography. The experimental conditions were as follows: T = 300°C, P = 2 MPa, τ = 0.1-0.5 s. The (Ni, Mo)/Al$_2$O$_3$ catalyst contained 2.7% of Ni and 13.9% of Mo.

OP-3-3

Kinetic model and results discussion

The proposed kinetic model is based on the following standpoints, which were revealed on studying the benzene hydrogenation reaction on the sulfide catalysts under unsteady state conditions [5-7]:

1. The active sites of the both reactions of benzene hydrogenation and thiophene hydrogenolysis are the nickel atoms, entering the composition of the sulfide bimetallic species, which is an active component of the sulfide hydrotreating catalysts.

2. The every Ni atom is an active site for adsorption and activation of both thiophene and benzene molecules and participates in catalysis.

3. The active sites are covered with the adsorbed molecule of either reagents or reaction products at the catalysis conditions.

4. The adsorption heat of molecules on the active site decreases in a row: thiophene > hydrogen sulfide > benzene > hydrogen > cyclohexane.

5. The both reaction of benzene hydrogenation and thiophene hydrogenolysis occur via the concerted mechanism and involves the interaction of bezene (thiophene) molecule with three (or four) molecules of hydrogen without the possible intermediates being desorbed into the gas phase.

6. When hydrogen sulfide is absent in the both gas phase and adsorbed state, the structure-forming sulfur atoms interact with hydrogen resulted in the destruction of the active component structure and the catalyst deactivation.

In accordance with this standpoints, the kinetic of both benzene hydrogenation and thiophene hydrogenolysis on sulfide Ni-Mo/Al$_2$O$_3$ catalyst is developed, which includes 7 following steps:

1) C_6H_6 + $[Z_{H2S}] \leftrightarrow [Z_{C6H6}] + H_2S,$

2) $C_6H_6 + 3H_2 + [Z_{C6H6}] \rightarrow [Z_{C6H6}] + C_6H_{12},$

3) $nH_2 + [Z_{C6H6}] \rightarrow [Z_X] + nH_2S + C_6H_6,$

4) $nH_2 + [Z_{H2S}] \leftrightarrow [Z_X] + (n+1)H_2S.$

5) $(n+1)C_4H_4S + (3n+4)H_2 + [Z_X] \rightarrow [Z_{H2S}] + (n+1)C_4H_{10},$

6) $C_4H_4S + 4H_2 + [Z_{C6H6}] \rightarrow [Z_{H2S}] + C_4H_{10} + C_6H_6,$

7) $C_4H_4S + 4H_2 + [Z_{H2S}] \rightarrow [Z_{H2S}] + C_4H_{10} + H_2S.$

The first step involves an interaction of benzene with adsorbed hydrogen sulfide with the site $[Z_{C6H6}]$ formation, which active in benzene hydrogenation. The benzene interacts with the activated hydrogen to yield cyclohexane (step 2). In the absence of hydrogen sulfide in the

122

gas phase and on the catalyst surface, the hydrogen from the gas phase can interact with sulfur atoms from the active component structure. This process involves the desorption of hydrogen sulfide into the gas phase and destruction of the active component structure, *i.e.* deactivation of the catalyst (steps 3, 4). There *[Z$_X$]* is the active site structures depleted of *n* sulfur atoms. Since the tiophene has most high the adsorption heat of molecule, it will displace of benzene and hydrogen sulfide molecules on a catalyst surface. Then, steps (1)-(4) one can add by (5)-(7) steps.
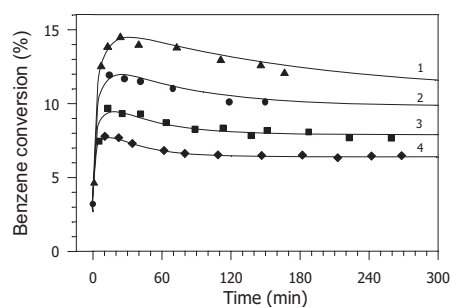
Fig. 1. Benzene conversion *versus* time at the different benzene/thiophene molar ratio in feed mixture: 1 – 140; 2 – 50; 3 – 35; 4 – 20. τ=0.18 s (points – experiments, lines – modeling).

Fig.1 shows benzene conversion *versus* time at different benzene/thiophene molar ratio in feed mixture. The catalyst in the reactor was preliminary treated with a mixture of hydrogen+benzene+thiophene until the steady-state conversion was achieved. It can see that maximum value of the benzene conversion increase with thiophene concentration decreasing. So, the rate of benzene hydrogenation is strongly inhibited by thiophene, which present in the feed mixture. For the modeling of the CSTR model was used.

Experimental and theoretical studies in heterogeneous catalysis during the last decades have given enough evidence that reactor performance under unsteady state conditions can lead to improvement in process efficiency if compared to optimal steady state operation. Using surface dynamics it is possible maintain the catalyst surface in an optimal state in order to increase the mean reaction rate and the selectivity towards a specific product formation. This can result in an increased yield of the desired product. On of the way of the catalyst unsteady state regulation is forced oscillations of reagents concentrations (periodic operations) [8,9].

The influence of various parameters like concentrations of thiophene, cycle split, period of forced oscillations and so on was investigated. It was shown that under periodic operations the mean reaction rate can exceed more the twice the steady state value.

Conclusion

The kinetic model of both HDA and HDS on the (Ni, Mo)/Al$_2$O$_3$ catalyst has been developed assuming that the catalyst surface contains only one type of active sites - nickel atoms found in the sulfide bimetallic complex - on which the reactions of hydrogenolysis of bond C-S and benzene hydrogenation occur. The number of active sites reduces due to both interaction between the network-forming sulfur atoms and hydrogen and destruction of the active site structure.

The model describes adequately the experimental data obtained at the preassure 2 MPa, temperature 573 K and variation of the contact time and ratio of benzene/thiophene in feed mixture.

The optimization of various parameters like concentrations of thiophene, cycle split, period of forced oscillations and so on was performed. It was shown that under periodic operations the mean reaction rate can exceed more the twice the steady state value.

References

1.   B.H. Cooper, B.B.L. Donnis: *Appl. Catal. A: General*, **137**, 203 (1996).

2.   C.Song, X.Ma. *Applied Catalysis B*: **41**, 207 (2003)

3.   N. M. Ostrovskii, K. S. Gulyaev, A. N. Startsev and O. A. Reutova: *Can. Jr. Chem. Eng.*, **74**, 935 (1996).

4.   M.V. Sidyakin, A.N. Cholodovich, E.A. Ivanov, S.I. Reshetnikov, A.N. Startsev: *React. Kinet. Catal. Lett,* **77**, 287 (2002).

5.   A.N. Startsev, V.N. Rodin, G.I. Aleshina, D.G. Aksenov: *Kinet. Katal.,* **39**, 238 (1998) (in Russian).

6.   A.N. Startsev, G.I. Aleshina, D.G. Aksenov, V.N. Rodin: *Kinet. Katal.,* **39**, 391 (1998) (in Russian).

7.   A.N. Startsev, I.I. Zakharov, V.N. Rodin, G.I. Aleshina, D.G. Aksenov,: *Kinet. Katal.,* **39**, 549 (1998) (in Russian).

8.   Renken, A. *Int. Chem . Eng*., **24**, (1984). 202-213.

9.   Silveston, P.L. Periodic operation of chemical reactors - a review of the experimental literature. Sadhana 10, (1987) 217-246.

NEW CATALYTIC SYSTEM FOR CONJUGATED OXIDATION OF CARBON MONOXIDE, SOLVENT, AND HYDROCARBOXYLATION OF CYCLOHEXENE

Lev G. Bruk, Elena A. Timashova, Sergey N. Gorodsky,

Irina V. Oshanina, Oleg N. Temkin

M.V. Lomonosov State Academy of Fine Chemical Technology, Pr. Vernadskogo 86,

119571 Moscow, Russia, Fax: (495)434-87-11; E-mail: lbruk@rol.ru

Introduction

Conjugated reactions are subject of theoretical and practical interest for creation of the new catalytic systems [1-3]. The oxidation of carbon monoxide by molecular oxygen is one of the simple available model reactions suitable for studying of fundamental regularities of the conjugated processes [2-4].

This report deals with the mechanistic study results of the conjugated reactions of carbon monoxide, water, and organic solvent oxidation, and cyclohexene hydrocarboxylation to cyclohexane carboxylic acid in catalytic systems: $PdBr_2$-1,4-dioxane-H_2O, $PdBr_2$–tetrahydrofuran-H_2O, PdI_2–LiI-1,4-dioxane-H_2O under very mild conditions (1 atm, 30°)(1-6).

$$CO + H_2O + O_2 \rightarrow CO_2 + H_2O_2 \qquad (1)$$

$$2CO + H_2O_2 \rightarrow CO_2 + HCOOH \qquad (2)$$

$$CO + 1,4\text{-dioxane} + O_2 \rightarrow CO_2 + 1,4\text{-dioxene} + H_2O \qquad (3)$$

$$CO + 1,4\text{-dioxane} + O_2 \rightarrow CO_2 + 1,4\text{-dioxan-2-ol} \qquad (4)$$

$$CO + \text{tetrahydrofuran} + 1,5\ O_2 \rightarrow CO_2 + \gamma\text{-lactone of butyric acid} + H_2O \quad (5)$$

$$CO + \text{tetrahydrofuran} + O_2 \rightarrow CO_2 + 1,4\text{-dioxane} \qquad (6)$$
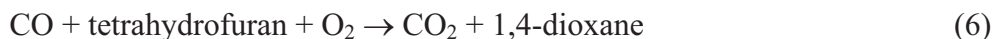
The effects of the nature of solvent, of anion, as well as the effects of inhibitors, and kinetics were studied. The hypothetical mechanisms of conjugated reactions in the above-mentioned systems were selected (discriminated). The best mechanism includes formation and transformations of hydride palladium complex (scheme 1). This hydride palladium complex is responsible for conjugation of the reactions of carbon monoxide, water, and

solvent oxidation. Experimental kinetic equation (1) does not contradict to proposed mechanism (scheme 1).

$$PdX_2 + H_2O \rightleftharpoons XPdOH + HX$$

$$XPdOH + CO \rightleftharpoons XPdCOOH$$

$$XPdCOOH \longrightarrow XPdH + CO_2 \qquad\qquad \text{scheme 1}$$

$$XPdH + O_2 \longrightarrow XPdOOH$$

$$XPdOOH + HX \longrightarrow PdX_2 + H_2O_2$$
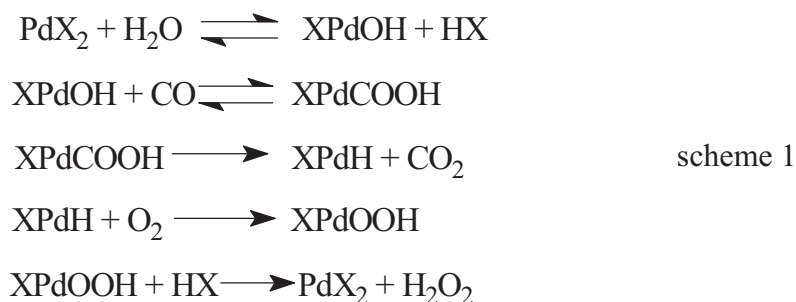
$$r_{CO2} = k_1[Pd]_\Sigma[H_2O] \, P_{CO}/([H^+](1 + k_2 \, P_{CO})) \qquad\qquad (1)$$

The correctness of this hypothesis was tested by experiments with addition of cyclohexene in the system $PdBr_2$ – tetrahydrofuran – H_2O. The synthesis of cyclohexane carboxylic acid is carried out in this system under mild conditions (30°, atmospheric pressure of CO and O_2 mixture) with rate up to 0.3 mol/l·h (fig 1). It is well known, that hydride complexes of palladium are truthful catalysts of alkene carbonylation reactions in the solutions of palladium complexes, for example [5].
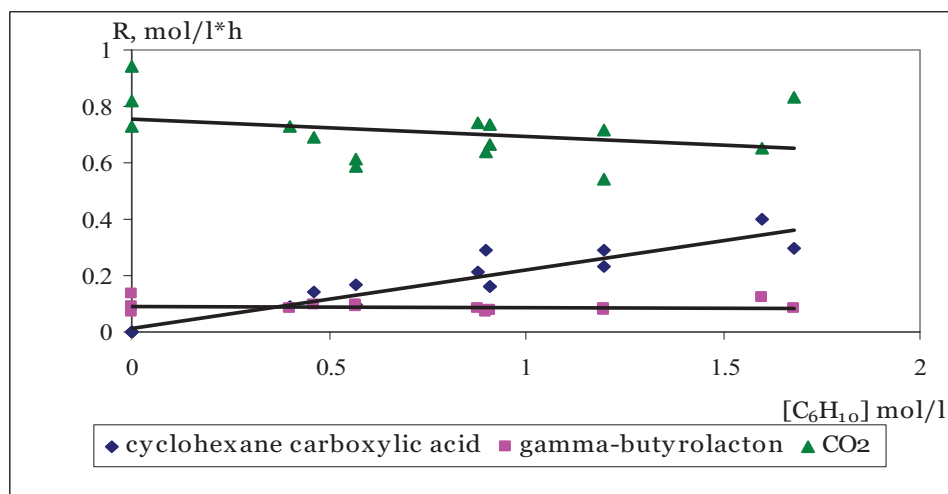
The overall mechanistic scheme of kinetic conjugation of the reactions under consideration includes three catalytic cycles (scheme 2).

scheme 2
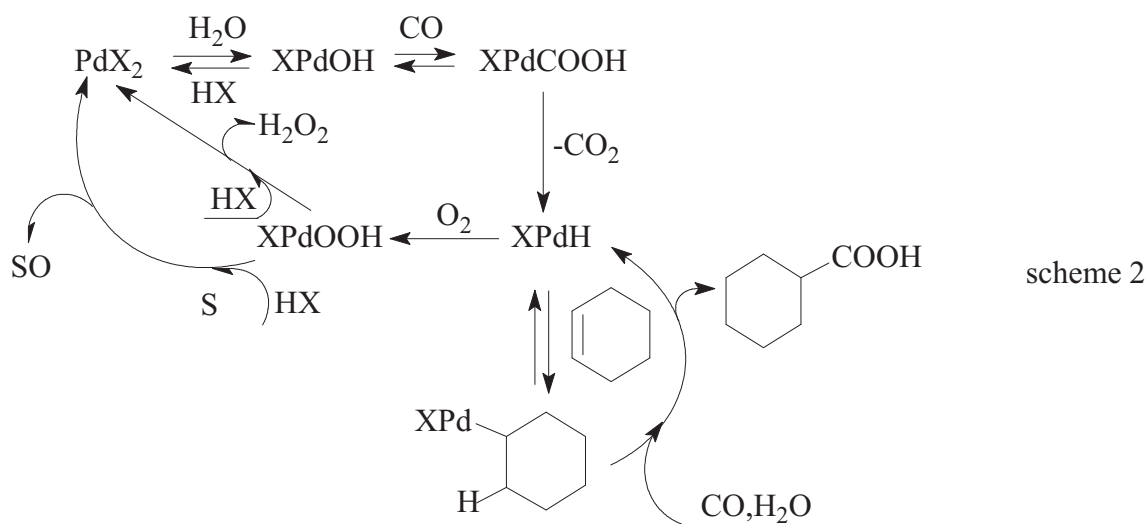
S-solvent

SO-product of solvent oxidation.

A number of alkenes were tested as substrates of hydrocarboxylation in these systems: oktene-1, hexene-1, styrene, 4-vinyl-cyclohexene, norbornadiene, norbornene. In the case of majority alkenes the products of hydrocarboxylation were identified.

Conclusion

It is possible to design catalytic systems for reactions with thermodynamic or kinetic limitations using information about probable mechanism of these reactions. It is necessary to find other reaction without thermodynamic or kinetic limitations (basic reaction), which would be capable to produce key intermediate for desirable reaction. If reagents of desirable reaction to introduce in the catalytic system of basic reaction under suitable conditions it would be possible to obtain desirable product under mild conditions. We term this approach "principle of kinetic conjugation of reactions".

Acknowledge

1. Nagiev N.A. Chemical conjugation. Moscow: "Nauka", 1989, p.35.(In Russian)
2. Zudin V.N., Likholobov V.A., Ermakov Y.I. Kinet. i Kataliz 1979, **20**, 1559.
3. Bianchi D., Bortolo R., D'Aloisio R., Rici M. J. Mol. Catal. 1999, **150**, 87.
4. Bruk L.G., Abdulaeva A.S., Vyrodov A.V., Temkin O.N. In: Abstracts 14-th Int. Symp. Homog. Catal. Munich, 2004, P0124.
5. Noskov Y. G., Simonov A.I., Petrov E.S. Kinet. i Kataliz 2000, **41**, 564.

CATALYTIC ACTIVITY OF HETEROPOLYTUNGSTIC ACID ENCAPSULATED INTO MESOPOROUS MATERIAL STRUCTURE

G. Gündüz[1], R. Dimitrova[2], S. Yılmaz[3]

[1]Department of Chemical Engineering, Ege University, 35100 Bornova, Izmir, Turkey

Fax: 00-90-232-3887776, e-mail: gonul.gunduz@ege.edu.tr

[2]Institute of Organic Chemistry, Bulgarian Academy of Sciences, 1113 Sofia, Bulgaria

Fax: 00-359-2-8700225, e-mail: zeolab@orgchm.bas.bg

[3]Department of Chemical Engineering, Izmir Institute of Technology, Izmir, Turkey

Fax: 00-90-232-750 6645, e-mail: selahattinyilmaz@iyte.edu.tr

1. Introduction

Tightening environmental legislation on the emission of hazardous pollutants is driving the industries to consider alternative processes such as heterogeneously catalyzed processes. Zeolites are widely used in chemicals industry in acid catalyzed processes. Unfortunately, the use of zeolites is restricted by their small pore sizes of around < 8 A^0, which makes them unsuitable for reactions involving bulky substrates. The discovery of the M41S family of mesoporous molecular sieves (MCM-41, MCM-48, MCM-50) offers pore sizes in the range of 20-100 A^0 which opens up new possibilities for liquid-phase acid catalyzed reactions of large molecules. Pure silica MCM-41 shows a one-dimensional, hexagonally arranged mesopore system (1.5-10 nm) with amorphous walls of the channels. It exhibits high thermal stability, a large surface area, a large adsorption capacity and it comprises silanol OH groups which are practically non acidic. Heteropoly acids (HPAs) are extremely strong acids. As molecules of Keggin type, the HPAs are spherical and with diameters around 1 nm. Thus, within the pore volume of MCM-41 molecular sieve, which is comparable to the HPAs size, can be effectively encaged and mobilized the Keggin type HPAs [1-4].

In this work, 12-tungstophosphoric acid (HPW), which is a Keggin type heteropoly acid, was immobilized in the pore volume of silicas MCM-41 molecular sieve and its catalytic activity was tested in the isomerization of the bulky α-pinene molecule, in methanol conversion and as a green chemistry example, in oxidation of ethyl acetate.

2. Experimental

2.1 Materials and Characterization

MCM-41 was synthesized in hydrothermal conditions by the method given in [3]. HPW was introduced into MCM-41 pores using the method described in [5] with some modification from the methanol solution containing 30 wt% of HPW. The concentration of HPW in the MCM-41 sample was estimated as 76 wt%. The SEM microphotographs of MCM-41 and HPW/MCM-41 samples were taken on Philips XL 30S Model Scanning electron microscope. XRD patterns of the samples were determined by Philips x'Pert diffractometer with CuK$_\alpha$ radiation. Nitrogen physisorption studies of the samples were performed at 77 K using micromeritics ASAP 2010 model static volumetric adsorption instrument. FTIR spectra of the samples were taken on a Brucker Spectrometer (Vector 22).

2.2 Catalytic Activity

The α-pinene isomerization was carried out at atmospheric pressure with 0.5 g of catalyst and 25 ml of α-pinene at 100 °C under a nitrogen atmosphere. Samples, taken from the reaction mixture, were analyzed with a gas chromatograph on a HP-Carbowax 20M capillary column.

Methanol conversion and ethyl acetate oxidation were performed in a fixed bed reactor (0.5 g of catalyst) at atmospheric pressure. On-line gas chromatographic analysis was made on a Porapak Q and a molecular sieve column using an absolute calibration method.

3. Results and Discussion

The introduction of HPW into MCM-41 channels reduced the pore volume and decreased the surface area of MCM-41 from 1030 m^2/g to 169 m^2/g. In the SEM images, the presence of HPW in MCM-41 structure were observed. Characteristic peaks of HPW appeared in the XRD reflections and the FTIR spectra of the HPW/MCN-41 sample, as the XRD signals of the initial MCM-41 sample almost disappeared. Similar results were reported in the literature [4, 6].

The overall conversion of α-pinene and the composition of reaction mixture after a reaction time of 3 h were presented in Table 1 for MCM-41 and HPW/MCM-41 samples. The corresponding data for HPW dried at 100 °C in vacuum for 7.5 h and for HPW calcined at 300 °C at atmospheric pressure for 2 h were given for comparison too.

As it was seen from the data in Table 1, the introduction of HPW into MCM-41 channels influenced significantly the catalyst activity in α-pinene isomerization, which was an acid catalyzed reaction. The results supported the knowledge that at high conversion levels of α-

pinene, limonene isomerized to terpinolenes and terpinenes and they were further transformed into HRTPs [2, 4].

Table 1. α-pinene conversion (x_α) and weight percentages of compounds after 3h reaction.

Catalyst	x_α	1	2	3	4	5	6	LRTP[a]	UP[b]	HRTP[c]
MCM-41	2.9	85.88	2.14	-	1.76	0.62	0.38	-	3.2	6.02
HPW/MCM-41	98.3	1.70	15.30	5.79	0.25	19.73	-	4.98	1.85	50.39
HPW(at 100 °C)	6.2	93.58	3.09	0.44	0.87	0.28	-	-	1.38	0.36
HPW(at 300 °C)	5.6	92.15	3.72	1.81	1.57	0.47	-	-	1.19	0.18

1, α-pinene; 2, camphene; 3, terpinenes; 4, limonene; 5, p-cymene; 6, terpinolenes

[a] Products with a retention time lower than α-pinene (low retention time products)

[b] Products with a retention time in the range between α-pinene and terpinolene (unidentified products)

[c] Products with a retention time higher than terpinolene (high retention time products)

The conversion of methanol at low reaction temperatures was dominated by the formation of dimethylether (DME). DME was registered at values greater than 80 % at temperatures above 450 K on HPW/MCM-41, Figure 1.
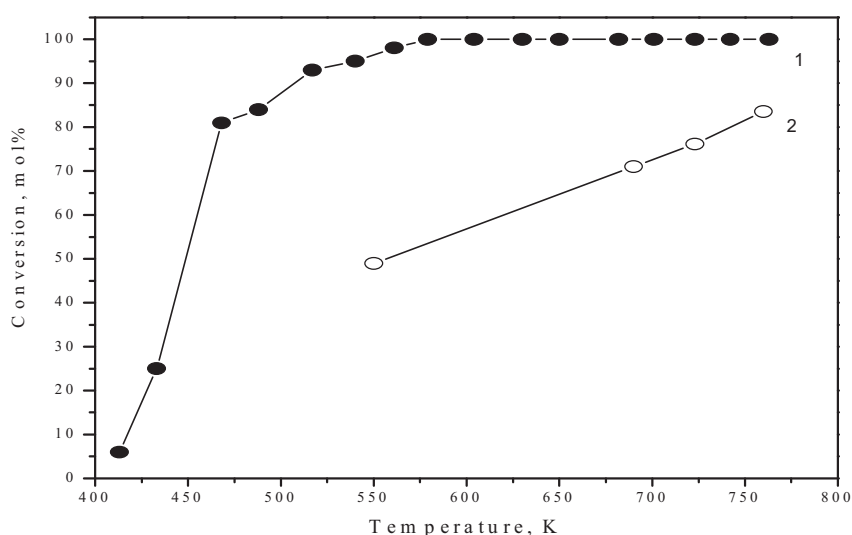
Figure 1 Methanol dehydration to dimethylether (DME) at different temperatures on HPW/MCM-line 1 and MCM-41-line 2.

The conversion of methanol to DME began at temperatures above 550 K on MCM-41 sample.The obtained data for methanol conversion and products distribution were in a good correlation with samples acidity. It was found that HPW/MCM-41 sample possessed higher

activity than MCM-41 in ethyl acetate conversion. Significant ethyl acetate conversion was found above 600 K, as ethanol, acetic acid and CO_2 were the main registered products.

The combined physicochemical and catalytic investigations clearly showed that the introduction of HPW on silica mesoporous MCM-41 sample influenced in a great extent the properties of the so obtained sample. The experimental data showed that HPW/MCM-41 was a very active catalyst in α-pinene isomerization, methanol conversion and in the oxidation of ethyl acetate.

References

[1] Wilson, K., Clark, J.H.; Solid acids and their use as environmentally friendly catalysts in organic synthesis, Pure Appl. Chem., 72 (7), (2000) 1313-1319.

[2] Dimitrova, R., Gündüz, G., Spassova, M.; A comparative study on the structural and catalytic properties of zeolites type ZSM-5, mordenite, Beta and MCM-41, J. Mol. Catal. A: Chemical 243 (2006) 17-23.

[3] Nowinska, K., Kaleta, W.; Synthesis of Bisphenol-A over heteropoly compounds encapsulated into mesoporous molecular sieves, Appl. Catal. A: Gen., 203 (2000) 91-100.

[4] Dimitrova, R., Gündüz, G., Dimitrov, L., Tsoncheva, T., Yılmaz, S., Urquieta-Gonzalez, E.A.; Acidic sites in beta zeolites in dependence of the preparation methods, J. Mol. Catal. A: Chem., 214 (2004) 265-268.

[5] Lin, H-P., Mou, C-Y.; Salt effect in post-synthesis hydrothermal treatment of MCM-41, Microporous and Mesoporous Materials, 55 (2002), 69-80.

[6] Kozhevnikov, I.V., Kloestra, K.R., Sirinema, A., Zandbergen, H.W., van Bekkum, H.; Study of catalysts comprising heteropoly acid $H_3PW_{12}O_{40}$ supported on MCM-41 molecular sieve and amorphous silica, J. Mol. Catal. A: Chemical, 114 (1996) 287-298.

HYDROGEN PURIFICATION FOR LOW TEMPERATURE FUEL CELLS BASED ON AN IRON REDOX CYCLE IN A PERIODICALLY OPERATED CATALYTIC REACTOR

V. Galvita[1], K. Sundmacher[1,2]

[1] *Max-Planck-Institute for Dynamics of Complex Technical Systems, Sandtorstraße 1, 39106 Magdeburg, Germany,*

Tel.: +49-391-6110-391, E-mail: galvita@mpi-magdeburg.mpg.de

[2] *Otto-von-Guericke University, Process Systems Engineering, Universitätsplatz 2, 39106 Magdeburg, Germany*

Fuel cell technology allows the highly efficient conversion of chemical energy into electrical energy without emissions of environmental pollutants, thereby making fuel cells one of the most promising sources for future power generation.

For the operation of the polymer electrolyte membrane fuel cell (PEMFC) the production of high-purity hydrogen is required. This hydrogen can be produced from hydrocarbon fuels or alcohols by reforming processes. These processes typically yield mixtures of hydrogen, carbon monoxide, carbon dioxide and steam. The carbon monoxide level in the gas has to be reduced below 20 ppm to avoid poisoning of the fuel cell electrodes [1, 2]. This is generally accomplished in a multi-step purification train including high and low temperature water-gas shift reactors (WGS) and a preferential oxidation reactor for CO removal (PROX) [1]. The WGS convert CO into CO_2 by the reaction with water over a suitable catalyst and yields additional hydrogen. The reaction nearly attains thermodynamic equilibrium. Two types of catalysts are commonly used in industry: a FeCr-based catalyst for high temperature WGS and a Cu-Zn catalyst for low temperature WGS. The volume of the WGS reactors steps takes a considerable part of the overall fuel processing due to the thermodynamic constraint to operate at the lowest possible temperatures to achieve high conversions. At these low temperatures most catalysts are not very active. In view of new applications such as on board hydrogen generation for PEM fuel cells, more active catalyst formulations are required for down-scaling the reformer, together with fast response behaviour, long catalyst lifetime and without use of pyrophoric materials.

As a novel alternative to this conventional technology, hydrogen purification from CO can be achieved by a novel process which is based on an iron redox cycle [4]. This process can be performed in a single reactor without any additional post-processing steps for the gas. The technology is based on a periodic reduction/re-oxidation cycle of iron oxides. During the first period (iron oxide reduction), CO reduces the iron oxide to iron, according to Eq.(1). During the second period (iron re-oxidation), steam is used as oxidizing agent for iron from which simultaneously hydrogen is being produced according to Eq.(2). This product gas also consists steam and could be supplied directly to a PEMFC. The overall reaction process is the water gas shift reaction according to Eq.(3).

$$4\ CO + Fe_3O_4 \rightarrow 4\ CO_2 + 3\ Fe \tag{1}$$

$$4\ H_2O + 3\ Fe \rightarrow 4\ H_2 + Fe_3O_4 \tag{2}$$

$$CO + H_2O \rightarrow CO_2 + H_2 \tag{3}$$
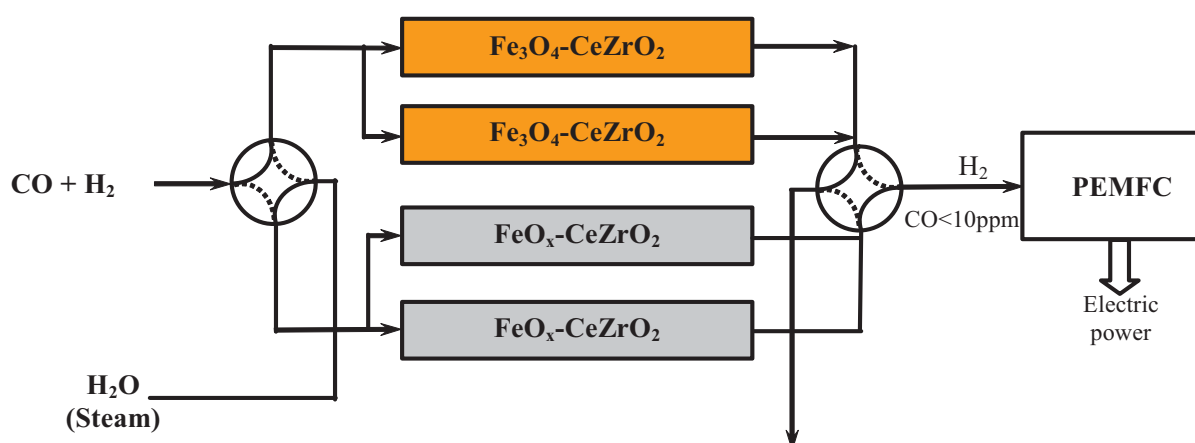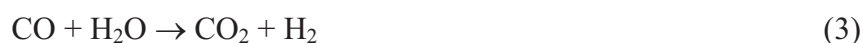
Fig. 1. Schematic diagram of novel concept of CO-free hydrogen production by a redox iron process in a periodically operated catalytic reactor for feeding a PEM fuel cell.

Fig.1 illustrates the novel concept of CO_x-free hydrogen production for polymer electrolyte fuel cells. The concept is based on a multi-tubular reactor system which is based on a bundle of simultaneously operating fixed bed reactors, some of them being in the reduction period of iron oxide (tubes filled with Fe_3O_4-$CeZrO_2$) and some of them being in the oxidation period (tubes filled with FeO_x-$CeZrO_2$). They are operated at temperatures from 700 to 800 °C. While the first tubes are fed with CO/H_2 gas which reduces the iron oxide, the latter are fed with steam for hydrogen production whereby taking up oxygen into the lattice of the solid material. When the reduction of the solid material in the reducing reactor tubes is completed, they are switched to the oxidation mode, i.e. they are fed with water vapour for

hydrogen production. Simultaneously, the other two reactor tubes are switched from steam feeding to CO/H$_2$ feeding. In this manner, a periodic redox cycle is established which requires the switching of the feed valve at discrete times.

As mentioned above, for use in PEM fuel cells the CO content has to be below 20 ppm. In our experiments, it was observed that directly after switching from reduction to oxidation the CO concentration was lower than 10 ppm. Some coke was produced on the catalyst surface by the Boudouard reaction. Subsequently, CO$_x$ was detected during the oxidation step due to the reaction of coke with water vapour. But the formation of carbon oxides could be minimized by keeping the catalyst oxygen conversion below a certain degree [3, 4]. The stability of iron oxides was observed during 1500 redox cycles (= 720 h time on stream) at a temperature of 750 °C.

The proposed process can be used as a downstream process for CO removal no matter by which process and from which primary hydrocarbon feed the hydrogen gas is being produced. I.e. methane, higher hydrocarbons, gasoline, alcohols (e.g. bioethanol) can be used for syngas production by steam, partial or autothermal reforming.

References

1. C. Song, *Catal. Today*, 77 (2002) 17.

2. J.N. Armor, *Appl. Catal. A: General*, 176 (1999) 159.

3. V. Galvita and K. Sundmacher, Hydrogen production from methane by steam reforming in a periodically operated two-layer catalytic reactor, *Appl. Catalysis A: General,* 289 (2005) 121.

4. V. Galvita, T. Schröder, B. Munder, K. Sundmacher, Production of CO$_x$-free hydrogen from methane by the iron-redox cycle for power stations on the basis of polymer electrolyte fuel cells. *Int. J. Hydrogen Energy*, submitted.

VARIOUS MODELS OF GAS-SOLID REACTION IN ESTIMATION OF SULFUR REMOVAL CATALYST BED SERVICE TIME

V.L. Hartmann

JSC "Novomoskovsk Institute of Nitrogen Industry", 301650 Novomoskovsk, Russia, Tula region, Kirova str., 11, vhart@yandex.ru

It has been shown [1], that the adjoint problem of modelling the reaction between minor impurity in a gas flow and the bed of porous granules of some absorbent (accepting irreversibility of the absorption and first order of reaction rate with respect to gaseous impurity content) can be reduced to two successive quadratures and one explicit relationship. This fact simplifies computing considerably and makes results more reliable; moreover it makes effects of some parameters more clear. For some cases even closed form solutions can be found.

Assuming shrinking core model for the reaction of gas admixture with spherical porous granule allows formulas for local reaction rate in the absorbent bed to be derived. We treat three cases of increasing complexity. First two of them are widely known [2].

Introducing below specific exposure E_{sp} allows results to be presented in a uniform manner.

Model 1

Only diffusion of impurity via fully reacted outer granule shell is rate-limiting. The absorbent in the bed is described by two parameters: adsorptive capacity P_0 per unit volume, kg/m^3, and diffusion time scale τ_D, s.

The well-known expression for local reaction rate w_b, kg/(m^3·s), is

$$w_b = \frac{c_0}{\tau_D}\, v\,\Box\,\varphi_1(\eta), \ \varphi_1(\eta) = 0.5\left(\eta^{-1/3}-1\right)^{-1}, \ \tau_D = \frac{R^2}{6(1-\varepsilon)D_S^*}, \ v = \frac{c}{c_0}, \ \eta = \frac{P}{P_0},$$

where c – gas impurity content, kg/m^3; c_0 – inlet gas impurity content, kg/m^3; ε – bed porosity; D_S^* – gas impurity effective diffusivity in the outer shell, m^2/s; R – granule radius, m; P – local adsorptive capacity per unit bed volume, kg/m^3.

Using results of [1] gives us the following pattern of bed behaviour. When frontal bed layer is still reacting ($\eta_0 > 0$),

$$E_{sp} = \tau_D T_1(\eta_0), \ \tau_{ac} = \tau_D\left[I(\eta) - I(\eta_0)\right], \ \eta = \left[1 - v(1-\eta_0)\right],$$

$$T_1(x) = 1 - 3x^{2/3} + 2x, \quad I(x) = 3\ln\left(1 + x^{1/3} + x^{2/3}\right) - 2\sqrt{3}\left(\arctan\frac{1 + 2x^{1/3}}{\sqrt{3}} - \frac{\pi}{6}\right).$$

Time of full exhausting the frontal bed layer is finite and corresponds to $E_{sp} = \tau_D$. After this moment

$$E_{sp} = \tau_{ac} + \tau_D\left[1 - I(1-v)\right],$$

where $E_{sp} = c_0 t / P_0$ – specific exposure, s; t – running time, s; η_0 – value of η in the frontal bed layer; $\tau_{ac} = V^{-1}$ – average contact time, s; V – space velocity, s^{-1}.

At first at the bed outlet $v=0$ for some time. After the moment corresponding to $E_{sp} = \tau_D + \tau_{ac}$ (time of full bed exhausting) $v=1$.

Model 2

Both diffusion and reaction on the core surface are limiting. The latter is first-order with respect to gas impurity content. One more absorbent parameter is needed there, namely kinetic scale τ_K, s.

The expression for local reaction rate is also well-known:

$$w_b = \frac{c_0}{\tau_D} v \square \varphi_2(\eta), \quad \varphi_2(\eta) = 0.5\left(\eta^{-1/3} - 1 + \frac{1}{3}\frac{\tau_K}{\tau_D}\eta^{-2/3}\right)^{-1}, \quad \tau_K = \frac{R}{(1-\varepsilon)K},$$

where K is a coefficient in an expression for the absorption rate w_s per unit surface of unreacted core, $w_s = Kc$, m/s.

As in the previous case the results of [1] allow pattern of bed behaviour to be found. When frontal bed layer is still reacting ($\eta_0 > 0$),

$$E_{sp} = \tau_D T_1(\eta_0) + \tau_K T_2(\eta_0), \quad \tau_{ac} = \tau_D\left[I(\eta) - I(\eta_0)\right] + \tau_K\left[F(\eta) - F(\eta_0)\right], \quad \eta = \left[1 - v(1-\eta_0)\right],$$

$$T_2(x) = 1 - x^{1/3}, \quad F(x) = \frac{1}{2}\ln\frac{(1-x)^{1/3}}{1 - x^{1/3}} - \frac{1}{\sqrt{3}}\left(\arctan\frac{1 + 2x^{1/3}}{\sqrt{3}} - \frac{\pi}{6}\right).$$

Time of full exhausting of the frontal bed layer is also finite and corresponds to $E_{sp} = \tau_D + \tau_K$. After this moment $E_{sp} = \tau_{ac} + \tau_D\left[1 - I(1-v)\right] + \tau_K\left[1 - F(1-v)\right]$.

v never reaches 0 except for $E_{sp}=0$. $v=1$ after the moment corresponding to $E_{sp} = \tau_D + \tau_{ac} + \tau_K$, i.e. time of full bed exhausting. Frequently used for rough estimations the so-called "stoichiometric time of exhausting" corresponds to $E_{sp} = \tau_{ac}$.

Model 3

Absorption is considered as occurring in the bulk of the unreacted core, its rate being proportional to the gaseous admixture content and the admixture being transported across the

core pores by diffusion. Such complication of model results in an extra parameter of absorbent such as characteristic depth λ of admixture penetration into the core.

In this case for local reaction rate we get [1]:

$$w_b = \frac{c_0}{\tau_D} v \square \varphi_3(\eta), \ \varphi_3(\eta) = 0.5 \left\{ \eta^{-1/3} - 1 + \frac{\tau_K}{\tau_D} \frac{\rho_0}{3\eta^{1/3}[\rho_0\eta^{1/3}coth(\rho_0\eta^{1/3})-1]} \right\}^{-1}, \ \rho_0 = \frac{R}{\lambda},$$

where $\lambda = \sqrt{D_O^*/k}$, m; D_O^* – gas impurity effective diffusivity in the unreacted core, m^2/s; k – coefficient in an expression for the absorption rate w_g inside the core, $w_g = kc$, s^{-1}.

For this model the description of bed behaviour is more complicated:

$$E_{sp} = \tau_D T_1(\eta_0) + \frac{\tau_K}{\rho_0} \left[L(\rho_0) - L(\rho_0\eta_0^{1/3}) \right], \ \tau_{ac} = \int_v^1 \frac{dx}{x\varphi_3 \left[1 - x(1-\eta_0) \right]},$$

$$L(x) = \ln \left(x \cosh x - \sinh x \right).$$

Neither time of full exhausting is finite. As well as in the previous case v never reaches 0 except for $E_{sp}=0$.

In order to evaluate the applicability of models mentioned above for estimation of sulfur removal catalyst bed service time they were used in calculations of "breakthrough curve", i.e. $v(E_{sp})$ relationship for the typical sulfur absorber of an ammonia plant using natural gas as a feedstock and charged with the commercial zinc-based absorbent.
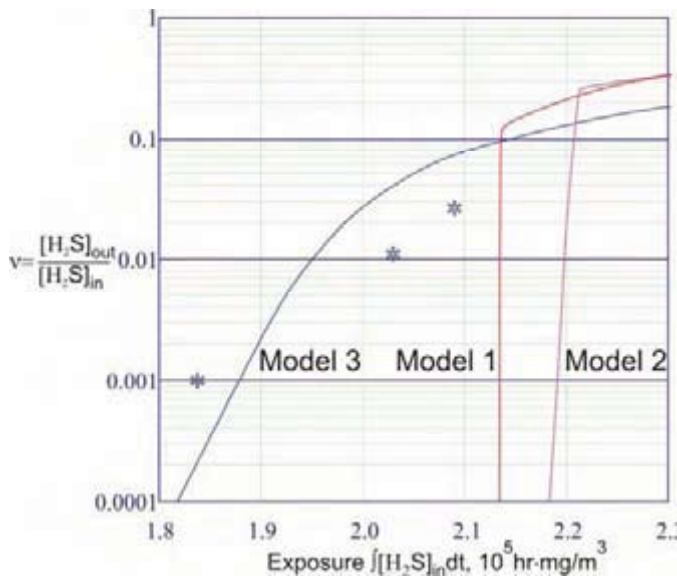
Fig.1. Sulphur removal catalyst bed output with gas analysis data of commercial absorber run.
✳ - gas analysis data.

Operating conditions in the absorber were as follows: pressure – 40 atm, temperature – 370°C, space velocity (at NTP) – 1300 hr^{-1}.

Feedstock sulfur content varied from 59 to 144 mg/m^3, which is a fairly severe condition, so the charge has run only 81 day, but for our purpose such data are most convenient.

Values of the given absorbent parameters were obtained by fitting the results of laboratory test using expressions for model 3 listed above. They were recalculated to absorber operating conditions by means of commonly used relationships for diffusivities [3]. The

coefficient k was assumed to depend on temperature and pressure like Knudsen diffusivity. Thus values used are: τ_D= 1.94 s, τ_K= 0.07 s (both at NTP), ρ_0= 62.4, P_0= 400 kg/m^3. "Breakthrough curves" thus obtained are shown in the Fig. 1 along with some gas analysis data. As x-coordinate it is more convenient to use exposure $E = E_{sp}P_0$.
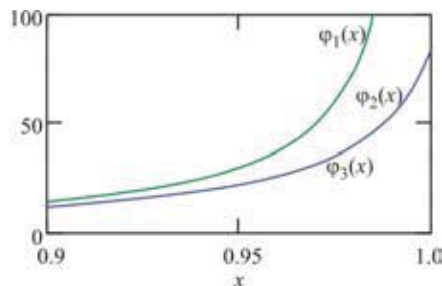
Fig.2. Local reaction rate behaviour in the vicinity of x=1.

Model 3 is obviously the most adequate here. Model 1 predicts prompt rise of v value from 0 up to 0.1. Model 2 is more realistic, but nevertheless output rise is too rapid and protective effect is too lasting.

In order to realize that the result obtained here can hardly be expected let us compare expressions for local reaction rate $\varphi_1(x)$, $\varphi_2(x)$ and $\varphi_3(x)$. Fig.2 shows their values in the vicinity of x=1, where $\varphi_1(x)$ differs appreciably and $\varphi_2(x)$ and $\varphi_3(x)$ merge. In the rest of the interval (0;1) all of them merge.

To find anyway more regions where they behave differently, the following functions can be plotted:

$$\psi_i(x) = \frac{\tau_K}{\tau_D \rho_0} \frac{\varphi_i(x)}{x}, \ i=1,2,3.$$

From Fig.3 it can be seen that even in such special form curves do not merge only for x<0.0001.

One can hardly expect such differences to be observed in the course of conventional laboratory study of the reaction kinetics. So data received in such a way

Fig.3. Local reaction rate behaviour in the vicinity of x=0.

are by no means reliable for use in estimation of commercial absorber service time. On the contrary, in the case of absorbent bed differences mentioned above can be observed definitely.

Therefore the laboratory tests of sulphur absorbents should be set up and interpreted as absorbent bed tests.
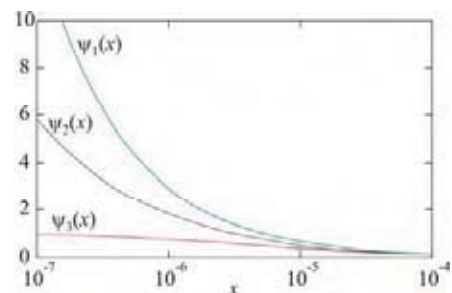
References

1. Hartmann V.L. Chem. Eng. J., v. 107, issues 1 – 3, 2005, p. 39

2. Beskov V.S., Safronov V.S. *General Chemical Engineering and Principles of Industrial Ecology*// Khimiya – Moscow, 1999.

3. Floarea O., Smigelschi O. *Calculations of Processes and Apparatuses of Chemical Engineering*// Khimiya – Moscow, 1971.

MAGNETIC FLUID MATERIALS FOR HOMOGENEOUS CATALYSIS

U. Laska[*], C.G. Frost[#], <u>P.K. Plucinski</u>[*], G.J. Price[#]

University of Bath, [*]Department of Chemical Engineering, [#]Department of Chemistry, Claverton Down, Bath, BA2 7AY, UK

Introduction

The separation of dissolved catalysts from reaction product(s) has been a major obstacle to the broader application of homogeneous catalysis in the production of bulk as well as speciality chemicals [1]. The sensitivity of many homogeneous catalysts to high temperatures often prevents the use of common techniques such as distillation. A number of separation technologies are available [2, 3]; filtration for separating supported catalysts (traditional filtration for insoluble support, ultrafiltration for soluble support), ultrafiltration or nanofiltration for unsupported catalysts. The main disadvantage of membrane separation is the necessity of passing the majority of the reacting phase through the membrane and the energy required to separate smaller molecules using moderate pressure nanofiltration. Another approach is to use biphasic systems using *e.g.* fluorous solvent, $scCO_2$, and ionic liquids. However, the necessary exclusive solubility of either the product or catalyst in one phase cannot always be realised and constraints are placed on the ligands that can be used to coordinate the catalyst. Not all reactions are amenable to the supercritical fluids approach.

The aim of this work reported here is to prepare a series of catalysts supported on nanosized magnetic particles. Their size means that they will operate in the same manner as homogeneous catalysts but they may be easily recovered by applying a magnetic field. For this proof of principle project, two reactions have been used: C-C bond coupling and hydrogenation, both using rhodium compounds as the catalyst.

Experiments

Magnetite nanoparticles (NP's) used for this work were prepared by two methods: (*i*) Nanoparticles coated with a surfactant were produced by chemical co-precipitation from an aqueous solution of ferrous and ferric salts in the presence of dispersed surfactant or in the aqueous cores of reverse micellar droplets. (*ii*) Bare magnetite nanoparticles were prepared by co-precipitation and stabilised by adsorption of an appropriate amphiphile by introduction of NO_3^- or OH^- ions onto the iron oxide crystallite surface. All the NP's have been easily separated *via* magnetic decantation using a permanent magnet.

OP-3-8

A number of methods have been used to immobilize catalytically active functional groups onto the NP's: (*i*) co-precipitation of NPs in the presence of unsaturated amphiphilic compounds followed by reaction with $[Rh(COD)Cl]_2$ or $[Rh(COD)_2]^+BF_4^-$ (COD=1,5-cyclooctadiene) or (*ii*) treatment of the bare NPs with separately prepared Rh-organic ligand (L_1–L_7, see Figure 1) complexes (ultra-sonication a mixture of Rh-complex and NP's in anhydrous methanol or THF at room temperature for 1 h under N_2).

Ligand functionalised nanoparticles were characterised by means of transmission electron microscopy (TEM – JEOL JEM-1200EX microscope) and X-ray diffraction (XRD – Phillips PW1740/00 diffractometer using CuKα radiation source).
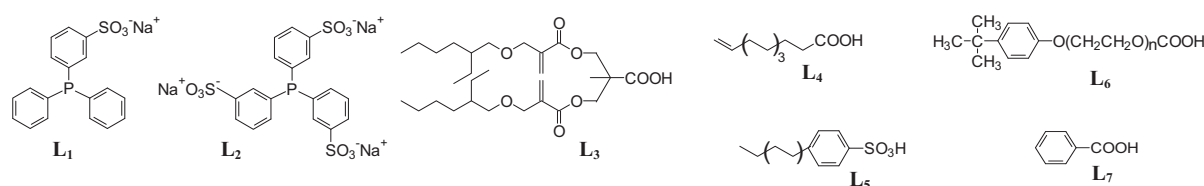
Figure 1. Organic ligands used for preparation of NP-supported catalysts.

Results and Discussion

Rh functionalised NP's were tested using the carbon-carbon coupling and hydrogenation reactions, initially using substrates shown in the Table.
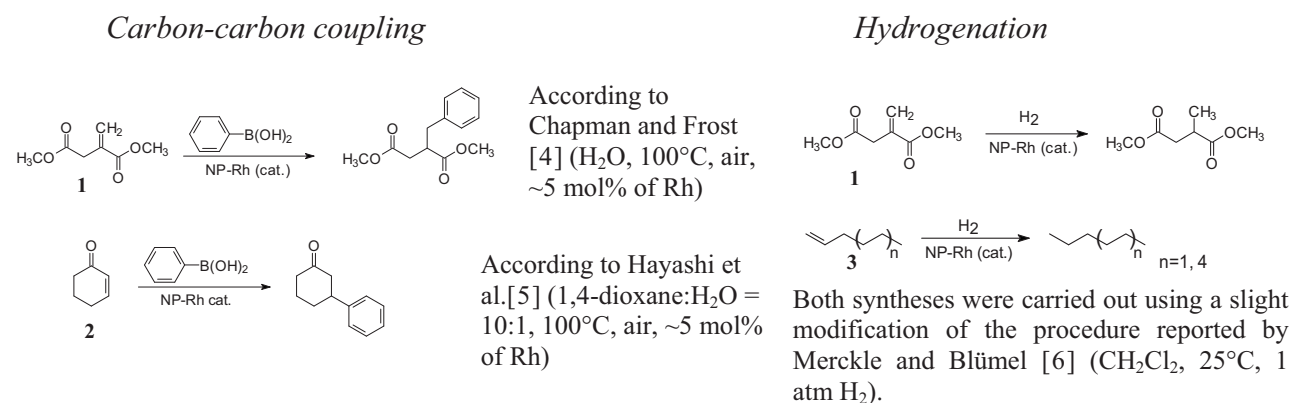
Dimethyl itaconate **1** or 2-cyclohexen-1-one **2** treatments with phenylboronic acid were chosen as model reactions for carbon-carbon coupling. The use of $[Rh(L_1)(COD)Cl]$-functionalised NP's resulted in excellent 100 and 97% conversion for **1** and **2**, respectively. The optimisation of the synthetic procedures as well as kinetic studies is presently underway and will be described in the report.

The search for an efficient hydrogenation NP-supported catalyst led us to use TPPTS (L_2) as the ligand. We have shown that **1** underwent hydrogenation in the presence of $[Rh(L_2)_3Cl]$-

modified NP's. The conversion after 4 h was < 60% [7], showing that further work to optimise the reaction conditions is necessary. However, the work establishes the principle of using Rh functionalised NP's as hydrogenation catalysts. More recent developments in this area will be included in the report.

After each reaction, the NP-supported catalyst was easily recovered by attraction with an external permanent magnet, making recovery extremely simple.
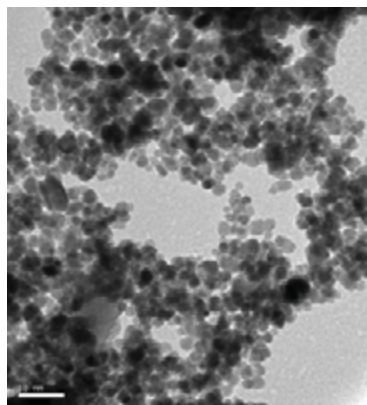
Figure 2:

TEM image for NP-

[Rh(L$_1$)(COD)Cl]

in toluene at magnification 200k.
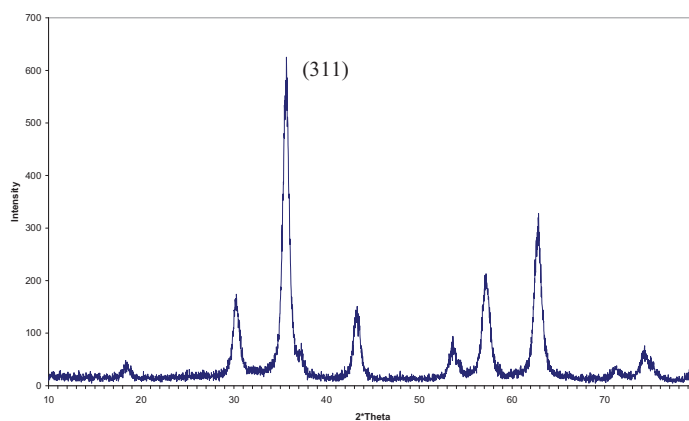
Figure 3:

XRD pattern for NP-L$_3$.

Ligand functionalised NP's have been examined by transmission electron microscopy and X-ray diffraction (Figures 2 and 3). Both methods show that we are producing NP's with sizes in the range of 7 – 17 nm depending on the system so that we have truly nanoparticulate catalysts. We are currently undertaking a full characterisation of their catalytic behaviour. However, significantly, initial work has showed that catalytic activity is retained on subsequent use after the NP's have been magnetically separated from the first reaction. While the activity is somewhat reduced, this is encouraging and demonstrates that metal is bound to the NP's. Optimisation and further study is underway.

Conclusions

A series of novel rhodium based catalysts supported on magnetite nanoparticles have been designed and studied. Nanosized magnetite particles (average diameter of 7-17 nm) were prepared using co-precipitation methods and were characterized using TEM and XRD. The nanoparticle cores comprise superparamagnetic iron oxide and thus can be simply and

efficiently separated from the reaction mixture. Among the various ligands immobilized on the particles surface, [Rh(**L₁**)(COD)Cl] has been found to catalyze the carbon-carbon coupling reactions with 100% conversion. [Rh(TPPTS)₃Cl] (**L₂**) appears to be most effective so far for hydrogenations, although efforts are currently being made to improve the reaction yields. Current work is aimed at fully characterising our systems as well as considering the engineering aspects of their use in realistic situations.

Acknowledgements

References

1) Cornils, B., Herrmann, W.A., *Applied Homogeneous Catalysis with Organometallic Compounds*, Willey-VCH, Weinheim, 2002.

2) Cole-Hamilton, D.J., *Science*, **2003**, *299*, 1702-1706.

3) Tzschucke, C.C., Markert, C., Bannwarth, W., Roller, S., Hebel, A., Haag, R., *Angew. Chem. Int. Ed.*, **2002**, *41*, 3964-4000.

4) Chapman, C.J., Frost, C.G., *Adv. Synth. Catal.*, **2003**, *345*, 35-355.

5) Hayashi, T., Takahashi, M., Takaya, Y., Ogasawara, M., *J. Am. Chem. Soc.*, **2002**, *124*, 5052-5058.

6) Merckle, C., Blümel, J., *Topics Catal.*, **2003**, *34*, 5-15.

7) Evaluated from the ^{1}H NMR spectra of the reaction mixtures by the ratio of the integral intensity of =CH₂ group of the initial substrate (δ 6.31 ppm) and –CH₃ group in the hydrogenated product (δ 1.21 ppm).

DEVELOPMENT OF NOVEL CATALYTIC SYSTEM FOR SELECTIVE HYDROGENATION OF "IMINE" TO SERTRALINE IN TRICKLE BED REACTOR

M.L. Kaliya, A. Erenburg, M. Herskowitz

Blechner Center for Industrial Catalysis and Process Development and Department of Chemical Engineering, Ben-Gurion University of the Negev, Beer-Sheva, Israel

mkaliya@bgumail.bgu.ac.il, Fax 972-8-6479427

Sertraline (1S-cis)-4-(3,4 dichlorophenyl)-1,2,3,4-tetrahydro-N-methyl-1 naphthalene- amine is a valuable pharmaceutically active substance. An important stage in sertraline production is the selective hydrogenation of imine to sertraline as shown in Fig. 1

Imine   Sertraline
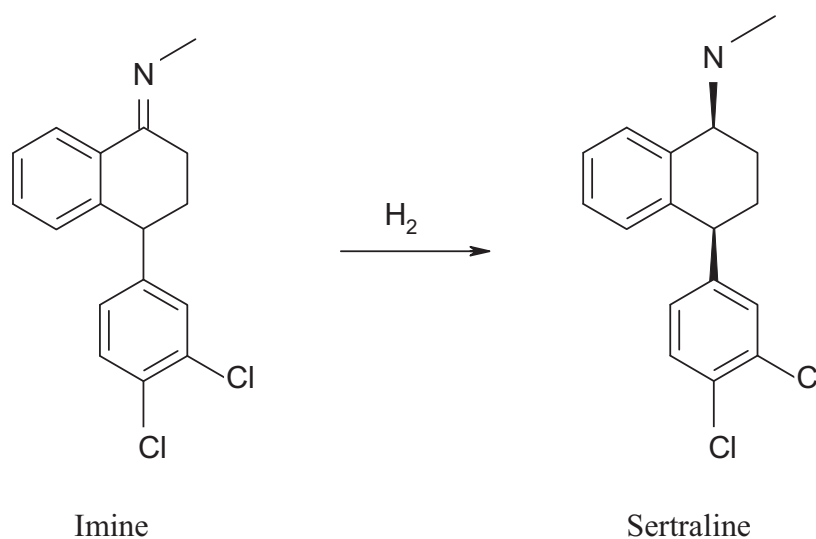
Fig. 1

The challenge in this hydrogenation process is achieving high selectivity to the cis isomer that is only active in antidepressant therapy. Furthermore, complete conversion of imine and elimination of by-products. High performance of sertraline production is achieved by combining the development of a highly selective and active catalyst along with a suitable reactor design.

OP-3-9

Patent literature includes Raney Ni and supported Pd catalysts yielding 75-78% and 0.8-1.3% of cis sertraline and dechlorinated (DCS) products respectively [1,2].

A novel catalyst containing 12wt% cobalt deposited on low surface area, 1.6 mm pellets alumina-silica was developed. Tests carried out at 120^0C and 15 atm both in the batch and trickle-bed reactor [3] yielded 90% cis sertraline at DCS (dechlorinated sertraline) products were less than 0.6%. Catalyst was prepared by deposition of cobalt nitrate the support, calcinations at 500^0C for 4 h and reduction in hydrogen at 450^0C for 5h. Tetrahydrofuran (THF) was selected as the most efficient solvent. Feed content of imine in THF was 30g/L

SEM, ESCA, XRD and TPR methods were used for characterization of the fresh and spent catalysts. It was found that metallic Co species (crystals 20-25nm in cubic form) provide selective hydrogenation. Increasing the reduction temperature to $>500^0C$ and decreasing of Co_3O_4 crystal size enhanced formation of hexagonal Co phase. This cobalt phase was less active and lowered selectivity to the cis isomer. Conversion of the cubic into hexagonal phase during imine hydrogenation and deposition of heavy organic products gradually deactivated the catalyst over 250 h on stream

Combustion of organic material on the catalyst by a air-nitrogen mixture containing 0.5-5% of O_2 at $300-350^0C$ following by catalyst reduction at 450^0C yielded complete regeneration of catalyst.

References

1. V. Kumar, G. Park, Patent WO 01/16089 A1, 1999.

2. G. Quallich U.S. Pat. No. 6,593,496, 2000

3. M. Herskowitz, M. Kaliya, Patent WO 2004/092110, 2004.

A NEW BASE APPROACH TO DEVELOPING POROUS BURNERS

V.S. Babkin*, I.G. Namyatov*, Yu.M. Maksimov**, A.I. Kirdyashkin**

* Institute of Chemical Kinetics and Combustion SB RAS, Novosibirsk, 3, Institutskaya str.,
Russia, fax: +7(383)3307350, e-mail: babkin@kinetics.nsc.ru.
** Department of Structural Macrokinetics TRC SB RAS, Tomsk, 10/3,
Akademicheskii pr., Russia,   fax: +7(3822)492838, e-mail: maks@fisman.tomsk.ru.

The term "porous burners" implies gas burners that employ a porous body to form a high-temperature chemical transformation zone in which the thermal energy of fuel is released. Usually, a porous body is produced from heat-resistant ceramics. Some burners include porous bodies in the form of a set of metallic meshes, the fillings of disperse material and perforated plates. At times, porous monoblocks are employed. A porous body can represent a set of complementary elements. There is a great variety of porous burners [1]. Those with the highest yield of a radiation component of a heat flux are called radiation burners. The porous burners are used not only as heat generators but also as chemical reactors e.g., to produce hydrogen [2], synthesis gas [3] and HCl [4].

Commonly, one-section burners are used with a layer of porous material which performs a series of various functions to provide the combustion of a combustible mixture, the stabilization and steadiness of combustion zone, the yield of effective IR-radiation, the completeness of burning-out, explosion safety, etc. over a wide range of operating parameters, i.e., the equivalence ratio, mixture flow rate, initial pressure.

A porous burner is a complex device which not only transforms chemical energy into the thermal one but satisfies also a great number of other requirements, i.e., the effective burning of a combustible mixture, process stability, power modulation over a wide range, the maximum yield of IR-radiation, etc. These requirements are, as a rule, contradictory and difficult to satisfy in the case of a one-section burner. On the other hand, the porous burner refers to a flowing system. Its functional problems are of different physicochemical origin and the various physicochemical processes run in the various zones of the burner and are separated in time. Therefore, it is reasonable to produce a multi-section, multi-zone burner each section (or zone) of which performs a certain function.

Some modifications of porous burners contain the elements of the section division of functions. These modifications are, however, of a sporadic character. In this respect, the two-section burners of the group of D.Trimis and F.Durst are most up-to-date [5].

In one-section porous burners, the conditions for flame front stabilization either over the surface of a porous body or inside this body, near the surface are realized most often. The former case is of no practical interest. Flame stabilization in a porous body is promising in many respects but displays its own disadvantages. First, front location depends on the parameters of a combustible gas. Second, minor variations of flow parameters can cause either flame blow-off or flashback.

The focus of attention in the present work is the novel methods of stabilization determined by boundary conditions. This term means conditions at the interface between two media with various physicochemical and structural properties: two inert porous media $(PM)_1/(PM)_2$; two porous media one of which is inert and the second one is active, e.g., catalytically active – $(PM)_i/(PM)_a$; two media one of which is a porous medium and the other is a structure, e.g., a set of meshes, perforated plates, (PM)/structure, etc.

A particular feature of this type of stabilization is its flexibility and great potentials because it is in agreement with the principle of porous burner structuring and the principle of a free choice of combustion regime. In this work, a flame front was stabilized using a (PM)/structure scheme with LVR in a fine-pore inert medium and HVR in a "structure" (coarse-porous medium).

The principles of gas burning are based on the steady-state regimes of gas combustion in inert porous media. At present, the following steady-state regimes are identified: low velocity regime (LVR, $u \approx 10^{-4}$ m/s), high velocity regime (HVR, $S \approx 10$ m/s), sound velocity regime (SVR, $S \approx 10^2$ m/s), low-velocity detonation (LVD, $D \approx 800\text{-}1500$ m/s), and normal detonation with heat and pulse losses (ND, $D > 1500$ m/s)[6]. These regimes have different parametric dependences of the propagation velocity of thermal wave, the nature of limits, the domains of existence, and the mechanisms of reaction transfer. The various properties of combustion waves offer a wide means of both organizing combustion process in porous burners of different applications and regulating thermal loading, the yield of a radiation component of heat transfer, and specific thermal capacity over a wide range of these characteristics.

The present work is concerned only with low and high velocity regimes realized experimentally in a two-section model setup: in a fine-porous layer (LVR) and in a coarse-porous medium (HVR) under combustion of methane-air mixtures.

When in the laminar flame the burning velocity is S_{u0}, in the LVR a corresponding combustion rate is $S_{uLVR} = (3-6)S_{u0}$. An increase in combustion rate in LVR with regard to the burning velocity of the laminar flame is determined by thermal interaction between a gas flow and a porous medium which depends on the properties of a porous medium and gas as well as on flow rate and interface heat exchange. As a result, in the reaction zone of a stabilized wave the temperatures and combustion rates are higher than those observed in the laminar flame. It is this regime that dominates in one-section burners.

In the case of HVR, the S_{uHVR}/S_{u0} ratio can amount to 30 which is due to the aerodynamic interaction between a gas flow and a porous medium which is also determined by the characteristics of a porous medium and a combustible mixture. However, the parameters that determine an increase in the combustion rate in LVR and HVR are different. The expected increase in the range of power modulation up to 1:30 can be one of the merits of section burners.

As far the unstable work of porous burners, note only one aspect, i.e., the burning-through upstream. It has been demonstrated that in addition to the common phenomenon of flashback observed at $d>d_{cr}$ there is the phenomenon of burning-through of flame-arresters and as a result, the passage of flame upstream even if $d<d_{cr}$, where d_{cr} is the critical diameter of flame quenching [7].

Potentialities of porous section burners have been studied in a series of experiments. A metallic flat burners with a cross-section of 48x48 had three sections, i.e., those of mixing, fire-extinguishing, and combustion. A flame-arrester was represented by a heat resistant monoblock of $48\times48\times20$ mm with a porosity of 0.4 and a characteristic pore size of 0.5 mm produced by the SVS method. A combustion section is composed of ceramic cylinders of 48 mm in length that were aligned in a row with a certain step. The cylinders of three diameters were employed: 3, 5, and 7 mm. A three-row porous structure was assembled in experiments which allows various combinations of structural elements, a simple change of element geometry and material, hydravlic resistance, radiation and other characteristics of a system.

Experiments indicate a stable work of the burner with the flow rate of stoichiometric methane-air mixture over the range of 0.5-5.5 l/s at a power of 1.7-18.7 kW. A corresponding range of power modulation is 1:11. The heating of ceramic elements in the combustion zone was 700-900 K. The radiation flux along the burner axis at a distance of 90 cm was 6-16 W/(cm^{2}s).

OP-3-10

Conclusions

Thus, a new concept of porous burners is that the principles of their functioning, design, solutions of the problems of combustion organization and efficiency and solutions of ecological problems should be based on the present data on combustion processes and, in particular, the processes of filtration combustion of gases. At such base approach, it appears that the widely adopted burners can be produced on the basis of a multi-section structure of a porous burner with a spatial distribution of inner functions, i.e., flame front stabilization, combustion efficiency, the yield of maximum radiation flux, and process stability.

Acknowledgement

References

1. V.P.Mikheev, Yu.P.Mednikov. Combustion of natural gas.//Leningrad,"Nedra", Leningrad Department, 1975.

2. J.P.Bingue, A.V.Saveliev, L.A.Kennedy. Optimization of hydrogen production by filtration combustion of methane by oxygen enrichment and depletion. //Int. J. of Hydrogen Energy 29 (2004) pp. 1365-1370.

3. M.K.Drayton, A.V.Saveliev, L.A.Kennedy,A.A.Fridman, Y-E Li. Syngas production using superadiabatic combustion of ultra-rich methane-air mixtures. //27-th Symp.(Int.)on Comb. Pittsburgh, 1998, pp. 1361-1367.

4. K.Wawrzinek, A.Kesting, J. Kunzel and et al. Experimental and numerical study of applicability of porous combustors for HCl synthesis. Catalysis Today, 69, 2001, pp 393-397.

5. D.Trimis, F.Durst. Combustion in a porous medium-advances and applications. //Combust. Sci. and Tech, 1996, v. 121, pp. 153-168.

6. V.S. Babkin. "Filtrational Combustion of Gases. //Present State of Affairs and Prospects". Pure and Applied Chemistry, 1993, Vol. 65, No 2, pp. 335-344

7. V.S. Babkin. The problems of porous flame – arresters.//V.E. Zarko et al. (eds.), Prevention of Hazardous Fires and Explosions, 1999, Kluver Academic Publishers, Netherlands, pp. 199-213.

ENHANCING CONSECUTIVE REACTIONS DURING THREE PHASE HYDROGENATION WITH A SEMIBATCH LIQUID PHASE

P. Mäki-Arvela, A. Denecheau, K. Alho, J. Wärnå, K. Eränen, T. Salmi, D. Yu. Murzin

Process Chemistry Centre, Åbo Akademi University, FIN-20500 Turku/Åbo, Finland, +358-2-2154479, paivi.maki-arvela@abo.fi

1. Introduction

In complex heterogeneously catalyzed liquid phase reactions the desired products can be formed in consecutive reactions. This is the case e.g. in the formation of citronellol as a second product from citronellal in citral hydrogenation [1]. There are several methods to enhance the reaction rates and to produce higher yields of the desired products, i.e. utilization of higher temperatures and pressures or application of higher amounts of catalysts. Another method to enhance the reaction rates is the use of temperature programmed experiments, which have, however, a potential drawback, since it can lead to increased amounts of side products. From the engineering point of view it might be beneficial to enhance the rates of secondary reactions giving the desired products, not by temperature increase, but by increasing the catalyst bulk density during the reaction. In this work the aim was to compare the effect of liquid phase pumping from the reactor during hydrogenation with a conventional case of constant liquid phase. Another aim was to develop a kinetic model, which could describe quantitatively the increasing catalyst bulk density.

2. Experimental

Citral hydrogenation kinetics (Figure 1) was investigated in an autoclave (V_L= 325 ml) in 2-pentanol as a solvent in the temperature and pressure range of 50 – 90°C and 5 – 21 bar, respectively. The Ni/Al$_2$O$_3$ (20.2 wt.% Ni) catalyst with a mean particle size of 13.5 μm (sieved below 100 μm) was reduced prior to the experiment in situ at 270°C for 90 min with flowing hydrogen.
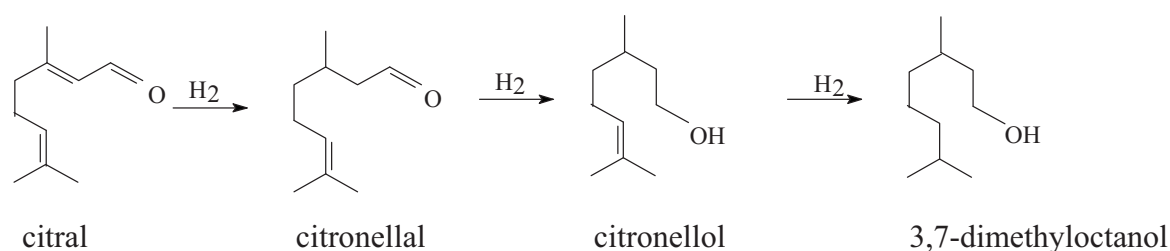
Figure 1. Scheme for citral hydrogenation.

Typically the initial citral concentration and the initial liquid phase volume were 0.1 mol/l and 325 ml, respectively. The catalyst mass was kept constant in all experiments (500 mg) and the stirring rate was 1500 rpm. In the experiments with increasing catalyst bulk density about 1 g/min liquid was continuously pumped out. Additionally in some experiments the temperature was increased during the hydrogenation by 0.8°C/min from 60°C to 90°C. The products were analyzed with a gas chromatograph equipped with a FI-detector.

3. Results and discussion

The effect of the pumping of the liquid phase from the reactor on the initial citral hydrogenation rates was the highest at 50°C, when the initial hydrogenation rate was 12.4 times higher than the rate observed in the absence of liquid phase pumping (Table 1, Figure 2). At higher temperatures (70°C and 90°C) the rate enhancement was 2.6 times higher in case of pumping.

Table 1. Comparison of the initial hydrogenation rates in citral hydrogenation under 10 bar hydrogen with and without liquid phase pumping at three different temperatures. The initial citral concentration was 0.10 mol/l and the solvent was 2-pentanol.

Working mode	Temperature (°C)	Initial hydrogenation rate (mmol/min/g Ni)	Conversion after 60 min (%)
Pumping	50	10.5	98.0
No pumping	50	0.85	67.9
Pumping	70	15.6	99.8
No pumping	70	6.11	70.6
Pumping	90	25.1	99.8
No pumping	90	9.8	99.8

The increased catalyst bulk density increased the concentrations of the desired products, citronellal and citronellol. The largest increase in citronellal concentration was observed at 70°C, when the liquid phase was pumped out from the reactor (Table 2).

The effect of liquid phase pumping together with a temperature programmed reaction was investigated in citral hydrogenation (Table 3).

a)
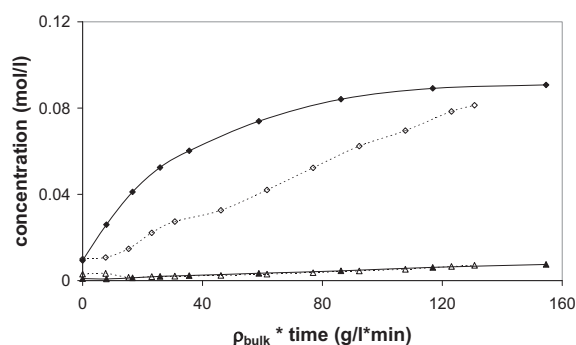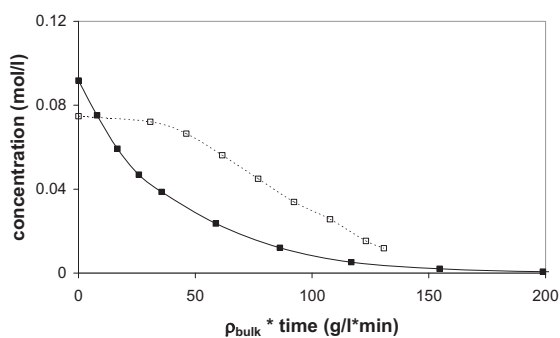
b)
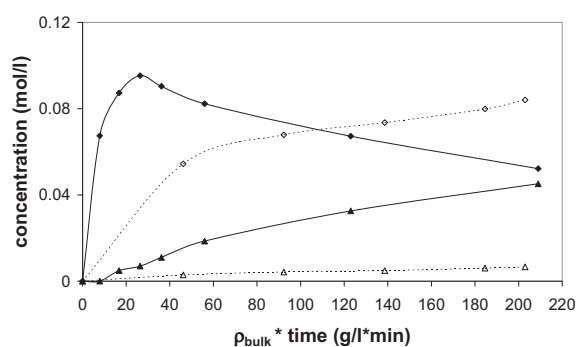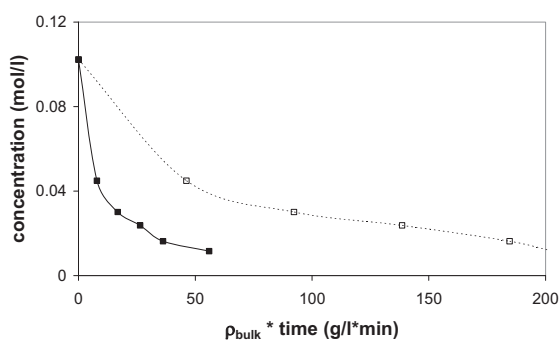
c)
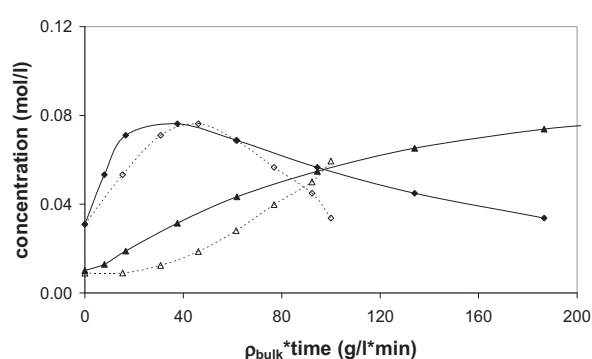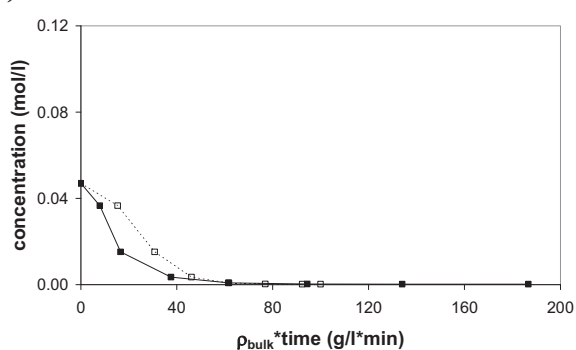
Figure 2. Kinetics for citral (■) hydrogenation, formation of citronellal (♦) and citronellol (▲) with (solid symbol, solid line) and without liquid phase pumping (open symbol, dashed line) in the hydrogenation of citral in 2-pentanol under 10 bar hydrogen at a) 50°C, b) 70°C and c) 90°C.

It turned out that the initial hydrogenation rate increased by 11% when the liquid phase was pumped out from the reactor compared to the constant liquid phase volume experiment.

Table 2. The effect of liquid phase pumping on the ratio of the concentrations of citronellal (CAL) and citronellol (COL) with pumping (wp) and without pumping (wop) at a defined ρ_{bulk}*time = 20 g/l*min.

Temperature (°C)	$c_{CAL,wp} / c_{CAL,wop}$	$c_{COL,wp} / c_{COL,wop}$
50	2.5	No effect
70	3.5	2.8
90	1.3	1.6

Table 3. Comparison of the initial hydrogenation rates in citral hydrogenation under 10 bar hydrogen with and without liquid phase pumping with a temperature programmed reaction from 60°C to 90°C. The initial citral concentration was 0.10 mol/l and the solvent was 2-pentanol.

Working mode	Initial hydrogenation rate (mmol/min/g Ni)	Conversion after 30 min (%)
Pumping	6.47	90.5
No pumping	5.75	73.8

4. Conclusions

The results for three-phase hydrogenation of citral indicated that the initial reaction rates can be enhanced by increasing catalyst bulk density, which is achieved by pumping out the liquid phase during a batch-wise experiment. In the studied temperature range the concentrations of the desired products at a normalized catalyst bulk density-time scale increased maximally at 70°C. A developed kinetic model containing the increase of catalyst bulk density can be used for quantitative description of the reactor operation.

References

1. P. Mäki-Arvela, L.-P. Tiainen, A. Kalantar Neyestanaki, R. Sjöholm, T.-K. Rantakylä, E. Laine, T. Salmi, D. Yu. Murzin, Appl. Catal. A: Gen. 237 (2002) 181.

WET AIR OXIDATION OF PHENOL AND ACETIC ACID IN THE TRICKLE BED REACTOR

N. Dobrynkin[1], M. Batygina[1], A. Noskov[1], V. Parmon[1], P. Tsyrulnikov[2],

D. Shlyapin[2], M. Besson[3] and P. Gallezot[3]

[1]*Boreskov Institute of Catalysis SB RAS, 5, Pr. Ak. Lavrentieva, 630090, Novosibirsk, Russia*

Fax: (7)-383 -330 68 78, E-mail: dbn@catalysis.nsk.su

[2] *Institute of Hydrocarbons Processing, SB RAS,*

54, Neftezavodskaya str., 644040, Omsk, Russia

[3]*Institut de Recherches sur la Catalyse, Centre National De La Recherche Scientifique, 2,*

avenue Albert Einstein, 69626 Villeurbanne Cedex, France

Abstract

The high-active catalysts PZ-65 (0.6%Ru+5%CeO$_2$/Sibunit), PZ-68 (0.6%Ru+8%CeO$_2$/Sibunit) were prepared by successive supporting CeO$_2$ and Ru on Sibunit-4 carbon and tested in catalytic wet air oxidation (CWAO) of phenol and acetic acid. Experiments were performed with catalysts PZ-65, PZ-68 and Sibunit-4 at 180 ^{o}C for phenol oxidation and at 200 ^{o}C for acetic acid oxidation at 50 bar air total pressure.

CWAO reactions runs were carried out in a continuous micropilot trickle-bed reactor for about 300 h. The initial concentrations of phenol and acetic acid were 1 g/L, catalyst loading was 1 g, and glass balls were used as an inert material. The treated solution was periodically analyzed, collected and submitted to a recycling run. Total organic carbon content (TOC), inorganic carbon content (IC) and concentrations of separate organic substances C$_i$ were analyzed by means of a TOC-meter and an HPLC.

All catalysts were rather active in oxidation of phenol and the activity was found very stable in all cases. No deactivation was observed. After several sets of recycling of treated solutions on catalyst PZ68, the oxidation activity measured on a fresh phenol solution was found similar to the initial activity. These experiments indicate directly that the catalyst is stable in phenol oxidation.

Wet air oxidation experiments were also carried out with acetic acid which is very resistant to degradation by WAO. The Sibunit catalyst did not exhibit catalytic activity up to temperature of 225 ^{o}C, whereas the promoted Ru-CeO$_2$/Sibunit catalysts exhibited high activity at 200 ^{o}C; however, their activity decreased significantly as a function of time on stream after 100 h.

TEM investigations of (Ru+CeO$_2$)/Sibunit catalysts have shown that 1nm-large Ru-particles are associated with 5 nm-large CeO$_2$ particles supported on the carbon surface. This association is probably very beneficial to the activity of the catalyst.

Introduction

The development of new Ru-CeO$_2$/carbon catalysts for deep oxidation of organic pollutants is carried out with the purpose of the creation of catalytic reactors of neutralization and processing of industrial waste water of high level of toxicity. The preliminary studies conducted with use of the perfect-mixing metal batch reactor have allowed us to evaluate the efficiency of catalysts, and to determine the initial levels of activity and selectivity of catalysts in WAO of variety substances during short-term experiments (some cycles of tests - totally within 3-12 hours) [1-2]. Nevertheless, owing to technical features of the reactor, the

catalyst in tests of this kind is subjected force to mechanical effects and crushed. Therefore, the additional long tests of the catalyst are necessary for objective further valuations of developed catalysts. Besides, the results of tests in a continuous micropilot trickle-bed reactor are very useful for the scaling of the process. Among the possible methods of long-term tests of a reactionary medium effect on the catalyst the continuous methods of a measurement of catalytic activity are most simple and convenient [3]. The experimental technique is well-described for differ cases of heterogeneous catalytic reactions in three-phase systems. In view of the aforesaid the trickle-bed reactors (TBR) are most suitable for laboratory and pilot tests of solid catalysts. The various aspects of TBR applications have been reviewed by Gianetto and Specchia [4]. Phenol and acetic acid were selected for oxidation as model systems of WAO reactions.

Experimental and Procedures

The catalysts $(Ru+CeO_2)/C$ were prepared by successive supporting CeO_2 and Ru on Sibunit-4 as has been described in [1]. The detailed description of the reactor (Hastelloy C22, length of 0.15 m, ID of 10 mm) and the test procedure used in this study has been given by Pintar et al. [5]. Reactions runs carried out for about 300 h, periodically the treated solution was collected, analyzed, and submitted to another WAO run for recycling it. Catalysts (1.0 g) : PZ-65 ($0.6\%Ru+5\%CeO_2$/Sibunit), PZ-68 ($0.6\%Ru+8\%CeO_2$/Sibunit), Sibunit-4); solutions: $PhOH/H_2O$, CH_3COOH/H_2O ($C^0_{SOLUTION}$ of 1.00 g/L); experiments were performed at $180\,^{\circ}C$ for phenol oxidation and at $200\,^{\circ}C$ for acetic acid oxidation , 5.0 L/h of V_{air}, 0.06 L/h of V_{liq}, 50 bar of air total pressure. The layer of catalyst was located in isothermal zone of the reactor, and the glass balls (D = 2.0 mm) were used as a top and bottom inert beds.

Analytically measured values were: content of total organic carbon - TOC, inorganic carbon - IC, (mg/L), concentrations of separate organic substances C_i (mg/L). Selectivity and conversion were used as calculated values: $S_{CO2} = (TOC_0-TOC_i)/TOC_0 = \Delta TOC/TOC_0$, $X = (C_o-C_i)/C_0 = \Delta C/C_0$.

Results and Discussion

Figures 1-5 shows the experimental data for phenol and acidic acid oxidation in the presence of catalysts Sibunit-4, PZ65 and PZ68. Data of the chromatographic analysis of the reaction mixture show the identical complicated composition of the components for phenol oxidation in all cases. Intermediate compounds identified are maleic, acetic and fumaric acids, hydroquinone + catechol at the beginning of the reaction.
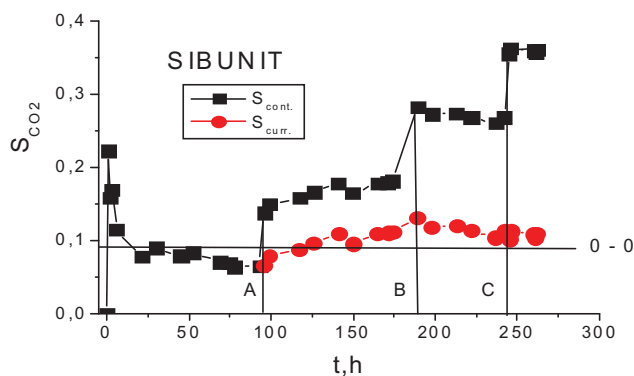
Fig. 1. Selectivity ("continuous" and "current" - for recycling) of CO_2 formation in long term test of Sibunit-4. Recycling (A, B, C) after 93, 174, 242 hours. Line 0-0 – is the initial level of the activity.
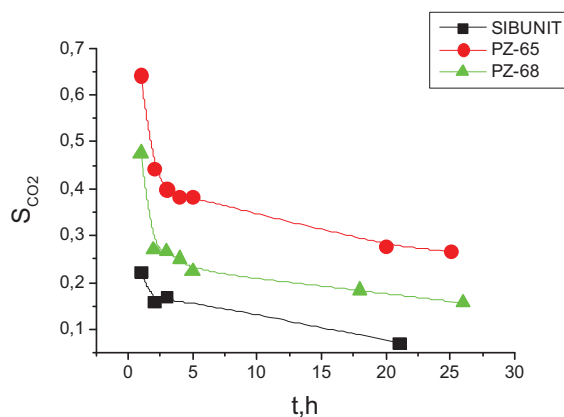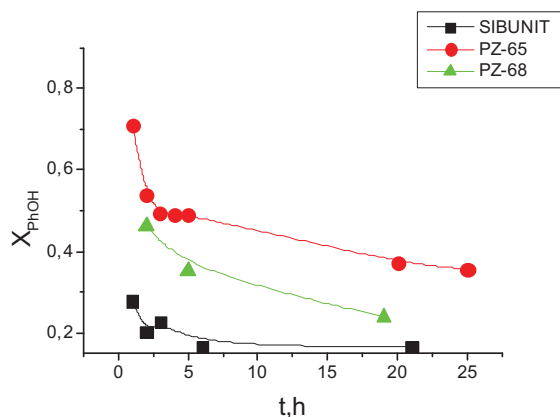
Fig. 2, 3. The comparison of initial levels of activity and selectivity of catalysts in phenol oxidation.
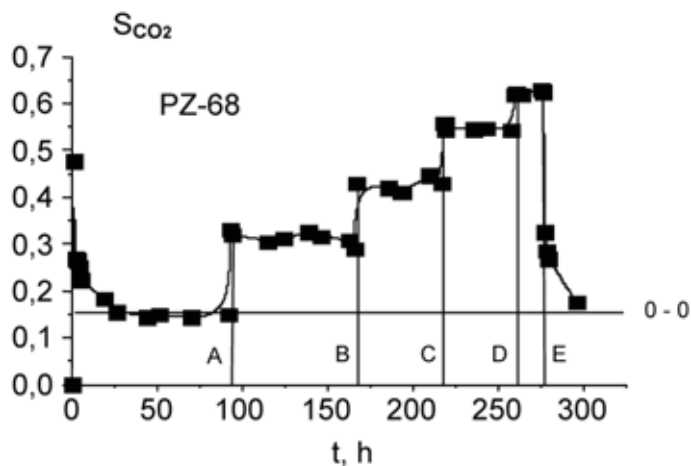
Fig. 4. Selectivity of CO_2 formation in long term test of Ru-CeO$_2$/C (PZ-68) catalyst in phenol oxidation. Recycling after 92 (A), 165 (B), 216 (C), 257 (D) hours; fresh solution after 276 h (E). Line 0-0 - initial level of activity.

As it was determined, all catalysts are rather active and are stable in oxidation of phenol. For each of them the observable regularities of activity and selectivity in deep oxidation, and also the composition of products are identical. The Sibunit catalyst did not exhibit catalytic activity in acetic acid oxidation up to temperature of 225 ^{o}C, whereas the promoted Ru-CeO$_2$/Sibunit catalysts exhibited high activity at 200 ^{o}C; however, their activity decreased significantly as a function of time on stream after 100 h. Atomic absorptive analysis showed the absence of Ru leaching, moreover the content of the supported metal (Ru) and promoter

(CeO_2) have exceeded the initial values for the catalyst samples used in acetic acid oxidation, that indicates considerable modification of the surface of carbon as a result of interaction of Sibunit with CH3COOH and oxygen. TEM investigations of ($Ru+CeO_2$)/Sibunit catalysts have shown that 1 nm-large Ru-particles are associated with 5 nm-large CeO_2 particles supported on the carbon surface. This association is probably very beneficial to the activity of the catalyst.
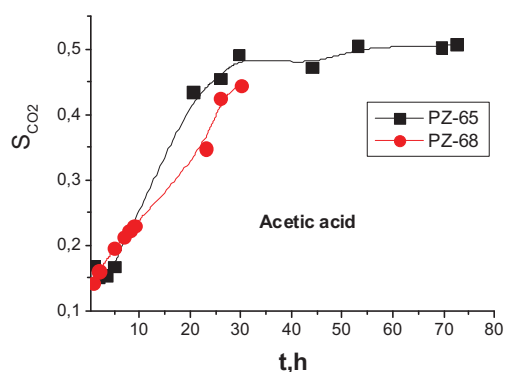
Fig. 5. The comparison of initial activity of ($0.6\%Ru+5\%CeO_2$) /Sibunit and ($0.6\%Ru+8\%CeO_2$) /Sibunit catalysts in acetic acid oxidation.

The results obtained have demonstrated the high efficiency and stability of all Ru-CeO_2/Sibunit catalysts in purification of phenol-containing wastewaters. Pure Sibunit is also very interesting for process economy because without precious metal it can degrade toxic effluents such as phenol into intermediate oxidation products that can be treated by conventional biological process. The research performed in this study presents a high potential impact for development of the reactors for the treatment of toxic industrial waste waters.

References

1. Dobrynkin N.M., Batygina M.V., Noskov A.S., Tsyrulnikov P.G., Shlyapin D.A., Schegolev V.V., Astrova, D.A., Laskin B.M., Topics in catalysis, 2005, Vol. 32, Nos. 1-4, p.69-76.
2. Batygina M., Dobrynkin N., Noskov A., Studies in Surface Science and Catalysis, 2003, Vol. 145, p.359-362.
3. Boreskov G. K. Heterogeneous catalysis. Moscow, Nauka, 1986, 304 p.
4. Gianetto A., Specchia V. Chem. Eng. Sc.,Vol. 47, Issues 13-14 , 1992, P. 3197-3213.
5. Pintar A., Besson M., Gallezot P., Applied Catalysis B: Environmental, 2001, Vol. 31, Issue 4, p. 275-290.

ISOPROPYLATION OF NAPHTHALENE OVER SEVERAL ZEOLITIC CATALYSTS: HY AND BIPOM'S

C. Bouvier and **W. Buijs**

Gebouw voor Scheikunde, Technische Universiteit Delft,

Julianalaan 136, 2628 BL Delft, The Netherlands.

Fax: +31 15 278 5006,   C.P.Bouvier@tudelft.nl

BIPOM is the acronym for BImodal POrous Material. These zeolitic materials with a MFI type framework exhibit unique structural features as a result of their very sophisticated synthesis [1]. BIPOM's can be obtained as so called zeogrids and zeotiles.

| zeogrid | zeotile-2 | zeotile-4 |
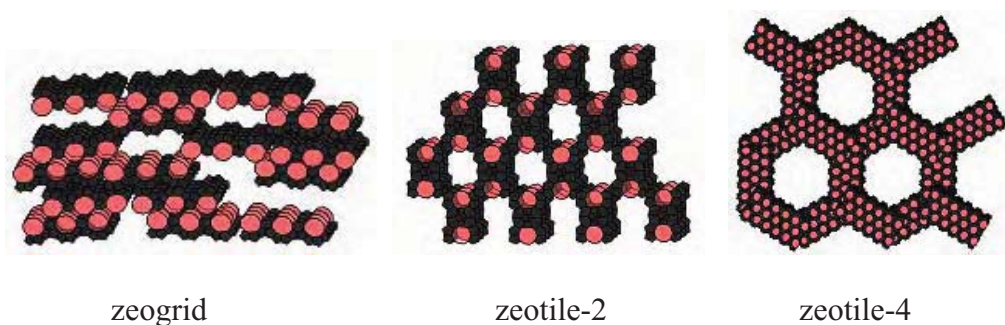
Their potential as sustainable catalyst is currently being investigated in our group. Their large mesopores should allow mass-transfer limitation free access of substrates to, and products from the catalytic sites. It might be expected that they exceed the performance of classical zeolite catalysts. As a model reaction isopropylation of naphthalene to 2,6-di-isopropyl naphthalene was chosen. A series of zeolitic systems has been tried on this reaction, and their performance will be compared with the first generation of BIPOM's.

Specific attention will be paid to the performance of HY and BIPOM-2, an Al zeogrid, because these catalysts showed a very good activity and selectivity depending on specific process conditions.

[1] Kirschhock, C.EA., Kremer, S.P.B., Vermant, J., Van Tendeloo, G., Jacobs, P.A. and Martens, J.A., Chem. Eur. J. 11 (2005) 4306.

THE AUTOTHERMAL SYNGAS PRODUCTION IN SOLID OXIDE FUEL CELLS UNDER FLOW REVERSAL CONDITIONS

F. Paloukis and <u>S.G. Neophytides</u>

FORTH/ICE-HT, Stadiou str., Platani P.O. Box 1414, Patras GR-26504, Greece.
Fax:+30-2610-965223, e-mail: neoph@iceht.forth.gr

1. Introduction

One of the inherent problems in processing methane selective oxidation to syngas in a fuel cell, is the low heating value of the reaction and the significantly larger in absolute values of the reaction free Gibbs energy change (ΔH_R=-5.127 kcal/mol and ΔG_R= -60.53 kcal/mol at 1173 K). In that respect the thermodynamic efficiency of the SOFC may far exceed unity, which is in a certain extend quite attractive. However the large positive entropy change of the reaction (ΔS_R=47.23 cal/mol·K at 1173 K) may cause a severe cooling effect in the SOFC as the reaction mixture will absorb heat from the SOFC. This may render the autothermal operation of the SOFC considerably difficult.

A proposed solution is to feed the cathode compartment with CH_4 lean CH_4/O_2 mixture where the complete oxidation of CH_4 will be catalyzed by the perovskite cathode electrode [1]. In that manner the direct and controlled supply of heat to the SOFC will be possible, so as to maintain the reactor ignited. This can be also combined with the SOFC operation under forced periodic reversal of the flow which was shown to be very successful for the autothermal processing of reaction mixtures with very low heating values [2]. Such a transient mode of operation may exploit the dynamic characteristics of the whole reactor, leading to the formation and propagation of temperature and concentration profiles along the reactor, which cannot be obtained in any steady state regime.

The reactions taking place at the anode and cathode compartments can be summarized as follows:

Anode: $CH_4 + O^{2-} \rightarrow CO + H_2 + 2e^-$ (8)

Cathode: $\frac{1}{2}O_2 + 2e^- \rightarrow 2O^{2-}$, $CH_4 + 2O_2 \rightarrow CO_2 + 2H_2O$ (9)
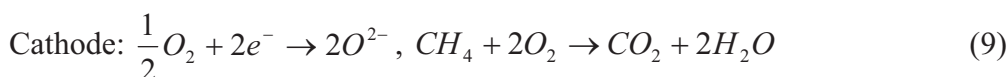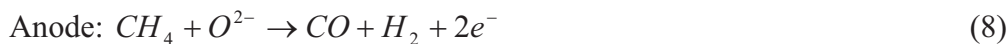
Since we are mostly interested in the proof of concept of the reversed flow operation of a partial oxidation SOFC, it is assumed that at the anode methane is selectively oxidised into CO and H_2 (eq. 8) while at the cathode compartment beyond the electrochemical reduction of

O_2 into O^{2-} the catalytic combustion of methane is considered to take place on the LSM perovskite surface (eq. 9), thus producing heat which will compensate the freezing effect of the positive entropy change of the partial oxidation reaction.

2. Mathematical model

The simulation is mathematically described by the following system of integro-diferential equations [3,4] which consists of the continuity equations, the energy balances of the gas streams and the solid electrolyte as well as the electron balance along the electrical and the electrochemical circuit:

(i)   Continuity equation in the gas streams

Fuel stream

$$v_f \frac{dy_{CH_4,f}}{dz} = \Theta_f \xi n_{CH_4,f} - y_{CH_4,f} \xi \Theta_f (n_{H_2} + n_{CO} + n_{CH_4,f})$$

Oxidant stream

$$v_{ox} \frac{dy_{O_2}}{dz} = \Theta_{ox} \xi n_{O_2}(1 - y_{O_2}) + n_{O_2} \Theta_{ox} r_{ox} \ , \qquad v_{ox} \frac{dy_{CH_4}}{dz} = -\Theta_{ox} \xi n_{O_2} y_{CH_4} + \Theta_{ox} r_{ox} n_{CH_4} \ ,$$

$$r_{ox} = \frac{k_0 L}{c1 N_{ox}^0} \exp(-\frac{E}{RT_{ox}}) y_{CH_4}$$

(ii)   Energy equation of the gas streams

Fuel stream

$$v_f \frac{d\Theta_f}{dz} = \Theta_f gh_f (\Theta_s - \Theta_f) \ , \ gh_f = \frac{2h_f L(b1 + c1)}{N_f^0 Cp_{tf} b1c1}$$

oxidant stream

$$v_{ox} \frac{d\Theta_{ox}}{dz} = \Theta_{ox} gh_{ox} (\Theta_s - \Theta_{ox}) \ , \ gh_{ox} = \frac{2h_{ox} L(b1 + c1)}{N_{ox}^0 Cp_{tox} b1c1} \ ,$$

(iii)   Evolution of the dimensionless gas velocity

Fuel stream

$$\frac{dv_f}{dz} = gh_f (\Theta_s - \Theta_f) + \Theta_f \xi (n_{H_2} + n_{CO} + n_{CH_4,f})$$

Oxidant stream

$$\frac{dv_{ox}}{dz} = gh_{ox}(\Theta_s - \Theta_f) + \Theta_{ox} \xi n_{O_2}$$

(iv) Energy balance of the solid electrolyte

159

$$\frac{d\Theta_s}{d\tau} = \frac{1}{Pe_{ha}}\frac{d^2\Theta_s}{dz^2} + sh_f(\Theta_f - \Theta_s) + sh_{ox}(\Theta_{ox} - \Theta_s) + H_{cp}\xi(\Theta_s - 1) + H_r\xi(1-\eta) + H_r'r_{ox} + H_{cp}'r_{ox}(\Theta_s - 1)$$

$$Pe_{ha} = \frac{\rho_s Cv_s L N_f^0}{k_s Ct_f^0}, H_{cp} = \frac{n\Delta Cp_R b1c1Ct_f^0}{Cv_s\rho_s A_s}, H_{cp}' = \frac{n\Delta Cp_R b1c1Ct_f^0}{Cv_s\rho_s A_s}, H_r' = \frac{b1c1Ct_f^0(-\Delta H_{R'}^0)n}{T_f^0 Cv_s\rho_s A_s},$$

$$H_r = \frac{b1c1Ct_f^0(-\Delta H_R^0)n}{T_f^0 Cv_s\rho_s A_s}, \quad sh_{ox} = \frac{2h_{ox}L(b1+c1)Ct_f^0}{N_f^0 Cv_s\rho_s A_s}, \quad sh_f = \frac{2h_f L(b1+c1)Ct_f^0}{N_f^0 Cv_s\rho_s A_s}$$

(v)Electron balance

$$\xi = [N1 + N2(\Theta_s - 1) + N3\Theta_s + N4\Theta_s\ln\Theta_s + N5\Theta_s\ln\frac{1}{k_p} - N6\xi_\tau]\exp(\frac{N7}{\Theta_s})$$

where the total dimensionless current density is defined as

$$\xi_\tau = \frac{\int_0^1\left\{[N1 + N2(\Theta_s - 1) + N3\Theta_s + N4\Theta_s\ln\Theta_s + N5\Theta_s\ln\frac{1}{k_p}]\exp(\frac{N7}{\Theta_s})\right\}dz}{1 + N6\int_0^1\exp(\frac{N7}{\Theta_s})dz}$$

The dimensionless parameters N1 through N7 are defined

$$N1 = \frac{nL(-\Delta H_R^0)}{(4F)^2 N_f^0\rho_0 d1c1}, \quad N2 = \frac{nL(-\Delta Cp_R)T_f^0}{(4F)^2 N_f^0\rho_0 d1c1}, \quad N3 = \frac{nL(\Delta S_R^0)T_f^0}{(4F)^2 N_f^0\rho_0 d1c1}, \quad N7 = -\frac{E_{act}}{RT_f^0}$$

$$N4 = \frac{nL\Delta Cp_R T_f^0}{(4F)^2 N_f^0\rho_0 d1c1}, \quad N5 = \frac{LRT_f^0}{(4F)^2 N_f^0\rho_0 d1c1}, \quad N6 = \frac{L[\text{Re}\,x + (Z+1)\text{Re}]b1}{Z\rho_0 d1}$$

The dimensionless cell potential or thermodynamic cell efficiency η is given by:

$$\eta = r_{ex}\xi_t$$

where r_{ex} is the dimensionless external resistance and is defined by:

$$r_{ex} = \frac{b1c1N_f^0(4F)^2[(Z+1)\text{Re} + \text{Re}\,x]}{nZ(-\Delta H_R^0)}$$

3. Simulation results
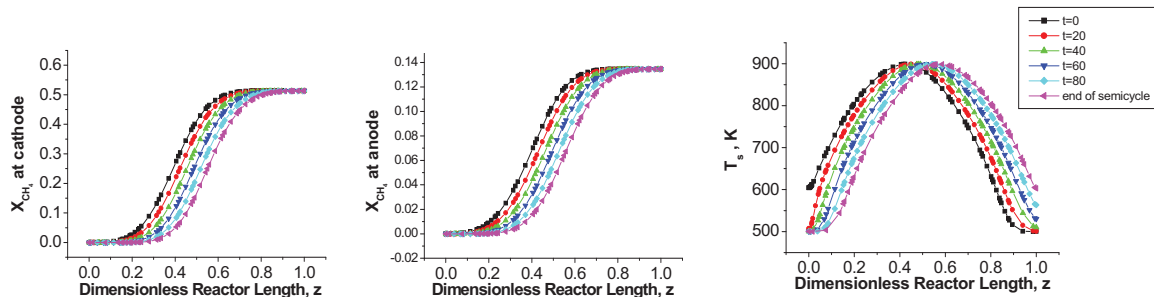
Figure 1: The temperature and concentration profiles are plotted for successive times thus depicting their movement along the reactor. $N_f^0 = 20$ mol/m²K, Rex=1 ohm, τ_p=100, y_{CH4}=0.024, $T_f^0 = 500$ K

Fig. 1 shows typical simulation results of the reversed flow operation of the SOFC. The temperature and concentration profiles are plotted for successive times thus depicting their movement along the reactor. The direction towards which the profiles move is defined by the direction of the flow. The features of these creeping profiles are quite similar with the behavior of the creeping heat fronts that are developed in an infinite catalytic bed [2]. However in the present case since the length of the reactor is not infinite by keeping the flow direction unchanged the creeping profiles will move out of the reactor thus resulting in the extinguish of the SOFC's operation. If prior to this the flow direction through the reactor is reversed the temperature and concentration profiles will start moving towards the opposite direction and the high temperature reaction zone will be confined inside, wondering back and forth along the reactor.

The beneficial operation of this transient mode of operation is depicted in Fig.2 where the reversed flow and steady state operation is compared in terms of fuel utilization, thermodynamic efficiency and power output plotted against inlet temperature. The steady state operation of the SOFC without the catalytic combustion of methane at the cathode compartment is presented too. It is clearly observed that both steady state operations result in an extinguished reactor at lower inlet temperatures while the reversed flow operation runs autothermally even at inlet temperatures as low as 300 K. In this way a more compact reactor system can be constructed since the use of heat exchangers for the preheating of the inlet gas streams at the SOFC is avoided.
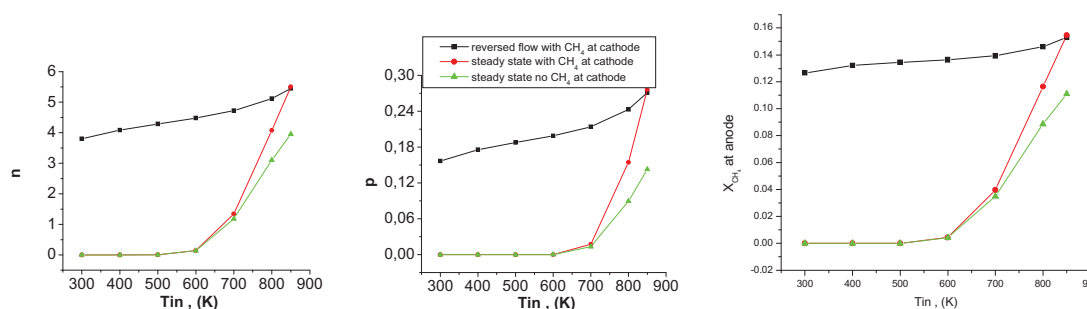
Figure 2: The reversed flow and steady state operation is compared in terms of fuel utilization, thermodynamic efficiency and power output plotted against inlet temperature. Inlet conditions as in Figure 1.

References

[1] R.F. Blanks, T.S. Wittrig, D.A. Petersen, Chem. Eng. Sci. 45 (1990) 2407-2413

[2] Y.S. Matros, in "Studies in Surface Science and Catalysis", Elsiever, Amsterdam (1989)

[3] S.G. Neophytides, A. Tripakis, Canadian journal of Chem. Eng. 74 (1996) 719-728

[4] S.G. Neophytides, Chem. Eng. Science 54 (1999) 4603-4613

DESIGN OF A CATALYST FOR THE DENITRIFICATION OF NATURAL WATER. THE IMPORTANCE OF THE REACTOR DESIGN

A.E. Palomares[a], J.G. Prato

Instituto de Tecnología Química, (UPV-CSIC), Valencia, Spain;

[a] *Departamento de Ingeniería Química y Nuclear, Universidad Politécnica Valencia, Avda. de Naranjos s/n, 46022 Valencia, Spain, fax: +34 963877639, e-mail: apalomar@iqn.upv.es*

Introduction

Nitrate concentration in water supplies has experienced an important increase in the last years, mainly caused by the use of fertilizers necessary for an intensive agricultural production. The increasing rigorousity of the drinking water quality standards, generates the urgent need to develop a new technology for the nitrate removal from aqueous solutions. Conventional techniques for ground water denitrification are relatively costly and they need in some cases a secondary post-treatment of the effluent and the sludge generated. Recently, it has been shown that the most adequate way to remove nitrates, from the environmental point of view, is to convert them into N_2 by liquid phase nitrate hydrogenation on noble metal catalysts [1-5]. However the catalyst has to be selective to avoid the production of NO_2^- and NH_4^+. Typically, metal-oxide supported bimetallic catalysts, combining a noble metal, usually Pd or Pt, and another metal, such as Cu, Sn or In, supported on alumina have been applied for this reaction [4-6], but it has been suggested that the kinetics and the selectivity of the process are severely limited by mass transfer limitations [2, 7]. The diffusion of the reactants towards the active centers is very influenced by the nature of the support and by the reactor, for this reason it is necessary an adequate selection of them to design an active catalyst.

In the present work, we have studied the influence of different supports on the activity of the catalysts to show that it is possible to diminish the problems associated with diffusion limitations by choosing an adequate support. After optimizing the catalyst design, the activity of this catalyst have been tested in different reactor types.

Experimental

Beta (Si/Al=12.5) and ZSM5 (Si/Al=15) zeolites were supplied by PQ Zeolites, ITQ2 zeolite (Si/Al=12) and hydrotalcites were synthesized in our laboratory and γ-Al_2O_3 was supplied by Merck. Palladium and copper were added to the support by standard impregnation methods in order to have a metal concentration of 5 % and 1.5 % respectively. The sample was calcined

in air at 500ºC for 1 hour and reduced in hydrogen flow at the same temperature. Powder catalyst was tested in a 1 liter glass reactor and the gas flow was introduced into the vessel below the impeller. In a typical run, 0.8 g of the catalyst was charged into the reactor containing 0.6 liters of distilled water with KNO_3, in order to have a nitrate concentration of 90 mg/l. The content of the reactor was purged with nitrogen and brought to reaction conditions, then a H_2/N_2 mixture was sparged continuously through the suspension at a metered rate. The concentrations of NO_3^-, NO_2^- and NH_4^+ in the aqueous-phase samples were determined by UV/VIS spectroscopy.

The optimized catalyst have been tested in different types of continuous reactors.

Results and discussion

The liquid phase nitrate hydrogenation has been studied on various catalysts based in a combination of Pd and Cu supported on various materials (Table 1). As it can be observed in Figure 1 the activity of the catalyst is very dependent on the support used. Catalysts supported on alumina or hydrotalcite show a fast reduction of the nitrates. On the other hand, those supported on zeolites exhibit a lower reaction velocity and only with the catalyst supported on a laminar zeolite, as ITQ2, the complete removal of nitrates is observed. The nature of the support is also influencing the selectivity of the catalyst and it is shown that with hydrotalcites the formation of intermediate products as nitrite or final subproducts as ammonia is much lower than with alumina.(Table 1).

It seems that hydrotalcites diminish the problems associated with diffusion limitations, since when calcined hydrotalcites are contacted with water, they recover its layered structure by capturing the anions present in the media (nitrates). The nitrates are located in the interlayer space next to the metallic active sites, overcoming in this way the problems related with mass transfer limitation. This does not occur when the support is alumina or zeolites.

Hydrotalcites can be prepared with different metals in its structure (Li-Al, Ca-Al, Zn-Al, Mg-Al), then the next step was to test these supports in order to optimize the design of the catalyst. The best results in activity and selectivity were obtained with Mg-Cu/Al hydrotalcites were copper is in the hydrotalcite structure substituting Mg atoms. Other noble metal as Pt was impregnated in the hydrotalcites substituting Pd, but the best results were obtained with the last one.

This clearly indicates that for an adequate behavior of the catalyst in the liquid phase nitrogen hydrogenation, it is necessary to look for a catalyst with the adequate metal active sites but in addition, all the factors that contribute to increase diffusion limitations has to be overcome. In order to do this, the first step has to be to choose an adequate support, as Mg-Al hydrotalcite,

but the next steps have to be related with an adequate reaction system where all the mass transfer problems, as the particle size, the stirring or the previous removal of particles and colloids, have been minimized.

In order to do this, different continuous reactor configurations were tested. It was observed that a good contact of the three phases present (the optimized solid catalyst, the liquid media containing the nitrates and the gaseous hydrogen) it is basic in order to obtain good results no only in the catalyst activity but also in its selectivity. In this way to obtain a very small diameter of the bubble gas when contacting with the solid catalyst it is the controlling step in order to obtain good results, similar to those obtained with the batch reactor.

Figure 1. NO_3^- concentration profile as a function of time for Cu/Pd catalysts.
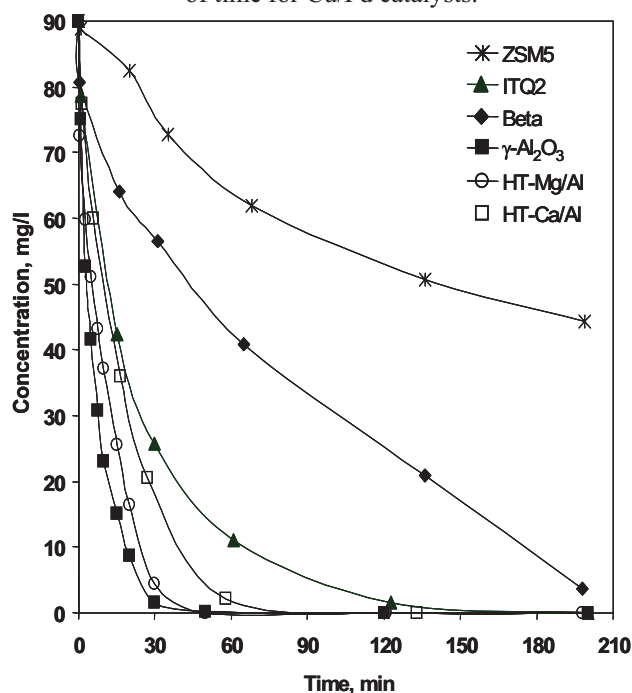
Table 1. Nitrite and ammonium concentrations after 200 min. of reaction.

Catalyst	NO_2^- (mg/l)	NH_4^+ (mg/l)
ZSM5 zeolite	13.6	2.3
Beta zeolite	23.7	1.6
ITQ2 zeolite	5.0	12.4
γ-Al_2O_3	2.0	18.7
Mg/Al hydrotalcite	0.05	7.4

Bibliography

[1] S. Hörold, K. D. Vorlop, T. Tracke and M. Sell, Catal. Today, 17 (1993) 21.
[2] A. Pintar, J. Batista, Catal. Today 53 (1999) 35.
[3] A.E. Palomares, J.G. Prato, F. Márquez, A. Corma, Appl. Catal. B, 41 (2003) 3.
[4] M.J. Chollier-Brym, R. Gavagnin, G. Strukul, M. Marella, M. Tomaselli, P. Ruiz, Cat. Today, 75 (2002) 49.
[5] U. Prüsse, M. Hälhein, J. Daum, K. D. Vorlop, Catal. Today, 55 (2000) 79.
[6] F. Epron, F. Gauthard, C. Pineda, J. Barbier, Appl. Catal. A., 237 (2002) 253.
[7] R. Gavagnin, L. Biasetto, F. Pinna, G. Strukul, Appl. Catal. B, 38 (2002) 91.
[8] U. Prüsse, K.D. Vorlop, J. Mol. Catalyst A, 173 (2001) 313
[9] O.M. Ilnitch, L. V. Nosova, V.V. Gorodetskii, V.P. Ivanov, S.N: Trukhan, E.N. Gribov, S.V. Bogdanov, F.P. Cuperus, J. Mol. Chem. 158 (2000) 237

PARTIAL OXIDATION OF METHANE TO SYNTHESIS GAS AT SHORT CONTACT TIMES IN AN AUTOTHERMAL REACTOR WITH MONOLITH CATALYSTS

S. Pavlova, V. Sadykov, Z. Vostrikov, O. Snegurenko, A. Shigarov, V. Skomorokhov, V. Kuzmin, V. Kirillov, S. Pokrovskaya

Boreskov Institute of Catalysis, Siberian Branch of the Russian Academy of Sciences, pr. Lavrentieva, 5, 630090, Novosibirsk, Russia, e-mail: pavlova@catalysis.nsk.su

Catalytic partial oxidation of methane (POM) at short contact times is now considered as an attractive technology for the small-scale and distributed production of syngas in the stationary and mobile fuel processing [1]. It is also of great practical interest to integrate POM into stage combustors of methane for gas turbines wherein, primarily, methane is partially oxidized to syngas in the fuel-rich combustor. Subsequent addition of syngas to ultra-lean feeds allows to stabilize combustion and reduce the nitrogen oxide content of exhaust to 1-5 ppm. Syngas may also be added to the conventional vehicle internal combustion engine in order to decrease pollutant emissions especially during the start -up period. In view of such applications, realization of POM at contact times < 0.1 sec to miniaturize the reactors is the most promising route, which determines the use of monolithic catalysts having a low pressure drop [2]. Furthermore, due to mild exothermicity, the process can be realized in an authothermal regime ensures a high yield of syngas.

Previous studies of POM using monoliths have been carried out mainly over small fragments of ceramic monolithic catalysts containing Pt or Rh [2]. Several problems associated with performance of such monolith catalysts exist. They are high contents of expensive Rh(Pt), their evaporation due to high temperatures developed in the inlet part of monolith, deactivation due to carbon build up in the outlet zone. Another problems associate with the insufficient thermal stability and conductivity of monolith ceramic supports. To solve these problems, new types of monolith support and more stable active components were developed earlier by the authors [3].

In this work, performance of developed catalysts comprised of CeO_2-ZrO_2 and $LaNiO_x$ promoted by Pt supported on different types of full-sized monolith substrates was studied in a POM autothermal reactor at transient and stationary conditions with its subsequent modeling.

OP-3-16

The effect of the linear velocity, feed composition and inlet temperature on the catalysts performance was elucidated.

Experimental. To prepare catalysts, two types of full-sized monolithic substrates were used: thin-wall corundum monoliths and honeycomb monoliths based on fechraloy foil. The corundum monoliths are a hexagon prism with a side of 40 mm and triangular channels with wall thickness of 0.2– 0.3 mm. The metallic support of 50 mm diameter is made of foils 20 to 50 μm in thickness and has the density of cells 200 - 400 per square inch. The foil surface is additionally protected by coating it with a protective nonporous film of thermally stable oxides, a few microns in thickness, using the unique technology of blast dusting [3]. Active components including both mixed oxides and platinum are supported by successive impregnation with appropriate suspensions or solutions followed by drying and calcination.

For POM experiments, the monolith catalysts along with front and back-end thermal shields were placed into a tubular stainless-steel reactor with required housing and thermal insulation. The axial temperature at selected points along the monolith was scanned by thermocouples located in the central channel plugged with alumina-silica fibers. The linear velocity of the feed was varied in the range of 0.5-6 m/s. The feed composition was CH_4 (natural gas) - 22-29 vol.%, air – balance. Gas composition was analyzed by GC method.

Modelling. For description of the monolith catalyst behavior, one-dimensional model was used. Reactor was assumed to be adiabatic. The kinetic model of partial methane oxidation includes the stages of complete methane oxidation shift and reforming reaction. All reaction stages occur independently and simultaneously [4]. Internal mass transfer control of reaction rates is negligible. External mass transfer control is significant and taken into account. The plug flow mode is assumed with respect to the gas phase, heat is dispersed along the monolith length due to thermal conductivity of substrate.

Results and discussion. To study the performance of the monolith catalyst during start-up, the air-natural gas mixture heated up to 200-450°C was continuously fed through the cold monolith catalyst until ignition occurred. At the ignition point, the rapid increase of the catalyst temperature, methane and oxygen conversion and syngas concentration is observed. For both catalysts based on corundum and metallic supports, the scan of the axial monolith temperature in the different points during start-up shows that at all linear velocities in the range of 0.25-6 m/s, ignition starts in the rear zone of a monolith. After ignition, the thermal front (maximal catalyst temperature) moves towards the monolith entrance until the stationary state is attained (Fig.1). At increasing the linear velocity, the time required to attain the steady

state decreases. At the same linear velocity, the temperature profile stabilizes more rapidly for the catalysts based on metallic substrate as compared to corundum ones due to

Fig.1. Temperature profile at different points of the catalyst based on the corundum substrate during ignition. Linear velocity – 1 m/s

Fig. 2. Axial temperature dependence on the monolith length for the catalysts based on different support types. Linear velocity for catalysts supported on Fechraloy-foil - 0.78 m/s, corundum – 1 m/s.
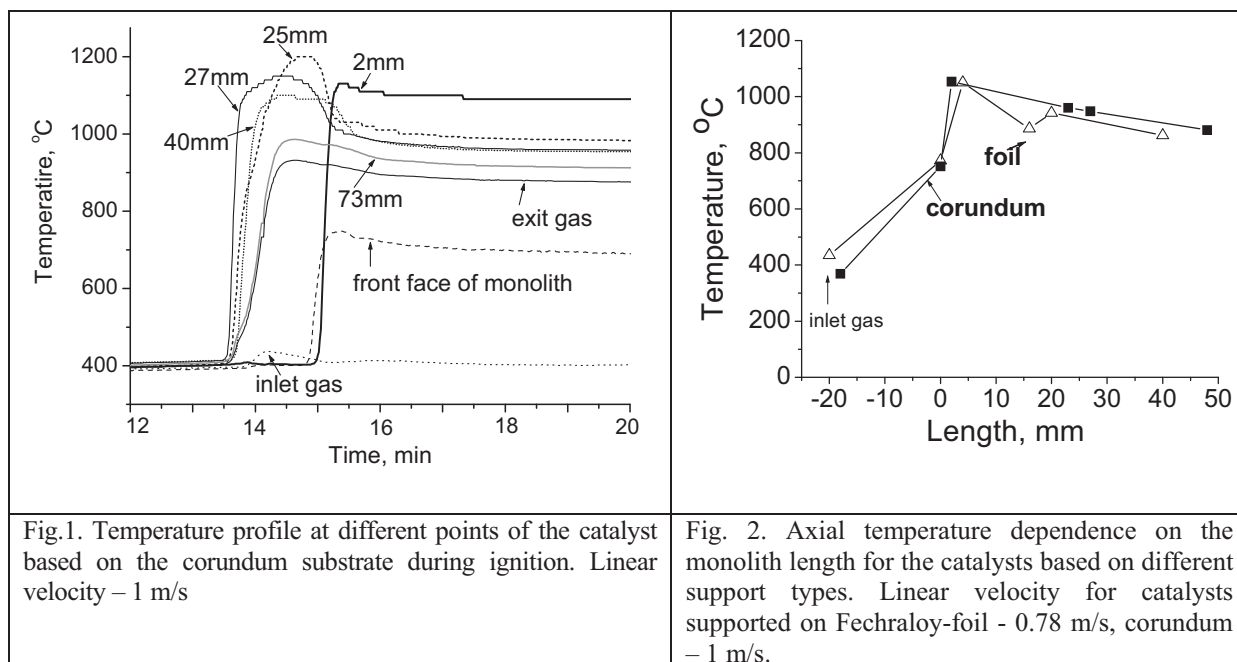
high thermal conductivity of the metal foil. However, the temperature profile at stationary state is the same for catalysts based on both corundum and metallic foil (Fig.2).

Fig. 3. Axial temperature profile along the catalyst based on corundum monolith at different linear velocities.

Fig. 4. Temperature profile of the solid and gas phase for the catalyst based on corundum monolith. Steady state regime, linear velocity- 1m/s, $CH_4 – 28\%$. Circles –measured catalyst temperature, lines – simulated temperature of catalyst and gas.
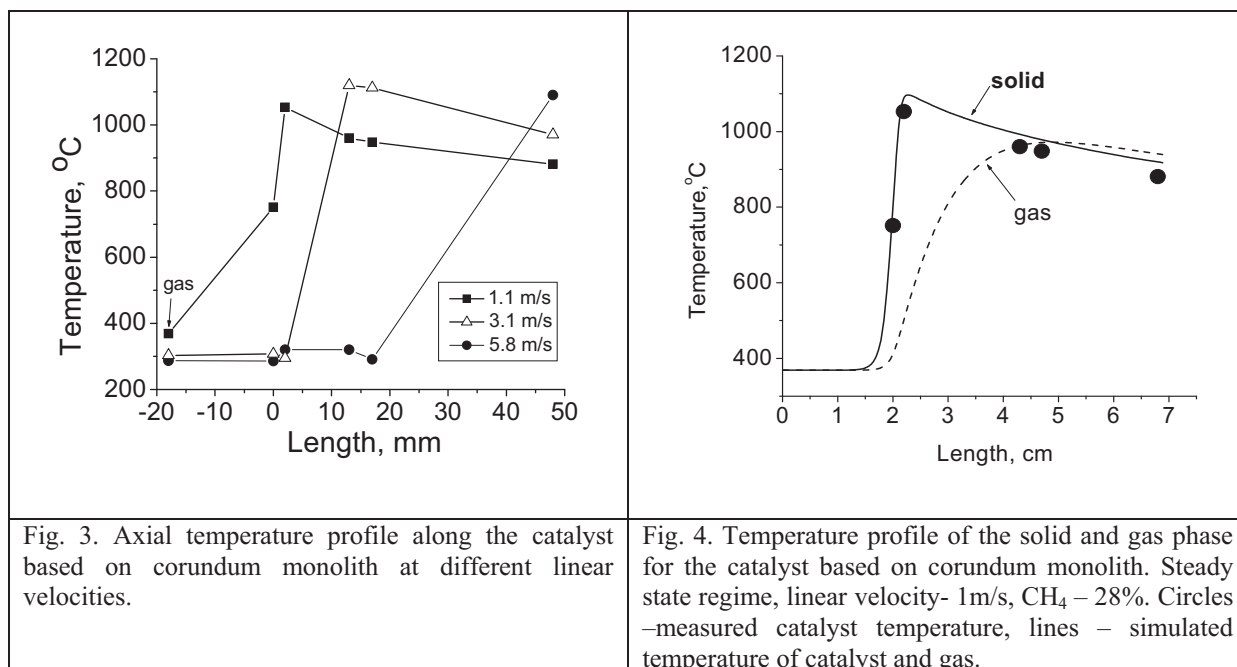
At the steady state regime, the location of the hottest monolith zone depends on the linear velocity. As the linear velocity increases, this zone moves to the monolith exit due to monolith cooling by the incoming gas (Fig.3). At the inlet gas temperature of 300°C and the

linear velocity in the range of 0.5-2 m/s, methane conversion and syngas concentration are nearly constant being equal to 77-72% and 45-41%, correspondingly. They decrease with decreasing the inlet gas temperature.

It is known that partial methane oxidation can occur through an indirect route including total oxidation of CH_4 to CO_2 and H_2O followed by steam and dry reforming of remaining CH_4 [1]. Hence, in the narrow hottest zone of the monolith, highly exothermic total oxidation occurs producing heat, which leads to the steep increase of the temperature. While oxygen is consumed in this zone producing mainly CO_2 and H_2O, syngas is formed further downstream via steam and, apparently, dry reforming of methane. The endothermic reforming reactions lead to the temperature decrease along the catalytic monolith.

The simulation of the temperature profile along the catalyst based on corundum monolith is in a good agreement with the experimental results (Fig. 4). In the exit zone of the monolith, the simulated temperature of the gas phase is shown to be lower than the catalyst temperature.

1. C. Song, Catal.Today 77 (2002) 17.
2. D. A. Hickman and L. D. Schmidt, J. Catal., 138 (1992) 267.
3. V.A. Sadykov, S.N. Pavlova et al. , Kinetics and Catalysis, Vol. 46, No. 2 (2005) 227.
4. A.M. De Groote and G.F.Froment, Appl. Catal. A 138 (1996) 245.

SIMULATION OF SELECTIVE REACTIONS PERFORMANCE IN TRANSIENT REGIMES WITH PERIODICAL SEPARATE FEEDING OF REAGENTS. CASE STUDY: PROPANE OXIDATIVE DEHYDROGENATION IN ADIABATIC V-Ti CATALYST BED

A.N. Zagoruiko

Boreskov Institute of Catalysis SB RAS, pr. Akad. Lavrentieva, 5, Novosibirsk, 630090, Russia
e-mail: zagor@catalysis.ru,   fax: +7-383-3306878

Introduction

Improvement of selectivity and desired product yield in complex reaction systems is one of the major problems in catalytic reaction engineering and also one of the main challenges in the catalytic reaction engineering area. Usually such problems are solved by development of new highly selective catalysts and by optimization of process operation parameters, though it cannot guarantee the desired results in all cases.

One of the most prospective approaches for solution of the problem is application of transient nonstationary regimes [1,2] and, in particular, periodical separate feeding of oxidant and reductant. Studies [3,4] on propane oxidative dehydrogenation at vanadia catalysts demonstrated that FFCC under isothermal conditions provided by periodical oscillations of propane/oxygen concentration ratio in feed leads to increase of propylene yield compared to steady-state conditions, with maximum C_3H_6 production at separate feeding of reagents.

Simulation of transient temperature and composition phenomena in an adiabatic packed catalyst bed arising under periodical separate feeding of reagents was earlier investigated by author for a complex consecutive system of model reactions [5]. The current research is devoted to the case study of selective oxidative dehydrogenation of propane to propylene.

Model formulation

As it was demonstrated in [4], the propane conversion at vanadia-titania catalyst may be described by Eley-Rideal mechanism, proposing that oxygen is involved into reaction via step of chemisorption, while hydrocarbon species react with chemisorbed lattice oxygen only (and not the gas phase one). In this case the reaction scheme may be formulated as follows [4]:

$$C_3H_8 + [V_2O_5] \Rightarrow C_3H_6 + H_2O + [V_2O_4] \tag{1}$$

$$C_3H_6 + 9 \, [V_2O_5] \Rightarrow 3 \, CO_2 + 3H_2O + 9 \, [V_2O_4] \tag{2}$$

$$C_3H_8 + 10 \, [V_2O_5] \Rightarrow 3 \, CO_2 + 4H_2O + 10 \, [V_2O_4] \tag{3}$$

$$[V_2O_4] + \tfrac{1}{2} \, O_2 \Rightarrow [V_2O_5] \tag{4}$$
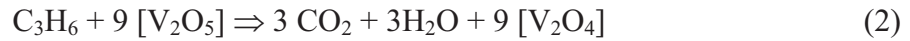
At formulation of the process mathematical model two important factors were taken into account: possibility of significant changing both the reaction mixture volume and heat capacity in course of reaction performance. To simplify the model at this stage of research, the dispersion factors (heat conductivity of the catalyst bed, mass transfer by gas diffusion), as well as inter-phase heat/mass exchange were excluded from the description. The bed was accounted as adiabatic and one-dimensional.

With account of these factors, the mass balance for species in the gas phase was expressed as:

$$\frac{\partial(uc_i)}{\partial l} = \sum v_{ij} w_j \tag{5}$$

with boundary conditions:

$$l = 0 \quad \Rightarrow \quad u = u_{in}; \quad c_i = c_i^{in} \tag{6}$$

where u – superficial gas velocity, c_i – molar concentrations of gas species ($i = C_3H_8$, C_3H_6, CO_2, H_2O, O_2, N_2), v_{ij} – stoichiometric coefficients of i-th species in j-th reactions, w_j – reaction rates ($j = 1\div4$ correspond to reactions (1-4)), index in specifies values at the bed inlet.

Mass balance for lattice oxygen at the catalyst surface was given by equation:

$$a_{max} \frac{\partial \theta}{\partial t} = \sum_j v_{ij} w_j \tag{7}$$

где a_{max} – maximum chemisorption capacity of catalyst surface in respect to lattice oxygen, θ - surface fraction of oxidized active sites $[V_2O_5]$ at the catalyst surface.

Kinetic equations (as well as values of their parameters) for w_j were taken in accordance with [4]:

$$
\begin{aligned}
w_1 &= k_1 c_{C3H8} \theta \\
w_2 &= k_2 c_{C3H6} \theta^2 \\
w_3 &= k_3 c_{C3H8} \theta^2 \\
w_4 &= k_4 c_{O2} (1-\theta)
\end{aligned}
\tag{8}
$$

Due to significant changing of gas heat capacity in course of reaction it was impossible to use conventional technique of adiabatic heat rise application, therefore, energy balance was formulated in enthalpy terms:

$$(1-\varepsilon)\frac{\partial H_{cat}(T,\theta)}{\partial t} = -\frac{\partial(uH_g(T,\overline{c}))}{\partial\ell} \tag{9}$$

$$(1-\varepsilon)\gamma\frac{\partial T}{\partial t} + a_{max}\Delta H_\theta\frac{\partial\theta}{\partial t} = -\frac{\partial(u\sum_i c_i h_i(T))}{\partial\ell} \tag{10}$$

with boundary conditions:

$$\begin{aligned}\ell = 0 &\Rightarrow u = u_{in}; \quad T = T_{in}\\ t = 0 &\Rightarrow T(\ell) = T_{init}(\ell); \theta(\ell) = \theta_{init}(\ell);\end{aligned} \tag{11}$$

where T – temperature, H_{cat} and H_g – enthalpies of catalyst and gas, respectively, γ - heat capacity of catalyst support material, $\Delta H_\theta = \Delta H_{V2O5}$ - ΔH_{V2O4}, h_i – enthalpies of individual (i-th) components of reaction mixture.

Analysis of thermodynamic data showed that it is possible to neglect temperature dependence for γ and ΔH_θ, and to simplify polynomial functions h_i (T) by linear dependencies. Thermodynamic properties of surface species (V_2O_4 and V_2O_5) were assumed to be equal to ones for the bulk state of these compounds.

Preliminary estimation of heat effects for reactions (1-4) showed, that stage of surface selective oxidation (1) has slightly negative heat effect (app. -1.1 kcal per mole of propane), while total exothermal character bulk selective oxidation (27.9 kcal/mole) is caused by high enough heat effect of catalyst reoxidation stage (4) – ~ 29 kcal per mole of [V_2O_4]. At the same time both deep oxidation stages (2,3) has fairly expressed positive heat effect (equal to ~ 200 kcal/mole for both stages).

Simulation results

Fig.1 represents the movement of heat front during feeding of pure propane with elevated inlet temperature in the cold bed of preliminary oxidized catalyst. It is seen that (due to practically zero heat effect of target reaction (1)) the maximum temperature of the catalyst does not significantly exceeds the inlet gas temperature. In such conditions the observed average-per-cycle selectivity of propane conversion into propylene is significantly higher than in steady-state processes. In turn, reoxidation of the reduced catalyst by air also occurs at moderate maximum temperatures (not exceeding 400°C), therefore, the process may be realized without catalyst overheating even in case of using undiluted propane as feed.

Evidently, application of undiluted propane feed together with higher selectivity provide higher unit propylene (per catalyst unit volume) output, compared to steady-state processes, despite lower observed average conversion.

Among other process advantages (compared to steady-state processes) the following may be stated:

- higher propylene concentration in outlet gases and absence of diluents will simplify separation of product propylene;

- absence of direct contact between hydrocarbon flammable species and oxygen, impossibility of catalyst overheating will improve process safety;

- air may be used as oxidative agent instead of pure oxygen without decrease of process efficiency;

- low coke formation (due to moderate process temperatures) as well as efficient incineration of deposited coke during each reoxidation cycle may lead to higher lifetime of the catalyst.
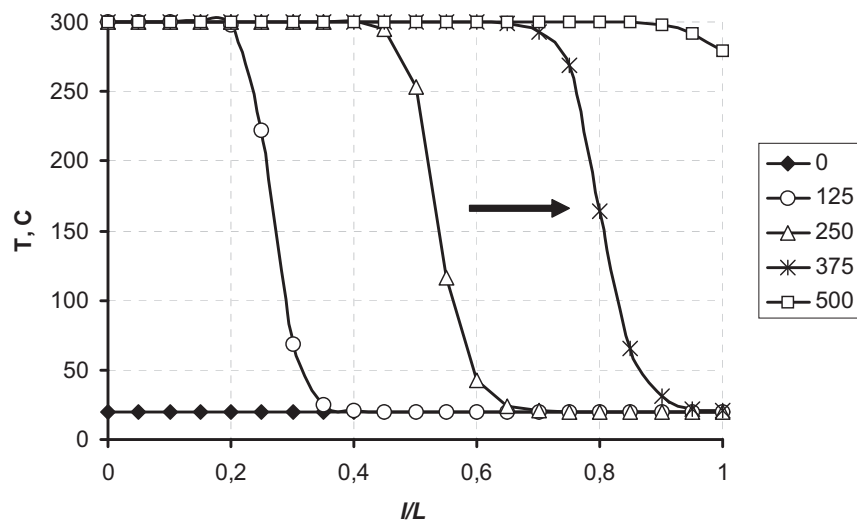
Fig. 1. *Temperature profiles vs catalyst bed length in different time points (time from cycle beginning is given at the right in seconds) under feeding of pure propane into oxidized catalyst bed. Conditions:*
$$c^{in}_{C3H8} = 1, c^{in}_{O2} = 0, \ T_{in}=300°C, \ T_{init}=20°C, \ \theta_{init}=1, \ L=1 \ m, \ u = 1 \ m/sec, \ a_{Max} = 20.8.$$
Gas filtration direction is shown by arrow.

References

1. Matros Yu.Sh. Catalytic Processes Under Unsteady-State Conditions, Elsevier Science Publishers, Amsterdam-New York, 1988.

2. P.L.Silveston. Composition modulation of catalytic reactors. Gordon and Breach Science Publishers, 1998.

3. D.Creaser et al. *App.Catal.A: General*, 187(1999), 147-160.

4. R.Grabowski, S.Pietrzyk et. al. *Appl.Catal.A: General*, 2002, 232, 277-288.

5. A.N.Zagoruiko. *Chemical Engineering Journal*, 2005, 107, 133-139.

NOVEL CATALYTIC PLASMA REACTOR FOR THE ABATEMENT OF DILUTED VOLATILE ORGANIC COMPOUNDS

Ch. Subrahmanyam, A. Renken and L. Kiwi-Minsker

Ecole Polytechnique Fédéral de Lausanne (LGRC-EPFL), CH-1015 Lausanne, Switzerland
Fax: +41-21- 693 31 90, subrahmanyam.challapalli@epfl.ch, lioubov.kiwi-minsker@epfl.ch

Abstract

The emission of industrial exhaust gases containing diluted Volatile Organic Compounds (VOCs) into the atmosphere is an important source of air pollution and an environmental concern. Abatement of VOCs needs highly efficient low cost processes. Conventional techniques for the abatement of VOCs mainly include thermal and thermo-catalytic oxidation. However, at low VOC concentrations (< 1000 ppm), these techniques are limited by the energy supply. Among the alternatives, non-thermal plasma (NTP) generated at atmospheric pressure is advantageous. The NTP selectively produces high energy electrons at ambient temperature without heating the flue gas. The NTP has been tested for the destruction of various VOCs, but the low selectivity (0.3 to 0.5) to total oxidation products (CO_2 and H_2O) limits the application. In order to improve the efficiency of NTP technique, plasma is often combined with a heterogeneous catalyst. In practice, the catalyst can be placed either in the discharge zone (in-plasma catalytic reactor) or after the discharge zone (post-plasma catalytic reactor). However, both reactors suffer due to the deactivation of the catalyst caused by carbonaceous deposits on the catalyst surface. Hence, novel reactors combining plasma with the catalytic action are needed. Present study deals with the design and performance of a novel dielectric barrier discharge (DBD) reactor for the destruction of VOCs. Influence the catalyst, voltage, frequency and energy input are studied for VOCs of different nature.

A novel DBD reactor with catalytic electrode is shown in Fig.1. The novelty is that the metallic catalyst made of sintered metal fibers (SMF) also serves as the inner electrode. The dielectric discharge was generated in a cylindrical quartz tube with a modified stainless steel filter (SMF) as the inner electrode. The SMF was doped by Mn and Co oxides. Typical discharge length was 10 cm and discharge gap was varied between 1.0 to 3.5 mm. The specific input energy (SIE) in the range 165-1650 J/l was applied by varying the AC high voltage (12.5-22.5 kV) and frequency (200-350 Hz). The V-Q Lissajous method was used to determine the discharge power (W) from which SIE was calculated. Destruction of model

VOCs (toluene, isopropanol (IPA) and trichloroethylene (TCE)) was carried out in the DBD reactor designed.
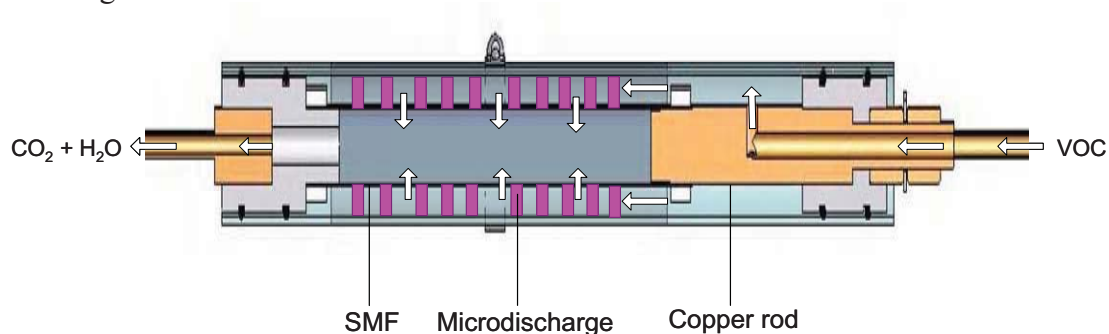
Fig. 1. Schematic representation of the novel DBD reactor

Typical results obtained show that under the same experimental conditions (discharge gap of 3.5 mm) MnOx and CoOx supported SMF electrodes shifted the product distribution towards total oxidation. At a fixed initial concentration of the VOCs, it has been observed that total oxidation of an alcohol (IPA) can be achieved at low SIE compared to an aromatic hydrocarbon (toluene) followed by chlorinated hydrocarbon (TCE). The optimized results with MnOx/ SMF electrode indicate that for 250 ppm of VOC, a SIE of 760 and 1650 J/l was required for the complete oxidation of IPA and toluene, respectively, whereas for TCE the selectivity to CO_2 was ~ 50 % even at 1650 J/l. The better performance of MnOx/ SMF might be due to the formation of active oxygen species by the in-situ decomposition of ozone on the catalyst surface. The selectivity to CO_2 during TCE destruction was further improved up to ~ 85 % at 650 J/l by modifying MnOx/SMF with TiO_2. The catalysts were characterized by different methods and the results will be presented in detail.

References

[1]. F. Holzer, U. Roland, F.D. Kopinke, Appl. Catal. B: Environmental 38 (2002)163.

[2]. B. Penetratnte, M.C. Hsiao, J.N. Bardsley, B.T. Merrit, G.E. Vogtlin, A. Kuthi, C.P. Burkhart, J.R. Bayless, Plasma Sources Sci. Technol. 6 (1997) 251.

[3]. S. Futamura, H. Einaga, H. Kabashima, L.Y. Jwan, Catal. Today 89 (2004) 89.

[4]. Ch. Subrahmanyam, M. Magureanu, A. Renken and L. Kiwi-Minsker, Appl. Catal. B: Environmental (in press).

SELECTIVITY OF OXIDATION PROCESSES IN FLUIDIZED BED REACTOR UNDER CATALYST UNSTEADY STATE

S.A. Pokrovskaya, M.G. Slinko*

Boreskov Institute of Catalysis SB RAS, Novosibirsk, pr. Akademika Lavrentieva, 5, Russia
**SPC "Karpov NIPCI", Voronzovo pole, 10, Moscow, Russia*
Phone: 007-3833-306278; fax: 007-3833-306878, E-mail: pokrov@catalysis.nsk.su

One of the specific features of heterogeneous catalytic processes in the reactors with fluidized bed is that catalyst particles move continuously in non-uniform field of gas concentrations. The concentrations of active species on the catalyst surface depend on the surrounding gas composition due to reaction stages and various physical processes on the surface and in the bulk of the crystalline lattice. The time scale required for attainment of steady state of the catalyst surface could be close or exceed the time scale of particles moving along the bed height. In this case, in spite of stationary operation conditions of fluidized bed reactor as a whole, the process is realized at unsteady coverage of the catalyst surface by reactive species with respect to reagent and product concentrations [1].

Under unsteady state of the catalyst the main process characteristics such as reagent conversion, selectivity to desired product, process productivity etc., could differ considerably from the ones for steady conditions. The studies illustrated the similar effects were fulfilled for the processes in the fixed catalyst bed with forced feed composition cycling. It was shown that such approach may provide enhancement of selectivity for a number of reaction systems [2,3,4]. But effects of unsteady state of the catalyst surface in fluidized bed reactors were studied only in a few works [1, 5, 6].

This work considers such effect on products selectivity in fluidized bed reactor (without inlet and outlet of catalyst particles) for the partial oxidation processes. At first the numerical simulation of the system behaviour is carried out for model kinetic scheme. Examples of the comparison of modeling and experimental results are discussed also for some processes of selective oxidation of hydrocarbons.

Mathematical model. The review of equation systems of material balance based on the kinetics with steady coverage of catalyst surface and used nowadays for process modeling in the reactor with fluidization regime is given in the publication of J. R. Grace with co-workers

[7]. To simulate the system behavior with catalyst unsteady state this mathematical description includes in addition the differential equation of the Focker-Plank type [1]. In studies presented below the simple two-phase model is applied to describe gas concentration profiles.

Model kinetic scheme. The simplified reaction scheme used for simulation contains two consecutive pathways of partial and deep oxidation: $A + \nu_1 B \rightarrow C$, $C + \nu_2 B \rightarrow D$, where is A – the reagent, B – the oxidant (oxygen), C – the desired product, D – the undesired product. These reactions were supposed to occur according the following steps:

a) $B + [\ ] \rightarrow [B]$ b) $A + \nu_1 [B] \rightarrow C + \nu_1 [\ ]$ c) $C + \nu_2 [B] \rightarrow D + \nu_2 [\ ]$

Catalytic step rates were in accordance with mass-action law assuming that activation energies may depend on the surface coverage [8].

Account runs were fulfilled using complete model, reflecting unsteady coverage of the catalyst surface, with variation of stoichiometric coefficients and step rate constants as functions of the fraction of surface oxidized sites. To reveal the effect of unsteady catalyst state, the results were compared with the data simulated for the steady coverage of the catalyst surface. For the second stage, as usually, the surface oxidant concentration was taken to be stationary with respect to gas concentrations and excluded from kinetics, all other parameters were the same. Summarizing results it is possible to choose three types of effects for studied system:

– Catalytic step rates are linearly dependent on surface oxidant concentration. Unsteady and steady catalyst state in fluidized bed lead to the same output yield of desired product C.

– The dependence is not linear, selectivity rises with the increase of the fraction of oxidized active sites. Process selectivity in the reactor declines because of more reduced unsteady state of the catalyst surface.

– Selectivity increases with the growth of the fraction of reduced surface sites. Unsteady surface coverage results in the rise of process selectivity and output yield of purposeful product C.

Thus, due to integral unsteady state of the catalyst the selectivity to purposeful product in the fluidized bed reactor might be considerably lower or higher as compared to that for corresponding stationary state. The state of the catalyst in the fluidized bed could be one of the main factors governing the product selectivity. The examples of such effects are given below.

Effect of unsteady state for the selective oxidation processes. Numerical simulation of three processes of selective oxidation of hydrocarbons was carried out comparing with the experimental results of laboratory and pilot setups with fluidized bed reactor.

Propylene oxidation to acrolein and acrylic acid

The process was realized on Co/Mo/Te/P catalyst in the pilot fluidized bed reactor. 11-12% decrease of the yield of acrolein and acrylic acid was obtained in comparison with the data simulated on the basis of stationary kinetic model.

Modeling has shown that the product selectivity decrease takes place as a result of mass transfer between a dense and bubble phase, by about 1-2%, and as a result of unsteady state of the catalyst, by about 10%. The special comparison experiments in laboratory reactors with a fixed and fluidized bed have confirmed these results. At studied operation conditions the catalyst surface was found to be more reduced in the fluidized bed reactor than one of the reactor with the fixed bed.

Propylene ammoxidation to acrylonitrile

The transient experiments obtained on 8-component catalyst (C-41 type) showed that the reduction of catalyst surface results in an increase of the selectivity to acrylonitrile. In the fluidized bed reactor, the state of the catalyst surface depends on the ratio of inlet concentration of ammonia to oxygen one. The optimal conditions were found by simulation to exclude unsteady state of the catalyst with a high degree of oxygen coverage and to provide maximum selectivity to acrylonitrile. The experiments in the pilot reactor confirmed the modeling results to demonstrate the 3-4% increase of the acrylonitrile selectivity.

O-xylene oxidation to phthalic anhydride

The simulation has been carried out based on the dynamic kinetic model. Quantitative estimations of surface species on V-Ti-O catalyst were received for the process in the fluidized bed reactor. Reactor modeling was performed for isothermal and nonisothermal fluidization regimes and for such regimes to assume steady catalyst state. Simulation results were in an agreement with experiments carried out in the lab fluidized bed reactor by A.A. Ivanov with co-workers [5].

At studied operation conditions the process occurs with unsteady state of the catalyst. This state generated for isothermal conditions results in significant decrease of phthalic anhydride selectivity in the reactor. The selectivity loweres by 6-8 % in comparison with one simulated with stationary kinetics. Conditions to form the unsteady selective state of the catalyst with the high yield of phthalic anhydride have been specified. In nonisothermal

regime the alteration of catalyst state takes place in comparison with isothermal conditions and phthalic anhydride yield increases by about 20%.

References

1. Slinko M.G., Pokrovskaya S.A., Sheplev V.S., *Dokl.AN SSSR.,* 221 (1975) 157-161; 244 (1979) 669-673.

2. Yu.Sh. Matros, Catalytic Processes Under Unsteady-State Conditions, Elsevier Science Publishers, Amsterdam,1988.

3. P.L. Silveston, Composition Modulation of Catalytic Reactors, Gordon and Breach Science Publishers, 1998.

4. A.N. Zagoruiko, Chemical Engineering Journal, 107 (2005) 133-139.

5. A.A. Ivanov and B.S. Balzhinimaev, In *Proceedings of the International Conference "Unsteady State Processes in Catalysis"* (1990) 91-113, Utrecht, The Netherlands, Tokyo, Japan: VSP.

6. Reshetnikov S.I., Balzhinimaev B.S., Gaevoi V.P., Ivanov A.A., Chemical Engineering Journal, 60 (1995) 131-139.

7. H.T.Bi, N.Ellis, I.A.Abba, J.R.Grace, CES, 55 (2000) 4789-4825.

8. A. Renken, In *Proceedings of the International Conference "Unsteady State Processes in Catalysis"* (1990) 183-203, Utrecht, The Netherlands, Tokyo, Japan: VSP.

MATHEMATICAL MODELING AND EXPERIMENTAL STUDY
OF HIGH PRESSURE ETHYLENE POLYMERIZATION REACTORS

A.M. Saveljev*, <u>Ju.N. Kondratjev</u>*, A.E. Sofiev*, S.S. Ivanchev**

*Central R&D Institute for Complex Automation

8, Mozhaisky Val, Moscow, Russia

fax: +7 (495) 2404206, e-mail: AMSAVELIEV@mtu-net.ru

**St-Petersburg Department of the Boreskov Institute of Catalysis SB RAS

14, prospect Dobrolubova, 197198, St-Petersburg, Russia

fax: +7 812 2330002, e-mail: ivanchev@SM2270.spb.edu

Mathematical models and experimental data are discussed for high pressure ethylene polymerizations in stirred tank and tubular reactors. The model is based on free radical mechanism of ethylene polymerization using material and energy balance equations as well as impact balance (for tubular reactors).

A stirred tank reactor is modeled taking into account mixing modes in the reactor on the basis of the segregation approach. Models for single- and double-zone stirred tank reactors are considered upon the comparison of the relating calculations with experimental data obtained using commercial polymerization reactors. The developed mathematical model was used to study the stability of stirred tank reactors and determine the range of the process parameters corresponding to their sustainable functioning. The possibility and conditions responsible for arising of bifurcation modes in the reactor at certain process parameters as well as the effect of the initiation and mixing modes upon the stable functioning ranges are theoretically revealed and experimentally confirmed.

The experimental data show that at the temperature increase in the top cross-section of the reactor (S1) due to the control of the initiator amount supplied in this zone the temperature growth profile in the next cross-section (S2) gradually drops and the polymerization zone continuously shifts towards S1. This phenomenon is accompanied by the decrease of the polymer molecular weight and initiator efficiency (Fig. 1, 2).
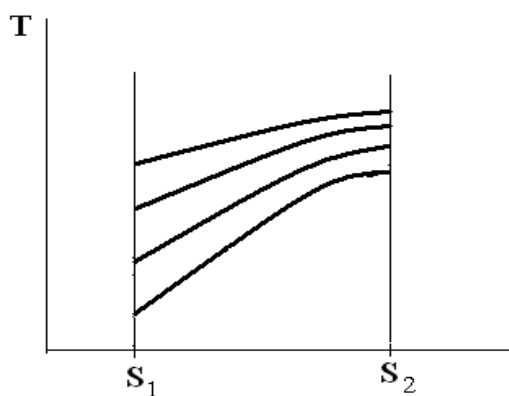
Figure 1. Temperature profiles in S1 and S2 cross-sections at temperature increase in S1
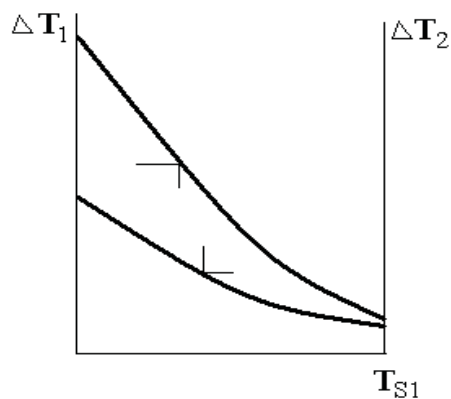
Figure 2. Temperature gradient in two cross-sections at temperature increase in S1

Industrial stirred tank reactors operate in a nearly adiabatic mode with the ratio $G*C_p/KF > 5$ and the temperature difference between the cross-sections S2 and S1 ($T_{s2} - T_{s1}$) being always positive. всегда положительна. ($G*$, C_p are the reaction medium mass flow and heat capacity accordingly and K, F are the heat transfer constant and surface area in the stirred tank reactor). However, for a pilot stirred tank installation at $G*C_p/KF \sim 0.5$ the temperature growth in the cross-section S1 leads to negative values of the temperature gradient between these cross-sections confirming the process shift towards S1.

At reduced temperatures in S1 zone for a certain initiator the process temperature should be controlled on the basis of the temperatures in this cross-section while at higher S1 temperatures the control can be based on the levels for either S1 or S2. The further increase of S1 temperature with S2-S1 temperature gradient approaching zero is undesirable in view of a high risk of the process thermal stability loss.

The considered changes in the polymerization behavior are qualitatively intrinsic to all the applied initiators, however a certain initiator type affects the temperature gradient value in S1 cross-section. For Trigonox-36 the low temperature level is 170-175°C whereas for Trigonox-42 this value is about 215°C.

For a multi-zone tubular reactor the mathematical model is based on the plug-flow admission and the following aspects are presented and discussed:

- calculation results and experimental data for a series of commercial ethylene polymerization reactors;

- recommendations for the selection of optimum technological conditions and modes for the exploration of such reactors as well as for their geometric (length, number of zones and their diameters) and heat exchange system design.

180

The adequacy of the developed mathematical models was tested using experimental data obtained for various commercial tubular polyethylene production reactors. First the sensitivity towards the main process parameters was analyzed followed by the determination of criteria to the experimental data. The studies were carried out relating to industrial high pressure reactors with a merely peroxide (stirred tank and tubular reactors), oxygen and complex (tubular reactors) initiation.

The results of mathematical modeling for a double-zone tubular reactor with different initiating systems are shown in Fig. 3 and fitting of the calculated and experimental temperature profiles are illustrated in Fig. 4. The theoretically expected and measured data for the initiator consumption, temperature profiles and process control parameters are found to be in a good agreement.
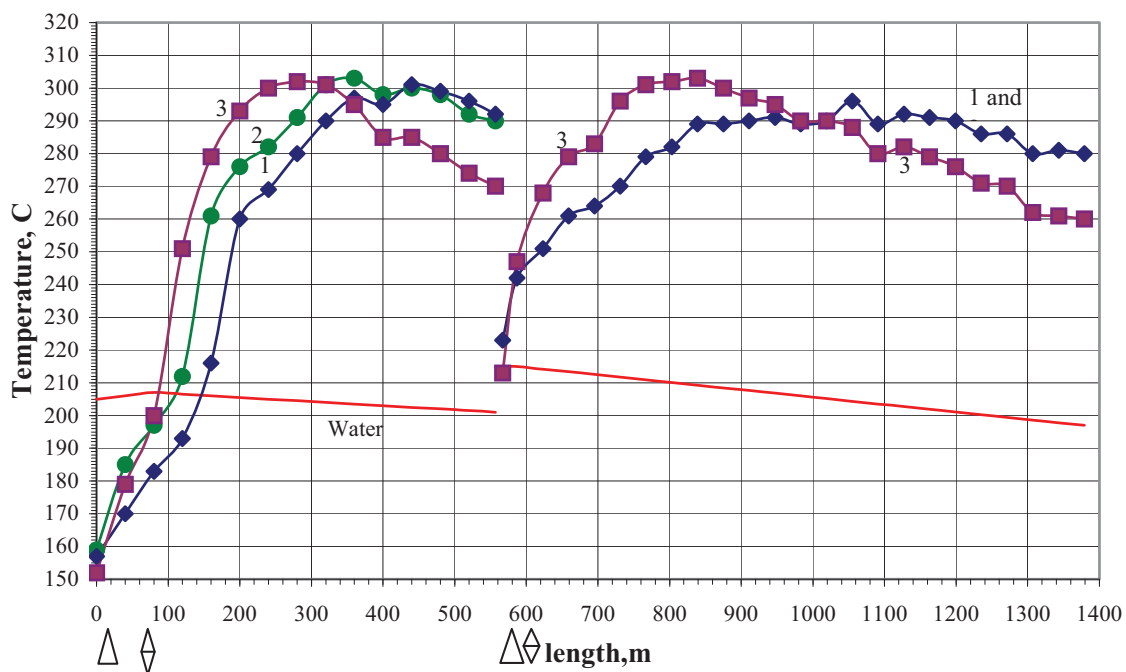
Figure 3. Temperature profiles in a double-zone tubular reactor with different initiating systems

1 – oxygen initiation in both zones;

2 – first zone: oxygem + Trigonox-36 (1.9 kg/h), second zone: oxygen;

3 – first zone: oxygen + Trigonox-36 (1.3 kg/h)+Trigonox-C (0.52 kg/h), second zone: oxygen + Trigonox-C (1.9 kg/h). Conversion growth up to 23 %.

△ - initiator solution input points; ◇ - control points.
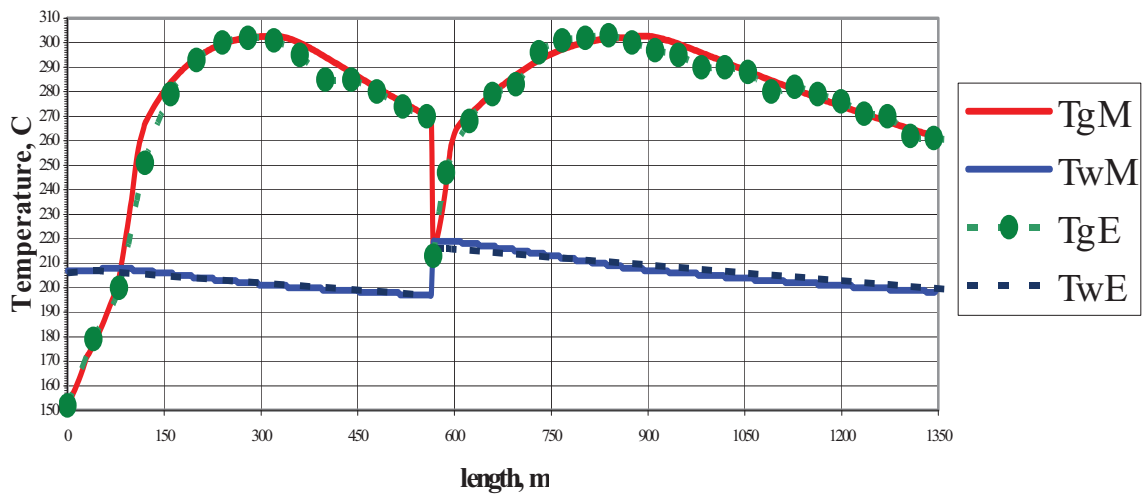
Figure 4. Comparison of experimental and modelling data.

Experiment: PE=10.9tons/h; first zone - Tr-36+Tr-C+O_2 (26+15.4+54.6) ppm;

second zone - Tr-C+O_2 (28+14.1) ppm

Modeling: PE=11.045 tons/h; first zone – Tr-36+Tr-C+O_2 (26+15.4+10.7) ppm;

second zone – Tr-C+O_2 (30.2+4.33) ppm

MODELING AND SIMULATION OF THE DIMETHYL CARBONATE (DMC) SYNTHESIS PROCESS IN REACTIVE DISTILLATION REACTOR WITH A NONEQUILIBRIUM MODEL

Feng Wang[1, 2], Ning Zhao[1], Junping Li[1], Wei Wei[1], <u>Yuhan Sun</u>[1,*]

[1] *State Key Laboratory of Coal Conversion, Institute of Coal Chemistry, Chinese Academy of Sciences, Taiyuan, 030001, P R China;*

[2] *Graduate School of the Chinese Academy of Sciences, Beijing, 100039, China*

* Corresponding author, e-mail yhsun@sxicc.ac.cn, fax +86 351 4041153

Dimethyl carbonate (DMC) has drawn considerable attentions as it is considered as an environmentally benign building block and has wide usage in chemical industry. It may be used as methylation reagent to substitute extremely toxic dimethyl sulfate or as carbonylation reagent for replacing phosgene [1-3]. However, the current routes of the DMC synthesis suffer from some drawbacks, such as using of poisonous and/or corrosive gases of chlorine, nitrogen oxides and carbomonoxide and bearing the possibility of explosion. Recently, a novel process for the synthesis of DMC from urea and methanol over heterogeneous solid bases catalyst has been presented and successfully carried out in packed reactive distillation at bench and pilot scale[1].

The packed reactive distillation (RD), a kind of reactive distillation, which combine a chemical reaction and distillation in a single unit, has become more important in the chemical processing industry for it can provide many advantages, such as high product conversion and selectivity, energy saving, simpler operation, overcoming of the azeotropic limitations and prolonging the catalyst lifetime[4]. Its application in chemical industry has increased rapidly in recent year. Up to now, a quite number of publications on nonequilibrium models have been presented on investigation of the performance of the RD.

In this work, a nonequilibrium model has been developed for the packed RD process of the DMC synthesis by urea methanolysis method over heterogeneous solid bases catalyst, which has been operated in the pilot scale. The mass and heat transfer between the vapor and liquid

surface is taken into account based on the Maxwell-Stefan theory. The heterogeneous reaction in the DMC synthesis process is considered as a pseudo-homogeneous description, so the total amount of the catalyst presented in the RD is the necessary parameter to meet the need of the chemical reactions [5]. The mathematical model has been solved by discretizing the differential equations along the spatial dimension using a high order finite-differential approach [6].

The synthesis of DMC from urea and methanol was considered to be a two-step reaction (shown as following). The intermediate methyl carbomate (MC) was produced with high yield in the first step and further converted to DMC by reaction with methanol in the second step. It was also found that the first step is much easier than the second step which might take place even without catalyst[1]. As a result, the first reaction of the DMC synthesis has been omitted in the kinetics model.

$$H_2N-CO-NH_2 + CH_3OH \longrightarrow H_3CO-CO-NH_2 + NH_3 \tag{1}$$

$$H_3CO-CO-NH_2 + CH_3OH \longrightarrow H_3CO-CO-OCH_3 + NH_3 \tag{2}$$
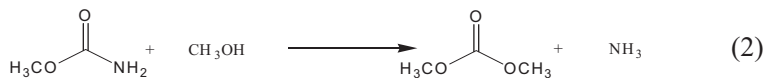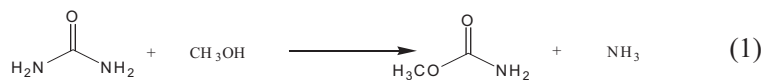
As can be seen from Eqs. (1) and Eqs. (2), the reaction system includes a light component ammonia and a binary azeotrope methanol-DMC. Considering the system nonideality, the Wilson model for the liquid activity and the Virial function for the gas fugacity are used to calculate the vapor-liquid equilibrium.

As a result, the following assumptions are made for the NEQ model:

(1) The process reaches steady state;

(2) The first reaction is omitted as the first step may be take place in the preheater without catalyst.

(3) The reactions take place entirely in the liquid bulk.

(4) The heat effect of the reaction is omitted in the model.

(5) Total mixing for liquid bulk.

(6) Vapor-liquid equilibrium occurs at the vapor-liquid interface and in the condenser and the reboiler.

(7) The reactions are considered to be pseudo-homogeneous.

(8) The pressure drop per meter along the RD column is considered as constant.

The nonequilibrium differential model equations are described below:

Material balance is defined as:

$$-\frac{dl_i}{dz} + f_i^L + R_i + N_i^L = 0 \tag{3}$$

$$\frac{dv_i}{dz} + f_i^V - N_i^V = 0 \tag{4}$$

The energy balance is defined as:

$$-\frac{d(LH^L)}{dz} + F^L H^L + e^L + Q = 0 \tag{5}$$

$$\frac{d(VH^V)}{dz} + F^V H^V - e^V + Q = 0 \tag{6}$$

where the vapor and liquid energy transfer rate is considered as equal. The vapor heat transfer rate is defined as:

$$e^V = -h^V a \frac{\partial T^V}{\partial \eta} + \sum_{i=1}^{C} N_i^V H^V \tag{7}$$

Vapor-liquid equilibrium occurs at the vapor-liquid interface:

$$y_i^I - K_i^I x_i^I = 0 \tag{8}$$

The equilibrium constant is computed by

$$K_i^I = \frac{P_i^0 \gamma_i f_i^0}{P f_i} \tag{9}$$

The mathematical model is discretized along the spatial dimension of the packed reactive distillation using a high order finite-differential approach to generate the differential-algebraic equations [6].

The simulated column is configured with two feeding inlets and a side outlet, two preheaters for each feeding inltet, in which the first step reaction of the DMC synthesis occur. The catalyst pellets are randomly packed in the reaction section. As for releasing the noncondensing gas of ammonia, the distillation has configured a partial condenser.

The process for the DMC synthesis has been operated at the pressure of 10-16 atm. and the

reactions took place at the temperature of 420-450 K. The mixture of urea and methanol and the pure methanol were fed to the RD respectively and the product was sampled from the side outlet. Based on the nonequilibrium model, the catalytic feasibility, effects of the feed locations of the reactants, the strong interaction of the components and the mass transfer in the packed RD column has been investigated. The predicted result was in accordance with the experiment data.

Conclusion: In this work, a nonequilibrium model of the packed reactive distillation has been carried out to investigate the process for the synthesis of DMC from urea and methanol by using solid base as catalyst. As the process includes a binary azeotrope, the reactive distillation has shown its advantages on the synthesis of the DMC and the product separation.

Notation

a	efficient interface area, m^2/m^3
e^l, e^v	liquid and vapor heat transfer rate, J/s
f_i^L, f_i^V	liquid and vapor feed of component i, mol/s
F^L, F^V	liquid and vapor feed, mol/s
h	heat transfer coefficient, $J\ m^{-2}s^{-1}K^{-1}$
H^L	liquid enthalpy, J/mol
H^V	vapor enthalpy, J/mol
K_i^I	equilibrium ratio
l_i	liquid flux of component i, mol/s
N_i^L, N_i^V	vapor and vapor mass transfer rate of component i, mol/s
P	pressure, kPa
P_i^0	vapor pressure of component i, kPa
Q	heat duty, J/s
T	absolute temperature, K
v_i	vapor flux of component i, mol/s
x	liquid composition, molar fraction
y	vapor composition, molar fraction

References

[1] W. Mouhua, W. Hui, Z. Ning, Catal. Comm. 7 (2005) 6.

[2] A.G. Shaikh, S. Sivaram, Chem. Rev. 96 (1996) 951.

[3] P. Tundo, M. Selva, Chemtech. 25 (5) (1995) 31.

[4] L. Huping, X. Wende, Chem. Eng. Sci. 56 (2001) 406.

[5] Higler, A, Taylor, R., & Krishna, R. Comput. Chem. Eng. 22 (1998) 113.

[6] Sebastien Lextrait, R. Bruce Eldridge, Ind. Eng. Chem. Res. 43(2004) 3860.

CITRAL HYDROGENATION OVER DIFFERENT ZEOLITES AND MCM-41 SUPPORTED Ni AND Ni-Sn CATALYSTS

Hilal Gülec[1], <u>Selahatttin Yilmaz</u>[1], Levent Artok[2]

[1] *Department of Chemical Engineering,* [2]*Department of Chemistry,*
İzmir Insitute of Technology, Gülbahçe Köyü, Urla,İzmir, Fax:00-90-232-7506645,
e-mail:selahattinyilmaz@iyte.edu.tr

1. INTRODUCTION

The selective hydrogenation of α-β unsaturated aldehydes is a difficult challenge since the C=C bond is much easily attacked then the C=O bond when a conventional heterogeneous catalysts used. Therefore, many efforts have been made to develop a suitable industrial catalyst that would be able to lead to the hydrogenation of C=O bond to get unsaturated alcohols. Citral hydrogenation was performed over noble metals (Pt, Rh, Ru, Pd and Ni) on different supports [1-5] over bimetallic catalysts such as Ni-Cu [5], Ru-Fe [3] and Ru-Sn [7,8] and over basic catalysts [9]. These studies showed that modification of the metal properties by promoter increased selectivity to unsaturated alcohols (nerol, geraniol, citronellol) and the support also affected the product distribution. Electronic effects and geometric effects have been suggested as explantaion for the improvement in the selectivity to unsaturated alcohols.

Zeolite supports induce the possibility of metal support interactions: active metals can be polarized by nearby cations or by metal support interaction [10]. Zeolite supported monometallic catalysts were tested in citral hydrogenation recently [4,5]. Maki-Arwela et al[2003] reported that the Ni supported on H or NH_4 forms of Y zeolite catalysts gave lower selectivities (<5%) and this was attributed to the presence of acid sites in the zeolite. However, in our study [5] Pd supported on clinoptiolite rich natural zeolite, the major product was citronellal (90 % selectivity). Further research is needed to determine the role of zeolite supports in citral hydrogenation reaction.

In the present study, monometalic (Ni) and bimetallic (Ni-Sn) catalysts supported on Na-Y, Na-Beta, Na-Mordenite (Na-MOR) and MCM-41 and clinoptilolite rich natural zeolite (CLINO) were prepared, characterized and tested in citral hydrogenation.

2. EXPERIMENTAL STUDY

2.1. Preparation of Catalysts

Clinoptilolite rich natural zeolites (Gördes-Manisa, Turkey) [4], Na-MOR (Süd-Chemie, MOR powder), Na-Y (Zeolyst, CBV100), and Na-β (Süd-Chemie, BEA powder) were calcined at 500 ^{o}C under N_2 flow (100 ml/min) for 5 h in a tubular reactor. MCM-41 was synthesised according to a method given literature[11] It was calcined at 560 ^{o}C with 1.5 ^{o}C/min heating rate for 6 h in order to remove the template.

Monometallic Ni catalysts were prepared by impregnation method from a ethanolic solution of 0.01 M Ni(NO$_3$)$_2$.6H$_2$O. Bimetallic catalysts were prepared by coimpregnation method. The Ni loading of the catalysts were kept constant (10 wt %) while the Sn/(Sn+Ni) mole ratio was 0.2. For this catalyst, the ethanolic solution of Ni(NO$_3$)$_2$.6H$_2$O and SnCl$_2$.2H$_2$O was used. The impregnated samples were dried at 120 ^{o}C overnight and then they were calcined at 500 ^{o}C under dry air (100 ml/min) for 5 h.

2.3 Catalyst Testing

Hydrogenation experiments were performed in a stirred, semibatch reactor (500 ml, 4574 model, Parr Instrument Co.). The catalysts (0.25 g for each test) were activated in situ. Citral (200 ml of 0.1 M citral in ethanol) was hydrogenated at 80 ^{o}C under 6 bar H_2 with a stirring rate of 600 rpm.The products formed were analyzed by a GC and were identified by GC-MS technique. The compositions of components in the reaction mixture were determined by internal standardization method.

3. RESULTS AND DISCUSSION

3.1. Catalyst Characterisation

Elemental and textural properties of supports, monometallic and bimetallic catalysts are given in Table 3.1. The Sn/Sn+Ni mol ratio of bimetallic catalysts are shown in brackets. The catalyst surface areas were found to decrease with the metal loading. This could be due to blockage and/or narrowing of some of the pores due to the loading.

SEM micrographs of zeolites showed that the morphologies of the samples were different. The crystallite sizes of Na-Y, Na-β, Na-MOR, MCM-41 and CLINO supports were around as 400 nm, 100 nm, 150 nm, 500 nm and 7 μm respectively. XRD diagrams showed that the structures of the support materials were preserved. The peak of Nickel Sin Alloy (Ni$_4$Sn) was also observed at $2\theta = 44.8$ ° for Na-Y and Na-MOR supported bimetallic catalysts.

Table 3.1. Properties maximum selectivities of UOL observed with the corresponding conversion and for the different catalysts tested.

Catalysts	Ni (wt %)	Sn (wt%)	Si/Al	BET Area (m^2/g)	V_p (cm^3/g)	X^1 (%)	$S_{UOL}{}^2$ (%)
Na-Y	-	-	2.6	886.1	0.463	-	-
Ni/Na-Y	8.2	-	2.6	785.7	0.404	57.6	1.5
Ni-Sn/Na-Y (0.2)	8.1	4.1	2.6	703.0	0.324	10.3	27.4
Na-β	-	-	12.4	558.8	0.413	-	-
Ni/Na-β	8.2	-	12.4	549.2	0.350	-	0.0
Ni-Sn/Na-β (0.2)	8.1	4.2	12.4	515.8	0.297	18.1	29.7
Na-MOR	-	-	9.0	390.2	0.233	-	-
Ni/Na-MOR	8.8	-	9.0	394.7	0.182	-	0
Ni-Sn/Na-MOR(0.2)	8.1	3.87	9.0	348.2	0.138	26.6	35.5
MCM-41	-	-	-	1449.0	0.866	-	-
Ni/MCM-41	8.5	-	-	1074.2	0.596	29.8	24.8
Ni-Sn/ MCM-41(0.042)	9.2	0.83	-	970.7	0.564	37.4	16.9
CLINO	-	-	5.3	43.3	0.065	-	-
Ni/CLINO	9.0	-	5.3	38.6	0.055	37.6	13.4
Ni-Sn/CLINO(0.2)	8.5	4.6	5.3	34.1	0.050	26.7	17.1

1) conversion at maximum selectivity to UOL, 2) maximum UOL selectivity observed

3.2 Activity and Selectivity of the Catalysts

Citral hydrogenation reaction over monometallic and bimetallic catalysts gave variety of products, which were citronellal, citronellol, nerol, geraniol, isopulegol, 3,7-Dimethyl-1-octanol, menthols and acetals. Unsaturated alcohols nerol and geraniol were reffered to as UOL in the text. The maximum selectivities to UOL observed for different catalysts with corresponding conversions are given in Table 2.

The major product over all monometallic catalysts and bimetallic catalysts was citronellal except for Ni/Na-β catalyst, which gave acetal as the main product. The product distribution was affected by the different supports. The acetal formation is related to presence of acid sites [5]. The high silica to alumina ratio of Na-β (compared to other supports) together with its smallest crystallite and irreqular morphology might be the reason for the acetal formation. Among the monometalic catalysts, geraniol and nerol formed only Ni/Na-Y, Ni-MCM-41 and Ni/CLINO. Their amounts were initially high and dropped with reaction time. The maximum selectivity to UOL was observed with Ni-MCM-41 (24.8%).

Monometallic catalysts showed high activity (conversions> 90 %) over the whole reaction time (300 min). Ni/Na-Y catalyst gave the highest conversion among the catalyst giving desired products. This could be related to its high surface area and its Al content compared to other catalysts.

The addition of Sn affected monometallic catalyst product distributions and activities differently. Selectivity to UOL significantly increased over Ni-Sn/Na-MOR (from 0 to 35.5 %), Ni-Sn/Na-Y (from 1.5 to 27.4 %) and Ni-Sn/Na-Beta (from 0 to 29.7)%. S_{UOL} was a little improved over Ni-Sn/CLINO. However, an unexpected trend was observed with Ni-Sn/MCM-41 for which S_{UOL} decreased by 1/3. The significant increase in the S_{UOL} was observed over the catlayst having Ni-Sn alloy formation. Probably these sites were responsible for enhance UOL formation [7,8]. Amount of acetal formation was also lowered with bimetallic catalysts. This implied that some of the active acid sites and metal sites were covered by the promoter. As a result asetal formation decreased

The activity of catalysts dropped with promoter addition except Ni-Sn/MCM-41, this was the catalyst for which Sn addition decreased S_{UOL}. This was the only catalyst that did not contain Al. The reason for the increase in activity was not clear. This awaits further invetigation.

5. REFERENCES

1. Armendia M. A., Borau, V., Jimenez, C., Marinas, J.M., Porras, A., Urbano F.J., J.Catal, 172 (1997) 46.

2. Singh U.K.and Vannice M.A., J. Catal. 189(2001)

3. Baeza, B.B., Guerrero-Ruiz, A., Wang, P. and Rodríguez-Ramos, I. Guerrero-Ruiz, A., App. Catal. A:Gen, 205(2001)227.

4. Yılmaz, S., Ucar, Ş., Artok, L., Güleç, H., App. Catal. A:Gen., 2005.

5. Mäki-Arvela, P., Tiainen, L.-P., Lindblad, M., Demirkan, K., Kumar, N., Sjöholm, R., Ollonqvist, T., Väyrynen, J., Salmi, T. and Murzin, D.Yu. , App. Catal. A:Gen., 241(2003)271.

6. Baeza, B.B., Guerrero-Ruiz, A., Wang, P. and Rodríguez, I. J. Catal., 204(2001)450.

7. Silva, A.M., Santos, O.A.A., Mendes, M.J., Jordão, E. and Fraga, M.A. App. Catal. A:Gen.,.241 (2003.)155.

8. Coupé, J.N., Jordão, E., Fraga, M.A. and Mendes, M.J. , App. Catal. A:Gen 199(2000)45.

9. Armendia M. A., Borau, V., Jimenez, C., Marinas, J.M., Ruiz J.R, A., Urbano F.J., J. Mol. Catal. A.171 (12001)153.

10. A.P. Jansen, R.A. van Santen, J. Phys. Chem 94 (1990)67.

11. Lin, H.P., Cheng, S. and Mou, C.Y. 2002. Microporous Matter. p. 10-11.

A TWO DIMENSIONAL STEADY-STATE MODEL OF THE GAS-SOLID-SOLID REACTOR. EXAMPLE OF THE PARTIAL OXIDATION OF METHANE TO METHANOL

Dallos C.G., Kafarov V., Maciel R.*

Universidad Industrial de Santander, Bucaramanga, Colombia
*Estadual de Campinas, Campinas-sp, Brazil

Partial oxidation of methane

The partial oxidation of methane to methanol has considerable potential for the utilization of vast natural gas fields in remote areas of the world. This process would not only be easier to of transport, but also increases the range of subsequent applications for further processing. The number of recent publications in this area reflects renewed interest in this reaction as an alternative to the two-stage steam reforming route to methanol [1-4]. The partial oxidation reaction is, potentially, a simpler and more energy-efficient process than the steam-reforming route, but in spite of the effort of investigators, no catalyst has been obtained to achieve desired levels of selectivity and conversion to take this process at industrial practice.

The gas-solid-solid reactor

Bearing this in mind, this work focuses in the way to increase the conversion of reversible reactions in a special kind of multifunctional reactors [5-7]: the gas-solid-solid reactors. In this reactor, a mixture of gaseous reactants is fed at the bottom of the packed column. The solid packing contains catalyst pellets. Another solid material, a selective product adsorbent, is fed at the top of the column and trickles down over the packing. The solids stream adsorbs the product immediately after it has been released from the catalyst surface. The reaction product therefore leaves the reactor in the adsorbed state at the lower end of the reactor. The unconverted reactants leave the reactor at the top, together with the non-adsorbed fraction of the product formed. With such design the reaction rates are not hampered by a reversed reaction and remain high. In this way, higher conversions and reaction rates can be expected. It may be possible even to find out operation conditions so that almost complete conversion can be achieved, so that the recycling is no longer necessary. This necessarily will result in considerable investment and operating costs savings.

OP-3-23

Model of the reactor

In this work this concept of reactor design is explored. A two dimensional steady-state model for the reactor is developed based on the mass and energy balance. The model was solved numerically through the finite difference method with software written in FORTRAN 90 with the NAG routines. The influence of the process parameters on the behavior of the reactor is discussed. The model was applied to the case of methanol synthesis directly from methane over ferric molybdate [8-9], with an amorphous silica-alumina powder as the methanol adsorbent [10]. The concentration of the adsorbed methanol was optimized at the exit of the reactor using as decision variables the feed relationship CH_4/O_2 and the supply rate of adsorbent. The results show that this reactor, in principle, must be cable to lead to high conversions of the feed gas to product in spite of unfavorable equilibrium.

On the basis of the results of this study, we conclude that a gas-solid-solid reactor offers a very attractive alternative to today's processes based on catalytic equilibrium reactions and deserves further evaluation in a pilot plant.

References

1. K. Otsuka, Y. Wang, Applied Catalysis A: General 222 (2001) 145
2. Q. Zhang et al, Fuel 81 (2002) 1599
3. T. Takemoto et al., Journal of Molecular Catalysis A: Chemical 179 (2002) 279
4. X. Wang et al., Journal of Catalysis 217 (2003) 457
5. K.R. Westerterp, Chemical Engineering Science 47 (1992) 2195
6. L.V. Barysheva et al., Chemical Engineering Journal 91 (2003) 219
7. N. Nikacevic and A. Dudukovic, Ind. Eng. Chem. Res. 44 (2005) 6509
8. A. Chellappa and D. Viswanath, Ind. Eng. Chem. Res. 34 (1995) 1933
9. A. Chellappa University of Missouri-Columbia, Doctoral Thesis (1997)
10. M. Kuczynski, A. van Ooteghem and K. R. Westerterp, Colloid Polymer Sci. 264 (1986) 362

SYNERGETIC USE OF HETEROGENEOUS PHOTOCATALYSIS AND CONSTRUCTED WETLANDS IN WASTEWATER TREATMENT: PRELIMINARY RESULTS OF COMPATIBILITY AND EFFECTIVENESS

A. Antoniadis[1], V. Takavakoglou[2], G. Zalidis[2], I. Poulios[1]

[1] *Laboratory of Physical Chemistry, Department of Chemistry,*

Aristotle University of Thessaloniki, 54124 Thessaloniki, Greece

[2] *Laboratory of Applied Soil Science, School of Agriculture,*

Aristotle University of Thessaloniki, 54124 Thessaloniki, Greece

Tel. +30 2310 997785, Fax. +30 2310 997709, e-mail: poulios@chem.auth.gr

Introduction

Wastewater has been recognized as one of the most important environmental pressures in Mediterranean region. The last decades centralized conventional wastewater treatment systems were typically provided to large cities and secondary towns. However, the establishment and operation of theses systems in the Mediterranean region have been costly and problematic (Ansola et al. 2003). As a result, the last decades several efforts have been made towards the development of alternative methods of wastewater treatment systems well established in the environmental and socioeconomic status of Mediterranean region. In order to fullfill the above mentioned expectations a low cost treatment system that is based on solar photocatalytic oxidation and natural processes has been developed. The system combines the synergetic action of the **heterogeneous photocatalytic oxidation** with the **surface flow constructed wetlands** in order to utilize the high solar irradiation (Malato et al. 2002) and the ability of the constructed wetlands to improve water quality through natural processes (Kadlec and Knight 1996). Comparing to conventional systems of wastewater treatment, the main advantages of the combined system are:

- Low cost of establishment and operation
- Ability to treat wastewater with great variability of hydraulic and pollutants load.
- Low requirements in chemicals and energy and utilization of solar energy and natural processes
- No need for additional disinfection method.

- Wastewater reuse opportunities

Aim of this work is to present the preliminary results regarding the compatibility of the two methods (heterogeneous photocatalysis/constructed wetlands) and the effectiveness of the combined system.

Materials and Methods

Experiments were conducted at laboratory scale using of both synthetic (OECD 1999) and cesspool wastewater. Each experiment consisted of two phases. In the first phase the wastewater was treated by using heterogeneous photocatalytic method, and the final effluent was channeled into surface flow constructed wetlands for the final purification. The photocatalytic treatment was tested using both artificial and natural irradiation in a lab-scale reactor able to treat 12 liters wastewater. For the needs of the experiment 9 surface flow wetlands were constructed. The dimensions of each wetland were 60 cm × 30 cm × 50 cm, the hydraulic residence time was 6 days, and the hydraulic loading rate was 1,5 lit/day. As wetland substrate a mixture of sandyloam soil and zeolite (5:1) was used and all wetlands were planted with *Typha spp*. Dissolved Organic Carbon analysis was performed using a TOC analyser (Shimadzu, model 5000A).Chemical Oxygen Demand (COD) and phosphates were measured according to APHA-AWWA-WEF (1992). COD was determined by the COD micromethod, while phosphates by the use of a spectrophotometer Perkin-Elmer Lambda 3. Nitrates and ammonium were measured using a Merck RQ Plus Reflectometer.

Results and Discussion

Preliminary experiments using synthetic wastewater under artificial irradiation revealed that the heterogeneous photocatalytic oxidation led to a 77 % reduction of the organic load, while the constructed wetlands led to a 17 % reduction **(Figure 1)**. The concentrations of ammonium and nitrate ions were increased in the treatment process but the final outflow was below the disposal limits **(Figure 2)**. The concentration of phosphate ions was reduced by 71,56 % in total. Experiments using real cesspool wastewater under solar irradiation revealed a 98,46 % decrease of the organic load in total **(Figure 3)**. The concentrations of ammonium and phoshate ions were decreased by 95,6 % and 84,1 % respectively. Nitrates were increased in the treatment process but the final concentration in the outflow of the combined system was below the disposal limits **(Figure 4).**
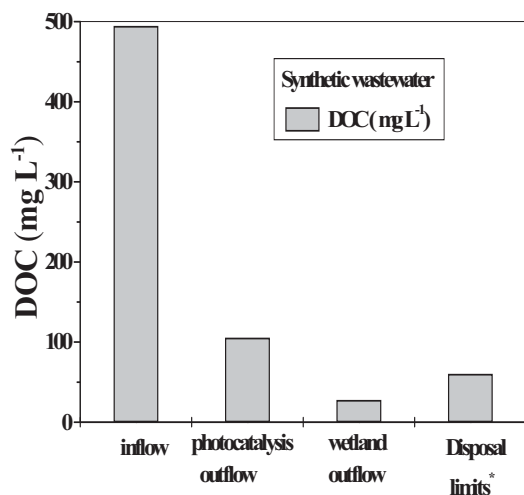
Figure 1. Organic load reduction of synthetic wastewater during the treatment phases of the combined system. (*limits set by Greek legislation PD/22374/91/94 for the disposal of the treated wastewater at Thermaikos Gulf)
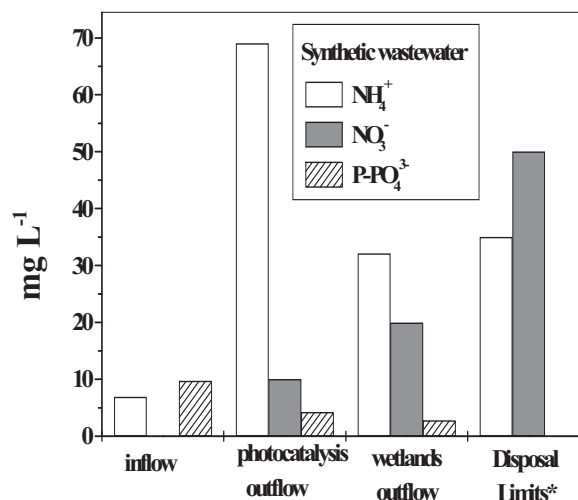
Figure 2. Nutrients concentration of synthetic wastewater during the treatment phases of the combined system.
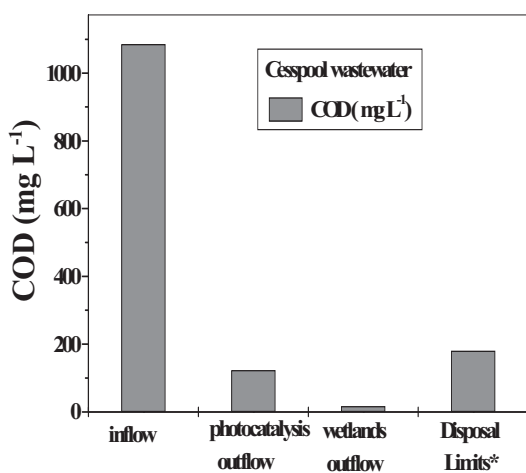
Figure 3. Organic load reduction of cesspool wastewater during the treatment phases of the combined system.
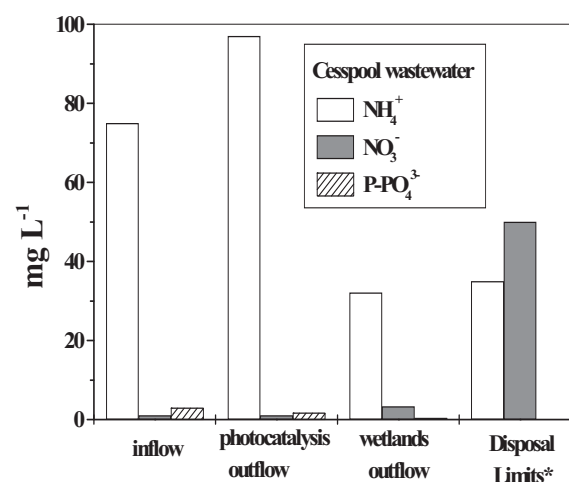
Figure 4. Nutrients concentration of cesspool wastewater during the treatment phases of the combined system.

Conclusions

The combined system effectively reduces the organic load and nutrients of both synthetic and cesspool wastewater. In all cases the quality of the outflows fulfilled the environmental legislative requirements in the region of Thessaloniki (Greece), where the system was tested.

The combination of homogeneous photocatalysis and constructed wetlands provides several advantages to each other, resulting in a flexible and operational system of wastewater treatment. The positive effects of Constructed Wetlands on Photocatalysis include: a) Reduction of treatment time, b) Reduction of the required amounts of chemical additives,

c) Lower cost of operation, d) Seasonal operation in touristic areas may effectively cope with peaks of hydraulic and pollutants load, and e) Reduction of nitrogen and phosphorous concentrations.

On the other hand the main positive effects of Photocatalysis on Constructed Wetlands include: a) Reduction of the required area, b) Lower cost of establishment, c) Elimination of clogging problems, d) Extension of operational lifetime, and e) Elimination of problems related to hard degradable substances (e.g. dyes, pesticides)

The preliminary results revealed that heterogeneous photocatalysis and constructed wetlands are compatible methods and their combination results in an effective treatment system for synthetic and cesspool wastewater. However further research is needed for the optimization of the system's performance and the operational evaluation at large scale.

References

1. Ansola G., J. M. González, R. Cortijo᾿ and Estanislao de Luis᾿ 2003. Experimental and full–scale pilot plant constructed wetlands for municipal wastewaters treatment. Ecological Engineering 21(1): 43-52

2. APHA-AWWA-WEF. 1992. Standard Methods for the Examination of Water and Wastewater. American Public Health Association, 18th edition, Washington D.C.

3. Kadlec, R.H. and R.L. Knight. 1996. Treatment wetlands. Lewis Publishers, CRC

4. Malato S., J. Blanco, A. Vidal, C. Richter. 2002. Photocatalysis with solar energy at a pilot-plant scale: an overview. Appl Catal B: Environ 37(1):1–15.

5. OECD. 1999. Guidelines for Testing of Chemicals,Simulation Test-Aerobic Sewage Treatment 303A.

Section 4.

Catalytic technologies in fuel and energy production

- ➤ *hydrogen production*
- ➤ *production of environmentally safe fuel*
- ➤ *environmentally friendly energetics*

SOLAR DRIVEN THERMOCHEMICAL REFRIGERATOR: AT THE INTERFACE BETWEEN CHEMICAL AND THERMAL ENGINEERING

Yu.I. Aristov[1], D. Chalaev[2], B. Dawoud[3], L.I. Heifets[4], O. Popel[5], G. Restuccia[6]

[1] *Boreskov Institute of Catalysis SB RAS, Pr. Lavrentieva, 5, Novosibirsk 630090, Russia fax: +7 383 330 9573, aristov@catalysis.nsk.su*

[2] *Institute of Engineering Thermophysics NASU, Bulahovsky str., 2, 03164 Kiev, Ukraine, fax: +380 44 424 31 77, trosh@imag.kiev.ua*

[3] *RWTH Aachen, Aachen, Germany*

[4] *Moscow Lomonosov State University, Moscow, Russia*

[5] *Institute of High Temperatures RAS, Izhorskaya str. 13/19, Moscow 125412, Russia fax: +7 495 484 2374, O_Popel@oivtran.iitp.ru*

[6] *Transformation and Storage of Energy CNR-ITAE, Santa Lucia sopra Contesse 5, 98126 Messina – Italy, fax: +39 090624247, giovanni.restuccia@itae.cnr.it*

This paper presents current activity of the six Institutes from the four countries on applying chemical reactions in modern devices for production of heat and cold, which are driven by solar energy. It is being performed within on-going project N 03-51-6260 "**Study of solar assisted adsorption cooling unit (SAACU) using new adsorbent materials"** supported by INTAS**.** The main objectives of the project are the development of new chemisorbents, belonging to a family of composite materials (known as Selective Water Sorbents, SWSs [1]), and the assessment of their utilization efficiency in a cooling thermochemical system driven by renewable energy sources, e.g. solar energy. The design of the chemisorption reactor and solar receiver in an integrated unit is also a paramount objective. A small experimental device is being under development.
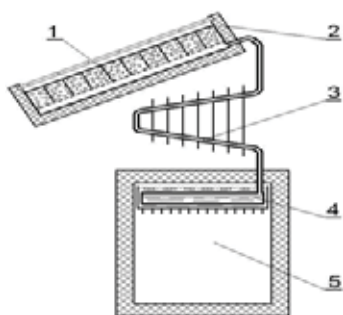
Fig. 1.
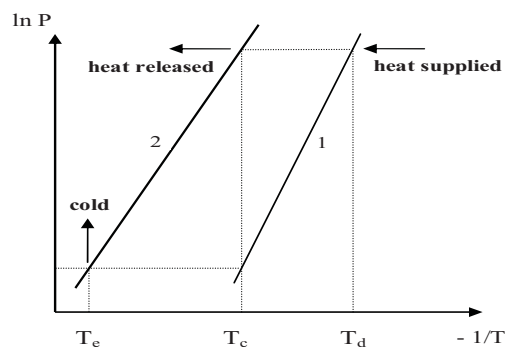
Fig. 2.

Solar cooling is one of one of the promising ways to transform solar heat for preservation of food and medicine, production of cold water and ice in arid areas, where other sources of energy are not available. A solar refrigerator consists of an adsorber 1 (Fig. 1), filled with solid sorbent and integrated with a flat solar receiver 2, a condenser 3 and an evaporator 4 integrated with an insulated cooling chamber 5 for food preservation.

An ideal cycle of thermochemical refrigerator includes two processes, namely, a monovariant vapour-solid chemical reaction S + G = G*S with the formation of non-volatile complex G*S (line 1 on Fig. 2) and, in simple version, an evaporation/condensation of pure vapour (line 2). The first process can be considered as a sorption of the vapour by the salt. Heat is consumed in the evaporator at T_e and released in the condenser at T_c, so that both cold and heat are produced. The cycle is driven by an external heat source, which causes the decomposition of complex G*S in chemical reactor (adsorber) at pressure Pc and temperature Td. First demonstration unit was realised by Michel Faraday in 1824 with a reaction between AgCl and NH_3 [2].

Sorption systems for heating and cooling based on chemical reactions are considered to be an alternative to vapour compression cycles using CFC's that are unacceptable any more according to the Montreal Protocol of 1988. One more reason concerns the effect of global warming (the Kyoto Protocol of 1997). Having zero Ozone Depletion and Global Warming Potentials, thermochemical systems are completely friendly for the environment, and their large scale dissemination requires searching new advanced chemical reactions, intensification of heat and mass transfer and improvement of interplay between chemical and thermal processes.
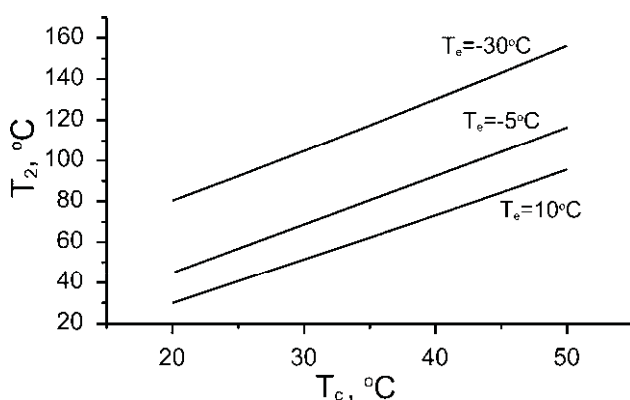
Fig. 3. Minimal decomposition temperature T_2 *vs.* T_c at various evaporator temperatures: deep freezing ($T_e = –30\ °C$), ice making ($T_e = –5\ °C$) and air conditioning ($T_e = 10\ °C$).

The new composites of SWS type (chemisorbents) have been described elsewhere [1, 3, 4], and here we focus on various aspects of chemical and thermal engineering of this advanced systems:

- thermodynamic criteria for choosing a chemical reaction proper for particular cooling cycle;
- thermodynamic, kinetic and thermal properties of new chemosorbents,
- model of the integrated system taking into account variable climatic conditions;
- detailed mathematical model of chemical reactor/solar receiver unit and exergy analysis;
- design of the thermochemical refrigerator driven by solar energy.

First, we analyzed a basic thermochemical cycle for choosing a proper vapour-solid reaction (or proper solid sorbent) [5]. The minimal temperature T_2 necessary to drive this cycle was found, to depend only on the condenser and evaporator temperatures, T_c and T_e, which are dictated by ambient climatic conditions. T_2 was calculated using the Trouton's rule (Fig. 3). The requirements to the optimal reaction are: a) complete decomposition should occur immediately at temperature T_2; b) amount of vapor desorbed at T_2 should be maximal. The optimal adsorbent for the cycle considered in this project is to be searched among the class of hydrated compounds, first of all, the dehydration of $CaCl_2 \cdot 2H_2O$, $Ca(NO_3)_2 \cdot 2H_2O$, $Ca(NO_3)_2 \cdot 3H_2O$ and $Na_2HPO_4 \cdot 2H_2O$.

These substances were confined to pores of various host materials (silica, alumina) to improve dynamics of mass transfer and avoid a hysteresis between the formation and decomposition reactions. Sorption equilibrium with water vapor was measured at T = 35-150 °C and $P(H_2O)$ = 6-70 mbar [7, 8]. Sorption kinetics is controlled by the intraparticle Knudsen diffusion of water. Appropriate diffusivities have been measured as function of temperature, water uptake and salt content [9, 10]. For $CaCl_2$/alumina a crossover to chemical reaction limitation was found at large salt contents. The equilibrium and dynamic data served as input parameters for further mathematical modeling.

One of the main peculiarities of a solar refrigerator is the variation of its working conditions (the ambient temperature and solar radiation). To put this factor in evidence we collected, systemized and processed climatic information for different sites (South of Russia, Italy, Germany, South-Eastern Asia, Africa, etc.) in formats necessary for the dynamic simulation of solar chiller. Typical Meteorological Years were generated for these selected sites for further utilization under the TRNSYS software [11]. Fig. 4 presents the averaged daily solar radiation for Messina.

Developed mathematical model of the thermochemical refrigerator allowed the simulation of the unit operation in real climatic conditions as well as the study on how different parameters affect the system thermal ratio STR and specific cooling power SCP at different

rated evaporator temperatures, varied in our calculations from 5 to 10 $^{\circ}$C. If use the composite CaCl$_2$/silica, the model for different sites predicted the SCP = 35 – 60 W/m^2 and STR $\approx$ 0.2, that is better than for common adsorbents. To reach these values the optimal mass of solid sorbent should be 12–16 kg/m^2 and the typical time for setting sorption equilibrium in the granulated sorbent layer should be less than 1 h. The latter value takes into account both heat and mass transfer in the layer as well as the rate of chemical reaction. Detailed analysis of these processes, which will carefully consider the effect of the vapor re-adsorption along the layer (the heat pipe effect), is on the way.
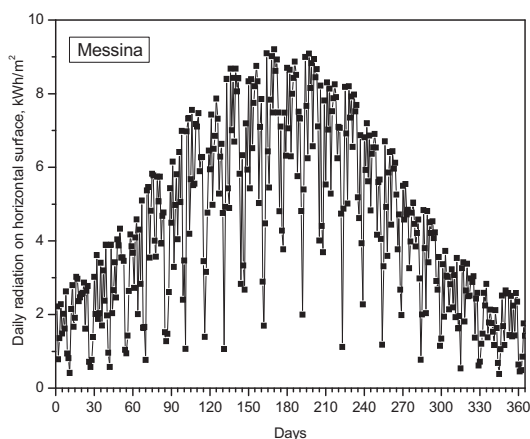
Fig. 4.

Fig. 5.

As a result of this comprehensive study a prototype of the thermochemical refrigerator driven by solar energy has been designed and built (Fig. 5). It will be tested in Crimea during summer 2006.

Literature

1. Yu.I.Aristov, G.Restuccia, G.Cacciola, V.N.Parmon, Appl.Therm.Engn., 2002, v.22, N 2, pp.191-204.
2. W.M.Raldow, W.E.Wentworth, *Solar Energy*, 1979, v.23, p.75-79.
3. L.G. Gordeeva, A.V. Gubar, L.M. Plyasova, V.V. Malakhov, Yu.I. Aristov, Kinetika i Kataliz (Russ. J. Kinetics and Catalysis), 2005, v. 46, N 5, pp. 736-742.
4. G.Restuccia, A.Freni, S.Vasta, Yu.Aristov, 2004, v. 27, N 3, pp. 284-293.
5. Yu.I. Aristov, Proc. VI Int. Seminar "Heat pipes, heat pumps, refrigerators", 12-15 Sept. 2005, Minsk, Belorus, pp. 342-353.
6. D.M. Chalaev, Yu.I. Aristov, Teploenergetika (Rus. J. Power Engineering), 2006, N 3, pp. 73-77.
7. I.A. Simonova, Yu.I. Aristov, Rus. J. Physical Chemistry, 2005, v. 79, N 8, pp. 1307-1311.
8. M.M.Tokarev, B.N.Okunev, M.S.Safonov, L.I.Heifets, Yu.I.Aristov, Rus. J. Physical Chemistry, 2005, v. 79, N 9, pp. 1490-1494.
9. Yu.I. Aristov, I.S. Glaznev, A. Freni, G. Restuccia, Chem. Engn. Sci., 2006, v.61, N 5, pp.1453-1458.
10. B.Dawoud, Yu.I.Aristov, Int.J.Heat& Mass Transfer, 2003, v.46, N 2, pp. 273-281.
11. TRNSYS – The Transient System Simulation Program // http://sel.me. wisc.edu/TRNSYS/.

FUEL PROCESSING IN MICROSTRUCTURED HEAT-EXCHANGER REACTORS - A PRACTICAL COMPARISON OF DIFFERENT FUELS FROM METHANOL TO DIESEL

G. Kolb, Y. Men, J. Schürer, D. Tiemann, M. Wichert, R. Zapf, V. Hessel, H. Löwe

Institut für Mikrotechnik Mainz GmbH (IMM), Carl-Zeiss-Str.18-20 D-55129 Mainz;
Germany; Tel.: ++49-6131-990-341; Fax.:-305; email: kolb@imm-mainz.de

Introduction

Size reduction is a critical issue for the applicability of mobile fuel cell and fuel processing systems, which is currently addressed by widespread international research. The benefits gained by microstructured heat-exchanger / reactor technology [1] are thus under investigation in numerous research projects related to fuel processing [2, 3].

Based upon experience with processing of methanol [4], ethanol, propane [5], gasoline [6] and diesel, a comprehensive study of advantages and drawbacks of different fuels is provided. It covers not only catalyst activity and durability issues [7, 8] and reactor design, but also the aspects of heat- and water management, start-up procedures, choice of reactor material, joining techniques and the aspects of future mass production of these devices, which are dedicated for the future distributed and clean energy production. Another issue, which needs to be taken into consideration, are the gas purification system requirements. This clean-up system needs to be installed downstream the reformer itself and deals mostly with the removal of carbon monoxide out of the reformate, at least as long as conventional PEM fuel cell systems are applied. In case catalytic CO-clean-up is chosen as strategy, it usually comprises water-gas shift and preferential oxidation of carbon monoxide, which both bear significant potential for improvement by the application of microstructured heat-exchangers [9, 10, 11, 12]. The efforts required for this purification system depend, once again, strongly on the fuel applied.

Alcohol Fuels

Alcohol fuels such as methanol and ethanol have significant advantages concerning the operating temperature of the reformer itself, which is significantly lower compared to hydrocarbon reforming. Methanol reforming, especially in case steam reforming, may well be operated at temperatures below 300°C. However, recent catalyst development work will be presented, which deals with new formulations allowing for a lower operating temperature for ethanol as well. Due to its lower toxicity and its potential production from organic waste, ethanol appears even more attractive than methanol on the longer term. The low operating temperature makes alcohol fuels attractive especially for portable energy generation systems. The smaller the size of the fuel processor the more drastic are the effects of heat losses on

system efficiency and consequently system size. Examples of the effects of heat losses on fuel processor efficiency will be presented.

However, the lower the operating temperature of the reforming reaction, the lower the activity of the catalytic systems is. A comparison of the activity of commercial and self-developed catalyst systems for different fuels will be provided. However, lower catalyst activity relates to higher reactor size, regardless if microstructured plate heat-exchanger technology, metallic or ceramic monoliths or even fixed beds are applied.

Finally, low operating temperatures allow for alternative choice of the reactor material different to stainless steel, such as aluminium, which helps to reduce the system weight. However, the laser welding procedure usually applied for joining microstructured plate stacks at IMM (see Fig.1) is not applicable for this novel material. Consequently, new joining techniques such as brazing (see Fig.2) and electron beam welding, which were so far only applied for stainless steel, need to be adopted for aluminium.
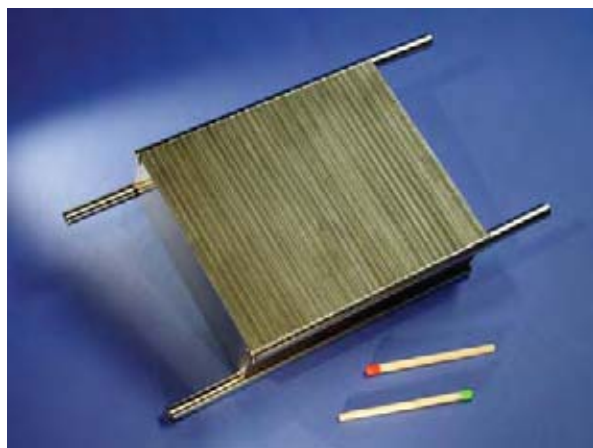
Fig.1: Integrated Methanol steam reformer / catalytic afterburner developed at IMM

Fig.2: Micro-structured heat-exchangers joined by brazing

Propane / Butane

Propane, butane and mixtures thereof are attractive fuels for small scale applications due to the existing distribution grid. Due to the higher operating temperature normally exceeding 700°C, catalyst activity is less an issue but rather rather catalyst stability, which is affected by sintering procedures. In fact, very high catalytic activity may be achieved even for steam reforming owing to the improved heat and mass transfer in microstructured reactors. WHSV values as high as 750 Ndm³/(h g_{cat}) have been realised at IMM for a duration of 1,000 hours over PGM catalyst formulations.

As soon as oxygen is added to the feed, the activity even increases. WHSV values up to 2400 Ndm³/(h g_{cat}) were achieved at IMM for the partial oxidation of propane.

Gasoline

Gasoline, even more than propane, has advantages owing to the existing distribution grid and is evidently most attractive to the automotive industry. Operating temperatures of a gasoline reformer are similar to the propane system, and thus catalyst stability issues are

similar as far as structural deactivation mechanisms such as sintering are concerned. However, deactivation by coking gets more an issue compared to light hydrocarbons. The addition of air to the reformer feed is one viable option to cope with coking problems. However, running a fuel processor in the autothermal mode (see Fig.3) has the drawback of a significantly lower hydrogen content compared to steam reforming owing to the dilution of the reformate by nitrogen.

Fig. 3 Autothermal microstructured reformer / gasoline developed at IMM

Fig. 4: Integrated catalytic steam reformer afterburner for diesel fuel developed at IMM

Diesel

Steam reforming of higher hydrocarbon fuels such as diesel requires advanced technology concerning catalyst coatings and reactor material due to the very high reaction temperature exceeding 800°C. At IMM, a microstructured heat-exchanger / reactor was developed and operated for more than 40 hours already, which completely converts diesel fuel (see Fig.4). The application standing behind this work is, once again, power generation for automotive applications.

References

[1] Kolb G., Hessel V, „Review: Micro-structured reactors for gas phase reactions" Chem. Eng. J. 98, 1-38 (2004).
[2] Hessel V., Löwe H., Müller, A., Kolb G., 2005, 'Chemical Micro Process Engineering- Processing, Applications and Plants', Wiley, Weinheim, ISBN-13 978-3-527-30998-6, p.281 ff.
[3] Reuse P., Renken A., Haas-Santo K., Görke O., Schubert K., Chem. Eng. J. 101, 133-141 (2004).
[4] Cominos V., Hardt S., Hessel V., Kolb G., Löwe H., Wichert M., Zapf R., Chem. Eng. Comm. 192 (2005) 685.
[5] Kolb G., Zapf R., Hessel V., Löwe H., Appl. Catal. A: General 277 (2004) 155.
[6] Kolb G., Cominos, V., Zapf R., Hessel V., Löwe H., *Proc. Of the 7th World Congress of Chem. Eng., Glasgow (2005)*, Paper O112-002, published on CD
[7] Zapf R., Becker-Willinger C., Berresheim K., Bolz H., Gnaser H., Hessel V., Kolb G., Löb P., Pannwitt A.-K., Ziogas A., Trans I Chem E Part A, 81 (2003) 721.
[8] Zapf R. and Kolb G., Chem Eng. Techn., in prep.
[9] TeGrotenhuis, W.E. King, D.L., Brooks, K.P., Holladay B.J., Wegeng, R.S. 6th International Conference on Microreaction Technology, 2002, AIChE, NY, 2002, p. 18
[10] Kolb G., Pennemann H., Zapf R., Catal. Today 110 (2005) 121
[11] Baier T. and Kolb G., Chem Eng. Sci., submitted for publ.
[12] Cominos V., Hessel V., Hofmann C., Kolb G., Zapf R., Ziogas A., Delsman E.R., Schouten J.C., Catal. Today 110 (2005) 140

CATALYTIC DECOMPOSITION OF NATURAL GAS FOR CO$_X$-FREE HYDROGEN PRODUCTION IN A STRUCTURED MULTILAYER REACTOR

G. Italiano[1], C. Espro[1], F. Arena[1], F. Frusteri[2], A. Parmaliana[1]

[1]*Dipartimento di Chimica Industriale e Ingegneria dei Materiali,*

Università degli Studi di Messina, Salita Sperone , 31, I-98166, Messina, Italy

[2] *Istituto CNR-ITAE "Nicola Giordano", Salita S. Lucia 39, I-98126 Messina, Italy*

Introduction

The catalytic decomposition of natural gas (CDNG) into hydrogen and carbon is currently attracting a great research interest since it appears a direct, mildly endothermic attractive route for producing high purity hydrogen avoiding any concern due to CO$_2$ emissions. The CDNG is the candidate process for fueling fuel cell systems as well a potential alternative to the conventional H$_2$ production processes owing to the higher energy efficiency and lower environmental duty [1-4].

Among transition metals and their alloys, Ni based catalysts feature high activity and the capability of producing carbon filaments or carbon nanotubes at moderate temperatures (500-700°C) [5]. The unavoidable carbon lay down on the catalyst surface leading to the reactor plugging is a serious issue which could limit the practical feasibility of the CDNG process. However, such hurdle can be overcome by using adequate catalyst configurations and reactor devices [6-7]. In this context, this contribution is aimed to highlight the suitability and potential of a novel class of Ni thin layer silica cloth catalysts in the decomposition of natural gas for producing CO$_x$-free hydrogen in a structured multilayer reactor (MLR).

Experimental

Ni Thin Layer Catalysts (Ni-TLC). A commercial silica fabric (OS 120, Thermal Material Systems (TMS) product; thickness, 0.15 mm; specific weight, 120 g/m^2) was washcoated with a colloidal SiO$_2$ (Ludox LS, Aldrich product; S.A., 215 m^2/g) solution in order to confer an adequate surface area for the dispersion of the active species. The weight ratio between SiO$_2$ layer and silica cloth was 34/100. Ni-TLC samples were prepared by stepwise incipient method impregnating the SiO$_2$/silica cloth support with a 0.1 M solution of Ni(NO$_3$)$_2$*6H$_2$O. After impregnation the samples were dried at 120°C for 12h and calcined at 550°C for 3h.

A series of Ni-TLC samples with Ni loading ranging from 0.5 to 50 wt%, referred to the weight of the SiO_2 layer, has been prepared.

Fresh and used Ni-TLC catalysts have been characterized by H_2 chemisorption, Temperature Programmed Reduction, SEM, TEM and Thermal Analysis.

Structured Multilayer Reactor (MLR), schematically shown in Fig.1, consists of a package of six Ni-TLC discs (Φ, 37 mm; W, 0.22 g) sandwiched between quartz rings (Φ_{ext}, 37 mm; thickness, 4 mm) set in a quartz tube (Φ_{int}, 39 mm; length, 600 mm). A heating wire was wrapped around the quartz tube providing the thermal conditioning of the reactor system. The influence of space velocity (GHSV, h^{-1}), reaction temperature and Ni loading on specific activity, catalyst performance and nature of the carbon nanostructures deposited on the catalyst surface has been evaluated.

Ni-TLC Testing was carried out at 500-600°C and atmospheric pressure using a 10% CH_4/5% N_2/85%Ar (vol/vol) reaction mixture. The activity of the catalysts was monitored until complete deactivation evaluating the trend of activity decay, the average H_2 Yield (STY_{H2}, kg_{H2}/kg_{Ni}*h) and the Carbon Capacity (C/Ni, number of CH_4 molecules decomposed for Ni atom along the catalyst lifetime).
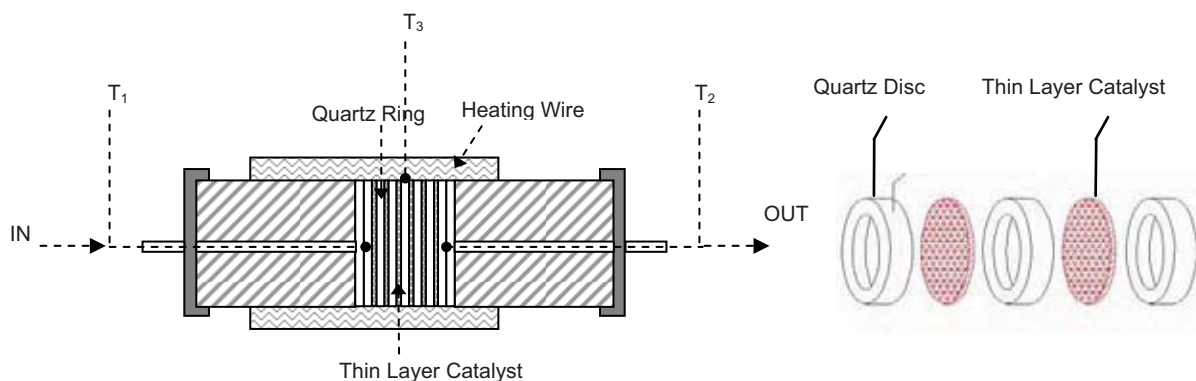
Fig. 1 - Schematic of Structured Multilayer Reactor (MLR)
(T_1, inlet Temperature; T_2, outlet Temperature; T_3, reaction Temperature)

Results and Discussion

The low magnification SEM micrographs, shown in Fig.2, accounts for the textural properties of the Ni-TLC systems. Silica cloth is constituted by fibres, 0.5 mm in diameter, interlaced each other (Fig. 2a). After the washcoating the fibres were randomly covered with SiO_2 aggregates (Fig. 2b). The subsequent impregnation with the aqueous solution of the Ni precursor (Fig. 2c) causes a redistribution of silica on fibres resulting in a more homogeneous catalyst surface. The physico-chemical characteristics of Ni-TLC samples are listed in Table 1.
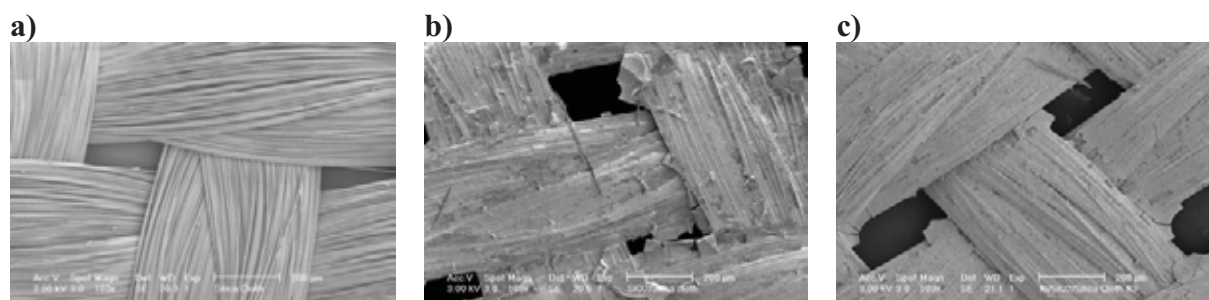
Fig. 2 SEM micrographs (magnification, 103x) of (a) bare silica cloth, (b) SiO_2/silica cloth and (c) Ni-TLC sample

Table 1 – Characteristics of Ni-TLC samples

Catalyst	Ni Loading (%)	SA_{BET} (m²/g$_{cat}$)	MSA (m²$_{Ni}$/g$_{cat}$)	[a]D_{Ni} (%)	[b]$d_{s, Chem}$ (nm)
TLC	-	71	-	-	-
N1-TLC	4.6	50	1.2	10.9	9.3
N2- TLC	11.4	51	2.3	8.1	12.5
N3- TLC	19.5	51	3.6	7.1	14.3
N4- TLC	41.1	48	2.3	1.8	56.6
N5- TLC	50.4	52	2.4	1.4	71.5

a) D_{Ni}, Ni dispersion; b) ds, mean diameter of Ni crystallites

A general overview of the performance of the Ni-TLC samples, in terms of Carbon Capacity (C/Ni) and initial and average STY_{H2} ($STY_{H2,i}$ and $STY_{H2,a}$, respectively) at 500°C, is presented in Table 2. The inevitable decay of the activity with the reaction time, at various reaction temperatures, for the N3-TLC sample is displayed in Fig. 3. The extent as well the trend of catalyst deactivation is controlled by reaction temperature, space velocity, Ni loading and nature/amount of coke laid down during the reaction time.

Table 2 – Activity data of Ni –TLC samples in the CDNG reaction at 500°C

Catalyst Code	Ni Loading (%)	C/Ni	$STY_{H2,i}$ [a] (kg$_{H2}$/kg$_{Ni}$*h)	$STY_{H2,a}$ [b] (kg$_{H2}$/kg$_{Ni}$*h)	Lifetime (h)
N1-TLC	4.6	1.3	$4.8*10^{-1}$	$1.8*10^{-1}$	0.5
N2-TLC	11.4	3.4	$5.6*10^{-1}$	$2.3*10^{-1}$	1.0
N3-TLC	19.5	61.3	$3.7*10^{-1}$	$3.1*10^{-1}$	13.6
N4-TLC	41.1	20.4	$1.6*10^{-1}$	$1.1*10^{-1}$	12.5
N5-TLC	50.4	16.0	$1.2*10^{-1}$	$8.2*10^{-2}$	13.3

a) $STY_{H2,i}$ refers the STY_{H2} calculated on the basis of the activity at reaction time of 0.5 min
b) $STY_{H2,a}$ refers the average STY_{H2} calculated on the basis of the activity along the entire reaction time
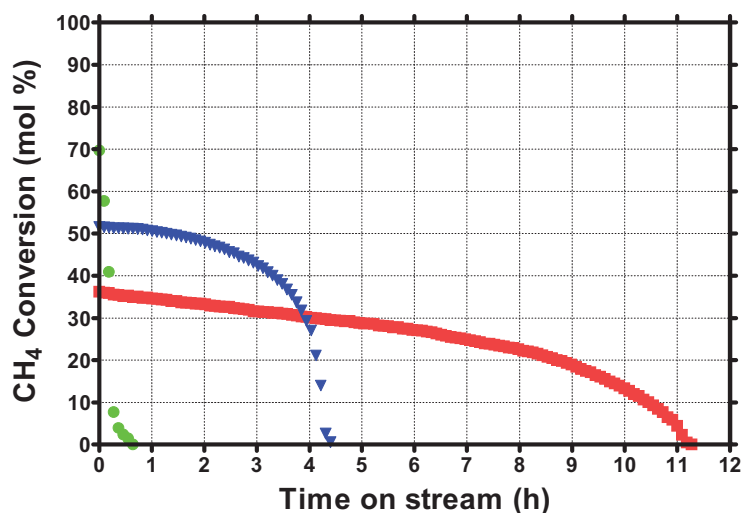
Fig. 3 Catalytic Decomposition of Natural Gas on N3-TLC sample. Methane conversion vs time on stream at (■) 500; (▼) 550 and (●) 600°C (GHSV, 1908 h^{-1}).

A detailed analysis of the coking of Ni-TLC systems, accomplished by SEM and TEM techniques, evidences the deposition of filamentous (whisker-like) carbon deposits at 500°C and encapsulating coke at 600°C with a mixed filamentous-encapsulating residues at 550°C.

References

[1] N. Z. Muradov, Energy & Fuels 12 (1998) 41

[2] R. Aiello, J. E. Ficus, H. Loye, M.D. Amiridis, App. Catal. A: General 192 (2000) 227.

[3] T.V. Choudhary, D. W. Goodmanm, J. Catal .192 (2000) 316

[4] N. Z. Muradov, T.N. Veziroğlu, Int. J. Hydrogen Energy 30 (2005) 225

[5] K. Otsuka, A. Mito, S. Takenaka, I. Yamanaka, Stud. Surf. Sci. Catal. 136 (2001) 215.

[6] A.Beretta, G. Groppi, L. Malocchi, P. Forzatti, Appl. Catal., A: General 187 (1999) 49

[7] L. Kiwi-Minsker, A. Renken, Catal. Today 110 (2005) 2

HYDROGEN PRODUCTION BY METHANOL STEAM REFORMING AND ETHANOL STEAM REFORMING IN MEMBRANE REACTORS: AN EXPERIMENTAL STUDY

A.Basile[1], A. Iulianelli[2], F. Gallucci[1], S. Tosti[3], E. Drioli[1,2]

[1] *Institute on Membrane Technology, ITM-CNR, c/o University of Calabria, via P. Bucci, Cubo 17/C, 87030 Rende (CS), Italy, Phone: (+39) 0984 492013 – Fax: (+39) 0984 402103 – a.basile@itm.cnr.it*

[2] *Department of Chemical Engineering and Materials, University of Calabria, via P. Bucci Cubo 42/A, 87030 Rende (CS), Italy, Phone: (+39) 0984 492039 – Fax: (+39) 0984 402103*

[3] *ENEA, Unità Tecnico Scientifica Fusione, C.R. ENEA Frascati, Via E. Fermi 45, Frascati, Roma 00044, Italy, Phone: +39 06 94005160 – Fax: +39 06 94005374*

Abstract

In this work a comparison between methanol steam reforming reaction (MSR) and ethanol steam reforming reaction (ESR) to produce hydrogen in membrane reactors (MRs) is discussed from an experimental point of view .

Both reaction systems have been investigated by considering the influence of the membrane characteristics as well as the influence of the operating temperature. In the case of the dense membrane, the sweep gas flow rate and the different fluxes configurations have also been analysed.

Experimental results, in terms of reactants conversion as well as hydrogen production and gases selectivity in MRs and in a traditional reactor (TR), are presented. The catalyst stability in both reaction systems was also tested.

1. Description of the process

The TR consists of a stainless steel tube, length 250 mm, *i.d.* 6.7 mm with the reaction zone 150 mm. The MR consists of a tubular stainless steel module, length 280 mm, *i.d.* 20 mm, containing different membranes, the first one (MR1) is a TiO_2-Al_2O_3 asymmetric porous commercial membrane (Inoceramic) with a Pd-Ag deposit. The second membrane (MR2) is a commercial asymmetric porous ceramic membrane with a Pd-Ag deposit. The third membrane (MR3) is a pine-hole free Pd-Ag thin wall membrane tube permeable only to hydrogen, having thickness 50 μm, *o.d.* 10 mm, length 150 mm.

2. Results and discussion

2.1 The membrane reactor MR1

Figure 1 reports the results, in terms of ethanol and methanol conversion, for both traditional reactor and membrane reactor MR1. Considering the conversion values for both reactions in the TR, it should be said that the catalyst shows higher activity for methanol steam reforming (MSR) than ethanol steam reforming (ESR). In fact, for the whole temperature range investigated the methanol conversion is higher than the ethanol conversion.
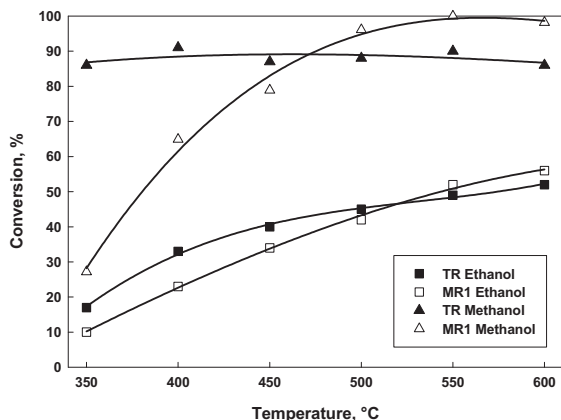
Fig 1 Methanol and Ethanol conversion versus temperature in MR1 and TR, H_2O/Alcool = 4.5/1, p_{lumen}=1.3 bar, p_{shell} = 1 bar (for MR)
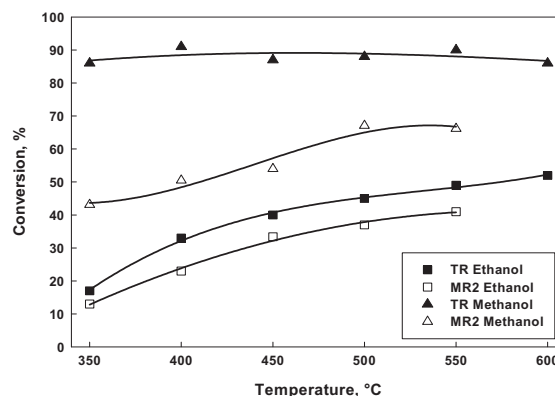
Fig 2 Methanol and Ethanol conversion versus temperature in MR2 and TR, H_2O/Alcool = 4.5/1, p_{lumen}=1.3 bar, p_{shell} = 1 bar (for MR)

2.2 The membrane reactor MR2

In Figure 2 the results, in terms of ethanol and methanol conversion, for both traditional reactor and membrane reactor MR2, are reported. For both MSR and ESR reactions, the results obtained in the MR2 are lower that the results obtained in the TR. In particular, the best conversion achieved by MSR in MR2 is 65% while it is 90% in TR (at T = 550°C); at this temperature, the conversion achieved by ESR it is 37% in MR2 and 47% in TR.

2.3 The membrane reactor MR3

The membrane reactor MR3 uses a dense Pd-Ag membrane with a perm-selectivity H_2/(other gases) infinite. For this membrane reactor there are at least two advantages: the first one is that the shell stream is CO-free and so it can be directly fed to a PEMFC. The second advantage is that, in order to improve the hydrogen recovery in this reactor, a sweep gas can be used in the shell side. The sweep gas can be used either in co-current and in counter-current mode and at different flow rates. The hydrogen production (Figure 3) is higher for the MSR reaction than the ESR reaction. In the best conditions, the MSR reaction is able to give an increase in the hydrogen production of around 80% with respect to the ESR reaction.

The same results are obtained by using the counter-current mode. In Figures 4, the comparison between ESR reaction and MSR reaction in terms of hydrogen production, are

reported, for the counter current mode. Also in this case the counter-current mode is able to give higher hydrogen production than the co-current mode. For the counter-current mode the best reaction system to be considered for producing hydrogen seams to be the MSR reaction system.
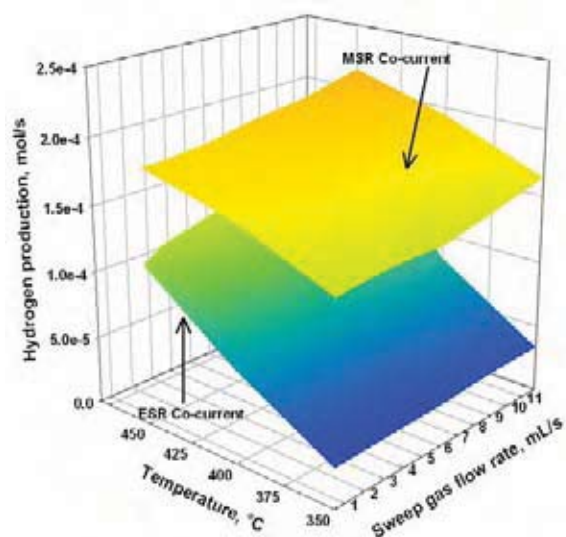
Fig 3 Hydrogen production versus temperature and versus sweep gas flow rate during ESR and MSR in MR3. Co-current mode
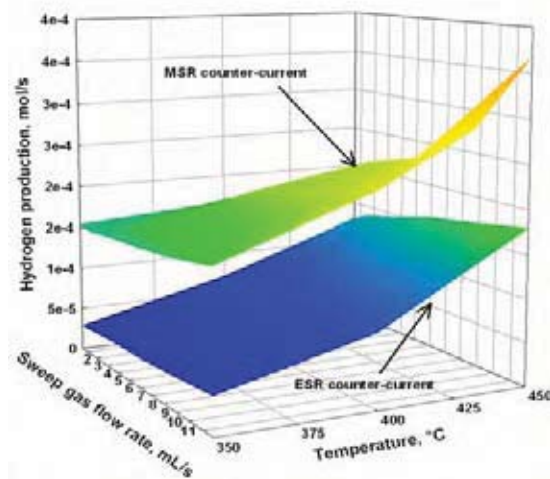
Fig 4 Hydrogen production versus temperature and versus sweep gas flow rate during ESR and MSR in MR3. Counter-current mode

3 Conclusions

The methanol and ethanol steam reforming reactions have been studied from an experimental point of view in TR and in three different MRs packed with commercial Ru-based catalyst. Two Pd/Ag supported membranes (MR1 and MR2) and a dense Pd-Ag membrane (MR3) were used in order to increase the reactant conversion and the hydrogen production. The experiments show that in both traditional and membrane reactors MSR conversions are higher than ESR. The ESR needs a higher reaction temperature than MSR in order to increase the ethanol conversion. With our membranes it is not possible to reach such high temperature. For MSR, the highest conversion is achieved in MR3 where, already at T = 400°C, in counter-current mode and sweep gas flow rate equal to 11.8 mL/s, 100% conversion is reached. For ESR, the highest conversion is achieved in MR3 at T = 450°C, in counter-current mode and sweep gas flow rate 11.8 mL/s, and it is equal to 50%. Also the total molar hydrogen flow rates, in both traditional and membrane reactors, for MSR are higher than ESR and the best results are obtained in MR3. By using Ru-Al$_2$O$_3$ 5% as a catalyst, ESR shows coke deposition with consequent deactivation of the catalyst. Finally, we can conclude that, in the conditions investigated in this work, the MSR reaction is much suitable than the ESR for producing hydrogen. However, a more in deep investigation, aided by a theoretical and an economical analysis, is necessary in order to find the best operative conditions for producing hydrogen.

FISCHER-TROPSCH SYNTHESIS FIXED-BED REACTOR:
A NEW CHANCE FOR OLD TECHNOLOGY

Kuz'min A.E.

A.V. Topchiev Institute of Petrochemical Synthesis RAS, 119991, Moscow,
Leninsky Av., 29, Russia, (495)954-47-98, tips@ips.ac.ru

In come XXI century the hydrocarbon synthesis from CO and H_2 for fuel and petrochemical purposes (Fischer-Tropsch synthesis, FTS), evidently, is one of the most dynamically developing processes of chemical industry; if at the end of XX century sum world capacity of FTS plants was about 7 million t/year (and its main part was concentrated in Southern Africa) then in the beginning of the present decade it will become worldwide and increase approximately in 10 times. Representing wide variety of the obtained products, applied catalysts and technological methods, FTS, in spite of the fact that it is known about one hundred years remains extremely interesting field both for fundamental researches and for applied developments.

FTS is an exothermal process ($\approx$170 kJ/mol CO), and one of the major problems of its industral realization is removal of generating heat from the reactor; insufficient heat removing followed by catalyst overheating quickly results to increased methane formation or catalyst coking (or to both phenomena together). Historically the first FTS reactor technology was fixed-bed one using granulated catalyst (at first with sheet-packed, then in a tubular reactor) and cooling condensate, but in this case temperature situation in a reactor becomes essentially non-isothermal both in axial and radial directions. This circumstance, obviously, imposes restrictions on a achievable CO conversion value per one reactor pass and on application of possible FTS catalysts with very high activity. Besides fixed-bed reactor has complex design (it is required to make several thousands of reaction tubes) and inconvenient for catalyst loading/unloading.

The most popular commercial SFT technology presented first in large-scale by Sasol (1993) and accepted in most of builded and commissioned plants is a reactor with three-phase suspended catalyst bed (slurry). Its basic advantages are near-isothermal reaction mode, an opportunity of use of fine catalyst powders, simplicity of its introduction into reaction and relative simplicity of reactor design (a bubble column). It appeared enough that FTS fixed-bed technology has considered now as a minor commercial opportunity.

Attempts to modify this type of process, however, were undertaken repeatedly. So, one variant of this technology is a reactor with adiabatic catalyst sections and intercoolers where one probably can more effective adjust a temperature profile of a reaction feed (the most

known development – the Lurgi reactor [1]). Other approach was recently presented in [2], where it is offered to use for FTS tubular reactor the syngas produced by air (instead of pure oxygen) conversion of methane and containing about 50 % of N_2 that is an inert at typical FTS conditions; application of such gas, besides its relatively low cost, allows to optimize non-isothermal reaction pattern a little. However, these both approaches are characterized by the specific problems: in the first case - inconvenience of reactor design in a whole (necessity of several intercoolers, tubular as a rule) and increase of section number at use of more active catalysts, in the second – expencive recirculation of syngas with ballast N_2 followed by necessity of achievement of 90-95 % CO conversion per pass and necessity of N_2 remove from gaseous FTS products.

Nevertheless, the fixed-bed technology, as it is represented, has more opportunites of upgrade. First, one can use two-section intertubular space of reactor and two vapor condensate feeds with different temperatures: lower one near reaction stream inlet, higher one near its outlet. Second, for this purpose it is possible to use as a coolant not the steam condensate evaporating at strictly determined temperature but heated cocurrent water with appropriate values of inlet temperature and velocity. In both cases at other parameters being equal one can calculate that CO conversion become higher and axial temperature profile become smoother in comparison with cooling by one-feed condensate; it is possible to tell that non-isothermicity of the coolant compensates non-isothermicity of reaction stream, eliminating both a characteristic temperature maximum within initial tube section and excessive cooling of tube "tail" where more effective conversion of the reactant-poor gas needs the raised temperature.

FTS technological features described above also cause lower average radial temperature difference in comparison with common fixed-bed reactor. It, in turn, can permit to increase diameter of a tube without excess of allowable temperature of catalyst at tube axis and, hence, to reduce number of tubes in an commercial reactor and to simplify its design.

Thus, for FTS tubular fixed-bed reactor one can sufficiently improve its temperature mode that can shift towards to one for slurry reactor and also to simplify reactor design. If to take into account that slurry reactor, besides obvious advantages, has also the specific lacks (the insufficient flexibility of working temperature that is caused by thickening or boiling away of a liquid phase; difficulty of application of catalysts with cracking function causing liquid phase destruction; certain difficulties concern separation and mechanical deterioration of the catalyst) which do not exist for fixed bed then one most to conclude that SFT fixed-bed technology still can remain efficient commercial alternative to three-phase one.

1. Chemierohstoffe aus Kohle (her. von J. Falbe), Stuttgart, 1977

2. A. Jess, R. Popp, K. Hedden/ Appl. Catal., A, 1999, v.186, p. 321

UPGRADING OF FLASH PYROLYSIS LIQUID BY REACTIVE DISTILLATION USING A HIGH-BOILING ALCOHOL IN THE PRESENCE OF SOLID CATALYSTS

F.H. Mahfud, I.V. Melian de Cabrera, H.J. Heeres*

Department of Chemical Engineering, Faculty of Mathematics and Natural Sciences

Rijksuniversiteit Groningen, Nijenborgh 4, 9747 AG, Groningen, The Netherlands

*Fax: +31-50-363 4479, Telephone: +31-50-363 4497, *E-mail: h.j.heeres@rug.nl*

Introduction

Anticipated future energy shortages and environmental concerns have boosted research on alternatives for fossil energy carriers [1]. This has encouraged the exploration of renewable resources like biomass for energy generation. Flash pyrolysis liquid, also known as bio-oil (BO), is a biomass-derived liquid energy carrier. It is produced via flash pyrolysis in yields up to 70%-wt [2-7]. A large variety of applications for BO have been proposed [8]. One of the challenging applications is the use as a liquid transportation fuel for internal combustion engines. For this application, the BO has to be upgraded to fulfill the stringent transportation-fuel product requirements. A number of BO upgrading technologies have been proposed and explored. For example, it is possible to treat bio-oil with hydrogen in the presence of solid catalysts to produce a diesel like transportation fuel (HDO process, see [[9-12]]). However, up till now, hydrogen consumption is excessive which negatively affects the economics of this process.

A number of studies have been reported dealing with chemical upgrading of crude bio-oil by reacting it with an alcohol (e.g. ethanol) at mild conditions using a liquid mineral acid catalyst like sulphuric acid [13-15]. From a chemical point of view, it is anticipated that reactive molecules like organic acids and aldehydes are converted to esters and acetals, respectively (Figure 1). Removal of water is essential to shift the equilibria to the right side. Radlein [15] has proposed the use of molecular sieves to capture the water and to drive the equilibria to the right side. Product studies indeed have shown that the product properties of bio-oil are significantly improved by this alcohol treatment.
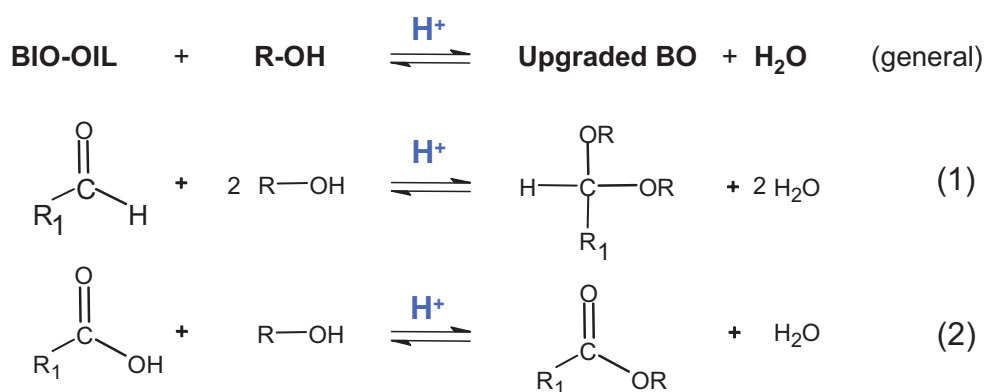
Figure 1. Reactions involve in bio-oil alcoholysis. (1) Acetalization, (2) Esterification.

However, the alcohol treatment concept also has some major drawbacks. The process applies a liquid mineral acid which has to be neutralised after reaction. This leads to an extra processing step and generates a large amount of waste salts. In addition, to be cost effective, the molecular sieves for water removal need to be regenerated, also leading to additional investments and processing costs. We here report our studies on the upgrading of bio-oil using an improved alcohol treatment concept.

Results and discussion

We have explored an improved upgrading technology using a solid catalysts and a high boiling alcohol (n-butanol). A schematic representation of the (batch)-concept is provided in Figure 2. The solid catalyst is retained in the reactor and thus the use of a post neutralisation step, necessary when using a liquid mineral acid, is avoided. The water formed during the reactions and the water present in the bio-oil feed is removed by distillation at reduced pressure. To avoid excessive alcohol vaporisation, a high boiling alcohol in the form of n-butanol is applied. This particular alcohol was selected as it can be produced from renewable resources.

Initially, a number of solid acid catalysts were screened (T= 60°C, P= 50 mbar, $t_{reaction}$= 1 hr). Among these, Nafion$^{®}$ SAC13 was found to be the preferred catalyst. The amount of water produced by the reactions as given in Figure 1 was highest, implying that this catalysts results in the highest reaction rates. To study the influence of operating conditions on product properties, an experimental design using a half fraction factorial method was applied. The investigations indicate that the optimum conditions are a 50%-v alcohol content, 1%-wt catalyst concentration, a reaction temperature of 70°C, a pressure of 50 mbar and a reaction time of 120 minutes.
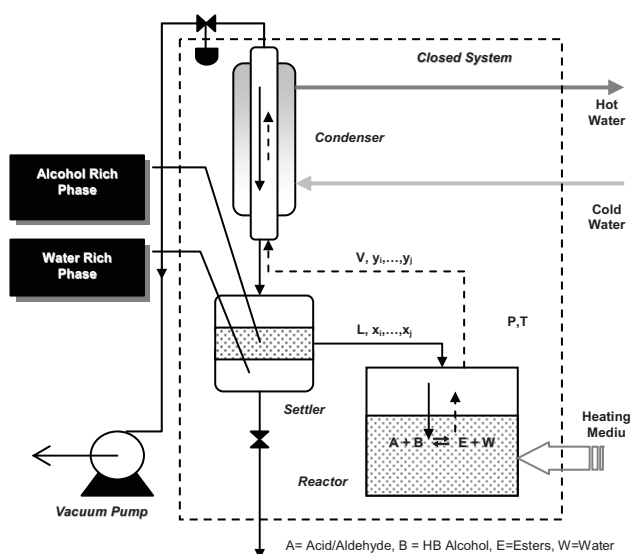
Figure 2. Batch reactive distillation set-up for high boiling alcoholysis.

The product properties for these optimised conditions are given in Table 1.

Table 1. Properties comparison for crude bio-oil, upgraded Bio-oil, diesel and biodiesel

Physical property	Bio-oil	Upgraded Bio-Oil	Diesel	Bio diesel
Viscosity40 'C, cSt	17	6.96	1.2 – 4.1	1.9 – 6.0
Water content	31.5 %wt	8.69 %wt	161 ppm	<0.05 %vol
Flash Point, oC	52.5	45	60 – 80	100 – 170
Density, kg/L	1.17	0.95	0.85	0.88
PH	3	3.22	7	7

It may be concluded that the alcohol upgrading procedure has led to a significant increase in the product properties. In particular, beneficial effects were observed on the viscosity and water content. Moreover, due to the presence of butyl esters, the pungent odor of the BO is absent and the product has a banana like odor.

Conclusions

A novel method of chemical upgrading of bio-oil by using reactive distillation with a high boiling alcohol and a solid catalysts has been explored in a batch set-up. The product properties of the upgraded bio-oil are significantly improved compared to the crude bio-oil. Engine tests are in progress and will also be provided.

References

1.   Ssen, Z., *Solar energy in progress and future research trends.* Progress in Energy and Combustion Science, 2004. **30**(4): p. 367-416.

2.   Agblevor, F.A., S. Besler, and A.E. Wiselogel, *Fast Pyrolysis of Stored Biomass Feedstocks.* Energy & Fuels, 1995. **9**(4): p. 635-640.

3.   Bridgwater, A.V., Czernik, S., Diebold, J., Meier, D., Oasma, A., Peackocke, C., Pizkorz, J., Radlein, D., *Fast Pyrolysis of Biomass: A Handbook.* 1st ed. Vol. 1. 1999: CPL Press, Newbury Berkshire, UK.

4.   Bridgwater, A.V. and G. Grassi, *Biomass pyrolysis liquids : upgrading and utilisation.* 1991, London ; New York, NY, USA: Elsevier Applied Science ; Elsevier Science Pub. ix, 377 p.

5.   Czernik, S., J. Scahill, and J. Diebold, *The Production of Liquid Fuel by Fast Pyrolysis of Biomass.* Journal of Solar Energy Engineering-Transactions of the Asme, 1995. **117**(1): p. 2-6.

6.   Onay, O. and O.M. Kockar, *Slow, fast and flash pyrolysis of rapeseed.* Renewable Energy, 2003. **28**(15): p. 2417-2433.

7.   Oasmaa, A., et al., *Fast pyrolysis of forestry residue. 1. Effect of extractives on phase separation of pyrolysis liquids.* Energy & Fuels, 2003. **17**(1): p. 1-12.

8.   Czernik, S. and A.V. Bridgwater, *Overview of applications of biomass fast pyrolysis oil.* Energy & Fuels, 2004. **18**(2): p. 590-598.

9.   Adjaye, J.D. and N.N. Bakhshi, *Production of Hydrocarbons by Catalytic Upgrading of a Fast Pyrolysis Bio-Oil .1. Conversion over Various Catalysts.* Fuel Processing Technology, 1995. **45**(3): p. 161-183.

10.   Bridgwater, A.V., *Production of high grade fuels and chemicals from catalytic pyrolysis of biomass.* Catalysis Today, 1996. **29**(1-4): p. 285-295.

11.   Elliott, D.C. and E.G. Baker, *Upgrading Biomass Liquefaction Products through Hydrodeoxygenation.* Biotechnology and Bioengineering, 1984: p. 159-174.

12.   Maggi, R. and B. Delmon, *A review of catalytic hydrotreating processes for the upgrading of liquids produced by flash pyrolysis.* Hydrotreatment and Hydrocracking of Oil Fractions, 1997. **106**: p. 99-113.

13.   Oasmaa, A., et al., *Fast pyrolysis of forestry residue and pine. 4. Improvement of the product quality by solvent addition.* Energy & Fuels, 2004. **18**(5): p. 1578-1583.

14.   Boucher, M.E., A. Chaala, and C. Roy, *Bio-oils obtained by vacuum pyrolysis of softwood bark as a liquid fuel for gas turbines. Part I: Properties of bio-oil and its blends with methanol and a pyrolytic aqueous phase.* Biomass & Bioenergy, 2000. **19**(5): p. 337-350.

15.   Radlein, D.J., Piskorz, J. Majerski, P., *Methode of Upgrading Biomass Pyrolysis Liquids for use as Fuels and as Sources of Chemicals Reaction with Alcohol*, E. Patent, Editor. 1996.

1, 2, 4-TRIMETHYLBENZENE TRANSFORMATION OVER Y-ZEOLITE BASED CATALYST: EFFECT OF ACIDITY

S. Al-Khattaf

Chemical Engineering Department King Fahd University of Petroleum & Minerals

Dhahran 31261, Saudi Arabia

In this study, the transformation of 1,2,4-Trimethylbenzene (TMB) over Y-based zeolite catalysts will be investigated in a novel riser simulator that resembles closely the operating conditions of large scale FCC units. The focus of the study will be on the effect of Catalyst acidity and reaction conditions on the variation of conversion and the ratios of isomerization to disproportionation products (I/D). Also, distribution of the trimethylbenzene (TMB) isomers and the variation of the different xylene ratios with changes in the reaction conditions will be reported.

All the experimental runs will be carried out in the riser simulator. This reactor is novel bench scale equipment with internal recycle unit [1] to overcome the technical problems of the standard micro-activity test (MAT). The products will be analyzed in an Agilent 6890N gas chromatograph with a flame ionization detector and a capillary column INNOWAX, 60-m cross-linked methyl silicone with an internal diameter of 0.32 mm. The Y zeolite to be used in this work is spray-dried using kaolin as the filler and silica sol as the binder. The resulting 60-μm catalyst particles have the following composition: 30 wt% zeolite, 50 wt% kaolin, and 20 wt% silica sol. The process of sodium removal was repeated for the pelletized catalyst. The catalyst was calcined for 2 hr at 600°C (CAT-C). Some part of CAT-C was then treated with 100% steam at 800°C for 6 hr producing CAT-S. Table 1 shows the physical and chemical properties of both catalysts.

1,2,4TMB conversion over CAT-C catalyst was found to be slightly higher than that over CAT-S due to the higher acidity of CAT-C. The initial experimental results show that both disproportionation and isomerization reactions are taking place over both catalysts. The disproportionation reaction involves the formation of xylenes and tetramethylbenzenes from 2 moles of 1,2,4-TMB. Subsequently, the xylenes (one of the disproportionation product) react with the TMB to form a transalkylation product Toluene. Isomerization reaction forms both 1,3,5 TMB and 1,2,3 TMB. Fig 1 shows the total xylene yields and total isomerization yields

over both catalysts. Dealkylation reaction was found to be inconsequential over CAT-S due to the very small amount of gases observed. However, dealkylation reaction was found appreciable over CAT-C. At 500C and 15 sec contact time, CAT-S forms a negligible amount of gases compared to 11.4 wt % over CAT-C. Moreover, coke yield over CAT-C and at the same reaction condition was found to be 14 times more than that formed over CAT-S. And as expected, these products increase with increasing conversion. Conversion was also observed to increase with increasing contact time and reaction temperature.

Table 1. Catalyst properties

	CAT-C	CAT-S
Steaming temperature (°C)	-	800
Steaming time (h)	-	6
Average crystal size (μm)	0.9	0.9
BET surface area (m^2/g)	187	155
Total acidity (mmol/g)	0.545	0.033
Unit Cell Size (A)	24.51	24.28

.
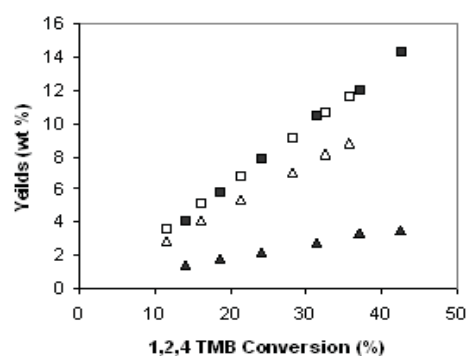
Fig. 1. Xylene and isomerization yield over both catalysts. ■ and □ are xylene yields over CAT-C and CAT-S respectively. ▲ and △ isomerization yields over CAT-C and CAT-S respectively.

While benzene yield was found low in both catalysts, toluene was produced in an appreciable amount over both catalysts. However, both catalysts have shown different toluene yeild. For example, at 500C and 15 sec reaction time, toluene yield was found 8.5 wt% over CAT-C compared to 1.5 wt% over CAT-S. This difference in toluene yield could be explained as follows; for CAT-S toluene is produced from only one reaction path (disproportionation). However, over CAT-C, toluene is produced via both the primary disproportination path and as well as the secondary dealkylation path. The initial experiments also suggest that toluene and ethylene are the main products for the dealkylation reaction which explains the low benzene selectivity over both catalysts.

References

[1] H.I. de Lasa, U.S. Pat. 5 102 (1992) 628.

WATER GAS SHIFT CATALYSTS FOR FUEL PROCESSOR:
FROM FIXED BED TO MICROCHANNEL REACTORS

S. Fiorot, C. Galletti, S. Specchia, G. Saracco, V. Specchia

Dipartimento di Scienza dei Materiali e Ingegneria Chimica,

Politecnico di Torino – Corso Duca degli Abruzzi, 24 – 10129 Torino, Italy.

Due to the increasing attention towards the emissions from the internal combustion engine, fuel cell technology is now standing out as a "clean" alternative for automotive pollution. The polymer electrolyte membrane fuel cell (PEMFC) is currently considered as the most suitable technology for vehicles application by the majority of the automotive companies due to its high power density, mechanical robustness, fast start-up, dynamic response characteristics.

Pure hydrogen is the ideal fuel as it offers some advantages for PEMFC: low operating temperature, high current density, low weight, compactness, long stack life, fast start-ups, satisfactory efficiency and truly "zero emissions" [1]. At the moment its utilization presents some problems due to lack of production plants and distribution nets and safety issues.

Therefore, the current way to feed vehicle FC transforms hydrocarbon feedstocks with a complex system based on reformate production and clean-up. The process considers a sequence of catalytic stages which reduces the reformate CO concentration to 10 ppm, limit value necessary to avoid poisoning of fuel cell Pt electrocatalyst.

The H_2 flow from reformer contains about 10% CO. Water gas shift (WGS) reaction (Eq. (1)) is the preferred one for CO removal; it reduces CO concentration to about 0.5–1% [2] and simultaneously increases the hydrogen one.

$$CO + H_2O \leftrightarrow CO_2 + H_2; \qquad \Delta H = -41.1 kJmol^{-1} \qquad (1)$$

Since at high temperatures CO conversion is equilibrium limited and at low temperatures is kinetically controlled, two types of WGS catalysts are commercially used. One for high temperature shift (HTWGS), based on Fe and Cr oxides, reduces at 400–500°C the CO concentration to about 2–5%. The second one for low temperature shift (LTWGS), with Cu and ZnO on alumina, is used at 200-400°C for reducing the CO concentration to about 1%.

A last preferential oxidation process (PROX) is yet necessary to reach 10 ppm CO.

Commercially a combination of the two catalysts is used with in between a cooling stage. However, they pose some disadvantages (low activity and some thermodynamic limitations at

high temperatures for the HT catalyst; pyrophoricity for the LT one) that render the catalysts unsuitable for residential or automotive applications, where fast start-ups dictate the use of reactors with low catalyst volume and therefore very active and non-pyrophoric catalysts [1].

If more active low temperature shift catalysts are developed, the CO conversion can then approach more favourable equilibrium limit.

Several other literature studies on catalysts for the WGS reaction considered noble (Pd, Au, Rh, Pt). In this work, some catalysts were prepared according to literature [3] as concerns the active elements and their catalytic activity was tested as powders in a fixed bed microreactor; the most active catalysts were then deposed and tested in a structured microchannel reactor.

Three preparation procedures were used: SCS (Solution Combustion Synthesis), IWI (Incipient Wetness Impregnation) and Deposition-Precipitation (DP). In all cases, the final powder obtained was calcined in oxygen flow and reduced in H_2 flow for 2 hours.

The feed mixture was prepared via mass flow controllers (MFC), for the gaseous components; water (dosed through a liquid-MFC) was added feeding it to an evaporator kept at a suitable temperature. The feedstock was delivered through a heated tube (above 110°C) to avoid water condensation. For powder catalysts, a pressure transducer measuring the inlet and outlet pressure checked any possible undesired clogging of the catalytic fixed bed.

The outlet gas stream was analyzed through a gas chromatograph (Varian CP-3800) equipped with a thermal conductivity detector (TCD). The feed mixture composition was varied depending on the temperature condition of the shift reaction: 10% CO, 6% CO_2, 40% H_2, 30% H_2O and He (balance) for HTWGS; 5% CO, 11% CO_2, 40% H_2, 25% H_2O and He (balance) for LTWGS. The total gas flow rate for the fixed bed microreactor was in any case equal to 200 Nml/min with a weight gas hourly space velocity WHSV = 78 Nl/h/g.

For LTWGS, the catalytic activity of Pt, Au, Rh on CeO_2 and TiO_2 on powder was investigated. Fig. 1 shows the CO residual concentration vs. temperature; the equilibrium conditions are also drawn to facilitate a quick glance estimation of the catalysts performance.

The lowest activity was shown by 2%Au-CeO_2 catalyst prepared by DP: 18% maximum conversion at 340°C. This result is in disagreement with the good activity data for literature Au-catalysts, prepared with synthesis procedures that allowed reaching a good dispersion of Au clusters on the support [4, 5]. HRTEM analysis of our Au catalyst showed the presence of large metal clusters size (about 20 nm), probably responsible for the not good performance.

A comparison between the catalytic activity of 2% Pt/CeO_2 catalysts prepared by IWI and SCS methods showed a better performance for the first one. Therefore, IWI was chosen as the synthesis method for the further catalysts preparation.
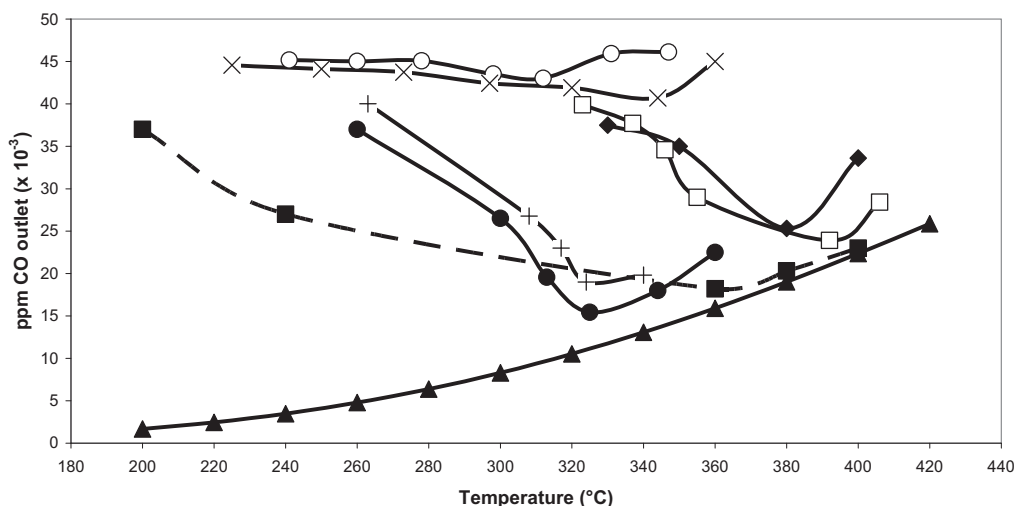
Fig. 1: CO outlet concentration vs. temperature for LTWGS on powder. (▲) thermodynamic equilibrium; (+) 2%Pt/CeO$_2$(SCS); (●) 2%Pt/CeO$_2$(IWI); (□) 2%Rh/CeO$_2$; (■) Cu/ZnO/Al$_2$O$_3$ commercial catalyst; (×) 2%Au/CeO$_2$; (○) 2%Pt/La$_2$O$_3$; (♦) 2%Pt/TiO$_2$.

For comparison, the activity of the LTWGS commercial catalyst Cu/ZnO/Al$_2$O$_3$ is also drawn in Fig. 1; its interesting performance was developed at rather high temperature. Moreover, the CO residual concentration in low temperature range, also if lower than that measured with the noble metal catalysts, proved to be not compatible with that required for PROX feeding. Some catalysts we prepared demonstrate to possess good activity. The 2%Rh/CeO$_2$ catalyst was particularly active at high temperature: the CO outlet concentration was about 2.3% at 390°C. The 2% Pt/TiO$_2$ reached, at 380°C, a residual CO concentration of about 2.5%, near to the thermodynamic equilibrium. These data proved the two above catalysts could be used for HTWGS reaction; therefore, they were tested for HTWGS and the obtained results (Fig.2) confirmed their satisfactory performance.
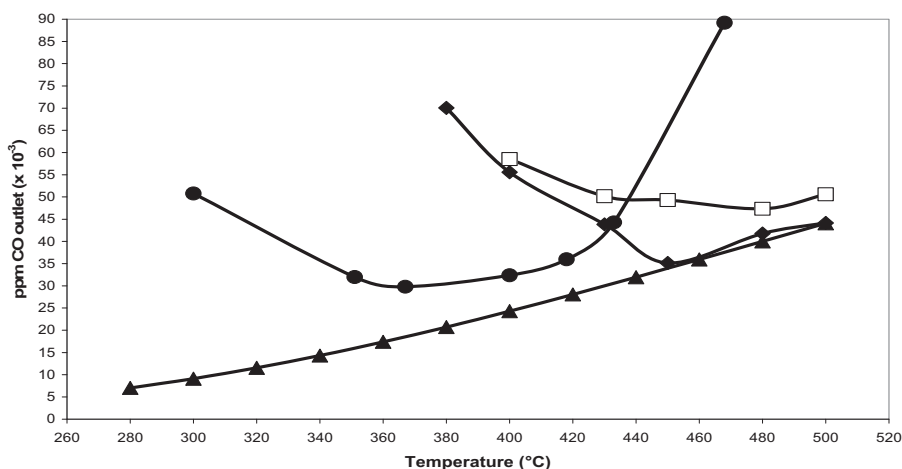
Fig. 2: ppm CO outlet vs. temperature for HTWGS on powder. (▲) thermodynamic equilibrium; (●) 2%Pt/CeO$_2$(IWI); (□) 2%Rh/CeO$_2$; (♦) 2%Pt/TiO$_2$.

In order to develop a structured system, preliminary catalytic activity tests on a microchannel laboratory reactor, equipped with six plates 50x50x1 mm with microchannels 0.26 mm width, were also carried out for HTWGS with 1%Pt catalyst on both CeO_2 and a modified mixed support $(50\%CeO_2+50\%TiO_2)$ for a stronger and better adhesion on the metallic surface of the microchannel plates (Fig.3). Each catalyst reached practically the equilibrium conditions, but at different temperature: 450°C with Pt-MIX and 530°C with Pt-CeO_2.
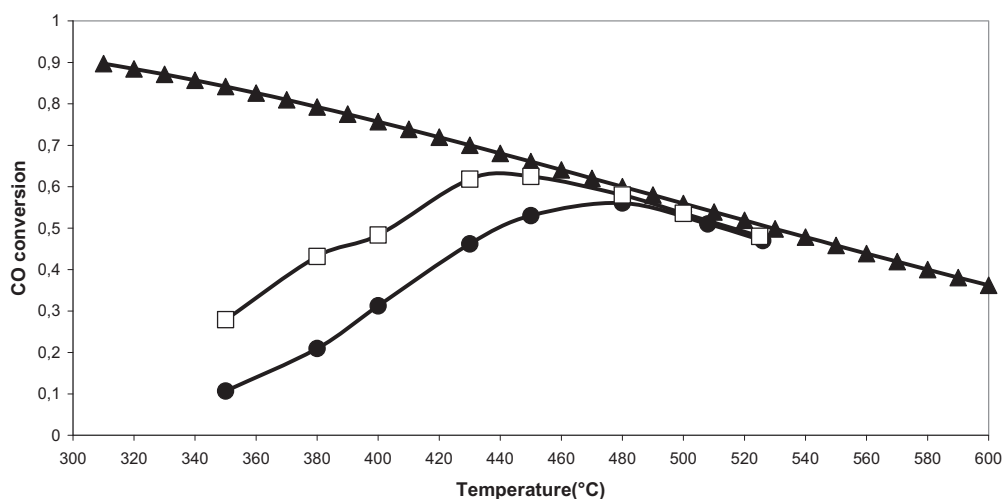
Fig. 3: CO conversion vs. temperature for HTWGS microchannel reactor with WHSV=50Nl/h/g. (▲) thermodynamic equilibrium; (●) 2%Pt/CeO_2(IWI); (□) 1%Pt-(50%CeO_2+50%TiO_2).

Since the catalysed plates used in the microchannel reactor showed good activity and a satisfactory potentiality for approaching the WGS equilibrium condition.

[1] A. F. Ghenciu, Current Opinion in Solid State and Materials Science, 6, (2002), 389-399;

[2] A. Luengnaruemitchai, S. Osuwan, E. Gulari, Catalysis Communications, 4, (2003), 215-221;

[3] G. Jacobs, L. Williams, U. Graham, G. A. Thomas, D. E. Sparks, B. H. Davis, Applied Catalysis A: General, 252, (2003), 107-118;

[4] A. Wolf, F. Schuth, Applied Catalysis A: General, 226, (2002), 1-13;

[5] T. Tabakova, F. Boccuzzi, M. Manzoli, J.W. Sobczak, V. Idakiev, D. Andreeva, Applied Catalysis B. Environmental, 149, (2004), 73-81.

PARALLIZED REACTOR SYSTEM FOR HIGH-THROUGHPUT-TESTING OF HYDROGEN STORAGE MATERIALS

A. Lange de Oliveira, P. Kolb

hte Aktiengesellschaft; Kurpfalzring 104; D-69123 Heidelberg; Germany

Fax. +49 (0)6221 7497-177; armin.oliveira@hte-company.de

A 2-fold-reactor was developed for simultaneous testing of hydrogen storage materials with respect to storage capacity and kinetics. The underlying base unit can be easily parallized to a manifold-reactor-system. Maximum temperatures and pressures are 300°C and respectively 200bar. Validation of the system was performed with a hydrogen-storage material (AB5-type) that is highly sensitive towards water.

Working principle

In Figure 1 the base unit of the 2-fold-reactor system is depicted. The unit mainly consists of two loops for absorption and desorption which are connected via automated 2-way-valves to the actual reactor. Pressure transducers in conjunction with thermocouples in both loops and the reactor allow calculation of the absorbed or desorbed amount of hydrogen by means of van-der-Waals-equation. Transfer tubes especially within the zone of thermal gradient into and out of the oven have low cross-section so that temperatures recorded are representative for the gas-phase in the reactor. The difference in mass-balance between amount of hydrogen introduced into the reactor respectively discharged from the reactor and the amount determined in the reactor´s gas-phase is accounted as absorbed respectively desorbed hydrogen.

Figure 1: scheme of base unit

Powder samples can be easily introduced into the reactor within glass vials. Thermocouple TI 2 is in contact with the sample thus exothermicity or endothermicity of the processes can be directly assessed.

The measurement itself consists of repeated cycles that involve following steps:

1. filling of V_1 with hydrogen up to p_0 by acting Valve 1, equilibration and subsequently acting Valve 1 again

2. filling of V_2 (reactor) with hydrogen from V_2 by acting Valve 2, equilibration and acting Valve 2 again

Desorption is measured accordingly by acting Valves 3 and 4.

Validation

In Figure 2 a) the typical course of pressure and temperature during absorption cycles is displayed. Initially high exothermicities are noticed upon charging cycles. From the pressure decrease within the cycles kinetics can be deduced. Figure 2 b) shows the high accuracy within six repetition experiments. In the first absorption cycle the full capacity of the storage material is not accessible. This phenomenon of activation upon the first charging and discharging processes is well known for AB5-type materials.
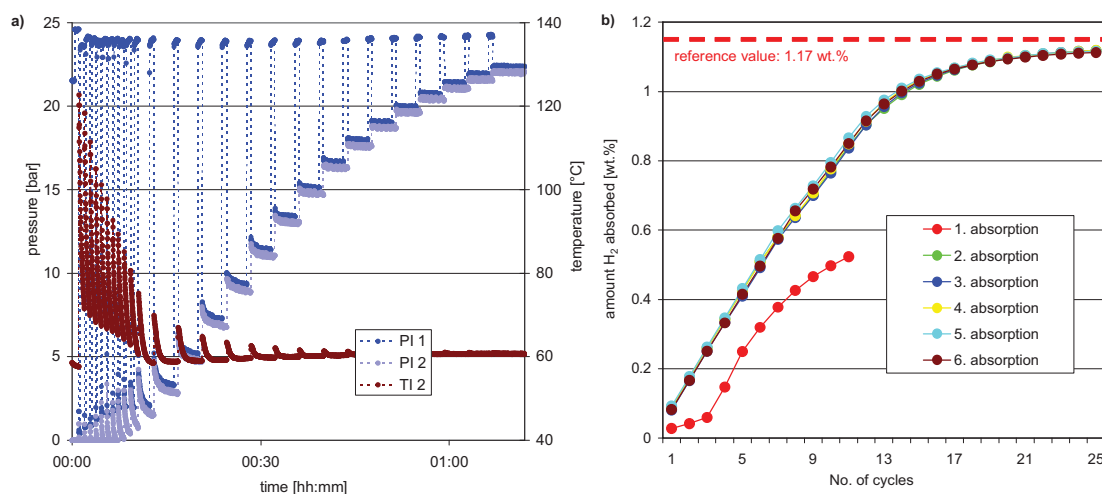
Figure 2: pressure and temperature course during absorption experiment (a) and calculated hydrogen-absorption in repetition experiments (b)

Summary

A 2-fold-reactor-system for testing of hydrogen-storing materials was successfully validated. The generic low-cost-approach allows for higher degree of parallelization and may be employed for other gas-absorptions-tests as well. Especially for hydrogen-storage materials the long-term cycling stability is an important issue. HTE supplies the necessary high testing capacities.

AROMATIZATION OF ISO-OCTANE ON Mo$_2$C CATALYSTS

<u>Frigyes Solymosi</u>*, Aleksander Széchenyi

Institute of Solid State and Radiochemistry, University of Szeged,

Szeged, H-6701, P.O.Box 168, Hungary

*Corresponding author. Tel/Fax :+36-62-420-678, fsolym@chem..u-szeged.hu

Introduction

Recently, we undertook the study of the aromatization of C$_2$-C$_7$ hydrocarbons on Mo$_2$C-containing catalyst [1]. This research program was initiated by the finding that Mo$_2$C on ZSM-5 exhibits a unique catalytic behaviour; it can convert methane with 80% selectivity into benzene at 10-15 % conversion [2-5]. In the present paper we give an account on the reaction pathways of iso-octane on various Mo$_2$C-containing catalysts.

Experimental

Mo$_2$C was prepared by the carburization of MoO$_3$ (products of ALFA AESAR) by C$_2$H$_6$/H$_2$. The oxide was heated under 10% v/v C$_2$H$_6$/H$_2$ gas mixture from room temperature to 900 K at a heating rate of 0.8 K/min. Afterwards the sample was cooled down to room temperature under argon. The carbide was passivated in flowing 1% O$_2$/He at 300 K. The surface area of Mo$_2$C is 20 m^2/g. In certain cases Mo$_2$C was prepared in situ, in the catalytic reactor, when the last step was missing. Supported Mo$_2$C catalysts have been made in the similar ways by the carburization of MoO$_3$-containing supports with C$_2$H$_6$/H$_2$ gas mixture. All the catalysts used in the study have been characterized by XPS measurements. The acidic properties of catalysts were evaluated by NH$_3$-TPD and FTIR methods using the adsorption of pyridine and CO. Catalytic reaction was carried out at 1 atm of pressure in a fixed-bed, continuous flow reactor consisting of a quartz tube connected to a capillary tube. The flow rate was 12 ml/min. The carrier gas was Ar. The hydrocarbon content was 2.0%. Generally 0.3 g of loosely compressed catalyst sample was used. Reaction products were analysed gas chromatographically using a Hewlett-Packard 6890 gas chromatograph with a 60 m long GS-GASPRO column.

Results

Pure Mo_2C prepared by C_2H_6/H_2 gas mixture exhibited relatively low activity. The decomposition of iso-octane started at ~623 K, and the conversion reached value of ~18-20 % at 873 K. At lower temperature, 623-723 K, the main process is the dehydrogenation with some cracking. At 723-873 K, however, aromatics, mainly p-xylene and toluene are also formed with 6-10 % selectivity. On Mo_2C/Al_2O_3 the product distribution was somewhat different. Although still the dehydrogenation of iso-octane was the dominant process as indicated the formation of octenes, aromatics were produced with higher selectivity. At 773-823 K the main aromatics were ethylbenzene and p-xylene, they formed with ~23-25 % selectivity. In contrast, on $Mo_2C/$ ZSM-5(80), which was the most effective catalyst, toluene and benzene were the dominant aromatics indicating the occurrence of the hydrogenolysis of C_8 aromatics on the acidic sites of ZSM-5. The selectivity of these compounds reached a value of 45-55 % at 773 K at a conversion level of ~20%. This catalyst exhibited a very stable activity: the conversion decayed only with few percent even after 10 hours, and the aromatizing capability also remained high. Interestingly, octenes were detected only in traces. This suggests that octenes formed in the dehydrogenation process have been rapidly converted into other compounds. This was confirmed by the study of the reaction of 1-octene on the $Mo_2C/ZSM-5$ catalysts. Applying ZSM-5 of different acidity showed that highest conversion and aromatics selectivity were attained using ZSM-5 of high Brønstead acid sites. The results are interpreted by the monofunctional (pure Mo_2C) and bifunctional mechanism (supported Mo_2C) of the aromatization of iso-octane. From the comparison of these results with those obtained on the aromatization of n-octane we can infer some interesting conclusion as concerns the influence of the structure of hydrocarbons on their reaction pathways.

References

[1] R. Barthos, F. Solymosi, J. Catal. 235 (2005) 60-68. and references therein

[2] L. Wang, L. Tao, M. Xie, G. Xu, J. Huang, Y. Xu, Catal. Lett. 21 (1993) 35.

[3] F. Solymosi, A. Erdőhelyi, A. Szőke, Catal. Lett. 32 (1995) 43.

[4] F. Solymosi, J. Cserényi, A. Szőke, T. Bánsági, A. Oszkó, J. Catal. 165 (1997) 150.

[5] D.W. Wang, J.H. Lunsford, M.P. Rosynek, J. Catal. 169 (1997) 347.

[6] F. Solymosi, A. Széchenyi, J.Catal. 223 (2004) 221.

A COMPARATIVE STUDY OF THE PRODUCTION OF ETHYL ESTERS FROM VEGETABLE OILS AS A BIODIESEL FUEL

A. Bouaid, M. Martinez and <u>J. Aracil</u>

Chemical Engineering Department, Faculty of Chemistry,

University of Complutense 28040 Madrid, Spain

E-mail: jam1@ quim.ucm.es.

In recent years, the development of alternative fuels from renewable resources, like biomass, has received considerable attention. Fatty acid methyl or ethyl esters, known as biodiesel, show large potential applications as diesel substitutes.

Ethyl esters are the product of transesterification of fats and vegetable oils with ethanol (obtained from fermentation in our case) in the presence of an acid or an alkaline catalyst. In addition, the process yields glycerol, which has large applications in the pharmaceutical, food and plastics industries.

In the present work, the process of synthesis of ethyl esters from High Oleic Sunflower Oil (HOSO), High and Low Erucic *Brassica Carinata* Oils (HEBO and LEBO), as alternative vegetable oils, using KOH as catalyst, has been developed and optimized by application of the Factorial Design and Response Surface Methodology. The effect of temperature, ethanol/oil molar ratio and catalyst concentration were studied. Catalyst concentration was found to have the most significant influence on conversion. A second order model was obtained to predict conversions as a function of temperature and catalyst concentration for LEBO process. The model has been found to describe the experimental range studied adequately.

PRODUCTION OF SYNTHESIS GAS BY REFORMING OF METHANE IN PRESENCE OF WATER OVER BIMETALLIC SUPPORTED CATALYSTS

Sh.S. Itkulova, G.D. Zakumbaeva, I.S. Chanysheva, L.V.Komashko

D.V. Sokolsky Institute of Organic Catalysis and Electrochemistry; 142, Kunaev str., Almaty, 050010, Republic of Kazakhstan, fax: +7-3272-915722, e-mail: itkulova@nursat.kz

Reforming of methane by carbon dioxide in presence of steam (steam-dry reforming or bi-reforming of methane) has been studied over the 5% bimetallic Co-containing catalysts promoted by a noble metal and supported on alumina with additives of NaZSM. It has been established that the introduction of steam into an initial gaseous mix (CO_2/CH_4) leads to decreasing the temperature of complete methane conversion ($<700^{o}C$), suppressing the coke deposition, and increasing the content of hydrogen in synthesis-gas formed ($H_2/CO > 1$). It has been shown that the introduction of 10% zeolite (NaZSM) into the $Co-M/Al_2O_3$ catalyst causes growing its activity.

Introduction

Synthesis-gas ($CO+H_2$) is a source being alternative to oil for the production of hydrocarbons and oxygenates by the well-known Fischer-Tropsch Synthesis (eqn. 1).

$$CO + 2H_2 \rightarrow C_nH_{2m} \qquad (eqn.1)$$

Synthesis-gas can be produced from available and abundant source - natural gas by 3 ways widely described in literature: 1) steam reforming (eqn.2); 2) partial oxidation (eqn.3); and 3) dry reforming (eqn.4).

$$CH_4 + H_2O \rightarrow CO + 3H_2 \qquad \Delta H = 206.3 \ kJ/mol \qquad (eqn.2)$$

$$CH_4 + 1/2O_2 \rightarrow CO + 2H_2 \qquad \Delta H = -35.6 \ kJ/mol \qquad (eqn.3)$$

$$CH_4 + CO_2 \rightarrow 2CO + 2H_2 \qquad \Delta H = 247.3 \ kJ/mol \qquad (eqn.4)$$
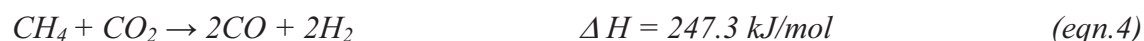
Carbon deposition occurring due to methane decomposition and/or disproportionation of carbon monoxide formed is a major problem of all abovementioned processes.

We have made an attempt to carry out the process combining both dry and steam reforming of CH_4 - steam-dry reforming, which can be called as the bi-reforming of methane. It was expected that the combining both processes can lead to a necessary ratio of $H_2/CO \leq 2$.

OP-4-12

Besides, the suppression of carbon deposition by water was also supposed. The Co-containing catalysts promoted by Pt-Group metal and supported on alumina modified by NaZSM zeolite have been used.

Experimental procedures

The Co-containing bimetallic catalysts supported on alumina promoted by zeolite (NaZSM) have been used in both dry reforming and bi-reforming of methane. The content of metals (Co and Pt-Group metal) is 5 wt. % from total catalyst amount. Co/M weight ratio is 8/2. The content of NaZSM in the support was varying from 10 to 20 wt. % from total mass of support (γ-Al_2O_3 + NaZSM). The catalysts were prepared by an impregnation method.

The processes were carried out at a flow quartz reactor supplied with the programmed heating and controlled feeding velocity under conditions: atmospheric pressure, space velocity - 1000 hr^{-1} and varying temperature from 200 to 800°C. The volume ratio of gases CO_2/CH_4/Ar/H_2O was 10/10/80/2 for bi-reforming and CO_2/CH_4/Ar = 10/10/80 for dry reforming of methane.

The initial and final gaseous reaction products have been on-line analysed by the gaseous chromatographs. Liquid products were collected in a special cooling trap and analysed after reaction by using the GC.

The physico-chemical properties of catalysts were studied by an electron microscopy, BET and IR-spectroscopy.

Results and Discussion

Dry reforming occurs with a slight activity at 300°C over all the catalysts studied. The complete conversion of methane is observed at temperature higher than 700°C. CO_2 conversion does not reach 100% and varied within 94.0-96.6%. The complete CO_2 conversion was not observed even at increasing temperature to 850-900°C.

Synthesis-gas is only one product of dry reforming over the 5%Co-M/Al_2O_3 catalyst. Over the zeolite containing catalysts, synthesis-gas, water, acetic acid, and non-significant amount of other oxygenates such as ethers, alcohols, and higher molecular carboxylic acids are formed. Selectivity to acetic acid is about 2% over both zeolite containing catalysts.

It has been observed that adding steam into the feeding mix promotes the CH_4 conversion. Temperature of the complete CH_4 conversion is decreased by 30 and 55°C with increasing the content of zeolite from 10 to 20 wt.% respectively. For the catalyst containing no zeolite, a decrease by 20°C is observed (Table 1). The comparison of both processes at the same temperatures demonstrates that CH_4 conversion in bi-reforming is higher than in dry reforming.

Table 1. Comparative characteristics of 5%Co-M$_2$/Al$_2$O$_3$+zeolites catalysts at the processes of dry reforming and bi-reforming of CH$_4$ (CO$_2$:CH$_4$=1:1; CO$_2$:CH$_4$:H$_2$O=1:1:0.2; V=1000 hr^{-1}; P = 1 atm)

Catalysts	Process	T,^{o}C	K$_{CH4}$,%	K$_{CO2}$,%	H$_2$/CO
5%Co-M/90%Al$_2$O$_3$-10%NaZSM	Dry reforming	500	34.5	39.5	1.5
		600	77.3	70.9	0.7
		725	~100	94.0	0.8
	Bi-reforming	500	36.6	26.7	2.1
		600	86.9	71.3	1.0
		695	**~100**	**87.3**	**1.1**
5%Co-M/80%Al$_2$O$_3$-20%NaZSM	Dry reforming	500	16.9	46.7	1.5
		600	87.8	86.5	1.1
		755	~100	94.9	0.9
	Bi-reforming	500	41.9	32.5	0.9
		600	89.7	74.4	0.7
		700	~100	81.2	0.9
5%Co-M/Al$_2$O$_3$	Dry reforming	500	23.8	17.4	2
		600	79.9	60.6	1.1
		740	~100	96.6	1.1
	Bi-reforming	500	40.6	31.3	2.3
		600	90.7	60	1.5
		720	~100	78	1.2

The conversion of CO$_2$, when K$_{CH4}$= 100%, is lower in bi-reforming as compared with dry reforming. It can indicate that the steam reforming begins to be prevalent at higher temperatures over all catalysts.

The main products of bi-reforming are carbon monoxide and hydrogen; also, oxygenates are formed over all the catalysts including containing no zeolite unlike the dry reforming. The yield of acetic acid is increased to 5-6% in bi-reforming. The yield of other oxygenates: methanol, ethanol, ethers, and carboxylic acids is not significant (less than 0.1%).

At adding steam (20 vol.%) to the CO$_2$-CH$_4$ feeding mix, yield of hydrogen is increased over the catalysts except the catalyst with 20% NaZSM. At temperature

corresponding to 100% CH_4 conversion, a ratio of H_2/CO is 1.1 and 1.2 over 5%Co-M/90%Al_2O_3-10%NaZSM and 5%Co-M/Al_2O_3 respectively that is higher than in dry reforming (0.8 and 1.1 respectively).

The effect of a reaction medium on the catalyst surface has been observed by TEM. In a fresh sample, the metal particles have a larger size than in the catalysts used in the dry reforming of methane. Adding water to the reacting mix leads to the following increase in dispersion. This effect has been observed over all catalysts.

Amorphous carbon has been observed in the catalysts after dry reforming of methane. No coke and no carbon have been determined after the bi-reforming of methane over all catalysts. It is possible to suppose that carbon formed reacts with water with the formation of an additional amount of carbon oxide and hydrogen. This reaction may be one of reasons of the positive effect of water.

IR-study of the catalysts showed the dissociative character of adsorption of CH_4 and CO_2 over the catalysts. The bands attributed to CO_{ads} (1920, 2000 cm^{-1}) and to CH_{xads} groups ($\sim$3000 cm^{-1}) are presented in IR-spectra. Also, OH_{ads} groups have been observed in the catalysts after both reactions. In case of dry reforming, OH_{ads} can be appeared due to the secondary surface reactions. During bi-reforming, also the dissociation of H_2O can take place.

Conclusions

The results of study show, that bi-reforming is more effective than dry reforming of CH_4 over the Co-containing supported catalysts. The presence of up to 20 vol.% water positively effects on the process. Temperature of complete methane conversion decreases by 20-55° depending on the zeolite content. Also, water prevents the coke formation. It gives a possibility to use the real natural and technological gases containing some amount of water for production of synthesis gas and oxygenates such as acetic acids by one step. Adding the 10% zeolite (NaZSM) into the Co-M/Al_2O_3 improves its performance in both processes. Temperature of complete methane conversion decreases to 695°C in bi-reforming of CH_4 over this catalyst.

STUDY OF OXIDATION OF ORGANIC COMPOUNDS
IN A MICROSTRUCTURED CATALYTIC REACTOR

Z.R. Ismagilov, E.M. Michurin, I.Z. Ismagilov, M.A. Kerzhentsev, A.N. Zagoruiko,
E.V. Rebrov*, M.H.J.M. de Croon*, J.C. Schouten*

*Boreskov Institute of Catalysis SB RAS, pr. Akad. Lavrentieva 5, 630090, Novosibirsk,
Russia; fax +7-383-339-73-52; e-mail: zri@catalysis.ru*
**Eindhoven University of Technology, Den Dolech 2, P.O.Box 513, 5600 MB Eindhoven,
The Netherlands; fax: +31-40-244-6653, e-mail: j.c.schouten@tue.nl*

Development of microstructured reactors is a prospective field in chemical technology, in particular for hydrogen production for fuel cells, fine chemical synthesis, high energetic materials synthesis and processes with participation of hazardous compounds.

This presentation refers mostly to the field of hydrogen energy, namely to one of the main stages – the catalytic conversion of fuels to produce hydrogen. The reaction of total oxidation is the first step in processes of fuel autothermal conversion and partial oxidation. On the other hand, the total fuel oxidation (catalytic combustion) is a important step in the fuel microprocessor network to provide heat for endothermic reaction of fuel conversion with steam and for utilization of anode gases. Therefore, we undertook systematic research for development of a catalytic microreactor for total oxidation of organic compounds, including:

- Fabrication of microstructured plates from the Al51st alloy;
- Preparation of a uniform anodic alumina coating on the plates;
- Impregnation of alumina coating with a catalyst precursor;
- Assembling of the microreactor;
- Microreactor testing in the reactions of total oxidation of organic compounds;
- Computer simulation of reaction kinetics.

Microstructured plates. Aluminum or its alloys were selected for the microreactor due to their high heat conductivity and possibility of preparation of a strong porous alumina layer by anodization. For the microreactor fabrication, plates with a length of 40 mm and a width of 28 mm made from AlMgSiCu1 alloy (6082 series, Al51 st) were taken. This alloy, being electro discharge machined (EDM) by the method of "2 incisions", provided a surface roughness of microchannel walls (Ra) below 2.0 µm. In each plate of 416 µm thickness, 45 semi-

cylindrical microchannels of 208 μm in radius with the distance in between of 150 μm were machined.

Coating Development. A porous alumina layer was produced by anodic oxidation of the AlMgSiCu1 alloy in 3.5 wt.% oxalic acid solution at 274±0.1 K for 23 hrs under current controlled conditions. The produced alumina layer has cylindrical pores with an average diameter of ca. 40 nm and very narrow pore size distribution. The layer has a uniform thickness of 29±1 μm.

Catalyst Development. The resulting coatings were impregnated with an aqueous solution of copper dichromate followed by drying and calcination at 450^oC to produce active catalysts. The coatings were characterized by XPS, ESDR, chemical analysis, X-ray microprobe analysis and SEM. The effect of a copper dichromate concentration, number of impregnation cycles (1 or 2), and different after-treatments on catalytic activity and stability in complete oxidation of butane was studied. The catalytic activity of the obtained coatings is comparable or superior to that of alumina supported pelletized catalysts even at much lower loadings of active metals. For the fabrication of the microreactor, microstructured catalysts containing 5 wt.% of Cu(II) and Cr(III) oxides (related to the mass of alumina layer) were prepared.

Microreactor fabrication The microreactor catalyst section is assembled from 63 microstructured plates with the catalytic coating. It has a size of ca. 28 x 34 x 40 mm^3 and contains 2835 semi-cylindrical microchannels. The microreactor has an inlet section with a diffuser and an outlet section with a cooler to cool gases leaving the catalyst section, preventing homogeneous gas phase reactions. The microreactor is connected to an automatic experimental setup equipped with mass flow controllers for preparation of reaction mixtures, temperature controllers and a GC.

Study of the kinetics of oxidation of organic compounds in a microreactor. Oxidation of n-butane, ethanol and isopropanol was studied at initial concentrations 0.5 -1.2 vol. %; GHSV in the range of 1600-10700 h^{-1}, temperature 150-360°C.

The oxidation of butane proceeds with the formation of the products of deep oxidation CO_2 and H_2O in the whole temperature range. No products of partial oxidation were detected. The dependencies of butane conversion on space velocities and temperatures (Fig. 1) were found to be in the best agreement with the reaction rate of first order with respect to butane. The kinetic parameters of the reaction: the rate constants and the apparent activation energy E_a (103 kJ/mol) were calculated.

Ethanol oxidation in the temperature range 200-325°C was shown to proceed with an intermediate formation of the products of partial oxidation: acetaldehyde and CO (Fig.2). In addition trace concentrations of acetone were detected. At higher temperatures, only products of deep oxidation: CO_2 and H_2O were formed.
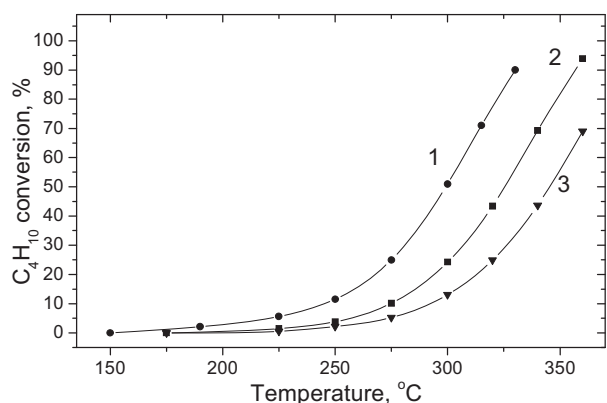
Fig. 1. Butane conversion at oxidation with air versus temperature at different GHSV: (1) 1600 h^{-1}, (2) 5360 h^{-1}, (3) 10700 h^{-1}, GHSV calculated with respect to the volume of catalyst coating
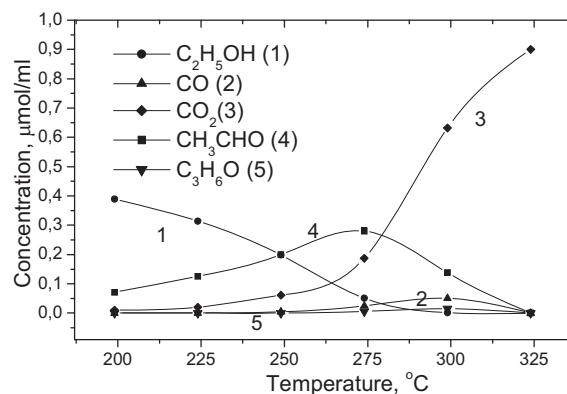
Fig.2. Composition of reaction products at the outlet of the reactor versus temperature during oxidation of ethanol with air at 5360 h^{-1}

The oxidation of isopropanol at T<325°C proceeded similarly with the formation of intermediate products of partial oxidation: acetone and CO. In addition, a parallel reaction of isopropanol dehydration on alumina support with propylene formation took place. At T>325°C mainly products of deep oxidation: CO_2 and H_2O were formed.

The kinetics of the reactions of alcohols oxidation was studied and tentative mechanisms of the reactions were proposed.

The oxidation reaction stimulation was done using the Mathcad 12 software, with the one-dimensional plug flow model including the Langmuir-Hinshelwood (L-H) kinetics and accounting for the variation of average temperature of catalyst, based on the pre-determined geometry of microchannels.

POST-SYMPOSIUM

"Catalytic Processing of Renewable

Sources: Fuel, Energy, Chemicals"

PLENARY LECTURES

PRECENT TRENDS IN CATALYTIC PROCESSING OF RENEWABLE PLANT BIOMASS INTO VALUABLE PRODUCTS

B.N. Kuznetsov

Institute of Chemistry and Chemical Technology SB RAS, Krasnoyarsk, Russia

Some features of catalyst application in the conversions of plant biomass

The main drawback of the conventional technologies of renewable plant biomass processing into chemicals, liquid hydrocarbons and carbon materials is their low productivity and selectivity as compared to catalytic petrochemical processes. The common approaches developed for liquid and gaseous reagents are not always suitable in catalytic conversions of solid plant polymers.

The processes of direct and indirect catalysis are used in catalytic conversions of plant biomass. For the direct action of catalyst on the transformation of chemical bonds in plant polymers the effective interaction between catalyst and polymer surface is demanded. The degree of catalyst and polymer interaction is increased in a sequence: solid catalyst < suspended catalyst < supported particles of catalyst < dissolved or molten and volatile catalysts < catalyst chemically bonded with polymer.

The other group of catalytic transformations proceeds via a route of indirect catalysis by means of the transfer of the catalyst action through the reaction medium:

catalyst $\rightarrow$ generation of active intermediates in the reaction medium $\rightarrow$ plant polymer $\rightarrow$ products.

The realization of indirect catalysis route simplifies the technology of the catalytic process, owing to the use a fixed or fluidized bed of heterogeneous catalysts for processing of powdery plant biomass.

Some examples of the successful use of catalysts in the novel processes of lignin oxidative depolymerization, polysaccharide acidic transformations, plant polymers thermocatalytic conversions are presented below.

Catalytic conversions of plant biomass to chemical products

Lignin oxidative destruction. The use of catalysts makes it possible to increase the efficiency of wood delignification processes. Two catalysts: antraquinone and 1,4-dihydro-9,10-dihydroxyanthracene disodium salt are used for the cellulose production in industry. But the many other different catalysts were successfully tested on a laboratory scale at the

PLS-1

conditions of alkaline pulping and oxidative delignification in the presence of metal salts, polyoxometalates, manganese complexes, etc.

The ecologically friendly process of wood delignification in the medium "acetic acids – hydrogen peroxide – water – catalyst" was developed. It was found that the delignification activity of oxidative –reductive catalysts is higher as compared to acidic catalysts. The conditions of one-step producing of pure cellulose and microcrystalline cellulose by wood delignification with powdery TiO_2 catalyst through the route of indirect catalysis were selected.

Low molecular-mass lignin of wood delignification process was used as raw material for producing aromatic hydrocarbons on zeolite catalyst HZSM. The maximal yield of liquid products (43 % mas.), containing toluene, xylenes, benzol was observed at 550 °C. Catalytic processes of lignin conversion were adapted to production of high-octane components of motor fuels: alkyl (C_7-C_{10}) benzoles and arylmethyl ethers.

Novel catalytic methods of aromatic aldehydes producing from wood lignin are under the development. The significant increase of vanillin and syringaldehyde yields was observed in the process of wood lignin and lignosulphonates oxidation by molecular oxygen in alkaline medium in the presence of copper catalysts. At selected conditions the yield of vanillin is by 2 times higher and the total duration of the process is about 10 times shorter in the comparision with the industrial non-catalytic process of vanillin production from lignosulphonates.

Wood polysaccharides acidic conversions. Catalytic reactions of hydrolytic splitting of wood polysaccharides in the presence of mineral acids are used in hydrolysis industry, mainly for ethanol and furfural producing. The important directions of the research at this area are connected with the products diversification and catalytic process simplification.

It was found the yield and the composition of wood steam-cracking products (furfural, acidic acid, alcohols, sugars, hydroxymethylfurfural e.a.) are changed in high extend under the action of metal sulfate catalysts at 150-350 °C. The degree of wood conversion at 200 °C is increased by 2-3 times in the presence of $Fe_2(SO_4)_3$, by 4 and 9 times in the presence of $CoSO_4$ and $Al_2(SO_4)_3$ accordingly. In a flow reactor the levoglucosenone is formed from wood with the yield up to 4.6 % mas. under the action of $Al_2(SO_4)_3$. In the autoclave reactor mainly furfural and levulinic acid are produced with yields 15-16 % and 30-35 %, accordingly. Sulfuric acid catalyzes the transformation of levoglucosenone to levulinic acid. The scheme of levulinic acid formation from wood cellulose was established: cellulose → → glucose → levoglucosenone → hydroxymethylfurfural → levulinic acid.

Sulfuric acid catalyst can be effectively used under the moderate temperature (98 °C) to synthesize levulinic acid with yields exceeding 35 % mol. for glucose and 50 % mol. for

sucrose. In the two-phases system "catalyst water solution – butanol" the continuous removal of carbohydrate conversion products from water phase by means of alkylation and extraction processes increases significantly (by 8-9 times) the yields of ethers of levulinic acid and hydroxymethylfurfural at high concentration of carbohydrates in the water solution.

Thermocatalytic conversions of plant biomass

Co-hydropyrolysis of biomass/plastic mixtures. The utilization of plant biomass residues and the waste plastics to liquid products was studied. The main task of the accomplished work was to establish the influence of co-liquefaction process conditions on the yield and composition of liquid products, in particularly: process operating parameters (temperature, gaseous medium, time of treatment, biomass/plastic ratio); nature of plant biomass (cellulose, lignin, beech-wood, pine-wood); nature of plastic (polyethylene, isotactic-polypropylene, atactic-polypropylene).

Hydropyrolysis of biomass/plastic mixture results in the higher degree of conversion and in the increased yield of light liquids with b.p. < 180 °C (by 1.6-1.8 times) as compared to co-pyrolysis in an inert atmosphere. The addition of activated iron ore catalysts also increases the degree of mixture conversion and the yield of light hydrocarbon fraction. Pyrhotite catalyst yields the highest amount of the light fraction (40 % wt. for beech-wood/PE mixture with ratio 1:1 at 400 °C). The highest degree of conversion (91% wt.) was observed for activated haematite catalyst. The formation of light liquids is promoted by H_2 pressure, which suppresses the char formation and facilitates the thermal cracking of heavy liquid products.

According GC-MS data the light liquids of biomass/plastic hydropyrolysis contain mainly normal paraffines C_7-C_{13} (about 75 % for pine-wood/i-PP mixture), alkylbenzenes and alkylfuranes compounds (about 10%) and non-identified compounds (about 15 %). The composition of heavy liquids of co-pyrolysis process significantly depends on biomass/plastic ratio. Wood pyrolysis liquids mainly contain polars (eluted with DCM) and polyaromatics (eluted with dichlormethane-THF mixture). The addition of plastic to wood biomass increases the concentration of saturates and light aromatics with synchronous decreasing by a few times the content of polar compounds.

The liquids of biomass/plastic pyrolysis and hydropyrolysis can be used as chemical feedstock and their light hydrocarbon fraction as motor fuel component.

Catalytic carbonization and grafitization. Different approaches are applied for the preparation of metal-containing porous carbons from cellulosic materials. Some methods are based on introducing of metal compound into cellulosic material with following pyrolysis at

elevated temperature. In this case the simultaneous carbonization of cellulosic material and chemical transformations of introduced metal take place.

In order to select an optimal parameters of pyrolysis process resulting in the formation of metal-containing porous carbons with high yield and high surface area the influence of carbonization temperature, rate and time of heating, type of pretreatment and methods of metal introducing into cellulosic material on the characteristics of obtained carbon products was investigated.

The most evident changes were detected at pyrolysis temperature 500-700 °C. They are connected with the destruction of C-O-C bonds and generation of polycondensed aromatic systems resulting in the formation of carbonaceous structure. Thermogravimetric analysis indicates the decreasing of the start of thermal decomposition process for metal-containing cellulose in the comparison with non-modified cellulose. SEM-data have shown that the carbonaceous products keep a fiber structure of the origin cellulose and their surface area can reach to 600 m^2/g.

The decrease of carbon material graphitization temperature was also detected at the presence of nickel and all resulting carbons have a turbostatic structure.

The thermocatalytic conversion of wood biomass in catalytic fluidized bed gives new possibilities for process intensification and for regulation an yield and composition of products. Oxide catalysts accelerate the oxidation of volatile compounds derived at the initial steps of biomass thermal transformation. Owing to intensive heat evolution the thermocatalytic process proceeds at autothermal conditions. Carbon products with the high porosity and surface area can be obtained. The formation of pyrolysis tars and polyaromatic compounds like benz-α-pyren was suppressed in the presence of catalysts. The integrated process of gaseous fuel and carbon porous material producing from wood biomass in catalytic fluidized bed was suggested.

The integration in an united technological cycle two processes: the oxidative carbonization of powder biomass in a fluidized bed of catalytically active slag and the steam gasification of produced char makes it possible to increase the effectiveness of plant biomass processing to fuel-gas and syn-gas. The continuous recirculation of hot char between carbonization and gasification reactors provides the gasification process by the additional heat. The advantages of integrated process of plant biomass gasification are the reduced consumption of oxygen and the higher quality of produced gas.

LOW COST PRODUCTION OF BIO-HYDROGEN
FROM AGRI-PELLETS

Grassi G., <u>Vasen N.N.</u>*, Conti L.**, S. Mascia**

European Biomass Association (EUBIA), Brussels, Belgium
*ETA – Renewable Energies, Piazza Savonarola 10, 50132 Florence, Italy
**University of Sassari, Via Vienna 2, 07100 Sassari, Italy

Introduction

The scope of this thesis is the technical-economical feasibility and the optimization of a prototype, four-steps process for the production of bio-hydrogen from low quality biomass.

The production of bio-hydrogen is very promising for sustainable development, and economically viable. Possible markets for hydrogen today are: petrochemical, steel, glass, etc. This market is supplied by conversion of fossil fuels. The large market of the future are not only vehicles but also many other applications where hydrogen can function as an energy vector (as electricity is, but this is not storable).

This short document has been elaborated to provide some elements of reflection on a promising and today viable integration of large-scale Biohydrogen production into the conventional hydrogen production capacity. The Russian Federation has huge renewable biomass resources that enable this extension.

Bio-hydrogen (or H2 derived from biomass) can be produced at competitive cost, with the commercially available technologies, in comparison of that derived from natural gas and at even very attractive conditions with the benefits of "CO_2 –trading".

It is of strategic importance to use the available time ($\sim$ 15/20 years), before the high demand of H2 will take place, for the development of a sustainable mass production capacity of bio-hydrogen.

In the framework of an international Renewable Energy Technology transfer network (see www.renewtransnet.com), supported financially by the European Commission, coordinated by Renew-Transnet (UK) and with Italian partner Tecnocentro Eng Srl in Terni, in Italy the market promotion of this process is undertaken. It is a method to bring innovations of SMEs from laboratory to commercial exploitation in the market.

Scheme of the 4-steps process
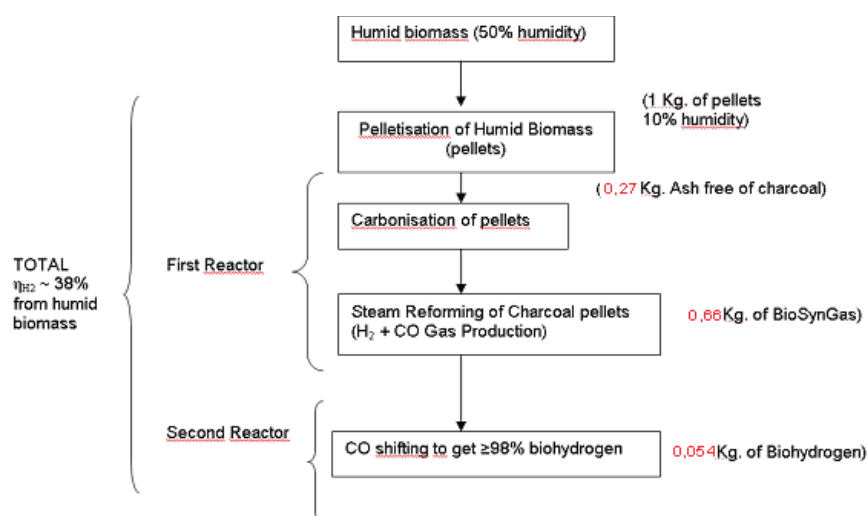
In the following sections, the four steps are explained singularly.

PLS-2

Step 1: biomass characterisation and pelletisation

In the Department of Chemistry of the University of Sassari some carbonisation and gasification tests of vegetal biomass were performed.

The pelletisation process is performed on inhomogeneous or small size biomass (chips, sawdust, agro-industrial wastes, etc.). The biomass is shattered and homogenised in an apparatus constituted of a riddled cylinder, where the biomass is compressed and transformed in little hard cylinders (See fig. 1). The bulk density is over 650 kg/Nm^3.
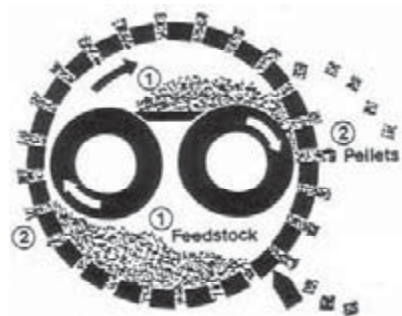
Fig. 1. Pelleting process

In the process there are losses of moisture, the pellets have an humidity content under 10%. The product is then easily transportable, storable and doesn't degrade. Before the carbonisation and gasification tests a characterisation of the pellets utilised was carried out. The results are reported in tab. 1.

Tab. 1. Analysis of the biomass

Ash	%wt	5,49
Moisture	%wt	9,95
C	%wt	42,11
H	%wt	5,20
N	%wt	0,51
O	%wt	36,74
H.H.V.	MJ/kg	18,534

Step 2: Pellet carbonization

Some carbonisation tests and following steam gasification of the obtained charcoal were carried on at laboratory scale. The employed equipment for these tests is shows in the figure below. The apparatus consists of four units:

1. Reactor with heating unit
2. Pneumatic device and gas flow controller
3. Gasification steam feeder
4. Effluents collection traps
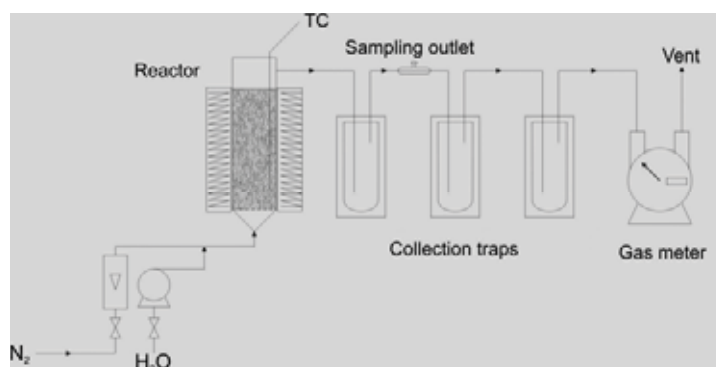
Experimental carbonisation and gasification device

During the tests gas samples were collected for the analysis. Produced gas was measured by a gas meter and vented. Liquid products were collected by cold traps, recovered and quantified.

The charcoal characteristics are showed in the table below.

Tab. 2. Analysis of charcoal pellets

Ash	%wt	19.38
C	% wt	72,15
H	% wt	1,49
N	% wt	0,36
O	% wt	6,62
H.H.V (mf)	kJ/g	25.5

Step 3: Charcoal gasification

Gasification[i,ii] is a thermal conversion process of biomass in gaseous products carried out with oxidant agents and steam at a temperature around 1000°C. As oxidant agents, air or oxygen are used. Produced gas is mainly made of carbon monoxide, hydrogen, carbon dioxide and a little percentage of methane. Little amounts of ethane, ethylene, water and several particles as char, ash, tars and oil drops are also produced.

Water gas is a mixture of carbon monoxide and hydrogen produced by passing steam through deep beds of incandescent coal (water gas reaction). The H.H.V.ranges around 11 MJ/Nm^3

$$C + H_2O \rightleftarrows CO + H_2 \qquad \Delta H^0 \ +118.0 \ kJ/mol$$
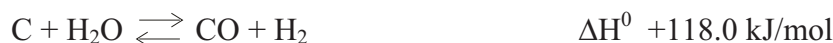
The water gas process is carried out in two alternate steps. In the first, air or oxygen are blew for 1-2 minutes; the charcoal burns and the temperature rises until 1000°C. in the second step steam was blown for 2-4 minutes until the temperature goes down under 900°C.

Steam reacts with charcoal at a temperature around 600°C producing a mixture of carbon dioxide and hydrogen

$$C + H_2O \rightleftarrows CO_2 + H_2 \qquad \Delta H^0 \ +76.2 \ kJ/mol$$

At higher temperature CO2 is reduced into CO by hydrogen

$$CO_2 + H_2 \rightleftarrows CO + H_2O \qquad \Delta H^0 \ +41.8 \ kJ/mol$$
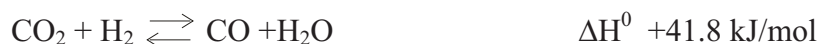
Also the following reaction occurs and a little percentage of carbon dioxide is found the in water gas.

$$C + CO_2 \rightleftarrows CO \qquad \Delta H^0 \ +159.8 \ kJ/mol$$
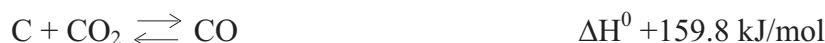
Reversible reactions producing water gases in dependence of the temperature bring to an equilibrium according to the mass reaction law:

$$K_p = \frac{p_{CO} \cdot p_{H_2O}}{p_{CO_2} \cdot p_{H_2}}$$

The figure below shows the calculated composition of pure water gas from charcoal at various reaction temperatures. The reactor on the right shows the new approach to integrate steps 2 and 3 in order to avoid cooling of the carbonised pellets, so that much energy is saved.
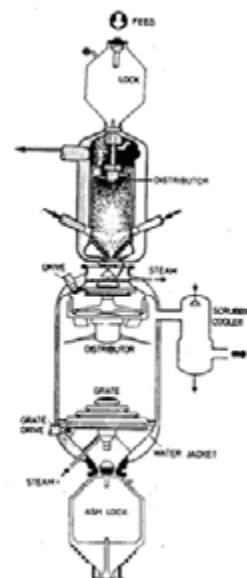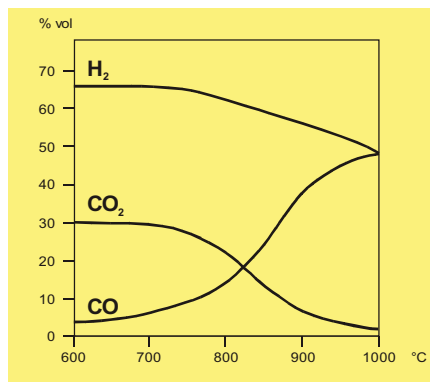
PLS-2

Step 4: Steam shifting syn-gas

A steam shift was carried out on the syn-gas, resulting in about 98 % pure hydrogen, so that the final amount of hydrogen was 5.4 gr, departing from 100 gr of pellets. The complete four step process in terms of mass balance is given in the flow diagramme below.
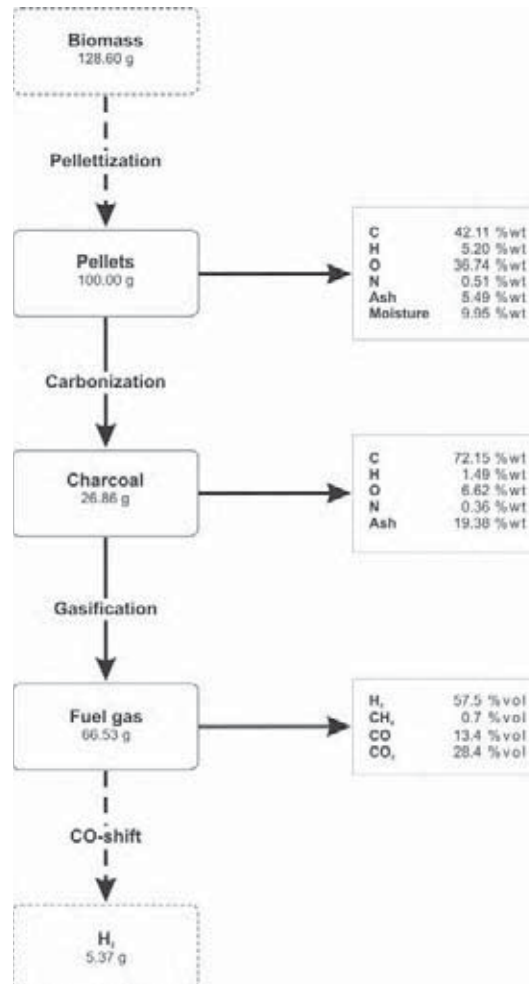
References

L. Conti, G. Grassi, S. Mascia, G. Scano, E. Maggioni, P.Pedani, R. Ostan, *Commercial Process for Low Cost Production of Charcoal, Activated Carbon, Bio-Hydrogen, from Low Value Biomass.* 12th European Conference and Technology Exhibition on Biomass foe Energy, Industry and Climate Protection, Amsterdam, The Nederlands, 17-21 June 2002.

[i] A. Kaupp / J. R. Goss "Small scale gas producer engine systems" Vieweg 1984 (ISBN 3-02001-6), pag. 25-96

[ii] T. B. Reed / A. Das "Handbook of biomass downdraft gasifier engine systems" The Biomass Energy Foundation Press, pag. 1-50

POST-SYMPOSIUM

"Catalytic Processing of Renewable Sources: Fuel, Energy, Chemicals"

ORAL PRESENTATIONS

CATALYTIC PYROLYSIS OF BIOMASS BY MESOPOROUS MATERIALS: EFFECT OF STEAM STABILITY AND ACIDITY OF Al-MCM-41 CATALYSTS

E.F. Iliopoulou[1,2], E.V. Antonakou[2], S.A. Karakoulia[3], A.A. Lappas[2]

I.A. Vasalos[2], K.S. Triantafyllidis[1,*]

[1] *Department of Chemistry, Aristotle University of Thessaloniki, 541 24 Thessaloniki, Greece*

[2] *Chemical Process Engineering Research Institute, CERTH, 570 01 Thessaloniki, Greece*

[3] *Department of Chemical Engineering, Aristotle University of Thessaloniki,*

Thessaloniki, Greece

Introduction

Biomass is a renewable source, expected to play a substantial role in the future global energy balance. It can provide energy either by combustion or by transformation to more valuable gaseous or liquid products (by gasification or pyrolysis). Among thermo chemical conversion processes biomass pyrolysis is the most emerging for the production of liquid oil (up to 75%wt on biomass). Bio-liquids can be used for energy production or as a source of high value chemicals. Fast pyrolysis of biomass is carried out in various types of reactors using an inert solid heat carrier for the fast heating of biomass particles [1]. However recently, various catalysts have been used both as heat carriers and for selectivity enhancement for the in-situ upgrading of biomass pyrolysis vapours. The use of catalysts usually leads to additional water and coke formation, at the expense of organic products but on the other hand it improves the quality of bio-oil [1,2]. Thus, tailoring of catalyst properties for simultaneous enhancement of the production and quality of biofuels would be a major accomplishment.

Aluminum substituted MCM-41 materials [3] seem to have promising properties (highly ordered mesoporosity, large surface area, and mild-to-moderate acidity). In recent studies [2] of our group, such materials were tested as catalysts in the biomass fast catalytic pyrolysis process, altering significantly the quality of pyrolysis products. The acid sites present in an Al-MCM-41 catalytic material can be of both Brönsted and Lewis type, each of them participating in the biomass pyrolysis via different mechanisms. However, water produced during biomass pyrolysis in combination with the relatively low hydrothermal stability of Al-MCM-41materials, could tentatively cause problems in their potential commercial use. In the present paper, various MCM-41 mesoporous aluminosilicate materials with different Si/Al

ratios were evaluated as catalysts for the fast pyrolysis of biomass. Furthermore, the effect of steaming of MCM-41 materials on their catalytic performance was also investigated.

Experimental

All MCM-type mesoporous materials were synthesized in the laboratory based on a modified procedure of the method that has been initially presented by Beck et al. [3]. In a typical synthesis of an aluminosilicate MCM-41 material (Al-MCM-41), a mixture of tetraethylorthosilicate (TEOS) and aluminum isopropoxide (AIP) was slowly added under stirring at room temperature to an aqueous solution of cetyltrimethylammonium bromide (CTAB) which has been previously become alkaline (pH=10-11) by the addition of ammonia solution. The formed gel was further stirred for 1 hour and was then transferred to a polypropylene bottle and was hydrothermally aged at 100^oC for five days. The white product was filtered, washed with double distilled water and dried at room temperature. The silicate MCM-41 sample (MCM-41) was synthesized following the above procedure with the absence of the Al source. All dried samples were further calcined at 540^oC for 7 hrs in air in order to combust the organic template (CTAB) and produce the H^+-form of the samples. The calcined samples were further steamed at 550 and 750^oC for 3 h at 20% steam partial pressures, in order to test the gradual effect of steaming on their acidic, porous and catalytic properties.

The biomass pyrolysis tests were performed on a bench-scale fixed bed reactor at 500°C, using a wood-based feed (LIGNOCEL). For comparison, tests with a non-catalytic solid (glass beads) were also performed. All experiments are ex-situ, using a piston to transfer the biomass into the pyrolysis zone [2], followed by direct contact of the produced pyrolysis vapours with the inert solid or the catalyst. The reactor was filled with 0.7 g glass beads or catalyst, for the non-catalytic or catalytic tests respectively, while the piston was filled with biomass (1.5 g). The gaseous products are directly measured by water displacement and sent to a GC for analysis. The liquid products are collected in a receiver immersed in a liquid bath (-17 °C) and then the two phases of the liquid product (organic and aqueous) are separated using an organic solvent (dichloromethane). Finally the amount of coke deposited on the catalyst is determined by weight difference method. Both gaseous and liquid products are analyzed using advanced GC and GC-MS techniques.

Results and Discussion

The porosity and acidic characteristics of the calcined MCM-41 –type materials are given in Table 1. As expected, all MCM-41 samples, both silicate and aluminosilicate, exhibit very

PS-1

high surface areas and mean pore diameters of ~ 28 Å. In addition, the number of acid sites increases with Al content of the samples, being negligible in the siliceous MCM-41 sample. Preliminary characterization results of the steamed MCM-41 materials have shown that even after steaming at 750^oC their structural and porosity properties, which greatly affect the catalytic performance, are not significantly altered (decrease of surface area less than 20 %). This is due to the relatively low steam partial pressure, which however, could simulate the hydrothermal conditions during biomass pyrolysis. On the other hand, a more than 50% decrease of the number of acid sites was noticed after steaming. In catalytic processes, such as the biomass pyrolysis, the acidic properties of the catalytic materials play an important role since the acid sites catalyze the cracking, isomerization, oligomerization-aromatization, decarboxylation and dehydration reactions.

Table 1. Properties of caclined MCM-41 – type catalytic materials

Samples	Surface area (m^2/g)	Pore size (Å)	Total acid sites (mmoles NH_3/g)
MCM-41 (siliceous)	946	27	0.02
Al-MCM-41 (Si/Al=50)	875	27	0.20
Al-MCM-41 (Si/Al=30)	869	28	0.28

The catalytic biomass pyrolysis tests with the inert solid (glass beads) and the MCM-41 materials showed that the use of the mesoporous catalysts induces a small increase in total liquid products, mainly due to higher water formation, leaving the organic phase almost unaffected. The total gases production is also similar between non-catalytic and catalytic pyrolysis tests. With regard, to the composition of the organic liquid phase, certain trends are observed in relation to the porosity and acidity characteristics of the MCM-41 samples. The yields of important compounds in the organic phase, which affect greatly the quality of the produced bio-oil, are shown in Table 2. As can be seen, the concentration of the high-added-value phenols in the organic phase increases with both Al-MCM-41 samples, compared to the non-catalytic runs, showing higher yields for the sample with Si/Al = 50. This indicates that a tuning of the Al content and consequently of the number of acid sites of Al-MCM-41 materials is necessary for higher phenol production. The above beneficial effect of Al-MCM-41 was eliminated after steaming of the samples which lowered their acidity.

Table 2. Product yields (wt. % on organic phase) in catalytic biomass pyrolysis tests

Catalysts	Phenols	Acids	Alcohols	PAH	Heavy
Glass beads	20.97	5.6	11.45	2.68	13.87
Al-MCM-41 (Si/Al=50)	30.09	1.48	9.16	0.98	9.03
Al-MCM-41 (Si/Al=30)	22.95	0.46	5.48	0.73	7.63
Al-MCM-41 (Si/Al=50), 20% steam 750°C/3h	19.96	0.34	8.96	-	15.09
Al-MCM-41 (Si/Al=30), 20% steam 550°C/3h	19.96	0.34	8.96	0.98	15.09
Al-MCM-41 (Si/Al=30), 20% steam 750°C/3h	19.57	0.42	9.53	-	-

In the case of the undesirable acids, alcohols and polyaromatic hydrocarbons (PAH) of the organic phase of the bio-oil, the use of both calcined and steamed Al-MCM-41 catalytic materials induces a significant reduction in their yields, which in most cases is enhanced with higher number of acid sites of the catalysts. As far as the heavy compounds are concerned, only the calcined samples reduce their yields, with the steamed samples having a minor effect.

Conclusions

The use of Al-MCM-41 materials as catalysts in biomass pyrolysis appears to be promising, with respect to improving the quality of bio-oil and the production of phenols. However, fine tuning of their acidic properties is required for optimization of the results. The relatively moderate steaming pretreatment of the catalytic materials before testing had a limited effect on products selectivity, which however was varied depending on the type of organic phase component.

References

1. S. Yaman, Energy Conv. Manage. 45 (2004) 651.

2. E. Antonakou, A.A. Lappas, M.H. Nilsen, A. Bouzga, M. Stöcker, submitted to Micropor. Mesopor. Mater., June 2005.

3. J.S. Beck, J.C. Vartuli, W.J. Roth, M.E. Leonowicz, C.T. Kresge, K.D. Schmitt, C.T.W. Chu, D.H. Olson, E.W. Sheppard, S.B. McCullen, J.B. Higgins, J.L. Schlenker, J. Am. Chem. Soc. 114 (1992) 10834.

PS-2

OXYGENATED ADDITIVES PRODUCTION FOR DIESEL FUELS

L. Spadaro[1], F. Arena[2,1], G. Bonura[1], O. Di Blasi[1], and <u>F. Frusteri[1]</u>

[1] *Istituto di Tecnologie Avanzate per l'Energia (CNR-ITAE) "Nicola Giordano",*

Messina, Italy;

[2] *Dipartimento di Chimica Industriale e Ingegneria dei Materiali,*

Università degli Studi di Messina, Italy

Introduction

Since a higher thermal efficiency and fuel economy, diesel engines are to date considered as the main power supply for heavy transportation and power-generation plants. Nevertheless the emission of pollutant compounds, such as NO_x, SO_x, HC, CO and mostly micro-particulate (*PM10*), highly noxious for both human health and environment, represent a major drawback for an intensive employment [1].

It is generally recognised that the addition of oxygenated compounds, like ethers or acetals, to diesel fuels allows improving engines combustion, ensuring much less pollutant emissions and a superior energetic efficiency [2]. Indeed, oxygenated additives imply a rise of the cetane number (CN) reflecting in better ignition quality and flammability of diesel fuels [3, 4]. In this respect, the 1,1-*di*-ethoxyethane (acetal) is considered as one of the most suitable *"CN improvers"* [3].

Actually, acetal is industrially produced *via* uneconomic homogeneous catalytic process, involving the reaction of two moles of ethanol with one of acetaldehyde to produce one mole of acetal. Like many other *high-value* chemicals industrial syntheses, this process still lies on the use of strong mineral acids, such as H_2SO_4 or HF, as catalysts [5]. Clearly, environmental and economic reasons [6,7] impose the adoption of cleaner and more selective process technologies deserving the replacement of homogeneous processes with safer heterogeneous catalytic technologies based on the employment of strong solid-acid catalysts [8]. Though zeolites and functionalized silicas catalyze several organic reactions [9-15], yet, in the case of acetal manufacture, the actual targets are still inadequate for industrial purposes [16,17].

Amongst various classes of potential solid-acid catalysts, in recent years a great interest has been focused on acid ion-exchanged polymers, such as Nafion®, characterized by terminal sulfonic groups, whose acidic strength is comparable with that of "concentrated" sulphuric acid [18,19]. However, the use of "pure" perfluorosulfonic-like solid acids is

generally limited by an intrinsic low surface exposure reflecting in poor process yields [20].

Therefore, this paper is aimed at assessing synthesis route and catalytic performance of silica-*heterogenized* perfluorosulfonic (PFS) acids in the synthesis of acetal.

Experimental

The PFS-*SiO₂* catalysts were prepared by the incipient wetness impregnation of a commercial silica sample (*Cab-O-Sil*) with an isopropanolic solution of the PFS-polymer. Catalysts were characterized by BET, XRD and SEM measurements, while loading, composition and *Brönsted's* acidity, were valued by TGA, CHNS and ZPC (*via* NaOH titration) techniques, respectively.

Testing in the acetal synthesis was performed at 4°C and a pressure of 3 atm using a 100 cm^3 batch reactor containing 0.05g of catalyst and 60 cm^3 of a reactant mixture of acetaldehyde/ethanol in the molar ratio 1:2, stirred at 2000 *rpm*. Reagents and products were analysed using a *HP 5890* gas chromatograph.

The list of the studied catalyst is reported in Table 1.

Table 1. List of the studied catalysts.

Code	[a] **Polymer (wt %)**	[b]**(meq H$^+$·g^{-1})**	**S.A. $_{BET}$ (m^{2}g^{-1})**	*Mean pore diameter* (Å)
6A-LM50	6	0.069	120	160
13A-LM50	13	0.150	111	155
18A-LM50	18	0.210	101	142
24A-LM50	24	0.282	97	135
30A-LM50	30	0.371	95	129

[a] *Polymer loading evaluated by TGA analysis;* [b] *Brönsted's acidity evaluated by ZPC analysis.*

Results and discussion

Rising the polymer loading from 6 to 30% (*wt/wt*) implies a progressive, though slight, decrease in surface area (120-95 m^{2}g^{-1}) and mean pore diameter (160-130Å), likely due to "filling" of larger pores by polymer molecules.

However, *Brönsted's* acidity data, as probed by electrochemical *Zero Point Charge* (ZPC) measurements, signal a straight-line increase in the concentration of acidic groups with the polymer loading (Fig. 1), diagnostic of a distribution of the active phase on the silica surface (e.g., dispersion) slightly, if any, affected by the loading.

The catalytic synthesis of acetal in the presence of PFS-*SiO₂* systems leads to the exclusive formation of acetal while no trace of PFS in the reacting solution, due to leaching phenomena, was detected.
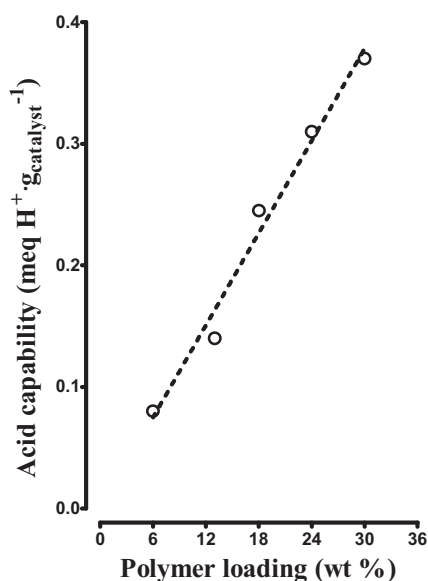
Fig. 1 Brönsted's acidity *vs* polymer loading.   Fig. 2 Activity data carried out at 30' of reaction time.
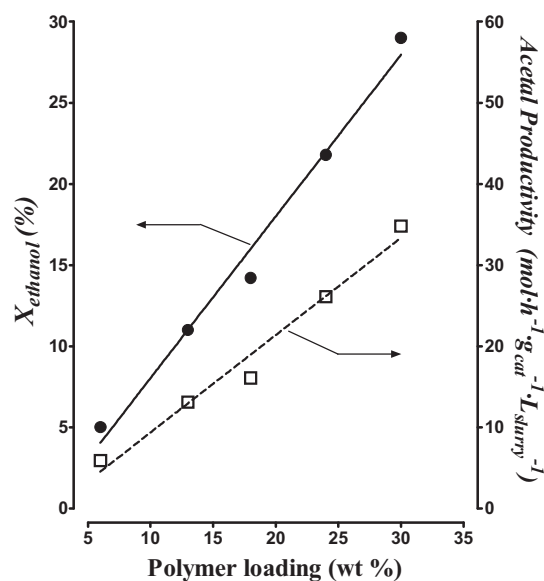
Catalytic data in the synthesis of acetal at 30 minutes of reaction time, using a catalyst/reagents ratio of 1/900 (*wt/wt*), are shown in Figure 2 in terms of ethanol conversion ($X_{ethanol}$ %) and *Acetal productivity* ($mol \cdot h^{-1} \cdot g_{cat}^{-1} \cdot L_{slurry}^{-1}$). Experimental data indicate that, at low reaction time, the catalytic activity depends linearly upon the *Brönsted* acidity, matching with a full availability of sulphonic acidic groups at the catalyst surface. Although the ethanol conversion is limited by thermodynamic constraints due to water formation:

$$2C_2H_5OH + CH_3CHO \xleftrightarrow{H^+} (C_2H_5O)_2CHCH_3 + H_2O$$
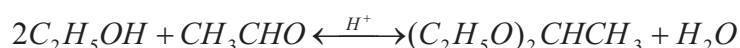
however, the maximum acetal productivity value (ca. 36 $mol \cdot h^{-1} \cdot g_{cat}^{-1} \cdot L_{slurry}^{-1}$) is remarkable, resulting higher by ca. two orders of magnitude than those recently reported in the literature using diverse solid acid catalysts for acetal systems [17].

Conclusions

The *heterogeneization* of PFS acid polymers on pre-formed SiO_2 carriers by a simple impregnation technique doesn't affect the acidic properties of the bare PFS polymer, leading to very significant improvement in the surface area which allows for a full availability of the sulphonic acidic groups in acid-catalysed liquid-phase reactions.

The suitability of PFS-*SiO$_2$* catalysts for the synthesis of acetal has been ascertained. PFS-*SiO$_2$* systems result very active and selective towards the production of acetal, denoting also a good mechanical and chemical stability under the typical process conditions.

References

[1] Pischinger FF. Compression-ignition engines. In: Sher E, editor. Handbook of air pollution from internal combustion engines. London, UK: Academic Press; 1998. p. 261–3.

[2] Peckham J. Diesel likeliest option for high-mileage car, says NRC. Fuels and Lubricants, Hart's Fuels and Lubes SAE Show Special, Potomac, MD: Hart Publication, May 1997.

[3] Owen K, Coley T. Diesel fuel additives, 2nd ed. Automotive fuels reference book; 1995. p. 503–10.

[4] L.N. Allard, N.J. Hole, G.D. Webster, T.W. Ryan, D. Otto III, A. Beregszazy, C.W. Fairbridge, J. Cooley, K. Mitchell, E.K. Richardson, N.G. Elliot, D.J. Rickeard, SAE Tech. Pap. Ser. 971636 (1997) 45.

[5] M. Kaufhold, M. El-Chahawi. Pat. DE 44 04 515 A1 (1995), to Huls AG, Germany.

[6] R.A. Sheldon, Chem. Ind. (1997) 12.

[7] R.A. Sheldon, H. Van Bekkum, Fine Chemicals through Heterogeneous Catalysis, Wiley VCH, Weinheim, 2000.

[8] A. Corma, H. Garcia, Chem. Rev. 103 (2003) 4307–4365.

[9] A. Corma, M.J. Climent, H. García, J. Primo, Appl. Catal. 49 (1989) 109–123.

[10] R. Fang, G. Harvey, H.W. Kouwenhoven, R. Prins, Appl. Catal. A 130 (1995) 67–77.

[11] K. Garre, D. Akporiaye, J. Mol. Catal. A 109 (1996) 177.

[12] K. Smith, Z. Zhenhua, P.K.G. Hodgson, J. Mol. Catal. A 134 (1998) 121.

[13] Y. Ma, W. Wang, W. Jiang, B. Zuo, Appl. Catal. A 165 (1997) 199.

[14] D. Das, S. Cheng, Appl. Catal. A 201 (2000) 159.

[15] Q.L. Wang, Y. Ma, X. Ji, Y. Yan, Q. Qiu, Chem. Commun. (1995)

[16] J. Andrade, D. Arntz, M. Kraft, G. Prescher. Pat. DE 34 03 426 A1 (1985), to Degussa AG, Germany.

[17] M. R. Capeletti, L. Balzano, G. de la Puente, M. Laborde, U. Sedran Applied Catalysis A: General 198 (2000) L1–L4

[18] G.A. Olah, NATO ASI Ser. C 444 (1994) 305.

[19] M.A. Harmer, W.E. Farneth, Q. Sun, Adv. Mater. 10 (1998) 1255.

[20] M. Alvaro, A. Corma, D. Das, V. Fornés, H. García, Journal of Catalysis 231 (2005) 48–55

BIOETHANOL AS AN ADVANCED FUEL FOR FUEL
CELL POWER PLANTS

V.A. Kirillov, V.D. Meshcheryakov and V.A. Sobyanin

Boreskov Institute of Catalysis SB RAS, Prosp. Akad. Lavrentieva, 5
Novosibirsk 630090, Russia

Bioethanol is a 12-14% aqueous solution of ethyl alcohol resulting from biochemical conversion of industrial wood residue and agriculture waste. In contrast to natural gas and oil refinery products, bioethanol is renewable fuel and practically has unrestricted resource. Therefore, bioethanol can be considered as one of the most promising fuels for generation of synthesis gas or hydrogen for fuel cell (FC) power plants. The role and significance of bioethanol have markedly increased in recent times in view of the development of high-temperature polymer fuel cells providing stable operation at CO concentrations up to 5 % in the hydrogen-containing gas.

Thermodynamics of the reaction. As follows from the available literature data, steam ethanol catalytic conversion is the most efficient method of synthesis gas generation applying to bioethanol. The complexity of the process performance is associated with its high endothermicity and possibility of carbon deposition caused by side reactions. The reaction of steam ethanol reforming can be carried out in a reactor with supported cobalt, rhodium, nickel or copper-nickel catalysts to yield CH_4, H_2, CO, CO_2, acetaldehyde and ethylene via the following equations:

$$C_2H_5OH = CH_4 + H_2 + CO$$
$$C_2H_5OH = CH_3CHO + H_2$$
$$CH_4 + 2H_2O = CO_2 + 4H_2$$
$$CH_3CHO + H_2O = 3H_2 + 2CO$$
$$C_2H_5OH = C_2H_4 + H_2O$$
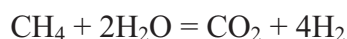
Choosing the catalysts and reaction conditions, it is possible to reduce of acetaldehyde and ethylene content in the reaction products.

At atmospheric pressure, temperature and molar ratio $H_2O:C_2H_5OH$ are factors governing the equilibrium mixture composition in the ethanol steam reforming.

As follows from refs. [1-3], at molar ratios $H_2O:C_2H_5OH$ = 4:1-10:1 and a temperature range of 300-950°C, the degree of ethanol conversion is higher than 99.9% and H_2O, CO,

CO_2, CH_4, H_2 are the main reaction products. Concentrations of the other reaction products are not exceed 10^{-3} vol.%. Since the reaction of ethanol steam reforming is an endothermal one, its equilibrium at moderate temperatures is shifted to the left and methane is the main hydrogen containing product. With rising of temperature the concentration of hydrogen increases, however, its concentration becomes noticeable at temperatures exceeding 300°C. Thus, the thermodynamic calculations suggest that at $H_2O/C_2H_5OH = 2$–4 and 700-800°C, the ethanol conversion is approached to100%, carbon does not formed, and H_2, CO, CO_2 are the main products of the steam ethanol reforming. In this case, the reaction products will contain (in terms of dry gas) about 65-69% of hydrogen, 8-9% of CO, 10-15% of carbonic acid gas, the methane residue being 0.5%.
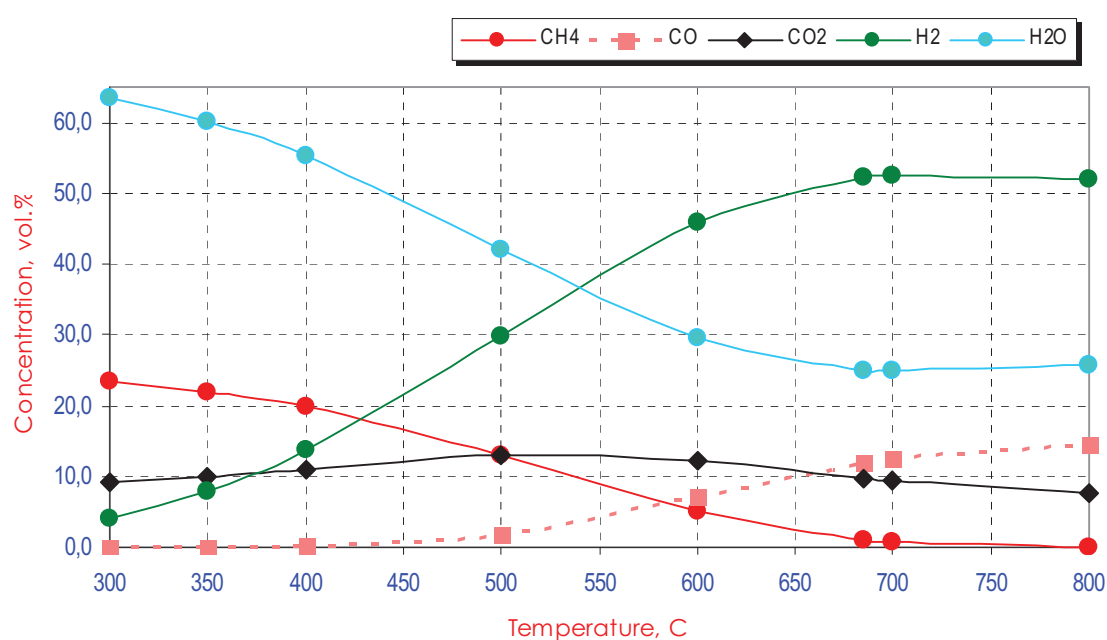
Fig. 1. Equilibrium composition of ethanol reforming products under 1 at and $H_2O:C_2H_5OH=4$.

Fig. 1 shows an equilibrium composition of the ethanol reforming products *versus* temperature under pressure of 1 at and molar feed ratio $H_2O:C_2H_5OH=4$ (according to data of ref. [2]).

The as-generated synthesis gas can be utilized as a fuel providing low NO_x emission in gas-turbine generators, internal combustion engines, and high-temperature polymer fuel cell (FC) power plants. However, because the CO concentration in the reaction products of the bioethanol reforming exceeds 10%, it complicates the direct utilization of this synthesis gas in high-temperature polymer fuel cells. To reduce CO concentration to 1%, it is necessary to apply additional step of the synthesis gas clean up, steam CO reforming. A two-step process involving (1) steam bioethanol reforming and (2) steam carbon monoxide reforming permits

one to produce hydrogen rich gas with CO content is not higher than 1%. Such synthesis gas can be used as feed for the high-temperature polymer fuel cells.

Catalysts of steam bioethanol reforming. Literature data suggest that reaction of steam ethanol reforming is usually performed in the presence of supported cobalt, rhodium, nickel, nickel-copper and palladium catalysts. Activity of the above catalysts supported on Al_2O_3, MgO, and TiO_2 is compared in refs. [4-7]. It emerged that the rhodium catalysts are most active and selective with respect to hydrogen. At ~800°C, the catalysts provide 100% conversion of ethanol, whereas and ethylene and acetaldehyde are not practically observed in the reaction products. Long-term testing of Rh catalysts at 700°C showed that the main process parameters such as degree of ethanol conversion and selectivity towards products do not substantially change during 100 h operation even after several process shutdowns without catalyst reload. Thus, rhodium holds the greatest promise as an active component to be used in the steam bioethanol reforming.

Version of the technology concept. Difficulties of the process performance are associated with high endothermicity of the reaction and necessity of evaporation of large volumes of water contained in the bioethanol. This requires the development of new types of heat conducting catalysts for bioethanol conversion and heat-coupled reactors. A heat-coupled reactor can be designed as an apparatus formed by two types of flat channels inside of which catalysts for steam ethanol conversion and ethanol deep oxidation are placed, accordingly. The reaction of deep ethanol oxidation will supply by heat the endothermal steam ethanol reforming process. Applying a high heat-conducting catalyst will improve the reactor performance. For that both catalysts are sintered with the metal walls of the channels. An example of the process flow sheet is given in Fig. 2. The operation principle is as follows: bioethanol (concentration is 14-15%) is fed from a reservoir to a converter of the first step of reforming. In heat exchangers TO1 and TO2, the mixture is evaporated and directed to a heat-coupled converter at 360°C. Combustion of ethanol rectificate provides heat for the endothermal ethanol conversion. A synthesis gas flow, containing H_2 (8%), CO (0.02%), CO_2 (5.4%), H_2O (78%) and CH_4 (8.30%), is directed to a high-temperature steam methane converter (the second step). Here, conversion is performed at 800°C. Needed heat for the endothermic steam methane reforming reaction is covered for expense combustion of the ethanol rectificate. The composition of the resulting synthesis gas is: H_2 (31.2%), CO (4.07%), CO_2 (7.72%), H_2O (57.01%), and CH_4 (0.004%). In heat exchanger TO1, synthesis gas is cooled to 350°C and directed to a reactor of steam carbon monoxide reforming. At the outlet

of this reactor, the gas flow has the following composition: H_2 (34.76%), CO (0.52%), CO_2 (11.28%), H_2O (53.45%, and CH_4 (0.004%) (dry gas is: H_2 74.66%, CO 1.11%, CO_2 24.22%, and CH_4 0.01%). The resulting hydrogen-enriched synthesis gas can be used for feeding of high-temperature polymer membrane fuel cells.
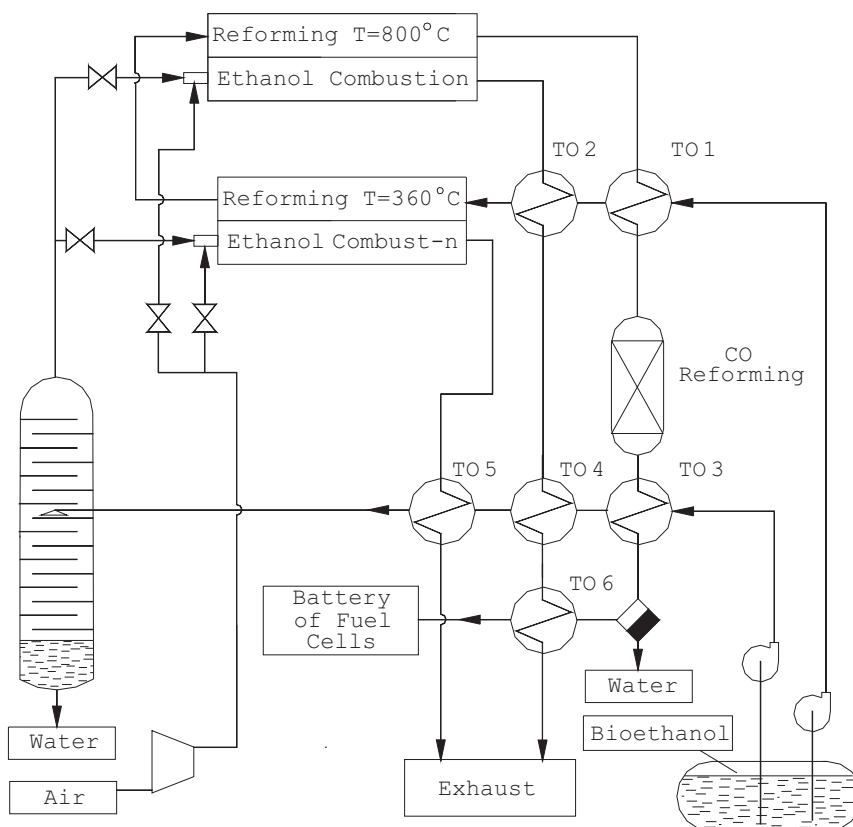
Fig. 2. Flow sheet of a fuel processor relaying on the two-step bioethanol reforming

References

1. E.Y. Garcia and M.A. Laborde // *Int. J. Hydrogen Energy,* 16 (1991) 307-312.

2. K. Vasudeva, N. Mitra, P. Umasankar, S. Dhingra // Int. J Hydr. Energy, 21(1996) 13-18.

3. I. Fishtik, A. Alexander, R. Datta, D. Geana // *Int. J. of Hydr. Energy,* 25 (2000) 31-45.

4. F. Frusteri, S. Freni, L. Spadaro, V. Chiodo, G. Bonura, S. Donato, S. Cavallaro // *Catalysis Communications, 5 (2004) 611-615* .

5. M.A. Goula, S.K. Kontou, P.E. Tsiakaras // *Applied Catalysis B: Environmental, 49 (2004) 135-144.*

6. J. P. Breen, R. Burch, H.M. Coleman //*Applied Catalysis B: Environmental, 39 (2002) 65-74.*

7. D.K.Liguras, D.I. Kondarides, X.E.Verykios //*Applied Catalysis B: Environmental, 43 (2003) 345-354.*

CATALYTIC PROCESSING OF BIOETHANOL COMBINED WITH FUEL CELL SYSTEM FOR ENVIRONMENTALLY FRIENDLY ENERGY PRODUCTION

L. Hernández, <u>V. Kafarov</u>

Center for Simulation and Control of Process, Industrial University of Santander

Cra 27 Cl 9. Fax: +57-7-6459647. A.A. 678, Bucaramanga, Colombia

Abstract

In this work, an environmentally friendly alternative for energy production from renewable sources is proposed. For this aim, an integration of catalytic bioethanol steam reforming and a fuel cell system (SOFC) was developed. For process integration, was taking into account that steam reforming of bioethanol is an endothermic and SOFC electrochemical reaction is exothermic. An integrated flowsheet was developed using heat integration of process streams improving the energetic efficiency.

1. Introduction

Electricity production from bioethanol and its steam reforming to hydrogen for fuel cells is a clean technology which offers high energy efficiency and zero emissions pollutants like SO_x, NO_x and CO_2 which is consumed for the biomass growth. This process has high energy efficiency, because the fuel cells are energy conversion devices which produce electricity from chemical energy of fuels. Among them the solid oxide fuel cells (SOFCs) has high efficiency (near to 60%), high rate in reaction kinetics and high quality heat.

The SOFC – based power plants fuelled by bioethanol have been studied for recent 3 years. The most of these researches are focused on SOFC direct ethanol fed (Gupta, et. al., 2005, Douvatzides, et. al., 2004, Assabumrungrat, et. al., 2004), but some operational problems must be solved. Other kind of these power plants is which the bioethanol reforming take place on external reformer at SOFC. The state of the art about this process is on developing and we can make mention of one work only of Douvartzides, et. al. (2003), although at the present on EU are going ahead several research projects as $BioH_2$.

2. Catalytic processing of bioethanol

The most of research made about bioethanol steam reforming is addressed to develop catalyst for this process and to study its behaviour, but only few works have been reported about the

development of reaction mechanisms and kinetics models. For catalyst development, different metals with several supports of metallic oxides have been probed among them: Rh/CeO_2, Rh/ZrO_2 and Rh/CeO_2-ZrO_2 (Diagne, et. al., 2004)(Diagne, et. al., 2002); Pt/CeO_2 (Freni, et. al., 2003); Ni/Al_2O_3 (Laborde, et. al., 2004 a), Ni/Y_2O_3 and Ni/La_2O_3 (Sun, et. al., 2005), (Sun, et. al., 2004), Ni/YSZ and Ni/MgO (Athanasios, et. al., 2002) (Athanasios, et. al., 2003) (Freni, et. al., 2003); Co/Al_2O_3, Co/SiO_2 and Co/MgO (Batista, et. al., 2004), Co/ZnO (Llorca, et. al., 2002), Co/Al_2O_3, Co/CeO_2, Co/SiO_2, Co/ZnO, Co/TiO_2, Co/V_2O_5, Co/La_2O_3, and Co/Sm_2O_3 (Llorca, et. al., 2003 b); Au/CeO_2 (Freni, et. al., 2003); Pd/Al_2O_3 (Goula, 2004), Pd/CeO_2 (Freni, et. al., 2003) and Ru/Al_2O_3 (Dimitris, 2003). Also, have been studied metallic oxides on metallic oxides as CuO/CeO_2 (Nishiguchi, et. al., 2005) and bimetallic catalyst as Cu-Ni/Al_2O_3 (Laborde, et. al., 2004 b) and Cu-Ni/SiO_2 (Fierro, et. al., 2002).

For feed ratio of ethanol/water have been probed experimentally ratios from 1:6 (Laborde, et. al., 2004 a) to 1:13 (Llorca, et. al., 2003 a), but for ratios superior at 1:8 was not registred an improving of conversion and selectivity for bioethanol steam reforming (Diagne, et. al., 2004). In relation to the discernment of reaction mechanisms for steam reforming of bioethanol, have been found only few such as for Nickel catalyst supported on La_2O_3 (Athanasios, et. al., 2004), Rhodiun on TiO_2 (Raskó, 2004), Nickel on Al_2O_3 (Laborde, et. al., 2004 b) and Cobalt on ZrO_2 (Benito, et. al., 2005). About kinetic models only have been found one complete work for Ni/Al_2O_3 catalyst (Therdthianwong, 2001) and this model was correlated for only one temperature of 400°C. On the other hand, for creation of kinetic model the following reaction scheme was used (equations 1 to 4).

$$CH_3CH_2OH \Leftrightarrow CH_3CHO + H_2 \qquad\qquad (1)$$

$$CH_3CHO \Leftrightarrow CO + CH_4 \qquad\qquad (2)$$

$$CH_4 + H_2O \Leftrightarrow CO + 3H_2 \qquad\qquad (3)$$

$$CO + H_2O \Leftrightarrow CO_2 + H_2 \qquad\qquad (4)$$

3. Solid oxide fuel cells (SOFC) system and co-generation

Solid oxide fuel cells with operating temperature of >800°C promotes rapid kinetics by no precious materials, and produces high quality by-product heat for cogeneration. For process integration was using SOFC with typical operational conditions: T=1000°C, fuel utilization: 85% and oxidant utilization: 25%.

4. Results: process description, design and integration

4.1. Process design

The process was designed to produce 1MW by SOFC on steady state conditions join with an additional cogeneration by gas turbine. As row materials were used liquid bioethanol, and water to feed the reformer and to produce hydrogen as fuel, and air to feed the SOFC as oxidant. This design was computer aided for HYSYS® software. The process flowsheet is showed on Figure 2.
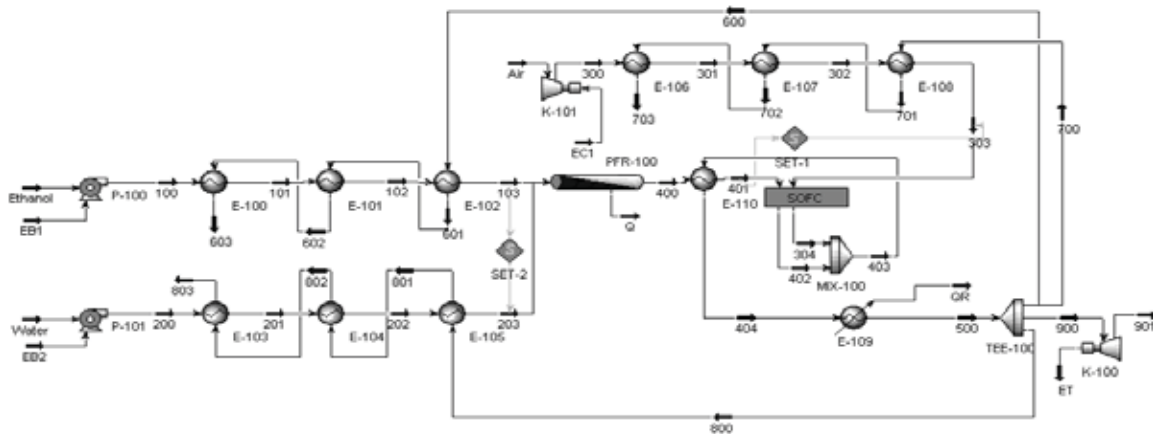
Name	Ethanol	Water	Air	100	103	200	203	300	303
Temperature(°C)	25	25	25	25	400	25	400	45,939	485
Pressure (kPa)	101,325	101,32	101,3	131	120,7	131	120,7	121,36	117,2
Molar flow (kgmole/h)	58,068	348,34	3198	58,068	58,07	348,3	348,3	3198,2	3198
Mass flow (kg/h)	2675,187	6275,3	92268	2675,2	2675	6275	6275	92268	92268
Name	304	400	401	404	500	603	703	803	901
Temperature(°C)	1000,012	400	485	985,58	903,3	82,75	64,73	108,14	895
Pressure (kPa)	110,3312	118,6	117,2	108,95	105,5	101,4	101,4	101,37	101,3
Molar flow (kgmole/h)	3055,737	629,83	629,8	3685,6	3686	165,9	1548	751,85	1220
Mass flow (kg/h)	87710,21	8950,5	8951	101218	1E+05	4555	42512	20649	33503

Figure 2. Electricity from bioethanol by steam reforming and fuel cell (SOFC) flowsheet

4.2. Integration of catalytic processing of bioethanol with fuel cell system

As SOFC operation temperature is 1000°C the fuel cell product streams have a high thermal potential. For this reason, two SOFC product streams were mixed and used to heat the steam reformer up to reaction temperature 400°C. The hot stream leaves the reformer at 903°C then; it is split on four streams to vaporize and preheat bioethanol, water, to preheat air and to feed a gas turbine. The process designed is a net energy exporter, which produce net 556.32 kW.

5. Conclusions

The environmentally friendly alternative for energy production proposed is a base to develop clean technologies to produce electricity by using renewable sources such as bioethanol. A new proposal of a clean technology to produce electricity from bioethanol by steam reforming

and SOFC using are designed. This alternative can produce net 556.32 kW and a burner to heat the steam reformer no is required.

6. References

1. Allied-Signal Aerospace Company, data (1992). In: Fuel Cells Handbook. EG&G Services Parsons, Inc. Science Applications International Corporation. U.S. Department of Energy. Office of Fossil Energy. National Energy Technology Laboratory. Fifth edition. Morgantown. 2000.
2. Assabumrungrat, S. et. al. (2004). Thermodynamic analysis for a solid oxide fuel cell with direct internal reforming fueled by ethanol. Chemical Engineering Science. 59 (24) 6015-6020.
3. Athanasios, N. et. al. (2002). Production of hydrogen for fuel cells by reformation of biomass-derived ethanol. Catalysis Today. 75.145–155.
4. Athanasios, N. et. al. (2003). Steam reforming of biomass-derived ethanol for the production of hydrogen for fuel cell applications. chemcomm communication.
5. Athanasios, N. et. al. (2004). Reaction network of steam reforming of ethanol over Ni-based catalysts. Journal of Catalysis. 225. 439–452.
6. Batista, M. et. al. (2004). High efficiency steam reforming of ethanol by cobalt-based catalysts. Journal of Power Sources. 134. 27–32.
7. Benito, M. et al. Bio-ethanol steam reforming: Insights on the mechanism for hydrogen production. Journal of Power Sources. Article in press.
8. Diagne, C., et. al. (2002). Hydrogen production by ethanol reforming over $Rh/CeO_2–ZrO_2$ catalysts. Catalysis Communications. 3. 565–571.
9. Diagne, C. et. al. (2004). Efficient hydrogen production by ethanol reforming over Rh catalysts. Effect of addition of Zr on CeO_2 for the oxidation of CO to CO_2. C. R. Chimie. 7. 61–622
10. Dimitris, K. (2003). Production of hydrogen for fuel cells by steam reforming of ethanol over supported noble metal catalysts. Applied Catalysis B: Environmental. 43. 345–354.
11. Douvartzides, S. et. al. (2004). Electricity from ethanol fed SOFCs: the expectations for sustainable development and technological benefits. International Journal of Hydrogen Energy. 29 (4) 375-379.
12. Douvartzides, S., Coutelieris, F. and Tsiakaras P. (2003). On the systhematic optimization of ethanol fed SOFC-based electricity generating systems in terms of energy and exergy. Journal of Power Sources. 114. 203-212.
13. Fierro, V. et. al. (2002). Oxidative reforming of biomass derived ethanol for hydrogen production in fuel cell applications. Catalysis Today. 75. 141–144.
14. Freni, S. et. al. (2003). Production of hydrogen for MC fuel cell by steam reforming of ethanol over MgO supported Ni and Co catalysts. Catalysis Communications. 4. 259–268.
15. Gaurav, G. Comparison of conversion and deposit formation of ethanol and butane under SOFC conditions. Journal of Power Sources, Article In Press.
16. Goula, M. (2004). Hydrogen production by ethanol steam reforming over a commercial $Pd/ -Al_2O_3$ catalyst. Applied Catalysis B: Environmental. 49.135–144.
17. Laborde, M. et. al. (2004 a). Bio-ethanol steam reforming on Ni/Al_2O_3 catalyst. Chemical Engineering Journal. 98. 61–68.
18. Laborde, M. et. al. (2004 b). Hydrogen production via catalytic gasifcation of ethanol. A mechanism proposal over copper–nickel catalysts. International Journal of Hydrogen Energy. 29. 67 – 71.
19. Llorca, J., et. al. (2002). Efficient Production of Hydrogen over Supported Cobalt Catalysts from Ethanol Steam Reforming. Journal of Catalysis. 209. 306–317.
20. Llorca, J., et. al. (2003 a). CO-free hydrogen from steam-reforming of bioethanol over ZnO-supported cobalt catalysts Effect of the metallic precursor. Applied Catalysis B: Environmental. 43. 355–369.
21. Llorca, J., et. al. (2003 b). In situ magnetic characterisation of supported cobalt catalysts under steam-reforming of ethanol. Applied Catalysis A: General. 243. 261–269.
22. Nishiguchi, T., et. al. (2005). Catalytic steam reforming of ethanol to produce hydrogen and acetone. Applied Catalysis A: General. 279. 273–27.
23. Raskó, J. (2004). Surface species and gas phase products in steam reforming of ethanol on TiO_2 and Rh/TiO_2. Applied Catalysis A: General. 269. 13–25.
24. Sun, J. et. al. (2004). Hydrogen from steam reforming of ethanol in low and middle temperature range for fuel cell application. International Journal of Hydrogen Energy. 29. 1075 – 1081.
25. Sun, J. et. al. (2005). H_2 from steam reforming of ethanol at low temperature over Ni/Y_2O_3, Ni/La_2O_3 and Ni/Al_2O_3 catalysts for fuel-cell application. International Journal of Hydrogen Energy. 30. 437 – 445.
26. Therdthianwong, A., Sakulkoakiet, T. and Therdthianwong, S. (2001). Hydrogen production by catalytic ethanol steam reforming. Science Asia. 27. 193-198.

BIODIESEL PRODUCTION FROM WASTE OILS BY USING LIPASE IMMOBILIZED ON HYDROTALCITE AND ZEOLITES

Yagiz F., Kazan D., <u>Akin A.N.</u>

Kocaeli University Engineering Faculty Chemical Engineering Department, Kocaeli, Turkey

Marmara University Engineering Faculty Chemical Engineering Department, Istanbul, Turkey

TUBITAK-Research Institute for Genetic Engineering and Biotechnology, Kocaeli, Turkey

Introduction

There is an increasing worldwide concern for environmental protection and for the conservation of non-renewable natural resources. Day by day fossil fuel resources deplete due to rapidly increasing population and industrialization all around the world. For this reason the possibility of developing alternative energy sources to replace traditional fossil fuels has been receiving a large interest in the last few decades. Fatty acid methyl esters (FAME), which are collectively named biodiesel and produced by methanolysis of triglycerides such as animal fats and plant oils, are shown as promising renewable sources of fuel [1]. Biodiesel can be used directly or mixed with conventional fuel for diesel engines, and as a heating fuel.

The main advantage of using biodiesel as fuel is that the amounts of SO_2, halogens, soot and CO contained in the exhaust gas, which are major contributors to environmental pollution, are much lower than those in petroleum diesel [2]. Furthermore, the recycling of waste oil will also contribute to alleviation of environmental problems.

Biodiesel is synthesized from direct transesterification of vegetable oils and animal fat, where the corresponding triglycerides react with a short-chain alcohol, usually methanol in the presence of a catalyst. Although conventional chemical technology using alkaline catalysts has been applied to biodiesel fuel production, there are several drawbacks to this approach, including difficulties in the recovery of glycerol and potassium and/or sodium salt, the need for catalyst exclusion, and the energy-intensive nature of the process. Utilization of lipase as a catalyst for biodiesel fuel production has great potential compared with chemical methods using alkaline catalyst, since no complex operations are needed either to recover the glycerol or to eliminate the catalyst and salt. In literature, the lipase enzyme has been used in biodiesel production in free form or immobilized on some different materials such as ceramics, kaolinites, silica, etc. [3]

In this work, immobilized lipase enzyme (Lipozyme IM) was used to produce diesel fuel from waste cooking oils. Lipase enzyme was immobilized on hydrotalcite prepared by coprecipitation method and four different types of commercial zeolites. Immobilization conditions such as temperature, pH, time and particle sizes on enzyme activity were investigated. Beside the immobilization conditions, the effect of reaction temperature and type of support for immobilization were also investigated.

Experimental

Lipozyme IM purchased from Novozyme was used without further purification for the experiments. Zeolite types 13-x, 5A, FM-8 and AW-300 kindly supplied by Altek Metal Ticaret A.Ş of Turkiye, Zeochem EU and Aldrich, respectively were used as different types of support for lipase immobilization. On the other hand, hydrotalcite was prepared by coprecipitation method from solutions of precursors by using precipitation reagents [4]. The coprecipitation was performed in a semi-batch system composed of an insulated cold water bath, a mechanical stirrer, a glass reaction beaker, a peristaltic pump and a pH-meter. The precipitation reagent was added to the precursor solutions using peristaltic pump while the solution mixed vigorously. After drying and calcination steps, hydrotalcite were ready to use for immobilization of enzyme.

Before immobilization all supports were grinded to different particle sizes. Enzyme solution was prepared by solving Lipozyme IM in potassium phosphate buffer pH 7.0 (for zeolite types) and Tris buffer pH 8.5 (for hydrotalcite). The hydrotalcite and zeolite particles were suspended in lipase solution for 5 h at different temperatures. The immobilized lipase was filtered and the supernatant was kept for protein and enzyme activity assays. The immobilized enzyme was stored at 4 °C until use.

The amount of protein content before and after immobilization was determined by Bradford method using BSA as a standard [5]. Lipase activity was estimated by the colorimetric method of Winkler and Stuckmann [6] by measuring the micromoles of 4-nitrophenol released from 4-nitrophenyl palmitate. The activities were expressed in IU (international unit) where 1 IU is defined as the amount of enzyme required to produce 1 μmol of 4-Nitro palmitate min-1 under assay conditions.

For the transesterification experiments, two types of waste cooking oil, kindly supplied by Saray Catering of Kocaeli, Turkey, and methanol (Merck) were used as reactants. Transesterification experiments were carried out in a stirred tank reactor provided with a reflux condenser to avoid methanol losses. Effects of immobilization materials and temperature on transesterification reaction were investigated.

PS-5

Feed and product analysis was performed on a Agilent 6890N Series Gas Chromatograph with Agilent 5973 Network Mass Selective Detector using a fused silica capillary column. Helium was used as carrier gas with a flowrate of 1.2 ml/min, oven temperature was raised from 190 to 300 °C with a heating rate of 4 °C min^{-1}.

Results

The results were discussed in terms of immobilization conditions, reaction temperatures and support type. The results obtained show that types of support affect the immobilization activity and reaction activity of lipase enzyme. Hydrotalcite was found to be the best support material for lipase than the other four types of zeolites. The maximum amount of protein bounded to the supporting material was 8.8 mg/g for zeolite FM-8 and 10.1 mg/g for hydrotalcite at 4 °C. It was found that the immobilized lipase on hydrotalcite yielded a lipolytic activity equivalent to 36% of initial activity of lipase that was measured after the seventh using as shown in Table.1.

Table 1. Stabilitiy of immobilized lipase on hydrotalcite in repeated use at 45 °C and pH:8.5

Number of cycle	1	2	3	4	5	6	7
Relative activity %	100	90	72	66	55	49	36

References

1. Taichi Samukawa, Masaru Kaieda, Takeshi Matsumoto, Kazuhiro Ban, Akihiko Kondo, Yuji Shimada, Hideo Noda, and Hideki Fukuda, Pretreatment of Immobilized Candida antarctica Lipase for Biodiesel Fuel Production from Plant Oil, Journal of Bioscience And Bioengineering Vol. 90, No.2, 180-183, 2000.

2. Cetinkaya M., Karaosmanoglu F., Today's position of biodiesel in Turkiye and EU, AOCS-94th Annual Meeting & Expo, Kansas City, USA, May 4-7, 2003.

3. Knezevic Z., Mojovic L., ve Adnadjevic B., Palm oil hydrolysis by lipase from Candida cylindracea immobilized on zeolite type Y, Enzyme Microb. Techol., 1998, 22, 275-280.

4. Tsyganok A.I., Inaba M., Tsunoda T., Suzuki K., Takehira K., and Hayakawa T., Combined partial oxidation and dry reforming of methane to synthesis gas over noble metals supported on Mg-Al mixed oxide, Applied Catalysis, 2004, 275, 149-155.

5. Bradford M.M., A rapid and sensitive method fort he quantitation of microgram quantities of protein utilizing the principle of protein-dye binding, Anal. Biochem., 1976, 72, 248-254.

6. Kumar S., Kikon K., Upadhyay A., Kanwar S.S., Gupta R., Production purification, and characterization of lipase from thermophilic and alkaliphilic Bacillus coagulans BTS-3, Protein Expression and Purification, 2005, 41, 38-44.

SYNTHESIS OF BIODIESEL WITH HETEROGENEOUS CATALYSTS: NaOH SUPPORTED ON ALUMINA AND SILICA

G. Arzamendi [a], I. Campo [a], E. Arguiñarena [a], M. Montes [b], <u>L.M. Gandía [a]</u>

[a] Departamento de Química Aplicada. Universidad Pública de Navarra. Edificio de los Acebos. Campus de Arrosadía s/n. E-31006, Pamplona, Spain. E-mail: lgandia@unavarra.es
[b] Departamento de Química Aplicada. Facultad de Ciencias Químicas de San Sebastián. Universidad del País Vasco. Pº Manuel de Lardizábal 3. E-20018, San Sebastián, Spain.

Introduction

Biodiesel could be an alternative renewable fuel for diesel engines. It consists of mono-alkyl esters usually produced by transesterification with an alcohol (most commonly methanol) of the triglycerides found in vegetable oils or animal fats. The European Union is the leading region of the world in terms of development of a biodiesel sector; 2.42 million tons were produced in 2004, representing a 25.7% increase compared to the 2003 figures [1]. Most of the commercial biodiesel is produced from plant oils (mainly colza, soybean and sunflower) using homogeneous base catalysts (NaOH or KOH), that is, catalysts soluble in methanol. However, production costs are still high and currently biodiesel is not cost-competitive with petrol diesel. This is largely due to the high vegetable oil prices, but there are also other drawbacks: the homogeneous catalyst cannot be recovered and must be neutralized giving rise to alkaline wastewaters and the formation of stable emulsions making separation of the methyl esters difficult, there is limited use of continuous processing technologies, and the synthesis is very sensitive to the presence of water and free fatty acids. Therefore, there is an increasing interest in the possibility to replace the homogeneous alkaline hydroxides, carbonates or metal alkoxides by heterogeneous solid catalysts that could potentially lead to lower production costs [2-5].

In this work, we report on the activity for the transesterification of sunflower oil with methanol of a series of basic solids consisting of NaOH supported on conventional alumina and silica catalytic carriers. Their performance will be compared with that of homogeneous NaOH under standard transesterification reaction conditions. We have also investigated the possible effect of the sampling procedure on the experimental results due to the heterogeneous character of the reaction (both methanol and vegetable oil are mutually immiscible).

PS-6

Experimental procedures

The catalysts were prepared by incipient wetness impregnation with aqueous NaOH solutions of the 212-300 μm size fraction of commercial alumina (Spheralite 505, Procatalyse) and silica (Aerolyst 350, Degussa) supports previously calcined in a muffle for 12 h at 500ºC. After impregnation the catalysts were dried at 120ºC under reduced pressure (10 kPa) and then, calcined at 400ºC for 12h in air. The nominal NaOH contents of the final solids were in the range from 10 to 26 wt.%.

The experiments were carried out at 50°C in two different experimental set-ups. When using the homogeneous NaOH catalyst, a 1 litre jacketed glass reactor fitted with a reflux condenser, a nitrogen inlet, a stainless steel agitator comprising a turbine (370 rpm), a thermocouple probe and a heated circulating water bath was employed. Edible-grade sunflower oil (ca. 300 g) and some methanol (ca. 40 g) were initially charged into the reactor to reach the reaction temperature. The catalyst (0.3g NaOH) was rapidly added into the reactor dissolved in the amount of methanol necessary to give overall alcohol/oil molar ratios of 3:1, 6:1 and 12:1. Samples were withdrawn during the experiment at various intervals. The sampling device consisted of a polyamide tube connected to a stainless steel one-way compression-nut stopcock and a 10 ml polypropylene syringe. A recirculation loop comprising a PTFE tube, a diaphragm-type metering pump working at 80 ml/min and a stainless steel three-way ball valve was also used for sampling purposes.

In the case of the heterogeneous catalysts a screening of the reaction conditions was carried out by performing series of 5 parallel reactions in closed glass flasks (60 ml) immersed in thermostatic water baths at 50ºC with magnetic stirring. 20 g of sunflower oil, 0.413g of supported catalysts (19.3 wt.% NaOH) and the volume of methanol required to reach alcohol/oil molar ratios of 6:1, 12:1, 24:1 and 48:1 were added into the flasks. The amount of NaOH in the 0.413g of solid catalyst is four times the NaOH relative to the oil mass used in the homogenously-catalyzed reaction (0.1%).

The reaction was short-stopped by addition of some drops of an acetic acid solution in tetrahydrofuran (THF). Once filtered and diluted with additional THF, the samples were analyzed at room temperature by size exclusion chromatography (SEC).

Results and discussion

Figure 1 illustrates the evolution of the SEC chromatograms with time for a typical transesterification reaction. This technique has allowed to determine simultaneously the total amounts of triglycerides (TG), diglycerides (DG), monoglycerides (MG), fatty acid methyl esters (ME), free glycerol (GLY) in samples of the transesterification reaction. Only one

266

chromatographic peak was obtained for each kind of compounds which resulted in an easy and accurate quantitation of these substances.
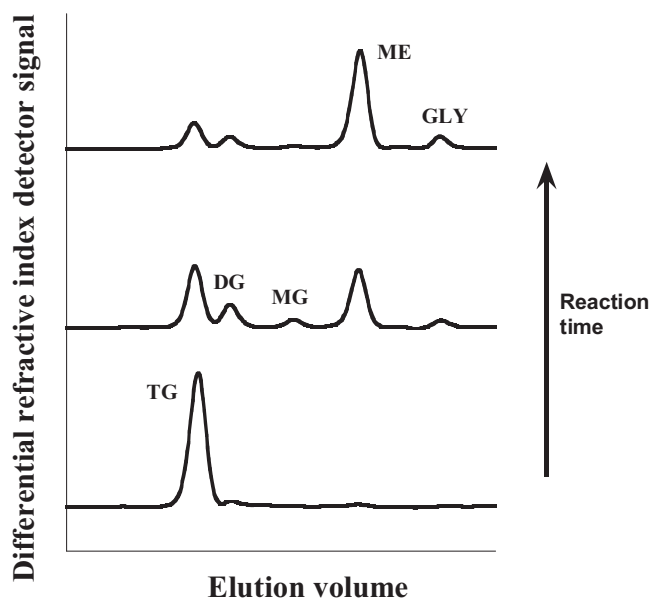
Figure 1. Evolution with reaction time of the SEC chromatograms of a typical transesterification reaction of sunflower oil using NaOH as homogeneous catalyst (50 ºC, methanol/oil molar ratio of 6:1).
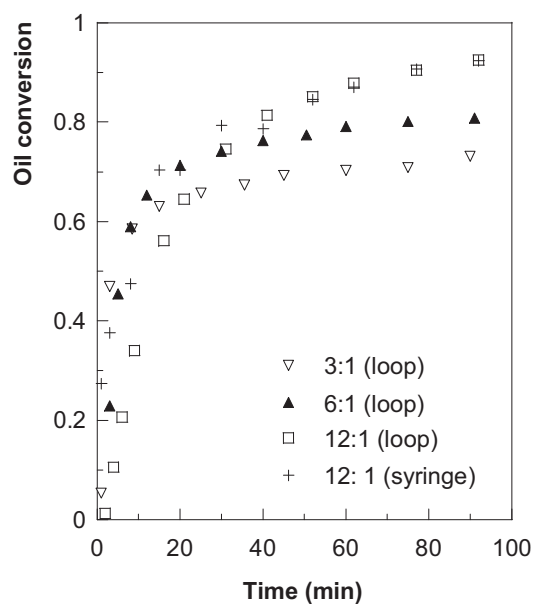
Figure 2. Effect of the methanol/oil ratio and sampling procedure in the transesterification of edible-grade sunflower oil using NaOH as homogeneous catalyst (50 ºC).

As regards the sampling procedure, some differences have been found between using a syringe or the recirculation loop only in the first instants, as shown in Figure 2. That is, when the viscosity of the reaction mixture is high. This allows some phase separation to take place in the tube used to extract the samples with the syringe. As the reaction progresses, the viscosity remarkably decreases and the results obtained with both sampling procedures are almost coincident. Also shown in Figure 2 is the effect of the methanol/oil molar ratio for transesterification reactions carried out with the same amount of homogeneous NaOH catalysts. As judged from the slope of the curves, the initial reaction rate decreases as the methanol/oil ratio increases which can be due to a lower concentration of active methoxide species. On the contrary, the final conversion increases with the methanol/oil ratio, as expected from the effect of the alcohol excess on the equilibrium conversion. Figure 3 shows the results obtained with the heterogeneous catalysts. A significantly better performance of the alumina supported catalysts compared to the silica supported ones has been found. In both cases, the performance improves when the catalyst is not calcined. The behaviour of the silica supported catalysts is very sensitive to the methanol/oil ratio. Although homogeneous NaOH

PS-6

gives the best results, it is remarkable that the behaviour of the non-calcined $NaOH/Al_2O_3$ catalyst is not far.
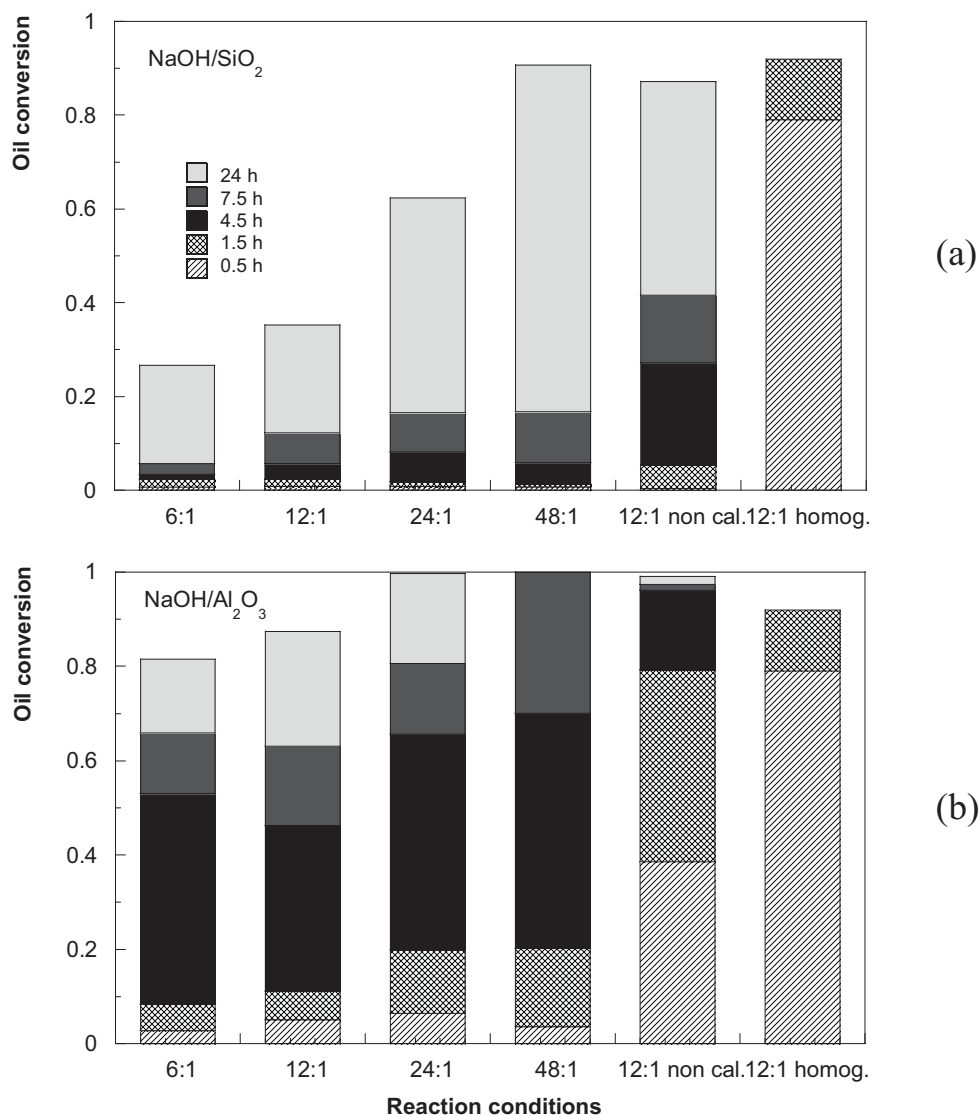
Figure 3. Evolution of the oil conversion for reactions performed with (a) $NaOH/SiO_2$ and (b) $NaOH/Al_2O_3$ catalysts calcined and non-calcined. The methanol/oil ratio used is indicated. It is also included for comparison the performance of homogeneous NaOH.

Acknowledgements

References

[1] EUROBSERV'ER, "Biofuels Barometer". June 2005, 39-50.

[2] T.F. Dossin, M.-F. Reyniers, G.B. Marin, Appl. Catal. B, 61 (2005) 178.

[3] D.E. López, J.G. Goodwin Jr., D.A. Bruce, E. Lotero, Appl. Catal. A 295 (2005), 97.

[4] P. De Filippis, C. Borgianni, M. Paolucci, Energy Fuels, 19 (2005) 2225.

STEAM REFORMING OF BIO-OIL IN A FIXED BED REACTOR FOR THE PRODUCTION OF HYDROGEN

P.N. Kechagiopoulos[(1)], **S.S. Voutetakis**[(2)], **A.A. Lemonidou**[(3)], **A.A. Iordanidis**[(4)] **and I.A. Vasalos**[(5)]

[(1,3,5)]*Department of Chemical Engineering, Aristotle University of Thessaloniki, P.O. Box 1517, University City, Thessaloniki 54124, Greece*

[(2,4,5)]*Process Engineering Research Institute, Centre for Research and Technology Hellas, P.O. Box 361, GR 57001, Thermi, Thessaloniki, Greece*

[(1)] *kechagio@cperi.certh.gr,* [(2)] *paris@cperi.certh.gr,* [(3)] *alemonidou@cheng.auth.gr,* [(4)] *arthouros.iordanidis@ch.abb.com,* [(5)] *vasalos@certh.gr*

Introduction

The continuously increasing pressure on the pollution of the environment from the use of conventional fuels, in conjunction with the concern for the depletion of oil reserves, has led to a necessity to intensify the search for alternative energy sources. Hydrogen is emerging as the energy carrier of the future since it can be used as a clean transport fuel as well as a means for the production of electricity via fuel cells. Nowadays, hydrogen is mainly produced from non-renewable sources leading to high CO_2-emissions. Hydrogen can present environmental benefits only when derived from renewable energy sources. Steam reforming of biomass pyrolysis oil (bio-oil) is a promising sustainable hydrogen production route. The main objective of this work was to study the reforming of bio-oil model compounds and the aqueous fraction of a bio-oil derived from beech wood in a pilot plant unit.

Experimental

The experiments for this study were conducted at the SYNGAS pilot plant unit of CPERI using a fixed-bed reactor. Gas chromatographs were used for the analysis of gas and liquid products. The reactor was heated electrically by a three-zone furnace. An industrial naphtha reforming catalyst supplied by Sud-Chemie (C11-NK) was used for the experiments Runs were conducted with ethylene glycol, acetone and acetic acid. The aqueous fraction of a bio-oil derived from catalytic pyrolysis of beech wood was also tested.

Results and discussion

Ethylene Glycol reforming: Complete conversion of ethylene glycol was attained for all the conditions studied. Hydrogen yield is presented as a function of H_2O/C ratio and temperature

in Fig.1a and b respectively. The approach to equilibrium for all of the conditions studied is very good with hydrogen yield always well above 80% reaching 93% at 700°C and a H_2O/C ratio of 6. Experiments terminated due to reactor blockage for H_2O/C ratios less than 3 after approximately 7 hours. Temperature variation experiments proceeded more smoothly. Coke formation was noticeably smaller due to the high $H_2O/Carbon$ ratio (equal to 6) that was used. We managed to sustain a continuous run even at temperature 600°C for more than 12 hours.
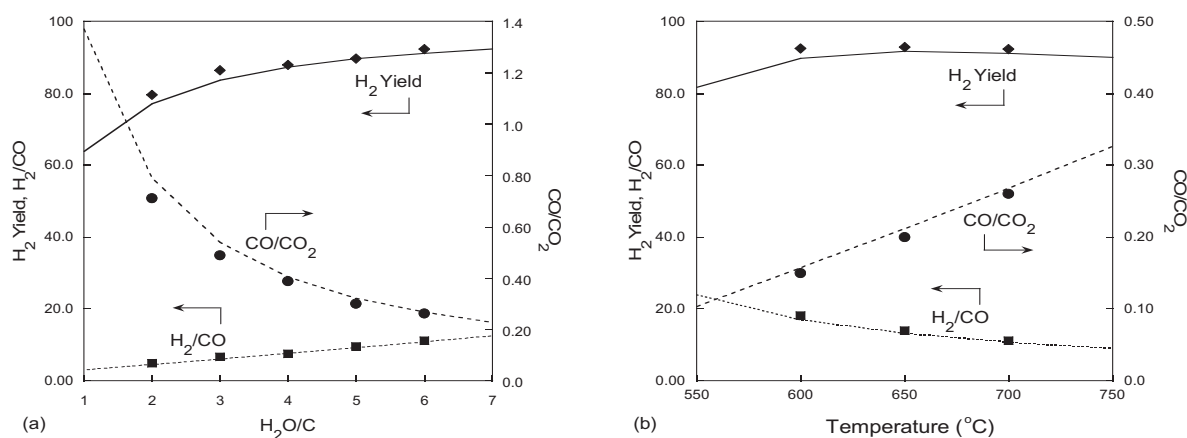
Figure 1. Ethylene glycol reforming at: (a) T=700°C and (b) H_2O/C=6. $G_{C1}HSV$ = 1500 hr⁻¹

Model compounds mixture reforming: An equimolar mixture of acetic acid, acetone and ethylene glycol was prepared. The results for variable H_2O/C ratio and temperature are depicted in Fig.2a and b respectively. Equilibrium product composition was attained under all the conditions used. Hydrogen yield as high as 90% is attained with the catalyst being able to convert completely the organic compounds. Steady runs in every experimental condition lasted for more than 4 hours. However, it was observed that coke formation was higher compared to ethylene glycol for the same conditions.
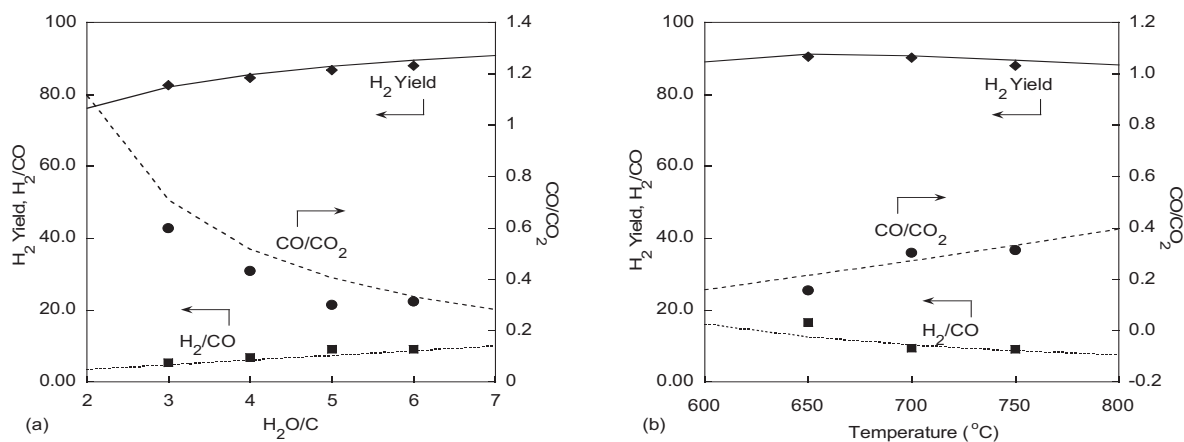
Figure 2. Mixture reforming at: (a) T=750°C and (b) H_2O/C=6. $G_{C1}HSV$ = 1500 hr⁻¹

Acetone reforming: Acetone is known to undergo aldol condensation reactions forming products such as mesityl oxide or produce ketene via decomposition. Both compounds can

undergo oligomerization forming carbonaceous deposits. Acetone being more susceptible for coke formation could be the reason for the higher carbon formation observed in the 3-component mixture experiments compared to ethylene glycol. This was validated in a separate set of experiments with acetone as the oxygenated feed stock (Fig.3a and b). At the same experimental conditions acetone showed increased formation of coke deposits. The approach to equilibrium is good for temperatures higher than $650^{o}C$ and H_2O/C ratios higher than 4. Coke formation restricted the TOS to 2h under which steady conditions could be attained. Nonetheless, conversion of acetone was complete in the entire spectrum of conditions covered under steady operation.
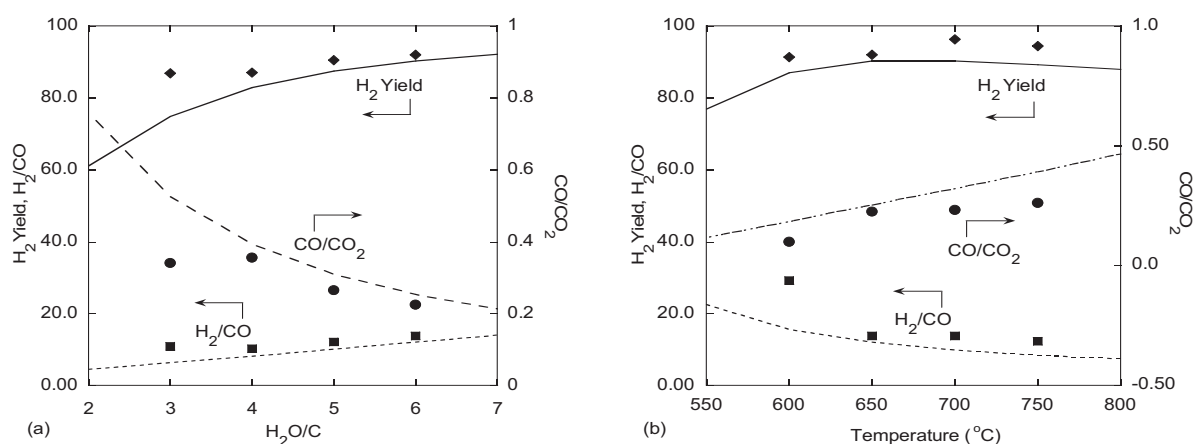
Figure 3. Acetone reforming at: (a) $T=650^{o}C$ and (b) $H_2O/C=6$. $G_{C1}HSV = 1500$ hr^{-1}

Bio-oil aqueous phase reforming: Bio-oil produced from the catalytic pyrolysis of beech wood was separated by adding water at a mass ratio equal to 2:1 in order to extract the aqueous fraction. The final aqueous mixture contained 16% wt organics ($CH_{2.48}O_{0.94}$), the rest being water, corresponding to a H_2O/C equal to 8.2. To avoid high extent of thermal decomposition an injection system was installed in the fixed bed reactor in order to feed the bio-oil at environmental temperature.

The first series of experiments with bio-oil as a feedstock were conducted in the absence of catalyst in order to investigate the extent of decomposition in the gaseous phase. The conversion of bio-oil to gaseous products was as low as 12% for $650^{o}C$ and increased up to 60% for temperatures higher than $850^{o}C$. More than 20% of the incoming carbon was deposited in the catalytic bed as coke at $650^{o}C$, with this number lowering to 12% above $800^{o}C$. Thus the total conversion of the bio-oil spanned from 35% to 80% with increasing temperature.

The catalytic tests with bio-oil were performed without any further addition of external water. The yield of hydrogen did not surpass 60% (Fig.4a) in all of the conditions studied with the

conversion of bio-oil being complete. The highest values were observed at the higher temperatures, while the flow of the organics did not seem to influence notably. According to thermodynamic calculations, hydrogen yield for these conditions is almost 90%. This deviation can be ascribed to the increased coke formation in the catalytic bed that amounted to around 30% wt of the incoming carbon. The majority of the experiments terminated after 4 hours in order to regenerate the catalytic bed.
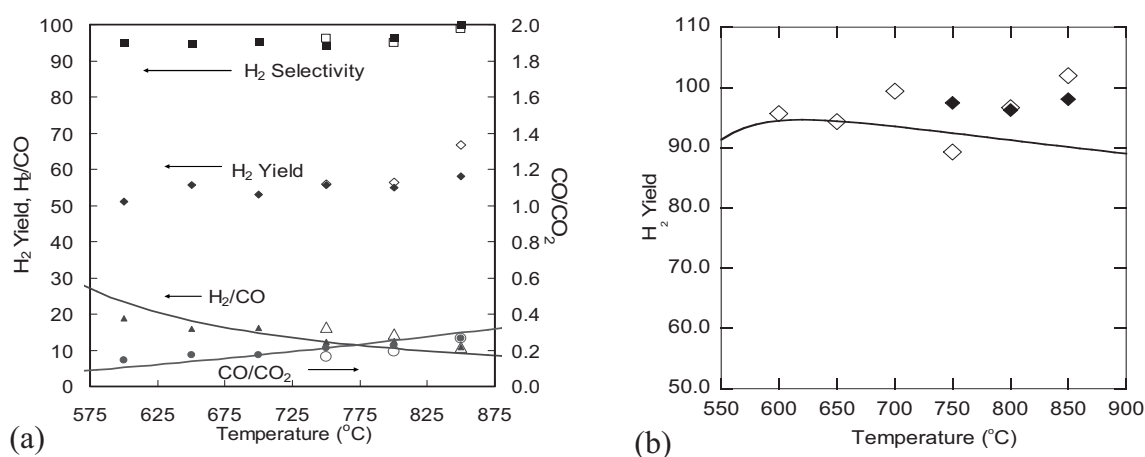
Figure 4. Catalytic reforming of bio-oil: (a) Effect of reaction temperature, (b) H_2 yield based on carbon moles at the outlet. $G_{C_1}HSV = 300$ hr^{-1} (solid), 600 hr^{-1} (blank). Lines: equilibrium

Worthy to note that the composition of the gaseous products follows very well the thermodynamically predicted, implying that the reactions of steam reforming and water-gas shift are at equilibrium. This can be proved by calculating the yield of hydrogen assuming that the incoming carbon moles are equal to the sum of those contained in the gaseous products (Fig.4b). It is clear from this diagram that hydrogen yield is equal to or greater than that theoretically predicted from equilibrium.

Conclusions

Biomass can be efficiently used for hydrogen production. Representative model compounds of bio-oil are effectively reformed in a fixed bed in the presence of commercial nickel-based catalysts. Hydrogen yields up to 90% can be achieved at reaction temperatures higher than 600°C and steam to carbon ratios higher than 3. Reforming of real bio-oil resulted in a much lower hydrogen yield around 60% due to the high extent of coking. The severe coking caused mainly from thermal decomposition of the unstable oxygenates, imposes the use of fluid bed reactors in processing the aqueous fraction of the bio-oil. By combining a proper reactor design with catalytic materials that minimize the catalytically produced coke, bio-oil has the potential to become an important and environmentally friendly hydrogen production method.

RENEWABLE HYDROGEN AND CHEMICALS BY AUTOTHERMAL REFORMING OF ALCOHOLS, ETHYLENE GLYCOL, AND GLYCEROL

P.J. Dauenhauer, J. Salge, E. Wanat and <u>L.D. Schmidt</u>

Department of Chemical Engineering & Materials Science
University of Minnesota – Twin Cities
151 Amundson Hall, 421 Washington Avenue SE
Minneapolis MN 55455, USA
Fax: 612-626-7246, schmi001@umn.edu

Autothermal reforming is a very promising method to convert biofuels into hydrogen and chemicals. [1-4] High conversion with residence times less than 10 milliseconds allow for very small reactors that operate without external heat sources. Flexible operation allows for start-up in a few seconds as well as in transient modes. [1]

We describe the reforming of alcohols (methanol, ethanol, n-propanol, and iso-propanol) as well as ethylene glycol and glycerol and consider the catalysts and reactor conditions that maximize either hydrogen or chemicals. All experiments exhibited greater than 90% conversion of fuel and oxygen and adiabatic temperatures greater than 700 °C. These fuels can be made to produce H_2, H_2O, CO, and CO_2 and less than 1% of any other species including olefins, alkanes, or aldehydes by tuning the carbon to oxygen ratio (C/O) to 1 for maximum H_2. By using larger pore diameters and operating at a C/O > 1, larger yields of chemicals can be obtained.

All alcohols can be converted into H_2 and CO with selectivities of at least 60% using rhodium (Rh) on a ceramic foam monolith support at C/O ~1. [2-4] The addition of a γ-alumina wash coat improves the hydrogen selectivity by up to 15% as observed with ethanol by increasing catalyst dispersion. The addition of cerium (Ce) to Rh has also been shown to dramatically improve hydrogen selectivity of ethanol and 1-propanol to 80% and 90% respectively. Alcohols can also produce chemicals such as ethylene in selectivities as high as 25% on Pd or Pt by increasing the C/O ratio beyond ~1. Furthermore, acetone can be produced from 2-propanol with selectivities up to 60%. [4] Few aldehydes have been observed from any of the alcohols under the range of reactor conditions.

PS-8

Addition of water improves H_2 selectivity from ethanol as high as 140%, based on the H atoms in the fuel. [2] The presence of water on a RhCe catalyst promotes water-gas shift, producing hydrogen molecules from all six H atoms of ethanol as well as H atoms from additional water molecules. The promoted shift reaction has the additional benefit of reducing the carbon monoxide selectivity from 80% to 40%, thereby reducing a fuel cell poison from the hydrogen rich product stream.

Ethylene glycol and glycerol have one carbon atom for every oxygen atom present as a hydroxyl group similar to larger biologically derived molecules. This class of molecules is restricted thermodynamically to H_2 selectivities of ~60%, achieved on RhCe catalysts with γ-alumina wash coat. Autothermal reforming with steam to carbon ratios as high as 4.5 have resulted in H_2 selectivities as high 90% and CO selectivities as low as 25% at 700 °C.

The high yield of H_2 without significant formation of any other chemicals appears to occur primarily by surface chemistry through the alkoxy bond with the Rh surface which is known to be the primary mechanism of alcohol bonding to noble metals. [4] β scission of the adsorbed alkoxy leads to complete dissociation and resultant formation of primarily H_2 and CO or to CO_2 in the presence of H_2O. Acetone is probably formed primarily by homogeneous chemistry within the pores of the catalyst, with the weak secondary C-H bond dissociation to form a radical species which eliminates H to form the ketone.

[1] K. Williams, C. Leclerc, and L. D. Schmidt, "Rapid lightoff of syngas production from methane: A transient product analysis," *AIChE Journal* **51,** 1, (2005).

[2] G. A. Deluga, J. R. Salge, and L. D. Schmidt, "Renewable hydrogen from ethanol by autothermal reforming," *Science* **303**, 993-997, (2004).

[3] J.R. Salge, G.A. Deluga, L.D. Schmidt, "Catalytic partial oxidation of ethanol over noble metal catalysts," *Journal of Catalysis*, **235**, 69-78, (2005).

[4] E.C. Wanat, B. Suman, L.D. Schmidt, "Partial oxidation of alcohols to produce hydrogen and chemicals in millisecond-contact time reactors," *Journal of Catalysis* **235**, 18-27, (2005).

OXIDATION OF α-PINENE WITH O$_2$ AND AQUEOUS H$_2$O$_2$ OVER SINGLE SITE CATALYSTS

N.V. Maksimchuk[1], M.S. Melgunov[1], J. Mrowiec-Białoń[2], A.B. Jarzębski[2], V.N. Parmon[1],V.A. Semikolenov,[†] and O.A. Kholdeeva[1]

[1]*Boreskov Institute of Catalysis SB RAS,*

Prospekt Akademika Lavrentieva 5, Novosibirsk, 630090, Russia

E-mail: nvmax@catalysis.nsk.su; Fax : +7 383 330 80 56

[2]*Polish Academy of Sciences, Institute of Chemical Engineering,*

44-100 Gliwice, Bałtycka 5, Poland

Introduction

α-Pinene is the main component of gum turpentine and is thus an inexpensive, readily available, and renewable starting material for producing a wide variety of valuable products, such as flavors, fragrances, medicines, and agrochemicals [1-2]. Specifically, its oxidation products, verbenol, verbenone, α-pinene epoxide, and campholenic aldehyde, are of high practical importance as flavor chemicals and key intermediates for manufacture of various fine chemicals, including citral, menthol, taxol, vitamins A and E [3-5].
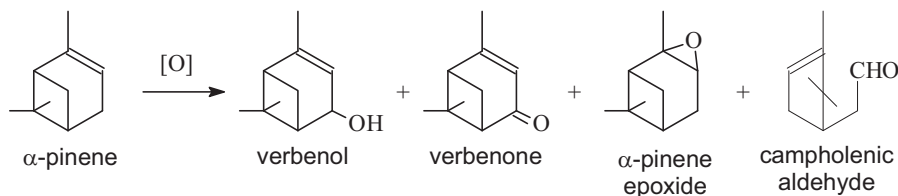
The development of methods for the selective oxidation of α-pinene using environmentally benign and cheap oxidants, such as O$_2$ and H$_2$O$_2$, over solid, easily recyclable catalysts is a challenging goal of fine chemistry.

Here we first report a comparative study of α-pinene autoxidation and oxidation by molecular oxygen (as well as its co-oxidation with isobutyraldehyde) over heterogeneous catalysts based on Co-containing polyoxometalate (Co-POM), TBA$_4$HPW$_{11}$CoO$_{39}$, and NH$_2$-modified mesoporous silicate matrixes (MMM, SBA-15, etc.). The catalytic properties of the single site catalysts, such as mesostructured metal-silicates Ti-MMM-2 and Fe-MMM-2, TiO$_2$-SiO$_2$ mixed oxides, Ti- and Zr-grafted on mesoporous silica cellular foams (Ti- and Zr-MCF), and the new composite material H$_5$PW$_{11}$TiO$_{40}$/silica prepared by a sol-gel method, in allylic oxidation of α-pinene with aqueous H$_2$O$_2$ are also reported. The effects of the reaction

conditions (temperature, concentration of reagents, solvent nature, etc.) on the product distribution and yield have been studied. The question on the catalyst stability and its reusability was addressed.

Experimental

The catalysts were prepared according to the literature procedures [6-8] and were characterized by elemental analysis, N_2 adsorption, XRD, IR and DRS-UV spectroscopy. Catalytic experiments were carried out in thermostated glass vessels under vigorous stirring. Aliquots of the reaction mixture were withdrawn periodically during the reaction course, and the reaction products were identified by GC-MS and ^{1}H NMR, and quantified by GC using internal standard. The leaching and stability tests were performed as described previously [9].

Results and Discussion

The kinetic peculiarities of α-pinene liquid-phase autoxidation by molecular oxygen have been studied (in the temperature range of 70-120°C and at oxygen pressure within 0.5-6 bar range). At a low α-pinene conversion (5.5%), the process of α-pinene oxidation by molecular oxygen proceeds selectively and gives two main products: α-pinene epoxide (39% selectivity) and verbenyl-hydroperoxide (55% selectivity), which can be catalytically hydrogenated to verbenol to increase its yield. The reaction conditions for selective reduction of verbenyl-hydroperoxide to verbenol by molecular hydrogen over the Pd/C catalyst without affecting the α-pinene C=C bond were found. The products ratio depends slightly on the temperature, oxygen pressure and α-pinene conversion. A kinetic equation for the reaction rate was inferred.

The catalytic α-pinene oxidation by molecular oxygen over Co-POM/silica catalysts leads to allylic oxidation products (50% selectivity at 56% conversion) while co-oxidation with isobutyraldehyde gives selectively α-pinene epoxide (90% selectivity at 100% conversion). The α-pinene oxidation by O_2 (both with and without isobutyraldehyde) without catalyst is slower and less selective than the catalytic process. The catalyst activity related to one Co center (TOF_{av}) in the α-pinene oxidation decreased in the order Co-POM/MCF ~ Co-POM/silica composite material > Co-POM/SBA-15 > Co-POM/silica (both with and without isobutyraldehyde). The catalysts can be used repeatedly without a significant loss in activity
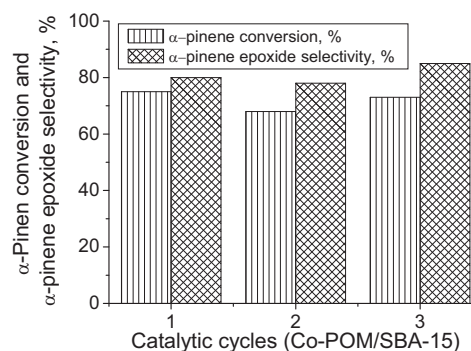
although minor leaching of the active component is observed.

The catalyst activity related to one active metal center (TOF$_{av}$) in the H$_2$O$_2$-based α-pinene oxidation decreased in the order H$_5$PW$_{11}$TiO$_{40}$/silica >> Ti-MCF > Ti-MMM-2 > Zr-MCF > Ti,Si-xerogel > Fe-MMM-2. The reaction selectivity strongly depends on the solvent, substrate/oxidant molar ratio, reaction temperature, and α-pinene conversion. In optimized reaction conditions (MeCN, 30°C), with H$_5$PW$_{11}$TiO$_{40}$/silica as catalyst, the selectivity toward verbenol/verbenone attains 82 and 68% at 8-15 and 28% conversion of the substrate, respectively. Interestingly, Co-POM/silica and Co-POM/SBA-15 yield the selectivity toward verbenol/verbenone as high as 67% at 16-21% of substrate conversion (MeCN, 50°C), so a higher selectivity level can be reached with H$_2$O$_2$. Meanwhile, in all the systems, the selectivity decreases with the substrate conversion indicating overoxidation processes.

The Ti-catalysts can be used repeatedly without a significant loss in activity, no leaching of the active component is observed.
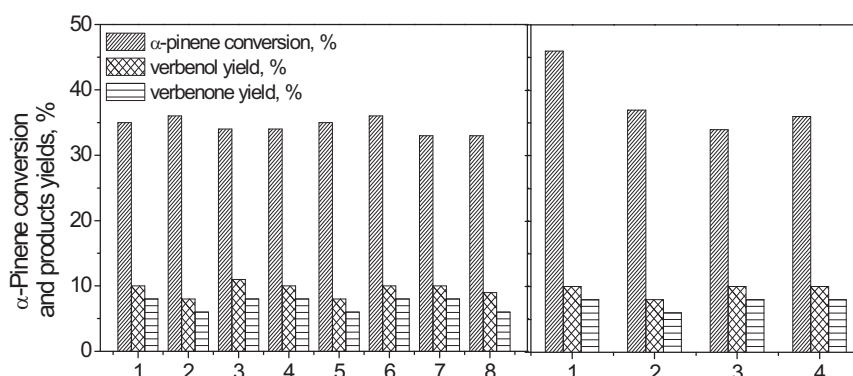
The experiments with a fast catalyst filtration at the reaction temperature showed that the oxidation is a true heterogeneous process. The reaction atmosphere (air, O$_2$ or Ar) and small amounts of the radical chain inhibitor, 2,6-di-*tert*-butyl-4-methylphenol, had no significant affect on the product distribution and the reaction rate indicating most likely radical non-chain mechanism of the oxidation or short chains.

Conclusion

In all the systems studied, the selectivity of allylic oxidation of α-pinene strongly depends on the substrate conversion. The highest selectivity to verbenol/verbenone (82% at 15% conversion) was obtained using heterogeneous composite catalyst H$_5$PW$_{11}$TiO$_{40}$/silica and aqueous H$_2$O$_2$ as oxidant. The catalyst behaves as a true heterogeneous one and can be used repeatedly without suffering its activity. Another advantage of this system is its non-chain

PS-9

radical mechanism (or mechanism with short chains). That ensures a good reproducibility of the catalytic results obtained with H_2O_2, which is in contrast to O_2-based processes proceeding via chain radical mechanisms.

References

[1] W.F. Erman, *Chemistry of the Monoterpenes: An Encyclopedic Handbook*, Marcel Dekker, New York, 1985.

[2] Bauer K., Garbe D., Surburg H., *Common Fragrance and Flavor Materials*, Wiley-VCH, New York, 1997.

[3] C. Mercier, P.Chabardes, *Pure and Appl. Chem.* 66 (1994) 1509.

[4] P.Z. Bedoukian, *Am. Perf. and Cosm.* 86 (1971) 25.

[5] P.A. Wender, T.P. Mucciaro, *J. Am. Chem. Soc*. 114 (1992) 5878.

[6] O.A. Kholdeeva, M.S. Melgunov, A.N. Shmakov, N.N. Trukhan, V.V. Kriventsov, V.I. Zaikovskii, V.N. Romannikov, *Catal. Today*, 91-92 (2004) 205.

[7] M.S.Morey, S.O'Brien, S.Schwarz, G.D.Stucky, *Chem. Mater.*, 12 (2000) 898.

[8] O. A. Kholdeeva, M. P. Vanina, M. N. Timofeeva, R. I. Maksimovskaya, T. A. Trubitsina, M. S. Melgunov, E. B. Burgina, J. Mrowiec-Białoń, A.B. Jarzębski, C. L. Hill, *J. Catal.,* 226 (2004) 363.

[9] N.N. Trukhan, V.N. Romannikov, E.A. Paukshtis, A.N. Shmakov, O.A. Kholdeeva, *J. Catal.* 202 (2001) 110.

REACTION OF THE NATURAL LIGNAN HYDROXYMATAIRESINOL OVER PALLADIUM ON CARBON NANOFIBRES

Heidi Markus[1], **Arjan Plomp**[2], **Päivi Mäki-Arvela**[1], **Narendra Kumar**[1],

Krijn P. de Jong[2], **Johannes H. Bitter**[2], **Dmitry Yu. Murzin**[1]

[1]*Laboratory of Industrial Chemistry, Process Chemistry Centre, Åbo Akademi University,*

Biskopsgatan 8, FIN-20500 Turku, Finland

[2]*Department of Inorganic Chemistry and Catalysis, Debye Institute, Utrecht University,*

P.O. Box 80083, Utrecht 3508 TB, The Netherlands

Introduction

Lignans can be found in many different parts of plants, such as the wooden parts, roots, leaves, flowers, fruits, and seeds. Most plants contain small amounts of lignans as glycosidic conjugates associated with fibre components, which complicates the isolation process [1]. Coniferous trees, on the other hand, contain large amounts of lignans in unconjugated forms, which can be more easily isolated. Knots of Norway spruce (*Picea abies*), i.e., the part of the branch that is embedded in the stem, contain large quantities of lignans, 6–24 wt-%, out of which hydroxymatairesinol (HMR) is the most abundant (65–85 wt-% of the lignans) [2]. Studies have suggested that lignans have a preventive effect against hormone-dependent cancers such as breast, prostate and colon cancers [3]. In addition to the anticarcinogenic effects, they also have antioxidative effects [4].

Matairesinol (MAT) can be found in small amounts in different plants, for example, in flaxseed and rye [5]. MAT can be produced through hydrogenolysis of HMR, which as indicated above, can be extracted in larger amounts from Norway spruce knots. Markus et al. [6] hydrogenolysed hydroxymatairesinol over palladium on active carbon, and it was concluded that the acidity of the carbon had a profound effect on the activity; the reaction rate increased with the acidity increase. However, carbon supported metal catalysts can exhibit large batch-to-batch variations due to, for example, natural variations in the starting material [7], and moreover the reproducibility of the catalyst preparation with respect to the surface groups might become difficult. To avoid this, synthetic carbons can be used. Examples on synthetic carbons are carbon nanofibres (CNF) and carbon nanotubes (CNT). Carbon nanofibres are graphite-like fibres grown from decomposition of carbon-containing gases on small metal particles and they contain neither micropores nor impurities [8]. The acidity of

this material can be modified by oxidation (creating acid sites) or reduction (removing acid sites). In this work, HMR was hydrogenolysed over palladium containing CNF, comprising different amount of acid sites.

Experimental

The carbon nanofibres were grown on a Ni/SiO$_2$ catalyst as described by Toebes et al. [9]. The deposition of palladium on the CNF was performed according to Winter et al. [10]. Three portions of the Pd/CNF were heat-treated in a N$_2$-flow at 300°C, 400°C, and 500°C during 2 hours (ramp 5°C/min). These catalysts and the non-treated Pd/CNF were having different concentration of acid sites; the most acidic was the non-treated catalyst, and the least acidic was the catalyst treated in N$_2$-flow at 500°C. The catalysts were tested in the hydrogenolysis of HMR under hydrogen atmosphere in stirred glass reactor at 70°C and using 2-propanol as solvent. The reaction scheme is presented in Fig. 1.
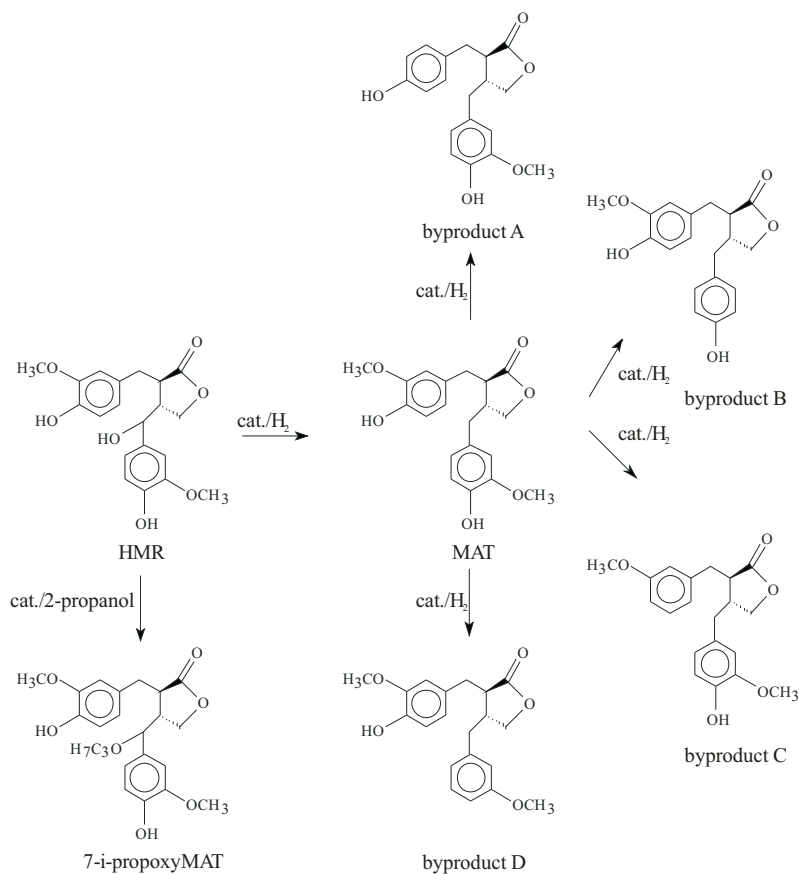
Fig. 1. Reaction scheme.

Results and discussion

As illustrated by Fig. 2, the least acidic Pd/CNF (treated in N$_2$-flow at 500°C) had the lowest activity and selectivity. The non-treated Pd/CNF had approximately the same activity as the catalyst treated at 300°C, but the non-treated catalyst was much more selective. It can

be concluded that a more acidic CNF support is preferred, and this is in agreement with the results obtained with Pd/C [6].

a)

b)
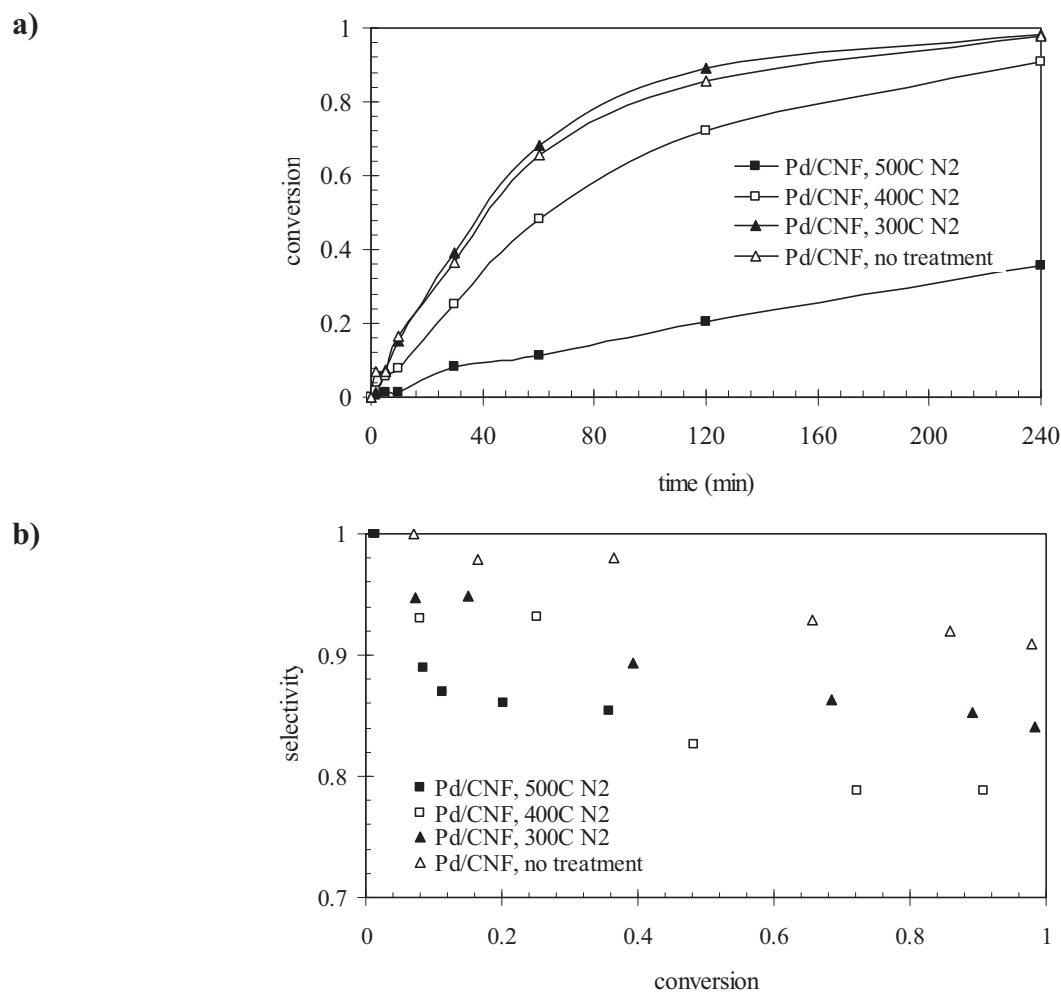
Fig. 2. Hydrogenolysis of hydroxymatairesinol to matairesinol: a) conversion versus time, b) selectivity to matairesinol versus conversion.

References

[1] N.M. Saarinen, A. Wärri, S.I. Mäkelä, C. Eckerman, M. Reunanen, M. Ahotupa, S.M. Salmi, A.A. Franke, L. Kangas, R. Santti, Nutr. Cancer 36 (2000) 207.

[2] S. Willför, J. Hemming, M. Reunanen, C. Eckerman, B. Holmbom, Holzforschung 57 (2003) 27.

[3] H. Adlercreutz, Lancet 3 (2002) 364.

[4] S.M. Willför, M.O. Ahotupa, J.E. Hemming, M.H.T. Reunanen, P.C. Eklund, R.E. Sjöholm, C.S.E. Eckerman, S.P. Pohjamo, B.R. Holmbom, J. Agric. Food Chem. 51 (2003) 7600.

[5] S. Heinonen, T. Nurmi, K. Liukkonen, K. Poutanen, K. Wähälä, T. Deyama, S. Nishibe, H. Adlercreutz, J. Agric. Food Chem. 49 (2001) 3178.

[6] H. Markus, P. Mäki-Arvela, N. Kumar, N.V. Kul'kova, P. Eklund, R. Sjöholm, B. Holmbom, T. Salmi, D.Yu. Murzin, Catal. Lett. 103 (2005) 125.

[7] N. Krishnankutty, M.A. Vannice, J. Catal. 155 (1995) 312.

[8] M.L. Toebes, J.M.P. van Heeswik, J.H. Bitter, A.J. van Dillen, K.P. de Jong, Carbon 42 (2004) 307.

[9] M.L. Toebes, J.H. Bitter, A.J. van Dillen, K.P. de Jong, Catal. Today 76 (2002) 33.

[10] F. Winter, A.J. van Dillen, K.P. de Jong, J. Mol. Catal. A 219 (2004) 273.

ENVIRONMENTALLY FRIENDLY NOVEL HYBRIDIZED CHIRAL ORGANO-INORGANIC CATALYSTS FOR EPOXIDATION AND ALKYLATION REACTIONS

Oriana Lanitou[1,2], Dimitra Dimotikali[1], Elina Yiannakopoulou[2], Kyriakos Papadopoulos[2]

[1]*Chemical Engineering Department, N.T.U. Athens, 15780 Athens, Greece,*
e-mail: oriana@chem.demokritos.gr, tel.: 210-6503634; fax.: 210-6511766.
[2]*Institute of Physical Chemistry, NCSR "Demokritos", 15310 Athens, Greece,*
e-mail: kyriakos@chem.demokritos.gr , tel.: 210-6503647; fax.: 210-6511766

Introduction

In recent years, methods for the stereoselective synthesis of epoxides as well as of α-amino acids have attracted widespread attention due to their importance as potential intermediates for the synthesis of natural or pharmaceutical products. Especially, numerous studies for the synthesis of α-amino acids, the "building blocks of life", have been made over the past quarter century [1-4].

In most cases the stereoselective formation of the aforementioned compounds has been extensively studied using chiral liquid-liquid phase-transfer catalysts on the basis of cinchona alkaloids [5,6]. However, these catalysts often cause problems related to their recovery and recycle. In the last years, the above mentioned catalysts are replaced by hybridized organo-inorganic ones which are insoluble in aqueous or organic solvents and thus easily removable from the reaction mixtures. Soai [7] and Lasperas [8,9] were of the first who described the use of such functionalized chiral organo-inorganic catalysts for enantioselective reduction reactions with very promising results. Encouraged by these results, we decided to prepare similar silica-functionalized chiral quaternary ammonium salts and test them on the asymmetric epoxidation of enones and asymmetric alkylations of glycine derivatives.

In this study, we present for the first time the synthesis of two novel chiral functionalized organo-inorganic catalysts **1** and **2** using the chiral auxiliaries (S)-(+)-cinchonine and (S)-(-)-nicotine, respectively, and their application in the asymmetric epoxidation reactions of chalcone **3** and asymmetric benzylation of ethyl N-(diphenylmethylene)-glycinate **5** (O'Donnell's-reagent).

Results and Discussion

The novel chiral hybridized organo-inorganic catalysts **1** and **2** have been synthesized in two steps. In the first step, 3-chloropropyl-triethoxysilane was bonded on activated silica gel (pore diameter 6.0 nm) by simple reflux in toluene. In the second step the isolated hybridized silica containing the chloropropylsilane-spacer was refluxed in toluene with the chiral auxiliaries, (S)-(+)-cinchonine or (S)-(-)-nicotine, filtered, washed and dried. Elemental analysis measurements showed that up to 1.5 mmol organic material was bound per gram silica. The existence of organic material on silica verified, also by infrared spectroscopy.
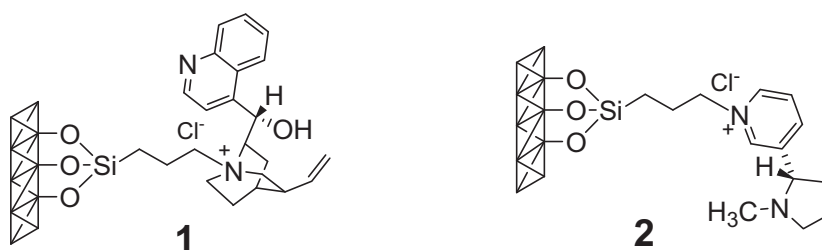
Scheme 1. Novel organo-inorganic chiral catalysts produced from activated silica gel and chiral auxiliaries, such as (S)-(+)-cinchonine **1** or (S)-(-)-nicotine **2**.

The novel hybridized organo-inorganic catalysts were tested on the asymmetric epoxidation of trans-chalcone **3** (Scheme 1) and on the asymmetric benzylation of ethyl N-(diphenylmethylene)-glycinate **5** (Scheme 2). These reagents have been chosen due to their often use in liquid-liquid phase-transfer reactions as well as for comparison reasons due to the known stereochemistry of their products.

In epoxidation reactions of chalcone, both catalysts lead to moderate chemical yields (50-60%), very high diastereoselectivities (de>96 %) but very low enantioselectivities (ee < 2 %). The extent of the diastereoselectivities (de) was determined by ^{13}C NMR spectroscopy, while the enantiomeric excess (ee) and absolute configuration after comparison of the measured optical rotation value of product **4** with that of authentic one given in the literature. The epoxide **4** showed the (-)-sign in optical rotation measurements which corresponds to the (2R, 3S)-configuration [10].
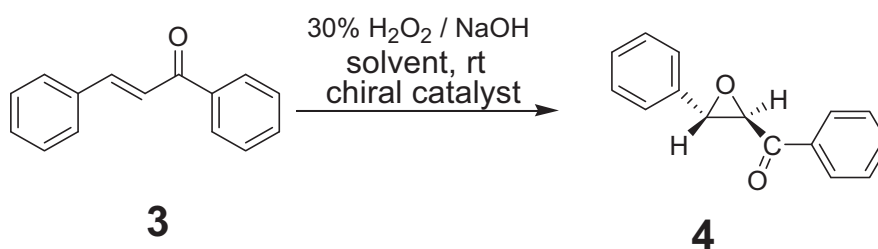
Scheme 1. Catalytic asymmetric synthesis of (2R, 3S)-2.3-epoxy-3-phenyl-propiophenone **4** using hybridized catalysts **1** and **2.**

PS-11

In benzylation reactions of ethyl N-(diphenylmethylene)-glycinate **5** (O'Donnell's-reagent) (Scheme 2), the cinchonine derived hybridized catalyst **1** leads to good overall chemical yields (35–48%) and moderate enantiomeric excess (15-55 %), while by using the nicotine catalyst **2** no reaction observed, even after 100 hours reaction time. The extent of the enantiomeric excess (ee) and the absolute configuration (R) were determined by comparison the measured optical rotation values of product **8** with authentic one [11]. The (-)-sign of product **8** in the literature corresponds to the (R)-configuration. All data of these reactions are shown in Table 2.
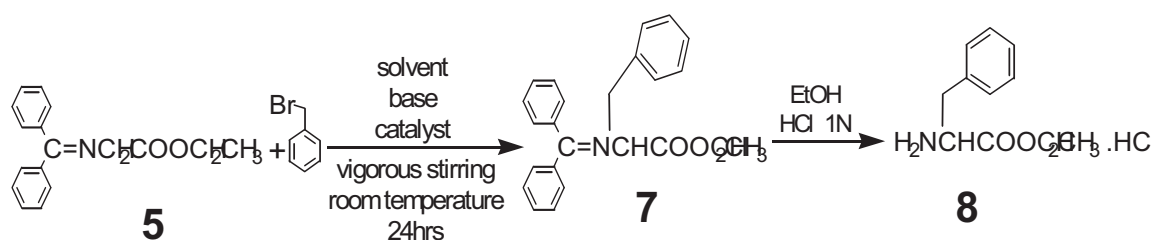
Scheme 2. Synthesis of (R)-α-amino phenylalanin by catalytic asymmetric benzylation of glycine iminoester derivative **5**.

The chemical as well as the stereochemical results depend strongly on the solvents and bases used. As shown in Table 2, the best results obtained in dichloromethane or mixture of it and toluene, while in protic solvents such as methanol the dialkylated product was obtained in good chemical yield. Best stereochemical results obtained by using caesium hydroxide as a base (ee up to 55 %).

Table 2. Chemical and stereochemical yields of amino acid ethyl ester salt **8** obtained by using the novel functionalised chiral silica catalysts.

Catalyst (10 mol%)	Solvent	Base	Chem. Yield [1] 8	Optical rotation [2] $[a]_D^{25}$	Enantiomeric Excess [3] (ee, %)	Absolute Configuration [3]
1	CH_2Cl_2	KOH/K_2CO_3	36%	- 8.7	25.80	R
1	CH_2Cl_2	$CsOH.H_2O$	40%	- 18.6	55.25	R
2	CH_2Cl_2	$CsOH.H_2O$	No reaction	-----	----	-----
2	toluene	aq. NaOH (10 %)	No reaction	-----	----	-----
1	MeOH	$CsOH.H_2O$	85% [5]	------	----	-----
1	CH_2Cl_2	NaH	48%	- 4.8	14.24	R
1	Toluene/CH_2Cl_2 7:3	aq. NaOH (10 %)	42%	- 12.1	35.94	R

[1]Overall yields; [2]measured in ethanol ($[a]_D^{25}$= + 33.7, c=2); [3]determined by comparison of measured optical rotation values of product **8** with that given in the literature [11]; [5]dialkylated product.

Conclusions

Although the first stereochemical results of the novel hybridized chiral organo-inorganic catalysts tested on the asymmetric epoxidation of chalcone and on the benzylation of ethyl N-(diphenylmethylene)-glycinate are not very impressive, nevertheless, the high chemical yields of these reactions and the advantage of the easy removal of the catalyst from the reaction mixture by simple filtration make such catalysts very attractive. The novel functionalized organo-inorganic catalysts can play an important role in the new greener industry by replacing hazardous and environmentally threatening chemicals. Further studies of these novel phase-transfer catalysts are now under investigation.

References

[1] R. O. Duthaler, *Tetrahedron,* **1994**, 50, 1539.

[2] A. Studer, *Synthesis,* **1996**, 793.

[3] D. Seebach, A.R. Sting, M. Hoffman, *Angew. Chem., Int. Ed. Engl.* **1996**, 35, 2708.

[4] M. J. O' Donnell, I.A. Esikova, A. Mi, D.F. Shullenberger, S. Wu, in *Phase-Transfer Catalysis; M.E. Halpern,* (Ed), ACS Symposium Series 659, American Chemical Society: Washington, DC, 1997, Chap. 10, pp. 124-135.

[5] B. Lygo, D. To, *Tetrahedron Lett.,* **2001**, 42, 1343-1346.

[6] E. J. Corey, F. Zhang, *Org. Lett.,* **1999**, 1, 1287-1290.

[7] K. Soai, M. Watanabe, A. Yamamoto, *J. Org. Chem.* **1990**, 55, 4832-4835.

[8] N. Bellocq, S. Abramson, M. Lasperas, D. Brunel, P. Moreau, *Tetrahedron: Asymmetry* **1999,** 10, 3229-3241.

[9] M. Lasperas, N. Bellocq, D. Brunel, P. Moreau, *Tetrahedron: Asymmetry,* **1998**, 9, 3053-3064

[10] B. Lygo, P.G. Wainwright, *Tetrahedron,* **1999,** 55, 6289-6300

[11] http://www.chemexper.com/chemicals/supplier/cas/3182-93-2.html

SYNTHESIS OF SATURATED FATTY ACIDS FROM NATURAL OIL RESOURCES OVER Pd/C CATALYST IN FIXED-BED FLOW CHEMICAL REACTOR

Simakova I.L., Deliy I.V., Romanenko A.V., Voropaev I.N.

Boreskov Institute of Catalysis SB RAS, Pr. Ak. Lavrentieva, 5, Novosibirsk 630090, Russia.
E-mail: simakova@catalysis.ru

Hardening of liquid vegetable oils and free fatty acids is one of the key operations in the fats and oils industry. The main objective is the partial or total saturation of the C=C double bonds of polyunsaturated oils:

$$CH_2\text{-O-CO-}(CH_2)_6\text{-CH=CH-}(CH_2)_8\text{-}CH_3$$
$$CH_2\text{-O-CO-}(CH_2)_6\text{-}(CH=CH)_2\text{-}(CH_2)_6\text{-}CH_3 \xrightarrow{H_2,\ Pd/C}$$
$$CH_2\text{-O-CO-}(CH_2)_6\text{-}(CH=CH)_3\text{-}(CH_2)_4\text{-}CH_3$$

$$CH_2\text{-O-CO-}(CH_2)_{16}\text{-}CH_3$$
$$CH_2\text{-O-CO-}(CH_2)_6\text{-CH=CH-}(CH_2)_8\text{-}CH_3$$
$$CH_2\text{-O-CO-}(CH_2)_6\text{-CH=CH-}(CH_2)_8\text{-}CH_3$$
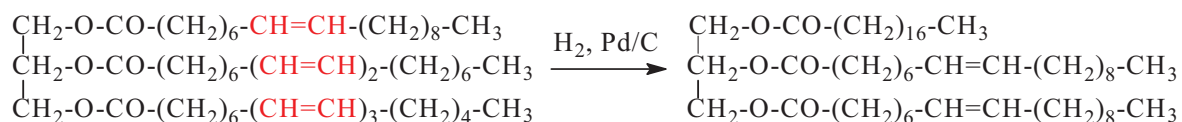
The physical-chemical properties of the final product depend on the unsaturations of the oil hydrogenated, type of catalyst and oil feedstock, residence time, hydrogen/substrate ratio, temperature and pressure. Hydrogenated oils of soft consistency are required for the manufacture of edible products: margarines, shortenings, light butters and fats. In recent years a monounsaturated and saturated fatty acids for tire and candle production, cosmetic and pharmaceutical industries are of great interest [1, 2]. At present, the process is carried out at high temperatures (180 – 250°C) over toxic nickel or nickel-copper catalysts and has serious disadvantages: low catalyst activity, contamination of products by carcinogenic Ni and inevitability of catalyst waste utilization. Earlier a batch method to produce edible hydrogenated oils in the presence of Pd/C catalyst was developed [3, 4]. Vegetable oils were hydrogenated periodically in autoclave in the presence of powdered Pd/C, after that hardening products were separated from the catalyst under filter presses. To solve this problem the method of continuous non-filtration hydrogenation over fix-bed palladium catalyst was suggested. Coming to practical industrial operational requirements we have made an attempt to work out an effective universal catalyst for hydrogenation of vegetable oil feedstock both in triglyceride form and in free fatty acid (FFA) form. However FFA are of less reactivity than triglycerides [5] and FFA saturation requires higher temperature and elevated hydrogen pressure to give carbon monoxide that can affect palladium sites activity [6].

The aim of this work is to develop a synthesis of saturated fatty acids based on industrial vegetable oil feedstock in form free fatty acids and triglycerides in fix-bed flow chemical reactor over Pd/C catalyst.

Industrial rapeseed oil and FFA were not distilled before catalytic runs. Samples of Pd/C catalyst with palladium content from 0.5 to 1.0% (wt) were prepared by an incipient wetness impregnation method which includes spraying the solutions H_2PdCl_4 and Na_2CO_3 onto the carbon granules (spheres by diameter of 2÷3 and 4÷6 mm) agitated in a rotating cylinder. The activated carbon "Sibunit" has been chosen as a carbonaceous support because of its high surface area and chemical inertness in acidic and basic media [7]. Preferable carbon granule's size was determined to be less than 4 mm according to previous simulator studying of carbon support grain size effect on hydrodynamic properties of triglyceride's feed.

Fig. 1. *General view of experimental set-up with fix-bed flow catalytic reactor for vegetable oil feed stock hydrogenation.*

To perform catalytic runs a catalytic set-up was working out and constructed (Fig. 1). The experiments were performed using stainless-steel up-flow reactor at temperature range from 146 to $180^{\circ}C$ and hydrogen pressure up to 8 bars. Reagents passed through a pre-heat reservoir and then flowed over the fixed catalyst bed. Hydrogen was metered into the system using a mass flow controller. Condensable products were collected in a water-cooled collector and analyzed by GLC method. To estimate C=C double bond saturation degree the melting point of fatty acid hydrogenated products (MPFA) was determined. This characteristic reflects the completeness of fatty acid hydrogenation (full C=C double bond saturation of FFA and rapeseed oil correspond to 61° and 65° of MPFA respectively).

It was found that the higher reaction temperature the more MPFA of hydrogenated product. Operation temperature was tuned to maintain a value of MPFA upper than 58° in

hydrogenation run. It was shown that the behavior of FFA and their triglycerides in hydrogenation reaction essentially depends on palladium metal content. A comparison of catalytic activity of 0.5 and 1.0% (wt) Pd/C shows that the latter is most effective and stable in FFA saturation under mild reaction conditions (Fig. 2). Fatty acids triglycerides are more chemical stable and can be hydrogenated at high temperature over the catalyst with 0.5% (wt) palladium content (Fig. 3). According to X-ray fluorescence spectroscopic data the content of palladium in fresh and spent catalyst samples practically didn't differ. It indicates no notable palladium leaching occurs during hydrogenation.
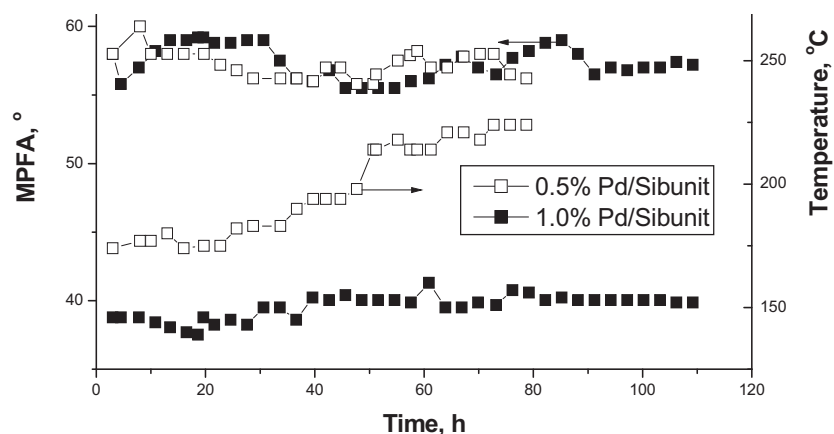
Fig. 2. FFA hydrogenation over Pd/C catalysts, fr. 2÷3 mm.
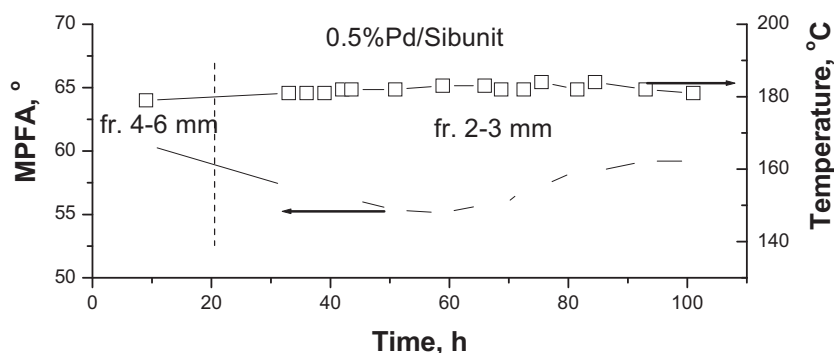
Fig. 3. Rapeseed oil hydrogenation over Pd/C catalysts, fr. 2÷3 and 4÷6 mm.

The samples of fresh and spent catalysts were analyzed by HREM and XRD methods to study palladium catalyst sintering during catalytic runs. The results obtained indicate that Pd dispersion was not changed: average palladium particle size of fresh samples, after long-term hydrogenation of triglycerides and FFA are 4.4, 4.3 and 4.8 nm respectively (Fig. 4).
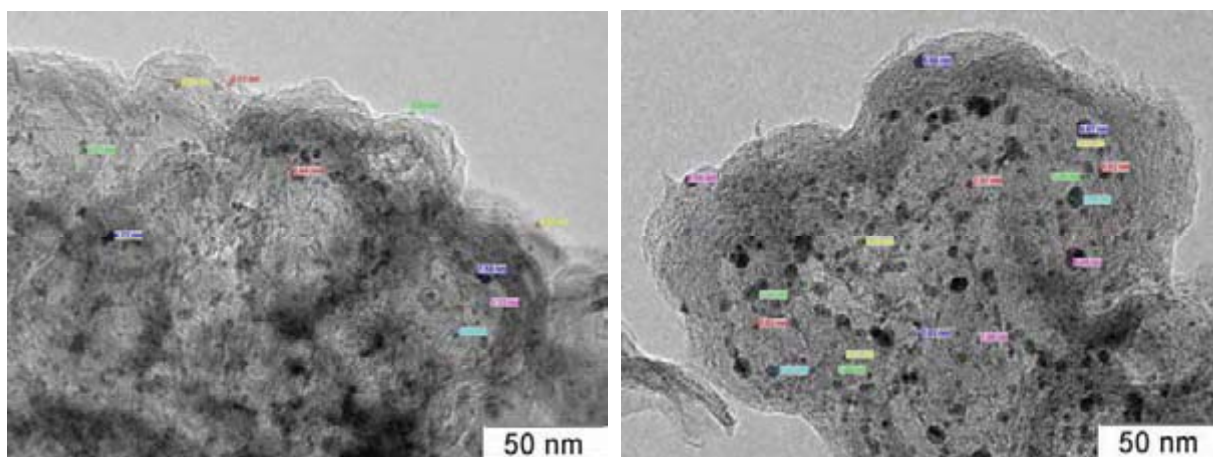
Fig. 4. *HREM images of the fresh (left) and spent (right) 0.5% (wt) Pd/C samples in FFA hydrogenation reaction.*

Notable amount of carbon monoxide was detected by GC analysis during FFA hydrogenation at temperature above 160°C. It indicates that decarbonylation reaction accompanies FFA hydrogenation to cause 0.5% (wt) Pd/C catalyst deactivation (Fig. 2). It is important to note that FFA saturation over 1.0% (wt) Pd/C shows quite stable value of MPFA during about 100 hours of catalyst performance at temperature below 160°C (Fig. 2). Obviously the effect of decarbonylation reaction is rather insignificant over 1.0% (wt) Pd/C at these reaction conditions. This can be explained by different carbon monoxide interaction with palladium particles depending on metal particle size and temperature. According to authors [8] carbon monoxide adsorbed on sufficiently small palladium particles disproportionates to surface carbon and carbon dioxide but this does not occur on large particles. Thus we can suggest plausibly that palladium particles of 1.0% (wt) Pd/C are large enough to be more resistant to carbon monoxide poisoning effect.

To conclude the method for synthesis of saturated fatty acids by hydrogenation of vegetable oil feedstock in form both free fatty acids and triglycerides in a fix-bed flow chemical reactor over the same 1.0% (wt) Pd/C catalyst was developed.

1. H.J. Dutton. *Chem. Ind.* 2 (1982) 9-17
2. H. Wagner, R. Luther, T. Mang. *Appl. Catal. A: General*. 221 (2001) 429-442
3. Russian Pat. No. 2105050, 1996
4. V.A. Semikolenov, I.L. Simakova and G.V. Sadovnichii. *Chimicheskaia promyshlennost`(“Russian chemical industry”)*. 3 (1996) 184.
5. F. Joo, L. Vigh, A.R. Cosins, J.A. Logue. *Biochimica et Biophysica Acta (BBA)/Biomembranes.* 1368 (1998) 41-51
6. J.B. Giorgi, T. Schroeder, M. Baumer, H.-J. Freund. *Surface Science*. 498 (2002) 171-177
7. A.F. Pérez-Cadenas, M.P. Zieverink, F. Kapteijn, J.A. Moulijn. *Carbon*. 44 (2006) 173-176
8. S. Ichikawa, H. Poppa, M. Boudart. *Catalytic Materials: Relationship between Structure and Reactivity, ACS Symp. Ser. Vol.248, eds. E.T.Whyte, R.A. Dalla Betta, E.G. Derouane, R.T.K. Baker (ACS, Washington, DC, 1984) 439-451*

PREPARATION AND INVESTIGATION OF NANOSTRUCTURAL CARBONACEOUS COMPOSITES FROM THE HIGH-ASH BIOMASS

Yakovlev V.A., Yelestky P.M., Lebedev M.Yu., Ermakov D.Yu., Parmon V.N.

Boreskov Institute of Catalysis, av. Akad. Lavrenteva, 5, 630090, Novosibirsk, Russia

Biomass is one of the most promising renewable energy resources for future as well as a convenient precursor of various valuable materials. Important sources of biomass are wood and vegetative residues (wheat and corn straw, chaff, rice and oat husk, etc.).

The most typical solid products of the biomass processing to valuable materials are active carbons which are used as efficient adsorbents to remove organic and inorganic impurities from liquid and gaseous media, etc.

At the processing of the high-ash biomass it is possible to produce also carbon-mineral composites with various textured characteristics. We have chosen rice husk as model feedstock for the production of several carbonaceous materials: carbon-silica composites, active carbons and nanostructural supermicroporous carbons with the maximum specific surface area. The Figure 1 demonstrates the developed pathways of the rice husk processing to target products as well as some characteristics of these materials.
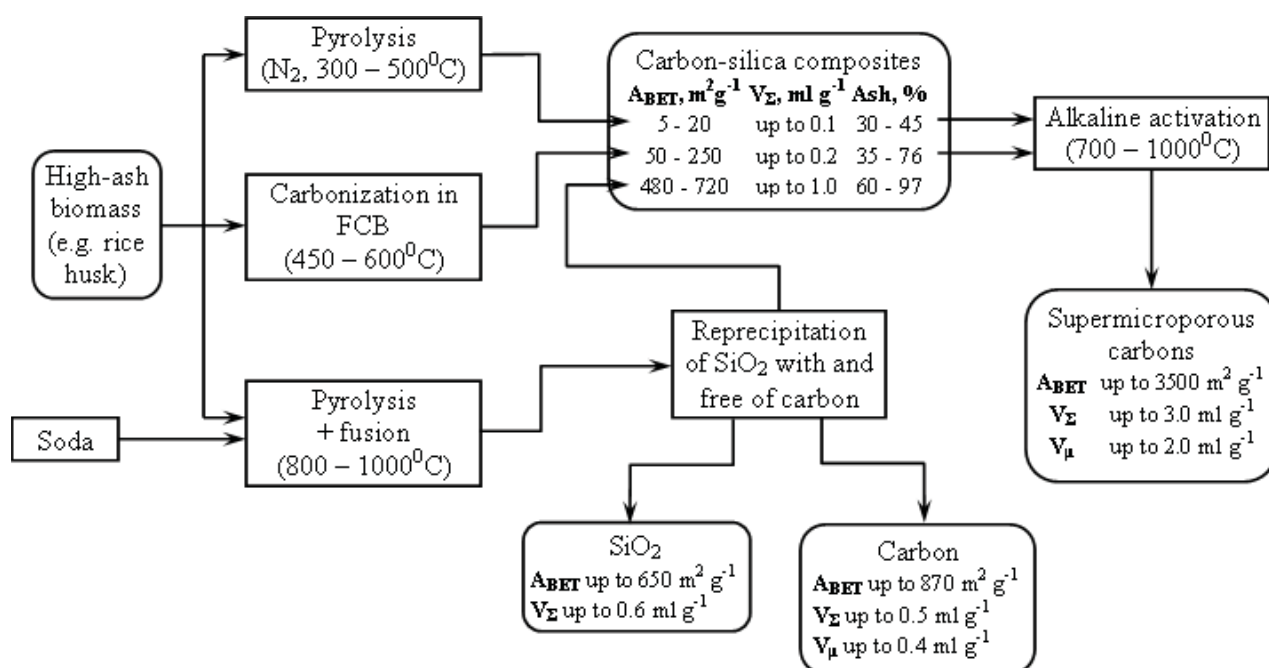
Figure 1. The developed pathways of the rice husk processing and the products obtained.

Microporous carbonaceous materials with the large specific surface area, A, are of particular importance among active carbons. Such materials, due to their large micropore volume, V_μ, are considered now as potential adsorbents for such poorly adsorbable gases as, for example, hydrogen, carbon monoxide and methane. The best among the currently produced microporous carbons are the

so called Maxsorb materials (Kansai Coke and Chemical Co Ltd., Japan), also known as AX-21 (Anderson Develop Co., USA). These carbons have $A_{BET} = 2670\pm600$ m^2/g, $V_\mu \sim 1.20$ cm^3/g [1,2].

The Boreskov Institute of Catalysis proposes a new method for the synthesis of supermicroporous carbons (SMPC's) with even higher adsorbability via treatment of agricultural high-ash lignocellulose wastes (like rice and oats husk, as well as wheat straw). In the new SMPC's, the specific surface area A_{BET} reaches 3460 m^2/g while micropore volume V_μ is up to 1.9 cm^3/g at the total of pore volume (not larger than 100 nm), V_Σ, as large as 3.0 cm^3/g.

The preliminary carbonization of mentioned wastes in inert atmosphere at 300–500 °C (pyrolysis) or in a fluidized catalyst bed (FCB) at 450–600 °C allows carbon-mineral composites to be synthesized with the different textural parameters [3]. In these composites, the ash residue contains mainly as nanospheres of amorphous silica which may behave as a mineral structure-forming agent – template – during the further treatment to synthesize microporous carbons, the carbon nanostructure with 1 to 1.5 nm graphenes being arranged around the template.

The obtained carbon-mineral composites are activated in melted KOH and/or NaOH at 700–900 °C to produce potassium silicates through the interaction between amorphous silica and KOH. After this activation, the materials are cooled and the silicate templates are removed by dissolving in water.

The similar interaction of silica template and carbon phase (template carbonization) can be observed at the fusion of rice husk and soda at 900°C. After that the obtained silicates are dissolved and silica is precipitated by CO_2. The TEM studies of these samples revealed that the carbonaceous phase consists of leaf-like, coral-like and hollow spheres of carbon, while silica is presented as microspheres with the average size up to 5 nm (Figure 2, 3).

One of the principal parameters affecting the textural characteristics of thus obtained SMPC's is the activation temperature [4]. Table 1 summarizes the data on the properties of SMPC's synthesized at different temperatures. A_{BET}, V_{pore} and V_μ are determined from the nitrogen adsorption isotherms at 77 K.

Table 1: Characteristics of carbonaceous nanostructural SMPC's materials synthesized at different temperatures

Activation temperature, ^{o}C	A_{BET}, m^2/g	V_{pore} /V_μ, cm^3/g	Micropore proportion %
700	3170	1.77/1.45	81.9
750	3450	2.01/1.68	83.6
800	3360	2.18/1.87	92.3
850	3170	2.26/1.74	77.0
900	3210	2.97/1.48	49.8

The total pore volume increases with the activation temperature. At the temperatures below 800°C, the increase is due to the micropore formation. At the further temperature elevation, the micropore volume decreases but the mesopore volume increases due to burning processes.

PS-13

In the synthesized microporous carbons, not only the specific surface areas and micropore volumes are superior to those of AX-21. The characteristic features of SMPC's are the much narrower pore size distribution as well as a higher contribution of micropores to the total pore volume (see Fig. 4). The differential surface area *vs* pore size is determined by the Ustinov method [5]; the authors [5] assert that this is the most appropriate method for large surface area carbons.
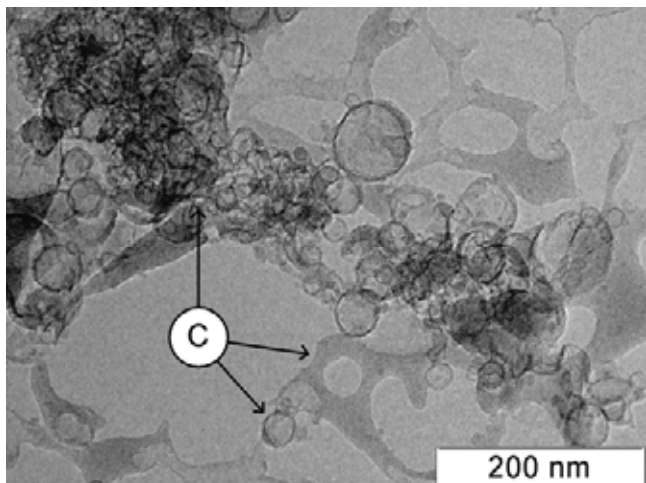
Figure 2: The TEM image of the carbonaceous phase after the rice husk fusion with Na_2CO_3 at $900^{\circ}C$.
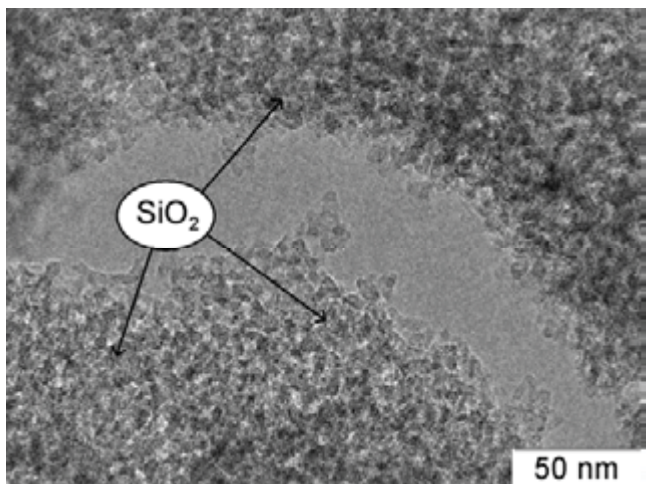
Figure 3: The TEM image of the silica phase after rice husk fusion and Na_2CO_3 at $900^{\circ}C$ following by the reprecipitation of SiO_2.
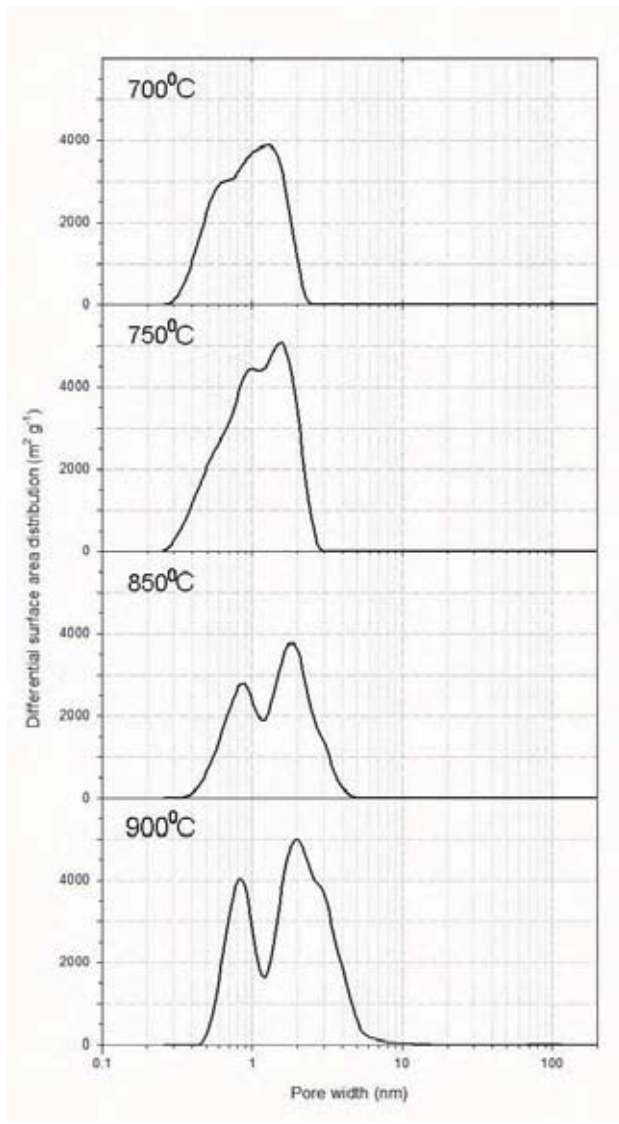
Figure 4: The differential surface area *vs* pore size of SMPC's prepared at different activation temperatures (calculated according to ref. [5]).

Now, we focus our studies on the preparation conditions of the new developed kind of microporous carbons to adopt it for particular applications such as membranes and sorbents for the gas separation as well as accumulators of power gases (hydrogen, methane etc.)

Indeed, the search for alternative energy sources for motor vehicles is an urgent problem of our days. A most thriving area is the substitution of hydrogen and natural gas for the traditional hydrocarbon fuels for motor vehicles. Therefore, much attention is paid to the development of safe and efficient on-board storage facilities. The adsorptive storage of hydrogen and methane seems to

be one of such methods with a good safety. Few systems based on the SMPC nanomaterials with high sorbability are developed at the Boreskov Institute of Catalysis for the accumulation and storage of hydrogen and methane.

Indeed, experimental studies on the adsorption of hydrogen and methane demonstrated a considerable sorption capacity of the SMPC materials. These carbons were shown to absorb up to 65 wt % of methane at room temperature and 60 atm and more than 6 wt % of hydrogen under mild cryogenic conditions (at 77 K).
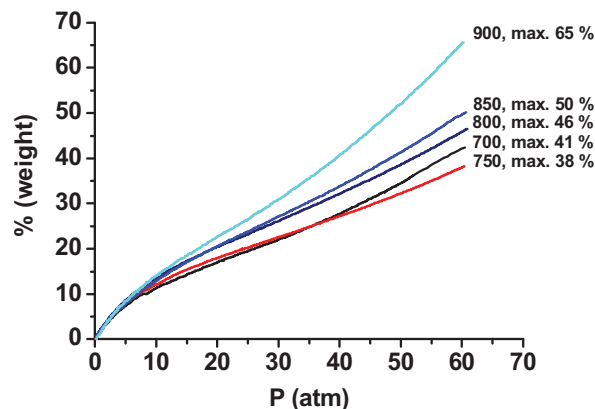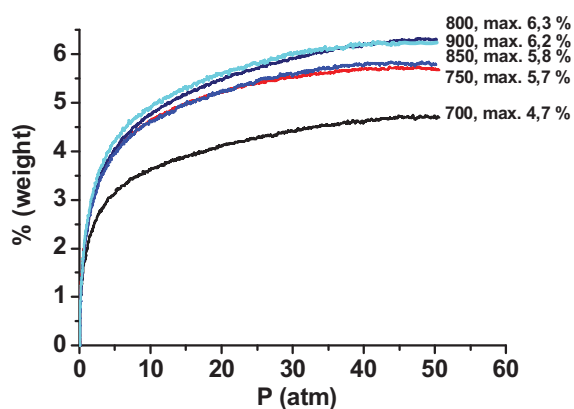
Figure 5: Isotherms of the hydrogen adsorption at 77 K for SMPC's synthesized at 700–900 °C.

Figure 6: Isotherms of the methane adsorption at 293 K for SMPC's synthesized at 700 – 900 °C.

The above data demonstrate the possibility of the synthesis of highly microporous carbons with the very large specific surface area from the high-ash biomass. The samples obtained are superior in their textural characteristics to the known best analogues synthesized by treating petroleum pitch with nitric acid. The expected practical application of the obtained carbon-silica composites may be first of all reinforcing rubber extenders and bifunctional sorbents for the gas and liquid purification.

References

1. March H., Van Davis S., O'Grandy T. M., Wennerberg A., Carbon, 22 (1984) 603

2. USA Patent 3,624,004 (1971) and 4,088,694 (1978)

3. Yakovlev V.A., Simonov A.D., Startsev A.N., Yeletsky P.M., Parmon V.N., Catalytic processing of biomass to heat, carbon materials and high-quality fuels, Proc. of 14th European Biomass Conference & Exhibition, October 17-21, Paris, France, (2005), 105-109.

4. Yakovlev V.A., Yelestky P.M., Parmon V.N., Nanostructural microporous carbonaceous material; RU patent application № 2006105038, priority 09.02.2006.

5. E.A. Ustinov, D.D. Do, V.B. Fenelonov, Carbon 44 (2006) 653.

THE DEVELOPMENT OF THE METHOD OF LOW–TEMPERATURE PEAT PYROLYSIS ON THE BASIS OF ALUMOSILICATE CATALYTIC SYSTEM

E. Sulman, V. Alfyorov, O. Misnikov, A. Afanasjev, N. Kumar[1], D. Murzin[1]

Tver State Technical University; A. Nikitin Str., 22, 170026, Tver, Russia,
phone/fax: +7 0822 449317, e-mail: sulman@online.tver.ru
[1]*Abo Akademi University; Biskopsgatan 8, 20500, Turku, Finland,*
phone: + 358 2 215 4985, fax: 358 2 215 4479, e-mail: dmurzin@abo.fi

Nowadays in many developed countries the programs on power systems transfer on new more available biogen fuel that can help to solve some ecological and technological problems have been developed. Peat – mineral compositions can become such fuel.

Physical – chemical study of composite granulated fuel on the basis of peat has been carried out. The granulation of organic mineral mixture by the method of palletizing allows to proportion exactly the initial components and to obtain solid bio-fuel with good technological characteristics (heat of combustion, humidity, strength, loosens and others).

The aim of the investigations is to study peat low – temperature pyrolysis in the presence of catalytic systems on the basis of natural alumosilicate materials and synthetic zeolites. In the present paper the following problems have been solved: to study the influence of temperature, nature and the catalyst amount on composition and calorific value of combustible gas mixture obtained and to choose optimal conditions of this process.

The study of peat low-temperature pyrolysis has been carried out in the presence of the catalysts – natural and synthetic materials with concentration 1, 2, 3, 4, 5 and 10 mass % at a temperature range of 350-480°C.

The best results have been observed at 2% alumosilicate minerals content of peat mass at a temperature of 480°C. Under such conditions of the experiment hydrocarbon yield as well as the heat of combustion of the pyrolysis gas obtained has been much higher than those of non-catalytic process. The value of activation energy for the catalytic process of peat pyrolysis has been approximately 2 times less than for the non-catalytic one.

As the result of the experiments carried out the application of natural and synthetic zeolite catalysts in peat catalytic pyrolysis was revealed to increase gaseous hydrocarbons yield by 2,1 – 2,5 times in case of natural catalysts and approximately by 4 times incase of synthetic ones. The heat of combustion has increased by 1,5 – 4 times on different catalysts.

NOVEL CHIRAL LIGANDS FOR CATALYSTS OF ASYMMETRIC REACTIONS DERIVED FROM NATURAL TERPENES

T.B. Khlebnikova, Yu.V. Sapegina, V.N. Konev, Z.P. Pai, A.G. Tolstikov

Boreskov Institute of Catalysis SB RAS, Akad. Lavrentiev Pr. 5, Novosibirsk, 630090, Russia, fax:(383) 330 80 56, E-mail: khleb@catalysis.nsk.su

Efficient use of renewable hydrocarbon raw materials is of topic importance at present time. Availability of numerous constituents of complex structure in vegetal feedstock opens the possibility to obtain compounds, synthesis of which starting from oil and gas processing products is impossible or economically unfeasible. Thus, the products of the integrated wood processing are the convenient starting material for the directional functionalization aimed at production of a whole series of substances with predetermined physicochemical properties and bioactivity.

Phytogenic diterpenes have been under intensive investigation for many years. Owing to their availability and unique structures, these compounds have been widely used as starting materials for the production of highly effective drugs and chiral reagents. The use of natural terpenoids as convenient chiral pools for the synthesis of optically active elementorganic compounds is the prospective approach to the creation of wide spectrum of available chiral ligands for the catalysts of asymmetric reactions.

Asymmetric catalysis is an attractive strategy of the synthesis of optically pure organic compounds and the dominant role in enantioselectivity of catalyst plays the structure of chiral ligand. Thus, design of the ligands of various structural types allows extending the field of application of asymmetric catalysis over the wide range of substrate and reactions. When preparing the ligands most attention was concentrated on the transformations of hydroxy- and amino acids, carbohydrates as well as binaphtyl, biphenyl, ferrocene derivatives. The synthesis of ligands based on steroids and terpenoids received lesser acceptance [1].

As a result of our investigations the synthetic procedure of preparing metallocomplex catalysts with the P-, N-containing ligands derived from terpenoids was developed [2]. Starting from tricyclic diterpenes, levopimaric and dehydroabietic acid, which are constituents of the composition of the galipot and colophony of the conifers of the *Pinus* genus, a number of chiral diphosphine, diphosphinite, amine, azomethine and urea ligands was prepared and used in complexes with Rh(I), Ru(II) and V(IV) as catalysts of asymmetric reactions.

PS-15

Levopimaric acid

Cat

conversion 80-100%
ee 10-40%
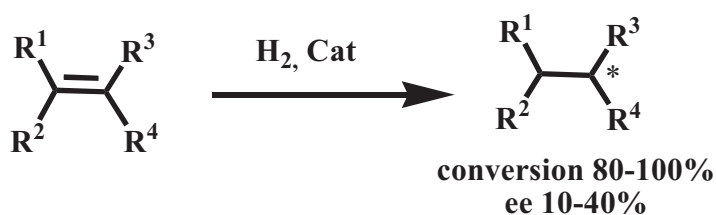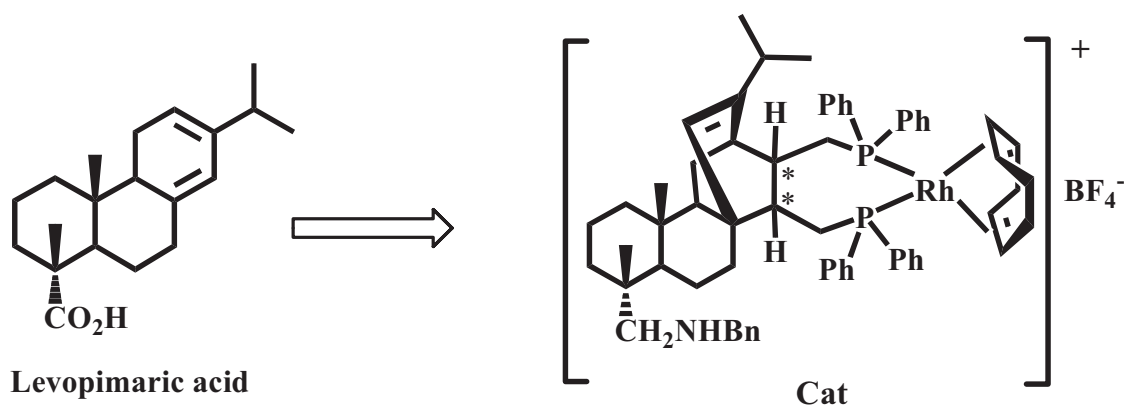
Scheme 1.

The additional functional group in diphosphine ligands presented on the Scheme 1 makes possible the immobilization of the complex catalysts by the covalent tethering onto the support surface (for example, mesoporous silica), which can be used as a coating of the interior surface of microreactors for the catalytic asymmetric reactions.

Dehydroabietic acid

X= O, S

[RhL(COD)Cl]₂ or [RuL(COD)Cl₂]₂

^{i}PrOH

conversion 10-90%
ee 10-60%
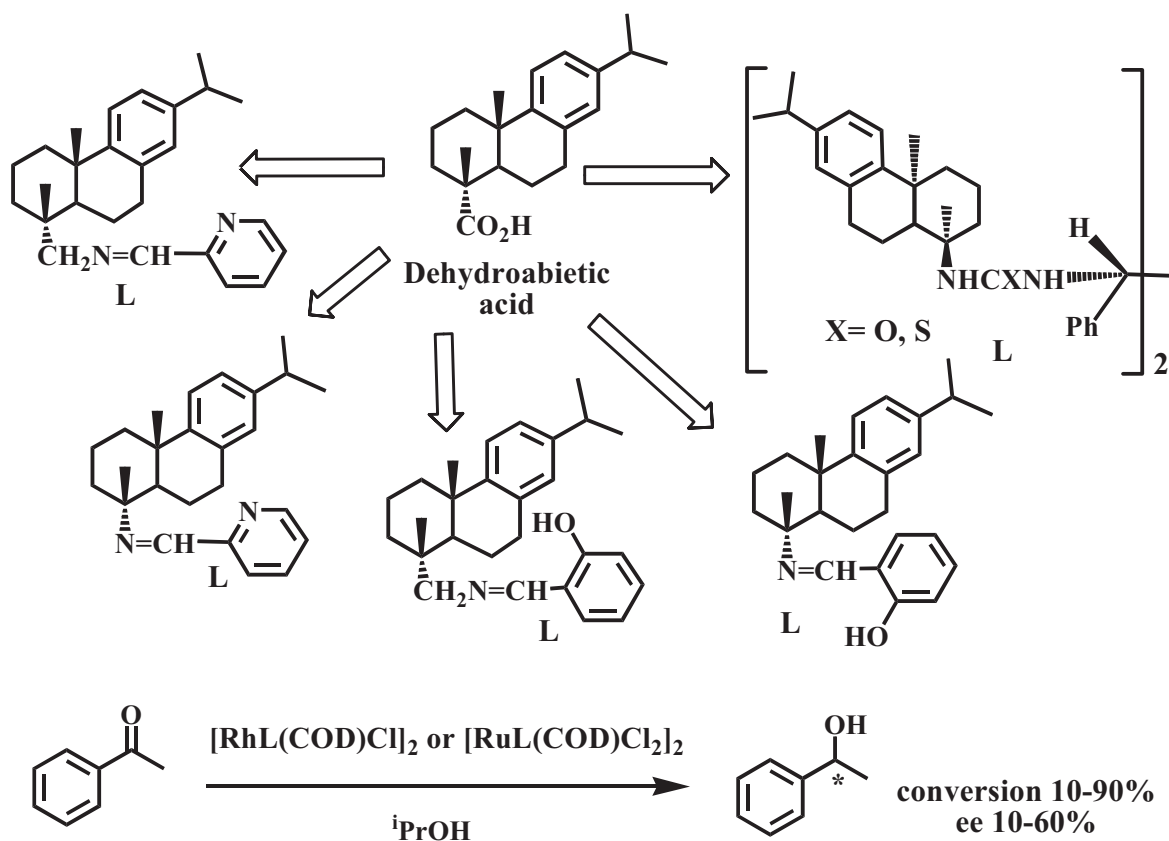
Scheme 2.

High molecular weight of the catalysts depicted on schemas 1 and 2 permits to carry out the asymmetric reduction reactions in membrane reactors with the use of catalyst during several cycles.

References

1. A.G. Tolstikov, T.B. Khlebnikova, O.V. Tolstikova, G.A.Tolstikov. Natural compounds in the synthesis of chiral organophosphorous ligands. // Russian Chemical Reviews.- 2003.- V. 72.- P. 803-822.

2. T.B. Khlebnikova, N.N. Karpyshev, O.V. Tolstikova, A.G. Tolstikov. Synthesis of New Chiral Phosphorous- and Nitrogen-containing Ligands from Resin Acids. // Chirality. Proceedings from the fifteenth International Symposium on Chirality (ISCD-15), Shizuoka, Japan, 2003.- 2004.- V. 16.- P. S40-S50.

PS-16

XANTHAN GUM PRODUCTION USING FED-BATCH CONTINUOUS RECYCLED PACKED BED BIOREACTOR

Awang Bono[1], Ng Lee Fong[1], Rosalam Hj. Sarbatly[2], Duduku Krishnaiah[1]

[1]*Chemical Engineering Programme, School of Engineering and Information Technology,*
University Malaysia Sabah, 88999 Kota Kinabalu, Sabah, Malaysia
[2]*Department of Chemical Engineering, Bath University, Bath, United Kingdom*
FAX: +60-88-320348, E-mail: krishna@ums.edu.my

Abstract

Xanthan gum is widely used as a thickening agent in food, pharmaceutical industries and chemicals (Becker et al.1998). It is a high molecular weight polysaccharides gum produced by a pure culture fermentation of carbohydrate with natural strains of exopolysaccharide derived from *Xanthomonas campestris* NRRL B-1459 (Leela and Sharma, 2000; Flores and Deckwer, 1999). The xanthan gum polymer consists of repeated units of five sugars, namely, two D-glucose, two D-mannose and one D-glucoronate and varying amounts of acetate and pyruvate (Flores and Deckwer, 1999). Xanthan also contains monovalent cations, which can be Na, K or ½ Ca (Flores and Deckwer, 1999; Nancy et al 1995). This polysaccharide produces *Xanthomonas campestris* high viscosity aqueous solutions which are also highly pseudoplastic.

Most studies on microbial exopolysaccharide production have been performed so far using batch incubation conditions (Lo et al. 1997; Lo et al 2001, Pollock et al 1997), the polymer macromolecules being recovered from fermentation broths by simple chemical and physical techniques, e.g. precipitation and centrifugation (Leela and Sharma, 2000). Some attempts have been made to apply immobilized-cell cultures for the production of xanthan gum (Yang et al. 1996 and Yang et al. 1998) and other bacterial polysaccharides (Saude et al. 2002; Stavros et al. 2003). Immobilization ensures the physical separation between microorganisms and the liquid phase containing nutrients and products, and facilitates continuous processes. In addition, high cell densities can be reached inside immobilized-cell particles, which may enhance productivities as compared with free-cell cultures. In the last few years, however, membrane processes have been increasingly used to separate microbial cells from the production medium.

Continuous experiments in membrane cell recycle bioreactors have been essentially devoted to the production of low-or moderate-molecular-weight molecules such as L-methionime (Yuan et al. 2002), lactic acid (Krishnan et al. 2001) and pediocin (Lebrun et al 1994;Cho et al. 1996).There are few studies of xanthan fermentation using immobilized cells. A large portion of the xanthan gum product was trapped in the bed and could not be easily separated from the cells(Yang et al. 1998). It is clear that cell entrapment is not an appropriate cell immobilization method for xanthan gum fermentation because of the high viscosity of xanthan solution.

In this work, a novel, continuous packed-bed bioreactor was developed for xanthan gum fermentation. Difficulties in agitation and aeration in the conventional stirred-tank bioreactor were overcome by continuous medium recirculation through a fibrous matrix, which contained immobilized cells. In this bioreactor, liquid media and air were passed through the porous fibrous matrix to ensure intimate contact with the immobilized cells, thus achieving high oxygen transfer and reaction rates.

Adsorption of Cell

Packing density of 0.026g/ml and 0.039g/l was used to determine the effectiveness of cell adsorption and its effect on the xanthan gum production. There are four lines denoted with different packing density and the inoculum's age. From the results, it is evident that, packing with 0.039g/ml gave better adsorption of cells where it decreases to zero at the fourth day of fermentation. From the literature, the xanthan gum production was not effected by the types of fibrous material used in the adsorption and fastest adsorption rate (Yang et al. 1998).

Effect of Inoculumn Age

A set of two different ages 24 and 48 hours immobilized inoculums was used in this study. The gum production was optimum with 36-48 hours old inoculum (Leela and Sharma, 2000.). The adsorption of cells to the fibers is more effective for 48 hours inoculumn which reduced from 1.75g/l to zero in five days. There is still 0.25g/l remaining cells on the broth for 24 hours age inoculum. This result also proves the statement that the cell still growing actively before reach 48 hour of inoculation(Leela and Sharma, 2000). The inoculum of 24 hours and 48 hours was immobilized on the cotton, yielded more production with higher packing density (0.039g/ml) on the 24 hours (20.63g/l) than 48 hours inoculum (18.75g/l). This is because of after 48 hours of incubation, the cells enter stationary phase and activity of cells growing decreases due to decaying. Production at lower packing density for 24hour and 48hour inoculum gives lower production because of low cell density on packing .

PS-16

Comparison Between Free Cell And Immobilized Cell Fermentation

For comparison batch fermentation with free cells repeated in conventional 200 ml Erlenmeyer flask(reactor) by shaking in incubator at 200 rpm, 30ºC and pH 7. Inoculum age of 24 hours and packing density of 0.039 g/ml was used. Figure 4 shows the typical time course of batch fermentation of *Xanthomonas campestris*. As fpund from the results, the xanthan gum was the product of fermentation with yield of 18.1g/ml. Exponential growth of production is observed with the free cell fermentation. Cell immobilized fermentation was conducted in packed bed and without packed bed. The concentration of cell and xanthan production in fermentation where cell is adsorbed on cotton but without packed bed. Figure 6 shows the concentration of cells and xanthan gum production where cell is adsorbed on cotton in packed bed.

Comparison with immobilized cells shows that, the immobilized cells fermentation production is higher than the conventional batch fermentation, mainly because of higher cell density in the reactor. The maximum xanthan obtained with free cells was only 18.1g/l, whereas 20.58g/l xanthan was obtained with immobilized cells. The adsorption rate from cotton that is packed into tube or bed gives results of higher rate than cotton without packing into bed. The productivity is highest (20.58g/l) in the fermentation using cotton that is packed into bed with a tube which supports the matrix .

Conclusions

Xanthan gum production by *Xanthomonas campestris* DSMZ using glucose as carbon source was studied in packed bed bioreactor.The cells were immobilized in order to improve xanthan gum quality. The results showed that the concentration of xanthan gum achieved by the immobilized cells in batch fermentation was 19.4 to 20.6g/l which is higher than the conventional batch fermentation without immobilized cells at 18.1g/l. However, the production of xanthan gum from fed-batch fermentation was comparable to batch fermentation and the highest concentration was obtained as 18.7g/l at the dilution rate equal to $1.44d^{-1}$.

References

1. Becker A, Katzan, F and Ielpi,L(1998): Xanthan Gum biosynthesis and application: a biochemical/ genetic prespective. Applied Microbial Biotechnology 50: 145-152.

2. Chia-Hua and Martin Lo, Y : (2003): Characterization of xanthan gum biosynthesis in a centrifugal flux analysis: Process Biochemistry : 38: 1617-1625.

3. Cho, H. Y., Yousef, A. E. & Yang, S. T., (1996): "Continuous production of pediocin by immobilized Pediococcus acidilactici in a packed bed bioreactor". Applied Microbiology and Biotechnology 45 : 589 – 594.

4. Cooney, C.L 1986, Continuous culture. Dlm. Perspective in Biotechnology and Applied Microbiology: 271-285, Elsevier Applied science publisher, London.

5. Flores Candia, J.L. & Deckwer, W.D., (1999): Dlm. Flickinger, M.C. & Drew, S.W.: Encyclopedia of Bioprocess Technology Fermentation, Biocatalysis and Bioseparation. Volume 5,John Willey & Sons Inc. USA

6. Harding, N.E., Clearly, J.M. & Luis, L., (1995): Genetics and Biochemistry of Xanthan Gum Production by Xanthomonas campetris. Dlm. Hui, Y.H. & Khachatourians, G. Food Technology Microorganisms: 495-514. John Wiley-VCH Inc. USA

7. Krishnan, S., Gowthaman, M.K., Misra, M.C. & Karanth, N.G., (2001): "Chitosan-treated polypropylene matrix as immobilization support for lactic acid production using *Lactobacillus plantarum* NCIM 2084", Chemical Technology and Biotechnology 76 :461-468.

8. Lebrun,L., Junter,G.A., Jouenne, T., Mignot,L (1994), Exopolysaccharide production by free and immobilized microbial cultures. Enzyme and Microbial Technology: 16 : 1048-1058.

9. Leela, J.K. & Sharma, G., (2000): "Studies on xanthan production from Xanthomonas campetris". Bioprocess Engineering *23*: 687-689.

10. Lo, Y.M., Hsu, C.H., Yang, S.T. & Min, D.B., (2001): "Oxygen transfer characteristics of a centrifugal, packed-bed reactor during viscous xanthan fermentation", Bioprocess and Biosystems Engineering 24: 187-193.

11. Lo, Y.M., Yang, S.T. and Min, D.B., (1997): "Effect of yeast extract and glucose on xanthan xanthan and cell growth in batch culture of *Xanthomonas campetris".* Application Microbial Biotechnology 47: 689-694.

12. Nancy E. Harding., Joseph M. Cleary and Luis Ielpi(1995): Genetics and Biochemistry of Xanthan gum production by Xanthomonas Comprestris: Food Technology Microorganisms, John Wiley- VCH Inc., USA

13. Pollock., T.J ., Yamazaki, M and Armentrout R.W (1997). Production of Xanthan gum by Sphingomonas bacteria carrying genes from Xanthomonas campestris: J. Industrial Microbiology and Biotechnology 19: 92-97.

14. Saude, N., Chèze-Lange, H., Beunard, D., (2002): Alginate production by *Azotobacter Vinelandii* in a membrane bioreactor. Process Biotechnology 38: 273-278.

15. Stavros Kalogiannis, Gesthimani ,I, Maria L.K, Dimitrios A.K and George, N.S: (2003): Optimization of xanthan gum production by Xanthomonas campestris grown in molasses: 39: 249-256.

16. Yang, S. T., Lo, M. Y. & Chattopadhyay, D., (1998): "Production of Cell-Free Xanthan Fermentation Broth by Cell Adsorption on Fibers". Biotechnology Progress 14: 259 – 264.

17. Yang, S. T., Lo, M. Y. & David B. Min., (1996): "Xanthan Gum Fermentation by Xanthomonas campestris Immobilized in a Novel Centrifugal Fibrous-Bed Bioreactor". Biotechnology Progress 12: 630 – 637.

18. Yuan, J.Y., Wang, S.H., Song, Z.X. & Gao, R.C., (2002): "Production of L-methionine by immobilized pellets of *Aspergillus oryzae* in packed bed reactor", Chemical Technology and Bi.

PS-17

PRODUCTION OF DIESEL FUEL FROM RENEWABLE FEEDS: KINETICS OF ETHYL STEARATE DECARBOXYLATION

<u>M. Snåre</u>, I. Kubičková, P. Mäki-Arvela, K. Eränen, H. Backman and D.Yu. Murzin

Laboratory of Industrial Chemistry, Process Chemistry Centre, Åbo Akademi University, Biskopsgatan 8 FIN-20500 Åbo/Turku, Finland, Tel.:+358 2 215 4985, Fax: +358 2 215 4479, E-mail: dmitry.murzin@abo.fi

Introduction

The extreme increase in energy consumption in the past decade and the growing environmental concerns have made renewable fuels an exceptionally attractive alternative as a fuel for the future. Several methods of producing fuels from renewable resources are nowadays well established, however, new innovative solutions are needed to satisfy the increasing energy demand and the well-being of our ecological system.

A novel method for production of diesel-like fuel from renewable resources, like vegetable oils and animal fats, is being investigated at our laboratory. It has recently been demonstrated that renewable feeds over heterogeneous catalysts in liquid-phase tend to decarboxylate [1]. The production of a deoxygenated biodiesel fuel involves removal of the carboxyl group in the fatty acid structure via carbon dioxide release, thus producing a linear hydrocarbon originating from the fatty acid alkyl group (typically C_6-C_{22}) [2]. The catalytic decarboxylation of fatty acids, fatty acid esters and triglycerides (comprising of three fatty acids and a glycerol group) is schematically illustrated below.

$$\text{Fatty acid:} \quad H-O-\overset{\overset{\displaystyle O}{\|}}{C}-R' \xrightarrow{\text{het. cat.}} CO_2 + R'\text{-H}$$

$$\text{Fatty acid ester:} \quad C_nH_{2n+1}-O-\overset{\overset{\displaystyle O}{\|}}{C}-R' \xrightarrow{\text{het. cat.}} CO_2 + C_nH_{2n} + R'\text{-H}$$

$$\text{Triglyceride:} \quad \begin{array}{l} CH_2-O-\overset{\overset{\displaystyle O}{\|}}{C}-R' \\ CH-O-\overset{\overset{\displaystyle O}{\|}}{C}-R'' \\ CH_2-O-\overset{\overset{\displaystyle O}{\|}}{C}-R''' \end{array} \xrightarrow{\text{het. cat.}} 3CO_2 + R'\text{-H} + R''\text{-H} + R'''\text{-H} + (\text{light HC})$$
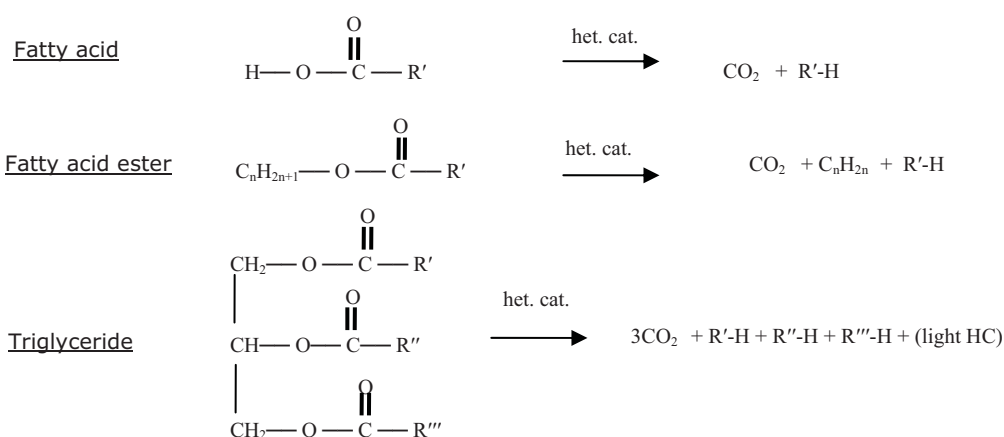
In the present work the kinetic behavior of ethyl stearate decarboxylation over a heterogeneous catalyst was investigated with the aim to verify the reaction mechanism and further optimize the chemical process.

Experimental

The kinetic study was carried out in a semi-batch reactor (300 ml Parr autoclave) over a fine powder catalyst (catalyst mass 1 g, particle size < 50 μm) which was reduced with hydrogen prior to reaction. The experiments were conducted at a stirring speed of 1100 rpm, which is proven to be efficient enough to avoid mass transfer limitations. The reaction temperature and pressure were kept constant during the reaction, in the range of 270-360 °C and 17-40 bar (the reaction pressure was adjusted according to the vapor pressure of the reaction mixture), respectively. The reaction was performed in a solvent (n-dodecane) under helium, nitrogen, hydrogen or argon- (5 vol%) hydrogen atmosphere, the total liquid volume in the reactor was 100 ml. The carrier gas was added with the volumetric flow of 25 ml/min.

Results and discussion

The decarboxylation of the fatty acid ester, ethyl stearate (A), proceeds via its corresponding fatty acid, stearic acid (B), which is subsequently decarboxylated to n-heptadecane (P_1). The produced paraffin is, however, simultaneously dehydrogenated to unsaturated olefins (P_2) and aromatics (P_3) (Figure 1).
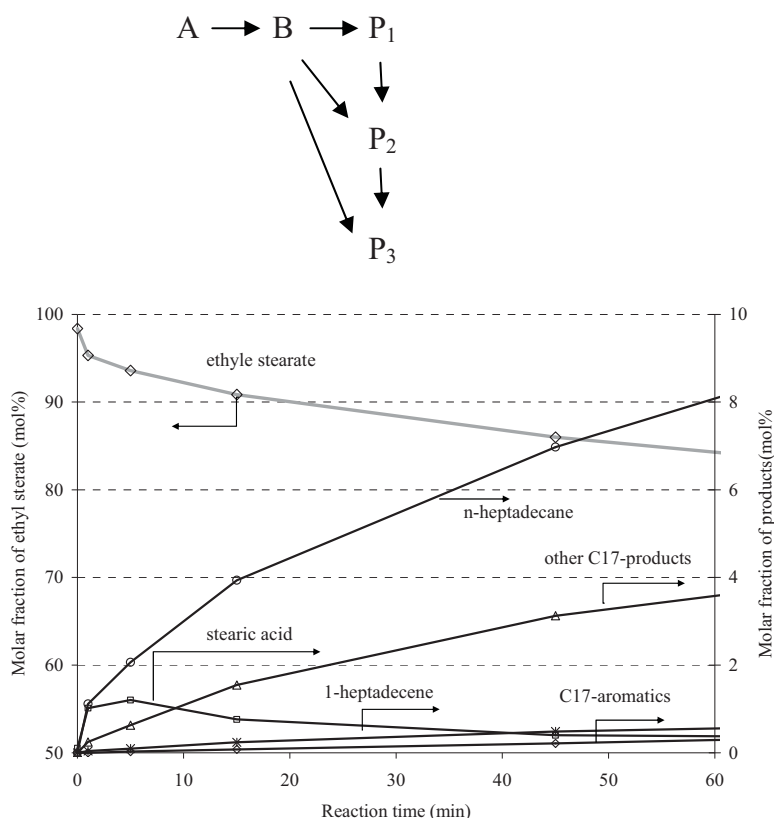
Figure 1. Concentration profile of ethyle stearate and products in the decarboxylation reaction. The reaction conditions: T = 300 ˚C, p= 17 bar (Ar-(5 vol%) H_2), $c_{ethyl\ stearate}$ = 1.6 mol/l, $m_{catalyst}$ = 1 g.

PS-17

As expected, the reaction rate increased with temperature when ethyl stearate was decarboxylated in a temperature range of 300-360 ˚C with apparent activation energy equal to 57.3 kJ/mol (Figure 2).
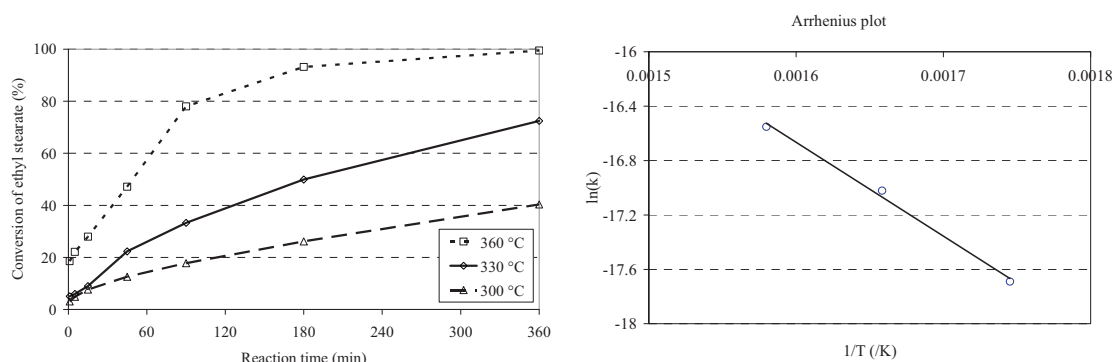
Figure 2. Effect of reaction temperature in the decarboxylation of ethyle stearate. The reaction conditions: T = 300-360 ˚C, p= 17 bar (Ar-(5 vol%) H_2), $c_{ethyl\ stearate}$ = 1.6 mol/l, $m_{catalyst}$ = 1 g.

In addition kinetic decarboxylation experiments with the intermediate product, stearic acid, were performed. The study showed that the reaction order of steraic acid is close to zero and the apparent reaction constant is approximately 0.0065 mol/l/min. However, with high initial concentrations (1.54 mol/l) of stearic acid, catalyst deactivation is observed (Figure 3), which is reflected in lower value of the corresponding rate constant. An earlier study of decarboxylation in a tubular reactor showed that the catalyst is indeed deactivated with a fatty acid feedstock [3].
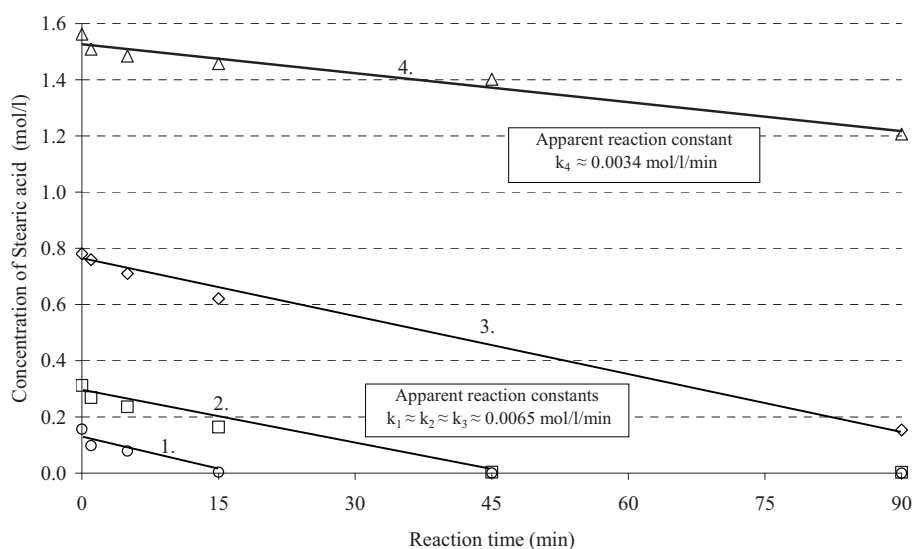
Figure 3. Effect of reactant concentration in the decarboxylation of stearic acid. T = 300˚C, p= 17 bar (inert atmosphere), $c_{stearic\ acid}$ = 0.154 – 1.54 mol/l, m_{cat} = 1 g

Conclusion

The kinetics of ethyl stearate decarboxylation was studied in a broad range of temperatures and pressures. Additionally decarboxylation of intermediate product, stearic acid, was investigated. The main kinetic regularities were established. The apparent activation energy in ethyl stearate decarboxylation was 57.3 kJ/mol.

[1] I. Kubičková, M. Snåre, P. Mäki-Arvela, K. Eränen and D. Yu. Murzin, Catalysis Today 106 (2005) 197-200.

[2] A. Demirbas, Fuel 77 (1998) 1117-1120

[3] M. Snåre, I. Kubičková, P. Mäki-Arvela, K. Eränen and D. Yu. Murzin, Proceedings of the14[th] European Biomass Conference and Exhibition on Biomass for Energy, Industry and Climate Protection, Paris (2005), in press

ISOMERIZATION OF n-BUTANE OVER Pd-H-MCM-22 AND H-MCM-22 ZEOLITE CATALYSTS: INFLUENCE OF ACIDITY AND CATALYST SYNTHESIS METHODS

[*1]Narendra Kumar, [1]Prem K. Seelam, [2]Teemu Heikkilä, [2]Vesa-Pekka Lehto, [1]Tapio Salmi, [1]Dmitry Yu. Murzin

[1]*Laboratory of Industrial Chemistry, Process Chemistry Centre, Åbo Akademi University, FIN-20500 Åbo/Turku, Finland,*

[2]*Department of Physics, Laboratory of Industrial Physics, Turku University, FIN-20014 Åbo/Turku, Finland,*

* Corresponding author, e-mail: nkumar@abo.fi, Fax: +358 2 2154555

Isomerization of n-butane to iso-butane was investigated over H-MCM-22 zeolite catalyst with varying acidities and Pd modified MCM-22 prepared by ion-exchange, impregnation and *in-situ* synthesis methods. The reaction was carried out in a fixed bed micro-reactor with hydrogen as a carrier gas. The influence of acidity, methods of Pd- modifications and pretreatment of Pd-H-MCM-22 and H-MCM-22 catalysts in n-butane isomerization were investigated. The conversion of n-butane and yield to iso-butane was observed to be influenced by the acidity of H-MCM-22 zeolite catalysts. The Pd- modified MCM-22 zeolite catalysts exhibited higher conversion of n-butane and yield to iso-butane than H-MCM-22. Pretreatment of the Pd-MCM-22 catalyst i.e. directly reduced or calcined and then reduced were observed to influence the conversion of n-butane and yield to iso-butane.

Na-MCM-22 zeolites with SiO_2/Al_2O_3 ratios 30, 50 and 100 were synthesized and transformed to H-MCM-22-30, H-MCM-22-50 and H-MCM-22-100 catalysts by ion-exchange with aqueous solution ammonium chloride, drying and deammoniation at elevated temperature. The Pd modified MCM-22 zeolite catalysts were prepared by ion-exchange, impregnation and *in-situ* synthesis methods. The catalysts were characterized using X-ray powder diffractometer, scanning electron microscope, nitrogen adsorption, X-ray fluorescency, direct current plasma spectrometer, TPD of ammonia and FTIR of adsorbed pyridine.

Introduction

Metal modified and proton forms of zeolite catalysts due to its unique properties of uniform pores, shape selectivity, thermal stability and coke resistant are used in several processes in oil refinery and has potential applications in synthesis of fine chemicals and environmental catalysis. The methods of metal introduction in zeolite and catalyst pretreatment have been reported to influence their state, dispersion, metal-zeolite interaction and consequently the catalytic properties.

Isomerization of n-butane to iso-butane is an important reaction from academic and industrial point of view. The direct conversion of n-butane to iso-butane can produce large amount of iso-butane which is a valuable raw material for the production of isooctane. There are several publications in open literature on Pt modified zeolite catalysts for n-butane isomerization [1]. However, there are only two publications regarding the Pd- modified zeolite catalysts in isomerization of n-butane [2]. In this work we report the synthesis and characterization of H-MCM-22 with varying acidities and Pd- modified MCM-22 zeolite catalysts prepared by ion-exchange, impregnation and *in-situ* synthesis methods. Further more isomerization of n-butane to iso-butane was investigated over H-MCM-22 and Pd- modified MCM-22 zeolite catalysts.

Experimental

Na-MCM-22 zeolite was synthesized with SiO_2/Al_2O_3 ratios such as 30, 50 and 100 in 300 ml autoclaves as mentioned in references [3-5] with some modifications. The Na-MCM-22 zeolites synthesized with varying acidities were transformed to H- forms by ion-exchange with ammonium chloride, followed by drying and calcination. Pd modified MCM-22 zeolite catalysts were prepared by impregnation, ion-exchange and *in-situ* synthesis methods using aqueous solution of palladium nitrate, followed by drying and calcinations. The catalysts were characterized using X-ray powder diffractometer, scanning electron microscope, nitrogen adsorption, TPD of ammonia and FTIR of adsorbed pyridine for acidity measurement. The state of Pd was investigated by XPS and crystallite size was determined by X-ray powder diffractometer. The isomerization of n-butane to iso-butane was carried out in a fixed bed micro reactors. Hydrogen was used as a carrier gas and Pd- modified MCM-22 molecular sieve catalysts were pretreated with hydrogen prior to the catalyst testings. The on-line analyses of the reaction products were carried out using a gas chromatograph equipped with a capillary column and FID.

PS-18

Results and discussion

The X-ray powder diffraction patterns of Na-MCM-22 micro-porous molecular sieves with SiO_2/Al_2O_3 ratios 30, 50 and 100 were similar to those reported in the literature. It was confirmed from the XRD patterns that modification of MCM-22 with Pd- using ion-exchange, impregnation and *in-situ* synthesis methods did not influence parent structure of MCM-22. Pd was highly dispersed in Pd-H-MCM-22-30-IE catalyst prepared by ion-exchange. The scanning electron micrograph of MCM-22 showed platelet like crystals. The acidity measurement by temperature programmed desorption of ammonia exhibited highest acidity for MCM-22 with SiO_2/Al_2O_3 ratio of 30 and lowest acidity for MCM-22 with SiO_2/Al_2O_3 of 100. The H-MCM-22 catalyst synthesized with SiO_2/Al_2O_3 ratio of 30 showed highest conversion of n-butane and yield to iso-butane among the three proton form catalysts. The lowest conversion of n-butane and yield to iso-butane was observed for H-MCM-22 with SiO_2/Al_2O_3 ratio of 100. It was observed that the Pd-H-MCM-22-30-IE ion-echanged zeolite catalyst exhibited higher conversion of n-butane and yield to iso-butane than the H-MCM-22-30 indicating the positive influence of Pd- modification of MCM-22 in isomerization of n-butane. The method of Pd introduction in MCM-22 was found to influence the conversion of n-butane and yield to iso-butane. The H- and Pd- modified MCM-22 catalysts showed deactivation in n-butane isomerization with time on stream. However, catalysts regained the activity after regeneration with synthetic air. The physico-chemical and catalytic properties of H-MCM-22 and Pd- modified MCM-22 catalysts in n-butane isomerization will be discussed in detail during the presentation.

Conclusions

Na-MCM-22 molecular sieve was synthesized with varying SiO_2/Al_2O_3 ratios of 30, 50 and 100. The H-MCM-22 catalyst synthesized with silica to alumina ratio 30 exhibited the highest conversion of n-butane and yield to iso-butane among the three H- forms. It was concluded that conversion of n-butane and yield to iso-butane was highly influenced by the acidic property of H-MCM-22 catalysts. The Pd- modified MCM-22 catalyst exhibited higher conversion of n-butane and yield to iso-butane than the proton forms of MCM-22 catalysts indicating the positive role of Pd in n-butane isomerization.

Reference

1. R. A. Asuquo, E. M. Gabriele, J. A. Lercher, Journal of Catalysis 155 (1997) 376.
2. P. Canizares, A. de Lucas, F. Dorado, J. Aguirre 42 (2001) 245.
3. Juttu G. G., Lobo R. F., Microporous and Mesoporous Material 40 (2000) 9.
4. Corma A., Corell C., Perez-Pariente J., Zeolites 15 (1995) 2.
5. Corma A., Fornes V., Martinez-Triguero J, Pergher S. B., Journal of Catalysis 186 (1999) 58.

LACTOSE OXIDATION ON GOLD CATALYSTS

A.V. Tokarev[a,b]**, E.V. Murzina**[b]** , J.-P. Mikkola**[a]**, J. Kuusisto**[a]**, L.M. Kustov**[b]**,**

D.Yu. Murzin[a]

[a]*Process Chemistry Centre, Åbo Akademi University, Biskopsgatan 8, FIN-20500, Turku/Åbo, Finland, fax: +358 2 215 4479, E-mail:dmurzin@abo.fi*

[b]*Department of Chemistry, Moscow Lomonosov State University, 119992, Moscow, Russia*

Inroduction

Lactose oxidation is a consecutive reaction, resulting first in lactobionic acid, and then to 2-keto-lactobionic acid. From industrial viewpoint this reaction is interesting because lactobionic acid possesses useful properties and can, thus, be used as acidulant, complexing agent or antioxidant in food, pharmacy and medicine. Lactose, an abundant disaccharide, is a by-product of dairy industry available in big amounts.

lactose → Na-lactobionate → 1-carboxy lactulose (2-keto-Na-lactobionate)
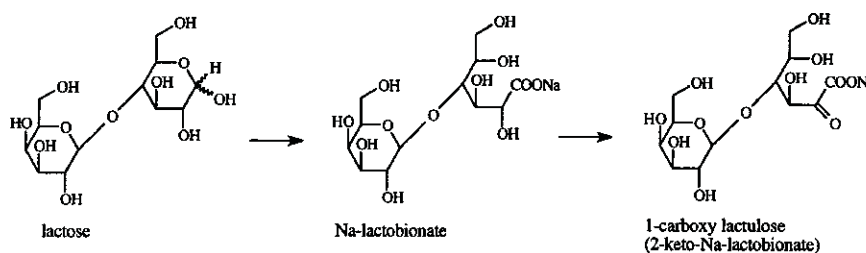
Oxidation of sugars is very sensitive to several factors such as pH of reaction media, since the formation of corresponding carbohydrate acids results into big pH change. Another important parameter is the oxygen feed rate, since the reaction rate can be retarded either due to the lack or due to "oversupply of oxygen (i.e. oxygen poisoning) at high oxygen feed rate. For such cases *"in situ"* catalyst potential measurements, applied in the present work, give important information about red-ox state of the catalyst surface. Among different supported metals used as catalysts in oxidation of sugars gold nanoparticles recently emerged as very effective and selective catalysts [1]. The present study is mostly concentrated on gold nanoparticles supported on different materials.

PS-19

Experimental

A shaker reactor for in situ catalyst potential measurements was used for lactose oxidation (Fig. 1). This reactor is an attractive alternative to other slurry systems. First of all, shaking helps to avoid appearance of stagnant zones of solution and improves gas to liquid mass transfer limitations. Moreover liquid to solid mass transfer limitations could be also eliminated. Second, the shaker is convenient for *"in situ"* catalyst potential measurements which provide information on the red/ox state of the catalyst surface during reaction. A continuous gas flow is used to ensure constant composition of a gas mixture over reaction media. Constant ratio between nitrogen and oxygen in gas mixture is maintained by mass flow controllers (Brooks 5850E). The stainless steel cup of reactor is used as an electrode collector for measurements of the catalyst potential. For this purpose all parts of the reactor are electrically isolated from shaking device (mechanical part of "3916 Hydrogenating Apparatus" Parr®). Potential
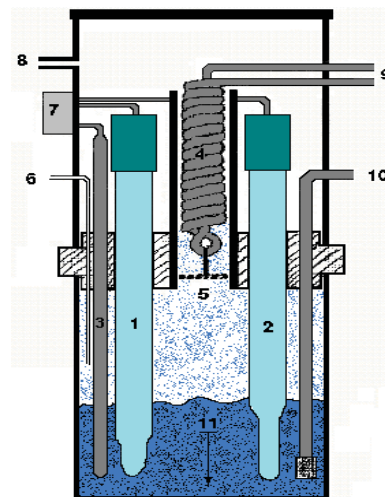
Figure 1. Shaker reactor: 1 - pH electrode, 2 - reference electrode, 3 - thermocouple, 4 - cooling coil, 5 - grid, 6 - alkaline inlet, 7 - electronics socket, 8 - gas outlet, 9 - inlets for cooling water, 10 - gas inlet.

measurements were performed versus Ag/AgCl electrode. Constant pH of reaction media was maintained by automatic titration device (Metrohm Titrino 751) at pH-stat mode.

For comparative catalysts testing, lactose oxidation was performed at 60°C in aqueous media. Gas flow was 20 cm^3/min, with an oxygen content 12.5 % (O_2/N_2 = 2.5/17.5). pH was maintained at a level higher than 8. For this purpose a 2.5 M NaOH solution was applied. In each experiment, the catalyst amount was 0.5 g, lactose concentration – 9.4 mM and the overall weight of the reaction mixture was 100 g.

Results and discussion

In the present study a number of gold catalysts prepared by different methods on a variety of support materials (active charcoal, alumina, ceria, zirconia, iron oxide) were tested. Catalytic activity, selectivity and time dependences of catalyst potential were obtained and compared. Additionally, the influence of catalyst deactivation on catalytic activity was evaluated for Au on alumina and ceria support and a reference Pd on alumina catalyst. In Fig. 2, the activities of gold catalysts is compared to a 5% Pd/Al_2O_3 catalyst. Taking into account higher metal loading of palladium catalyst, it can be concluded that gold is more active, selective and more resistant to deactivation.

Qualitative difference in reaction products caused by different metal nature is visible from dependence of selectivity on conversion (Fig.3). The main feature of lactose oxidation on gold is that there is almost no formation of the product of the consecutive oxidation (2-keto-lactobionic acid).

Figure 2. Kinetic curves of lactobionic acid formation over Pd and Au catalysts.

"In situ" measured catalyst potential correlate well with catalysts activity (Fig.4).
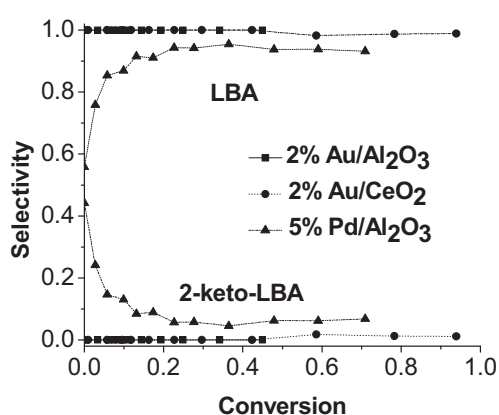
Figure 3. Selectivity as a function of conversion for Au and Pd catalysts.
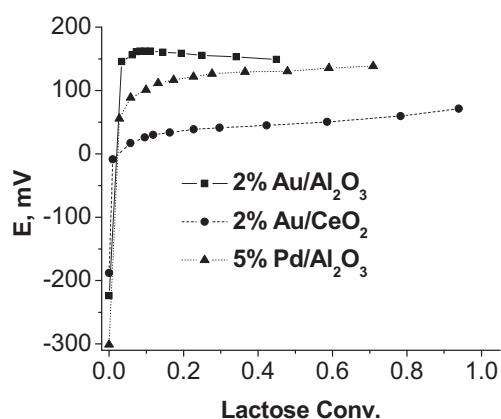
Figure 4. Potential on conversion dependences for Au and Pd catalysts.

PS-19

Dependences of electrochemical catalyst potential on time shown in Fig. 5 have linear parts with different slopes. These slopes characterize rate of accumulation of non-reacted oxygen on the surface. From curves of LBA formation (Fig. 6) it is visible that in the beginning of experiment reaction rate is proportional to oxygen feed rate. However, decrease of lactose concentration makes reaction slower and non-reacted oxygen accumulates on the catalyst surface. Deactivation state is reached faster in case of higher oxygen feed rates.
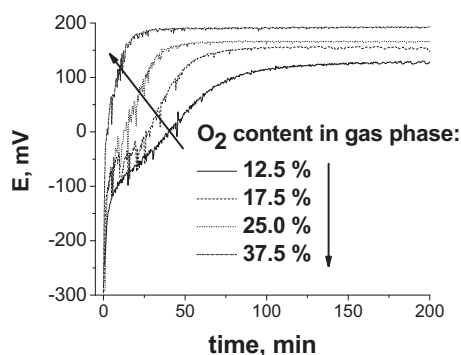
Figure 5. Catalyst potential transients for experiments with different oxygen feed rate.
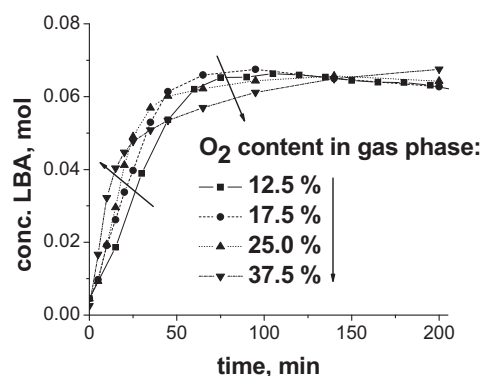
Figure 6. Concentration of lactobionic acid in experiments with different oxygen feed rate.

Conclusions

Gold catalysts were successfully applied in lactose oxidation. The results of performed research show that on gold catalysts lactobionic acid can be obtained with high yields and selectivity.

References

[1] H. Berndt, A. Martin, I. Pitsch, U. Prüsse, K.-D. Vorlop, Catalysis Today 91-92 (2004) 191.

BIOETHANOL FROM HAZELNUT HUSK

<u>Selim Ceylan</u>, Dilek Kazan, Sevil Ünal and A. Alp Sayar

Marmara University, Faculty of Engineering, Chemical Engineering Department

Göztepe 34722 Istanbul, TURKEY

In order to obtain a better exploitation of raw material for bioethanol production, the most favorable conditions were explored for saccharification of the residues of hazelnut, an abundant agricultural product in Turkiye. Hazelnut husk was pulverized and treated with sulphuric acid. Different times of treatment (30 min – 90 min), different concentrations of sulphuric acid (1% to 5%, by wt) and different concentrations of sample (1/5, 1/10, 1/15, 1/20 solid/liquid ratio) were tested.

The maximum yield of sugar (g reducing sugar/g dry mass %) was obtained as 18.63 ±0.51% for 1.5 hour incubation at an acid concentration of 4% and a sample concentration of 1/20 for hazelnut husk. The sugar composition of hydrolysed hazelnut husk was analysed using Thin Layer Chromatography (TLC). Four mono-sugars, arabinose, glucose, mannose and xylose were determined in acid hydrolyzed hazelnut husk.

Hydrolyzates obtained after saccharification were used in ethanol production by *S.cerevisiae*. The highest ethanol yield as 7.65 g/L was obtained using acid hydrolyzate of hazelnut husk.

ENVIRONMENTALLY FRIENDLY FUEL FROM RENEWABLE RAW MATERIALS

Yandieva F.A., Tsodikov M.V., Kugel V.Ya., *Gekhman A.E., *Moiseev I.I.

A.V. Topchiev Institute of Petrochemical Synthesis, RAS, Moscow, Russia
**N.S. Kurnakov Institute of General and Inorganic Chemistry, RAS, Moscow, Russia*
E-mail: yand@ips.ac.ru

Investigation results of recently discovered [1,2] aliphatic alcohol (C_2-C_5) reductive dehydration reaction proceeding at 300-400°C and 0,3-0,5 MPa in the presence polymetallic hydride-forming systems leading to formation of hydrocarbons are reported.

In the case of ethanol this new reaction proceeds via the following scheme:

$$n\ C_2H_5OH + C_2H_5OH \longrightarrow C_{2n}H_{4n+2} + CH_3CHO + n\ H_2O, \text{ where } n \geq 1$$
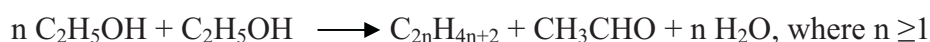
The target reaction products represent the main components of gasoline fraction. The yield of hydrocarbon fraction, comprising more than 90% isoalkanes, most valuable high-octane fuel components, attained 50% mass.

The initial alcohol nature exerts the considerable influence on the reaction product composition. Thus, 2-methylpropanol-1 or 3-methylbutanol with high selectivity has been transformed to isooctane or isodecane, respectively, representing doubling products of alcohol carbonic skeleton:
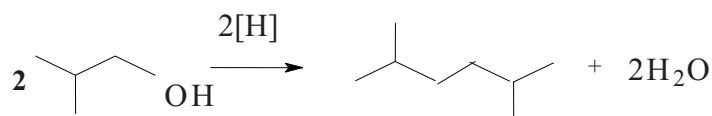
where hydrogen source could be an alcohol molecule, generating H_2 in the course of dehydrogenation reaction.

New one-stage cross-condensation reaction between aliphatic and cyclic alcohols with formation of alkylcycloalkanes, representing gasoline valuable components, was developed:
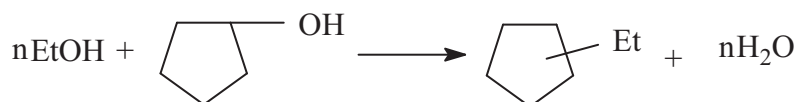
The main source of aliphatic alcohols represents biomass being renewable raw material.

Submitted data demonstrate actual possibility for future utilization of new approach for production of ecologically clean and high-quality motor fuels from raw-materials of non-oil origin.

References:

1. M.V. Tsodikov, V.Ya. Kugel, F.A. Yandieva, G.A.Kliger, L.S. Glebov, A.I. Mikaya, V.G. Zaikin, E.V. Slivinskii, N.A. Plate, A.E. Gekhman I.I. Moiseev // Kinetics and Catalysis, 2004, vol. 45, № 6, p.854-866.

2. I.I. Moiseev, A.E. Gekhman, M.V. Tsodikov, V.Ya. Kugel, F.A. Yandieva et all. In "Multimetallic Catalysts in Organic Synthesis" (Eds: M.Shibasaki, Y.Yamamoto), WILEY-VCH, 2004, 249-290.

POSTER PRESENTATIONS

XVII International Conference on Chemical Reactors

THE PROCESS OF SYNTHESIS OF PREMIUM MOTOR FUELS FROM HIGH-SULFUR STRAIGHT-RUN DISTILLATES OVER COMBINATION OF ZEOLITE CATALYST WITH HYDROTREATING CATALYST – THE BIMF-2 PROCESS

Dmitry G. Aksenov, Oleg V. Klimov and Gennadii V. Echevsky

Boreskov Institute of Catalysis SB RAS, pr. Lavrentieva, 5, Novosibirsk 630090 Russia

E-mail: Aksenov@catalysis.ru

Manufacture of non-polluting high-quality motor fuels is one of actual and priority tasks of oil refining. Boreskov Institute of Catalysis has developed a new catalytic process for the one-stage conversion of gas condensates or of oil distillates with boiling points up to 360 °C to high-octane gasoline, diesel fuel (winter grade) and liquefied gases C_3-C_4 [1]. This technology, named as BIMF (Boreskov Institute Motor Fuels) process, allows one to reduce essentially the power consumption for the manufacturing of motor fuels. The process is carried out over a zeolite catalyst (IC-30-BIMF) not containing a noble metal in a temperature range of 350–450 °C and pressure of 50 – 250 MPa. The gasoline produced at these conditions contains as a rule less than 35 wt.% of aromatic compounds, up to 10 wt.% n-alkanes, with the rest being i-alkanes and naphthenes. The produced diesel fuel consists mainly of i-alkanes and naphthenes, with the content of n-alkanes lower than 5 wt.%, and the content of aromatic compounds lower than 10 wt.% [2].

Recently we have showed that gasoline produced from wide-fractional gasoline feedstocks with different sulfur content always fall into allowed sulfur content range prescribed by the Russian standards on gasoline quality [3]. The obtained results agree very well with those of other researchers [4] who found the upper limit of 150 mg/kg for sulfur content in gasoline produced on zeolite catalysts. However, the similar situation with diesel fuel is more complicated. In the case of application of the basic IC-30-BIMF catalyst sulfur content in diesel fuel may be reduced as much as in two times compared with fed hydrocarbon raw material. That sulfur reduction efficiency doesn't always allow to meet the required on the Russia territory parameter – less than 0.2 %wt. This observation may be explained by the presence in hydrocarbon feedstocks of sulfur-containing compounds which may be divided to two groups:

1. Chemically inert compounds of thiophene derivatives group.

2. Rather reactive S-containing compounds of aliphatic derivatives group – thiols, mercaptanes, sulfides.

The main problem in production of high-quality diesel fuel is to convert the sulfur-containing compounds of the first group. While compounds of the second group rather easily react on zeolite catalysts to give hydrogen sulfide and respective hydrocarbons at moderate temperatures and pressures without necessity in hydrogen, compounds of the first group to be removed from fuels require not only rather high temperatures and pressures but presence of hydrotreating catalyst and some hydrogen pressure also.

For the basic variant of the BIMF process it was shown that conversion of thiophene and dibenzothiophene, the typical representitatives of the first class compounds, was rather low [5]. As a consequence, in **Boreskov Institute of Catalysis** the new variant of the BIMF process of premium motor fuels synthesis from high-sulfur hydrocarbon feedstocks has been developed – the BIMF-2 process. This process is based on application of the two essentially different components of the complex catalyst:

A)   zeolite component responsible for the conversion of n-paraffins with low octane number (ON) and high melting temperature to hydrocarbons with high ON:

B)   hydrotreating component responsible for sulfur reduction in motor fuels.

Under the reaction conditions of the BIMF process (350 – 450 °C, 0,5 – 2,5 MPa) in presence of zeolite catalyst normal paraffins C_5^+ are converted mainly to aromatic hydrocarbons C_7-C_{10} with formation of some hydrogen. Conversion of other feedstock's components is rather low [6]. As a result, there are suitable conditions in the BIMF reactor for hydrotreating catalyst functioning.

The BIMF-2 process may be realized in two main practical variants.

First variant. Two different catalyst are charged into BIMF-2 reactor, for example, zeolite catalyst IC-30-BIMF and any hydrotreating or hydrocracking catalyst according to [7]. Charging of the reactor is possible in several ways as depicted in Fig. 1.

In accordance with variant 1(a), the upstream part of reactor is filled with zeolite catalyst and the bottom part is filled with hydrotreating catalyst. In the upper part n-paraffins are converted to aromatic hydrocarbons and hydrogen. Thiophenes are converted in the bottom part of the reactor under the action of hydrotreating catalyst and hydrogen giving hydrogen sulfide and hydrocarbons.

PP-1

Feedstock ... Feedstock

Z - zeolite catalyst, **HC** - hydrotreating catalyst
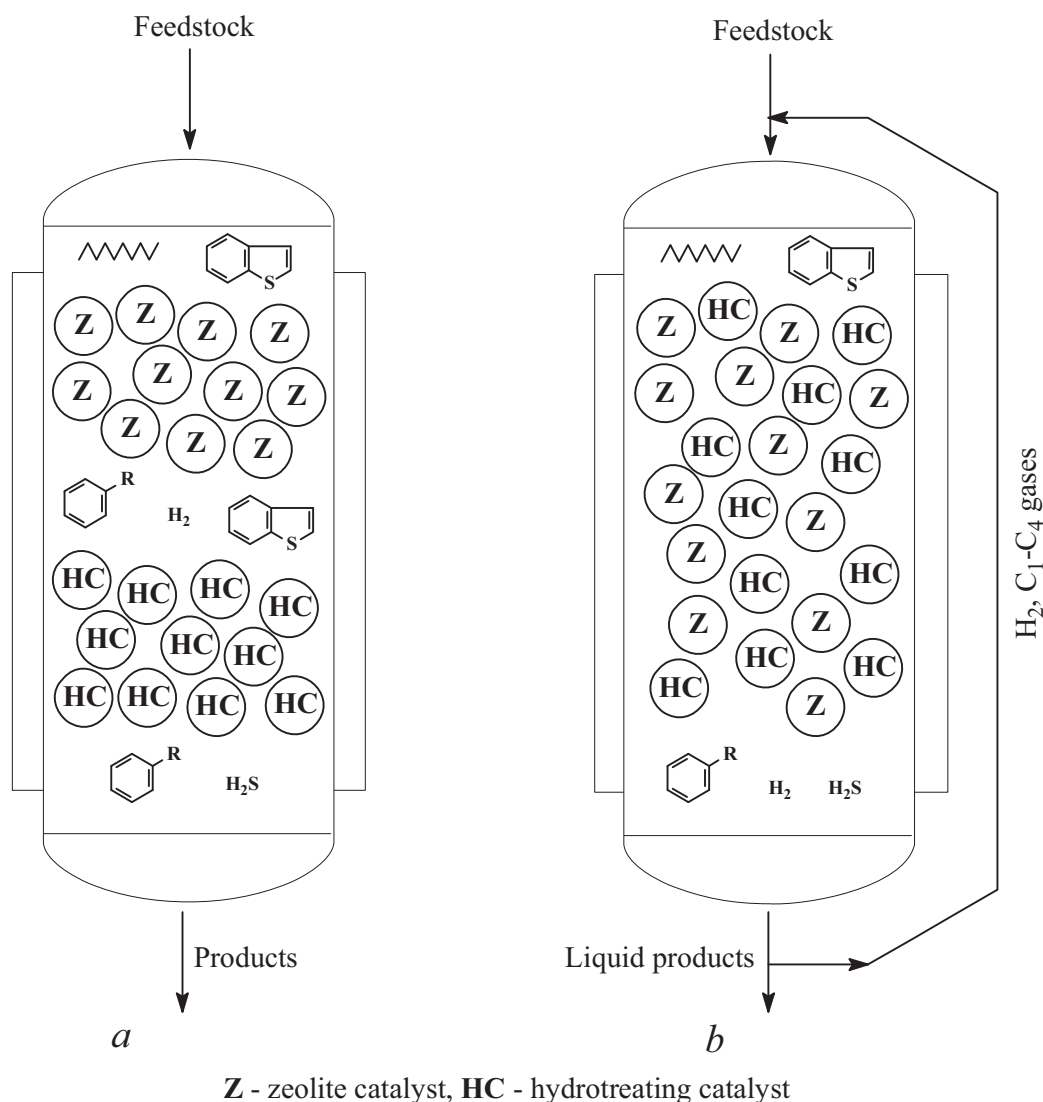
Figure 1.

In accordance with variant 1(b), reactor is loaded with a mechanical mixture of both catalysts, and conversion of n-paraffins and thiophenes proceeds simultaneously. For this case circulation of part of the reacted gases, containing hydrogen, through the reactor is necessary.

Second variant. The BIMF-2 reactor is loaded with bifunctional catalyst which contains zeolite and hydrotreating component and binder (Fig.2). The method of preparation of such catalyst is described in [8]. It has been shown [9] that the hydrotreating component is localized on the binder particles only and has no influence on zeolite component's performance. In the process by variant 2 the circulation of the reacted gas, containing formed hydrogen, through the reactor is necessary as well.

Feedstock

H₂, C₁-C₄ gases

BFC - bifunctional catalyst

Liquid products
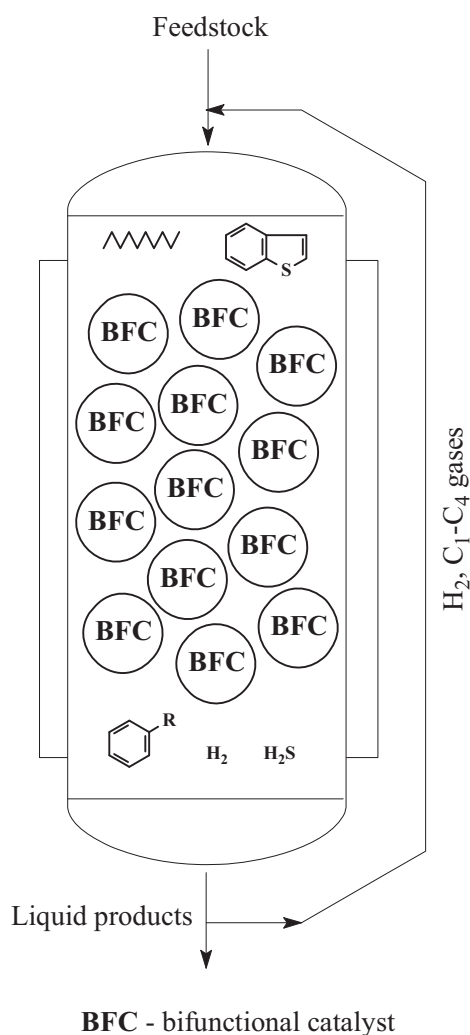
In conclusion, synthesis of premium motor fuels from high-sulfur straight-run distillates, the BIMF-2 process, may be realized in several variants, differing in applied catalysts and charging schemes of the reactor. For all variants of the BIMF-2 process realization in our experiments the sulfur content in gasoline products didn't exceed 150 mg/kg, and that in diesel fuels was less than 0.1 %wt. Synthesis of motor fuels with more lower sulfur content is also possible, but other than described in [7 – 9] hydrotreating components or catalysts are required.

Figure 2.

References

[1]   Echevsky G.V.// Science and Technologies in Industry №.2 (2002) 62 (In Russian).

[2]   Echevsky G.V., Klimov O.V., Kikhtyanin O.V. et al.// Catalysis in Industry, №2 (2003) p.60.

[3]   Klimov O.V., Kikhtyanin O.V., Aksenov D.G. et al.// Chemistry and technology of fuels and oils, №5 (2005) p.20.

[4]   Stepanov V.G., Ione K.G.// Catalysis in Industry, №2 (2003) p.55.

[5]   Aksenov D.G., Klimov O.V., Echevsky G.V.//Petroleum and Coal, v. 45, 3-4 (2003) 200.

[6]   Aksenov D.G., Klimov O.V., Kikhtyanin O.V., Echevsky G.V.// Scientific base and technology of BIMF. In "New challenges in catalysis", IV, P.Putanov ed., Belgrade, 2006, p.123.

[7]   Aksenov D.G., Klimov O.V., Kikhtyanin O.V. et al.// Russian Patent №2219219.

[8]   Klimov O.V., Aksenov D.G., Dudarev S.V. et al.// Russian Patent №2235591.

[9]   Klimov O.V., Aksenov D.G., Prosvirin I.P. et al.// Studies in Surface Science and Catalysis, v.158 (2005) 1779.

EFFECT OF GOLD LOADING ON THE PHYSICOCHEMICAL AND CATALYTIC PROPERTIES OF Au/α-Fe$_2$O$_3$ CATALYSTS FOR THE PREFERENTIAL CO OXIDATION REACTION

G. Avgouropoulos[1], J. Papavasiliou[1], Ch. Papadopoulou[2], T. Ioannides[1], H. Matralis[1,2]

[1] *FORTH/ICE-HT, Stadiou str., Platani P.O. Box 1414, Patras GR-26504, Greece*
Fax: +30-2610-965223, e-mail: geoavg@iceht.forth.gr
[2] *Department of Chemistry, University of Patras, GR-26504 Patras, Greece*
Fax: +30-2610-996322, e-mail: matralis@chemistry.upatras.gr

1. Introduction

Contamination of H$_2$, produced from fuels such as methanol, with 1-2 % CO results in anode poisoning of H$_2$-fuelled solid polymer fuel cells. The acceptable concentration of CO at CO-tolerant alloy anodes is < 100 ppm [1, 2]. Preferential CO oxidation reaction (PROX) is the simplest and most cost effective method for removing CO from H$_2$-rich fuels. An efficient PROX catalyst must fulfill three requirements: (i) high oxidation rate, (ii) high selectivity with respect to the undesired H$_2$ oxidation side reaction and (iii) stability with reaction time.

Most of the reports in the literature for the PROX reaction are related with Pt group catalysts [1, 3]. However, these systems can't avoid significant losses of H$_2$ due to oxidation. CuO-CeO$_2$ catalysts have been also proposed as one of the best candidates for the PROX reaction [1, 2]. These catalysts are able to operate at 100-200 °C with almost ideal selectivity and stability. They can also tolerate high concentrations of CO$_2$ and H$_2$O. On the other hand, highly dispersed Au nanoparticles (<3-5 nm) supported on reducible metal oxides [4, 5], such as Fe$_2$O$_3$, CeO$_2$, TiO$_2$ and MnO$_x$, were found to be superior than Pt group catalysts, since they are able to remove CO from reformed fuels with extraordinarily high oxidation rate and better selectivity at much lower temperatures (<100 °C). Precipitation techniques are able to bring a strong interaction of gold particles with the support. The strong interaction leads to the stabilization of small gold particles through a wider contact area and often gives the longest perimeter interface around gold particles [4, 5]. The support provides additional O$_2$ adsorption sites at the perimeter interface around gold particles and supplies it to the gold surface, in order to facilitate the oxidation of CO in the presence of H$_2$. In this work, a series of Au/α-Fe$_2$O$_3$ catalysts were prepared by the coprecipitation method, and their physicochemical and catalytic properties were investigated for the PROX reaction. The main parameter of this study was the Au content of Au/α-Fe$_2$O$_3$ catalysts.

2. Experimental

A series of Au/α-Fe$_2$O$_3$ catalysts were prepared via the coprecipitation method [1]. The obtained solids were calcined in flowing air at 400 °C and sieved in the desired fraction (90<d<160 μm). The catalysts were characterized by atomic adsorption spectroscopy (AAS), N$_2$ adsorption, X-ray powder diffraction (XRD) and X-ray photoelectron spectroscopy (XPS).

The catalytic performance for the PROX reaction was studied in a fixed-bed reactor system [1] at 1 atm and in the temperature range of 30-270 °C. The contact time was 0.03-0.144 g s cm^{-3} and the reaction mixture consisted of 1 % CO, 1.25 % O$_2$ and 50 % H$_2$ in He. The effects of CO$_2$ and H$_2$O were also investigated, at separate runs, by adding 15 % CO$_2$ and 10 % H$_2$O in the reaction mixture. Gas analysis was carried out by a gas chromatograph. Details on the experimental techniques employed can be found elsewhere [2].

Table 1. Physicochemical properties of Au/α-Fe$_2$O$_3$ catalysts.

Catalyst	Au loading^a (wt. %)	S$_{BET}$ (m^2 g^{-1})	V$_P$ (cm^3 g^{-1})	D$_P$ (nm)	$10^3 \cdot$[Au/(Au+Fe)]$_{XPS}$	$10^3 \cdot$[Au/(Au+Fe)]$_{AAS}$
Au1	0.7	44.2	0.2	7-30	1.2	3.0
Au2	2.1	49.4	0.2	6-30	3.9 (2.9^b)	9.1
Au3	2.9	49.8	0.2	6-30	7.3 (3.5^b)	12.2
Au4	4.0	44.9	0.2	7-30	2.8	17.0
α-Fe$_2$O$_3$	0.0	2.0	-	-	-	-

^{a} measured by AAS, ^{b} measured after exposure in realistic reaction conditions for 7 days

3. Results and discussion

Various physicochemical properties of Au/α-Fe$_2$O$_3$ catalysts are reported in Table 1. For all catalyst samples, the isotherms of nitrogen adsorption/desorption were of type II and had type B hysteresis loops, which closed at P/P$_o$ = 0.65-0.70. Significant enhancement of surface area is observed in supported catalysts (S$_{BET}$ = 44-50 m^2 g^{-1}) compared to pure α-Fe$_2$O$_3$ (S$_{BET}$ = 2 m^2 g^{-1}). Strong interaction between gold and iron oxide hinders the tendency of each other towards agglomeration and formation of large crystalline particles. The pore size distribution, D$_P$, as estimated using the BJH method, was in the range 7-30 nm and the total pore volume, V$_P$, was equal to 0.2 cm^3 g^{-1}. XRD measurements of supported catalysts showed no gold peaks implying that the metal particle size is less than 3 nm. XPS analysis of Au 4f, Fe 2p and O 1s spectra of all the fresh samples indicated the presence of metallic gold and Fe$_2$O$_3$. More specifically, the Au 4f$_{7/2}$, Fe 2p$_{3/2}$ and O 1s binding energies were equal to 83.9, 711 and 530 eV, respectively. Neither gold loading nor exposure in reaction conditions affected these values. A broad shoulder at a higher BE region of O 1s spectra was evident in all the samples. This shoulder is attributed to oxygen in hydroxyl groups. Table 1 compares the atomic ratio Au/(Au+Fe), as determined by XPS, with the corresponding bulk concentration, as determined by AAS. The surface concentration of gold is significantly lower than the bulk concentration. The linear increase in the loading region of 0-3 wt.% implies constant

PP-2

dispersion of gold on the catalyst surface of Au1, Au2 and Au3 samples. Further increase of gold loading (Au4 sample) resulted in lower metal dispersion, probably due to the formation of bigger gold crystallites.
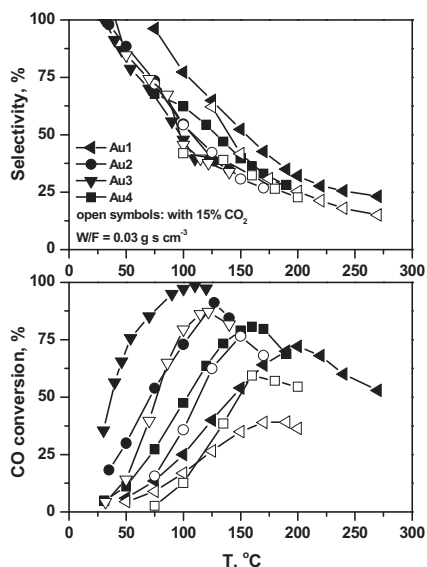
Figure 1. *Activity-selectivity of Au/α-Fe₂O₃ catalysts for the PROX reaction.*
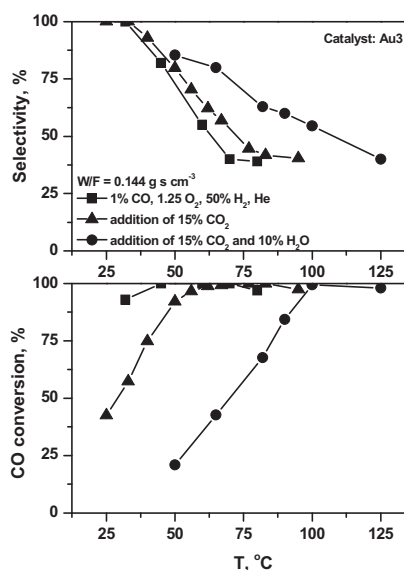
Figure 2. *Effect of CO_2 and H_2O on the activity-selectivity of Au3 catalyst for the PROX reaction.*

Fig. 1 shows the activity and selectivity of four Au/α-Fe₂O₃ catalysts, namely Au1, Au2, Au3 and Au4 under PROX conditions, while the CO oxidation rates and T_{50} values are presented in Table 2. The Au3 catalyst appeared to be the most active. The activity decreases in the order Au3> Au2> Au4> Au1, regardless of the presence of 15% CO_2 in the feed (open symbols in Fig. 1). The presence of CO_2 had a negative effect on the performance of all the samples and it lowered their catalytic activity by 1-2 orders of magnitude. The observed trends in activity with variation of Au loading correlate well with surface measurements by XPS. The reaction rate increases monotonically and almost linearly with the gold surface concentration. Therefore, the high activity of Au/α-Fe₂O₃ is due to the presence of highly dispersed gold nanoparticles. In what concerns the selectivity towards CO_2 production, the increase of the reaction temperature from 30 to 270 °C is accompanied by a continuous decrease of the selectivity from 100 to 15 %, indicating a higher apparent activation energy for H_2 oxidation than for the CO oxidation. Maximum CO conversion, i.e. 99%, was achieved over the Au3 catalyst at 110 °C with 40 % selectivity (W/F = 0.03 g s cm⁻³). Using a W/F ratio of 0.144 g s cm⁻³, complete CO conversion was obtained over the Au3 catalyst at 45 °C with 82 % selectivity (Fig. 2). By adding 15 % CO_2 in the feed, complete CO removal can be achieved at higher temperature, i.e. at 77 °C (45 % selectivity). Addition of both 15 % CO_2 and 10 % H_2O provoked further decrease in the Au3 activity, probably due to competitive adsorption of CO, CO_2 and H_2O on the catalyst surface [1, 2]. The presence of H_2O also

diminishes H_2 oxidation activity. Thus, 99.5 % CO conversion is obtained at 100 °C with 55 % selectivity.

Table 2. CO oxidation rates, r_{CO}, in the absence (at 50 °C) and presence (at 100 °C) of 15 % CO_2 in the feed.

Catalyst	r_{CO} at 50 °C (μmol_{CO} s^{-1} g_{cat}^{-1})	T_{50} [a] (°C)	r_{CO} at 100 °C (μmol_{CO} s^{-1} g_{cat}^{-1})	T_{50} [a] (°C)
	In the absence of CO_2		In the presence of 15% CO_2	
Au1	0.9	143	0.8	[b]
Au2	2.2	92	3.6	127
Au3	>10.0	36	9.0	77
Au4	1.9	104	1.8	149

[a] W/F = 0.03 g s cm^{-3}, [b] maximum CO conversion = 39 %

A 7-days catalytic run was performed with the Au2 and Au3 catalysts, in order to examine their stability under realistic reaction conditions. Both samples lost a significant part (15 and 30 % for Au2 and Au3 catalysts, respectively) of their initial activity during the first 75 h. The deactivation with reaction time for Au can be explained by taking into account the surface gold concentration values after exposure in PROX conditions (Table 1), which are significantly lower than those of fresh samples. This effect is much more pronounced in the case of Au2 catalyst, implying a higher degree of gold agglomeration during reaction.

4. Conclusions

The effect of Au loading on the catalytic performance of Au/α-Fe_2O_3 catalysts in PROX reaction correlates well with the characterization results. The reaction rate increases almost linearly with the Au surface concentration (in the region of 0-3 wt.% Au). Further increase of Au loading causes agglomeration phenomena, which are also responsible for the deactivation behaviour. The catalyst with 2.9 wt.% Au showed the best catalytic performance, remaining very active at low temperatures and with good selectivity and tolerance towards deactivation.

References

[1] G. Avgouropoulos, T. Ioannides, Ch. Papadopoulou, J. Batista, S. Hocevar, H. Matralis, Catal. Today 75 (2002) 157.

[2] G. Avgouropoulos, T. Ioannides, Appl. Catal. A 244 (2003) 155.

[3] P. Snytnikov, V. Sobyanin, V. Belyaev, P. Tsyrulnikov, N. Shitova, D. Shlyapin, Appl. Catal. A: Gen. 239 (2003) 149.

[4] M. Haruta, Cat. Tech. 6 (2002) 102.

[5] G.C. Bond, D.T. Thompson, Gold Bull. 33 (2000) 41.

PP-3

ON THE THEORY OF SPATIAL-TEMPORAL INSTABILITY IN CATALYTIC TRANSFORMATIONS ON ELECTRODES OF HYDROGEN-HYDROCARBONS FUEL CELLS

V.Barelko, A.Ivanova, K.Pribitkova, Z.Andrianova

Institute for Problems of Chemical Physics RAS, Chernogolovka, Russia

The presented work is developing the earlier created theoretical notions about non-linear phenomena (travelling waves, domain structures, oscillations, "ignition" effects) in catalytic combustion reactions (oxidation of hydrogen, hydrocarbons, ammonia etc.) on platinum containing catalysts (see [1,2] and the cited references). This instability problem is a most important subject for theory of chemical reactors. Now, it is obviously, the question about appearing of spatial-temporal structures on catalytic electrodes of fuel cells is a very essential aspect of this devices engineering and exploitation. Nevertheless, this non-linear feature of fuel cells systems was long time out attention of scientists and engineers acting in this field.

A theoretical analysis of critical conditions of "ignition" of exothermic heterogeneous catalytic reaction by thermal action on a local part of catalytic surface was carried out in this work on base of numerical experiments. One- and two-dimensional catalytic elements (catalytic filament-wire and flat surface of catalyst) were used as physical models of the process. The studied equations systems for thermal and substances balances uses two types of nonlinear kinetic schemes of the process which are typical ones for the practical important class of catalytic combustion reactions with Pt-containing catalysts for fuel cell systems (hydrogen & hydrocarbons oxidation reactions): i – reactions with hysteresis kinetics; ii – reactions with braking by initial reagent. We investigated the named models in relation of bifurcation features of them, autowave transitions between steady state regimes, phenomena of domain instability and spatial-temporal patterns. The present report describes threshold conditions of "ignition" and dynamics of the transient process depending on energy value of local thermal perturbation. There was shown that in a definite parametric region "ignition" process does not be finished by a homogeneous steady state regime. The "ignition" results by a single domain of reaction that is not accepted for fuel cell process. This domain regime may be a stationary and stable or unstable oscillating one. The results explain the existing phenomena "hot spots" in catalytic transformations. Such phenomena are rather probable for

catalytic process on cathode of fuel cell. These results may be used as a tool for search of technological ways for suppressing of the nonlinear effects.

The work form an initial theoretical base for describing of macrokinetic features of "two-dimensional catalysis" on fuel sells electrodes. Full model will demand to include additional stages description in the equations system: ions emission, diffusion of them through layer of solid electrolyte, charges recombination.

1. K.V.Pribitkova, V.V.Barelko // Himicheskaya fizika 2002, v.21, No 3, p.68.
2. A.N.Ivanova, Z.S.Andrianova, V.V.Barelko // Himicheskaya fizika, 2004, v.23, No 1 p.73

PP-4

NEW TYPE OF PLATINOID CATALYTIC GAUZES FOR OXIDIZING CONVERSION OF AMMONIA (nitric acid industry)

V.V. Barelko*, <u>L.A. Bykov*</u>, V.Ya. Onischenko*,

A.G. Ivanyuk**, V.N. Chepelenko**, M.G. Kurbatov**,

N.V. Gorshkova***, V.A. Shults***, R.Yu. Bogidaev***, L.V. Spakhova***

*Institute for Problems of Chemical Physics RAS,
JSC "Chemphyst-Splav", Chernogolovka, Russia
**"Moscow Special Alloys Processing Plant", Moscow, Russia
***JSC "Acron", V.Novgorod, Russia

We proposed a new geometric structure for platinoid woven gauze catalysts of oxidizing ammonia conversion in nitric acid production technology. A main difference of the proposed catalytic gauze in comparison with traditional one is using of a rectangular woven cell instead of the conventional square one. Realized up to now pilot tests confirmed the theoretical predicted advantages of the new catalytic gauze type. The catalytic materials have a highest competitive market potential because:

- decreasing of platinum mass in catalytic reactor packet by 20-50 %;
- decreasing of ammonia losses in conversion process by 1,5-2 times;
- decreasing of platinum losses by 15-20 %.

We have started industrial production of the catalysts.

The developed platinoid catalytic gauze is protected by patent:

Russian patent No 2212272, 20.09.2003, Bull. No 6;

International application No PCT/RU03/00527, 08.12.03

MEASUREMENT OF TIME CONSTANT FOR OXYGEN ELECTRODE

S. Bashir, E. Edreder

Petroleum Research Centre, Tripoli, Libya

Mass transfer coefficient has been estimated by many different methods, the physical method is one of them. The principle of this method is to measure the change of the yield of gas solved in liquid with respect to time in the oxygen electrode, the gas was transferred into the membrane which is inside of the electrode, therefore the error for measuring device has been formed, this error explained by the diffusion of gas into the liquid more rapid than to the membrane. Most of the research which has been reported in the literature weren't carried out this state, and also were not advert it. Therefore the objective of this work is to find the mechanism how to evaluate the time constant and the relationship between the measured value CE for the oxygen electrode and the real value CL has been derived. Experimental setup has been constructed to perform this work and the numerical results were fitted with the measuring values to estimate the time constant. From the experimental data we can be seen that the difference between the measured values CE and the real values CL until the 30 sec after that the measured and real values are the same.

PREPARATION AND STABILITY OF COATED CERAMIC MONOLITHS FOR HYDROGEN PRODUCTION BY STEAM REFORMING OF ETHANOL

Albert Casanovas, Jordi Llorca

Institut de Tècniques Energètiques, Universitat Politècnica de Catalunya

Av. Diagonal 647, Ed. ETSEIB, 08028 Barcelona, SPAIN

Fax : (0034)934017149   E-mail : jordi.llorca@upc.edu

Introduction

Our current energy model, based mainly on fossil fuels and combustion processes, will be no longer sustainable. Hydrogen has been proposed as a possible energy carrier between renewable energy sources and applications[1]. However, apart from the development of technologies that transform the chemical energy of hydrogen, like fuel cells, it is necessary to produce hydrogen in an efficient, clean, cheap and safe way.

Bio-fuels appear as an alternative to fossil fuels for hydrogen production. Among them, bio-ethanol offer several advantages. When obtained from biomass sources, ethanol can be considered as a renewable fuel; it is liquid, safe, easy to manipulate and has a high H/C ratio, yielding up to 6 mol of hydrogen per mol of ethanol consumed in steam reforming processes (1).

$$CH_3CH_2OH + 3\ H_2O \rightarrow 6\ H_2 + 2\ CO_2 \qquad \Delta H = 173\ kJ \cdot mol^{-1} \qquad (1)$$

Different materials have been proposed as catalysts for the ethanol steam reforming reaction. Commonly these materials are metals supported on high surface area inorganic oxides (M/oxide). Several studies demonstrate the influence of both the metal and oxide phases, depending on their nature and properties. It is known that a redox exchange between M^0 and $M^{\delta+}$ species are required for the metallic phase to be active, and that strong redox properties of the oxide are also advantageous. This is the case, for example, for ZnO-supported cobalt catalysts which exhibit good catalytic performance for ethanol steam reforming reaction at moderate temperature[2-4]. These systems have been tested in powder form, like different supported catalysts based on Ni, Cu, Rh, Pd, etc.[5-8]. However, for practical applications, these catalysts must be deposited or anchored on structured supports, like pellets or monoliths[9-10], in order to obtain good structural and thermal stability. In this

work, ceramic monoliths of 400 cells per square inch are used as a structured support and are loaded with zinc oxide and Co/ZnO catalyst. Different tests are carried out in order to evaluate thermal and mechanical stability of the resulting monolithic catalysts, which are also characterized with various techniques.

Previous catalytic results with powders

Several catalytic tests were performed over the Co/ZnO catalyst at atmospheric pressure in the temperature range 548-723 K. A constant ethanol vapour flow of 0.5 mL·min^{-1} and different H_2O/EtOH molar ratios (between 3 and 13) were used. Furthermore, an air flow inlet was used to evaluate oxidative steam reforming of ethanol (2) with different O_2/EtOH molar ratios (up to 0.5). Temperature was controlled by a thermocouple inside the catalyst bed.

$$CH_3CH_2OH + \tfrac{1}{2} O_2 + 2 H_2O \rightarrow 5 H_2 + 2 CO_2 \qquad \Delta H = - 50 \text{ kJ·mol}^{-1} \qquad (2)$$

Although it is demonstrated that temperature, space velocity, and different H_2O/EtOH and O_2/EtOH ratios in the reactant mixture influence catalytic performance, Co/ZnO catalyst exhibits high activity and selectivity towards H_2 under the different conditions tested. For example, at the reaction temperature of 673 K, the hydrogen yield is between 5 and 6 mol of hydrogen per mol of ethanol introduced under steam reforming conditions, and around 4.5 mol of hydrogen under oxidative steam reforming at low water contents.

Functionalized ceramic monoliths

Ceramic 400 cpsi monoliths were coated with ZnO and Co/ZnO by different methods:

a) Washcoating: Co/ZnO (10% w/w) powder catalyst was first prepared by incipient wetness impregnation using cobalt nitrate as precursor. Solid was dried at 373 K overnight and calcined in air at 673 K for 6 h. Monoliths were dipped several times in a dense suspension of ZnO or Co/ZnO in de-ionized water. After each immersion monoliths were dried with continuous rotation and calcined at 673 K. At the end of the washcoating process the resulting monolith was reduced under H_2 flow at 673 K.

b) In-situ precipitation: Monoliths were exposed under rotation to a solution with nitrate metal salts, and the precipitating agent, urea. The temperature of the solution was increased to decompose urea (3), which resulted in a pH increase and the deposition of precursors inside the monolith channels (4).

$$CO(NH_2)_2 + 3 H_2O \rightarrow CO_2 + 2 NH_4^+ + 2 OH^- \qquad (3)$$

$$M^{2+} + 2 OH^- \rightarrow M(OH)_2 \qquad (4)$$

PP-6

After that, monoliths were dried, calcined in air at 673 K and reduced under H_2 flow at 673 K.

Stability of monolithic catalysts

Stability tests over the monolithic catalysts are currently being developed under the experimental conditions tested for the powder Co/ZnO sample in order to examine possible technological applications of these catalysts for the production of hydrogen from ethanol steam reforming processes. To evaluate thermal stability, the functionalized monoliths are exposed to different vapour treatments with H_2O, $EtOH+H_2O$ (ethanol steam reforming) and $EtOH+H_2O+O_2$ (ethanol oxidative steam reforming) at various temperatures between 573 and 873 K. Functionalized monoliths have also been subjected to thermal cycles to simulate continuous switch on and shut down of the reformer.

In order to evaluate mechanical stability, vibration tests are conducted by ultrasound exposure with monoliths immersed in ethanol or water.

In all cases, weight loss is monitored. In addition, scanning electron microscopy (SEM) is used to study in detail the morphology of the monolithic catalysts, both as prepared and after the stability tests. Electron probe for microanalysis (EPMA) is used to analyze catalyst composition inside the monolith channels.

Acknowledgments

References

[1] J.N. Armor, Applied Catalysis A: General, 176 (**1999**) 159.

[2] J. Llorca, N. Homs, J. Sales and P. Ramírez de la Piscina, Journal of Catalysis, 209 (**2002**) 306.

[3] J. Llorca, P. Ramírez de la Piscina, J.A. Dalmon, J. Sales and N. Homs, Applied Catalysis B: Environmental, 43 (**2003**) 355.

[4] J. Llorca, N. Homs, J. Sales, J.L.G. Fierro and P. Ramírez de la Piscina, Journal of Catalysis, 222 (**2004**) 470.

[5] V. Klouz, V. Fierro, P. Denton, H. Katz, J.P. Lisse, S. Bouvot-Mauduit and C. Mirodatos, Journal of Power Sources, 105 (**2002**) 26.

[6] G.A. Deluga, J.R. Salge, L.D. Schmidt and X.E. Verykios, Science, 303 (**2004**) 993.

[7] C. Diagne, H. Idriss and A. Kienemann, Catalysis Communications, 3 (**2002**) 565.

[8] M.A. Goula, S.K. Kontou and P.E. Tsiakaras, Applied Catalysis B: Environmental, 49 (**2004**) 135.

[9] D.K. Liguras, K. Goundani, X.E. Verykios, International Journal of Hydrogen Energy, 29 (**2004**) 419.

[10] D.K. Liguras, K. Goundani, X.E. Verykios, Journal of Power Sources, 130 (**2004**) 30.

EXPERIMENTAL STUDY OF TURBULENT REGIMES
IN FLUIDIZED BED OF MICROSPHERICAL CATALYST

V.A. Chumachenko, V.N. Kashkin, A.S. Samarina*

Boreskov Institute of Catalysis SB RAS, address: pr. Akademika Lavrentieva, 5, Novosibirsk, 630090, Russia; e-mail: vachum@catalysis.ru, fax: +7 383 3306878

*JSC Katalizator, Tikhaya St. 1, 630058 Novosibirsk, Russia

Introduction

Dehydrogenation of low alcanes C_4-C_5 in fluidized beds of catalyst is the main stage of production of many synthetic rubbers monomers and MTBE. Large capacity industrial facility comprise reactor-regenerator unit with some hundred tons of microspherical catalyst which is circulating between reactor and regenerator. For better quality of fluidization, both vessels are equipped with several rows of horizontal grids. Hydrodynamic regimes of fluidization play a key role in reactor performance, being strongly depended on physical properties and particle size distribution. In some cases, gas-particle interaction [1] may seriously affect gas-solid contacting and transport processes.

The comparative study of fluidization regimes of 2 commercial dehydrogenation catalysts was performed at the lab-scale setup.

Experimental procedure

A sketch of experimental setup is shown in **Fig.1**. It consists of 6-m long vertical column, 0.15 m ID equipped with 1.8-m long transparent glass lower section, followed by stainless steel upper section and a particle wide separator at the top. At the outlet of column gas enters into the battery of cyclones that was installed to ensure separating of entrained fine solids from the gas. Particles captured by the cyclones were returned back through the discharging tube to the bottom of column.
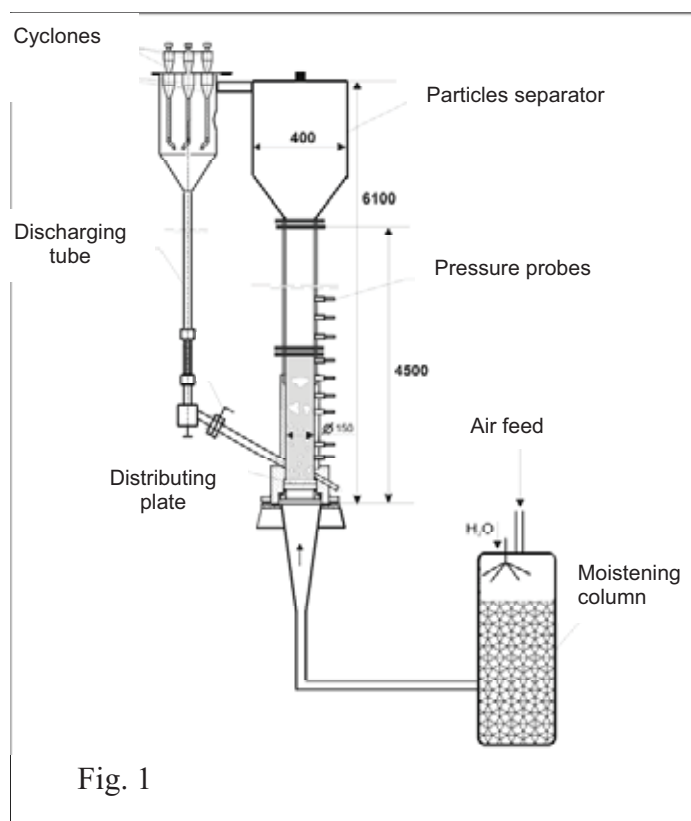
Fig. 1

PP-7

Ports with pressure probes were mounted every 50 mm along the column height. Differential pressure fluctuations were measured between ports located at various distances. Absolute pressure fluctuations were measured at heights of 0.16, 0.41, 0.715 and 0.915 m above distribution plate. Low-inertial differential pressure sensors *Motorola* MPX 2010DP and 2050DP were used for both absolute and differential measurements. In each run pressure fluctuations were detected at a frequency 100 Hz during 40 sec. Electric signals from the pressure probes were transformed and recorded by computer controlled device. To ensure more statistical validity of information, experiments at a given gas velocity were repeated up to 20 times. Then the average values of the pressure drop in the bed at given conditions, and its standard (mean square) deviations were fixed.

Experiments were made at ambient temperature and pressure. To reduce static charge, air supplied to the setup was humidified to 70-80% in a separate moistening column. The following parameters of fluidization of various catalysts were determined in the course of experimental studies:

- gas velocity demarcating the transition from bubbling to turbulent fluidization;
- apparent bulk density along the bed height;
- relative expansion of the bed;
- effect of horizontal grids on the quality of fluidization.

Specifications of commercial C_4-C_5 dehydrogenation catalysts are shown in the Table 1.

Table 1

Size, % wt.	Catalyst IM	Catalyst AOK	Catalyst AOK 80/20	Catalyst AOK 70/30
1	*2*	*3*	*4*	*5*
< 63 mcm	8.3	-		
63-71 mcm	4.2	1.4	12.6 (< 63)	17.9 (< 63)
71-90 mcm	7.5	5.6	9.0	10.7
90-160 mcm	37.7	77.1	78.4 (>90)	71.4 (>90)
> 160 mcm	42.3	16.0		
Bulk density, kg/m^3	1400	1312	1328	1332

Results and discussion

At the *first stage* of experimental runs hydrodynamic properties of catalysts IM-2201 and AOK-73-21 were compared under the following conditions:

Table 2

Nomenclature	Catalyst IM	Catalyst AOK	Catalysts AOK modif.
1	*2*	*3*	*4*
Packed bed height, m	0.94	0.73	0.66-0.76
Range of gas velocities, m/s (S.T.P.)	0.2-1.4	0.2-1.4	0.2-1/2
Relative humidity of air, %	60	65	65
Pressure in the column, kg/cm^2	1-1.2	1-1.2	1-1/2
Minimum fluidization velocity, m/s	0.013	0.02	
Bulk density at minimum fluidization velocity, kg/m^3	897	1084	1103
Points of measuring the pressure fluctuations above distributor, m	0.16-0.915 0.41-0.915	0.16-0.715 0.41-0.715	0.36-0.715

Relative expansion of the bed depending on superstitial gas velocity is rather similar for both catalysts, in spite of different size distribution and bulk density, see **Fig.2**.
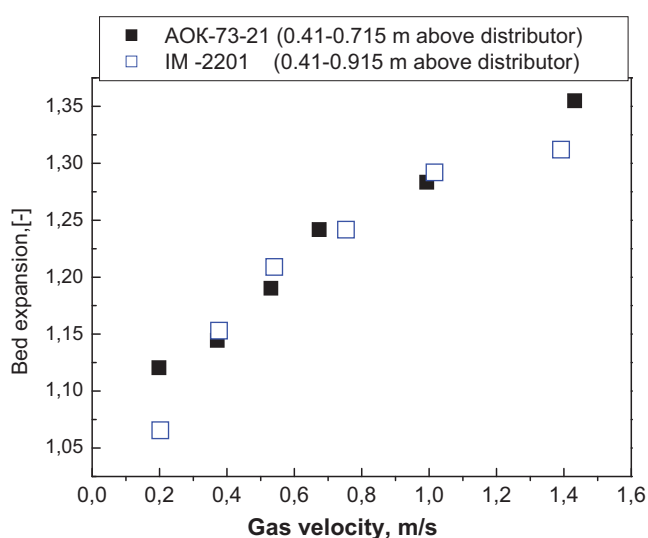
Fig. 2
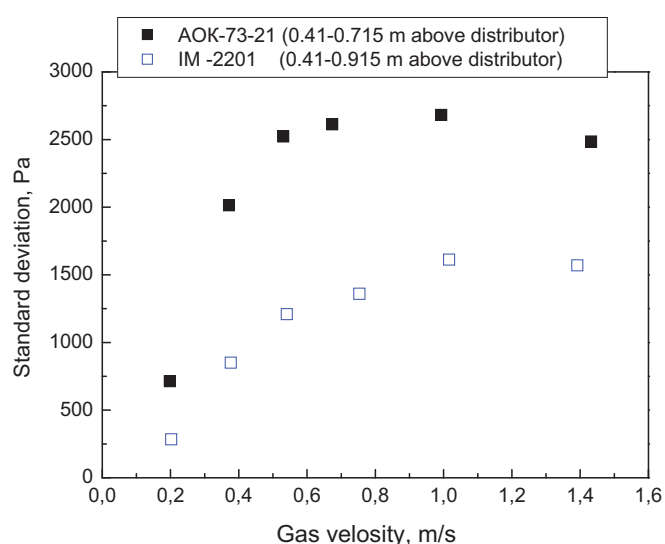
Fig. 3

The transition from bubbling to turbulent regime in the terms of gas velocity can be identified when a maximum value of the standard deviation (SD) of pressure fluctuation is reached. Standard deviation can be regarded as a qualitative measure of fluidization uniformity of various particles: the less SD, the smoother fluidization occurs.

As shown in **Fig.3**, for both catalysts SD reaches its maximum within 0.8-1.0 m/s, although its value is larger for catalyst AOK, as a consequence of larger average particles sizes, narrow size distribution, and larger bubbles in the bed. Catalyst efficiency in fluidized bed strongly depends on mass exchange between bubbles and dense phase, so that it seems reasonable to increase it by adding a definite fraction of fine particles to existing catalyst.

PP-7

At the *second stage* of experiments three modifications of catalyst AOK distinguished by various size distribution were tested: initial catalyst AOK, mixture of AOK with 20 % wt. of small fines <60 mcm (AOK 80/20), and mixture of AOK with 30 % wt. of small fines <60 mcm (AOK 70/30), see Table 1. Experimental conditions are shown in Table 2.

Standard deviation of pressure fluctuations (see **Fig.4**) is rather close for all 3 catalysts at gas velocities <0.5 m/s. At higher velocities SD for catalysts AOK 80/20 and AOK 70/30 is 15-20% less than that for initial AOK. This may be explained by smaller size bubble formation, due to a greater fraction of small particles in these mixtures. In the total range of velocities there was found no significant difference in SD between catalysts AOK 80/20 and AOK 70/30, while they approach to catalyst IM.
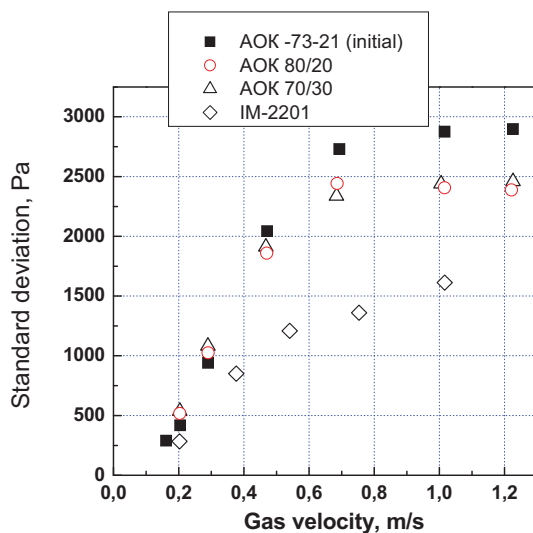
Fig.4
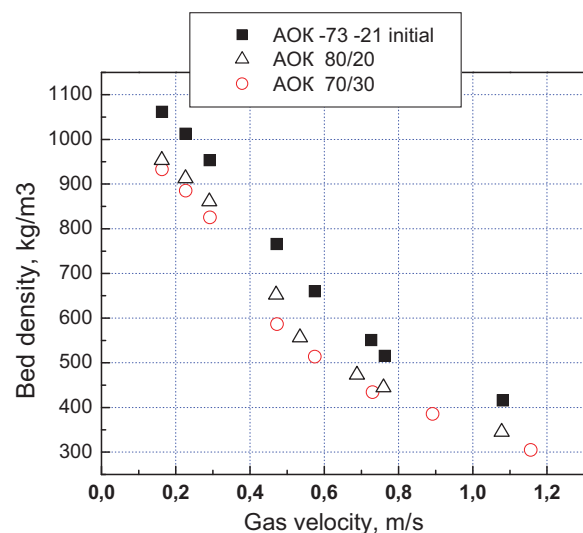
Fig. 5

In the *third series* of experiments the effect of multi-sectioned grid on apparent bed density (see **Fig.5**) and bed expansion of 3 catalysts AOK was studied. At gas velocities >0.5 m/s relative expansion of a sectioned bed is 2-3 times higher, standard deviation of pressure fluctuations is 5-10 times less compared to a freely bubbling bed. Transition to the turbulent regime in sectioned bed occurs at lower velocity, maximum SD shifts from 1.0 to 0.3 m/s. Fluidization regimes of catalysts AOK 80/20 and 70/30 are just without distinctions, while they remarkably differ from initial AOK.

References

1. Jie Li, J.A.M.Kuipers. *Chemical Engineering Science*, 58 (2003), 711-718.

KINETICS OF PHENOL OXIDATION OVER HYPERCROSSLINKED POLYSTERENE IMPREGNATED WITH Pt NANOPARTICALS

Doluda V., Sulman E., Matveeva V., Sulman M., Lakina N., Sidorov A., Valetskiy P., Bronstein L.

Biotechnology and Chemistry Department, Tver State Technical University, A. Nikitina str., 22, Tver, 170026, Russia. Tel./ Fax: 7 0822 449317. E-mail sulman@online.tver.ru.

Nowadays there is a large amount of phenols in the noosphere, hence, novel technologies based on the conversion of phenols to non-hazardous or useful substances should be developed and implemented at industrial scale. Catalytic wet air oxidation (CWAO) of phenols compounds are the most significant methods for wastewater treatment. A great challenge for solving problem of phenol compounds waste water treatment is to design a highly selective catalyst comprising of an active site with the correct ensemble of metal atoms and other active components[1-3]. The advantages of a nanocatalyst prepared in organic functional polymers are not only the "nanoscale" size control of metal crystallites, but also the easy tailoring via variation of the polymer nature[4-5]. Nanostructures in a polymeric composite are defined as regular nanosized heterogeneous domains (i.e., certain regions of the polymeric material that are separated by some interface)[6,7]. Due to the presence of nanostructures one can control the growth of nanoparticles, the particle size distribution and interfacial interactions and control phenol wastewater treatment rate. The main goal of our research work was investigation of efficient catalyst and study of it's kinetics for waste waters treatment.

Synthesis of the catalyst for CWAO

Platinum nanoparticle formation in cavities (pores) of a polymer matrix was carried out with hypercrosslinked polystyrene (HPS). The controlled growth of metal nanoparticles in a polymer matrix is possible if it occurs in cavities or pores. In this case, the size of the growing particles can be limited to the cavity size. HPS is the representative of cross-linked polymers that gives the possibility for nanoparticle growth control. In this study we investigate HPS purchased from Purolite inc. (MN-270) as organic support. Synthesis of Pt catalysts was performed the following way. First step is dissolving of platonic acid $H_2[PtCl_6]$ in complex solvent ($H_2O/THF/CH_3OH = 1/4/1$), then follows solubilization of salt solution by HPS

PP-8

matrix and stirring of HPS suspension for two hours. Then follows drying of the catalyst (t=60^{0}C, 0,5 atm) and reduction of the catalyst with different types of reducing agents (N_2H_4, $NaBH_4$, H_2). And the last step is catalyst drying (T=60^{0}C)

Oxidation of the phenol

Phenol oxidation is carried out in laboratory set up shown in fig. 1.

1 - reactor,
2 - reverse refrigerator,
3 - burette hydrogen peoxide,
4 - oxygen cylinder,
5 - magnetic stirrer,
6 - laboratorial transformer,
7 - rotameter,
8 - pH-meter,
9 - electrodes,
10- automatical titration block,
11 - electromagnetic valve
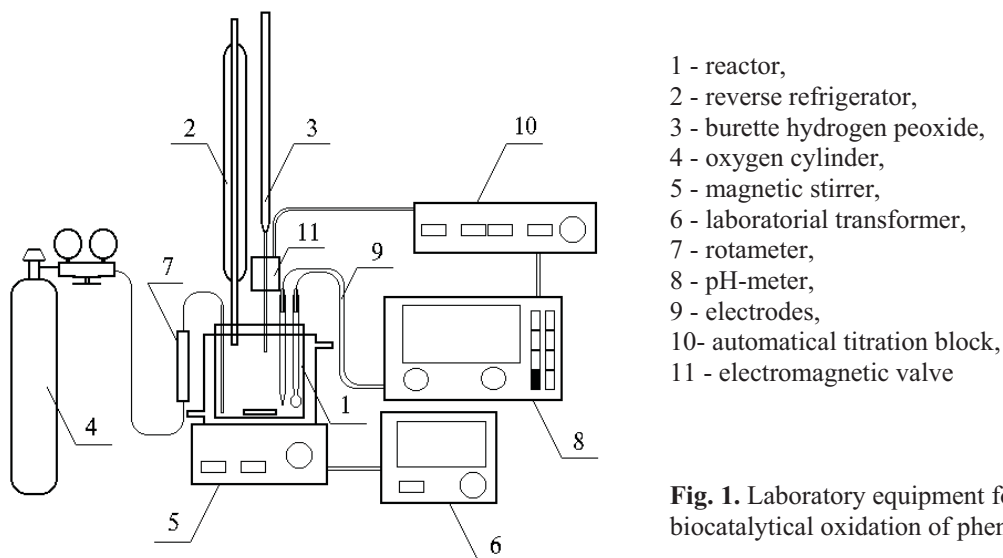
Fig. 1. Laboratory equipment for catalytical and biocatalytical oxidation of phenol compounds.

Kinetics of phenol oxidation

For investigation of CWAO kinetics we used phenol as a main pollutant from the phenol compounds. Reaction that is proposed for CWAO is shown in fig. 2.
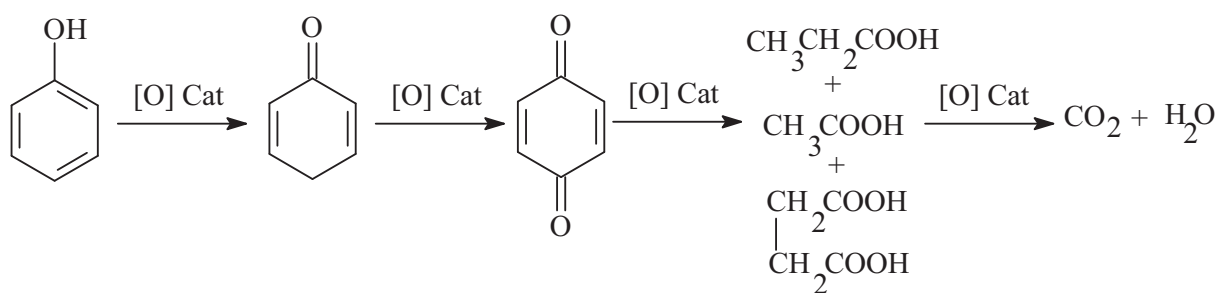
Fig. 2. Wet air oxidation of the phenol

For finding optimal conditions of phenol CWAO we varied following parameters: temperature, catalyst concentration, oxygen flow rate and phenol concentration. On fig. 3 it is possible to see increasing of phenol conversion with increasing of temperature. CWAO oxidation of phenol is characterized with low activation energy level compare to non-catalytic oxidation Fig. 4.
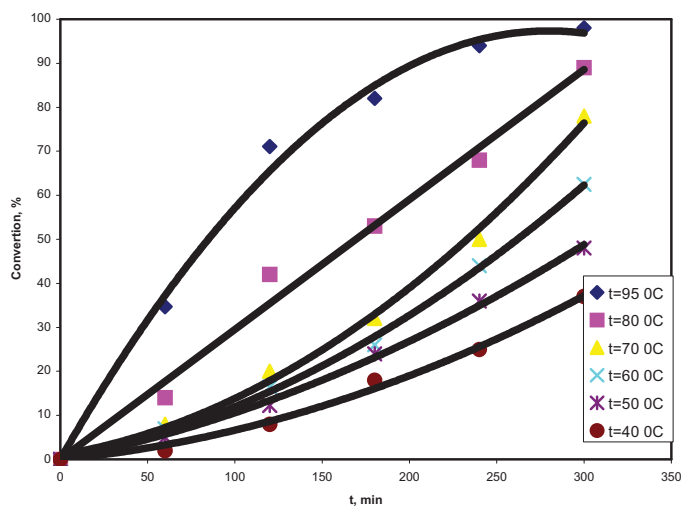
Fig. 3. Kinetics curves of phenol oxidation with temperature variation 40-95^{0}C. Catalyst -HPS-5,9%-Pt, m(Cat)=0,1g, C(Phenol)=20 g/l, V(Phenol)=25 ml, P(O$_2$)=1 bar, W=400 1/c, W (O$_2$)=8 ml/sec
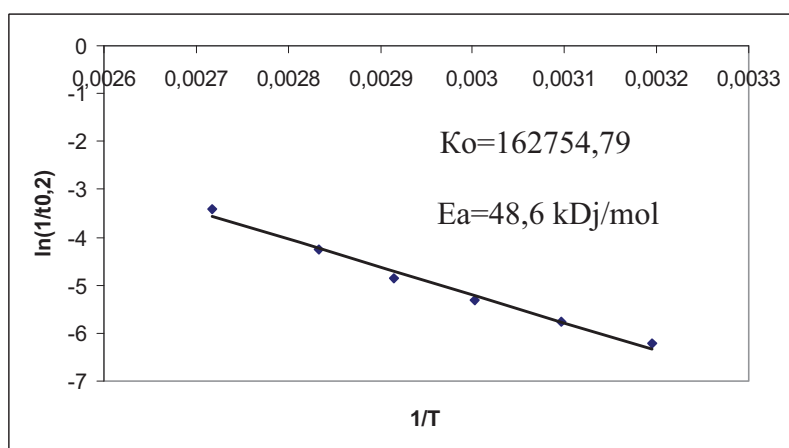
Activation energy equation. Catalyst -HPS-5,9%-Pt, m(Cat)=0,1g, C(Phenol)=20 g/l, V(Phenol)=25 ml, P(O$_2$)=1 bar, W=400 1/c, W (O$_2$)=8 ml/sec

CWAO treatment of phenol compounds leads to full (concentration of left phenol compound is less then 5 ppb) conversion in non-hazardous substances. Implementation of the results can present a new attractive possibility to decrease the phenol content of industrial wastewaters. The successful development of novel, inexpensive should lead to their use by phenol producing plants.

References

1] Bronstein, L.M.; Goerigk, G.; Kostylev, M. Pink, M.; Khotina, I.A.; Valetsky, P.M.; Matveeva, V.G.; Sulman, at. Al*J. Phys. Chem. B* (2004), 108(47), 18234-18242.

2] Okhapkin I.M., Bronstein L.M., Makhaeva E.E., Matveeva V.G., Sulman M.G., Sulman E.M., Khokhlov A.R. Macromolecules (2004), 37, 7879-7883

4] Sulman, E., Matveeva, V., Bronstein, L., Sidorov, A., Lakina, N., Sidorov, S., Valetsky, P. *Green Chemistry* 2003, 5(2), 205-208.

5] Matveeva V.G., Sulman E.M., Sulman M.G. Catalytic oxidation of *Catalysis in Industry* 2002, 5, 50-60. – *In Russian*.

6] Sulman E.M., Semagina N.V., Matveeva V.G. Bulletin of the Tver State Technical University, 2002, 1, 28-31. – In Russian.

7] *Sulman E.M., Valetsky P.M., Bronstein L.M., Lakina N.V., Matveeva V.G., Sidorov S.N., Chernyshov D.M., Ankudinova T.V., Kirsanov A.T., Sidorov A.I., Sulman M.G. Patent № 2185369 Priority at 02.04.2001. (Russia)*

THE EFFECT OF GROWTH REGULATORS AND CHEMICAL MODIFICATION ON CHLOROPLAST FERREDOXIN-NADP REDUCTASE OF CHENOPODIUM ALBUM

El-Shora H.M.

Botany Department, Faculty of Science, Mansoura University, Mansoura, Egypt

Chloroplast ferredoxine-NADP reductase from Chenopodium album was investigated under the effect of four growth regulators namely kinetin, gibberellic acid (GA3), 6-benzyladenine and 2,4-D. These regulators were investigated at 5×10^{-4} M, 2×10^{-4} M and 10^{-3} M. The four compounds induced the enzyme activity in leaves particularly at 5×10^{-4} M. Gibberellic acid was the strongest stimulator. This stimulation was corroborated in the leaves by inhibition of the enzyme activity with 10 mM b-chloroethyltrimethylammonium (CETA), and the reconstitution of the enzyme activity when GA3 was added with CETA. The enzyme activity was inhibited by cycloheximide, actinomycin D, and methylpurine and this suggests that protein synthesis is involved in the enzyme induction. Chemical modifications of the enzyme with N,N-dicyclohexylcarbodi-imide (DCCD), citraconic anhydride (CAN) and N-bromosuccinimide (NBS), which are respective chemical modifiers of carboxylic, lysine and tryptophan residues, were examined. Incubation of the enzyme with increasing concentration of each tested modifier resulted in a progressive decrease in enzyme activity. Kinetics data for the inactivation demonstrated that each of carboxyl, lysine and tryptophan residues is essential for catalytic activity of the enzyme. The protective effect of NADP against the inactivation by the three compounds suggests that functional carboxyl, lysine and tryptophan residues are located in the active site.

DEVELOPMENT OF AN ACTIVE Pt BASED CATALYST FOR H$_2$ PRODUCTION BY HYDROLYSIS OF NaBH$_4$

Ersoz Y., Yildirim R., <u>Akin A.N.</u>

Kocaeli University, Department of Chemical Engineering, Kocaeli, Turkey

Bogazici University, Department of Chemical Engineering, Istanbul, Turkey

Introduction

In the future, hydrogen is to become a major source of energy. In the search for efficient, clean and safe energy resource, hydrogen draws attention with its advantages such as high energy density (142 kj/g) and electronegative properties. Recently, the use of hydrogen is applied to various industries and will be used more and more if the research and development of it is continued. Hydrogen production and storage technologies are developed parallel to the developments in fuel cell technologies. Especially, PEM fuel cells are attractive and alternative options for producing clean energy by using hydrogen as fuel. Hydrogen needed for PEM fuel cell can be stored somewhere or produced from a source on demand. However, the currently used hydrogen is mostly produced from natural gas via catalytic reforming, which produces a mixture of H$_2$, H$_2$O, N$_2$, CO$_2$, and CO [1,2]. The performances of PEM fuel cell are sensitive to the concentration of carbon monoxide in hydrogen. Even a few parts per million CO can cause the catalyst poisoning in PEM fuel cell [2]. Therefore, a fast and clean hydrogen supply method is required, especially for a mobile PEM fuel cell. At this point a chemical hydrate sodium borohydrate is seen as a safe and portable alternative route because it is stable under ordinary conditions and liberates pure H$_2$ in a safe and controllable way [3]. NaBH$_4$ contains 10.8%wt hydrogen. In the presence of a selected catalyst, hydrolysis reaction of NaBH$_4$ solution gives 4 moles of H$_2$ and the half of the produced hydrogen comes from water. The by-product NaBO$_2$ does no harm to the environment, and can be recycled as the raw material for producing NaBH$_4$ [2,3]. Thus, the hydrolysis reaction of NaBH$_4$ is an environmentally friendly and renewable process. It is a zero order reaction and without a catalyst the reaction is very slow (half life is about 430 days in pH=14 and 25 °C) [4]. Therefore, development of an effective catalyst is the focal point of the researches in the literature.

Various type of catalysts are being used by different researchers such as metal halides (NiCl$_2$, CoCl$_2$), colloidal platinum, Co and Ni boride, active carbon, Raney nickel, Ru

supported on ion exchange resin beads, and uorinated particles of Mg-based material [3-8]. Pt-LiCoO$_2$ (among the others) was found to work as an excellent catalyst for releasing hydrogen by hydrolysis of NaBH$_4$ solution [5]. In all these studies, Pt-LiCoO$_2$ catalysts were prepared by impregnation of Pt precursor on commercial LiCoO$_2$ support material.

The aim of this study is to develop of an effective Pt/LiCoO$_2$ catalyst by investigating the preparation conditions of support material. LiCoO$_2$ as catalyst support material was prepared by solid state reaction of lithium and cobalt precursors and effects of preparation parameters on catalyst activity and hydrogen production rate in the hydrolysis reaction were determined. Effects of hydrolysis reaction parameters on hydrogen production rate were also investigated.

Experimental

In this study 1.5% Pt/LiCoO$_2$ catalysts were prepared and their activities were tested in hydrolysis reaction of NaBH$_4$. LiCoO$_2$ was prepared as support material by solid state reaction of Li$_2$O and Co(NO$_3$)$_2$.6H$_2$O. Commercial LiCoO$_2$ was also used for comparison. Pt impregnation on LiCoO$_2$ was done by incipient to wetness impregnation method. In solid state reaction method, Li$_2$O, Co(NO$_3$)$_2$.6H$_2$O precursors and heat generating material were mixed in appropriate amounts and heated in a muffle furnace [6]. Amount of reactants, existence and type of the heat generating material and calcination temperature were chosen as preparation parameters. Prepared catalysts characterized by different methods. The total surface areas and the total pore volumes were determined by N$_2$ adsorption from N$_2$-He mixtures using a multipoint technique together with the BET equation and by the N$_2$ adsorption-desorption method, respectively. XRD analysis were performed to determine the catalyst structure. The activities of catalysts in hydrolysis of NaBH$_4$ were measured in a semi-batch jacketed reactor at atmospheric pressure and room temperature.

Results

LiCoO$_2$ as catalyst support material was prepared by solid state reaction of lithium and cobalt precursors and effects of preparation parameters on catalyst activity and hydrogen production rate in the hydrolysis reaction were determined. The results were discussed in terms of preparation conditions. Amount of reactants, existence and type of the heat generating material and calcination temperature were preparation parameters. The amount and type of heat generating material was found as an important parameter. Equal amount of heat generating material to the reactants was determined as optimum amount and using 1 ml of water in the mixture of solid materials improves the mixing quality, however does not affect hydrogen production rate so much. Catalysts prepared by using NH$_4$NO$_3$ as heat generating material, compare to urea, gives higher hydrogen production rates. Calcination procedures

with wide temperature ranges were investigated and 500-600 °C were found as ideal calcination temperatures. Type of Pt precursor was also investigated. $Pt(NH_3)_4^.(NO_3)_2$ gave better results. Effect of addition of Pt precursor in the preparation of solid mixing rather than impregnation was also investigated. Hydrogen production rate measured by using the catalyst prepared by solid state reaction showed a different profile. It was slow at the beginning and accelerated by time. However, all the other catalysts prepared by impregnation gave similar H_2 production profiles which have high acceleration rate at the beginning and then remain constant. According to the results of the catalyst development studies catalysts prepared by impregnation Pt on $LiCoO_2$ prepared by solid state reaction gave the highest H_2 production rate comparing to the catalyst prepared by commercial $LiCoO_2$ studied both in our work and literature [2,5,7]. In this study, effects of hydrolysis reaction parameters on hydrogen production rate were also investigated. The parameters studied were concentrations $NaBH_4$ and NaOH solutions, reaction temperature and catalyst amount. Results showed that: Decreasing concentrations of $NaBH_4$ and NaOH solutions increased H_2 production rate. Increasing reaction temperature and catalyst amount was also increased the rate as expected.

References

(1) Amor J.N., Applied Catalysis 176, p.169. 1999

(2) Chuan Wu ., Huaming Zhang, Baolian Yi, Catalysis Today 93–95 p. 477–483, 2004

(3) Amendola S.C., Sharp-Goldman S.L., Janjua M.S., Spencer N.C., Kelly M.T., Petillo P.Jbinder. M., Int. J. Hydrogen Energy 25, p. 969, 2000

(4) Amendola S.C., Sharp-Goldman S.L., Janjua M.S., Kelly M.T., Petillo P.J. and Binder M. J. Power Sources 85, p. 186, 2000

(5) Kojima Y., Suzuki K., Fukumoto K., Sasaki M., Yamamoto T., Kawai Y. and HAYASHI H., Int. J. Hydrogen Energy 27, p. 1029, 2002

(6) S. Suda, Y.M. Sun, B.H. Liu, Y. Zhou, S. Morimitsu, K. Aral, N. Tskamoto, M. Uchida, Y. Caudra, Z.P. Li, Appl. Phys. A 72, 209. 2001

(7) Kojima Y., Kawai Y., Nakanishi H., Matsumoto S., J. Power Sources 135, p.36, 2004.

(8) Kaufman C.M., Sen B., J. Chem. Soc., Dalton Trans. p.307 1985 .

CATALYTIC PERFORMANCE OF Au-TiO$_2$ CATALYSTS PREPARED BY DEPOSITION-PRECIPITATION FOR CO PREFERENTIAL OXIDATION IN H$_2$-RICH GASES

C. Galletti, S. Fiorot, S. Specchia, G. Saracco and V. Specchia

Dipartimento di Scienza dei Materiali e Ingegneria Chimica, Politecnico di Torino – Corso Duca degli Abruzzi 24, 10129 Torino, Italy – fax. +390115644699 –

camilla.galletti@polito.it

The use of PEM fuel cells as a power source for electrically operated vehicles is currently of major interest due to their ability to produce virtually no pollutants. The H$_2$ fuel gas for the PEM fuel cell is required to be "nearly CO free" as the platinum fuel cell anodes are poisoned by traces of CO. H$_2$ rich gas produced by catalytic steam reforming of fossil fuels, followed by water gas shift reaction, requires the final catalytic selective CO oxidation to remove CO content. Selective oxidation of CO to CO$_2$ (CO-PROX) is carried out to reduce the CO content of the reformate gas to a concentration not higher of 10 ppm [1, 2].

The main goal is the study of suitable catalysts for the CO-PROX reaction.

Until the end of the 1980s, only very limited attention has been paid to catalysis with gold metal because of its electronic configuration of noble metal, which is usually accompanied by very low activities [3]. This situation changed in recent years with the discovery of the catalytic activity of gold nanoparticles [4]. Remarkable catalytic properties of supported gold were first obtained for the reaction of CO preferential oxidation at sub-ambient temperature by Haruta et al. [5]. The most studied catalyst for preferential CO oxidation is gold supported on TiO$_2$ because it is one of the most active catalysts for this reaction at low temperature, and it may allow to operate at temperatures compatible with those of PEM fuel cell (80-100°C). The optimum gold particle size in these catalysts was found to be 2–3 nm [6-8]. Such particle sizes can be achieved owing to suitable preparation methods and a careful control of the running conditions during preparation.

Up to now, for the preparation of Au-TiO$_2$ catalysts, the best method was the deposition-precipitation with NaOH [9], particularly because it allowed the size of the gold particles to be adjusted towards very small values by controlling the pH during the preparation.

In this work, Au-TiO$_2$ catalysts were prepared by means of deposition-precipitation method, with NaOH, varying pH and some other parameters in the preparation procedure.

Titania prepared in our laboratory by gel combustion method was used as support and solid HAuCl$_4$*3H$_2$O (Sigma-Aldrich) as Au precursor. The gold load on TiO$_2$ was 2 wt%.

Two different methods were used. In the first one, an aqueous solution of HAuCl$_4$ (4.2*10^{-3} M) was adjusted to pH = 10.4 by drop wise addition of NaOH, then a suitable amount of TiO$_2$ particles was dispersed in the solution which was then heated to 70°C and in the same time the pH lowered till 8.6. Then the solution was filtered and the separated particles washed with H$_2$O.

With the second method an aqueous solution of HAuCl$_4$ (4.2*10^{-3} M) was firstly heated up to 80°C, then its pH was adjusted to 7 by drop wise addition of NaOH (1 M). A suitable amount of TiO$_2$ was dispersed in the solution and the pH was readjusted to 7 with NaOH. The suspension thermostated at 80°C was vigorously stirred for 2 h, then filtered and the separated particles washed with H$_2$O. After preparation, all the Au-TiO$_2$ catalysts were calcined in air at 200 and 300°C for 2 hours and therefore characterized by means of XRD, SEM and TEM analyses.

Catalytic activity tests were carried out on catalysts in powder: a suitable amount of catalyst was placed in a fixed bed tubular micro-reactor, heated up by a PID regulated oven, and the feed gas was set at a composition similar to that of a reformate gas: 37%vol H$_2$, 5%vol H$_2$O, 18%vol CO$_2$, 1%vol CO, 2%vol O$_2$ and He as balance. The λ value ($\lambda = 2O_2/CO$) was fixed equal to 4. The outlet gas stream was analyzed through a gas chromatograph equipped with a thermal conductivity detector (TCD); CO and O$_2$ conversions and O$_2$ selectivity toward CO oxidation were determined in the 40°C-180°C temperature range.

A first comparison was performed on catalysts prepared through the first method and calcined at 200 and 300°C (2% Au-TiO$_2$-1-200, 2% Au-TiO$_2$-1-300) feeding 100 ml/min of synthetic reformate gas; the obtained results are shown in Fig. 1.
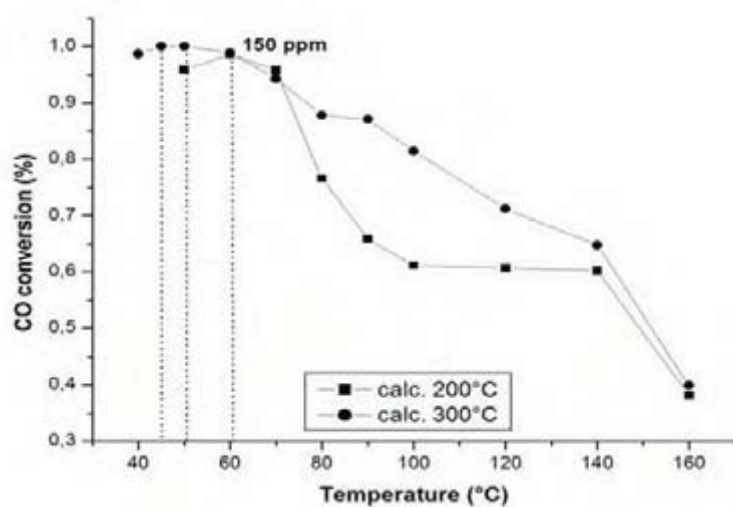
Fig. 1: CO conversion for 2% Au-TiO$_2$-1 calcined at different temperatures.

PP-11

The complete CO conversion was reached in the range 40-45°C with sample calcined at 300°C, whereas the minimum CO residual amount for the catalyst calcined at 200°C was 150 ppm at about 60°C. However, the complete conversion with 2% $Au-TiO_2-1-300$ was obtained at too low temperature, as the operating temperature of PEMFC is in the range 80-100°C.

Therefore, the second preparation method, as indicated above, was used and catalytic activity tests were carried out on the catalyst calcined at 300°C, identified as 2% $Au-TiO_2-2-300$. The obtained results are shown in Fig. 2: a complete CO conversion was achieved in the temperature range 60-80°C.
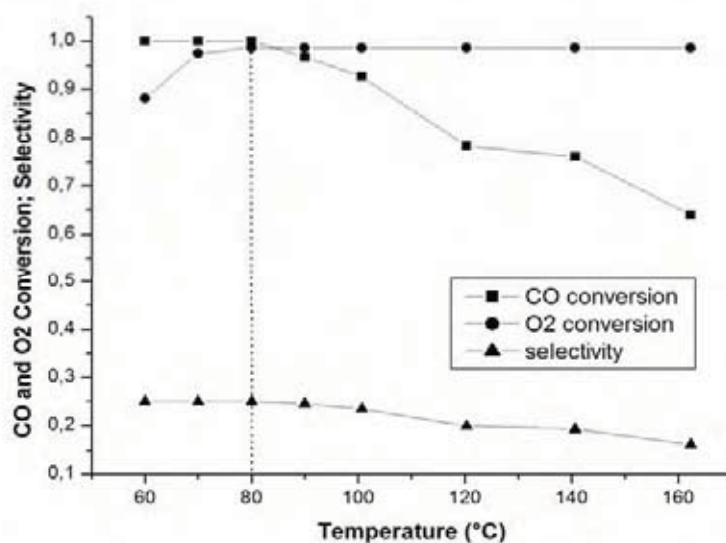
Fig. 2: CO and O_2 conversion and O_2 selectivity vs. temperature for 2% $Au-TiO_2-2-300$.

Then, on this promising catalyst, the research activity was deepened varying some parameters, as λ, weight space velocity and inlet CO concentration.

Test performed at λ = 3 showed still complete CO conversion, but only at 60°C, again a little bit low temperature for PEM applications.

In sight of industrial applications, weight space velocity was increased. Unfortunately, catalytic test did not show complete conversion: the CO residual concentration was about 600 ppm with a doubled weight space velocity.

As outlet CO concentration from WGS step could be lower than 1%, following tests were carried out with an inlet CO concentration of about 0.5%, feeding 100 ml/min of synthetic reformate gas at two different λ values (Fig. 3).
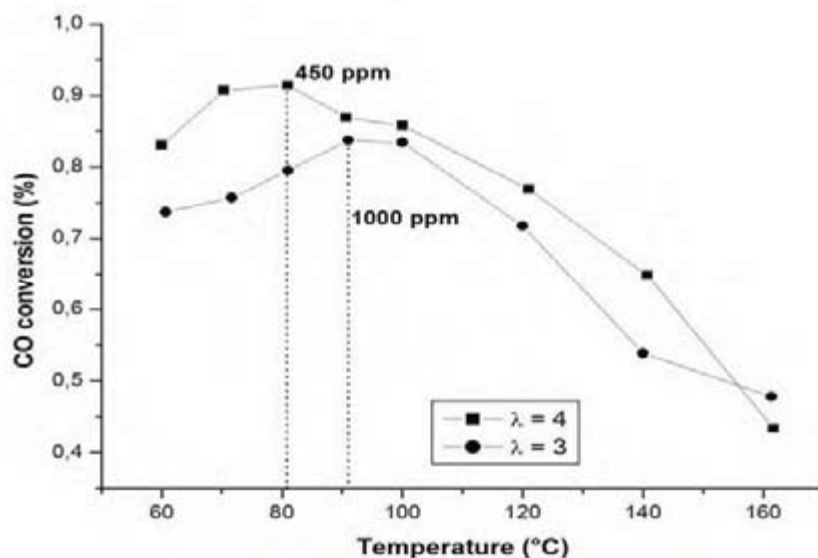
Fig. 3: Performance of 2% Au-TiO$_2$-2-300 at two different λ values; CO inlet concentration 0.5%.

As shown in Fig. 3, by decreasing the inlet CO concentration complete CO conversion was not reached: with $\lambda = 4$ residual CO was about 450 ppm, and it increased to 1000 ppm with $\lambda = 3$.

The above results could probably be explained by the lower CO concentration: in this case the parasite RWGS reaction (CO$_2$ + H$_2$ $\rightarrow$ CO + H$_2$O) could be favoured, then decreasing the CO conversion.

Therefore, the 2% Au-TiO$_2$-2 catalyst calcined at 300°C and operating at $\lambda = 4$ could potentially be used for CO-PROX applications at low temperature: the catalyst was able to reduce the CO concentration to below 10 ppm in the 60°C-80°C temperature range.

[1] Oetjen H.F., Schmidt V.M., Stimming U., Trila F., J. Electrochem. Soc. 143 (1996) 3838.

[2] Dudfield C.D., Chen R., Adcock P.L., J. Power Sources 86 (2000) 214.

[3] B. Hammer, J.K. Norskov, Nature 376 (1995) 238.

[4] M. Haruta, Catal. Today 36 (1997) 153.

[5] M. Haruta, T. Kobayashi, H. Sano, N. Yamada, Chem. Lett. 2 (1987) 405.

[6] G.R. Bamwenda, S. Tsubota, T. Nakamura, M. Haruta, Catal. Lett. 44 (1997) 83.

[7] M. Valden, X. Lai, D.W. Goodman, Science 281 (1998) 1647.

[8] T. Tabakova, F. Boccuzzi, M. Manzoli, J.W. Sobczak, V. Idakiev, D. Andreeva, Appl. Cat. B: Environmental, 149, (2004), 73-81.

[9] S. Tsubota, D.A.H. Cunningham, Y. Bando, M. Haruta, Stud. Surf. Sci. Catal. 91 (1995) 227.

SIMULATION STUDY OF A MEMBRANE METHANOL REFORMER FOR HYDROGEN PRODUCTION: HIGH RECOVERY IN COUNTER-CURRENT MODE

Fausto Gallucci[1], Angelo Basile[1], A. Iulianelli[1,2], Enrico Drioli[1,2]

[1] *Institute on Membrane Technology, ITM-CNR, c/o University of Calabria, Via P. Bucci, cubo 17/C, I-87030 Rende (CS) Italy. Phone: (+39) 0984 492011 – Fax: (+39) 0984 402103, E-mail: f.gallucci@itm.cnr.it   a.basile@itm.cnr.it*

[2] *Department of Chemical Engineering and Materials, University of Calabria, via P. Bucci Cubo 42/A, 87030 Rende, (CS), Italy, Phone: (+39) 0984 492039 – Fax: (+39) 0984 402103*

Abstract

In this simulation study, methanol steam reforming reaction to produce synthesis gas has been studied in a membrane reactor when shell side and lumen side streams are in co-current mode and in counter-current mode. The simulation results for both co-current and counter-current modes are presented in terms of methanol conversion and molar fraction versus temperature, pressure, H_2O/CH_3OH molar feed flow rate ratio and axial co-ordinate.

Although the methanol conversion is sometimes higher in the membrane reactor operated in co-current mode than in the counter-current one, in the last case it is possible to extract more hydrogen from the reaction zone. With this theoretical analysis we present a set of parameters which permit to have a CO-free hydrogen stream and a complete recovery of the hydrogen from the lumen side of the reactor.

Theoretical Model of Methanol Steam Reforming

The model was developed using all the thermodynamic values for the reaction species and the kinetic expressions; hydrogen removal was calculated using experimental permeabilities [1].

The rate equations are taken from Peppley *et al.* [2], as well as kinetic and adsorption parameters. A mass balance for a differential reactor volume along the z axis of MR for both co-current and counter-current mode has been written for the reaction zone (lumen) and for the permeating zone (the last mass balance changes for the two modes). The set of differential equations has been solved using a IV order Runge-Kutta method with variable step. The counter-current mode has been solved using the shooting method. The code was written in Fortran 95 by using the Salford Plato3 platform.

Results and discussion
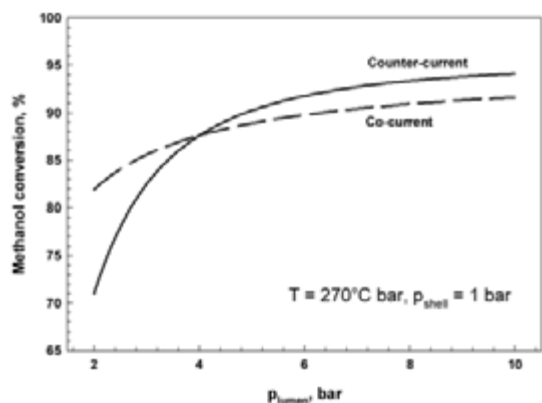
Fig. 1 Methanol conversion versus lumen pressure. p_{shell} = 1 bar, H_2O/CH_3OH feed ratio = 3, T = 270°C
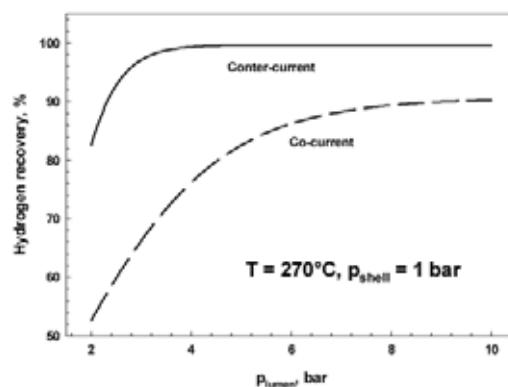
Fig. 2 Hydrogen recovery versus lumen pressure. p_{shell} = 1 bar, H_2O/CH_3OH feed ratio = 3, T = 270°C

Fig. 1 reports the methanol conversion versus the reaction pressure at 270°C. It shows that at pressures higher than 4 bar the methanol conversion in the counter-current mode is higher than the one in the co-current mode, vice versa, for pressures lower than 4 bar the co-current mode gives a higher conversion than the counter-current mode. Although the conversion is an important parameter in the reactor's performances evaluation, the key parameter in the CO-free hydrogen production is the hydrogen recovery, calculated as the percentage of hydrogen recovered in the shell side of the reactor with respect to the total hydrogen produced. Fig 2 shows the hydrogen recovery versus reaction pressure for the same operative conditions of the previous figure. For both co-current and counter-current mode the hydrogen recovered in the shell side increases by increasing the reaction pressure. This is because, by increasing the reaction pressure the hydrogen permeation is promoted. In this case, one can see that hydrogen recovery in counter-current mode is always higher than the hydrogen recovery in co-current mode. In particular, at pressure of 2 bar the hydrogen recovery in co-current mode is about 51% while in the counter-current mode it is more than 80%.
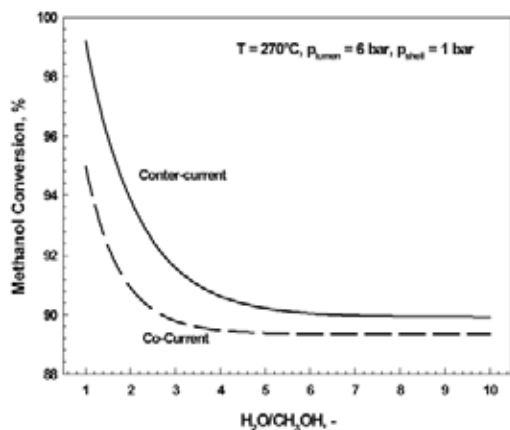
Fig. 3 Methanol conversion versus H_2O/CH_3OH feed ratio. p_{lumen} = 6 bar, p_{shell} = 1 bar, T = 270°C
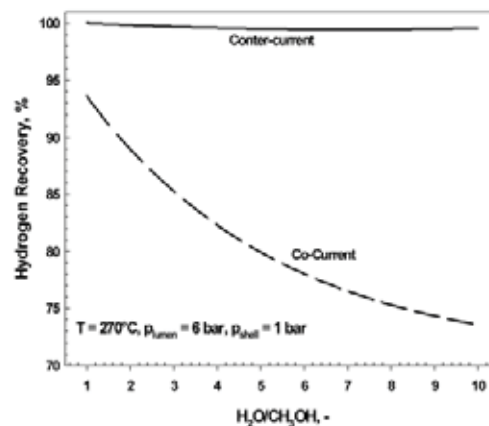
Fig. 4 Hydrogen recovery versus H_2O/CH_3OH feed ratio. p_{lumen} = 6 bar, p_{shell} = 1 bar, T = 270°C

PP-12

Figg. 3 and 4 report the methanol conversion and the hydrogen recovery versus the H_2O/CH_3OH feed flow rate ratio, respectively, for a temperature of 270°C, reaction pressure 6 bar and shell-side pressure 1 bar. Methanol conversion decreases with increasing the feed flow rate ratio for both co-current and counter-current modes. The counter-current mode gives methanol conversions always higher than the co-current mode. Although the difference in the methanol conversion between the counter-current mode and the co-current one is practically not so high, the hydrogen recovery in the counter-current mode is almost 100% in all the H_2O/CH_3OH range considered, while the hydrogen recovery for co-current mode quickly decreases with increasing H_2O/CH_3OH.

Conclusions

Hydrogen production by methanol steam reforming reaction and its recovery have been studied in a membrane reactor when shell side and lumen side streams are in co-current mode or in counter-current mode. The theoretical results show that the counter-current mode gives a methanol conversion often comparable with the co-current mode one. The difference in the hydrogen production depends on parameters such as reaction temperature and pressure and molar feed flow rate ratio. In general, counter-current mode can give hydrogen production higher than co-current mode. The most interesting result is the hydrogen recovery. In fact, in the case of counter-current mode it is possible to have 100% of hydrogen recovered in the permeate stream. This results are very interesting because, if steam is used as sweep gas in the membrane reactor, it is possible to recover all the hydrogen produced in the reactor as a pure stream and to use it directly in a fuel cell. It should be noted that the theoretical results suggest that it is possible to improve the MR performance also by changing the feeding mode between lumen and shell side of the membrane reactor.

References

[1] Gallucci, A.; Paturzo, L.; Basile A. Hydrogen Recovery from Methanol Steam Reforming in a Dense Membrane Reactor: Simulation Study. *Ind & Eng Chem Res.*, **2004**, *43(10)*, 2420-2432.

[2] Peppley, B.A.; Amphlett, J.C.; Kearns, L.M.; Mann, R.F. Methanol steam reforming on $Cu/ZnO/Al_2O_3$ catalysts. Part 2. A comprehensive kinetic model. *Appl. Catal. A: Gen.* **1999**, *179*, 31-49.

KINETIC ANALYSIS OF TOTAL OXIDATION OF BENZENE USING MIXED OXIDES TYPE CATALYSTS Cu-Cr SUPPORTED ON Al_2O_3 + SiO_2

V. Georgescu, G. Dobrescu, F. Papa and V.T. Popa

Institute of Physical Chemistry "I.G.Murgulescu", Romanian Academy,

Spl. Independentei 2o2, Bucharest, Romania

E-mail: frusu@icf.ro; vgeorgescu@icf.ro

Total oxidation of basic organic compounds for the depopluation of industrial environments is an acute problem. Using rare metals catalysts for oxidation through heterogeneous catalysis turned out to be successful.

However, the higher prices of these catalysts stimulated the searching other alternatives, one of them being the mixed oxides type catalysts with spinel structure, deposited on support.

In this work a mixed oxide type catalyst of Cu-Cr supported on Al_2O_3 + 20% SiO_2 from the complex precursor with tartaric acid $[CrCu_4Ta_6].5H_2O$ was prepared [1]. After calcinations at 650 °C, a catalyst with spinel structure and specific surface of 175 m^2/g was obtained. The catalyst was characterized by Infrared Spectroscopy (IR), X-Ray diffraction (XRD), UV-VIS Spectroscopy (UV-VIS), thermoprogrammed reduction (TPR) and thermoprogrammed desorption (TPD) studies; the thermogravimetric analysis (TGA) evidenced the spinel phase $CuCr_2O_4$ that is the active phase of the catalyst [2,3].

The catalyst has been used in the oxidation reaction of benzene in a laboratory installation with continuum flux; the reaction products were chromatographic analysed.

A good activity and stability of the catalysts has been evidenced by testing different benzene concentrations in the reaction mixture and different spatial velocities [4].

The chemical reactor was designed to simulate the industrial total oxidation reactors with pre-heating of the reaction mixture.

The chemical reaction was initiated in the catalyst thin layer and it is continuated in the gaseous-phase, in the inner part of the reactor. The contribution of the homogeneous process to the total conversion X, is more important as the reaction temperature increases.

Taking into account the space where the heterogeneous catalytic initiated reaction can be continued in gaseous-phase (homogeneous), the spatial velocities: heterogeneous s_1 and

PP-13

homogeneous s_2, respectively, and the contact times: τ_1 and τ_2 are related by the following equation: $s_1/s_2 = \tau_2/\tau_1 = 20$.

The chemical reactor can be modeled as a two series-bounded tubular reactors system: the first reactor is working as a differential reactor (at $X \leq 0.1$) or as a integral reactor (at $X > 0.1$); the second one, the un-catalytically reactor, is a integral reactor. These contributions have been evidenced by kinetic analysis using some simplifying assumptions.

Also, the preliminary analysis of the oxidation results is based on the selection of the experimental domains where the assumption of the higher importance of the heterogeneous reaction versus the global process is valid.

Differential analysis

The experimental results for lower conversions ($X \leq 0.1$) were used to compute the apparent kinetic constants. The Arrhenius curves lead to computing of the activation energies.

Integral analysis

The apparent kinetic constants corresponding to the integral reactor were computed using an Excel-based computer code from the $F(n,X) - \tau_1$ curves.

The conversion integral function $F(n,X)$ was computed using the trapezium-method with a step of $\Delta V = 0.001$.

Conclusion

The values of the activation energies of the total oxidation of benzene, within the kinetic temperature domain, {where a weak variation of activation energy on reaction rate is observed} are in agreement with our results obtained from work function data.

Bibliografie

1. V.Pocol, L.Patron and P.Spacu, Rev. Roumaine de Chim., 39 {1994} 1113.
2. M.I.Vass, V.Georgescu, Catal. Today 29 {1996} 463-470.
3. M.Teodorescu, I.Sitaru, V.Georgescu, M.I. Vass, E.Segal, Thermochimica Acta 282/283 {1996} 61-68.
4. D.Mehandjiev, K.Cheskova, A.Naydenov and V.Georgescu, React. Kinet. Catal. Lett. 76(2) {2002} 287-293.

HETEROPOLY ACID $H_3PW_{12}O_{40}$/SiO$_2$ CATALYZED SYNTHESIS OF BENZOCAINE UNDER SOLVENT-FREE CONDITION

A. Gharib, F.F. Bamoharram, M. Roshania, M. Jahangir

Department of Chemistry Science, School of Science, Islamic Azad University,

Mashhad - Iran, aligharib5@yahoo.com

Microwave heating and its application in organic chemistry for reaction is currently being developed successfully and in recent years, there has been a tremendous interest in this area. Remarkable decrease in reaction times and in some cases cleaner reaction have been reported with microwave irradiation. The use of heteropoly acid (HPA) as catalysis for fine organic synthesis process in developing synthesis of antioxidant and biologically active substance for instance have been reported [1]. Heteropoly acids are more active catalyst for various reaction in solution than conventional inorganic and organic acids [2]. Herein we report the esterifacation P-amino benzoic acid with Ethanol to corresponding Ethyl-4-amino benzoate which has local anesthetic commonly used as topical pain reliever. It is active ingredient in many over –the-counter analgesic ointments and sprays[3]. This work describe the application of silica support $H_3PW_{12}O_{40}$(PW). The strongest HPA in the Keggin series against silica supported sulfuric acid and other heterogeneous catalyst like zeolite, HZSM-5 for esterificiation of 4-amino benzoic acid with ethanol under microwave irradiation and traditional thermal condition.

References

1 .Onous Y., MizutanY.,S.Akiyam,Y. Izumi, Chem.Ttechnol, 8, (1978) 432.

2. I. V. Kozhevnikov, K. I. Matveev Appl.Catal, 5, (1983) 135.

3. F.Y, W.O.principles of Medicinal chemistry, Philadelphia. Leaond febiger.1974, chap14 (local Anesthatica)

PREYSSLER HETEROPOLYACID AS GREEN, ECO-FRIENDLY AND REUSABLE CATALYST FOR HIGHLY SELECTIVE SYNTHESIS OF PHENYLSALICYLATES

F.F. Bamoharram, M. Roshani, <u>A. Gharib</u>, M. Jahangir

Department of Chemistry, School of Science, Islamic Azad University of Mashhad - Iran.

aligharib5@yahoo.com

Generally phenylsalicylates are prepared under liquid phase, refluxing the reactants in the presence of small amount of conc. H_2SO_4, HCl, $POCl_3$ or sulfonic acid as the catalyst [1]. Solid acids such as zeolites, oxides, aluminophosphates and their modified forms have been extensively studied as possible alternatives to conventional Lewis/ Bronsted acid catalysts [2-4]. Although many effective and reliable methods for the preparation of aromatic esters exist, there is still a good scope for research towards finding eco-friendly and economically viable processes.

Polyoxometalates, and particularly the heteropolyanions, can function as effective catalysts whose redox properties can be controlled by alteration of their compositions. They are remarkably stable both in the solid state and in solution, making them useable as heterogeneous or homogeneous catalysts. All reports show that heteropolyacids, like Keggin and Dawson structures, are efficient "Supper acid" catalysts which can be used both in the homogeneous or heterogeneous phase [5] and the catalytic applicability of Preyssler's anion with exclusive properties has been very limited, with only a few demonstrations of catalytic activity. This heteropolyanion with fourteen acidic protons, is an efficient "supper acid" solid catalyst which can be used both in the homogeneous and heterogeneous phases [6].

In continuation of our research on exploring the application of this catalyst and application of heteropolyacids in organic syntheses [7], in the present work we have studied performance of sodium-30 tungsto pentaphosphate, the so-called Preyssler's anion as catalyst for highly selective preparation of phenyl esters of salicylic acid from aromatic alcohols. The performance of the Preyssler catalyst as pure, mixed addenda and silica supported was compared against known classical catalyst: sulfuric acid. We have found that this green solid and recyclable catalyst in an organic solvent, render effective reaction better than sulfuric acid under different temperatures. Both homogeneous and heterogeneous catalysts are discussed

and compared and the results show that the catalytic performance of this catalyst is excellent. The effects of various parameters such as catalyst type, reaction time, temperature, molar ratio and solvent type have studied and the optimum conditions have been obtained. All different forms of this green solid catalyst can be easily recovered and recycled with retention of their initial structure and activity.

References

1. A. Rodriguez, M. Nomen, B. W. Spur Tetrahedron Lett, 39 (1998) 8563.

2. P. B Venuto Micropor Mater, 2(1998) 297.

2. M. E. Davis, Micropor Mesopor Mater, 21(1998) 12657.

4. S. E. Sen, S. M. Smith, K. A. Salivan, Tetrahedron. 55, (1998) 12657.

5. N. Mizuno, M. Misono J. Mol. Catal, 86, (1994) 319.

6. M. H. Alizadeh, H. Razavi, F. F. Bamoharram, M. K. Hassanzadeh Kinet. Catal, 44, (2003) 524.

7. a) M. M. Heravi, F. Derikvand, F. F. Bamoharram J. Mol. Catal. 242, (2005) 173.
   b) Alizadeh, H. Razavi, F. F. Bamoharram, K. Daneshvar J. Mol. Catal, 206, (2003) 89.

SPECIFIC CATALYST INFLUENCE TO PROCESSES FOR AEROSOL NANOCATALYSIS TECHNOLOGY

Glikina I., Glikin M.

Vladimir Dal Eastern-Ukrainian National University, Severodonetsk Technological Institute,
av. Sovetskiy, 59A, Severodonetsk, Ukraine
e-mail: irene555@mail.ru, glikin@sdtcom.lg.ua

The successful development chemical industry for processing various raw material is connected to application heterogeneous catalysis on carriers [1]. During 150 years the main attention of a science and practice in catalysis is concentrated on improvement of technology of carriers reception with given structure and ways of fixing on catalytic active components on their surface. On this period the engineering of definition of properties stability, activity and selectivity of the received samples in researched reactions was constantly improved. Simultaneously there was the complication of reception desired result and a growth of catalysts cost. In the scientific literature, at domestic and international conferences and symposiums the problems of activity, aging, poisoning and regeneration of catalysts [2, 3] were regularly examined. As a result of experimental and practical data for traditional catalysis on carriers have revealed a lot of complex and difficultly soluble problems. In general view they subdivide to three blocks: reduction of potential possibilities of catalysis; fast catalyst deactivation; the reactions, which not speeding up catalysis on carriers.

From the end of XX centuries our specialists developed new ideology of heterogeneous and catalytic manufactures creation, which free from these problems, is named aerosol nanocatalysis (AnC) [3, 4]. The chemical reaction will be carried out with catalytic system application. It consists the moving inert material and catalytic active substance. The particles sizes in reaction zone are 8-100 nm. Were used the reactors with mode of a fluidized and vibrating bed. One of the first reactions which systematic investigating was the deep oxidation of acetic acid reaction by use of the catalyst on carriers and in aerosol catalyst [3].

The major industrial synthesis are detailed investigated and is studied them kinetics for the reactions of aerosol nanocatalysis technology. Thus are revealed new phenomenon for catalysis. The results of oxidation reagents, taking place in gaseous, liquid and solid condition are given on Fig. 1. For all reagents irrespective of aggregate state are fixed new properties

for heterogeneous catalysis, such as dependence of reaction rate on catalyst concentration, insignificant catalyst concentration, presence of a maximum rate for each reaction at catalyst concentration up to 5 g/m^3. It notes a successful reaction realization with active silt containing solid oxidizing components. The left part direction of lines is natural. It was not represented possible to predict the subsequent rate decrease in the right part of dependence. The results

Table 1. The process of acetic acid deep oxidation at temperature 600^{0}C

№	Acid concentration, %vol.	Maximal loading mode, kg/(kg$_{cat}$*h)		Aerosol of catalyst and moving inert material
		Fluidized catalyst bed on γ-Al$_2$O$_3$		
		Pt	CuCrO$_4$	Fe$_2$O$_3$
1	98	1,5	0,8	-
2	60	-	0,65	3,6*10^4
3	30	-	0,37	2,6*10^4
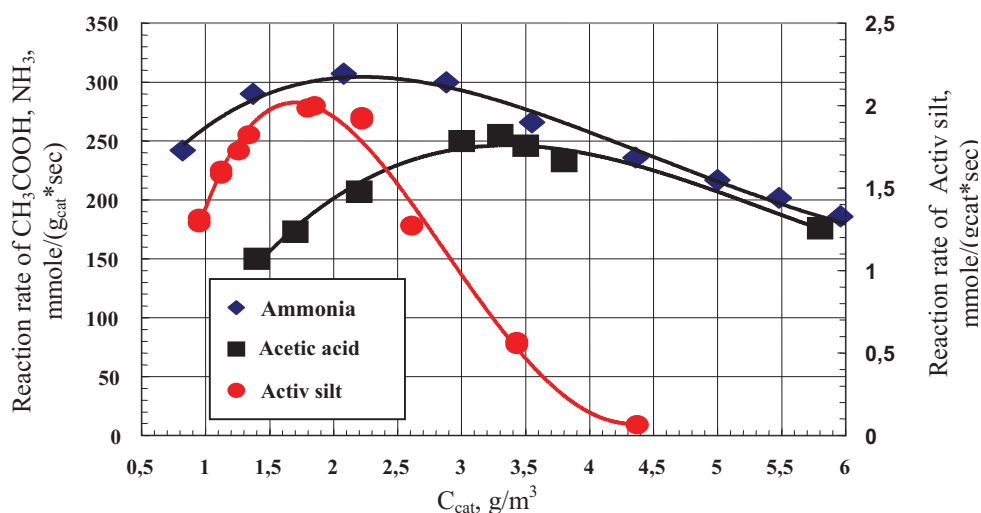
Fig. 1. Dependence of reaction rate of ammonia, acetic acid and active silt oxidation processes on aerosol catalyst concentration in reactor with fluidised bed.

were unexpected. Probably, it is connected to some reasons, such as energy change to catalyst surface and reagents from moving inert materials, braking of diffusion, increase of the influence of convective carry to rate of the process. Probably, displacement of process balance is influenced during destruction and agglomeration of catalyst particles in fluidized bed. Thereof the active catalyst surface decreases. The further study of this phenomenon is necessary.

The similar dependence of chemical processes studying by aerosol nanocatalysis technology with vibrating bed (Fig. 2) was received. In this case it was show an opportunity

of chemical reaction stopped. It is necessary to note, the reaction rate does not decrease even at concentration 0,3 g/m^3$_{r.vol.}$.

At the results the AnC technology has shown a new opportunity to manage activity and selectivity of catalysis of chemical processes. The reaction rate is constant at catalysis on carrier, as the amount of active component is constant. It can be changed even during chemical reactions for AnC technology.
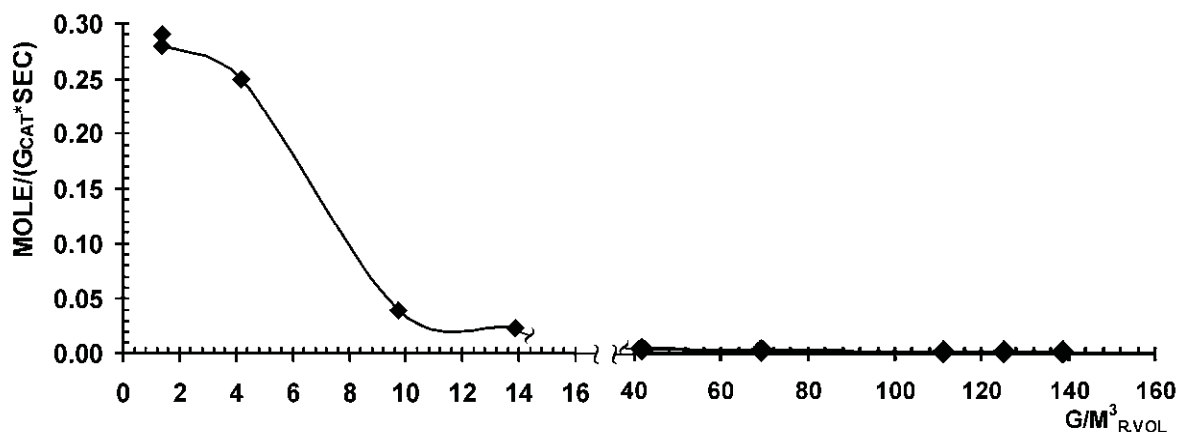
Fig. 2. Dependence of reaction rate of acetic acid oxidation on catalyst concentration in reactor with vibrating bed by frequency 6 sec^{-1} and amplitude 7 mm.

There is a maximum catalyst quantity (3-4 g/m^3 for fluidised bed and 0,3-2 g/m^3 for vibrating bed at realization of acetic acid oxidation process. The vibrating bed allows receiving the more active catalyst than fluidized bed. Previously, it is necessary to define a dependence of reaction rate on catalyst concentration up to kinetic studying of chemical reactions. It is possible to ensure a constant catalyst activity for the practically unlimited time for AnC technology.

The vibrating bed has allowed increasing reaction rate in 10^6 times and probably more. It has resulted in new features of aerosol nanocatalysis technology:

− minimization of catalyst concentration (0,3-2 g/m^3);
− management of mechanical and chemical activation in situ (frequency, amplitude, size of inert material, efforts of influence to catalyst particles);
− decrease of hydraulic resistance of reactor practically up to zero;
− decrease of reactor volume in 3-10 times.

The reaction rate and selectivity depends on concentration of active oxygen on contact surface by viewing of the mechanism of oxidation process. The degree of surface filling by active oxygen depends on catalyst concentration, active centers of surface and diffusion conditions in a reaction zone at a constant ratio of reagents in mixture. Nanoparticles have a

plenty of the active centers at the moment of formation, so it explains catalyst activity in aerosol nanocatalysis technology [5].

The studying of catalyst influence to reaction rate on aerosol nanocatalysis technology opens a new sight on kinetic of gas-phase processes.

Also it influences to the basic theoretical and practical parameters for technology and equipment development. By analyzing experimental results, it came to a conclusion about introduction catalyst concentration in the mathematical description of chemical process.

The modern evolutionary development of a scientific idea in chemistry and chemical technology is created by enterprises satisfaction by an actual level of engineering. It's not stimulated essentially new energy- and cost-saving scientific development. It reminds you, that XXI century, is called as nanotechnology century. The nanochemistry reviews [5] are rather pessimistic. Probably, the given work will change this opinion and will expand numbers scientific engaged aerosol nanocatalysis technology.

References

1. Крылов О.В. Мировой кризис ресурсов, загрязнение окружающей среды и проблемы катализа // Российский химический журнал. – 1997. - № 3 – С. 124 – 136.

2. Островский Н.М. Кинетика дезактивации катализаторов. М., Наука, 2001.334 с.

3. М.А. Гликин. Аэрозольный катализ // Теоретические основы химической технологии. – т. 30, №4, 1996. – С. 430-434

4. Glikin M., Kutakova D., Prin E. Unsteady-process and aerosol catalysis // Chemical Engineering Science, 1999, P. 4337-4342

5. Бухтияров В.И., Слинько В.Г. Металлические наносистемы в катализе // Успехи химии. - 2001, Т. 70. - №2. - С 167–181.

PP-17

HYDROGEN PRODUCTION TECHNOLOGY BY NATURAL GAS PYROLYSIS WITH ENERGY SAVING

Tarasov V., Glikin M., Glikina I.

Vladimir Dal Eastern-Ukrainian National University, Severodonetsk Technological Institute, av. Sovetskiy, 59A, Severodonetsk, Russia
e-mail: vatarasov@ramblrer.ru, glikin@sdtcom.lg.ua, irene555@mail.ru

Hydrogen is a widely used reagent. The yearly increase of its consumption in Europe is above 8% [1]. Large-scale hydrogen producing enterprises are necessary for the hydrogenation of chemical compounds in chemical, petrochemical, metallurgy and a number of other industries. The prospects of hydrogen use in internal combustion engines is extensively discussed. The efficient solution of these problems would require the reduction of capital invested in the hydrogen production and the decrease of its prime costs. At present, the basic hydrogen producing technology worldwide is the natural gas conversion. Of alternative methods, the steam conversion is mainly preferred. The small-scale hydrogen consumers, previously relied upon the water electrolysis and ammonia or methanol decomposition processes become more inclined to the natural gas conversion.

The schemes of steam-based natural gas conversion were gradually improved during past 70 years. Their most efficient versions were implemented in several generations of the ammonia-producing technology. However, the underlying chemical process remains essentially the same, and consists of four chemical stages and one mass-transfer stage. During this time, the energy consumption in commercial conditions was decreased from 170 to 6,5 GJ per one ton of ammonia, and more than 70% of this energy is spent at the conversion stage. One can hardly expect any significant improvements of technological and economical parameters at natural gas conversion stage in the ammonia production process.

The alternative to known multistage technologies of the hydrogen production for its use in industry and transportation should be the pyrolysis of the same natural gas and, possibly, other hydrocarbons [2-4]:

$$CH_4 = C\!\downarrow + 2H_2 \qquad\qquad\qquad (1)$$

The temperature dependence of the monomolecular rate constant of the methane pyrolysis was studied in a number of works; the Ea values obtained therein are varied in the

range of 263 to 435 kJ/mol. The pre-exponential factor value is $(3.0\pm1.0)\cdot10^{12}$, which agrees with the activated complex theory for the monomolecular reaction. The expression derived for the monomolecular constant of reaction rate in steady state conditions (closed system) fits the experimental data obtained for the temperature range 1100-1600 K quite well. However, all the carbon formed as the result of chemical reaction was accumulated at the reactor walls. This would certainly affect the experimental results [2].

One of the methods of pyrolysis is the contact pyrolysis (CP) of natural gas in liquid-high temperature heat carrier (LHC). The pyrolysis is performed in the "gas-melt" system. The contact heat exchange based on mixing is implemented, which determines a number of parameters and processes of the pyrolysis. For these conditions there is a lack of reliable experimental and calculation methods to determine the time and area of the contact between the phases, and the heat transfer regime [3]. However, these parameters determine the rate and the extent of chemical transformations. Therefore, the development of technology would require the experimental studies, on which reliable kinetic models could be based.

The studies were performed on the continuous flow unit in the bubbling-type reactor made of quartz [4]. The main parameters of the reaction zone are: diameter 40 mm, the melt bed height (h_0) up to 70 mm. The gas-off is performed from the melt surface. Gaseous products of the reaction were analyzed using the gas chromatograph. The composition of natural gas used in the study was: methane (95.6% $_{vol.}$), ethane (3.3% $_{vol.}$) and other gases (less than 1.1% $_{vol.}$). The influence of oxygen on pyrolysis rate was explored in number of experiments by temperature is 1233 K. The experiments shown, the rates of methane and hydrogen formation is not depended from oxygen concentration, if it changed from 0,1 to 5%vol. Relative oxygen rate spending approximately complies with relative methane rate spending. Under enough high additive of the oxygen ($[O_2]$ =5 %) was fixed CO formation. The experiments with mixtures of the composition $CH_4 : N_2$ = 1:1 (1:2 and 1:3) were organized by changing of velocities of gas flow in free reactor volume from 0,003 to 0,051 m/s and the height of fixed melting bed from 10 to 70 mm (fig.). The change of H_2 contents in products of reactions did not exceed 1% when the heights of heat carrier layer change in 7 times. This fact explaining that when entering raw material in melt is instant heating (the heat explosion) from temperature into reactor. Herewith the chemical reactions is run, and certain chemical balance reached in "gas - melt" system (the gas bubble). The further bubble moving under the Arhimed power influence do not bring to offset of the balance (fig.). The change of methane partial pressures has allowed defining the order of NG in LHC pyrolysis reactions. The importance of reactions order fits to the literary dates and is 1. The results obtained in the

experiments are summarized in Table 1. These data were used to derive an expression for the rate constant of the natural gas decomposition reaction which takes place during the CP in the sodium chloride melt:

$$r = k * C_{CH4} \tag{2}$$

$$k = (2,8 \pm 1,0) \ 10^7 \ e^{-134000 \pm 5000/RT}, \ c^{-1} \tag{3}$$

The value of energy $E_a = (134 \pm 5)$ kJ/mol, and remains constant for various gas dynamic modes. The significant changes in the values of activation energy and pre-exponential factor imply that the mechanism of the pyrolysis process in the "gas-surface" system is different from that in the "gas-melt" system
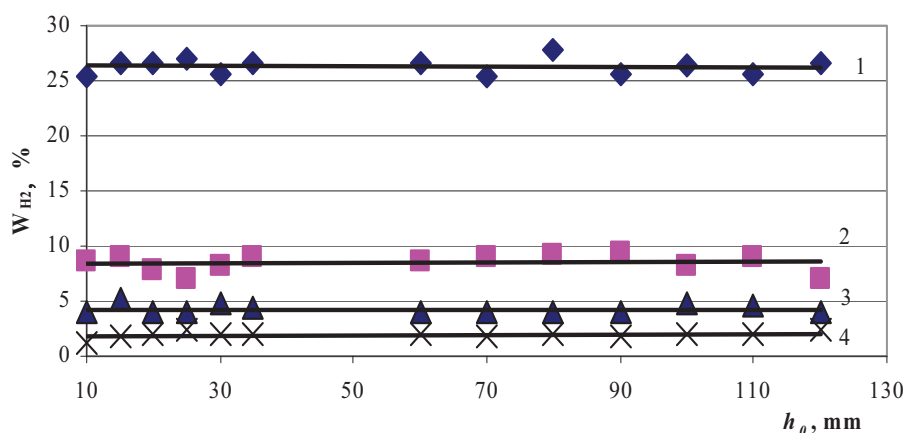
Fig. The Dependency of the contents H_2 in product of the reactions from height layer heat carrier at the temperature 1233K and its concentrations: 1 - 95,6 %$_{vol.}$; 2 - 50 %$_{vol.}$; 3 - 33 %$_{vol.}$; 4 - 25 %$_{vol.}$.

Table 1

Composition (%$_{vol.}$) of gaseous products of natural gas pyrolyses process at height an bubbling bed of LHC 40 mm

Temperature, K	Component	Consumption of natural gas , l/h											
		4,7			10,7			21,5			34,9		
		Diameter of natural gas output, mm											
		1	2,5	5	1	2,5	5	1	2,5	5	1	2,5	5
1113	H_2	19,5	28,7	35,7	13,8	23,0	30,0	9,0	18,6	25,2	6,1	18,4	22,0
	CH_4	79,4	70,3	63,2	85,1	75,9	69,0	89,9	80,4	73,7	92,9	80,6	77,0
1153	H_2	25,2	32,5	42,3	18,9	29,6	35,2	14,9	25,1	32,1	12,3	23,3	31,2
	CH_4	73,7	66,5	56,6	80,0	69,2	63,8	84,0	73,9	66,8	86,7	75,7	67,8
1213	H_2	36,2	51,2	66,5	27,2	36,2	43,3	25,2	34,2	41,2	21,2	32,3	40,2
	CH_4	62,7	47,8	32,5	71,8	62,7	55,7	73,8	64,8	57,7	77,8	66,6	58,7
1263	H_2	48,0	59,4	75,4	44,6	56,6	61,2	32,2	39,2	46,2	29,8	36,3	44,2
	CH_4	50,9	39,6	23,5	54,3	42,2	37,8	65,7	59,8	52,7	69,2	62,7	54,8
1353	H_2	79,4	85,0	92,0	74,8	79,6	85,2	65,0	74,6	81,2	58,0	68,0	76,2
	CH_4	19,5	14,0	7,0	24,1	19,2	13,8	33,9	24,4	17,7	40,9	30,9	22,8

.

And the sequence of the stages of methane transformation in the pyrolysis process in static conditions proposed in [2]:

$$CH_4 \rightarrow C_2H_6 \rightarrow C_2H_4 \rightarrow C_2H_2 \rightarrow C$$

seems to be inapplicable to CP in LHC. However, to verify this supposition, more accurate experimental data should be obtained.

Conclusions: The comparison of the results obtained in this study with the data for various schemes of the hydrogen production by natural gas conversion shows that:

- the two-stage process of hydrogen production by natural gas pyrolysis can be used in industry instead of the five-stage conversion process, which will decrease the capital investments more than twice;

- it is possible to reduce the prime costs of hydrogen by 60% due to the decrease of the expenses for capital investments, power resources and maintenance.

References

1. G. Lipkin. Shortly about Various Things: Energy Utilities as the PCO's 'Stepsons', Neftegazowyje technologii, No.2(2001)119.

2. V.S. Arutyunov, V.I. Vedeneev, R.I. Moshkina, V.A. Ushakov, Kinetics and catalysis, 32(1991)267.

3. United States Patent 5,435,814. Molten metal decomposition apparatus.

4. Tarasov V.Yu., Glikin M.A., Glikina I.M. The synthesis of hydrogen by methane pyrolysis process using the liquid heat-carrier technology / Book of abstracts of the VII Ukrainian-Polish Symposium "Theoretical and experimental studies of interfacial phenomena and their technological application", September 2004, P.350-352.

THE CRITICAL PHENOMENA IN THE DYNAMICS
OF THE HOMOGENEOUS CATALYTIC PROCESSES

Gorodsky S.N., Bruk L.G., Temkin O.N.

Lomonosov State Academy of Fine Chemical Technology

Vernadsky av. 86, 119571, Moscow, Russia; +7(495)434-87-11; Gorodsky@yandex.ru

Introduction

By the study of homogeneous and heterogeneous catalytic reaction kinetics in increasing frequency nontrivial dynamic behaviour of reacting systems (the critical phenomena) is observed - occurrence of intermediates, products and reactions rates self-oscillations, multiple steady states, hysteresis, chaotic behaviour [1, 2]. Reactions, in which the critical phenomena are found out (mostly oscillations of concentrations) in homogeneous isothermal conditions, in general concern to organic substrates oxidation processes by strong oxidants ($KBrO_3$, KIO_3, H_2O_2, O_2), catalyzed by metals ions of variable valency (Ce (IV)/Ce (III), Mn (III)/Mn (II), Fe (III)/Fe (II), Co (III)/Co (II) and others), and to inorganic reactions with participation of H_2O_2 [1]. Self-oscillations are discovered also in typical reaction of benzaldehyde liquid-phase oxidation by oxygen at the presence of Co (II) complexes [3].

Experimental

Participants of our team discovered the critical phenomena in typical reactions of the organometallic catalysis by metals complexes in which no substrates destruction, but synthesis of complex molecules occurs. So, in acetylene carbalkoxylation reaction in the system $PdBr_2$ – KBr – HBr – butanol-1 – dimethylsulphoxide proceed the reactions:

$$CO + (CH_3)_2SO \longrightarrow CO_2 + (CH_3)_2S \qquad (1)$$

$$2CO + C_2H_2 + 2ROH \longrightarrow ROCOCH=CHCOOR \ (E, Z) + (CH_3)S + H_2O \qquad (2)$$
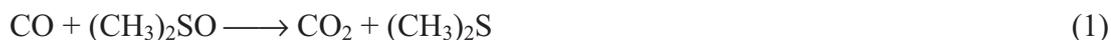
with periodic change of carbon monoxide and acetylene absorption rate, values of platinum electrode electric potential (E_{Pt}), pH and color of a reaction solution [4]. By the study of various alkynes oxidative carbonylation reaction in the system PdI_2 - KI - MeOH on reaction (3)

$$RC \equiv CH + 2CO + 2MeOH + \tfrac{1}{2} O_2 \longrightarrow MeOCOC(R)=CHCOOMe + H_2O \ (E, Z) \qquad (3)$$

oscillations of E_{Pt} and pH have been found out [5-7]. The multiple steady states phenomenon in reaction of maleic anhydride synthesis from acetylene and CO was discovered [8].

Discussions

The analysis of the information concerning reaction mechanism with the critical phenomena and experience of such processes studying [5-7] allow us to formulate the features of homogeneous catalytic reactions mechanisms which can become the reason of nontrivial dynamic behaviour:

1) Presence of nonlinear stages in the process mechanism (reaction between intermediates, presence of one or more catalysts);

2) Participation of active particles formation and destruction stages, i.e. chain mechanisms of the catalytic process;

3) Presence in the mechanism schema the positive (autocatalysis) and negative (autoinhibition) feedbacks.

The study of reaction (3) in solutions of Pd (II) iodide complexes allow us to suppose an autocatalysis by hydride particles HPdI, the presence of active particles formation and destruction stages, and features of the chain multiroute process display.

Conclusions

We are thinking, that mechanisms of many processes in organometallic catalysis allow to expect occurrence of self-oscillations and other critical phenomena. The searching of such phenomena is important for development of the catalytic reactions mechanisms theory, and their presence is the powerful tool of hypotheses discrimination [7].

Acknowledges

References

[1] R. J. Field, M. Burger, *Oscillations and Travelling Waves in Chemical Systems*, Wiley, New York, 1985.

[2] M. M Slin'ko, N. Jaeger, *Oscillating Heterogeneous Catalytic Systems*, Elsevier, *Studies in Surface Science and Catalysis*, 1994, <u>86</u>, 1 – 408.

[3] M. G. Roelofs, E. Wasserman, J. H. Jensen, A. E. Nader, *J. Am. Chem. Soc.,* 1987, <u>109</u>, 4207 – 4217.

[4] G. M. Shul'akovsky, O. N. Temkin, N. V. Bykanova, A. N. Nyrkova, in book: Chemical kinetics in catalysis: Kinetic models of liquid-phase reactions, Chernogolovka: IPC, 1985, 112.

[5] A. V. Malashkevich , L. G. Bruk, O. N. Temkin, *J. Phys. Chem., A*, 1997, <u>101</u>, 51, 9825 - 9827.

[6] S. N. Gorodskii, A. N. Zakharov. A. V. Kulik, Bruk, O. N. Temkin, *Kinetics and Catalysis*, 2001, <u>42</u>**,** 2, 280 – 291.

[7] S. N. Gorodskii, E. S. Kalenova, L. G. Bruk, O. N. Temkin, *Russ. Chem. Bull.*, 2003, <u>52</u>, 7, 1534 - 1543.

[8] L. G. Bruk, I. V. Oshanina, A. S. Zakieva, A. P. Kozlova, O. N. Temkin, *Kinetics and Catalysis*, 1998, <u>39</u>**,** 2, 183 – 186.

NEW OSCILLATING REACTION - OXIDATIVE CARBONYLATION OF PHENYLACETYLENE TO ANHYDRIDE OF PHENYLMALEIC ACID

Gorodsky S.N., Kasatkina O.V., Bruk L.G., Temkin O.N.

M.V. Lomonosov State Academy of Fine Chemical Technology
Vernadsky av., 86, Moscow, Russia; *+7(495)434-87-11; Gorodsky@yandex.ru*

Introduction

In solutions of palladium complexes a reaction oxidative carbonylation of phenylacetylene to anhydride of phenylmaleic acid proceeds in soft conditions: at 40 °C and 1 atm. CO and O_2 [1]. Using methylacetylene in the same conditions results in formation of citraconic acid anhydride. Both products are valuable reagents in organic chemistry. Recently by study this reaction we been a success to find out a mode in which periodic changes of intermediate concentration are observed. It allows to speak that one more oscillatory system among typical catalytic processes with metal complexes is found [2, 3]. Thus, it is possible to assert, that the oscillatory mode for reactions with participation of complexes of transitive metals is not the exclusive phenomenon and advise to peer into other processes which were earlier described with the help of linear mechanisms [4] more steadfastly.

Experimental

Experiments were carry out in glass thermostating at 40 °C closed reactor with 180 ml volume. The stirring of a gas and liquid phases was made by magnetic mixer. During the experiments potential differences glass (pH) and platinum electrodes (E_{pt}), immersed into catalytic solution, in relation to standard chlorine-silver electrode in saturated solution of KCl are measured. Gases volume absorbed during the reaction is measured by calibrated burette. Structures of initial and reactionary gas by method gas chromatography are determined. Experiments with phenylacetylene are carried out; as solvent the acetone containing 0,55 M of water was used (1).

$$\text{C}_6\text{H}_5\text{-C}\equiv\text{CH} + 2\text{CO} + 1/2\text{O}_2 \xrightarrow{\text{PdBr}_2\text{-LiBr-(CH}_3)_2\text{CO-H}_2\text{O}} \quad (1)$$
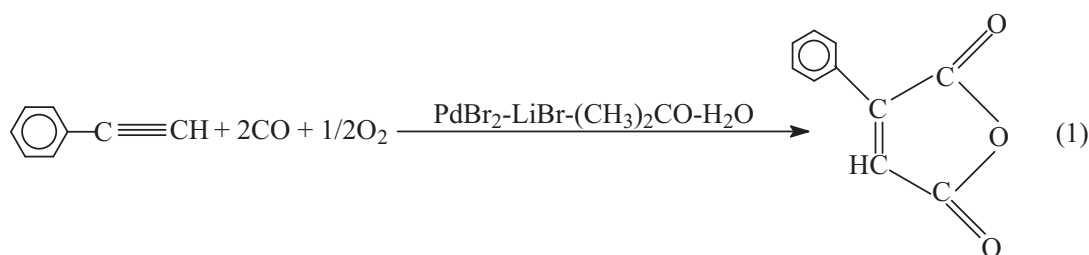
The products of phenylacetylene oxidative carbonylation are identified by chrom-mass-spectrometry. It was used Agilent Technologies (USA) gas chromatograph, equipped by Agilent 5973N mass - detector. As a basic product of phenylacetylene oxidative carbonylation phenylmaleic anhydride was found.

Discussions

Oxidative carbonylation of phenylacetylene (PhA) in system $PdBr_2$-LiBr-H_2O-acetone, as it has been shown, can proceed in an oscillatory mode. In researched system oscillations of values E_{Pt} and pH, and also the characteristic periodic absorption of a gases (CO, O_2) mixture have been found out (fig. 1).
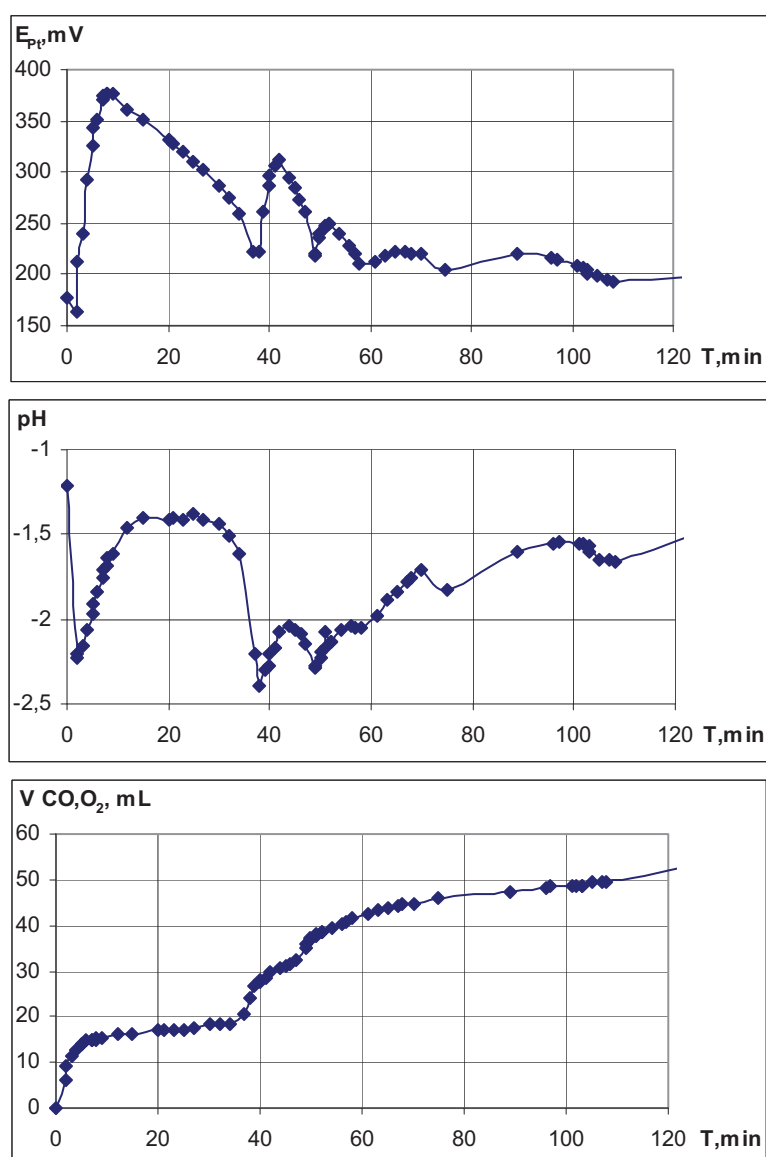
Fig. 1. Oxidative carbonylation of phenylacetylene in system LiBr-$PdBr_2$-H_2O- acetone
LiBr=0,2M; $PdBr_2$=0,01M; ФА=0,1M; H_2O = 0,75M; $V_{(CH3)2CO}$=10мл; $[CO]_0$: $[O_2]_0$ = 1:1

PP-19

Oscillations in researched process have an unusual form and quickly fade. Thus the solution remains homogeneous; the palladium in a course of experiments is not reduced, that can speak about the reason of oscillations attenuation may be other. Oscillations E_{Pt} occur at values 150 - 400 mV; and pH - in an interval of values -2,5 – 0. Values pH decrease from 4 – 5 to -2,5 – 0 directly after an expulsion of system with gases mixture (CO, O_2) for the first 5 - 7 minutes of experiments.

By studying of gases mixture composition influence on an oscillatory mode of the reaction we find oscillations in experiments with the percentage of CO in gas mixture no more than 50 %. In these xperiments used mixtures $CO:O_2$ which composition changed from 1,5 : 1 up to 1 : 1,3.

Conclusions

The new oscillatory system - reaction of oxidative carbonylation of phenylacetylene to anhydride phenylmaleic acid is found out. Independence of a mode of oscillations of a gases mixture composition is shown at the percentage of CO no more than 50 %. Ranges of E_{Pt} and pH in which the oscillations have fading character are revealed. An immediate task are researches of oscillating reaction kinetic, and also research of behavior in this system of methylacetylene and others alkynes.

Acknowledges

References

[1] Zargarian D., Alper H., Organometallics, 1991, v. 10, pp. 2914-2921.

[2] S.N. Gorodsky, A.N. Zaharov, A.V. Kulik, L.G. Bruk, O.N. Temkin, Concentration limits of the oscillations occurrence in process phenylacethylene carbonylation and possible mechanisms of process, *Kinetic and Catalysis*, 2001, v. 42, № 2, pp. 285-293.

[3] S.N. Gorodsky, E.N. Kalenova, L.G. Bruk, O.N. Temkin, Oxidative carbonylation of alkynes in an oscillating mode. The substrate nature influence on the dynamic behavior of reaction system. *Russ. Chem.Bull.* 2003, v.52, № 7, pp. 1534-1542.

[4] O.N. Temkin, L.G. Bruk, Complexes Pd (II, I, 0) in catalytic reactions of the Oxidative carbonylation. *Kinetic and Catalysis*, 2003, v. 44, № 5, pp. 661-676.

CATALYTIC WET OXIDATION OF ETHANOL BY H_2O_2 ON NANOSIZED Mn_2O_3/SBA-15 - PREPARATION, CHARACTERIZAION AND KINETICS

Yi-Fan Han*, Fengxi Chen, Zi-Yi Zhong, Effendi Widjaja, Lu-Wei Chen, Wong Wan Ling and Dou Jian

Institute of Chemical and Engineering Sciences, 1, Pesek Road, Jurong Island, Singapore, 627833; E-mail: han_yi_fan@ices.a-star.edu.sg

Removal of organic compounds from wastewater is of importance, because organic substances, i.e., benzene, alcohols etc., may lead to serious intimidate to human and animal health by drinking the contaminated water. Currently, a Fenton reagent, consisting of homogenous iron ions and hydrogen peroxide, is used as an effective oxidant in the purification of industrial effluents containing organic compounds [1]. However, several problems raised by the homogenous Fenton system, i.e., disposing the iron-containing waste sludge, limiting the pH value of the aqueous solutions, and irreversible losing reactivity of the regent, are of great challenge. Recently, a heterogeneous Fenton reagent using metal ions exchanged zeolites, i.e., Fe/ZSM-5 catalysts, has been proved to be a promising alternative in the remediation treatment of wastewater, since it has showed a comparable reactivity with the homogenous Fenton system [2] without encountering the above problems. Inspired by those studies, we will explore an alternative heterogeneous catalytic system using manganese oxides as catalysts, which has rarely been addressed.

In this study, nano-crystalline Mn_2O_3 was prepared inside the mesopores of SBA-15. The catalyst as prepared has been examined for wet oxidation of ethanol in aqueous solution. For comparison, the reactivity of several standard bulk manganese oxides was also examined under the same reaction conditions. The structure of nano-crystalline Mn_2O_3 has been characterized with a series of techniques.

The synthesis of SBA-15 is adopted from literature method [3] that employs Pluronic P123 (BASF) surfactant as template and tetraethyl orthosilicate (TEOS, 98%) as silica source. First, manganese (III) acetylacetonate ($[CH_3COCH=C(O)CH_3]_3Mn$, Aldrich, denoted as MnAc) was

dissolved in acetone (C.P.) at room temperature, then SBA-15 powder was put into the solution. The ratio of MnAc/SBA-15 is 2.5 mmol/g. The mixture was vigorously stirred until the solvent was evaporated completely. Finally, the precursor was heated in an oven at 773 K for 5 h with a ramping rate of 1 K/min. Through calcination the organic compound was decomposed into Mn_2O_3 crystalline. Note that by the similar process for heating MnAc, only a mixture of oxidation state of Mn_xO_y (mainly MnO_2, dark color) was formed. Characterizing the catalysts was performed through several techniques, including powder X-ray diffraction (PXRD, Bruker D8 diffractometer), N_2 adsorption-desorption isothermals, transmission electron microscopy (TEM, Tecnai TF 20 S-twin with Lorentz Lens), laser Raman spectroscopy (LRS, JY Horiba LabRAM HR) and X-ray photoelectron spectroscopy (XPS, VG ESCALAB 250 spectrometer).

The activity measurements were carried out in a glass batch reactor equipped with a magnetic stirrer and thermostat. The analysis of the reactant was done with a GC (Agilent 6890N) equipped with a HP-5 column.

The existence of sole Mn_2O_3 phase is confirmed by the Raman and XPS spectra. Raman spectra obtained for the bulk Mn_2O_3 (99.99% Aldrich) and the Mn_2O_3/SBA-15 catalyst are presented in Fig. 1. The bands at 309, 502, and 641cm^{-1} correspond to the bending modes of Mn_2O_3, asymmetric stretch of Mn-O-Mn, symmetric stretch of Mn_2O_3 groups, respectively [4]. It is worthy to note that the band at 974 cm^{-1} (Fig. 1b), which is ascribed to stretch of terminal Mn=O, is an indicative of the isolated Mn_2O_3 [4]. Furthermore, the strong intensity for the peak at 974 cm^{-1} indicates that nano-crystalline Mn_2O_3 is highly dispersed inside the channels; therefore, it is understandable that almost no diffraction peak is visualized in XRD patterns. It is well known that the minimum size of crystalline determined by XRD is ca. 3 nm [5]. So, most of single Mn_2O_3 crystalline inside the SBA-15 is estimated to be consisted of about three unit cells (the lattice parameter for Mn_2O_3 (cubic), a=0.941 nm). On the other hand, XPS analysis of the Mn 2p core level and split of Mn 3s proved the predominant species is Mn(3+) in the Mn_2O_3/SBA-15 [6].

The high dispersion of Mn_2O_3 and the location of these nano-crystallines are also verified by PXRD, TEM and N_2-adsorption experiments. PXRD patterns at low angles suggest that the SBA-15 still has a high degree of hexagonal mesoscopic organization even after forming Mn_2O_3 nano-crystallines [3]. N_2 adsorption measurements confirmed that the Mn oxide particles indeed were inserted in the pores of SBA-15, because the pore volume of the SBA-15deceased from

1.27 cm^3/g to 0.49 cm^3/g after the deposition of Mn$_2$O$_3$; meanwhile, the average pore size of the bare SBA-15 is 7.7 nm, deceasing to 6.3 nm after the insertion of Mn$_2$O$_3$. The morphology and structure were further characterized by TEM. The SBA-15 employed has typical *p6mm* hexagonal morphology with the well-ordered 1D array (Figs. 2a and 2b). The estimated average pore size of the SBA-15 is ca. 8.0 nm from the TEM measurement, very close to the value (ca. 7.7 nm) determined by N$_2$ adsorption. Furthermore, along [001] and [100] orientation, we can see the pores are filled with Mn$_2$O$_3$ nano-crystallines (Figs. 2c and 2d), while the features for the SBA-15 nanostructure are little affected in the process of preparation.
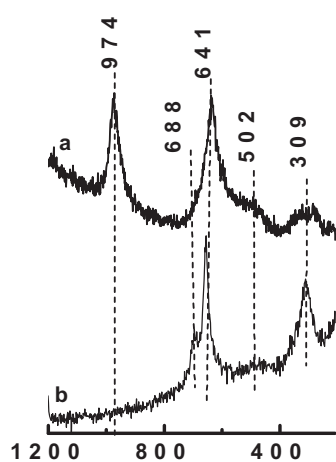
Fig 1. Raman spectroscopy of Mn$_2$O$_3$/SBA-15 (a) and single crystalline Mn$_2$O$_3$ (b).
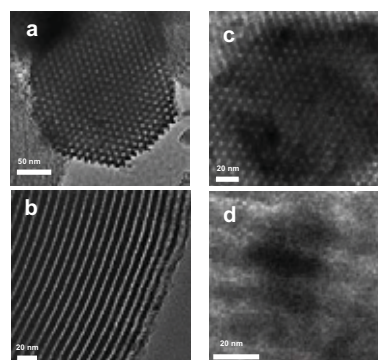
Fig 2. TEM images recorded along the [001] and [100] of SBA-15 (a and b), Mn$_2$O$_3$/SBA-15 (c and d)
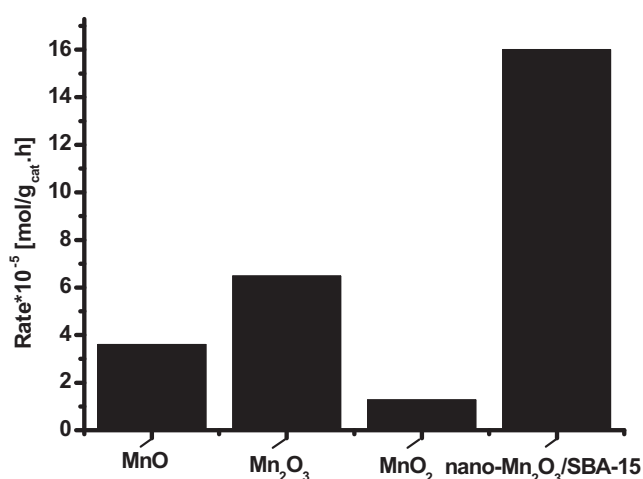
Fig 3. Reactivity of bulk manganese oxides and Mn$_2$O$_3$/SBA-15 for the wet oxidation of ethanol in aqueous solution. Reaction conditions: 100 ppm of ethanol, 8000 ppm of H$_2$O$_2$, 0.25 g/L of catalyst, at 363 K for 1 h, pH of 7

Fig. 3 shows that the reactivity of the standard manganese oxides, such as MnO (aldrich, 99.99%, 1.1 m^2/g), Mn$_2$O$_3$ (aldrich, 99.999%, 4.0 m^2/g) and MnO$_2$ (aldrich, 99.999%, 0.9 m^2/g),

exhibit an order of $Mn_2O_3 > MnO > MnO_2$. Interestingly, the reactivity of the Mn_2O_3 nano-crystalline is about three times higher than the bulk Mn_2O_3.

In summary, a method has been developed to prepare highly dispersed Mn_2O_3/SBA-15 catalysts. Preliminary results indicate that most of the Mn_2O_3 particles are located in the channels of SBA-15. The prepared catalyst exhibits high catalytic activity in the wet oxidation of ethanol, and is a promising Fenton-type catalyst material.

Notes and references

[1] Centi, G.; Perathoner, S.; Torre, T.; Verduna, M. T. *Catal. Today* 2000, **55**, 61.

[2] Kuznetsova, E. V.; Savinov, E. N.; Vostrikova, L. A.; Parmon, V. N. *Appl. Catal.* B 2004, **51**, 165

[3] (a) Zhao, D. Y.; Huo, Q. S.; Feng, J. L.; Chmelka, B. E.; Stucky, G. D. *J. Am. Soc. Chem.* 1998, **120**, 6024. (b) Zhao, D. Y.; Feng, J. L.; Huo, Q. S.; Melosh, N.; Fredrickson, G. H.; Chmelka, B. F.; Stucky, G. D. *Science*, 1998, **279**, 548.

[4] (a) Chua, Y. T.; Stair, P. C.; Wachs, I. E. *J. Phys. Chem. B* 2001, **105**, 8600. (b) Bernard, M.-C.; Goff, A. H.; Thi, B. V.; De Torresi, S. C. *J. Electrochem. Soc*. 1993, **140**, 3065. (c) *Handbook of Viberational Spectroscopy*; Chalmers, J. M.; Riffiths, P. R.; Eds.; Jim Wilkie, J & R Press, UK, 2002.

[5] (a) *Handbook of Heterogeneous Catalysis*; Ertl, G.; Knözinger, H.; Weitkamp, J.; Eds.; VCH, Weinheim, Germany, 1997. (b) *Handbook of Chemistry and Physics*; Lide, D. R.; Eds.; 2000, CRC Press LLC.

[6] (a) Zhao, L. Z.; Young, V. *J. Electron Spectrosc. Relat. Phenom*. 1984, **34**, 45. (b) Elp, J. van; Potze R. H.; Eskes, H.; Berger, R.; Sawatzky, G. A. *Phys. Rev. B* 1991, **44**, 1530.

GAS TO LIQUIDS (GTL) AS AN OPTION IN MONETIZING STRANDED GAS FIELD. FEASIBILITY ANALYSES USING INTEGRATED PROCESS ROUTES

A. Hanif[a], A. Thaib[a], A.D. Yagus[a], W.W. Purwanto[b], K. Mulia[b], A.H. Saputra[b]

[a]*PERTAMINA EP, 14th Kwarnas Build. Jl.Merdeka Timur no. 6 Jakarta, 10110, Indonesia*
Email : ahanif@pertamina.com
[b]*Chemical Engineering Department, University of Indonesia, Depok 16424, Indonesia*

Indonesia has wealth of natural gas resources; part of these resources are stranded and located in remote regions outside Java Island that is still untapped, with excellent prospective for further utilization of natural gas. The main obstacle of this kind of natural gas reserves development is high cost of transportation. Gas to Liquids (GTL) technology offers some superb opportunities to bring Indonesia's remote natural gas reserves to markets by converting the gas into high quality liquid fuels, sulfur free, ultra low aromatics and high centane number that can be transported using conventional petroleum infrastructures.

This paper, first reviews emerging gas technologies and its economic considerations. Second analyses technical and economical aspects of integrated GTL application on Indonesia's gas reserves with the case study of Matindok block gas fields. In the technical aspect, five integrated GTL process routes are proposed, producing simultaneously ultra clean liquid fuels (diesel and naphtha), electricity and valuable chemicals. This analysis is conducted using mainly CHEMCAD process simulator in evaluating technical performances of each integrated process routes such as their synthesis gas characteristic, carbon efficiency and energy efficiencies. Profitability analyses are conducted by evaluating economical parameters such as NPV and IRR for some process routes. In addition, sensitivity analyses are also carried out to find the most sensible parameters such as gas price, product prices or crude oil price, and plant capacity, affecting the profitability of integrated GTL plant.

The analyses results revealed that some integrated GTL process routes producing synthetic fuels, electricity and chemicals (urea) are feasible for certain natural gas reserves with modest gas price (~ 1.2 – 1.8 US$/MMbtu) with 30.000 bpd capacity corresponding to ~ 3 tcf of gas reserves. And for natural gas reserve with high content of carbon dioxide up to 40%, integrated GTL process with co-product acetic acid is very promising due to high price of co-product for even at higher gas prices and smaller gas fields. Finally, the energy policy needed to capitalize Indonesia's stranded gas is also discussed.

PP-22

MATHEMATICAL MODELLING OF PHENOL PHOTOOXIDATION. KINETICS OF THE PROCESS TOXICITY

Oscar Primo, María J. Rivero, <u>Inmaculada Ortiz*</u>, Angel Irabien

Departamento de Ingeniería Química y Química Inorgánica, E.T.S.I.I. y T.,

Universidad de Cantabria, Avenida de los Castros s/n, 39005 Santander, Spain.

Phone: 34 942201585   Fax: 34 942201591   E-mail: ortizi@unican.es

ABSTRACT

This work reports the kinetic analysis of the photochemical degradation of phenol considering the evolution of parameters such as the total organic carbon, *TOC*, toxicity of the treated water, *TU*, and oxidant concentration H_2O_2. The experimental study was carried out working with an initial concentration of phenol of 1000 mg L^{-1}, with a constant flux of radiation of 8.8×10^{-5} einstein s^{-1} and a variable initial concentration of the oxidant in the range between 17000 mg L^{-1} and 51000 mg L^{-1}. The obtained results of *TOC* fitted to a first order kinetic law whereas zero order kinetics was found to describe H_2O_2 evolution. The decrease of the toxicity followed a constant trend related to *TOC*, being the ratio *TU*/*TOC* dependant on the initial H_2O_2 concentration.

1. INTRODUCTION

Phenol is usually taken as a model compound in research studies dealing with advanced wastewater treatments due to its toxicity, the frequency of its presence in industrial wastewaters and the fact that it is an intermediate in the oxidation route of higher molecular weight aromatics. The combination of ultraviolet light and H_2O_2 has great potential and could be applicable for the conversion of many types of organic contaminants into mainly CO_2 and H_2O. Degradation of phenol by different advanced oxidation processes, including UV-based processes, has been reported in literature [1-4]. When studying oxidation reactions, attention has to be paid not only to the removal of the main compound but also to the reduction of the toxicity of the final products because it is well known that phenol oxidation treatments lead to the generation of highly toxic intermediate products. Besides, generally there is excess of H_2O_2 over the stoichiometric ratio in the reaction, and it also contributes considerably to the toxicity of the final product. In this sense, bioassays can complete the chemical characterization of the reaction products.

In this work, the degradation process of phenol in polluted water by UV/H_2O_2 has been studied. An experimental design was carried out to investigate the influence of operation variables. Finally, a generalized kinetic model is developed in order to determine the kinetic behaviour of the main operation variables.

2. EXPERIMENTAL SECTION

Phenol (99%, *Panreac*) and H_2O_2 (35 % w/w, *Solvay Interox*) were used as reagents. Deionized water supplied by a *Milli-Q* water purification unit (*Millipore Waters*) was used.

The experiments were performed in a batch cylindrical glass photoreactor of 0.8 L. It included a medium-pressure Hg lamp TQ 150 (150 w) with a wavelength emission at 200 – 450 nm (*Heraeus Nobelight*) immersed in a quartz sleeve placed in the middle of the reactor. The photon flux entering the reactor was 8.8×10^{-5} einstein s^{-1} estimated from hydrogen peroxide actinometry. A magnetic stirrer (*Selecta Agimatic-S*) was used to provide proper mixing.

For a standard run, 0.75 L of aqueous solution were used. The initial phenol concentration was 1000 mg L^{-1}. The H_2O_2 concentration varied in the range of 0 – 1.5 M. The initial pH value was in a range of 3.5 – 4. The reaction was carried out at no buffered pH and constant temperature (293 K).

Total organic carbon (*TOC*) analyses were carried out using an analyzer *Euroglas model TOC 1200*. Phenol and identified reaction intermediates (catechol, hydroquinone and p-benzoquinone) were measured by a *Waters* high-pressure liquid chromatograph (HPLC). A Dionex 120 ion chromatograph (IC) equipped with a column IonPac AS9-HC and a conductivity detector was used for organic acids analyses. H_2O_2 concentration was analyzed by iodometric titration. The toxicity of the samples was determined by means of a bioassay following the standard ISO 11348-3 (1998) [*21*] based on the decrease of light emission by *photobacterium phosphoreum* with a *Microtox M500* analyzer (*Azur Environmental*).

3. RESULTS AND DISCUSSION

H_2O_2 concentration had two opposing effects on the reaction rate. Increasing the initial hydrogen peroxide concentration enhanced the oxidation process up to a certain concentration, when hydrogen peroxide started to react with hydroxyl radicals. At higher hydrogen peroxide concentrations, hydrogen peroxide acted as a free-radical scavenger itself decreasing the hydroxyl radicals concentration so, there was an optimum H_2O_2 concentration. For all the experiments more than 88 % of phenol removal was achieved after 60 minutes of irradiation and total degradation was achieved after 120 minutes. An optimum H_2O_2 concentration of 1.0 M (initial H_2O_2/phenol molar ratio = 100) was found.

PP-22

The reaction rate constants k_{ph} were calculated based on the pseudo-first-order kinetics assumption (*equation 1*) by linear regression of the experimental data obtaining values from 3.7×10^{-2} min^{-1} to 6.7×10^{-2} min^{-1}.

$$- dC_{ph}/dt = k_{ph} \, C_{ph} \tag{1}$$

where C_{ph} is the phenol concentration at time t. *Figure 1* illustrates the photodegradation of phenol and *Figure 2* shows formation and degradation of reaction intermediates.
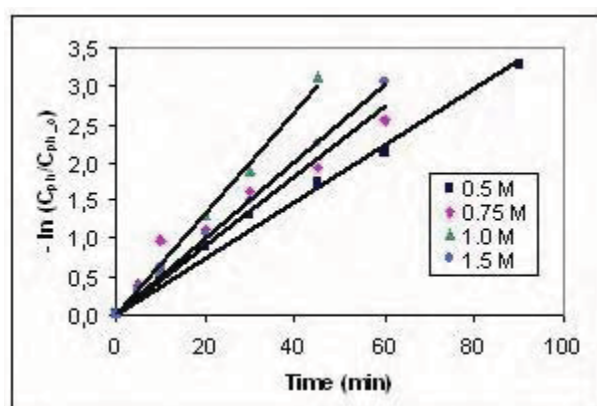
Fig. 1. Pseudo-first-order kinetic for phenol oxidation for several H_2O_2 initial concentrations
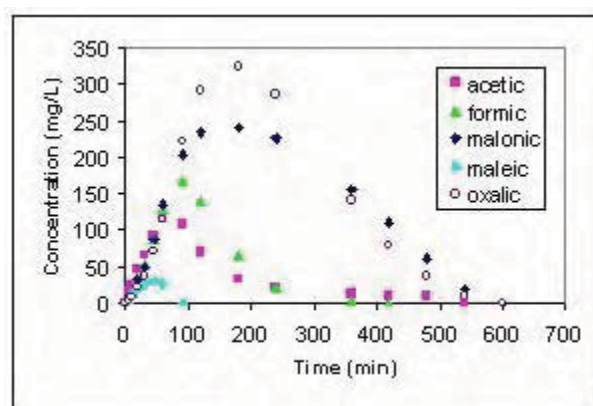
Fig. 2. Organic acids concentration (Initial $H_2O_2 = 1.0$ M)

But due to the intermediate species formation, the total degradation of the target compound does not always correspond to the total mineralization of the organics to CO_2 and H_2O. So, TOC is a global parameter that is frequently analyzed. The decrease of TOC was slower than phenol decrease. The pseudo-first-order kinetic constants k_{TOC} were determined for TOC removal obtaining values between 3.2×10^{-3} min^{-1} and 4.8×10^{-3} min^{-1}.

Related to a kinetic model for H_2O_2 evolution, a zero-order kinetic expression was found (equation 2). The values of the kinetic parameter k_{H2O2} ranged between 1.1×10^{-3} Mmin^{-1} and 2.1×10^{-3} Mmin^{-1}.

$$[H_2O_2] = [H_2O_2]_o - k_{H2O2} \, t \tag{2}$$

The k_{H2O2} dependence on the initial H_2O_2 concentration could be understood considering that phenol and its degradation intermediates could compete with hydrogen peroxide for the available radiation and the value of the H_2O_2/TOC ratio was different in each experiment.

Moreover, an empirical relationship between H_2O_2 and TOC was found (equation 3a). The value of the H_2O_2/TOC ratio was dependent on the initial H_2O_2 concentration (equation 3b) in the range of operation variables (H_2O_2 concentration between 0.5 M and 1.5 M) (*Figure 3*).

$$\text{(a) } H_2O_2 = R_1 \times \text{TOC}; \quad \text{(b) } R_1 = 17.68 \, [H_2O_2]_o \quad (r^2 = 0.99) \tag{3}$$
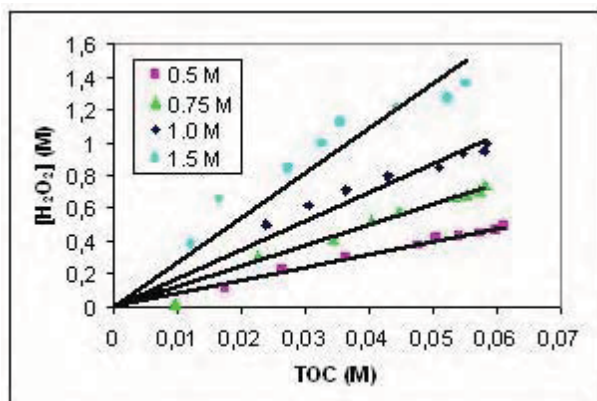
Fig.3. Empirical H_2O_2/TOC relationship.   Fig. 4. Empirical TU/TOC relationship.
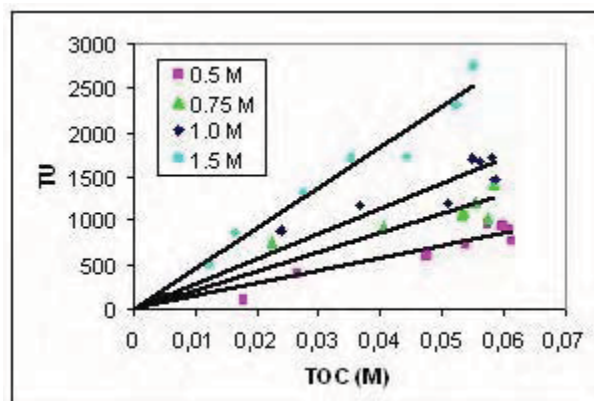
During the experiments a linear relationship between the values of TU and TOC was also found (equation 4a), as it is shown in *Figure 4*. The TU/TOC ratio (R_2) (M^{-1}) depends on the initial H_2O_2 concentration in the range of operation variables (equation 4b)

$$\text{(a) } TU = R_2 \times TOC; \quad \text{(b) } R_2 = 2.99 \times 10^4 \, [H_2O_2]_o \quad (r^2 = 0.99) \tag{4}$$

4. CONCLUSIONS

Thus, a simple predictive model based on the description of the kinetics of the main operation variables of the photochemical oxidation process, i.e., *TOC*, *TU* and oxidant concentration has been proposed.

REFERENCES

[1] R. Andreozzi, V. Caprio, A. Insola, R. Marotta, Advanced oxidation processes (AOP) for water purification and recovery, Catal. Today 53 (1999) 51 – 59.

[2] P. R. Gogate, A. B. Pandit, A review of imperative technologies for wastewater treatment I: oxidation technologies at ambient conditions, Adv. Environ. Res. 8 (2004) 501 – 551.

[3] O. Legrini, E. Oliveros, A. M. Braun, Photochemical processes for water treatment, Chem. Rev. 93 (1993) 671 – 698.

[4] R. Alnaizy, A. Akgerman, Advanced oxidation of phenolic compounds, Adv. Environ. Res. 4 (2000) 233 - 244.

PP-23

SYNTHESIS OF CATALYSTS ON THE BASE OF CERIA-ZIRCONIA OXIDES IN MOLTEN AMMONIUM NITRATE BY USING MICROWAVE IRRADIATION

Ishmaev N.M.[1], Morozov I.V.[1], Lermontov A.S.[2], Fedorova A.A.[1], Burdeynaya T.N.[2], Tretyakov V.F.[2]

[1]*Moscow Lomonosov State University, Chemistry Department, Moscow, Russia, fax: 939-09-98*

[2] *A.V. Topchiev Institute of Petrochemical Synthesis RAS, Moscow, Russia*

morozov@inorg.chem.msu.ru; fedorova@inorg.chem.msu.ru

Now special attention is paid to searching of three-way catalysts for neutralization of dangerous wastes of motor transport (mixture of CO, light hydrocarbons and NO_x). One of the most perspective catalytic systems is system on the base of solid solutions of zirconium and cerium dioxides. This system possesses high thermal and mechanical stability. Besides one of the most important property of cerium dioxide is its ability to regulate the partial oxygen pressure by oxidation – reduction transformation: $CeO_2 \leftrightarrow CeO_{2-x} + x/2\ O_2$ ($0 \leq x \leq 0.5$) [1]. Intercalation of ZrO_2 in crystal lattice of cerium dioxide leads to increase sintering temperature of cerium dioxide [2, 3]. Besides that, solid solutions on the base of cubic or tetragonal modification of ZrO_2 possess high ionic oxygen conductivity and have higher oxygen capacity as compared with pure CeO_2 [4].

The catalysts on the base of ceria-zirconia oxides were synthesized by decomposition of nitrate mixtures in molten NH_4NO_3 using microwave radiation for the first time in this work. One of the advantages of this method is that excess of ammonium nitrate can be easily eliminated from the reaction mixture during heating that leads to formation pure samples without any admixtures. Besides that, mixtures containing NH_4NO_3 absorb microwave radiation that permit to carry out decomposition in microwave furnace. Microwave treatment provides uniform heating of reaction mixture all over the volume that leads to formation high homogeneous products and decreases time of the synthesis.

In all cases, reaction mixture was heated at 130 ºC to prepare homogeneous solution before decomposition in microwave furnace.

Support **A** with average composition $Ce_{0.5}Zr_{0.5}O_2$ was obtained by decomposition of mixture $Ce(NO_3)_3 \cdot 5.7H_2O$, $ZrO(NO_3)_2 \cdot 2H_2O$ and NH_4NO_3 (molar ratio 1:1:6). Support **B** with the same average composition was prepared from reaction mixture that contained $ZrOCl_2 \cdot 8H_2O$ instead of $ZrO(NO_3)_2 \cdot 2H_2O$ and monohydrate of citric acid $C_6H_8O_7 \cdot H_2O$ (**CA**) was added in it in molar ratio Ce:Zr:CA:NH_4 = 1:1:5:20. Both supports were annealed in furnace at 500 °C (2 h). A specific surface area of support **A** was 51.1 m^2/g and of support **B** - 12.1 m^2/g.

Supports A and B were used for preparation supported samples **I-VII**. Samples **I-IV** with composition $CuO/Ce_xZr_{1-x}O_2$ contained 1 mol. % CuO. Samples **I** and **II** were synthesized by impregnation of support **A** with aqueous solution of $Cu(NO_3)_2 \cdot 3H_2O$ or $Cu(CH_3COO)_2 \cdot H_2O$ accordingly. Sample **III** was prepared by impregnation of support **A** with solution $Cu(NO_3)_2 \cdot 3H_2O$ in molten NH_4NO_3 (molar ratio Cu:NH_4 = 1:4). Sample **IV** was synthesized by impregnation of support **B** with aqueous solution of $Cu(NO_3)_2 \cdot 3H_2O$. Sample **V** $CuO/Ce_xZr_{1-x}O_2$ was prepared by the same way with sample **IV** but copper oxide content in sample **V** was 5 mol. %. Sample **VI** was obtained by simultaneous decomposition of cerium nitrate, zirconium oxonitrate, copper (II) nitrate and ammonium nitrate mixing in molar ratio 1:1:0.8:12 accordingly. Sample **VII** was synthesized from cerium nitrate, zirconium oxonitrate, iron (III) nitrate and ammonium nitrate taking in molar ratio 1:1:0.8:12 accordingly. Both samples **VI** and **VII** were washed in concentrated HNO_3 to remove copper (II) oxide and iron (III) oxide accordingly.

Samples were annealed at 500 °C (1 h) and at 600 °C (2 h).

Investigation of decomposition process was carried out by thermo-gravimetric (TGA) and differential-thermal (DTA) analyses. Samples obtained were investigated by X-ray powder diffraction (XRD). Samples were tested in carbon monoxide oxidation reaction (gas volume rate was 10000 $sm^3 \cdot h^{-1}$, gas mixture composition was 4 vol. % CO and 2 vol. % O_2 in He).

According to XRD support **A** consists of two phases: $t-ZrO_2$ and solid solution on the base of CeO_2 ($t-Ce_{0.81(3)}Zr_{0.19(3)}O_2$). At the same time support **B** is monophase and its composition is the same with average composition $Ce_{0.5}Zr_{0.5}O_2$.

According to the results of TGA and DTA temperatures of the formation of ZrO_2 and CeO_2 are close but CeO_2 forms at lower temperature. So decomposition of solution of cerium and zirconium nitrates in molten NH_4NO_3 does not lead to formation of monophase sample $Ce_{0.5}Zr_{0.5}O_2$ and formation of two different phases takes place (support **A**). Monophase sample $Ce_{0.5}Zr_{0.5}O_2$ was obtained when citric acid was added in reaction mixture (support **B**). Perhaps it connects with the formation of stable chelate citrate complexes including

simultaneously both cations. Besides that, decomposition of reaction mixture containing citric acid proceeds in combustion regime because of oxidation of citrate-ions by ammonium nitrate.

Temperatures of 50 % and 95 % conversion of CO over samples prepared are presented in table 1.

Table 1. Results of catalytic measurements.

Sample	I	II	III	IV	V	VI	VII
	CuO/**A**, 1 %	CuO/**A**, 1 %	CuO/**A**, 1 %	CuO/**B**, 1 %	CuO/**B**, 5 %	(Cu,Ce,Zr) O_x	(Fe,Ce,Zr) O_x
$m_{catalyst}$, g	0.170	0.182	0.075	0.116	0.116	0.253	0.140
$V_{catalyst}$, cm^3	0.3	0.3	0.3	0.6	0.7	0.3	0.3
$T_{50\%}$, °C	130	127	157	165	147	99.5	217
$T_{95\%}$, °C	161	163	207	202	178	124	497

Investigation of catalytic activity of samples prepared has shown that samples supported on monophase support do not possess higher activity than samples supported on polyphase one. So samples **I** and **II** supported on diphase support **A** possessed higher catalytic activity than sample **IV** with the same composition supported on monophase support **B** (table 1, figure 1). Impregnation of the support **A** by solution of $Cu(NO_3)_2$ in molten NH_4NO_3 (sample **III**) occurred less effective as compare with commonly used way of impregnation in aqueous solution (samples **I**, **II**). Perhaps it connects with less wettability of supported by melt and as a result, CuO is not uniformly dispersed on the surface.
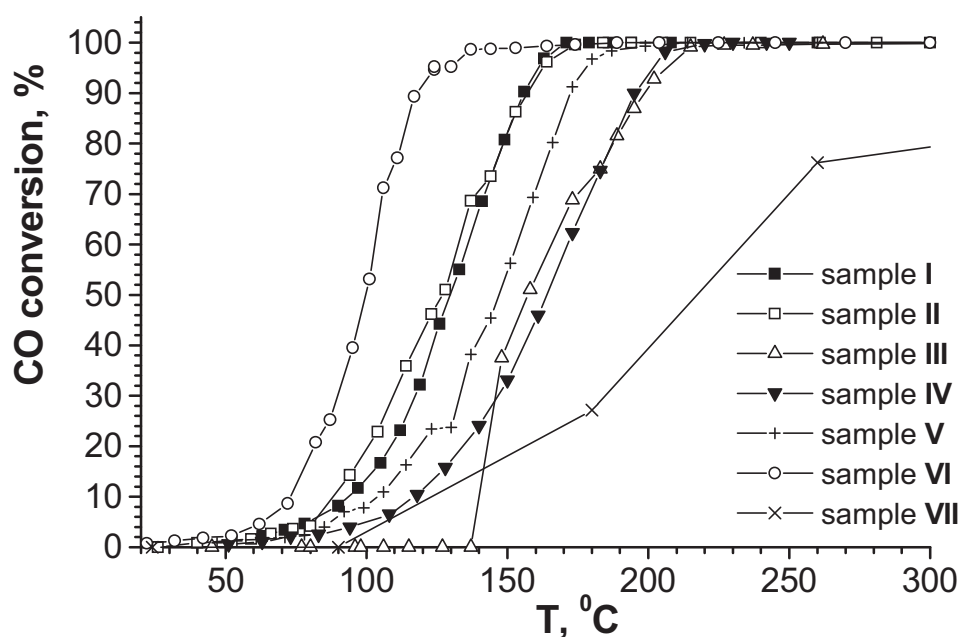
Fig. 1. Carbon monoxide oxidation over samples synthesized.

Sample **VI** demonstrated the highest catalytic activity ($T_{50\%}$ = 99.5 °C). Perhaps it connects with high catalytic activity of copper oxide clusters (distance Cu - Cu < 5 Å) that are formed in $CuO-ZrO_2$ system [5]. At the same time sample **VII** synthesized by the analogous way demonstrated less catalytic activity ($T_{50\%}$ = 217 °C). It can be explain by that decomposition of $Fe(NO_3)_3 \cdot 9H_2O$ to Fe_2O_3 proceeds near 100 °C. Therefore, zirconium and cerium dioxides, which decompose at much higher temperature, precipitate on the surface of Fe_2O_3 particles. This scheme is confirmed by that Fe_2O_3 from sample **VII** does not dissolve in concentrated HNO_3. So different distribution character of oxides CuO and Fe_2O_3 in samples **VI** and **VII** accordingly is in good agreement with catalytic activity data.

Thus, oxide samples, which possess good catalytic activity in carbon monoxide oxidation reaction, can be obtained by synthesis in molten NH_4NO_3 using microwave radiation. It was shown that this new way of oxide synthesis permits to obtain pure products in short time.

1. Fukui K., Namai Y., Iwasawa Y. // Applied Surface Science. 2002. V. 188. P. 252-256.

2. Masui T., Ozaki T., Machida K., Adachi G. // Journal of Alloys and Compounds. 2000. V. 303-304. P. 49-55.

3. Pichinger S. // Topics in Catalysis. 2004. V. 30-31. P. 5-15.

4. Bernal S., Blanco G., Calvino J.J., Gatica J.M., Perez Omil J.A., Pintado J.M. // Topics in Catalysis. 2004. V. 28. P. 31-45.

5. Vasenin N.T., Fedorova A.A., Anufrienko V.F., Larina T.V., Morozov I.V., Paukshtis E.A., Ismagilov Z.R. // Russian Journal of Physical Chemistry. 2005. V. 79. № 8. P. 1417-1423.

FORMATION OF THE Pt(O)/Si(Ca)O₂ NANOFIBERS UPON THE REACTION OF PLATINUM AEROSOL PARTICLES WITH A CALCIUM- AND SILICON-CONTAINING MATERIAL

A.S. Ivanova, **E.M. Slavinskaya, V.I. Zaikovskii, I.N. Polukhina,**
O.V. Chub, and A.S. Noskov

Boreskov Institute of Catalysis, Novosibirsk, Russia
E-mail: iva@catalysis.nsk.su

1. Introduction

The high-temperature oxidation of ammonia carried out on platinum gauzes under pressure [1] is accompanied by platinum evaporation and mechanical entrainment as aerosol particles. To reduce the irretrievable loss of platinum, its particles are trapped, in particular, by mounting a granular layer of refractory calcium oxide. The reaction of platinum and platinum oxide vapors with CaO yields compounds like $CaO \cdot PtO_2$, $3CaO \cdot PtO_2$, etc. A macroscopic study of the surface of calcium oxide grains after trapping has shown that Pt particles are located on the surface of the oxide grains and almost do not penetrate inside the grains. To increase the efficiency of using CaO by increasing its surface area, it was proposed [2] to apply CaO on a high-temperature silicon-containing material (glass fabric).

In this work, we studied the interaction between platinum aerosol particles formed upon the oxidation of ammonia on a platinum catalyst and calcium oxide supported on a high-temperature silicon-containing material (glass fabric) at about 900°C.

2. Experimental

The high-temperature oxidation of ammonia was carried out on model Pt-containing catalysts (16--45% Pt/SiO₂) with simultaneous capture of platinum aerosol particles by a material (filter) containing 12--14 wt % CaO applied onto a glass fabric. Ammonia oxidation proceeded in a flow-type reactor as follows: a reaction mixture containing 10 vol % ammonia, 14.6 vol % oxygen, and balance helium was passed through a Pt catalyst bed at a temperature of 900°C and a pressure of 2 atm for 1 to 5 h. The hot reaction gases formed traveled through a filter layer. After the experiment, the reactor was cooled to room temperature in a helium flow.

The unloaded Pt-containing catalyst and the filter were analyzed by X-ray fluorescence on VRA-30 analyzers using a Karl-Zeiss-Jena X-ray tube with a Cr anode; by scanning electron microscopy on an REM-100U instrument (Selmi, Ukraine); and by high-

resolution (0.14 nm) transmission electron microscopy (TEM) on a JEM-2010 instrument (Jeol, Japan) coupled with energy dispersive X-ray microanalysis (EDX).

3. Results and discussion

According to scanning electron microscopy, the initial glass fabric is composed of interlaced threads consisting of fibers 6.5 - 7 μm in diameter (Fig. 1a). In the thread structure, the fibers are evenly arranged at distances of 3 - 4 μm from each other (Fig. 1a). After application of CaO, the general pattern changes (Fig. 1b): the distance between the fibers increases to 6 - 18 μm. This is due to the fact that calcium oxide penetrates both into the thread fibers and between them (Fig. 1b). The CaO particles between the thread fibers are distributed nonuniformly. In the sites with greater CaO concentration, aggregation of its particles takes place to form larger agglomerates (Fig. 1b). The average diameter of the smallest particle is 2 - 4 μm, that of the agglomerate is 9 - 17 μm.

a)   b)
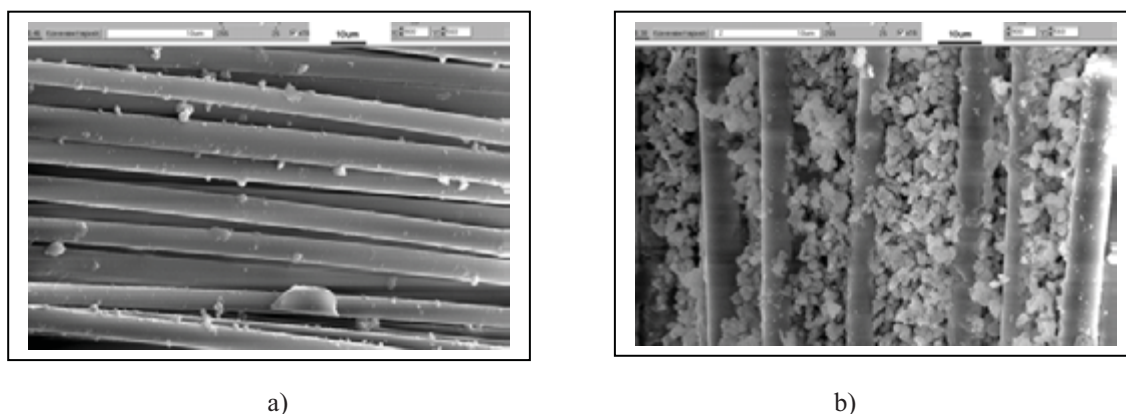
Fig.1. Images of (a) the initial glass fabric sample and (b) glass fabric with applied CaO.

In chemical reactor new material is formed in process of ammonia oxidation at 900°C as a result of platinum evaporation from model Pt- containing catalyst. To elucidate the state of platinum on the filter, the filter was examined under an electron microscope after the reaction. High-resolution images show (Fig. 2a) that CaO occurs on the glass fiber surface as porous particles with a size of 20 - 70 nm; simultaneously, crystalline rods (nanofibers) about 50 nm in diameter and up to 1000 nm

Fig.2. TEM image of the filter: (a) silica nanofibers grown on the CaO/glass fabric surface; (b) EDX spectrum of nanofibers (the sites for the spectra were taken inside the circles).

high with different orientations of the growth axes can b e detected. The EDX spectrum of

these sites (Fig. 2b) shows that the nanofibers contain Si : O = 1 : 2 (atomic ratio); in addition, they contain Ca. Thus, the composition of nanofibers can be represented as $Si(Ca)O_2$; i.e., this is quartz containing dissolved calcium. The crystal structure of nanofibers includes a multitude of planar defects (stacking faults) normal to the growth axis (Fig. 3). The formation of the nanofibers may be catalyzed by platinum that has been entrained from the model Pt-containing catalyst of ammonia oxidation and deposited on the CaO/glass fabric filter. This is indicated by TEM data (Fig. 4): the active platinum deposited on CaO is carried by the growing nanofibers during the reaction from the filter surface toward the fiber top. As this takes place, platinum exists as metal particles with a size of ~5 nm under the $Si(Ca)O_2$ layer (Fig. 4b). The oxidation of platinum is apparently favorable for the termination of the growth of the $Si(Ca)O_2$ rods and the emergence of the oxidized platinum on the $Si(Ca)O_2$ surface (Fig. 4c). According to EDX data (Fig. 4d), the Ca concentration in $Si(Ca)O_2$ is much higher on the nanofiber top.
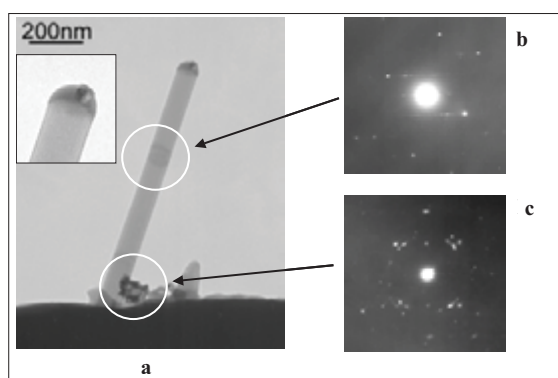
Fig.3. TEM image of the filter (a) and electron diffraction patterns from the nanofiber sites (in the circles): (b) one-dimensional diffraction demonstrating multiple stacking faults of $Si(Ca)O_2$ nanofiber layers; (c) diffraction by a CaO particle.
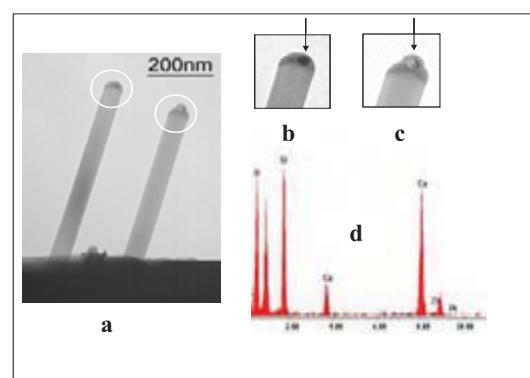
Fig.4. TEM image of the filter: (a) sites for the microanalysis of the nanofiber top (shown in the circles); (b) Pt metal particle incorporated into the top; (c) oxidized Pt; (d) EDX spectrum.

The possibility of formation of rods (or whiskers) of, for example, alumina has long been known [3, 4]. It has been found [5] that, depending on the synthesis conditions, one can prepare alumina rods differing in shape, size, and crystallographic orientation of the growth axes. One synthetic procedure includes oxidation of aluminum in the presence of dry hydrogen and coreagents, such as mullite or another silicon-containing material. The presence of these coreagents is considered to be crucial for the growth of the rods, because this ensures the reaction between the "aluminum" vapor and volatile silicon monoxide.

In our case, the formation of $Pt(PtO)/Ca_xSi_yO_2$ nanofibers upon the reaction of active platinum with the CaO/glass fabric material during ammonia oxidation may occur in the

following way.

- The platinum removed from the Pt-containing catalyst is apparently oxidized by the steam resulting from the oxidation of ammonia: $Pt + 2H_2O \rightarrow PtO_2 + 2H_2$;

- the oxidized platinum interacts with the filter: $PtO_2 + CaO/glass\ fabric \rightarrow$ $PtO_2\ CaO/glass\ fabric$;

- in the presence of hydrogen, a part of the oxidized platinum is reduced, and the reaction between platinum metal and calcium oxide deposited on silicon dioxide, capable of some volatility, might give the nanofibers.

Thus, our findings show that the CaO/glass fabric material can capture platinum aerosol particles entrained from the Pt-containing catalyst and stabilize them as the oxide distributed at the end of the $Si(Ca)O_2$ nanofibers. The newly formed Pt-Ca-O/glass fabric composition opens up the way for the production of new generation catalysts in which the active component (Pt) is located at the ends of nanofibers at a distance of up to 1000 nm above the substrate surface. This design of the catalyst would, on the one hand, prevent the aggregation of particles of the active component and, thus, increase its thermal stability and, on the other hand, increase the catalyst stability against poisoning, in particular, by sulfur-containing compounds by preventing blocking of the active sites through sulfatation of the substrate.

4. Conclusions

It was found that crystalline nanofibers (up to 1000 nm high and about 50 nm in diameter) are formed on the surface of the calcium-and-silicon--containing high-temperature material upon its interaction with platinum aerosol particles at $900^{o}C$. The nascent nanofibers represented quartz containing dissolved calcium, $Si(Ca)O_2$, the calcium concentration being higher on the top of the fibers. Platinum is also present on the top of the nanofibers, in particular, oxidized platinum occurs on the surface and metal particles (~5 nm) are located under the $Si(Ca)O_2$ layer.

References

1. Karavaev, M.M., Zasorin, A.P., and Kleshchev, N.F., Kataliticheskoe okislenie ammiaka (Catalytic Oxidation of Ammonia), Moscow: Khimiya, 1983.
2. Noskov, A.S., Ivanova, A.S. Slavinskaya, E.M., Polukhina, I.A., Karasyuk, N.V., and Chub, O.V., RF Patent No. 2 266 858, Byull. Izobret., No. 33 (2005).
3. Webb, W.W. and Forgang, W.D., //J. Appl. Phys., 1957, vol. 28, p. 1449.
4. Wiedemann, H.G., Sturzenegger, E., Bayer, G., and Wessicken, R., //Naturwissenschaften, 1974, vol. 61, pp. 65--68.
5. Wiedemann, H.G., Nerbel, J., and Reller, A., //Thermochim. Acta, 1998, vol. 318, pp. 71--82.

PP-25

DESIGN OF THE TWO-STAGE AMMONIA OXIDATION CATALYTIC SYSTEM FOR MEDIUM PRESSURE NITRIC ACID PLANTS

L.A. Isupova, I.A. Zolotarskii, N.A. Kulikovskaya, A.A. Marchuk,

E.F. Sutormina, V.A. Sadykov, A.S. Noskov

Boreskov Institute of Catalysis SB RAS, pr. Lavrentieva, 5, Novosibirsk, Russia, 630090

Ammonia oxidation process in nitric acid production ($4NH_3 + 5O_2 \rightarrow 4NO + 6H_2O$) is realized on Pt gauzes. There are three types of ammonia oxidation reactors working under atmospheric, medium and high pressure, their operation conditions are presented in the Table 1.

Table 1. Industrial operation conditions for ammonia oxidation process

Pressure	Temperature of Gauses, ^{o}C	NH_3 content, vol.%	NO yield, %	Pt loss, g/t HNO_3	Operating time, month
Atmospheric	810-850	11-12	97-98	0.04-0.05	10-12
Medium, 3-5Bar	850-890	10-11	95.0-96.5	0.10-0.11	5-6
High, 7-11 Bar	900-940	10-11	92-95	0.15-0.30	3-4

Due to high temperature operation conditions, Pt losses occur (Table 1). At that, the last gauzes in the catalyst layer polish ammonia conversion while still lose a sound portion of noble metals. Therefore, an idea to replace them by less expensive oxide catalyst is evident. In 1960th the two stage catalytic system (1 gauze + layer of palletized oxide catalyst) was developed by GIAP for normal pressure plants [1]. For medium and high pressure plants honeycomb catalysts seem to be more attractive providing uniformity of gas flow, low pressure drop and low dust formation. Boreskov Institute of Catalysis has developed the iron oxide based honeycomb catalyst BIC-42-1 in 1990th [2,3]. This catalyst has found wide application in high pressure UKL-7 plants. It is shaped as a 70x70x50 mm monolith with square cannels (5x5 mm) and wall thickness 1.8-2.2 mm. Its application results in 25-30% saving in gauzes loading and 15-20% reduction of Pt losses at near the same product yield and longer gauzes life time [4]. However, as it will be shown below, its application for medium pressure plants is questionable due to its geometry.

Mathematical modelling of a two-stage catalytic system consisting of different numbers of Pt gauzes and honeycomb catalyst layers of different geometry was performed at conditions corresponding to the ammonia oxidation reactor of the typical Russian medium pressure plant AK-72 (operation pressure – 3.5 Bar). This reactor is loaded by 7 woven Pt gauzes with an

initial fibre diameter of 0.092 mm traditionally. The mathematical model applied presumes mass transfer limitation of the reaction both on Pt gauzes and a honeycomb catalyst.

Calculations show that ammonia conversion reaches 98.8% when a standard catalytic system with 7 sheets is used. The aim of calculations was to find out a configuration of a honeycomb catalyst bed when 3 sheets of Pt gauzes are removed. Table 2 shows calculation results for 3 types of a honeycomb catalyst.

Table 2. Ammonia conversion for different configuration of a honeycomb catalyst bed. Number of channels per square inch: I – 15, II – 30, III – 200. Height of one layer – 50 mm.

Type of catalyst	Number of honeycomb catalyst layers		
	1	2	3
I	96.9	98.1	98.8
II	97.7	99.0	99.6
III	98.6	99.6	99.9

One can see that a two-stage catalytic system comprising 4 Pt gauzes and 2 layers of the catalyst III or 3 layers of the catalyst II provides ammonia conversion higher than a standard Pt system. Such system can be applied in industry if the oxide honeycomb catalyst meets the following requirements:

– high activity;

– high selectivity;

– robustness in operation conditions (strength and resistance to thermoshocks);

– manufacturability.

It is hardly possible to fulfill these requirements, especially thermoshock resistance, for a bulk iron oxide based honeycomb monolith catalyst with cell density corresponding to catalyst II and III because of its rather high thermal expansion coefficient (TEC). Therefore, a comprehensive study of different catalytic materials was carried out. The frame structured cordierite ($2MgOx2Al_2O_3x5SiO_2$) honeycombs are characterized by the low TEC ($2*10-6$ 1/K) and often used as a refractory carrier for high temperature catalyst applications [5]. Results of this study for impregnated on cordierite catalyst including results of a life test in real operation conditions were published in [6].

This paper presents results of ammonia oxidation process study for another kind of catalytic materials – cordierite-like frame structured ones.

A frame structure allows to obtain modified materials with 3d active cations (Fe, Co, Mn) instead of Mg, that may be active in ammonia oxidation. Meanwhile frame structured materials can be directly shaped as monoliths.

PP-25

Therefore, this paper deals with investigation of ammonia oxidation process with modified frame structured honeycomb monoliths. A draw plate used for monoliths preparation had a triangle channel side of 2.5 mm and wall thickness of 0.4 mm that gives approximately 200 channels per square inch. Monolith height was 50 mm. Three types of honeycomb catalysts with Co, Fe and Mn cations ($2CoOx2Al_2O_3x5SiO_2$, $2FeOx2Al_2O_3x5SiO_2$, $MnOx2Al_2O_3x5SiO_2$) were prepared.

Ammonia oxidation process was carried out in a bench scale quartz tubular reactor with inner diameter of 26 mm at temperature 700-900 ^{o}C and atmospheric pressure. Samples of honeycomb catalysts in the form of fragments with diameter of 21-22 mm and length of 50 mm were tested with and without one Pt sheet. Before the reaction starts up, catalysts were preheated at 700 ^{o}C in air for 30 minutes. Then reaction gazes (5% ammonia in the air preheated at 450°C in a quartz mixer) were flowed through the catalyst with 7.6 l/min flow rate (standard gas velocity 0.33 m/s). The ignition of the catalyst was determined by temperature increase. Ammonia, NO and NO_2 concentrations were analyzed by the on-line spectrophotometer analysis [6, 7].

All such prepared catalysts provide 100 % ammonia conversion degree even without Pt gauzes at temperature higher 850 ^{o}C. The two-stage system (with one Pt gauze) provides NO yield higher than 94%. $2FeOx2Al_2O_3x5SiO_2$ and $MnOx2Al_2O_3x5SiO_2$ frame structured catalysts (BIC-42-4) was shown not to be deactivated after living tests in UKL-7 plant as compared with supported catalysts.

References

1. M.M. Karavaev, A.P. Zasorin, N.F. Klesev. Catalytic oxidation of ammonia. Moskow, Khimiya, 1983.232 c.(In Russian)

2. V.A. Sadykov, E.A. Brushtein, L.A. Isupova, et al. Khimicheskaya promyshlennost', No 12 (1997) 33 (In Russian).

3. V.A. Sadykov, L.A. Isupova, I.A. Zolotarskii et al. Applied Catalysis A: General 204 (2000) 59.

4. V.I. Chernyshev, E.A. Brushtein, Cataliz v Promyshlennosti (Catalysis in Industry), 3 (2001) 30 (in Russian).

5. E.G. Avakumov, A.A. Gusev. Kordierite- advanced ceramic material. Novosibirsk, SB RAS, 1999 166c

6. L. A. Isupova, E.F. Sutormina, N.A. Kulikovskaya, L.M. Plyasova, N.A.Rudina, I.A. Ovsyannikova, I.A. Zolotarskii, V.A. Sadykov Catalysis.Today105(2005) 436.

7. E. F. Sutormina, Zurnal Analiticheskoi Khimii (J. Analytic Chem.) 59/4 (2004) 1 (In Russian).

PtNi CATALYSTS FOR DRY REFORMING OF METHANE

<u>S. Damyanova</u>[1], K. Arishtirova[1], B. Pawelec[2], J.L.G. Fierro[2], L. Petrov[1]

[1] *Institute of Catalysis, Bulgarian Academy of Sciences, 1113 Sofia, Bulgaria*

[2] *Instituto de Catalis y Petroleoquimica, CSIS, Cantoblanco, 28049 Madrid, Spain*

Fax: 359 2 9712967, E-mail: soniad@ic.bas.bg

Introduction

Hydrogen offers a potentially non-polluting, inexhaustible, efficient, and cost attractive fuel for energy demands. Hydrogen is the "fuel of the future". However, the use of hydrogen as a fuel depends on how it is produced. Of all the potential sources of hydrogen, natural gas offers many advantages. The main processes used to transform natural gas to hydrogen are: steam reforming, dry reforming, partial oxidation and autothermal reforming of methane.

The catalytic reforming of methane with carbon dioxide ($CH_4 + CO_2 \rightarrow 2CO + 2H_2$) has several advantages compared to other methane reforming reactions, such as: (i) production of low H_2/CO ratio, suitable for synthesis gas; (ii) providing a practical method for consumption of the both greenhouse gases (CH_4 and CO_2); (iii) opportunity for combination with steam reforming and/or partial oxidation of methane, etc. [1, 2].

Unfortunately, no industrial technology for CO_2 reforming of methane has yet been developed, because no effective, economic catalysts have been discovered. One of the main problems for the preparation of effective reforming catalysts is the prevention of coke formation. The parameters responsible to enhance the catalytic performances of the catalysts include the kind of the components and their concentration, type of the support, temperature of reaction.

The subject of this work is to develop new effective Ni-containing catalysts supported on a suitable support and modified with a small amount of noble metal that can result in a non-expensive bimetallic supported system assuring both high activity of catalyst for hydrogen production and low carbon deposition. The effect of the method of preparation and of the ratio Ni/noble metal on the surface and catalytic properties of the nickel-based catalysts in the process of dry reforming was investigated.

Experimental

Zeolite-supported Ni-containing catalysts modified with Pt were prepared by sequential impregnation and co-impregnation techniques using aqueous precursor solutions of

PP-26

$Ni(NO_3)_2.6H_2O$ and solution of $H_2PtCl_6.6H_2O$ in ethanol. Zeolite ZMS-5 was used as carrier. After impregnation the samples were dried at 384 K and calcined at 823 K. The amount of Pt was 0.5 or 0.3 wt%. The amount of Ni was in the range of 1-12 wt%.

The samples were characterized X-ray diffraction (XRD), temperature-programmed reduction (TPR), infrared spectroscopy (IR) and by S_{BET} method. The catalytic properties of the catalysts were evaluated in the reaction of reforming of methane with CO_2 at 773 K.

Results and discussion

The textural properties of bimetallic PtNi samples presented in Table 1 show that the S_{BET} surface area and pore volume decrease with increase of Ni content, which is caused by the plugging of the pores with nickel oxide particles. There was no influence of the presence of Pt on the textural properties of the samples. However, the method of preparation influences the change of S_{BET} and pore volume; the PtNi sample prepared by co-impregnation shows higher S_{BET} and pore volume compared to those of the sample prepared by consecutive impregnation method.

Table 1. Textural properties of zeolite-supported PtNi samples

Samples	S_{BET} m^2/g	Pore Volume cm^3/g	D_{XRD}, NiO nm	H_2/CO
ZSM-5	401	0.66	-	-
Pt1Ni	389	0.61	-	0.4
Pt3Ni	374	0.61	-	0.4
Pt6Ni	345	0.49	8.7	0.9
Pt12Ni	335	0.50	11.1	0.6
0.3Pt6Ni	367	0.55	9.7	0.7
Pt6Ni-co	367	0.55	10.3	0.6
6Ni	341	0.53	11.1	0.2
Pt	399	0.62	-	0.4

The IR spectra showed no change in the structure of zeolite framework of the supported samples.

XRD patterns of bimetallic zeolite-supported PtNi samples with Ni loading ≤ 3 wt% did not show any diffraction peak of NiO phase that means that NiO is in amorphous state. Diffraction peaks of NiO at 2θ=43.8° were detected in the spectra of the samples with higher Ni content of 6 and 12 wt% Ni. The latter is confirmed by the change of the values of the calculated particle size of NiO phase based on the diffraction peak broadening (Table 1); the size of NiO increases from 8.7 to 11.1 nm for samples with 6 and 12 wt%, respectively. No diffraction peaks due to formation of platinum oxide species were observed for all calcined samples, that means well dispersed Pt on the surface of PtNi catalysts.

The TPR results demonstrated that the reducibility of supported Ni species depends on the amount of nickel, method of preparation and the presence of Pt. The hydrogen consumption for supported samples increased with increasing the agglomeration of NiO. The PtNi sample prepared by co-impregnation showed TPR peak at temperature of 689 K, which is higher compared to that for samples prepared by consecutive impregnation. The effect of the presence of Pt in Ni catalysts was revealed by easy reduction of NiO.

It was clear that the addition of small amount of Pt in Ni catalysts led to increasing of the catalytic activity in the reaction of reforming of CH_4 with CO_2 at 773 K and $CH_4:CO_2=1$. With exception of the Ni/zeolite catalyst all catalysts showed high stability. The ratio H_2/CO was lower than one for all catalysts. The values of CO_2 conversion were higher than those of CH_4 conversion as a consequence of the participation of the reverse of water-gas shift reaction. The reason for the lowest activity of the low-loaded Ni samples was related to less accessible metal surface area. The highest activity for zeolite-supported Pt6Ni catalyst was connected with the existence of interaction between Pt and Ni revealed by XPS data.

Conclusions

The presence of small amount of noble metal (Pt) in zeolite-supported Ni catalysts leads to: (*i*) formation of nano-sized NiO particles; (*ii*) better dispersion of NiO particles and (*iii*) easy reduction of nickel species. The obtained bimetallic PtNi catalysts are good catalysts for hydrogen production by the process of methane reforming with CO_2.

References

1. S.M. Gheno, S. Damyanova, B.A. Riguetto, C.M.P.Marques, C.A.P. Leite, J.M.C. Bueno, Mol. Catal.A: Gen. 198 (2003) 263.

2. S. Damyanova, J.M.C. Bueno, Appl. Catal. A: Gen. 253 (2003) 135.

EFFECT OF H$_2$O ON ABSORPTION OF FLUE GAS SO$_2$ OVER A CuO/γ-Al$_2$O$_3$ CATALYST – A MICRO-KINETICS STUDY

Zhehua Jia, <u>Zhenyu Liu</u>, Youhua Zhao, Jianli Yang

State Key Laboratory of Coal Conversion, Institute of Coal Chemistry

Chinese Academy of Sciences, Taiyuan, Shanxi 030001, P.R. China

zyliu@sxicc.ac.cn Fax: +86-351-4048571

Introduction

CuO/γ-Al$_2$O$_3$ has been studied for simultaneous removal of SO$_2$ and NO$_x$ from flue gases emitted from stationary sources [1-4]. The adsorption characteristics of SO$_2$ over CuO/γ-Al$_2$O$_3$ are of importance to the overall performance and have been studied mostly in water-free conditions[3,4], However, flue gases always contain some amount of H$_2$O, 2-18%, and the presence of H$_2$O may affect the behavior of SO$_2$ adsorption on this catalyst-sorbent. Therefore, understanding of SO$_2$ adsorption behavior of CuO/γ-Al$_2$O$_3$ in the presence of H$_2$O is fundamental and important.

In this work, effect of H$_2$O on SO$_2$ adsorption behavior of CuO/γ-Al$_2$O$_3$ is studied. Before the study being made, the catalyst-sorbent are subjected to SO$_2$ removal and NH$_3$-regeneration to simulate a continued SO$_2$ removal process where the adsorbed SO$_2$ is converted to ammonium-sulfur salts by regeneration in NH$_3$. The micro-kinetics study performed include a surface-coverage model and a non-ideal adsorption model.

Experimental

The SO$_2$ removal experiments are performed in a thermogravimetric analyzer (Setaram TGA92). The CuO/γ-Al$_2$O$_3$ (containing 8wt% CuO and termed R-CuO/γ-Al$_2$O$_3$) is prepared by heating up a SO$_2$-adsorbed CuO/γ-Al$_2$O$_3$ to 400°C in 5 vol% NH$_3$/Ar in a fixed bed reactor. The TGA tests use 3~5 mg of R-CuO/γ-Al$_2$O$_3$ and are carried out at a total flue gas flow of 400 ml/min. The flue gas contains 3000ppm SO$_2$, 5% O$_2$, various amounts of H$_2$O and balance Ar. H$_2$O vapor is fed to the TGA by passing an Ar stream through a temperature-controlled gas-wash bottle containing de-ionized water.

Results and discussion

Effect of H_2O concentration on SO_2 adsorption over the R-CuO/γ-Al$_2$O$_3$

The SO_2 removal from the gas phase is accomplished by reacting the gaseous SO_2 with CuO in the presence of O_2 to form $CuSO_4$, during which the weight of R-CuO/γ-Al$_2$O$_3$ increases. Figure 1 shows the weight increase in R-CuO/γ-Al$_2$O$_3$ during SO_2 removal at various H_2O concentrations. The SO_2 adsorption rate and the maximum SO_2 adsorption capacity increase with increasing H_2O concentration in the H_2O concentration range of 0-10%, at a H_2O concentration of 20%, however, the SO_2 adsorption rate and the maximum SO_2 adsorption capacity are significantly lower. These behaviors seem to suggest that the effect of H_2O on the SO_2 adsorption at high H_2O contents follows a different mechanism compared to that at low H_2O contents. It is likely that the promoting effect of H_2O at the low H_2O contents results from increased oxidation activity of R-CuO/γ-Al$_2$O$_3$, and the reduced SO_2 adsorption at H_2O content of 20% results from high coverage of H_2O over R-CuO/γ-Al$_2$O$_3$ surface, which reduces the rates of SO_2 and O_2 adsorption, but these suggestions need to be verified.
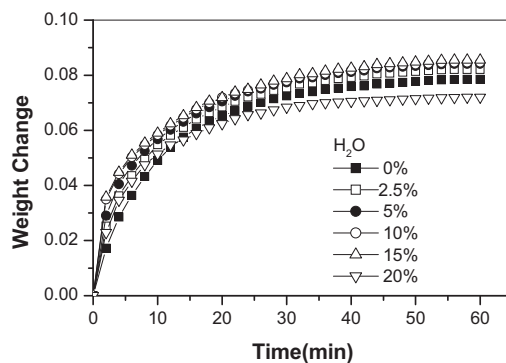
Figure 1. Weight increase in R-CuO/γ-Al$_2$O$_3$ during SO_2 adsorption at 400°C
at various flue gas H_2O concentrations

Kinetics analysis using the surface coverage model

For water-free conditions the surface coverage model has been used to study the kinetics, which assumes that the SO_2 adsorption rate is controlled by surface chemical reaction and the reaction takes place only on the active sites which are not covered by product. This model is used here as the first step to correlate the data. Equation (1) is the form of the model:

$$X = k_1 t / (1 + 0.5 k_1 k_2 t) \tag{1}$$

where, X is defined as $X = \dfrac{W_t - W_0}{W_{max} - W_0}$, W_0, W_{max} and W_t are weight of R-CuO/γ-Al$_2$O$_3$ before

the SO_2 adsorption, at the maximum SO_2 adsorption and at reaction time t, respectively. The rate constant k_1 represents SO_2 oxidation and adsorption activities, and is a function of the

reactants (gas and solid) concentration and temperature; k_2 is a function of solid reactants concentration and temperature. In the presence of H_2O, k_1 may be expended to include the H_2O concentration.

The fitting of the experimental data to Equation (1), shown in Figure 2, indicates that the experimental data at H_2O concentrations of 0%, 2.5% and 5% are well represented by the model, and the value of k_1 increases with increasing H_2O concentration. But the fitting increasingly deviates from the data when the H_2O concentration is increased further to 10% and 20%. This seems to suggest that the SO_2 adsorption is no longer controlled by the surface reaction, and changes in surface texture may have occurred at the high H_2O concentrations.
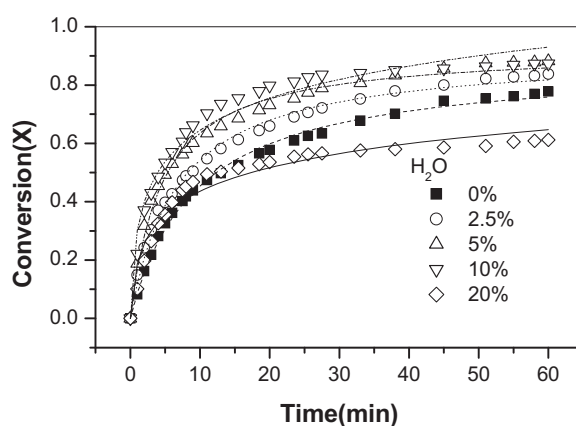
Figure 2. Fitting of the surface coverage model to the experimental data

Kinetics analysis using a non-ideal adsorption model

To account for the inability of the surface coverage model, a non-ideal adsorption model is used to fit the experimental data, and the fitting results are shown in Figure 3. The non-ideal adsorption model assumes that the adsorption of SO_2 on the surface is the rate-controlling step, and the active sites on the surface are different and interacts to each other.
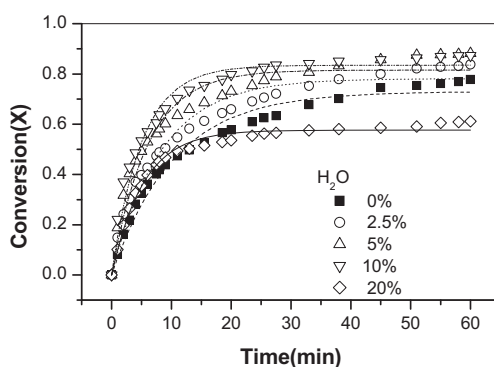
Figure 3. Fitting of the non-ideal adsorption model to the experimental data

In the nonideal adsorption model, the adsorption rate of SO_2 is expressed as[5]:

$$r = ky(1 - X_t)\exp(-g_s X_t) \tag{2}$$

where, X_t can be expressed by the the solid-phase balance:

$$\frac{dX_t}{dt} = \upsilon r_s S_e M \tag{3}$$

Introduction of Equation (2) into Equation (3) yields:

$$t = \frac{1}{\upsilon S_e M} \int_0^{X_t} \frac{dX_t}{ky(1 - X_t)\exp(-g_s X_t)} \tag{4}$$

Figure 3 show the fitting results of Equation (4) to the experimental data. Apparently, this model is suitable to the data of high H_2O concentrations. Dependence of the parameters in the model to the H_2O concentration and the chemical nature of the kinetics are to be discussed in the conference.

Conclusion

Micro-kinetics of SO_2 adsorption over a NH_3-regenerated CuO/γ-Al_2O_3 in the presence of H_2O is firstly studied. H_2O promotes SO_2 adsorption at H_2O concentrations of 15% or below, but inhibits SO_2 adsorption at H_2O concentrations of 20%. The surface-coverage model used for H_2O-free conditions fits the data well for H_2O content of less than 10%. A non-ideal adsorption model however is suitable for the data of high H_2O concentrations. The study suggests that the effect of H_2O on the SO_2 adsorption over CuO/γ-Al_2O_3 follows different mechanisms at low and high H_2O concentrations.

Acknowledgments

References

[1] Yeh, J.T.; Drummond,C.J.; Joabert, J.I. Process Simulation of the Fluidized-Bed Copper-Oxide Process Sulfation Reaction. Envi-ron.Prog. 1987, 6, 44.

[2] Waqif, M.; Saur, D.; Lavalley,J.C.; Perathoner, S.; Centi, G. Nature and Mechanism of Formation of Sulfate Species on Copper/Alumina Sorbent-Catalyst for SO_2 Removal. J.Phy.Chem. 1991, 95, 4051.

[3] Centi,G.; Passarini, N.; Perathoner,S.; Riva,A. Combined $DeSO_x/DeSO_x$ Reactions on a copper on Alumina Sorbent-Catalyst. 1. Mechanism of SO_2 Oxidation-Adsorption. Ind. Eng. Chem. Res.1992, 31, 1947.

[4] Centi,G.; Passarini, N.; Perathoner,S.; Riva,A. Combined $DeSO_x/DeSO_x$ Reactions on a copper on Alumina Sorbent-Catalyst. 2. Kinetics of the $DeSO_x$ reaction.Ind. Eng. Chem. Res.1992, 31, 1956.

[5] Murzin,D.Y.; Modeling of adsorption and kinetics in catalysis over induced nonuniform surfaces. *Ind. Eng. Chem. Res.* 34, 1208-1218.

SCR OF NO OVER A HONEYCOMB CuO/Al$_2$O$_3$/CORDIERITE – EFFECT OF AMMONIA PRETREATMENT ON Al$_2$O$_3$ COATING AND SCR ACTIVITY

Junhua Su, <u>Zhenyu Liu</u>, Xiaohang Zhang, Qingya Liu

State Key Laboratory of Coal Conversion, Institute of Coal Chemistry

Chinese Academy of Sciences, Taiyuan, 030001 P.R. China

zyliu@sxicc.ac.cn , Fax: +86-351-4048571

Introduction

Selective catalytic reduction (SCR) of NO with ammonia is an effective approach to solve stationary NO$_X$ emission problems. Vanadium oxide supported on honeycomb TiO$_2$ is the current state of art for such a purpose [1, 2]. However, this catalyst is of high cost, which hampers its broader application. Low cost catalysts are therefore widely studied. CuO/Al$_2$O$_3$ has been reported to be an alternative, which is active for the SCR at 400°C [3]. Since packing of the pellet type CuO/Al$_2$O$_3$ catalyst in a fixed-bed reactor causes high flow resistance and plugging problems due to trapping of particulates in flue gas, honeycomb type CuO/Al$_2$O$_3$ is also preferred. One of the methods that have been used in preparing honeycomb CuO/Al$_2$O$_3$ is to support CuO over an Al$_2$O$_3$ coated cordierite honeycomb. The literature shows that the SCR activity and stability of this type of catalyst are strongly affected by the amount and type of Al$_2$O$_3$ coatings [4]. In this works, we report a new method for coating of Al$_2$O$_3$, which involves pre-treatment of a cordierite with ammonia. This new approach significantly increases the amount of Al$_2$O$_3$ loaded over the cordierite but results in lower SCR activity.

Experimental

Preparation of the catalysts

The honeycomb cordierite used in this work is a commercial product with a cell density of 200 cells per square inch (cpsi) and a BET surface area of 0.7 m^2/g. It is treated with oxalic acid [5] (marked CHC) to increase its surface area to 164 m^2/g before been used. The alumina

sols used for coating are prepared by pseudo-boehmite (known as SB powder commercially) and nitric acid.

Two preparation methods are used. In one case CHC is directly dipped into the alumina sol for a certain period of time and then subjected to drying and/or calcinations (marked SB). In another case CHC is treated in ammonia (pH=11.6) for 5s before being dipped into the alumina sol (marked SB-NH$_3$). These two samples obtained are then impregnated with a cupric nitrite solution and then dried and calcined to yield catalysts with a Cu loading of about 1wt%. The catalysts prepared are named Cu1/SB and Cu1/SB-NH$_3$, respectively.

Catalyst activity measurement

The SCR activity measurements are carried out in a fixed-bed reactor (0.02m i.d.) system. When the system reaches steady state at a desired temperature, a feed containing 1600 ppm SO$_2$, 600ppm NO, 600 ppm NH$_3$, 5.0% O$_2$, 2.5% H$_2$O and balance N$_2$ are introduced into the reactor. In all the runs, the total flow rate is maintained at 450 ml/min, corresponding to a superficial space velocity of 7800 h^{-1}. The concentrations of NO, SO$_2$ and O$_2$ in the reactor outlet are measured online with a flue gas analyzer (KM96006, Germany).

Results and discussion

Figure 1 shows the amounts of Al$_2$O$_3$ loaded onto CHC by the two methods. Clearly the ammonia pretreatment significantly increases the Al$_2$O$_3$ loading. This phenomenon may be attributed to changes in surface acidity/basicity of CHC. Since CHC is obtained by oxalic acid treatment of the cordierite, its surface is acidic; the ammonia treatment however makes the surface basic. This surface basicity certainly would result in strong interaction with the weakly acidic alumina sol SB, and increase the Al$_2$O$_3$ loading.

The SCR activity of the catalysts prepared, Cu1/SB and Cu1/SB-NH$_3$, are shown in Figure 2. It is rather surprise to see that Cu1/SB, with a smaller amount of Al$_2$O$_3$, shows higher SCR activities than Cu1/SB-NH$_3$, with a larger amount of Al$_2$O$_3$, does.

Further studies using TPR indicate that Cu1/SB-NH$_3$ is more difficult to be reduced in H$_2$ than Cu1/SB, and this difference is not resulted from difference in Al$_2$O$_3$ loading. NH$_3$ oxidation experiments show that Cu1/SB-NH$_3$ produces significantly more NO and less N$_2$ than Cu1/SB does at the SCR temperatures.
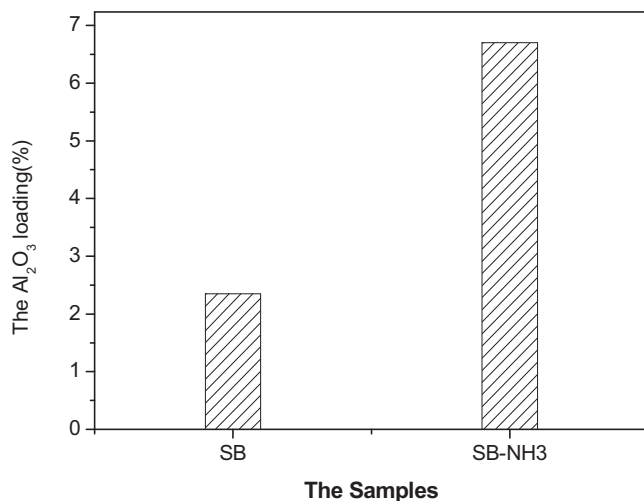
Figure1. The Al_2O_3 loading of SB and SB-NH$_3$
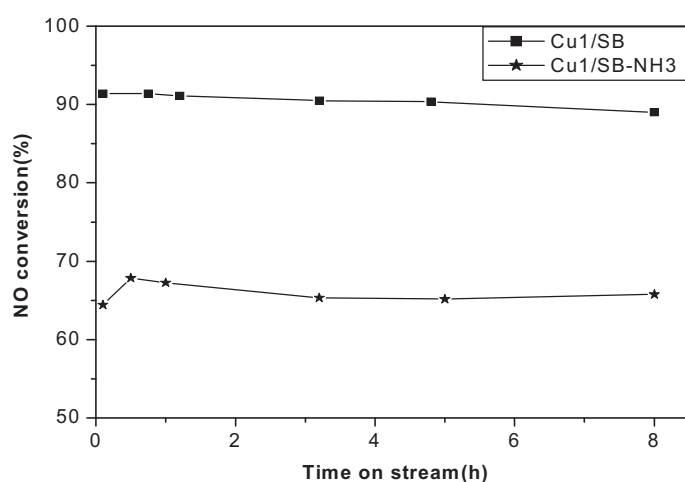
Figure2. The SCR activity of Cu1/SB and Cu1/SB-NH$_3$

Conclusion

NH$_3$-pretreatment to a cordierite honeycomb significantly increases the amounts of Al_2O_3 coated from an acidic SB alumina sol. The catalyst prepared, however, shows low SCR activity towards NO reduction, which is due mainly to the over oxidation of NH$_3$ to NO.

Acknowledgments

References

1   C. J. Pereira, K. W. Phumlee, Grace Camet® metal monolith catalytic emission control technologies, Catal. Today, 13(1992): 23-32.

2   J. Svachula, N. Ferlazzo, P. Forzatti, E. Tronconi, F. Bregani, Selective reduction of nitrogen oxides (NO$_x$) by ammonia over honeycomb selective catalytic reduction catalysts, Ind. Eng. Chem. Res., 32(1993): 1053-1060.

3   G. Xie, Z. Liu, Z. Zhu, Q. Liu, Simultaneous removal of SO$_2$ and NO$_x$ from flue gas using a CuO/Al$_2$O$_3$ catalyst sorbent II. Promotion of SCR activity by SO$_2$ at high temperature, J. Catal., .224(2004): 36-41.

4   Q. Liu, Z. Liu, Preparation and performance of cordierite honeycomb based CuO/Al$_2$O$_3$ for SO$_2$ and NO removal from flue gas, Doctor Paper 62 (2004)

5   Q. Liu, Z. Liu, Z. Huang, Catal. Today, 93-95(2004): 833-837.

PRODUCTION OF ELEMENTAL SULFUR BY H$_2$-REGENERATION OF SO$_2$-ADSORBED CuO/Al$_2$O$_3$

Youhua Zhao, <u>Zhenyu Liu</u>, Zhehua Jia, Jianli Yang

State Key Laboratory of Coal Conversion, Institute of Coal Chemistry

Chinese Academy of Sciences, Taiyuan, 030001, P.R. China

zyliu@sxicc.ac.cn, Fax: +86-351-4048571

Introduction

As an effective catalyst-sorbent for SO$_2$ removal or simultaneously SO$_2$ and NOx removal from flue gas, CuO/Al$_2$O$_3$ has been studied since 1970s [1-3]. The process consists of three stages, SO$_2$ adsorption from flue gas or sulfation, regeneration of the SO$_2$-saturated CuO/Al$_2$O$_3$ and sulfur recovery into marketable products. In the Shell process, both sulfation and regeneration are carried out at 400°C [1]. The regeneration yields concentrated SO$_2$ gas, which is further treated in another unit. Reduction of SO$_2$ to elemental sulfur by hydrogen is regarded to be a better choice compared to other options for sulfur recovery [4-6]. However, the requirement of additional catalyst and reactor for such a purpose results in increased cost. Carrying out the three operation stages in one unit certainly will result in significant cost reduction. To achieve such a goal, new catalyst-sorbent and reactor strategy need to be developed which are capable of removing (adsorb) SO$_2$ in flue gas in one operation mode and reducing the SO$_2$ released during H$_2$-regeneration to form elemental sulfur in another operation mode. Here, we report recent work on such a process which uses CuO/Al$_2$O$_3$ as the catalyst-sorbent. Effects of regeneration temperature and H$_2$ feed strategy on elemental sulfur yield and SO$_2$ removal capacity are mainly discussed.

1. Experimental

A commercial γ-Al$_2$O$_3$, 30-60 mesh with a BET surface area of 200 m^2/g, is impregnated with an aqueous Cu(NO$_3$)$_2$·3H$_2$O solution and subjected to drying at 110°C for 8 h and calcination at 500°C for 8 h to yield a CuO loading of 8.0 wt.%.

The reactor configuration is shown in Figure 1. A flue gas containing 2200 ppm SO$_2$, 6% O$_2$ and balance N$_2$ is introduced into the fixed-bed reactor for sulfation of CuO/Al$_2$O$_3$ at 400°C. Upon SO$_2$ saturation of the catalyst-sorbent the reactor is purged with N$_2$ and then

switched to H_2 to initiate the H_2-regenration and elemental sulfur production processes. The effluent gas is cooled in a cold trap to collect elemental sulfur formed, and the rest of the gas is recycled back to the reactor. This process is carried out in two modes, a continuous H_2 feed mode (C) and an intermittent H_2 feed mode (I). Changes in the gas composition in the system are monitored on-line by mass-quadrupole detector (OmmiStar 200, Blazers).
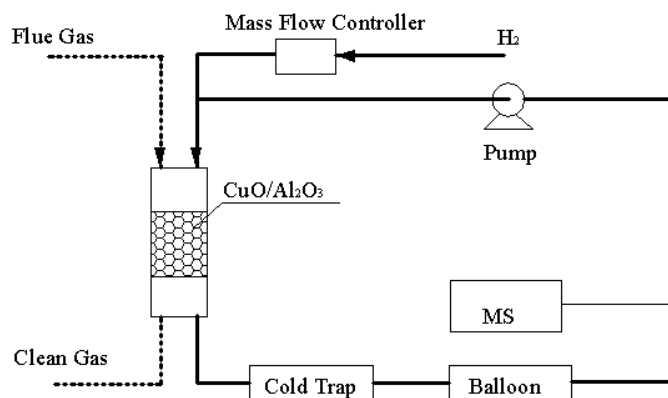
Figure 1. Experimental apparatus

Elemental sulfur yield Y is defined as $Y = 100\, m/M$, where m is the mass of elemental sulfur collected and M the total amount of sulfur generated from the regeneration.

2. Results and discussion

Effect of regeneration temperature

Figure 2 shows elemental sulfur formation at various regeneration temperatures on operation mode C. It can be seen that no elemental sulfur is collected at regeneration temperatures of lower than $350^{\circ}C$, but in the regeneration temperature range of $350\text{-}440^{\circ}C$ the elemental sulfur collected increases with increasing temperature, corresponding to elemental sulfur yields of 55-90%. These data indicate that the process works well, which is capable to desorb SO_2 from the catalyst-sorbent and then reduce the released SO_2 to elemental sulfur. The optimum regeneration temperature is $420^{\circ}C$ or higher.

Another purpose of the H_2-regeneration is to restore the catalyst-sorbent's activity for SO_2 adsorption in the subsequent cycles. Figure 3 shows the effect of H_2-regeneration temperature on the SO_2 adsorption capacity at $400^{\circ}C$. Apparently, H_2-regeneration of the SO_2-adsorbed catalyst-sorbents is not very effective at temperatures of $420^{\circ}C$ or lower, which results in SO_2 adsorption capacities less than that obtained at higher temperatures. These observations correlate well with the elemental sulfur yield data shown in Figure 2.
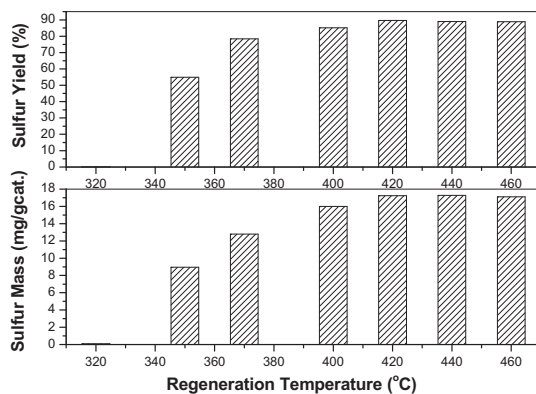
Figure 2. Effect of regeneration temperature on sulfur yield
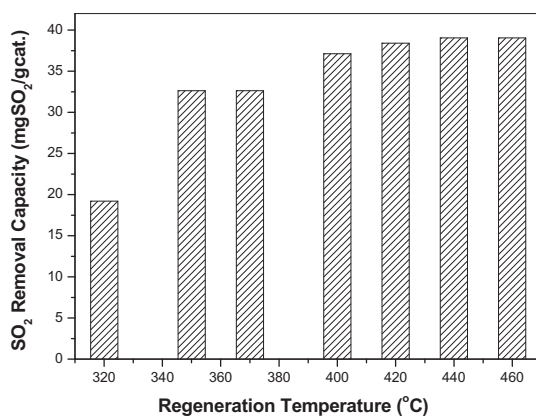
Figure 3. Effect of regeneration temperature on SO_2 removal capacity

Effect of H_2 feed strategy

Since the whole H_2-regeneration process may involve desorption of sulfur species from the catalyst-sorbent to form gaseous SO_2, reduction of some amounts of SO_2 by H_2 to form H_2S, and reaction of the H_2S with the rest of SO_2 to form elemental sulfur, the amounts of H_2 fed into the reactor is a very important operation parameter, which affects the H_2S/SO_2 ratio and the yield of elemental sulfur. Figure 4 shows the elemental sulfur yields obtained from operation modes C and I at a H_2-regeneration temperature of $400^{\circ}C$. It can be seen that the intermittent H_2 feed mode (filled symbol) yields better results than the continuous H_2 feed mode (open symbol) does and the catalyst-sorbent has a good stability for elemental sulfur formation.
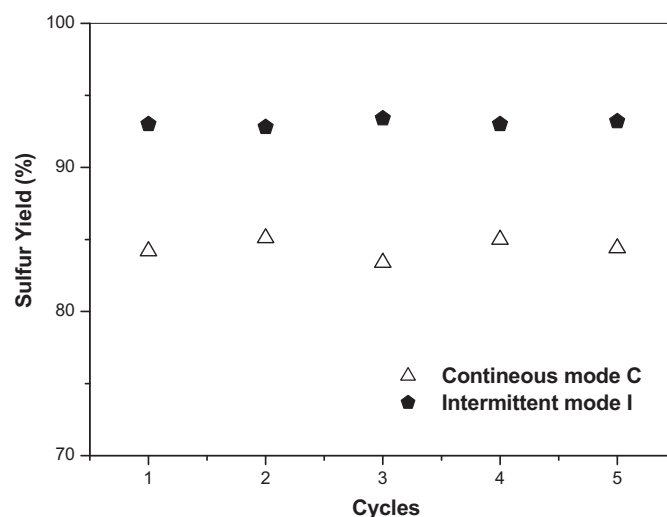
Figure 4. Effect of H_2 feed strategy on elemental sulfur yield, $400^{\circ}C$

3. Conclusions

CuO/Al_2O_3 catalyst-sorbent can be used for flue gas SO_2 removal and elemental sulfur production if H_2-regeneration is used and the effluent gas from the regeneration operation is recycled back to the reactor. Temperatures greater than $420^{\circ}C$ are necessary for high elemental sulfur yield and high SO_2 removal capacity. Elemental sulfur yield of greater than 90% can be obtained if the H_2-regeneration temperature and H_2 feed strategy are properly selected. Intermittent H_2 feed mode shows better results than continuous H_2 feed mode.

References

[1] F.M. Dautzanberg J.E. Nader and A.J. van Ginneken, Chem. Eng. Prog. 67 (1971) 86.
[2] P.S. Lowell, K. Schwitzgebel, T.B. Parsons and K.J. Sladek, Ind. Eng. Chem. Process Des. Dev. 10 (1971) 384.
[3] D.H. McCrea, A.J. Forney and J.G. Myers, J. Air Pollut. Control Assoc. 20 (1970) 819.
[4] T.F. Doumani, R.F. Deery and W.E. Bradley, Ind. Eng. Chem. 36 (1944) 329.
[5] S.C. Paik and J.S. Chung, Appl. Catal. B 5 (1995) 233.
[6] S.C. Paik and J.S. Chung, Appl. Catal. B 8 (1996) 267.

EXPERIMENTATION IN INDUSTRIAL HYDROTREATMENT REACTOR WITH APPLICATION OF ARTIFICIAL INTELLIGENCE FOR SELECTION OF CATALYSTS WITH DESIRED PHYSICO-CHEMICAL PROPERTIES

F. Jiménez[1], V. Kafarov[1], M. Nuñez[2]

[1]*Industrial University of Santander, Kra. 27 Calle 9, Bucaramanga, Colombia*
Tel. +57 +76344746, Fax +57 +76344684, E-mail: kafarov@uis.edu.co
[2]*Colombian Petroleum Institute –ICP, Piedecuesta, Colombia*

Abstract

The complexity of heterogeneous catalytic systems doesn't allow, nowadays, forecasting the catalytic activity for the hydrotreatment processes based on rigorous laws of heterogeneous catalysis, expressed in quantitative form. In this paper is presented a strategy for prediction of the catalytic activity based on a combination of computational tools such as Artificial Neural Networks (ANN), Fuzzy Logic, traditional and non traditional statistic regression methods with an industrial experimental methodology developed by the Colombian Petroleum Institute, based on aging of catalysts with different textural and chemical properties, inside industrial reactor during the normal length of the run. The methodology was validated for twenty four different hydrotreatment catalysts.

Introduction and Proposed Methodology

The strategic methodology developed to selection catalysts with desired physic-chemical properties is presented in Figure 1. Twenty four fresh hydrodemetallation catalysts samples were tested during the investigation. Six physic-chemical properties were measures: Porosity (%), superficial area (mc/g), pore diameter (A), equivalent size (mm), initial content of Molybdenum (%) and initial content of Nickel (%). The samples were submitted inside the industrial reactor to the real conditions during approximately eight months. Then the aged samples were recovered and repetitively was measured their capacity to retain metals like Ni, Mo, and V (catalytic activity). The reliability of the obtained database is made through the application of statistics filter, like Hotelling T^2 Multidimensional Method. Next, is proposed the training of a suitable Neural Network to obtain the rank of influence of each one of physic-chemical properties on the metals removal. The tools to predict the catalytic activity based on the reliable experimental information acquired are:
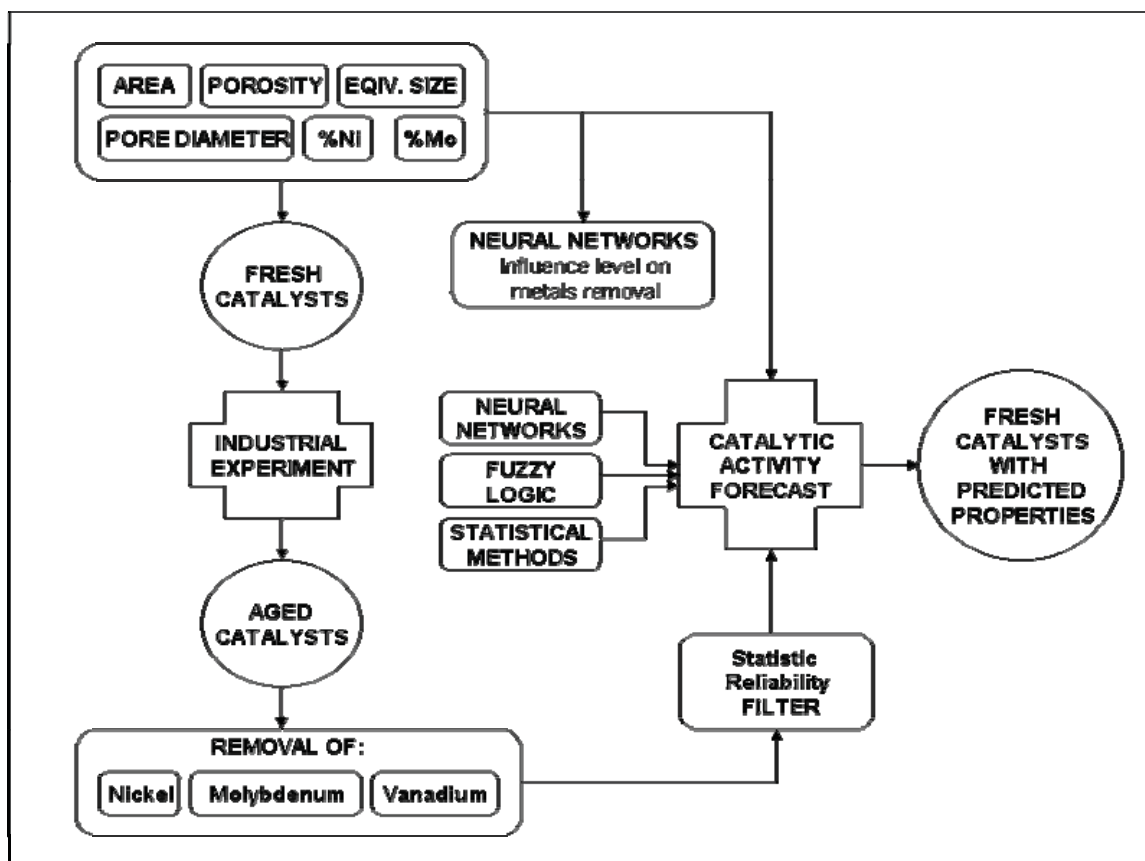
Figure 1. Strategic Methodology of Research

- *Statistic Filter*: is proposed the Hotelling Method (Johnson, 1998) to evaluate if the differences among the repeated measurements taken for metals removal (Ni, V, Mo) in a catalyst sample, are statistically less than the differences among averages values from others samples. Then, is possible to compare simultaneously all the activities measurements (Ni, V, Mo) and to determine if there are irregular data, that must be reviewed or not considered.

- *Neural Network*: Is proposed the application of a neural network to predict the catalytic activity. Also, when the final model be obtained, the sequential importance of physic-chemical variables in activity will be determined from the sequential elimination of each variable, the error in final prediction will be useful to attribute a place in importance order.

- *Statistic Methods:* Is proposed the Brandon Method (Johnson, 1998) to define the catalytic activity as a product of six expressions. Each expression is function of each selected parameter, and the order depends on the sequential importance on the activity (obtained by ANN). Likewise, forty one (41) traditional statistical models to establish dependence between catalytic activity and physic-chemical properties (multiple lineal regressions with 1-6 parameters, regression by steps, polynomial regression with two interactions, etc.) are proposed to compare the results with results from others proposed methods.

- *Fuzzy Logic Method*: Large part of qualitative data about catalysts selection, presents some uncertainty, and hampers often a strict mathematical statement. The application of Fuzzy Logic in combination with other mathematical methods can promote the efficiency of catalyst activity prediction due to formalization of such knowledge (Qian et al, 1995).

The combination of this methods are introduced like hypothesis to take decisions about selection of catalysts with desired physic-chemical properties for very complexes processes, in this case the hydrodemetallation of heavy petroleum fractions.

Experimental part

The fresh catalysts samples are introduced during the load and are recovered during unload of industrial reactor (Nuñez et al, 2000). The samples were aged inside the fixed-bed industrial catalytic reactor with a catalyst load of approximately 40 tonnes. The process was operated at LHSV of $1.0h^{-1}$, total pressure of 1500 psia and maximum temperature of 400°C. The recovered baskets were identified and were determined in repetitive way (with the purpose of obtain replicas for statistical analysis) by Atomic Sorption (Perkin Elmer 5-100), the contents of Nickel, Vanadium and Molybdenum. Finally, the measures for activity, and the physic-chemical properties conform the main database of this investigation.

Results

Based on the Hotelling-T2 Method, was developed specific software, and was achieved the comparison of twenty four hydrotreatment catalysts. Was deduced that the database from compared catalyst, have sufficient reliability to assure the utilization in the research.

- *Artificial Neural Network Method (ANN):* Eight different tables with aleatory data were organized. Eighteen data sets were useful for network training and six data sets were useful like test or validation. Three different architectures were selected for network training, and a hidden layer with 3-5 nodes was defined (Quick-Propagation rulers, and Dot-Product input functions were used; Hilera et al, 1995). The normalized data sets were applied with the best table and more efficient network architecture. After more than 2000 iterations and a low forecast error, was defined the final model. With this model, and the proposed methodology, the level influence on activity for input variables was: porosity, surface area, pore diameter, equivalent size, and initials Ni and Mo contents.

- *Statistics Methods*: Specific software for application of Brandon Method and Multiple Lineal Regression was developed. Comparative results (sum of quadratic errors) of some methods are showed in Table 1. Is observed that statistical methods are not viable in this forecast. The Brandon method demonstrated be good, since were obtained results that present a real physical sense. The equations confirm that the retention of metals is

associated with an optimum porosity, high superficial area and pore diameter, and a small equivalent size. On the other hand, the ability of ANN provides a more exact prediction than other traditional prediction methods, and is possible to establish isolated effects and dependences of the chosen variables. However, the effective learning depends on the supplied information, quality and quantity.

Table 1. Sum of quadratic errors for some regression methods (Training and test data)

	Multiple Regression	Regression by steps	Back Elimination	Brandon Modified	ANN
$\Sigma\varepsilon^2_1$. Training data (16)	20669,05	20844,28	19387,29	632,97	359,11
$\Sigma\varepsilon^2_2$. Test data (8)	5633.27	6377.46	6121,94	440.96	276.22

- *Fuzzy Logic Method*: Quantitative ranks, fuzzy vocabulary and trapezoidal type belonging functions were defined for all the parameters. To formalize correlation between parameters, nineteen rules from literature were obtained (Absi-Halabi et al., 1995; Bogdanor, 1986; Do, 1984; Furimsky et al., 1999; Nunez et al., 2000; Pazos et al., 1983; Pereira et al., 1987). Numerical values were referent to compare with experimental data. The fuzzy model was created by dialogue of expert with computer. The developed model, predict qualitatively the experimental activity for 22 from 24 data set.

Acknowledgement

References

1. Absi-Halabi M., Stanislauss A., Qamra A., 1995. Fuel, 74 (8) 1211-1216.
2. Bogdanor J. 1986, Eng. Chem. Prod. Res. Dev., 25, 220-226.
3. Do D., 1984. AIChe J. 30: 849-854.
4. Furimsky E., Massoth F., 1999. Catalysis Today, 52 (4): 381-386
5. Hilera J., Martínez J., 1995. "Redes Neuronales Artificiales", Addison Wesley Ib., Madrid, 1995, 388p.
6. Johnson D., 1998. "Métodos Multivariados Aplicados al Análisis de Datos", Thompson ed., México, 566p.
7. Núñez, M., Pachón, Z., Kafarov V., Resasco D. 2000, Appl. Catal. A, 5057: 1-10.
8. Pazos, J. M., Gonzalez J.C., Salazar-Guillen A.J., 1983, Ind. Eng. Chem. Process Des. Dev., 22: 653-661.
9. Pereira C., Donelly R., Hegedus L., 1987. Catalyst Deactivation. Edit. Marcell Dekker. 315 p.
10. Qian Y., Tessier P., 1995. Chem. Eng. Technol., 18: 1-7.

MODELING OF INDUSTRIAL REACTOR FOR HYDROTREATMENT OF VACUUM GAS OILS.
JOINT HYDRODESULFURIZATION, HYDRODENITROGENATION AND HYDRODEAROMATIZATION REACTIONS

F. Jiménez[1], <u>V. Kafarov</u>[1], M. Nuñez[2]

[1]*Industrial University of Santander, Kra 27 Calle 9, Bucaramanga, Colombia*

Tel. +57 +76344746, Fax +57 +76344684, E-mail: kafarov@uis.edu.co

[2]*Colombian Petroleum Institute -ICP, Piedecuesta, Colombia*

Abstract

Simultaneous reactions for hydrodesulfurization (HDS), hydrodenitrogenation (HDN) and hydrodearomatization (HDA) were investigated during hydrotreating of vacuum gas oil. The results include the modeling of Trickle Bed Reactor based on experiments carried out under typical industrial conditions at pilot plant, and the inhibition effects among different molecules such as decahydro-naphtalene, naphthalene, anthracene, (mono, di, tri-aromatic), carbazole (non basic nitrogen), acridine (basic nitrogen), dibenzotiophene (sulfur), and water, mixed in a vacuum gas oil severely hydrotreated (matrix feed), according to the elaborated factorial experimental design. The analytical techniques selected for this research were Nuclear Magnetic Resonance-NMR (for aromatic content and other analysis), Gas chromatography coupled with high performance mass spectrometry-GC-MS (for aromatic families distribution-including sulfur families), Ultra violet-visible spectrometry-UV/VIS (for aromatic families), Simulated distillation (SimDis), analysis of Saturates-Aromatic-Resin (SAR), and Standard Tests (ASTM) to determinate basic nitrogen, total nitrogen, total sulfur, and other physic-chemical properties in vacuum gas oils (VGO).

Introduction

Hydrotreatment (HDT) is used in refining industry to remove contaminants such as sulfur, nitrogen, metals, etc., by technical and environmental reasons. Better understanding about HDS has been acquired during the process development over the last decades; however, the most of available information has been obtained from study of light fractions, or synthetic solvents and model molecules. Thus, mathematical models for heaviest fractions, like vacuum

gas oil, and for joint HDS, HDN and HDA are limited in literature, probably because of the necessity of specific data for heaviest fractions, and to the incomplete or less precise information about mutual inhibitions. For these reasons, and based on the inevitability to process heavy oils in refining industry, the purpose of this work reside in confront some of challenges concerning with modeling taking into account the inhibitions or promotion effects, during HDT of vacuum gas oils.

Experimental part

A gas oil from an intermediate crude oil (Naphtenic/Paraffinic, 27°API, 0.8%S) was selected like main feed for kinetic and inhibition analysis. Six pure reactive (based on technical evaluation): decahydro-naphtalene, naphthalene, anthracene, carbazole, acridine and dibenzotiophene, were purchased. Also, one part of selected gas oil was split in six fractions (in liquid-liquid extraction pilot plant) and each one was separated in aromatic and saturate fraction with the purpose of use like additional reactive. Likewise, water emulsify was used in high concentrations (5-10% vol.). To detect inhibition or promotion effects, the selected reactive were mixed (in comparables concentrations with real feedstock) with the severely hydrotreated vacuum gas oil, under the elaborated factorial design of experiments. All the hydrotreatment test were made in Pilot Plant (ICP) using the catalyst in their original size (Ni-Mo/Al$_2$O$_3$, trilobe shape, equivalent size of 1,8mm, length 4,1mm). The reactor has an inside diameter of 1,9cm and a length of 73,5 cm. The normal operating conditions selected for inhibition test were: T:350°C, P:10MPa, LSHV:1.1h^{-1}, gas/oil ratio:6.24, whereas the severe operating conditions consider 370°C of temperature. Finally, 46 tests, involving different operational conditions, were made for kinetic analysis, and other 32 tests were made to detect inhibition effects (2^5 factorial design).

Reactor modeling

As well known the Trickle Bed Reactor (TBR) for HDT process has a lot of advantages in comparison with other types of reactors. A set of several three-phase reactor models were evaluated (Cheng et al, 2004; Lange et al, 2004, Avraam and Vasalos, 2003; Chowdhury et al, 2002, Korsten and Hoffman, 1996; Medjell et al, 2001; Chen et al, 2001; Cotta et al, 2000; Froment et al, 1994; Tsamatsoulis and Papayannakos, 1998; Van Hasselt et al, 1999). In this work, for liquid and gas phase, was selected the model proposed by Korsten and Hoffman, and was combined with model reported by Froment et al., for solid phase. Specific numerical package was developed for the evaluation of thermodynamic and physic-chemical properties

of hydrocarbon compounds and mixtures, and for calculation of interfacial mass transfer rates, using information reported in literature (Rodriguez & Ancheyta, 2004; Avraam and Vasalos, 2003; Korsten and Hoffman, 1996). Specific software also was developed for integration of equation of model based on Orthogonal Collocation Method for solid phase, and Runge-Kutta-Gill for gas and liquid phase. Similarly, to apply Sequential Design of Experiments for kinetic analysis, a user-friendly computational program was developed, which, supplemented with a statistical analysis, discriminated among nine models from literature (Broderick and Gates, 1981; Cheng et al, 2001; Medjell et al, 2001; Cotta et al, 2000; Girgis and Gates, 1991; Froment et al, 1994; Avraam and Vasalos, 2003; Tsamatsoulis and Papayannakos, 1998; Van Hasselt et al, 1999) and minimized the volumes of the confidences intervals. The developed kinetic model for simultaneous hydrodesulfurization, hydrodenitrogenation and hydrodearomatization reactions was based on unification of the kinetic models for HDS hydrogenation and hydrogenolysis proposed by Broderick and Gates (1981) joint with HDN and HDA kinetic expressions of Avraam and Vasalos, 2003.

Results

Simulation Performance

The software showed excellent agreement between theoretical and experimental data, and it was observed a behavior similar to showed in literature. The increase in temperature or pressure, or the decrease in space-velocity, improves the conversion of sulfur and nitrogen compounds. The concentrations profiles for selected compounds along the reactor show an increment in mono-aromatic, whereas the H_2S concentration increases rapidly, and sulfur, nitrogen, and di plus tri-aromatics decrease.

Inhibition Effects

The proposed methodology of use a VGO severely hydrotreated (less than 120 ppm sulfur, 20 ppm basic nitrogen, 1% total nitrogen) like matrix to carry the pure molecules led to interesting results. The matrix re-hydrotreatment doesn't produce significant changes in concentrations. Initially, the solubility of pure molecules in matrix wasn't complete, then was necessary make test at high pressures and agitation velocities, and make some emulsions with the reactive, until good solubility was observed. Based on this methodology, were detected inhibitions for HDS reactions by low and high concentrations of different aromatic molecules such as anthracene, naphthalene, and decahydro-naphthalene, likewise inhibition by basic nitrogen (acridine) and non-basic nitrogen (carbazole), in different extensions. In similar way

PP-31

were detected inhibitions for HDN by sulfur and aromatics molecules. Also, it was observed that water markedly enhanced the capacity to remove sulfur and nitrogen compounds during HDT of VGO's.

Conclusions

A heterogeneous model for industrial reactor was developed to carry out the simulation of hydrotreatment of vacuum gas oils, where simultaneous HDS, HDN and HDA reactions have been included. A sequential design of experiments was used for kinetic model discrimination and estimates their parameters from pilot plant tests. Likewise, was investigated the mutual influence of different model molecules (mono, di, tri-aromatic, basic nitrogen, non basic nitrogen, sulfur, water) mixed properly, under a factorial design of experiments, in a severely hydrotreated vacuum gas oil. The simulation shows good agreement with experimental data and with information available in literature. Were detected mutual inhibitions for HDS and HDN by pure molecules used, and a promoter effect of water for all the HDT reaction.

Acknowledgement

References

1. Avraam D., Vasalos I., 2003. Catalysis Today, 79–80: 275–283.
2. Broderick D., Gates B., 1981. AIChE Journal, Vol 27, No 4. 663 -672.
3. Chen J., Ring Z., 2001. Ind. Eng. Chem. Res, 40: 3294-3300.
4. Cheng Z., Fanga X., Zeng R., Han B., Huang L., Yuan W, 2004. Chem. Eng. Sci, 59: 5465–5472
5. Chowdhury R., Pedernera E., and Reimert R., 2002, AICHE Journal, 48 (1) 126-135.
6. Cotta R., Wolf-Maciel M., Maciel Filho R., 2000. Computers and Chemical Engineering, 24: 1731 – 1735.
7. Froment G., Depauw G., Vanrysselberghe V., 1994. Ind. Eng. Chem. Res., 33 (12): 2975 – 2988.
8. Girgis M., Gates B., 1991. Ind. Eng. Chem. Res., 30 (9) 2021-2058
9. Khadilkar M., Mills P., Dudukovic M., 1999. Chemical Engineering Science, 54: 2421 – 2431
10. Korsten H., Hoffman U., 1996. AICHE Journal, 42 (5) 1350-1360
11. Matos E., Guirardello R., 2000. Brazilian Journal of Chem Eng, 17 (2) 1-14
12. Medjell T., Myrstad R., Steiner P.,2001. Studies in surface science and catalysis 133. Elsevier Sc. 189-194.
13. Rodriguez M., Ancheyta J., 2004. Energy & Fuels, Vol 18, No. 3, 789 – 794
14. Tsamatsoulis D., Papayannakos N., 1998. Chem. Eng. Sci, 53 (19): 3449–3458.
15. Van Hasselt B., Lebens P., Calis H., Van Den Bleek C., 1999. Chem. Eng. Sci, 54: 4791- 4799

CATALYSIS OF THE HYDROCARBON AND OIL OXIDATION BY TETRAALKYAMMONIUM SALTS

Kasaikina O.T., Maximova T.V., Kartasheva Z.S., Pisarenko L.M.

Institute of Chemical Physics RAS, Moscow, Russia

The recent studies showed that additives of surfactants can affect substantially the rate and mechanism of hydrocarbon oxidation. Surfactant molecules form microaggregates of a reverse micelle type in a nonpolar hydrocarbon medium in which polar oxidation products, viz., water, alcohols, hydroperoxides, and others, are concentrated. Quaternary ammonium salts (quats) accelerate the oxidation of hydrocarbons and oils and possess a bactericidal effect.

The catalytic effects of cetyltrimethylammonium halides (CTABr, CTACl), $CTAHSO_4$, dicetyldimethyl ammonium bromide (DDABr), as well as acethylcholine chloride (AcC) on the oxidation of various hydrocarbons (dodecane, cumene, limonene, RH) and sunflower (TGSO) and olive (TGOO) oil triacylglycerols have been studied thoroughly. The hydroperoxide (ROOH) decomposition was found to be a key stage affected by surfactants. We found that the catalytic effect of quats on the oxidation is caused by the accelerated decomposition of ROOH in mixed ROOH-quats micelle microreactors with escape of $RO_2\bullet$ radicals to a hydrocarbon bulk followed by the chain-radical oxidation of the hydrocarbon.

The inhibitor method equipped with proprietary radical acceptors was used to study the kinetics of free radical formation during the hydroperoxide decomposition catalyzed by quats combined with NMR, GC-MS and TLC methods to analyze the oxidation products obtained. The rate of free radical formation was found to depend strongly on the counterion of quats.

CTACl exceeds considerably CTABr and especially $CTAHSO_4$ in catalytic activity in free radical initiation. It contradicts the published assumptions on a special role of bromide ions in the decomposition of hydroperoxides. A lower rate of radical formation in the case of CTABr can be related to the influence of bromine as a heavy atom facilitating the intracellular (microreactor) recombination of radicals, which decreases the apparent initiation rate.

The increase of free radical escape has been found for the systems CTABr+ cumene hydroperoxide and CTABr+limonene hydroperoxide in magnetic field. An unusual magnetic-field effect points out the spin selectivity of a radical producing reaction and the generation of ion-radical couple via electron transport. It is established that free radical escape in these systems 2.5-fold decreases under oxygen atmosphere. This fact can be caused by oxygen spin-catalysis for the decay reactions (recombination/disproportionation) of free radicals generated inside micelle microreactors.

INVESTIGATION OF REACTION KINETICS AND INTRAPARTICLE DIFFUSION LIMITATION OF β-PICOLINE OXIDATION TO NICOTINIC ACID

V.N. Kashkin, E.V. Ovchinnikova, <u>A.P. Kagyrmanova</u>, V.N. Bibin, G.Ya. Popova,

I.A. Zolotarsky, G.A. Zenkovetz, T.V. Andrushkevich

Boreskov Institute of Catalysis of Siberian Branch of Russian Academy of Sciences,

Pr. Ak. Lavrentieva, 5, Novosibirsk, 630090, Russia, e-mail: kashkin@catalysis.ru

1. Introduction

Nicotinic acid (NA) is used as a vitamin in medicine, in the food-processing industry and as an intermediate in synthesis of some pharmaceuticals. NA is produced by a hazardous technology of liquid-phase oxidation mainly. The Boreskov Institute of Catalysis (BIC) has developed the one-stage gas-phase process of NA production by oxidation of β-picoline (βP) over the V_2O_5/TiO_2 catalyst. [1]. The main goal of this work was to investigate kinetics of β-picoline oxidation over this ring – shaped vanadia-titania catalyst and to clarify the effect of intraparticle diffusion limitation on catalyst performance.

2. Experimental

2.1. Catalyst

The catalyst was prepared by spray drying of an aqueous suspension of vanadyl oxalate and TiO_2 (anatase) followed by extrusion into rings 2 mm ID, 4 mm OD and 5 mm length and calcination at 450 °C. The resulted catalyst contained V_2O_5 and TiO_2 in a weight ratio 1:4. The original TiO_2 was prepared by a sulfate-based technology and contained 3.3 % wt. of $(SO_4)^-$. The BET specific surface area of the catalyst was 25 m^2/g. Average pore radius, measured by N_2 adsorption was 34 nm.

2.2. Kinetic measurements

Kinetics of βP oxidation to NA was investigated in a differential reactor with external circulation loop providing ideal mixing regime. Kinetics was studied at ambient pressure and temperature 270 °C, βP conversion was 20-85%. Initial concentrations of the components were varied as follows: 0.09 - 1.82 % vol. of βP, 9 - 28 % vol. of oxygen, 5 - 25 % vol. steam, and nitrogen – balance.

3. Reaction network and kinetics data processing

The main products of βP oxidation over V_2O_5/TiO_2 catalyst are nicotinic acid, 3-pyridine aldehyde (PA), 3-pyridine nitrile (PN) and CO_2. The high catalyst surface acidity due to high content of $(SO_4)^-$ of the catalyst under investigation was assumed to be responsible for the

significant amount of PN formed. Previously studied catalyst samples containing 0.04 % wt. $(SO_4)^-$ were shown to form PN at a trace level.

Using FTIR *in situ* technique it was shown that formation of NA from βP and PA proceeds through the sequence of a similar surface compounds (SC2, SC3, SC4) [2]:
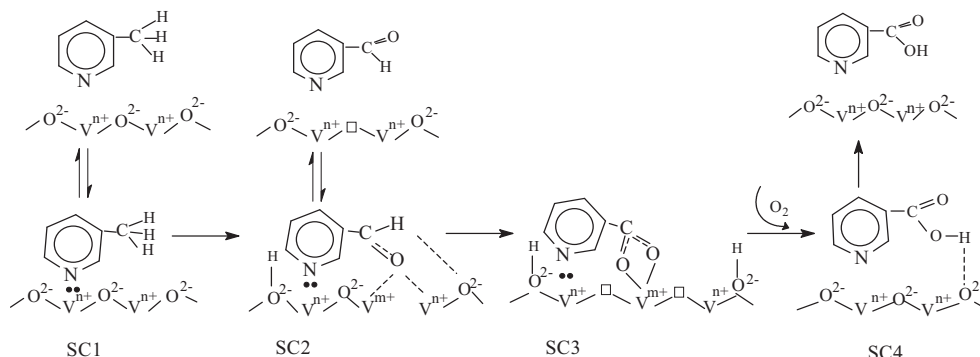
According to the previous work [3] the overall reaction network could be represented as follows:
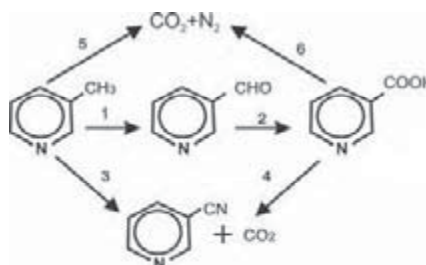
Reaction mechanism data and experimental kinetics data obtained resulted in the following kinetics equations for the reaction rates according to reaction network scheme showed above (eq. 1-6). Equations 1-6 were obtained applying the graph theory and using the following assumptions:

1. Reactions (1), (2) occur on the different active centers and reactions (3,4,5,6) occur on the same active centers.
2. Surface compounds (SC2, SC3) are formed with a participation of surface oxygen.
3. Decomposition of the carboxylic compound (SC3) proceeds according to the associative mechanism with participation of gas phase oxygen of combined stage of catalyst reoxidation and NA desorption.

$$\omega_1 = \frac{k_1 P_{\beta P}}{1 + k_2 \dfrac{P_{\beta P}}{P_{O_2}} + k_3 P_{\beta P} + k_4 \dfrac{P_{\beta P}}{P_{H_2O}}} \ (1); \quad \omega_2 = \frac{k_5 P_{PA}}{1 + k_6 P_{PA} + k_7 \dfrac{P_{PA}}{P_{O_2}} + k_8 \dfrac{P_{PA}}{P_{H_2O}}} \ (2); \quad \omega_3 = \frac{k_9 P_{\beta P}}{DEN} \ (3);$$

$$\omega_4 = \frac{k_{10} P_{NA}}{DEN} \ (4); \quad \omega_5 = \frac{k_{13} P_{\beta P}}{DEN} \ (5); \quad \omega_6 = \frac{k_{14} P_{NA}}{DEN} \ (6); \quad DEN = 1 + \frac{k_{11} P_{\beta P}}{P_{O_2}} + \frac{k_{12} P_{NA}}{P_{O_2}}$$

where ω_i – reaction rates [mole/(m³s)]; k_i – kinetic parameters; $P_{\beta P}$, P_{O2}, P_{PA}, P_{H2O}, P_{NA} – partial pressure of components [atm].

Intraparticle diffusion limitation was accounted by a general dusty gas model:

$$\frac{\partial}{\partial \rho}(D_{ri}^* \frac{\partial C_i}{\partial \rho}) - \frac{RT}{P}\frac{\partial}{\partial \rho}(V_i^* C_i) = \sum_{j=1}^{6}\gamma_{ij}\omega_j , \quad i \equiv C_{\beta P}, C_{O_2}, C_{PA}, C_{H2O}, C_{NA}, C_{PN} \quad (7)$$

with boundary conditions: $\rho = 0 : \frac{\partial C_i}{\partial \rho} = 0; \quad \rho = \rho_{grain} : C_i = C_i^{surface}$, C_i − component

concentration [mole/m^3].

In equation (7), $D_{ri}^* = \dfrac{1}{\dfrac{RT}{P}\sum_{k=1}^{6}\dfrac{C_k}{D_{ik}^*} + \dfrac{1}{D_i^{kn*}}}$ is a diffusivity of a component i in a mixture,

$V_i^* = \dfrac{\dfrac{RT}{P}\sum_{k=1}^{6}\dfrac{J_k}{D_{ik}^*}}{\dfrac{RT}{P}\sum_{k=1}^{6}\dfrac{C_k}{D_{ik}^*} + \dfrac{1}{D_i^{kn*}}}$ is a hydrodynamic velocity of a component i. Effective binary and

Knudsen diffusivity are defined as: $D_{ik}^* = \Pi D_{ik}$; $D_i^{kn*} = \Pi D_i^{kn}$, where Π is permeability. The kinetic parameters k_i as well as permeability Π were evaluated by minimizing the function F (eq.8) which represents the difference between the experimental and the calculated apparent rates W_i of main components transformations:

$$F = \frac{1}{N \cdot 4}\sum_{j=1}^{4}\sum_{i=1}^{N}\left(\frac{W_i^{\exp} - W_i^{calc}}{W_i^{\exp}}\right)^2 \quad i \equiv \beta P, PA, PN, CO_2 \quad (8)$$

Calculated apparent rate of component i transformation was defined as:

$$W_i^{calc} = \frac{1}{\rho_{grain}}\int_{0}^{\rho_{grain}}\sum_{j=1}^{6}\gamma_{ij}\omega_j(\rho)d\rho \quad (9)$$

4. Results

Kinetic parameters calculated by described above procedure are given at the Table. The kinetic parameters provide mean average deviation of 14.2 % between calculated and experimental reaction rates.

Table   Values of kinetic parameters

constant	dimension	values	constant	dimension	values
k_1	mole m^{-3} s^{-1}atm^{-1}	0.0572	k_8	dimensionless	330.5
k_2	dimensionless	0.0012	k_9	mole m^{-3} s^{-1}atm^{-1}	0.0023
k_3	atm^{-1}	0.0069	k_{10}	mole m^{-3} s^{-1}atm^{-1}	0.0003
k_4	dimensionless	0.0014	k_{11}	dimensionless	0.00001
k_5	mole m^{-3} s^{-1}atm^{-1}	0.5922	k_{12}	dimensionless	1.449
k_6	atm^{-1}	0.5454	k_{13}	mole m^{-3} s^{-1}atm^{-1}	8×10^{-7}
k_7	dimensionless	0.0005	k_{14}	mole m^{-3} s^{-1}atm^{-1}	0.0002
			Π	dimensionless	0.03

Effect of intraparticle diffusion limitation was studied for an isothermal plug flow reactor numerically. Product selectivities for two different catalyst sizes are shown at the Figs. 1-3.

The following operation conditions were used for the modeling: T=270 °C, inlet concentrations: βP-1%, O_2-18%, H_2O-20% (vol.).
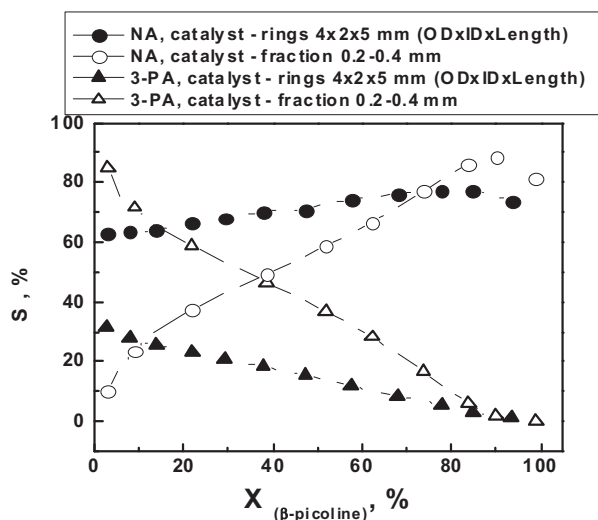
Fig. 1. Simulated selectivity of NA and PA vs. βP conversion in isothermal plug flow reactor
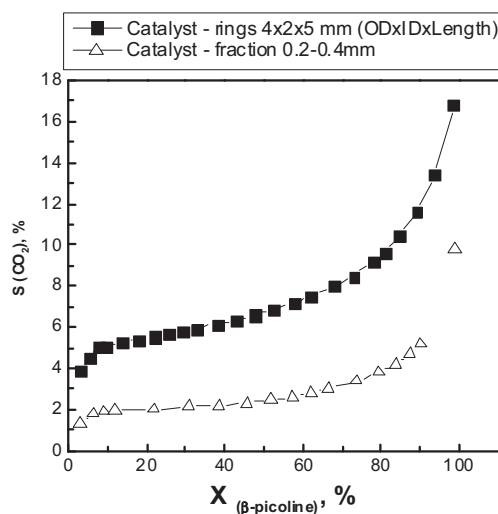
Fig. 2. Simulated selectivity of CO_2 vs. βP conversion in isothermal plug flow reactor
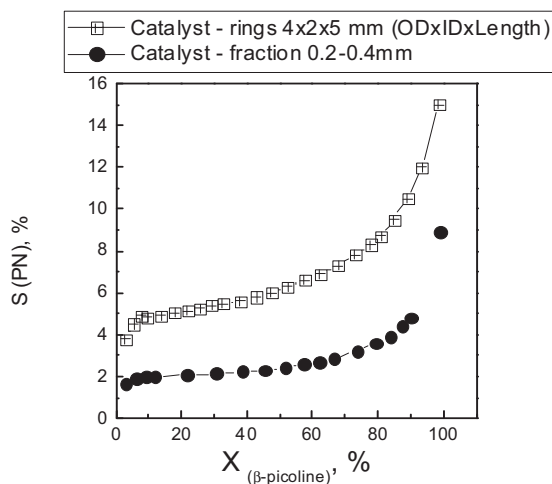
Fig. 3. Modeling of catalyst size effect on PN selectivity in isothermal plug flow reactor

The increase of catalyst pellet size evidently results in enhancement of intraparticle diffusion limitations, which causes dramatic changing in product selectivities. The only kinetic route of NA formation is through the intermediate PA. For a catalyst fraction 0.2-0.4 mm, modelled PA selectivity is 85% and NA selectivity is only 11 % at $X_{βP}$ = 3 % (Fig. 1). Low mass transfer resistance is observed. For a ring-shaped catalyst a new pseudo route of direct βP-oxidation into NA appears due to significant intraparticle mass-

transfer limitation. At βP conversion close to zero, modelled NA selectivity consists of 62 % (Fig.1). An apparent share of consecutive transformation PA into NA is less than 40 %. The corresponding changes take place with the selectivities of deep oxidation products – CO_2 and PN. Increase of catalyst pellet size results in significant rise of their selectivities (Fig.2, 3).

Thus, intraparticle diffusion limitation decreases the yield of desired product (NA). For increasing the yield of NA the change of catalyst porous structure and optimization of catalyst pellet shape and size are required.

[1]   E.M. Alkaeva, T.V. Andrushkevich, G.A. Zenkovetz, M.G. Makarenko, Russian Patent 2049089,1995; Euro Patent 0747359 A1 WO 95/20577; US Patent 5,728,837,1998.

[2]   G.Ya. Popova, Yu. A. Chesalov, T.V. Andrushkevich, E.V. Ovchinnikova, React. Kinet. Catal. Lett., V.87, № 2, 287-386, 2006

[3]   E.V. Ovchinikova, T.V. Andrushkevich, L.A. Shadrina, React. Kinet. Catal.Lett.,V.82, № 1, 2004,191-197.

THEORETICAL BASIS FOR STEAM REFORMING CATALYST SIZING

A.P. Kagyrmanova, I.A. Zolotarsky, E.I. Smirnov, N.V. Vernikovskaya

Boreskov Institute of Catalysis SB RAS,

Pr. Ak. Lavrentieva, 5, Novosibirsk, 630090, Russia, e-mail: aigana@catalysis.ru

1. Introduction

Catalyst shape and dimensions have an extremely high importance in performance of steam reformers. Catalysts of different sophisticated shape are widely used in industry for steam reforming of natural gas and higher hydrocarbons [1]. But theoretical optimization of catalyst dimensions is strictly restricted by lack of correlations for heat transfer parameters of beds packed by shaped particles. This gap was closed by recently derived correlations based on a hydrodynamic model of gas flow through holed particles [2,3]. That made possible to carry out theoretical optimization of dimensions for different catalyst shapes.

This paper presents optimization of shaped catalyst dimensions with technologically imposed restrictions for industrial operation conditions of a typical methanol plant reformer. A three-hole cylinder was taken as an example (height H, the outer diameter D and the hole diameter d of the particle), general conclusions on steam reforming catalysts sizing being made.

2. Optimization criteria and restrictions

From economical point of view the following criteria are most important:

- ✓ **the maximum methane conversion;**
- ✓ **the low pressure drop along the catalyst bed.**

But requirements of process reliability and safety place additional restrictions on catalyst mechanical strength and uniform packing. Nonuniform catalyst packing results in maldistribution of gas flow through reformer tubes and a risk of tubes overheating. According to [4], **for cylindrical particle the ratio of tube diameter to height D_{tube}/H and the ratio of height to diameter H/D should be kept within $D_{tube}/H \geq 5$ and $0.75 \leq H/D \leq 1.5$ for providing uniform catalyst packing.**

Poor catalyst strength results in catalyst damage and dust formation worsening reformer performance and shortening catalyst life time. Thus, catalyst strength should be kept constant during an optimization procedure. It is known from the resistance of materials, that generatrix

crushing strength of a holed cylindrical particle depends on the hole diameter to outer diameter ratio d/D only and does not depend on the outer dimension characteristics of the pellet (D and H). It means that **varying a height H and an outer diameter D of the particle and keeping the ratio d/D the same for all calculations, the mechanical strength is not changed.**

Steam reformer operation strongly depends on furnace chamber conditions. Enhanced catalyst heat transfer and activity properties ensure effective heat sink from reformer tubes and high conversion. Wall temperature was assumed to be constant for purposes of this work. In this case the optimization criteria is methane conversion at some fixed tube length.

3. Simulation procedure

Optimization of three-hole cylinder dimensions was performed by using the previously elaborated comprehensive mathematical model of a single reformer tube [5]. The two-dimensional pseudo homogeneous model accounts for a heat transfer between the tube wall and catalyst bed, conductivity and diffusivity in the radial direction in the packed bed and intraparticle diffusion.

Process parameters correspond to a typical methanol reformer, operation pressure being 25 Bars and tube diameter being 100 mm. Therefore, dimensions of three-hole cylinders were varied as $D = 5 \div 15$ mm and H=$10 \div 20$ mm.

Numerous simulations with different sizes of three-hole cylinder were performed at constant tube temperature for industrial conditions of a typical methanol plant reformer. Since the diameter of the reformer tube in our simulations was 100 mm, the varying range of three-hole dimensions was of $D = 5 \div 15$ mm and H=$10 \div 20$ mm. The holes were placed to have the same wall thickness between holes and between a hole and outer surface. Their diameter is defined from the ratio $d/D = 0.30$. This ratio provides the same mechanical strength of three-hole particles as that for Rahig rings with $d/D =$ (corresponding to commercial catalysts).

4. Results and discussions

Figures 1 and 2 present the effect of three-hole cylinder dimensions on the optimization criteria. The methane conversion is characterised by a ratio of methane concentration at a fixed bed tube length (L=2.4 m) to an equilibrium one at tube wall temperature (X).
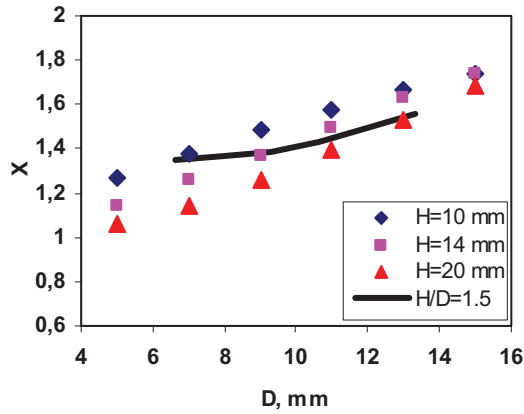
Fig.1. Effect of three-hole cylinder dimensions on degree of approaching equilibrium X at the tube length L = 2.4 m
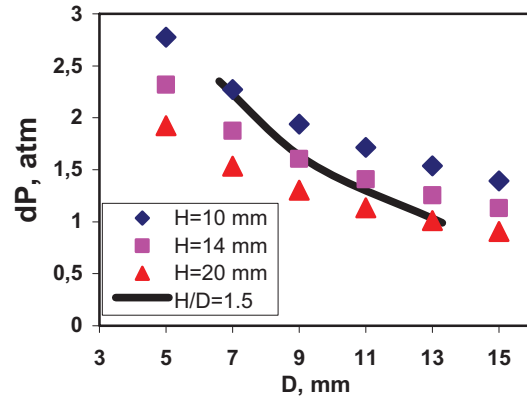
Fig.2. Effect of three-hole cylinder dimensions on pressure drop along the tube length ΔP.

As can be seen from Figs.1, 2, increasing of the height H results in the rise of methane conversion and reduction of pressure drop along the catalyst bed except the region with a large particles with $D > 13$ mm. Increase of the outer diameter D results in pressure drop reduction, but at the same time the methane conversion considerably decreases.

These dependences result from complex effects of catalyst dimensions on heat transfer parameters and catalyst effectiveness factor. The effectiveness factor is proportional to the geometric surface area of pellet, increasing of both height and diameter diminishing the effectiveness factor. Catalyst height and diameter have the same effect on radial thermal conductivity λr also (Fig.3). Their increase rises λr, which is substantially determined by a convective mechanism with a small contribution from radiation. The convective radial heat conductivity is enhanced with catalyst size due to gas mixing intensification.
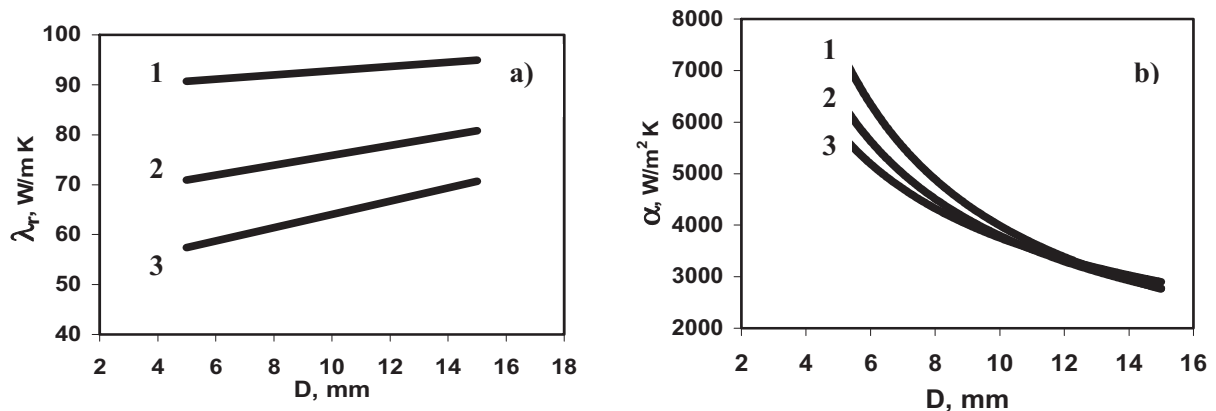
Fig.3. Effect of three-hole cylinder dimensions on (a) radial heat conductivity; (b) heat transfer coefficient from the tube to catalyst bed. (1) H=20 mm; (2) H=14 mm; (3) H=10 mm.

The effect of catalyst dimensions D and H on a wall heat transfer coefficient α has a more complicated character (Fig. 3b). It monotonically decreases with the growth of D but

has an opposite trend from the height *H* in the range of practical interest with D < 13 mm. At D >13 mm dependence of α from H is divergent. This effect is caused by redistribution of gas flow through holes and around particles according to the mathematical model applied. Since process performance is more sensitive to α than to λr, this effect strongly determines methane conversion curves shown at Fig. 1. Namely, height rise does not decrease the conversion at D >14 mm in spite of effectiveness factor drop.

Therefore, the height to outer diameter ratio *H/D* in the optimized catalyst should be maximal. Solid lines on Figs 1 and 2 correspond to isolines with maximum allowed *H/D* = 1.5. Since methane conversion changes slightly along the isoline in comparison with the pressure drop, optimal catalyst dimensions are determined by pressure drop dependence mainly and restricted by maximum catalyst height. Therefore, optimal dimensions of the three-hole cylindrical catalyst are: *H*=20 mm; *D* = 13.3 mm, *d* = 3.9.

The similar results were obtained for different holed cylindrical catalysts – for optimal catalyst sizing one can choose a maximum catalyst height and minimum diameter with restrictions determined by requirements of uniform catalyst packing. Numerical results obtained for Rashig rings and trilobed catalyst will be presented in the paper.

[1] J.R. Rostrup-Nielsen, Catalytic Steam Reforming, Berlin: Springer, 1984.

[2] E.I. Smirnov, A.V. Muzykantov, V.A. Kuzmin, A.E. Kronberg, I.A. Zolotarskii, Chem. Eng. J., 11,2003, 243-248.

[3] E.I. Smirnov, V.A. Kuzmin, I.A. Zolotarskii, Chem. Eng. Research Des., 82,2004, 293-296.

[4] S. Afandizadeh, E.A. Foumey, Applied Thermal Eng., 21, 2001, 669-682.

[5] A.P. Kagyrmanova, I.A. Zolotarskii, N.V. Vernikovskaya, E.I. Smirnov, V.A. Kuzmin, N.A. Chumakova, Theoret. Found. Chem. Eng., 2, 2006, 1-14.

PP-35

METHOD OF DEFINITION OF MOISTURE CONTENT IN OIL PRODUCTS

R.M. Kasimov, E.M. Mamedov

Institute of Chemical Problems, Azerbaijan National Academy of Sciences,
Baku, AZ0143, 29 Husein Javid Prospect, Azerbaijan Republic
Phone: 994 12 439 41 59, E-mail: baku@bk.ru

Oil products used during processing require the preliminary control of the water in them in allowable limits. Existing laboratorial chemical and physicochemical methods of definition of moisture content in oil products are difficult enough and demand much time for processing the received information. In this connection, because of simplicity of technical realization there was preferable an application of physical methods of the analysis which are based on measurements of dielectric coefficients of oil products in capacitor cells or under characteristics of reflection from them microwave radiation. Sensitivity of these methods is connected to essential distinction in dielectric coefficients of water and dehydrated oil product. However, the complex and not always simple dependence between required and measured sizes, and also necessity of application of the products purified from water at carrying out of calibration of a scale of the device complicates carrying out of settlement operations by these methods.

With the purpose of elimination of these lacks of a physical quality method of control the new variant of a microwave method of definition of moisture content in oil products which is based on the analysis of peak characteristics of the wave reflected from a layer adjustable on thickness of researched substance is offered. By preliminarily carried out researches of modeling binary solutions of polar liquids in non polar solvents, and in particular solutions of water in non polar dioxan, it has been established, that at the set temperature and frequency of radiation in these solutions at certain, selective values of thickness of a layer of a solution and concentration in it of a polar component the effect of full or unreflecting absorption of falling radiation takes place. Thus their product appears in invariant size for the given solution. Existence of such selective values of structure and thickness of a layer in similar binary solutions and invariance of their product allows to carry out a quantitative estimation of a

polar component without carrying out preliminary procedure of measurement of dielectric coefficients of pure components.

The method of definition developed on the basis of carried out researches small (0,01–10 % weight.) content of water in oil product is reduced to the removal of dependence on thickness of a layer of a product of amplitude of the microwave radiation reflected from it and definitions of such thickness of a layer at which it is feasible or the condition of full absorption of radiation in a layer of this substance. Thus for finding out the percentage content of water in oil product the measured values of amplitude of the reflected signal in two points of a minimum of the removed dependence located on both sides from found boundary area of thickness of a layer of substance are used. Approbation of the developed method is carried out in a range of microwaves at lengths of waves 1,5 and 0,8 sm. Reliability of the carried out analyses on moisture of some samples of oil product is confirmed with the data control distillation method of the analysis of the same products.

REDUCING OF AN ENERGY CONSUMPTION IN THE PROCESS OF THE VAPOR-PHASE DEHYDRATION OF METHYLPHENYLCARBINOL BY THE USE OF A COMPOSITE HEAT CARRIERS

Kharlampidi Kh., Karalin E., Abramov A., Ksenofontov Dm.

Kazan State Technological University, Russia, Kazan, 420015, K. Marks st. 68;
fax (843)2314162; e-mail: karalin@kstu.ru; karalin@yandex.ru)

Up to the present are known 3 industrial methods for receiving of propylene oxide and the best one among them is the method of simultaneous receiving of propylene oxide and styrene monomer (POSM) on account at relatively low costs of production **[1]**. A similar production in Russia was introduced in the mid 1980s in "Nizhnekamskneftechim" (Nizhnekamsk, Tatarstan), where today about 60000 tons of propylene oxide pro year are produced **[2]**. Home technology of this process (POSM), worked up under heading of M.A. Dalin and B.R. Serebryakov, doesn't differ from foreign analog processes in principle and includes the stage of vapor-phase catalytic dehydration of methylphenylcarbinol (MPC). Dehydration of MPC is realized in the presence of alumina (gamma-oxide) catalyst under adiabatic conditions by temperature at the entry of the reaction vessel $280 \div 320°C$. For lowering of partial pressure of hydrocarbons and compensation of endothermic effect of the basic reaction there is used a water excess of 10 mol for 1 mol of MPC.

For reducing of power capacity at the dehydration stage there is proposed a partial replacement of water steam with a methane -hydrogen fraction by mass correlation MPC : water : hydrogen = $1 : 1 : 4{\cdot}10^{-4} \div 4{\cdot}10^{-2}$ **[3,4]**. It should be note that there is an alternate reducing method of water consumption by its partial replacement not with a gasiform but with a hydrocarbon diluter as this there can be used, for example, ethylbenzene which is an intermediate product by the POSM process.

Taking in account the proper thermal and hydrodynamic parameters, which ensure the maximally permissible fall in temperature by the work with water steam in an industrial installation, it must be one of the urgent task by replacement of heat carrier to hold the adiabatic fall in temperature in optimal limits appointed for water steam.

The object of this paper is to value the realization possibility of both methods of partial water replacement taking in account the adiabatic fall in temperature.

The maximal temperature of reaction mixture, which is possible in adiabatic conditions, when the reaction proceeds to the end (ΔT_{ad}), is determined from equation:

$$\Delta T_{ad} = \frac{\Delta H \cdot m}{M \cdot C_p \cdot m_{mix}} \qquad (1),$$

where m is reagent mass, kg /hour; M – mol mass of the reagent, kg /kmol; m_{mix} – mass of base mix, which comes into the reaction vessel, kg /hour; C_p – thermal capacity of the mixture, kJ /(kg·K); ΔH – thermal effect of reaction, kJ /mol.

When taking as row material a binary mix, which consists of 82% - mass MPC and 18% - mass acetophenone (ACP) **[5, 6]** with $\alpha_{MPC}=1$, for a system with only water as heat carrier, we convert the product $C_p \cdot m_{mix}$ for base and final mix composition as:

$$\left(\sum \overline{C}_{Pi} \cdot m_i\right)_{base} = m_{0MPC} \cdot \overline{C}_{PMPC} + m_{ACP} \cdot \overline{C}_{PACP} + m_{0water} \cdot \overline{C}_{Pwater}$$

$$\left(\sum \overline{C}_{Pi} \cdot m_i\right)_{end} = m_{ST} \cdot \overline{C}_{PST} + m_{ACP} \cdot \overline{C}_{PACP} + m_{0water} \cdot \overline{C}_{Pwater} + m_{1water} \cdot \overline{C}_{Pwater},$$

where C_{pi} is medium thermal capacity of i-th component at interval $500 \div 600$ K $(227 \div 327°C)$, kJ/ (kg·K); m_{0water} – water mass at the reaction vessel entrance, kg; m_{1water} – water mass separated during the reaction, kg; m_{ACP} and m_{ST} are masses of ACP and styrene, kg.

Since reagent MPC and reaction products – styrene and water – have practically the same thermal capacity and accordingly the products $(\sum C_{pi} \cdot m_i)$ at entrance and outlet of the reaction vessel don't differ, then we have:

$$\left(\sum \overline{C}_{Pi} \cdot m_i\right)_{base} = \left(\sum \overline{C}_{Pi} \cdot m_i\right)_{end} = const + m_{0water} \cdot \overline{C}_{Pwater}$$

It is evident, that by the fixed value of ΔT_{ad} and replacing a part of water with an inert heat carrier the next condition must be carried out:

$$m_{0water} \cdot \overline{C}_{Pwater} = m_{2water} \cdot \overline{C}_{Pwater} + m_{hc} \cdot \overline{C}_{Phc} \qquad (2),$$

where m_{2water} is water mass by its partial replacement with a heat carrier, kg; m_{hc} – mass of an inert heat carrier, kg; C_{Phc} – medium thermal capacity of an inert heat carrier at interval $500 \div 600$ K $(227 \div 327°C)$, kJ/ (kg·K).

By calculation for 1 kg MPC-fraction of above mentioned composition m_{0water} for an industrial process is 1,210 kg (10 mol of water on 1 mol MPC), m_{2water} – by partial replacement of water with hydrogen **[3, 4]** – 0,820 kg (6,8 mol of water on 1 mol MPC). Under these conditions, we see from equation (3) that it is necessary to put into the system 0,373 kg of ethylbenzene or 0,054 kg of hydrogen (what considerably exceeds the maximum quantity of hydrogen in accordance with patents **[3, 4]**) to compensate the 0,34 kg lowering of water quantity.

Heat quantity Q_Σ used for warming of a heat carrier up to work temperature of the dehydration process by utilizing of a liquid heat carrier includes heat for warming the heat carrier up to the boiling temperature Q_1, heat for evaporation of heat carrier vapor up to the work temperature Q_3. When a gasiform heat carrier is used two former components aren't necessary and heat is consumed only for worming gas up to the work temperature.

PP-36

A calculation example to water:

$$Q_1 = m_{0water} \cdot \overline{C}_{Plwater} \cdot (t_{boil} - t_{initial}) \qquad (3)$$

$$Q_2 = m_{0water} \cdot \Delta H_{vb} \qquad (4)$$

$$Q_3 = m_{0water} \cdot \overline{C}_{Pwater} \cdot (t_{work} - t_{boil}) \qquad (5),$$

where $t_{initial}$ is initial temperature of the up heat carrier (about 40°C); t_{boil} – normal boiling temperature of the heat carrier; t_{work} – work process temperature (at the entrance of the reaction vessel); $C_{Plwater}$ – medium thermal capacity of liquid water at interval $t_{initial} \div t_{boil}$, kJ/(kg·grad); C_{Pwater} – medium thermal capacity of water steam at interval $t_{boil} \div t_{work}$, kJ/(kg·grad); ΔH_{vb} – evaporation enthalpy by normal boiling temperature, kJ/kg.

Calculation results from the equations (1-5) for different combinations of heat carriers by the work temperature 300°C are given in the table 1. It is seen that the total heat consumption for warming of a heat carrier by a partial replacement of water is practically the same (regardless of replacing water with hydrogen or ethylbenzene) and makes about 75% of heat consumption in an active process.

At the same time, 54 g of hydrogen for 1 kg of row material are equivalent to 600 dm³ (normal conditions) of gasiform hydrogen, it means that cooling and separation of such gas quantity will require a considerable complication of technological equipment. Increase of explosion danger is another negative side of hydrogen application.

The alternate version with the partial replacement of water with hydrocarbon doesn't require principal changing in the technological scheme, but by using of ethylbenzene there will be higher requirements to equipment for separation of dehydration products on account of close boiling temperatures of styrene and ethylbenzene.

In our option, it is preferable to utilize aliphatic hydrocarbon with boiling temperature lower than styrene has (for example n-hexane or n-octane).

Table 1. Heat consumption for warming of a heat carrier

№	Quantity of a heat carrier on a basis of 1 kg MPC-fraction, kg			Q, kJ			
	Water	H₂	Ethylbenzene	Q_1	Q_2	Q_3	Q_Σ
1	1,210	0	0	304	2730	482	3516
2	0,820	0,054	0	206	1850	531	2587
3	0,820	0	0,373	280	1977	454	2711

References

[1] Lyondell Chemical Company (http://www.lyondell.com)
[2] "Nizhnekamskneftekhim" INC (http://www.nknk.ru/about_company_en.asp)
[3] RU Patent 2,083,543 (1997)
[4] RU Patent 2 104 991 (1998)
[5] USA Patent 4 521 635 (1985)
[6] Lange, Jean-Paul. Mass transport limitations in zeolite catalysts: the dehydration of 1-phenyl-ethanol to styrene / J.P. Lange, Carl M.A.M. Mesters // Appl. Catal. A: General. – 2001.– 210. – P. 247–255.

AN EFFECTIVE CoOx-CuOx-CeO2 CATALYST FOR PREFERENTIAL OXIDATION OF CO

Kibar M.E., Ozdemir E., Yildlrim R.*, Akin A.N.

Kocaeli University, Department of Chemical Engineering, Kocaeli, Turkey

*Bogazici University, Department of Chemical Engineering, Istanbul, Turkey

Introduction

There is a worldwide interest in the development and commercialization of polymer electrolyte membrane fuel cells (PEMFC) [1]. The PEMFCs require hydrogen as its fuel source in order to avoid storing high pressure hydrogen be generated on board [2]. The hydrogen produced by steam reforming or partial oxidation of hydrocarbons or renewable fuels contains 0,5-2,0 vol.% CO. Hydrogen mixtures for fuel cell should be free of CO because it adsorbs on anode catalysts and decrease the performance [3].

As a fact, CO should be removed to ppm level (<10 ppm) and preferential oxidation of CO (PROX) has been recognized as one of the most strong and cost effective method for removing of CO in hydrogen in feed gas [4]. Different types of catalysts have shown their efficiency for the preferential oxidation of CO. This can be classified into four general groups: noble metal-based catalysts, perovskites, spinels, solid dispersions/solutions of transition metal oxides and lanthanide oxides [5]. Among these catalysts, CuO/CeO_2 have shown to be very active for CO oxidation and therefore, they are superior to Pt-based catalysts [6]. CeO_2 is used as promoter or support based on its high oxygen capacity. The activity and selectivity of CeO_2-based catalysts are greatly enhanced by base metals, especially copper [7]. Also, cobalt oxide shows very high CO oxidation activity in CO/O_2 mixtures even at ambient temperature [8].

The catalyst properties which influenced the activity/selectivity of catalyst, vary by the preparation methods and conditions. Most commonly used methods are impregnation and precipitation. For product homogenity, high metal loading, small crystalline form of metals and the reproducibility of the process, co-precipitation can also be used as catalyst preparation method [9].

Experimental

In this study a co-precipitation method has been developed and modified for the preparation of $CuOx – CoO_x – CeO_2$ catalysts developed for CO oxidation in H_2 rich environment in the presence of CO_2 and water. Catalysts were prepared by coprecipitation of metal nitrates in a semi-batch reactor by using NaOH as precipitation reagent. Two important

precipitation parameters pH and temperature are optimized for the activity and the selectivity of mixed oxide catalyst. Experimental design is performed to two factors and three levels (pH : 8,5-10,0-11,5 and T = 5,0-37,5-70,0 °C) by using central composite design for the preparation of 20%CuO-20%CoO-60%CeO_2 catalysts.

To determine the effect of metal interactions in the prepared catalysts to catalyst activity, new catalysts were prepared at optimum pH and temperature by using statistical experimental design techniques. For this purpose, 14 catalysts were prepared at six metal levels of 0,17, 33, 50, 67, 100 % for all Co, Cu and Ce metals to perform mixture design.

Prepared catalysts characterized by different physical and chemical methods. Metal contents of the catalysts were measured by atomic absorption spectrometer. The total surface areas were determined by N_2 adsorption using multipoint technique with BET equation. SEM and XRD analysis were performed to determine the catalyst structure.

Catalytic activity tests were conducted in a microreactor flow system, including an online gas chromatograph for feed and product analysis. The effect of reaction conditions such as temperature, CO, O_2, CO_2, and H_2O concentrations in the feed mixture, time-on-stream, space velocity were also investigated.

Results

Optimum catalyst preparation conditions (pH and temperature) and metal contents are determined according to catalytic activity and selectivity at PROX. The activity and selectivity results for prepared catalysts were correlated with their physical and chemical properties measured to understand the effects of metal loadings and preparation conditions. The catalyst preparation conditions were also optimized using activity as the response considering that achieving full conversion of CO is the primary goal for this catalyst. The results show that the addition of Co as a second metal leads to bimetallic interaction which gives way to enhanced activities at very low temperatures. Optimum conditions for catalyst preparation are found as 37.5 °C and pH 10. 100 % conversion in PROX of CO at 150 °C was obtained. H_2O and CO_2 in the feed cause a decrease in activity and selectivity. However, water vapor dramatically decreases the activity of the catalyst compared to CO_2.

References

1. J. D. Kim, Y. I. Park, K. Kobayashi, M. Nagai, M. Kunimatsu, Solid state Ionics, 140 (2001) 313
2. P. K. Cheekatamarla, W. S. Epling, A. M. Lane, J. Power Sources, 147 (2005) 178
3. F. Marino, C. Descorme, D. Duprez, App.Catal B: Environ., 58 (2005) 175
4. A. Martinez-Arias, A. B. Hungaria, M. Fernandez-Garcia, J. C. Conesa, G. Munuera, J. Power Sources, 151 (2005) 32
5. G. Marban, A. B. Fuertes, App. Catal. B: Environ. 57 (2005) 43
6. G. Avgouropoulos, T. Ioannides, H. K. Matralis, J. Batista, S. Hocevar, Cat. Lett., 73 (2001) 33
7. X. Tang, B. Zhang, Y. Li, Y. Xu, Q. Xin, W. Shen, App. Catal. A: Gen, 288 (2005) 116
8. J. Jansson, A. E. C. Palmqvist, E. Fridell, M. Skoglundh, L. Osterlund, P. Thormahlen, V. Langer, J. Catal, 211 (2002) 387
9. M.Campanati, G. Fornasari, A. Vaccari, Catal. Today, 77 (2003) 299

IMPROVEMENT OF TEMPERATURE CHARACTERISTICS OF DIESEL FRACTIONS AND LUBE CUTS BY THEIR HYDROISOMERIZATION ON Pt-SAPO-31 CATALYST

O.V. Kikhtyanin, A.V. Toktarev, G.A. Urzuntsev, L.A. Vostrikova and G.V. Echevsky

Boreskov Institute of Catalysis, SB RAS, Lavrentyev Ave., 5, Novosibirsk, 630090, Russia
kihtanin@catalysis.nsk.su

Low temperature properties of diesel fuels and base oils are one of their main working characteristics which allow fuel and oil systems of engines to operate at extreme temperature conditions. There are a number of processes oriented on production of diesel fuels and base oils with improved temperature characteristics. The main task of these methods, named deparaffinization, is a decrease of n-paraffins content in final product. Long-chain n-paraffins as a substantial part of a raw material possess undesirable temperature properties and, hence, should be removed to get high-quality goal product with low pour point.

Several processes concerning conversion of n-paraffins using zeolite catalysts are known. These catalysts usually contain noble metals, Pt or Pd, and the reaction is carried out in the presence of hydrogen. In the course of the reaction over zeolites n-paraffins meet two pathways of their transformation, hydrocracking and hydroisomerization.

When n-paraffins content in initial hydrocarbon mixture is not very high it is possible to carry out deparaffinization by means of catalysts on the base of pentasil zeolites, ZSM-5, ZSM-11, etc. Removing of n-paraffins occurs via their hydrocracking producing light hydrocarbons, and in this case an yield of the aim low-freezing product depends on the percentage of linear compounds in the starting material.

However, when content of n-paraffins is high, direct deparaffinization via cracking is not suitable due to the significant yield loss of the goal product. In this case hydroisomerization is more convenient as soon as long-chain linear hydrocarbons are not transformed to shorter molecules but are converted to branched isomers making unchanged fractional composition of the product comparatively with the feed.

Zeolitic unidimentional substituted aluminophosphates attract a lot of attention for this case due to their unique pore structures and acidic properties of moderate strength.

Hydroisomerization catalyst on the base of Pt-SAPO-11 is known as one of the examples of successful industrial application [1].

Boreskov Institute of Catalysis during several years has been working out its own hydroisomerization catalyst on the base of SAPO-31 silicoaluminophosphate. This catalyst possesses high activity in conversion of long-chain paraffins to corresponding isomers with very low content of cracked products. The present work presents some results on hydroconversion of diesel fraction and gatch (wax concentrate) on Pt-SAPO-31 catalyst in dependence on reaction conditions and properties of initial feed.

Synthesis of SAPO-31 sample was carried out according to [2]. Calcined silicoaluminophosphate powder was impregnated with $Pt(NH_3)_4Cl_2$ solution to get 1 wt.% of Pt loading followed by granulation with 20% of pseudoboehmite and calcining of the resulted extrudates at 550°. Catalytic tests were carried out using a flow installation with a fixed catalyst bed (catalysts volume - 10 cm^3). Prior to experiments catalyst was pretreated in a hydrogen flow at 400°C. Reaction products were analyzed using HP-5890 unit equipped with DB-1 capillary column.

Prepared Pt-SAPO-31 catalyst was tested in hydroconversion of diesel fraction (b.p. 170-350°C) used as an initial feed. Reaction conditions and results of the experiments are presented in Table 1.

Table 1. Hydroconversion of diesel fraction on Pt-SAPO-31 in dependence on reaction temperature. $P_{reac.}$ – 3.0 MPa, WHSV – 1.2 h^{-1}, volume ratio H_2 : feed = 2000.

Reaction temperature, °C	Yield of diesel fraction, wt%.	n-Paraffins content, wt%.	Pour point of diesel fraction, °C	Calculated Cetane Number [3]
Feed	100	22,5	-10	54,0
290	98,8	15.5	-28	53,2
300	98,3	12,7	-35	52,7
310	97,6	10,1	-46	52,4
320	96,8	8,1	-55	51,7
330	96,2	6,2	-58	51,1
340	95,1	3,9	-61	50,5
350	93,6	not determ'd	-65	50,1

Table 1 shows high hydroconversion activity of Pt-SAPO-31 sample. Transformation of initial diesel fraction is observed at reaction temperatures even below 300°C what is seen from the lowering of pour point of the obtained diesel products. It is seen that decrease of n-paraffins content in the products is greater than loss of the yield of the aim fraction. This proves that during hydrotreatment of the feed n-paraffins undergo isomerization rather than cracking. This is due to moderate acidity and unique pore structure of SAPO-31 material what substantially minimizes secondary hydrocracking.

Hydrotreating of sulfur containing hydrocarbon fractions is seems to be another problem in production of high-quality products. Sulfur presented in nearly all refinery feeds affects the properties of hydroisomerization catalyst, so it would be desirable that Pt-containing catalyst stays active when initial feed contains increased amounts of sulfur.

Runs were carried out with diesel fractions with 0-500 ppm of sulfur (dibenzothiophene specially added to initial sulfur-free feed). Figure 1 shows the effect of S content in the feed on activity of Pt-SAPO-31 which is represented in the terms of pour points of resulted products.
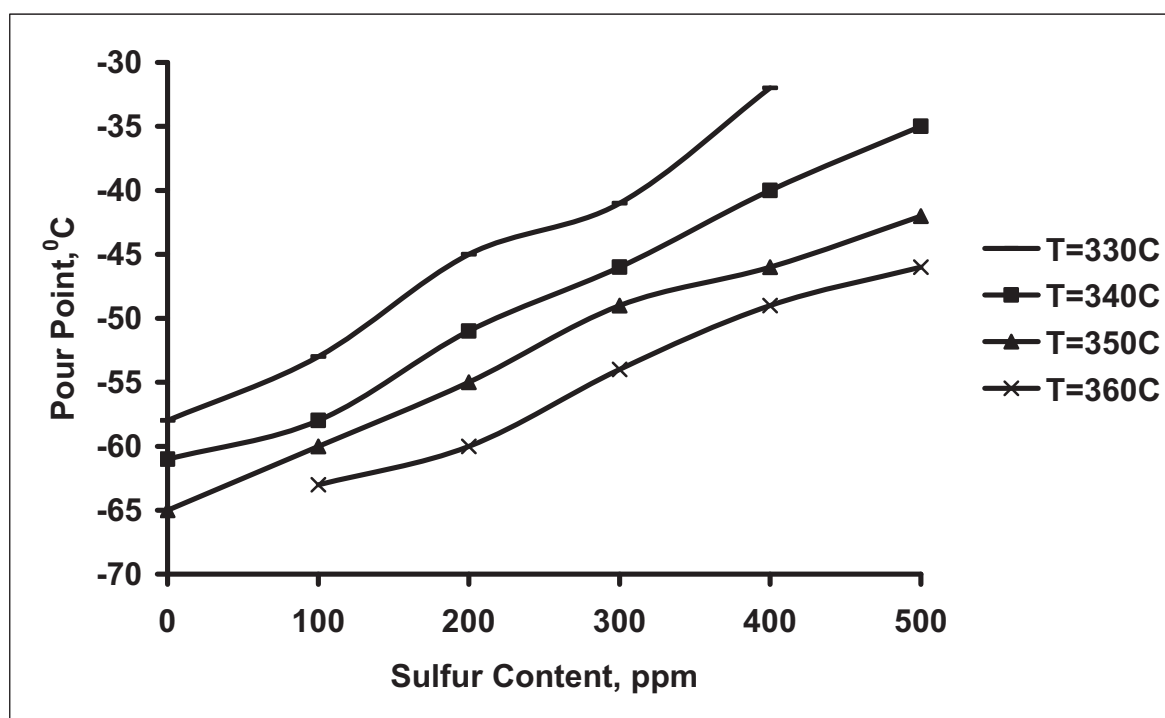
Figure 1. Influence of sulfur content in initial feed on pour point of resulted diesel fractions. Catalyst - Pt-SAPO-31, P = 3.0 MPa, WHSV = 1.2 h^{-1}, volume ratio H$_2$: feed = 2000.

Obviously, in the case of S-containing feed to produce diesel fuel with improved temperature properties it is necessary to increase reaction temperature. On the other hand, this is a reason of decreasing yield of the desired fraction due to secondary cracking of isomerized product. In the case of high sulfur feed such decrease may amount as much as 15%.

Pt-SAPO-31 was also used to isomerize wax concentrate – gatch (b.p. 360-480°C) which is considered as a feed to produce high quality high viscosity base oil. Content of n-paraffins in this feed attains 72.5 %wt. From data presented in Table 2 it is seen that lowering of the pour point from 56°C in the feed to below zero results in a lube yield of more than 75 %wt. The main by-product in this case is low-freezing diesel fraction >150°C. Decrease in reaction temperature improves yield of the desired product but simultaneously pour point increases up to 12-16°C.

Table 2. Hydroconversion of wax concentrate (gatch) on Pt-SAPO-31 in dependence on reaction temperature. $P_{reac.}$ – 3.0 MPa, WHSV – 1.2 h^{-1}, volume ratio H_2 : feed = 2000.

Reaction temperature, °C	Yield of lube, wt%.	Pour point of lube, °C
Feed	100	56
310	89.7	15
320	82.3	6
340	76.1	-1
350	62.4	-8

The presented data prove that Pt-SAPO-31 catalyst is highly effective for improving temperature characteristics of fuels and lubes by hydroisomerization of n-paraffins in the feed. Isomerization properties of the catalyst are decreased by sulfur presenting in the starting material, but increasing the reaction temperature it is possible to produce products with the desired pour point characteristics starting from feed with S content up to 500 ppm.

References

1. S.J. Miller, et al, NPRA Natl. Fuels and Lubr. Mtg. (1992), Paper No. FL-92-109.

2. Patent of Russian Federation, No. 2,264,859 (2005).

3. S.V. Cherepitsa, et al, Khimiya i Technologiya Topliv i Masel (Rus.), No. 6 (2003), p. 45.

MODELING OF A HEAT-COUPLED CATALYTIC REACTOR WITH CONCURRENT OXIDATION AND CONVERSION FLOWS

Kirillov V.A.[*], Fadeev S.I.[**], Kuzin N.A.[*], Shigarov A.B.[*]

[*]*Boreskov Institute of Catalysis SB RAS, Prosp. Akad. Lavrentieva, 5, Novosibirsk, Russia*
V.A.Kirillov@catalysis.ru
[**]*Sobolev Institute of Mathematics SB RAS, Prosp. Akad. Koptyuga 4, Novosibirsk 630090,*
Russia

Development of a compact catalytic reactor for conversion of hydrocarbon fuels into synthesis gas with following production of hydrogen for fuel cells has become a highly topical problem in recent years. Steam conversion provides the maximal hydrogen yield, but it requires heat supply to the endothermal reaction zone. One promising solution of the problem is that heat coupling of the endothermal reaction of steam natural gas conversion, for instance, and catalytic afterburning of the hydrogen-containing anode gas unspent in the fuel-cell stack in one reactor. In this case, the reactor is designed as a combination of flat catalytic channels. A number of the channels are ment for endothermal steam conversion of natural gas (endothermal channels). Oxidation of the anode gas to evolve heat proceeds in the neighboring exothermal channels. The evolved heat is transferred to the neighboring endothermal channels due to heat conductivity. This type of reactors was considered in several publications [1-3] and a number of mathematical models were suggested to describe steady state regimes. However, the amount of available experimental data confirming the validity mathematical models is insufficient. In this work we present a more detailed model as compared to the earlier reported in ref. [3] and a comparison of the experimental and simulation data. Fig. 1 schematically shows the reactor of synthesis gas generation. The experimental conditions were: natural gas flow rate 60 cm^3/s, steam flow rate 0.32 g/s, flow rates of hydrogen and air at the reactor inlet 310 and 2250 cm^3/s, respectively. The experiment was described in detail in [3].
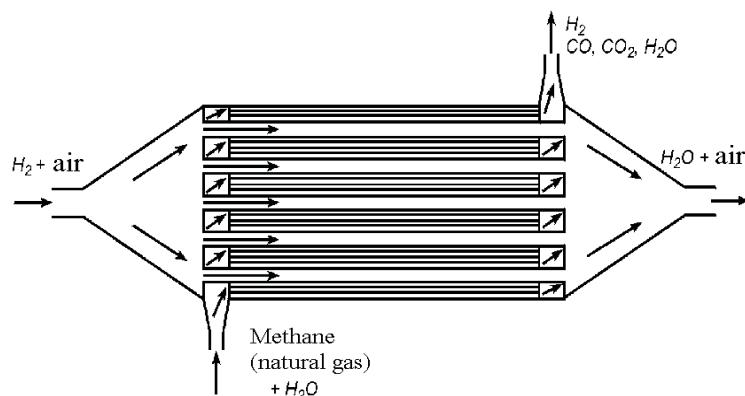
Fig. 1. Heat coupled reactor.

PP-39

Mathematical model

The following equation set was used to describe the processes occurred in the endothermic channels: $0 \leq z \leq H, \ 0 \leq \ell \leq L$,

$$c_p^{en} G_{en} \frac{\partial T_g^{en}}{\partial \ell} = \alpha_{en} S\left(T_c - T_g^{en}\right), \qquad \lambda_z \frac{\partial^2 T_c}{\partial z^2} + \Delta H_{con} W_{con} + \Delta H_{sh} W_{sh} = \alpha_{en} S\left(T_c - T_g^{en}\right),$$

$$G_{en} \frac{\partial y_i}{\partial \ell} = \left(\nu_i^{con} W_{con} + \nu_i^{sh} W_{sh}\right) m_i, \qquad i = \left\{CH_4, H_2O, CO, H_2, CO_2\right\}, \tag{1}$$

The processes in the exothermal channels were described by: $z = H, \ 0 \leq \ell \leq L$,

$$c_p^{ex} g \frac{dT_g^{ex}}{d\ell} = \alpha_{ex}\left(T_W - T_g^{ex}\right), \qquad g \frac{dx_j}{d\ell} = \nu_j^{hyd} w_{H_2}^{ex} m_j, \qquad j = \left\{O_2, N_2, H_2, H_2O\right\}, \tag{2}$$

The heat-balance equation for the wall between the channels is: $z = H, \ 0 \leq \ell \leq L$,

$$\lambda_z \frac{\partial T_c}{\partial z} + \alpha_{ex}\left(T_W - T_g^{ex}\right) = w_{H_2}^{ex} \Delta H_{H_2} + \lambda_W \delta_W \frac{d^2 T_W}{d\ell^2}. \tag{3}$$

Краевые условия: $y_i = y_{i0}, \quad x_j = x_{j0}, \quad T_g^{en} = T_{g0}^{en}, \quad T_g^{ex} = T_{g0}^{ex}$ at $\ell = 0$;

$$\frac{\partial T_c}{\partial z} = 0 \text{ at } z = 0; \ T_c = T_w \text{ at } z = 1; \ \frac{dT_W}{d\ell} = 0 \text{ at } \ell = 0 \text{ and } \ell = L. \tag{4}$$

Coefficients of heat-mass transfer, heat conductivity, kinetics of the reaction were determined from the dependences described elsewhere [3]. Definition of the boundary problem does not belong to a standard type. Therefore, the problem solution called for the development of an ingenious numerical method.

Results

Figure 2 shows temperature profiles along the reactor length. Note that at the reactor inlet, one can observe rather high temperature differences between the gas and the catalyst and through the endothermic unit thickness between its wall (z=1) and center (z=0). Fig. 3 shows changes in calculated «dry» mole fractions of CH_4, H_2, CO, and CO_2 in the gas flow along the endothermal channel length and the experimental values at the outlet. Fig. 4 shows a hysteresis dependence of the reactor temperature regime *versus* oxidation catalyst activity k_{ox}^0. The wall temperature profiles were obtained for eight solutions in the range $6 < k_{ox}^0 < 30$ m/s. Calculations were performed as parameter k_{ox}^0 gradually changed from its maximal value of 30 m/s to 6 m/s, and then in reverse sequence. The upper solution branch (normal operation mode of reactor) exists if activity of the oxidation catalyst is rather high ($k_{ox}^0 > 6$ m/s). However, if activity is very high ($k_{ox}^0 > 15$ m/s), the catalyst undergoes dangerous overheating $>1000^{\circ}$C. If the catalyst activity decays to a critical value ($k_{ox}^0 \sim 6$ m/s), the reactor operation changes from the high-temperature mode to the low-temperature one, that is the reactor stops its operation. The reverse process is possible if $k_{ox}^0 \sim 13$ m/s. Interestingly, the actual values of parameter k_{ox}^0 are just in the range between the points of ignition and

extinction, i.e. in the domain of regime multiplicity. This indicates that in order to start up such a catalytic reactor, it should be initially heated.

Thus, our mathematical model adequately describes the experimental data and permits one to predict regimes of the process performance in the thermally-coupled catalytic reactors, which undoubtedly hold much promise as generators of synthesis gas for fuel cells.
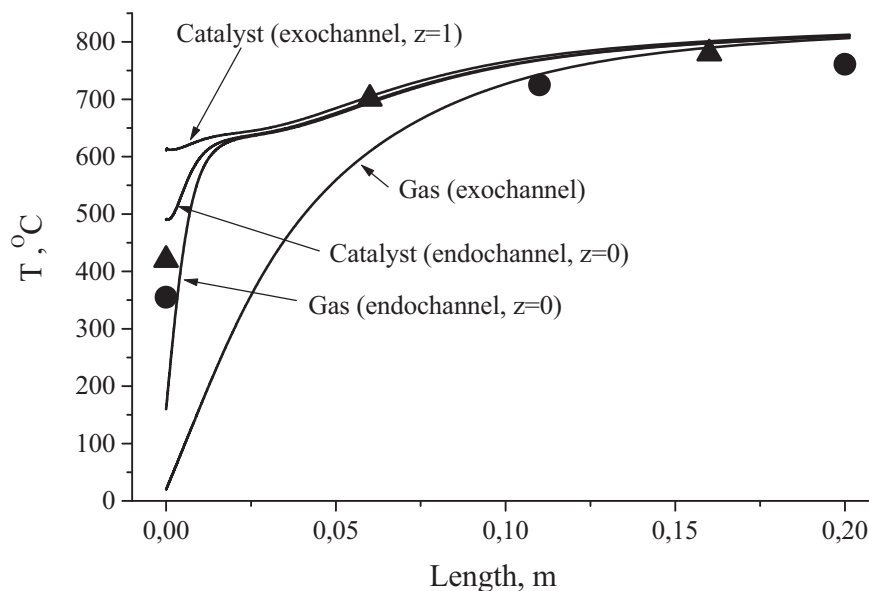
Fig. 2. Temperature profiles along the reactor length. Experimental data are denoted by the following symbols: Δ - exothermic channels, O - endothermic channels, solid lines denote calculations made at k^0_{ox}= 7 m/s.
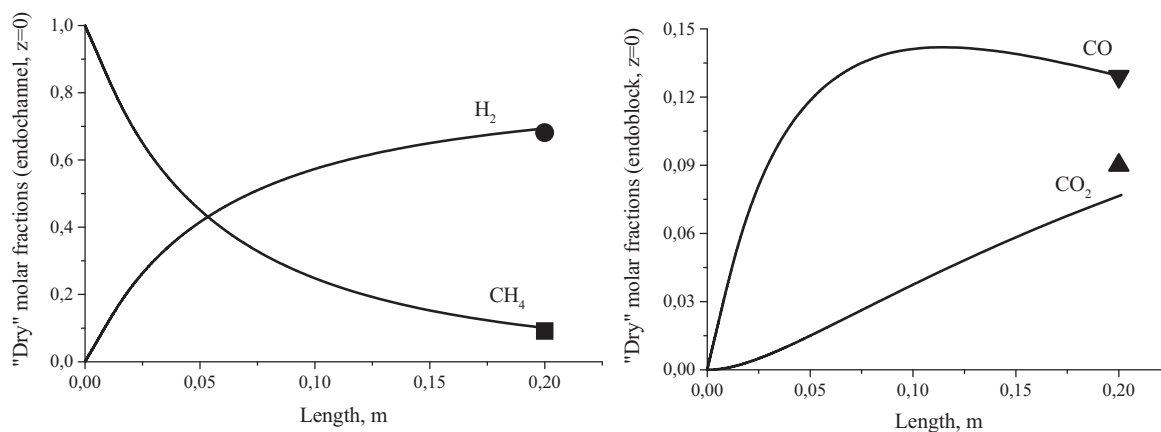
Fig. 3. Profiles of dry gas concentrations calculated for endothermic unit (at the symmetry plane z=0) and experimental data obtained at the outlet at k^0_{ox}=7 m/s.
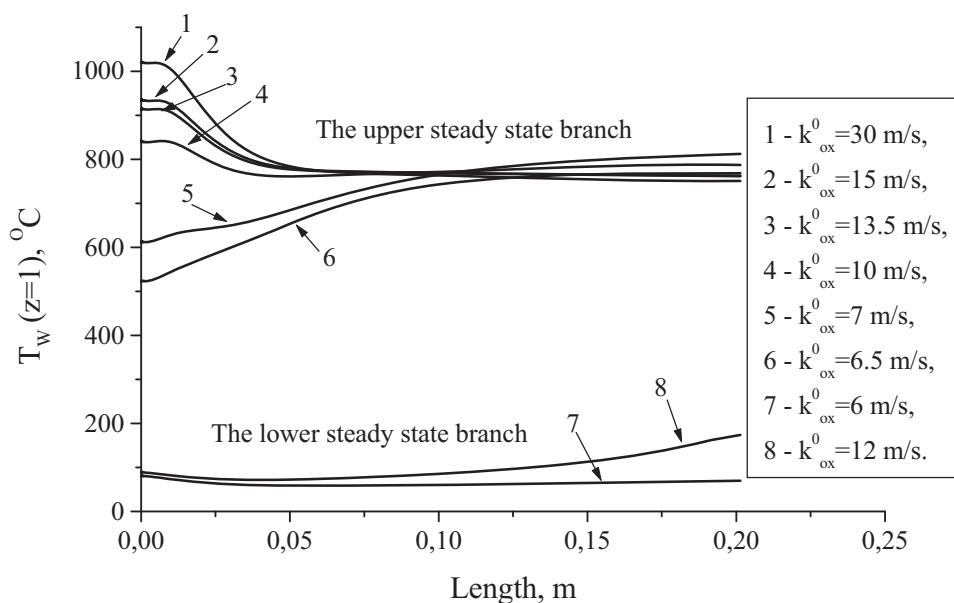
Fig. 4. Calculated profiles of wall temperature T_W under variation of oxidation catalyst activity k^0_{ox}.

Reference

1. Frauhammer J., Eigenberger G., Van Hippel L., Arntz D. A new reactor concept for endothermic high-temperature reactions //Chem.Eng.Sci. 1999. V. 54. P.3661-3670.

2. Zanfir M., Gavriilidis A. Modelling of a catalytic plate reactor for dehydrogenation-combustion coupling //Chem. Engng. Sci. 2001. V. 56. P 2671-2683.

3. Kirillov V.A., Kuzin N.A., Kulikov A.V., Fadeev S.I., Shigarov A.B., Sobyanin V.A. Thermally coupled catalytic reactor for steam reforming of methane and liquid hydrocarbons: experiment and mathematical modeling. // Theor. Found. Chem. Eng., 2003, V. 37, P. 276-284.

A SIMULATION OF THE STEADY-STATE FLOW AND CHEMISTRY IN THE PACKED BED REACTOR

O.P. Klenov, A.S. Noskov

Boreskov Institute of Catalysis SB RAS, Novosibirsk, 630090, Russia

Fax: +7(383) 330 68 78, e-mail: klen@catalysis.nsk.su

The objective of this paper is to simulate the steady-state flow and chemistry in the packed bed reactor. An influence of inlet nonuniformity and heat transfer through the reactor wall was examined. The complete Navier-Stokes model, considering 3D mass, momentum and energy transport and 1-step heterogeneous catalyst reaction was used.

Fig. 1 shows the sketch of a typical single bed catalytic reactor, using for a gas pollutant emissions purification. The inner diameter of reactor is equal 1.3 m. The reactor has both side inlet and outlet. The height of packed bed of catalyst particles is equal 0.8 m. The distinctive size of catalyst particles and the bed void fraction are equal $15 \cdot 10^{-3}$ m and 0.4 accordingly.
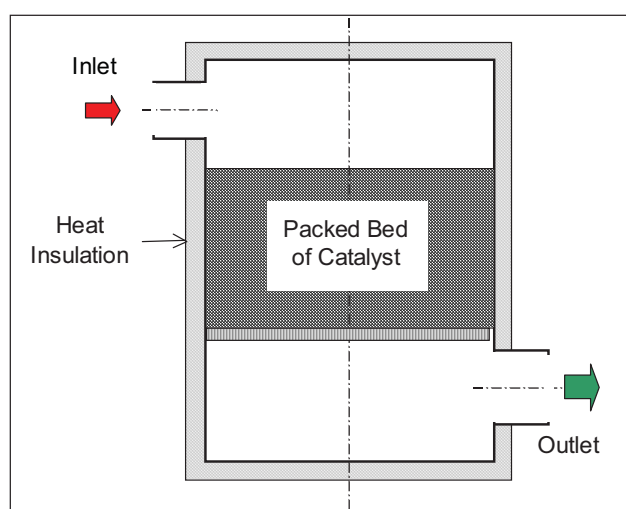
Fig.1. The sketch of the packed bed reactor

The inlet flow consists of 0.007 mass fraction C_2H_2, 0.23 – O_2, 0.0015 H_2O and N_2 – remaining. The inlet temperature and static pressure are equal 673 K and 101325 Pa accordingly. A Reynolds number based on inlet conditions is $Re=2.2 \cdot 10^5$, that corresponding to a turbulent mode.

The reaction mechanism for acetylene combustion based on 1-step catalytic reaction was used.

$$C_2H_2 + 2.5O_2 \rightarrow 2CO_2 + H_2O$$
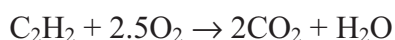
The reaction rate **r** was described by first-order equation $r=k \cdot C_{C2H2}$, where the rate constant **k** was computed using the Arrhenius expression. The Arrhenius parameters for the rate constants are a pre-exponential factor $k_0=6.38 \cdot 10^6$ s^{-1} and an activation energy $E_0=7.45 \cdot 10^7$ J/(kgmol).

The radial void fraction distribution inside a packed bed was used in a reactor model [1].

PP-40

A model was used perfect-gas behavior, the turbulent, multi-component, chemically reacting Navier-Stokes equations. A model solver is based on the FLUENT software using a finite-volume approach [2]. The distinctive size of mesh of 3D reactor model is equal $2.5 \cdot 10^{-3}$ m.

A flow distribution

The case of heat insulated reactor with outside temperature 273K is discussed. Fig. 2 shows the flow distribution inside reactor by path lines of stream. The jet from a side inlet tube spreads through a over bed space, runs up to opposite reactor wall and divides on two parts, generating a two symmetrical eddy flows and nonuniform pressure distribution above packed bed. There is a reason of flow nonuniformity in a bed inlet.
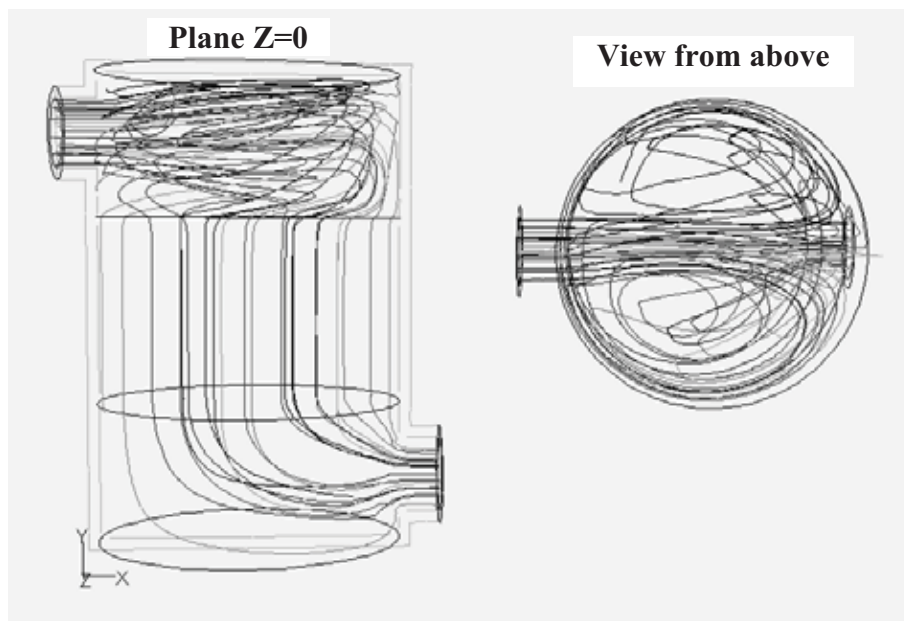
Fig. 2. Flow distribution inside reactor shown by path lines of stream.

The temperature distribution in vertical cross section z=0 and level cross sections of packed bed is shown on Fig. 3.

The Influence of Heat Transfer through the Reactor Wall

The three cases of heat transfer through the reactor wall are discussed. There are two limit cases, firstly is an adiabatic reactor, secondly – a no insulated reactor with wall temperature T_{wall}=273K-const, and in the third place a heat insulated reactor with outside temperature T_{out}=273K-const.

Fig. 4 shows the radial distributions of temperature on different heights of packed bed for three cases discussed here.

The total conversion N of C_2H_2 was determined as N=($C_{inlet} - C_{outlet}$)/$C_{inlet} \cdot 100\%$, where C is a mass-weighted average of acetylene mass fraction. The conversions of acetylene for discussed cases shows on Fig. 5.
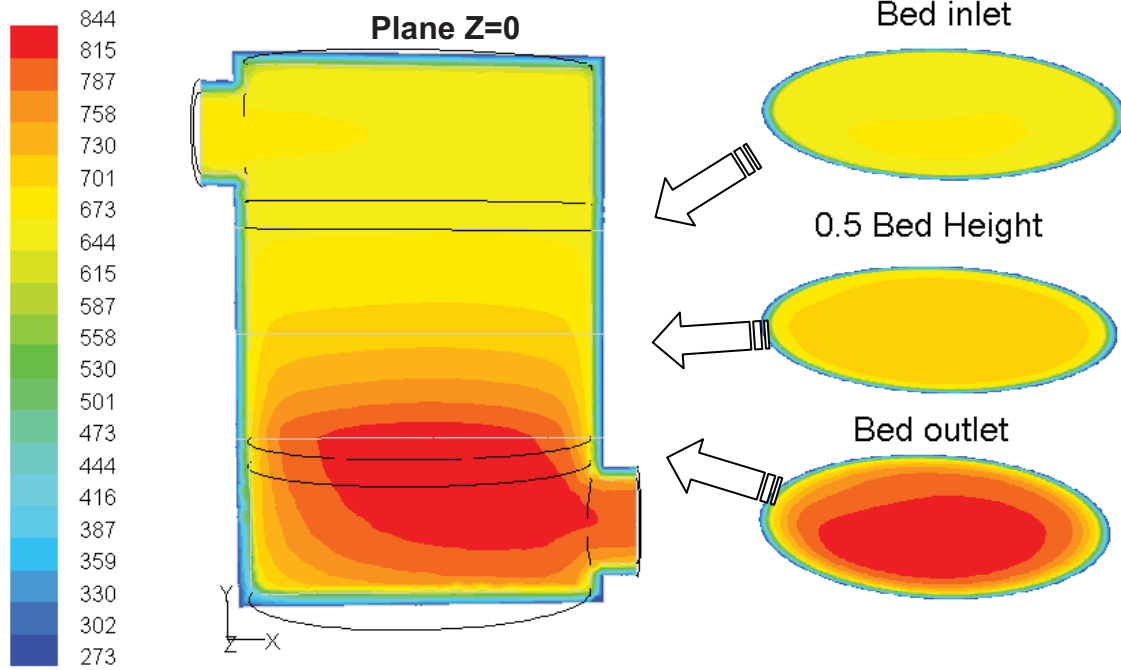
Fig. 3. Temperature distribution maps in packed bed reactor. Values of temperature are in compliance with the colour scale on left.

Conclusions

A main behavior of catalytic reactor depends on a heat exchange between reactor and surroundings. A conversion of pollutant emissions can reach to critical value over poor heat insulation.

A hydrodynamic nonuniformity based on inlet condition does not sufficient effect on behavior of reactor as a heat leakage.
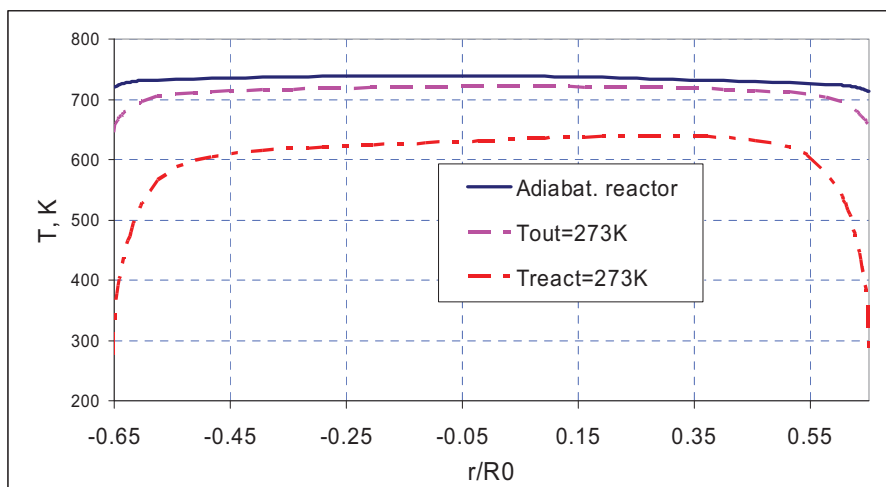
Fig. 4. Radial distributions of temperature on 0.5 height of packed bed.
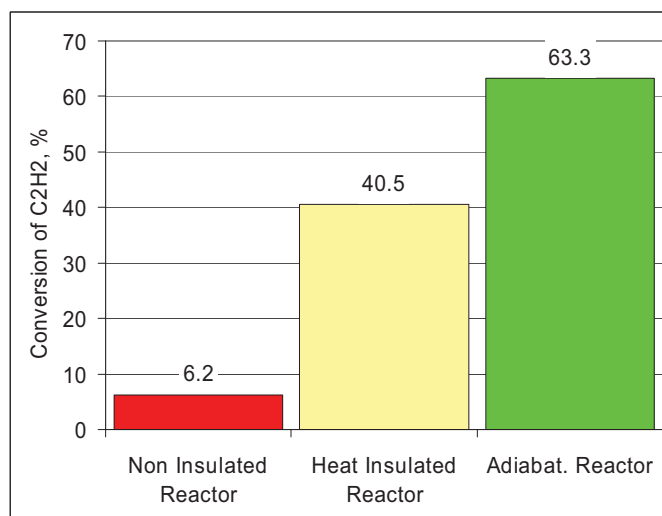
Fig. 5. Influence of heat transfer through the reactor wall
on the C_2H_2 conversion

References

1. R.F.Benenati, C.B.Brosilow. Void Fraction Distribution in Beds of Spheres. AIChEJournal, Vol 8, No3, p. 359-361, 1962.

2. Fluent Version 6.1. Fluent Inc., Lebanon, New Hampshire, 2003.

MULTI-VARIANT PRODUCTION OF HIGH-OCTANE GASOLINE AND LOW-FREEZING DIESEL FUEL BY "BIMF" TECHNOLOGY

O.V. Klimov, D.G. Aksenov, E.G. Kodenev, G.V. Echevski, A.A. Meged*,

S.N. Korsakov*, G.N. Tlekhurai*, A.Yu. Adzhiyev*

Boreskov Institute of Catalysis SB RAS, Novosibirsk, Russia

**NIPIgaspererabotka, Krasnodar, Russia*

E-mail: klm@catalysis.nsk.su

Recently in the Boreskov Institute of Catalysis it has been developed the new catalytic process of one-stage refining of wide-cut oil hydrocarbons to high quality motor fuels – the "BIMF" process (**B**oreskov **I**nstitute **M**otor **F**uels) [1]. In this process hydrocarbon feedstocks with end boiling point (EBP) of 360 °C (in some cases EBP of 400 °C), distillated from crude oil or gas condensate, are converted in a fixed-bed catalyst reactor to gasoline with desired octane number, winter diesel fuel and some amount of gas product consisting mainly from C_3-C_4 hydrocarbons [2]. The process was successfully tested largely up to pilot plant scale with production capacity of 4000 tons of feedstock per year [3].

The process utilizes IC-30-BIMF catalyst based on ZSM-5 zeolite with molar silica-to-alumina ratio of 80 and is carried out at following parameters in the reactor: start temperature 350 °C, pressure up to 2.5 MPa, WHSV = 1.5 – 4 h^{-1}. With decrease of catalyst's activity, realizing in decrease of gasoline octane number and resulted from blocking of active surface by coke deposits, temperature in reactor is periodically increased by 5 or 10 °C steps up to 450 °C. After that, under the condition of progressive decrease of gasoline octane number, feeding is stopped and catalyst regeneration is carried out by the known methods. Production of gasoline with desired octane number is achieved by appropriate combination of feed velocity, temperature and time intervals between temperature ramps. The background chemistry data and typical product yields for different types of hydrocarbon feedstocks are given in [3–8]. It is important to mention that in all experiments the produced diesel fuel fraction has freezing point below -50 °C.

In present work we describe variants of BIMF process, characterizing by increased motor fuel yields and differing from the base variant of the process given in [9]. Schematic diagram of the base variant of the BIMF process is presented in Fig. 1. According to this

variant the products from reactor come to separator with following rectification of liquid product for gasoline and diesel fuel. In the base variant of the process under production of gasoline with MON (**M**otor **o**ctane **n**umber) = 83 – 85, the overall production of gas products may reach the value of 18 wt% and more [8, 9]. Furthermore, the produced gasoline contains appreciable amount of C_5 hydrocarbons whose MONs don't exceed 77. To compensate the negative influence of those low-octane number components one should increase the content of high-octane number aromatic hydrocarbons in gasoline by hardening of the process regime what, in turn, leads to increased gas production. Usually gas product after separator S-1 contains an appreciable amount of C_5^+ hydrocarbons and needs in additional purifying in accordance with standards on liquefied gas.
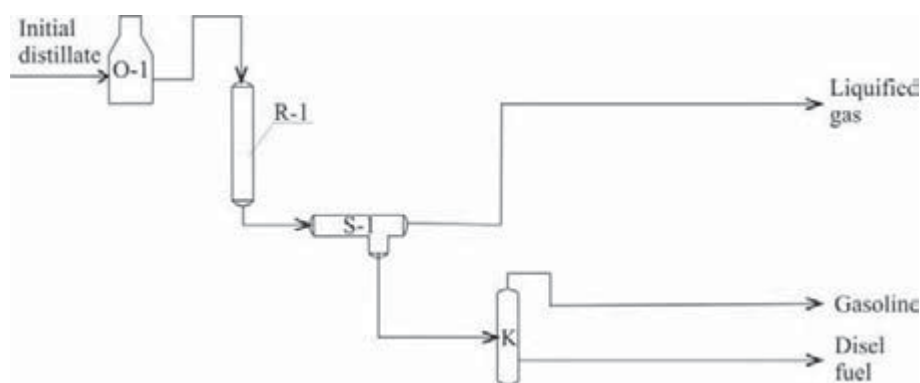
Fig. 1. Based variant

From the other hand, it is possible to organize the processing regime in separator in such way when most of C_5 hydrocarbons will be in gas phase, similar to that described in [3] where outlet gas from separator operating at 35– 40 °C and <0.3 MPa contained 12.3 wt% of C_5^+ hydrocarbons. There are different variants for processing of such gas. In all variants the outlet gas from separator is heated in furnace O-2 and comes to reactor R-2 charged with a catalyst for aromatization, for example with IC-17-M catalyst based on modified high-alumina ZSM-5 zeolite. Operating parameters for reactor R-2 are those to produce either aromatics or liquid products with maximal yield. Generally, process in reactor R-2 is carried out at <0.5 MPa, 475–550 °C and volume feed velocity of <2000 h^{-1}. In such regime the yield of liquid hydrocarbons may reach 60 % and more based on the converted gas. The produced in reactor R-2 liquid product has MON as high as 104, and gas product mainly consists of C_1-C_2 hydrocarbons and may be utilized as a fuel for furnaces.

There are three main variants of the BIMF process aimed on processing of gas product produced in the first reactor. The are illustrated in Figs. 2 -4. In accordance with the first variant reactor R-2 operates in most hard regime to produce the maximal yield of concentrate

of aromatics, which contains at least 88 wt% of benzene, toluene and xylenes in sum and is a marketable product itself.
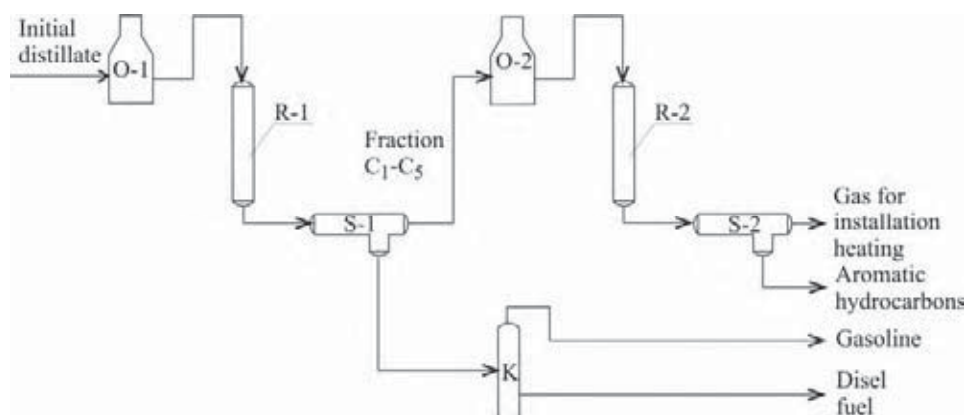
Fig. 2. Variant 1

In second and third variants the maximal yield of liquid products (not only aromatic ones) in reactor R-2 is provided. In accordance with the second variant (Fig. 3) those liquid products are compounded with gasoline fraction after rectification column K to get commercial gasoline. The operating parameters for reactors are those to produce gasoline with desired MON.
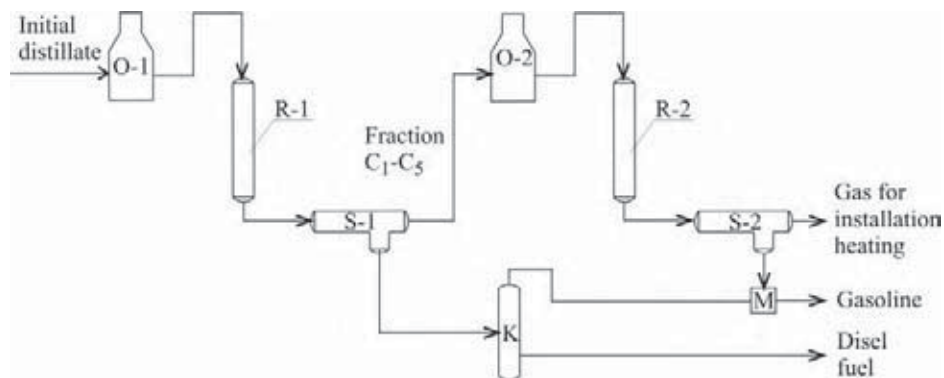
Fig. 3. Variant 2

In accordance with the third variant (Fig. 4) only part (about 20 wt%) of fed on column K-1 hydrocarbons is initially separated, which represents mainly light hydrocarbons of $C_5 - C_6$ composition with MON of 70 – 75. The rest 80 % of hydrocarbons comes to reactor R-1, gas product, including C_5^+ hydrocarbons, after separator S-1 is converted in reactor R-2 and the produced liquid products are compounded with above obtained on column K-1 light hydrocarbons fraction to get commercial gasoline, specified as Gasoline-1. Two commercial products, diesel fuel and gasoline-2, comes out from column K-2. Necessary to mention that it is most rational to organize operation of BIMF unit in such way when MON of gasoline-2 is

PP-41

higher than that of gasoline-1, for example, gasoline-1 corresponds to AI-92 (Russian index) and gasoline-2 – to AI-95.
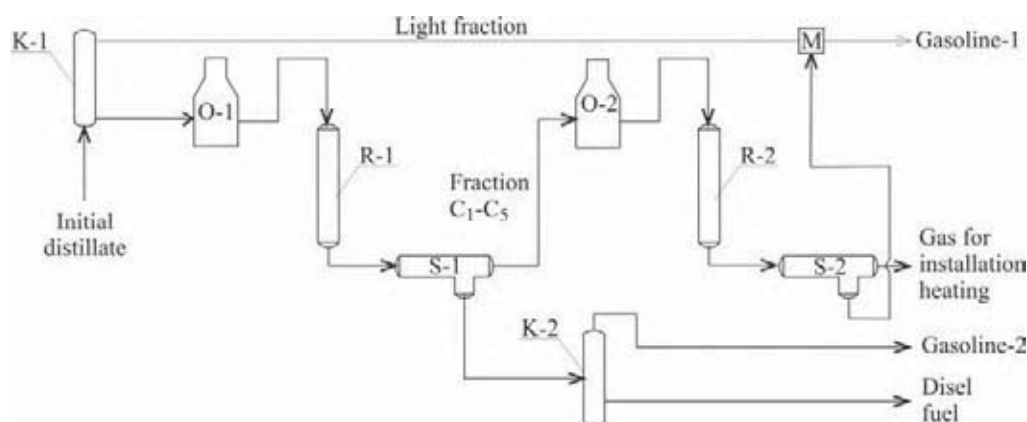
Fig. 4. Variant 3

All three variants of processing of C_1-C_5 hydrocarbons formed in BIMF reactor provide the overall yield of liquid products in the process exceeding 90 wt%, what is higher for 5 – 10 wt% than typical yield for the base BIMF process. For all that, quality of motor fuels remains high.

References

1. Echevsky G.V., Klimov O.V., Kikhtyanin O.V. et al.// Russian Patent №2181750.

2. Echevsky G.V., Klimov O.V., Kikhtyanin O.V. et al.// Catalysis in Industry, №2 (2003) p.60.

3. Klimov O.V., Aksenov D.G., Kodenev E.G. et al.// Catalysis in Industry, №1 (2005) p.18.

4. Klimov O.V., Kikhtyanin O.V., Aksenov D.G. et al.// Chemistry and technology of fuels and oils, №5 (2005) p.20.

5. Klimov O.V., Aksenov D.G., Echevsky G.V. et al.// XVI Russian Conference on Chemical Reactors "Chemreactor-16", 17-20.06.2003 Kazan, Russia, Thesis, p. 299.

6. Klimov O.V., Pimonova M.N. and Echevsky G.V.// 13th international congress on catalysis, Paris 11-16 July 2004, P4-015.

7. Klimov O.V., Kikhtyanin O.V., Aksenov D.G. and Echevsky G.V.// "EUROPACAT-VI" (Innsbruck, 31.08-4.09.2003). A3, 044.

8. Klimov O.V., Aksenov D.G., Kikhtyanin O.V., Echevsky G.V.// Aktualnye problemy neftekhimii, Second Russian Conference,11-13.10.2005. Ufa, Russia, Thesis p.186.

9. Klimov O.V., Aksenov D.G., Kodenev E.G. et al. // Russian Patent №2265042.

KINETICS OF BENZENE HYDROGENATION ON Rh/C

S.R. Konuspayev[1], **M. Schaimardan**[1], **H. Backman**[2], **D.Yu. Murzin**[2]

[1]*A.B. Bekturov Institute of Chemical Sciences, Almaty, 480100, Sh.Ualikhanov st. 106, Kazakhstan, srkonuspayev@mail.ru*

[2]*Åbo Akademi University, Turku, Biskopsgatan 8, 20500, Finland, dmurzin@abo.fi*

Introduction

Hydrogenation of aromatic hydrocarbons has become a key process for the production of environmentally acceptable transportation fuels in the recent years. As soon as the connection between aromatics and formation of harmful emissions was recognized, tighter environmental regulations were imposed on gasoline and diesel fuel compositions [1– 3]. The reduction of aromatics content in diesel results in an improved quality of the fuel since aromatics, owing to their stability, are not suitable for combustion in ignition engines. In addition, the saturation of aromatic hydrocarbons brings further benefits: the cetane number is increased and the fuel density decreased [2, 3]. The improvement of these properties has been shown to suppress formation of particulate matter and NO_x emissions, which are connected with serious health risks. Hydrogenation of aromatics has been studied by many researchers both in the liquid and gas phase [4–7], with benzene being the most frequently studied system.

Experimental

The kinetic experiments were performed in a well-mixed 170 ml autoclave assuring that the reaction took place in the external diffusion free region. All experiments were carried out under isothermal and isobaric dead-end conditions. The hydrogen pressure and temperature were varied between 2.0 and 10.0 MPa and 15-100°C respectively. Ethanol was used as diluent. Some experiments were done with water and octane as solvents as well as in neat solvent. The reactor was equipped with special hydrogen containing vessel (10 l) allowing monitoring hydrogen consumption during the reaction (the values of hydrogen consumption in what follows refer to standard temperature and pressure conditions). In a typical run 2 ml of benzene and 0.3 g of 3%Rh/sibunit in 50 ml of the solvent were put into the reactor. The use of activated carbon "sibunit" in the recent years has been due to its high surface area, chemical inertness both in acidic and basic media, and by the absence of very strong acidic centers on its surface which in principle could promote undesirable side reactions. The catalysts particles were less then 50 μm. A fresh portion of catalyst was taken for each

experiment. For selected runs during the course of the reaction samples of the solution were taken for analysis by gas chromatography.

Results and Discussion

A typical profile of hydrogen consumption in benzene hydrogenation is shown in Fig. 1.
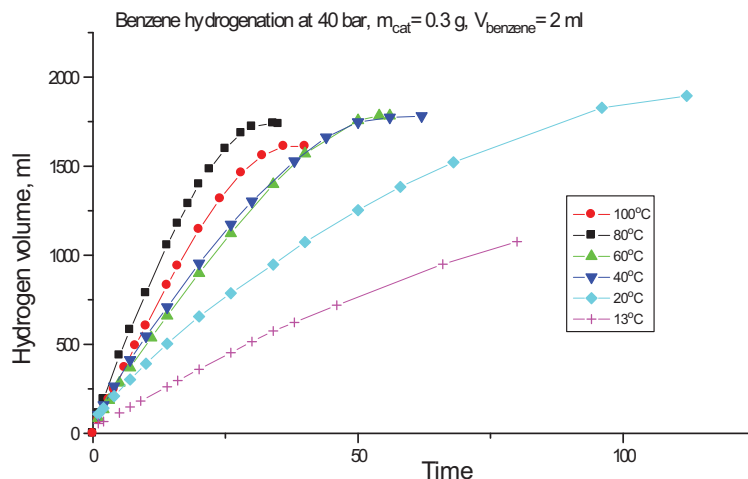
Figure 1. Temperature dependence in benzene hydrogenation in ethanol.

It can be observed that the hydrogen consumption goes through maximum as a function of temperature. Similar dependences were previously reported for gas-phase hydrogenation of aromatics being a result of an interplay between kinetics and adsorption [7] and for the liquid phase citral hydrogenation due to catalyst deactivation [8].

Hydrogen pressure dependence (Figure 2) is less pronounced, than temperature dependence.
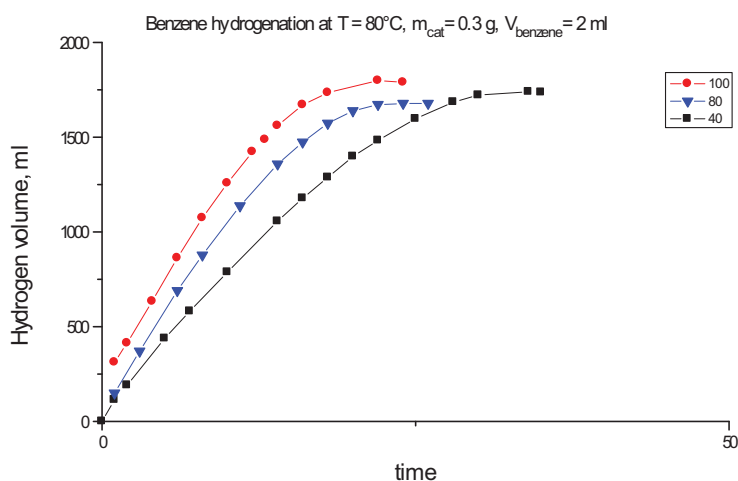
Figure 2. Pressure dependence in benzene hydrogenation in ethanol.

Concentration of benzene in a mixture with cyclohexane exhibits a linear dependency on reaction time up to high conversions levels (Figure. 3).
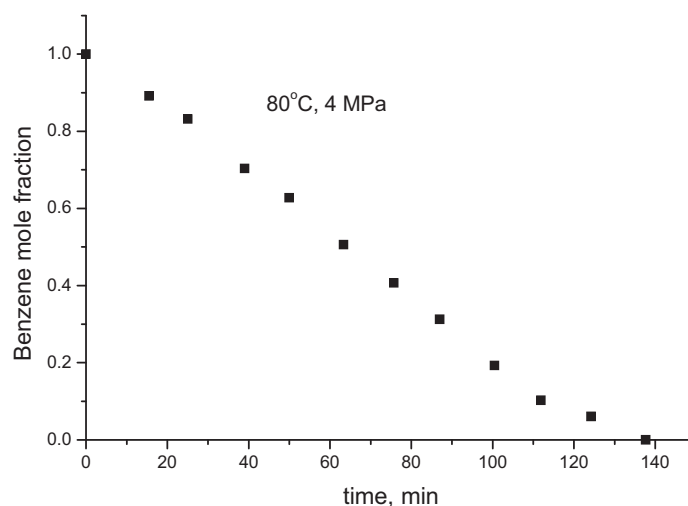
Figure 3. Hydrogenation of benzene in solvent-free conditions.

This means that the reaction order with respect to benzene is equal to zero, i.e., the reaction rate is independent of the aromatics concentration. Similar behavior was reported previously for liquid-phase hydrogenation of other aromatic hydrocarbons on several VIII group metal catalysts [9], where the zeroth order dependence on the concentration of aromatics was ascribed to a very high surface concentration of these compounds due to their strong adsorption on the active sites .

Conclusions

Hydrogenation of benzene was performed over a wide range of temperatures and pressures with a rhodium catalyst supported on a special carbon sibunit. Kinetic regularities were established. Several previously advanced kinetic models were tested and compared to experimental data.

References

[1] Quality of European Gasoline and Diesel Fuels. EU Fuels Directive 2003/17/EC.

[2] A. Stanislaus, B.H. Cooper, Catal. Rev.- Sci. Eng. 36 (1994) 75.

[3] B.H. Cooper, B.B.L. Donnis, Appl. Catal. A: Gen. 137 (1996) 203.

[4] U.K. Singh, M.A. Vannice, AIChE J., 45 (1999) 1059.

[5] S. Toppinen, T.-K. Rantakylä, T. Salmi, J. Aittamaa, Ind. Eng. Chem. Res. 35 (1996) 1824.

[6] H. Backman, A.Kalantar, D.Yu. Murzin, J.Catal. 233 (2005) 109.

[7] A. Kalantar, P. Mäki-Arvela, H. Backman, H. Karhu, T. Salmi, J. Väyrynen, D.Yu. Murzin, J.Catal., 218 (2003) 267

[8] P. Mäki-Arvela, N. Kumar, K. Eränen, T. Salmi, D.Yu. Murzin (in preparation).

[9] D.Yu.Murzin, N.V.Kul'kova, Catalysis Today, 24 (1995) 35.

VORTEX REACTORS FOR HETEROGENEOUS DIFFUSION-CONTROLLED PROCESSES.

ENZYMATIC LIQUID-SOLID PROCESS OF STARCH SACCHARIFICATION

Kovalenko G.A., Sukhinin S.V., Perminova L.V., Tanashev Yu.Yu.

Boreskov Institute of Catalysis SB RAS, 630090 Novosibirsk, Russia

E-mail: galina@catalysis.ru

R&D of novel types of reactors are at the heart of modern heterogeneous biotech processes performed by immobilized enzymes. The main directions of the reactor design are the enhancement the productivity of the processes due to the overcoming diffusion limitation by significant intensification of mass transfer of substrate to biocatalyst and elimination of stagnant zones in bioreactor.

The exploitation of renewable feedstock such as starch to produce the sweeteners for food industry is still of great importance. Now the all stages of starch–feedstock processing relies at homogeneous conditions. The heterogeneous regimes of the starch saccharification to treacle performing with the immobilized enzyme glucoamylase are more attractive and feasible for economy.

The two types of vortex reactors – rotor-inertial bioreactor (RIB) and vortex-immersed reactor (VIR), were designed for heterogeneous diffusion-controlled processes. These types of reactor were investigated in the enzymatic liquid-solid process of starch saccharification.

Rotor-inertial bioreactor (RIB) was designed for the heterogeneous biocatalysts prepared on the base of macrostructured inorganic supports, in particular foam-like ceramics.
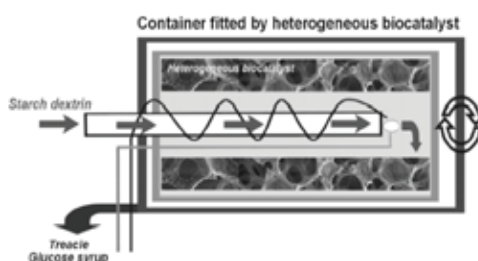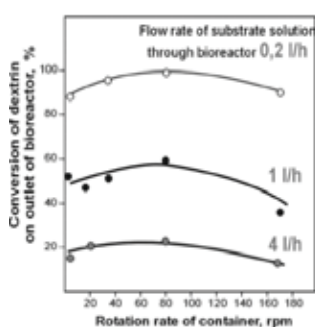
Rotor-inertial bioreactor was consisted of rotated container fitted by foam-like heterogeneous biocatalyst. The rate of starch saccharification was maximal at the rotation rate

of container of ca. 80 rpm (Fig. attached to Paragraph). At continuous mode of RIB operation full conversion of 10w/w% starch dextrin to glucose syrup was observed at the slow flow rate (< 0,2 l/h) of substrate solution through the bioreactor (Fig. attached to Paragraph).

Vortex-immersed reactor (VIR) was designed for the biocatalysts prepared on the base of granulated inorganic supports. Vortex-immersed reactor was consisted of rotated body filled by granules of heterogeneous biocatalyst. Rate of starch saccharification was constant at rotation rate of the body more than 300 rpm (Fig. attached to Paragraph), e.g. at these conditions the external diffusion limitation was overcome. The internal diffusion restriction was eliminated when size of the support granules did not exceed 1 mm. Thus, the observed rate of starch saccharification increased in order of magnitude when the carbon support was grinded from 3 mm-granules to 0,6 mm-granules (Fig. attached to Paragraph). In periodic mode of VIR operation full conversion of 32w/w% dextrin to glucose syrup was observed for ca.4 hours.
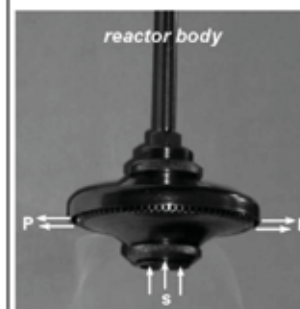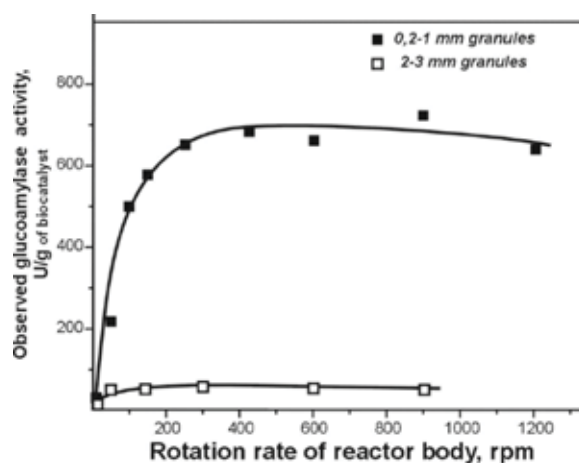
As a result, the activities of heterogeneous biocatalysts observed in the vortex reactors and productivity of the heterogeneous diffusion-controlled processes, in particular enzymatic liquid-solid process of starch saccharification have been found to be of 1,2-1,5-fold higher if to compare with the actively engaged fixed-bed reactor.

SIMULATION OF THE CATALYST DEACTIVATION IN SELECTIVE ETHYLENE GLYCOL PRODUCTION

V.F. Shvets[1], <u>R.A. Kozlovskiy</u>[1], I.A. Kozlovskiy[1], M.G. Makarov[1], J.P. Suchkov[1], A.E. Kapustin[2], D.E. Zavelev[1]

[1]*D.I.Mendeleev University of Chemical Technology of Russia, Chair of Basic Organic and Petrochemical Synthesis, 9 Miusskaya Square, Moscow, 125047, Russia, kra@muctr.edu.ru*
[2]*Azov State University, Mariupol, 87500, Ukraine, 000044@pstu.edu*

Abstract

The model of the tube fixed bed catalytic reactor for ethylene glycol production was used for analysis how process conditions influence on catalyst life time. The model includes equations describing catalyst's deactivation. The catalyst is a cross-linked styrene-divinylbenzene anion-exchange resin in carbonate/bicarbonate form. Various process conditions (temperature, substance's concentrations), heating regimes (isothermal, adiabatic) and a stream direction were simulated. The optimal conditions concerning minimum of the catalyst consumption were determined.

Introduction

Hydration of ethylene oxide is an industrial approach to glycols in general, and ethylene glycol in particular. Ethylene glycol is one of the major large-scale products of industrial organic synthesis, with the world annual production of about 15,3 million ton/y. Today ethylene glycol is produced in industry only by a noncatalyzed reaction. As it follows from numerous investigations [1-3] hydration of ethylene oxide catalyzed by anion-exchange resin is one of the most promising methods for ethylene glycol production as alternative for traditional industrial noncatalytic process. Catalytic method provides significant energy saving in comparison with noncatalytic one due to much higher selectivity. But the main disadvantage of such a catalyst is it's deactivation that consists of two undesirable processes: loss of catalytically active sites and catalyst's swelling. In our previous works the models of the tube fixed bed catalytic reactor [4] and of catalyst deactivation [5] were elaborated.

In the present work above mentioned models were used for analysis how process conditions influence on catalyst life time.

Results

The main parameters influencing on of the catalyst and its activity are temperature and concentrations of ethylene oxide and glycol. Series of calculations were made for two types of reactors – isothermal and adiabatic. Process conditions were varied in the following ranges: temperature 80-100°C; initial concentration of ethylene oxide 3-10 % mass.; initial concentration of glycol 0-29 % mass. In each case selectivity, catalyst's capacity, catalyst's volume, catalyst productivity (kmole of glycol per m^3 of catalyst per h) and catalyst consumption (m^3 of catalyst per kmole of glycol) were calculated. Results of simulation showed that adiabatic reactor is more favorable than isothermal. It was found that most profitable conditions for production of outlet stream containing 35% mass of glycol are follows: installation consisting of several (up to 5) consecutive adiabatic tube reactor with distributed ethylene oxide input in each reactor and intermediate heat exchangers; initial concentration of ethylene oxide in each reactor is not exceed 6 % mass. These conditions provide selectivity about 95 %, catalyst productivity about 2,4 (kmole of glycol per m^3 of catalyst per h) and catalyst consumption about 7×10^{-5} (m^3 of catalyst per kmole of glycol) and catalyst life time up to 6000 h.

Simulation was also used in order to investigate how stream direction influence on catalyst deactivation. Result of simulation have showed that periodically changing of direction of feed stream allows to decrease catalyst consumption per ton of glycol up to 10 %.

References

1. Shvets V.F., Makarov M.G., Koustov A.V., et al. Method for obtaining alkylene glycols. RU Patent 2149864, 2000.

2. Van Kruchten E. M. G. Process for the preparation of alkylene glycols. US Patent 5874653, 1999.

3. Iwakura T., Miyagi H. Production of alkylene glycol. JP Patent 11012206, 1999.

4. Shvets V.F., Kozlovskiy R.A., Makarov M.G., Koustov A.V., Selective catalytic hydration of ethylene and propylene oxides. XV International Conference on Chemical Reactors Chemreactor-15, Helsinki, Finland, June 5-8, 2001, c 102.

5. Shvets V.F., Kozlovskiy R.A., Kozlovskiy I.A., Makarov M.G., Suchkov Y.P., Koustov A.V., The Model of Catalytic Reactor of Ethylene Glycol Production. Organic Process Research & Development (2005), 9(6), 768-773.

CATALYTIC EPOXIDATION OF CYCLOOCTENE BY IMMOBILIZED SALEN COMPLEXES

T. Luts, W. Suprun, H. Papp

Institute of Technical Chemistry, University of Leipzig

Linnéstraße 3, 04103 Leipzig, Germany

Fax: +49(0341)9736349; e-mail: luts@chemie.uni-leipzig.de

Introduction

The oxidation of alkenes to epoxides and their products is both of academic and industrial interest. Consequently, several groups work in this field using different catalysts such as supported metal oxides [1,2] as well as homogeneous transition metal complexes [3]. The metal Salen complexes have been reported as very efficient catalysts in asymmetric catalytic reactions and they are also widely used for the epoxidation of olefins [4.5]. Due to the problems to separate the homogeneous catalysts from the products, significant efforts were undertaken to immobilize them. The catalyst immobilization helps to overcome the problems of catalyst separation, recovery and recycling. In the present study covalent bonding techniques were chosen as a very efficient approach to design stable immobilized catalysts on an amorphous mesoporous silica gel. The results about synthesis, characterization and application of homogeneous and immobilized metal (Mn and Mo) Salen complexes in epoxidation are presented.

Experimental

(3-aminopropyl)trimethoxysilane and (3-iodopropyl)trimethoxysilane were preliminary used in a post-synthesis grafting method to prepare organosilane-modified porous materials. Peptide (1) and ester (2) bonding were employed to anchor the Salen complex to the silica framework using amino- and iodo-functionalized groups, respectively (Fig. 1).

To characterize and to prove the presence of immobilized Salen complexes on the surface FTIR, atomic absorption spectroscopy (AAS), electrospray ionization mass spectroscopy (ESI MS), CNHO elemental analysis and termogravimetry analysis (TGA) were used. The amount of manganese and molybdenum content on the silica surface was determined by elemental analysis of metal using AAS. The presence of only covalently coupled molecules of Salen complex excluding non-bound ones in porous material was proven by ESI MS approach. FTIR spectroscopy allows to observe the presence of specific bonds of immobilization process.

To test the catalytic activity of the immobilized Mn and Mo-Salen complexes the catalytic epoxidation of cyclooctene (CycO) with *tert*-butylhydroperoxide (TBHP) as well as cumene hydroperoxide as an oxidant was studied. Gas chromatography was used for the identification and the quantification of the reaction products. The influence of different reaction conditions on the epoxide yield was studied.
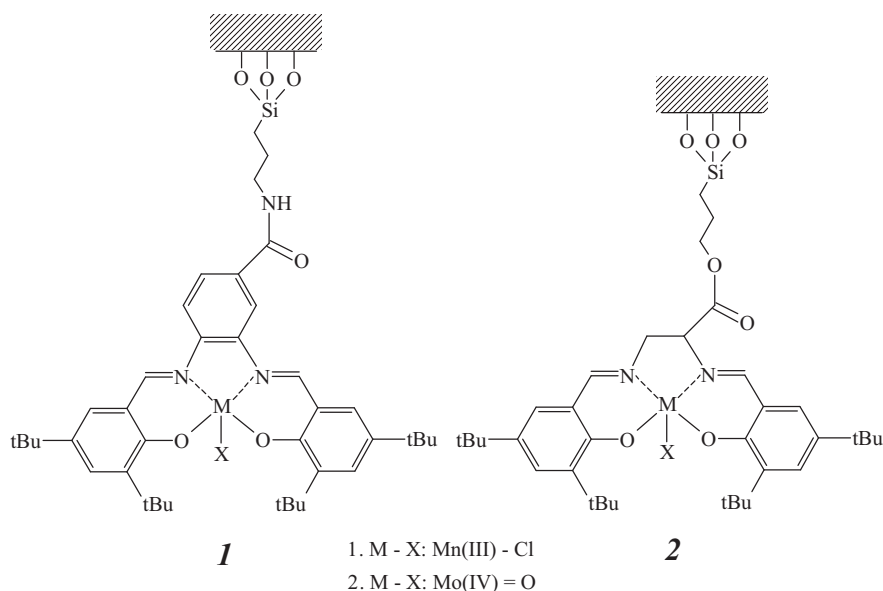
Fig. 1. The structures of Salen complexes immobilized *via* peptide (1) and ester (2) bonding.

Results and discussions

Manganese and molybdenum Salen complexes were successfully immobilized in amorphous mesoporous silica support with high yield of heterogeneous catalyst. The obtained immobilized Salen complexes were found to be stable at the temperature up till 100°C, towards different solvents (polar, nonpolar) as well as oxidative agents (TBHP, cumene hydroperoxide).

Using AAS, FTIR, ESI MS as well as TGA and elemental analysis the definitive structure of catalyst with its characteristic groups were proven. The presence of metal and its content in immobilized complexes were determined by AAS. The characteristic bonds, typical only for the immobilized complex were observed by FTIR. ESI MS experiments were carried by treatment of immobilized metal Salen complexes with formic acid, triethylamine and also in neutral condition in different solvent systems (chloroform/acetonitrile, chloroform/acetonitrile+Na, tetrahydrofuran/acetonitrile and methanol) to explicitly prove the catalyst structure.

In the current study the effects of reaction temperature, solvent, adduct proportions on the catalytic activity were investigated. Epoxidation of cyclooctene was performed at 25, 45, 60 and 75°C in following solvents: toluene, chlorobenzene and tetrachloroethane (Tab. 1).

PP-45

Experiments in which the immobilized catalyst was used for three consecutive runs in the epoxidation of cyclooctene were also carried out (Fig. 2). The results demonstrate constant stability and activity of spent catalyst after several uses.

Tab. 1. Influence of reaction parameters on the epoxidation of cyclooctene (reaction conditions: CycO (2.7 mmol), TBHP (6.0 mmol), catalyst (0.045 mmol of active centers) and 1 ml of solvent).

Catalyst	T (^{o}C)	Reaction time (h)	Solvent	Yield* (%)
	75	35	Toluene	26
Homogeneous	60	35	Toluene	34
Mn-Salen	45	35	Toluene	45
	45	35	Chlorobenzene	35
	45	35	Tetrachlotoethane	48
Immobilized Mn-Salen	45	35	Toluene	39
Immobilized Mo-Salen	45	3	Tetrachlotoethane	89

* Yield of epoxide was calculated according to initial amount of olefin.

Conclusions

Manganese and molybdenum Salen complexes were immobilized on the silica support. The defined structure of the resulting heterogeneous system was proven by spectroscopic analysis (FTIR, ESI MS, AAS and TGA). The immobilized catalysts were tested for the epoxidation of cyclooctene and found to be active. A comparison of the results obtained

Fig. 2. Epoxidation of CycO by immobilized Mn-Salen complex in 3 consecutive runs at 45°C. Reaction conditions: see legend of Tab.1.

with the homogeneous and the immobilized catalyst showed that there was no significant loss of cyclooctene conversion in epoxidation by immobilization (Tab. 1). The influence of the immobilized catalyst, solvent, temperature and adduct proportion was studied. Although the systems were not completely optimized, the catalyst based on the silica surface could be used in at least three consecutive runs. The mechanism of the epoxidation in presence of homogeneous and heterogeneous Salen complexes was discussed.

References

1. F. Chiker, *et al., Appl. Catal. A: Gen.*, 2003, **243** (309).
2. R. Ghosh, *et al., J. Catal.*, 2004, **224** (288).
3. L. Canali, *et al., Chem. Soc. Rev.*, 1999, **28** (85).
4. J. F. Larrow, *et al., J. Org. Chem.,* 1994, **59** (1939).
5. T. Katsuki, *Chem. Soc. Rev.,* 2004, **33** (437).

OVERALL PERFORMANCE OF THE CATALYST IN A MICROREACTOR FOR THE METHANE PARTIAL OXIDATION

L.L. Makarshin, D.V. Andreev, S.N. Pavlova, V.A. Sadykov, O.I. Snegurenko,

V.V. Privezentsev*, A.V.Gulevich*, V.Yu. Ulianitsky**, V.A. Sobyanin, V.N. Parmon

Boreskov Institute of Catalysis, Prosp. akad. Lavrentieva 5, 630090 Novosibirsk, Russia

makarshin@catalysis.nsk.su

* SSCRF – Institute for Physics and Power Engineering named after acad. A.I. Leypunsky Sq. Bondarenko 1, Obninsk, Kaluga Region, 249020, Russia

** Lavrentyev Institute of Hydrodynamics, Prosp. akad. Lavrentieva 15, 630090 Novosibirsk, Russian

Introduction

Use of natural gas as a source of syngas is a perspective direction in the hydrogen energy development and gas-to-liquid (GTL) processes. Generally, methane is converted to syngas by steam reforming, but this endothermic process requires a large heat input, while the H_2/CO ratio obtained (about 3) is too high for fuels synthesis via Fischer–Tropsch reaction or methanol route [1]. Due to its exothermic nature, the methane partial oxidation is an advantageous route for syngas production, since it is less energy intensive and more cost-efficient [2]. Moreover, H_2/CO ratio (about 2) in syngas is favorable for GTL processes. Microfabricated chemical reactors with at least one typical dimension in the sub-millimeter range are of a great promise for the partial oxidation reactions and processes of chemicals production. Their distinct advantages over conventional reactors are associated with their high surface-to-volume ratio, which increases the heat transfer and thus, reduces thermal gradients in the reactor. Due to small channel dimensions, their heat-exchanging efficiency is rather high allowing fast heating and cooling of reaction mixtures, so that development of hotspots or reaction heat accumulation within microstructures is prevented [3]. Development of methods of the microchannel plate (MCP) manufacturing and procedures for the catalyst supporting is a paramount problem in manufacturing the microreactor. Though a variety of methods for MCP design and catalyst layers supporting are described in literature, their majority could not be applied for design of a microreactor for syngas generation due to high ($>700^0$C) operation temperatures. High operation temperatures impose also restrictions on selection of construction materials. The methane partial oxidation is catalyzed by transition

group (Ni, Co) [5] and noble (Ru, Rh, Pd, Pt and Ir) metals [6]. However, they are rapidly deactivated by carbon deposition.

The combined structures and various metal additives to basic Ni-Al$_2$O$_3$ composition allowed to improve essentially performance of this catalyst ensuring a high activity and selectivity in methane partial oxidation at high (10^5 – 10^6 ml/(g·h) space velocities and temperatures (> 700 ^{o}C) [7,8]

The purpose of the present work was to elucidate main features of methane partial oxidation into syngas at ms contact times in a microchannel reactor as dependent upon the design of catalytic microchannel plate.

Experimental

The performance of the catalyst supported onto a microchannel plate was estimated in a microreactor manufactured from stainless steel (Fig. 1) equipped with one MCP of 21×21
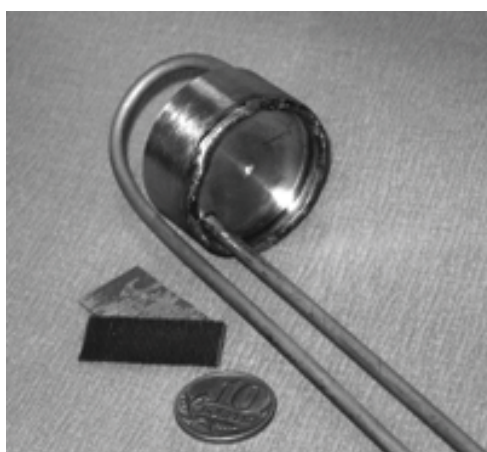
Fig 1
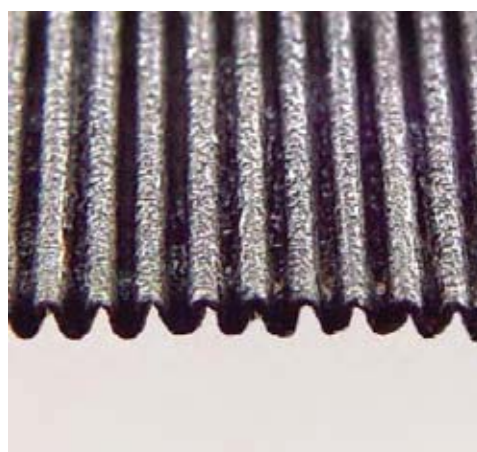
Fig. 2

mm size. The goffered microchannel plate was made of fechraloy foil with 50 microns thickness (Fig. 2). Corrugation produces a plate slab of 0.6 mm thickness with nearly triangular (sides 0.3×0.6 mm) channels. The foil surface was precovered by continuous non-porous buffer corundum layer via blast dusting deposition. The catalyst was supported in two steps: first, the complex oxide support was deposited, and second, an active component was supported by the incipient wetness impregnation. One MCP contained 80 mg of the active metals. The MCP was finally calcined at 900^{0}C for 2 h [9]. Microreactor was thermally insulated by siliceous plates with thickness of 20 mm. The reactor temperature was controlled between 200 and 900 ◦C by placing it within a furnace. The temperature was measured by a thermocouple fixed at the microreactor external wall. Air - methane mixture with O$_2$/CH$_4$ ratio 0.55 was fed into the microreactor. The methane partial oxidation ignites at heating a

microreactor up to 600^{0}C (Fig. 3). After achieving the microreactor temperature 820-830^{0}C, the furnace was cooled to a room temperature. However, the temperature of a microreactor practically did not change due to heat generation by exothermic reactions of deep and partial oxidation. Feed rate of the mixture varied within 2-35 ml/s being controlled with a flow-mass controller. The GHSV (gas hourly space velocities) were calculated with respect to the volume of reactants in the gas phase at 25^0 C. The time of contact of reagents with a layer of the catalyst varied in the range of 175-10 ms corresponding to GHSV ~ 20000-360000 h^{-1}. The reaction feed components were analyzed by GC.

Using material balance equations the conversions of oxygen and methane as well as CO selectivity were calculated:

$$X_{CH4} = 100\% \cdot \frac{CH_4^0 - \frac{N_2^0}{N_2} \cdot CH_4}{CH_4^0} \qquad (1)$$

$$X_{O2} = 100\% \cdot \frac{O_2^0 - \frac{N_2^0}{N_2} \cdot O_2}{O_2^0} \qquad (2)$$

$$S_{CO} = \frac{CO}{\frac{N_2}{N_2^0} \cdot CH_4^0 - CH_4} \qquad (3)$$

where N_2^0, O_2^0 and CH_4^0 - initial concentrations of the feed gases, N_2, O_2, CO and CH_4 - outlet concentrations of the products.

Results and discussion
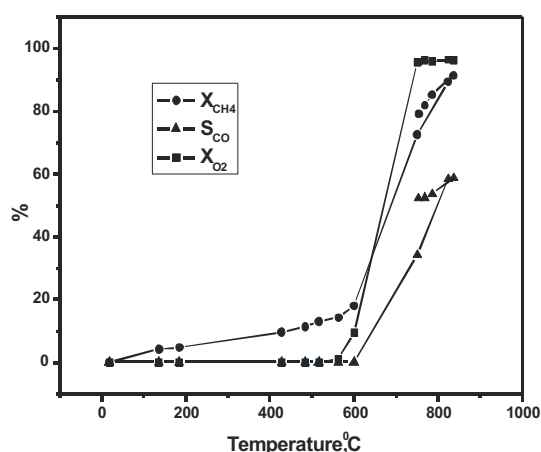
Fig 3 Temperature dependence of the methane and oxygen conversion and CO selectivity at feed rate 35 mL/s

The plots of methane conversion and CO selectivity versus space velocity are shown in Fig. 4. It should be noted that at sufficiently high values GHSV = 360000 h^{-1}, methane conversion X_{CH4} remains at 86 %. This fact indicates a high efficiency of the microreactor. In this case the amount of hydrogen produced by one MCP is equal to 48 L/h. At MCP volume equal to 0.35 cm^3, this corresponds to hydrogen capacity 139 L/(h·cm^3). This value allows estimating the size of the microreactor with required hydrogen production capacity. Specific hydrogen productivity of a microreactor related to the weight of

PP-46
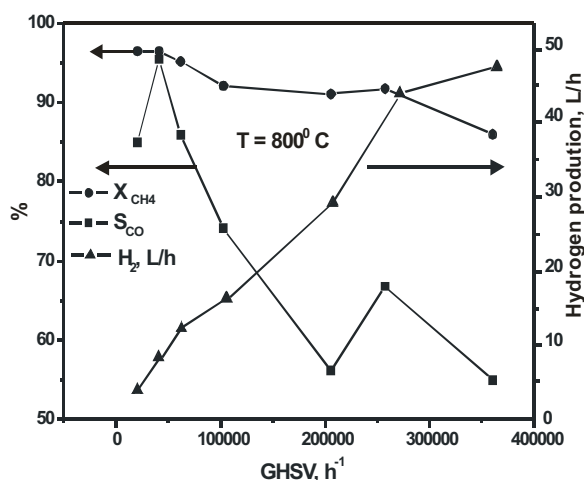
Fig 4. Conversion characteristics of the microchannel catalyst in hydrogen production by methane partial oxidation direct methane oxidation into syngas [9].

the catalyst is equal to $6 \cdot 10^5$ ml/(g·h), which is close to the best published date. At the same time, with increasing GHSV up to 360000 h^{-1}, S_{CO} decreases to 56 %, which corresponds to 20.7 L(CO)/h of the microreactor capacity. This decline of CO selectivity with space velocity suggests that at least a part of syngas is formed via consecutive occurring combustion-steam/dry reforming reactions, the latter being somewhat slower than the rate of

References

1. R.J. Rostrup-Nielsen, Catal. Today 18 (1993) 305.

2. L.D. Schmidt, M. Huff, S.S. Bharadwaj, Chem. Eng. Sci. 49 (1994), 3981.

3. K.F. Jensen, Chem. Eng. Sci. 56 (2001) 293.

4. M. Fichtner, J. Mayer, D. Wolf, K. Schubert, Ind. Eng. Chem. Res. 40, (2001), 3475.

5. D. Dissanayake, M.P. Rosynek, K.C.C. Kharas, J.H. Lunsford, J. Catal. 132 (1991) 117.

6. P.M. Torniainen, X. Chu, L.D. Schmidt, J. Catal. 146 (1994),1.

7. S. Tang, J. Lin, K.L. Tan, Catal. Lett. 51 (1998) 169.

8. P. Chen, H.B. Zhang, G.D. Lin, K.R. Tsai, Appl. Catal. A, 166 (1998) 343.

9. V.A. Sadykov, S.N. Pavlova et al. Kinetics and Catalysis, Vol. 46, No. 2 (2005) 227.

EQUATION-FREE BIFURCATION ANALYSIS OF THE LATTICE-GAS MODELS OF CATALYTIC REACTIONS

Alexei G. Makeev and Ioannis G. Kevrekidis*

Faculty of Computational Mathematics and Cybernetics, Moscow Lomonosov State University, Moscow, 119992, Russia; Tel. +7 495 9394079; e-mail: amak@cs.msu.su
*Department of Chemical Engineering, Princeton University, Princeton, NJ 08544, USA; Tel.: +1 609 2582818; e-mail: yannis@princeton.edu

Kinetic Monte Carlo (kMC) simulations may provide an atomically detailed description of catalytic chemical reactions. With the increasing power of computers, kMC simulations become more and more prominent in modeling of catalytic systems, which may exhibit complex reaction dynamics. However, traditional nonlinear dynamics tools, such as bifurcation analyses and parameter continuation, are not directly applicable to the stochastic models represented on a microscopic level by means of kMC algorithms. This feature is considered as one the main disadvantages of kMC simulations as compared to the traditional mean-field type deterministic equations.

Over the last several years we have worked on developing a novel computational framework [1, 2] that allows one to bypass the derivation of explicitly closed macroscopic equations in order to address problems for which macroscopic equations conceptually exist but are not explicitly available. The inner component of this methodology is the best available microscopic simulator of the process, such as a kMC simulator. This framework bridges traditional, continuum numerical analysis with atomistic simulation codes, allowing tasks like stability and bifurcation analysis, control and optimization to be performed using the fine scale code directly. Our approach trades functions evaluation (these functions are explicitly unavailable!) with estimation based on short, appropriately initialized kMC simulations. The proposed computational framework consists of the following basic elements:

a) translation (lifting) of a macroscopic initial condition to an ensemble of consistent microscopic configurations;

b) evolution of each initial microscopic configuration in the ensemble according to a microscopic simulator for the same short time period;

c) averaging over the ensemble of the evolved microscopic configurations to provide a macroscopic evolved system state;

d) execution of the previous three steps over a finite set of macroscopic initial conditions corresponding to nearby values of the operating parameter set (in this way, numerical evaluation of a Jacobian matrix is performed).

These steps are supplemented by the Newton-Raphson iterations, which, in turn, may converge to the stable or unstable steady states.

We illustrate an equation-free framework for the study of the complex models of heterogeneous catalytic reactions; our illustrative examples are the stochastic kMC lattice-gas models of the $CO+O_2$ and $NO+CO$ catalytic surface reactions. Beyond the practical importance, these reactions have enjoyed long-standing academic interest, because they exhibit complex reaction dynamics, such as bistability and kinetic oscillations. In the presence of adsorbate-adsorbate interactions the mean-field closures for these models are not accurate over relevant ranges of operating conditions. The numerical bifurcation analysis of the coarse-grained microscopic dynamics was performed using the "coarse time-stepper" approach in order to link kMC simulations with deterministic, continuum computational tools such as Newton-Raphson iterations, parameter continuation and eigenanalysis.

The continuation algorithm was able to produce the complete one-parameter bifurcation diagrams during a single simulation run. The calculated diagrams exhibit saddle-node and Hopf bifurcations and demonstrate that our algorithm succeeds in finding both the coarse stable and unstable stationary states. The coarse unstable states as well as the complex shape of the bifurcation diagrams would be practically impossible to reproduce using only the direct kMC simulations. In addition, we discuss the relevance of the studied lattice-gas models for the description of the experimental data obtained under UHV conditions over single-crystal Pt surfaces.

[1] A.G. Makeev, D. Maroudas, I.G. Kevrekidis. "Coarse" stability and bifurcation analysis using stochastic simulators: Kinetic Monte Carlo examples. Journal of Chemical Physics 116 (2002) 10083-10091.

[2] A.G. Makeev, D. Maroudas, A.Z. Panagiotopoulos, I.G. Kevrekidis. Coarse bifurcation analysis of kinetic Monte Carlo simulations: A lattice-gas model with lateral interactions. Journal of Chemical Physics 117 (2002) 8229-8240.

DYNAMICS OF THE METHANE PARTIAL OXIDATION INTO SYNGAS AT SHORT CONTACT TIMES ON MONOLITHIC CATALYSTS: EFFECT OF THE LATTICE OXYGEN MOBILITY AND ITS MODELING

N. Mezentseva, S. Reshetnikov, V. Sadykov, Yu. Frolova-Borchert, V. Muzykantov, E. Paukshtis, G. Alikina, A. Lukashevich, T. Kuznetsova, S. Pavlova, O. Snegurenko, Z. Vostrikov, S. Tikhov and V. Parmon

Boreskov Institute of Catalysis SB RAS, Pr. Lavrentieva, 5, 630090, Novosibirsk, Russia.
E-mail: mnv@catalysis.nsk.su

At present, selective oxidation and autothermal (steam–oxygen or steam–air) reforming of hydrocarbons into synthesis gas are considered to be promising alternatives to conventional steam reforming [1]. Advantages of this process are mild exothermicity, superiority to steam reforming in terms of efficiency (productivity), and, hence, smaller reactor sizes (lower capital investments).

Catalysts comprised of doped ceria-zirconia oxides with supported Pt were recently shown to be very efficient and stable in these reactions [2]. A high activity of these systems is explained in the frame of a bi-functional scheme [4]. It includes methane activation on Pt clusters into CH_x fragments followed by their subsequent interaction with the lattice oxygen of the oxide support at the Pt– support interface. Hence, ability of oxide systems to provide fast oxygen diffusion from the bulk to the surface could be important for these catalysts performance especially in dynamic conditions. Incorporation of low-valence cations (La, Gd, Pr) into the lattice of ceria-zirconia solutions is expected to create anion vacancies, thus improving catalytic properties of these systems [3].

On the other hand, start-up of syngas generators where selective oxidation of the natural gas occurs, is known to be accompanied by the temperature excursions often exceeding stationary values, which could cause break-up or even melting of monolithic catalysts. To avoid it, relation between such an overheat (caused by domination of deep oxidation during start-up period) and mobility of the lattice oxygen is to be elucidated, and factors controlling this mobility in complex oxide supports are to be clarified.

In this respect, it is of interest to make a quantitative estimation of the scope of the lattice oxygen diffusion coefficients at which the greatest deviation of the transient regimes from the

stationary one is observed. These results will be of primary importance for the tailor-made design of nanostructured catalysts based upon Ce-Zr complex oxide supports via controllable tuning the lattice oxygen mobility by variation of their chemical composition and real/defect structure parameters.

This work present results of studies of the relaxation characteristics for the process of methane selective oxidation into syngas at short contact times and their mathematical modeling aimed at elucidating their interrelation with the lattice oxygen mobility in doped $CeO_2 –ZrO_2$ complex oxides as well as effects of the Pt –complex oxide supports interaction.

Experimental

Samples of complex oxides $Ce_{0.5-x/2}Zr_{0.5-x/2} Me_xO_{2-y}$ (Me = La, Gd or Pr, x=0÷0.3) were prepared via the polymerized precursor route with modifications of procedures described earlier [5, 6] and calcined at 500-700 ^{o}C. Pt (1.4 wt. %) was supported by the incipient wetness impregnation with H_2PtCl_6 solution followed by drying and calcination at 500 ^{o}C.

Dynamic isotope oxygen exchange was carried out in a static installation with MS control in the temperature-programmed mode as described elsewhere [5].

The surface features of sample were characterized by Fourier Transform Infra-red Spectroscopy (FTIRS) of CO adsorbed and earlier described procedures [6].

Experimental procedures of catalytic activity characterization in the reaction of CH_4 partial oxidation for both dispersed active components and real-size monolithic catalysts on different substrates were described earlier [5]. The catalysts were pretreated in O_2 at 500 C for 1 h and tested in the isothermal (or autothermal) mode (steady-state and transient experiments) as well as temperature -programmed mode using feeds with CH_4/O_2 ratio 2 either diluted by He (CH_4 concentration 1-5%) for dispersed samples or stoichiometric methane-air mixture for monolithic catalysts.

Results and discussion

Catalytic transients.   In all experiments, after contact of reaction mixture with oxidized catalysts studied here, deep oxidation products are formed simultaneously with syngas, its selectivity increasing with the temperature. Among studied systems, the active component based on Pt-supported Ce-Zr-La-O sample with an optimum (20 at.%) content of La was shown to be the most active and selective in the partial oxidation of methane into syngas. In diluted feeds, prolonged (up to   60 min) relaxations are observed at temperatures ~ 650 ^{o}C, while decreasing up to 10 min at temperatures exceeding 800 ^{o}C in concentrated feeds. Shorter relaxations were observed for deep oxidation products suggesting mainly participation of highly mobile

surface/near surface oxygen forms in methane combustion, while syngas relaxations seem to be controlled by the lattice diffusion.

__Theoretical analysis of effect of the lattice oxygen mobility in oxide supports on the transient dynamics of fast catalytic reactions.__ Red-ox scheme of the reaction mechanism [8] was used as a basis for this analysis. Parameters of kinetic and mathematical models were derived from the experimental data on steady-state and transient methane selective oxidation in diluted feed on powdered $1.4\%Pt/Gd_{0.2}Ce_{0.4}Zr_{0.4}O_x$ catalyst.

Key parameter defining dynamics of change of the catalyst surface due to diffusion, parameter Tiele is $\varphi^2=L^2k_s/D$ (D - effective coefficient of the lattice oxygen diffusion, L - characteristic size of the oxide crystallite/domain, k_s-reaction rate constant for reoxidation of the surface site by oxygen from the bulk). For efficient operation of a catalyst in the bifunctional mode of syngas generation (vide supra), diffusion of oxygen in the bulk should not limit the transient dynamics, so Tiele parameter should be small. Nevertheless, our task is to define area in which effect of the oxygen diffusion is the most pronounced.

At the initial contact of the reaction feed with the catalyst, only oxygen of the near-surface layers takes part in oxidation. At small φ values (a fast bulk diffusion), the catalyst reduction proceeds uniformly within all depth of crystallites. At a large φ (a slow bulk diffusion), the oxygen mobility is insufficient for reoxidation of the reduced surface. For this reason, at bigger φ values, the surface coverage by oxygen and reagent (CH_4) conversion declines faster (Fig. 2).

Modeling revealed that there is a range of the Tiele parameter variation ($\varphi \in [0.3 \div 7]$) in which the greatest effect of the oxygen diffusion on the process dynamics is observed. This range corresponds to the values of the oxygen diffusion coefficient $D \sim 10^{-18} \div 10^{-13}$ cm^2/s close to the typical values for the oxygen diffusion in oxides [9].

__Oxygen mobility and Pt-support interaction.__ Fig. 2 presents dynamic degree of the oxygen exchange [7] for nanocrystalline ceria-zirconia system doped with La, Gd, or Pr. As amount of the easily exchanged oxygen is mainly below a monolayer, this oxygen appears to be mainly located in the surface layer or in the vicinity of disordered domain boundaries of these nanocrystalline systems. The most mobile near-surface oxygen is revealed for Ce-Zr-La-O system, which correlates with the biggest size of La cation and, hence, the biggest lattice parameter, which decreases the energy barrier for the oxygen diffusion.

For Pr-doped ceria-zirconia, after decline of the lattice mobility at a low doping level (up to xPr = 0.1), it increases again at a higher Pr content (Fig. 2). This phenomenon can be
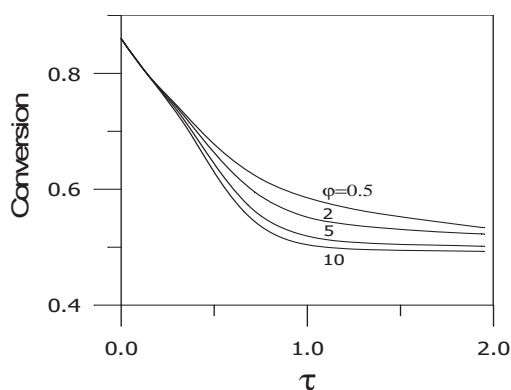
Fig. 1. Dependence of conversion CH_4 versus time at various values of module Tiele ($\varphi = 0.5, 2, 5, 10$).
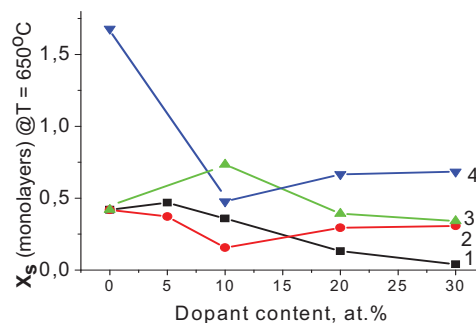
Fig. 2. The dynamic degree of exchange (Xs) at 650 ^{o}C versus the dopant content (mole fraction, x) for ceria – zirconia (1:1) oxide systems doped with Gd (1), Pr (2) or La (3). 4-Pt/Ce-Zr-La-O system.

assigned to the effect of red-ox Pr^{3+}/Pr^{4+} couple ensuring a mixed ionic-electronic conductivity in the mixed oxide when a high doping level is achieved.

Pt supporting strongly affects the oxygen mobility, apparently via facilitating the bulk oxygen transfer to the surface. This suggests a strong Pt interaction with support. Indeed, IR Spectroscopy of CO adsorbed at 77K as a test molecule revealed bands at 2175-2180 cm^{-1} (Pt^{2+}- CO complexes), 2125-2132 cm^{-1} (Pt^{+}- CO complexes) and 2041-2046 cm^{-1} (Pt^o –CO complexes) [6]. The highest concentration of cationic Pt species is observed for Ce-Zr-O system doped by La, which correlates with the highest oxygen mobility and shortest relaxations of catalytic activity as well as the highest specific activity and syngas selectivity. Cationic Pt^{2+} species dominate for studied systems, which are associated with their nanocrystallinity, namely, ability to stabilize these cations at surface defects, probably, in vicinity of domain boundaries.

References

1. V. A. Sadykov, S. N. Pavlova, R et al. Kinetics and Catalysis 46 (2005) 227

2. M. Krumpelt, S. Ahmed, R. Kumar and R. Doshi, US Patent 6,110,861 (2000).

3. J. Kašpar, P. Fornasiero, In Catalysis by Ceria and Related Materials.

4. Pantu P., Kim K., Gavals G.R. App. Catal. A 193(2000)203.

5. V. A. Sadykov, Yu. V. Frolova, et al, Mater. Res. Soc. Symp. Proc. 835, (2005) 199.

6. V. A. Sadykov, S. N. Pavlova, R et al. Kinetics and Catalysis 46 (2005) 227.

7. V. A. Sadykov, Y.V. Frolova et al, React. Kinet. Catal. Lett., 85, 375 (2005).

8. N.M. Ostrovskii, Kinetic of catalyst desactivation. M.: Nauka, 2001.

9. P.Kofstad. "Nonstoichiometry, diffusion and electrical conductivity in binary metal oxides". Willey-Interscience, New-York, 1972.

RECENT DEVELOPMENT OF CONVENIENT METHODS OF SYNTHESIS OF CHLORO CARBOXYLIC ACIDS ON THE BASIS OF LIQUID PHASE OXIDATION OF SUBSTITUTED VINYL CHLORIDES

A.R. Mikaelyan, N.L. Asatryan, S.S. Akarmazyan, G.H. Torosyan

State Engineering University of Armenia (SEUA), Department of Chemical Technologies and Environmental Engineering, 105 Terian St., B. 1, Yerevan, 375009, Republic of Armenia.

gtorosyan@seua.am

Introduction: Application of selective oxidation of alkenes by molecular oxygen is one of the current challenges in the manufacture of organic building blocks and industrial intermediates [1,2]. According to literature [3], the data relating to auto-oxidation of series of activated alkenes without halogen substitutes by oxygen is known. The involvement of styrene, α- methylstyrene, methyl acrylate, methyl methacrylate, butyl acrylate, etc. results usually in their polymerization into the oxidation process at 70-120 °C.

Liquid phase non-catalytic direct oxidations by molecular oxygen or by air of chlorovinylic compounds, have been presented in our recent reports [4,5]. Present work has established that for a great number of compounds studied, the chloroanhydrides of α-chloroacids are the main products of the reaction:

$$RCX=CCl_2 \xrightarrow{O_2} RCXClCOCl$$

R= CH$_2$Cl, CH$_2$OAc, CH$_2$C$_6$H$_5$, (CH$_2$)$_3$Cl, (CH$_2$)$_3$OAc; X=H
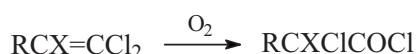
The high yield ($\approx$ 80 %) and the selectivity of formation of chloroanhydrides brings to the forefront the direct oxidation reaction of halogenvinylic compounds from a practical point of view. A possible problem might be the formation of peroxides; however, explosion of peroxide intermediate was not noticed because of they are mainly converted into the chloroanhydrides of corresponding carboxylic acids above 100-110 °C. From the presented data, one can see that liquid phase direct oxidation of halogenvinylic compounds by air is a simple and convenient method for synthesis of α-halogen- and α,α-dihalogencarboxylic acids and their derivatives. It should be noticed that in recent years many halogenvinyl compounds have already become available and cheap raw materials due to introduction of new and effective methods of chlorination of alkenes, alkynes, alkadienes, and other petrochemicals.

We hope, that this way vinylhalogen organic molecules oxidation can be use also in various field, which are extended to drinking water treatment, advance treatment of sewage water, treatment of waste water.

Thus the problem of development of new effective methods of their selective oxidation is becoming more actual.

Results and Discussion: The kinetics of oxidation of 1,1,3-trichloropropene **(I)**; 1,1-dichloro-3-phenyl-1-propene **(II)**; 1,1,5-trichloro-1-pentene **(III)** and 1,1-dichloro-5-acetoxy-1-pentene **(IV)** by oxygen has been studied [6,7,8]. Kinetic studies of liquid phase oxidation reaction of halogenolefines are based on measurements of oxygen absorption rate (manometric method) and speed of consumption of halogenvinyl compounds, and formation of the products by GLC method. The correlation of products, dynamics of their formation and changes in quantities of intermediary products are determined by the following methods: peroxides- by iodometric method, halogenanhydride of halogencarboxylic acids, halogenoxiranes and the starting halogenvinyl compounds - by GLC method in isothermal and programming regimes.

The obtained experimental data shows that the increase of oxygen flow speed does not affect the process itself furthermore substitution of oxygen with air causes increase of chloroanhydrides yield. The most reactive was trichlorpropene, which over the 20-70 °C temperature range oxidizes with average rate of 0,5-1,5$*10^{-4}$ mol/(l.$*$sec). The calculations show that the oxidation process proceeds selectively below 70 °C and when conversion of the compounds reaches 100% yield of chloroanhydrides of α-chlororganic acids exceeds 90%. It has been established that in early stages of oxidation the peroxides are formed, amount of which reaches maximum values (40-42 %, iodometric method) at 65-70% of the reaction conversion.

The quantitative analysis of thermal treatment products of peroxides by GLC method shows that *hem*-dichlorolefine oxide and chloranhydride of the corresponding acid are the products of following rearrangement reaction.

$$RCH=CCl_2 + O_2 \longrightarrow RCH\overset{\overset{\displaystyle O—O}{|\quad\;|}}{—}CCl_2 \longrightarrow RCH\overset{O}{—}CCl_2 + RCHCl—COCl \longrightarrow$$

$$\xrightarrow{\text{distillation}} RCHCl—COCl$$

$$R=CH_2Cl, (CH_2)_3Cl$$
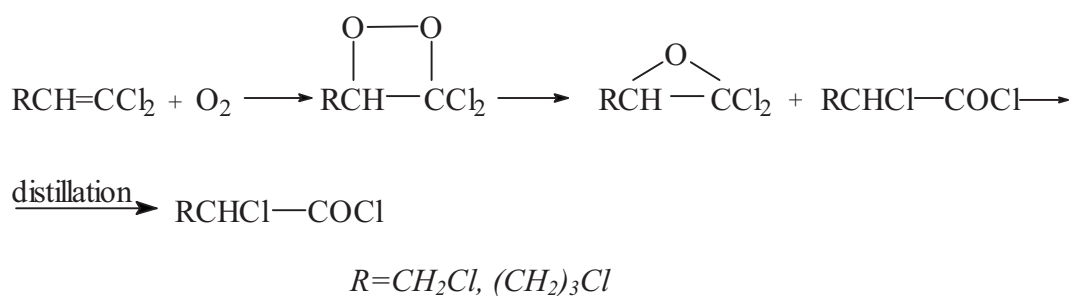
We carry out also the hydrolysis, alcoholysis and aminolysis of the oxidate into the acids, esters and amides of α-chlorocarboxylic acids, respectively.
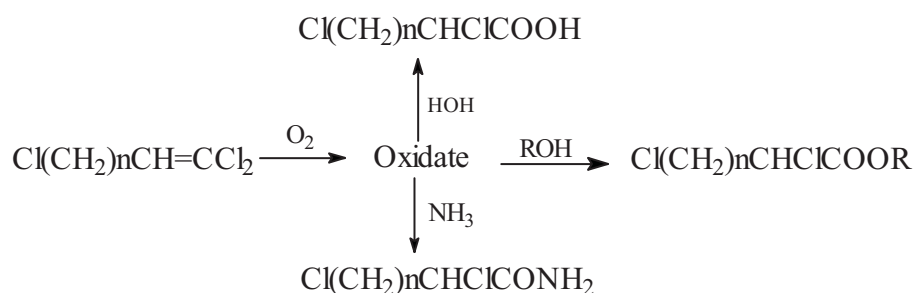
It is obviously, that the increasing of oxidation speed and prevention of long time thermal influence on intermediates leads to increasing of the yield an selectivity aimed products.

In this goal the non-catalytic liquid phase oxidation of 1,1-dichloro-5-acetoxy-1-pentene by molecular oxygen in reactor with oxygen-spray has been investigated [8]. It has been shown that the main products of the reaction are ω-acetoxyvalerianic acid chloride and the olygomer, which is obtained as a result of poly-condensation of the chloride with abstraction of acetyl chloride. It has been determinate, that in case of application of oxygen-spray reactor with glass-ring packed, the yield of ω-acetoxyvalerianic acid chlorid is approximately two-time higher.

In addition, the catalytic (TiO$_2$) liquid phase oxidations of 1,1,5-trichloro-1-pentene (as a model compound) by molecular oxygen in glass-ring packed reactor with oxygen-spray have been investigated.
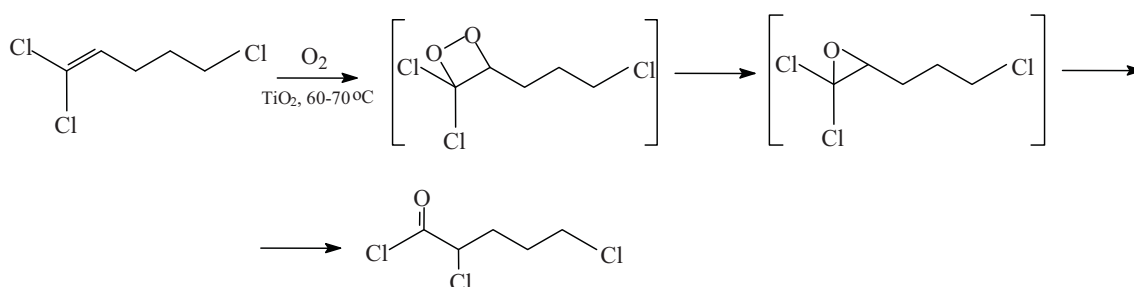
The investigations of kinetics of oxidation processes (consumption of 1,1,5-trichloro-1-pentene and formation of α,ω-dichlorovaleric acid chlorides by GLC method) have been performed.

PP-49

It has been shown, that titanium dioxide (10mg TiO_2 to 1mmol substrate) have catalytic activity in this oxidation reactions, so by 60 °C after 5.5 hour the yield of acid chloride 6 arrived at 61% (by non-catalytic oxidation this rate have been attained more then 9 hour reaction time).

It has been proposed that this oxidation process will offer synthetic utility since reaction proceeds readily, does not require any solvent (which would usually introduce problems for purifying of products) and provide selective formation of chlorides of α-halogenalkenoic acids. On the basis of the obtained results on direct liquid phase oxidation of halogenolefines by oxygen in air it is supposed to find the opportunities for application of these reactions for solution of environmental problems related particularly to the problems of utilization, mineralization and metabolism in the biosphere of halogenorganic compounds wastes.

References

[1] R.A. Sheldon, J.K. Kochi.//Metal-Catalyzed Oxidation of Organic Compounds, Academic: New York, 1981.

[2] G.W. Parshall, S.D. Ittel. // Homogeneous Catalysis, Wiley: NewYork,1992.

[3] E.M.Pliss, V.M.Troshin. // Neftekhimiya 1982, v.22, N 4, pp. 539-542.

[4] B. Bayatyan, A. Mikaelyan, N. Asatryan et al. // Book of abstracts of annual scientific conference of SEUA, 25-29 October 1999, Yerevan, p. 40, 41.

[5] B.E. Bayatyan, A.R. Mikaelyan, E.S. Voskanyan, Sh.O. Badanyan. // "Chemistry in Armenia on the Threshold of the XXI Century", Book of Abstracts (NAN of RA), 18-20 May 2000, Yerevan, p. 121.

[6] B. Bayatyan, A. Mikaelyan et al. // Book of abstracts of annual scientific conference of SEUA, Vol. 1, 29 October -2 November 2001, Yerevan, pp. 66-68, 68-70.

[7] A.G. Ayvazyan, A.R. Mikaelyan, N.L. Asatryan, B.E. Bayatyan, R.M. Mirzakhanyan, Sh.O. Badanyan. // Information Technologies and Management, (Series chemical technologies and ecological engineering), Yerevan, 2002, N1, pp.191-196.

[8] A. Sarksyan, A. Mikaelyan. // Book of abstracts of annual scientific conference of SEUA, 28-30 April 2003, Yerevan, pp. 3-5.

PERMEABLE CATALYTIC MEMBRANE FOR COMPACT APPARATUS FOR HYDROGEN-RICH GASES DEEP CLEANING FROM CO

Minyukova T.P., Itenberg I.Sh., Khasin A.A., Sipatrov A.G., Dokuchits E.V., Terent'ev V.Ya.*, Khristolyubov A.P.*, Brizitskii O.F.*, Yurieva T.M.

Boreskov Institute of Catalysis SB RAS, 5, Pr. Lavrentieva, Novosibirsk, 630090, Russia, fax. +7-383-3308056, min@catalysis.ru
*Russian Institute for Experimental Physics (VNIIEF), 37, Mira ave, Sarov, 607190, Nizhegorodskoi obl., fax +7-831-3040032, trn@gatestc.sarov.ru

In order to provide a wide application of the PEMFC technology, reduce cost and improve characteristics of PEMFC-based power plants, it is necessary to create a compact and economic apparatus for deep cleaning (to 20 ppm) of converted fuel from carbon monoxide. In the existent technologies of hydrogen conditioning for fuel cells WGSR and deep purification by CO selective oxidation follow the stage of hydrocarbon steam reforming. Method of selective CO hydrogenation for deep purification is the alternative one to the selective CO oxidation. It doesn't demand the addition of the air (therefore, the dilution by nitrogen is excluded) and provides more high-calorie hydrogen fuel, that leads to the higher overall efficiency of electric power plant.

Method of selective CO hydrogenation is not so developed, but some publications and patents are known [1-5]. The hydrogenation is carrying out in one or two stages on the catalysts based on Ru, Rh, Pt, Fe. In these studies the necessary depth of purification is not reached and so a problem is solved by the subsequent selective oxidation. In [6] the required purity is achieved on Ni/Al_2O_3 catalyst at GHSV 300 h^{-1}. A compact apparatus for hydrogen deep purification can't be designed on the base of such a low active catalyst.

The present study is devoted to:

(1)   the search of the catalyst, providing the CO hydrogenation to the content below 20 ppm and having the selectivity not less than 0.3 at GHSV above 6000 h^{-1};

(2)   the development of the permeable catalytic membrane on the base of this catalyst.

CO hydrogenation occurs by the reactions (1) and (2) forming methane (and some amounts of higher hydrocarbons) and is complicated by reaction (3):

$$CO + 3H_2 = CH_4 + H_2O \qquad\qquad (1)$$
$$CO_2 + 4H_2 = CH_4 + 2H_2O \qquad\qquad (2)$$
$$CO_2 + H_2 = CO + H_2O \qquad\qquad (3)$$
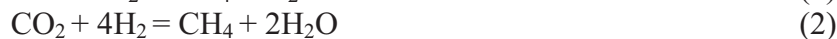
The obstacle of the selective CO hydrogenation consists in the presence along with 1 vol.% CO about 20 vol.% of CO_2 and the same amount of water vapours. The following criteria were adopted for estimation of the effectiveness of the catalysts for selective CO hydrogenation for the compact apparatus of hydrogen-rich gas conditioning for fuel cells:

(1) **depth of purification**: CO outlet gas content not higher than 20 ppm;

(2) **selectivity** 0,3; i.e. not more than 70% of methane may be formed from CO_2;

(3) **activity**: GHSV not less than 6000 h^{-1}.

Experimental part. The catalysts were obtained by the thermal decomposition of appropriate hydroxocompounds. For the comparison commercial Ru-containing catalyst RC-3 (0.5% Ru/Al_2O_3) known as effective methanation catalyst was tested in the same conditions. The catalytic tests were carried out in the unit with flow reactor at 0.1 MPa. Gas Chromatograph Cristall-2000 was used for fuel gas analysis. The threshold of sensitivity by CO was 10 ppm. Inlet gas composition was: $CO:CO_2:H_2O:H_2 = 1:21:18:60$.

Results. The series of nickel- and cobalt-containing catalysts with different composition, thermal treating and activation parameters have been prepared and tested. in selective CO hydrogenation [7]. On the base of results of catalytic tests in the kinetic field (catalyst granules 0.25-0. 5 mm) the composition of optimal catalyst has been revealed. This catalyst was denoted as NM-1.

It was shown that in the kinetic field at 190-210^{0}C and GHSV from 2000 to 17000 h^{-1} CO hydrogenation on NM-1 catalyst occurs up to 10-20 ppm with selectivity about 0.7. However, while using larger granules of 2-3 mm, especially pellets of 5x5 mm, it was ascertained that abrupt decrease of selectivity takes place, i.e. the methane amount produced by CO_2 hydrogenation increases by several times. This is a result of the influence of diffusion resistance on the catalyst surface state, in particular, reduction of the catalyst surface coating with adsorbed carbon monoxide.

To solve the problem we used the developed in BIC approach to improving mass exchange by application of a permeable catalytic membrane (PCM) [8]. The contact of reaction gas with the catalyst's particles of 70-150 μm occurs in the (PCM), i.e. the conversion takes place in the kinetic field. Such membranes can be prepared from a composite, containing a catalytic active component (NM-1 catalyst in our study); metal, providing the strength and high thermal conductivity of membrane; and porophore

component. PCM may be prepared in the form of the plates or hollow cylinder. In the last case the gas flow is radially directed.

The procedure of PCM preparation includes a sequence of operations commonly used in powder metallurgy: 1) preparation of a mixture of powders of a catalytic active oxide component, a metal and a porophore component; 2) mixture densification; and 3) sintering at elevated temperatures. In present research the powder of NM-1 catalyst was mixed with electrolytic metallic Cu powder of 20 - 50 μm in size having dendrite structure and malachite (as porophore), then pressurized at ~200 MPa to the hollow cylinder of 13 mm in height and 18 mm in diameter. After all it was sintered at 450°C in flowing argon. Figure 1 shows the appearance of PCM-NM-1 based.
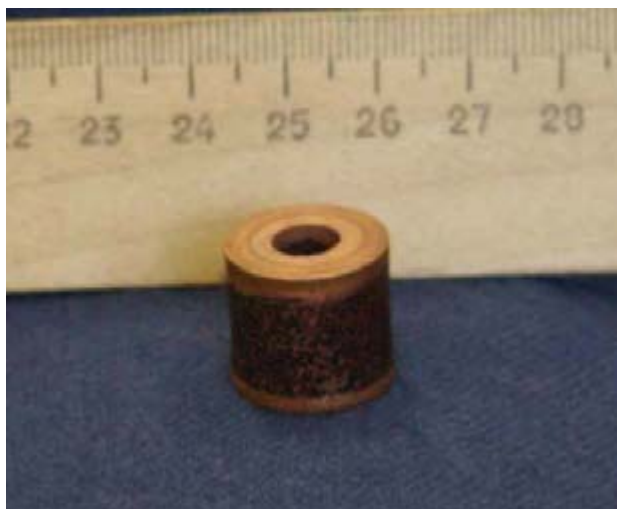
Figure 1. Permeable catalytic membrane based on the NM-1 catalyst

Figure 2 shows the dependence of CO outlet content and the selectivity of CO hydrogenation from GHSV for permeable catalytic membrane PCM-NM-1. It can be seen that in the wide range of GHSV from 15 000 to 30 000 h^{-1}, PCM-NM-1 has the selectivity above 0.3 and the CO content in the outlet gas below 20 ppm. Therefore, PCM-NM-1 meets the criteria of the effective catalyst for selective CO hydrogenation in a compact apparatus.

Furthermore, it should be noted that PCM has high thermal conductivity, comparable with the thermal conductivity of metals. It provides the isothermal catalytic bed. The application of PCM in the form of rings allows constructing a tubular reactor with low hydrodynamic resistance.
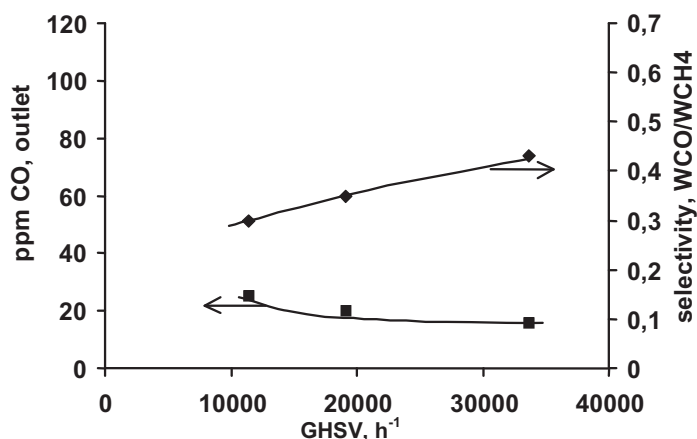
Figure 2. Dependence of CO outlet content and selectivity (W_{CO}/W_{CH4}) from GHSV for permeable catalytic membrane based o NM-1 catalyst (PCM-NM-1) at 200^{0}C. Inlet fuel gas composition: CO: CO_2:H_2: H_2O = 1:21:60:18

PP-50

The tests of RC-3 catalyst as commercial granules (3-5 mm) were performed varying GHSV and temperature. The results have shown that the lowest CO outlet content for this catalyst is 60 ppm and the best selectivity 0.6-0.8 at 270-280^{0}C in a very narrow GHSV 2000-5000 h^{-1}. It implies subsequent selective CO oxidation for achievement the required 20 ppm CO.

Figure 3 shows the advantage of PCM-NM-1 catalyst in comparison with commercial RC-3. Note, that our results on Ru-based catalyst RC-3 are in good agreement with the results of [3,4] while developed permeable catalytic membrane based on NM-1 catalyst (PCM-NM-1) is characterised by the wider effective range of GHSV in comparison with nickel-containing catalyst in [6].
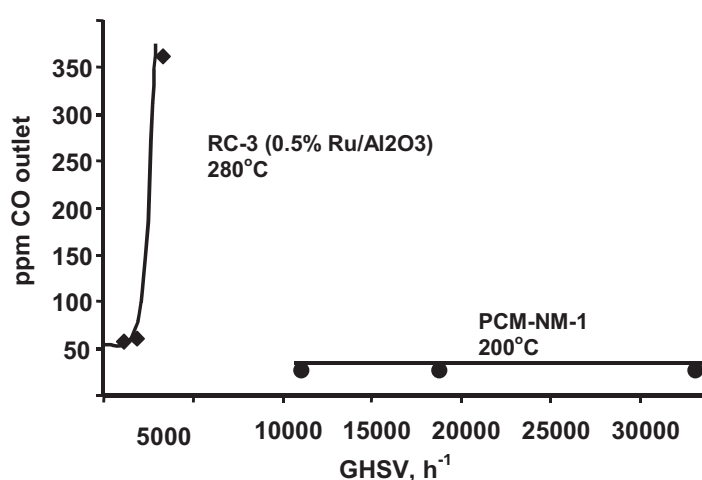
Figure 3. Comparative studies of RC-3 catalyst as commercial granules at 280^{0}C (♦) and PCM-NM-1 at 200°C (●). Inlet fuel gas composition: CO: CO$_2$:H$_2$: H$_2$O = 1:21:60:18

So, the developed NM-1 catalyst in the form of permeable catalytic membrane (PCM) provides the fine fuel gas purification to CO concentration 20 ppm and below in the wide range of GHSV from 6000 to 30000 h^{-1} and has selectivity above 0.5.

References:

1. R. Wangerow, C. Sishtla, A.H.Hill, M. Onischak. US Patent 2003/0086866, 2003.
2. K. Heikrodt, S. Wieland, P.Britz, F. Baumann. EP 1246286, 2002.
3. V. Keulen. US Patent 6,207,307, 2001.
4. M.Echido, O.Yamazaki, H.Sasaki, T. Tabata. Fuel Cell Seminar 2003. Extended Abstracts, p.98-101.
5. J.Wagner, H.Takeda. Fuel Cell Seminar 2003. Extended Abstracts, p.245-248.
6. H. Ashiro, K. Nagaya K. Mitani. Fuel Cell Seminar 1996. Extended Abstracts, p.319-322.
7. T.P.Minyukova, I.Sh.Itenberg, M.P.Demeshkina, N.V.Shtertser, T.M. Yurieva. Chem. Sust. Dev. 13(6) (2005) 793-796.
8. A.A. Khassin, A.G. Sipatrov, T.M. Yurieva, G.K. Chermashentseva, N.A. Rudina, V.N. Parmon. Catal. Today, 105(3-4) (2005) 362-366.

NOVEL ZnBiGaO$_4$ PHOTOCATALYST FOR VISIBLE LIGHT PHOTOCATALYTIC HYDROGEN PRODUCTION

Jin-Ook Baeg, <u>Sang-Jin Moon*</u> and Hyunju Chang

Korea Research Institute of Chemical Technology (KRICT)
100 Jang-dong, Yuseong-gu, Daejeon 305-343, Republic of Korea
*e-mail; moonsj@krict.re.kr, fax; 82-42-860-7590

Introduction

The hydrogen generation by photocatalytic decomposition of hydrogen sulfide (H$_2$S) is one of the considerable interest due to environmental hazardness of H$_2$S. Photocatalytic decomposition of H$_2$S using oxide photocatalysts provides a good method for the removal of the pollutant, H$_2$S and leads to the production of hydrogen, which is a clean fuel and a starting material for many industries. H$_2$S is considered to be a potential source of hydrogen in the future hydrogen economy. An ubiquitous Claus process is currently used for the decomposition of hydrogen sulfide.[1] This conventional Claus process comprises the proportionation reaction between H$_2$S and SO$_2$ yielding elemental sulfur and water vapor. If hydrogen can be recovered from H$_2$S instead of oxidizing it into H$_2$O (Claus process), immense amount of hydrogen can be produced.[2] Photocatalytic splitting of H$_2$S to H$_2$ using solar energy is a challenging, interesting and an eminent topic of research with the potential to provide clean and renewable alternate energy to the mankind. This process requires less photoelectrochemical energy compared to the photocatalytic decomposition of water.[3-6]

In this paper, we are reporting first time the photocatalytic decomposition of H$_2$S by using a novel spinel oxide photocatalyst, ZnBiGaO$_4$. We have synthesized this photocatalyst by solid-state and hydrothermal methods and characterized its crystalline property and surface morphology by using XRD and FE-SEM. The characteristics of crystal and band structure were studied using computational analysis. This paper also describes the novelty in synthesis of new product, its characterization and evaluation for the photocatalytic decomposition of H$_2$S to generate hydrogen under visible light irradiations.

PP-51

Experimental Section

Materials

In our studies, $ZnBiGaO_4$ was prepared by two methods. One is the solid-state reactions between stoichiometric amounts of ZnO, Bi_2O_3 and Ga_2O_3 (all are Aldrich grade). Another compound was prepared by hydrothermal method using a stoichiometric amounts of $Zn(NO_3)_2 \cdot 5H_2O$, $Bi(NO_3)_3 \cdot 6H_2O$, $Ga(NO_3)_3 \cdot xH_2O$.

Photocatalytic Studies under UV and Visible Irradiations

In all experiments, 500 mg of the photocatalyst was dispersed in 250ml of 0.50M KOH aqueous solution with the H_2S flow (2.5ml/min.) in a Pyrex glass photoreactor with a water-cooled quartz immersion well and thermostated water jacket. The excess hydrogen sulfide was trapped in NaOH solution. The solution mixture was thermostated at 25°C and vigorously stirred and the dispersion was purged with argon gas for 1h and then hydrogen sulfide (H_2S) was bubbled through the dispersion solution mixture for about 1h. The dispersion solution mixture was irradiated with 450 W xenon-arc lamp (Oriel) in the case of visible light irradiation which produces a line-free continuum from 350 to 2500 nm. The IR radiation and UV radiation were filtered by a water jacket IR filter and 420nm cut-off light filter(Oriel), respectively. The amount of evolved hydrogen was measured using graduated gas burette and the collected gas was detected as hydrogen by GC (Model Shimadzu GC-14B, MS-5Å column, TCD) by using argon as the carrier gas.

Results

Characterization

Powder XRD patterns for $ZnBiGaO_4$ (s-s) and $ZnBiGaO_4$ (h-t) are shown in fig. 1(a) and fig.1(b). The XRD patterns of $ZnBiGaO_4$ (s-s) and $ZnBiGaO_4$ (h-t) contain peaks at 24.7°, 27.7° and 32° and these peaks matches with the theoretical values.[7] The major peak at 27.7° shows the formation of $ZnBiGaO_4$. XRD results of $ZnBiGaO_4$ shows that it is cubic spinel structure.

Fig.1c and fig.1d depict the FESEM micrographs of $ZnBiGaO_4$ (s-s) and $ZnBiGaO_4$ (h-t). SEM micrograph of $ZnBiGaO_4$ (s-s) shows the unique layered structure. The aggregation of particles was observed, which suggests the homogeneity of the solid solution with fairly good crystallinity. The very hard nature of the products suggests that there may be formation of highly crystalline glass ceramics having the particle size in the range of 0.2-1.0μ.

ZnBiGaO$_4$(h-t) shows little different morphology with layered structure having the particle size in the range 50-150nm which is smaller than ZnBiGaO$_4$ (s-s) due to low processing temperature.
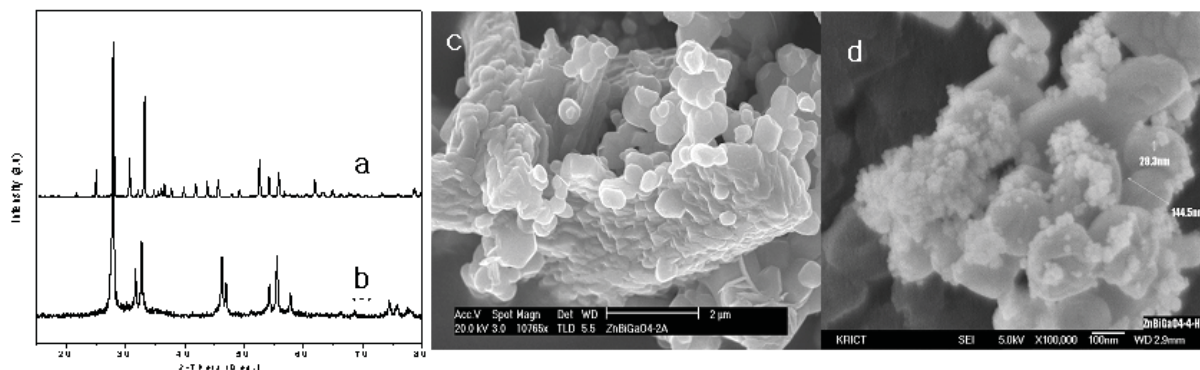
Fig. 1: XRD pattern of {(a) ZnBiGaO$_4$ (s-s) and (b) ZnBiGaO$_4$ (h-t)} and FESEM image of {(c) ZnBiGaO$_4$ (s-s) and (d) ZnBiGaO$_4$ (h-t)}

The band gap energy of ZnBiGaO$_4$ (s-s) and (b) ZnBiGaO$_4$ (h-t) were determined by the UV–VIS diffused reflectance spectra. The estimated band gap energies for ZnBiGaO$_4$ (s-s) and ZnBiGaO$_4$ (h-t) are the same i.e, 2.80 eV (440nm).

Photocatalytic Studies of ZnBiGaO$_4$

Table 1. Photocatalytic decomposition of H$_2$S by using ZnBiGaO$_4$ for H$_2$ evolution under Visible light irradiation

Photocatalyst	Band gap energy (eV)	H$_2$ evolution rate (μmol/h)
ZnBiGaO$_4$ (s-s)	2.80	3030
ZnBiGaO$_4$ (h-t)	2.80	3022

In this paper, the photocatalytic decomposition of hydrogen sulfide by using ZnBiGaO$_4$ as photocatalyst is presented. Different series of experiments were carried out using photocatalysts of ZnBiGaO$_4$ (s-s) and ZnBiGaO$_4$ (h-t). By using ZnBiGaO$_4$ as new photocatalyst, we have studied the photocatalytic activity under visible light of radiations. Table 1 presents the photocatalytic decomposition of H$_2$S of ZnBiGaO$_4$ (s-s) and ZnBiGaO$_4$ (h-t) under visible light irradiation. From the table 1, we understand that the both photocatalysts have more or less similar photocatalytic activities. This implies that there is no size effect of particle on the photocatalytic activity. ZnBiGaO$_4$ (s-s) seems to be more

crystalline than the ZnBiGaO$_4$ (h-t) as observed in XRD and SEM. From the above studies, we concluded that the photocatalytic activity is more dependent on crystallinity and good microstructure than the smaller particle size and high surface area.[8] Low light absorption and unsatisfactory stability in time are, unfortunately, typical for smaller particle sized (nanoparticles) photocatalysts.

Acknowledgements

References

(1) Elsner, M. P.; Menge, M.; Muller, C.; Agar, D. W. *Cata. Today* **2003***, 79*, 487.

(2) Linkous, C. A.; Muradov, N. Z.; Ramser, S. N. *Int. J. Hydrogen Ener.* **1995,** *20*, 701.

(3) Kudo, A.; Kato, H.; Tsuji, I. *Chem Lett.* **2004**, *33*, 1534.

(4) Kato, H.; Kudo, A. *J. Phys Chem. B*. **2002**, *106*, 5029.

(5) Kim, J.; Hwang, D.W.; Kim, H.; Bae, S.W.; Ji, S. M.; Lee, J. S. *Chem. Commun.* **2002**, 2488.

(6) Ishii, T.; Kudo, H.; Kudo, A. *J. Photochem. Photobiol. A*. **2004,** *163*, 181.

(7) JCPDS file, 38-1240.

(8) Beydoun, D.; Amal, R.; Low G.; McEvoy, S. *J. Nanoparticle Res.*, **1999,** *1*, 439.

PHOTOCATALYTIC HYDROGEN PRODUCTION
OF CdS COMPOSITE FILMS BASED ON TITANIA-NANOTUBE

Sang-Jin Moon*, Hyun-Mi Lee, Won-Wook So, Jin-Ook Baeg, and Hyunju Chang

Korea Research Institute of Chemical Technology (KRICT)

100 Jang-dong, Yuseong-gu, Daejeon 305-343, Republic of Korea

*e-mail; moonsj@krict.re.kr, fax; 82-42-860-7590

1. Introduction

Recently, TiO_2 nanotubes have been prepared by a rather simple hydrothermal processing using NaOH aqueous solution [1]. Since this TiO_2 form has a larger surface area, it is of particular interest in the respect of catalytic or photocatalytic application. In the present study, we prepared TiO_2 nanotubes following the previous hydrothermal process under the basic condition [1] but using KOH solution instead of NaOH solution, resulting in longer TiO_2 nanotubes with a very strong thermal resistance at higher temperatures. Thus, their applicability as a catalyst scaffold for photo-production of hydrogen from aqueous H_2S solution was studied and the activities were tested after preparing CdS-TiO_2 nanotube composite films as visible-light sensible photocatalysts.

2. Experimental

Nano-crystalline CdS sol was prepared by a precipitation reaction of 0.5 M $Cd(NO_3)_2$ and 0.5 M Na_2S aqueous solutions at room temperature and a subsequent hydrothermal treatment at 240°C for 12 hr [2]. TiO_2 nanotubes were prepared by the hydrothermal reaction under strongly basic condition. A commercial TiO_2 powder (P-25, Degussa) was used as a starting material. For alkali-treatment of the TiO_2 raw material, concentrated (10~15 M) KOH or NaOH aqueous solution was used. Hydrothermal treatment was conducted for 12 hr at 120°C in a sealed Teflon-lined S.S. vessel containing about 50 cc of KOH or NaOH aqueous solution.

PP-52

The resulting TiO_2 slurry was washed with deionized water and further treated with an inorganic acid like HCl (~0.1 M), and then washed again repeatedly with deionized water to obtain the final TiO_2 nanotube slurry. These CdS sol and TiO_2 nanotube slurries were mixed together mechanically using ultrasonification with variation of the mole ratio, r = TiO_2 nanotube/(CdS + TiO_2 nanotube). Using these CdS-TiO_2 nanotube composite sols, CdS-TiO_2 nanotube composite films were prepared by casting the final sol onto fluorine doped SnO_2 conducting glass (F:SnO_2), and a subsequent heat-treatment at 450°C for 30 min under air. The physico-chemical properties of the composite films were measured by using SEM, TEM, XRD, and the BET method (Micromeritics, ASAP 2400). The photocurrent was measured in a water-jacketed cell of three-electrodes system consisting of the composite film electrode (photo-anode), a saturated calomel electrode (SCE), and Pt gauze. The light was illuminated on the photo-anode with the intensity of 100 mW/cm^2 (A.M. 1.5) using a Xe lamp (ILC Technology, U.S.A). Hydrogen production experiments were carried out in a closed circulation system [3] using an aqueous solution of 0.1 M Na_2S and 0.02 M Na_2SO_3 as a reference feedstock for comparison of water photo-splitting activity of these composite films which was coated with Pt particles as co-catalyst by plasma sputtering (80 watt, 30 sec., $3x10^{-3}$ torr of Ar).

3. Results and Discussion

Figure 1 shows typical TEM images for the microstructure of TiO_2 nanotubes prepared. Depending on the kind of the basic solution used, the nanotubes (Figure 1b) prepared with KOH solution revealed a different morphology with smaller outer diameter (~5 nm) and longer length (~500 nm) compared to the nanotubes (Figure 1a) prepared with NaOH solution. After calcination of the nanotubes under air at 450°C, the surface areas of nanotubes prepared with NaOH solution reduced to about 30 % of the initial surface area (376 → 134 m^2/g), while that of the nanotubes prepared with KOH solution was not so much variant (352 → 296 m^2/g). The nanotubes prepared under KOH solution were apparently more resistant to

heat treatment at a higher temperature.

Figure 2 shows SEM photographs of CdS-TiO$_2$ nanotube composite films, whose nanotube was prepared in KOH solution. The pure TiO$_2$ nanotube film (r = 1) showed a rather dense shape consisting of thin and long nanotubes, which were aligned uniformly. The CdS-TiO$_2$ nanotube composite films (Figure 2b and 2c) revealed that CdS particles and TiO$_2$ nanotubes were well mixed homogeneously without any severe agglomeration among TiO$_2$ nanotubes. Their photocatalytic performances such as the photocurrents and the hydrogen photo-production rates were measured. The values measured under the present experimental conditions varied in the range of 0.05 ~ 4.95 mA/cm^2 and 0.03 ~ 0.23 cc/cm^2·hr with r, respectively, and showed the maximum hydrogen production rate at r = 0.2 (Figure 3). As a result of higher resistance of the present TiO$_2$ nanotubes to the acid etching and thermal treatment at higher temperatures, the CdS-TiO$_2$ nanotube films showed stable and strong film properties, although their photocatalytic performances were not so remarkable compared to the previous CdS-TiO$_2$ particulate films [4].

References

[1] T. Kasuga, M. Hiramatsu , A. Hoson , T. Sekino, K. Niihara, *Adv. Mater.*,11(15),1307 (1999).

[2] W.W. So, J.S. Jang, Y.W. Rhee, K.J. Kim, S.J. Moon, *J. Colloid Interface Sci.,* 237, 136 (2001).

[3] S.J. Moon, W.W So, H.Y. Chang, *J. Electrochem. Soc.,* 148(9), E378 (2001).

[4] W.W. So, K.J. Kim, S.J. Moon, *Int. J. Hydrogen Energy,* 29, 229 (2004).
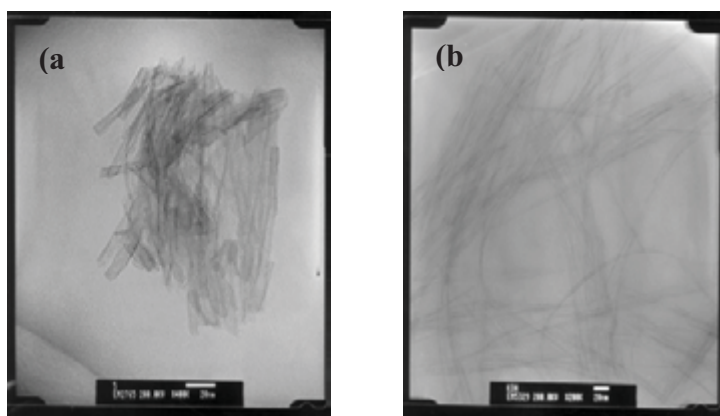
Figure 1. TEM images of TiO$_2$ nanotubes prepared by the hydrothermal treatment with (a) NaOH aqueous solution and (b) KOH aqueous solution.
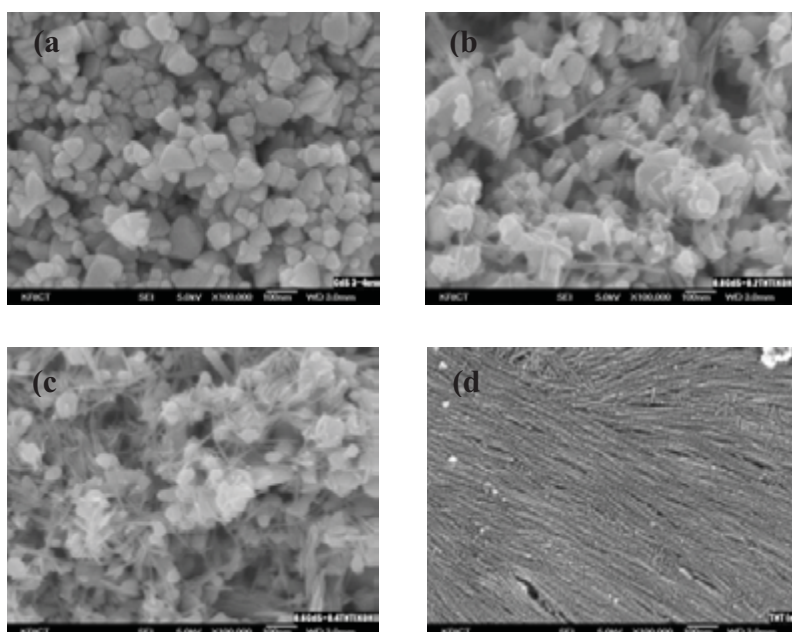
Figure 2. SEM photo-graphs of composite films with variation of the mole ratio, r = TiO$_2$ nanotube/(CdS + TiO$_2$ nanotube): (a) r = 0, (b) 0.2, (c) 0.4, (d) 1.
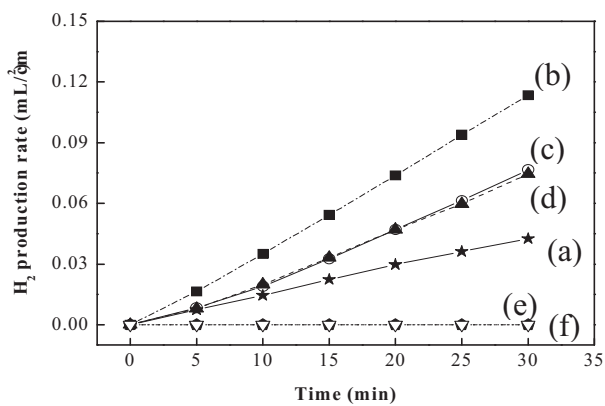
Figure 3. The amount of hydrogen produced from CdS-TiO$_2$ nanotube composite films: (a) r = 0, (b) 0.2, (c) 0.4, (d) 0.6, (e) 0.8, (f) 1.

EFFECT OF PREPARATION PARAMETERS ON ACTIVITY OF La$_{1-x}$Ce$_x$CoO$_3$ PEROVSKITES FOR ENERGY PRODUCTION BY THE CATALYTIC FLAMELESS COMBUSTION OF METHANE

C. Oliva[a], G.L. Chiarello[a], S. Cappelli[a], I. Rossetti[a], A. Kryukov[b], L. Forni[a]

[a]*Dipartimento di Chimica Fisica ed Elettrochimica, Università degli Studi di Milano,*

and CNR Institute, via C.Golgi, 19 20133 Milano, Italy. Fax:+39-02-70638129

[b]*D.I. Mendeleev University of Chemical Technology of Russia, Moscow, Russia.*

Introduction and aim of the investigation

Perovskite-like La$_{1-x}$Ce$_x$CoO$_3$ samples are well-known catalysts for several applications [1, 2] and particularly for the catalytic flameless combustion (CFC) of methane [3,4]. However, samples with the same nominal composition, but prepared by different procedures, can show very different catalytic performance. In a few cases the XRD patterns of catalysts prepared by the traditional sol-gel (SG) method show traces of La$_2$O$_3$, CeO$_2$, and/or Co$_3$O$_4$ [3]. This does not occur with samples with the same composition, but obtained by innovative methods based on flame-hydrolysis (FH) [4] or flame pyrolysis (FP) [5]. However, these impurities are present in a very low concentration, so to be hardly detectable by XRD. Furthermore, to the best of our knowledge, no clear connection has been ever established between the presence of those low-concentration phases and catalytic performance. In addition, some SG-prepared La$_{1-x}$Ce$_x$CoO$_3$ catalysts showed an Electron Paramagnetic Resonance (EPR) line at $g \cong 2$, Lorentzian-shaped at low temperature and broadening with increasing it (L line, Fig.1(a)). This feature was observed with some low-performance catalysts both when fresh and after use for the CFC of methane [3] but it was noticed only after the catalytic reduction of NO by CO with other nominally identical SG-prepared samples [2]. Furthermore, L was never observed with FH- or with FP-prepared La$_{1-x}$Ce$_x$CoO$_3$ catalysts [4, 5]. In any case, no connection between L and catalytic performance has been proposed up to date with La$_{1-x}$Ce$_x$CoO$_3$ catalysts. Lines like L have been reported in literature also with SG-prepared La$_{1-x}$M$_x$MnO$_3$ samples (M = Ce, Eu, Sr) [6]. In that case the EPR line broadening was attributed to polaron propagation involving Mn^{3+}($3d^4$; S = 2) and the nearest neighbour Mn^{4+}($3d^3$; S = 3/2), among which a conduction electron hops (Double Exchange mechanism) and a connection between this line, activity and durability of those catalysts has been proposed [7]. However, in the here examined case of La$_{1-x}$Ce$_x$CoO$_3$, the $3d^6$ Co^{3+} ions

are stable in the low spin ($S = 0$, t^6_{2g}, e^0_g) state when octahedrally coordinated to 6 oxygen atoms in an ideal $LaCoO_3$ structure. Therefore, no EPR line at all would be expected with ideal samples of this kind and the considerations above reported for $La_{1-x}M_xMnO_3$ cannot be simply applied to $La_{1-x}Ce_xCoO_3$ catalysts. The aim of this investigation was then to better understand this complicate situation and to find a connection between these phenomena and catalytic activity of $La_{1-x}Ce_xCoO_3$ in the CFC of methane.

Experimental

The $La_{1-x}Ce_xCoO_3$ samples (x = 0; 0.1) have been prepared both by the traditional SG route, followed by calcination at 800°C for 8 h (SG0 and SG1 samples) and by the mentioned FP method [5], recently proposed by us (FP0 and FP1 samples). The last were prepared by employing n-octanol or ethanol as fuel, obtaining identical results. All the prepared samples have been then activated at 600 °C for 1 h in flowing air and tested as catalysts for the CFC of methane. After reaction, the samples underwent three deactivation cycles under reaction conditions, but at 800 °C for 1 h (samples SG0U, SG1U, FP0U and FP1U) and then re-examined by XRD and by EPR spectroscopy.

Results and discussion

Catalytic activity was always lower with the SG samples than with the FP ones (Fig.2). The XRD patterns revealed a pure perovskite-like structure for SG0 and FP0 samples, as well as for FP1, (see for example Fig.3(a)). On the contrary, traces of CeO_2 and Co_3O_4 phases were noticed in the SG1 (Fig.3(c)).

In our opinion, these can form through the decomposition reaction:

$$120 \ La_{0.9} \ Ce_{0.1}CoO_{3+\delta} \rightarrow 12 \ CeO_2 + 54 \ La_2O_3 + 40 \ Co_3O_4 + 7 \ O_2 \qquad (1)$$

in which δ = 0.05 to obtain charge neutrality. Usually, not all the right-hand solid phases of Eq.(1) can be detected by XRD, due to their low amount and dilution in the main perovskite-like phase. Furthermore, CeO_2 and Co_3O_4 impurities appear also in the FP1U samples (Fig.3(b)).

No EPR *L* signal has been observed with SG0, nor with FP0, SG0U and FP0U. By contrast, both SG1 (Fig.1(a)) and SG1U (Fig.1(b)) showed a *L* feature, though the latter showed a *g* value higher than the former. FP samples behaved in a different way. In fact, the EPR signal was noticed with FP1U (Fig.1(c)), but not with FP1. The former was characterised by a *g* value comparable to that measured with SG1U and higher than that of SG1.

Therefore, *L* does not appear with pure mono-phasic perovskite-like $La_{1-x}Ce_xCoO_3$ samples. It appears only when La_2O_3, CeO_2 and Co_3O_4 or similar species form in them, due to catalytic use (as with FP1U) and/or to the preparation method (as with SG1U and SG1).

Indeed, a $g \cong 2$ Lorentzian-shaped L line has been noticed since long time with Co_3O_4 [8, 9] and its origin has been described satisfactorily [10]. The formation of units like:

$$- O^{2-} - Co^{3+} - O^{2-} \underline{- Co^{2+} - O^{2-} - Co^{3+} - O^{2-} - Co^{2+}} - O^{2-} - \qquad \text{(Scheme 1)}$$
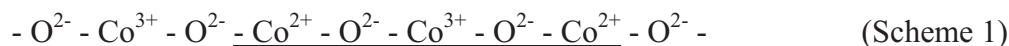
has been hypothesised, in which two Co^{2+} ($3d^7$, S = 3/2) ions, localised in tetrahedral sites, would interact with each other through $O^{2-} - Co^{3+} - O^{2-}$ bridges, Co^{3+} ($3d^6$, S = 0) being localised in an octahedral field. Two sets of units like that underlined in Scheme 1 would form, characterised by antiferromagnetic and ferromagnetic coupling, respectively. The former would possess multiplicity 12, the latter multiplicity 24. Furthermore, polarons would propagate also in Co_3O_4 [9], accounting for broadening of L with increasing temperature. Therefore, the presence of the L line in fresh catalysts marks the presence of Co_3O_4 or, in any case, that of Co^{2+} magnetic ions mixed with diamagnetic Co^{3+} ones. The former, when clustered, could constitute ferromagnetic (FM) domains. These would cause an internal magnetic field in the sample, leading to the increased apparent g value of the used catalysts. Therefore, the L line in fresh samples (as here with SG1) indicates that the reaction (1) has occurred and, therefore, that the sample has lost a part of its oxygen, becoming a worse catalyst. Analogously, the appearance of L after reaction (as here with both SG1U and FP1U) indicates that the catalyst loosed its oxygen through Eq.(1) and that it did not re-oxidize completely. Furthermore, in the latter cases the increased apparent g value suggests also the formation of disordered FM clusters of Co^{2+} and/or other magnetic impurities.

EPR spectroscopy shows then an useful tool to probe the influence of preparation method on performance of these perovskite-like catalysts, as well as to monitor their re-oxidation state after the present catalytic reaction.

References

[1] L.Forni, C.Oliva, F.P.Vatti, M.A.Kandala, A.M.Ezerets, A.V.Vishniakov, Applied Catalysis B: Environm., 7 (1996) 269.

[2] L.Forni, C.Oliva, T.Barzetti, E.Selli, A.M.Ezerets, A.V.Vishniakov, Catalysis B: Environm., 13 (1997) 35.

[3] C.Oliva, L.Forni, A.D'Ambrosio, F.Navarrini, A.D.Stepanov, Z.D.Kagramanov, A.I.Mikhailichenko, Applied Catal.A: General, 205 (2001) 245.

[4] R.Leanza, I.Rossetti, L.Fabbrini, C.Oliva, L.Forni, Applied Catal.B: Environm., 28 (2000) 55.

[5] C.Oliva, S.Cappelli, A.Kryukov, G.L.Chiarello, A.V.Vishniakov, L.Forni, J.Molecular Catal.A: Chemical, 2005, in press.

[6] C.Oliva, L.Forni, P.Pasqualin, A.D'Ambrosio, A.V.Vishniakov, Phys.Chem.Chem.Phys., 1 (1999) 355.

[7] C.Oliva, L.Forni, Catalysis Commun., 1 (2000) 5.

[8] S.Angelov, E.Zhecheva, S.Stoyanova, M Atanasov, J.Phys.Chem. Solids, 51 (1990, 1157.

[9] C.Oliva, L.Forni, L.Formaro, Applied Spectroscopy, 50 (1996) 1395.

[10] W.L.Roth, J.Phys.Chem.Solids, 25 (1964) 1.
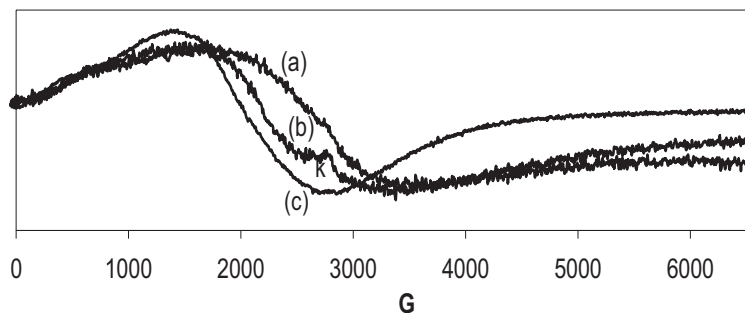
Fig.1   R.T. EPR spectra of some $La_{0.9}Ce_{0.1}CoO_3$. Samples (a) SG1, (b) SG1U, (c) FP1U. (a) and (b): Intensity x 3; k is a bump due to the instrument cavity, and not to the sample.
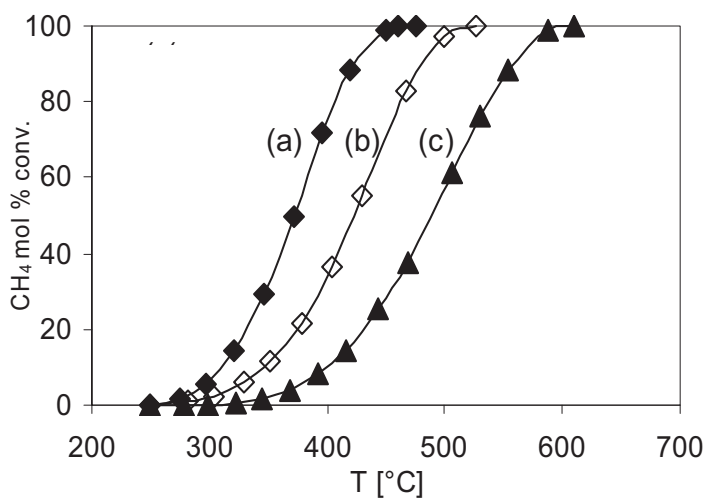
Fig.2   Activity of $La_{0.9}Ce_{0.1}CoO_3$ for CFC of methane: (a) fresh FP1; b) FP1 after three deactivation cycles (activity decreases significantly only after the first cycle); (c) SG1: activity curves are identical for fresh sample and after three deactivation cycles.
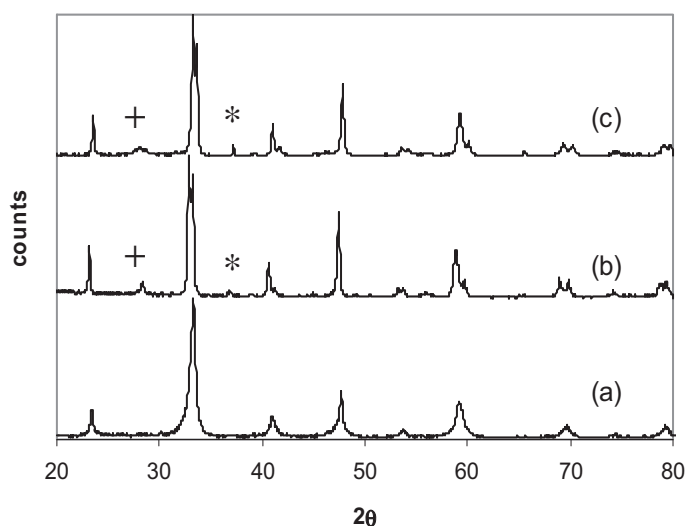
Fig.3   XRD of $La_{0.9}Ce_{0.1}CoO_3$: (a) FP1, (b) FP1U, (c) SG1. (*) Co_3O_4; (+) CeO_2 phases.

FUNGICIDE (FUNAC-S) TECHNOLOGY USING
THE PHASE-TRANSFER CATALYSIS METHOD

Z.P. Pai and **B.M. Khlebnikov**

Boreskov Institute of Catalysis SB RAS, Prosp. Akad. Lavrentieva, 5, Novosibirsk 630090

Russia, Fax: +7(383) 330 8056 E-mail: zpai@ catalysis.nsk.su

The prospects for the sulfur production speed-up in Russia (2006) are estimated at 6.5 million tons, which is associated with the development of gas-processing, oil-refining and metallurgy industries. Besides, more rigid ecological standards on sulfur emissions into the atmosphere [1] can become a cofactor of the sulfur output increase.

However, taking into account the fact that sulfur is not highly profitable commodity, as compared to oil products, it is reasonable and commercially viable to develop and commercialize new sulfur-processing technologies providing an increase in the production of agrichemicals.

In this work we report on the development of a new agrochemical micro-structured composite FUNAK-S. To develop a pesticides composite, one should prepare a water-soluble emulsion containing elemental sulfur (by product of the gas-production, oil-refining, by-product-coking and metallurgy industries) as the main initial component. In order to improve functional properties of the product, we added to the mixture a number of ammonium salts of lignin sulfonic acids (wood residue) and ameliorant (a special additive), acting as a phase-transfer catalyst. Adding the phase-transfer catalyst, it is possible to prepare sulfanmonosulfonic acids, which provide both stabilization of the resulting colloidal system and improve its acaricide activity.

On the development of a reactor, we used a number of unique technical solutions, which permit one to reduce the process time by integrating several technological steps; to improve the quality of the resulting product due to formation of particles <1 micron in size, the yield being 80%. Note that the best analogue-prototypes contain 70-80% of granules 6 micron in size and 20-30%, 12 micron in size [2].

«FUNAK-S» is a multipurpose chemical because of its fungicidal, acaricidal and insecticide properties. Using the "FUNAK-S", it is possible to

a) increase activity due to formation of sulfur-containing acids, which improve stability of the suspension with time;

PP-54

b) improve LD_{50} indexe (the corresponding dose or concentration of the solution that provide demise of 50% of organisms) with respect to analogues by not less that two times;

c) increase selectivity and persistence (ability to preserve in the surrounding for some time and to keep biological activity).

In contrast to the known pesticides, «FUNAK-S» does not enter plant fruits!

The product can be manufactured as powder or paste with the moisture up to 15-20%. For treatment of plants, one should prepare a solution: 10-20 g of FUNAK-S per 10 L of water.

References

1.   www/rcc/ru/Rus/Chemicals/
2.   kagol.chat.ru/garden/prilov.htm

SYNTHESIS OF EPOXIDE COMPLEXES FROM RENEWABLE RAW MATERIALS

Z.P. Pai, Yu.V. Sapegina, N.V. Selivanova, T.B. Khlebnikova, A.G. Tolstikov

Boreskov Institute of Catalysis SB RAS, Pr. Ak. Lavrentieva, 5, Novosibirsk 630090 Russia

Fax: (383) 330-80-56, E-mail: july@catalysis.ru

Utilization of renewable raw materials, such as industrial wood residue, offers possibilities of manufacturing of epoxy compounds of commercial value. The field of application of epoxides is rather wide. Epoxides are efficient plasticizers (modifiers, stabilizing agents and diluents) of plastics and epoxy resins as well as precursors in the synthesis of different pharmaceutical products. One of the most promising processes for preparing of epoxides from raw materials is the method of phase-transfer catalysis, providing direct oxidation of different organic substrates in the presence of peroxopolyoxotungstate based catalysts [1].

The present work reports screening of substrates of different nature (unsaturated aliphatic compounds, terpenoids and coumarins) in the reaction of oxidation in a two-phase solution in the presence of methyltri-*n*-octylammonium tetrakis(oxodiperoxotungsto)phosphate.

It was established that epoxidation of oleic (**1**), ricinoleic (**2**) acids and their ethers (**3, 4**) (scheme 1) provides 90 % selectivity with respect to epoxide.

Scheme 1.

1, 2, 3, 4

H_2O_2
$[Cat]$

5, 6, 7, 8

1, 5 - R^1, R^2 = H
2, 6 - R^1 = H, R^2 = OH
3, 7 - R^1 = CH_3, R^2 = H
4, 8 - R^1 = CH_3, R^2 = OH
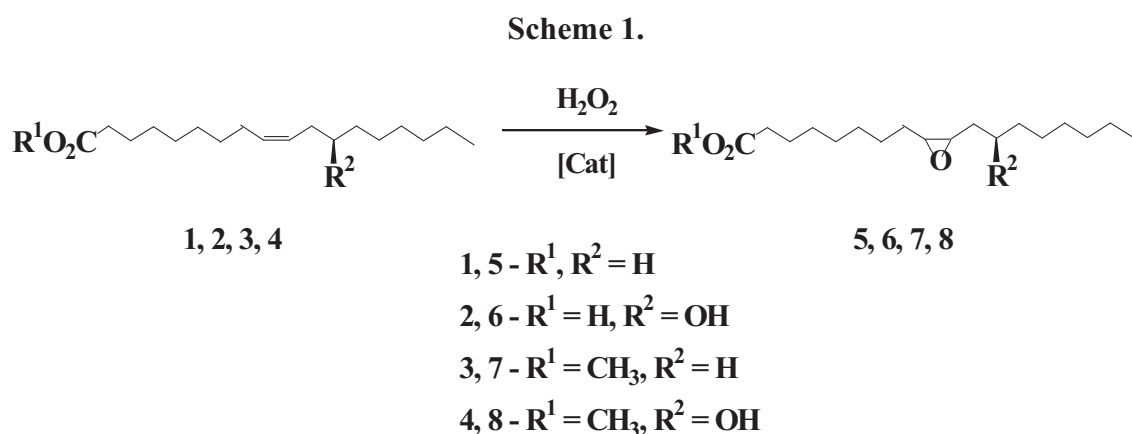
Epoxidation of coumarins was performed using peucedanin (**9**) as an example. It was oxidized to yield unstable epoxide (**10**), which transforms into ketol hydroxyoreozelon (**11**) under reaction conditions (Scheme 2).

Scheme 2

        9   **10**   **11**
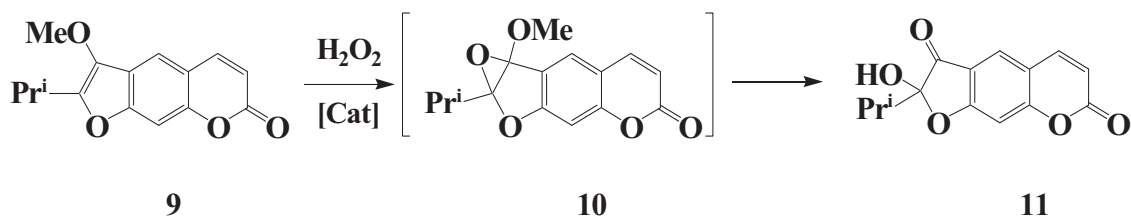
The process of oxidation of natural terpenoids (such as betulin isolated from birch bark) results in the formation of a number of products, including epoxide, the yield of which is not higher than 30 %. By contrast, the oxidation of betulin diacetate (**12**) provides 90% selectivity with respect to epoxide (**13**).

Scheme 3

        12   **13**
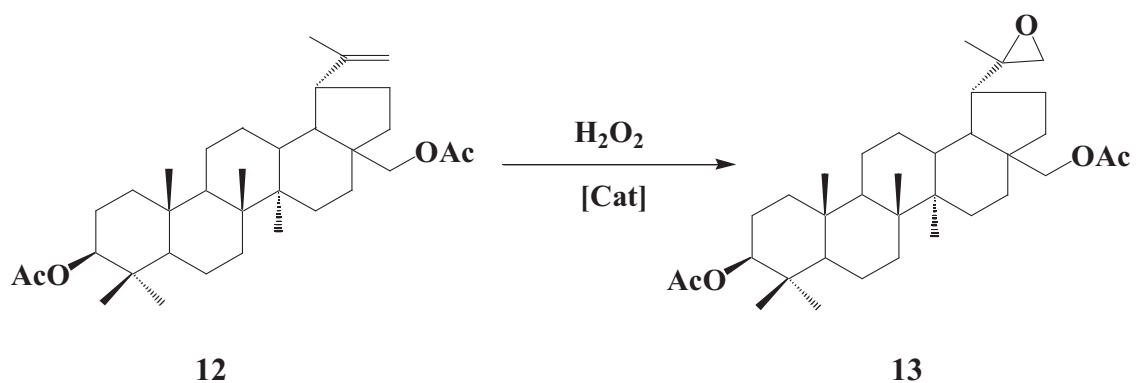
Since the above betulin derivatives exhibit antiphlogistic, antiviral and antineoplastic activity, they are of profound interest for medicinal chemistry [2].

References

1. Z.P.Pai, A.G. Tolstikov, P.V. Berdnikova, G. N. Kustova, T.B. Khlebnikova, N.V. Selivanova, A.B. Shangina, and V.G. Kostrovskii// Russian Chemical Bulletin, International Edition, 2005, **54**, 8, P. 1847-1854.

2. Achrem-Achremowicz J., Janeczko Z. Betulin – a pentacyclic triterpene // Wiadomosci Chemiczne, 2003, **57**, 3-4. P. 223-246.

WATER-GAS SHIFT ACTIVITY OF DOPED Pt/CeO$_2$ CATALYSTS

P. Panagiotopoulou[1], J. Papavasiliou[1,2], G. Avgouropoulos[2], T. Ioannides[2],

D.I. Kondarides[1]

[1] Department of Chemical Engineering, University of Patras, GR-26504 Patras, Greece

[2] FORTH/ICE-HT, GR-26504 Patras, Greece

Fax:+30-2610-965223, e-mail: jpapav@iceht.forth.gr

1. Introduction

Conventional low-temperature (Cu/ZnO/Al$_2$O$_3$) and high-temperature (Fe$_3$O$_4$/Cr$_2$O$_3$) water-gas shift (WGS) catalysts cannot be used in power generation systems for transportation and residential fuel cell applications due to restrictions related to their volume and weight and also due to the requirements for reduced start-up times, durability under steady state and transient conditions and stability to condensation and poisons [1,2]. Catalyst formulations based on cerium oxide seem to be promising alternatives [3-5], exhibiting activity comparable to that of Cu/ZnO/Al$_2$O$_3$ catalysts [5]. However, most ceria-supported noble metals are not sufficiently stable under conditions typical of a reformer outlet [6] and progressively deactivate, possibly due to irreversible reduction of the support [6] and/or sintering of the dispersed metallic phase [7]. As a result, efforts are made to further increase catalytic activity and to improve structural stability of ceria-supported noble metal catalysts.

In our previous studies [8,9] it was shown that the WGS activity of supported noble metals depends strongly on the nature and physicochemical characteristics of the support. In particular, it was found that activity is significantly improved when the noble metal is supported on "reducible" rather than on "irreducible" metal oxides [9]. In the present study, we report on the WGS activity of Pt catalysts supported on metal (Me)-doped cerium oxide prepared by the urea-nitrate combustion method [10]. The catalytic performance of these Pt/Ce-Me-O catalysts is investigated with respect to the physicochemical characteristics of the support, in particular reducibility and primary crystallite size of ceria.

2. Experimental

Metal-promoted cerium oxide supports were synthesized by the urea-nitrates combustion method [10] by mixing the nitrate salt of the promoter [Me(NO$_3$)$_z$·XH$_2$O] (Me: Yb, Gd, Zr, Mg, La, Ca, Y, Zn) with cerium nitrate [Ce(NO$_3$)$_3$·6H$_2$O] and urea (CH$_4$N$_2$O) in appropriate molar ratios (Me/(Me+Ce) = 0.10, 75% excess of urea). In order to obtain pure,

well-crystallized supports, the resulting powders were calcined in air at 550°C for 1 h. Catalysts were prepared employing the wet impregnation method with the use of the above promoted cerium oxide powders and $(NH_3)_2Pt(NO_2)_2$ (Alfa) as a platinum precursor salt.

Materials were characterized with respect to their specific surface area, primary crystallite size of the support and platinum dispersion, employing nitrogen physisorption at the temperature of liquid nitrogen (BET method), X-ray diffraction (XRD) and selective chemisorption of CO, respectively. Temperature-programmed reduction (TPR) experiments were performed under a flow of a 3% H_2/He mixture (50 cm^3 min^{-1}) over 200 mg of preoxidized catalyst using a heating rate of 10°C/min. The catalytic performance for the WGS reaction was investigated in the temperature range of 100-550°C using a feed stream consisting of 3%CO and 10%H_2O (balance: He, total flow: 150 cm^3/min, m_{cat}= 75 mg). Measurements of intrinsic rates were obtained under differential reaction conditions. Details on the techniques and methods employed can be found elsewhere [8].

3. Results and discussion

Results of catalyst characterization are summarized in Table 1. It is observed that doping results in a substantial increase of the BET surface area, compared to that of undoped Pt/CeO$_2$, which is accompanied by a parallel decrease of the primary crystallite size of ceria.

Table 1. *Results of catalyst characterization and of kinetic measurements obtained from the 0.5%Pt/(Ce-Me-O) catalysts investigated.*

Promoter (Me)	S_{BET} ($m^2.g^{-1}$)	d_{CeO2}(*) (nm)	Pt dispersion (%)	Rate at 250°C ($\mu mol.s^{-1}.g^{-1}$)	TOF at 250°C (s^{-1})	Activation Energy ($kcal.mol^{-1}$)
Yb	41	7.9	40	13.1	1.28	18.8
Gd	42	9.4	52	11.1	0.83	20.5
Zr	27	11.0	100	10.7	0.42	19.9
Mg	33	10.2	58	10.1	0.68	20.4
La	50	8.9	73	9.65	0.52	19.2
Ca	43	8.0	45	6.22	0.54	20.9
Y	28	11.2	48	5.21	0.42	20.5
Zn	20	15.5	37	1.33	0.14	20.0
Undoped	8	18.5	46	6.53	0.55	18.2

(*) *Primary particle size of CeO$_2$ determined by XRD line broadening.*

XRD patterns obtained from the Pt/Ce-Me-O catalysts are shown in Fig. 1. It is observed that the diffraction peaks of ceria in the doped samples are shifted towards higher or lower diffraction angles, compared to that of the undoped catalyst. This depends on the ionic radius of the dopant cation and implies that the dopant cation is incorporated in the ceria lattice.
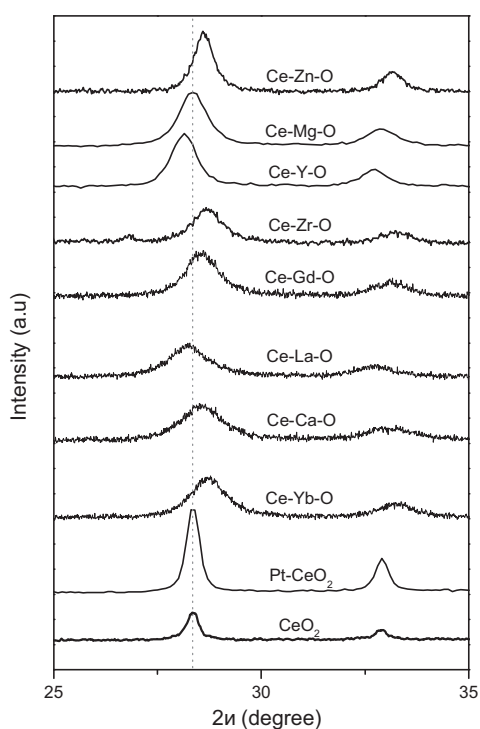
Figure 1. XRD profiles of Pt/Ce-Me-O catalysts.
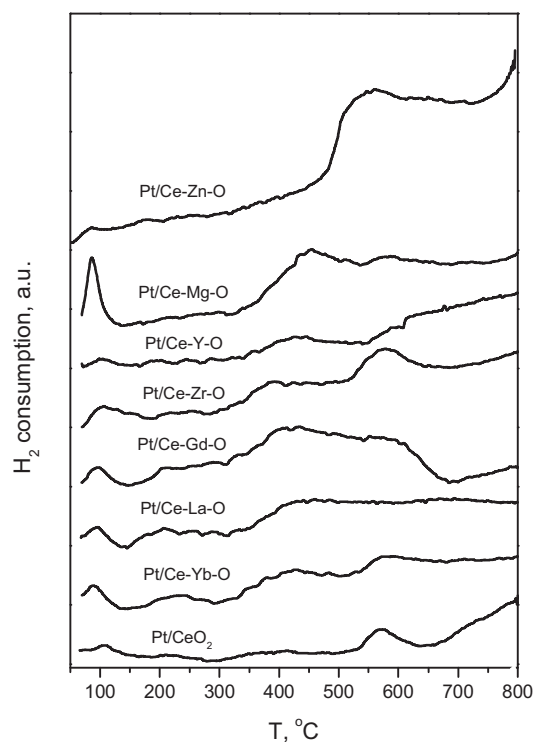
Figure 2. TPR profiles of Pt/Ce-Me-O catalysts.

The TPR profiles (Fig. 2) of Pt/Ce-Me-O catalysts are characterized by features at high ($>600^{o}$C) and low ($<150^{o}$C) temperatures, assigned to reduction of bulk ceria and platinum oxide, respectively, and by broad peaks at intermediate temperatures (200-600°C), attributed to the Pt-catalyzed reduction of the surface cell of ceria. The amount of H_2 consumed during TPR is larger for doped catalysts, indicating that doping enhances the reducibility of ceria.

Results of catalytic performance tests are presented in Fig. 3. It is observed that doping of Pt/ceria with Ca (line 3), Gd, Mg, La (line 2) and, especially, Yb (line 1) results in a shift of the conversion curves toward lower reaction temperatures, compared to the one of the unpromoted catalyst (line 4). Similar was the effect of addition of Zr, which gave a conversion curve located between lines 1 and 3 (not shown for clarity). In contrast, doping with Y (line 5) and Zn (line 6) results in a decrease of catalytic activity, which is much more pronounced for the latter sample.

Results of kinetic experiments (Table 1) show that the apparent activation energy (E_a) of the WGS reaction does not vary significantly, taking values between 18 and 21 kcal.mol^{-1} for all samples investigated. In contrast, the specific reaction rate (per gram of catalyst) depends strongly on the nature of the promoter, following the order of Yb> Gd> Zr> Mg> La> Ca> CeO$_2$(undoped)> Y> Zn, with the Yb-promoted catalyst being about one order of

magnitude more active than the Zn-promoted one, at 250°C. Comparison with the TPR results of Fig. 2 shows that a general correlation between catalyst activity and ceria reducibility does not exist.
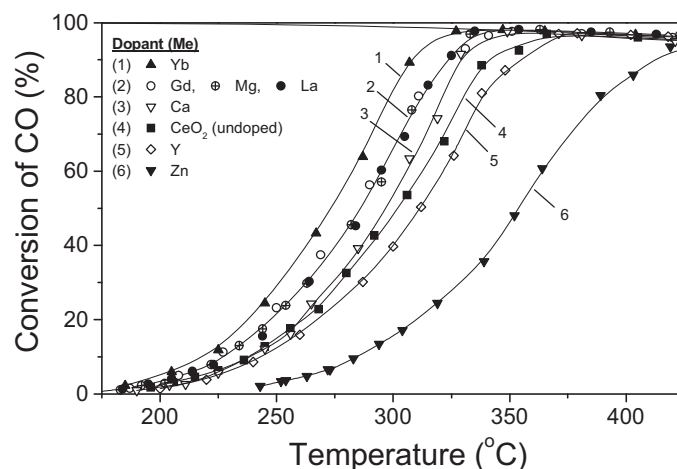
Figure 3. Catalytic performance of the indicated 0.5%Pt/(Ce-Me-O) catalysts for the WGS reaction.

4. Conclusions

The WGS activity of Pt/Ce-Me-O catalysts depends strongly on the nature of the dopant employed, following the order of Yb> Gd> Zr> Mg> La> Ca> CeO_2(undoped)> Y> Zn, with the Yb-promoted catalyst being about one order of magnitude more active than the Zn-promoted one at 250°C. Although ceria becomes more reducible upon doping, the enhanced reducibility does not seem to be the only factor influencing activity in doped catalysts.

References

1. A.F. Ghenciu, Curr. Opin. Solid State Mater. Sci. 6 (2002) 389.

2. J.M. Zalc and D.G. Löffler, J. Power Sources 111 (2002) 58.

3. T. Bunluesin, R.J. Gorte, Appl. Catal. B 15 (1998) 107.

4. Y. Li, Q. Fu, M. Flytzani-Stephanopoulos, Appl. Catal. B 27 (2000) 179.

5. Q. Fu, H. Saltsburg and M. Flytzani-Stephanopoulos, Science 301 (2003) 935.

6. J.M. Zalc, V. Sokolovskii, D.G. Löffler, J. Catal. 206 (2002) 169.

7. T. Bunluesin, R.J. Gorte, G.W. Graham, Appl. Catal. B 15 (1998) 107.

8. P. Panagiotopoulou, D.I. Kondarides, J. Catal. 225 (2004) 327.

9. P. Panagiotopoulou, D.I. Kondarides, Catal. Today, in press.

10. G. Avgouropoulos, T. Ioannides, Appl. Catal. A 244 (2003) 155.

MESOPOROUS ZrO$_2$-TiO$_2$-Y$_2$O$_3$ FOR FUEL CELLS APPLICATIONS

<u>**V. Parvulescu**</u>[a], **N. Cioatera**[a], **S. Somacescu**[a], **G. Telipan**[b], **M. Ignat**[b],

B.G. Albu[c] **and B.L. Su**[d]

[a]*Institute of Physical Chemistry, Spl. Independentei 202, Bucharest, Romania*

e-mail:vpirvulescu@chimfiz.icf.ro

[b]*Rcesearch Institute for Electrical Engineering-Advanced Research, Bucharest, Romania*

[c]*Research Center for Macromolecular Materials and Membranes, Bucharest, Romania*

[d]*Laboratoire de Chimie des Matériaux Inorganiques, The University of Namur (FUNDP),*

61 rue de Bruxelles, B-5000 Namur, Belgium

ABSTRACT: Y$_2$O$_3$-ZrO$_2$, Y$_2$O$_3$-TiO$_2$ and Y$_2$O$_3$-TiO$_2$-ZrO$_2$ oxides with various composition, structure and morphology were prepared using a surfactant templating strategy. The obtained binary and ternary oxides were characterized by XRD, TEM and SEM microscopies, adsorption and N$_2$ desorption of. Characterization revealed that the mesoporous powder, calcined at 873 K was weakly agglomerated and had a high surface area.

INTRODUCTION

Zirconia based ceramics have been widely used for several advanced and structured applications such as solid-oxide fuel cells (SOFC), gas sensors and automotive [1-3]. One of the most successful semiconducting oxygen sensors in automotive application is the TiO$_2$. For these applications it is desirable to control the porosity of the materials to obtain a homogeneous structure and a good packing of powders. Colloidal processing is accepted as an ideal route [4, 5]. These materials must be able to operate in harsh conditions, such as high temperature and the presence of aggressive gases. One of the possibilities to operate at lower temperatures is the introduction of the porosity by the preparation of nanoscaled materials. Here we describe and discuss the synthesis and characterization of mesostrucured yttria-zirconia and yttria-titania-zirconia with 8 wt. % yttria. The mesoporous oxides are obtained as materials for anode in SOFC applications.

MATERIALS AND METHODS

Y$_2$O$_3$-ZrO$_2$, Y$_2$O$_3$-TiO$_2$ and Y$_2$O$_3$-TiO$_2$-ZrO$_2$ were synthesized by two methods using sol-gel procedure. The surfactant used in the first method was cetyltrimethhylamonium bromide-CTAB and in the second poly(alkylene oxide) block copolymer-Pluronic. The reagents used as precursors were zirconium propoxide or ZrCl$_4$, titanium isopropoxide or

$TiCl_4$ and $Y(NO_3)_3 \cdot 6H_2O$. In the first method the oxides were obtained by partial hydrolysis of alkoxides in the presence of water resulting from an esterification reaction between propylic alcohol and acetic acid. The sols with various $ZrO_2/TiO_2/Y_2O_3$ molar ratios were mixed with CTAB solution in alcohol. In the second method the solutions of inorganic precursors were added with vigorous stirring in to block copolymer alcoholic solution. The resulting sol solution was gelled at 313 K in air for hydrolysis and polymerization of the inorganic precursors. The gels were supported by dip coating method on CeO_2-Ta_2O_5 support (Φ=1.0 mm, h=10 mm), dried at 373 K and calcined at 873 K. The obtained powders and films were characterized by XRD, TEM and SEM microscopy and N_2 adsorption-desorption.

RESULTS AND DISCUSSION
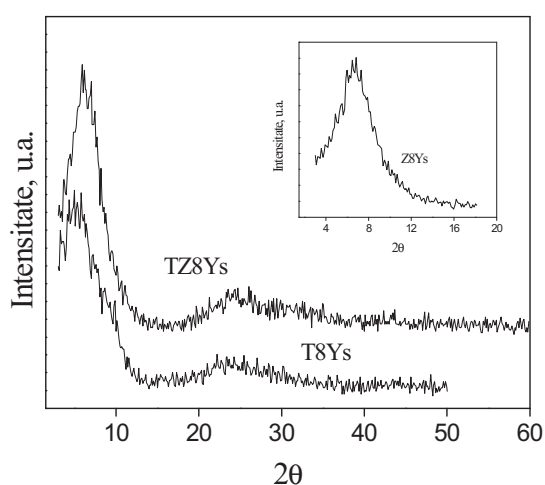
Fig. 1. XRD patterns of binary and ternary oxides

XRD patterns of Y_2O_3-ZrO_2, Y_2O_3-TiO_2 and Y_2O_3-TiO_2-ZrO_2 materials reveal the presence of amorphous phase with a mesoporous structure (Fig.1). The low-angle diffraction indicates that mesoscopic order is preserved in the calcined oxides. This is confirmed by nitrogen adsorption-desorption isotherms (Fig.2) and transition electron microscopy (TEM) images (Fig.3). The isotherms of the calcined samples obtained by the first method (Fig.2) are typical for the mesoporous materials with narrow pore distribution. The isotherms of the samples obtained by the second method exhibit distinct hysteresis loop in the P/Po ranging from 0.4 to 0.9, typical for the mesoporous materials with larger pore distribution. This binary and ternary mesoporous materials display a high surface area (134-182 m^2/g). The mesoporous structure is stable up to 873 K for the oxides obtained by the first method. The samples obtained by the second method are more stable. The evolution of the mesoporous structure was examined by TEM and SEM for the samples calcined at 873 K and 973 K. In Fig. 3 are clearly observed the ordered array. For the formation of low-densified Y_2O_3-TiO_2-ZrO_2 oxides from mesoporous powder, at higher temperature, it may consider that the mesopores grew into larger connected channel during calcination and sintering process.
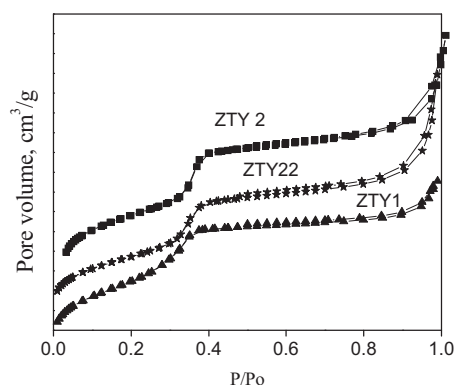
Fig. 2. N$_2$ adsorption-desorption isotherms of the powders obtained by the method 1
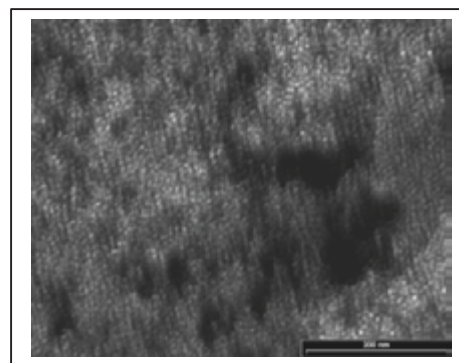
Fig. 3. TEM images of ZTY22 sample

A **B**
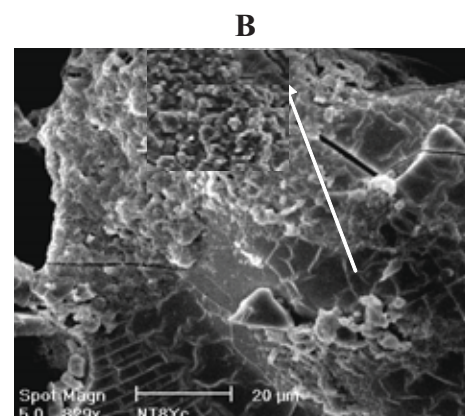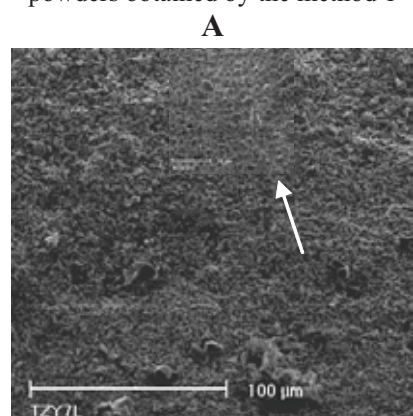
Fig. 4. SEM images of ZTY22 oxide film (A) and powder (B)

The morphology of binary and ternary powders and films are typically for the mesoporous materials. Figures 4 presents SEM images of Y$_2$O$_3$-TiO$_2$-ZrO$_2$ film (A) and powder (B) obtained by the first method.

The mesoporous powders obtained by the second method are weakly agglomerated and all the films obtained are very homogeneous. Such materials with open structure may be used as the skeleton of SOFC electrodes in order to reduce the concentration polarization. Further coming, mesoporous Cu-CeO$_2$-YTZ and Ni-YTZ anodes will be prepared by this method and its effect on the concentration polarization will be investigated.

CONCLUSIONS

The nanocrystalline mesoporous oxides with Y$_2$O$_3$, TiO$_2$, ZrO$_2$ oxides were prepared using CTMA or block copolymer as surfactants. The obtained oxides are mesoporous materials with high surface area and highly stable structure.

REFERENCES

1. R.J. Gorte, J.M. Vohs, S. McIntosh, Solid State Ionics, 175 (2004) 1.
2. S.D. Kim, S.H.H. Yun, J. Moon, J-H. Kim, R.H. Song, J. Power Sources 139 (2005) 67.
3. C-W. You, Y-H. Lee, K-Z. Fung, M-C. Wng, J. Non-Crystal. Solids, 351 (2005) 304.
4. N. McN. Alford, J.D. Birchall, K. Kandall, Nature, 330 (1987) 51.
5. J. Zhang, F. Ye, J. Sun, D. Jiang, M. Iwasa, Colloid Surf. A Physicochem Eng. Aspects, 254 (2005) 199.

PP-58

BENZENE TO PHENOL OXIDATION ON TRANSITION METALS INCORPORATING MESOPOROUS SILICAS

V. Pârvulescu[a], S. Todorova[b], G. Kadinov[b], K. Tenchev[b], Cr. Tablet[a] and B.L. Su[c]

[a]*Institute of Physical Chemistry, Spl. Independenței 202, FAX: 402131*

vpirvulescu@chimfiz.icf.ro, R-060021 Bucharest, Romania

[b]*Institute of Catalysis, Bulgarian Academy, Acad. G. Bonchev St., Block 11, Sofia, Bulgaria*

[c]*Laboratoire de Chimie des Matériaux Inorganiques, ISIS, The University of Namur (FUNDP), 61 rue de Bruxelles, B-5000 Namur, Belgium*

ABSTRAC: Mono- (Ti, V, Cr, Mn, Fe, Ni, Cu) and bimetallic (V-Ti, V-Co, V-Cu, Cr-Ni, Cr-Ru, Ni-Ru, Cu-Ru)- MCM-41 molecular sieves, obtained by hydrothermal synthesis, are active in selective oxidation of benzene to phenol. Benzene hydroxylation temperature and time were varied from 293 to 343K and from 12 to 48 h, respectively. The incorporation of the second metal increases the activity of the Me-MCM-41 catalysts. The effects are significantly for V on Ti and Co and Ru on Cu containing molecular sieves. The main reaction product is phenol. Leaching for the ruthenium and chromium was only evidenced.

INTRODUCTION

The oxidative hydroxylation of aromatic compounds is a very attractive way to produce phenol by one-step oxidation of benzene [1, 2]. A new process to produce phenol without by-product and with high selectivity has therefore been explored, under mild conditions, by catalytic hydroxylation of benzene over transition metal or transition metal complex containing micro/mesoporous materials [3, 4]. The common feature of these biomimetics reactions is activated species with oxygen. Of the environmentally benign materials, hydrogen peroxide is the most attractive for hydroxylation reactions realized at small-scale procedures [5].

In this paper, direct hydroxylation of benzene with hydrogen peroxide on mono- and bimetallic MCM-41 mesoporous molecular sieves was investigated. Especially, improvement of the catalytic activity was explored by incorporation of the second metal (another 3d transition metal or ruthenium) into MCM-41 network.

EXPERIMENTAL

The mono- and bimetallic MCM-41 molecular sieves were prepared by hydrothermal treatment [4,6] on the basis of molar gel composition of 1.0 SiO_2: x M: 0.48 CTMAB: 0.28

Na$_2$O: 3.7 TMAOH: 222.0 H$_2$O (where x= 0.02-0.1 for M= Co, x= 0.02 for M=Ti, V, Cr, Mn, Fe, Ni, Cu, and x= 0.04 for M=V-Ti, V-Co, V-Cu, Cr-Ni, Cr-Ru, Ni-Ru, Cu-Ru with M$_1$/M$_2$ molar ratio=1). The solid products were recovered by filtration, washed, dried in air at 373 K and calcined in a flow of N$_2$ followed by air at 823 K. The obtained materials and the metal states were characterized by XRD, N$_2$ adsorption/desorption, SEM and TEM microscopy, TPR, XPS and DRS methods.

Phenol hydroxylation experiments were run in a glass reactor equipped with a reflux condenser and a magnetic stirrer. The reaction temperature and time varied from 293 to 343 K and from 12 to 48 h, respectively. The molar ratio of phenol /hydrogen peroxide was 1/3. After reaction, the catalyst was separated by centrifugation and the oxidation products were analyzed on gas chromatography. The catalysts were reutilized in the oxidation reactions and characterized after each utilization. Hydrogen peroxide consummation was determined by iodometric titration and metal ions leaching were also verified.

RESULTS AND DISCUSSION

The activity, at 323 K, of monometallic redox molecular sieves and the effect of ionic ratio on the conversion of benzene are presented in Figure 1. A higher conversion was obtained for the cation with lower $R_{M(n+)}/R_{O(2-)}$ ratio. A comparison of the XRD patterns and the cell parameter a$_0$ (calculated from a$_0$ =2d$_{100}$(3)$^{-1/2}$), for the obtained monometallic samples, show a highly ordered and stable hexagonal phases when the oxidation state of the cation, introduced during synthesis, is favorable for a tetrahedral coordination and the $R_{M(n+)}/R_{O(2-)}$ ratio varies between 0.3 and 0.5. Conversion of benzene to phenol increases with the quantity of the incorporation of the metals in the silica framework (see Fig. 1) for different values of $R_{M(n+)}/R_{O(2-)}$ ratio). The highly ordered array of MCM-41 molecular sieves and metal state are modified with metal loading and activity increase. The maximum activity was obtained al 7.4 % Co. In the low loaded Me-MCM-41 catalysts the metal is in one oxidation state in tetrahedral position. The increase in the metal content results in the appearance of the oxide extra-framework phase. Increasing of the metal loading changes the ratio between two kinds of the metal: extra-framework and in the framework (Fig.2). The high can be favorable to the homolyticaly decomposition of H$_2$O$_2$ and the reaction of the hydroxyl radicals with benzene.
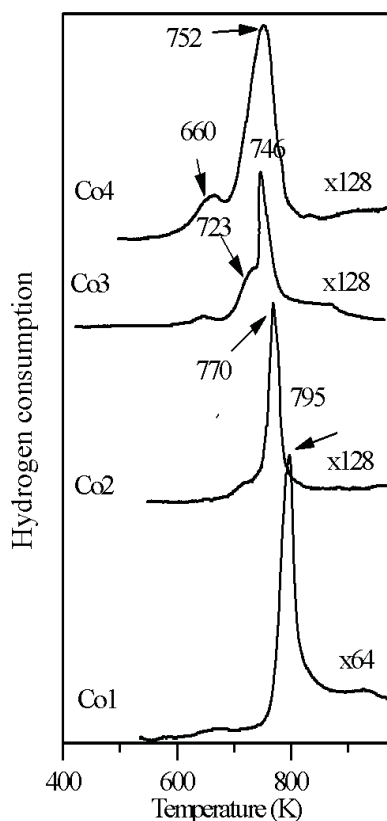
Fig. 1. Effect of transition metal modification and ionic ratio on the conversion of benzene
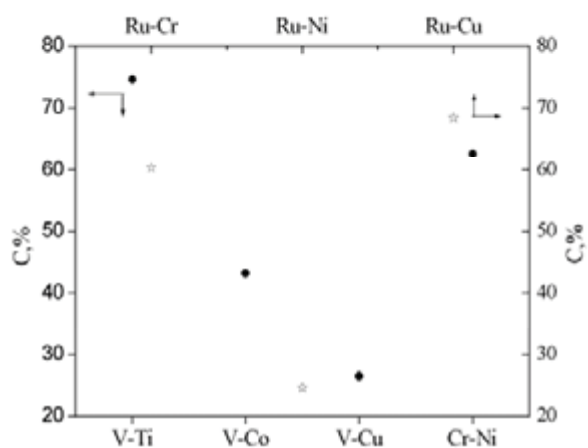
Fig. 2. Variation of TPR profiles with loading of cobalt
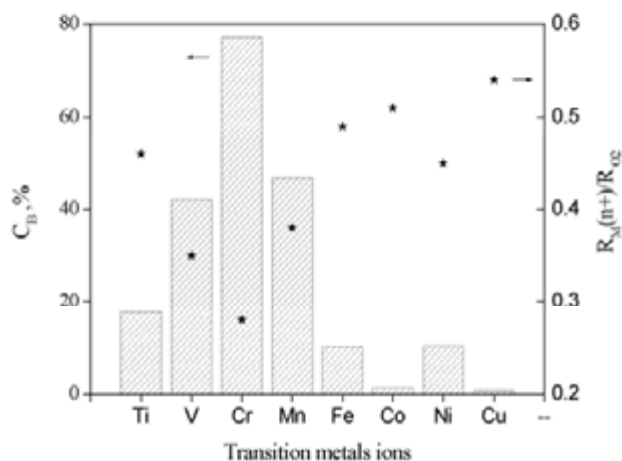
Fig. 3. Effect of the second metal on the conversion of benzene to phenol

In the reaction of benzene oxidation the conversion on the monometallic cobalt catalysts increased with the cobalt content. As is mentioned above, several oxide phases and Co_3O_4 are formed in the samples with high cobalt content. It is possible that the key factor in the benzene oxidation with hydrogen peroxide on the cobalt modified catalyst to be the formation of cobalt oxide interacting weakly with the siliceous framework.

The longer induction period of the catalysts was modified by changing the addition method for H_2O_2. The second metal increases the activity of the Me-MCM-41 catalysts. The effects are significantly for V on Ti and Co and Ru on Cu containing molecular sieves (Fig.3). The main reaction product is phenol and selectivity to phenol is high for all the catalysts.

The effect of reaction temperature was also evidenced. The selectivity to phenol is lower for all the catalysts with Cr. Leaching for the ruthenium and chromium was only evidenced.

CONCLUSIONS

XRD patterns of the monometallic samples show a highly ordered and stable hexagonal phase. The monometallic samples form several oxide phases, which differ in their interaction with the support and are placed outside the molecular sieve framework. A higher conversion was obtained for the cation with lower $R_{M(n+)}/R_{O(2-)}$ ratio. Conversion of benzene to phenol increases with the quantity of the incorporation of the metals in the silica framework. The activity increase with metal content and the maximum value was obtained for Co-MCM-41 catalysts with 7.4 % wt. Co. An increase in cobalt content leads to a decrease in the interaction of CoO phase(s) with MCM-41 and to the appearance of Co^{3+} in Oh symmetry. The second metal increases the activity of redox molecular sieves.

REFERENCES

1. V.Parvulescu, C. Anastasescu, B.L. Su, J. Mol. Catal A Chem ., 211 (2004) 143.

2. J. He, W-P Xu, D.G. Evans, X. Duan and C-Y. Li, Microporous Mesoporous Mat., 44-45 (2001) 581.

3. T. Miyake, M. Hamada, Y. Sasaki and M. Oguri, Appl. Catal. A: Gen. 131 (1995) 33.

4. V. Parvulescu, C. Anastasescu, C. Constantin and B. L. Su, Stud. Surf. Sci. Catal, 142 (2002) 1213.

5. V.van de Velde, I.W.C.E. Arends and R.A. Sheldon, J. Inorg. Biochem., 80 (2000) 81.

6. V. Pârvulescu and B. L. Su, Stud. Surf. Sci. Catal., 143 (2002) 575.

HYDROGEN PRODUCTION BY STEAM REFORMING OF METHANOL OVER GRANULATED AND PLATE-TYPE Cu-BASED CATALYSTS

**S. Pavlova, P. Yaseneva, V. Sadykov, V. Sobyanin, Sukhe, L. Makarshin,
A. Gribovskii, D. Andreev, E. Moroz, E. Burgina**

Boreskov Institute of Catalysis SB RAS, Pr. Lavrentieva, 5, 630090, Novosibirsk, Russia
E-mail: pavlova@catalysis.nsk.su

Steam reforming of methanol is a promising route to produce hydrogen for small solid polymer fuel cells which can be an attractive power source for on-board or portable devices [1]. To develop an effective compact fuel processor, an integrated approach combining the endothermic SRM with the exothermic combustion of methanol or H_2 in the fuel cell anode off-gases is the most promising. Such a system requires the metal-supported catalysts ensuring high thermal conductivity and yet ensuring high yield of hydrogen containing low amounts of CO (not exceeding a few ppm). To miniaturize a fuel processor, microreactors with microchannels are more applicable. Micro-structured reactors ensure high performance especially for periodic operation due to the short residence time, which also allows a quick response to dynamic changes in the inlet conditions [2]. Recently, a number of works concerning this field were published, however, development of effective microchannel catalysts for SRM and the methods of their preparation are still a problem to discuss.

Commercial Cu-Zn-based catalysts supported on plate-type metallic substrates are commonly used for SRM. However, these catalysts have the low thermal and long-term stability especially at temperatures up to 300°C. The catalysts based on mixed oxides of Cu, Ce, Y and Zr were found to be more active and selective for SRM than CuO-ZnO catalysts [3]. In this study, to prepare the mixed oxide catalysts with high activity, selectivity and stability, alumina and Cr were added. Their effect on the SRM performance of the granular mixed oxides and these systems supported on the porous steel plates with microchannels was studied.

Experimental

The urea-nitrate combustion method [4] was used to synthesize pure $Cu_{0.2}Ce_{0.5}Y_{0.2}Zr_{0.1}O_y$ (CCYZ) sample and that with Al_2O_3 and Cr additives. Urea $CO(NH_2)_2$

(doubled quantity as compared with a stoichiometric value) was added to a mixed solution of $Cu(NO_3)_2$ $Ce(NO_3)_3$, $ZrO(NO_3)_2$, $Y(NO_3)_3$ and $Cr(NO_3)_3$ in the appropriate molar ratios. Al_2O_3 powder (10-40 w.%) was added to the mixed solution with urea and then it was steamed until a gel formation followed by calcination in air at 400°C for 3 h. Granular catalysts were prepared by crushing the pressed pellets obtained from a catalyst powder. To obtain plate-type catalysts, steel porous plates (~0.7 mm thickness, 30 mm width and 40 mm length) with microchannels were dipped into alcohol suspension containing a catalyst powder and glycol and treated in the ultrasonic bath followed by drying. The phase composition of the catalysts was characterized using XRD and IR spectroscopy. Granular catalysts were tested in a fixed-bed flow reactor at 250-350°C and GHSV 10000 h^{-1} in N_2:CH_3OH:H_2O=20:40:40%vol. reaction mixture. Plate type catalysts were tested in a brass square microreactor in the feed of CH_3OH:H_2O=1:1 at a liquid rate ~0.1-2 µmol/min. The reaction products were analyzed by GC.

Results and discussion

Phase composition of the catalysts. According to XRD data, in all catalysts, the solid solutions of fluorite structure are present. Though reflections of γ-Al_2O_3 are absent in all XRD patterns, the IR data reveal the presence of γ-Al_2O_3 with a poor crystallinity. Highly dispersed CuO is also present in samples that is verified by XRD, IR and UV–vis spectra. In the Cr-containing catalysts, the chromate also is revealed by IR. The specific surface area (SSA) increases from 30 to 140 m^2/g at increasing alumina content in the range of 10-40%. The addition of Cr favours the increase of SSA up to 170 m^2/g.

SRM activity of the granular catalysts. The methanol conversion and selectivity depend on the catalyst composition and temperature. At all temperatures, addition of Al_2O_3 increases methanol conversion which reaches 86% at 300°C for samples containing 40% Al_2O_3. The incorporation of Cr in the solid solution as well as the increase of Cu-content up to 12% leads to higher methanol conversion. The most effective catalysts comprised of Al_2O_3 and Cr ensure at 300°C the hydrogen production rate ~10 l/h·g$_{cat}$. For catalysts without additives, CO_2 selectivity is 100% at 250-300°C and decreases to 98-98.7% (CO concentration ~0.25-0.3%) at 350°C. For samples containing Al_2O_3 and Cr, CO_2 selectivity decreases at temperatures above 250°C depending on the catalysts composition. Note that formation of CO starts only above 250°C even though this is permitted thermodynamically at much lower temperatures. These results indicate that the reaction sequence is such that CO_2 and H_2 are the primary products of the reaction and

that CO is formed at higher temperatures by the reverse water-gas shift reaction. Addition of Al_2O_3 and Cr ensures a stable performance of the catalysts in SRM (Fig.1).
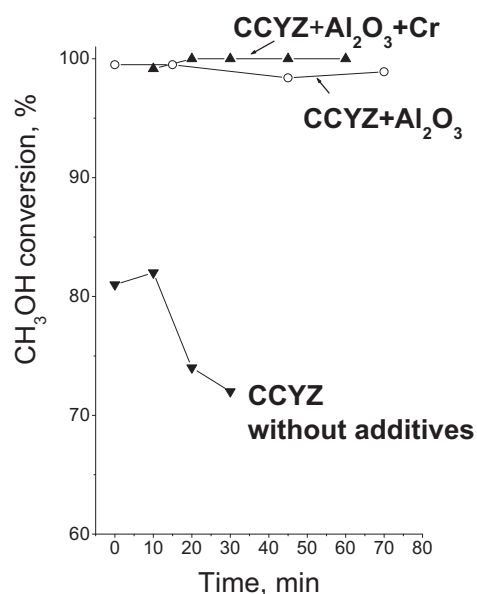
Fig.1. Time dependence of methanol conversion over granular catalysts with different composition. $10000h^{-1}$, 300°C.

Plate-type catalysts. The performance of the powder catalysts supported on plate-substrates differs from that of the pellets. The catalysts with only Al_2O_3 additive show poor hydrogen production, selectivity and stability. The catalysts comprised of both Al_2O_3 and Cr ensure high stability, higher methanol conversion and lower CO concentration as compared with $CuO-ZnO-Al_2O_3$ especially at short contact times (Fig.2).
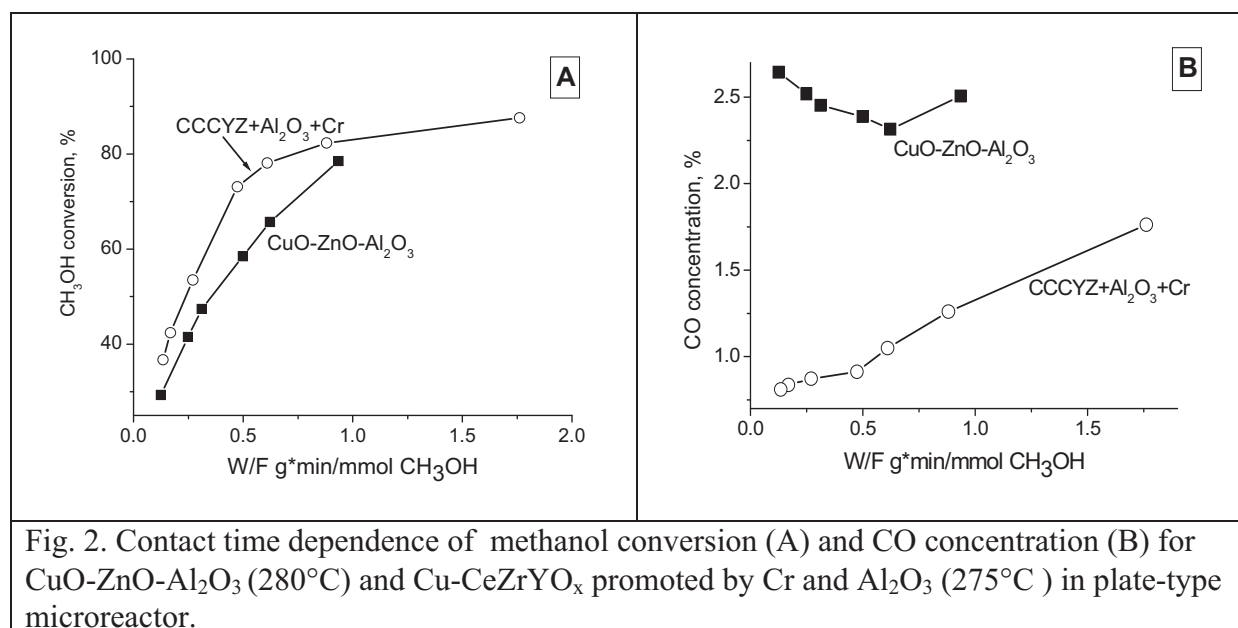
Fig. 2. Contact time dependence of methanol conversion (A) and CO concentration (B) for $CuO-ZnO-Al_2O_3$ (280°C) and $Cu-CeZrYO_x$ promoted by Cr and Al_2O_3 (275°C) in plate-type microreactor.

For all catalysts, the hydrogen production (per gram of the active component) over plate-supported catalysts is less than that for pellet catalysts. Such a difference could be due to various testing conditions for granular and plate-type catalysts. In the latter case, higher methanol and water concentration in the feed could be one reason of the methanol conversion decreasing. Another cause of the catalysts activity decline could be the internal diffusion limitation.

References.
1. D. L. Trimm and Z. I. Onsan, Cat. Rev., 43 (2001) 31.
2. P. Reuse, A. Renken, K. Haas-Santo, O.Gorke, K. Schubert, Chem. Eng. Jour. 101 (2004) 133
3. Y. Liu, T. Hayakawa, K. Suzuki, S. Hamakawa, et.al, Appl. Cat. A 223 (2002) 137.
4. J. Papavasiliou, G. Avgouropoulos, T. Ionnides, Cat. Commun. 5(2004) 231.

PP-60

KINETIC EVALUATION OF CARBON FORMATION IN A MEMBRANE REACTOR FOR METHANE REFORMING

Marisa N. Pedernera, Juliana Piña, <u>Daniel O. Borio</u>

Planta Piloto de Ingeniería Química (UNS - CONICET), Camino La Carrindanga Km. 7, (8000) Bahía Blanca, ARGENTINA. Fax: 0054-291-4861700 Ext: 210/265
E-mail: julianap@plapiqui.edu.ar

Introduction

Methane steam reforming is one of the most important processes for the production of hydrogen and synthesis gas. It may be represented by the reversible reactions (1) to (3).

Deactivation of Ni catalysts by carbon formation is a significant problem in CH_4 reforming, caused by fouling of the Ni surface, blockage of the pores of the catalytic particle and disintegration of the support material [1]. Thermodynamically, the more probable reversible reactions for carbon formation are equations (4) to (6).

$CH_4 + H_2O \leftrightarrow CO + 3H_2$	(1)	*CH_4 Cracking*	$CH_4 \leftrightarrow C + 2H_2$	(4)
$CO + H_2O \leftrightarrow CO_2 + H_2$	(2)	*Boudouard*	$2CO \leftrightarrow C + CO_2$	(5)
$CH_4 + 2H_2O \leftrightarrow CO_2 + 4H_2$	(3)	*CO Reduction*	$CO + H_2 \leftrightarrow C + H_2O$	(6)

When CO_2 is available at large quantities and low costs, it can be used to replace the steam partially (*mixed reforming*) or totally (*dry reforming*). However, the presence of CO_2 augments the risk of carbon formation [1].

An alternative to increase the CH_4 conversion is the membrane reactor (MR), in which the chemical equilibrium is shifted through selective permeation of reaction products. For the CH_4 reforming, the composed membranes constitute an adequate choice due to their high permeation flows and selectivity [2]. However, it has been demonstrated by means of a thermodynamic criterion that the removal of H_2 from the products stream tends to augment the risk of carbon formation [3].

In this work, the risk of carbon formation for a MR is kinetically analyzed and compared with that corresponding to a conventional fixed bed reactor (CR).

Mathematical Model

Figure 1 shows a scheme of the MR under study. It consists in two concentric tubes, an external shell installed in an electric furnace and an internal supported Pd membrane tube. The Ni catalyst is packed in the annular space and a parallel flow configuration is supposed on both sides of the membrane. The reactor geometry is detailed in Table 1.
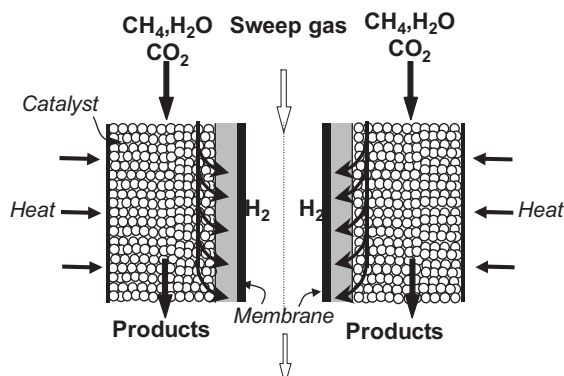
Figure 1: Scheme of the membrane reforming reactor.

To represent the MR, a 1D heterogeneous model is adopted subject to the following assumptions: a) non-isothermal conditions on the reaction side, b) plug-flow, c) isothermal and isobaric conditions for the permeate side, d) ideal membrane (infinite selectivity to H_2) [2, 4]. The intrinsic kinetics reported by Xu and Froment [5] is selected for reactions (1)

to (3). The effectiveness factors are calculated after solving the mass balances inside the catalyst particle [6]. The hydrogen permeance is evaluated using the Sievert Law [2, 4].

Table 1: Geometric parameters and operating conditions used to simulate the CR and MR.

Parameter	Value	Parameter	Value
Reactor length	20 cm [2]	Overall heat transfer coefficient	227 W/m² K [2]
Shell internal diameter	32.6 mm [2]	Furnace temperature	500 ºC [2]
Tube internal diameter	21 mm [2]	Feed flow rate	200 SSCM [2]
Tube external diameter	25 mm [2]	Feed temperature	500 ºC [2]
Catalyst	30% Ni/Al$_2$O$_3$ [4]	Pressure	100 kPa [2]
Diameter/height of pellet	1 / 3 mm [4]	Sweep flow rate	2000 SSCM [2]
Thickness of Pd film, δ	7.5 µm [2]	Sweep gas temperature	500 ºC [2]

The performance of the MR is compared with that of a conventional reactor (CR), which is modeled by assuming the parameters of Table 1 and null H_2 permeation. The trends of the main variables of the MR model were validated against experimental and numerical results from the literature [4]. The net rate of carbon deposition (reactions 4 to 6) is evaluated by means of the kinetic expression reported by Snoeck et al. [7].

$$r_{c,net} = \frac{r_{c,4} + r_{c,(5+6)}}{DEN^2} \qquad (7)$$

The first term of the right-hand side of equation (7) represents the carbon formation by CH_4 cracking and its gasification by H_2 (reaction 4). The second term $r_{c,(5+6)}$ groups the carbon formation by reactions (5) and (6), and its gasification by CO_2 and H_2O. According with this kinetic criterion, if $r_{c,net} \geq 0$ at any axial position along the reactor, carbon deposition occurs.

Results and Discussion

The influence of the CO_2 content in the feed stream is shown in Table 2, where the equilibrium conversion, the outlet conversion for MR and CR and the carbon formation prediction through the kinetic criterion are included. For all the studied operating conditions, the conversion for the MR is higher than that of the CR and even higher than the equilibrium value. For conditions 1 and 2 (high H_2O/CH_4 ratios) carbon formation does not occur in any of the reactors. Conversely, for condition 4 (high CO_2/CH_4 ratio) carbon deposition appears in MR and CR. For condition 3, carbon formation is only predicted in the MR.

Table 2: Influence of the H_2O/CH_4 and CO_2/CH_4 ratios on X_{CH4} and the carbon formation in the CR y MR.

Operating condition	H_2O/CH_4	CO_2/CH_4	X_{CH4}^{eq}	X_{CH4}^{CR}	X_{CH4}^{MR}	(Carbon formation)^{CR}	(Carbon formation)^{MR}
1	2.9	0.1	0.441	0.405	0.477	NO	NO
2	2	1	0.322	0.305	0.389	NO	NO
3	0.9	2.1	0.264	0.247	0.326	NO	YES
4	0.2	2.8	0.283	0.250	0.320	YES	YES

To compare the carbon deposition phenomenon in both reactors, Fig. 2 shows the $r_{c,net}$ curves along the reactor length. As it can be seen, no carbon formation takes place in the CR ($r_{c,net} < 0$ for $r = 0$ and $r = 1$) while in the MR carbon appears from the critical axial position $z_c = 0.117m$ towards the reactor outlet. This behavior can be explained by inspection of Fig. 3. The diminution in p_{H2} caused by the H_2 permeation through the membrane, increases the rate of carbon deposition by CH_4 cracking. Besides, p_{H2O} is lower for the MR as a consequence of the higher CH_4 conversion and the shift to the right of the WGS reaction (2). The lower p_{H2O} values promote carbon formation by CO reduction (reaction 6). As the axial temperature profiles for both reactors are very similar, it is not possible to attribute the differences observed in $r_{c,net}$ to a thermal effect.
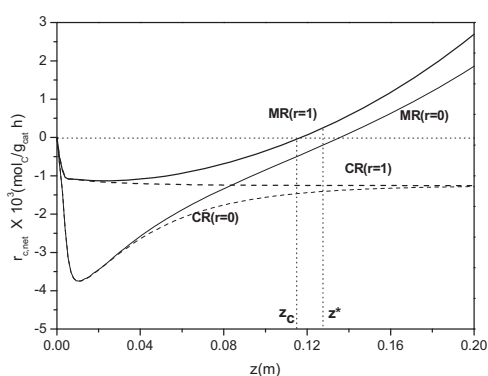
Figure 2: Axial profiles of the net carbon deposition rate in CR and MR (Condition 3 of Table 2). $r = 0$: catalyst surface; $r = 1$: catalyst center.
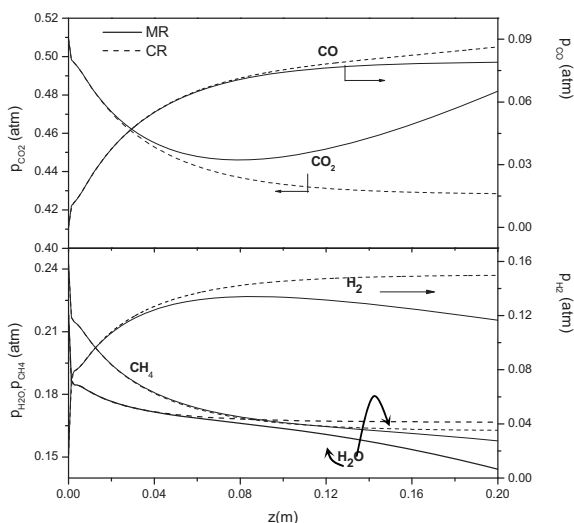
Figure 3: Axial variation of composition for CR and MR (Condition 3 of Table 2).

As it can be seen in Fig. 2, the $r_{c,net}$ values at the particle center ($r = 1$) are higher than those corresponding to the catalyst surface ($r = 0$) for both reactors. For the MR, Fig. 4 shows the rates of carbon formation within the catalyst particle at $z^* = 0.128$m. From the catalyst surface and up to $r = 0.005$m, the rate of carbon deposition by reaction (4) is lower than the rate of carbon gasification by reactions (5) and (6), thus $r_{c,net}$ is negative. From this radial position to the particle center, the model predicts carbon formation. This result is a consequence of the composition profiles within the catalyst (see Fig. 5). The decrease in p_{CH4} and the increase in p_{H2} cause the diminution in $r_{c,4}$ towards the catalyst center shown in Fig. 4. However, the increase in p_{CO} and the decrease in p_{H2O} with the radial coordinate are responsible for the continuous augment in the $r_{c,(5+6)}$ and $r_{c,net}$ curves. The results shown in Figs. 4 and 5 demonstrate the importance of taking into account the intraparticle diffusional limitations to evaluate the risk of carbon formation in MRs.
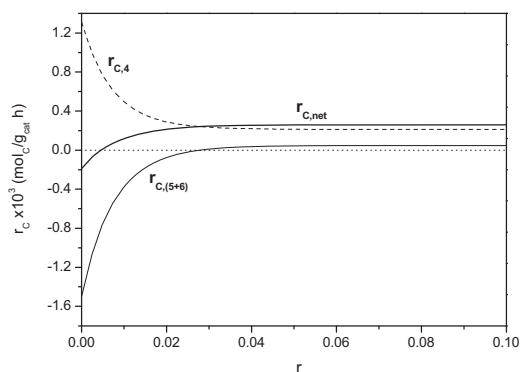
Figure 4: Profiles of $r_{c,net}$, $r_{c,4}$ and $r_{c,(5+6)}$ within the catalyst at z^*=0.128 m for MR (Condition 3).
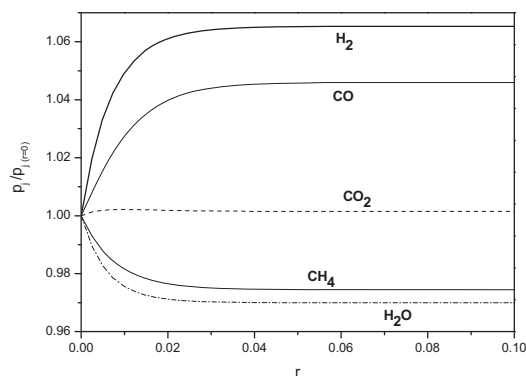
Figure 5: Partial pressures (dimensionless values) within the catalyst particle at z^*=0.128 m for MR (Condition 3).

The influence of the tube wall temperature and the inlet temperature on the carbon formation phenomenon was also analyzed (results not shown in this abstract).

Conclusions

The kinetic analysis has demonstrated that the hydrogen permeation through the membrane increases the risk of carbon formation with respect to the conventional fixed bed reactor. This risk should be carefully evaluated along the reactor, not only at the catalyst surface but also within the particle and considering simultaneously the three possible sources of carbon formation (reactions 4 to 6).

References

[1] J.R. Rostrup Nielsen, *Catalysis Science and Technology*, 1, (1984), 1.
[2] G. Marigliano, G. Barbieri, E. Drioli, *Catalysis Today*, 67 (2001) 85.
[3] K. Hou, M. Fowles, R. Hughes, *Chem. Eng. Sci.*, 54 (1999) 3783.
[4] G. Madia, G. Barbieri, E. Drioli, *The Can.J.Chem.Eng,* 77 (1999) 698.
[5] J. Xu, G.F. Froment, *AIChE J.*, 35 (1989) 88.
[6] J.Piña, V. Bucalá, D.O. Borio, *Int. J. Chem. Reactor Eng.*, A25, (2003), 1.
[7] J.-W. Snoeck, G.F. Froment, M. Fowles, *Int. J. Chem. Reactor Eng.*, A7, (2003), 1.

PP-61

MONTE CARLO SIMULATION OF METALLIC NANOPARTICLE OXIDATION

<u>N.V. Peskov</u>, A.P. Chernavsky*, P.A. Chernavsky*

Department of Computational Mathematics and Cybernetics, Moscow Lomonosov State University, Moscow, Russia
*Department of Chemistry, Moscow Lomonosov State University, Moscow, Russia

Metallic particles of nanometer size are often used in modern catalysts. The process of the metallic nanoparticles oxidation is now a matter of great interest both in practical and theoretical points of view. In practice, it is important to know the optimal conditions for the passivation of catalysts after their preparation. Also in the course of catalyst exploitation there can occur the oxidation of metal used as the active part of the catalyst. These and some other aspects require deeper understanding of the process of metallic nanoparticles oxidation. From a theoretical point of view, the oxidation process of metallic nanoparticles could be considered as a suitable object for investigations of the size effects in topochemical reactions.

There are a lot of studies devoted to the investigation of thermo-oxidation of massive metals as well as thin metallic films (see, for example, the review [1]), while the number of works devoted to the oxidation of tiny metallic particles is rather small [2,3,4]. Most of these works are related with the comparatively high temperatures (upper 573 K) where the oxidation proceeds in the "Wagner region" and is controlled by the diffusion in the oxide layer. Besides, the investigators have to do, as a rule, with sufficiently coarse particles of micrometer size.

Applicability of the general theory of metal oxidation to the particles of nanometer size is questionable due to many reasons. For example, one could mention high complexity of the particle surface and the interface between metal and oxide layer as well as more importance of the initial stage of oxidation in the case of nanoparticle in comparison with massive metals oxidation. It should be noticed that the detailed theory of the initial stage of metal oxidation is under construction now and one of the first models was presented in [5]. In addition, a finite and relatively not large number of atoms (μ 103) are involved in the process of oxidation of nanoparticle that is why the process cannot be correctly described by the mean field approximation used in the theory. The goal of our presentation is to present the new model of

metal nanoparticle oxidation based on the Monte Carlo simulation of main elementary stages involved into the process.

The presented model is based on the atomistic concepts of the Cabrera-Mott [6] theory of metal oxidation applied to the case of nanoparticle. Our main goals are to reproduce the experimentally observed dependencies of Co nanoparticles oxidation kinetics on the temperature of oxidation and on the size of particles [7].

We consider a metal crystalline particle with fcc crystal structure. Many metals with high catalytic activity have crystal lattice of such type. Moreover, crystal lattice of some metals (e.g. Co), which ordinary have the hex crystal structure, reconstruct to fcc structure in nanometer size particles. It is known that the equilibrium form of fcc crystal (at zero temperature) is cubo-octahedron form. In real catalyst the metal particles sit on a passive substrate. Therefore, neglecting the interaction metal-substrate, one can consider only half of cobo-octahedron particle. The particle surface consists of four hexagonal (111) faces, and one quadratic (top) and four triangle (100) faces separated by sixteen edges.

According to the Cabrera-Mott theory the kinetic scheme of metal oxidation consists of the following elementary stages.

Dissociative adsorption of O_2 molecule on the metal surface.

Surface oxidation and formation of oxide film.

Ionization of adsorbed O atoms on the oxide-gas interface.

Formation of metal ions on the metal-oxide interface.

Migration of metal ion in oxide layer under influence of electric field.

Reaction of metal and oxygen ions on the oxide-gas interface and grows of oxide film.

These elementary stages are simulated with the help of the 3D lattice gas model.

The rate of O_2 adsorption on metal and oxide surface is extracted from the kinetic gas theory. Two neighboring empty adsorption centers are needed for O_2 adsorption. The adsorbed atom O is supposed to be immobile.

Surface oxidation is treated as the reaction $O + M \rightarrow MO$ between neighboring atoms O and M (metal). The oxide molecule MO is placed in the site of atom M and the crystal lattice parameters are supposed unchanged. The activation energy of this reaction is supposed to be dependent on the population of the first neighbor of metal atoms. This supposition allows one to simulate the dependence of oxidation rate on the atom position on surface, and reproduce the island mechanism of oxide film growth.

According to Cabrera-Mott the ionization of adsorbed oxygen proceeds owing to electron tunneling from metal to surface through the oxide film: $O + 2e- \rightarrow O_2-$. The ionization creates

surface charges on the interfaces gas-oxide and metal-oxide. The rate of ionization is assumed to depend on average diameter of metallic core of particle, width of oxide film, and local electric field. These dependences allow one to simulate the size effects in nanoparticles oxidation observed experimentally.

The process of metal ions creation on the interface metal-oxide is simulated for simplicity via the position interchange of neighboring metal atom M and oxide molecule MO: $M + MO \rightarrow MO + M^{2+}$. The rate of this process is supposed to depend on local population of M and MO.

The migration of metal ions in the oxide layer is also simulated via lattice position interchange: $M^{2+} + MO \rightarrow MO + M^{2+}$. The activation energy of metal ion hop depends on the hop direction via dependence of hop's activation energy on local electric field.

When the migrating metal ion occurs in the first neighboring position with oxygen ion the reaction $M^{2+} + O_2- \rightarrow MO$ can happen. The new MO molecule occupies the site of M^{2+} increasing the mass of the oxide layer.

The process of metal oxidation is simulated be the dynamic Monte Carlo algorithm with continuous time. Local electric field is computed as the sum of electric field from point charges corresponding to oxygen and metal ions and surface charge of metallic core of the particle.

Thus the simplified electro-chemical model of metallic nanoparticle oxidation based of contemporary concept of metal low temperature oxidation mechanism is constructed. The model is devoted, in the first turn, to the description of particle size effects on the oxidation kinetics. The simulation results demonstrate a qualitatively agreement of model oxidation kinetics with available experimental data. Future development of the model will be connected with the problem of determination of size distribution of particles in real catalyst from the oxidation kinetics data.

References

1. A. Atkinson, Rev. Mod. Phys. 57, (1985), 437.
2. R. van Wijk, et al., Appl. Surf. Sci. 90, (1995), 261.
3. S. Ohno, H. Okuyama, Y. Sakka, J. Jap. Inst. Met. 60, (1996), 318.
4. R. Karmhag, G.A. Niklasson, M. Nygren, J. Appl. Phys. 89, (2001), 3012.
5. R. Chakarova, D.E. Oner, I. Zoric, B. Kasemo, Surf. Sci. 472, (2001), 63.
6. N. Cabrera, N. F. Mott, Rep. Prog. Phys. 12, (1948), 163.
7. P.A. Chernavsky, Russian J. Phys. Chem. 77, (2003), 636.

ISOMERIZATION OF XYLENES OVER DIFFERENT ZEOLITES: TEMPORAL ANALYSIS OF PRODUCTS STUDY

P. Poladli, H. Papp

Institut für Technische Chemie, Universität Leipzig, Linnestrasse 3, 04103 Leipzig, Germany

Introduction

Xylene isomerization allows one to meet the high demand for *p*-xylene (which is eg. a precursor of polyesters) by converting the much less needed *m*- and *o*- xylenes [1]. The selective production of *p*-xylene by isomerization of *o*- and *m*-xylene over modified zeolites has been a subject of many investigations. The product distribution of isomerization depends on the prevailing mechanism and on the diffusion rate of intermediates and products. The temporal analysis of products (TAP) reactor system is tool for investigating "gas-solid" reactions, particularly reactions on catalysts. TAP experiments are one method to determine the diffusion coefficients [3]. In this work the isomerization of xylenes on zeolites with different pore sizes was investigated and correlated with the diffusion coefficients of educts and products determined by the TAP experiments.

Experimental

The zeolites were characterized by DTA/TG, BET-N_2, elementary analysis, and XRD. The xylene isomerization (*m*-xylene, *o*-xylene, *p*-xylene) was investigated on different zeolites (HZSM-5, HFER, HFAY, H-beta) in the temperature range from 200 to 350°C, at atmospheric pressure and at various space velocities (4-7 g/h*g_{cat}). The test of the activity of zeolites was carried out in a flow apparatus with a glass tube reactor connected on-line to a gas chromatograph. Before the reaction the catalysts were activated *in situ* by N_2 (50 ml/min) for 2 h at 450°C.

The principle of the TAP II reactor system has been described in detail elsewhere [3]. Single pulse experiments were performed with SiMCM-41 and the zeolite under vacuum conditions at 10^{-9} mbar in a temperature range from 200 to 300°C. The outlet pulses were detected by QMS. A fraction of granulated sample of about 0.2-0.315 mm of equivalent diameter was used. The sample grains were placed between two layers of inert, nonporous corundum of the same grain size.

Results

The isomerization was performed over different zeolites to study the influence of the pore structure on the product distribution. Results of the isomerization of pure xylene isomers over HZSM-5 (26) at 250°C are given in Table 1. The conversion of *p*-xylene and selectivity to *p*-xylene in *m*-xylene isomerization is higher than that of the other isomers. From literature it is known that the minimum van der Waals diameter of *p*-xylene is smaller than that of the other

PP-62

isomers that seems to be the determining factor for higher conversion of *p*-xylene and higher yield of *p*-xylene than for the other isomers in the isomerization reactions.

Table 1. Isomerization of different xylene isomers over HZSM-5 (26)

reaction	*o*-xylene isomerization	*m*-xylene isomerization	*p*-xylene isomerization
Yield (%):			
toluene	~1	~1	~1
p-xylene	13	23	-
m-xylene	27	-	55
o-xylene	-	17	14
trimethylbenzene isomers	~1	~1	~1
conversion	42	42	71
p-xylene selectivity	31	55	-
m-xylene selectivity	64	-	77
o-xylene selectivity	-	40	20

Reaction conditions: He/*m*-xylene =11.5, T=250 °C, WHSV 4,4 h^{-1}

The small size of *p*-xylene allows it to diffuse easier into the pores and also easier out from the pores of the zeolite than the other isomers. The conversions of all three isomers increased with increasing temperature. HZSM-5 showed the highest activity and selectivity for the isomerization reaction. At 250°C isomerization is the favoured reaction over HZSM-5. With increasing temperature the rate of disproportionation of xylenes increased over HZSM-5. Mainly disproportionation is found

Figure 1. Comparison of area normalized responses for pulsing *m*-xylene and *p*-xylene over SiMCM-41 (40 mg)

over H-beta and HFAU zeolites. The activity of HFER is low at the investigated temperatures. The difference of the diffusion rates of reactants and products is the main reason for the observed differences in reactivity. The diffusion coefficients of educts and products in the different zeolites were determined by pulse experiments in the TAP II reactor system. Figure 1 shows a comparison of area normalized responses for pulsing *m*-xylene and *p*-xylene over SiMCM-41 at 573 K. It can be seen that the *m*-xylene response is broader than that of *p*-xylene, indicating that *m*-xylene diffuses slower than *p*-xylene. Over corundum the *m*-xylene and *p*-xylene responses are approximately the same.

Acknowledgment

References

1. M.Guisnet *et al.* J. Micropor. Mesopor. Mater. 35-36 (2000) p.50
2. A.S.Araujo *et al.* J. React. Kinet. Catal. Lett. 73, (2001) p.283
3. G.S.Yablonsky *et al.* J. Catal. 216 (2003) p.121

DEVELOPMENT OF OXYGEN PERMEABLE MEMBRANE REACTOR

O.Yu. Podyacheva, A.P. Nemudry[*], N.V. Shikina, V.V. Kuznetsov, E.A. Schevchenko, N.Z. Lyakhov[*] and Z.R. Ismagilov

Boreskov Institute of Catalysis SB RAS, prosp. Akad. Lavrentieva, 5, 630090 Novosibirsk, Russia, Fax: +7-383-339-73-52, e-mail: pod@catalysis.ru

[*]*Institute of Solid State Chemistry and Mechanochemistry SB RAS, Kutateladze st. 18, 630128, Novosibirsk, Russia*

Presently the main source of pure oxygen production is purification of air in cryogenic plants. This technology is rather costly and requires specific storage and transportation equipment to the main processes where the pure oxygen is utilized. One of the promising large scale oxygen consumption technologies is partial oxidation of methane to syngas as downstream processing requirements cannot tolerate nitrogen. The use of oxygen permeable membrane for the separation and its combination with catalytic conversion in one catalytic membrane reactor is a new approach worked out intensively now [1]. This approach can decrease the cost of the syngas produced via partial methane oxidation by 45% [2]. It was found that mixed electronic-ionic conducting perovskites exhibit high oxygen permeability and can be successfully used as oxygen permeable membranes. As estimated, the industrial reactors for methane partial oxidation comprising 1000 perovskite membrane tubes of 1 m length with oxygen fluxes not less than 10 cm^3/cm^2 min will demonstrate methane capacity about 500 kg/hour. It is foreseen that increase of reactor capacity by several times is possible if thickness of the membrane layer is reduced to the level of 20-50 μm, and the application of reactor with supported membrane layers is favorable. The successful industrial application of tube membrane reactors requires preliminary detailed study and optimization of oxygen fluxes in a simple plate perovskite reactor.

The subject of this paper is testing of a membrane reactor with oxygen permeable plates based on bulk and supported perovskite membranes.

The scheme of the reactor for the study of oxygen fluxes through membranes is shown in
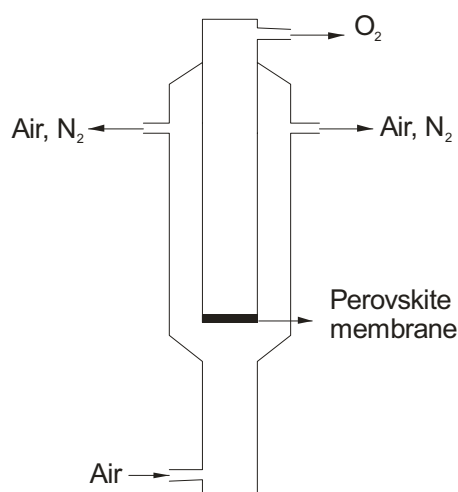
Fig.1. Oxygen permeable perovskite membrane reactor

PP-63

Fig.1. For this reactor, the samples in the shape of plates having diameter of 13-18 mm were fabricated. The plates were composed of $Sr_{1-x}Co_{0.8-y}Fe_{0.2}O_{3-z}$ perovskite as a parent material. The parent perovskite was doped by Nb, Al, La metals, and stability of the materials was studied. It was found that partial substitution of Co by Nb or Al and Sr by La in the parent perovskite stabilizes the perovskite phase in a wide oxygen nonstoichiometry window (z=0-0.4). Partial substitution of parent perovskite was also accompanied by a substantial increase of material stability in the reducing atmospheres (5%H_2/95%Ar and 10%CH_4/90%Ar), the temperature of perovskite degradation shifted to the high temperature region by 50-250°C depending on the perovskite composition. The formation of specific microdomain texture was registered in the chosen perovskites.

The oxygen mobility in perovskite materials was tested. A technique of measuring kinetic parameters of oxygen mobility along microdomain boundaries and inside defect-free domains by the use of electrochemical relaxation methods was developed. Using the kinetic model developed to describe the diffusion of oxygen in perovskites, the potentiostatic relaxation curves of the oxidation of $SrCo_{0.5}Fe_{0.3}Nb_{0.2}O_{3-z}$ have been analyzed. It was demonstrated that the current transients are described in the frame of interdiffusion regime and the limiting stage is the supply of oxygen along the domain boundaries. On the basis of studies of electrochemical oxidation at different temperatures, it was shown that the oxygen diffusion along domain boundaries is described by the following Arrhenius equation: D= $2 \cdot 10^{-4}$ exp[-(74± 3 kJ/mole)/RT] cm^2/s.

Oxygen permeable membrane reactor based on perovskite membrane deposited on the surface of appropriate support, i.e. zirconia, hexaaluminate or perovskite plates, is being developed, Fig.2. Plasma spraying and sol-gel techniques [3] were used for the fabrication of supported perovskite membranes with membrane layer thickness of 10-50 μm. The formation of gas-tight membrane perovskite layers on zirconia and hexaaluminate supports was observed if sol-gel technique was used, but partial interaction of membrane layer with both zirconia and hexaaluminates was found to occur. The influence of membrane composition and thickness of membrane layer on oxygen flux in plate reactor based on bulk or supported membranes was studied.

The process of the methane partial oxidation on $Sr_{1-x}Co_{0.8-y}Fe_{0.2}O_{3-z}$ catalysts was investigated in a flow reactor with fixed catalyst bed and reaction mixture 20%CH_4/10%O_2/Ar at GHSV=50000 h^{-1}. The highest reaction rate was achieved when $Sr_{1-x}La_xCo_{0.8-y}Fe_{0.2}Al_yO_{3-z}$ was used: considerable syngas formation with 20% yield, was observed starting from 600°C, the maximum methane conversion amounted to 50% at 900°C

with CO and H_2 selectivity 90 and 80% respectively, Fig.3. It was found that in this case the main process of syngas production is not impeded by the reaction of coke formation.
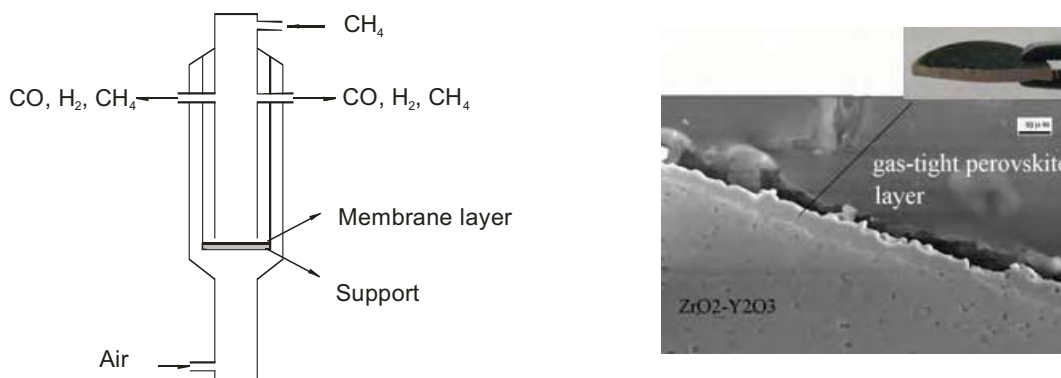
Fig. 2. Design of oxygen permeable reactor and supported membrane for methane partial oxidation.
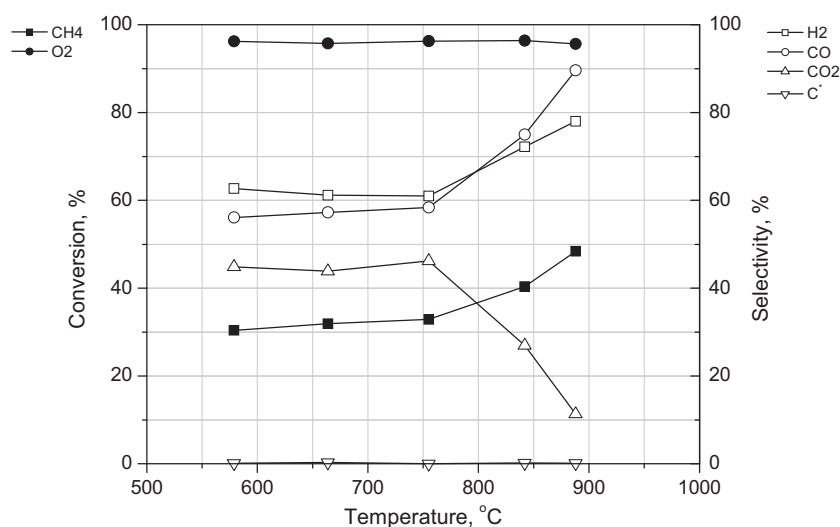
Fig. 3. Methane partial oxidation parameters on perovskite $Sr_{1-x}La_xCo_{0.8-y}Fe_{0.2}Al_yO_{3-z}$.

Summarizing, the operation of plate membrane reactor based on perovskites $Sr_{1-x}Co_{0.8-y}Fe_{0.2}O_{3-z}$ where x= La and y= Nb, Al has been studied. The effective membrane layer thickness to optimize oxygen flux has been proposed and reactor with supported perovskite membrane of 10-50 μm thickness has been developed. The highest reaction rate of syngas production has been observed over $Sr_{1-x}La_xCo_{0.8-y}Fe_{0.2}Al_yO_{3-z}$ catalyst caused by the suppression of the reaction of coke formation.

Acknowledgements

Literature

1. J.E.ten Elshof, H.J.M.Bouwmeester, H.Verweij, Appl.Cat. A 130 (1995) 195.
2. P.V.Hendriksen, P.H.Larsen, M.Mogensen, F.W.Poulsen, K.Wiik, Catalysis Today 56 (2000) 283.
3. Z.R.Ismagilov, O.Yu.Podyacheva, O.P.Solonenko, V.V.Pushkarev, V.I.Kuzmin, V.A.Ushakov, N.A.Rudina, Catalysis Today, 51 (1999) 411.

DYNAMIC SIMULATION OF SOLAR DRIVEN THERMOCHEMICAL REFRIGERATOR IN DIFFERENT CLIMATIC CONDITIONS

O.S. Popel, **S.E. Frid, S.S. Sharonov**

Institute of High Temperatures RAS, Izhorskaya str. 13/19, Moscow 125412, Russia
fax: +7 495 484 2374, O_Popel@oivtran.iitp.ru

This paper concerns the on-going INTAS project No. 03-51-6260 "**Study of solar assisted adsorption cooling unit (SAACU) using new adsorbent materials**" [1] and represents some results of mathematical simulation of an adsorption solar cooler operation in real climatic conditions.

The solar cooler under consideration (Fig. 1) consists of an adsorber integrated with a flat solar receiver, a condenser and an evaporator of cooling chamber. Principle and ideal cycle of solar adsorption cooler operation have been described [2] and its preliminary thermodynamic analysis which demonstrates advantages of selective water sorbents (SWSs [3]) application has been carried out [4].
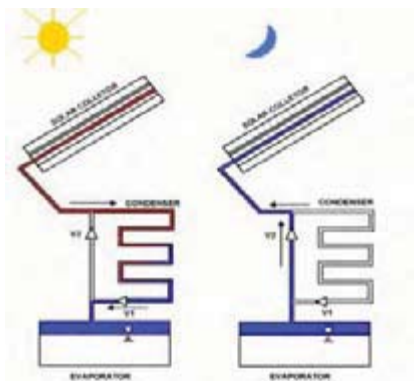
Fig. 1.
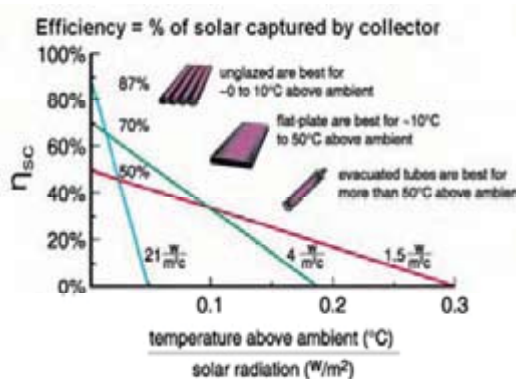
Fig. 2.

At the same time influence of variable climatic conditions (daily and seasonal variations of solar irradiation and ambient temperature) on solar cooler performance has not been studied. The target of this work was development of simplified mathematical model of the solar adsorption cooler to predict its thermal efficiency in different climates and to define critical parameters affecting on its performance. The following 2 indicators are most important to characterize thermal efficiency of solar cooler: achievable average for the considered period of time (month, season, whole year) cooling capacity counting on 1 m^2 of solar receiver (SCP)

and total thermal efficiency characterised by average System Thermal Ratio (STR) that is the ratio of heat extracted from evaporator due to water evaporation to solar heat that falls on solar collector-absorber aperture. Coefficient of performance (COP), which is ratio of amount of heat extracted from evaporator to amount of solar heat usefully used in solar receiver-adsorber for water desorption, is also useful indicator to better understand energy conversion stages efficiencies.

Real SAACU operation conditions are non-stationary and all working parameters vary in wide ranges. Intensity and amount of solar radiation collected by solar receiver-adsorber dramatically affect on temperature of adsorbent and amount of sorbate which is desorbed during day time cycles from sorbent. Ambient air temperature from one side has impact on efficiency of solar energy conversion into heat in solar collector (Fig. 2) and from another side influences on heat exchange and sorbate temperature in condenser as well as on intensity of desorption processes in adsorber during night time cycles.

To evaluate efficiency of adsorbtion/desorbtion cycle application for solar cooling a mathematical model of SAACU providing its hour by hour operation dynamic simulation during the year for variable climatic conditions of 7 sites, located in different areas of the world (Messina, Stuttgart, Kiev, Novosibirsk, Cairo, Bangkok, Colombo) has been developed. The TRNSYS software [5] with specially constructed solar adsorption cooler component models of flat-plate solar collector-adsorber, vapour condenser and evaporator has been used for hour by hour simulation of its operation during the year in variable climatic conditions. Hour by hour sequences of weather data have been generated by specialized TRNSYS climatic module.
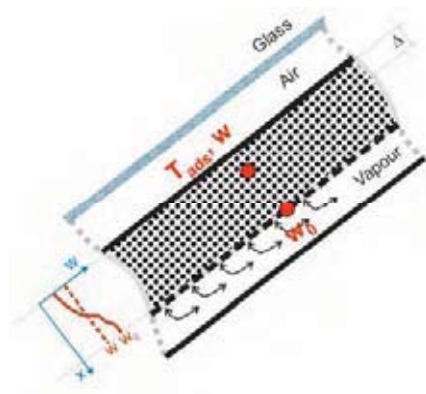
Fig. 3
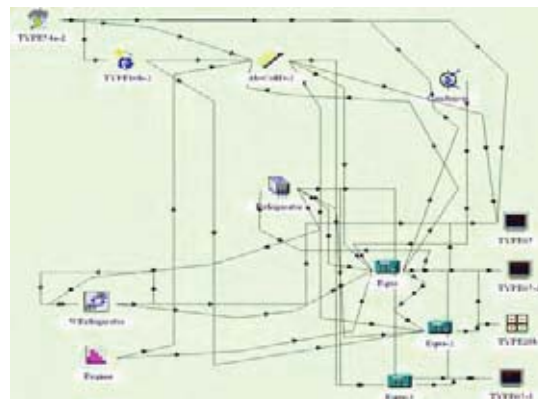
Fig. 4

PP-64

One node solar collector-adsorber model (Fig. 3) was used describing the adsorber heat balance by equation:

$$\frac{M_{ads}}{A_c}\frac{\partial}{\partial t}[(c_{ads}+c_w w)T_{ads}] = F_\lambda[S(\tau\alpha)-U_L(T_{ads}-T_a)]+\frac{M_{ads}}{A_c}H_{des}\frac{\partial w}{\partial t},$$

where c_{ads}, c_w – specific heat of adsorbent and adsorbed water, M_{ads} – mass of adsorbent, w – mean water content of adsorbent, $(\tau\alpha)$ – optical efficiency of solar adsorber-collector, A_c – its area, S – solar radiation flux, U_L – adsorber heat loss coefficient, T_{ads} – mean adsorbent temperature, T_a – ambient air temperature, H_{des} – the heat of desorption. The factor F_λ was introduced to use the mean adsorbent temperature instead of solar flux adsorbing plate temperature.

The Linear Driving Force model [6] was used for description of the kinetics of vapor sorption/desorption:

$$\frac{\partial w}{\partial t}=k(w_0-w),$$

where equilibrium water content (w_0) is determined by sorption curves for given sorbent and Polani equation.

The condenser model assumes vapour condensation at the temperature of ambient air. The evaporator was considered to stay at constant temperature varied as parameter in range of 5–10°C. In both cases the vapour pressure is equal to saturation pressure for corresponding temperatures.

Only SWS-1L selective water sorbent [7] was considered at this stage of study. It is clear from the model description that at the chosen evaporator rated temperature there are 2 main parameters defining the SAACU operation efficiency at the given climatic conditions of considered sites: the specific sorbent mass counting on 1 m² of solar receiver aperture and the effective mass transfer coefficient k, which were correspondingly varied in our calculations in ranges of 4–20 kg/m² and 0,1–2,5 h⁻¹.

Typical curves illustrating the received summarized results of SAACU mathematical simulation during whole year of its operation are presented at Fig. 5 (Messina, evaporator temperature 5°C, k=0.8 h⁻¹,) and Fig. 6 (Messina, absorbent mass 10 kg/m², evaporator temperature 5°C). The following 2 most important conclusions could be made: (1) – an optimal specific adsorbent mass exists providing maximal average specific cooling capacity of solar cooler; (2) – there is a critical minimal value of effective mass transfer coefficient below which heat and mass transfer processes of sorption/desorption are too slow to provide

effective production of cold. It has been also shown that for considered sites and different periods of solar cooler operation optimal specific mass of SWS-1L adsorbent has to be 12–16 kg/m^2 and design and construction of adsorber has to provide effective mass transfer coefficient not less than 0,5–1,0 h^{-1}. If these requirements are satisfied the specific average cooling capacity SCP of considered solar cooler 35–60 W/m^2, total system thermal ratio STR up to 0,2 and COP up to 0,5–0,8 could be achieved in different climatic conditions.
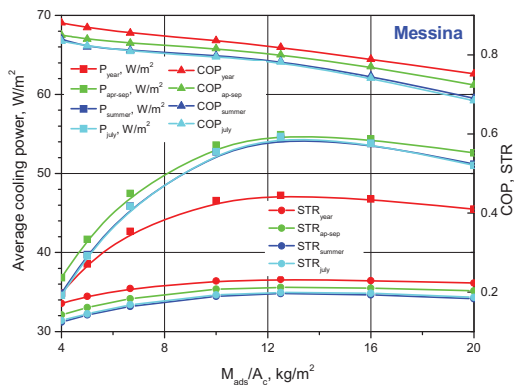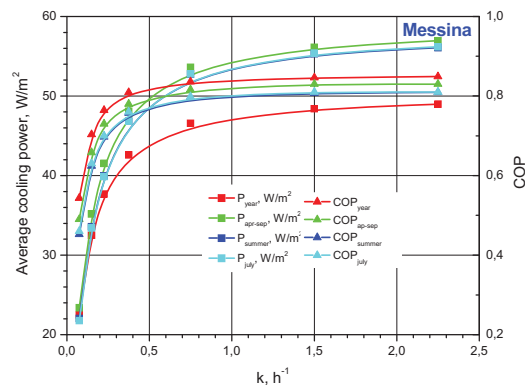
Fig. 5.	**Fig. 6.**

Next stages of the study will be devoted to comparison analysis of different sorbents influence on solar cooler performance to justify their optimal choice and SAACU mathematical model improvement to provide more detailed simulation of heat and mass transfer processes in adsorber as well as in cooling chamber.

Literature

1. Yu. I. Aristov, D. Chalaev, B. Dawoud, L. I. Heifets, O. Popel, G. Restuccia, Proc. CHEMREACTOR-17

2. Yu.I.Aristov, G.Restuccia, G.Cacciola, V.N.Parmon, Appl.Therm.Engn., 2002, v.22, N 2, pp.191-204.

3. W.M.Raldow, W.E.Wentworth, *Solar Energy*, 1979, v.23, p.75-79.

4. Yu.I. Aristov, Proc. VI Int. Seminar "Heat pipes, heat pumps, refrigerators", 12-15 Sept. 2005, Minsk, Belorus, pp. 342-353.

5. TRNSYS – The Transient System Simulation Program // http://sel.me. wisc.edu/TRNSYS/.

6. E. Glueckauf, Part 10. Formulae for diffusion into spheres and their application to chromatography, Trans. Faraday Soc. 1955. V.51. part 11, pp. 1540-1551.

7. M.M.Tokarev, B.N.Okunev, M.S.Safonov, L.I.Heifets, Yu.I.Aristov, Rus. J. Physical Chemistry, 2005, v. 79, N 9, pp. 1490-1494.

THE FORMALDEHYDE OXIDATION TO FORMIC ACID. IN SITU FTIR KINETIC STUDY OF SURFACE COMPOUNDS TRANSFORMATION ON VANADIA –TITANIA CATALYST

G.Ya. Popova, T.V. Andrushkevich, Yu.A. Chesalov

Boreskov Institute of Catalysis SB RAS, Novosibirsk 630090, Russia, gyap@catalysis.nsk.su

INTRODUCTION

Formaldehyde is found to be oxidized with a high selectivity to formic acid over the vanadia-titania catalysts at the temperature range of 100 to 140°C [1].

Figure 1 shows the plot of selectivities to formic acid and carbon oxides versus the formaldehyde conversion at 120, 130 and 140°C. At 120°C the selectivity to formic acid slightly decreases with increasing formaldehyde conversion. At higher temperatures, an increase in the conversion is accompanied by a decrease in the selectivity to formic acid and by an increase in the selectivity to carbon oxide due to the formic acid decomposition to CO and H_2O.
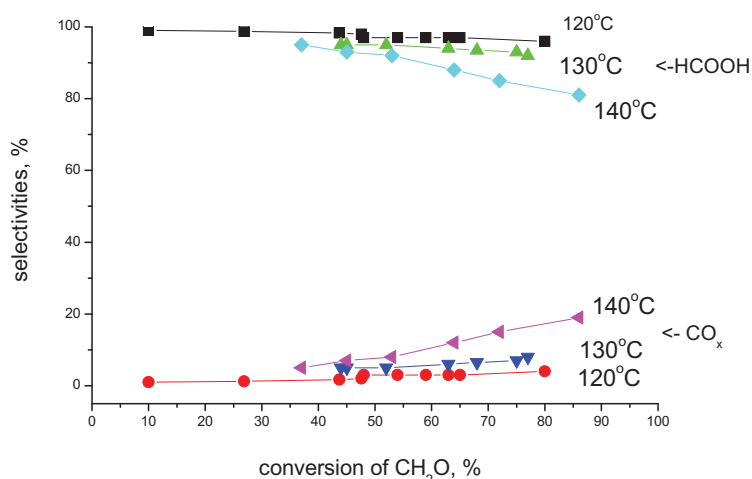
Fig.1. Dependences of the selectivities to HCOOH and CO$_x$ *versus* the CH$_2$O conversion.

Earlier, we study mechanism of formaldehyde oxidation reaction and decomposition of formic acid by kinetic, in situ FTIR spectroscopy, TPD and quantum chemical methods [2-4]. Formic acid may form two paralled pathways: by an associative mechanism through the oxidative elimination of bidentate formates (BF1) and by a stepwise redox Mars van Krevelen mechanism through the decomposition of asymmetrical formates (AF). This mechanism presumes the existence of active centers of two types. The vanadyl oxygen (-V=O) participates in the formation of BF1 while the bridge oxygen (-V-O-V-) participates in the formation of AF. The decomposition of formic acid occurs through the thermal decomposition of bidentate formates (BF2). It is the product of readsorption of formic acid on the support TiO_2.

In this work we studied the kinetics of formation and decomposition of surface formates BF1 and AF in formaldehyde oxidation to formic acid and surface formate BF2 during formic acid decomposition.

RESULTS AND DISCUSSION

FTIR spectra of surface species recoding at passing the reaction mixture of 2% CH_2O in air and 1% HCOOH in air through the IR cell-reactor are shown in Fig. 2.
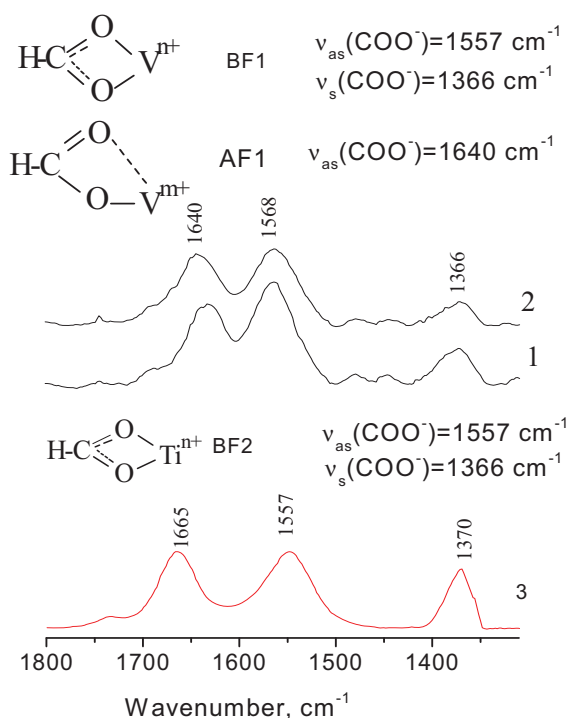
Fig.2 In situ FTIR spectra of V-Ti-O catalyst during CH_2O oxidation (1,2) and HCOOH decomposition (3)

The kinetic curves of formation and decomposition surface formates BF1, AF and BF2 determined by optical density D changes of adsorption bands $\nu_{as}(COO^-)$ =1568 cm^{-1} (BF1), $\nu_{as}(COO^-)$=1640 cm^{-1} (AF) and $\nu_{as}(COO^-)$=1557 cm^{-1} (BF2).

Time dependencies of relative intensities of adsorption bands $\nu_{as}(COO^-)$ =1568 cm^{-1} (BF1), $\nu_{as}(COO^-)$=1640 cm^{-1} (AF) and that of $\ln(1-D/D_o)$ during BF1 and AF formation in the reaction mixture of CH_2O in air are shown in Fig. 3,4. The data are satisfactorily processed in the coordinates of first order reaction.
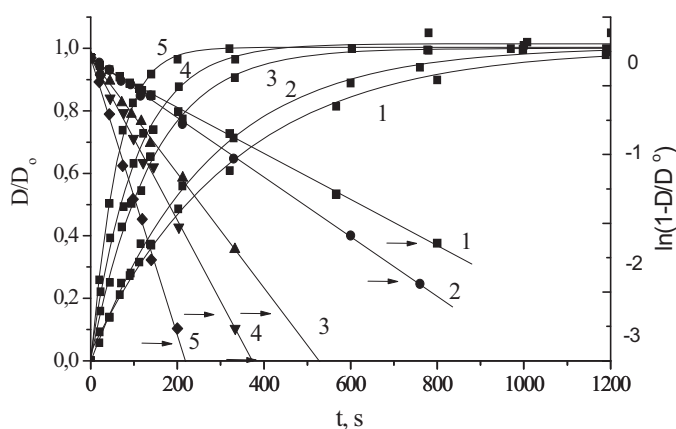
Fig.3 The kinetic curves of BF1 formates formation
1 - 70, 2 - 100, 3 - 120, 4 - 150, 5 - 190°C
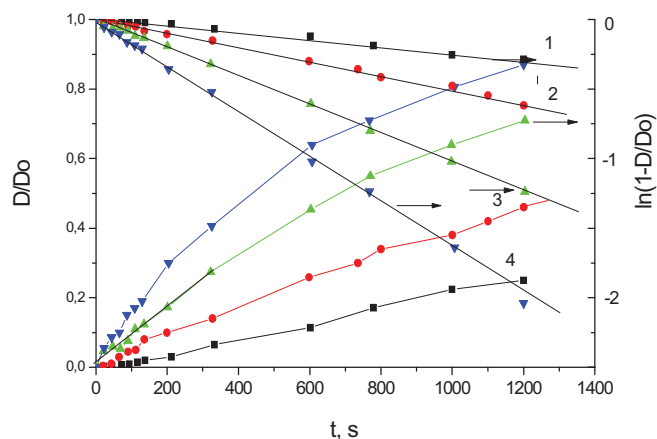
Fig.4 The kinetic curves of AF formates formation
1 - 100, 2 - 120, 3 - 150, 4 - 170°C

Time dependencies of relative intensities (D/Do) of adsorption bands $\nu_{as}(COO^-)$ = 1568 cm^{-1} (BF1) and $\nu_{as}(COO^-)$=1640 cm^{-1} (AF) in the air flow at different temperature are shown in Fig. 5,6 (a). The kinetic dependences of surface species decomposition are processed in the coordinates of first order rate reaction (Fig. 5,6 b).
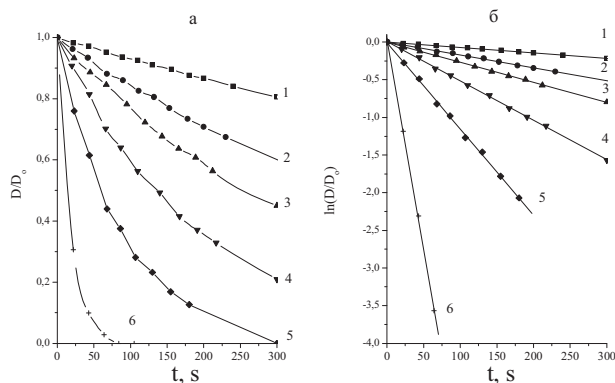
Fig. 5. Kinetic curves of the decomposition of surface formats BF1.
1-70, 2-100, 3-120, 4-150, 5-190°C.
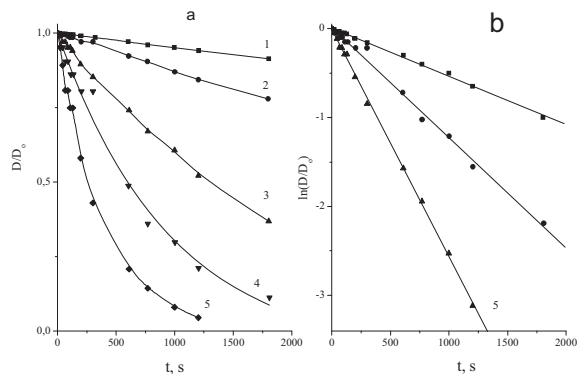
Fig. 6. Kinetic curves of the decomposition of surface formats AF.
1-100, 2-120, 3-150, 4-170, 5-190°C.
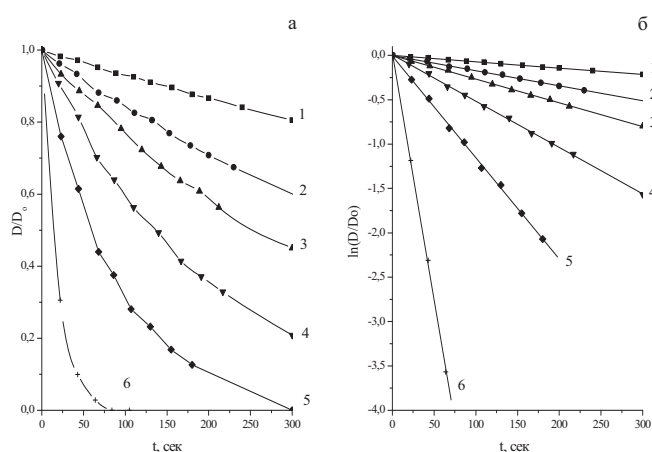
Fig. 7. Time dependence of relative intensity (D/Do) of band BF2 (a) and that of ln(D/Do) (b) during the decomposition of HCOOH in the air flow: 1-50, 2-75, 3-100, 4-125, 5-130, 6-150°C.

Figure 7,a shows kinetic curves of surface species HCOOH (BF2) decomposition in air flow at 50-150°C. The BF2 decomposition rate is described by the first order equation of reaction rate (Fig. 7 b).

The rates of the BF1 and AF decomposition (W_s) and the rates of the formic acid and CO formation (W_k) at the formaldehyde oxidation (sample 1,2) and the rate of BF2 decomposition and the rate of the CO formation at the formic acid decomposition (sample 3) are listed in Table. The rate of the formic acid formation in the gas phase is close to the rate of the BF1 decomposition in flowing air at 100 °C (sample 1). and to the sum of the rates BF1 and AF decomposition at 120 °C (sample 2). The rate of the CO formation in the gas phase is close to the rate of the BF2 decomposition at 150 °C (sample 3).

Table. The rate of the surface compounds decomposition (W_s) and the rate of the reaction products formation (W_k) on the V-Ti-O catalyst.

Sample	T,°C	$N^* \cdot 10^{-18*}$, molecules $\cdot$ m^{-2}			$W_s \cdot 10^{-15}$, molecules $\cdot$ m$^{-2} \cdot$ s^{-1}			$W_k \cdot 10^{-15}$, molecules $\cdot$ m$^{-2} \cdot$ s^{-1}	
		BF1	AF	BF2*	BF1	AF	BF2	HCOOH	CO$_x$
1	100	3.0			3.1			2.9	0.03
2	120	3.3	2.4		5.0	0.4		5.1	0.10
3	150**			2.5			14.3		11.8

*N is the surface formate concentration, **decomposition of HCOOH.

Schema describes the formation of formic acid by formaldehyde oxidation and decomposition of formic acid to CO$_x$ on V-Ti-O catalyst. The temperature dependences of the rate constants in Scheme take the following values:
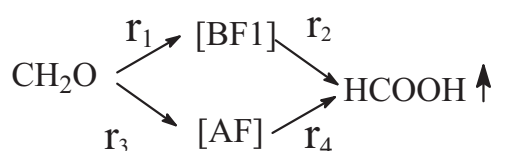
$$K_1 = 3,34 \times e^{-4,9/RT} \text{ s}^{-1}$$

$$K_2 = 8,16 \times e^{-6,9/RT} \text{ s}^{-1},$$

$$K_3 = 1,28 \times 10^2 e^{-9,8/RT} \text{ s}^{-1},$$

$$K_4 = 3,67 \times e^{-15,1/RT} \text{ s}^{-1}$$

$$K_5 = 2,4 \times 10^{10} e^{-26,4/RT} \text{ s}^{-1}.$$

Acknowledgements

References

1. G.Ya. Popova, T.V. Andrushkevich and G.A. Zenkovets, *Kinet. Catal.*, 1997, **38**, 285.

2. G.Ya. Popova, Yu.A. Chesalov, T.V. Andrushkevich and E.S. Stoyanov, *Kinet. Catal.*, 2000, **41**, 601.

3. G.Ya. Popova, Yu.A. Chesalov, T.V. Andrushkevich, I.I. Zakharov and E.S. Stoyanov *J. Mol. Catal. A: Chemical,* 2000, **158**, 345.

4. G.Ya. Popova, T.V. Andrushkevich, I.I. Zakharov and Yu. A. Chesalov, *Kinet. Catal.*, 2005, **46**, 217.

PP-66

EVALUATION OF CO AND CO$_2$ BASED METHANOL SYNTHESES USING ASPEN PLUS SIMULATION SOFTWARE

Riitta Raudaskoski, Esa Turpeinen & Riitta L. Keiski

Department of Process and Environmental Engineering, Mass and Heat Transfer Process Laboratory, P.O.Box. 4300, FIN-90014 University of Oulu, Finland. Fax. +358 8 553 2369. E-mail address: riitta.raudaskoski@oulu.fi

Introduction

Kyoto protocol and emissions trading closely related to it entered into force during the year 2005, which has increased the interest to CO$_2$ utilization. Among those bulk chemical processes in which CO$_2$ can be used as a feedstock, methanol synthesis is one of the most potential methods to utilize CO$_2$ separated from flue gases. Methanol is an important product and feedstock in chemical industry. It is used for example as a refrigerant, as a synthetic fuel, as a solvent and in the manufacturing of formaldehyde as well as dimethyl terephthalate (DMT) [1]. Currently methanol is commercially produced from synthesis gas (CO + H$_2$) over Cu-Zn oxide based catalysts using gas phase fixed bed reactors [1]. In this process CO$_2$ is commonly used only to adjust the feed composition. Although commercial methanol synthesis is well known and several companies offer commercial technologies (e.g. ICP, Lurgi and Mitsubishi processes [1]), methanol synthesis from CO$_2$ and H$_2$ has also gained a wide attention during the last decade mainly because of the possibility to utilize CO$_2$ as a feedstock in this process. Several articles have already been published around this area [e.g. 2-6], but more research work is needed. The objective of the present study is to evaluate, using Aspen Plus (version 2004.1) simulation software [7], two different ways to produce methanol. These two Cases are following: a typical natural gas based production route (a commercial process) and methanol synthesis directly from CO$_2$ and H$_2$.

Simulations

Thermodynamic calculation is a useful and practical tool for designing new or alternative processes, particularly in determining favourable reaction conditions and in evaluating required material and energy flows. In this study material and energy balances are calculated using Aspen Plus simulation software for two different methanol processes, which are a typical natural gas based production route (Case A) and methanol synthesis directly from CO$_2$ and H$_2$ (Case B). Economic efficiencies of these Cases are evaluated based on the material

and energy balances as well as average list prices of raw materials and electricity. Flow sheets of the simulated Cases and the used reaction conditions are shown in Figures 1 and 2.
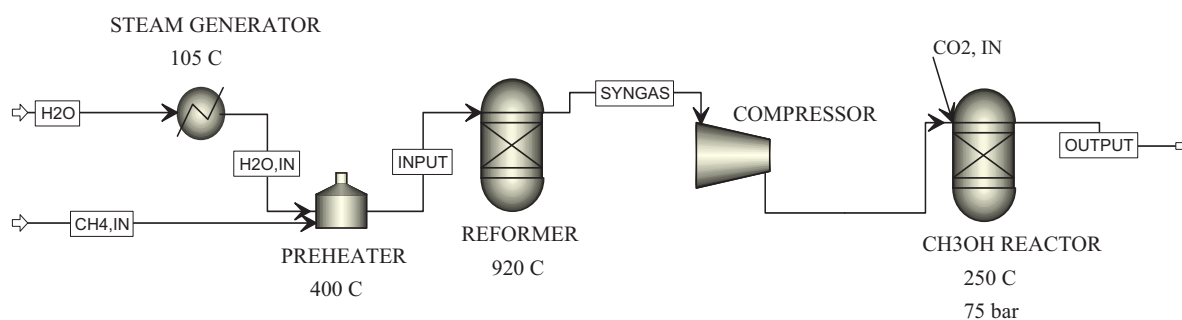
Figure 1. Natural gas based production route, Case A.
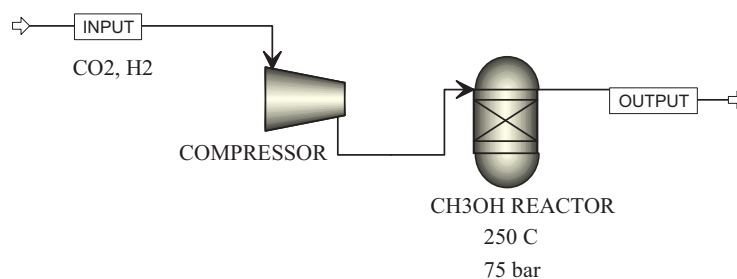
Figure 2. Methanol synthesis from CO_2 and H_2, Case B.

The used reaction conditions for the reformer and the methanol reactor have been selected based on thermodynamic calculations and typical commercial processes [1], respectively. Results from thermodynamic calculations reveal that suitable reaction conditions are high temperature and low pressure in the reformer and low temperature and high pressure in the methanol reactor. Although high temperature is favourable in the reformer, e.g. increase in energy consumption sets limits to the temperature level. For many years numerous hydrogen plants have operated with reformer outlet temperatures of about 920°C [8]. This temperature is also used in this study. The rate of reaction at low temperature in the methanol reactor is very slow over most catalysts and high operation temperature becomes almost mandatory [1]. Because of that, the reaction conditions used in typical commercial methanol processes have been selected for the methanol reactor. Primary reactions involved in the two Cases are:

Reformer $\quad\quad\quad CH_4 + H_2O \leftrightarrow CO + 3H_2 \quad\quad$ (1)

Methanol reactors $\quad CO + 2H_2 \leftrightarrow CH_3OH \quad\quad$ (2)

$\quad\quad\quad\quad\quad\quad CO_2 + 3H_2 \leftrightarrow CH_3OH + H_2O \quad$ (3)
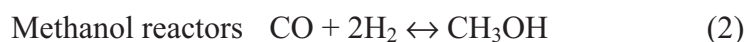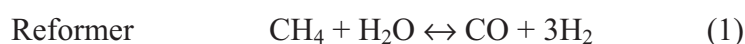
PP-66

The stoichiometry of the reformed gas can be conveniently characterized by the ratio M (M= (H_2-CO_2/(CO+CO_2)). Stoichiometry of the methanol synthesis (reactions 2 and 3) requires that M ≈ 2 [9]. To reach the stoichiometry necessary for the methanol reactor, CO_2 is mixed with the exit gas from the steam reformer (Case A). In the Case B, the stoichiometric ratio of the feed gas has been used. In both Cases, it is assumed that the only carbon containing product in the methanol reactor is CH_3OH which means that reactions are selective to methanol. In order to compare these two Cases to each other, the yield of methanol is set to 1.0 kmol/h.

Simulation results and discussion

Calculated material and energy balances are summarized in Table 1 and 2, respectively. Operation costs are shown in Table 3. Energy losses are excluded in calculations and heat transfer efficiency is assumed to be 100%.

Table 1. Material balances.

	Case A	Case B
Input (kmol/h)		
CH_4	1.36	-
CO_2*	0.41	3.54
H_2O	1.36	-
H_2	-	10.63
CO	-	-
Output (kmol/h)		
CO_2	0.42	2.54
H_2O	0.030	1.01
H_2	1.96	7.61
CO	0.31	-
CH_3OH	1.00	1.01

* It is assumed that CO_2 (pure enough) is available without extra expenses, e.g. the methanol synthesis plant is near the CO_2 emission source.

Table 2. Energy balances.

	Case A	Case B
Energy balance (MJ/h)		
Reformer*	475	-
Methanol converter*	-221	43.8
Feed **	1088 (CH_4)	2570 (H_2)
Total net energy (MJ/h)	1342	2614

* Heat duty
** Lower heating value

Table 3. Operation costs.

	Case A	Case B
Operation costs (€/h)		
Feed*	4.90 (CH_4)	12.86 (H_2)
Electricity **	4.94	0.85
Total operation costs	9.84	13.71

* CH_4 0.45 snt/MJ [10], H_2 0.5 snt/MJ [11]
** 1.94 snt/MJ [12], heat duty required in reactors is produced by hydrogen

Calculations indicate that energy needed to produce 1 kmol/h methanol is in the Case B almost twice as high as in the Case A. If recycling is taken into account Case B becomes more energy efficient than without recycling, because un-reacted hydrogen can be reused and thus the competitiveness increases compared to the Case A. Operation costs are also higher in the Case B than in the Case A. Operation costs in the Case B will decrease, if cheaper hydrogen is available since this Case consumes quite a lot H_2. Merchant hydrogen prices vary considerably depending on the volume and form of the feedstock. Hydrocarbon based steam reforming is the cheapest way to produce hydrogen [13] and hydrogen produced by this technology can cost as little as 0.5 €/kg [11], which value is used in this study. CO_2 emissions trading can also affect the cost-effectiveness of the Case B, because this Case can exploit theoretically more CO_2 than Case A. In addition, emissions trading favour the Case B, because of larger net CO_2 consumption.

To conclude the presented results: Nowadays, with the selected assumptions, Case A (commercial natural gas based methanol synthesis) is economically more attractive, but decisions in energy politics can change the situation in the future.

Acknowledgements

References

[1] Lee, S. Methanol synthesis technology. United States 1990, CRC Press, Inc. 236 p.

[2] Chen, G. & Yuan, Q. Separation and Purification Technology, 34 (2004) 227-237.

[3] Liu, J., Shi, J., He, D., Zhang, Q., Wu, X., Liang, Y., Zhu, Q. Applied Catalysis A: General, 218 (2001) 113-119.

[4] Ma, Y., Sun, Q., Wu, D., Fan, W.-H., Zhang, Y.-L., Deng, J.-F. Applied Catalysis A: General, 171 (1998) 45-55.

[5] Ma, L., Tran, T., Wainwright, M.S. Topics in Catalysis, 22 (2003) 287-293.

[6] Mignard, D., Sahibzada, M., Duthie, J.M. & Whittington, H.W. International Journal of Hydrogen Energy, 28 (2003) 455-464.

[7] http://www.aspentech.com/

[8] Rostrup-Nielsen, T. Catalysis Today, 106 (2005) 293-296.

[9] Kroschwitz, J.I.(edit.) Kirk-Othmer Encyclopedia of Chemical Technology. Volume 16. 4. edition. United States 1995, John Wiley & Sons. 1117 p.

[10] http://www.energiamarkkinavirasto.fi/data.asp?articleid=1104&pgid=188 (in Finnish)

[11] Dincer, I. International Journal of Hydrogen Energy, 27 (2002) 265-285.

[12] http://www.energia.fi/page.asp?Section=2772 (in Finnsh)

[13] Rostrup-Nielsen, J.R. & Rostrup-Nielsen, T. Cattech, 6 (2002) 150.

MATHEMATICAL MODELING OF TOLUENE
OXYDATION ON VANADIA/TITANIA CATALYST
UNDER UNSTEADY STATE CONDITIONS

<u>Reshetnikov S.I.</u> and Ivanov E.A.

Boreskov Institute of Catalysis, Pr. Lavrentieva, 5, 630090, Novosibirsk, Russia.

E-mail: reshet@catalysis.ru

Experemental and theoretical studies performed in a last decades have proved that unsteady state operation of heterogeneous catalytic reactors can be an effective tool to improve reactor performance [1, 2]. The physical basis for such improvement lies in the ability to regulate the concentration of adsorbed species by reaction conditions.

One of the ways to perform the process of hydrocarbon catalytic oxidation is to divide the reaction space in a few separate zones, for instance, a zone of the catalyst reduction by hydrocarbon and a zone of its oxidation by oxygen and catalyst circulation between zones (see, for example [3, 4]). This operation was industrially used in the DuPont process of butane oxidation to maleic anhydride over vanadium-phosphorous catalysts [3].

Second way is regulation (or periodic operations) when the reagents concentrations, gas flow rates are changed periodically in the fixed bed catalytic reactor input - cyclic reduction and re-oxidation of a catalyst [1,5]. The possible objectives of the use of periodic operation of catalytic reactors are to provide an increased conversion, improved selectivity, and reduced deactivation. Aditionally, an important information could be extracted from the transient behavior of the reaction after the fast change of the composition of reaction mixture over the catalyst. Modeling of the transient phenomena allows obtaining valuable kinetic constants, which often could not be determined from the steady state experiments.

For the toluene oxidation by the same researchers it was shown that benzaldehyde (BA) and some CO_2 are formed in the flow of toluene, while after consecutive oxygen introduction only maleic anhydride and carbon dioxide are observed. These data were explained by a conjugated oxidation of the catalyst and desorption/formation of the products. In [6] during the toluene interaction with a V/Ti-oxide catalyst found that BA is formed for a long time with a very high selectivity (around 100%) while CO_2 is evolved only during the first moments of the reaction. This was assigned to different surface oxygen species.

The aim of this work is modeling of toluene interaction with a pre-oxidized vanadia/titania catalyst under periodic operation.

The catalyst was prepared via a well-known grafting technique by the vapor deposition of $VOCl_3$ on the surface of TiO_2 (Aldrich). The BET specific surface area was equal to 9 m^2/g, the amount of vanadium was found to be 0.57 wt. % that corresponds to 0.75 of a monolayer (ML) [7] . It is important that this catalyst contained only about a monolayer of the surface vanadia species and did not contain any bulk crystalline V_2O_5.

An experimental set-up used for the transient response study has been described in [8]. The catalyst (1 g) was loaded into a fixed bed reactor of i.d. 6 mm. Before each experiment, the catalyst was pretreated in an oxidative atmosphere (20 vol. % O_2 in Ar) at 673 K for 30 min. Then the flow was switched to Ar and the catalyst was cooled to the reaction temperature. The reaction was carried out with a 2 vol. % toluene/Ar mixture (1 ml/s). The products were analyzed with a quadrupole mass spectrometer and a gas chromatograph.
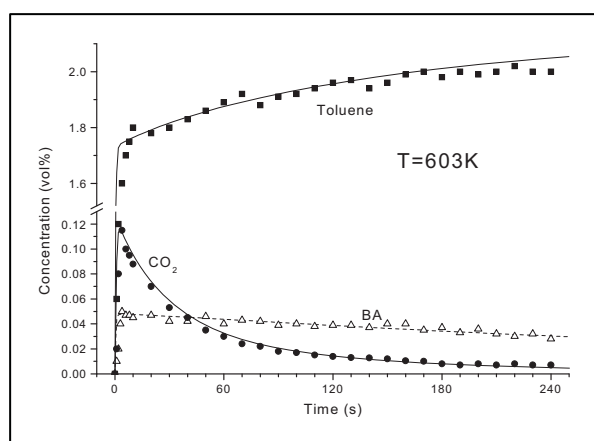
Fig.**1.** Toluene interaction with the pre-oxidised *0.75 ML* catalyst at Symbols – experiments, lines – modelling .

A typical transient behavior of the toluene, benzaldehyde and CO_2 concentrations as a result of interaction of toluene with the 0.75 ML V/Ti-oxide catalyst is demonstrated in Fig. 1 [8]. The main products of the interaction of toluene with the pre-oxidized vanadia/titania catalyst in the temperature range 523-633 K are benzaldehyde (BA), CO_2, CO and H_2O. The transient behavior of CO is similar to CO_2, but the CO concentration is 5–6 times lower. Hence, it was not taken into account. It is seen that the dynamics of the CO_2 and benzaldehyde formation are different. CO_2 is formed during the initial time of the reaction, declining quickly with time, while BA is formed for a prolonged time.

For mathematical modeling of periodic operation the kinetic model of the interaction of toluene with a pre-oxidized vanadia/titania catalyst was used. The model is based on the

following main assumptions [8]: (i) Benzaldehyde and CO_2 are formed mainly on different active sites; (ii) the ratio of these active sites is independent of the temperature; (iii) adsorbed benzoates and other coke-like species are formed on the surface of vanadia/titania during the interaction; (iv) diffusion of oxygen from the bulk of the catalyst is not important in the studied temperature range.

A kinetic scheme with the minimal amount of steps that appropriately describes the response curves of toluene and reaction products was chosen. It includes 5 steps [8]:

1) $C_6H_5CH_3 + 2 [YO] \rightarrow 2 [Y] + C_6H_5CHO + H_2O$,

2) $2 C_6H_5CHO + 3 [YO] \rightarrow 2 [YC_6H_5COO] + [Y] + H_2O$,

3) $C_6H_5CH_3 + 18 [ZO] \rightarrow 18 [Z] + 7 CO_2 + 4 H_2O$,

4) $C_6H_5CH_3 + [ZO] \rightarrow [ZOC_7H_8]$,

5) $[ZOC_7H_8] + 17 [ZO] \rightarrow 18 [Z] + 7 CO_2 + 4 H_2O$.

Toluene from the gas phase interacts with nucleophilic oxygen sites [YO] of the catalyst with the formation of benzaldehyde (step 1). Then, benzaldehyde interacts with the same oxygen sites forming benzoate on the catalyst surface (step 2). Toluene can be adsorbed with its aromatic ring parallel to the surface on a group of electrophilic sites [ZO]. Electrophilic oxygen may provide a fast formation of CO_2 by fission of the aromatic ring (step 3). Toluene may also be adsorbed on [ZO] sites (step 4). Adsorbed toluene interacts slowly with [ZO] sites forming the total oxidation products (step 5).

The kinetic equations corresponding to steps 1–5 are as follows:

$$r_1 = k_1 C_T \theta_{YO}^m, \quad r_2 = k_2 C_{BA} \theta_{YO}, \quad r_3 = k_3 C_T \theta_{ZO}^n, \quad r_4 = k_4 C_T \theta_{ZO}, \quad r_5 = k_5 \theta_T \theta_{ZO},$$

where C_T and C_{BA} are the concentrations of toluene and benzaldehyde in the gas phase (mole fractions); θ_{YO}, θ_{ZO}, θ_{YB}, θ_{ZT} are the fractions of adsorbed species, benzoate and toluene on the catalyst surface, correspondingly; θ_Y, θ_Z are the fractions of not occupied sites of the monolayer; k_j are the rate constants of the corresponding steps (s^{-1}); m, n are the reaction orders in the kinetic equations r_1 and r_3.

To describe the transient behavior of interaction of toluene with pre-oxidized catalyst, the mathematical model of the continuous stirred tank reactor was used.

The response curves presented in Fig. 1 indicate that the dynamics of the CO_2 and BA formation are different. The CO_2 formation declines quickly, while BA is formed over extended period of time. Except for gaseous products, the coke-like species are formed on the catalyst surface. This follows from the balance calculations as well as from the oxygen

introduction experiments after the toluene interaction. After the oxygen introduction, CO_2, CO и H_2O were found in the products, while benzaldehyde was never observed.

On the base kinetic model the modeling of the interaction of toluene with the pre-oxidized vanadia/titania catalyst has been performed. It was shown, that under periodic operation it is possible to increase selectivity towards to BA essentially with comparison steady state ones. This was due to presence a different surface oxygen species: nucleophilic lattice species and electrophilic surface species participating in the parallel routes of the toluene oxidation. The latter species could be formed easier in the presence of gaseous oxygen providing the decrease of BA selectivity.

References

1. G.K. Boreskov, Yu.Sh. Matros: *Catal. Rev.-Sci. Eng.*, **25**, 551 (1983).

2. P. Silveston, R.R. Ross, A. Renken: *Catal. Today*, **25**, 91 (1995).

3. R. M. Contractor, A.E. Sleight. *Catal. Today. 1*, 587 (1987).

4. S.I. Reshetnikov, N.M. Ostrovsky: *React. Kinet. Catal. Lett.*, **71**, 129 (2000).

5. Silveston, P.; Hudgins, R. R.; Renken, A. *Catal. Today*, **25**, 91 (1995).

6. Bulushev, D. A.; Kiwi-Minsker, L.; Renken, A. *Catal.Today*, **61**, 271 (2000).

7. Bulushev, D. A.; Kiwi-Minsker, L.; Zaikovskii, V. I.; Lapina, O. B.; Ivanov, A. A.; Reshetnikov, S. I.; Renken, A. *Appl. Catal. A: General*, **202**, 243 (2000).

8. Bulushev, D. A., Ivanov E.A., Reshetnikov S.I., Kiwi-Minsker, L., Renken, A. *Chem. Eng.J.,* **107,** 147 (2005).

PP-68

KINETICS OF THE N-HEXANE SKELETAL ISOMERIZATION OVER NEW SULFATED ZIRCONIA CATALYSTS IN FIXED-BED REACTOR

G.G. Volkova, L.N. Shkuratova, A.A. Budneva, E.A. Paukshtis, <u>S.I. Reshetnikov</u>

Boreskov Institute of Catalysis SB RAS, Pr. Akademika Lavrentieva 5,
Novosibirsk, 630090, Russia

Naphtha isomerization is a simple and cost effective technology for increasing octane number of gasoline. Isomerization of naphtha is composed mainly of conversion of n-pentane and n-hexane into iso-pentane, mono-methyl and di-methyl hexane. Di-methyl hexane has higher octane number than mono-methyl hexane, and is preferentially produced at low temperature subject to chemical equilibrium. Recently new acid catalyst based on sulfated zirconia have been developed and successfully commercialized by UOP LLC [1-2]. This catalyst revealed higher activity for light naphtha isomerization at lower temperature and is less sensitive to the amount of water in feed oil than conventional catalysts. By the large demand of desired isomerization products development of new more active catalysts has been continued [3]. Group of researchers from Boreskov Institute of Catalysis and Institute of Hydrocarbons Processing has developed new sulfated zirconia catalysts with high density of Lewis acid sites [4].

The aim of this work was to investigate the kinetics of n-hexane skeletal isomerisation over $Pt/SO_4^{2-}/Al_2O_3/ZrO_2$ catalysts with different density of Lewis acid sites.

Catalysts were evaluated in fixed-bed flow reactor. Study of the kinetics of isomerization of the n-hexane on solid superacids [5] has shown that it is the possible to divide process into three stages. The first, most fast stage, is formation of 3-methyl pentane (3MP) from 2-methyl pentane (2MP), and then, 2,3-methyl butane (2,3DMB) formation up to thermodynamic equilibrium. The reactions of the isomerization of n-hexane and the formation of 2,2- methyl butane (2,2DMB) has the comparable rates. Third stage is the side products formation.

For the kinetic analysis the following reaction network was used:

$$\text{n-C}_6 \underset{k_{-1}}{\overset{k_1}{\leftrightarrow}} \text{2MP} + \text{3MP} + \text{2,3 DMB} \underset{k_{-2}}{\overset{k_2}{\leftrightarrow}} \text{2,2 DMB}$$

$$\downarrow$$

$$\text{C}_1\text{-C}_5$$
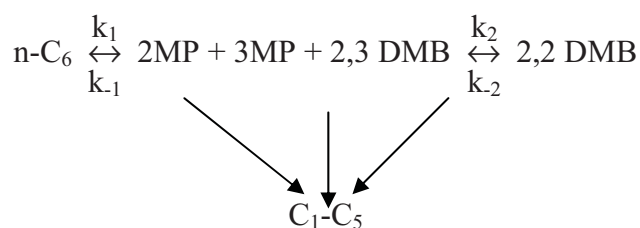
$$\frac{dC_1}{d\tau} = -k_1 C_1 (1 - \frac{C_2}{C_1 K_{e1}}) \, ,$$

$$\frac{dC_2}{d\tau} = k_1 C_1 (1 - \frac{C_2}{C_1 K_{e1}}) - k_2 C_2 (1 - \frac{C_3}{C_2 K_{e2}}) - k_3 C_3,$$

$$\frac{dC_3}{d\tau} = k_2 C_2 (1 - \frac{C_3}{C_2 K_{e2}}),$$

$$\frac{dC_4}{d\tau} = k_3 C_2,$$

Where C_1 – mole fraction of n-hexane; C_2 - 2MP + 3MP + 2,3 DMB; C_3 - 2,2 DMB; C_4 – cracking products; τ - contact time; k_i, k_{-i} – rate constants of direct and reverse reactions of n-hexane isomerisation and 2,2 DMB formation; K_{ei} – equilibrium constants.

The calculation of the rate constants, characterizing the catalyst activity and selectivity was performed on the base of mathematical model of plug flow reactor. It is assumed that the reactions are pseudo-first order in reagents. The kinetic constants and activation energies were determined. The results of mathematical modeling are in good agreement with experimental data.

Table 1. Kinetic data for catalysts Pt/SO$_4^{2-}$/Al$_2$0$_3$/ZrO$_2$ in n-hexane skeletal isomerization at the pressure 3 atm and temperature 200°C.

Sample	Lewis acid sites N μmol g^{-1}	Rate constant k_1 ,c^{-1}	Rate constant k_2,c^{-1}
1	220	0.810	0.066
2	240	0.850	0.065
3	250	0.909	0.073
4	150	0.224	0.033
5	50	0.103	0.011

The data presented in Table 1 show that rate constant of n-hexane isomerization (k_1) for Catalyst 1-3 is fourfold as those for Catalyst 4-5, and k_2 which characterized the rate of desired product (2,2DMB) formation for Catalyst 1-3 (Lewis acidity 220-250 μmol g^{-1}) is also higher than for Catalyst 4-5 (Lewis acid sites 50-150 μmol g^{-1}). From these data it may be concluded that the rate of n-hexane isomerization is mainly determined by the density of Lewis acid sites on the surface of Pt/SO$_4$/ZrO$_2$ catalysts.

References

1. T. Kimura, Catal.Today, 81 (2003) 57.
2. S.A. Gembicki, Stud. Sur. Sci. Catal., 130 (2000) 147.
3. Patents:US 5,036,035, US 6,495,733, US 6,448,198, US 5,629,257, US 6706659
4. G.G. Volkova, L.N. Shkuratova, L.S. Egorova, E.A. Paukshtis, A.A. Budneva, G.N. Kustova, S.I. Reshetnikov, V.K. Duplyakin, V.A. Likholobov, Russian Patent 28.09.2005, application 2004132964.
5. D.M. Brouwer, J.M. Olderik, Reac. Trav. Chim. 1968, 87, 721.

KINETIC STUDY OF AMMONIA SYNTHESIS OVER Ru/C CATALYST

Ilenia Rossetti[1], Francesco Ferrero[2], <u>Nicola Pernicone</u>[3] and Lucio Forni[1*]

[1]*Dipartimento di Chimica Fisica ed Elettrochimica, Università degli Studi di Milano,*

v. C. Golgi 19   I-20133 Milano, Italy

[2]*v. Turbigo, 2   I-28100 Pernate (NO), Italy*

[3] *v. Pansa, 7   I-28100 Novara, Italy*

*lucio.forni@unimi.it

Introduction

Ru-based catalysts for ammonia synthesis are gaining growing attention, due to a significant increase of productivity with respect to the traditional Fe-based catalyst [1-3]. This is mainly due to the kinetic inhibition of the Fe catalyst by ammonia [4,5]. Though the availability of reliable kinetic equations is of utmost importance for both design and operation of catalytic reactors, only some fundamental papers on the main reaction steps have been published [6,7] and, to the best of our knowledge, no kinetic model has been reported so far for the industrially employed Ru/C catalyst. To fill this gap we undertook a kinetic test program aiming at evaluating the performance of a Ru/C catalyst under widely different reaction conditions of industrial relevance. Modelling of the results allowed us to propose a possible kinetic model for the present reaction, suitable for reactor design.

Experimental

A 3.8 wt% Ru on C catalyst, promoted with K, Cs and Ba [8], diluted with quartz powder, was employed for the collection of kinetic data. Catalytic activity was measured in a microreactor [2,8], by varying GHSV between 50,000 and 400,000 h^{-1}. The test program included 20 runs, during which we varied temperature (370, 400, 430, 460°C), pressure (50, 70, 85, 100 bar) and H_2/N_2 feeding ratio (1.5 or 3 vol/vol). Data elaboration was accomplished by non linear regression and subsequent Runge-Kutta numerical integration of the model rate equations, with the usual objective function based on the minimization of the mean square sum of the differences between calculated and experimental data.

Results and Discussion

Different kinetic models have been tested. As expected, fitting of experimental data of our Ru-based catalyst by the classical Temkin equation was not satisfactory, the Fe-based

catalyst being inhibited by ammonia and Ru by H_2. Further attempts were carried out by varying the value of α in the Temkin equation, in order to obtain at least a better data fitting, but the model did not show satisfactory results even with α as low as 0.15 and therefore it was abandoned.

A LHHW approach was then tried, in order to better highlight the role of single reaction steps on the overall kinetics [5,9], but it did not allow a physically meaningful representation of every adsorption parameters.

Therefore, we tried to introduce terms accounting for the competitive adsorption properties of the Ru-based catalyst, by modifying the classical Temkin equation. The general form of the proposed model is the following:

$$\frac{d\eta}{d\tau} = k_f \cdot \lambda(q) \frac{(a_{N2})^n \cdot \left[\frac{(a_{H2})^{3n}}{(a_{NH3})^{2n}}\right]^{\alpha} - \frac{1}{(Ka)^{2n}} \cdot \left[\frac{(a_{NH3})^{2n}}{(a_{H2})^{3n}}\right]^{1-\alpha}}{1 + K_{N2} \cdot \frac{1}{(Ka)^{2n \cdot w3}} \frac{(a_{NH3})^{2n \cdot w3}}{(a_{H2})^{3n \cdot w2}} + K_{H2} \cdot (a_{H2})^{3n \cdot w2} + K_{NH3} \cdot (a_{NH3})^{2n \cdot w3}}$$

The best fit of our experimental data was obtained with $n = 0.5$, $\alpha = 0.25$ and $w2 = w3 = 0.2$. This resulted in the following three-parameters equation:

$$\frac{d\eta}{d\tau} = k_f \cdot \lambda(q) \frac{(a_{N2})^{0.5} \cdot \left[\frac{(a_{H2})^{0.375}}{(a_{NH3})^{0.25}}\right] - \frac{1}{Ka} \cdot \left[\frac{(a_{NH3})^{0.75}}{(a_{H2})^{1.125}}\right]}{1 + K_{H2} \cdot (a_{H2})^{0.3} + K_{NH3} \cdot (a_{NH3})^{0.2}}$$

It should be remarked that no significant effect of N_2 adsorption was observed, while, as expected, H_2 competition with N_2 was important. The best values of the various constants for our Ru/C catalyst have been determined, obtaining an average agreement around 5% between calculated and experimental data. Some typical examples are shown in Fig. 1. The consistency of the optimised parameters was checked through the Arrhenius or Van't Hoff equations, which allowed to obtain reliable kinetic and thermodynamic parameters, with excellent correlation coefficients. The values of ΔH_{ads} derived from this model confirm H_2 inhibition, although the NH_3 adsorption term cannot be neglected. The value of the activation energy obtained with the present analysis for our Ru-based catalyst was $E_a = 23$ kcal/mol.

The present data were compared with those of a commercial Fe-based catalyst, tested under its usual reaction conditions, *i.e.* 100 bar, 430°C and H_2/N_2=3 (vol/vol). Our Ru-based catalyst outperformed both the traditional and the innovative Fe-based samples, mainly by noticeably decreasing the activation energy required for N_2 dissociation (35 kcal/mol for the magnetite-based catalyst and 32.5 kcal/mol for the wustite-based one). This allows to strongly improve catalyst productivity. Indeed, when fixing, *e.g.*, operating conditions such as

PP-69

$\tau = 0.0010$ h L mol^{-1}, H$_2$/N$_2$ = 3 (vol/vol) and T = 460°C, the same ammonia content in the exit gas obtainable with the Fe-magnetite catalyst at 100 bar (6.6%) can be obtained at 57 bar with the Ru/C catalyst (Fig.2). Hence our Ru-based catalyst allows to decrease by 40-50% the working pressure with respect to a commercial magnetite-derived catalyst. Similar considerations can be extended to calculate the increase of NH$_3$ concentration in the reactor outlet gas at the fixed pressure of 100 bar. Such an increase is +28% and +42% at 430 and 460°C, respectively. If preferred, it is also possible to decrease the bed volume of Ru-based catalyst. In this case the same conversion of the magnetite-based catalyst is attained, under identical operating conditions, with bed volumes –34% and –54% at 430 and 460°C, respectively.

Conclusions

The present results show that with our Ru/C catalyst the equilibrium conversion can be attained at 460°C by feeding under-stoichiometric H$_2$/N$_2$ mixture. The simple addition of adsorption terms for H$_2$ and NH$_3$ in the Temkin equation allowed to obtain a reliable kinetic model, useful for both design and operation of industrial reactors. An activation energy value as low as 23 kcal/mol for the ammonia synthesis reaction was obtained, showing that the activation barrier for N$_2$ dissociation on Ru is by far lower than for the traditional Fe-based catalyst, prepared from either magnetite or wustite precursor. When comparing our Ru/C catalyst with the best commercial Fe catalysts, it must be concluded that a substantial reduction of the reaction pressure can be obtained with the same plant productivity.

References

1. Z. Kowalczyk, J. Sentek, S. Jodzis, E. Mizera, J. Goralski, T. Paryjczak, R. Diduszko, Catal. Lett. 45, 65 (1997)

2. L. Forni, D. Molinari, I. Rossetti, N. Pernicone, Appl. Catal. A: Gen. 185, 269 (1999).

3. C.Liang, Z.Wei, Q.Xin, C.Li, Appl. Catal. A: General 208, 193 (2001).

4. S.R. Tennison, in: "Catalytic Ammonia Synthesis" (J.R. Jennings, Ed.), Plenum Press, New York, 1991, p. 303.

5. G. Gramatica, N. Pernicone, in: "Catalytic Ammonia Synthesis" (J.R. Jennings, Ed.), Plenum Press, New York, 1991, p.211.

6. O. Hinrichsen, F. Rosowski, A. Hornung, M. Muhler, G. Ertl, J. Catal. 165, 33 (1997).

7. O. Hinrichsen, Catal. Today, 53, 177 (1999).

8. I. Rossetti, N. Pernicone, L. Forni, Appl. Catal. A: Gen. 208, 271 (2001).

9. G. Buzzi Ferraris, G. Donati, F. Rejna, S. Carrà, Chem. Eng. Sci., 29 (1974) 1621.
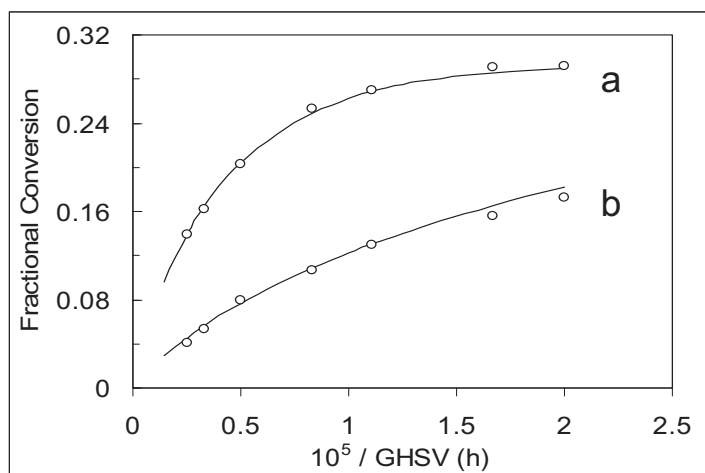
Figure 1: Calculated kinetic curves (Modified Temkin Equation) and experimental points under the following working conditions: a) P=100 bar, T=460°C, H_2/N_2=1.5 (vol/vol); b) P=85 bar, T=430°C, H_2/N_2=3 (vol/vol)
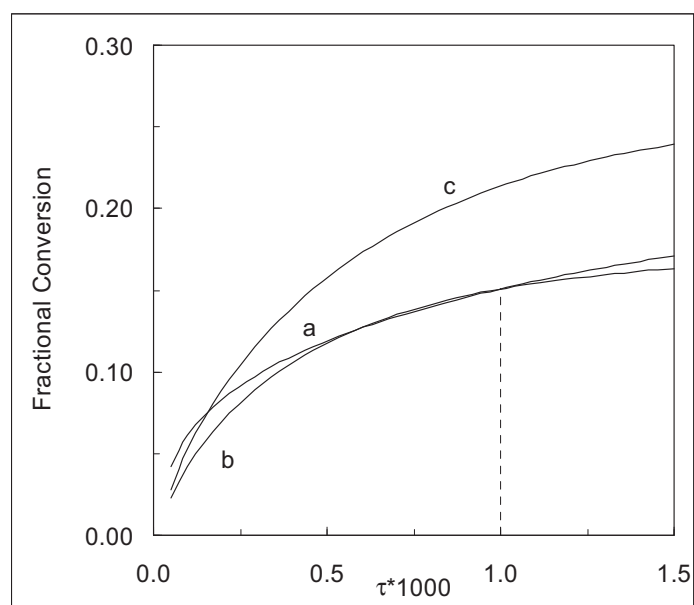
Figure 2: Performance of Fe-based catalysts and of Ru/C catalysts at 460°C, H_2/N_2 = 3: a) Fe at 100 atm; b) Ru/C at 57 atm; c) Ru/C at 100 atm.

EXPERIMENTAL STUDY OF FEATURES OF THE ETHYLENE GLYCOL OXIDATION PROCESS

M.A. Salaev, V.S. Shmotin, A.S. Knyazev, O.V. Vodyankina, L.N. Kurina

Tomsk State University, pr. Lenina, 36, Tomsk, Russia

Fax: (3822) 52-95-85, e-mail: vodyankina_o@mail.ru

Partial oxidation of organic compounds is one of the most important methods of synthesis of such available compounds as formaldehyde, ethylene oxide, acetic acid, etc. Recently the interest to the process of ethylene glycol oxidation into glyoxal on silver catalysts has also increased.

Glyoxal is a highly active bifunctional organic compound widely used for production of pharmaceuticals and pesticides; it proved to be a valuable intermediate especially in the preparation of heterocyclic compounds. It is most widely used as a cross-linker in the production of permanent press resins for textiles. It has also found application in the production of moisture resistant glues and adhesives as well as moisture resistant foundry binders. It is also used to improve the wet strength of paper and the moisture resistance of leather [1].

The world production of glyoxal is approximately 170000 tones per year. At present the production of glyoxal in Russia is absent while the requirement in it is over 10000 tones per year. Main producers of glyoxal are Germany, China and USA. Detailed information about glyoxal technology is not published in literature. There are sparse patent data describing the preparation of catalytic systems and the realization of the process of glyoxal synthesis in a laboratory reactor. The experimental study of the ethylene glycol oxidation process in flow reactor with a fixed catalyst bed is necessary to elaborate the macrokinetic model.

The aim of the present work is the detailed investigation of the regime of ethylene glycol oxidation process into glyoxal on the polycrystalline silver catalyst.

In the present work the experimental study of the influence of contact time, partial pressures of components in the reaction mixture and temperature on the main factors of the process such as ethylene glycol conversion and glyoxal selectivity has been performed. The investigations in a flow fixed bed reactor with i.d. of 16 mm. (height of catalyst bed was 20 mm, reactor length was 100 mm) [2] have been carried out, the temperature interval was 500-650 $^{\circ}$C. In each experiment the peak of the temperature gradient along the reactor under steady operating conditions has been measured and recorded as the reaction temperature.

The influence of the weight hour space velocity of the reaction mixture on the behavior of the temperature gradient along the reactor has been studied. The decrease of the contact time up to values lower than 0.01 sec leads to the shift of the "hot" zone to the bottom part of reactor. The approaching of the "hot" zone to the heat-treatment cooler, which is immediately located under the catalyst bed, increases instability of the temperature regime in reactor and, finally, leads to the "dying-away" of reaction.

In this work the boundaries of stable realization of the ethylene glycol oxidation process into glyoxal on the polycrystalline silver catalyst have been characterized. The manners of temperature regime realization management in the laboratory level by changing of reaction mixture composition have been developed. The control is provided:

- *firstly*, due to the increase and decrease of partial pressure of components at the constant ratio between them;

- *secondly,* due to changing of oxygen/alcohol (O_2/EG) molar ratio under inert gas constant dilution of reaction mixture that allows to vary the ratio between the reactions of partial and deep oxidation of ethylene glycol. The variation of O_2/EG molar ratio, in its turn, changes the amount of emitting heat and decreases/increases the silver catalyst heating-up temperature.
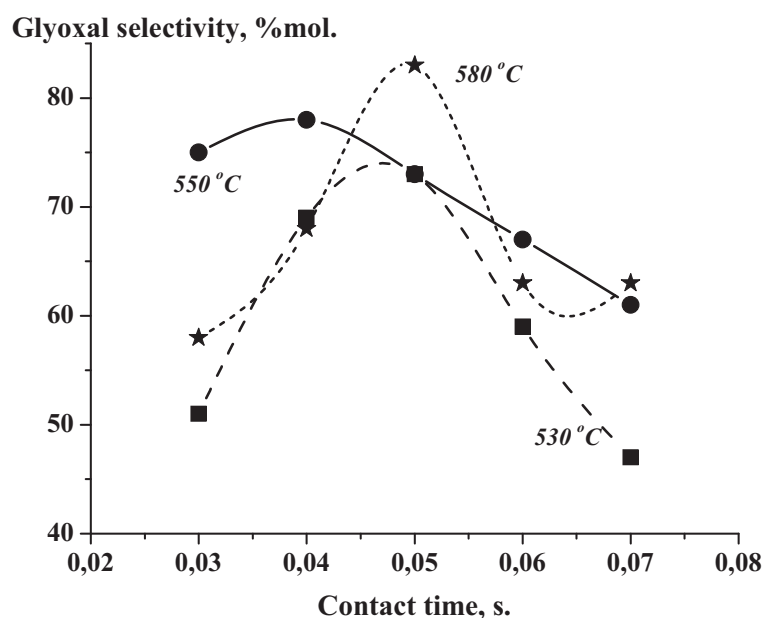
Fig. 1. Effect of the contact time on the glyoxal selectivity.

The contact time variation exerts its influence on the selectivity of the process of ethylene glycol partial oxidation into glyoxal (*Fig. 1*). At all investigated temperatures the extreme dependences with the maximum glyoxal selectivity in the range of 0.04-0.05 s. have been obtained. Under contact times higher than aforementioned the glyoxal selectivity is decreased due to the deep oxidation reaction of the desired product up to CO_2 or because of the participation of glyoxal in processes which lead to the occurrence of carbon-content deposits on the silver catalyst surface as it was shown

earlier [3]. The decrease of the contact time leads to the incomplete interaction of the reaction mixture with the catalyst surface that is accompanied by the reduction of the glyoxal selectivity.

It is interesting to note that the increase of the contact time of the reaction mixture with the catalyst leads to the insignificant reduction of the ethylene glycol conversion (*Fig. 2*). Possibly the obtained result is associated with the formation of carbon deposits on the silver surface. These deposits particularly poison the active centers of the catalyst surface under investigated conditions ($O_2/EG/N_2$ =1.1/1.0/20.0). Lack of oxygen-content in the reaction mixture does not allow removing the carbon deposits from the catalyst surface completely. And under long-continued contact times the rate of the carbon deposit formation dominates over their burning-out rate. As a result a part of the active silver surface is inaccessible to the selective ethylene glycol transformation.

Fig. 2. Effect of the contact time on the ethylene glycol conversion.

In the present work the thermodynamic analysis of routes of the ethylene glycol transformation such as dehydrogenation, partial oxidation, and oxidative dehydrogenation has been carried out at $550^{\circ}C$. Both partial oxidation and oxidative dehydrogenation of ethylene glycol routes have been mainly realized. Kinetic equations describing the glyoxal formation routes have been derived. Physical-chemical properties of individual components and its mixtures have been calculated. The hydrodynamic modes of steams of reaction mixtures and products in the reactor branch pipe and in the catalyst bed have been estimated.

Literature

1. Mattioda G., Metivier B., Guette J.P. What can you do with glyoxal // Chemtech. 1983 V.13(8) 478 – 481.

2. Vodyankina, O. V.; Kurina, L. N.; Izatulina, G. A.; Arkatova, L. A. Vapor-phase catalytic oxidation of ethylene glycol to glyoxal. // Zhurnal Prikladnoi Khimii (Sankt-Peterburg) 1997. 70(12) 2007-2010.

3. Vodyankina, O.V.; Koscheev, S.V.; Yakushko, V.T.; Salanov, A.N.; Boronin, A.I.; Kurina, L.N. // Journal of Molecular Catalysis A: Chemical 2000 158(1) 381-387.

MODEL OF THE REACTOR FOR BUTYL LACTATE PRODUCTION

S.V. Schactlivaya, D.N. Kondratiev, V.F. Shvets, R.A. Kozlovskiy

D.I. Mendeleev University of Chemical Technology of Russia, Chair of Basic Organic and Petrochemical Synthesis, 9 Miusskaya Square, Moscow, 125047, Russia, kra@muctr.edu.ru

Abstract

Esterification of lactic acid with butanol-1 (eq. (1)) in presence of strong-acid cation-exchange resin "Levatit" as a catalyst was investigated. Kinetic equations in batch reactor (in kinetic region) and in a tube fixed-bed reactor were found. Mathematical model of circulating semibatch installation for butyl lactate production was elaborated. The model describes experimental data adequately.

Introduction

Butyl lactate is one of the promising "green" chemical which successfully replaces toxic and environmentally harmful solvents (for example chloro-organic solvents). Butyl lactate is biodegradable substance and is synthesized from lactic acid which is produced from renewable resources. That's why there is great interest for highly efficient technology for butyl lactate production. In other hand strong-acid cation-exchange resins are expected to be very suitable heterogeneous catalysts for esterification reactions. The aim of present work was obtaining of kinetic description and, on this basic, elaboration of mathematical model of a reactor for butyl lactate production.

$$\text{(1)}$$
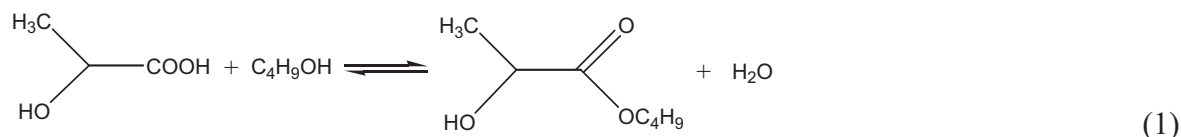
Results

At the beginning kinetics of esterification was investigated in a batch reactor in kinetic region. Strong-acid cation-exchange resin "Levatit" was used as a heterogeneous catalyst. The Lengmuir-Hinshelwood like kinetic equation, well describing all experimental data, was obtained:

$$\frac{dC_{BL}}{d\tau} = \frac{C_{cat}\left(k_1 C_B C_L - k_2 C_{BL} C_W\right)}{1 + b_W C_W} \tag{2}$$

Where C_{cat} – catalyst concentration, g/L; C_B, C_{BL}, C_L, C_W - concentrations of butanol-1, butyl lactate, lactic acid and water respectively, mol/L; k_1, k_2 - constants of direct and back reactions respectively; b_W - water adsorption constant.

At the next stage the kinetics of reaction was investigated in a fixed-bed tubular reactor. It was found that experimental data were described adequately by equation (3), which differed from kinetic equation for batch reactor (1) by presence coefficient $\beta = 0.14$. All the rest kinetic parameters (k_1, k_2, b_W) remained the same. The coefficient β evaluates diffusion resistance for mass transfer between liquid flow and catalyst's grains.

$$\frac{dC_{BL}}{d\tau} = \beta \frac{C_{cat}\left(k_1 C_B C_L - k_2 C_{BL} C_W\right)}{1 + b_W C_W} \tag{3}$$

The kinetic equation (3) was used for making of mathematical model of laboratory circulating semibatch installation for butyl lactate producing (Fig. 1). Operating mode of the installation was following: Reaction mixture (at the start of experiment: butanol and lactic acid) was circulated continuously by peristaltic pump (point 9) through thermostated fixed-bed tubular reactor and boiling still (point 10). In the reactor catalytic esterification took place. The reaction mixture continuously boiled in the still and butanol-water azeotropic vapor moved up into the backflow condenser (point 2) where it condensed and flowed down into phase separator (point 4). In the separator heteroazeotropic liquid divided into organic and water layers. Water layer was continuously removed through outlet cock and organic one flowed back to the still. Water removing shifted equilibrium of esterification (eq. 1) to the right and made possible to achieve high conversion of lactic acid up to 99.5 %.
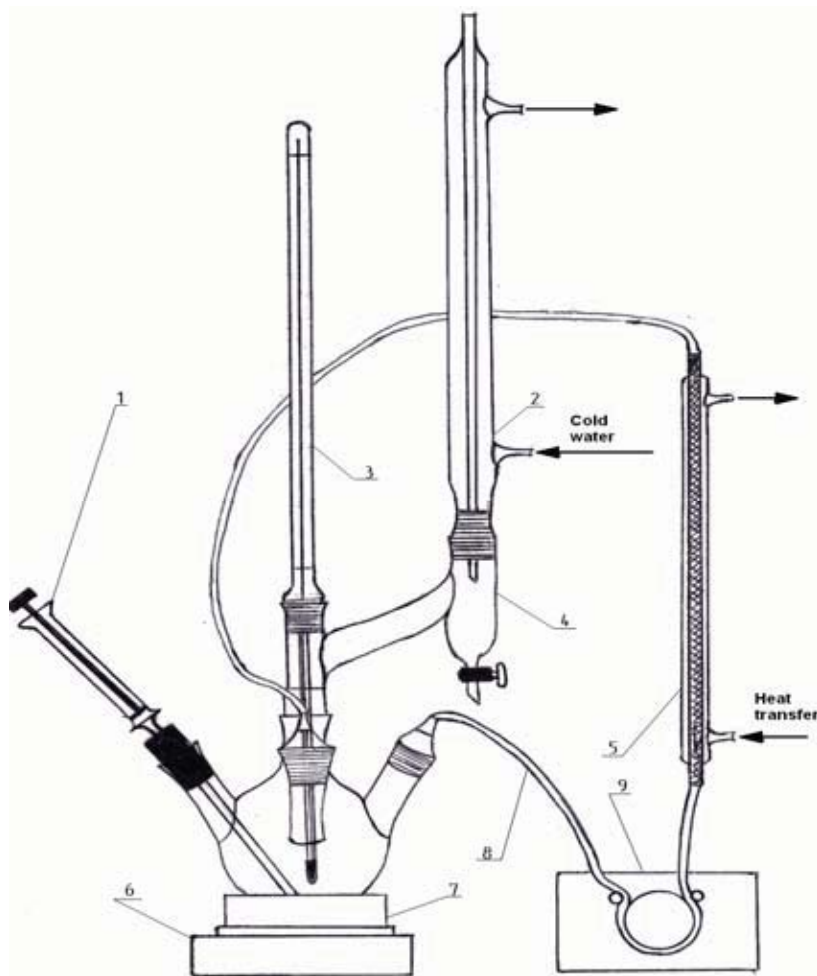
Mathematical model including equations of reaction kinetics (3), liquid-vapor equilibriums (in the boiling still) and mutual solubility (in the phase separator) was made. This model describes experimental data obtained on laboratory installation sufficiently adequate.

THE DEVELOPMENT OF PORTABLE HYDROGEN GENERATORS

Simagina V.I., **Storozhenko P.A.**[1], **Komova O.A.**, **Netzkina O.V.**

Boreskov Institute of Catalysis SB RAS, Novosibirsk, Russia
[1]*State Scientific Research Institute of Chemistry & Technology of Organoelement Compounds, Moscow, Russia*

Growing market of the mobile devices calls for safety effective sources of energy providing prolonged working period. Maximum gravimetric energy density of nickel-hydride and lithium-ion batteries used now does not exceed 0.2 Wh/g. Application of portable fuel cells allows to increase the energy density, but the problem of creation of hydrogen compact sources appears. At present several types of portable hydrogen generators are offered, including the generators based on hydrolysis of hydrides. Among the hydrides sodium borohydride ($NaBH_4$) is desirable due to its high hydrogen density – about 0.112 g/cm^3, whereas the density of liquid hydrogen is only 0.07 g/cm^3. The hydrolysis of $NaBH_4$ provides the amount of hydrogen twice more than in case of thermal decomposition of the hydride. Furthermore, alkaline solutions of sodium borohydride are stable during storage. The hydrolysis of $NaBH_4$ is observed even at room temperature, but for the complete hydrolysis the using of catalysts is necessary.

The works on creation of portable hydrogen generators were begun at the end of 90s. *Millennium Cell* company (USA) [1, 2] and *Central Research & Development Laboratorie*s (*Toyota)* [3, 4] achieved the most results in this area. However, essential disadvantages of proposed constructions are unsatisfactory mass and size properties. Overcoming of this problem is possible by development of active and stable catalysts, optimization of the catalytic bed and application of new engineering solutions.

Joint efforts of specialists of Boreskov Institute of Catalysis and State Scientific Research Institute of Chemistry & Technology of Organoelement Compounds allow to develop portable systems for hydrogen generation on the basis of sodium borohydride hydrolysis with optimized mass and size properties.

It was found that Pt and Rh catalysts supported on untraditional $LiCoO_2$ carrier show the highest activity in $NaBH_4$ hydrolysis in comparison with catalysts prepared using traditional supports – γ-Al_2O_3, TiO_2 and carbonaceous material. It should be mentioned that using of

$LiCoO_2$ provides stable hydrogen generation by request both in uninterrupted and in periodic modes of operation. As a result of performed investigations the preparation conditions of catalysts providing stable working of 100 Watt portable fuel cell were found.

The optimization of initial support geometry and the catalysts packing method allows to form the catalytic bed, providing uniform hydrogen generation both in uninterrupted and in periodic modes of operation.

It was showed that fixed-bed reactors can be used to provide a continuous, controllable reactions for generation of hydrogen from sodium borohydride. The reactor consists of a hollow tube with a top and bottom end caps, and screens to contain a catalyst material. The feed solution is pumped through the reactor. Upon contact with the catalyst, the hydrolysis reaction is initiated resulting in the generation of both the hydrogen and reaction by-products. The type and quantity of catalyst, the feed rate and the feed solution concentration are all key parameters in the reactor operation.

Carried out studies have permitted to develop the optimized design of hydrogen generators with automatic control system. During the testing it was shown that generator with mass of 300 g can provide work of 100 Watt portable fuel cell during 1 hour under one-time refueling by 150 ml of sodium borohydride solution.

References

[1] Amendola S.C., Sharp-Goldman S.L., Janjua M.S., Kelly M.T., Petillo P.J. Binder M., J. Power Sources 2000, 85, 186-189.

[2] Richardson B.S., Birdwell F.J., Pin F.G., Jansen J.F., Lind R.F., J. Power Sources 2005, (in press).

[3] Kojima Y., Suzuki K., Fukomoto K., Sasaki M., Yamatomo T., Kawai Y., Hayashi H., Int. J. Hydrogen Energy 2002, 27, 1029-1034.

[4] Kojima Y., Suzuki K., Fukumoto K., Kawai Y., Kimbara M., Nakanishi H., Matsumoto S., J. Power Sources 2004, 125, 22-26.

DEVELOPMENT OF BIOBASED CATALYTIC PROCESS: PECULIARITIES OF LACTIC ACID TO 1,2-PROPANDIOL HYDROGENATION OVER VARIOUS COPPER-CONTAINING CATALYSTS

Simakova I.L., Simonov M.N., Minyukova T.P., Khassin A.A.

Boreskov Institute of Catalysis SB RAS, Pr. Ak. Lavrentieva, 5, Novosibirsk 630090, Russia
E-mail: simakova@catalysis.ru

1,2-Propanediol has uses in a wide variety of applications including as monomers in polyester resins; in antifreeze and deicing fluids; in the manufacture of food, drug and cosmetic products; and in liquid detergents. The demand for 1,2-propanediol has recently increased as it could replace toxic ethylene glycol in these applications. Commercial production of propylene glycol is currently petroleum-based and involves the high pressure and high temperature hydrolysis of propylene oxide that is manufactured by either chlorohydrin's process or the per-oxidation process [1]. Successful attempts to replace petrochemicals are recently undertaken to produce 1,3-propanediol. DuPont, the creator of nylon products and the famous Lycra[®], has successfully manufactured a "smart" ingredient 1,3-propanediol for its newest polymer Sorona™ using a fermentation process based on corn sugar. Fabrics made with Sorona™ fiber are soft to the touch, exhibit excellent stretch and recovery characteristics, can be dyed readily and feature the easy care attributes of polyester and stain resistance for a wide variety of uses in the apparel and carpet industry. Because the corn is a renewable resource and can be produced anywhere in the world 1,3-propanediol becomes 40% less expensive to manufacture. At the same time a catalytic method of 1,2-propanediol synthesis has been in progress where promising starting material is a refined lactic acid obtained by fermentation of crude biomass. However high pressure up to 350 bar and temperature till 350°C is necessary for reasonable lactic acid conversion over Re, Ni Reney and Ru catalysts [2-4]. Silica-supported copper is a high selective catalyst to convert lactic acid carboxylic group to 1,2-propanediol hydroxyl one at less hydrogen pressure [5].

The goal of the present work is to study catalytic behaviour of various copper-containing catalysts in hydrogenation of a crude lactic acid in order to develop high selective catalytic process of 1,2-propanediol synthesis in mild reaction conditions.

Four samples of copper-containing oxides were chosen as copper catalyst precursors (*Table 1*): copper chromite with a tetragonally distorted spinel structure (Cu-Cr), copper-zinc

oxide (Cu-Zn), copper hydroxysilicate with Chrysocolla mineral structure (Cu-Si), copper-zinc hydroxysilicate with Zincsilite mineral structure (Cu-Zn-Si) [6]. Besides a sample of porous copper was tested to compare catalytic properties of unsupported copper catalyst.

Table 1. Copper-containing catalysts tested in lactic acid hydrogenation

Code	Catalyst precursor	Copper loading, at. %
Cu-Cr	$CuCr_2O_4$	33,3
Cu-Zn	$Cu_{0.08}Zn_{0.92}O*$	8
Cu-Zn-Si	$(Cu_{0.3}Zn_{0.7})_3[Si_4O_{10}](OH)_2*nH_2O$	12,9
Cu-Si	$Cu_8(OH)_{12}[Si_4O_{10}]*nH_2O$	50

The catalytic properties of the samples were studied in the fix-bed flow chemical reactor at atmospheric hydrogen pressure in a temperature range from 130 to 220°C. Catalyst grains of size 0.25-1.00 mm mixed with the quartz spheres of the size 0.63-1.6 mm were loaded in the glass reactor for the vapor phase hydrogenation of lactic acid. Before the catalytic run every sample of copper-containing oxide was reduced in pure hydrogen flow (1000-2000 h^{-1}) under a programmed temperature regime (2 K/min). An aqueous solution of lactic acid was supplied to the reactor by a syringe pump, vaporized in a heated line and brought to catalyst bed with hydrogen flow. Hydrogen was deoxygenated by passage through a deoxo unit. Condensable products were collected in a glass trap and analyzed by a GLC method (FID). Direct method of quantitative GLC analysis for carboxylic acids and glycols mixture was worked out.

According to GLC analysis 1,2-propandiol (PG) and propionic acid (PA) are the main products of lactic acid hydrogenation. Catalytic activity and selectivity obtained for different catalyst samples are presented on *Fig. 1*. Sample Cu-Cr with copper loading 33 % exhibited very low conversion of lactic acid and deactivated rapidly. Despite the fact that copper content in Cu-Zn-Si and Cu-Si catalyst samples is quite the same (13 and 14%), lactic acid conversion of the latter is essentially higher. It was not observed any catalytic activity of Cu-Zn catalyst sample.
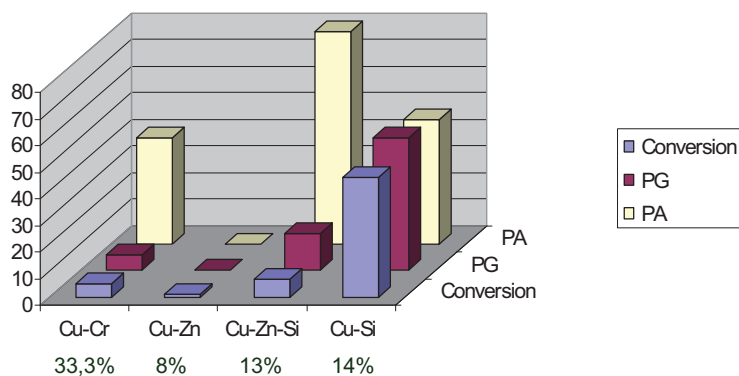
Fig. 1. Comparison of catalytic activity and selectivity of catalyst samples in lactic acid hydrogenation. Reaction conditions : T=200°C, P_{H2}= 1 bar, WHSV=0,08 h^{-1}

It was found that the maximum conversion of lactic acid was achieved over Cu-Si catalyst sample. Since all the catalyst samples exhibit catalytic activity in lactic acid hydrogenation only after reductive activation by hydrogen, it seemed to be reasonable to relate their catalytic activity difference with that in copper content and surface area of copper. Metallic copper content is the same in Cu-Si and Cu-Cr, but the latter shows very low catalytic activity. Difference between metallic copper surface area in Cu-Zn-Si and Cu-Si does not match the difference in their catalytic activity also (*Table 2 and Fig. 1*).

Table 2. *The copper metal content and copper surface area in reduced samples*

Catalyst sample	Cu-Zn-Si	Cu-Si	Cu-Cr	Cu-Zn
Cu^o content (at.%)	8.4	14.0	14.0	8.0
Cu^o surface area (m^2/g catalyst)*	~13	~27	~8	~2.6
Cu^o surface area (m^2/g catalyst)**	7.0	31.0	6.0	2.0

*Copper surface area was calculated from structural data

**Surface area was determined by N_2O titration

Lactic acid conversion was found to correlate with Cu^o surface area of copper-containing samples reduced. Similar catalytic behaviours were observed for these catalysts in dehydrogenation reaction of cyclohexanol to cyclohexenone as well as in dehydrogenation reaction of methanol [9]. It seems that similar active sites are responsible for the hydrogenation-dehydrogenation reaction performance.

With respect to Cu-Zn-Si sample, copper cations are known to occupy two structural positions in the "interlayer" and "layer" that differ by reduction temperatures. Copper cations from the "interlayer" and that from the "layer" are known to reduce at 270^oC and 380^oC respectively. According to the literature data copper atoms formed by the reduction of copper cations from the Zincsilite "layer" are crystallized mainly at the copper particles formed in the course of reduction of copper cations from the "interlayer". It was assumed that low Cu-Zn-Si specific catalytic activity may be explained by a partial decoration of copper particles, probably Si-O$_x$ clusters. The decoration indicates a strong metal-support interaction (SMSI), which may change the electronic and catalytic properties of copper [9]. Thus, we are inclined to assume that SMSI is responsible for low catalytic activity of Cu-Zn-Si catalyst.

Copper loading effect on PG and PA selectivity as well as lactic acid conversion was studied in the presence of the most active Cu-Si catalyst sample. PG selectivity slightly increases with the copper loading growth up to 50% (*Fig. 2*). Further increasing of copper content causes sharp decreasing of PG selectivity. Note that lactic acid conversion does not depend on copper loading at value more than 20%. Sample of porous unsupported copper was
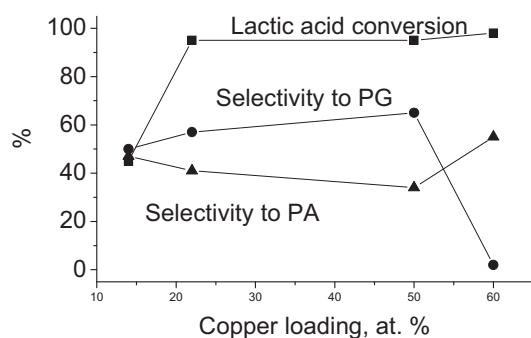
Fig. 2. Effect of copper loading on lactic acid conversion and selectivity of PG and PA. Reaction conditions: T=180°C, P$_{H2}$= 1 bar, WHSV=0,08 h^{-1}

found to be not active in 1,2-propandiol synthesis. Thus the highest conversion of lactic acid and PG selectivity is observed over copper-silica if ratio Cu/Si is equal to 1:1 as that is in nature Chrysocolla mineral.

During Cu-Si catalytic performance it was shown selectivity to PG and PA practically does not change during several hours that indicates promising catalytic activity (*Fig. 3*).

Effect of temperature and residence time on reaction rate and PG selectivity were studied. It is noteworthy that catalytic activity was very low at 160°C and the formation of pyrolysis products was not observed up to 220°C. Temperature growth causes lactic acid conversion increase but PG selectivity decrease.
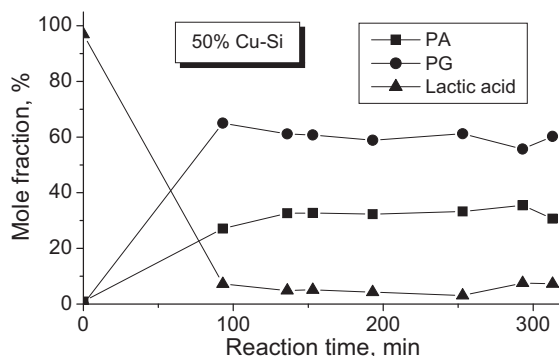
Fig. 3. Hydrogenation of lactic acid over Cu-Si sample. Reaction conditions : T=200°C, P$_{H2}$= 1 bar, WHSV=0,08 h^{-1}

To conclude catalytic behaviour of copper-containing catalysts to develop far-reaching process of biomass-derived crude lactic acid hydrogenation has been studied. Catalyst samples prepared via reductive activation of various copper oxides strongly differed in catalytic activity. The most active catalyst precursor was found to be chrysocolla-like copper hydroxosilicate with copper loading 50% at. provided 95% lactic acid conversion and 65% PG selectivity in mild reaction conditions [10]. To compare the known copper-silica catalyst provides 7% lactic acid conversion and 75% PG selectivity in these reaction conditions [5].

1. A.I. Rakhimov. Chemistry and technology of organic peroxide compounds. M.: Khimia. 1979.
2. WO 2000030744
3. US 6455742
4. US 6479713
5. R.D. Cortright et al. Applied Catalysis B 39 (2002) 353-359
6. T.M. Yurieva. Mat. Res. Innovat. 5 (2001) 74-80
7. T.P. Minyukova et al. Appl. Cat.A: G 237 (2002) 171-180
8. RF Appl. N 2005 141791

AUTOTHERMAL REFORMING OF GASOLINE FOR VEHICLES APPLICATION

E.I. Smirnov[1], V.V. Kireenkov, Yu.P. Ermakov, V.A. Kuzmin, N.A. Kuzin, V.A. Kirillov

Boreskov Institute of Catalysis, SB RAS, pr. Lavrentieva, 5, 630090, Novosibirsk, Russia
[1]E-mail: esmirnov@catalysis.ru

Introduction

While stoichiometrically operated gasoline spark ignition engines (SI-engines) equipped with three-way catalysts (TWC) are capable to fulfill the most stringent emission standards, the fuel consumption of SI-engines has to be lowered considerably for successful competition with diesel engines and fuel cell systems in vehicle application [1]. In order to reach fuel economy and to reduce CO_2 emissions the gasoline engines will need to switch from stoichiometrically to lean (with oxygen excess) operation. Unfortunately, TWC does not work in lean mixtures and for this reason emission standards for NO_x could not be achieved in the engine by operating lean, using only gasoline. This will require development of lean NO_x aftertreatment systems that complicates design of the engine, increases its cost and reduces its operating efficiency. On the other hand, mixtures of hydrogen and gasoline can burn lean enough to meet this requirement without any exhaust aftertreatment [2]. Combining the increase in heating value, lean operation and higher compression ratios provides a potentially high increase in thermal efficiency (as high as 56% according to [3], for example) for the hydrogen-enriched fuels. Thus hydrogen has good potential and great environmental advantages not only for vehicle fuel cell systems in the future but also as a supplemental fuel for SI-engines today.

Synthesis gas (syngas) with a high H_2 content can be on-board generated via autothermal steam reforming of the preliminary evaporated gasoline. Thus, there appears a chance to develop vehicle system with partial substitution of gasoline by syngas that improves thermal efficiency and ecological characteristics of SI-engines operation.

The aim of this work was to develop catalysts of autothermal reforming of gasoline into syngas, which will be stable to coke formation and provide a high productivity of hydrogen with his high content in the reforming products.

PP-74

Results

The lab-scale axial-type syngas reactor for autothermal steam reforming of gasoline was made of a stainless steel tube with heat insulation, which encloses monolith reinforced metal porous catalyst. The outer tube diameter is 84 mm, and the reactor length is 160 mm. The reactor design permits one to test catalysts of the standard size: 53 mm diameter and 57 mm length.

The technology of preparation of monolith reinforced metal porous catalysts has been recently developed at the Boreskov Institute of Catalysis for synthesis gas generation from natural gas [4]. This technology was used to prepare a catalyst sample for the autothermal reforming of gasoline also. To prepare the catalyst, one used a stainless steel net formed as a strip covered with Al_2O_3 and SiO_2. Then the support was impregnated with active components. The as-prepared catalytic strips were used to manufacture a multi-channel monolith by sintering a couple of spiraled flat and corrugated strips. The general view of catalytic strips and monolith reinforced metal porous catalysts presented on Fig. 1.

Fig. 1. General view of catalytic strips and monolith reinforced metal porous catalysts.

The setup for the catalysts testing (see testing scheme on Fig. 2) provides feed of the inlet air-gasoline-water mixtures with different concentration of the initial reagent amounts. The system of conditioning and preparation of the air-gasoline-water mixture includes both

gas and liquid flow mass controllers and an evaporator. The initial reagents are fed through a nozzle into the evaporator, heated with waste gases released by the catalytic burner, then into the catalytic reformer.
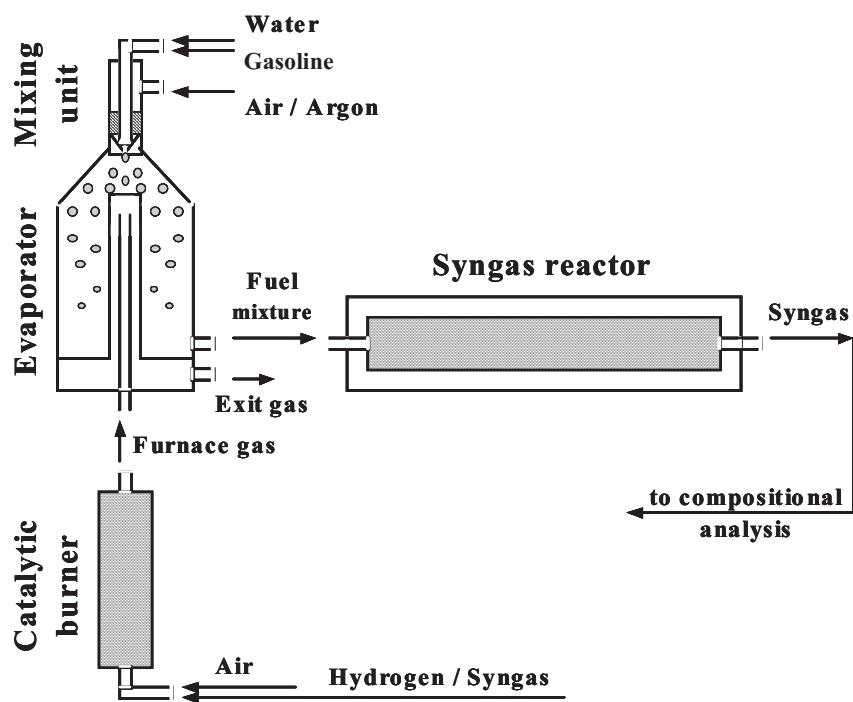
Fig. 2. Scheme of the developed catalysts testing.

After the catalysts testing it was accepted that the promising are the samples of monolith reinforced metal porous catalysts containing Pt, Co and Mn as an active component. The process of autothermal reforming of gasoline into syngas is not accompanied by coke formation for these catalysts. The most promising catalysts provide hydrogen productivity at least 2.5 $Nm^3/l_{cat}/h$ with more than 30 vol.% H_2 in the dry reforming products.

The obtained solutions will be used in future developments of vehicle versions of the on-board syngas generator in order to provide high SI-engines efficiency and low pollutants emission in exhaust gas.

References

[1] S. Pischinger. The future of vehicle propulsion – combustion engines and alternatives. *Topics in Catalysis*, **30**, p. 5-16 (2004)

[2] Y. Jamal and M.L. Wyszynski. On-board generation of hydrogen-rich gaseous fuels – a review. *Int. J. Hydrogen Energy*, **19**, p. 557-572 (1994)

[3] H.B. Mathur and L.M. Das. Performance characteristics of a hydrogen fueled SI engine using timed manifold injection. *Int. J. Hydrogen Energy*, **16**, p. 115-127 (1991)

[4] V.A. Kirillov, A.S. Bobrin, N.A. Kuzin, V.A. Kuzmin, A.B. Shigarov, V.B. Skomorokhov, E.I. Smirnov, V.A. Sobyanin. Compact radial reactor with a structured metal porous catalyst for conversion of natural gas to synthesis gas: experiment and modeling. *Industrial & Engineering Chemical Research*, **43**, p. 4721-4731 (2004)

PP-75

DEHYDROGENATION OF ETHANE TO ETHYLENE
IN A WALL-LESS REACTOR

V.N. Snytnikov, Vl.N. Snytnikov, T.I. Mischenko, O.P. Sklyar, V.N. Parmon

Boreskov Institute of Catalysis SB RAS, Novosibirsk, Russia

The mechanism of the endothermic dehydrogenation of ethane to ethylene is usually associated with generation of radicals. In the thermal cracking of ethane, the radicals are most probably generated and perish on the reactor inner walls through which the energy is supplied. While considering pyrolysis in reactors, it is of great interest to distinguish between homogeneous reactions of hydrocarbons in the reactor volume and heterogeneous processes on the reactor walls, as well as to study the gas-phase thermal reactions in order to improve further the industrially important methods for synthesis of C_2–C_3 and other olefins.

Dehydrogenation of ethane was studied under conditions of a wall-less reactor when heterogeneous processes are excluded. We designed a reactor of 6.5 cm^3 in volume where the heat energy was supplied directly to the gas at atmospheric pressure using a continuous CO_2 laser with the radiation power up to 120 W at the power density up to 10^4 W/cm^2. Since ethane does not absorb radiation of the CO_2 laser, it was mixed with ethylene or propylene which are characterized by a strong absorption band at 10.6 µm. In our experiments, the vibration energy of radiation-excited olefin molecules was transferred to ethane molecules due to fast relaxation through collisions. The reactor design ensured the gas bifunctionality, i.e. a part of the high-dense mixture behave as a heat insulator between the quartz walls at the temperature not higher than 125 °C and the reaction zone at the temperature not higher than 1000 °C.

The product analysis using chromatographic technique revealed that the absorption of the laser radiation by the ethane-ethylene mixture containing more than 5 vol % of ethylene gave rise to the chemical reaction of dehydrogenation of ethane into ethylene to generate hydrogen. The ethane conversion depended on the radiation energy and reached 90%. The selectivity for ethylene decreased from 90% to 70% as the energy supply increased. The decrease in the selectivity was accounted for by synthesis of methane. Propylene was formed in amount of 1–1.5 vol % under any conditions of the ethane pyrolysis. At a low laser energy supply, butane was detected in trace amount among the products nearby the point of initiating the chemical reactions; it disappeared as the ethane conversion increased. Acetylene was detected at high conversions of ethane. No other product was detected.

The possibility of the autocatalytic effect to occur in the system is discussed along with the radical chain mechanisms of the ethane pyrolysis to be used in technological applications. The obtained experimental data on ethane dehydrogenation in the wall-less reactor demonstrate applicability of the selective CO_2-laser radiation to control endothermic chemical reactions.

MATHEMATICAL MODELING OF A MULTIPHASE REACTOR
OF AN AQUEOUS ALKALI OXIDATION OF PRIMARY ALCOHOLS

Staroverov D.V., Varlamova E.V., Suchkov Yu.P., Shvets V.F.

D.I. Mendeleyev University of Chemical Technology of Russia,

Miusskaya Sq. 9, 125047 Moscow, Russia;

phone/fax +7 495 978 95 54; E-mail: stardv@muctr.edu.ru

Introduction

Oxidation of primary alcohols with oxygen in aqueous alkali solutions on noble metals is attractive method for preparation of valuable acids [1–5]:

$$RCH_2OH + O_2 + NaOH \longrightarrow RCOONa + 2\,H_2O.$$

These processes are environmentally friendly, especially in comparison with stoichiometric oxidation, and can be performed with high selectivity under mild operating conditions. Studies of oxidation of the alcohols on Pd/C–catalysts was carried out.

Results

Alcohols examined are differred by chemical structure and physico-chemical properties:

- the water-soluble 2-methoxyethanol (methyl cellosolve) and ethylene glycol;
- boundedly water-soluble *n*-butyl, *i*-butyl and isoamyl alcohols;
- micellar ethylene oxide adducts of fatty alcohols (Syntanols ALM) and alkyl phenols (Neonols AF9)

are greatly differred by chemical structure and physico-chemical properties. It was established, that in all cases the main reaction, and also mutually inverse over-oxidation and reactivation of the catalyst, occur on a water-wetted catalyst surface. The rates of reaction (r_{Ox}), over-oxidation (r_{Ox}) and reactivation (r_{Re}) is described by equations:

$$r_{Ox} = k_{Ox} \cdot (1 - X_{Ov}) \cdot C_S \cdot C_{Ox}/(1 + b \cdot C_S), \tag{1}$$

$$r_{Ov} = dX_{Ov}/dt = k_{Ov} \cdot (1 - X_{Ov}) \cdot (C_{Ox})^{1/2}/(1 + b \cdot C_S), \tag{2}$$

$$r_{Re} = -dX_{Ov}/dt = k_{Re} \cdot X_{Ov} \cdot C_S \cdot C_B/[(1 + b \cdot C_S)(1 + K \cdot C_B)], \tag{3}$$

where C_S, C_{Ox}, C_B are substrate, oxygen and base concentrations; X_{Ov} is catalyst over-oxidation degree; k_{Ox}, k_{Ov}, k_{Re}, b, K are coefficients.

As is known in a kinetic mode the catalyst rapidly lose activity because of over-oxidation, especially when micellar adducts is oxidized [1, 2, 5]. In many cases the current catalyst activity is essentially increased if oxidation process was carried out under limited oxygen

mass transfer conditions [6]. For oxygen mass transfer limitation we used remote trickle-bed reactor in semi-periodical circulation scheme (Fig. 1).
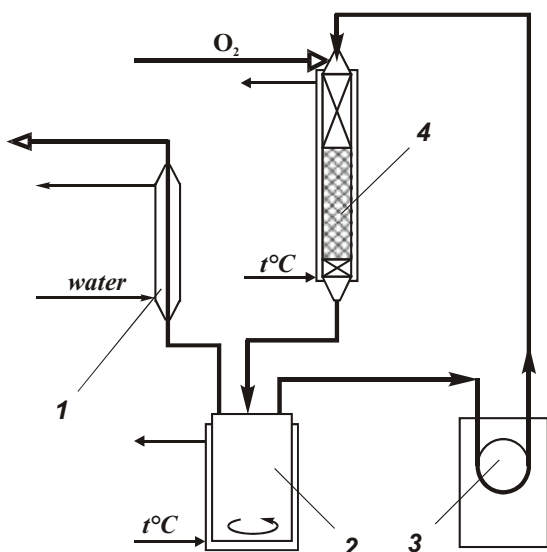
Fig. 1. Circulation apparatus for alcohols oxidation:

1 — condenser; *2* — mixer;
3 — pump; *4* — trickle-bed reactor.
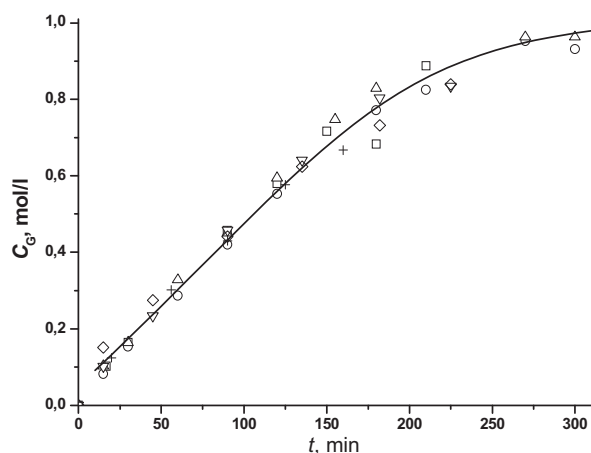
Fig 2. Kinetic curves of glycol oxidation:

$T = 35°C$; $u_{sG} = 1{,}54 \cdot 10^{-2}$ m/s; $u_{sL} = 6{,}99 \cdot 10^{-3}$ m/s; $C_{S,0} = C_{NaOH,0} = 1$ mol/l.

In the course of process a volume portion of reaction solution in flow circuit wasn't more 10% and current passage conversion wasn't more of 10%. In this case we accepted the catalyst is in state of dynamic balance over-oxidation–reactivation (2)–(3), that is

$$dX_{Ov}/dt \approx 0, \tag{4}$$

and concentration change at mixer *2* is described as for batch reactor.

Kinetic equations (1)–(3) with corresponding simplification and assumption (4) was used for modeling of circulation oxidation process.

For glycol and 2-methoxyethanol oxidation was established: $b \cdot C_S \gg 1$, $K \cdot C_B \gg 1$.

Correspondigly, the oxidation rate equation is

$$dC_G/dt = (m/V) \cdot k'_1 \cdot C_S/(1 + k'_2 \cdot C_S), \tag{5}$$

where m is the catalyst amount at trickle-bed; V is the reaction solution volume.

Accordance of equation (5) with experimental data is presented on Fig. 2. One can see up to glycol conversion 70–90% the kinetic curves is linear, that is $1 \ll k'_2 \cdot C_S$.

At the same time the oxidation rate is depended on hydrodynamic parameters of gas–liquid flow at trickle–bed, first of all on superficial liquid velocity u_{sL} (Fig. 3). The form of this dependence indicate the oxidation rate is limited by oxygen transfer from gas to catalyst

particle surface through flow film of reaction solution. Keeping in mind the form of catalyst (Pd/Sibunite) particles is near spherical, we used the Otake & Okada correlation [7]. Correspondingly, observed reaction rate coefficient k'_1 we calculated on basis of kinetic rate coefficient:

$$k'' = k_{Ox}/(1+(k_{Ox}/\beta)\, u_{sL}{}^{0.676}, \tag{6}$$

where β is oxygen transfer coefficient 'gas–particle'.
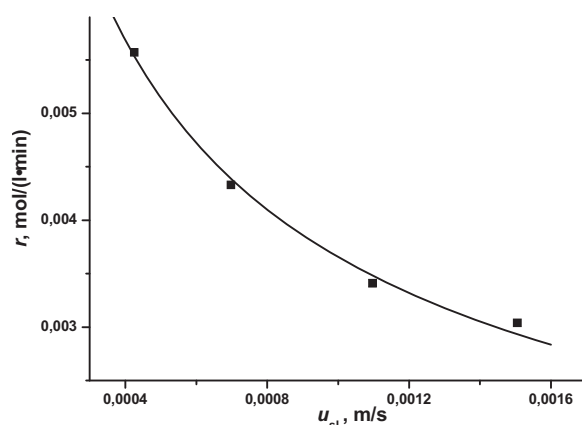
Fig. 3. Glycol oxidation rate *vs* superficial liquid velocity:

$T = 35°C$; $u_{sG} = 1,54 \cdot 10^{-2}$ m/s;
$C_{S,0} = C_{NaOH,0} = 1$ mol/l.
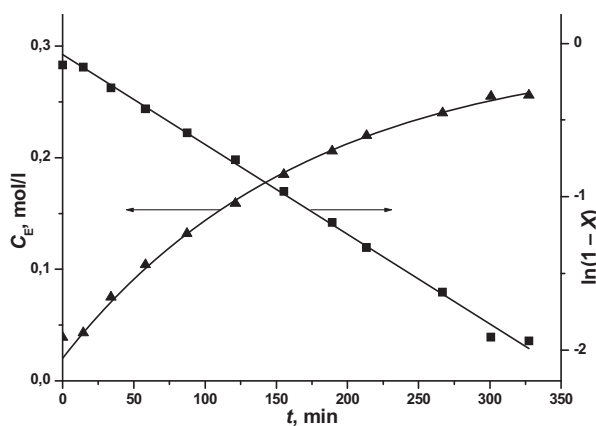
Fig. 4. Kinetic curves of Neonol AF–12 oxidation:

$T = 90°C$; $u_{sG} = 3.76 \cdot 10^{-3}$ m/s;
$u_{sL} = 2.48 \cdot 10^{-3}$ m/s;
$C_{S,0} = C_{NaOH,0} = 0.28$ mol/l.

For boundedly water-soluble alcohols oxidation in a kinetic mode was observed partial 'capsulating' of catalyst particles into drops of organic phase. This 'capsulating' resulted in rate rapid decrising with incrising of alcohol content in reaction mixture over solubility. But this effect wasn't appeared when boundedly water-soluble alcohols was oxidated in trickle-bed reactor. The modeling principles for this case are similar to water-soluble alcohols oxidation.

For Syntanols and Neonols oxidation was established: $b \cdot C_S \ll 1$, $K \cdot C_B \gg 1$.

Correspondigly,

$$dC_E/dt = (m/V) \cdot k''_1 \cdot (C_S)^2/(1 + k''_2 \cdot C_S) \tag{7}$$

True solubility of micellar surfactants is the critical micelle-formation concentration (CMC). For mixtures of compatible surfactants it may accept that components solubilities are proportional to respect concentrations in micellar phase. The CMC values for adducts and ether carboxylates are very small, namely 10^{-5}–10^{-2} mol/l. So Neonol concentration in aqueous phase is $C_S \sim (1 - X)$, where X is conversion of Neonol.

'Micellar' part of kinetic curve is linearized as semi-logarithmic anamorphosis (Fig. 4), i. e.

$$dC_E/dt = (m/V)\cdot(k''_1/k''_2)\cdot(1 - X). \tag{8}$$

Correspondigly, $1 \ll k''_2 \cdot C_S$.

Neonol oxidation rate isn't depended from hydrodynamic prameters, and the ratio (k''_1/k''_2) for makeup catalyst is well agreed with value calculated from kinetic data.

Conclusions

1. Aqueous alkali oxidation of different primary alcohols with oxygen on Pd/C-catalyst at kinetic mode is described by unified model including oxidation rate equation as well as equations of catalyst over-oxidation and reactivation rates.

2. Oxidation rate in circulation reactor with remote trickle-bed reactor for different substrates may be modelled on base of kinetic data taking into account a dynamic balance between over-oxidation and reactivation of catalyst.

3. In case of low-reactive alcohol oxidation a process rate is near kinetic, and in case of high-reactive substrate one is limited by oxygen transfer 'gas–particle'.

Acknowledgement

References

1. T. Mallat and A. Baiker, Catal. Today, 19 (1994) 247.

2. M. Besson and P. Gallezot, Catal. Today, 57 (2000) 127.

3. J.H.J. Kluytmans et al., Catal. Today, 57 (2000) 143.

4. Nonionic Surfactants (Surf. Sci. Ser.,V. 72), N.M. Van Os ed. New York – Basel – Hong-Kong: M. Dekker, 1998. 291.

5. D.V. Staroverov et al., Chim. Prom., 1 (2000) 58.

6. H.E. van Dam, H. van Bekkum, React. Kinet. and Catal. Lett., 40 (1989) 13.

7. G.F. Froment, K.B. Bischoff. Chemical Reactor Analysis & Design. J. Wiley & Sons. 1990.

SYNTHESIS OF 1,5-NAPHTHALENE DICARBAMATE BY METHOXYCARBONYLATION OF 1,5-NAPHTHALENE DIAMINE WITH DIMETHYL CARBONATE IN THE PRESENCE OF ZINC CYCLOHEXANEBUTYRATE DIHYDRATE

Fukui Xiao[a, b, c], Desheng Zhang[c], Zhenshun Piao[c], Ning Zhao[a], Wei We [a], Yuhan Sun[a] *

[a] *State Key Laboratory of Coal Conversion, Institute of Coal Chemistry, Chinese Academy of Sciences, Taiyuan 030001, China;*

[b] *Graduate School of Chinese Academy of Sciences, Beijing 100039, China;*

[c] *Research Institute of Jilin Petrochemical Company of Petrochina , Jilin 132021,China;*

*Corresponding author, Tel: +86-351-4053801, Fax: +86-351-4041153, E-mail: yhsun@sxicc.ac.cn;   fukuixiao@hotmail.com

Abstract

The catalytic performances of zinc compounds for the methoxycarbonylation of 1,5-naphthalene diamine (NDA) with dimethyl carbonatec (DMC) to 1,5-naphthalen dicarbamate (NDC) were examined. The results showed that zinc carboxylates dihydrate, especially zinc cyclohexanebutyrate dihydrate, had high catalytic activities toward the methoxycarbonylation. But the oxides, hydroxides, carbonatebasic and inorganic acid salts of zinc hardly were active towards the methoxycarbonylation. When the methoxycarbonylation was catalyzed by zinc cyclohexanebutyrate, the conversion of 1,5-naphthalene diamine and the selectivity of 1,5-naphthalene dicarbamate could reach 100% and 99%, respectively.

1. Introduction

1,5-naphthalene diisocyanate (NDI)/ester elastomers are known for high performance and long service life in particularly demanding dynamic applications, and have a wide usage prospect.[1, 2] But the material NDI are industrially produced from 1,5-naphthalen diamine (NDA) and phosgene,[3] which is a very poisonous gas,[4] the use in bulk quantities will bring about enormous menace to the entironment and life. Fortunately, the non-phosgene route for the NDI through the pyrogenation of 1, 5-naphthalene dicarbamate (NDC) has been opened out, which represents an attractive synthetic route.[5-7] Thus, it is very important to synthesize NDC in green chemistry pattern. NDC can be prepared in non-phosgene method by the methoxycarbonylation of NDA with dimethyl carbonate (DMC) in the presence of organic or

inorganic zinc salts (see Scheme 1).[8] However, relative research in the open literature was few and less systemic. Here, the catalytic performances of zinc compounds, especially the catalytic performances of zinc cyclohexanebutyrate dihydrate in the methoxycarbonylation were explored in detail for the synthesis of NDC with higher yield than that reported.

Scheme 1 The methoxycarbonylation of NDA with DMC to NDC
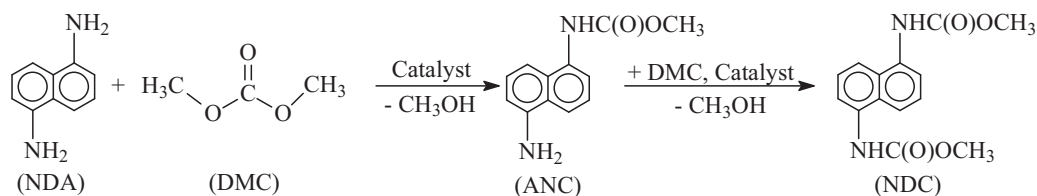
2. Experimental

The reaction was carried out in a 75 ml stainless steel autoclave with a magnetic stirrer under a nitrogen atmosphere. An excess quantity of DMC with respect to NDA was preferably used in the reactions as it also acted as a solvent. The conversions of NDA and the selectivity of ANC and NDC were determined by high-performance liquid chromatography (HPLC) with external standard method, which was performed on Waters 510 LC connected with a photodiode array detector under the condition of Zorbax Bonus-RP C_{18} column (4.6×250 mm, 5μm), methanol/water=45:55 (v/v) mobile phase and 0.8 ml min^{-1} flow. The selectivity of ANC and NDC are expressed based on the amount of NDA charged.

3. Results and discussion

3.1 Catalytic performances of zinc compounds for the methoxycarbonylation

As shown in Table 1, zinc carboxylates dihydrate showed high catalytic activities. However, though the oxides, hydroxides, carbonate, and inorganic acid salts of zinc could promote the conversion of NDA more or less, they could not promote the methoxycarbonylation of NDA with DMC.

Table 1 Catalytic performance of zinc compounds for the methoxycarbonylation

Catalyst	Conversion of NDA (%)	Selectivity of ANC (%)	Selectivity of NDC (%)
$Zn(NO_3)_2 \cdot 6H_2O$	17.34	0	0
$Zn_3(PO_4)_2 \cdot 4H_2O$	11.51	0	0
$ZnSO_4 \cdot 7H_2O$	12.84	0	0
ZnO	23.19	0	0
$ZnCO_3$	20.28	0	0
$3ZnCO_3 \cdot 2 Zn(OH)_2$	21.15	0	0
$Zn(OH)_2$	15.84	0.07	0
$Zn(OOCH)_2$	15.79	0	0
$Zn(OOCCH_3)_2 \cdot 2H_2O$	100	0.85	92.94
$Zn(OOC(CH_2)_3C_6H_{11})_2 \cdot 2H_2O$	100	1.17	95.44
$Zn(OOC(CH_2)_{16}CH_3)_2 \cdot 2H_2O$	74.63	18.17	50.46

Reaction conditions: 6.33 mmol NDA, 0.46 mmol catalyst, 356.67 mmol DMC, at 170°C for 3 h.

3.2 The Catalytic performance of zinc cyclohexanebutyrate dihydrate

As shown in Fig. 1, the reaction of NDA with DMC proceeded slowly when the reaction temperature below 130°C, but with the rise of temperature, NDA conversion increased and reached at 100% at 170°C. When the temperature below 150 °C, the dominant carbamate product was ANC, and the selectivity of ANC reached a maximum of 56% at 150 °C. The formation of NDC was observed at reaction temperatures higher than 130 °C, and reached a maximum at 170°C. At 190°C, the selectivity of NDC became lower due to its decomposition. Therefore, the suitable temperature range was 150°C to 170°C.

When the reaction was carried out at 150°C, the conversion of NDA was fast and ANC was the dominant product in the initial 3 h. When the reaction time over 3 h, the conversion of NDA became slow and the selectivity of ANC decreased, but the selectivity of NDC sharply increased and reached maximum (98%) at 5 h, and then decreased slightly (see Fig. 2). Thus, 5 h was a suitable reaction time for the formation of NDC.
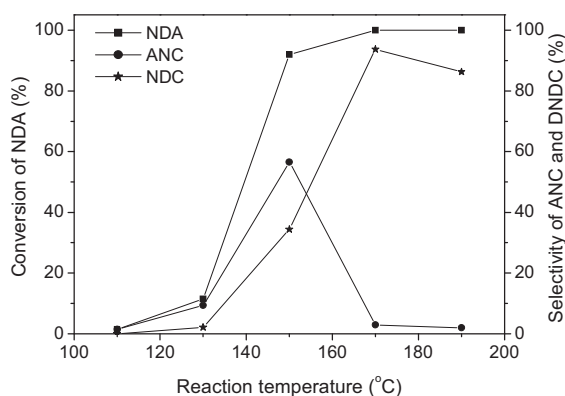
Fig. 1 Effect of reaction temperature on NDA conversion and selectivity of ANC and NDC. Conditions: 6.33 mmol NDA, 356.67 mmol DMC, 0.23 mmol Zinc cyclohexanebutyrate dihydrate, 3 h.
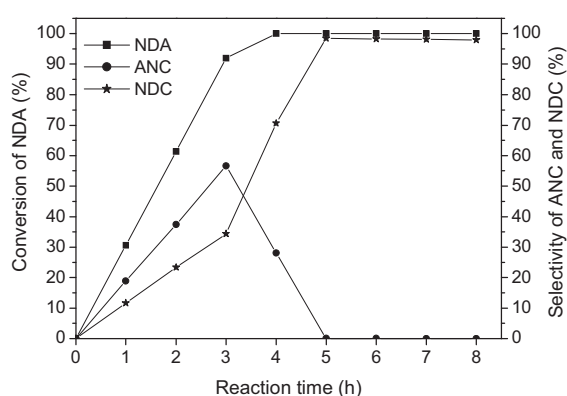
Fig. 2 Effect of reaction time on NDA conversion and the selectivity of ANC and NDC. Conditions: 6.33 mmol NDA, 356.67 mmol DMC, 0.23 mmol Zinc cyclohexanebutyrate dihydrate, 150°C.

The amount of the catalyst showed a great effect on the reaction when it was carried out at 150 °C and reacting for 5 h (see Fig. 3). The conversion of NDA and the selectivity of NDC were both low at the zinc cyclohexanebutyrate dihydrate/NDA molar ratio of 0.01. With increasing the catalyst amount, the conversion of NDA and the selectivity of NDC both increased sharply, and reached 100% and 99%, respectively at the zinc cyclohexanebutyrate dihydrate/NDA molar ratio of 0.03. With further increasing the catalyst amount, the selectivity of NDC decreased gradually. Therefore, the optimum molar ratio was around 0.03.

The conversion of NDA and the selectivity of ANC and NDC were also strongly dependant on the amount of DMC (see Fig. 4). The conversion of NDA and the selectivity of NDC were

both low at the DMC/NDA molar ratio of 10, and the selectivity of ANC was relatively high (16%). With increasing the mount of DMC, the conversion of NDA and the selectivity of NDC increased and reach at 100% and 99%, respectively at the DMC/NDA molar ratio of 37, and the selectivity of ANC decreased to a minimum of 0.4%. With further increasing the amount of DMC, the selectivity of NDC decreased and the selectivity of ANC increased slightly again. Therefore, the optimum molar ratio of DMC/NDA was around 37.
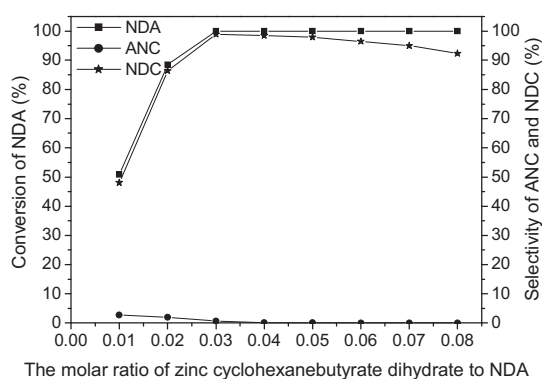
Fig. 3 Effect of zinc cyclohexanebutyrate dihydrate amount on NDA conversion and the selectivity of ANC and NDC. Conditions: 6.33 mmol NDA, 356.67 mmol DMC, 150°C, 5 h.
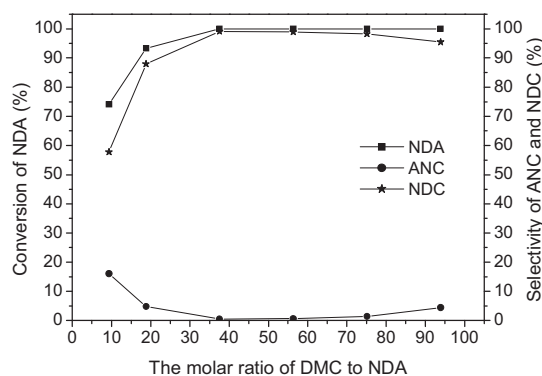
Fig. 4 Effect of DMC amount on NDA conversion and the selectivity of ANC and NDC. Conditions: 6.33 mmol NDA, 0.03 of Zinc cyclohexanebutyrate dihydrate/NDA molar ratio, 150°C, 5 h.

Conclusion

NDC could be synthesized with high yield by the methoxycarbonylation of NDA with DMC using zinc cyclohexanebutyrate dihydrate as catalyst.

References

(1) Kultys, A.; Podkoscielny, W.; Pikus, S. Polyesters containing sulfur. VI. Synthesis and characterization of polyesters from naphthalene-1,4- or naphthalene-1,5-bis(methylthioacetic acid) and aliphatic diols. *J. Polym. Sci. Part A* **1998**, 36 (13), 2359.

(2) Kozlova, T.V.; Letunovskii, M.P.; Zharkov, V.V. Effect of isocyanate structure on the mechanical and orientational characteristics of polyurethane elastomers. *Polym. Sci. USSR* **1989**, 31 (12), 2766.

(3) Li, F.; Chong, J. S.; Xue, W.; Zhao B. The synthesis state of 1,5-naphthalene diisocyanate. *china chem. Comm.* **2002**, 65, 83

(4) Babad, H.; Zeiler, A. G. The chemistry of phosgene. *Chem. Rev.* **1973**, 73 (1), 75

(5) Franz, M.; Friedrich, T. Thermal decomposition of aryl urethanes Thermal decomposition of aryl urethanes. U.S. Patent 4,330,479, 1982.

(6) Hamnen, F. W. D. Process for the preparation of polyisocyanates. EP Patent 0396976, 1990.

(7) Butler, D. C. D.; Alper, H. Synthesis of isocyanates from carbamate esters employing boron trichloride. *Chem. Commun.*, **1998**, 23, 2575.

(8) Cong, J. S.; L, F.; Zhao, B.; Xue, W.; Zhao, X.; Zhao, X. Q.; Wang, Y. J. The synthesis method of 1,5-naphthalene dicarbamate. CN Patent 1176065C, 2004.

MECHANIZM OF PHOTO-DRIVEN NO SCR WITH AMMONIA OVER TITANIA PHOTOCATALYST

TsunehiroTanaka, **Seiji Yamazoe, Kentaro Teramura**

Department of Molecular Engineering, Kyoto University, Kyoto 615-8510, Japan
E-mail: tanakat@moleng.kyoto-u.ac.jp, Fax: +81-75-383-2561

Introduction

Recently, it is desirable to develop the low temperature SCR systems. We have reported that photoassisted selective catalytic reduction of NO with NH_3 in the presence of O_2 proceeds at room temperature over $Rb_2O-V_2O_5/SiO_2$[1], TiO_2/SiO_2[2] and TiO_2[3,4]. Above all in the case of TiO_2, photo-SCR took place efficiently in a conventional fixed bed flow system (83% NO conversion and 96% N_2 selectivity were 83 % and 96 %). We have reported that the reasonable

Scheme 1 Reaction scheme of photoassisted selective catalytic reduction of NO with NH_3 in the presence of O_2 under irradiation

reaction mechanism of the photo-SCR with NH_3 over TiO_2 by means of various spectroscopic methods and kinetics[4,5]. Scheme 1 shows the photo-SCR reaction mechanism over TiO_2. NH_2 radical formed by the photo-activation of NH_3 adsorbed on TiO_2 (step 2) is an intermediate and this NH_2 radical plays an important role in photo-SCR. In this study, we attempted to unveil the role of thes paramagnetic NH_2 radical by ESR and analysis of effective wavelength to formation of NH_2 radical.

Experimental

TiO_2 samples used in this study were supplied from the Japan Catalysis Society (JRC-TIO-4 and 11). The measurement of the life times of NH_2 radical at each temperature (113-143 K) was carried out by analysis of decay curve of ESR signal. Before ESR measurements, TiO_2 sample was heated in air and evacuated for 30 min at 673 K, followed by treatment with 90

torr O_2 for 60 min and evacuation for 30 min at 673 K. ESR spectra of NH_2 radical were obtained by illumination of NH_3 adsorbed TiO_2. As a light source, 500 W ultrahigh-pressure mercury lamp equipped UV-33 cut filter was used.

Catalysts were filled up in quartz reactor, which had flat facet (50 x 15 x 1 mm^3), and were fixed with quartz wool. Before photocatalytic reaction, catalysts were pretreated at 673 K by flowing 10% O_2 diluted with Ar at flow rate of 50 ml/min. The composition of the reaction gas was NO: 1000ppm, NH_3: 1000ppm and O_2: 2% (Ar balance). As a light source in the reaction, PERKIN-ELMER PE300BF 300 W Xe lamp was used and samples were illuminated from the flat face side of the reactor with this lamp at room temperature.

The measurement of action spectrum of the photo-SCR was measured by measuring the product yield in a conventional fixed bed flow reactor irradiated through the monochromator from Xe lamp.

Fig. 1 ESR spectrum of TiO_2 adsorbed NH_3 under irradiation at 123 K.

Results and discussion

Fig. 1 shows the ESR spectrum obtained by illumination to TiO_2 adsorbed NH_3 at 123 K. The signals in the range of $g = 1.980$-2.021 are assigned to NH_2 radical formed by photo-activation of NH_3 adsorbed on TiO_2. At 15 min irradiation, the lamp was turned and the decay curve of the NH_2 radical signal was measured. The life time of NH_2 radical at 123 K was evaluated to be 4.3 min from the decay curve analysis. In the same way, the life times of NH_2 radical at 113, 133 and 143 K were 5.0, 3.8 and 3.2 min respectively. We evaluated the life time of NH_3 at reaction temperature by extrapolation of Arrhenius plot of half-lives. Consequently, the life time of NH_2 radical was estimated to be 1.4 min in the reaction condition. This shows

Fig. 2 Action spectrum of photo-SCR over TiO_2 (●) and UV-Vis spectrum of TiO_2 (curve).

the time span for the recombination of photoformed holes and electrons is 1.4 min since NH_2 radical is formed by capturing a hole generated by photo-excitation of TiO_2. In comparison

with the life time (< 100 psec) of charge separation of TiO_2[6], the adsorption of NH_3 elongates the charge separation of TiO_2 extremely.

Fig. 2 shows the action spectrum of photo-SCR together with the UV-Vis spectrum of TiO_2. In region of the wavelength less than 385 nm, the both plots are consistent with each other. However, the action spectrum exhibits the shoulder peak at around 425 nm while UV-Vis spectrum shows the typical band gap absorption edge of TiO_2. The feature of the action spectrum is very similar to that of UV-Vis spectrum of nitrogen-doped titanium oxides[7]. We guess analogously that electron donor level of N $2p$ is formed in the forbidden band by the adsorption of NH_3 and electron transition occurs from N $2p$ of NH_3 adsorbed on TiO_2 to Ti $3d$ directly. This process promotes the oxidation of NH_3 resulting in the formation of NH_2 radical. Actually, the formation of NH_2 radical by visible light (> 400 nm) was confirmed by ESR. Therefore, photo-SCR can be operated by irradiation of both UV and visible light.

4. Conclusions

The photo-activation of NH_3 exhibits two characteristic features. One is that the elongation of life time of charge separation in TiO_2 by capturing holes resulting in the formation of NH_2 radicals. This is the direct cause of the high activity. The other is that the effective wavelength for driving photo-SCR is longer than that corresponding to band gap energy (3.2 eV) of TiO_2 photoctalyst. This is concluded to be caused by electron transfer from N $2p$ by NH_3 adsorbed on TiO_2 to Ti $3d$.

References

1) T. Tanaka,K. Teramura,T. Funabiki, *Phys. Chem. Chem. Phys.,* **2** (2000) 2681.
2) T. Tanaka,K. Teramura,T. Yamamoto,S. Takenaka,S. Yoshida,T. Funabiki, *J. Photoch. photobio. A,* **148** (2002) 277.
3) T. Tanaka,K. Teramura,K. Arakaki,T. Funabiki, *Chem. Commun,* (2002) 2742.
4) K. Teramura,T. Tanaka,T. Funabiki, *Langmuir,* **19** (2003) 1209.
5) K. Teramura,T. Tanaka,T. Funabiki, *Chem. Lett,* **32** (2003) 1184.
6) S. Ikeda,N. Sugiyama,B. Pal,G. Marci,L. Palmisano,H. Noguchi,K. Uosaki,B. Ohtani, *Phys. Chem. Chem. Phys.,* **3** (2001) 267.
7) R. Asahi,T. Morikawa,T. Ohwaki,K. Aoki,Y. Taga, *Science,* **293** (2001) 269.

THE CENTRIFUGAL FLASH REACTORS OF NEW DESIGN AND LOW-WASTE PREPARATION OF ALUMINA FROM THE CTA PRODUCT

Yu.Yu. Tanashev, V.S. Lakhmostov, V.V. Danilevich, V.A. Balashov, V.I. Pinakov*,

A.S. Ivanova, L.A. Isupova, V.Yu. Kruglyakov, I.A. Zolotarsky, V.N. Parmon

Boreskov Institute of Catalysis SB RAS, Novosibirsk, Russia, E-mail: tanashev@catalysis.ru

*Lavrentiev Institute of Hydrodynamics SB RAS, Novosibirsk, Russia

Very rapid heating of powdered materials (hydroxides, salts, clays, etc.) with consequent thermal quenching is known as an efficient way of their reactivity rising [1] and can be used as an initial stage of the multi-step catalysts preparation. The high heating rate, the short time of treatment at the temperature of a phase transition and the high rate of the following cooling are essential for the formation of a substance that is characterised by a high stored energy, considerable chemical activity and amorphous structure.

The fast thermal treatment of powders is usually provided by the contact with hot gas. To improve the conditions of the heating, the special type of Centrifugal Flash Reactor (CEFLAR^{TM}) has been recently proposed [2,3] and used in the BIC for the rapid thermal treatment of the aluminium hydroxide (gibbsite) powder at temperature T = 300-700°C. The heating is provided by a hot rotating solid heat carrier with the rate more than 1000 degrees per second, the contact time τ is about 0.5-1.5 s and can be varied by centrifugal forces. The solid products of thermal treatment are quenched in contact with cooled surface, the gaseous products (steam) are separated and move away.

At the present day, the design of CEFLAR has been considerably improved, so that two modifications of the reactor are now under operation in the BIC. In the first one, the reagent moves over the hot rotating plate with special profile ("tulip"), in the second one it moves along the inner surface of the hot rotating cylinder barrel, as it is shown on Fig.1. In previous presentation [2] we reported only about reactor with conic plate. According to the change of plate' shape the increase in product output as well as the decrease in energy consumption are achieved.

It has been found that treated in CEFLAR gibbsite Al(OH)$_3$ is partially dehydrated and transformed to the so called "centrifugally thermally activated" (CTA) product. The CTA products have been investigated by a lot of methods including X-ray and thermal analysis, BET, electron microscopy, IRS, NMR. It has been shown that the crystal structure of gibbsite is completely destroyed at T > 400-500°C, τ > 1.0 s and the initial powder particle size

< 0.12 mm. The CTA product is mainly amorphous, it can include pseudoboehmite-like or boehmite-like constituents, its phase composition essentially depends on thermal treatment conditions and its specific surface area can achieve 250-300 m^2/g.

The CTA products are shown to be promising starting materials for the preparation of various alumina-based compounds including catalysts and catalyst supports. Active alumina can be prepared by ordinary calcination of CTA product; spherical alumina can be obtained by using plate granulator. Also, CTA products possess essential reactivity in the rehydration process. The conditions of pseudoboehmite or bayerite synthesis have been established. These hydroxides are used for preparation of γ-Al$_2$O$_3$ or η-Al$_2$O$_3$ with regulated porous structure and low impurities content.

The main merits of the CEFLAR^{TM} are the following: compactness and simple design; the provision of no environment pollution; the short contact of the reagent with the rotating heat carrier will not lead to the appearance of additional impurities in the activated products; the product output (tens kg per hour) and the energy consumption (about 5 kJ/g) of the tested reactors are suitable for an industrial coping of the devices.
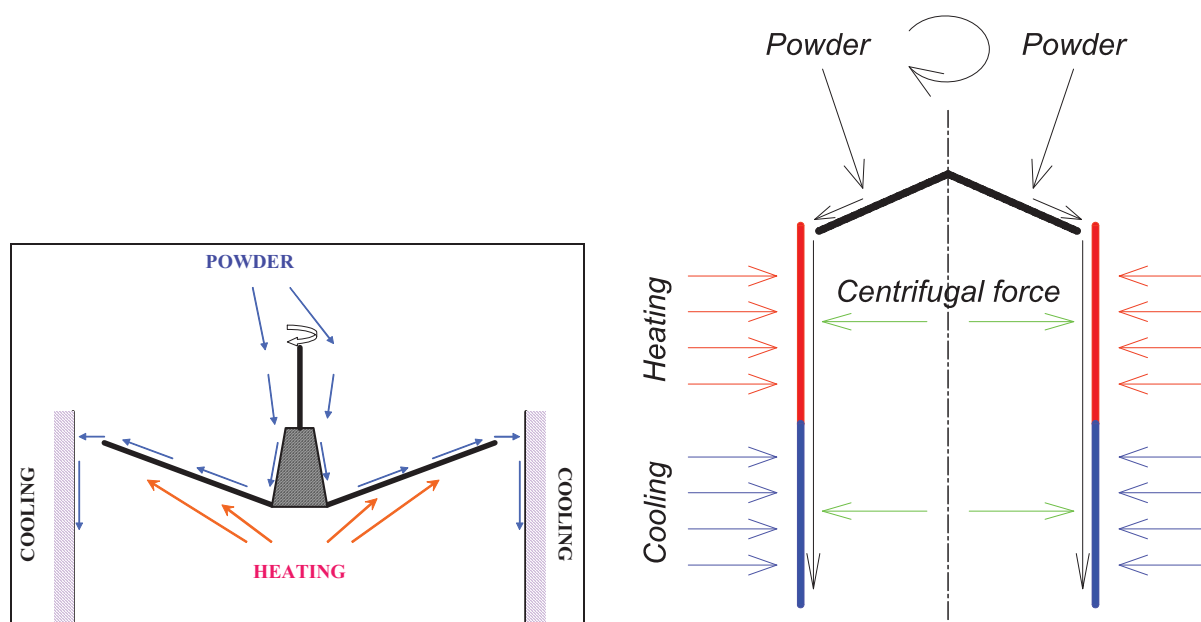
Fig.1. Principle of operation of CEFLAR with different heat carriers: hot rotating plate (left) and hot rotating barrel (right).

References

1. Rhone Poulenc, US patent 2,915,365 (1959).

2. V.I. Pinakov, O.I. Stoyanovsky, Yu.Yu. Tanashev et al // XVI International Conference on Chemical Reactors CHEMREACTOR-16, December 1-5, 2003, Berlin, Germany. P.364-367

3. V.I. Pinakov, O.I. Stoyanovsky, Yu.Yu. Tanashev et al // *Chemical Engineering Journal*, 2005, v. 107, issue 1-3, pp. 157-161.

PP-80

PROPANE OXIDATION BY CHEMICALLY BOUND OXYGEN OVER Pt/TiO$_2$/Al$_2$O$_3$ AND Pt/CeO$_2$/Al$_2$O$_3$

V.V. Sinelnikov, A. Yu. Stakheev, N. N. Tolkachev

N.D. Zelinsky Institute of Organic Chemistry RAS, Moscow, 119991, Leninsky pr. 47, Russia

fax: +7(095)135-5328, e-mail: nick33@ioc.ac.ru

Experiments

Oxidative transformation of light alkanes (C$_1$-C$_3$) to valuable products is one of the most important problems in heterogeneous catalysis nowadays. One of the promising approaches to improve oxidation selectivity is to carry the reaction under conditions of alternative supply of an oxidant (e.g. oxygen) and a hydrocarbon containing feed to a catalyst. The overall catalytic process passes through two stages. At the first stage the catalyst accumulates oxygen and at the second stage the interaction of hydrocarbon with catalyst active sites and accumulated oxidant occurs. This makes it possible to increase selectivity of the partial oxidation due to a suppression undesirable gas phase total oxidation process. However, two main problems arise: 1) low efficiency due to **small oxygen storage capacity** of the catalyst and 2) **low activity in hydrocarbon oxidation** of catalytic systems studied so far. Former problem can be solved by introduction of oxygen storage component (OSC) into a catalyst composition. The second restriction can be avoided using noble metal for hydrocarbon activation (Pt) [1].

In this research we study propane oxidation under conditions of continuous flow (simultaneous supply of C$_3$H$_8$ and O$_2$) and alternative supply of propane and oxygen (air) on the catalyst. The performances of two catalysts were compared: conventional three-way catalyst Pt/CeO$_2$/Al$_2$O$_3$ and Pt/TiO$_2$/Al$_2$O$_3$ containing TiO$_2$ as OSC component [2]. In addition to that we estimate an impact of oxygen desorption from OSC on the propane oxidation under conditions of alternative supply of reagents.

Catalytic data demonstrate a principal difference in propane oxidation under conditions of continuous flow and alternative supply of reagents. Propane oxidation under continuous flow results in a deep C$_3$H$_8$ oxidation and formation of CO$_2$ and H$_2$O as a reaction products. On the other hand, under conditions of alternative supply of C$_3$H$_8$ and O$_2$ a significant amount of CO and the products of propane oxidative dehydrogenation were detected (Fig. 1). Noteworthy, that Pt/TiO$_2$/Al$_2$O$_3$ was found to be more selective toward propane oxidative dehydrogenation as compared to Pt/CeO$_2$/Al$_2$O$_3$.
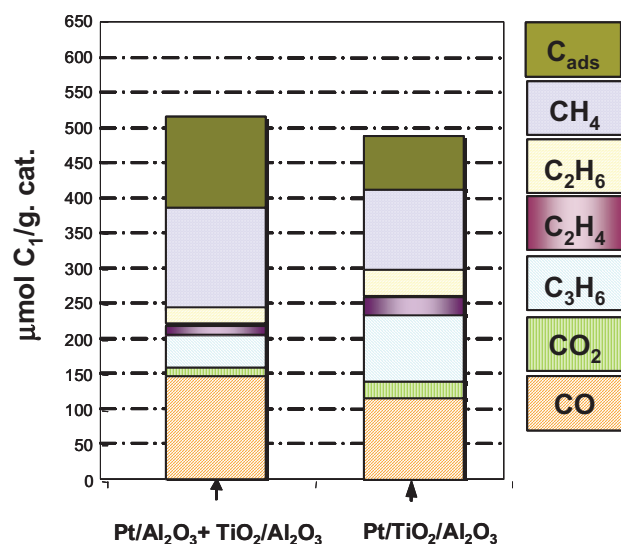
Fig.1 Cumulative product distribution of 10 pulses of propane reacting with TiO_2 containing catalysts.

Experiments with O_2-TPD indicate that an influence of oxygen desorption on the overall reaction mechanism is negligible under conditions of alternative supply of C_3H_8 and O_2. Evidently, propane is oxidized by oxygen tightly bound by OSC component of the catalyst.

Additionally, we compare the catalytic data obtained for $Pt/CeO_2/Al_2O_3$ and $Pt/TiO_2/Al_2O_3$; mechanically mixed Pt/Al_2O_3 + CeO_2/Al_2O_3 and Pt/Al_2O_3 + TiO_2/Al_2O_3 (Fig. 1); CeO_2/Al_2O_3 and TiO_2/Al_2O_3. The comparative study indicates that a hypothetical reaction scheme includes propane activation over Pt followed by a transfer of intermediates through gas phase toward oxygen storage component where intermediates undergo oxidation by chemically bound oxygen (Fig. 2).
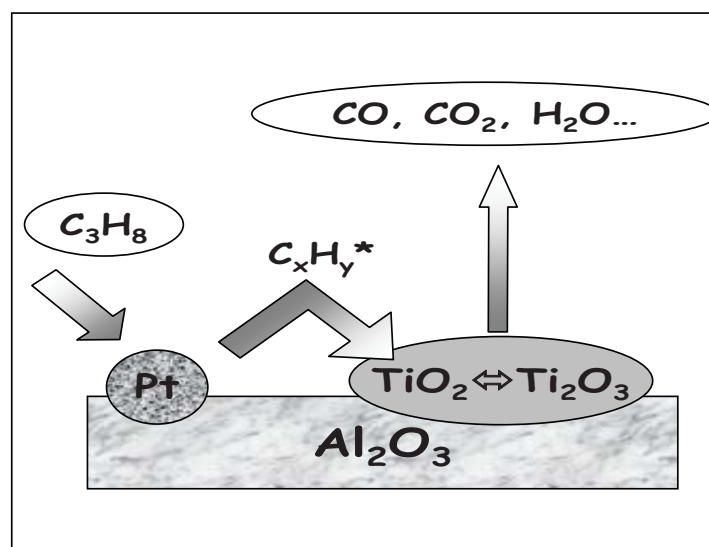
Fig.2 Reaction pathway

Data analysis

Chemical process running under conditions of alternative reagent supplying has several peculiarities. Main of them is interaction of the reagent supplied into the reactor with the reagent preadsorbed on the catalyst surface. Hence, analysis of the performance and

PP-80

selectivity of the catalytic process becomes more complicated in comparison with conditions of continuous reagent supplying.

It was found that during propane oxidation stage several processes can run sequentially. Interaction of propane with the catalyst is started by oxidation (partial oxidation) of the hydrocarbon followed by cracking when stored oxygen was consumed. Simple approach was developed to estimate impact of these two different reaction on target process efficiency. In framework of this approach unselective consumption of preadsorbed oxygen (X_O) and unselective non-oxidative consumption of hydrocarbon (X_{HC}) were taken into account. It was shown that overall unselective consumption of the preadsorbed oxygen differs significantly for the catalyst containing different oxygen storage components (Fig. 3).
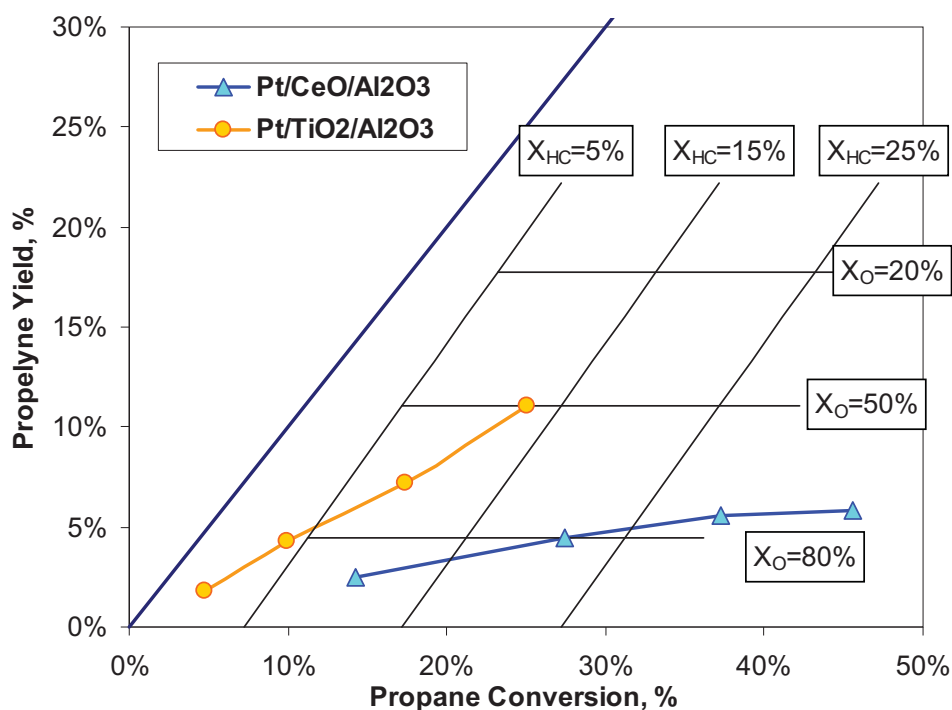
Fig. 3. Performance of different catalyst under conditions of periodic supply in the propane oxidation process.

References

1. P. Pantu, K. Kim, G.R. Gavalas, Appl.Catal A: General, 193 (2000) 203-214.

2. Sinelnikov V.V., TolkachevN.N, Stakheev A.Yu., *Kinetics and Catalysis*, 2005.**v. 46**, #4, p. 585

3. Sinelnikov V.V., TolkachevN.N, Telegina N.S., Goryashenko S.S., Stakheev A.Yu., *Kinetics and Catalysis*, 2006.**v. 46**, #1, p. 104

METHANOL CONVERSION TO HYDROGEN ON INDUSTRIAL CATALYSTS: SURFACE REACTIONS AND MECHANISM

Tretyakov V.F., Berezina L.A., Lermontov A.S., Burdeynaya T.N., Matyshak V.A.[*]

A.V. Topchiev Institute of Petrochemical Synthesis, RAS, Leninsky pr., 29, 119991, Moscow, Russia; fax 7 (495) 230-2224; tretjakov@ips.ac.ru

[*] *N.N. Semenov Institute of Chemical Physics, RAS, Russia*

At present, proton exchange membrane fuel cells (PEMFC) are considered for the purpose of replacing the engines of internal combustion in cars as promising energy sources for automobiles. The most preferable fuel for such elements is pure hydrogen. However, its unrestricted use is inhibited by a number of difficulties. Therefore, it was proposed to generate hydrogen on-board by methanol reforming. Gas flow exiting the reformer typically contains 40–75 vol.% H_2, 20–25 vol.% CO_2, up to 10 vol.% H_2O and 0.5–2 vol.% CO. However, even such low content of CO in gas has negative effect on PEMFC performance. Traditionally, copper containing catalysts are the most promising for methanol to hydrogen conversion process. However, there are a few copper containing industrial catalyst which can be used in methanol conversion. We have shown that SNM-1 ($CuO/ZnO/Al_2O_3$) it is most active and selective one among the others. But its activity and selectivity in methanol conversion to hydrogen and CO_2 still need to be enhanced; therefore we try to make a direct investigation of mechanism of this process on SNM-1 surface using *in situ* IR-spectroscopy techniques.

The main task of investigation is identifying the surface species (intermediates) in reactions of methanol catalytic decomposition over Al_2O_3, Cu/Al_2O_3 and industrially made SNM-1 ($CuO/ZnO/Al_2O_3$) systems with the help of spectrokinetic method. This method includes the simultaneous measurement of the rate of surface species transformation and of the rate of products formation in the reaction. IR-Fourier spectroscopy (transmission, diffuse reflectance) *in situ* is used for these tasks.

Adsorption of methanol on these catalytic systems, the influence of temperature and reaction mixture composition on activity and properties of surface species, and reactivity of surface complexes of adsorbed methanol were investigated. It was found on the first stage methanol or adsorbed methoxy species are decomposed on catalysts surface forming at least

three first intermediate species – formate, aldehyde and carbonate complexes. Then these initial intermediates on the surface of the catalysts are converted by different reaction routes.

Fig. 1. Mechanism of methanol conversion reactions on industrial SNM-1 (CuO/ZnO/Al2O3) catalyst revealed by IR-spectroscopy *in situ*.
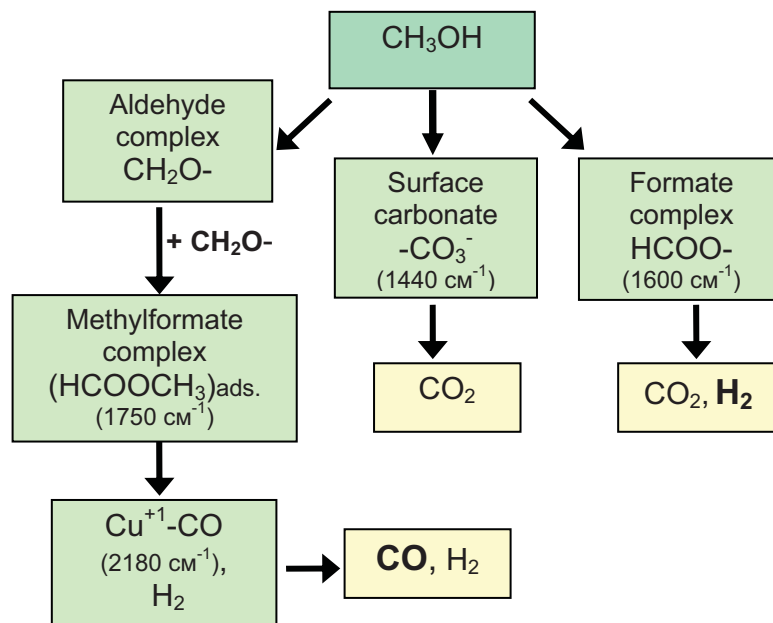
The main product of methanol conversion on γ-Al$_2$O$_3$ is dimethyl ether forming via two bridged methoxy species interaction or via interaction of gas phase methanol molecule with bridged surface methoxy specie. Linear methoxy species are transformed to formiate and aldehyde surface complexes, which are the main source of CO_2 in a gas phase. On 10% Cu/γ-Al$_2$O$_3$ the very same complexes were found, but the products composition is different – beside dimethyl ether, there are large quantity of CO_2, H_2 and some CO. CO_2 is formed from formate surface complexes, but CO is formed from surface aldehyde species. Hydrogen is produced via H-atoms recombination on surface of copper clusters. On SNM-1 catalyst some new reaction pathways was observed (Fig.1). Most of aldehyde surface species are transformed to methylformate, which then is decomposed forming small quantities of gaseous CO. Carbonate species are transformed to CO_2, and formate species generate H-atoms, the last recombine to molecular hydrogen on copper surface.

As a main result of this investigation is a proposed mechanism of H_2 formation via methanol transformation on industrial SNM-1 catalyst. Knowledge of detail mechanism is a great advantage for industrial technology design and reactors construction and optimization.

THE INFLUENCE OF METAL OXIDE ADDITION TO INDUSTRIAL H-ZSM-5 CATALYST ON ETHANOL CONVERSION TO MOTOR FUELS AND AROMATIC HYDROCARBONS

Tretjakov V.F., Burdeynaya T.N., Lermontov A.S., Mastyunina T.N.

A.V. Topchiev Institute of Petrochemical Synthesis, RAS, Leninsky pr., 29, 119991, Moscow, Russia; fax 7 (495) 230-2224; tretjakov@ips.ac.ru

Last fifty years the main source of aromatic compounds for industry was petroleum processing. Nowadays with the continuous growth of the world market petroleum prices and ecology friendly orientation of the industrial countries the bio-resources have a great preference on petroleum based technologies. Plant derived ethanol is the good alternative to the petroleum from ecological, industrial and agricultural viewpoints. The first is CO_2 consumption by plants which can be transformed to ethanol, so this is only one route to bring CO_2 from atmosphere to the industrial use. The second is a prices, despite of years of ethanol production from ethylene, today's situation on the market is a 700-900$ for the metric ton of ethylene comparing to 200-400$ for the metric ton of ethanol. The third is agriculture; years of optimization bring us to a great overload of its products so the conversion of the part of them to ethanol gives a new interest in this economy sector.

However, ethylene is not only one product [1], which can be derived by ethanol conversion. A significant amount of ethanol can be converted to various aromatic products over H-ZSM-5 zeolite based catalysts. In recent work [2] we have show that using pure H-ZSM-5 zeolite up to the 20% of ethanol can be converted to the aromatics mixture mainly consisted of toluene and xylenes.

In this work we have tried to investigate the influence of various oxides addition to H-ZSM-5 on the ethanol conversion. Experiments were performed in the continuous flow fixed-

Fig.1 Yield of liquid fraction during 2h of ethanol conversion on 65%H-ZSM-5+4%B2O3/Al2O3 modified by various oxides
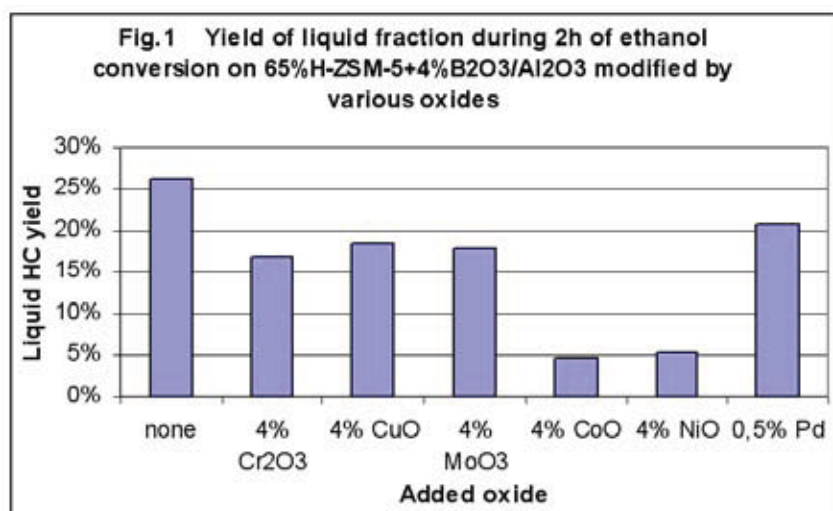
bed reactor at 420°C and 3 atm with ethanol flow 10 h^{-1}. Industrial catalyst - 65%H-ZSM + 4%B$_2$O$_3$ /Al$_2$O$_3$, doped by 4% of Cr$_2$O$_3$, CoO, CuO, MoO$_3$, NiO and 0,5%Pd (maked by Irkutsk SU via impregnation of corresponding metal salts) were used in this study. Compound analysis of liquid and gaseous products was carried out by GC-MS. The activation of the catalysts carried out in air stream at 550 C for 1 hour, the same procedure was applied for catalysts reactivation.

Fig.2 Composition of liquid HC fraction obtained by ethanol conversion on promoted 65%HZSM-5+4%B2O3/Al2O3 catalysts
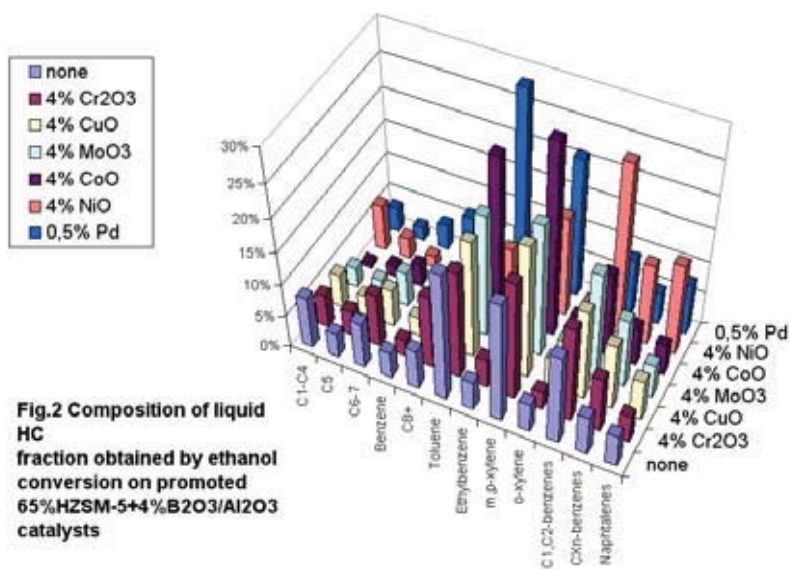
The conversion to hydrocarbons in all cases was nearly complete because of relatively high temperature of the reaction. However most of the catalysts, except undoped, copper and Pd containing ones completely lost their selectivity to liquid hydrocarbons after 2 hours of reaction due to high amount of carbon deposits on their surface. However, selectivity can be nearly completely recovered by reactivation in air, except Co and Ni doped catalysts. In all cases addition of the oxides to the industrial zeolite catalyst have negative influence on selectivity to liquid hydrocarbons (Fig.1).

As it can be seen from Fig. 2 the composition of liquid hydrocarbons fraction does not change significantly with nature of added component. Only in the case of chromia and copper significant amount of long aliphatic products was greater than on unpromoted catalyst. The addition of metals – Pd, Co, Ni leads to increase in aromatics yield, however only Pd can be a promoter due to

Fig 3. Gas phase products concentration changes during ethanol conversion on 0,5%Pd/65%HZSM-5+4%B2O3/Al2O3 catalyst
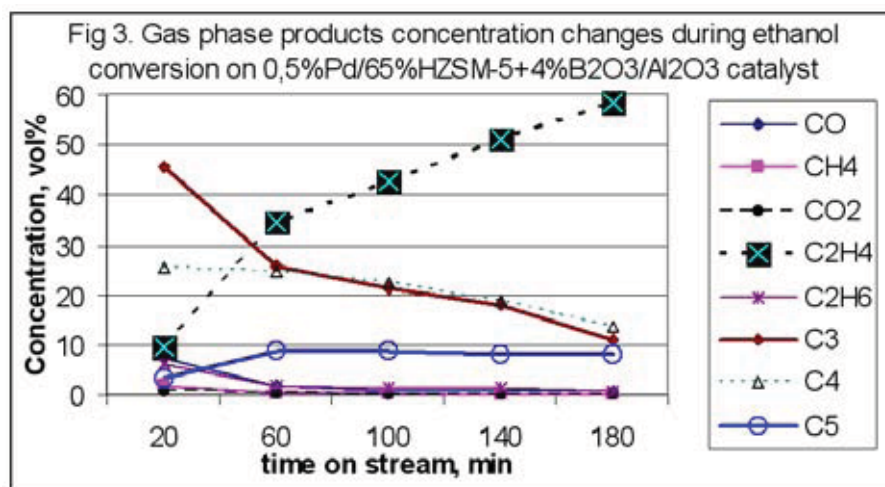
irreversible lost of selectivity in the case of Co and Ni. Very similar behavior of gaseous

products concentration changes was observed for all of the catalysts. Looking onto gas phase changes during the time of experiment, we can observe only a few types of species mainly gaseous hydrocarbons and CO and CO_2 (Fig 3). At the first moments of reaction hydrogen was also observed. The lost of selectivity increase an ethylene yield, so the final gas composition is 100% ethylene. It is an important observation, that C3 products are the main reaction products in gaseous phase when any of the catalysts have maximum selectivity to liquid hydrocarbons. Propane, hydrogen and CO observations are in contradiction to the previously proposed reaction mechanisms [3,4], so this can be the object for further study.

As the result of this work we have found that aromatics yield in ethanol conversion on HZSM-5 containing catalyst can be increased by addition of palladium. Also it is possible to increase the yield of aliphatic hydrocarbons adding copper or chromia to the catalyst.

References

1. T.M. Nguen, R. Le Van Mao, Appl. Catal., 1990, V.58, pp.119-129
2. V.F. Tretyakov et al., Catalysis in Industry 2006, №.5 (in press).
3. C. Tsakiris et al, Revista de Chimie, 1995, V.46 (3) pp. 214-218
4. S. Bun et al, Appl. Catal. 1990, V.59, pp.13-29

OXIDATIVE CONVERSION OF METHANE TO SYNTHESIS-GAS AND HYDROGEN OVER POLYCOMPONENT OXIDE CATALYSTS

Tungatarova S.A., <u>Dossumov K.</u>, Salakhova R.Kh., Masalimova B.K. and Turlygazhaeva D.Zh.

D.V.Sokolsky Institute of Organic Catalysis and Electrochemistry, 142 D.Kunaev str., Almaty, 050010, Republic of Kazakhstan. Fax: 7(3272)915722. E-mail: tungatarova58@mail.ru

Powerful raising of economy in XX century is the result of availability of oil, the main power resource of hydrocarbons and other chemicals. However the reserve of oil is not unlimited. Processing of the natural gas, containing C_1-C_3 alkanes, is actual at the present moment.

Production of synthesis-gas from methane. Ni-Cu- and Ni-Cu-Cr-catalysts on Al_2O_3 and other carriers are widely used in red-ox processes: deep oxidation of CO and organic compounds, combustion of methane, reduction and decomposition of nitrogen oxides, hydrogenation of fats, and decomposition of methane up to carbon /1-3/. According to physical-chemical data, the initial Ni-Cu-Cr-catalyst after reduction at temperature higher than 673 K forms the alloy of Ni with Cu with face-centered cubic lattice, in internodes of which the chromium is introduced. /4,5/.

In our report the results of investigation of the partial oxidation of CH_4 to synthesis - gas in micro-reactor at atmospheric pressure on micro-dispersed (20-25 microns) 9 % Ni-Cu-Cr/2%Ce/($\theta+\alpha$)Al_2O_3, received by method of capillary impregnation of the carrier by water solutions of metal nitrates with the subsequent heating on air and reduction in a current of a H_2+Ar mixture at a ratio H_2:Ar=40:60 at 1173 K within 1 hour are presented /6/. The amount of the catalyst was 0,01 g, which was diluted by SiO_2 in the ratio 1:43. The investigations were carried out at 1173 K at ratio CH_4:O_2:Ar = (1,4÷2,2):(0,6÷0,8):(97÷98) (vol. %), variation of ratio CH_4:O_2 from 2 up to 3,75, contact time (τ) from 2 up to 8 ms and space velocity (W) from 1,8 10^6 up to 4,5 10^5 h^{-1}.

In figure 1 the results of investigation of reduced Ni-Cu-Cr catalyst within 180 minutes at a ratio CH_4:O_2=2,79 in a reaction mixture and contact time 2 ms (W=1,8 10^6 h^{-1}) are presented. From figure it is visible, that on the catalyst there is a stable conversion of methane to mixture of CO and hydrogen with high selectivity by products (S_{CO}=96,26-99,13%,

S_{H_2}=89,0-95,65%), which slightly varied within 3 hours. The ratio H_2/CO in a received mixture made 1,85÷1,93.

The investigation of increase of a ratio CH_4:O_2 in a mixture from 2,07 up to 3,75 has shown that the oxygen completely reacts with methane at contact time 2,0-2,6 ms (W= 1,8 10^6-1,38 10^6 h^{-1}). The conversion degree of oxygen is close to 100 %, and the conversion
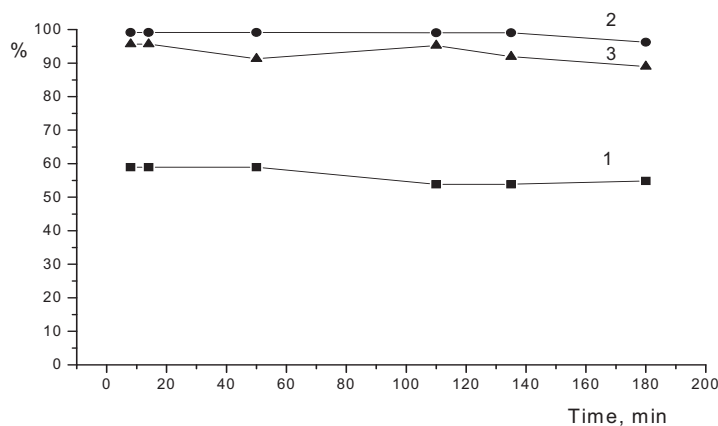
Fig. 1 Change of methane conversion, selectivity by CO and hydrogen on reduced 9 % Ni-Cu-Cr/2%Ce/(θ+α)Al$_2$O$_3$ during experiment. τ=2 ms, CH$_4$:O$_2$=2,79, T=1173 K.
1 – methane conversion, 2 – selectivity by CO, 3 – selectivity by hydrogen.

degree of CH_4 to synthesis - gas falls from 80,6 up to 48,5 % at high selectivity by CO and H_2 (S_{CO}=90,9-99,9% and S_{H_2}=87,7-99,6 %). A ratio H_2/CO made 1,9-2,1 in a received mixture.

The conversion degree of methane is increased up to 97-100 % at preservation of high selectivity by CO and hydrogen (S_{CO}=96,6-100%, S_{H_2}=79,3-99,7%) and at a ratio H_2/CO in a received mixture ~ 2,0 during reduction of space velocity from 1,44 10^6 h^{-1} up to 1,02 10^6 h^{-1} (τ from 2,49 up to 3,5 ms). Further reduction of space velocity up to 4,5 10^5 h^{-1} (τ=8 ms) results in appearance in composition of a received mixture of CO and hydrogen the 0,03 % CO_2 (S_{CO_2}=2,0%) too and reduction of selectivity by H_2 up to 75,9%.

The received data testify that reduced Ni-Cu-Cr catalyst supported on promoted by cerium the alumina, is capable to carry out the selective oxidation of methane to synthesis - gas at very short contact times.

Production of hydrogen from methane and propane-butane mixture. The hydrogen formed in composition of products of oxidative conversion of alkanes, represents independent interest as a marketable product. The rapt attention is given to synthesis of hydrogen and hydrogen-containing mixtures for producing of hydrogen fuels. Hydrogen is practically inexhaustible renewed source of energy. The hydrogen exceeds on power consumption all compounds, which can serve as fuel: 2,6 times - natural gas, 3,3 times - liquid hydrocarbons

of oil, 5 times - coal, 6,6 times - methanol etc. The hydrogen is unique ecologically clean fuel and reagent, product of which oxidation is water vapor or liquid water /7,8/. Using the hydrogen addition into different types of fuel points to perspective of such direction for intensification of combustion processes. Delphi (USA) and Toliyati Technical University (Russia) have developed a method for reduction of harmful gas emissions via addition of hydrogen to gasoline. The partial oxidation of fuel without essential modifying of engines and more effective catalytic work is provided at optimum temperature /9-11/.

Catalytic action of supported catalysts on the base of the Mo and W polyoxometallates and mixed oxides of Mo, Ni, Fe, Cr for the processes of partial oxidative conversion of CH_4 to H_2-cotaining mixtures was carried out. It is known that using of the gas fuel with H_2 as addition to gasoline and diesel fuel increases combustion efficiency of fuel and decreases exhaust of CO, NO and other waste gases. It improves ecological situation of regions. Tests were realized in reaction mixture, containing methane, oxygen and inert gas (Ar) with water vapor or without it. Granulated and block ceramic carriers are used for preparation of catalysts. The concentration of active component is varied from 1 to 20 vol.%. The size of catalytic granules, contact time and relation of components are varied widely.

Increase of temperature up to 850°C sharply raises conversion of CH_4 (to 67,1%), yield and selectivity by H_2. It was established that the activity of investigated compositions of catalysts in synthesis of H_2 are increases in series: $[BiSiMo_{12}]$ (Y=2,5%, S=44%) < $[ZnSiMo_{12}]$ (Y=12,8%, S=43,6%) < $[MgSiMo_{12}]$ (Y=19,4%, S=61%) < $[NH_4NiMo_6]$ (Y=56,9%, S=84,8%), Fig.2.
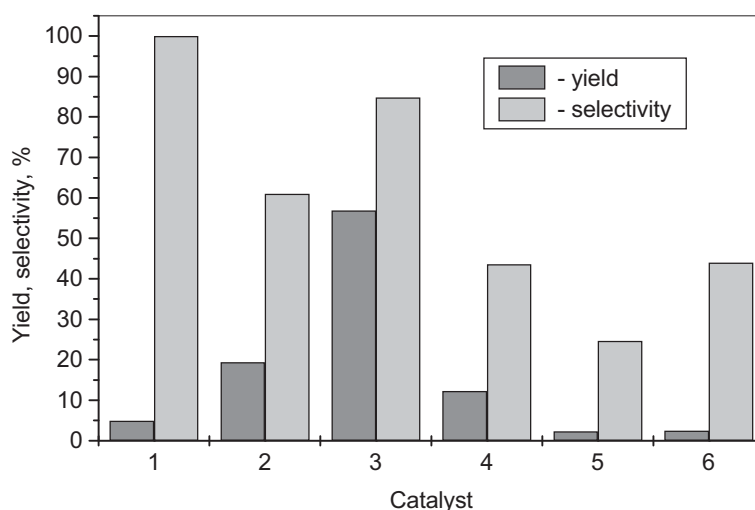
Fig.2. Influence of the composition of 10% Mo containing catalysts, supported over aluminosilicate on oxidative conversion of methane. W = 4000h^{-1}, τ = 0,9c, CH_4:O_2:Ar = 70:30:100, vol.
1 – $Fe_2Mo_6O_x$, 2 – $MgSiMo_{12}O_x$, 3 – $NH_4NiMo_6O_{24}$, 4 – $ZnSiMo_{12}O_{40}$, 5 – $Na_6PV_3Mo_9O_{40}$, 6 – $BiSiMo_{12}O_x$.

W-containing polyoxometallates of different composition was investigated in the process of oxidative conversion of CH_4 to H_2-containing mixtures too. Yield of H_2 on the catalyst $Ba_x[PW_{11}Ni]$ attains 80,8% (850°C). Aluminosilicate as carrier was more active and selective from the series of carries (silica gel, aluminosilicate, alumina, fluorinated alumina, cordierite, zeolite with clinoptilolite structure).

Block carrier from cordierite was investigated in the process of oxidative conversion of methane. As a result of investigation it was shown that supporting method of active component over block porous carrier by variation of secondary carrier, binding agent, protective layer play an important part in the process of selective production of hydrogen. The yield of H_2 on $5\%(NH_4)_4NiMo_6O_{24}$ over carrier attains 53,0%. W-containing samples supported over block porous carriers are more perspective. It was carried out the investigation of the physical-chemical properties of catalysts by complex methods (IRS, XRD, ESDR, TPR) and determined the correlation between catalytic and physical-chemical properties.

The prospecting investigations of catalytic oxidative conversion of methane to hydrogen-containing mixtures have allowed to show an opportunity for application of low percentage catalysts supported on granulated carriers on a base of polyoxometallates and production sufficiently high yields of hydrogen from methane.

References

1. G.R.Kosmambetova, N.M.Popova, E.A.Marchenko, K.Dosumov, Z.T.Zheksenbaeva. Int. Symp. "Combustion and Plasmochemistry". Almaty. (2001) 217.

2. T.V.Reshetenko, L.B.Avdeev, Z.R.Ismagilov. EUROPACAT-V. Book 4. Limerick, Ireland. Symposium 5. (2001) 5-P-01.

3. N.M.Popova. Influence of the carrier and structure of metals on adsorption of gases. Nauka. Almaty. (1980) 15.

4. E.Z.Golosman, V.N.Efremov, V.I.Jakerson. Khimicheskaja promyshlennost. 1 (1996) 25.

5. N.M.Popova, Z.T.Zheksenbaeva, A.S.Sass, K.Dosumov, R.Kh.Salakhova. Izvestija MON RK, NAN RK. Ser. Khimicheskaja. 5 (2003) 50.

6. S.N.Pavlova, N.N.Sazonova, V.A.Sadykov et.al. Kinetika i kataliz. 45 (2004) 1.

7. L.F.Kozin, S.V.Volkov. Hydrogen energy and ecology. Naukova Dumka. Kiev. 2002, P.336.

8. J.N.Armor. The multiple roles for catalysis in the production of H_2 // Applied Catalysis A: General 176 (1999) 159-176.

9. Bortnikov L.N., Rusakov M.M., Shaikin A.P., Pelipenko V.N. Chemical Physics of combustion and explosion, 12-Symp. on combustion and explosion, Chernogolovka, Russia, Sept. 11-15, 2000, Part. 3, 170.

10. Weniger Emissionen durch Wasserstoffzusatz zum Benzin, Erdol-Erdgas-Kohle, 118 (2002) 386.

11. B.Ibrahimogli, A.O.Mekhrabov, I.M.Akhmedov, R.Alibekli et.al. ICHMS'2003. Sudak, Kiev. Sept.14-20, 2003, 982.

PP-84

ISOMERIZATION OF LIGHT PARAFFINES OVER ANION-DOPPED MIXED OXIDES

G.A. Urzhuntsev, O.V. Kikhtyanin, A.V. Toktarev and G.V. Echevsky

Boreskov Institute of Catalysis SB RAS, Novosibirsk, Russia

Nowadays the requirements to modern refinery products are becoming more and more ecologically complex. Latest world-wide regulation even call for low concentration level of sulfur, benzene and MTBE in gasolines and therefore refiners have to find improved pathways to develop processes of production of clean high-octane gasoline.

In this context, acid-catalysed alkane isomerization has become an increasingly important in producing high-octane blending fraction because of low investments, possibly using idle reactors from either catalytic reforming or hydroprocessing.

Traditionally, process of light paraffins isomerization is based on a choice between Pt-zeolite catalysts and Pt-chlorinated alumina oxide which is much more active than zeolite catalyst. Chlorinated alumina is more preferable to use for low-temperature isomerization in favorable equilibrium condition producing high-octane gasoline.

Zeolite catalysts are characterized by outstanding tolerance to feedstock impurities such as sulfur and water, chlorinated alumina catalyst suffering from extreme sensitivity to all feed contaminants.

At the present, several companies such as UOP, Exxon-Mobil, Sud-Chemie develop metal oxide catalysts for paraffin isomerization based on anion-dopped zirconia. These catalysts possess outstanding activity and high sulfur and water resistance at low-temperature isomerization.

Some isomerization catalysts and process features are presented in Table 1.

Table 1. Isomerization catalysts and process features [1].

Process features	Platinum on Chlorinated Alumina	Metal oxide (Platinum on sulphate – dopped zirconia)	Pt-zeolite
Temperature, $^{\circ}C$	130-150	180-210	250-280
Pressure, atm	15-35	15-35	15-35
LHSV, h^{-1}	1-3	1-3	1-3
H2/hydrocarbons molar ratio	1-2	1-2	1-1.5
Sulfur contaminants ppmw	<1	30	200
Water contaminants ppmw	<1	30	200
Isomerizate yield, %	>96	>96	>96
Isomerizate octane number	82	80	78

During several years Boreskov Institute of Catalysis has been working out its own isomerization catalyst on the base of sulfate-dopped zirconia, dispersed in porous alumina matrix. This catalyst possesses high activity in conversion of different paraffins to highly branched isomers at low reaction temperatures. The present work contains some results on isomerization of light paraffins and paraffin fraction over Pd promoted SO_4-ZrO_2/Al_2O_3 catalyst in dependence on reaction conditions and properties of initial feed.

Synthesis of Pd promoted SO_4-ZrO_2/Al_2O_3 catalyst was carried out according to [2].

Catalytic tests were carried out on a flow installation with a fixed catalyst bed (catalysts volume - 5 cm^3). Prior to experiments a catalyst was pretreated in a hydrogen flow at 150°C. Reaction products were analyzed using HP-6850 unit equipped with DB-1 capillary column.

Pd promoted SO_4-ZrO_2/Al_2O_3 catalyst was tested in isomerization of n-butane, n-pentane, n-hexane at different temperatures. Results of the reaction are presented in Picture 1.
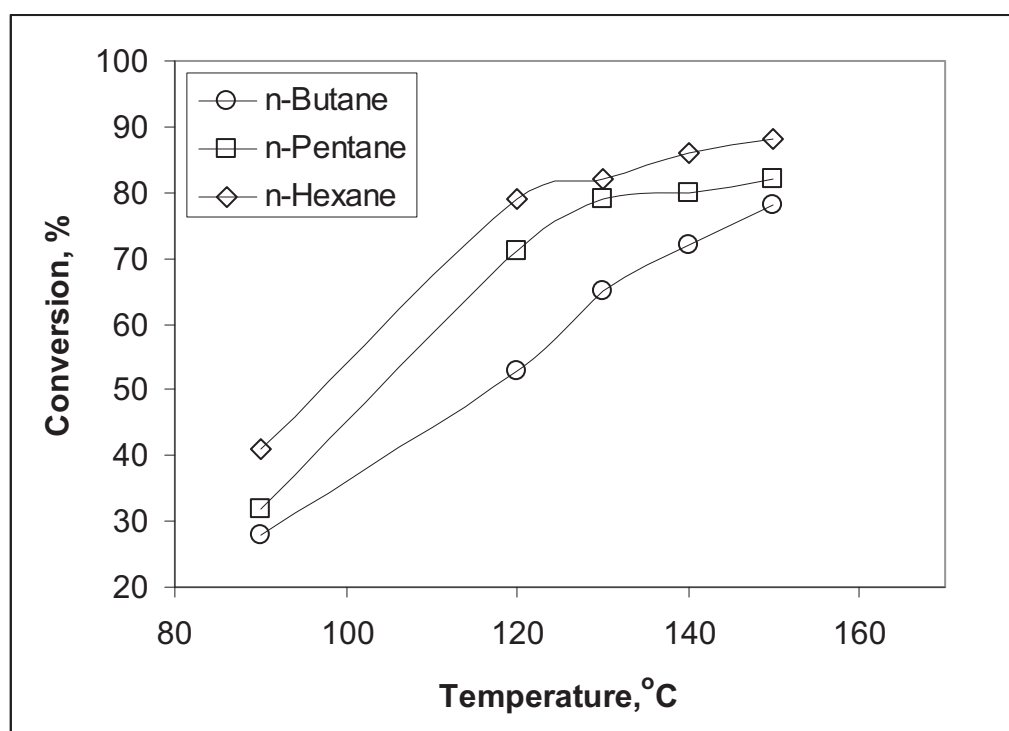
Picture 1. Isomerization of light paraffins over Pd promoted SO_4-ZrO_2/Al_2O_3 catalyst at different temperatures. Isomerization condition: reaction pressure – 1,5 MPa, WHSV – 3 h^{-1}, H_2/hydrocarbon molar ratio – 0.5

Picture 1 shows high isomerization activity of Pd promoted SO_4-ZrO_2/Al_2O_3 catalyst. Significant conversion of light paraffins C_4-C_6 is observed at reaction temperatures even below 100°C. Equilibrium conversion of light paraffins is observed at 130-140°C at more favorable temperature conditions than isomerization over typical non-dispersed sulfated zirconia.

PP-84

Pd promoted SO_4-ZrO_2/Al_2O_3 catalyst was also used to isomerize model paraffin fraction C_5-C_6 in the presence of some impurities such as naphthenes, aromatics, water and sulfur. Characteristics of a feed composition are presented in Table 2.

Table 2. Typical feed composition

Component	Wt%
iC5	0,24
nC5	40,60
2Methylpentane	0,27
3Methylpentane	0,53
nC6	48,34
Cyclohexane	5,72
Benzene	1,94
C_{7+}	2,36
Water, ppmw	80
Sulfur (as thiophene), % wt	0.15

Results on isomerization of model hydrocarbon mixture are presented in Table 3.

Table 3. Reaction product composition
(130°C, WHSV = 3 hr $^{-1}$, P=1,5 MPa, TOS=50 hours)

Component	Wt%
iC5	32,2
nC5	7,3
2.2Dimetilbutane	18,9
2.3Dimethylbutane	4,8
2Methylpentane	15,5
3Methylpentane	6,3
nC6	3,9
MethylCyclopentane	3,6
Cyclohexane	4,0
Benzene	0
C_{7+}	3,4

Results presented in Table3 shows that activity of the prepared catalyst at chosen reaction conditions is close to theoretical calculations and ensures a thermodynamic attainment of content of multi-branched paraffin hydrocarbons during isomerization process.

Fig. 2 contain data on catalyst stability when converting a model C_5-C_6 feed with added 80 ppmw of water and 0.15% wt. of sulfur (thiophene). An activity decrease is observed when water concentration in the catalyst reaches 3-3.3% wt. Regeneration in a flow of a dry hydrogen at 160°C resulted to an initial activity of the catalyst.
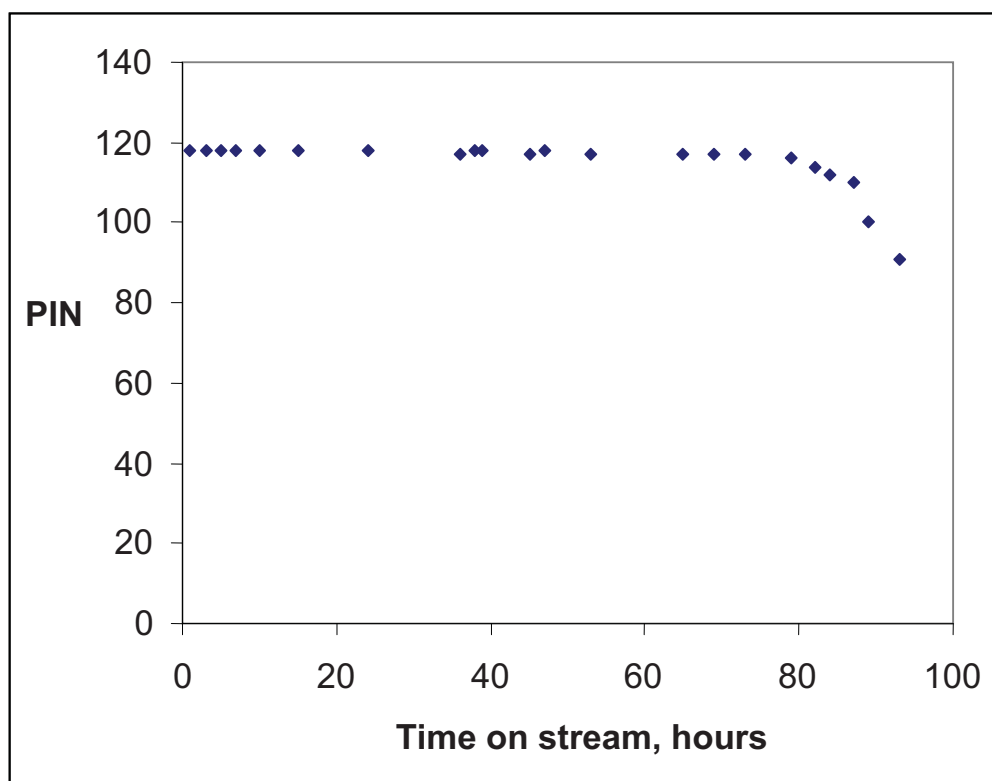
Figure 2. Stability of prepared catalyst in a process of n-paraffins isomerization when using a model feed with 80 ppmw of water and 0.15% wt. of sulfur (thiophene). PIN= {(i-C_5/n-C_5)+ (2,2 DMB+2,3 DMB)/(n-C_6)}*100, where: i-C5 – weight content of isopentane in C_5 reaction products; n-C5 – weight content of n-pentane in feed; 2,2 DMB- weight content of 2.2-dimethylbutane in C_6 reaction products; 2.3 DMB- weight content of 2.3 dimethylbutane in C_6 reaction products, n-C_6 - weight content of n-hexane in feed

The presented data prove that Pd promoted SO_4-ZrO_2/Al_2O_3 catalyst is highly effective for isomerization of light paraffins at low reaction temperatures and it is stable to poisoning action by feed contaminants.

References

1. Jeff Beck " EMICT, a Regenerable Paraffin Isomerization Catalyst", MCCJ 15th Anniversary Symposium, 2000.

2. Patent of Russian Federation, No. 2,264,256 (2005).

TRANSIENT BEHAVIOR OF THE METHANE PARTIAL OXIDATION IN A SHORT CONTACT TIME REACTOR: MODELING ON THE BASE OF CATALYST DETAILED CHEMISTRY

N.V. Vernikovskaya, L.N. Bobrova, I.A. Zolotarskii

Boreskov Institute of Catalysis SB RAS, Pr. Akademika Lavrentieva, 5,
630090,Novosibirsk, Russia, Fax: 007 3833 308056, vernik@catalysis.nsk.su

In particular at short contact times, a complex interaction of transport and reaction kinetics can occur at partial oxidation of methane (POM) in a monolith reactor. The implications of the reliable detail kinetic model for reactor design and scale up are significant. Detailed elementary-step kinetic models should be coupled with appropriate reactor models and the simulation results should then be tested against available experimental data such as conversions and selectivities for the specific reactor configurations [1].

The goal of this paper is the study of the transient behavior of POM by mathematical modeling of the reaction on the base of catalyst detailed chemistry to assist a sound understanding of the interaction between chemical and physical processes inside a short contact time monolith reactor. The 1D reactor model is developed on the base of differential equations of mass and energy changes. The reactor model contains one-dimensional detailed species mass and energy balances for both gas and solid phases. The model implements molecular, nonsteady-state kinetics. Accumulation terms were considered in all equations. The following assumptions are considered in the model: a fixed bed adiabatic reactor; non steady-state heat– and mass transfer; heterogeneously of the system; both the axial and thermo diffusions in the gas phase; thermal conduction of solid phase by means of effective axial thermal conductivity; heat loss due to radiation.

Model equations, boundary and initial conditions are listed below:

The mass balance equations

gas phase:

$$\varepsilon \frac{\rho_g \partial \omega_i}{\partial t} = -\varepsilon \frac{\rho_g \upsilon \partial \omega_i}{\partial z} - \varepsilon \frac{\partial J_i}{\partial z} - S_{sp} \beta_i (z) \rho_g (\omega_i - \widehat{\omega}_i) + \varepsilon \sum_{j=1}^{Nr_g} \nu_{ij} r_j + S_{sp} \omega_i \rho_g \sum_{i=1}^{N_g} \beta_i (z)(\omega_i - \widehat{\omega}_i),$$

$$J_i = -\rho_g \frac{M_i}{M_{mix}} D_{im} \frac{\partial x_i}{\partial z} - D_i^T \frac{1}{T} \frac{\partial T}{\partial z}, i = 1, N_g \tag{1}$$

solid phase:

$$\widehat{\varepsilon}\widehat{\rho}_g\,\frac{\partial\widehat{\omega}_i}{\partial t} = S_{sp}\beta_i(z)\rho_g(\omega_i - \widehat{\omega}_i) + S_c f_{pt} M_i\sum_{j=1}^{Nr_s}\mu_{ij}\widehat{r}_j - S_{sp}\widehat{\omega}_i\rho_g\sum_{i=1}^{N_g}\beta_i(z)(\omega_i - \widehat{\omega}_i) -$$

$$\widehat{\omega}_i S_c f_{pt}\sum_{i=1}^{N_g} M_i\sum_{j=1}^{Nr_s}\mu_{ij}\widehat{r}_j,\quad i = 1, N_g \tag{2}$$

The energy balance equations

gas phase:

$$\varepsilon\rho_g c_{p_g}\frac{\partial T_g}{\partial t} + \varepsilon\upsilon\rho_g c_{p_g}\frac{\partial T_g}{\partial z} = S_{sp}\alpha(z)(T_s - T_g) - \varepsilon\sum_{j=1}^{Nr_g}\Delta H_j r_j - \varepsilon\sum_{j=1}^{N_g} c_{p_i} J_i\frac{\partial T_g}{\partial z} \tag{3}$$

solid phase:

$$(1-\varepsilon)\rho_s c_{p_s}\frac{\partial T_s}{\partial t} = (1-\varepsilon)\frac{\partial}{\partial z}\lambda_{eff}\frac{\partial T_s}{\partial z} - S_{sp}\alpha(z)(T_s - T_g) - S_c f_{pt}\sum_{j=1}^{Nr_s}\Delta H_j\widehat{r}_j \tag{4}$$

Species mass balance equations

$$\frac{\partial\theta_k}{\partial t} = \sum_{j=1}^{Nr_s}\nu_{kj}\widehat{r}_j,\quad k = 1, N_s \tag{5}$$

Boundary conditions:

$$z = 0\;:\;\; T_g = T_{in};\; \omega_i = \omega_{i_{in}};\; \lambda_{eff}\frac{\partial T_s}{\partial z} = \sigma\varepsilon'\left(T_s^4 - T_w^4\right);$$

$$z = L\;:\;\; \frac{\partial\omega_i}{\partial z} = 0;\; -\lambda_{eff}\frac{\partial T_s}{\partial z} = \sigma\varepsilon'\left(T_s^4 - T_w^4\right). \tag{6}$$

Initial conditions:

$$t = 0\;:\;\; \omega_i = \omega_i^0;\; \widehat{\omega}_i = \widehat{\omega}_i^0;\; T_s = T_s^0;\; T_g = T_g^0;\; \theta_i = \theta_i^0. \tag{7}$$

A surface reaction mechanism of POM on a platinum catalyst described in [2], which contains 10 intermediates, 13 gaseous compounds and 31 reactions, was taken for the unsteady-state kinetic model. The gas phase reactions can be neglected for the atmospheric pressure. The monolith transport properties were accounted for by specific heat and mass transfer correlations published in literature. The balance equations represent a system of differential equations in partial derivatives, which solved numerically by the method of lines. Numerical experiments have been carried out on the base of the dynamic 1D heterogeneous diffusive mathematical model with complex chemistry and heat conduction along the reactor. Figure 1 illustrates the time dependencies of main components in the product gas. It can be seen that at first total oxidation of CH_4 to CO_2 and H_2O occurs during the first 5 seconds, which may enhance significantly the process exothermicity in this period.

PP-85
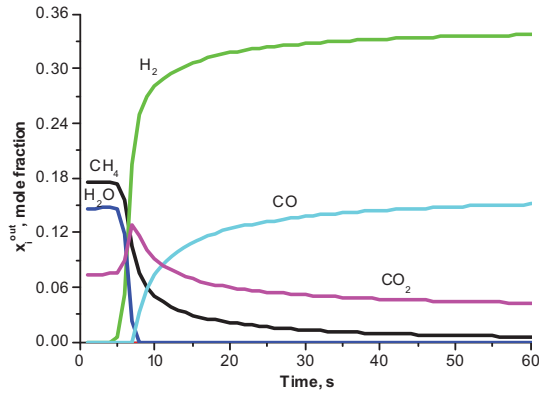
Figure 1. Time dependencies of main components in the product gas at using a honeycomb monolith with triangular channels. T_{in}=400°C, P=1atm, $x_{CH_4}^{in}$ =0.25 mole fr., $x_{O_2}^{in}$ =0.15 mole fr., d_{eq}=0.67 mm, ε=0.59, υ =0.5 m/s.

Fig. 2 reveals the numerically predicted both temperature and species distribution in the monolithic structure as function of time. There is no H_2 and CO produced in the first few second after ignition. At 5 s the temperature is high enough for hydrogen formation, CO is appeared in 2 s later. The model includes the calculation of the surface coverage with adsorbed species as function of time as well. Complex dynamic behavior of the surface species is revealed. Figure 2f shows that the vacancies coverage is settled rather slowly due to the multi-step heterogeneous reaction mechanism. The adsorption–desorption equilibrium of the species shifts with increasing the temperature leading to changing the rate-limiting steps and prevailing reaction rout in the surface reaction kinetics.

In this work the influence of such parameters as linear velocity, equivalent channel diameter and effective thermal conductivity of the monolith on the POM dynamics has been studied. The mathematical model developed is essential to capture the underlying physics of the process and explain the transient behavior of the POM in a monolith reactor.

Nomenclature: c_p – heat capacity, J/gK; D_{im} – mixture-averaged diffusion coeff. between species i and the remaining mixture; m²/s; D_i^T – thermal diffusion coefficients of i-th compound, g/m s; d_{eq} – equivalent channel diameter, mm; f_{pt} – the molar site density for Pt, mol/m²; ΔH_j – heat of reaction j, J/mol; J_i – mass flux of i-th compound, g/m²s; M_i – molecular weight of i-th compound, g/mol; P – pressure, atm; $r_j, \hat{r}_j$ – j-th reaction rate in gas and solid phase, g/m³s, mol/mol$_{pt}$s; S_{sp} – specific surface area, m²/m³; S_c – specific surface area occupied with Pt, m²/m³; T – temperature, K; t – time, s; x_i –mole fraction in gas phase; z – reactor axial coordinate, m; **Greek letters:** α – heat transfer coefficient, J/m²sK; β – mass transfer coefficient, m/s; ε, $\hat{\varepsilon}$ – void fraction in monolith and in coverage pores; ε' – emission coefficient; λ_{eff} – effective heat dispersion coefficient, J/msK; μ_{ij}, ν_{ij} – stoichiometric coefficients; θ_j– surface coverage; $\rho_g, \hat{\rho}_g$ – density in gas phase and in coverage pores, g/m³ ; υ – velocity, m/s; σ– Stefan-Boltzmann constant, J/m²sK⁴; $\omega_i, \hat{\omega}_i$– weight fraction in gas phase and in coverage pores.

Subscripts: g –gas phase; s – solid phase; w – surrounding; in – inlet; mix – mixture; o – initial; out – outlet.
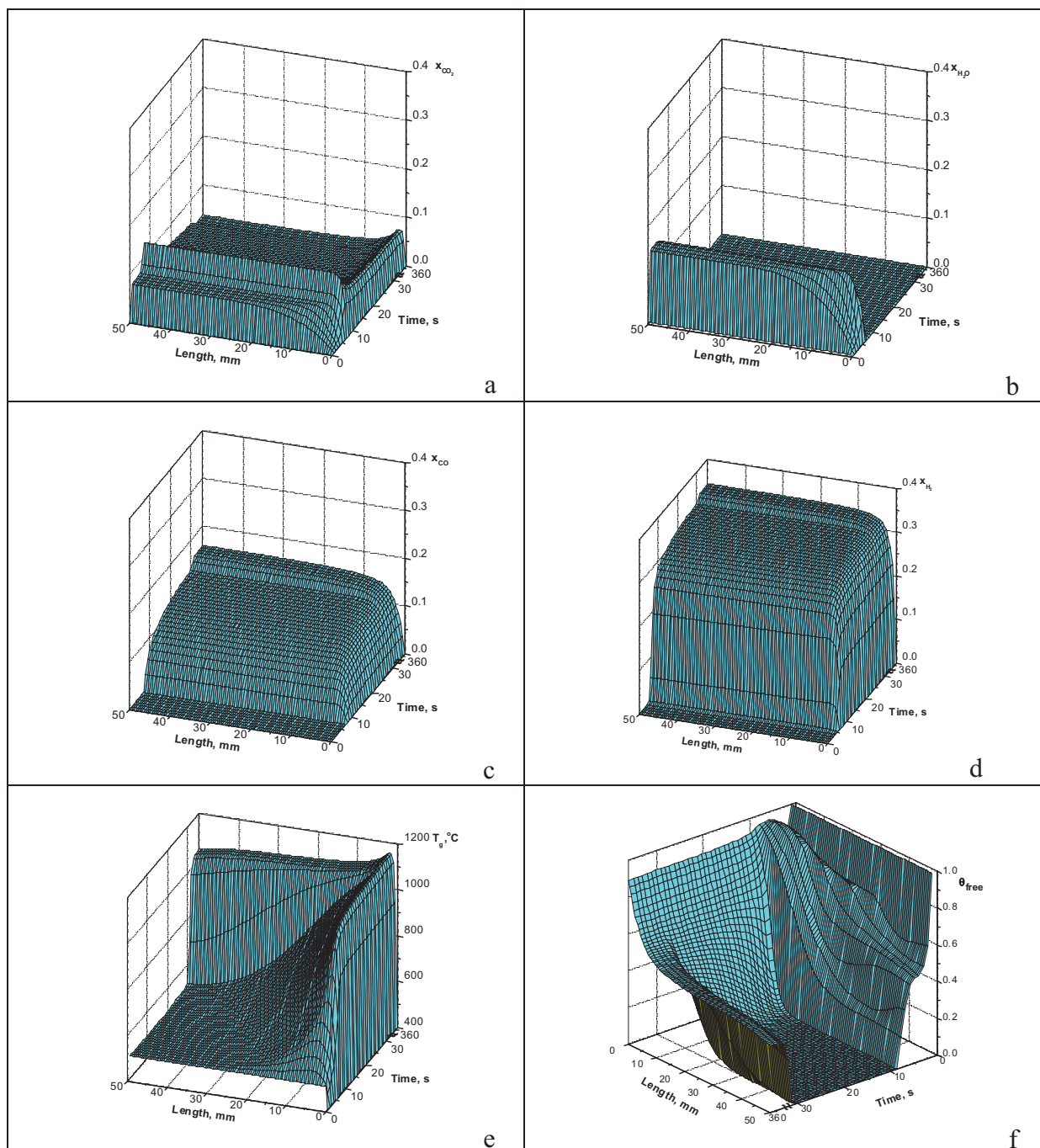
Figure 2. Axial gas-phase species mole fractions, surface temperature and free surface species distributions with time in the monolith with triangular channels. T_{in}=400°C, P=1atm, $x_{CH_4}^{in}$ =0.25 mole fr., $x_{O_2}^{in}$ =0.15 mole fr., d_{eq}=0.67 mm, ε=0.59, v =0.5 m/s.

References

1. I.A. Dumesic, D.F. Rud, L.M. Aparicio, J.E. Rekoske, A.A. Revino, The Microkinetics of Heterogeneous Catalysis, American Chemical Society, Washington, DC, 1993.

2. P. Aghalayam, Y.K. Park, N. Fernandes, V. Papavassiliou, A.B. Mhadeshwar, D.G. Vlachos. A C1 mechanism for methane oxidation on platinum//Journal of Catalysis 213, 2003.

CATALYTIC CONVERSION OF LIGHT HYDROCARBONS INTO VALUABLE LIQUID PRODUCTS

A.V. Vosmerikov[1], **A.M. Masenkis**[2], **A.I. Vagin**[1], **L.N. Vosmerikova**[1], **G.V. Echevskii**[3], **S.P. Milostnov**[2], **Ya.Ye. Barbashin**[1], **A.P. Popov**[2], **V.V. Kozlov**[1], **Y.G. Kodenev**[3]

[1]*Institute of Petroleum Chemistry SB RAS,*

634021, 3, Akademichesky Avenue, Tomsk, Russia

fax: (3822)491-457; e-mail: pika@ipc.tsc.ru

[2]*Soyuzprominvest Ltd, 109544, 17A, Bolshaya Andronievskaya Street, Moscow, Russia*

[3]*Boreskov Institute of Catalysis SB RAS, 630090, 5, Pr. Ak. Lavrentiev, Novosibirsk, Russia*

The problem of the synthesis of petrochemical products from natural and associate gases of petroleum and gas-producing industries is very urgent. Today Russia possesses great resources of gaseous hydrocarbons whose conversion is non-efficient when using the conventional technologies, and the simplest recycling causes serious environmental problems. Most of these hydrocarbons are used at best as a fuel or are burnt in the flares. The search for the ways of conversion of low-value and cheap raw material into practically important products is one of the primary goals of Russian petroleum and gas companies. The processes developed for the conversion of gaseous hydrocarbons must meet some obligatory conditions: be non-expensive and quick-payable (in 2-3 years), give the products that may be used in-situ (high-octane gasoline and low cold-test diesel fuel) or those whose transportation to long distances is profitable. The latter include the valuable petrochemical raw materials: benzene, ethylbenzene and other aromatic products.

The conventional technologies of the conversion of associate gas and wide fractions of light hydrocarbons (WFLH) are based on the processes of separation of hydrocarbon mixtures, though the obtained commercial products (propane, butane or their mixtures) do not find a wide application in the regions of gas and oil production, which results in serious problems of their marketing. In addition, the liquid phase isolated using the gas-liquid fractionation plants, is not a commercial product and requires further conversion. Almost all the known developments on the conversion of light hydrocarbons into higher compounds have some limitations for raw composition, their technical solutions are incomplete and the requirements to the catalysts are too strong rising the catalyst cost.

One of the promising directions for conversion of the components of natural gas and C_2-C_5 end gases of petroleum production and refining is their transformation into liquid C_6-C_{12} hydrocarbons over the zeolite-containing catalysts. The main advantages of zeolite-containing catalysts and processes on their base are non-sensitivity of the catalytic systems to different poisons contained in the initial feedstock; application of a fixed-bed catalyst that significantly simplifies the design of the reactor and regeneration blocks; high yield of the desired product obtained in one step; a versatile technology allowing both natural and associate gases to be used as the feedstock. The liquid products obtained as a result of the chemical transformation of gaseous products may be used as a high-octane additive to gasolines or a valuable feedstock for petrochemical industry.

The present paper gives the results of the study into the process of the production of aromatic hydrocarbons from a mixture of light C_1-C_6 hydrocarbons using the zeolite-containing catalysts. The composition of these hydrocarbons maximally approaches that of the stabilization gas obtained at the stabilization of the gas condensate. Discussed are the problems of the influence of the process parameters (temperature, pressure, raw material consumption), component ratio in the initial raw, service period of catalysts, and oxidative regeneration on the composition and yield of the end products obtained.

The tests of the zeolite-containing catalysts (ZCC) R-1, R-2 and their mixture (1:1) were carried out in a flow-circulation installation OL-120 with the reactor volume of 100 cm^3 equipped with the system of water coolers and separator with a coil submerged in the thermostat bath filled with a liquid cooled to –15 ^{o}C. The reaction products were analysed using the gas chromatography. The products were sampled as a gas-vapor mixture using a heated 6-way valve at the output of the catalytic reactor that allowed excluding the loss of the high-boiling aromatic hydrocarbons caused by their rapid condensation on the connecting pipes of the installation. During the study three process parameters were changed: temperature (300-650 ^{o}C), pressure (0.1-2.0 MPa), and gas hourly space velocity (50-500 h^{-1}).

Figure 1 shows the comparative data on the ZCC catalytic activity in the process of the conversion of C_1-C_6 hydrocarbon mixture. It is seen that the greatest values of yield and selectivity of aromatic hydrocarbon formation are observed over the catalyst R-2 and are, respectively, 55.6 and 84.2% at the 66% conversion. Figure 2 shows the conversion, yield and selectivity of arene formation over R-2 catalysts *vs*. time. During 96 h this catalyst demonstrated a high operation stability: conversion and arene yield reduced by no more than 6%.
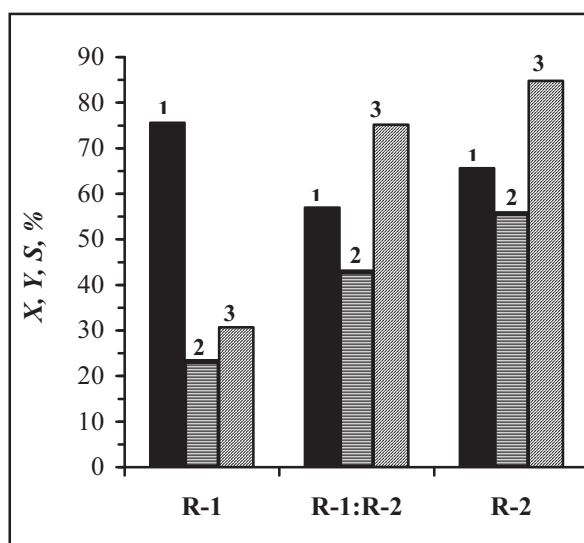
Fig. 1. Conversion (X) of the mixture of C_1-C_6 hydrocarbons (1), yield (Y) of C_{6+} arene (2) and selectivity (S) of C_{6+} arene formation (3) over different catalysts.
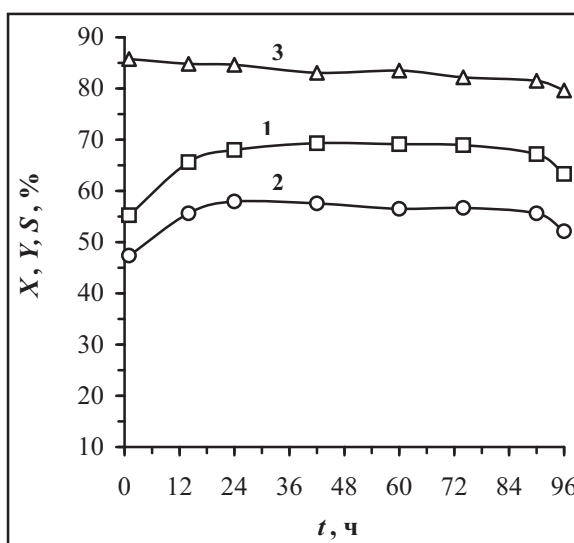
Fig. 2. Changes in the conversion (X) of the mixture of C_1-C_6 hydrocarbons (1), yield (Y) of C_{6+} arene (2) and selectivity (S) of C_{6+} arene formation (3) *vs.* the period (t) of R-2 catalysts operation at a gradual temperature rise of reaction.

The Table gives the data on the thermal analysis of catalysts operated for different periods of time in the process of conversion of gaseous hydrocarbon mixture. Endothermal effects at 100-110 ^{o}C and corresponding maximums on DTG curves are caused by water removal. Intensive exothermal effects and peaks on the DTG curves observed above 410-420 ^{o}C correspond to the coke burnout. The results obtained evidence that a significant amount of carbon deposits was formed over the R-1 catalyst operated for 56 h (37.2%). Although the period of its operation is almost 2 times less than for other catalysts, there is significantly more coke on it. The coke formed on the catalysts for different operation periods is very similar, which is proved by a close position of DTA peak maximums corresponding to the coke burnout (635-645 ^{o}C). Higher coke content on the R-1 catalysts as compared with another samples and the shift of the temperature of the coke burnout end into the high-temperature region evidence that the process of coke formation is very intensive on this catalyst, and the coke formed is characterized by a high polycondensation degree. The smallest coke amount is formed on the R-2 catalyst and it completely burns out at a lower temperature that for other samples.

Table – Temperature and weight data on the catalysts treated by a mixture of gaseous C₁-C₆ hydrocarbons for different period of times*

Catalyst	Weight changes, %	
(period of operation, h)	Water removal	Coke removal
R-1 (56 h)	− 4.9 (110 ^{o}C)	− 37.2 (625 ^{o}C and a shoulder to 960 ^{o}C)
R-1: R-2 (100 h)	− 2.3 (105 ^{o}C)	− 21.4 (645 ^{o}C and a shoulder to 920 ^{o}C)
R-2 (100 h)	− 1.8 (100 ^{o}C)	− 20.3 (632 ^{o}C and a shoulder to 835 ^{o}C)

* In parentheses given are the corresponding temperatures of maximums on the DTG curves. The Table gives the weight changes as compared to the weight of 'clean' catalysts (after coke burnout to 1000 ^{o}C).

The study performed established that the conversion of gaseous hydrocarbons and the yield of aromatic hydrocarbons greatly depend on the process temperature and gas hourly space velocity of the feedstock, the pressure influencing less the process indices. Under optimal process conditions one reaches a high conversion of gaseous hydrocarbons into the mixture of aromatic compounds consisting mainly of benzene, toluene, xylene and naphthalene as well as of small amounts of C_{9+}, methyl- and dimethylnaphthalenes. It was established that the introduction of 5-30 wt% of pentane-hexane fraction into the initial gaseous mixture results in the rise in conversion and yield of aromatic hydrocarbons. The service cycle of catalysts is no less than 96 h and, despite of the formation of a significant coke amount on their surface, the oxidative regeneration allows the activity of ZCC to be restored almost completely.

Thus, the direct catalytic conversion of associate gases and WFLC over zeolite-containing systems into a mixture of aromatic hydrocarbons is the most promising method for their processing. The application of the proposed method will allow building up of a new structure of the gas-processing plant to manufacture the marketable products.

PHYSICO-CHEMICAL CHARACTERISTICS OF Mg-Al-Fe LAYERED DOUBLE HYDROXIDE BASED CATALYSTS IN CORRELATION TO N$_2$O ABATEMENT

T. Vulic[1], A. Reitzmann[2], M. Hadnadjev[1], Y. Suchorski[3], R. Marinkovic-Neducin[1], H. Weiss[3]

[1]*University of Novi Sad, Faculty of Technology, Bul. Cara Lazara 1, 21000 Novi Sad, Serbia & Montenegro, fax: +381 21 450413, E-mail: tatjanavulic@yahoo.com*

[2]*University of Karlsruhe (TH), Institute for Chemical Process Engineering, Karlsruhe, Germany*

[3]*Otto-von-Guericke Universität, Chemisches Institut, Magdeburg, Germany*

Introduction and motivation

Layered double hydroxides (LDH), also known as hydrotalcite-like-materials belong to a group of anionic clays. They consist of stacked hydroxide layers with charge-balancing anions in the interlayer, presented by general formula: $[M(II)_{1-x} M(III)_x(OH)_2](A^{n-})_{x/n} \cdot m\ H_2O$, where M(II), M(III) represent divalent and trivalent cations; A^{n-} interlayer anion (usually carbonate) and $x = M(III) / [(M(II)+M(III)]$. [1,2,3].

Tailoring possibilities of flexible properties enable design and synthesis of LDH based catalysts for environmental friendly processes. Derived mixed oxides, after thermal treatment of LDHs, have homogeneous interdispersion of constituting elements, developed surface area and enhanced resistance to sintering compared to supported catalysts. [3,4,5,6,]. The flexibility of layer composition accomplished by different M(II) and M(III) ions isomorphic substitution, variation of M(II)/M(III) ratio and interlayer anion explains wide field of application, as acid-base and redox reaction catalysts, catalyst supports, anion exchangers, adsorbents, fillers (stabilisers for polymers) to medical-pharmaceutical employment [3,4,5]. LDH phase synthesis is considered to be possible in the range $0.1 < x < 0.5$; the single phase LDH synthesis is limited to $0.2 \leq x \leq 0.33$ [3,5,7]. The structure and surface properties of LDHs and derived mixed oxides, depend strongly on the extent of M(III) substitution, chemical composition and synthesis procedures [5]. Exceeding the mentioned range for single phase LDH synthesis the formation of additional single hydroxide phase (e.g. Al(OH)$_3$ and Mg(OH)$_2$) proceeds [5]. The stability of the LDH matrix is reduced, especially concerning metal to oxygen bonds, leading to metastable state of interest in catalytic act.

Mg-Al-Fe-LDH based materials were investigated as potential catalysts for nitrous oxide abetment, as one of the important sources of the greenhouse effect. Two catalytic reactions are considered: decomposition to N_2 and O_2 and reduction with ammonia to N_2 and H_2O. Introduction of iron (5 mol%) into LDH matrix enabled the redox properties necessary for both mentioned processes. The influence of Mg/Al ratio on properties of Mg-Al-Fe-LDHs was investigated in order to find a correlation between physico-chemical properties of Mg-Al-Fe-LDH based materials and N_2O catalytic abatement process.

Experimental

Among many different preparation methods presented in the literature [5,8,9], low supersaturation coprecipitation with constant pH was selected for the synthesis of LDHs [10] (denotation LS). The samples with different Mg:Al:Fe compositions, with x ranging from 0.15–0.7 were prepared. Magnesium, Aluminum and Iron nitrate salts solution (1M regarding to metal content) was added continuously (4 cm^3 min^{-1}), and the constant pH (ca. 9.6–9.9) was maintained by simultaneous addition of Na_2CO_3 and NaOH (CO_3^{2-}/(M(III)+Mg) = 0.67 and OH$^-$/(M(III)+Mg) = 2.25). The precipitates were calcined 5h, at 500°C in air.

The physico-chemical characterization of untreated and calcined samples was performed by structural (XRD) and morphological analysis (SEM), X-ray photoelectron spectroscopy (XPS) of iron species and temperature programmed reduction with H_2 (TPR).

Catalytic tests, N_2O decomposition (1000 ppm N_2O) and N_2O reduction with NH_3 (1000 ppm N_2O, 1000 ppm NH_3), were followed in a fixed bed micro reactor with 0.8 g catalysts loading in temperature range from 300 to 500°C, at atmospheric pressure and modified space velocity, GHSV$_{mod}$ from 2.17 to 6.25 cm^{3}g$_{(cat)}^{-1}$s^{-1} (NTP). The concentrations of the gas mixture were analyzed with non dispersive IR.

Results

XRD patterns of all untreated samples are typical for LDH compounds; only in $x = 0.7$ sample an additional aluminum hydroxide phase, $Al(OH)_3$, was observed. Well defined structure with the most intensive and sharpest peaks is observed in the sample $x = 0.3$ (25 mol% Al; 5 mol% Fe) of LS-0.3-Fe5.
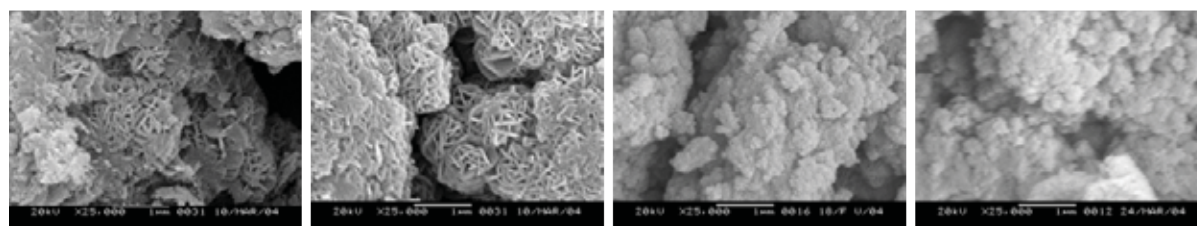
Figure 1. SEM from samples: LS-0.15-Fe5 (left); LS-0.3-Fe5 (middle left), LS-0.5-Fe5 (middle right) and LS-0.7-Fe5 (right); magnification 25000x

The morphology of all samples is characterized by agglomerates of plate-like particles whose dimensions vary with M(III) content (Figure 1). The largest particles are observed in the previously mentioned $x = 0.3$ sample. Exceeding the optimal range for single LDH phase synthesis, the size of particles diminishes.

Oxidation state of iron species in LDH derived catalysts was evaluated with XPS analysis in accordance to the calibration curve of the reference iron oxide which determined the positions of Fe^{3+} oxidation state peaks and Fe^{2+} oxidation state peaks. In all catalyst samples the positions of iron peaks and corresponding binding energies suggest the presence of iron in the 3+ oxidation state, as presented in Figure 2 for the LS-0.3-Fe5 sample ($Fe2p_{1/2}$ at binding energy of 724.5eV and $Fe2p_{3/2}$ at 710.8 eV).
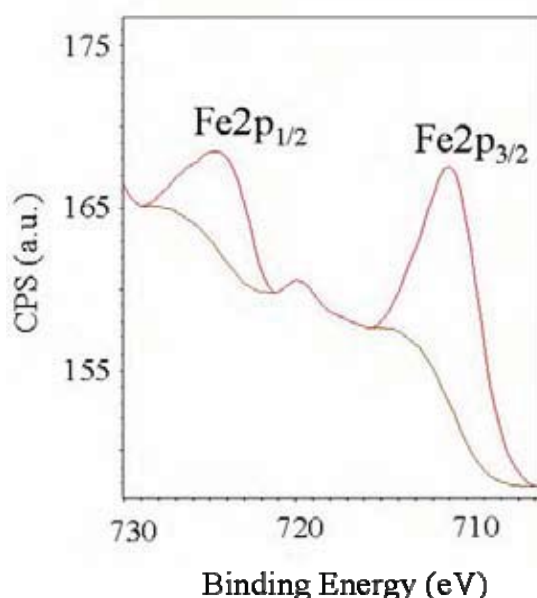
Figure 2. XPS spectra of LS-0.3-Fe5 measured using Mg-anode.

Equations 1-3 describe the sequence for catalytic decomposition of N_2O adsorbed on active center giving N_2 and surface oxygen O^* (eq. 1). Surface oxygen then desorbs reacting with another oxygen atom or in direct reaction with another N_2O (eq. 2 and 3) [11]:

$$N_2O + {}^* \rightarrow N_2 + O^* \qquad \text{adsorption on active center *, giving surface oxygen } O^* \qquad (1)$$

$$N_2O + O^* \rightarrow N_2 + O_2 + {}^* \qquad \text{desorption and reaction} \qquad (2)$$

$$2O^* \leftrightarrow O_2 + 2^* \qquad \text{desorption and reaction} \qquad (3)$$

The decomposition of N_2O at Mg-Al-Fe-LDH derived catalysts is based on iron redox cycle $Fe^{3+} \leftrightarrow Fe^{2+}$ [11]. The results of catalytic tests are presented in Figure 3. Low iron containing samples (5 mol%), independent on Mg/Al-ratio, have very low N_2O conversion. The increase of iron content (sample LS-0.3Fe; 30 mol% of iron) improves conversion. The higher

conversion of catalyst with increased iron content confirms the crucial role of iron in the catalytic act.
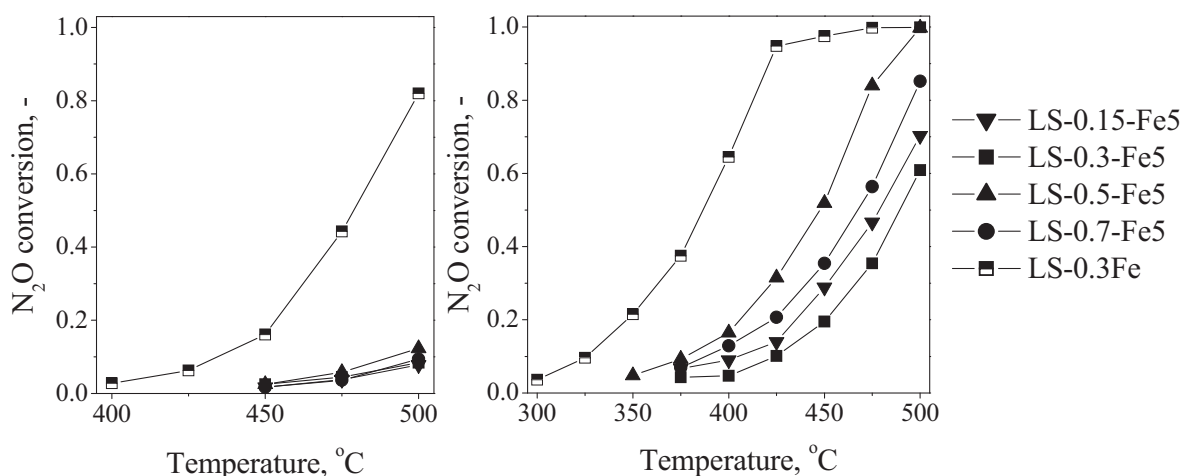
Figure 3. N_2O decomposition (left) and N_2O reduction with NH_3 (right) at $GHSV_{mod}$=2.17 cm^3_{NTP} g_{cat}^{-1} s^{-1}

The other reaction path with reducing agent has overall higher activity, since the presence of reducing agent e.g. ammonia, boosts the removal of surface oxygen (eq. 4) [*12*]:

$$2NH_3 + 3O^* \leftrightarrow N_2 + 3H_2O + 3^* \tag{4}$$

In this reaction path, the crucial role of iron is also confirmed, but the activity of samples with lower iron content is generally increased being dependent on the Mg/Al-ratio among the series. Differentiation of lower iron content samples could be made depending on the stability of LDH matrix structure and *x* value, since the N_2O conversion in these series decreases with the exceeding from the optimal range for single LDH phase synthesis. Conversion was the highest in case of $x = 0.5$ sample (LS-0.5-Fe5) with *x* value nearest to the limit for the incorporation of M(III) into LDH matrix. The presence of the additional single hydroxide phase, $Al(OH)_3$, in x = 0.7 sample (LS-0.7-Fe5), does not improve catalytic act.

References

1. Reichle, W.T. Solid States Ionics 1986, 22, 135-141
2. Newman, S. P.; Jones, W. In Supramolecular Organisation and Material Design; Jones, W.; Rao, C.N.R.; Eds.; ISBN: 0-521-66240-0; Cambridge University Press: Cambridge, UK, 2002, pp 295-331
3. Vaccari, A. Catal. Today 1998, 41, 53-71
4. Serwicka, E.M., Bahranowski, K. *Catal. Today* **2004**, *90,* 85-92
5. Cavani, F.; Trifiro, F.; Vaccari, A. *Catal. Today* **1991,** *11,* 173-301
6. Carrado, K.A.; Kostapapas, A. *Solid State Ionics* **1988**, *26,* 77-86
7. Miyata, S. *Clays Clay Min.* **1980**, *28,* 50-56
8. Olsbye, U., Akporiaye, D., Rytter, E., Ronnekleiv, M., Tangsatd, E. *Appl. Catal.* **2002**, *224* , 39-49
9. Prineto, F.; Ghiotti, G.; Durand, R.; Tichit, D. *J. Phys. Chem.* **2000**, *104,* 11117-11126
10. Chen. Y.Z.; Hwang, C.M.; Liaw, C.W. *Appi .Catal.* **1998**, *69,* 207-214
11. Kapteijn, F.; Rodriguez-Mirasol, J.; Moulijn, J.A. *Appl. Catal.* **1996,** *9,* 25-64
12. Coq, B.; Mauvezin, M.; Dalay, G. ; Kieger, S. *J. Catal.* **2000**, *195,* 298-303

PP-88

INVESTIGATION OF REACTION CONDITIONS ON BIODIESEL PRODUCTION WITH HYDROTALCITE, ZEOLITE AND SULPHATED OXIDES

Yildiz M., Boz N., Canakci M., <u>Akin A.N.</u>

Kocaeli University Engineering Faculty Chemical Engineering Department, Kocaeli, Turkey

Kocaeli University Technical Education Faculty Mechanical Education Department, Kocaeli, Turkey

Introduction

The suggested shortage of fuels encouraged the researches for substitutes for petroleum derivatives. These researches resulted in "biodiesel" as an alternative fuel [1]. Biodiesel is an alternative fuel that is made from renewable biological sources such as vegetable oils and animal fats by chemically reacting with an alcohol. The reaction, named as transesterification, requires a catalyst that is usually a strong base. The final product is called as methyl esters that have come to be known as biodiesel [2, 3]. Because of higher oxygen content than petroleum diesel, biodiesel has shown great reduction in emission of particulate matter, carbon monoxide, sulphur, poly aromatics, hydrocarbons, smoke and noise in diesel engines [4].

Transesterification reactions can be alkali-catalyzed, acid-catalyzed or enzyme-catalyzed. The first two types have received the greatest attention. Most current biodiesel research concentrates on the alkali-catalyzed technology carried out on a bench scale. Apart from the transesterification reaction, the actual process of biodiesel production includes many process steps from raw material refining to product separation and purification [5].

In this study, the effect of reaction temperature on transesterification of canola oil and waste cooking oil was investigated at four different temperatures in the presence of zeolite, hydrotalcide and sulphated oxide catalysts. Beside the temperature effect, oil/methanol ratio and catalyst amount were also investigated as reaction parameters.

Experimental

In this study, solid acid and base catalysts were prepared and their activities were tested in transesterification reaction of canola oil. Hydrotalcide was used as solid base catalyst, while sulphated zeolites and oxide catalysts were used as solid acid catalysts. Hydrotalcite and oxides were prepared by coprecipitation method from solutions of precursors by using precipitation reagents. The coprecipitation was performed in a semi-batch system composed of an insulated

cold water bath, a mechanical stirrer, a glass reaction beaker, a peristaltic pump and a pH-meter. The precipitation reagent was added to the precursor solutions using peristaltic pump while the solution mixed vigorously. After drying and calcination steps catalysts were ready to use in transesterification reaction. Sulphated zeolites and oxides were prepared by kneading of a mixture of known amounts of zeolite and oxides with sulphuric acid.

Prepared catalysts characterized by different physical and chemical methods. The total surface areas were determined by N_2 adsorption using multipoint technique with BET equation. XRD analysis were performed to determine the catalyst structure.

The transesterification reactions were performed in batch reactor system including a gas chromatograph for feed and product analysis. The effect of reaction conditions such as temperature, oil/methanol ratio and catalyst amount were also investigated. Freezing point, flash point, free glycerine, kinematical viscosity and density determination methods were also used to investigate the fuel properties of product.

Results

The results were discussed in terms of catalyst types, reaction temperatures, oil/alcohol ratio and catalyst amount. The results obtained show that types of catalyst affect the reaction conditions and yield. Results were also compared with the results obtained by using homogeneous catalysts in literature and in our laboratories.

Acknowledgement

Ahmet Duran Çelik and İsmail Dinçer are acknowledged for their help in catalyst preparation.

References

[1] A.C. Pinto, L.L.N. Guarieiro, J.C. Rezende, N.M. Riberio, E.A. Torres, W.A. Lopes, P.A. Pereira, J.B. Andrade, J. Braz. Chem. Soc., 16 (2005) 1313.

[2] J.V.Gerpen, Fuel Processing Technology, 86 (2005) 1097.

[3] F. Ma, M.A. Hanna, Bioresource Technology, 70 (1999) 1.

[4] S. Zullaikah, C. Lai, S.R. Vali, Y. Ju, Bioresource Technology, 96 (2005) 1889.

[5] Y. Zhang, M.A. Dube, D.D. McLean, M. Kates, Bioresource Technology, 89 (2003) 1.

PP-89

THE SKELATAL ISOMERISATION OF 1-BUTENE OVER
H-ZSM-5 MODIFIED BY ION EXCHANGE AND IMPREGNATION

Öniz Birsoy[1], <u>Selahatttin Yilmaz</u>[1], Levent Artok[2], Oğuz Bayraktar[2]

[1] Department of Chemical Engineering, [2]Department of Chemistry,

İzmir Insitute of Technology, Gülbahçe Köyü, Urla, İzmir,

Fax:00-90-232-7506645, e-mail:selahattinyilmaz@iyte.edu.tr

1. Introduction

Isobutene is an important raw material for the production of polyisobutane-additive for lubricating oils, butyl rubber and polybutene. It is the primary component for the production of methyl *tert*-butyl ether (MTBE). The supplies of isobutene are not sufficient to meet the increasing demand of for isobutene [1,2]. Therefore, considerable interest has been devoted to finding a new isobutene source via skeletal isomerization of n-butene [3,4] and in the development of new skeletal isomerization catalyst and processes to give optimum results of various industrial requirements.

Zeolites having suitable acidity and pore size are active and selective for this reaction [2,5]. The most suitable zeolites for skeletal isomerization of *n*-butenes are in the group of 10-membered ring (MR) molecular sieves include ZSM-22, SAPO-11, ferrierite, and ZSM-5. Their pore sizes are suitable to achieve high activity and selectivity [3-7]. ZSM-5 has straight channels (5.3x5.5 Å) which are interconnected by zig-zag channels (5.1x5.5 Å). They are very stable. Ferrierite is a two dimensional zeolite with main channels (4.2x5.4 Å) which are interconnected via smaller 8 MR side channels (3.5x4.8 Å). H-FER is also very stable. The pore structure of zeolites may hinder or restrict the access of reactant to some of the potentially active sites.

An other important parameter that effects the activity and selectivity of a catalyst is its acidity. The catalytic activity of acid solids is not only related to the surface concentration of acid sites, but also depends on their nature (i.e. Brønsted or Lewis type) and strength. The skeletal isomerization of 1-butene is mainly catalyzed by acid sites of Brønsted type [2], whereas Lewis surface acid sites seem to be less important in this reaction [8]. Product selectivity and activity depend strongly on the strength distribution of Brønsted acid sites. The production of isobutene from this reaction is selectively achieved by a monomolecular

mechanism, [8,9] and the byproducts (e.g., C3-C5 or C2-C6) are produced by a bimolecular mechanism that involves dimerization of butenes and isobutene, followed by breakdown of the octenes formed. Therefore, modification of the acid strength is a potential way to increase the selectivity.

In this study, the effect of zeolite acidity on n-butene isomerization was investigated. Catalysts were prepared by ion exchange (Co, Ni, Zn or Cu) and impregnation (Co) of H-ZSM-5. For comparision, H-FER was also tested. The catalysts were characterized by XRD, N_2 adsorption, FTIR (pyridine adsorption) and ICP-AES, Scanning Electron Microscopy (SEM).

2. Experimental

2.1. Catalyst preparation and characterization

The parent H-ZSM-5 materials were supplied by Süd-Chemie (MFI-50). Ion exchange was performed from 0.01 M aques solution of metal salts ($Co(NO_3)_2.6H_2O$, $Ni(NO_3)_2.6H_2O$, $Zn(NO_3)_2.6H_2O$ or $Cu(NO_3)_2.2H_2O$) at 80°C for 4 hours in a water bath equipped with a shaker. Only Co was loaded by incipient wetness. Appropriate amount of Co was taken so that it gave about 1.5 % metal loading. The amount of solution was calculated by using the pore volume of the catalyst. The samples were then dried at 110°C over night and calcined at 500°C (temperature increment 5°C/min) for 4 hours. Ferrierite was supplied from Zeolyst in NH_4 form (CP 914C, Si/Al=20). It was calcined at 540 °C for 4 h with a temperature ramp of 3 °C/min. The acidity of the catalysts were determined by pyridine adsorption/desorption using FTIR spectroscopy.

2.2. Catalyst testing

1-butene (98%, 8 ml/min) was sent together with N_2 (99.99%) in to a packed bed reactor (WHSV of 22 h^{-1}). The catalyst amount (125-250 μm) was 0.050 g and n-buten isomerization was carried out at 375 ºC. The products were online analyzed by a Gas Chromatogragphy. Conversions and selectivities were calculated on a carbon basis.

3. Results and Discussion

3.1 Characterization Results

The ion exchanged sampled were labeled as M-H-ZSM-5 where M indicates the metal ion used. The impregnated sample was labeled as Co-Imp/ZSM-5. The similar XRD patterns of ion exchanged samples with the parent ZSM-5 zeolite indicated that the crsysrtal structure was preserved. However, when the zeolite was impregnated with Co, the intensities of the peaks at $2\theta = 7.9°$ and $8.5°$ decreased in comparison to those for H-ZSM-5. The catayst surface area and pore volume changed with the ion metal loading, Table 1. The reason for the

decrease in the surface area may be due to partial blockage of the channels and pores by the metals loaded. Ferrierite catalyst had lower surface area than ZSM-5 catalysts.

The relative amounts of Lewis and Brönsted acid sites of the catalysyts measured are given in Figure 1. The band at 1548 cm^{-1} is assigned to Brønsted acid sites. The intense band at 1490 cm^{-1} assigned to Brønsted and Lewis acid sites. It was observed from each spectrum that the zeolite in its metal loaded and H form had Brønsted and Lewis acid sites. None of the H-ZSM-5 catalysts presented the band at 1455 cm^{-1} which is related to Lewis acidity. Acidities of the catalysts varied with the type of the metal loaded. H-ZSM-5 and H-FER showed the highest acidity when compared to other modified samples of ZSM-5. Co-Imp/ZSM-5 showed the lowest acidity. The catalyst relative acidities was found decrease in the following order;

H-FER > H-ZSM-5 > Co-ZSM-5 > Ni-ZSM-5 > Zn-ZSM-5 > Cu-ZSM-5 > Co-Imp/ZSM-5.

Table 1. Physico-chemical properties , activities and selectivities to isobutene at 3 h over different catalysts.

Sample Code	Metal Loading (wt%)	BET Surface Area (m^2/g)	H.K. Pore volume (cm^3/g)	Conversion (%)	Selectivity (%)
H-ZSM-5	-	455.7	0.210	82.5	25.0
Co-ZSM-5	1.12	460.49	0.209	82.7	22.4
Ni-ZSM-5	1.33	414.49	0.196	79.0	24.6
Zn-ZSM-5	1.42	394.78	0.185	79.0	23.4
Cu-ZSM-5	1.35	447.62	0.189	76.5	30.5
Co-Imp/ZSM-5*	1.78	429.57	0.172	66.0	28.4
H-FER	-	339.25	0.172	57.0	68.9

3.2. Activity and Selectivity Results

The activity of ion exchanged zeolite did not change significantly with the metal type loaded, see Table 1. Apart from Co-H-ZSM-5 which gave similar conversion to H-ZSM-5, conversion dropped with the other metal loaded. The lowest conversion over the catalyst prepared by ion exchange was observed with Cu-H-ZSM-5. Co-Imp/HZSM-5 gave a lower activity. H-FER showed some deactivation at the beginning of the reaction: conversion dropped from 70.5 to 57 % in 40 min and then stabilized. The selectivity to isobutene changed little with the metal loading, Table 1. Only the Cu loading by ion exchange and Co loading by impregnation improved H-ZSM-5 selectivity while it decreased for the others. Cu-H-ZSM-5 and
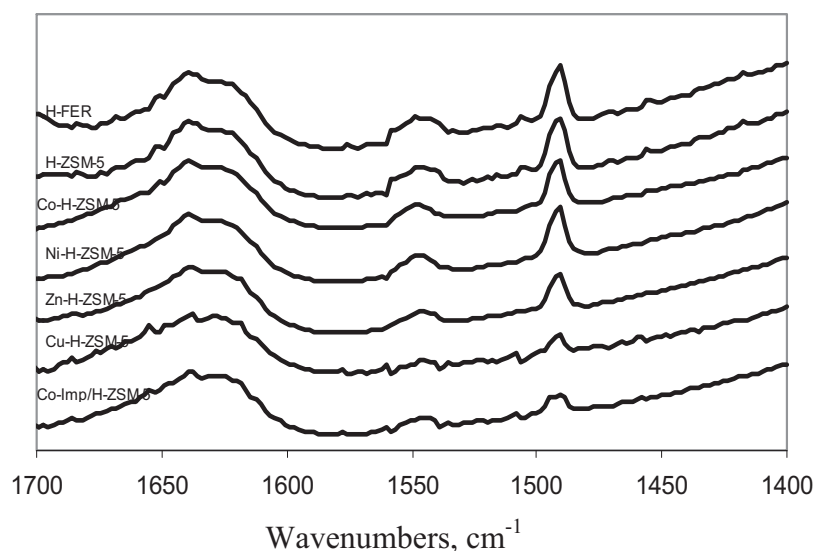
Figure 1. IR spectra of pyridine adsorbed the catalysts.

Co-Imp/H-ZSM-5 did not posses as much Bronsted and Lewis sites as others. On the other hand, H-FER which relatively had higher amount of Bronsted and Lewis sides gave higher selectivity to isobutene (68.9 %). It was suggested that strong acid sites of this catalyst were deactivated by coke formation at the beginning of the reaction, as a result high selectivities were observed.

The product distribution obtained changed with the catalyst used. Propylene was the major by-product with parent (20.6 %), M-H-ZSM-5 (from 21.8 to 25.5 %) and with Co-Imp/HZSM-5 (28.1%) catalysts. Then followed propane, n-butane and ethylene which were about 5 % each. More propylene and ethylene formed over the modified catalysts. Since there was no pentane formation, one could suggest that dimerazation reaction were not taking place. This indicated that the reaction took place following a monomolecular mechanism which takes place on weak and medium acid sites.

References

[1] Seddon, D. "Reformulated Gasoline, Catalysis Today 1992, 15, 1.

[2] Houzvicka, J.; Ponec, V. *Catal. Re*V.s*Sci. Eng.* **1997**, *39*, 319.

[3] Szabo J., Perrotey J., Szabo G., Duchet J.C., Cornet D., J. Mol. Catal. 67 (1991) 79.

[4] Houzvicka, J.; Hansildaar, S.; Ponec, V., J.Catal, 167(1997)273.

[5] Xu, W.-Q.; Yin, Y.-G.; Suib, S. L.; Edwards, J. C.; O'Young, C.-L. J. Phys. Chem. 99(1995)9443.

[6] Seo, G., Park, S.-H., Kim, J.-H Catal. Today 44 (1998) 215-222

[7] Byggningsbacka R.; Kumar, N.; Lindfors, L.E., J. Catal. 178(1998)611-620.

[8] Cheng, Z. X.; Ponec, V. *J. Catal.* **1994**, *148*, 607.

[9] Houzvicka, J.; Ponec, V. *Ind. Eng. Chem. Res.* **1998**, *37*, 303.

COMPACT REACTOR FOR WATER GAS SHIFT REACTION
OVER THERMAL-CONDUCTING CATALYSTS

T.M. Yurieva[a], **N.A. Baronskaya[a]**, **T.P. Minyukova[a]**, **M.P. Demeshkina[a]**, **A.A. Khassin[a]**,

S.V. Dimov[b], **V.V. Kuznetsov[b]**, **V.Ya Terentiev [c]**, **A.P. Khristolyubov [c]**, **O.F. Brizitskiy[c]**

[a] *Boreskov Institute of Catalysis, Pr. Ac. Lavrentieva, 5, 630090, Novosibirsk, Russia,*

fax: +7-383-3308056, e-mail: yurieva@catalysis.ru

[b] *Kutateladze Institute of Thermophysics, Pr. Ac. Lavrentieva, 1, 630090, Novosibirsk, Russia*

[c] *Russian Institute for Experimental Physics (VNIIEF), Sarov, Russia*

Decreasing the size of the reactors for the synthesis gas conditioning (water gas shift reaction, WGSR, and fine CO removal) makes an appeal to the researches due to the need in compact generators of pure hydrogen for fuel cell applications. For this purpose, a rather small scale reactor with optimal productivity related to a reactor volume is needed. In this case, the tubular bed reactors having the optimal temperature profile along the catalyst bed may be fruitful. Such an approach to optimizing the WGSR reactor was reported in [1] and [2]. For effective reactor heat abstraction tubular reactors with the tube diameter 50-60 mm are used. Since the effective heat conductivity coefficient of a catalyst bed in the direction perpendicular to the gas flow does not exceed 0.5-1 $W(m^.K)^{-1}$, the radial temperature difference in the tubular catalyst bed for WGSR reaches 20-30°C [3, 4].

In our present contribution we report on the possibility of efficient solution of the problem of intensive heat abstraction in the catalyst bed in the radial direction by: (1) using of a catalyst with high thermal conductivity of the catalyst body and (2) effective organization of the catalyst by using the catalyst body with perpendicular dimensions comparable with the reactor size. The effective catalytic activity of such thermal-conductive catalyst bodies is even higher than that of the commercial size catalyst grains.

The reported catalyst for water-gas shift reaction is a composite with high catalytic activity and thermal conductivity no less than 1 $W(m^.K)^{-1}$, which consists of particles of a catalytically active oxide component and heat conducting metal particles acting simultaneously also as reinforcing component. Such composites were prepared by a sequence of operations commonly used in powder metallurgy that includes: 1) preparation of a mixture of powders of a catalytically active oxide component, a metal and a porophore component; 2) mixture densification; and 3) sintering at elevated temperatures. In present research the

powder of Cu-Zn-Zr WGSR catalyst containing 40 at. % of Cu was mixed with electrolytic metallic Cu powder of 20 - 50 μm in size having dendrite structure and malachite (as porophore), then pressurized at 170-220 MPa to the 2.4-2.6 mm plate, which after all was sintered at 450°C in flowing argon. Fig. 1 shows the optical and scanning electron microscope images of a typical thermal-conducting catalyst plate (TCP).
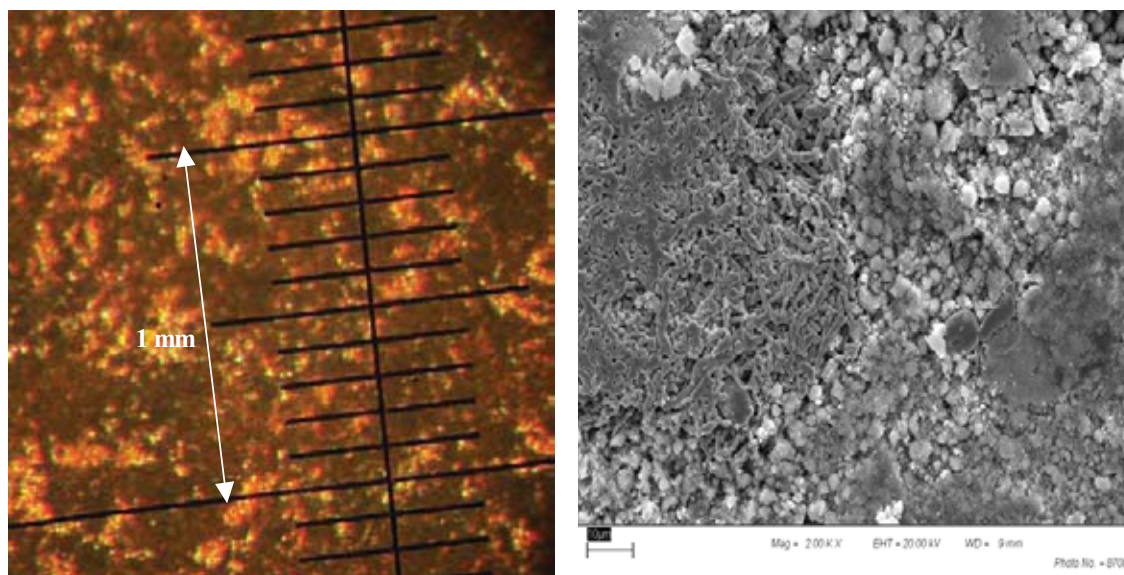
Fig. 1. Optical (left) and scanning electron (right) micrographs of a typical heat conducting catalyst plates. Scale bar at the right graph is 10 micrometers.
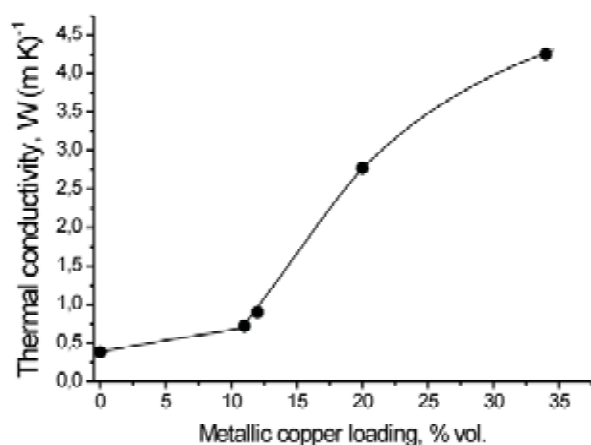
Fig. 2. The correlation between the metallic copper loading and thermal conductivity of the TCP catalyst. The plates were pressed at 170 MPa and sintered at 410°C.

The thermal conductivity of the TCP catalyst obviously correlates to the metallic copper content. Fig. 2 shows that an improvement in the composite thermal conductivity can be obtained by introducing above 10-12 % vol. of metallic copper. It is noteworthy, however, that higher metallic copper loading is needed to prepare strong plates. The plates discussed below contain 20-25 % vol. (50-55 % wt.) of metallic copper. The density of the WGSR catalyst loading is approx. 1.1 g cm^{-3}.

PP-90

The prepared TCP catalysts have rather high porosity (> 55 % vol.), which makes the diffusion constrains rather mild. Their WGSR catalytic performance was studied in the circulating-flow gradientless reactor and the first order kinetic constants were calculated from the experimental data. The ratios of the observed kinetic constants to those observed on the fine catalyst powder (0.25-0.5 mm), i.e. effectiveness factors of the catalyst usage are compared in Table 1 to the corresponding values for a traditional cylindrical catalyst pellet (5 mm x 5 mm). The performance of TCP catalysts is good when they were sintered at temperatures of $410^{o}C$ and below.

Table 1. Comparison of the catalytic performance of the TCP catalyst to that of the traditional catalyst pellet. CO content in dry gas 12 % vol., steam : gas ratio 0.6, atmospheric pressure. The figures in the TCP notation mean the conditions of its preparation: pressure (MPa) and temperature (^{o}C).

Reaction temperature, ^{o}C	270	300	330	350
First order kinetic constant, s^{-1}				
Cu-Zn-Zr catalyst	24.2	36.1	45.1	62.2
Effectiveness factor of catalyst usage				
Traditional pellet, 5mm x 5mm	0.41	0.37	0.36	0.34
TCP-220-380	0.47	0.44	0.35	0.29
TCP-170-380	0.53	0.46	0.36	0.39
TCP-170-410	0.60	0.48	0.40	0.40
TCP-220-440	0.39	0.38	0.28	0.24
TCP-170-440	0.51	0.40	0.33	0.33

The shape of the TCP catalyst and the way of its arrangement in the reactor may play significant role for the TCP reactor performance. Figure 3 shows the calculated gas velocity fields for two different TCP shapes, firmly arranged in a reactor tube. In Fig. 3.1 disks with one hole are interchanged with those having four holes, in Fig. 3.2, all plates are disk segments interchanging symmetrically (Fig. 3.2). The velocity of gas mixture is considered as 1 m^3/h. At these conditions, the reactor with 66 TCP plates is expected to convert CO from 12 % to 1 % vol. One can see that in Fig 3.1 only forefront of the plate is washed by the gas flow, while at the backside gas is stagnant. It forces one to expect twice worse performance of the arranged TCP catalyst comparing to that of an "unarranged" one. This expectation agrees with the experimental data on the TCP reactor arranged with square TCP catalyst (Table 2).

On the other hand, the both sides of a TCP plate are well washed in Fig. 3.2. It presents modelling of the TCP reactor with the catalyst of a disk segment shape. This calculation allows us to hope for better performance. The experimental catalytic study of the reactor with TCP of disk segment shape is now under preparation.
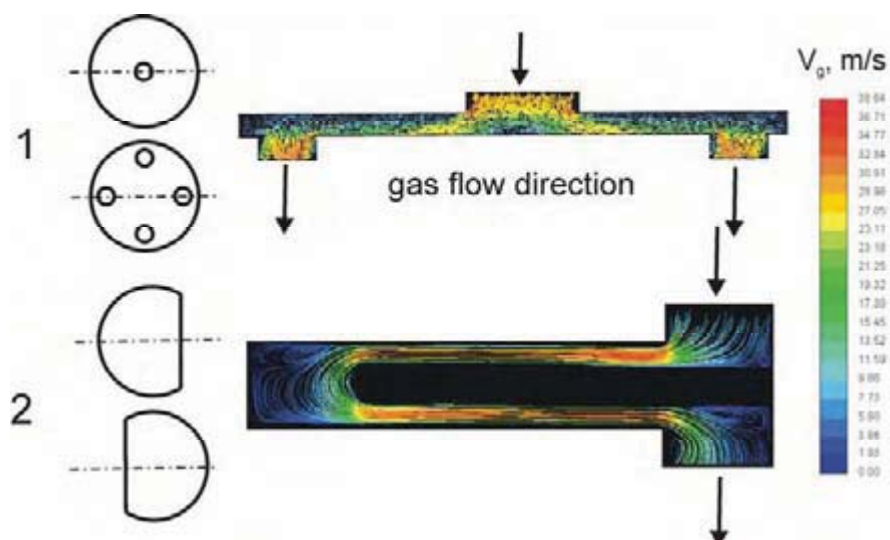
Fig. 3. Gas velocity fields for two different schemes for heat conducting plates arrangement in the tubular reactor: 1 – interchange of disks with one and four holes; 2 – interchange of disk segments. Gas flow 1 m^3/h. Disks are of 25 mm in diameter, the gap between disks is 1 mm.

Table 2. Comparison of the catalytic performance of the reactor with square TCP catalyst. CO content in dry gas 12 % vol., steam:gas ratio 0.6, atmospheric pressure, gas velocity 0.4 m^3/h.

Reaction temperature, ^{o}C	270	300	330	350
Effectiveness factor of catalyst usage				
TCP-170-440-square "unarranged"	0.45	0.41	0.33	0.25
Arranged in the TCP reactor	0.30	0.25	0.24	0.20

Conclusions. Thermal conductive catalyst plates (TCP) for compact WGSR reactors were prepared and studied. High thermal conductivity of 2.5–5 W $(m\ K)^{-1}$ can be achieved, while the effective catalytic activity of TCP catalysts is even higher than that of the commercial size catalyst grains. The TCP shape is important for the overall reactor performance and should be in the focus of our future studies.

References:

[1] D. Myers, T. Krause, J.-M. Bae, and C. Pereira. D. Myers, T. Krause, J.-M. Bae and C. Pereira. Extending Abstracts. 2000 Fuel Cell Seminar. p. 280-283, 2000.

[2] X.D. Hu, J.P. Wagner, US Pat. 5'990'040, 1999, to United Catalysts Inc.

[3] S.D. Beskov, Technological Calculations. Vysshaya Shkola, Moscow, 1968 (in Russian);

[4] G.K. Boreskov, Heterogeneous Catalysis. Nauka, Moscow, 1988 (in Russian)

SELECTIVE CATALYTIC OXIDATION OF HYDROGEN SULFIDE FOR CLEANUP OF CLAUS TAIL GASES: STARTUP OF INDUSTRIAL INSTALLATION AT OMSK REFINERY

A.N. Zagoruiko, V.V. Mokrinskii, N.A. Chumakova, G.A. Bukhtiarova, S.V. Vanag,

T.V. Borisova*, G.G. Isaeva*, P.G. Tsyrulnikov**, M.D. Smolikov**, B.G. Kozorog***

Boreskov Institute of Catalysis SB RAS, pr. Akad. Lavrentieva, 5, Novosibirsk, 630090,

Russia; e-mail: zagor@catalysis.ru, fax: +7-383-3306878;

*JCS «Katalizator», Novosibirsk, Russia;

** Institute for Problems of Hydrocarbon Processing, Omsk, Russia;

*** JSC "Omsk Refinery", Omsk, Russia

Introduction

Decrease of atmospheric emissions of volatile sulfur-containing compounds remains an actual environmental problem worldwide. One of the most important challenges in this area is cleanup of tail gases of Claus units which are widely applied in oil refinery and gas processing industry. Though during last decades numerous tail gas cleanup processes were developed and put into operation [1], there still exists the demand for the technology, combining low capital and operating cost with appropriate cleanup efficiency. The most promising way in this area is application of catalytic selective oxidation of H_2S into sulfur by oxygen.

Catalyst selection and testing

The typical industrial processes of selective hydrogen sulfide oxidation are based on application of iron oxide (SuperClaus process [2]), vanadia (Selectox process [1]) or titania (MODOP process [1]) catalyst. In the scope of preliminary catalyst selection in our study there were taken 9 own catalyst samples, including those based on oxides of iron, cobalt and vanadium, with one reference iron oxide commercial catalyst.

Catalyst selection experiments were performed at laboratory installation in isothermal microreactor with loading of each catalyst sample, equal to 2.5 cm^3. Условия проведения экспериментов: inlet reaction mixture composition: H_2S – 1.2% (vol.), O_2 – 5%, H_2O – 30%, SO_2 – 0.1%, balance – helium; catalyst pellets size – 3-4 mm; residence time – 2 sec; temperature range – 200-300^{0}C; duration of each experiment – not less than 8-10 hours. Outlet gas composition was controlled by GC (with measurement of H_2S, SO_2, O_2, H_2O concentrations). Achievement of steady-state catalyst performance was checked by periodical

control of reaction mass balance. The significant excess of oxygen in reaction mixture (almost an order of magnitude over stoichiometry) was made to provide selection of the most selective and stable to deactivation catalyst.

The criteria for comparison of tested catalysts were observed H_2S conversion and oxidation selectivity.

The selection experiment showed that all cobalt oxide based catalysts demonstrated significant discrepancy of mass balance even after 10 hours of testing, which may be attributed to their intensive sulfation. Vanadia catalyst showed much higher stability, but failed to provide high oxidation selectivity – practically all H_2S at temperatures higher than 250°C was converted into SO_2.

The best results, both in sulfur yield and stability were demonstrated by iron-oxide based catalysts. One of such samples, optionally called M-1, showed practically similar performance as commercial reference sample. This sample was chosen for further testings.

Resource testings of M-1 and reference sample (optionally marked as RP) were performed in two experimental cycles with duration of each cycle not less than 200-300 hours. The comparative results are shown at Fig.1.
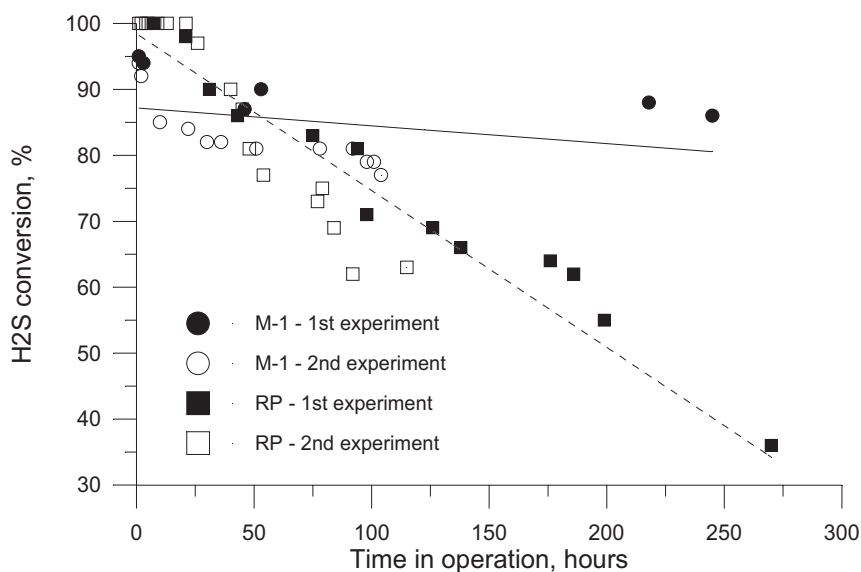
Fig. 1. Hydrogen sulfide conversion during comparative resourse testing.

It is seen that M-1 visibly shows higher operation stability than the reference sample. It should be also stated that M-1, dislike reference sample, contains no chromium oxide and other toxic additives. Therefore, we may state that proposed sample provides better performance than known commercial catalyst and its industrial application is worthy.

The industrial technology of production of chosen catalyst was afterwards developed by JSC "Katalizator" and the developed catalyst has received commercial trademark ICT-27-42.

PP-91

Process simulation and development

The proposed process flow-sheet was traditional and quite simple – it included device for mixing of Claus tail gases with air, reaction mixture preheater, H_2S oxidation reactor with a packed bed of ICT-27-42 catalyst and sulfur condenser. Process simulation was performed on the base of kinetic model, applying nonstationary kinetic equations to description of steady-state experiments [3].

Separate modelling studies showed that selectivity of H_2S oxidation into sulfur under observed kinetic regularities may rise with the increase of the catalyst pellet size. Substantially, deep oxidation reaction (with formation of SO_2) requires stoichiometrically three times more oxygen than selective oxidation reaction. Therefore, diffusion resistances (both intra/extraparticle) rising with a catalyst pellet size, will limit oxygen access to catalyst surface and favor selective oxidation. Of course, it will also cause decrease of total H_2S conversion rate, so there exists the optimal pellet size, providing maximum process operation efficiency and maximum sulfur yield. Under studied process conditions such optimal pellet equivalent diameter lies within the range 5-10 mm [4].

Industrial installation creation and startup

The developed installation was created and put into operation at the JSC "Omsk Refinery" site to provide cleanup of combined flow of tail gases from two Claus units.

The oxidation reactor was charged with 5 tonnes of ICT-27-42 catalyst (cylinders 10x10 mm), produced by JSC "Katalizator".

The startup of the installation was performed in November 2004. The tail gases from Claus units contatined upto 1-2% (vol.) H_2S, 0-0.5% SO_2, ~30% H_2O.

Temperature regime of reactor operation was quite stable. Pressure control showed reasonably low pressure drop both in the reactor and in the installation in total. Moreover, the pressure regime was also quite stable, showing no evidence of catalyst destruction or soiling.

Sulfur condenser showed good operation efficiency and reliability. Direct measurements of the condensed sulfur volume (upto 70-90 kg/hour) was in good coincidence with design data. Information on observed process operation parameters is given in the table below.

Process operation parameters

No.	Parameter	Units	Value
1.	Total acid gas (90-95% H_2S) processing capacity at two Claus units	st.m^3/hour	1800-3200
2.	Total volume of tail gases from two Claus units	st.m^3/hour	5000-9000
3.	Flow rate of air, fed to H_2S oxidation reactor	st.m^3/hour	105-250

4.	Gas temperatures:
	    inlet of gas heater (outlet from last Claus condenser)
	    H_2S oxidation reactor inlet
	    H_2S oxidation reactor outlet
	    sulfur condenser outlet
		°C	
			~ 130
			170-180
			200-240
			125-135

5.	Pressure drop at maximum gas loading:
	    H_2S oxidation reactor
	    cleanup installation in total
		mm WC	
			40-80
			200-250

Gas composition analysis showed that observed sulfur recovery level (in general, with Claus units) after introduction of the cleanup unit was increased from 90-92% to 95-99%. It should be noted that minimum sulfur recovery efficiency (95-97%) was observed during significant deviation of tail gas composition from optimal one, being a result of unsatisfactory control of flow rate of air fed to the Claus furnaces, i.e. non-optimal operation of Claus units. In the regimes meeting the tail gas composition requirements sulfur recovery level was observed at predicted level (98.5-99.2%).

In general, startup of tail gas cleanup installation provided decrease of sulfur emissions into atmosphere from refinery site by a factor of 4-5 or by almost 2000 tonnes SO_2 per annum.

References

1. J.Wieckowska. Catalytic and adsorptive desulphurization of gases. *Catalysis Today*, 1995, 24(4), 405-465.

2. P.F.M.T. van Nisselrooy, J.A.Lagas. Superclaus reduces SO_2 emission by the use of a new selective oxidation catalyst. *Catalysis Today*, 1993, 16(2), 263-271.

3. A.N.Zagoruiko, V.V.Mokrinskii. Non-steady-state approach to steady-state kinetics: case study of H2S oxidation by oxygen. // XVI International Conference on Chemical Reactors (CHEMREACTOR-16), Berlin, Germany, December 1-5, 2003, pp.399-402.

4. A.N.Zagoruiko, V.V.Mokrinskii, N.A.Chumakova. Method of selective catalytic oxidation of hydrogen sulfide into sulfur. Russian Patent Application No.2003122581, 2003.

KINETIC INSTABILITIES AND INTRA-THREAD DIFFUSION LIMITATIONS IN CO OXIDATION REACTION AT Pt/FIBER-GLASS CATALYSTS

A.N. Zagoruiko, S.A. Veniaminov, I.N. Veniaminova, B.S. Balzhinimaev

Boreskov Institute of Catalysis SB RAS, pr. Akad. Lavrentieva, 5, Novosibirsk, 630090, Russia; e-mail: zagor@catalysis.ru, fax: +7-383-3306878

Introduction

Novel catalysts comprising noble metals (Pt and Pd), supported on fiber-glass woven support [1] has attained a lot of attention recently both from theoretical and applied points of view. Though the research of their catalytic properties is developing very fast, still there is a lack of understanding of heat/mass transfer processes in various packing of fibrous catalysts. Earlier non-trivial influence of external mass transfer limitations in woven catalyst packing was reported for SO_2 oxidation reaction [2]. Though these results were obtained at pilot plant tests with low accuracy level, nevertheless, it may be stated that diffusion limitations may influence significantly the efficiency of processes in fiber-glass beds.

The situation becomes especially complicated for reactions with strongly non-linear kinetics, such as CO oxidation by oxygen at noble-metal catalysts. Earlier studies of these reaction at Pt/FG[3] and Pd/FG [4] catalysts showed that reaction kinetics may expressed by an equation with second-order inhibition term, being a source of kinetic instabilities (reaction rate hysteresis, oscillations etc.). Such instabilities are generally typical for CSTR reactor, though they may be also observed in plug flow reactor under influence of external diffusion limitation factors [5].

Experiments
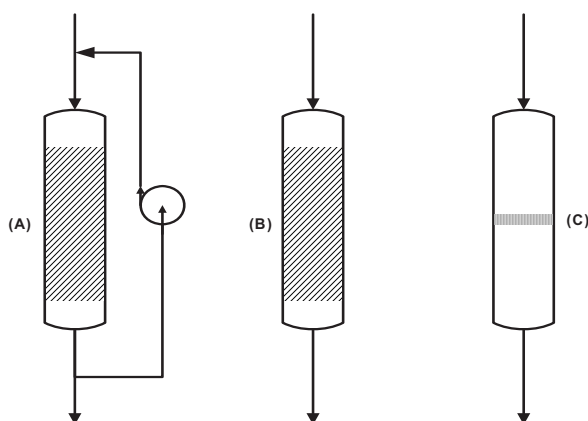
The Pt/FG catalysts (~0.01% mass Pt at high-silica glass fibers) were tested at experimental installation, using three types of reactor and catalyst arrangement (see Fig.1).

Fig. 1. Types of reactor and catalysts arrangement. A – loop reactor with separate catalyst threads, B – direct flow reactor with separate catalyst threads, C – direct flow reactor with a single layer (disc) of woven catalyst fabric.

Type A arrangement may be identified as CSTR, while B was expected to behave like plug-flow reactor and probable behavior of C was not predominantly clear (at the same time it was interesting to study this type as a prototype of commercial thin-bed reactors). The tests were performed with mixture of 900/500 ppm CO, 10% vol. oxygen and balance helium.

The experimental results obtained are given in Fig.2.

Fig.2. CO conversion vs temperature in different types of reactor arrangement.
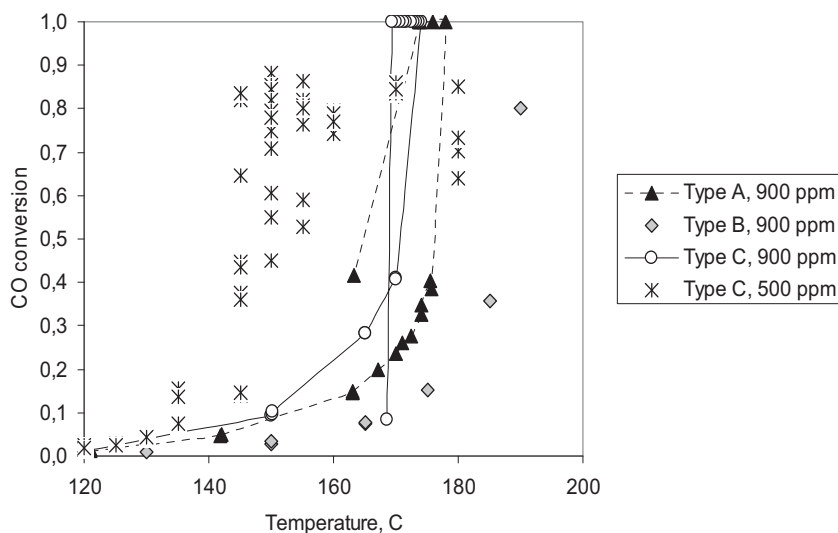
It is seen that kinetic instabilities typical for noble-metal catalysts (such as reaction "light-off", reaction rate hysteresis both with changing of temperature and residence time) are clearly observed for CSTR (Type A reactor). The well-known reason of these instabilities is strong non-linearity of kinetic equation with second-order inhibition term in combination with CSTR type equation for reactor. The Type B reactor shows plug-flow behavior with lower conversions and without conversion instability, what also is in good correspondence with theory. The best description of experimental data for Types A and B was provided by conventional kinetic equation $w = k_1 C_{CO} / (1 + k_2 C_{CO}^2)$.

The operation of disc (Type C) reactor is less predictable. For mixtures with higher CO content (900 ppm) that some experimental points are close to Type A performance, though some definitely belong to Type B curve. Therefore, it may be stated that kinetic instabilities in this case may be complicated by oscillations between CSTR/plug-flow reactor operation modes.

Type C operation is even more unstable in case of lower CO inlet concentration (500 ppm). In this case the "light-off" is observed at lower temperature, but further increase of temperature does not lead to achievement of complete conversion and results in chaotic conversion oscillations in the range of ~80-90%, most probably, being a result of the same oscillations between CSTR/plug-flow modes with influence of external mass-transfer limitations.

Simulation of diffusion limitations inside the catalyst thread

The important question of prediction of fiber-glass catalysts behavior is influence of heat and mass transfer inside the knitted thread of the catalyst.

As soon as it seems impossible to measure these effects experimentally, this problem was studied by means of numerical simulation. Earlier it was shown that important difference of fibrous catalyst from conventional granular ones is possibility of existence of the convective flow inside the thread except the usual conductive diffusion [2]. Nevertheless, under studied experimental conditions influence of such flows may be neglected as soon as they may play significant role only at high gas linear velocities, as it was demonstrated in [6].

In our model formulation we proposed the single catalyst thread with internal diffusion of reagents and internal heat conductive transfer.

The results of simulation are given in Figs.3-5. In general it was found that diffusion limitations maybe significant even at low CO concentrations and moderate temperatures, leading to existence of two reaction modes with "high" and "low" reaction rates and temperature nonuniformity of the thread.
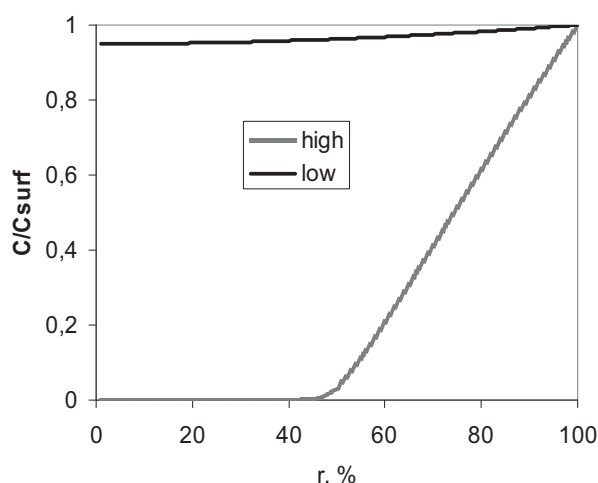
Fig. 3. Calculated relative local CO concentrations (related to concentration at the surface) vs catalyst thread radius.
0% - thread axis, 100% - thread surface. Surface conditions: temperature 150°C,
CO concentration – 500 ppm,
thread diameter – 3 mm.

In low conversion mode the thread is practically uniform and influence of diffusion limitations is negligible. To the contrary, high conversion mode is characterized with strong concentration nonuniformity, when the major part of conversion occurs in the thin zone between thread surface and thread axis. The well expressed temperature gradient is also observed, being quite significant, if compared with low adiabatic heat rise of diluted mixture (~ 5°C).

Integral reaction rate in case of "high" conversion mode is higher than reaction rate at thread surface conditions and formal observed effectiveness factor may reach the values as high as 7-8. The value of temperature difference inside the thread may rise up to 50-80% of adiabatic heat rise. Taking into account that, according to experimental data, the reaction

"light-off" in definite temperature area may be caused by temperature changing by <1°C, the thread temperature nonuniformity may impose significant influence on reaction performance.

<div align="center">
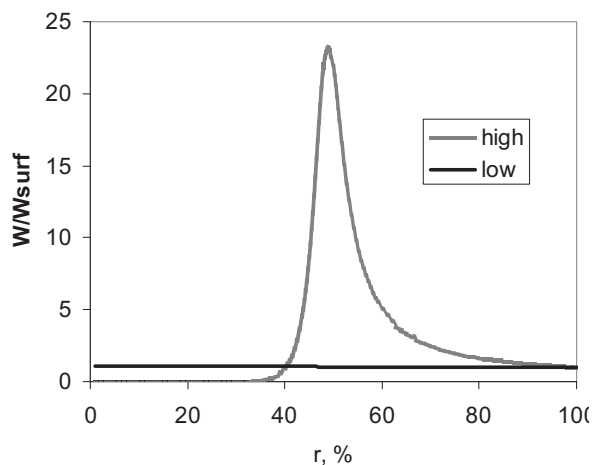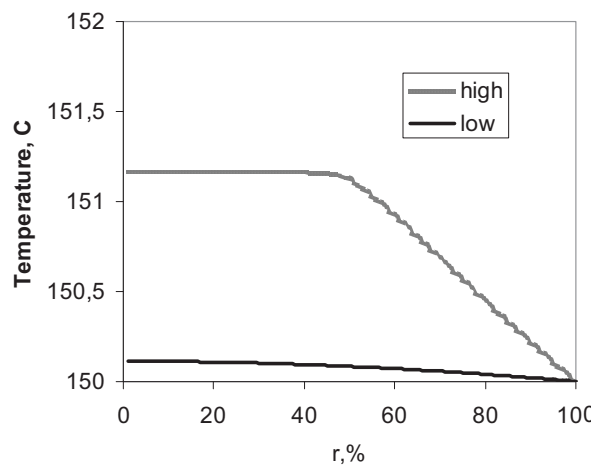
Fig.4   **Fig.5**

*Calculated relative local reaction rates (fig.4) and catalyst temperature (fig.5)
vs catalyst thread radius. Conditions – see fig.3*

</div>

The values of nonuniformities inside the thread depend upon many reaction conditions – thread diameter, CO concentration, temperature etc. Notably, the simulation results vary very much in simulations cases when balance gas was changed from helium to nitrogen (due to quite different viscosity and heat conductivity of these gases). It means that investigations of practically important reactions (e.g. purification of gas exhausts, assuming oxygen and nitrogen as balance gases), using helium as balance gas in lab experiments may lead to erroneous conclusions.

References

1. L.G.Simonova, V.V.Barelko, A.V.Toktarev, V.I.Zaikovskii, V.I.Bukhtiarov, V.V.Kaichev, B.S.Balzhinimaev. *Kinetics and catalysis*, 2001, v.42, No.6, p.917.

2. A.N.Zagoruiko, V.D.Glotov, N.N.Meniailov, Yu.N.Zhukov, V.M.Yankilevich, B.S.Balzhinimaev, L.G.Simonova. // XVI International Conference on Chemical Reactors (CHEMREACTOR-16), Berlin, Germany, December 1-5, 2003, pp.395-398.

3. S.A.Veniaminov, A.N.Zagoruiko, L.G.Simonova, A.V.Toktarev, I.N.Veniaminova, B.S.Bal'zhinmaev. // 7th European Congress on Catalysis, 2005, Sofia, Bulgaria, Book of Abstracts, P9-25, p. 283.

4. I.Yuranov, L.Kiwi-Minsker, M.Slin'ko, E.Kurkina, E.D.Tolstunova, A.Renken. *Chem.Eng.Sci*, 55(2000), pp.2827-2833

5. F.Duprat. *Chem.Eng.Sci*, 57(2002), pp.901-911.

6. O.V. Chub, E.S. Borisova, O.P. Klenov, A.S. Noskov, A.V. Matveev, I.V. Koptyug. *Catal.Today*, 105(2005), pp. 680-688.

PP-93

ACTIVITY AND REGENERABILTY OF SULFATED ZIRCONIA AS A FUNCTION OF CATALYST PRECURSOR AND PRETREATMENT CONDITIONS

A. Zarubica[1*], M. Kovacevic[1], P. Putanov[2], G. Boskovic[1]

[1]Faculty of Technology, University of Novi Sad, 21000 Novi Sad, Serbia & Montenegro;
oskovic@uns.ns.ac.yu

[2]Serbian Academy of Sciences and Arts, 11000 Belgrade, Serbia & Montenegro

* on leave from Faculty of Natural Sciences and Mathematics, University of Nis,
18000 Nis, Serbia & Montenegro; zarubica2000@yahoo.com

Introduction

Supply of high octane number (ON) fuel is a challenging task for refineries due to strong environmental restrictions initiated by EU. Mainly, elimination from gasoline harmful but at the same time high-ON substances forces ON-issue to be solved by alternative processes. Hydroisomerization of straight C_5-C_7 paraffins producing high-ON components for gasoline blending is one possibility [1]. The reaction requires a byfunctional catalyst: a noble metal on an acidic support, preferentially on zeolites due to their resistance to impurities [2]. M/zeolites catalysts, however, demonstrate lower activity than corresponding chlorided-alumina-based catalysts. Therefore, for the near future an important challenge is to develop a new environmental friendly and active catalyst. Solid acids as sulfated zirconia (SZ) are potential candidates for isomerization of light alkanes [3]. The problem with zirconia, however, is rapid deactivation due to accumulation of coke [4], loss of acidity [5], and removal of active sulfur entities [6]. The aim of this work is to correlate catalytic and physicochemical properties of series of SZ samples as a function of catalyst precursor and pretreatment temperature.

Experimental

Three types of SZ catalysts were prepared from different commercial precursors following the identical procedures for the equivalent sequences required to obtain the particular sample: the catalyst (1) from SO_4-$Zr(OH)_4$ (97%, Aldrich) by its calcination; the catalyst (2) from $Zr(OH)_4$ (Aldrich) by first its sulfation and further calcination; and the catalyst (3) from $ZrO(NO_3)_2 \cdot xH_2O$ (Aldrich) by its precipitation, followed by sulfation of the obtained hydroxide and its further calcination. The hydroxide for the catalyst starting from nitrate salt (catalyst 3) was obtained by its precipitation with 25% NH_4OH. The sulfation of

both hydroxides (one synthesized from nitrate - catalyst 3, and the commercial one - catalyst 2) was done by wet-impregnation of 0.5M H_2SO_4 for intended S content of 3%. All three sulfated $Zr(OH)_4$ catalyst precursors were finally calcined, for 3h in air flow. Consequently, total of 9 samples of SZ catalysts were obtained, denoted as (1), (2) and (3) depending on precursor, followed by A, B and C depending on applied calcination temperature, 500, 600 and 700 ºC, respectively.

Catalysts activity in n-hexane isomerization was measured in a fixed-bed micro reactor. The reaction was performed at 200-350 ºC, p=1bar, with 60.5 mbar $n\text{-}C_6$ partial pressure, molar ratio $He(H_2)/n\text{-}C_6$=15, and space velocity $6 \cdot 10^{-2} - 8 \cdot 10^{-2}$ mmol $n\text{-}C_6$/g·min. The feed was premixed by bubbling He (alternatively H_2) through a saturator with $n\text{-}C_6$. Reaction products were separated using 30m long PONA column and identified by FID (Hewlett Packard 5890). As a rule 0.5 g of a catalyst sample was loaded into the reactor and was *in situ* activated in 20 ml/min flow of air at 500 ºC for 1h.

Surface area and average pore diameter were determined by BET (Micromeritics ASAP 2010). Thermogravimetric (TG) studies were performed on a Baehr STA 503, in temperature range 30-1000 ºC, by using temperature ramp of 10 ºC/min.

Results and discussions

In Table I initial catalyst activities and corresponding textural characteristics are given, together with weight loss attributed to SO_4 release during TG analysis. Corresponding initial temperatures for SO_4 take-off are given as well. All samples follow surface area decrease and average pore diameter increase with rise of calcination temperature. On another hand, elevated calcination temperature is beneficial for the initial activity of all catalysts: it is 600 ºC for both catalyst 1 and catalyst 2 (samples 1B and 2B), and in the case of catalyst 3 preferences are even to the highest calcination temperature of 700 ºC (sample 3C).

A typical steady-state composition of isomers for the case of catalyst 1 is shown in Figure 1. The composition hardly change in the region of calcination temperatures preferred for activity (500-600 ºC), showing mostly mono-branched isomers (CH_3x1). A minor fraction of highly desirable dimethyl-butanes (CH_3x2) might be understood in terms of low acidity of this catalyst. Consequently reaction probably doesn't occur via byfunctional isomerization mechanism, but rather by transfer of methyl group on the hydrogenation catalyst function. The similar isomer composition for samples 1A and 1B indicates the active sites of comparable quality and quantity (Figure 1). Indeed, SO_4 take-of temperatures for both samples are very close each other (Table I).

Table I. Catalysts performances and weight loss of SO₄ during TG analysis

	Surface area, m^2/g	Average pore diameter, nm	Conversion, % (SV=$6.45\cdot10^{-2}$ mmol n-C_6/g·min)			SO₄ loss, %	Initial T for SO₄ release, ^{o}C
			200 ^{o}C	300 ^{o}C	350 ^{o}C		
1A	130	2.3	14	50	18	5.0	620
1B	103	3.3	15	22	58	3.8	652
1C	69	5.7	0	-	0	2.1	730
2A	82	2.6	0	1	-	2.3	675
2B	68	3.9	4	11	17	2.3	675
2C	67	5.0	2	3	-	1.9	675
3A	144	3.2	1*	-	0	2.6	750
3B	117	4.4	1	10	14	2.6	750
3C	89	6.0	1*	25	25	2.4	750

*SV=0.13 mmol n-C_6/g$_{cat}$·min

Superacidic features of zirconia modified with ions, e.g. SO_4^{2-}, depend on preparation methods and activation procedure [7]. Temperature treatment above 500 ^{o}C brings decomposition of some of the sulfates by forming SO_2 [8], but increases the acidic strength of SZ [9]. The effect of calcination temperature on sulfates can be followed by rest of sulfates decomposition by means of TG; difference in SO₄ take-of temperatures indicates various types of sulfur created due to diversity in pretreatment temperatures for different samples (Table I). The superior activity of sample 1A might be connected to higher amount of total S (5% towards 2.3 and 2.6 for catalysts 2 and 3, respectively), but also to the different structure of incorporated S into the ZrO_2 matrix of different samples [10].
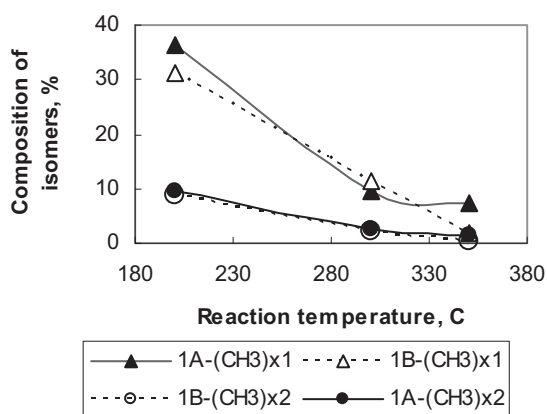
Fig. 1. Isomers composition as a function of calcination temperature for catalyst (1)
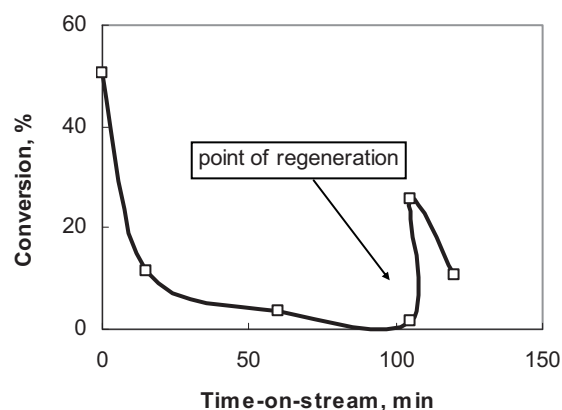
Fig. 2. Activity of catalyst 1A at 300 ^{o}C before and after regeneration

All samples showed no even traces of activity when H_2 was used as a carrier gas for saturation with n-C_6, confirming some previous findings [11]. This can be explained by H_2 affinity towards S, and extraction of the former from the catalyst in form of H_2S. By using He premixed with n-C_6 substantial activities were obtained (Table I), followed, however, with fast deactivation (Figure 2). On Figure 2 activity of the best catalyst in the whole series (1A) at its optimal reaction temperature of 300 ^{o}C is shown. After 100 min of time-on-stream activity fools nearly to zero; the black color of the sample indicates coking as the cause for the deactivation. Obviously, lack of hydrogenation function due to H_2 deficiency takes away auto-regeneration ability of the catalyst. Regeneration of the same catalyst was performed in air flow at 500 ^{o}C for 2 h, restoring, however, only about 50% of the initial activity (Figure 2). The similar regeneration procedure with catalyst 2B following its participation to the reaction at 350 ^{o}C failed, implicating deactivation mechanism other then coking. Namely, with the presence of He isomerization reaction can start with production of water, forcing S from +6 to +4 oxidation state, the last being known of lower activity [11].

Acknowledgments

References

[1] I.E.Maxwell, J.E.Naber, K.P.de Jong, Appl.Catal. A: General, 113(1994)153

[2] G.Boskovic, R.Micic, P.Pavlovic, P.Putanov, Catal.Today 65(2001)123

[3] T.Yamaguchi, Appl.Catal.A: General, 222(2001)237-246

[4] R.A.Keogh, D.E.Sparks, B.H.Davis, in: B.Delmon, G.F.Froment (Eds.), Catalyst Deactivation, Stud.Surf.Sci.Catal., vol. 88, Elsevier, Amsterdam, 1994, p. 647.

[5] C.Li, P.C.Stair, Catal.Lett,. 36 (1997) 119.

[6] V.Adeeva, J.W. de Haan, J.Janchen, G.D. Lei, G.Schunemann, L.J.M. van de Ven, W.M.H.Sachtler, R.A. van Santen, J. Catal. 151 (1995) 364.

[7] A.Corma, J.M.Serra, A.Chica, Catal.Today 81 (2003) 495.

[8] F.R.Chen, G.Coudurier, J.F.Joly, J.C.Vedrine, J.Catal. 143 (1993) 616.

[9] V.Bolis, G.Magnacca, G.Cerrato, C.Morterra, Tops.Catal. 19 (2002) 259.

[10] P.Nascimento, C.Akratopoulou, M.Oszagyan, G.Coudurier, C.Travers, J.F.Joly, J.C.Vedrine, in: L.Guczi (Ed.), Proceedings of Tenth International Congress on Catalysis, New Frontiers in Catalysis (1993) 2585.

[11] K.Fottinger, G.Kinger, H.Vinek, Appl.Catal. A: General 226 (2004) 195.

PP-94

PREPARATION OF Au/γ-Al$_2$O$_3$-NANOFIBERS CATALYST FOR OXIDATION OF CO AT LOW TEMPERATURES

<u>Ziyi Zhong*</u>, Shoucang Shen, Yi-Fan Han

Institute of Chemical and Engineering Sciences, 1 Pesek Road, Jurong Island, Singapore 627833. Fax: +65- 6316 6182, e-mail: Zhong_ziyi@ices.a-star.edu.sg

In last decade there has been a dramatic increase in the number of publications related to the study of Au-based catalysts, though traditionally supported Au catalysts were almost marginal value. However, this view is only partially true when the Au particles size is larger than about 10 nm, in which the intrinsic size effects and the interactions between Au and oxide supports are only weakly expressed [1, 2]. The quantum size-effects for supported Au catalysts has been verified by Goodman et al. [3], and the remarkable reactivity at low temperatures, e.g., oxidation of CO below 100°C, is only observed when the size of Au particles is below 5 nm. CO oxidation at low temperatures is of great importance for producing pure H$_2$ on-board supplying to fuel cells derived vehicles, because the maximum concentration of CO that the electrodes in the fuel cells can tolerate is ca. 10 ppm in the feed gas [3]. Up to now, for this purpose TiO$_2$ and other supported Au catalysts have been studied widely [4]. Among them, Au/Al$_2$O$_3$ catalyst shows advantageous performance [5]. In particular, Al$_2$O$_3$, as one of widely applied supports, is superior to TiO$_2$ and other supports in several aspects, such as strong mechanical strength, high thermal conductivity, etc. Obviously, its properties in the preparation of supported Au catalyst have not been addressed enough. In the study, we aim to develop an active Au/Al$_2$O$_3$ catalyst for CO oxidation.

Al$_2$O$_3$ nano-fibers were synthesized by a modified literature method [6]. Typically, 15g of Al(NO$_3$)$_3$·9H$_2$O (Merck, >98.5%) was dissolved in 100 mL of de-ionized water, then mixed with 20% TEAOH (tetraethylammonium hydroxide, Merck-Schuchardt, Germany) solution under rigorous stirring till the pH value reached 5.0. The mixture was continuously stirred for 30 min before transferred into an autoclave equipped with a Teflon-liner. The hydrothermal treatment was conducted at 170°C for 72 h. The as-prepared sample was calcined at 750°C for 5 h with a heating rate of 5°C/min. While, a commercial γ-Al$_2$O$_3$ (Acros Organic, surface area of 104m^2/g) was used for comparison.

The immobilization of Au colloids onto the catalyst substrate was conducted employing own invented method [6]. The loading amount of Au in the Au/Al$_2$O$_3$ catalyst was ca. 1.0wt%.

The measurement of catalytic oxidation of CO was carried out in a fixed-bed microreactor. Prior to the testing, the catalyst was treated in air at 200°C for 1 h. Reactant gas containing CO was passed through the catalyst bed at a GHSV of 15000h^{-1}. The outlet gases were analyzed with an on-line GC (Shimadzu) equipped with one TCD and one FID detector. For kinetic study, the catalyst was diluted with 90% of α-Al$_2$O$_3$.

The morphology and size of the Al$_2$O$_3$ samples and the Au/ Al$_2$O$_3$ catalyst were observed by a transmission electron microscope (TEM, Tecai TF20 Super Twin, 200kV) and Scanning electron microscope (SEM, JEOL-6700F). The powder XRD analysis was conducted on a Bruker D8 Advance X-ray diffractometer with CuK$_{\alpha1}$ radiation. The surface area was measured at 77K (liquid nitrogen) on a Quantachrome Autosorb-6B Surface Area & Pore SizeAnalyzer.

TEM in Fig. 1 shows that the Al$_2$O$_3$ nanofibers as prepared have 1-dimensional morphology, with a diameter of 8-15 nm, and their length in the range up to 1μm. XRD result (Fig.2) demonstrates that the calcined sample 750°C is γ-Al$_2$O$_3$(JCPDS 04-0858), and its BET surface area is ca. 210 m^2/g. The TEM images of the Au/Al$_2$O$_3$ catalysts in Fig. 3 reveal that the Au particles (black dots) are highly distributed over the two types of the catalyst support, and most of the Au particles size are successfully controlled in the range of 2-5 nm.

The catalytic activity of the Au/Al$_2$O$_3$-nanofibers catalyst is much higher than that of the Au/Al$_2$O$_3$-commercial catalyst. The temperatures for 50% and 100% conversion of CO (denoted as T$_{50}$ and T$_{100}$, respectively) for Au/γ-Al$_2$O$_3$-nanofibers catalyst were measured at 26 and 40°C, respectively, while the corresponding temperatures were 65 and 140°C respectively for the Au/Al$_2$O$_3$-commercial catalyst. XPS spectra revealed that before and after the reaction gold existed as metallic state. However, the apparent active energies, Ea, are different for the two Au catalysts.
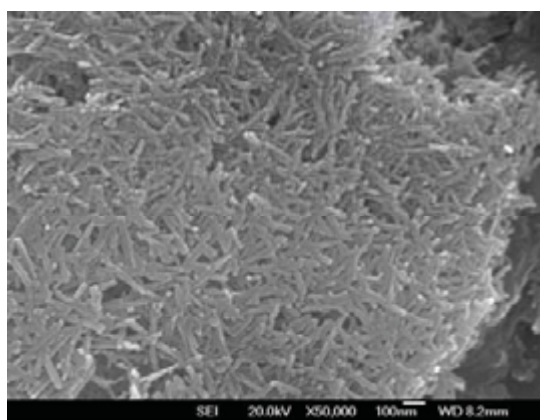
Fig.1. SEM image of the as-prepared γ-Al$_2$O$_3$. Nanofibers.
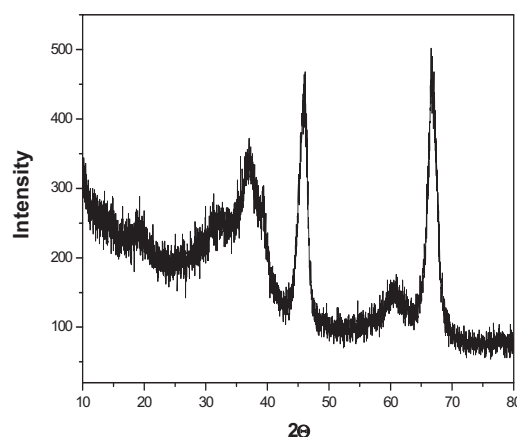
Fig.2. XRD pattern of the as-prepared γ- Al$_2$O$_3$ nanofibers.
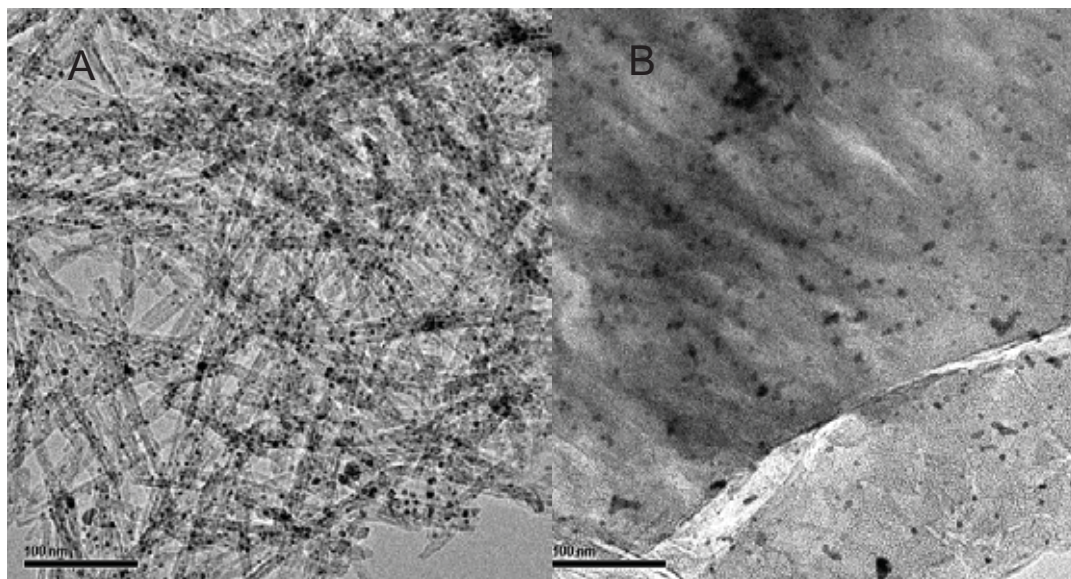
Fig.3. TEM images of the Au/γ-Al₂O₃-nanofibers (A) and Au/γ-Al₂O₃ commercial powder.

In conclusion, Au nanoparticles are successfully deposited on the γ-Al$_2$O$_3$ supports with controlled particle size in the range of 2-5 nm. The Au/Al$_2$O$_3$-nanofibers catalyst exhibited much higher catalytic activity for CO oxidation than the Au/γ-Al$_2$O$_3$ commercial powder as prepared in the same way. XPS results show that in the Au/Al$_2$O$_3$ catalysts the chemical states of Au(0) is quite stable in the reaction, and kinetic data hint that the active sites for CO oxidation may be different for the two catalysts. Oxidation of CO in the presence of H$_2$ is underway.
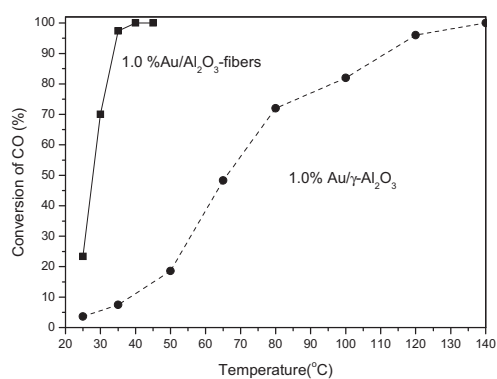
Fig.4. Comparison of CO oxidation activity for the two Au/γ-Al₂O₃ catalysts. The feed gas is 1% CO in air and the GHSV is 15000h⁻¹.

References

1. G. Ertl et al, Handbook of Heterogeneous Catalysis, Weinheim: VCH, 1997, vol 4, 1159-1693. (b) D. Ciuparu, et al, Catalytic Combustion of Methane over Pd-based Catalysts, *Catal. Rev.*, 2002, **44** , 593.
2. V. Raman, *Chem. Ind.* 1997, 771.
3. (a) Y.-F. Han, M. Kahlich, M. Kinne, and R. J. Behm, *Appl. Catal.* B **50** (2004) 209. (b) Y.-F. Han, M. Kahlich, M. Kinne, and R. J. Behm, *Appl. Catal*. B **52** (2004) 123.
4. (a) M. Valden, X. Lai, D. W. Goodman, *Science*, 1998, **281**, 1647. (b) M. Haruta, *Catal. Today*, 1997, **36**, 153.
5. (a) Q. Xu, K. C. C. Kharas, A. K. Datye, *Catal. Lett.*, 2003, **85**, 229. (b) C. K. Costello, J. H. Yang, H. Y. Law, Y. Wang, J.-N. Lin, L. D. Marks, M. C. Kung, H. H. Kung, *Appl. Catal.* A 2003, **243**, 15. (c) J. T. Calla, R. J. Davies, *Ind. Eng. Chem. Res.* 2005, **44**, 5403.
6. B. S. Gevert, Z.S. Ying, *J. Porous Mater*. 1999, **6**, 63.
7. Ziyi Zhong*, Jizhong Luo, James Highfield, Ang Thiampeng, Jianyi Lin, Preparation of HighlyDispersed Gold Catalysts for CO Oxidation, 13rd International Catalysis Conference(ICC) in Paris, July, 2004.

PRODUCTION OF HYDROGEN BY CATALYTIC DECOMPOSITION OF WATERMETHANOL MIXTURES

A.L. Lapidus, <u>S.N. Antonyuk</u>*, E.V. Egorova*, E.Z. Golosman**

N.D. Zelinsky Institute of Organic Chemistry RAS, 119991, Moscow, Leninsky avenue, 47, Russia, fax +7(495)-135-53-03, E-mail:albert@ioc.ac.ru
*M.V. Lomonosov State Academy of Fine Chemical Technology, 119571, Moscow, Vernadsky avenue, 86, Russia, fax: +7 (495)-246-48-23 E-mail: nhsigt@mitht.ru
**Novomoskovsk JSC "Institute of Nitrogen Industry", 301650, Novomoskovsk, Kirova avenue, 11, Russia, fax: +7(08762)-7-16-61, E-mail:gez@novomoskovsk.ru

Further expansion of methanol manufacturing is connected now not only with providing of raw material for a number of chemical enterprises (formaldehyde, dimethylterephthalate, methylamines, methyl methacrylate), but solution of some current problems in power engineering, transport, and ecology as well [1].

In the long term, methyl alcohol may become the universal energy carrier as well as a kind of raw material for manufacturing of hydrocarbon fuel, a wide spectrum of oxygen-containing compounds and derivatives on their basis [2,3].

Alongside with it, development of highly effective catalysts for methanol decomposition into H_2 is of great importance to create the closed cycles of chemithermal power transfer (with utilization of nuclear power plant heat) as well as increase the efficiency of methanol internal combustion engines [3,4].

Besides, methanol decomposition holds much promise for preparative manufacturing of gas synthesis to be applied in technologies of limited tonnage and research practice.

Our research is devoted to investigation of water-methanol mixtures decomposition over catalysts on the basis of Cu, Zn,- Cu-cement catalysts as well.

Catalytic decomposition of water-methanol mixtures was carried out in flow-type fixed-bed reactor at atmospheric pressure and temperature of 200-400 °C. Space velocity of the stock (WHSV) was varied from 0.6 to 7 h^{-1}.

Catalyst samples prepared by chemical mixing of basic carbonates of copper and zinc with Cement Fondu-Talum, consisting of calcium mono- and dialuminates (NTK-10), were

used in experiments. Samples were preliminary calcined in flowing air at 400 °C for 5 h. Before the tests, catalysts were treated with methanol vapors at 200 °C for 3 h.

In investigation of methanol steam conversion on catalyst NTK-10, a series of experiments overall temperature range of 200-300 °C and initial feedstock volumetric rate of 0.6-7 h^{-1} was carried out (Table 1) Equimolar water-methanol mixture was used as initial feedstock. Formation of hydrogen-containing gas proceeds according to Reaction 1, in turn, can be considered as a sum of Reactions 2 and 3.

$$CH_3OH + H_2O \Leftrightarrow 3H_2 + CO_2 \qquad (1)$$

$$CH_3OH \Leftrightarrow CO + 2H_2 \qquad (2)$$

$$CO + H_2O \Leftrightarrow CO_2 + H_2 \qquad (3)$$

Investigation of the process shows that as temperature rises from 200 to 250 °C, methanol conversion increases up to 100 % at feedstock flow rate of 0.6 h^{-1}. As water-methanol mixture rate increases from 0.6 to 7 h^{-1} at 225 °C, degree of methanol conversion is reduced from 99.8 down to 93.7 %. At the same time, hydrogen-containing gas yield increases from 778.8 up to 9889.2 $l/l_{cat}h$ and carbon monoxide content simultaneously decreases from 1.8 down to 1.1 vol. %

Table 1 Products of methanol-water mixture transformation at 225 ^{o}C at different flow rate (Feedstock is methanol-water mixture: 64 wt.% of methanol and 36 wt.% of water).

C_{CH_3OH}, wt. %	W_{CH_3OH}, h^{-1}	Gas composition, vol. %			Gas yield, $l/l_{cat}h$
		H$_2$	CO	CO$_2$	
99.8	0.6	73.4	1.8	24.8	778.8
99.6	1.5	73.9	1.5	24.6	1972.3
98.6	3.0	74.5	1.2	24.3	4222.5
95.4	5.0	74.6	1.2	24.2	5889.3
93.7	7.0	73.9	1.1	25.0	9556.2

Because carbon monoxide steam conversion is reversible and proceeds with heat evolution, of interest was to shift it towards formation of hydrogen and carbon dioxide by introduction of water excess. Experiments were carried out at 225 °C, initial mixture volumetric rate was 3.0 h^{-1}, and water content in feedstock was 15, 30, 36, 42, 50, 70 and 90 wt. %.

As followed from Table 2, methanol conversion at 225 °C is increased with water content in initial mixture and attains 98.6 % at 36 wt. %. At the same time, residual carbon monoxide in products is reduced down to 1.2 vol. %. Further enrichment of initial feedstock with water results in complete carbon monoxide conversion with formation of practically stoichiometric hydrogen-containing mixture.

Table 2 Products of methanol-water mixture transformation at different water content

$$(T = 225 \,^{\circ}C, \, W_{CH_3OH} = 3.0 \, h^{-1})$$

C_{H_2O}, wt. %	C_{CH_3OH}, %	Gas content, vol. %			Liquid products, wt. %			Gas yield, $l/l_{cat}h$
		H_2	CO	CO_2	$HCOOCH_3$	CH_3OH	H_2O	
15	53.3	73.7	5.9	20.4	3.4	96.2	0.4	2554.6
30	85.9	73.8	2.9	23.7	0.1	91.2	8.7	3720.9
36	98.6	74.5	1.2	24.3	0	14.6	85.4	4225.5
42	99.8	74.7	1.0	24.3	0	0.3	99.7	3665.4
50	99.8	74.9	0.8	24.3	0	0.3	99.7	2996.9
70	99.8	75.0	0.3	24.7	0	0.2	99.8	2415.8
90	99.8	75.0	0.1	24.9	0	0.1	99.9	888.5

Thus, dehydrogenation (Reaction 2) is completely suppressed at water-methanol mixture decomposition.

$$2 \, CH_3OH \Leftrightarrow HCOOCH_3 + 2H_2 \qquad\qquad (4)$$

As water grows up to 90 %, methanol in liquid products decreases down to 0.1 % and gas yield passes through a maximum of 4225,5 l/l_{cat}·h, which corresponds to the equimolar content in initial mixture.

Flow chart of water-methanol mixture transformation into hydrogen

Based on the results above a flow chart of methanol processing has been developed (Fig. 1).The flow chart consists of several standard components – a tank farm for initial feedstock and intermediate products (1-2), feedstock heating and evaporation section (heat exchangers 3-5), reaction section (reactor of methanol decomposition 6) and separators 8.

Methanol from tank 1 and water from tank 2 with the mass ratio of 1.8:1 are pumped into heat exchanging section and then into reactor 6 with NTK-10 catalyst (225 °C). After cooling and separation, hydrogen-containing gas enters gas separation unit (not displayed at the scheme). The gas containing 98-99 vol. % hydrogen goes to consumer.

Literature

1. L. P. Strahova and T. G. Bitkova. Market research at grounds of investments in methanol manufacturing. Proceedings of the 4th International Conference "Current problems of management – 96," Moscow, 139, (1996).

2. Asinger F. Methanol-Chemie und Energierohstoff: Die Mobilisation der Kohle. Berlin, (1987).

3. G. A. Terent'ev, V. M. Tyukov, and F. V. Smal'. Motor Fuel from Alternative Feedstock. Moscow, Chemistry, 186, (1989).

4. N. S. Pechuro, V. D. Kapkin, and O. Yu. Pesin. Chemistry and Engineering of Synthetic Liquid Fuel and Gas. Moscow, Chemistry, 323, (1986).

Fig. 1 Flow chart of water-methanol processing
(See position and flow designations in the text)
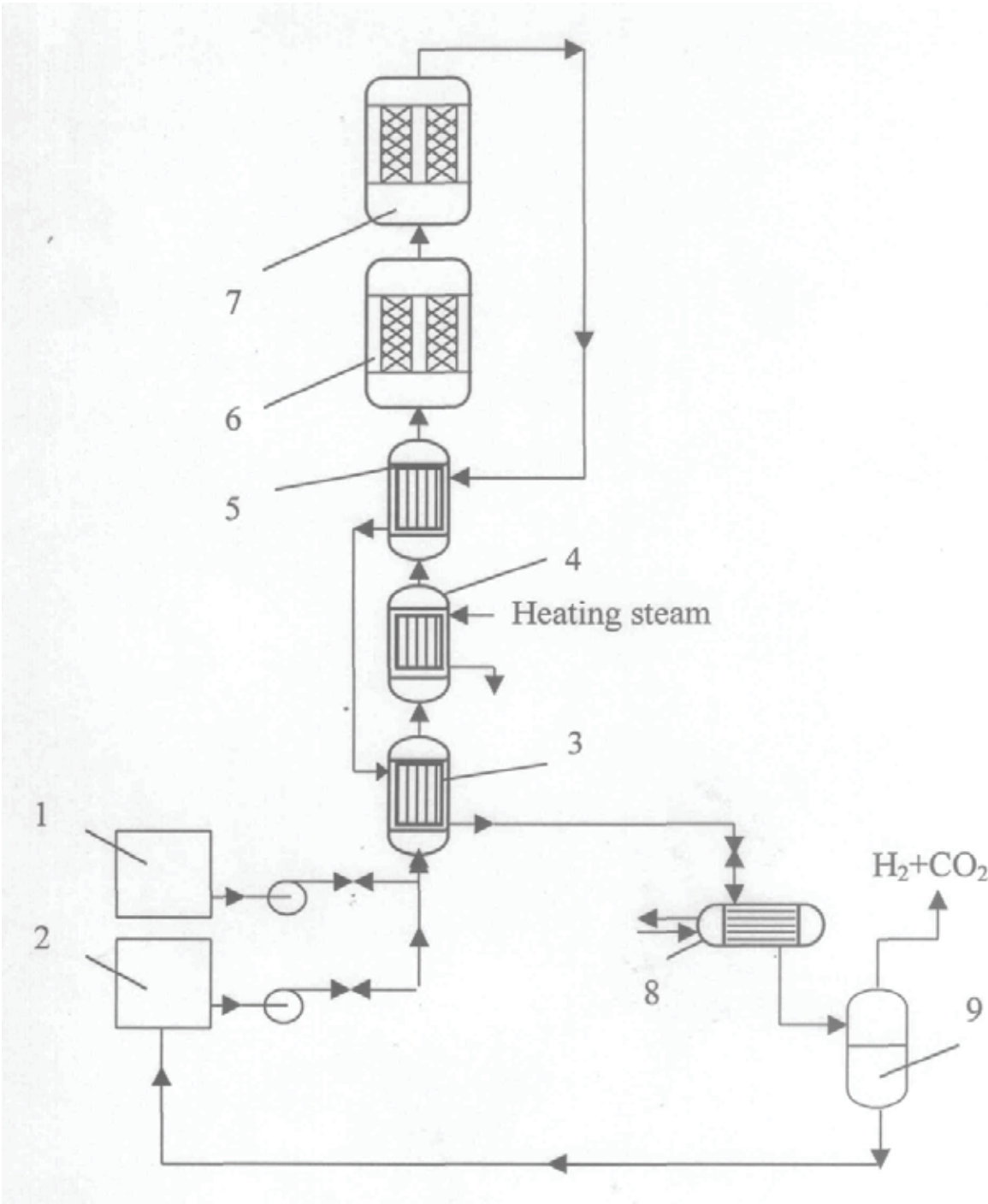
LIMONENE EPOXIDATION OVER PW-AMBERLITE IN A TRIPHASIC SYSTEM

Rolando Barrera Z., **Aída L. Villa de P., Consuelo Montes de C.**

Departamento de Ingeniería Química, Universidad de Antioquia, Medellín-Colombia
Calle 67 Nº 53-108. Tel: + 574 2106606, Fax: + 574 2106609, e-mail: rolando@udea.edu.co

Abstract

The effect of several reaction parameters on limonene epoxidation and hydrogen peroxide decomposition over PW-Amberlite in a triphasic system was studied. Parameters evaluated were average particle diameter and concentration of limonene and hydrogen peroxide. Empirical reaction rates for limonene epoxidation and hydrogen peroxide decomposition were estimated in terms of concentration and activities.

Introduction

Limonene is an abundant monoterpene extracted from citrus oil. It is usually epoxidized as an intermediate step for obtaining fragrances, perfumes, and food additives.[1] High limonene conversion (> 80 %) and limonene epoxide selectivity (> 90 %) have been obtained over PW-amberlite using aqueous H_2O_2 as oxidizing agent and acetonitrile as solvent.[2] Upon addition of 81 wt %, acetonitrile, in a biphasic system, the reaction rate is first order with respect to limonene, oxidant and catalyst concentration[3]. Notwithstanding, due to environmental and economic reasons it is desirable to minimize the amount of solvent and a triphasic reaction system which consists of two liquid phases and a solid catalyst is formed. Here, we report on the influence of several reaction parameters on limonene epoxidation and hydrogen peroxide decomposition in a triphasic system. Studied parameters were: limonene and hydrogen peroxide concentration, temperature and catalyst recycling. Internal mass transfer limitations were avoided following the Weisz-Prater criterion.

Experimental

PW-Amberlite catalyst was synthesized as reported elsewhere.[2] All catalytic experiments were carried out in magnetically stirred glass flasks (8 mL) immersed in a thermally controlled oil bath. Flasks were sampled at different times, between 0 and 120 minutes. Catalytic tests were carried out with different catalyst particle sizes and hydrogen peroxide concentration was varied between 0.73 – 1.92 mol/L. Acetonitrile concentration was 4.05

mol/L, (71 wt %) which gives a maximum in the initial limonene epoxidation[4]. After reaction, samples of the two liquid phases were analyzed by gas chromatography (Varian Star, 3400) equipped with a flame ionization detector (FID) and a 50 m DB-1 capillary column. H_2O_2 concentration at different times was determined by cerimetric titration using a 0.1 N $CeSO_4$ aqueous solution.

Results and discussion

First, internal and external diffusion limitations on initial reaction rate were investigated. Stirring speed was varied for determining external mass transfer resistances. Above 800 rpm no effects on limonene epoxidation in a triphasic system were observed. Thus, stirring speed was set at 1000 rpm for all further experiments in order to avoid external mass transfer resistances. The effect of internal diffusion on initial reaction rates was determined by measuring reaction rates for different catalyst particle sizes (Table 1). It was observed that initial reaction rates did not significantly vary when catalyst particle size was lower than 425 µm (fractions III to VI). Besides the estimated Weiz-Prater criterion is lower than 1. So, particle sizes corresponding to fraction III was used in all further experiments.

Table 1. The effect of catalyst particle size on the initial reaction rates.

Fraction	Particle size range (µm)	Average diameter, (µm)	Initial reaction rate of limonene epoxidation, mmol/h.g dry cat [a]		
			Aqueous phase	Organic phase	Bulk
I	600 – 830	715	3.77	3.8	7.57
II	425 – 600	512	3.78	3.54	7.32
III	250 – 425	337	4.13	3.77	7.90
IV	180 – 250	215	4.15	3.78	7.93
V	125 – 180	152	4.11	3.80	7.91
VI	90 – 125	107	3.98	3.85	7.83

[a] Reaction conditions: $[C_{10}H_{16}]_0 = 0.66$ mol/L, $[H_2O_2]_0 = 1.33$ mol/L, $[H_2O] = 5.84$ mol/L, $[cat] = 18$ g/L, $[CH_3CN] = 14.05$ mol/L, 306 K.

The initial reaction rate of limonene epoxidation increased with temperature; however, above 306 K the higher the temperature, the higher the hydrogen peroxide decomposition (table 2). Figures 1a and 1b show that initial reaction rate of limonene epoxidation increased, and H_2O_2 decomposition decreased as limonene concentration increased. However, limonene epoxidation decreased when hydrogen peroxide concentration increased, figure 1c. As illustrated in figure 1d, hydrogen peroxide decomposition was proportional to concentration. Results from figures 1c and 1d may be explained from LLE of water + limonene + acetonitrile system,[5] indicating limonene dilution in the aqueous phase because of hydrogen peroxide.

Table 2. Effect of temperature on the initial reaction rate.

Temperature (K)	Initial limonene epoxidation rate (mmol/g.h)			Initial H_2O_2 decomposition rate (mmol/g.h)
	Aqueous phase	Organic phase	Bulk reaction mixture	
296	3.40	3.00	6.40	1.47
306	4.40	3.62	8.02	2.81
316	6.36	5.06	11.4	17.1
323	8.00	7.00	15.0	38.4

Reaction conditions: $[C_{10}H_{16}]_0 = 0.66$ mol/L, $[H_2O_2]_0 = 1.33$ mol/L, $[H_2O] = 5.84$ mol/L, $[cat] = 18$ g/L, catalyst particle size:250 – 425 μm, $[CH_3CN] = 14.05$ mol/L.
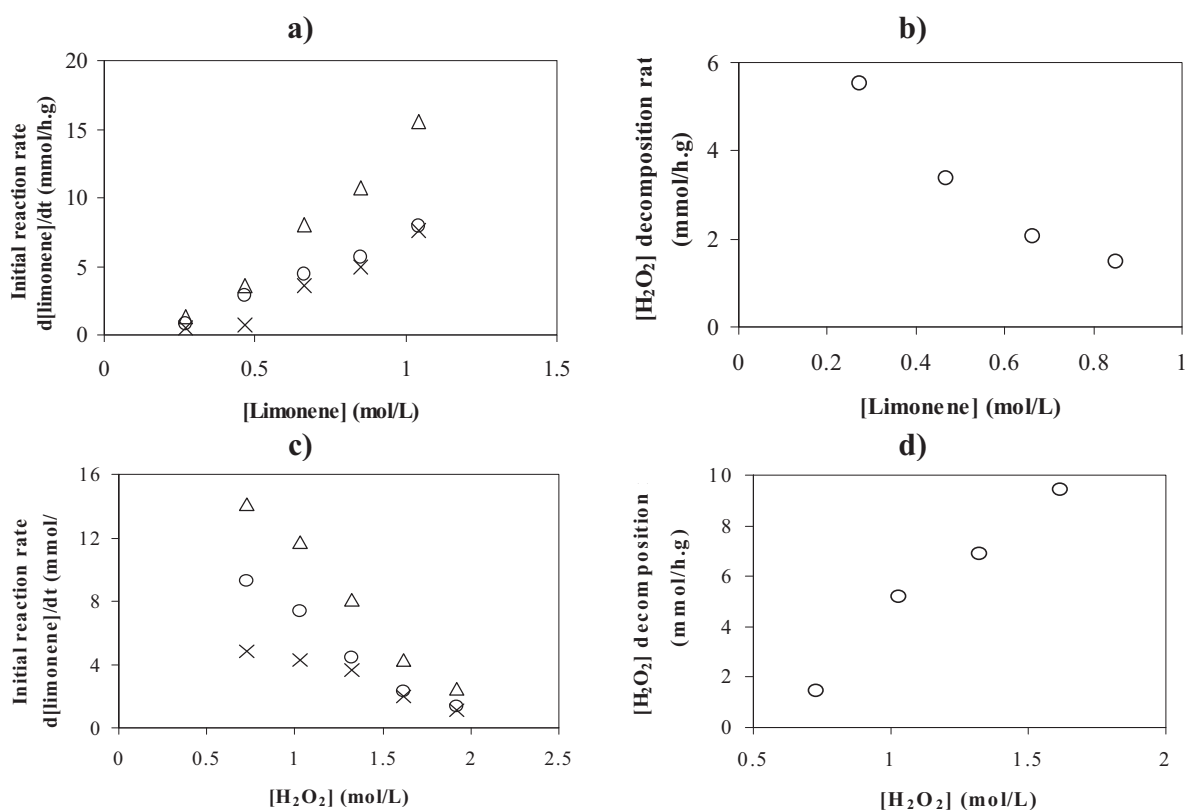
Figure 1. The effect of limonene concentration (a and b) and H_2O_2 concentration (c and d) on the initial reaction rate of limonene epoxidation (a and c) and H_2O_2 decomposition rate (b and d). **x**, Organic phase; **o**, aqueous phase; **Δ**, bulk reaction mixture. $[C_{10}H_{16}]_0 = 0.27$ - 1.04 mol/L (a and b) or $[C_{10}H_{16}]_0 = 0.66$ mol/L (c and d), $[H_2O_2]_0 = 1.33$ mol/L (a and b) or $[H_2O_2]_0 = 0.73$ - 1.92 mol/L (c and d), $[H_2O] = 5.84$ mol/L, $[cat] = 18$ g/L, catalyst particle size:250 – 425 μm, $[CH_3CN] = 14.05$ mol/L, 306 K.

PW-Amberlite was recycled up to three times under the same reaction conditions. Catalytic activity was recovered after catalyst washing with acetone; no significant change in the initial limonene reaction rates was observed. The initial reaction rate for limonene epoxidation was 8×10^{-3} mol/h.g with fresh catalyst and after three reactions it decreased to 7×10^{-3} mol/h.g.

Empirical reaction rate expressions for limonene epoxidation and hydrogen peroxide decomposition are estimated in terms of concentrations and activities, to account for the nonideal character of liquid mixtures using the optimization toolbox slqnonlin from Matlab 6. Empirical kinetic parameters for limonene epoxidation and hydrogen peroxide decomposition are listed in Table 3.

Table 3. Empirical kinetic parameters for limonene epoxidation and hydrogen peroxide decomposition

Equation	SSR × 10⁵	SE × 10³	Parameter with 95 % confidence interval		
			k	α	β
$-r_L = k[A]^\alpha [B]^\beta$	3.7	1.4	0.021 ± 0.007 [a]	1.934 ± 0.006	-1.410 ± 0.005
$-r_{des} = k[A]^\alpha [B]^\beta$	4.8	0.7	1.581 ± 0.006 [b]	-0.436 ± 0.007	2.475 ± 0.006
$-r_L = ka^\alpha{}_A a^\beta{}_B$	6.2	1.2	$(9.479 \pm 0.001) \times 10^{-7}$ [c]	2.869 ± 0.017	-2.407 ± 0.043
$-r_{des} = ka^\alpha{}_A a^\beta{}_B$	5.5	0.6	1.57 ± 0.005 [c]	-0.371 ± 0.011	2.399 ± 0.016

[a] In $mol^{0.476}L^{0.524}$ $(g.h)^{-1}$. [b] In $mol^{-1.039}L^{2.039}$ $(g.h)^{-1}$. [c] In mol $(g.h)^{-1}$. SSR = square sum of residuals, SE: standard error. $-r_L$: limonene epoxidation rate, $-r_{des}$: H_2O_2 decomposition rate. [A] is limonene concentration and [B] is H_2O_2 concentration; a_i is the activity of component i.

Interestingly, empirical reaction rate constant and order for hydrogen peroxide decomposition are little affected when non-ideal reaction mixture is considered, in contrast to those corresponding to limonene epoxidation.

Conclusions

Limonene epoxidation with aqueous H_2O_2 in the presence of acetonitrile in a triphasic system was studied over PW-amberlite. External mass transfer problems were avoided using a stirring speed of 1000 rpm. According to Weiz-Prater criterion, mass transfer limitations were insignificant for catalyst particle sizes lower than 425 μm. Empirical kinetic parameters for limonene epoxidation are different when concentration or activity data was fitted, while those of hydrogen peroxide decomposition are almost the same independent of whether concentration or activity data were used. The apparent activation energy of limonene epoxidation was 25.16 KJ/mol, three times lower than that found previously in biphasic system; for hydrogen peroxide decomposition the estimated apparent activation energy was 100.6 KJ/mol. PW-amberlite was recycled three times and no significant decrease on catalytic activity was detected.

References

(1) Derfer, J. M.; Derfer, M. M. *Encyclopedia of Chemical Technology Kirk-Othmer*, *Vol 22, 3rd edition*; Wiley: New York, 1978.

(2) Sels, B. F.; Villa, A. L.; Hoegaerts, D.; De Vos, D. E.; Jacobs, P. *Top. in Catal.* **2000,** *13*, 223.

(3) Villa, A. L.; Taborda, F.; Montes de C., C. *J. Mol. Catal. A*. **2002**, *185*, 269.

(4) Barrera R.; Villa A. L.; Montes de C., C. The effect of the amount of solvent in the epoxidation of limonene over PW-amberlite, *19th North American Meeting*, Philadelphia, Pennsylvania, may 22-27 **2005**, poster 306.

(5) Barrera, R.; Villa A. L.; Montes de C., C. *J. Chem. Eng. Data.* **2005**, *50*, 1353.

THE CRITICAL PHEMOMENA AND THE CATALYST SURFACE TOPOLOGY

V.I. Bykov, N.V. Kisilev*, S.B. Tsybenova**

Bauman Moscow State Technical University, Moscow, 105005, Russia

E-mail: vibykov@mail.ru

*Krasnoyarsk State Technical University, Krasnoyarsk, 660074, Russia

** Russian State Social University, Moscow, 107150, Russia

The two-dimentional model of diffusion and reaction of intermediates on a surface of the solid-state catalyst is offered. This model takes into account an opportunity of a jump of adsorbed molecules with occupied on the next free active place. The coefficients of two-dimentional diffusion depend from degrees of a covering. Nonlinearity of model is determined generally nonlinear kinetics of reactions between substances adsorbed on a surface of the catalyst. For a case autocatalytic oscillator are carried out illustrating the calculations showing an opportunity of existence of structures and autowaves on a surface of the catalyst. We considered four basic surface topology: plane, sphere, cylinder, torus.

In the elementary case the mathematical description of diffusion and reaction on surfaces of the catalyst is under construction on a basis of lattice model [1]. As a surface of the catalyst the square lattice of active places is considered [2−5]. Each place has 4 neighbours of the nearest environment. We yet do not consider neighbours of more distant levels of an environment. Except for that we assume, that everyone intermediate takes one active place. Process of diffusion is considered as jump of a molecule with occupied on any free place. The probability of this process depends on a degree of a covering of an active surface adsorbed molecules.

The model of reaction and diffusion of intermediates on a surface of the catalyst has the form:

$$\frac{\partial x_i}{\partial t} = D_i(z\Delta x_i - x_i\Delta z) + f_i(x, z), \qquad i = 1, \ldots, n, \qquad (1)$$

where $z = 1 - x_1 - \ldots - x_n$ is a share of free place, a vector $x = (x_1, \ldots, x_n)$, x_i are degrees of intermediates covering, Δ is Laplas's operator for a plane.

PP-97

As an example of general model (1) the model of reaction and diffusion for the scheme of transformations [3]:

$$1)\ A + Z \Leftrightarrow X, \quad 2)\ X + 2Z \rightarrow 3Z + A, \quad 3)\ B + Z \Leftrightarrow Y, \tag{2}$$

where A, B are substances in a gas phase (A, B = $const$), X, Y are intermediates, Z is the catalyst, is considered. Model (1) for scheme (2) in the assumption of diffusion X has the form:

$$\frac{\partial x}{\partial t} = k_1 z - k_{-1} x - k_2 x z^2 + D(z \Delta x - x \Delta z),$$

$$\frac{\partial y}{\partial t} = k_3 x - k_{-3} y, \qquad z = 1 - x - y, \tag{3}$$

$$\Delta x = \frac{\partial^2 x}{\partial \xi_1^2} + \frac{\partial^2 x}{\partial \xi_2^2}, \qquad \Delta z = \frac{\partial^2 z}{\partial \xi_1^2} + \frac{\partial^2 z}{\partial \xi_2^2}.$$

Autocatalytic character of the kinetics for reaction (2) results to that the steady homogeneous condition in the system at presence of diffusion in the distributed system can lose stability that is characterized by presence in (3) steady non-homogeneous solutions (dissipative structures) [6,7]. These structures can be stable in time or periodically vary, that answers autowaves on the catalyst surface. In the latter case adsorbed substances form in claster which periodically arise, grow, decrease and disappear. Such "blinking" of intermediates on catalyst surfaces results in complex dynamics of total catalytic reaction rate. It macro-characteristic essentially depends from a ratio of parameters of nonlinear interaction of intermediates and their diffusions at a microlevel.

We have for the spherical surface the Laplas's operator

$$\Delta = \frac{1}{R^2} \left(\frac{\partial^2}{\partial \varphi^2} + \frac{1}{\cos^2 \varphi} \frac{\partial^2}{\partial \psi^2} - \operatorname{tg} \varphi \frac{\partial}{\partial \varphi} \right), \tag{4}$$

where φ, ψ are spherical coordinates. The dissipative structures and traveling waves on the spherical catalyst surface are investigated. We considered also the cylinder and torus.

References

1. Zhdanov V. P. // Surf. Sci. Rep., 2002, vol.45, p. 231-326.
2. Gorban A.N., Bykov V.I., Yablonskii G. S. Sketches about a chemical relaxation. Novosibirsk: Nauka, 1986. 320 p.
3. Bykov V.I. Modelling of the critical phenomena in chemical kinetics. M.:Nauka, 1988. 264 p.
4. Yablonskii G.S., Bykov V.I., Gorban A.N., Elokhin V.I. Kinetic models of catalytic reactions. Amsterdam: Elsevier.1991. 400 p.
5. Gorban A.N., Bykov V.I., Yablonski G.S. // Chem. Eng. Sci. 1980, vol. 35, №11, p. 2351.
6. Bykov V.I., Tsybenova S.B., Slinko M.G.// DAN. 2003, vol. 388, №6, p. 769.
7. Bykov V.I., Tatarenko A.A., Slinko M.G.// DAN. 2003, vol. 392, №5, p. 645.

THE THERMOCATALYTIC OSCILLATORS

V.I. Bykov, S.B. Tsybenova[*]

Bauman Moscow State Technical University, Moscow, 105005, Russia

E-mail: vibykov@mail.ru

* Russian State Social University, Moscow, 107150, Russia

E-mail: tsybenova@mail.ru

We considered the thermokinetic models of the catalytic reactions:

$$\frac{dx}{dt} = \sum \gamma_s w_s(x,T),$$

$$\rho C_p \frac{dT}{dt} = \sum (\Delta H_s) w_s(x,T) + \alpha(T_o - T),$$

(1)

where $x = (x_1,\ldots, x_n)$ is the concentration vector; T is the temperature of catalytic surface; w is the reaction rate. The dynamic system (1) for $T=const$ have one or more steady states [1-3]:

$$\sum \gamma_s w_s(x,T) = 0.$$

(2)

The equations (2) determine a function $x=x(T)$. So for steady state temperature we have equation:

$$\sum (\Delta H_s) w_s(x(T),T) = \alpha(T - T_0).$$

(3)

The temperature balance (3) gives a possibility to determine the steady states and sometimes their stability [4-8]. In this paper we consider a set of thermokinetic models (1) for the basic catalytic reactions. The mathematical model (1) consists of two subsystems – the kinetic and thermal subsystems [9-12]. For the steady state it is (2) or (3).

1. Linear mechanism: 1) $A+Z \rightarrow AZ,$ 2) $AZ \rightarrow Z+B.$ (4)

The dimensionless model for (1), (4) has the form:

$$\frac{dx}{d\tau} = f_1(y)(1-x) - f_2(y)x,$$

$$\frac{dy}{d\tau} = \beta_1 f_1(y)(1-x) + \beta_2 f_2(y)x + s(1-y),$$

(5)

where x, y, τ are the dimensionless concentration, temperature and time;

$$f_i(y) = Da_i \exp(\gamma_i(1-\frac{1}{y})), \qquad i = 1,2;$$

β_i, γ_i, Da_i, s are the dimensionless parameters. The parametrical analysis method gives a possibility for thermokinetic model (5) to build the bifurcation curves, parametric and phase portraits, oscillation regimes. We study the nonlinear dynamic system (5) like the famous classic models CSTR – Aris-Amundson model [6] and Semenov-Zeldovich model [5].

2. Autocatalytic trigger: 1) $Z \leftrightarrow X$, 2) $X+2Z \to 3Z$, $\qquad$ (6)
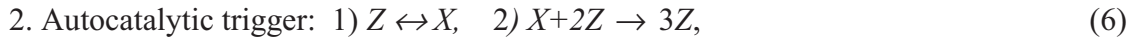
where Z is a catalyst, X is an intermediate. The dimensionless thermokinetic model corresponds to (6):

$$\frac{dx}{d\tau} = f_1(y)(1-x) - f_{-1}(y)x - f_2(y)x(1-x)^2,$$
$$\frac{dy}{d\tau} = \beta_1 f_1(y)(1-x) + \beta_{-1} f_{-1}(y)x + \beta_2 f_2(y)x(1-x)^2 + s(1-y).$$
$$\qquad (7)$$

We consider more detail two separated cases for system (7):

$$\frac{dx}{d\tau} = k_1(1-x) - f(y)x - k_2 x(1-x)^2,$$
$$\frac{dy}{d\tau} = \beta f(y)x + s(1-y),$$
$$\qquad (8)$$

and

$$\frac{dx}{d\tau} = k_1(1-x) - k_{-1}x - f(y)x(1-x)^2,$$
$$\frac{dy}{d\tau} = \beta f(y)x(1-x)^2 + s(1-y),$$
$$\qquad (9)$$

where k_i are the dimensionless reaction rate constants. The dynamic system (8) has a limit cycle for example for parameters: $\beta = 0.4$, $\gamma = 75$, $s = 4$, $Da = 0.1$, $k_1 = 0.6$, $k_2 = 1$. The system (9) has the oscillations for example for parameters: $\beta = 0.395$, $\gamma = 65$, $s = 4.5$, $Da = 0.5$, $k_1 = 0.6$, $k_{-1} = 1$.

3. Autocatalytic oscillator: 1) $Z \leftrightarrow X_1$, 2) $X_1 + 2Z \to 3Z$, 3) $Z \leftrightarrow X_2$, $\qquad$ (10)
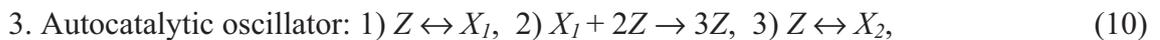
where X_1, X_2 are the intermediates on the catalyst surface Z. The thermokinetic model corresponds to scheme (10):

$$\frac{dx_1}{d\tau} = k_1 z - k_{-1}x_1 - f(y)x_1 z^2,$$
$$\frac{dx_2}{d\tau} = k_3 z - k_{-3}x_2,$$
$$\frac{dy}{d\tau} = \beta f(y)x_1 z^2 + s(1-y),$$
$$\qquad (11)$$

where $z = 1 - x_1 - x_2$, x_1, x_2, y are the dimensionless concentrations and temperature. The dynamic system (11) has the oscillations for example for parameters: $\beta = 0.4$, $\gamma = 65$, $s = 4.5$, $Da = 0.56$, $k_1 = 0.6$, $k_{-1} = 1$, $k_3 = 0.001$, $k_{-3} = 0.03$.

4. Catalytic trigger: 1) $2Z \leftrightarrow 2X_1$, 2) $Z \leftrightarrow X_2$, 3) $X_1 + X_2 \rightarrow 2Z$. (12)
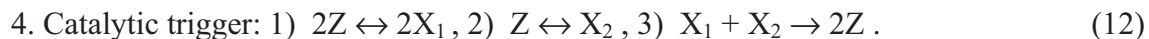
For (12) the thermokinetic models has for example the form:

$$\frac{dx_1}{d\tau} = 2k_1 z^2 - 2k_{-1} x_1^2 - f(y)x_1 x_2,$$

$$\frac{dx_2}{d\tau} = k_2 z - k_{-2} x_2 - f(y)x_1 x_2, \qquad (13)$$

$$\frac{dy}{d\tau} = \beta f(y)x_1 x_2 + s(1-y).$$

5. Catalytic oscillator: the scheme (12)+ buffer step

$$4)\ Z \leftrightarrow X_3 . \qquad (14)$$

is a catalytic oscillator [1,3]. The thermokinetic models for (12) and (12)+(14) may have a complex dynamic behavior.

References

1. Bykov V.I. Modelling of the critical phenomena in chemical kinetics. M.:Nauka, 1988. 264 p.

2. Yablonskii G.S., Bykov V.I., Gorban A.N., Elokhin V.I. Kinetic models of catalytic reactions. Amsterdam: Elsevier.1991. 400 p.

3. Bykov V.I.//Zh.Phys.Chem. 1985, vol.54, №11, p. 2712.

4. Bykov V.I., Pushkareva T.P.//React.Kinet.Catal.Lett. 1994, vol. 52, №1, p. 87.

5. Bykov V.I., Pushkareva T.P.//React.Kinet.Catal.Lett. 1995, vol. 54, №1, p. 145.

6. Bykov V.I., Tsybenova S.B.//Phys.Gor.Vzryv. 2001, vol. 37, №5, p. 36.

7. Bykov V.I., Tsybenova S.B.//Teor.Osn.Chem.Techn. 2003, vol.37, №1, p. 64.

8. Bykov V.I. Tsybenova S.B.// DAN. 2000, vol. 374, №5, p. 640.

9. Bykov V.I., Tsybenova S.B., Slinko M.G.// DAN. 2001, vol. 378, №2, p. 214.

10. Bykov V.I., Tsybenova S.B., Slinko M.G.// DAN. 2001, vol. 378, №3, p. 355.

11. Bykov V.I., Tsybenova S.B.//Zh.Phys.Chem. 2003, vol. 77, №9, p. 1566.

12. Bykov V.I., Trotsenko L.S.//Zh.Phys.Chem. 2005, vol. 79, №5, p. 792.

STUDY OF THE COMBINED ZEOLITE-CONTAINING ADSORBENT LAYER FOR SWEETENING OF NATURAL GAS UTILIZED AT THE «ORENBURGGAZPROM Ltd»

S.N. Filimonov[1], S.R. Khairulin[2], Z.R. Ismagilov[2]

[1]*Orenburggazprom Ltd., Orenburg, Russia*
[2]*Boreskov Institute of Catalysis, SB RAS, Novosibirsk, Russia*
S.Filimonov@ogp.gazprom.ru

Introduction

Sweetening of sour natural gases is a key problem of production of pollution free fuels. One of the most promising technologies/processes is that removal of sulfur containing complexes (hydrogen sulfide and mercaptans) by synthetic zeolite-based adsorbents which successfully runs at the Orenburg Gas Processing Plant (OGPP). Prior to entering the natural gas-sweetening and drying plant of the (OGPP), natural gas was passed through amine treatment plants and glycol dehydration units of the gas processing/refining plant. Cleaning was performed over the NaX zeolite containing adsorbent in vertical cylindrical adsorbers. The zeolite loading is 70 tons, the gas flow rate through the adsorber was 250–360 thousand m^3/h. A stage of adsorption lasts for 20 h, regeneration and cooling last for 10 h each taken separately. The process of regeneration is performed by preheated purified natural gas at temperatures ranging from +270 to +320° C.

Upon the operation period of 18–24 months, adsorption capacity of the layer to all components, including the main component such as sour sulfur, reduced from 3.2 to 1.6 wt.% because of accumulation of coke deposits.

Deactivation of the layer is primarily caused by decomposition of mercaptans, however, DEA and glycol also significantly contribute to this process (15 to 20% of the total coke deposition), even if both amine and glycol plants operate stable and the concentration of DEA and glycol does not exceed the limit 16 mg/m^3 (in total).

Carbon deposit is non-uniformly throughout the zeolite height. The main portion of carbon is deposited on the front layer part (7–10% of the loading height) where sorption of almost all DEA and glycol, supplied to the adsorber, proceeds.

Experimental

In order to optimize the process conditions, we proposed the following order of the adsorber loading: 10% of the layer (along the gas movement) length at the inlet is formed by zeolite adsorbent NaY, the rest being NaX.

To test the suggested load using the actual raw gas to be cleaned from sulfur compaunds and dried, the pilot plant was designed and constructed (Fig. 1). The main units are two parallel adsorbers designed for the zeolite load of 10-12 g. The size of zeolite fractions in both adsorbers was 0.5-1.0 mm.

Both adsorbers are designed as a tube, the inner diameter is 10 mm, the zeolite bed height is 200-250 mm.

A feed gas flow was directed to the both adsorber inlets at the pressure 50 kilogram-force/cm^2. The gas flow rate through the adsorber was 50 l/h, monitoring of the gas supply was performed by gas meters, the variation in gas supply to the adsorbers was maintained at ± 0.2 l/h.

Adsorber 1 was loaded with two zeolite layers: the first layer (along the gas flow) contains zeolite adsorbent NaY (1.18 g), the second layer contains commercial zeolite adsorbent NaX (10.57 g).

Adsorber 2 (reference) was loaded with the NaX adsorbent (11.7 g). The size of zeolite fractions in both adsorbers was 0.5-1.0 mm.

We were forced to use paralleling of the adsorbers in order to equalize differences in the natural gas composition at the reactor inlet, because components of the gas flow and concentrations of sulfur complexes in the gas vary within a rather wide range, thus the hourly variations attain to 20%. The inlet and outlet flows were analyzed to determine:

- gas composition by a chromatography method (State Standard # 23781-87) using a "TSVET 2000M" chromatograph. We registered hydrocarbons C_{1+6}, CO_2 and non-hydrocarbon components;

- concentration of the sour sulfur and hydrogen sulfide by an iodimetric method (State Standard # 22387.2 – 97);

- concentrations of amine and glycol in the feed flow by the standard technique for mass concentrations of glycol and amines in gases (M 005 – 123 – 00).
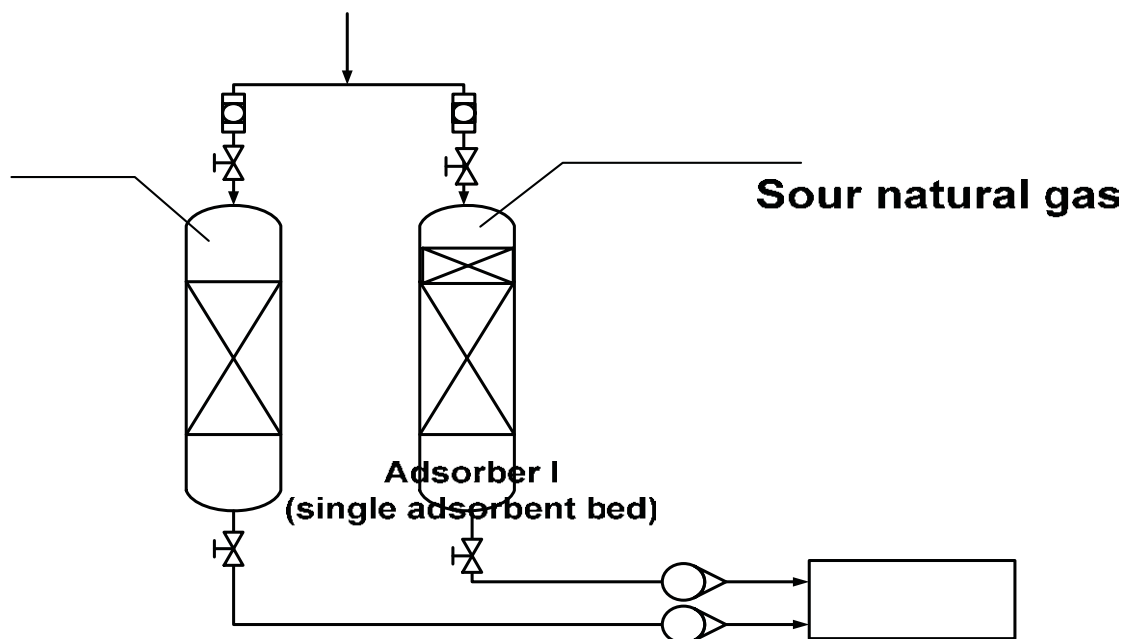
Fig. 1. Pilot setup for studying the process of adsorptive natural gas cleaning

Results and discussion

Processing of experimental data suggests that dynamic capacity of the composite layer to sour sulfur exceeds that of the reference layer by 2 % and reaches 3.27% under experimental conditions. Dynamic capacity to hydrogen sulfide and carbonic acid gas of both loads was practically equal.

To study stability of the load characteristics, we performed a number of runs with varied adsorption-regeneration cycles using the natural gas. The total number of cycles was 50. After each ten cycles, the amount of coke deposits on the layer was determined by the weight method. After 50 cycles, dynamic capacity of loads 1 and 2 was determined from the sour sulfur.

The content of coke deposits vs cycle number is shown in Table 1

Number of cycles	Content of coke deposits		
	NaY layer	NaX layer (loading 1)	NaX layer (loading 2)
10	0.023 g - 1.91 %	0.164 g - 1.53 %	0.191 g - 1.60 %
20	0.046 g - 3.75 %	0.271 g - 2.50 %	0.312 g - 2.60 %
30	0.058 g - 5,45 %	0.361 g - 3.30 %	0.425 g - 3.50 %
40	0.091 g - 7.16 %	0.418 g - 3.80 %	0.513 g - 4.20 %
50	0.110 g - 8.52 %	0.446 g - 4.05 %	62 g - 4.58 %

As follows from the table data, the total concentration of coke on both loads is almost equal. For load 1, coke deposits more intensively on the NaY zeolite layer than on the NaX layer due to decomposition of DEA and glycol. The underlying NaX layer is fed by a gas flow cleaned from both DEA and glycol. After 50 adsorption-regeneration cycles, the dynamic capacity of the partially carbonized loads to sour sulfur was: 2.07 and 1.93 wt.% for loads 1 and 2, respectively.

Conclusion

As follows from the pilot tests, the combined zeolite load permits one to increase the adsorbent life serving in the natural gas sweetening plant. An application of zeolite NaY as a protective layer made it possible to preserve the value of dynamic capacity of the load that exceeds that on the industrial load by 7.3%.

EXPERIMENTAL-COMMERCIAL STUDIES OF CATALYTIC SYSTEMS FOR AMMONIA OXIDATION PROCESS

Brushtein E.A., <u>Golovnya E.V.</u>, Vanchurin V.I.

«ALVIGO-M» Ltd; 38, Shosse Entuziastov, 111123 Moscow, Russia

Tel./Fax: (+7 495) 232-1465, 232-9906

E-mail: Alvigom@alvigo.ee;   Web: http://www.alvigo.ee

For decades, ammonia oxidation process in Russian domestic nitric acid plants was performed with two variants of catalytic system - either over conventional stack of platinoid catalyst gauzes, or over two-stage system comprising platinoid gauzes and non-precious oxide catalyst. In the early 90s, the non-precious oxide catalyst for 2nd stage of ammonia oxidation in the form of honeycomb-structured blocks have been developed for the first time in Russia. Implementation of regular honeycomb catalyst instead of bulk beds of pelleted catalyst types has allowed then to take the full advantage of using two-stage systems for ammonia oxidation, namely to reduce the noble metal catalyst costs and losses of platinoids, as well as to lower converter's hydraulic resistance. On the other hand, the industrial tests have shown that there is a room for performance improvement of ammonia oxidation units lying in replacement of a part of conventional stack of platinoid catalyst gauzes by less expensive palladium catchment gauzes, which are capable of absorbing noble metals aerosols.

Nevertheless, the costs of platinoid catalyst required for nitric acid production remain high, and therefore a research aimed at reduction of both catalytic system initial cost and losses of platinoids during operation is still of great importance today.

The possible new direction in development of ammonia oxidation process is the using of new advanced catalytic system which have been designed taking into account the operating experience of nitric acid plants with conventional catalyst options. Obviously, the new system can not be marketed without carrying out very detailed and reliable operation tests under conditions similar to those at commercial operation. The results of such tests can be of both theoretical and practical value as they allow to discover and examine the new properties of multi-stage catalytic system and significantly contribute to saving of precious metals.

Some results are given in this paper of such experimental-commercial studies of various catalytic systems for ammonia oxidation process which have been carried out at the

installation mounted at JSC ACRON industrial site in Novgorod, Russia with the participation of ALVIGO-M Ltd.

The main device of the installation was an ammonia converter reactor with effective inner diameter of 0.15 m, operating under process conditions equal to those in UKL-7 type commercial nitric acid plant. Platinoid catalyst and catchment gauzes were fixed by special flange in the converter, and oxide catalyst in the form blocks' fragments was loaded in the separate basket under the gauzes inside the converter. The stack of gauzes was separated from a layer of the oxide catalyst by a Megapure gauze. The distance between the gauzes and thermocouple was approx. 10 mm. The installation was also equipped by all the necessary instrumentation and devices for process control, maintaining the preset technological parameters, measurement and sampling.

The following types of catalytic system were studied:

Conventional types:

1. Platinoid system of 7-12 catalyst gauzes.

2. Platinoid system of 7 catalyst gauzes and 3-5 catchment gauzes (Pd/W-5 alloy).

3. Two-stage system, comprising 6-9 platinoid catalyst gauzes and a layer of the IK-42-1 honeycomb block oxide catalyst.

New advanced type:

4. Two-stage system comprising 9 platinoid catalyst gauzes, 3 catchment gauzes (Pd/W-5 alloy), and a layer of the honeycomb block oxide catalyst.

The graph is shown below (See Fig. 1) for the obtained values of ammonia conversion rate over conventional catalytic systems against catalyst gauzes number, under the process conditions of 500 nm^3/hr flow rate of Ammonia-Air Mixture (AAM), temperature 880-890 ºC and ammonia concentration in AAM 10.53 – 10.69 vol.%.

It is evident from the diagram that for the conventional platinoid gauze catalyst system (curve 1) there is a linear dependence between the ammonia conversion rate and the number of gauzes for the system containing 7 to 10 gauzes, and for the number of gauzes 10 to 12 the conversion rate changes insignificantly, which is in accordance with earlier studies results. With the two-stage system of 9 platinoid catalyst gauzes and a layer of block oxide catalyst (curve 2), the conversion rate is comparable to that with conventional stack of gauze catalyst, or even slightly higher. It is obvious that the improvement of ammonia oxidation in this case is due to effect of hydrodynamic conditions stabilization of AAM flow through the converter by the layer of regular blocks of oxide catalyst.
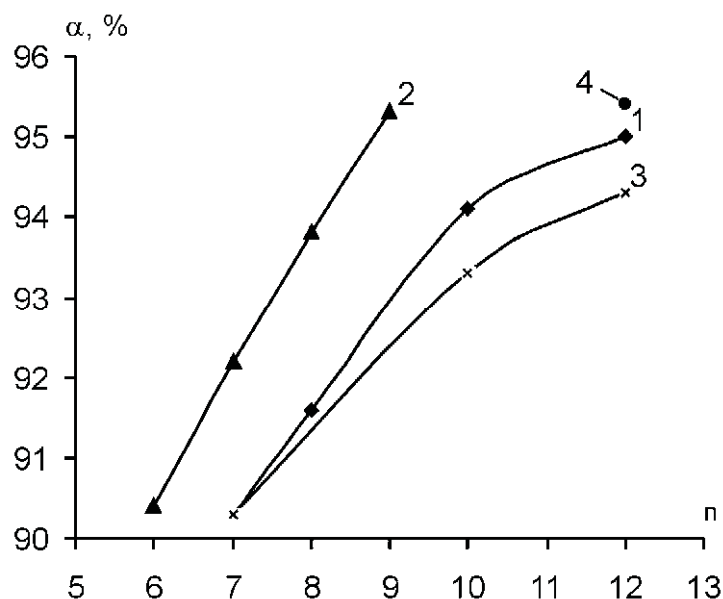
Fig. 1 Ammonia conversion rate (α, %) dependence on catalyst gauzes number (n):
1. – platinoid catalytic system of 7-12 catalyst gauzes;
2. – two-stage catalytic system of 6-9 catalyst gauzes and a layer of blocks of IK-42-1 oxide catalyst;
3. – platinoid catalytic system in combination with 3-5 catchment gauzes (Pd/W-5 alloy): p.7 – 7 platinoid gauzes, p.10 – 7 platinoid + 3 catchment gauzes, p.12 – 7 platinoid + 5 catchment gauzes;
4. – two-stage catalytic system of 9 platinoid gauzes in combination with 3 catchment gauzes (Pd/W-5 alloy) and a layer of the block oxide catalyst.

Also, it can be concluded from curves 1 and 3 comparison that in terms of selectivity the combined systems of 10 gauzes (7+3) and 12 gauzes (7+5) generally slightly concede to the systems of 10 and 12 platinoid catalyst gauzes. As an example, the obtained ammonia conversion with the system of 12 platinoid gauzes amounts to 95.0 %, while the combined system of 7 platinoid and 5 catchment gauzes has achieved 94.2 %. It is evident however that no considerable decrease of system catalytic properties is observed at replacement of catalyst gauzes by catchment ones, even of considerable part of stack. It testifies that catchment gauzes possess the certain catalytic activity in desired reaction of ammonia conversion into nitrogen oxide, i.e. their operation is bifunctional.

The interesting data have been obtained concerning ammonia slip. It have been found that ammonia concentration in catalytic system effluent gas equaled to 0.016 vol. % with 12 platinoid gauzes system and 0.011 vol.% with the system of 7 platinoid catalyst and 5 catchment gauzes. The decrease in ammonia conversion rate and in ammonia concentration in system effluent gas (ammonia slip) at using the catchment gauzes can point at the possible occurrence of undesirable reaction:

$$4NH_3 + 6NO \rightarrow 5N_2 + 6H_2O$$
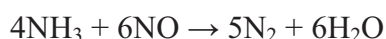
The point 4 on Fig. 1 illustrates the efficiency of two-stage system of 9 platinoid catalyst and 3 catchment gauzes and a layer of the block catalyst. The ammonia conversion rate in this case have reached 95.4 %, which is by 0.4 % than the calculated value for the system of 12 platinoid catalyst gauzes and by 1.2 % higher than for system of 7 platinoid catalyst and 5 catchment gauzes. It is assumed that this effect is conditioned by the favourable influence of block oxide catalyst layer placed under gauzes stack on the gas flow hydrodynamics inside the converter which results in excluding the selectivity decrease observed in the systems not containing such layer.

The further research of the two-stage catalytic systems containing platinoid catalyst and catchment gauzes along with the layer of block oxide catalyst will surely be very promising for further improvements in ammonia oxidation process in nitric acid production.

RELATIONAL DATABASE SYSTEM MANAGER OF COMPLEX REACTIONS IN THE PRESENCE OF ZIRCONIUM CATALYST $(C_2H_5)_2ZrCl_2$

Irek M. Gubaydullin[1], Il'dar I. Gubaydullin[2]

[1]*Institute of Petrochemistry and Catalysis, Laboratory «Mathematical chemistry»,*
Ufa Scientific Centre of RAS, address: Prosp. Oktyabrya, 141, 450075, Ufa, Russia,
phone/fax: 7-3472-312750, e-mail: irekmars@mail.ru.
[2]*Ufa State Aviation Technical University, address: K.Marx str, 12, 450000, Ufa, Russia,*
phone/fax: 7-3472-730672, e-mail: ildargubaydullin@mail.ru.

Any mathematical model comprise a structure and algorithms of the investigated process. In the heart of current technology of database underlie use of the relational model of data (RMD), based on the strict apparatus of the relational algebra and the mathematical logic. Such approach is the most effective at the decision of problems of modelling of complex systems [4].

Under the direction of a member correspondent of Dzhemilev U.M. in the Instutute of Petrochemistry and Catalysis (INK) of the Russian Academy of Science are studied complex mechanisms of catalytic cycloaluminizing [1] and hydroaluminizing [2] of olefines in the present of zirconium catalyst Cp_2ZrCl_2. The developed kinetic models for above specified mechanisms, and also for reaction of oligomerization of alpha-methylstyrene [3], formed a relational database system manager (RDBSM).
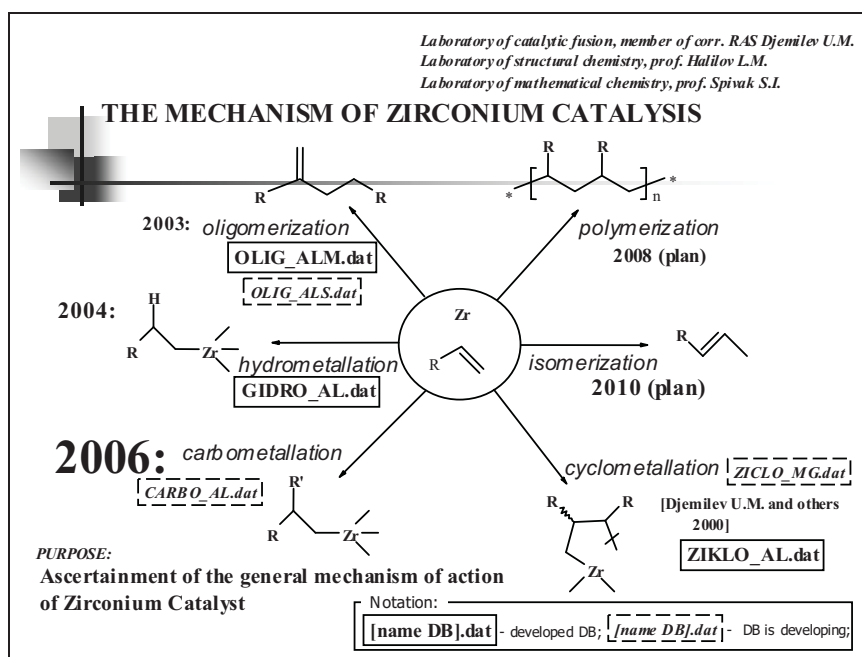
Fig. 1 – The mechanism of zirconium catalysis

In figure 1 strategy of studying of the general mechanism of action of zirconium catalysts is presented. In process of modelling separate reactions of all complex mechanism with participation of zirconium catalysts [1, 2, 3], there was a necessity not only to keep numerous experimental data, but also to analyze and synthesize connections both between data in one reaction, and between data of several reactions. The data taken from a database on the basis of established connections, are the information. Outside of connections data are the information only in the event that they are typified, or classified, and the applied classification scheme is known. In figure 2 it is presented static part of a DB of the new considered complex mechanism of cyclomagnezing of olefines.
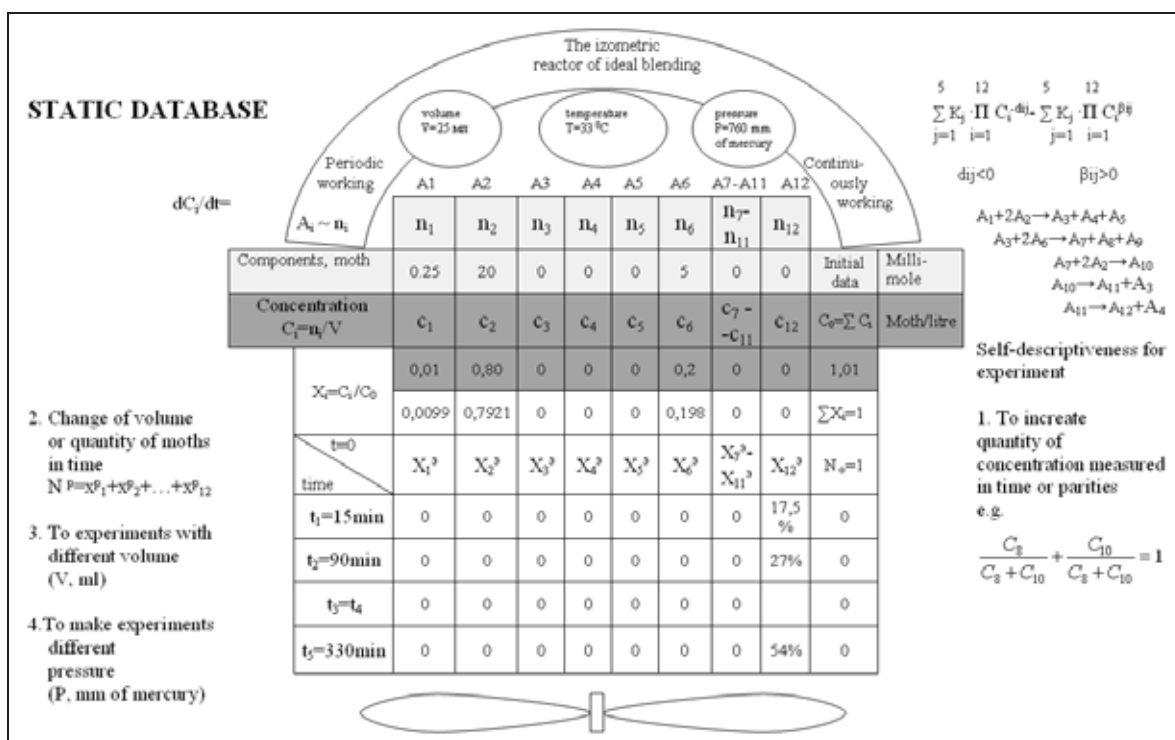
Fig. 2 – The elementary input informational flow for to computing experiment by definition of the kinetic constants of mechanism cyclomagnezing of olefines and alens RMgR, catalyzed by complexes Ti and Zr

The natural language reflecting stoichiometry of chemical reactions, language of linear algebra is. An atomically-molecular matrix mirror chemistry of agent, and stages of chemical reaction - a stoichiometric matrix. Change in time of concentration of substances participating in reaction too is set by matrix tables. During search of a minimum of functional conformity of experimental and calculated concentration it is used Volpert's A. bipartite graphs which are set by matrixes of an adjacency and incidence.

PP-101

In view of above specified, the relational approach is justified at designing a DB in an opportunity of their future integration in the integrated distributed databases (IDDB).

First of all the RDBSM orientate for convenience of work of the chemical experimenter (the technologist at a factory).

In figure 3 the superficial scheme of working user from RDBSM is presented. Deeper and full description of structures of RDBSM will be presented in the subsequent works.
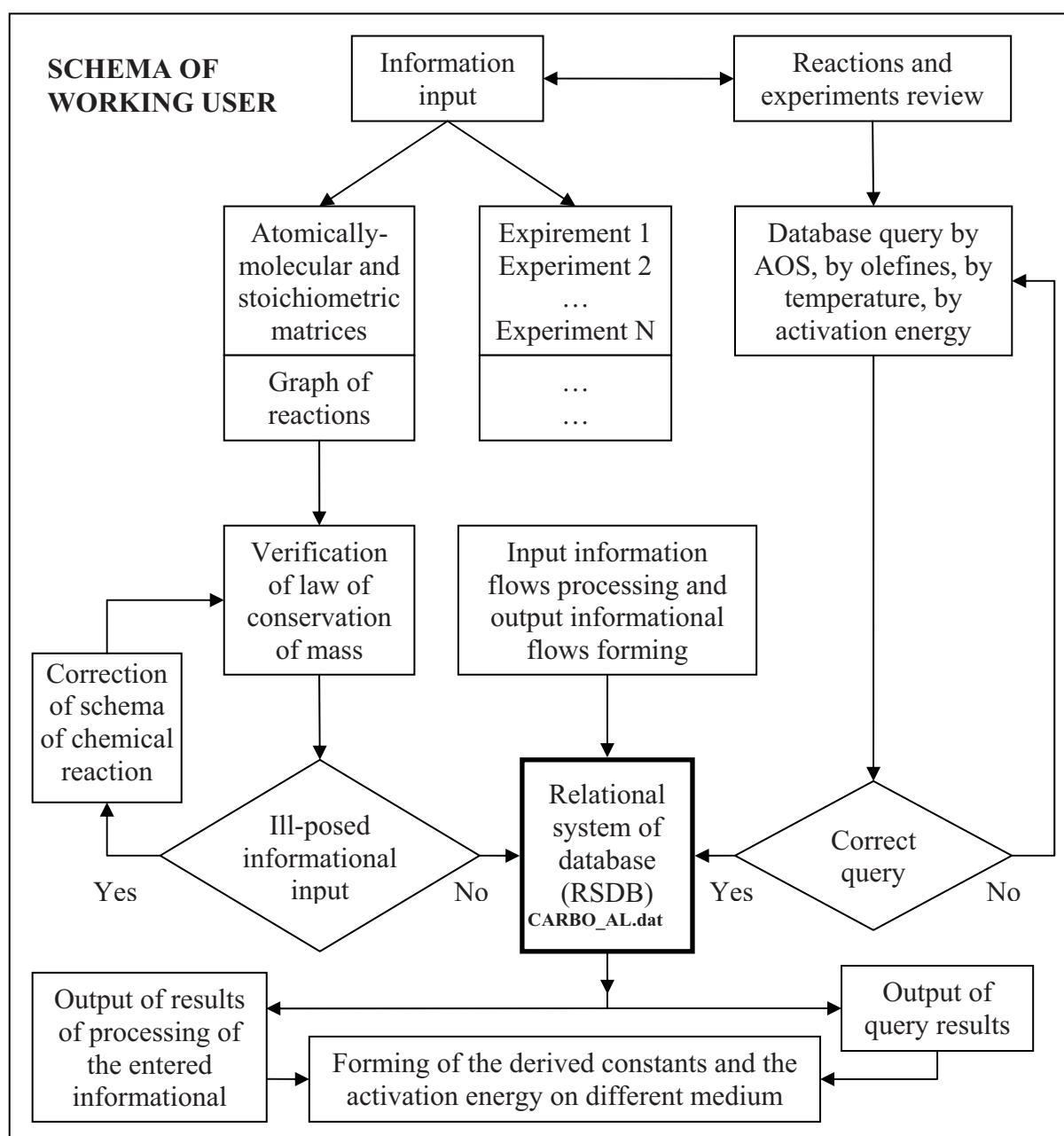
Fig. 3 – Schema of working user from RDBSM

The structure and the maintenance of each experiment is presented in figure 2.

At present the first group of total of methods and means of definition of the connected data is developed. The group contains the formal description of structures of data, and also administration of a DB.

Following DB are developed:

1) OLIG_ALM.dat – alpha-methylstyrene oligomerization in the presence of NaHY Zeolite;

2) ZIKLO_AL.dat – cycloaluminizing of alkylalanes by $AlEt_3$ in alumocyclopentane in the presence of Cp_2ZrCl_2;

3) GIDRO_AL.dat – olefin hydroalumination by alkylalanes in the presence of Cp_2ZrCl_2.

In a stage of development are:

1) OLIG_ALS.dat – styrene oligomerization in the presence of NaHY Zeolite;

2) KARBO_AL.dat – carboaluminizing;

3) ZIKLO_MG.dat – of olefines and alens RMgR, which catalysting at complexes Ti and Zr.

References

1. А.В.Балаев, Л.В.Парфенова, И.М.Губайдуллин и др. Механизм реакции циклоалюминирования алкенов триэтилалюминием в алюмациклопентаны, кактализирумеой Cp_2ZrCl_2 // ДАН, 2001, том 381. №3, с.364-367.

2. Парфенова Л.В., Губайдуллин И.М., Печаткина С.В. и др. Механизм гидроалюминирования под действием Cp_2ZrCl_2 // Тезисы докладов XVI Всероссийской конференции по химическим реакторам "Химреактор-16", Казань, 2005, стр. 17-20.

3. Kutepov B.I., Balaev A.B., Grigor'eva N.G., Gubaydullin I.M. Kinetic model of a-Methylstyrene oligomerization in the presence of NaHy zeilite // XVI International Conference on Chemical Reactors "CHEMREACTOR-16", Berlin, Germany December 1-5, 2003, p.305-307.

4. Дейт К.Дж. Введение в системы баз данных: Пер. с англ. - 7-е изд. - Киев: Диалектика, 2001. - 784 с.

APPLIED SOFTWARE PACKAGE OF CHEMICAL HETEROGENIC-CATALYTIC PROCESSES' COMPUTER MODELLING

I.U. Ibadzadeh, V.V. Bogatov

Institute of Chemical Problems of NAS of Azerbaijan, Department of Automation of Chemical Experiment, Baku, 370143, Husein-Javid ave, 29, Azerbaijan Republic
phone. +994 439-41-59

For behaviour prediction of complex chemical heterogenic-catalytic processes with non-stationary catalytic activity, scientific studies use methods of kinetic research computer modeling after all reduced to numeric techniques including automatic data collection for processing and display output.

The task arising therein is complex and multi-parametric, for which solution we develop the package of applied software providing parametric identification of the kinetic models and estimation of their reliability, finding model target parameters and estimation of disturbing influences.

The package of applied software is written and developed by us in Visual Basic 6.0 and functions in Windows XP environment, in dialogue mode allowing to:

- solve mathematical models describing complex chemical processes, consisting of over 100 simple differential equations, and equations in partial derivatives down to the fourth order unit with variable factors according to Runge Kutt method with automatic step change providing an approximated error estimation at each integration step;
- build graphic dependencies of target parameters and process disturbing influences, directly in dialogue mode;
- carry out model adequacy confirmation by means of data processing for finding optimum conditions of researched process course.
- investigate process kinetic laws.

The given package of applied software has been approved using the mathematical model of acetoxillation process of ethylene into vinyl-acetate and propylene into allylacetate on PdCuZn catalyst. Thus the found target parameters under the reactor process working pressure change (conversion of acetic acid, selectivity of target product from acetic acid, output of acetone from acetic acid), and changes of reagent partial pressure values differed only by 5% from the experimental values obtained using pilot installation, that is quite acceptable in engineering calculations.

On the basis of the data received, researched process optimization has been achieved where the output of vinyl-acetate and allylacetate was selected as optimization criterion, and temperature and reagent partial pressure as managing parameters. On the basis of the found conducting process optimum mode the reactor unit constructive dimensions have been calculated.

MATHEMATICAL MODELLING OF THE EPITAXIAL REACTOR STABILITY

Itskova P.G.

Al-Farabi Kazakh National University, Department of Mechanics and Mathematics,

CIS, Kazakhstan, 480078, Almaty, Al-Farabi, 71

E-mail: laskoz@nursat.kz, Polina@kazsu.kz

In the present work approximately - analytically and numerically the critical phenomena and stability of the steady states in the process of the chemical deposition from a gas phase in a cylindrical reactor of final length [1,2] are investigated. The kinetic mechanism accepted in [3] is used. The analysis of the dynamic behaviour of the system is carried out on the basis of the zero - dimensional analogue of the two-dimensional model by methods of the qualitative theory of the ordinary differential equations. The received results are used in designing numerical experiments for the investigation of the influence on process of parameters and periodic external perturbations.

The cylindrical vertical epitaxial reactor of finite length is considered. The temperature of the on the surface of the reactor is supported by a constant. Is supposed that the gaseous mixture is incompressible, dynamic viscosity, a specific thermal capacity, factors of diffusion and heat conductivity are constant. The Soret and Dufour effects are neglected. Reynolds numbers are in a range 10-100, therefore effects of turbulence are not taken into account. The limit stages of the exothermal chemical reactions in a gas phase [4] and on the deposition surface are considered. The rates of the homogeneous and of the heterogeneous reactions are described by the Arrhenius law and have the first order on the concentration of the reagents.

The problem is mathematically formulated by a system of the two-dimensional dimensionless conservation equations of the mass, impulse, energy, of the mixture component:

$$\xi \text{Pe} \frac{\partial \widetilde{U}}{\partial \widetilde{x}} + \frac{\partial \widetilde{V}}{\partial \widetilde{r}} + \frac{\widetilde{V}}{\widetilde{r}} = 0,$$

$$\frac{\partial \widetilde{U}}{\partial \widetilde{t}} + \xi \text{Pe} \widetilde{U} \frac{\partial \widetilde{U}}{\partial \widetilde{x}} + \widetilde{V} \frac{\partial \widetilde{U}}{\partial \widetilde{r}} = M + \text{Pr}(\frac{\partial^2 \widetilde{U}}{\partial \widetilde{r}^2} + \frac{1}{\widetilde{r}} \frac{\partial \widetilde{U}}{\partial \widetilde{r}}), \qquad (1)$$

$$\frac{\partial \widetilde{T}}{\partial \widetilde{t}} + \xi \text{Pe} \widetilde{U} \frac{\partial \widetilde{T}}{\partial \widetilde{x}} + \widetilde{V} \frac{\partial \widetilde{T}}{\partial \widetilde{r}} = \frac{\partial^2 \widetilde{T}}{\partial \widetilde{r}^2} + \frac{1}{\widetilde{r}} \frac{\partial \widetilde{T}}{\partial \widetilde{r}} + \widetilde{q} \widetilde{W}_1,$$

$$\frac{\partial C}{\partial \tilde{t}} + \xi \text{Pe}\tilde{U}\frac{\partial C}{\partial \tilde{x}} + \tilde{V}\frac{\partial C}{\partial \tilde{r}} = \text{Le}\,(\frac{\partial^2 C}{\partial \tilde{r}^2} + \frac{1}{\tilde{r}}\frac{\partial C}{\partial \tilde{r}}) + \tilde{W}_1 \ .$$

The initial conditions are taken in the form

$$\tilde{t} = 0:\ 0 \leq \tilde{r} \leq 1,\ 0 \leq \tilde{x} \leq 1,$$

$$\tilde{U} = \tilde{U}_{_H},\ \tilde{T} = \tilde{T}_{_H},\ \ C = C_{_H}. \tag{2}$$

The boundary conditions are formulated as

$$\tilde{t} > 0: 0 < \tilde{r} < 1,$$

$$\tilde{x} = 0:\ \tilde{U}_0 = 1,\ \tilde{V}_0 = 0,\ \tilde{T}_0 = 1,\ C_0 = 1,$$

$$0 \leq \tilde{x} \leq 1,$$

$$\tilde{r} = 0:\ \frac{\partial \tilde{U}}{\partial \tilde{r}} = 0,\ \frac{\partial \tilde{T}}{\partial \tilde{r}} = 0,\ \ \frac{\partial C}{\partial \tilde{r}} = 0, \tag{3}$$

$$\tilde{r} = 1:\ \tilde{U} = \tilde{V} = 0,\ \tilde{T} = \tilde{T}_n,\ -\frac{\partial C}{\partial \tilde{r}} = \text{Sh}_1 C,$$

where

$$\tilde{W}_1 = \text{Da}(1 - C)\exp\!\left(\frac{-\beta}{\tilde{T}}\right) \text{ - the rate of the homogeneous reaction.}$$

For the analysis of the dynamic behaviour the simplified analogue of system of the equations (1) - (3) - zero - dimensional model was constructed

$$\frac{d\tilde{U}}{d\tilde{t}} = 2\tilde{U}(\tilde{V} - 3\text{Pr}) + M \equiv P_1(\tilde{U}),$$

$$\frac{d\tilde{T}}{d\tilde{t}} = (-2\xi\text{Pe}(2\tilde{U} - 1) - 6)\tilde{T} + (-\tilde{V} + 6)\tilde{T}_n + 2\xi\text{Pe}\tilde{U} + \tilde{q}\tilde{W}_1 \equiv P_2(\tilde{U}, \tilde{T}, C),$$

$$\tag{4}$$

$$\frac{\partial C}{\partial \tilde{t}} = \left(-2\xi\text{Pe}\tilde{U} + \frac{\text{Sh}_1(\tilde{V} - 6Le)}{1 + \text{Sh}_1}\right)\hat{C} + 2\xi\text{Pe}\tilde{U} + \tilde{W}_1 \equiv P_3(\tilde{U}, \tilde{T}, C),$$

where

$$\tilde{V} = -2\xi\text{Pe}(\tilde{U} - 1).$$

On the basis of the zero - dimensional model (4) coordinates, number, static and dynamic instability of the process regimes are studied.

The steady states of system (4) are determined by the decision of system of the algebraic transcendental equations

$$P_1(\tilde{U}_S) = P_2(\tilde{U}_S, \tilde{T}_S, C_S) = P_3(\tilde{U}_S, \tilde{T}_S, C_S) = 0. \tag{5}$$

The bifurcation diagrams on a plane $\tilde{T}_n, \tilde{T}_s$ are used.

The bifurcation diagrams show that in dependence on numerical values of parameters is possible the existence of the crisis-free regimes and the process with hysteresis (with the critical phenomena such as "ignition" and "extinction").

From bifurcation diagrams and condition of the existence of theirs extremum are received the parametrical equations of the boundary of multiple steady states on the plane $\widetilde{q}, \widetilde{T}_S$. The stability of the steady states of the system with multiple parameters is analyzed by first Lyapunuv' s method on the plane of two parameters under the fixed values of the others. With the help of criteria Routh-Hurwitz are received the parametrical equations of four boundaries of the stability $\Delta = 0$, $\theta = 0$, $\sigma\Delta - \theta = 0$ are received.

It is established, that the parametrical equations of boundary $\theta = 0$ coincide with the equations of boundary of the multiple steady states. The boundary $\theta = 0$ looks like a wedge inside which parameters gives the multiple steady states, and outside of - the unique steady states. Other boundaries allocate areas of the parameters with asymptotically stable and self-oscillatory regimes. On a plane of two parameters of process $(\widetilde{q}, \widetilde{T}_n)$ the boundaries $\sigma = 0$, $\Delta = 0$ and one of boundaries $\sigma\Delta - \theta = 0$ are lines with a loop. The area of the parameters inside of the loops belong to the dynamically unstable steady states. The boundary $\sigma = 0$ gives the narrowest area of the dynamically unstable steady states while boundary $\sigma\Delta - \theta = 0$ gives the widest area.

It is established that areas of instability take places between areas of steady process. The influence of Sherwood, Damkohler, Lewis, Peclet, Prandtl numbers, relations of radius of the reactor to its length, of the pressure differential, of the temperature on the reactor input upon the form and the disposition of the stability boundaries on the plane $\widetilde{q}, \widetilde{T}_n$ is revealed. On some critical values of the Lewis, Sherwood, Prandtl numbers the loops on the curves $\sigma = 0, \Delta = 0, \sigma\Delta - \theta = 0$ disappear and dynamic instability becomes impossible.

It is shown that self-oscillatory regimes are possible under condition for the effective factors of the mass- and heat transfer

$$m_C < m_{\widetilde{T}},$$

where

$$m_C = 2\xi\,\mathrm{Pe}\,\widetilde{U}_s + \frac{\mathrm{Sh}_1}{\mathrm{Sh}_1 + 1}[6\,\mathrm{Le} - 2\xi\,\mathrm{Pe}(1 - \widetilde{U}_s)],$$

$$m_{\widetilde{T}} = 6 - 2\xi\,\mathrm{Pe}(1 - 2\widetilde{U}_s).$$

The given parametrical analysis is used for planning numerical experiments on the base of

the zero - dimensional model (4) and of the two-dimensional model (1) - (3). From the numerical solution of these problems is confirmed the existence of the attractors such as stable limit cycles in case of self-oscillatory regimes and such as stable steady state in the parametrical areas of the unique and non-unique regimes.

Figure1 shows results of numerical solutions of the zero - dimensional problem (4) and a two-dimensional problem (1) - (3) for the self-oscillatory regime. In case of the two-dimensional problem the solution on an axis of the reactor near to its input $\tilde{x} = 0,2$, $\tilde{r} = 0$ is presented. The limit cycles illustrate the relaxational oscillations. The period of the self-oscillations received as a result of the solution of the zero - dimensional problem (4), coincides with received of the analytical solution and one order with received at the solution of the two-dimensional problem. Self-oscillations occur near to the steady state with the coordinates found with the help of the bifurcation diagram.
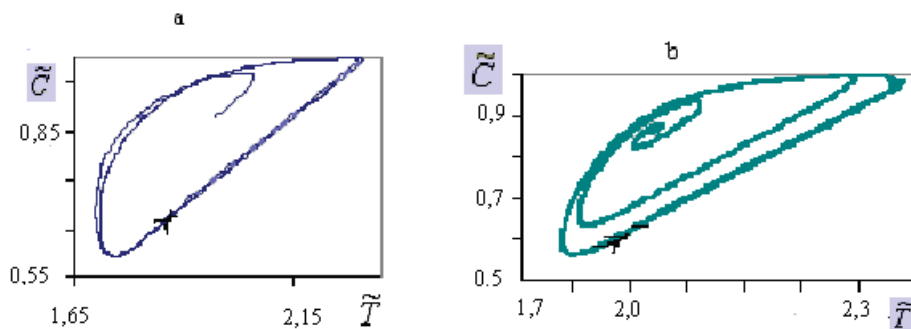
Fig. 1. Phase portraits of the system for a self-oscillatory regime:
a - the solution of the problem (4), b - the solution of the problem (1)-(3)

The possible responses of the oscillations regime (self-oscillation and slowly damped oscillations) on the pulsation of the temperature of the reactor surface under the law

$$\tilde{T}n = \tilde{T}n_1(1 + A_1 \sin \omega_1 \tilde{t}) \tag{6}$$

(where A_1, ω_1 - the amplitude and the frequency of the influence) are investigated.

The specific effects of influence of the frequency and the amplitude of the perturbation at the character of the forced oscillations, at their form, amplitude and frequency are established. Almost periodic oscillations, synchronization of system with external influence, reduction of amplitude of an initial self-oscillatory regime, the nonlinear resonant phenomena are received etc.

The amplitude-frequency characteristics (figure 2) illustrate the influence of the disturbances of the kind (6) on the regime of slowly damped temperature oscillations.
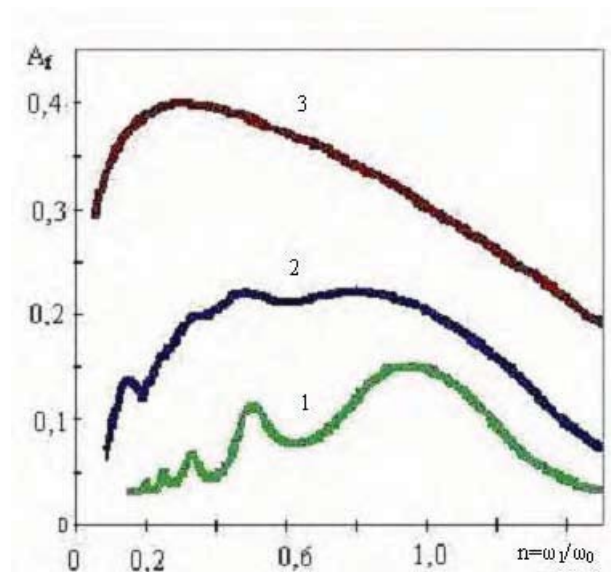
Fig. 2. Change of amplitude of the forced oscillations of the temperature depending on the relation
of frequency of influence (6) to the frequency of damped oscillations. A_1=0,01 (1); 0,02 (2);0,05

The received results can find application for the process control of chemical deposition
from a gas phase.

References

1. Itskova P.G. Numerical modeling of regimes of operation of tubular epitaxial reactor // Computing technologies 2003, V. 8, 72-80 (Novosibirsk – Almaty - Ust-Kamenogorsk, joint publication).

2. Itskova P.G. Mathematical modeling of disturbances influence on the operation regimes of chemical reactors// Computing technologies, T.9 2004, 263-271 (Novosibirsk - Almaty, joint publication).

3. Itskova P.G. Numerical modeling of stability of processes of transport with by exothermal chemical reactions // Computing technologies, 2002, т.7, 52-60 (Novosibirsk - Almaty, joint publication).

4. Minkina V.G. Macrokinetics of process of chemical deposition from the gas phase, accompanying with homogeneous reactions // *Theoretical Foundations of Chemical Engineering*, 1999,V.33, №1, 54-61.

RESEARCH OF INFLUENCING OF CATALYTIC SOLUTIONS ON THE PROCESS OF OXIDIZATION OF CYCLOHEXANE

Ivaschuk O.S., Skachko S.V., Mel'nyk J.R., Reutskyy V.V.

National University „Lvivs'ka Polytechnika", Institute of Chemistry and Chemical Technology, Department of Technology of Organic Products, Lviv, 12, St. Bandery str., Ukraine, ivaschuk@rambler.ru

The binary catalytic systems on the basis of cobalt naftenate and different superficial-active substances (SUS) which were created on a department of technology of organic products in NU „Lvivs'ka polytechnika" allow improving the indexes of process of oxidization of cyclohexane. However the use of these catalytic systems in industry is complicated in cause with bad and different solubility of cobalt naftenate (CN) and additions in cyclohexane. Therefore preparation of catalytic solution is offered in cyclohexanon, which enables its previous activating.

Process of liquid oxidization of cyclohexane in the presence of the catalytic systems of cobalt naftenate (CN) – polyethyleneglycol (PEG) – cyclohexanone (CON) was studied at temperature 418 K and pressure of 1,0 MPa.

During the research the factor of change of catalytic solution during its protracted storage was studied. Influence of fresh prepared solution and solution, that was stored, was analysed. The results of spectrography indicates the formation OH-bonds, changes in concentration of bonds C=O and C-H. This indicates the formation of complex compound in solution.

The results of experiments testify that the use of the preliminary prepared catalytic solution NC in CON affects on speed and selectivity of process of oxidization of cyclohexane, and also on ratio of purpose products of cyclohexanol (COL) / cyclohexanone (CON).

Initial acceleration of elementary stages of oxidation reaction (at k=2%) is observed at application catalytic solutions $C(CN+CON)=5\times10^{-4}$ mol/l and $C(CN+PEG+CON)=5\times10^{-5}$ mol/l, at the simultaneous insignificant rise of total selectivity and displacement of ratio of purpose products to cyclohexanone. The industrial value of conversion of k=4% is achieved by the use of catalytic solution $C(CN+PEG+CON+TPN^*)=5\times10^{-5}$ mol/l comparing with above-mentioned catalytic solutions. There is observable smoothing of indexes of total

selectivity in comparison with base experiment and accumulation of cyclohexanol in a reactionary environment. The use of TPN addition loses the expedience at k=6%, which is desired for achievement in industry. At this level of conversion catalytic solution with addition of polyglycol displaces the ratio of purpose products to COL. Application of solution C(CN+CON)=5×10^{-4} mol/l leads to increase concentrations of ceton.

Influence of preliminary ultrasonic activation of catalytic solutions is negatively represented on the kinetic indexes of process. However selective action of the ultrasound is brightly expressed in accumulation of CON in a reactionary environment.

Catalytic effect of application of solutions on the basis of CN, PEG and CON increases during their storage, although influence of ultrasonic treatment on the given mixtures is expressed negatively. These questions need the subsequent detailed study.

Influence of some analysed catalytic mixtures on kinetics and selectivity of process of oxidization of cyclohexane is evident. The detailed influencing of application of catalytic solutions on the basis of cobalt naftenate, ultrasonic activating and storage of the catalytic systems will be explored.

*– tripolyphosphate Na

INCREASE OF REACTOR BLOC RUN EFFECTIVENESS OF GASOLINE REFORMING PROCESS BY APPLICATION OF COMPUTER CONTROL SYSTEM OF Pt-CATALYSTS

A.V. Kravtsov, E.D. Ivanchina, <u>S.A. Galushin</u>, E.P. Filintseva

Tomsk Polytechnic University

30, Lenin Avenue, Tomsk, 634050, Russia

Tel.: +7 (3822)563443; Fax: +7(3822)563435; E-mail: bird@tpu.ru

The mathematical formulation proves that it is possible to increase the effectiveness of the reactor bloc of gasoline reforming process by means of regulation of kinetic and hydrodynamic values [1].

Last years, besides widely used experimental and statistical methods of estimation of the technology of high-octane gasoline production, new simulation systems have been introduced very intensively. These systems are intended for maintenance of catalytic reforming process [2].

The computer-based simulation system of the reforming process is developed by us. This system significantly differs from others by taking into consideration the nonstationary kinetics of the carbohydrates conversion at the platinum catalysts surface. This makes possible not only evaluate the effectiveness of reactor bloc run [3], but also to introduce the system controlling the Pt-catalysts work that is a relevant task nowadays. Technologists can monitor and predict major effectiveness indexes such as: optimum and current activity of the Pt-catalysts, rate of coke formation, and on the whole, productivity and selectivity of the catalyst reforming process.

As a result of fundamental researches in catalytic gasoline reforming, a theoretical limit of Pt-catalysts activity was almost reached and as a consequence, the majority of catalysts (both domestically produced and imported) have close indexes of activation energy. Therefore, the perspective of an increasing productivity of the Pt-catalysts can be reached by means of perfection of the preparation technology and of their exploitation at the optimum activity level [2]. It must be underlined that demonstration of these regularities mainly depends on real conditions and, most of all, on composition of raw material, conditions of catalyst forming, preparation and elaborating in each particular process.

The analysis of the work of platinum catalysts of the same type proved that particular technological figures can alter a lot from one oil-refining plant to another. It was found that integral selectivity – octane-tons (octane number multiply by number of tons of reformed gasoline per 1 tone of raw material) – may differ by 1–4 octane-tons under the same composition of raw material. On the other hand, variation of the raw materials composition may result in difference in selectivity up to 2–6 octane-tons.

In view of the aforesaid, it should be mentioned that control of catalyst run on plant by optimum activity must be provided by developed computer system for testing various modifications of Pt-catalysts.

Practical realization of developed computer system is software product connected with factory automatic control system on "Kirishinefteorgsintez" Ltd. It allows using in automatic mode both operational figures of units Lch-35-11/1000 and Lg-35-8/300B and chromatographic composition of raw materials and reformed gasoline.

Consequently, the effectiveness increase of process run is reached by keeping optimum conditions of processes: reactivation, oxidative chlorination, sulfuration – essential for initial Pt-catalysts activity creation and continual calculation of current and optimum activity level during work cycle. Obviously that level of activities must be similar as much as possible. At the same time, the task of estimation of coke formation and duration of work cycle is being solved.

References

1. Kravtsov A.V., Ivanchina E.D. Computer-based forecasting and optimization of benzine processing.-Tomsk: STT, 2000. – 191 p.

2. Kravtsov A.V., Ivanchina E.D. Introduction of technological computer systems is a new stage in the control of hydrocarbon material refining process //Oil refinement and petrochemistry, № 9, 2005. – P. 40–43.

3. Kravtsov A.V., Ivanchina E.D., Galushin S.A., Poluboyartsev D.S., Voropaeva E. N., Melnic D. I. Evalution of the reactor bloc effectiveness for gasoline reforming process by application of mathematical model process // Proceedings of TPU, Tomsk. – 2004. – v. 307, – №1, – P. 119–121.

DESIGN OF COMPACT GENERATORS OF SYNGAS BY PARTIAL OXIDATION OF THE NATURAL GAS

A.P. Khristolyubov, O.F. Brizitskii, V.Ya. Terentyev, V.A. Sadykov*,

S.N. Pavlova*, Z.Yu. Vostrikov*, V.A. Kuzmin*

Institute of Experimental Physics, Sarov (VNIIEF), Russia

*Boreskov Institute of Catalysis, SB RAS, pr. Lavrentieva, 5, 630090, Novosibirsk, Russia,

e-mail: pavlova@catalysis.nsk.su

Introduction

Design of compact inexpensive reactors for syngas generation by partial oxidation of hydrocarbons including natural gas for mobile and stationary power-generating engines is now among the top priority problems of chemical engineering [1]. Syngas can be directly fed to solid oxide fuel cells or used as a fuel or fuel additive in the internal combustion (including diesel) engines [2]. Approaches to the reactor design including selection of a certain type of a catalyst depend upon the field of syngas generators application. For stationary fuel processors, generators should have replacement life not less than 40,000 h, while operation requirements are rather soft including start-up time up to several hours and a narrow range of steady-state performance variation (~ 0.75 of the nominal regime). For mobile application, replacement life could be shorter (not exceeding 5,000 h), while exploitation conditions are tougher including fast (less than 1 min) start-up along with a broad variation of the performance/load and environment conditions.

This paper presents results of research aimed at development of approaches to design of compact syngas generators for mobile and stationary fuel cells with capacity up to 10 kWt as well as for replacing a part of logistic fuel in the internal combustion engines.

Experimental

The basic approach to design of compact syngas generators was based on the integration of functions played by all their parts (a catalyst, an incorporated heat exchanger, feed preparation and start-up systems) as well as on the concept of conjugation of heat fluxes in the reactor. Design of generators for different application areas (mobile and stationary power – generating devices) was carried out with a due regard for the specific requirements to the capacity, size, start-up dynamics, replacement life, pressure drop, heat capacity and allowed thermal regimes.

Designed and manufactured generators were bench-tested using facilities of VNIIEF and BIC equipped with systems of feeds preparation and supply. Continuous control of the temperature profiles within selected parts of reactors and reformed feed composition was carried out using thermocouples, GC and sensors for O_2, H_2, CO_x , CH_x with the data acquisition and processing by PC.

Designed generators were equipped with a variety of catalysts including structured ones on different substrates (extruded ceramic honeycombs, fechraloy foil monolith, fechraloy ring plates and gauzes) or granulated catalysts on alumina supports (microspheres, granules or rings). The active components were comprised of mixed fluorite-like ceria-zirconia oxides with supported lanthanum nickelate and Pt [3].

Results and discussion

Axial-type syngas generators. Design of generators of this type (Fig. 1) was primarily aimed at achieving an efficient conjugation between the heat fluxes in different parts of the reactor, while minimizing the pressure drop. Such problem as a fast warming - up of the inlet feed by using a heat of the converted mixture was solved by using an in-built recuperative heat exchanger and heat-conducting catalysts on monolithic substrates made of fechraloy foil with the thickness varying along the layer length in the inlet zone. For the rear part of the layer where more slow endothermic reactions of methane steam and dry reforming occur, catalysts on high-surface-area monolithic corundum substrates were situated. Fig. 2 presents a general view of this reactor. A total volume of loaded monolithic catalysts is below 200 cm^3, which allows to convert up to 24 m^3/h of stoichiometric methane –air feed. At a room inlet temperature of the feed, methane conversion not less than 80% was achieved with the outlet temperature ~ 600 ^{o}C. The yield of syngas was in the range of 45-50% even at very high gas linear rates (Fig. 3). Such characteristics of syngas generator exceed those for known prototypes [1].

| **a** | **b** |
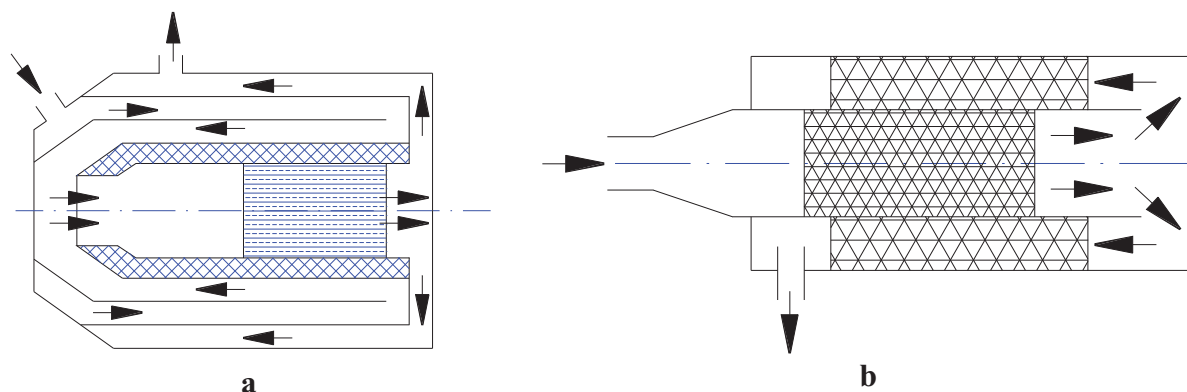
Fig. 1. Main schemes of the axial type reactors. a- reactor with incorporated heat exchanger; b – reactor with the reverse of the direction of the gas flowing through the catalytic layers with different compositions.

Fig. 2. A general view of the reactor with in-built heat exchanger
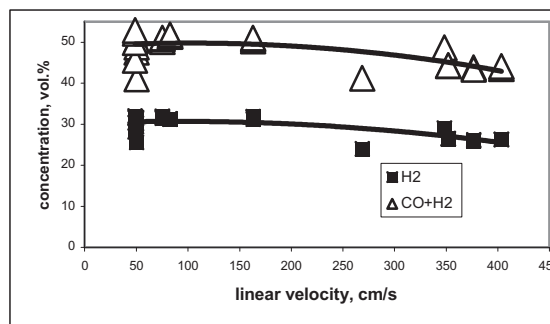
Fig. 3. Dependence of syngas and H_2 concentration on gas linear velocity. Contact time 0.03-0.3 s. 28 % of CH_4 in air, no feed preheat.

Such additional feature as incorporated fuel mixer situated immediately before the catalytic layer allows to efficiently mix pre-heated air and cool natural gas thus ensuring explosion safety and preventing undesirable ignition of the methane-air mixture in the heat exchanger at high loads.

Passing the electric current through the fechraloy spiral situated before the catalytic monoliths allows to make a fast cold start-up reaching a steady-state performance within 4 minutes.

Syngas generator with the reverse of the gas stream and system of a fast start-up

Design of this generator (Fig. 1b) was aimed at further minimizing the start-up time by warming the catalytic layer with the products of the natural gas combustion. Since in transient regimes the catalytic layer overheating could occur, this generator was equipped with thermally stable corundum-supported catalyst with the active component based upon lanthanum nickelate. A lean fuel –air mixture was ignited by using a car spark- plug, and resulted flame allowed to rapidly warm-up the inlet part of the catalytic layer. A minimum start-up period required for syngas appearance in the products was ~ 40 sec. A reverse of the gas stream allows to ensure an efficient transfer of heat through the internal reactor wall (Fig. 1b) from the inlet exothermic zone (where oxygen is consumed) into the outlet zone (where endothermic reactions of methane steam and dry reforming occur). Due to such a conjugation, even at the room inlet temperature of the feed, a yield of syngas up to 45 % was achieved.

Syngas generators of the radial type. A principal scheme of such a generator is shown in Fig. 4. A hollow internal part could be warmed up by an electric heater or by a flame burner. Several options of the catalytic layer design were checked including those where a central part is comprised of a stack of microchannel fechraloy ring plates covered by a catalyst able to efficiently transfer heat from the inlet part where the oxygen is consumed. This allows to avoid overheating of the metal support causing its burning out in oxygen at T> 1100 C.
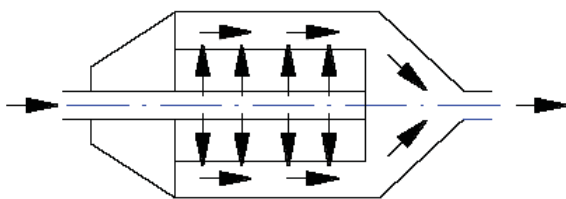
Fig. 4. A principal scheme of the syngas generator of the radial type
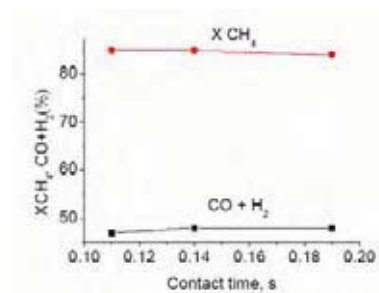
Fig. 5. Methane conversion and syngas yield vs. contact time for radial-type syngas generator with combined (ring plates + microspherical catalyst) layer

Around the central part, catalytic layers of a different types were situated including those on heat-conducting substrates (Fe-Cr-Al gauzes or felt with supported active component), granulated catalysts based upon alumina microspheres or rings etc, or their combination. This allows to ensure an efficient heat transfer in the radial direction as well as to minimize the pressure drop. At the feed rate up to 10 m^3/h of the stoichiometric natural gas –air mixture, this design allows to achieve syngas yield up to 50% at contact times up to 0.1 s (Fig. 5).

Conclusions

Approaches to design of compact syngas generators of the axial and radial types to be used in fuel processors for mobile and stationary fuel cells with the capacity up to 10 kWt were developed, experimental prototypes were manufactured and bench-tested. Integration of the start-up systems for start-up, reaction feed preheat and using of original heat-conducting catalysts and reactor parts to conjugate the heat fluxes within processor allowed to ensure a compact size of reactors (not exceeding 1L per 5 kWt of syngas thermal power) with syngas yield in the range of 45-55%.

References

[1] C. Song, Catal.Today 77 (2002) 17.

[2] V. Sobyanin, V. Sadykov, V. Kirillov et al. Proc. Intern. Hydrogen Energy Congress and Exhibition IHEC 2005, Istanbul, Turkey, 13-15 July 2005.

[3] V. Sadykov et al, Kinetics and Catalysis, 46 (2005) 227.

QUANTUM-CHEMICAL RESEARCH OF INHIBITOR ACTION MECHANISM

Kukueva V.V., Kirillov A.A.

Fire Safety Institute, Onoprienko 8, Cherkassy, Ukraine, 18034
FAX: +380472-55-09-71, e-mail: kukueva@yahoo.com

Inhibitors use for the delay, but sometimes and packed stops of chain reactions. Study of inhibition actions of fire suppressant powder on processes of combustion presents a big interest for the chemical kinetics, as far as hard surface of particles of powder can serve a good catalyst of heterogeneous ruins of carriers of reactionary chains. In the gas phase of molecule of powdered inhibitor (in the event of the evaporation) or their "splinter" (in the event of the decomposition), entering in reactions with active centers of flame ($H^\bullet$, $O^\bullet$, $CH_3^\bullet$, $OH^\bullet$), can slow a process of spreading a combustion in gas mixtures.

Action of powder can be stipulated as an increasing of velocity heterogeneous ruins of carriers of reactionary chains, so and homogeneous reactions following after the evaporation of particles of powder. For the clarification of question on that, through what channel is realized inhibition action of powder on processes of combustion - homogeneous or heterogeneous, vital importance has information on warm up particles of powder in the flame. Necessary condition to realization of homogeneous mechanism is having warmed up particles before such temperatures, which will ensure sufficiently greater velocity of evaporation. Unfortunately reliable experimental methods for execution of the similar measurements are very limited therefore greater value gain approximate theoretical calculations. The general goal is the prediction of measurable catalytic kinetics based on mechanistic information for every elementary reaction step in the overall cycle, as well as competing phenomena operative at catalytic conditions. A competition exists between the rate of dissociation and the rate of recombination with negative catalyst. Quantum-chemical methods are reliable tools which can be used to probe ideas and predict properties, that is, structure and energetic. They have made important contributions toward mechanistic understandings of various catalytic chemistries through reaction mode analysis in terms of detailed orbital interactions [1].

The present model stresses the importance of gas phase reactions of hydrogen atoms. A critical review of the literature is in progress and some of the preliminary observations are presented. Important hydrogen atom reactions can be divided into three categories:

(1) The rate limiting branching reaction, $H^\bullet + O_2 \rightarrow OH^\bullet + O^\bullet$.

(2) Bimolecular reactions, $H_2 + RX \rightarrow H_2$ or $HX + R'$, with inhibition expected if the new radical, R', is less reactive than the hydrogen atom.

(3) Recombination reactions, $H^{\bullet} + R + M \rightarrow HR + M$.

The mechanism of homogeneous inhibition of flame was discussed from three standpoints: first, the possibility that flame inhibition is an equilibrium phenomena was investigated by calculating adiabatic flame compositions and temperatures; second, the possibility that a partial equilibrium established before three body reactions become important was investigated; and third, the possibility that inhibition is controlled by kinetic phenomena early in the flame was investigated using an ultra simple flame model. It was concluded that neither equilibrium nor partial equilibrium changes in radical concentration and temperature were large enough to account for the effects of chemical inhibitors. Therefore, inhibition was believed to be kinetic phenomena.

The model proposed for examining the kinetic effects and understanding the details of the inhibition process consists of two reaction regions: (1) a low temperature initial region where radicals are destroyed; recombination is dominate here because of the negative temperature dependence of the reaction rate; and (2) a branching zone where high radical concentrations are produced. This region occurs at temperatures higher than the recombination region, but still significantly below the final adiabatic flame temperature. The two regions are coupled by diffusion. The boundary between the two regions is the point at which the rate of the branching reaction first balances the recombination reaction. The action of the inhibitor is postulated to be the addition of terms in the initial radical sink region. This forces the cross over temperature up and radical concentrations down in agreement with observations. If radical scavenging reactions are dominant in inhibition, the model predicts that the reduction the burning velocity is significant. The scavenging effectiveness of inhibitor molecules is very difficult to investigate experimentally. Besides it is impossible predict correctly if inhibition happens by whole molecules or separated particles after decomposition. Theoretical methods give us possibility to research such unstable reactions.

The scavenging agent can be the inhibitor itself, or its stable and unstable breakdown products. The elementary reactions during the flame inhibition have been investigated by the ab initio method with 6-31 G basis set. The scavenging efficacy during intermolecular interaction between active centers of flame ($O^{\bullet}$, $OH^{\bullet}$, $H^{\bullet}$) and flame inhibitors destruction products have been estimated by the binding energy value. The most effective fire suppressants have been choosing for the study: diethyl amine ((C_2H_5)$_2$NH) and three fluorine bromine methane CF_3Br. The destruction ways of the inhibitor molecules shows the active inhibition agents. For the diethyl amine the more probable reaction channel for destruction:

$(C_2H_5)_2NH \rightarrow 2C_2H_5^\bullet + NH$: ($\Delta H^0_{298} = 39,19$ kcal/mol), three fluorine bromine methane: $CF_3Br \rightarrow CF_3^\bullet + Br^\bullet$ ($\Delta H^0_{298} = 33,77$ kcal/mol). The following step of research was the calculation of intermolecular interaction between active centers of flame (ACF) and active inhibiting components. The results of calculations are shown in the table 1.

Table 1. The calculation by ab initio method in the 6-31 G basis set of the interaction between active centers of flame and destruction products of fire suppressants

№ п/п	ACF	Active inhibiting components			
		$NH^\bullet$	$C_2H_5^\bullet$	$CF_3^\bullet$	$Br^\bullet$
2	$H^\bullet$	0.0935	0.1344	0.1398	0.0819
3	$OH^\bullet$	0.3949	0.0781	1.7278	0.0077
5	$O^\bullet$	0.1194	0.1811	-	9.8216

As we can see from the calculation results the most efficient scavenger of active centers of flame is bromine atom because it can to bind as well as $H^\bullet$ and $OH^\bullet$. For the diethyl amine destruction leads to three active components, which can interact with $H^\bullet$ ($NH^\bullet + 2H^\bullet \rightarrow NH_3$) and $OH^\bullet$ ($C_2H_5^\bullet + OH^\bullet \rightarrow C_2H_5OH$). So, the inhibiting activity has been explained by the quantum-chemical calculations. In generally the fire suppressants destruction products can be arranged in such order by their activity: $Br^\bullet \rightarrow C_2H_5^\bullet \rightarrow NH^\bullet$. As far as the halogenated fire suppressants are dangerous for ecology of the environment, we can recommend the application of the diethyl amine as inhibitor agents in the chain combustion. These results are in good agreement with experimental results [1].

Thus, results of our research can confirm the inhibition mechanism [2] as following:

$$X + Inh\ (+M) \rightarrow InhX\ (+M) \qquad (R.1)$$
$$X + InhX \rightarrow X_2 + Inh \qquad (R.2)$$
$$X + X \rightarrow X_2 \qquad (R.3)$$
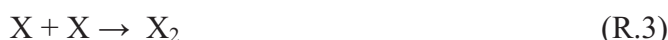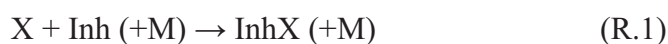
where X – active centre of flame, and Inh represents the inhibiting species. Inherent in these reactions is not only the scavenging of the radical be the inhibitor species but also its regeneration. Hence, an amplifying effect occurs, as each inhibitor molecule is able to neutralize more than one reactive radical. So among investigated in our work inhibitors the most effective is diethyl amine, because almost all of destruction products act on the all of active reaction centers, in spite of the fact that for molecule CF_3Br destruction and interaction energy significantly less.

References

1. N.Vora, J.E.Siow, N.M.Laurendeau, Combustion and flame 126: 1393-1401 (2001)
2. Babushok V., linteris G.T., Tsang W., and Reinelt D., Combustion and flame, 115: 551-560 (1998)

NANOFIBROUS CARBON AS A CATALYST
FOR SELECTIVE OXIDATION OF HYDROGEN SULPHIDE

Gennady G. Kuvshinov*, Vasiliy V. Shinkarev**, Alexey M. Glushenkov*,

Maxim N. Boyko*, Dmitriy G. Kuvshinov*

*Novosibirsk State Technical University, Department of Chemical Engineering, Pr.Karla Marksa, 20, Novosibirsk, Russia, 630092, fax: 007(383)3460801, email: tpa@ngs.ru

**Boreskov Institute of Catalysis SB RAS, Group of Catalytic Technologies of Carbon Materials Synthesis, Pr.Akademika Lavrentieva, 5, Novosibirsk, Russia, 630090, fax: 007(383)3308056, email: shinkarevv@mail.ru

1. Introduction

Hydrogen sulphide is one of the most toxic and dangerous for ecosphere materials. The most common way for it to get into atmosphere is through man-caused factors, since most of the natural resources, including copper ore and energy resources (such as oil, gas, coil, geothermal vapor etc.) comprise considerable amounts H_2S. Processing of hydrogen sulphide into sulphur is preferable from the ecological standpoint, because elementary sulphur is a safe, universal and easy transported raw material for various manufactures. The only large-scale technology for obtaining the sulfur from the sulfur-bearing gas today is the Clauss multi-stage process [1]. Though because of the process's reversibility it is impossible to obtain the 100% conversion of hydrogen sulphide for one stage. The direct selective oxidation of H_2S by molecular oxygen makes it possible to reduce the number of stages and to rise the efficiency of desulfurization, to miniaturize the equipment.

It is known that for direct H_2S oxidation the metal-oxide catalysts and activated carbons [2] can be used. The significant disadvantage of metal-oxide catalysts is their deactivation, or considerable reduction of selectivity, or unstability in excess of oxygen and water vapors. The application of activated carbon is effective in low temperatures only (lower the 150 °C), that is why they can be used in periodic mode only.

Nanofibrous carbonaceous materials (NFC) produced in the hydrocarbons decomposition with 8-group metals catalysts are the materials of the new class and can be applied in various spheres. Recently the unique properties of NFC have been discovered. NFC can catalyze the reaction of selective molecular oxygen oxidation of hydrogen sulphide[3].

PP-108

The goal of the research was to study the influence of the NFC samples' structure, of the remains of metal phase of original catalyst of NFC synthesis and water vapor content in reaction medium on activity and selectivity of hydrogen sulphide direct oxidation into sulfur.

2. Samples

NFC samples were obtained in the result of decomposition of methane over nickel-containing catalysts in the form of mesoporous granules of diameters less then 0,5 mm, which consist of tightly twisted graphite-like fibers or nanotubes of diameters of 5-150 nm. The inner surface of granules is made of graphite basal planes or edges of graphite basal planes, which orient to the surface angularly dependent of NFC origin catalyst. The **NFC-1, NFC-2 and *NFC-3*** samples was synthesized form methane in the temperature of 675 and 550 ^{0}C correspondingly.

Table 1 - Samples description.

Sample	Original catalyst composition, %	Carbon yield, g_{CFC}/g_{cat}	Specific surface area A_{BET}, m^2/g
NFC-1	62 Fe – 8 Ni / Al$_2$O$_3$	122	155
NFC-2	10 Cu – 80 Ni / Al$_2$O$_3$	230	251
NFC-3	90 Ni / Al$_2$O$_3$	80	110

3. Experimental techniques

Catalytic properties of NFC were investigated in flow reactor. The catalyst bed was fluidized by the reactor oscillating in an axial direction. The typical conditions are: temperature of 200 °C, gas mixture 1 % vol. H$_2$S + 15 % vol. O$_2$ (30-times excess oxygen to stoichiometric content), the rest is helium, gas hourly space velocity (GHSV) 3100 hr^{-1}.

4. Results and discussion

The obtained data on the change of conversion of hydrogen sulphide and selectivity of its transformation into sulfur against time are presented on the Fig. 1. The highest selectivity (about 89 %) is typical for **NFC-1**. There is an interesting initial fall of selectivity and its posterior rise to almost the same level. It is the evidence of the fact that there was possibly the gradual formation of non-selective compounds on which the total oxidation of hydrogen sulphide took place. This corresponds the area of falling selectivity. Then there was a rapid formation of selective surface compounds – it corresponds the area of selectivity's rise to the previous level. **NFC-2** sample demonstrated the lower but stable selectivity. **NFC-1** sample shows higher selectivity due to the fact that its surface (graphite planes) has less surface energy comparing to the one of **NFC-2** (the ends of basal planes). **NFC-3** proved to be the least selective and stable.

The most active sample is **NFC-2** (Fig. 1), where hydrogen sulphide conversion was about 95 %. It is possible to suppose that the difference between **NFC-1** and **NFC-2** as in the case of selectivity can be linked with the difference of structure of carbonaceous fibers, and their surface in particular: the ends of basal planes have higher surface energy comparing to the surface energy of basal planes, and due to this the processes of reagents sorption can go faster on the surface of **NFC-2**, and this results in the rising activity. Moreover the specific surface area of **NFC-2** sample is 1,6-times bigger than the one of **NFC-1** (Table 1).
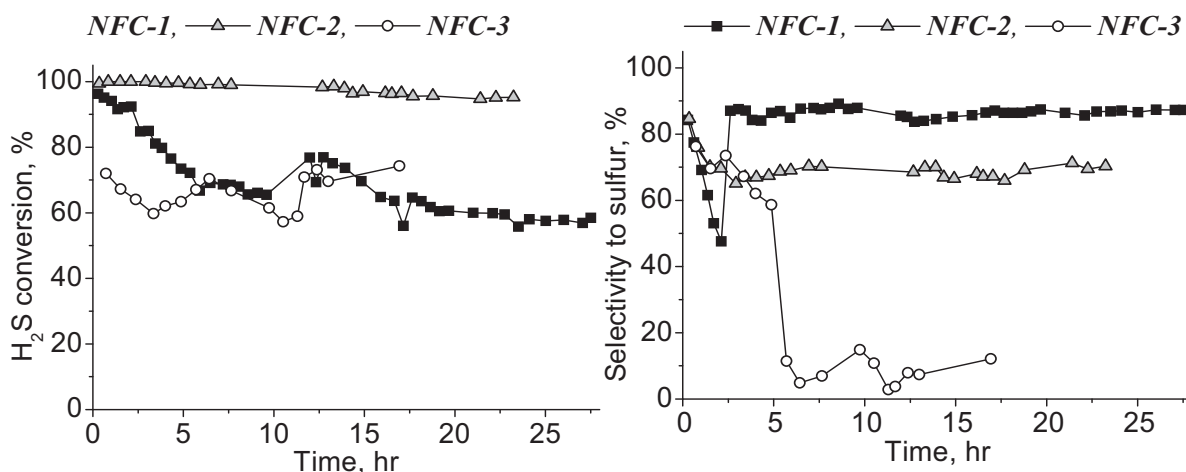
Figure 1 -Deactivation patterns with time on stream. GHSV=3100 hr^{-1}, T=200 ^{0}C
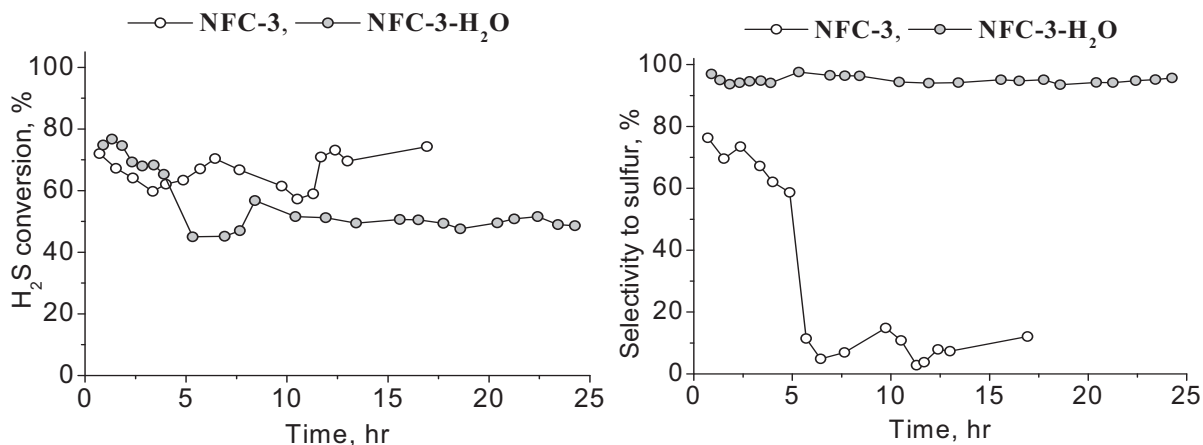
Figure 2 - Deactivation patterns with time on stream. GHSV=3100 hr^{-1}, T=200 ^{0}C

The study of samples, obtained over copper-nickel catalysts with different carbon yields demonstrated that with the growth of the yield the selectivity rises and the conversion falls [5]. Indeed, it is known that the hydrogen sulphide oxidation over nickel catalysts can be realized quite effectively in temperature of already 100 °C [6], that is why even non-significant access of hydrogen sulphide and oxygen to metal surface in 200 °C can lead to the decrease of selectivity due to the oxidation of H_2S into SO_2. It can explain the low selectivity of **NFC-3**, and the samples with low specific yield of carbon per weight unit of catalyst. The

unstable work of **NFC-3** can be explained by the sulfur accumulation on the surface and its cyclic burning in the conditions of excess oxygen under the catalytic influence of the metal phase.

Catalytic properties of the **NFC-3-H₂O** with addition of the 40 % vol water vapor in gas stream was significant changed (Fig. 2), catalyst began to work more stable. Selectivity with time on stream practically didn't decreased and was about 95 % during whole experiment. At the same time some falling of the activity of the **NFC-3-H₂O** sample have taken place.

5. Conclusion

Thus the samples with the highest activity and selectivity are those with graphite planes which are situated perpendicularly to the axis of fiber and nanotube. And nanotubes have higher selectivity, though copper-nickel sample possess higher activity. An addition of the 40 % vol. of water vapor in initial gas mixture significantly improves catalytic properties of the NFC formed by the set of put one into another coned graphite basal planes. It is possible to increase the selectivity by decreasing the influence of metal phase, i.e. by obtaining the NFC with the bigger specific yield of carbon. It is possible to additionally increase the selectivity by synthesizing the NFC samples with more ordered structure of the surface: the defects bear higher activity and can catalyze the total oxidation of hydrogen sulphide. The activity of samples can be increased by decreasing the diameters of fibers.

References

[1]   British Patent Application No.3608, 1882.

[2]   O.Bankovski and R.Pastemak, Ger. (East) Pat.12.805, Mar. 1, 1957.

[3]   Kuvshinov G.G., Moguilnykh J.I., Lebedev M.J., Kuvshinov D.G., Zavarukhin S.G. The method to obtain the elemental sulfur. Patent № 2111164, 1997.

[4]   Mogilnykh Yu. I., Kuvshinov G. G., and Lebedev M. Yu. //Filamentary carbon as a catalyst of hydrogen sulfide oxidation to sulfur. Extended abstracts of conference "EUROCARBON '98", Strasbourg, France, pp. 445-446, 1998.

[5]   G.G. Kuvshinov, V.V. Shinkarev, A.M. Glushenkov, M.N. Boyko, D.G. Kuvshinov. Catalytic Properties of Nanofibrous Carbon in Selective Oxidation of Hydrogen Sulphide. // The Seventh World Congress on Recovery, Recycling and Re-integration is held in Beijing, People's Republic of China, September 25~29, 2005. p. 8.

[6]   N. Keller, C. Pham-Huu, C. Crouzet, M.J. Ledoux, S. Savin-Poncet, J.B. Nougayrede, J. Bousquet. Direct oxidation of H2S into S. New catalysts and processes based on SiC support. Catalysis Today, 53 (1999) 535-542.

C7 HYDROISOMERIZATION ON ZIRCONIA SUPPORTED CATALYSTS

Yan Liu

Applied Catalysis Group, Institute of Chemical and Engineering Sciences, 1 Pesek Road, Jurong Island, Singapore 627833; Email: liu_yan@ices.a-star.edu.sg; Fax: 0065-63166182

New environmental regulations impose the elimination of regulated gasoline additives such as tetraethyl lead and the reduction of aromatic compounds because of their detrimental environmental effects [1], which may be accompanied by a loss in the octane number. Consequently there has been a sharp rise in the requirements for octane enhancement processes. One potential way is to isomerize the straight-chain paraffins, which are a major constituent in some crude oil fractions, with a low octane number, into their branched isomers with a higher octane number. Such isomers are ready to be used as a blending stock for gasoline obtained from reforming to produce "ultra clean" fuel.

The current catalytic processes for alkane isomerization and alkylation require liquid acids (e.g., H_2SO_4, HF, $AlCl_3$) or halogen-promoted metal oxides (e.g., $Cl-Al_2O_3$), which pose significant containment, corrosion, and environmental challenges [2]. These problems can be circumvented by the development of strong solid acid catalysts consisting of metal oxides. Recently, metal oxides promoted by sulfur compounds have been studied as strong solid acid catalysts, especially SO_x promoted zirconia containing noble metal to inhibit deactivation [3]. However, their low isomerization selectivity for C_7-alkanes, their poor stability, and their tendency to form volatile sulfur compounds during catalysis and regeneration limit their applicability in isomerization and alkylation process. Tungesten oxide based materials comprise another interesting class of solid acids. The small and highly charged W^{6+} cations are found in several solid acids such as WO_x dispersed on Al_2O_3 and ZrO_2 [4,5]. In this work, ZrO_2 supported Pt/WO_3 solid acid catalysts promoted by Y_2O_3 and ZnO, in addition to ZrO_2 supported Pt/PO_4^{3-} catalysts, were studied and compared with Pt/β catalysts for n-C_7 hydroisomerization.

Experimental

$Zr(OH)_4$, $Y(OH)_3-Zr(OH)_4$, $Zn(OH)_2-Zr(OH)_4$ were prepared by precipitation. Pt, WO_3, and PO_4^{3-} were introduced by impregnation. XRD, XPS, SEM, and an automated adsorption apparatus were employed for characterization. Catalytic activity analysis was

carried out at atmospheric pressure in a tubular quartz glass, fixed-bed reactor. Before catalytic measurements, the catalysts were reduced by hydrogen for activation. The outlet gas mixture was analyzed using on-line GC.

Results and Discussion

Pt/WO$_3$/ZrO$_2$ catalysts modified by Y$_2$O$_3$ and ZnO are employed in n-C$_7$ hydroisomerization reaction and compared with Pt/PO$_4^{3-}$/ZrO$_2$ and Pt/β catalysts. It is found that Pt/WO$_3$/ZrO$_2$ shows good activities for n-C$_7$ hydroisomerization. N-C$_7$ conversion and C$_7$ isomers selectivity can be 78.5% and 75.1%, respectively, at 250 °C. It is comparable with that for Pt/β catalysts with Si/2Al ratio at 100, which is 87.1% for n-C$_7$ conversion and 75.5% for C$_7$ isomers selectivity. When 1% Y$_2$O$_3$ is introduced to Pt/WO$_3$/ZrO$_2$ catalysts, n-C$_7$ conversion keeps almost the same at 79.2% while C$_7$ isomers selectivity obviously increases to 89.1%. It is due to Y$_2$O$_3$ can stabilize the tetragonal phase [6,7]. However, the n-C$_7$ conversion decrease with large amount of Y$_2$O$_3$ added while the C$_7$ isomers selectivity increase along with the amount of Y$_2$O$_3$, as shown in Fig. 1 (250 °C). It is also found that the precipitation agent can affect the activities for Pt/WO$_3$/Y$_2$O$_3$-ZrO$_2$ catalysts. The catalysts using NH$_3$ as the precipitate show much higher activities than the catalysts using urea and NaOH as the precipitates.
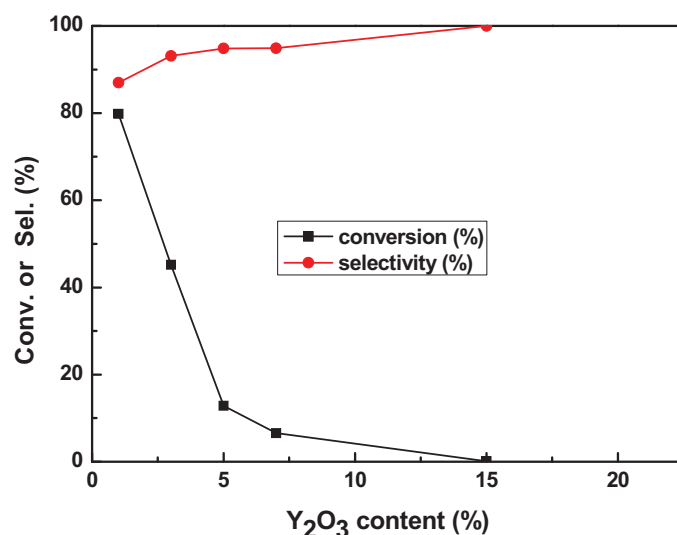
Fig. 1 The effect of Y$_2$O$_3$ amount on n-C$_7$ catalytic performance.

Among the catalysts investigated, Pt/PO$_4^{3-}$/ZrO$_2$ shows the lowest activity for n-C$_7$ hydroisomerization. The n-C$_7$ conversion and C$_7$ isomers selectivity can only be 2.2% and 36.2% at 250 °C (42.1% and 37.1% at 300 °C), which is much lower than those for Pt/WO$_3$/ZrO$_2$ and Pt/β catalysts. It is due to the weak acidity for PO$_4^{3-}$. The further

experiments found that the activity for Pt/PO$_4^{3-}$/ZrO$_2$ decrease with the reaction time at 300 ^{o}C. After 48 h, the n-C$_7$ conversion and C$_7$ isomers selectivity can only be slightly higher than 30%. It is suggested PO$_4^{3-}$/ZrO$_2$ has the low stability. Previous investigation indicates the activity for Pt/WO$_3$/ZnO-ZrO$_2$ can keep stable at least 82 h with 80.9% n-C$_7$ conversion and 89.1% C$_7$ isomers selectivity at 250 ^{o}C.

References:

1. I. E. Maxwell, J. E. Naber, *Catal. Lett.* **12** (1992) 105.

2. J. M. Thomas, *Sci. Am.* **266** (1992) 112.

3. E. Iglesia, S. L. Soled, G. M. Kramer, *J. Catal.* **144** (1993) 238.

4. S. L. Soled, G. B. Mc Vicker, L. L. Murrell, L. G. Sherman, N. C. Dispenziere, S. L. Hsu, D. Waldman, *J. Catal.* **111** (1998) 286.

5. M. Hino, K. Arata, *J. Chem. Soc. Chem. Commun.* (1987) 1259.

6. M. Li, Z. Feng, P. Ying, Q. Xin, C. Li, *Phys. Chem. Chem. Phys.* **5** (2003) 5326.

7. A. Gedanken, R. Reisfeld, E. Sominski, O. Palchik, Y. Koltypin, G. Panczer, M. Gaft, H. Minti, *J. Phys. Chem. B* **104** (2000) 7057.

PP-110

PREPARATION AND CHARACTERIZATION OF HETEROGENEOUS ENZYMATIC CATALYST FOR BIODIESEL PRODUCTION

*<u>A. Macario</u>[1], G. Giordano[1], L. Setti[2], A. Parise[3], E. Perri[3], J.M. Campelo[4], D. Luna[4]

[1]*Dip. Ing. Chim. & Mat., Università della Calabria, I-87030 Rende (CS), Italy*
[2]*Dip. Chim. Ind. & Mat., Università degli Studi di Bologna, I- 40136 Bologna – Italy*
[3]*Exsperimental Institute of Olive-Growing, I-87030 Rende (CS), Italy*
[4]*Dip. Org. Chem., Cordoba University, Av. San Alberto Magno s/n, E-14004 Cordoba - Spain*
*Corresponding author. Fax +39.0984.49.66.55; e-mail: macario@unical.it

In this paper, the preparation and characterization of the *Rhizomucor miehei* Lipase/zeolite catalyst is reported. In order to obtain an efficient heterogeneous enzymatic catalyst two different immobilization method of Lipase enzyme on zeolite type supports are investigated. Concerning the adsorption method, the zeolite materials have been prepared in order to obtain supports having different physical-chemical surface properties. The immobilization test shows that the zeolitic support prepared in F^- media allow to attach the highest protein amount (280 mg/g) with respect to those ones obtained in alkaline system (200 mg/g). An immobilization yield of 99% by covalent attachment is obtained. A simple and fast method for testing the catalytic activity by an alkyl ester hydrolysis reaction was used in order to investigate the interactions between the enzyme and the support. Stability, leaching and total productivity of the immobilized enzyme were also measured. These preliminary catalytic results let to choose the more suitable Lipase/Support system to use as catalyst for tuning of the heterogeneous enzymatic transesterification reaction of olive oil.

Introduction

The conventional biodiesel technology involves the use of inorganic homogeneous basic catalyst (sodium hydroxide, potassium hydroxide and sodium or potassium methoxide) and methanol. Particularly, the potassium hydroxide is the most efficient basic catalysts, because its highest reaction kinetic rate compared to the NaOH and NaOMe catalysts [1]. The main disadvantages of a homogeneous basic catalyst is the presence of saponification reaction during the transesterification process, that reduce the biodiesel production efficiency. The amount of soap-products increases as a function of free fatty acids into the triglycerides source. Moreover, if the vegetable oil and the alcohol used are not water-free, the biodiesel yield decreases because the hydrolysis of esters could take place. At the contrary, the

enzymatic transesterification allows to obtain a process without any by-product and starting from any triglycerides source. In presence of an alcohol (methanol, ethanol, etc.) lipases are able to catalyze the alcoholysis reaction. Glycerol is the by-product of the reaction which can be easily separated from the produced esters by centrifugation. In general the reaction conditions of an enzymatic process needs less energy consuming and neutral pH. In order to improve the lipase stability, the enzyme immobilization is an attractive method for industrial applications. There are several method for the enzymatic immobilization: adsorption, covalent binding, cross-linking and containment in a barrier (e.g. microencapsulation, entrapment and confinement). The zeolites and related materials have potentially interesting properties, such as hydrophobic/hydrophilic behavior, acid/basic character, mechanical and chemical resistance so that the use of these materials as enzyme-support is of great interest. Additional advantages is represented by their easy water dispersion/recuperation. Therefore, the compositional and structural variances of molecular sieves offer a powerful tool for tuning the carrier adsorption properties. The immobilization of Lipase enzyme in biodiesel production combines the enzymatic transesterification advantages with those of a heterogeneous catalysis. Moreover, the particularly conformation of lipase enzyme suggests that the most suitable immobilization method of this enzyme have to involve the "*lid*" region of the same enzyme in order to obtain the activation of its catalytic center [2]. Immobilization by adsorption technique permits a suitable interaction between enzyme and support surface that allow to obtain the request enzyme adsorbed in the "open" conformation. At the contrary, the covalent attachment presents a stable enzyme immobilization without its "interfacial activation". In the present work the adsorption of lipase enzyme on Silicalite-1 type zeolites and the covalent attachment of the same enzyme on functionalized Sepiolite/AlPO$_4$ material, are described. The preliminary catalytic results show that the acid-basic interactions between enzyme and the external surface of the support allow the opening of the *lid*-enzyme and the activation of the catalytic enzyme centre. The performance of the so prepared heterogeneous biocatalyst are evaluated in the biodiesel production by the transesterification of olive oil with methanol and in solvent-free system.

Experimental

The preparation of Silicalite-1 type zeolites and the Sepiolite/AlPO$_4$ functionalized material were carried in according to the procedure published elsewhere [3-5]. The amount of adsorbed enzyme was evaluated by UV adsorption method ($\lambda = 280$ nm), while the amount of the enzyme covalently attached was determined by the measurements of the hydrolysis esters activity using a fast and simple colorimetric method of the initial immobilization solution and

the supernatant obtained after immobilization. The hydrolysis of methyl myristate to myristic acid, carried at 40°C and pH 7, is the preliminary catalytic test used to know the immobilized enzyme conformation. The transesterification reaction was carried out at 40 °C and with methanol/oil molar ratio equal to 5/1. The triglycerides source has been the olive oil (79.9 % in oleic acid and 16.1% in palmitic acid). At pre-determined time, 2 µl aliquots of reaction medium were taken and diluted in n-hexane for GC-analysis. For quantitative analysis, the methyl pentadecanoate was used as standard ester.

Results and discussion

The results of the immobilization technique by adsorption show that the protein is preferably adsorbed on the surface of the support synthesized in fluoride media (F-S2 containing 280 mg/g of Lipase). For these materials, the presence of five-coordinate silicon $[SiO_{4/2}F]^-$ units might generate electrostatic bonds between the amino acid of the enzyme and the support surface. Concerning the materials synthesized in alkaline media (S2 containing 200 mg/g of Lipase), the weak acid silanol groups constitute the main support surface sites involved during the protein adsorption. However, the highest immobilization yield was obtained by the covalent technique on Sepiolite/AlPO4 in the presence of 433 mg/g of Lipase. These different kind of enzyme bindings have a strong influence on the immobilized lipase conformation and, then, on the catalytic activity of the heterogeneous biocatalyst (Figure 1). In fact it is possible to observe that the highest methyl ester conversion occurs when the enzyme is physically adsorbed on the support S2 (Silicalite-1 synthesized in alkaline system) (Figure 1). For this support type, the binding forces with the enzyme are the acid-basic ones and, probably, occur between the acid Si-OH zeolite groups and the basic aminoacid *Arginina* that constitutes the hinge region of the lid-enzyme [6].
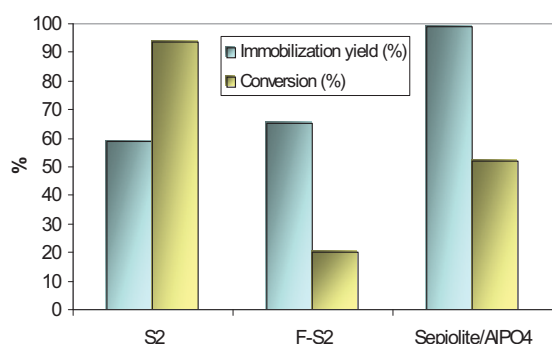
Figure 1. Lipase immobilization yield and methyl myristate conversion after 24 h of reaction at 40°C.
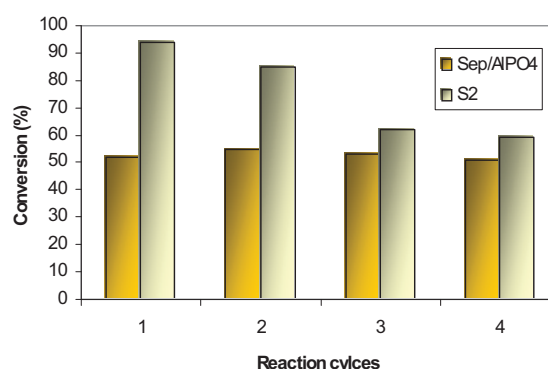
Figure 2. Stability of immobilized Lipase during four batch reuses in the hydrolysis of methyl myristate reaction.

When the enzyme is covalently attached on the functionalized Sepiolite/AlPO4 support, the highest amount of enzyme is immobilized by very stable bonds, no leaching occurs until

four reaction cycles but the total productivity of the enzyme is lower than that obtained with the lipase adsorbed on the S2 support by acid-basic interaction (Figure 2 and 3). These last results suggest that the most covalently immobilized enzyme is not completely active.
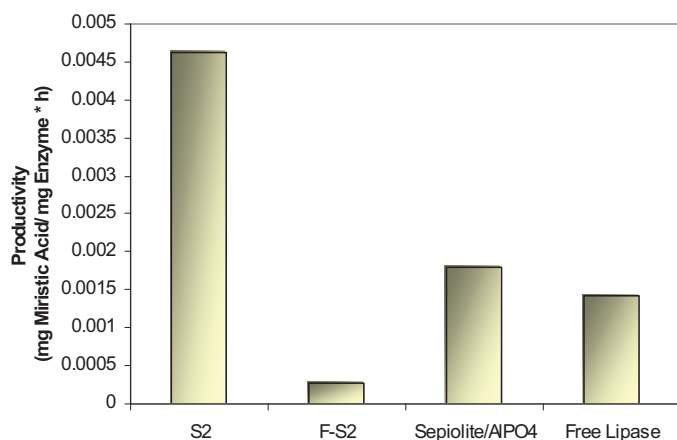
Figure 3. Productivity of heterogeneous Lipase catalyst in the methyl myristate hydrolysis reaction (four batch reuses). Comparison with the productivity of 100 mg of free lipase for each batch use.

After these preliminary activity test, the Lipase/S2 and Lipase/Sepiolite/AlPO$_4$ catalyst are used in the transesterification reaction. The Lipase adsorbed (80 mg) by acid-basic interaction on the S2 support shows the same oleic acid conversion (69%) which was obtained by the free enzyme (100 mg) after only 2 hour of reaction at 40 °C. Concerning the Lipase covalently attached on the Sepiolite/AlPO$_4$, about the same immobilized enzyme amount (73 mg) allows to obtain a oleic acid conversion of 22%. These preliminary transesterification tests confirm the results obtained by the hydrolysis reaction about the final conformation of the immobilized enzyme. The simple regeneration of the support used for the Lipase immobilization is an important aspect to be considered in the heterogeneous catalyst preparation. The deactivated enzyme on the support S2 was completely removed by simple thermal treatment (4 hours at 400 °C in air) and the regenerated support showed the same immobilization yield as in the first application. Moreover, the activity of the Lipase adsorbed on the regenerated support remains unaltered. Finally, the optimization of the transesterification parameters are necessary in order to increase the methyl esters produced by the understudied immobilized biocatalysts prepared.

References

[1] B. Freedman, E.H. Pryde, T.L. Mounts, J. Am. Oil Chem. Soc., 61 (1984) 1638-1643.

[2] R. Fernandez-Lafuente, P. Armisen, P. Sabuquillo, G. Fernandez-Lorente, J.M. Guisan, Chem. Phys. Lipids, 93 (1998) 185-197.

[3] Macario A., Katovic A., Giordano G., L. Forni, F. Carloni, A. Filippini, L. Setti, Stud. Surf. Sci. Catal.,155 (2005) 381-394

[4] Frontera P., Macario A., Katovic A., Crea F., Giordano G., Stud. Surf. Sci. Catal., 158/A (2005) 383-390

[5] F.M. Bautista, M.C. Bravo, J.M. Campelo, A. Garcia, D. Luna, J.M. Marinas, A.A. Romero, J. Chem. Technol. Biotechnol, 72 (1998) 249-254

[6] S. Herrgard, C.J. Gibas, S. Subramaniam, Biochemistry, 39 (2000) 2921-2930

PP-111

PRODUCTION OF HYDROGEN BY STEAM REFORMING OF ETHANOL USING Co AND Ni CATALYSTS SUPPORTED ON PEROVSKITE-TYPE OXIDES

M. Matsukata, K. Urasaki, K. Ishikawa, K. Tokunaga, Y. Sekine and E. Kikuchi

Department of Applied Chemistry, Waseda University, 3-4-1, Okubo, Shinjuku, Tokyo, 169-8555, Japan; *Tel&Fax: +81-3-5286- 3850, E-mail: mmatsu@waseda.jp

Abstract

H_2 production by steam reforming of ethanol was examined using Co or Ni catalysts supported on $LaAlO_3$, $SrTiO_3$ and $BaTiO_3$. Their catalytic activities and resistance to coking were compared to those of conventional Co or Ni catalysts supported on MgO and γ-Al_2O_3. Co and Ni catalysts supported on $LaAlO_3$ and $SrTiO_3$ showed higher catalytic activities and better long-term stabilities than those supported on MgO. We found that $LaAlO_3$ and $SrTiO_3$ could suppress carbon deposition, which caused the deactivation of Co and Ni catalysts supported on MgO. $Co/BaTiO_3$ showed a lower catalytic activity and poorer coke resistance. TEM study indicated that the particle size of Co over $BaTiO_3$ was larger than that over $SrTiO_3$. We consider that the lattice oxygen in perovskites may play positive roles in hindering coking and $Co/SrTiO_3$ has more frequent participation of lattice oxygen in ethanol steam reforming in comparison with $Co/BaTiO_3$.

Introduction

In recent years, H_2 production by the catalytic steam reforming of ethanol (equations (1) and (2)) has been studied as one of effective methods for utilizing biomass–derived ethanol without energy intensive and rather expensive distillation processes. Among non-precious metals, supported Co and Ni catalysts are catalytically active for the steam reforming of ethanol, while coke formation and sintering often cause catalyst deactivation[1,2]. An effective approach to developing a highly active and stable catalysts is to focus on the selection and modification of catalyst supports. Several researchers pointed out that La_2O_3[3], ZnO[4] and MgO[5] were effective as supports for Co or Ni in the steam reforming of ethanol.

$C_2H_5OH + H_2O \rightarrow 2CO + 4H_2$ (1)

$C_2H_5OH + 3H_2O \rightarrow 2CO_2 + 6H_2$ (2)
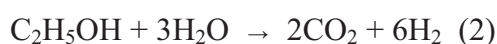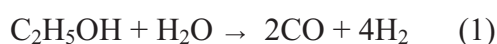
We have previously reported that $Ni/LaAlO_3$ and $Ni/SrTiO_3$ show high catalytic activities and durabilities for the steam reforming of methane at 1073 K possibly because the lattice oxygen in perovskites promotes the oxidation of CHx and hinders the production of inactive carbonaceous species[6]. Based on these results, we have tried to apply $SrTiO_3$ to Co and Ni catalysts for the steam reforming of ethanol at 823 K and found that $SrTiO_3$ is suitable as the support of Co and Ni in comparison with conventional MgO[7]. The aim of this study was to investigate the catalytic activities and stabilities of Co and Ni catalysts supported on perovskites including $SrTiO_3$, $LaAlO_3$ and $BaTiO_3$ for the steam reforming of ethanol in detail.

Experimental

The preparation methods of Co and Ni catalysts supported on $LaAlO_3$, $SrTiO_3$ and $BaTiO_3$ were described elsewhere[6,7]. The amounts of Co and Ni loaded were 5 wt% as metal. Catalytic activities were tested in a continuous flow reactor with a fixed bed of catalyst at 823 K and atmospheric pressure, and a molar H_2O/C_2H_5OH fed was 10. Before starting the activity test, catalysts were reduced at 873 K for 1 h in a hydrogen stream.

Results and Discussion

Steam reforming of ethanol has been performed using Co catalysts supported on perovskite-type oxides including $LaAlO_3$, $SrTiO_3$ and $BaTiO_3$, MgO and γ-Al_2O_3. Table 1 summarizes the results. Hydrogen yield was defined as $F_{H2out} \times 100 / (3 \times F_{C2H5OH}^{in} + F_{H2O}^{in})$, where F_{H2out} is the formation rate of hydrogen, F_{C2H5OH}^{out} is the feed rate of ethanol, and F_{H2O}^{in} is the feed rate of H_2.

Catalytic activities of Co and Ni catalysts significantly depended on the kind of catalyst support. Although Co/γ-Al_2O_3 gave the highest ethanol conversion among the catalysts tested, a larger parts of ethanol was consumed to give C_2H_4 resulting in a low H_2 yield. It is known that the dehydration of ethanol ($C_2H_5OH \rightarrow C_2H_4 + H_2O$) dominantly proceeds on an acidic Al_2O_3 support to give C_2H_4 selectively[3,4,9–11]. On the other hand, the products over other catalysts tested were composed of H_2, CO, CO_2 and CH_4. Other products such as oxygenated compounds and acetylene were not detected.

Co/MgO and Ni/MgO featured similar levels of conversion. While the levels of ethanol conversion over Co/MgO and Ni/MgO after 15 min on stream were 54% and 49%, respectively, both catalysts deactivated rapidly in the first hour of reaction. Deactivation, which occurred in both cases of Co/MgO and Ni/MgO, was hardly observed in the cases of $Co/SrTiO_3$ and $Co/LaAlO_3$, both of which kept higher conversion levels of ethanol of ca. 63 % and 58 %, respectively, even after 300 min. Although deactivating rapidly during the first hour of reaction,

Ni/LaAlO$_3$ and Ni/SrTiO$_3$ showed better durability than Co/MgO and Ni/MgO, keeping higher ethanol conversion levels of 45.6 and 49.7 %, respectively, after 300 min.

The deposition of coke is one of the major reasons for catalyst deactivation in the steam reforming of ethanol. We evaluated the amounts of coke deposited on the Co and Ni catalysts. Fig. 1 shows the quantities of deposited coke after the reaction for 2 and/or 5 h. Almost of coke accumulated on Co/MgO and Ni/MgO in the early stage of reaction and the amounts of coke after 2 h of reaction were hardly changed. The amounts of deposited coke on Co or Ni catalysts supported on perovskite were smaller than Co/MgO or Ni/MgO. Among the perovskite-supported catalysts, the amounts of coke deposited on Co/SrTiO$_3$ and Co/LaAlO$_3$, which kept the levels of high ethanol conversion during reaction were much smaller, 9 and 11 mg, respectively. We supposed that the lattice oxygen in perovskites may play a positive role in oxidation of deposited coke and/or CH$_x$ fragment adsorbed on Co or Ni as previously proposed[6] with study of the steam reforming of methane.

As described above, SrTiO$_3$ and LaAlO$_3$ were suitable as the support of Co and Ni catalysts in the steam reforming of ethanol, while BaTiO$_3$ caused both the decrease in ethanol conversion and carbon deposition. For the purpose of examining such large differences in catalytic activities among Co/perovskite catalysts tested, both the size distribution and the average size of Co particles were determined by counting more than 100 particles observed in TEM micrographs. Fig. 2 shows Co particle size distributions for Co/SrTiO$_3$ and Co/BaTiO$_3$. The Co particle size over SrTiO$_3$ was obviously smaller than that over BaTiO$_3$; the average Co particle sizes over SrTiO$_3$ and BaTiO$_3$ were 39 and 79 nm, respectively. These results imply that the dispersion of Co governs both the catalytic activity and coke resistance of Co/perovskite in the steam reforming of ethanol. As previously described[6,7], we consider that the lattice oxygen in perovskites plays positives roles in hindering coking. It can, thus, be deduced that more frequent participation of lattice oxygen due to higher dispersion of Co on SrTiO$_3$ contributed to its higher catalytic activity and durability in comparison with Co/BaTiO$_3$.
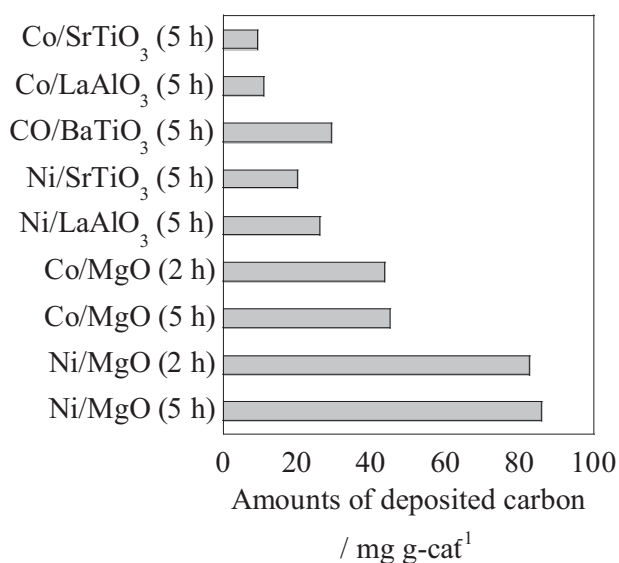
Fig. 1. Amount of deposited carbon.

Table 1. Catalytic activities of Co and Ni catalysts for the steam reforming of ethanol

Catalyst	[a]TOS /min	Conv. / %	Yield / %				
			CO	CO_2	CH_4	C_2H_4	H_2
Co/MgO	15	54.0	16.7	31.9	5.5	0	19.5
	300	30.1	11.1	15.7	3.2	0	10.5
Ni/MgO	15	49.3	15.4	26.3	7.7	0	15.1
	300	27.2	8.6	14.5	4.1	0	8.2
Co/SrTiO$_3$	15	60.9	27.3	24.2	9.4	0	19.8
	300	67.7	21.0	38.2	8.5	0	23.9
Ni/SrTiO$_3$	15	60.3	18.8	30.6	11.0	0	18.5
	300	45.6	16.4	23.0	6.2	0	15.0
Co/LaAlO$_3$	15	58.3	16.3	36.7	5.3	0	22.5
	300	56.0	15.7	34.9	5.5	0	20.7
Ni/LaAlO$_3$	15	62.1	13.1	40.2	8.8	0	22.3
	300	49.7	11.4	31.8	6.5	0	17.7
Co/BaTiO$_3$	15	39.9	22.1	12.4	5.4	0	18.1
	300	24.8	12.2	9.2	3.4	0	9.3
Co/γ-Al$_2$O$_3$	180	98.4	6.1	2.0	3.8	86.5	0.8

[a] Time on stream
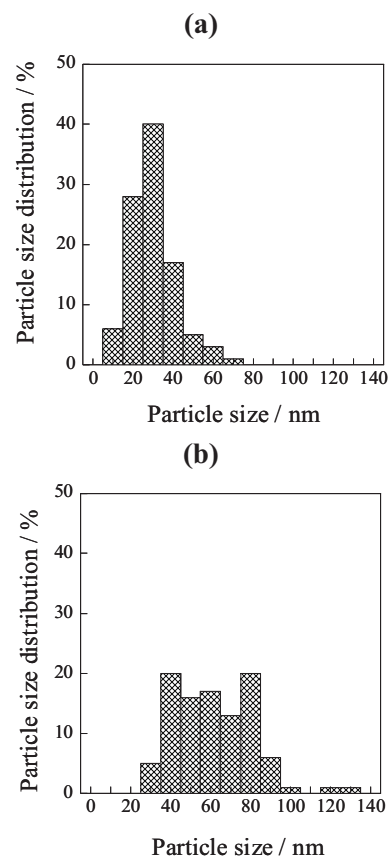
Fig. 2. Size distribution for (a) Co/SrTiO$_3$ and (b) Co/BaTiO$_3$.

References

1. A. Haryanto, S. Fernando, N. Murali, S. Adhikari, *Energy & Fuels*, **19**, 2098 (2005).
2. F. Haga, T. Nakajima, H. Miya, and S. Mishima, *Catal. Lett*. **48,** 223 (1997).
3. A. N. Fatsikostas, D. I. Kondarides, X. E. Verykios, *Chem. Commun.*, 851 (2000).
4. J. Llorca, N. Homs, J. Sales, P. R. Piscina, *J. Catal.*, **209**, 306 (2002).
5. S. Cavallaro, N. Mondello, S. Freni, *J. Power Sources,* **102**, 198 (2002).
6. K. Urasaki, Y. Sekine, S. Kawabe, E. Kikuchi, M. Matsukata, *Appl. Catal. A*., **286**, 23 (2005).
7. K. Urasaki, T. Tokunaga, Y. Sekine, E. Kikuchi, M. Matsukata, *Chem. Lett.*, **34**, 668 (2005).

MICROWAVE PLASMA REACTOR FOR PRODUCTION OF HYDROGEN AND NANODISPERSIBLE CARBON MATERIAL FROM NATURAL GAS

[1]Polygalov Yu. I., [1]Stepanov V.P., [1]Medvedev Yu. V., [2]Galanov S.I., [2]Sidorova O.I., [3]Zherlitsyn A.G., [3]Shejan V.P.

[1]*Joint Stock Company "Tomskgazprom", 73, Bol´shaya Podgornaya, 634000, Tomsk, Russia, E-mail: medvedevjv@vostokgazprom.ru*

[2]*Tomsk State University, 36, Lenin Ave., 634050, Tomsk, Russia, E-mail: galanov@xf.tsu.ru*

[3]*State Scientific Institution "Nuclear Physics Institute" (NPI), 2a, Lenin Avenue, 634050, Tomsk, Russia, E-mail: Zherl@npi.tpu.ru*

The opportunity of the production of nanodispersible carbon material and hydrogen from natural gas was considered. In process was used the combination of metallic catalysts and the influence of microwave field on catalyst and methane. In the course of reactions occurs accumulation of hydrogen, which promotes origination of hydrogen plasma. The hydrogen plasma cleans the surface of catalyst from formed carbon with carrying out carbon from a reactor.

The dependence of methane conversion, velocity of carbon formation from a material of the catalyst gives in table 1.

Table 1. The parameters of reaction (temperature of the catalyst 600 °C)

The catalyst	Conversion of methane, %	Concentration of H_2, %vol.	Concentration of C_{2+}, %vol.	Velocity of carbon formation, g/cm^3·h
TiNi	42.4	52.3	8.8	0.27
AlNi	15.8	28.3	2.2	0.1
Ni	79.6	84.9	4.0	0.51
Fe	54.6	69.4	2.2	0.35
Mo	77.6	84.6	3.1	0.5
Ti	27.9	43.4	2.5	0.18
Si (granule)	29.3	43.3	4.2	0.19
W (strand)	15.7	25.7	4.7	liquid

The combination of catalytic processes with plasma processes results to the occurrence of complex dependences for endothermic reactions of decomposition of methane. The reduction of time of contact of gas mixture with the catalyst at preservation of linear speed of methane

results to the reduction of methane conversion and concentration of hydrogen at the concentration C_{2+} hydrocarbons is constant (figure 1, 2).
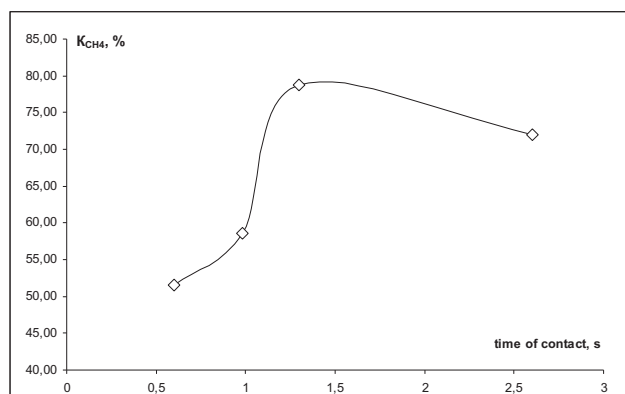
Figure 1.
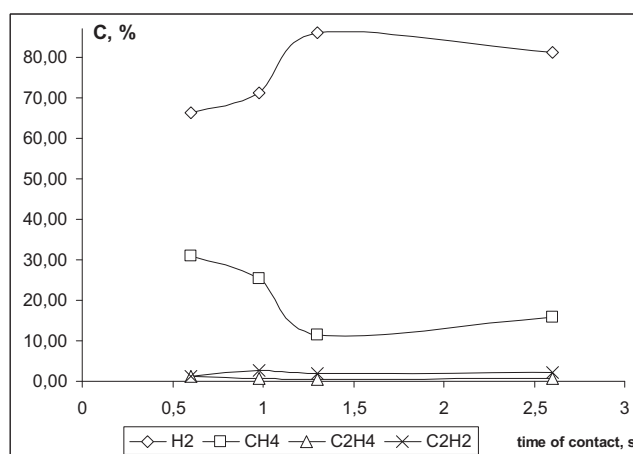
Figure 2.
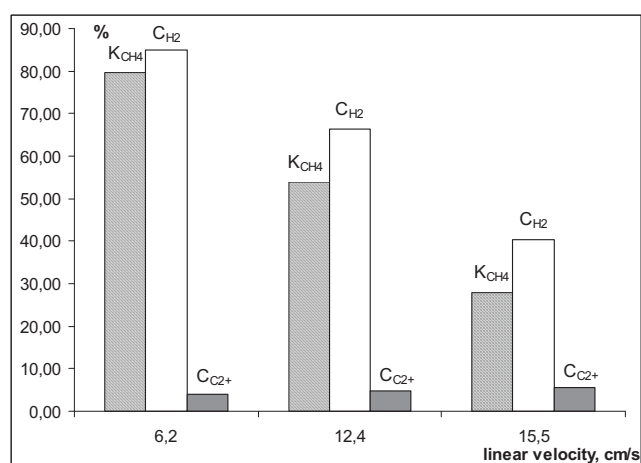
Figure 3.

The increase of linear velocity of methane results to the reduction of methane conversion and yield of hydrogen at the increase of concentration C_{2+} hydrocarbons in reactionary gases (figure 3).

The structure of nanodispersible a carbon material is depending on the used catalyst (table 2).

Table 2. The dependency of correlation amorphous carbon and nanotubes from used catalysts

Composition of catalyst	Contents of carbon nanotubes (%) and size (nm)		Contents of amorphous carbon (%)
	%	nm	
TiNi	46.13	9.12	45.00
AlNi	33.14	10.57	55.00
Ni	56.51	7.12…14.92	21.24
Fe	78.24	3.70…12.40	4.04
Mo	24.91	26.26…37.22	64.89
Ti	23.05	5.8…11.6	-

The rest is a graphite and ortacarbon.

The ortacarbon is formed only on Ni containing catalysts – Ni, AlNi and TiNi.

When carrying out of reaction without catalyst in plasma category occurs the change of methane conversion from 1.5 before 17 % and is accompanied formation C_2-C_4 hydrocarbons and fluid hydrocarbons.

THE KINETICS OF HOMOGENEOUS CATALYTIC METHANE OXIDATION

Beata Michalkiewicz

Szczecin University of Technology, ul. Pulaskiego 10, 70-322 Szczecin, Poland,
fax: 489144946 86, beata.michalkiewicz@ps.pl

Introduction

Despite being the most abundant and least expensive hydrocarbon feed stocks available, methane finds limited use as a starting material for the chemical industry. The heterogeneous catalytic oxidation of methane to methanol and formaldehyde at high temperatures has been investigated by many authors [1-3]. However, both conversion and selectivity are too low (yield below 10%) [3]. The methane activation requires high temperature, where the chemistry is dominated by radical pathways. Under such conditions, reactivity is determined by C–H bond strength. The desired products – oxygenates – are unstable intermediates, which in the presence of oxygen suffer fast consecutive reactions to carbon oxides. The relative reactivity of methane compared to methanol over heterogeneous catalyst is at last 20–fold higher.

A novel high-yield system for the catalytic conversion of methane to methanol was published in 1992 by Catalytica Inc. [4]. Homogeneous reaction took place at $180^{o}C$ and 3.5 MPa in concentrated sulfuric acid and was catalyzed by mercuric sulfate. The desired intermediate reaction product was methyl bisulfate, which was hydrolyzed to methanol. The highest methanol yield was 43%. The great advantage of using a strong acid as a solvent is that the alcohol formed is protected either as the ester or by protonation [5]. The better results were achieved when catalytic system dichloro(η-2{2,2'-bipyrimidyl} platinum(II) – fuming sulfuric acid was applied by Catlytica Inc. (72% yield) [6]. The palladium trifluoroacetate-trifluoroacetic acid mixture resulted in achieving $CF_3CO_2CH_3$ with a 60% yield [7].

Experimental

The aim of the investigation is to examine the kinetics of the methane conversion to methyl bisulfate. The process was carried out at 160oC in the autoclave containing 100 cm^3 of oleum. Platinum chloride(IV) was used as a catalyst. In a typical experiment concentration of PtCl4 was 0.0015 mol·dm-3. Methane partial pressure was varied from 3.0 to 6.8 MPa. Sulfur trioxide concentration in oleum was ranging from 0.40 – 5.65 mol·dm-3. The experiments last 2 – 22 h.

The mixture of oleum and $PtCl_4$ was sealed into a stainless steel autoclave lined with

Teflon and then pressurized with methane. The process was terminated by stopping the heating and stirring, and cooling the reactor with water. The gases and liquid postreaction mixture after treatment with water were analyzed by gas chromatography. Methyl bisulfate was analyzed quantitatively as methanol after water treatment. CH_3OSO_3H presence as the reaction product was confirmed by ^{13}C NMR.

Results and discussion

It was found that the following reactions took place:

$CH_4 + SO_3 + H_2SO_4 \rightarrow CH_3OSO_3H + SO_2 + H_2O$

$CH_4 + 4SO_3 \rightarrow CO_2 + 4SO_2 + 2H_2O$

$H_2O + SO_3 \rightarrow H_2SO_4$
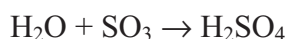
Only when the process lasted 18 h or longer carbon dioxide was observed. The highest carbon dioxide yield was 2% after 22 h. Practically, the only product of methane oxidation is oleum CH_3OSO_3H.

In order to investigate the influence of the sulfur trioxide concentration in oleum on the methyl bisulfate concentration, the first series of the experiment were carried. In this study time of the reaction was 2 hours and the initial methane pressure 4.5 MPa. In the second series, the dependence of the reaction rate on sulfur trioxide concentration and the methane pressure was investigated. In this case the initial pressure of methane was altered, and the initial sulfur trioxide concentration in oleum (5.95 mol/dm^3) and reaction time remained the same.

Therefore the reaction rate (r) equation in this system was postulated as follows:

$$\frac{dC_E}{dt} = r = r_{(SO_3)} \cdot r_{(p_{CH_4})} = f_1(C_{SO_3}) \cdot f_2(p_{CH_4}) \qquad (1)$$

C_E, C_{SO_3} – methyl bisulfate, sulfur trioxide concentration [mol·dm^{-3}]

p_{CH_4} – methane partial pressure [MPa]

$r_{(SO_3)} = f_1(C_{SO_3})$ – function of the sulfur trioxide concentration in the reaction rate equation

$r_{(p_{CH_4})} = f_2(p_{CH_4})$ – function of the methane partial pressure in the reaction rate equation

The next experiments were carried out by initial pressure of methane 4.5 MPa, 5.95 mol/dm^{3}sulfur trioxide concentration in oleum. Only the reaction time was modified (Fig. 1).

It was found that for the first three hours the ester concentration and time exhibited the linear dependence. The value of the slope is 0.144. One can conclude that the reaction rate after two hours is 0.144 (the initial pressure 4.5 MPa, the initial SO_3 concentration 5.95 mol/dm^3). The same value of the reaction rate was obtained by the division of the ester

concentration after two hours by the factor of two. We can generalize that the experimental reaction rate (r^{exp})can be obtain by the division of the value of the ester concentration by the reaction time (up to three hours): $\dfrac{dC_E}{dt} \approx \dfrac{\Delta C_E}{\Delta t} \approx r^{exp}$
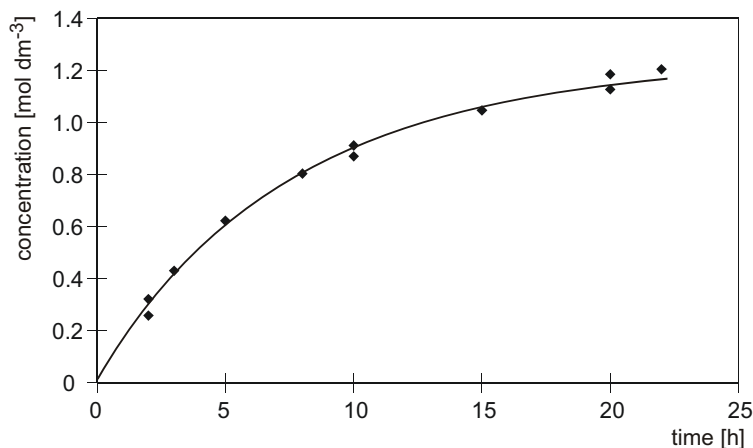
Fig. 1. The plot of ester concentration vs. time. Temperature 160°C, SO$_3$: 5.95 mol/dm^3, CH$_4$: 4.5 MPa.

For the first and second series of experiments the values of r^{exp} were calculated basing on the above-mentioned equation. The average values of the C_{SO_3} and p_{CH_4} were taken into further consideration. It was found that $r_{(SO_3)} = f_1(C_{SO_3})$ is linear function. The slope is equal 0.0226 and y-intercept 0.0251.

The function of methane partial pressure in reaction rate equation (1) –

$f_2(p_{CH_4}) = \dfrac{r^{exp}}{f_1(C_{SO_3})}$ can be determine from a plot, where y=$\dfrac{r^{exp}}{f_1(C_{SO_3})}$ and x=p_{CH_4}.

It was found that: $f_2(p_{CH_4}) = 0.0033(p_{CH_4})^4 + 0.2$

The rate of the methane to the ester conversion is a function of the sulfur trioxide concentration and the methane partial pressure:

$$r = \left(0.0226\,C_{SO_3} + 0.0251\right)\left(0.0033(p_{CH_4})^4 + 0.2\right) \qquad (2)$$

After applying of the initial values of sulfur trioxide concentration and methane partial pressure:

$$r = \frac{dC_E}{dt} = 0.000076\left(C_{0\,SO_3} - 2C_E + 1.11\right)\left[\left(p_{0\,CH_4} - 2.37\,C_E\right)^4 + 59.76\right] \qquad (3)$$

$C_{0\,SO_3}$ – the initial SO$_3$ concentration in oleum [mol dm^{-3}]

$p_{0\,CH_4}$ – the initial methane partial pressure [MPa]

The calculation of the theoretical rate of methane to ester conversion when reaction lasted

longer than two hours, was based on equation (3).

The experimental values of the reaction rate was obtained by graphical differentiation of the parameters plotted in figure 1. The comparison of the experimental and theoretical values of the rate versus time are shown in Fig. 2.
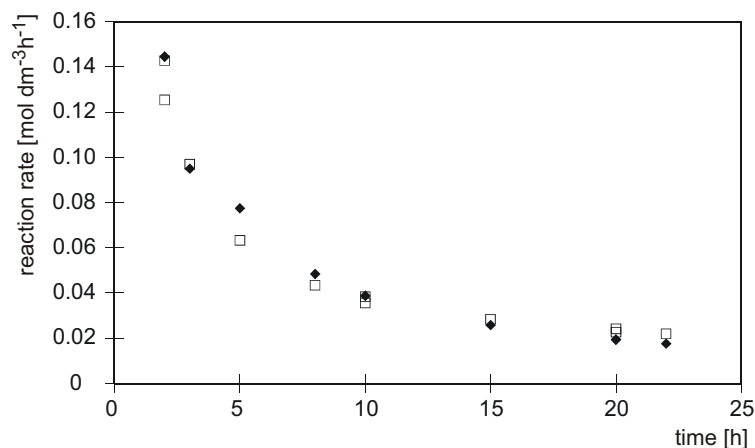
Fig. 2. The experimental and theoretical reaction rate vs. time. □ - experimental, ♦ - theoretical

Conclusion

Theoretical equation of the reaction rate for methane to ester conversion was found. The model provide an excellent agreement between the experimental and theoretical rate versus time in the process of the methane to ester conversion. This observation let one calculate the reaction rate and the ester concentration in any moment of the process up to 22 hours. The estimation of the equation (3) is a step towards the projection of the industrial reactor for the mass production of the methyl bisulfate.

References

1. US Patent 5 220 080

2. Labieger, J.A., *Fuel Processing Technology* 1995, **42**, 325.

3. Kiyoshi O., Wang Y. *Appl. Catal. A,* 2001, **222**, 145–161.

4. WO14738 (1992)

5. Sen, A, Benvenuto, M.A., Lin, M., Hutson A.C., Basickes, N. *J. Am. Chem. Soc*. 1994, **116**, 998.

6. Periana, R. A.; Taube, D. J.; Gamble, S.; Taube, H.; Satoh, T.; Fujii, H. *Science* 1998, **280**, 560.

7 Gretz, E.; Oliver, T. F.; Sen, A. *J. Am. Chem. Soc.* 1987, **109**, 8109.

TWO PHASE PROCESS OF PROPYLENE DIMERIZATION IN IONIC LIQUIDS USING NICKEL-CONTAINING DITHIOSYSTEMS

F.A. Nasirov, F.M. Novruzova, A.M. Aslanbeyli, A.H. Azizov

Institute of Petrochemical Processes of Azerbaijan National Academy of Sciences,

30, Khodjaly av., AZ 1025, Baku, Azerbaijan, phone/fax: (99412) 4904204

E-mail: fizulin52@rambler.ru

Ionic liquids offer the potential for ground-breaking changes to synthesis routes and unit operations in the chemical industry. Ionic liquids are liquid at room temperature, highly polar, yet no coordinating (ideal for catalytic reactions), they can be made immiscible with water and/or a number of organic solvents (providing flexibility for a number of reaction and separation schemes), and they do not emit volatile organic compounds, providing a basis for "green chemistry." This creates new opportunities for two phase catalytic reactions, and combined reaction/separation processes.

The nickel-catalyzed dimerisation of lower olefins in ionic liquids containing chloroaluminate anions is probably the most investigated reaction in ionic liquids. As early as 1990 the group of Chauvin Y. at the Institut François du Petrole (IFP) reported the nickel-catalyzed dimerisation of propene in 1-butyl-3-methyl-imidazolium chloroaluminate ionic liquid (bmimAlCl$_4$) [1,2]. The catalyst precursor consisted of L$_2$NiCl$_2$ (L=Ph$_3$P or pyridine) in combination with EtAlCl$_2$ (bmimCl/AlCl$_3$/EtAlCl$_2$=1/1.2/0.25) and the active catalyst is a cationic nickel (II) complex, [LNiCH$_2$CH$_3$]$^+$AlCl$_4^-$, formed by reaction of L$_2$NiCl$_2$ with EtAlCl$_2$. Since ionic liquids promote the dissociation of ionic metal complexes it was envisaged that they would have a beneficial effect on this reaction. This proved to be the case: at 5 °C and atmospheric pressure productivities (~ 250 kg dimers/ g Ni) much higher than those observed in organic solvents were achieved (25 kg dimers/g Ni.hour). The mixture of dimers obtained contains 2,3-dimethylbutenes as the major component (83%).

Therefore development of propylene dimerisation process in ionic liquids using nickel-containing catalytic dithiosystems on the base of organic dithiocompounds of nickel (DTC-Ni, such as O,O-dithiophosphates, N,N-dithiocarbamates, xhantogenates) and aluminum organic compounds (AOC, such as dialkylaluminum chlorides, alkylaluminumdichlorides, aluminoxanes) – DTC-Ni+AOC, along with the possibility for creation of new technology favours also elimination of the existing economic, technological and ecological problems

caused by purification and drying of solvents as well as by washing off, isolation and drying of reaction products, etc.

As a solvent were used chloroaluminate and zinc chloride type ionic liquids based on pyridine or imidazole. In their presence nickel-containing catalytic dithiosystems show very high catalytic activity and the process productivity reaches 720-1000 kg of dimers/g Ni.hour whereas the productivity of usual process in organic solvents reaches 25-50 kg of dimers/g Ni.hour, and that of the analog of commercial process "Dimersol" carrying out in ionic liquids is 250 kg of dimers/g Ni.

In the process along with propylene dimers, trimers and tetramers are also obtained but portion of dimers fraction in reaction products achieves 92-96 %. Such high-octane components as 4-methylpentenes, 2-methylpentenes, 2,3-dimethylbutenes prevail in dimers fraction. The octane number of dimers fraction obtained is 95-97 and it may be used as a high-octane additive to motor gasolines or in isoprene production.

Unlike the usual homogeneous process in organic solvents the technology of two-phase propylene dimerisation process in ionic liquids is very simple and insolubility of the reaction products obtained in ionic liquids allows separating them easily from catalyst that reduces significantly the energetic expenses.

The nickel-containing catalytic dithiosystem remains selectively dissolved in the ionic liquid phase, which permits both simple extraction of pure products and efficient recycling of the liquid catalyst phase. In addition to the ease of product/catalyst separation, the key benefits from using the ionic liquid solvent are the increased activity of the catalyst (productivity >1000 kg dimers/g Ni.hour), better selectivity to desirable dimers (rather than higher oligomers), and the efficient use of valuable catalysts through simple recycling of the ionic liquid. The possibility for catalyst regeneration and its reuse considerably reduces its consumption and cost of the main product, not causing the ecological problems.

Propylene dimerisation process was conducted either batch wise or in a semi-continuous way. Batch experiments were carried out in a 500 mL autoclave flask containing a magnetic stirring bar and the flask was immersed in a cooling bath. Semi-continuous experiments were carried out in a 150 mL double walled glass reactor containing a magnetic stirring bar with constant supply of neat gaseous propylene at atmospheric pressure.

References

1. Chauvin Y., Gilbert B., Guibard I.. Catalytic dimerisation of alkenes by nickel-complexes in Organochloroaluminate molten-salts. J. Chem. Soc., Chem. Commun., 1990, 1715–1716.
2. Chauvin Y., Einloft S., Olivier H. Catalytic dimerisation of propene by nickel-phosphine complexes in 1-butyl-3-methylimidazolium chloride/AlEt$_x$Cl$_{3-x}$ ionic liquids. Ind. Eng. Chem. Res. 1995, 34, 1149–1155.

BUTADIENE GAS PHASE POLYMERISATION WITH COBALT-CONTAINING CATALYTIC DITHIOSYSTEMS

F.A. Nasirov, F.M. Novruzova, S.S. Salmanov

Institute of Petrochemical Processes of Azerbaijan National Academy of Sciences, 30, Khodjaly ave., AZ 1025, Baku, Azerbaijan, phone/fax: (99412) 4904204.
E-mail: fizulin52@rambler.ru

Recently, processes of gas phase polymerization of olefins using heterogenized highly efficient homogenous catalytic systems have become widespread. Solvents are not used in these processes, therefore there are no technological, economic and ecological problems concerning cleaning and drying the solvent, washing off catalyst residues from the polymerizate, polymer degassing, polymer solubility, viscosity of reaction medium, etc.

Because gas phase polymerization is conducted without solvent in the process, the complicate procedures of aggregation and separation of polymer from solution, which are needed in solution polymerization, are excluded from gas phase polymerization. This leads to not only cutting down the cost of construction and operation, but also reducing environmental pollution. On the other hand, it also avoids the shortages of bulk polymerization such as low conversion, polymer quality difficult to control and the danger of violent polymerization, which are due to system viscosity enhancing rapidly with the increase of conversion and reaction heat being difficult to diffuse in bulk polymerization. Although the gas phase polymerization technology of ethylene and propylene has been industrialized for a long time, gas phase polymerization of butadiene has just been studied.

Study on gas phase polymerization of butadiene was firstly carried out by Berlin Technical University and Bayer Company in 1994 with a getraegerten neodymium catalyst [1,2]. The main reasons for delaying transfer of production of polydienes from liquid phase technology to gas phase one, are low activity of the known catalytic systems and deterioration in quality indices of the polymers obtained because of catalyst residues. Bifunctional homogeneous nickel- and cobalt-containing dithiosystems developed IPCP of Azerbaijan National Academy of Sciences have high catalytic activity in the process of butadiene solution polymerization as well as high stabilizing efficiency in the process of photo- and thermo oxidative ageing of the end product, therefore they are free of the abovementioned shortcomings. In this connection, development of new technologies for gas phase polymerization of butadiene into 1,4-cis polybutadiene using homogenous highly effective

cobalt-containing catalytic dithiosystems heterogenized upon different supports is a topical problem and has a scientific and practical importance.

Bifunctional catalytic dithiosystems on the base of organic dithiocompounds of cobalt (DTC-Co, such as O,O-disubstituted dithiophosphates, N,N-dithiocarbamates, etc.) and aluminum organic compounds (AOC, such as dialkylaluminumchlorides, alkylaluminum-dichlorides, aluminoxanes, etc.) - DTC-Co+AOC, has been heterogenized on aluminum oxides or silica gels supports (dehydrated by heating at 25-105, 105-170 and above 170^0C) by the methods of direct deposition or pre-alumination. Catalysts heterogenized on various samples of supports show a very high activity, and polybutadiene containing 1,4-cis links 93-96% is formed. Output of gas phase polymerization of butadiene using heterogenized cobalt-containing dithiosystems reaches 1700 kg PBD/g. Co. hour, this is much higher than the output of liquid phase process using the same homogenous catalysts (40 kg PBD/g. Co. hour) and gas phase process of Berlin Technical University (250 kg PBD/mole. Nd. hour).

Gas phase polymerization of butadiene was carried out in a fluidized-bed 200 ml reactor, which has been long recognized as one of the main roads for producing polyolefins. In this process small catalyst particles are continuously fed into a fluidized-bed reactor. They grow due to reaction with the incoming fluidizing gas. The larger product particles are continuously withdrawn at the bottom.
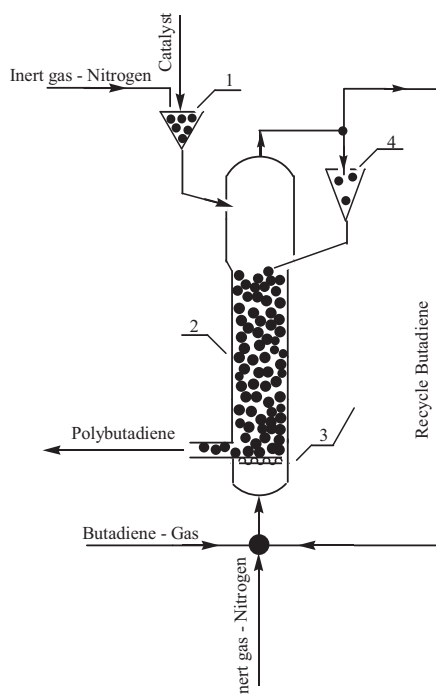
Fig. Principal scheme of butadiene gas phase polymerization laboratory unit

1 – equipment for fresh-made catalyst;
2- reactor;
3 – net-filter;
4 – equipment for carried away catalyst and polymer.

References

1. Sylvester, G., Vernalekeu, H., Eur. Pat. Appl., EP 647657.
2. Eberstein, C., Garmatter, B., Reichert, K. H. et al. Gas-phase polymerization of butadiene, Chemie Ingenieur Technik, 1996, 68, 820.

DEVELOPMENT OF CATALYTIC SYSTEMS FOR ACETALDEHYDE PRODUCTION BY ETHANOL DEHYDROGENATION

Nougmanov Evgeniy, **Egorova Ekaterina, Antonyuk Sergey**

M.V. Lomonosov Moscow State Academy of Fine Chemical Technology

Russia, 119571, Moscow, Vernadskiy avenue, 86, fax: 246-48-23,

E-mail: nhsigt@mitht.rssi.ru

Last years in the world chemical industry the necessity of the decision of environmental problems is got a special urgency. These problems can solved due to creation of the new, alternative manufactures described by a minimum quantity of harmful waste products and basing renewed sources of raw material.

One of the most perspective directions of chemical industry development is application of bioethanol for manufacture of valuable chemical compounds. It allows to leave from oil dependence. The biotechnology developing by fast rates already now enables to make ethanol on non-polluting technologies from organic waste products and biomass by their conversion by enzymes of a microbic origin. The vegetative biomass is a renewed source of organic raw material and due to a huge annual gain is capable to solve completely human needs for fuel and chemical products. The opportunity of use for biological processing waste products and by-products allows to create practically without waste manufactures. Huge progress has been achieved by Danish company Novozymes. It managed to reduce in 30 times cost and to increase efficiency of enzymes used at bioethanol production. Worldwide conducted researches allow to speak about substantial growth of competitiveness of manufacture of bioethanol which in the modern conditions demanding reduction of use of oil products can take a key place in industrial organic synthesis.

One of ways of bioethanol processing is its catalytic dehydrogenation with production of acetaldehyde - important intermediate product of organic synthesis. The main industrial method of acetaldehyde reception is ethylene oxidation in the presence of $PdCl_2$ and $CuCl_2$ water solutions. It has a number of lacks. It is characterized by formation of a lot toxic chlororganic by-products and a plenty of sewage. Besides, ethylene used as initial raw material is based on processing of oil raw that results to rise of its price. At the same time, acetaldehyde production by ethanol dehydrogenation in the presence of heterogeneous catalysts has a number of advantages: absence of toxic wastes, soft conditions of the process

and formation of hydrogen, which can be used in other processes. Initial raw material is only ethyl alcohol, which production from biomass allows not using oil raw. However the development of new highly active, selective and stable catalytic systems is necessary for effective realization of ethanol dehydrogenation with all set forth above advantages.

This study is devoted to development of new catalysts for acetaldehyde synthesis with application of carbon material sibunit as a support. Sibunit represents a new class of porous carbon-carbon composite and it is very perspective for using in catalysis. Most important advantage of sibunit is its high chemical purity that can render essential beneficial effect on selectivity of catalytic systems prepared on its base.

Earlier carried out research have shown, that the most effective in acetaldehyde synthesis is the sibunit supported catalyst containing 3 wt.% of copper. Yield of acetaldehyde was 54,4%. As it is known, one of the primary goals of catalytic systems development is search of optimum conditions of catalysts pretreatment, during which the formation of an active component occurs. Therefore, the influence of calcination and reduction conditions of cooper-containing catalysts on its activity and selectivity in the ethanol dehydrogenation was studed. Calcination of copper-containing catalysts was carried out in argon flow at temperatures 200, 300 and 400˚C. Then all samples was reduced in hydrogen and researched in ethanol dehydrogenation. Researches have shown, that introduction of a stage of pre-calcination renders significant influence on process parameters, increasing both activity, and selectivity of catalysts. The selectivity of catalysts increased when calcination temperature raised, and reached maximum values in the presence of the sample calcinated at 400˚C (Fig. 1). The stage of previously reduction of catalysts in hydrogen flow results in increasing of the main product
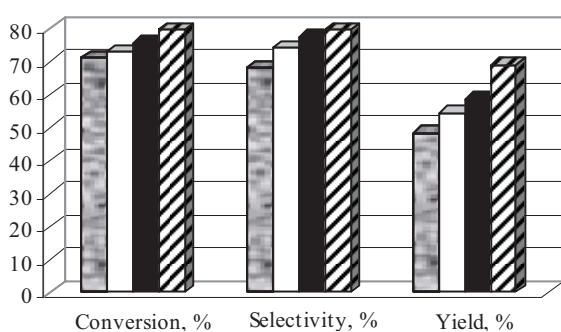
Fig. 1. Ethanol conversion, selectivity and yield of acetaldehyde in the presence of copper-containing catalysts calcinated at different temperatures

⬜ without calc. ☐200˚C ⬛ 300˚C ▨400˚C
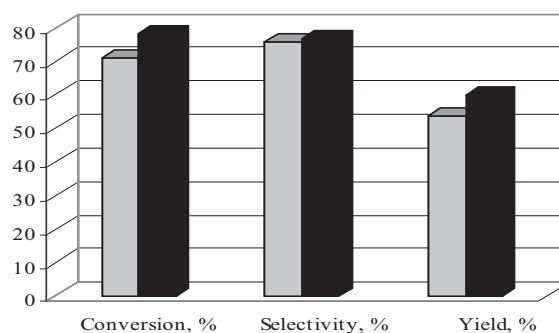
Fig. 2. Ethanol conversion, selectivity and yield of acetaldehyde in the presence of reduced and unreduced copper-containing catalysts

⬜ without reduction ⬛ reduced

yield only by increase of initial alcohol conversion comparing with unreduced catalyst (Fig. 2). The temperature of reduction does not influence. Thus, the maximum yield of acetaldehyde was 69,2% in the presence of the sample, which was previously calcinated in argon flow and reduced in hydrogen flow at 400˚C.

The extremely important characteristic of catalysts which is necessary for introduction of new systems in the industry is their stability. However based on sibunit copper-containing catalysts sharply decreased the activity in the field of high temperatures. As have shown by researches, this fact is caused by change of a degree of copper oxidation under action of the reactionary environment. Duration of stable work of such catalyst in optimum conditions was only 30 hours. Then activity of the catalyst decreased.

Introduction of promotional additives is one of the ways to increase the catalytic systems stability. We investigated an opportunity of chrome oxide introduction into copper-containing catalysts as a promotional additive.

Addition of chrome oxide into catalyst has allowed to raise activity of system in the field of temperatures above 400˚C. Alcohol conversion was more than twice above than in the presence of unpromoted catalyst. Yield of acetaldehyde was 63,3% despite of smaller selectivity. Besides, introduction of chrome oxide additive has allowed to increase duration of stable work of the catalyst considerably. In the conditions of process providing the maximal yield of acetaldehyde such system, can work stably not less than 80 hours.

Thus, as a result of the done work the effective copper-containing catalysts based on carbon material sibunit for acetaldehyde synthesis by ethanol dehydrogenation have been developed. It will allow to make acetaldehyde by ecologically purer technology independent of oil raw material.

Fe_2O_3-MODIFIED/SiC AS A NEW AND ACTIVE CATALYST FOR DEEP SELECTIVE OXIDATION OF HIGH CONCENTRATIONS OF H_2S INTO ELEMENTAL SULFUR

Patrick Nguyen[1], **Jean-Mario Nhut**[1], **David Edouard**[1], **Marc-Jacques Ledoux**[1], **Cuong Pham-Huu**[1], **Charlotte Pham**[2]

[1]*Laboratoire des Matériaux, Surfaces et procédés pour la Catalyse (LMSPC), UMR 7515 du CNRS-ECPM, 25, rue Becquerel, F67087 Strasbourg, France*
[2]*European Laboratory for Catalysis and Surface Science (ELCASS)*
Sicat, 14 , avenue Hoche, 75008 Paris, France

Due to its high toxicity, hydrogen sulfide (H_2S) must be removed as much as possible before being released from natural gas plants and petroleum refineries into the atmosphere. The catalytic selective oxidation of trace amount of H_2S by air has been extensively studied and details concerning this process were summarized in a series of review articles (1-2). The general trend is to selectively transform the H_2S into elemental sulfur by the equilibrated Claus process: $2\ H_2S + SO_2 \leftrightarrow (3/n)\ S_n + 2\ H_2O$ (**1**). However, thermodynamic limitations of the Claus equilibrium reaction fix the maximum conversion level to about 97 %. This led to the development of new processes to deal with the Claus tail-gas, based on the direct oxidation of the remaining traces (≤ 1 vol. %) of H_2S in order to meet ever stricter legislation requirements. In the tail-gas processes, the remaining H_2S is catalytically oxidized into elemental sulfur in the presence of oxygen. Recently, it has been reported that silicon carbide based catalyst exhibits a high catalytic activity for this reaction either in a discontinuous-mode (reaction temperature ≤ 100 °C) or in a continuous-mode (reaction temperature ≥ 180 °C) (3-4).The aim of this work is to present the latest development of the SiC based catalyst. The drastic reaction conditions were deliberately chosen in order to illustrate the extremely high performance of such catalyst compared to traditional catalysts supported on alumina or silica. The catalytic results obtained will be compared with those available in the open literature. It has been observed that under these extreme conditions (high temperatures and high H_2S concentrations) the Fe_2O_3/SiC catalyst still exhibits high catalytic performance compared to those observed on the traditional catalysts supported on alumina or silica. The high intrinsic thermal conductivity and the high chemical inertness of the support were advanced to explain the observed results. The advanced hypothesis was also confirmed by

theoretical simulation experiments based on the evolution of the thermal profile of the catalyst bed in an industrial micropilot setup.

The support employed is a β-SiC (face cubic centred) synthesized according to the gas-solid reaction between the SiO vapour and solid carbon finely dispersed throughout the matrix of the precursor (5,6). The support was in an extrudate form (2 x 6 mm, diameter x length) with a specific surface area measured by BET of 24 m^2/g and was mainly constituted by a meso- and macropores while no trace of micropores was observed. The active phase was deposited on the support via an incipient wetness impregnation method using a $Fe(NO_3)_3,6H_2O$ dissolved in a solution containing water and glycerol (80:20 v:v %). After impregnation the solid was oven dried at 100 °C and calcinated in air at 350 °C for 2 h in order to decompose the salt precursor into its corresponding oxide.

The influence of the reaction temperature was conducted between 230 and 320 °C and the results obtained are presented in Figure 1. On the alumina based catalyst the sulfur selectivity is high at low reaction temperature and then rapidly drops when the reaction temperature attains 280 °C and higher. The SiC-based catalyst exhibits a different trend as the sulfur selectivity (81%) remains almost higher at the reaction temperature of 300 °C. This exceptional behaviour was attributed to the high thermal conductivity of the β-SiC which avoids local hot spots formation.
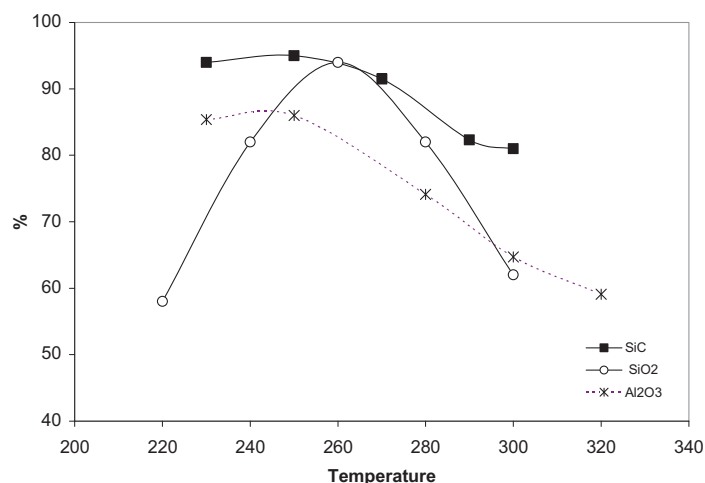
Figure 1: Sulfur yield of the silicon carbide based catalyst (SiC), alumina based catalyst (Al_2O_3) and the most active catalyst which is the commercial one (SiO_2).

The influence of the H_2S concentration on the activity and sulfur selectivity was carried out between 1 and 2.7 vol.% of H_2S. The O_2-to-H_2S molar ratio was kept constant at 5. As shown in Table 1, even at high H_2S concentration, the sulphur selectivity remains very high. Catalysts based on isolating supports i.e. alumina and silica are not able to treat more than 1.5% H_2S in the feed.

687

[H$_2$S] (vol.%)	Conversion (%)	Selectivity (%)	Yield (%)
1.0	98	96	94
2.0	97	96	93
2.7	97	93	90

Table 1: Conversion, selectivity and yield of the catalyst as a function of the concentration of H$_2$S in the feed.

For analysis effect of chemical reaction on the temperature profile in the catalytic bed, a simple dynamic heterogeneous model is proposed (7). This model takes in account the heat transfer (between fluid and solid phases) and thermal conductivity of the solid phase. The following heterogeneous model is described by equations (1)–(5)

Basic balance equation for the heterogeneous model:

- Energy balance for the fluid:

$$u_g \rho_g C p_g \frac{\partial T_g}{\partial z} + h a_c \left(T_g - T_s \right) = 0 \tag{1}$$

- Energy balance for the solid phase:

$$(1-\varepsilon)\rho_s C p_s \frac{\partial T_s}{\partial t} = h a_c (T_g - T_s) + h_{in} a t (T_s - T_{owen}) + \lambda_{ax}^{eff} \frac{\partial^2 T_s}{\partial z^2} + a_c (-\Delta H) r_s (T_s, \omega_s) \tag{2}$$

- Mass balance for the fluid:

$$u_g \rho_g \frac{\partial \omega_g}{\partial z} + \rho_g k_d a_c (\omega_g - \omega_s) = 0 \tag{3}$$

- Mass balance for the solid phase:

$$k_d (\omega_g - \omega_s) = M \frac{r_s}{\rho_g} \tag{4}$$

A first order kinetic may be generally assumed for chemical reaction:

$$r_s = k_0 \exp\left(-\frac{E_a}{RT_s}\right) C_s = k_0 \exp\left(-\frac{E_a}{RT_s}\right) \frac{\omega_s \rho_g}{M} \tag{5}$$

The boundary conditions:

$$\left.\frac{\partial T_s}{\partial z}\right|_{z=0} = \left.\frac{\partial T_s}{\partial z}\right|_{z=H} = 0; \; T_g\big|_{z=0} = T_0 = 593,15K \; ; \; \omega_g\big|_{z=0} = \omega_0 \; ; \forall z, \frac{1}{h_{in}} = \frac{1}{h_{ex}} + \frac{e}{\lambda_{tube}} + \frac{1}{h_{int}}$$

Initial conditions are t=0, $T_s = T_g = T_0 = 593.15$

For the simulations, the feed composition of the gas was similar to these used in the experiment plant and only the inlet flow rates are changed (industrial conditions). As predicted, the silicon carbide based catalyst exhibits a very smooth temperature profile as shown in Figure 3.a (1% H$_2$S in the feed) and 3.b (2.7% H$_2$S in the feed). In the case of the alumina based catalyst, a gradient of temperature from the top to the end of the bed is

observed. This difference of temperature $(\Delta(T_{s(z=0)}- T_{s(z=H)}=22K)$ is more pronounced with 2.7% of H_2S (i.e $\Delta Tad=40K$) versus 15K for 1% of H_2S. This increase of temperature on the catalyst surface was expected to be responsible for the bad selectivity (oxidation of the sulphur witch leads to the formation of SO_2).
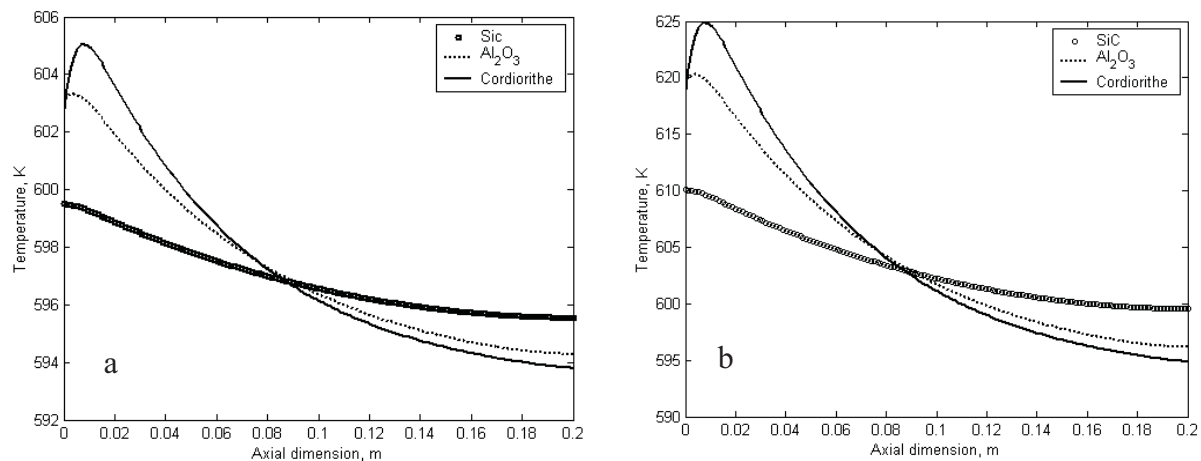
Figure 3. Simulations of temperatures profiles of the catalyst bed from different catalyst;
a. 1% H_2S in the feed, b. 2.7% H_2S in the feed.

Conclusion

In summary, we have shown that SiC supported iron-based active phase represents a new and extremely selective catalyst for performing a high-temperature selective oxidation of H_2S into elemental sulfur. The combination of the high thermal conductivity and the chemical inertness of the support avoids hot spots formation during the reaction leading to the high activity and sulfur selectivity even at high reaction temperature and in the presence of high H_2S concentration. The high desulfurization activity of the SiC-based catalyst allows envisaging the possibility to suppress the last Claus reactor which represents a great advantage regarding the cost investment of the desulfurization process.

References

1. J. Wieckowska, Catal. Today 24 (**1995**) 405

2. Sulphur, 250, (**1997**). 45.

3. N. Keller, C. Pham-Huu, C. Estournes, M.J. Ledoux, Applied Catal. A :Gen. 234 (**2002**) 191.

4. N. Keller, C. Pham-Huu, M.J. Ledoux, Applied Catal. A :Gen. 217 (**2001**) 205.

5. M.J. Ledoux, J. Guille, S. Hantzer, D. Dubots, U.S. Pat. No. 4914070 (**1990**).

6. M.J. Ledoux, S; Hantzer, C. Pham-Huu, J. Guille, M.P. Desaneaux, J. Catal.., 114 (**1988**) 176.

THE INVESTIGATION OF STATIONARY STATES NUMBER
OF CATALYTIC REACTIONS

Patmar E.S. and **Koltsov N.I.**

Department of Physical Chemistry, Chuvash State University, Cheboksary, Russia
e-mail: koltsov@chuvsu.ru

One of the important problems of reaction kinetics of heterogeneous catalysis characterised by critical phenomena is the investigation of their internal stationary states stationary states (ISS) - stationary states having no zero coordinates. The wide-spread way of investigating ISS is constructing kinetic curves in the coordinates - rate (r) to one of reagents (C_A) concentration. The kinetic curves can have complex forms: S - hysteresis, isola, self-crossing and mushroom. The characteristic peculiarity of these curves is the possibility of existing not less than three ISS, two of them are stable and one is unstable. Besides the above-mentioned curves there can exist kinetic curves of more complex form. This proves that more than three ISS can appear. The method of the estimation of ISS number both upper and lower is described in this paper. It helps to determine their real number. The lower bound is based on the action that at first an arbitrary stage complex of the investigated scheme is taken the boundary stationary stages (BSS) number is analysed (BSS are stationary states having at least one zero coordinate). Then the types (zero coordinates number) of these BSS are determined. After that the investigated mechanism stages (not included into the initial stage complex) are added in succession. The appearing of new BSS and the motion direction of the obtained at the previous stage BSS in a reaction simplex are fixed. There are some cases. If a BSS type does not decrease, then ISS formation does not take place. If the type decrease then the possibility of BSS converting into ISS arises. Sometimes it converts into the non-physical region (one of the coordinates becomes negative). It is worth noting that BSS can disappear that is it transfers into a complex plane. This happens, however, if BSS is multiple. This is a rare case because multiple roots are degeneration ones. The previous ISS can disappear but we are able to avoid it if to take small values of rate constants of added stages. Thus adding stages in succession we get a mechanism at each step which approaches to the initial one. The number at some steps can increase, this helps to estimate the lower bound of the ISS number for the reaction initial mechanism.

The ISS upper bound estimation is the following. For example, there is an algebraic equation system which describes the stationary behaviour of a concrete catalytic reaction. At first this equation system is brought to a trinomial form. Let some equation has more than three terms (monomials). Let's choose any two terms and take a new variable which is equal to these monomials sum. Then in the initial equation the term number decreases by unity because instead of two terms a new one equal to their sum appears. Having done this action several times we get a system in which every equation has not more than three members. Then the base variable and equation are selected, the differentiation of the base equation via the base variable take place. We get an equation of the initial system variables and their derivatives. To find these derivatives the equation system which is obtained from the initial one by excluding the base equation is differentiated. The number of solutions of the initial system is not more than by unity surpasses the number of solutions of the obtained system. Consequently the analysis of the obtained system decision shows if this system can have two solutions. If the obtained system is unsolvable then the research work is over. If it is solvable then with the new system (after some steps of the above-mentioned procedure) we learn if the initial system has tree solutions.

Let's analyse the application of this method for a reaction of carbon monoxide catalytic oxidation proceeding via the following scheme:

1. $CO + K \Leftrightarrow KCO$,

2. $2K + O_2 \Rightarrow 2KO$,

3. $KCO + KO \Rightarrow KCO_2 + K$,

4. $2KCO_2 + KO + CO \Rightarrow 3KCO_2$,

5. $KCO_2 \Rightarrow K + CO_2$,

$$(1)$$
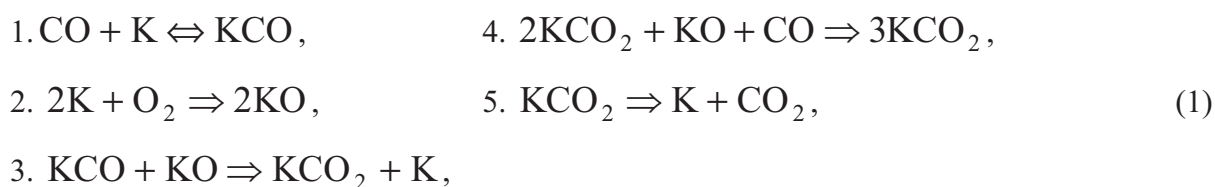
where K - are active centres on the catalyst surface. Having applied the above described methods to scheme (1) we get the data that the ISS lower bound is equal to six and upper bound is equal six too. This results in the fact that the maximal possible ISS number for an experimental reaction is equal to six. Fig. 1 illustrates this fact.

Applying this method reaction mechanisms of carbon monoxide and hydrogen catalytic oxidation are selected which ISS number can be more than five. Some of these reactions schemes are given in the table.
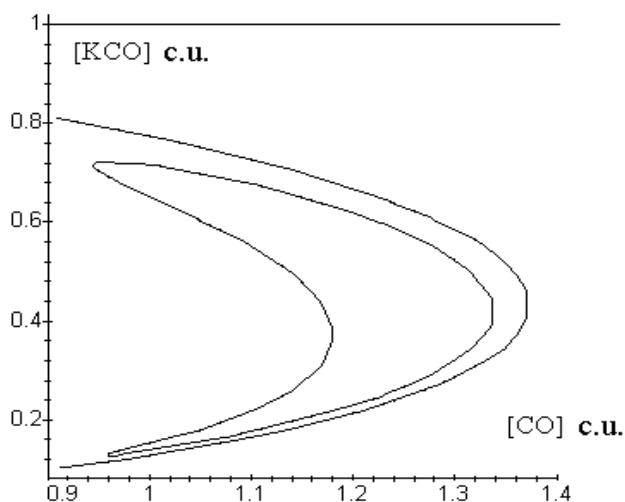
Fig. 1 The dependence of the concentration of absorbed carbon monoxide
on the catalyst surface from the concentration of gas CO

Reaction mechanism	Lower bound	Upper bound
1. $O_2 + 2K = 2KO$, 2. $KO + KCO = 2K + CO_2$, 3. $CO + K + KCO = 2KCO$, 4. $2CO + KO_2 + K = 2KCO_2$, 5. $O_2 + KO_2 + KCO_2 = 2KO_2 + CO_2$, 6. $2KCO_2 = 2K + 2CO_2$	9	9
1. $2K + O_2 \Rightarrow 2KO$, 2. $K + H_2 = KH_2$, 3. $KO + KH_2 + H_2O + O_2 \Rightarrow 2K(OH)_2$, 4. $2K(OH)_2 = 2KH_2O + O_2$, 5. $K(OH)_2 + KH_2O + H_2 = 2K + 3H_2O$	5	8

In some cases the lower and upper bounds do not coincide. This shows that there is some limitation of this method. The main peculiarity is determination of ISS number without numerous numerical experiments. Thus we have developed the method which can be used for stationary states number estimation of heterogeneous catalytic reactions.

SURFACE CHARACTERISATION OF ALKALINE-EARTH METAL OXIDE CATALYSTS BY TEST REACTIONS

A. Saadi[*], **R. Merabti, Z. Rassoul**

Laboratoire de Chimie du Gaz Naturel, Institut de Chimie, USTHB, BP32 El-Alia, 16111 Bab-Ezzouar, Algeria. Fax:+ 213 21 24 73 11, E-mail address: adel_saadi@yahoo.fr.

The acid-base properties of metal oxides play a key role in catalysis[1]. The adsorption and reaction of alcohols on metal surfaces plays an important role in determining the surface chemistry of a number of important catalytic processes[2] because of its application to produce a various intermediates and compounds[3]. In the past few years, various reduction reactions in gas phase have been studied to synthesize valuable intermediate products on fine chemicals[4]. Benzaldehyde reduction is one of theses reactions who can provide information about nature and properties of surface centers[5].

The present work deals with acid-base properties of alkali-earth metal oxide catalysts (MgO, CaO, BaO, SrO). Isopropanol decomposition and benzaldehyde reduction were used as probe reactions for characterizing the surface properties. They were characterized by their BET specific area, XRD and FTIR spectra. The catalytic performances were carried out in a quartz fixed bed reactor with 0,2g samples (P= 1 atm, $T_{reaction}$ = 100 – 350°C) after H_2 or N_2 pre-treatment at 350°C.

The results obtained by isopropanol decomposition show propene and acetone were produced competitively with yields depending on nature of the oxide and reaction temperature. The obtained order of acetone productivity was attributed to basic surface and propene productivity to acid surface character of alkali earth metal oxides. The different studies have provided evidence of the dissociative adsorption of isopropanol and the formation of isopropoxide species which decompose at high temperature to acetone and/or propene.

The results obtained by benzaldehyde reduction show that benzyl alcohol is produced by the Cannizzaro reaction under nitrogen flow on MgO oxide and by direct hydrogenation under dihydrogen on irreducible oxides such as CaO, BaO, and SrO. The Cannizzaro reaction involves the basic hydroxyl groups and is followed by the reduction of benzoate species by H_2 to benzaldehyde. Toluene and benzene were produced at high temperature reaction under nitrogen and dihydrogen flow over alkali earth oxides from a reaction involving benzyl alcoholate species, under H_2 by means of consecutive reduction reactions and under N_2 by alkoxy species.

[1] R.M.Rioux, M.A.Vannice, J.Catal. 216 (2003) 362-376.
[2] D.Haffad, A.Chambellan, J.C.Lavalley, J.Mol.Catal. A : Chemical 168 (2001) 153.
[3] A.Gervasini, J.Fenyvesi, A.Auroux, Catal.Lett. 43 (1997) 219.
[4] A.Saadi, Z.Rassoul, M.M.Bettahar, Stud.Surf.Sci.Catal. 130 (2000) 2261.
[5] A.Saadi. R.Merabti, M.M.Bettahar, Z.Rassoul. J.Soc.Alg.Chim. 11 (2) (2001) 231-240.

PP-120

MATHEMATICAL MODELING OF REACTIVE DISTILLATION COLUMN FOR THE PRODUCTION OF ETHYLENE GLYCOL

Samoilov N.A.[1], Mnushkin I.A.[2], Mnushkina O.I.[2]

Ufa State Petroleum Technical University[1] and "Peton" Company[2],
Kosmonavtov St., 1, Ufa, 450062, Russia, E-mail OLES@LI.RU

At the last time years have received increased attention for elaboration of reactive distillation apparatuses which joint chemical process and separation of reaction products in the same column. This is allowed essential intensify the process because simplify of technological scheme of unit and carrying out its optimization. Reactive distillation columns can be attractive and employment in such processes chemical technology as etherification, hydrolyze, oxidation, isomerization et all in which chemical stage of process carrying out in range of boiling temperatures of components reaction mixture on a few contact mass transfer trays [1], in particular in process production of ethylene glycol.

The direct hydrolysis of ethylene oxide be most widespread method production of ethylene glycol. The glycols produced can further reacting with ethylene oxide to produce the unwanted by-products: di-ethylene, three-ethylene and tetra-ethylene glycols.

Synthesis of ethylene glycol carrying out in liquid phase at increasing temperatures (near 480 K) and pressure (1.5-2 MPa) at surplus of water.

Technological scheme of process is sufficiently cumbersome and include besides reactor three vaporizers and block rectification columns for removal of unwanted components from goods ethylene glycol. That complicated technological scheme in principle can be replaced by one apparatus – reactive distillation column.

It is peculiarity of reactive distillation column working that appearing possible circulation of water plenty in column by practical total conversion of ethylene oxide. In that case, upper part of column is working in regime of infinity reflux ratio (total reflux) what increasing efficiency of rectification [1].

Modeling of reactive distillation column is can complicated as well that that simulation model of reaction and rectification processes usually are fulfill by a different methodical fundamentals. Rectification process as a rule calculated by models of static on the base of conception of theoretical tray which ensure improvement of equilibrium between vapor and

liquid passed in infinity time ; that maybe allowed avoid of using such difficult characteristics as surface contact phases, coefficient of mass transfer, hydrodynamic structure of currents on the real contact tray, etc. From another side, modeling of chemical process required take into account kinetics of process. We united both considered approach to decision of problem in one combined static-kinetics model of reactive distillation column.

The kernel of combined static-kinetics model is model of rectification process in complicated composition column which be equivalent for any system of simple columns [2]. Where that model was elaborated, there are foreseeing bring feed on the every tray, partial or total remove vapor and liquid phases out of tray after finishing of mass transfer. That phases can bring as feeds on the other trays of composition column. Working out model of column was adapted to present problem by supplement of algorithm with blocks of mixture of feed with circulate stream and calculation of chemical transformation on the theoretical tray which at the same time play a part of reaction zone (Fig. 1).

It is adoption following assumption by work out of mathematical model of reactive distillation column:

- hydrodynamic of streams on the tray is described with model ideal oust;

- relative volatility of fractionate components is receive as constant by high of column. Ethylene glycol is using as standard component.

Reactive distillation column can efficient put into practice by overcome twine difficulties:

- necessary limitatio – time of reaction

- is not more than time being of streams in reaction zone;

Fig.1. Scheme streams of model reaction tray for calculation of reactive distillation column: 1 – mix part, 2 – reaction part, 3 – fractionating part.
— - liquid streams, ⟶ - vapor streams.

- sufficient limitation – composition of reaction mixture mast guarantee high purity of main product.

Plate to plate calculations of columns are used the modified relaxation method. At first the column is fill up with clear water.

It is bring to light following peculiarity of working reactive distillation column.

PP-120

Calculations of compositions reaction mixture arriving at maximum going out of ethylene glycol (at typical for industrial conditions correlation water : ethylene oxide in feed near 6 : 1 [3] are showed that maximum concentration ethylene glycol do not dependence from temperature of hydrolysis and equal 12.5-12.7 %mol. Increase of temperature in range 373-493 K is reducing concentration of un-reacting ethylene oxide nearly on the three cut above.

Increase of multiple water: ethylene oxide in range 2-100 is essential increasing concentration ethylene glycol (from 68 to 99 % mol) in potential residual fraction. Residuum of high degree of purity with concentration of ethylene glycol 99.2 % is correspond to goods product of first quality and may it using without supplementary purification. Thus, limitation by purity of ethylene glycol which may receive in reactive distillation column is overcome by selection of correlation water: ethylene oxide in initial reaction feed mixture.

On the base of results modeling of process receiving ethylene glycol may be recommend level of correlation water: ethylene oxide in reaction zone entrance after mixed feed with recycling water (that water have only small soiling of organic substances) in the reactive distillation column on the level (30-40) : 1. Further increasing maintenance of water in feed can not give essential positive effect and only lead to increasing of energetic expenditure for realization of process (Fig. 2). The appraisal of ensure necessary residence time in reaction zone on rectification tray of column is carry out on the base calculation kinetics of ethylene glycol synthesis
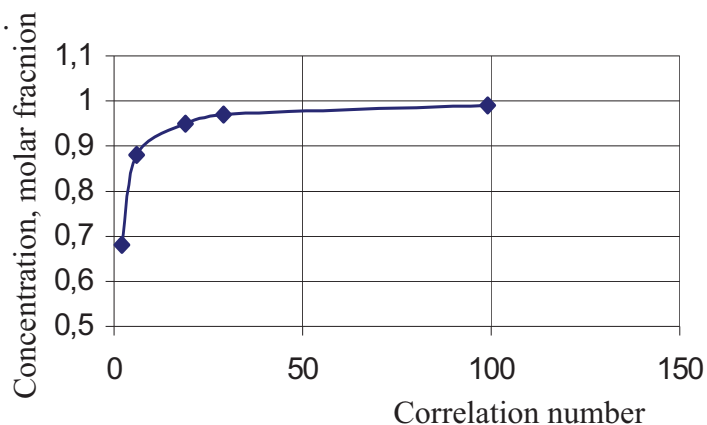
Fig.2.Dependence of maximum concentration ethylene glycol in potential residuum of column from correlation number water : ethylene oxide in initial feed mixture at temperature in reaction zone 493 K

For all that, achievement maximum quantity of ethylene glycol is very stable from residence time near 0.4 min. because practical absence ethylene oxide in reaction mixture is suppressing unwanted reactions. Calculation of real stay time stream of reflux in reaction zone of column with productivity by ethylene glycol 6.2 t/h at correlation water : ethylene oxide at range (30-70):1 said that residence time of reaction mixture near 0.56 min (Fig.3).

Such, working out model of reaction distillation column is guarantee realization of examined limitations and assumptions.

696

It is compare results of calculation reactive distillation column by work out static-kinetics model with data of paper [1] in which are take into account only two from four reactions of process hydrolysis from ethylene oxide. The acceptable likeness profiles temperature and concentration water and ethylene glycol by trays of column is indirect testify about adequacy of work out combined mathematical model of column (Fig. 4).

Fig.3. Kinetic syntheses of ethylene glycol at 493 K and correlation water: ethylene oxide 29.3 : 1.
1 – ethylene glycol, 2 – water. τ_R – residence time reaction mixture on the tray
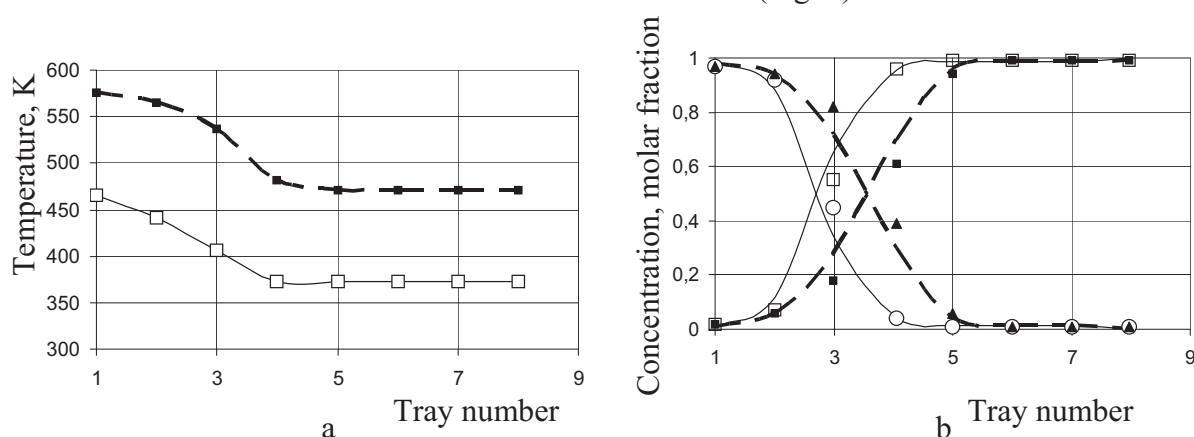
Fig.4. Profiles temperature (a) and concentration (b) water (1) and ethylene glycol (2) by trays of column
Continuous lines – is calculations by model at 0.1 MPa,
punctuated lines – is calculations by model at 1.5 MPa , points – data of [1].

Conclusion

1. It is work out adequacy combine static-kinetics model of reactive distillation column for production ethylene glycol.
2. The residence time of reaction mixture on the tray is enough for completely finishing of reaction. Limitation by purity of ethylene glycol which may receive in reactive distillation column is overcome by selection of correlation water: ethylene oxide in initial reaction feed mixture and temperature of process.

References

1. Cardoso M.F., Salcedo R.L., Feyo de Azevedo S. et al. Optimization of reactive distillation processes with simulated annealing. //Chem. Engineering Sci., 2000, v.55, p.5059.
2. Kondratjev A.A., Samoilov N.A. Rectification columns with intermediate heat- and mass transfer section. // Journal of Applied Chem. , 1997, v. 70, № 9, p. 1512 (In Russian).
3. Diment O.N., Kazansky K.S., Miroshnikov F.M. Glycols and other products from ethylene and propylene oxides. Moscow : Chemistry , 1976, 373 p.

PP-121

DEVELOPMENT OF THE MATHEMATICAL MODEL OF PROCESS OF PYROLYSIS OF DEAROMATIZED DISTILLED GASOLINE IN THE PRESENCE OF FUEL GAS

Aliyev A.M., Babayev A.I., Tairov A.Z., Mamedov Z.A.

Institute of Chemical Problems of National Academy of Science of Azerbaijan,
Baku, Azerbaijan, itpcht@itpcht.ab.az

The purpose of the present work is to increase the efficiency of process of the pyrolysis by added to dearomatized distilled gasolene of fuel gas. Dearomatized gasoline is a distilled gasoline which is alkilated with &-olefins C_9-C_{12} in the presence of catalyst – $AlCl_3$; the obtained alkilaters are extracted as highindex alkilbenzene oils.

The investigation of process of pyrolysis of dearomatized distilled gasoline in the presence of fuel gas was carried out at temperatures, 800-840^{0}C and contact times 0.5÷0.9 sec at different ratio; gasoline: fuel gas (85:15; 90:10; 95:5).

The results of analysis of carried out experiments showed that pyrolysis gasoline in the presence of fuel gas allows increasing the yield of ethylene 5.0÷6.0%. Under these conditions the gasification was increased on 10-12% also increased the yield of the light resins and the yield of heavy resins was decreased.

The increasing of partial pressures of methane and hydrogen in the system increases of the rate reaction of demethylation as a result the yield of benzene increases.

An addition of fuel gas to dearomatized distilled gasoline decreases the coke deposition in the process of pyrolysis because of termination of the reaction of growth of highconcentrated semiproducts of coke deposition. In addition the fuel gas contains 0.22 mg/m^3 sulfur compounds which are inhibitors for reaction of formation of pyrolysis reactor on 5-7 days.

While pyrolysis of the distilled gasoline fractions a large number of the reactants take part and it is not possible to describe all their conversions. For developing of mechanism of this process we have used the method of chemical generalization of the reactants on group hydrocarbon composition [1]. While investigation of continuous mixtures such generalization

is convenient. The composition of raw gasoline fraction was characterized the following groups:

1. Paraffin hydrocarbons (P)

2. Naphthenes (N)

3. Aromatic hydrocarbons (A)

The main of primary products while pyrolysiz of gasoline in our work were taken: hydrogen, methane, ethylene, propylene, butadiene, butenes, normal paraffin hydrocarbons. The listed products of primary reaction take part also in the secondary conversions.

Acetylene is a product of dehydrogenation of ethylene. Aromatic hydrocarbons were formed while secondary interactions of low olefin hydrocarbons; their concentrating between each other and with dien hydrocarbons form the high molecular compounds.

Taking into account chemical generalization of initial substances, the products of the reaction and the most essential chemical conversion we have suggested the generalization chemical and secondary reactions of pyrolysis conversion of gasoline:

$$P \xrightarrow{W_1} v_{11}H_2 + v_{12}CH_4 + v_{13}C_2H_4 + v_{14}P_{2-4} + v_{15}C_3H_6 + v_{16}C_4H_6 + v_{17}C_4H_8$$

$$N \xrightarrow{W_2} v_{21}H_2 + v_{22}CH_4 + v_{23}C_2H_4 + v_{24}P_{2-4} + v_{25}C_3H_6 + v_{26}C_4H_6 + v_{27}C_4H_8 + A$$

$$C_4H_{10} \xrightarrow{W_3} v_{31}H_2 + v_{32}CH_4 + v_{33}C_2H_4 + v_{34}P_{2-3} + v_{35}C_3H_6$$

$$C_3H_8 \xrightarrow{W_4} v_{41}H_2 + v_{42}CH_4 + v_{43}C_2H_4 + v_{44}P_2 + v_{45}C_3H_6 \qquad (1)$$

$$C_2H_6 \xrightarrow{W_5} v_{51}H_2 + v_{52}CH_4 + v_{53}C_2H_4 + v_{54}C_3H_6 + v_{55}C_4H_6$$

$$C_2H_4 \xrightarrow{W_6} v_{61}H_2 + v_{62}C_2H_4$$

$$v_{71}C_2H_4 + v_{72}C_3H_6 + v_{73}C_4H_8 \xrightarrow{W_7} v_{74}A + v_{75}H_2$$

$$v_{81}C_4H_6 + v_{82}A \xrightarrow{W_8} C$$
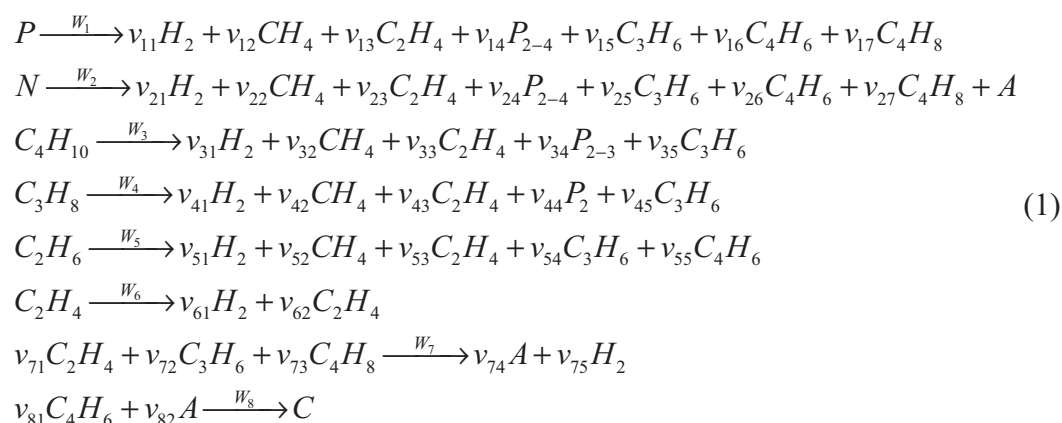
P_{2-3}- parafins with 2-4 carbon atoms; C – high molecular compounds; V_{ij} – mass coefficients equal the mass fractions of the products formed while pyrolysys of gasoline; W_j – rate of reaction.

In accordance with mechanism (1), pyrolysys of dearomatized distilled gasoline are described by 8 reactions primary and secondary conversions with 12 current components. Mathematical model of the process can be presented the following form:

$$\frac{G_c dg_1}{dV} = v_{11}W_1 + v_{21}W_2 + v_{31}W_3 + v_{41}W_4 + v_{51}W_5 + v_{61}W_6 + v_{75}W_7$$

$$\frac{G_c dg_2}{dV} = v_{12}W_1 + v_{22}W_2 + v_{32}W_3 + v_{42}W_4 + v_{52}W_5$$

$$\frac{G_c dg_3}{dV} = v_{13}W_1 + v_{23}W_2 + v_{33}W_3 + v_{43}W_4 + v_{53}W_5 - W_6 + v_{71}W_7$$

$$\frac{G_c dg_4}{dV} = v_{14}W_1 + v_{24}W_2 + v_{34}W_3 + v_{44}W_4$$

$$\frac{G_c dg_5}{dV} = v_{15}W_1 + v_{25}W_2 + v_{35}W_3 + v_{45}W_4 + v_{54}W_5 - v_{72}W_7 \qquad (2)$$

$$\frac{G_c dg_6}{dV} = v_{16}W_1 + v_{26}W_2 + v_{55}W_5 - v_{81}W_8$$

$$\frac{G_c dg_7}{dV} = v_{17}W_1 + v_{27}W_2 - v_{73}W_7$$

$$\frac{G_c dg_8}{dV} = v_{28}W_2 + v_{74}W_7 - v_{82}W_8$$

$$\frac{G_c dg_9}{dV} = v_{62}W_6$$

$$\frac{G_c dg_{10}}{dV} = W_8$$

$$\frac{G_c dg_{11}}{dV} = -W_1$$

$$\frac{G_c dg_{12}}{dV} = -W_2$$

where $g_i(i=1,12)$ – mass fraction of hydrogen, methane, ethylene, paraffin hydrocarbons C_2-C_4, propylene, butadiene, butanes, aromatic hydrocarbons, acetylene, high molecular compounds, paraffin and naphthene hydrocarbons of the gasoline.

Suggested mathematical model (2) have given possibility to take account of regime parameters, compositions and expenditure of raw material while calculating of material balance of the process pyrolysis and can be used for control of the process.

Literature

1. Yu.M.Zhorov, Modeling of Physico-Chemical Processes of Oil Processing and Petrochemistry, M., Khimiya, 1978, 375 c

STUDY OF KINETIC REGULARITIES OF N-PROPYL ALCOHOL OXIDATION REACTION OVER POLYFUNCTIONAL ZEOLITE CATALYST CuCaA

A.M. Aliyev, <u>D.B. Tagiyev</u>, S.S. Fatullayeva, S.M. Mejidova, F.A. Kuliyev

Department of Biophysical and Bioorganic Chemistry, Azerbaijan Medical University
23, Bakikhanov str, 1022, Baku, Azerbaijan
fax: (99412)4903520; e-mail: dtagiyev@hotmail.com

Summary

The results of investigations of oxidative conversion of n-propyl alcohol with participation of molecular oxygen over synthetic and natural zeolites of the different types modified by cations Cu^{2+}, Pd^{2+}, Sn^{2+}, Zn^{2+} have shown that by the regulation of zeolite structure, nature and concentration of promoted metals and also temperature, contact time, mole ratio of reagents, oxidation of n-propyl alcohol can be directed to the formation of propionic aldehyde, propionic acid or propylpropionate. It has been established that polyfunctional zeolite catalyst CuCaA containing 3.0 wt.% Cu^{2+} shows a high activity and selectivity in the direct oxidation of n-propyl alcohol into propionic acid at relatively low temperatures.

Introduction

The heterogeneous catalytic oxidative conversion of aliphatic alcohols is a highly perspective method of obtaining of carboxylic acids. The known catalysts (transition metals over the different carriers, oxides of the transition metals and etc.) are not effective for the given process because of the proceeding of the numerous side reactions under their influence and high temperature of the process [1]. Although, zeolite catalysts modified by cations of the transition metals decrease temperature of the process and show a high acti-vity, however, the selectivity regulation of heterogeneous catalytic conversion of aliphatic alcohols with the aim of the preferential formation of one of the valuable products (aldehyde, acid, ester) is embarrassed with insufficient studying of the mechanism of these processes [2]. The present paper is dedicated to the study of kinetic regularities of proceeding of the oxidative conversion reaction of n-propyl alcohol into propionic acid over polyfunctional zeolite catalyst CuCaA containing 3.0 wt.% Cu^{2+} ions.

Experimental

Both natural – clinoptilolite (SiO_2/Al_2O_3=8.68) of Aidag field and mordenite (SiO_2/Al_2O_3=9.6) of Chananab field of Azerbaijan and synthetic zeolites – NaA

(SiO$_2$/Al$_2$O$_3$=2.0), CaA (SiO$_2$/Al$_2$O$_3$=1.9), NaX (SiO$_2$/Al$_2$O$_3$=2.9), NaY (SiO$_2$/Al$_2$O$_3$=4.2) modified by ion-exchange method with Cu^{2+}, Pd^{2+}, Sn^{2+}, Zn^{2+} cations have been studied in this reaction. The catalytic tests of the activity of the synthesized samples of metalzeolite catalysts and study of the kinetic regularities of the reaction of n-propyl alcohol oxidation were carried out on a flow installation with the fixed bed of catalyst. The experimental kinetic investigations of vapor-phase oxidation reaction of n-propyl alcohol into propionic acid were carried out over zeolite catalyst CuCaA (Cu^{2+}-3.0 wt.%) at pressure 101.325 kPa, in the range of the reaction temperatures 453-523 K, space velocity 900-4500 h^{-1} and partial pressures of reagents P$_{O_2}$ = 5-40 kPa, P$_{C_3H_7OH}$ = 5-40 kPa and under the conditions ensuring the running of the reaction in the kinetic area. Catalyst CuCaA (Cu^{2+}-3.0 wt.%) was prepared by ion-exchange method. Before studying catalyst CuCaA (2 cm^3) was activated by air current at 723 K, GHSV=2400 h^{-1} for 2 hours and then cooled up to the reaction temperature. The reaction products were analyzed by GC and IR-spectroscopy.

Results and discussion

Catalysts prepared on the basis of zeolite CaA are highly more active in the reaction of direct oxidation of n-propyl alcohol into propionic acid than ones prepared on the basis of synthetic and natural zeolites of X, Y types, clinoptilolite and mordenite. Comparison of obtained data has shown that zeolite CuCaA containing 3.0 wt.% Cu^{2+} cations is the most effective catalyst for the given reaction. The kinetic regularities of the reaction of oxidative conversion of n-propyl alcohol into propionic acid have been investigated over zeolite catalyst CuCaA (Cu^{2+}-3 wt.%). The given results showed that with increasing of partial pressure of n-propyl alcohol selectivity of process on propionic acid is increased at temperatures 453-498 K. The yield of propionic acid reaches maximal value (66.4%) at partial pressure of n-propyl alcohol 10 kPa (T=498 K) and then yield of propionic acid begins to decrease. The decrease of yield of propionic acid can be explained in such way that at the given partial pressure of oxygen (P$_{O_2}$ =30 kPa) relatively high partial pressures of n-propyl alcohol prevent to the coordination of oxygen to the active centers of metalzeolite catalyst. The increase of partial pressure of oxygen at temperatures T= 453-498 K results in the negligible increase of selectivity of the process on propionic acid and increase the yield of propionic acid. The results of the carried out investigations have also shown that the greatest yield of propionic acid and the greatest selectivity of the process on propionic acid are observed at relatively low space velocity (900 h^{-1}) and reach to maximal value in the range of temperatures 488-498 K.

On the basis of the experimental data the total kinetic scheme of reaction proceeding of oxidation of n-propyl alcohol over catalyst CuCaA can be depicted as:

$$C_3H_7OH + \frac{1}{2}O_2 \xrightarrow[-H_2O]{k_2} CH_3CH_2CHO \begin{cases} \xrightarrow{+4O_2} \xrightarrow{k_4} 3CO_2 + 3H_2O \\ \xrightarrow{+\frac{1}{2}O_2, k_3} CH_3CH_2COOH \xrightarrow[-H_2O]{+C_3H_7OH} \xrightarrow{k_1} CH_3CH_2COOC_3H_7(1) \end{cases}$$
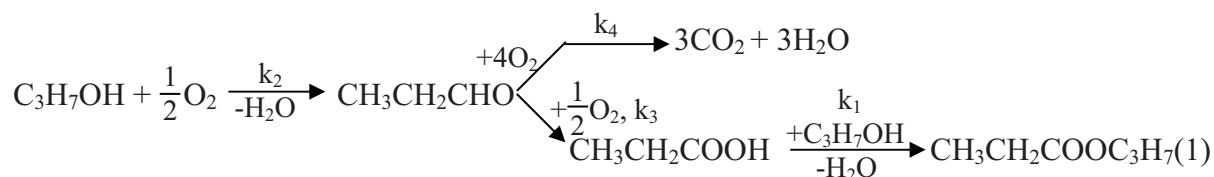
The kinetic stage schemes of products formation of n-propyl alcohol oxidative conversion may be presented in the following view:

Kinetic equation corresponding to kinetic scheme of propionic aldehyde formation is presented as:

$$r_1 = \frac{k_2 K_2 K_3 P_1 P_2}{(1 + K_2 P_1 + K_3 P_2 + K_1 P_3 + K_4 P_4)^2} \tag{2}$$

Kinetic scheme of propionic acid formation is presented by the following kinetic equation:

$$r_2 = \frac{k_3 K_3 K_4 P_2 P_4}{(1 + K_2 P_1 + K_3 P_2 + K_1 P_3 + K_4 P_4)^2} \tag{3}$$

Kinetic equation corresponding to kinetic scheme of propylpropionate formation is offered as:

$$r_3 = \frac{k^*_1 K_1 K_6 P_1 P_3}{(1 + K_1 P_3 + K_6 P_1)^2}$$

$$K_1 \gg K_6; \qquad K_6 k^*_1 = k_1 \qquad r_3 = \frac{k_1 K_1 P_1 P_3}{(1 + K_1 P_3)^2} \tag{4}$$

Kinetic scheme of carbon dioxide formation is presented by stated below kinetic equation:

$$r_4 = \frac{k_4 K_5 P_4 P_2}{1 + K_5 P_4} \tag{5}$$

On the basis of kinetic equations the composed kinetic model of process of n-propyl alcohol oxidation over zeolite catalyst CuCaA is presented as:

$$W_{aldehyde} = r_1 - r_2 - r_4 = \frac{k_2 K_2 K_3 P_1 P_2}{(1 + K_2 P_1 + K_3 P_2 + K_1 P_3 + K_4 P_4)^2} \quad -$$

$$- \frac{k_3 K_3 K_4 P_2 P_4}{(1 + K_2 P_1 + K_3 P_2 + K_1 P_3 + K_4 P_4)^2} - \frac{k_4 K_5 P_4 P_2}{1 + K_5 P_4} \tag{6}$$

$$W_{acid} = r_2 - r_3 = \frac{k_3 K_3 K_4 P_2 P_4}{(1+K_2 P_1 + K_3 P_2 + K_1 P_3 + K_4 P_4)^2} - \frac{k_1 K_1 P_1 P_3}{(1+K_1 P_3)^2} \qquad (7)$$

$$W_{ester} = r_3 = \frac{k_1 K_1 P_1 P_3}{(1+K_1 P_3)^2} \qquad (8) \qquad W_{co_2} = r_4 = \frac{k_4 K_5 P_4 P_2}{1+K_5 P_4} \qquad (9)$$

where P_1, P_2, P_3 и P_4 – partial pressures of alcohol, oxygen, acid and aldehyde; k_1, k_2, k_3 и k_4 – constants of the reaction rate of ester, aldehyde, acid and carbon dioxide; K_1, K_2, K_3 и K_4 – constants of adsorption equilibrium of acid, alcohol, oxygen and aldehyde.

This model was subjected to statistical analysis on the basis of experimental kinetic data. On the basis of aforecited kinetic equations of n-propyl alcohol oxidation reaction into propionic acid by means of comparison of experimental and calculated kinetic data the kinetic parameters of the given model have been determined.

Conclusion

The results of investigations of catalytic oxidative conversion reaction of n-propyl alcohol with the participation of molecular oxygen have shown that, from the number of catalysts prepared on the basis of natural and synthesized zeolites, the process of oxidative conversion of n-propyl alcohol into propionic acid proceeds with the high activity and selectivity over zeolite CaA containing 3.0 wt.% Cu^{2+}. The kinetic regularities of the reaction over zeolite catalyst CuCaA have been studied. On the basis of experimental data kinetic scheme of n-propyl alcohol oxidation reaction has been proposed and kinetic model of the present process has been developed.

References

[1] M.A.Wassel, N.Kh.Allahverdova, K.Y.Adjamov, Collect.Czechosl.Chem.Commun., 57 (1992) 446.

[2]L.Jinglin, L.Bin, L.Jiang and et al., J.Catal., 20 (1999) 429.

CATALYTIC PROPERTIES OF THE PROTON CONDUCTORS:

$Sr_3CaZr_{0.5}Ta_{1.5}O_{8.75}$, $BaCe_{0.9}Y_{0.1}O_{2.95}$ AND $Ba_3Ca_{1.18}Nb_{1.82}O_{8.73}$

FOR REVERSE WATER GAS SHIFT

Hermenegildo de A.L. Viana, John T.S. Irvine

School of Chemistry, University of St. Andrews, KY16 9ST, Scotland

jtsi@st-andrews.ac.uk

A renewable hydrocarbon-based hydrogen economy is a very promising scenario. Such a technology is acceptable if it does not generate additional CO_2. However, there are two key barriers for the implementation of a hydrocarbon-based hydrogen economy: separation and concentration of CO_2 from air exhaust stream and efficient conversion of CO_2 to hydrocarbon fuels.

Solid oxides with high surface areas have been used as supports for precious metals as catalysts. One of the most common catalysts for this reaction is ceria supported catalysts due to oxygen exchange properties. Among the precious metals, Pt supported by ceria has been well studied; however, Pd, Rh or even Au have been shown to be effective also.[1]

This study shows that the cerate $BaCe_{0.9}Y_{0.1}O_{2.9}$ or other proton conductors $Sr_3CaZr_{0.5}Ta_{1.5}O_{8.75}$, ₅ and $Ba_3Ca_{1.18}Nb_{1.82}O_{8.73}$ are active heterogeneous catalysts for the reverse water gas shift (RWGS) reaction.

The reaction studied was the reverse water gas shift (RWGS) reaction (reaction 1) which allows the reduction of CO_2 to CO. This CO might be used as a chemical feedstock for the Fischer-Tropsch synthesis of higher hydrocarbons, the oxy-synthesis or the synthesis of oxygenates.[2]

$$CO_2 + H_2 \Leftrightarrow CO + H_2O \quad \Delta H^o_{298}=41kJ/mol \quad [1]$$
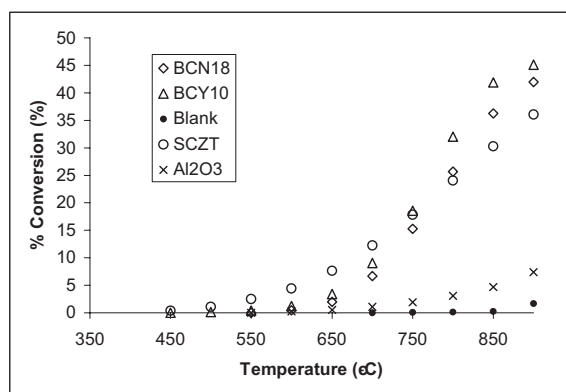
Figure 1 – RWGS reaction rate of conversion against temperature

Their maximum rate of conversion of CO_2 to CO is obtained with BCY10 reaching 45% CO conversion by 900ºC (figure 1). Both BCN18 and SCZT have shown smaller rates of conversion. At low temperatures, SCZT has shown a good conversion onset temperature, starting to convert CO_2 into CO at 400ºC. Their stability and degradation after being exposed to H_2/CO_2 atmospheres is also investigated.

[1] – D. Tibiletti, S.P. The, G. Rothenberg, Journal of Catalysis 225 (2004) 489-497

[2] – D.J. Moon, J.W. Ryu, Catalysis Today 87 (2003) 255-264

ANALYSIS OF GENETIC ALGORITHM OPERATORS IN THE PRODUCTIVITY OF AN INDUSTRIAL REACTOR

Victorino, I.R.S. and Maciel Filho, R.

Laboratory of Optimization, Design and Advanced Control.

Department of Chemical Processes. School of Chemical Engineering.

State University of Campinas (UNICAMP)

P.O. Box 6066, 13081-970, Campinas, SP, Brazil,

Tel.:+55-19-37883971; Fax: +55-19-3788396

E-mails:igor_rsv@yahoo.com.br / maciel@feq.unicamp.br

Introduction

Genetic Algorithms (GAs) have obtained great popularity in the last decades, since this have shown great potential and ability to solve complex problems of optimization in diverse industrial fields, including chemical engineering process. Several optimization classic techniques have been used with this objective, but generally these techniques are not efficient, mainly when the complexity of the problem is large due to non-linearity and process variable interactions.

The genetic algorithms are based on the genetics and natural evolution principles of the species. The mechanism of the Genetic Algorithms technique occurs with successive modifications of the individuals or chromosomes (artificial structures) of population through the application of selection, crossover, and mutation operators. The application of Genetic Algorithms needs to develop a representative objective function of the reactor model, where this objective function evaluates the quality of determined solutions, being used as main criterion in approaches of great potential in industrial applications.

This work has as objective the development of an optimization methodology, using genetic algorithms, as evolutionary technical coupled with the concepts of evolutionary operation to be applied in deterministic mathematical models.

The process considered is a multiphase catalytic reactor, where hydrogenations reactions take place. A series of parallel and consecutive reactions may happen, so that the

reactor has to be operated in a suitable way to achieve high conversion as well as high selectivity. The reactor is constituted of a series of tubes, which are immersed in a boiler. In fact, they consist of concentrical tubes. The reactants flow through the tubular as well as through the external annular region, while the thermal fluid flows inside the other regions. The model is considered in the steady-state.

The study was related to a specific cyclic alcohol (CA) production, optimizing some important operational parameters. A deterministic model based on the equations of mass conservation, energy and moment was developed and validated with real operational data.

The study was made analyzing the genetic operators sensibility and influence in the specific cyclic alcohol productivity. In order to do this, some genetic operators and parameters had been studied and analyzed as: two crossover types (one-point and uniform) and the variation of crossover rates, the presence or not mutation operator types, the variation mutation rates and the consequences in the increase of the production.

This study observed the influence of some genetic operators and parameters in the improvement of the reactor performance. The results showed an increase in the CA productivity (considerable increase CA production) with changes in the operational parameters analyzed and showing that this optimization procedure is very robust and efficient.

Results

The GA procedure revealed to be very efficient and robust for all the considered situations. Several testes with different population sizes, crossover and mutation values allow to conclude that the optimization by GA works well without be so dependent of its design values as well as the initial value. Optimization of the same problem by conventional methods (as SQP) was not possible to be obtained in all the cases considered in this work.

In the Figures 1 and 2 are shown some results considering the influence of the population size (npz), crossover rates (%) and the crossover form in the CA productivity (mass rate normalized). It is verified in this study that using the one-point crossover form, values better of CA rates are reached, meaning more raised productivity of the desired product. This situation is important therefore the amount produced to the long time is considerable, diminishing costs and increasing the profitability.

Level 1

Level 1
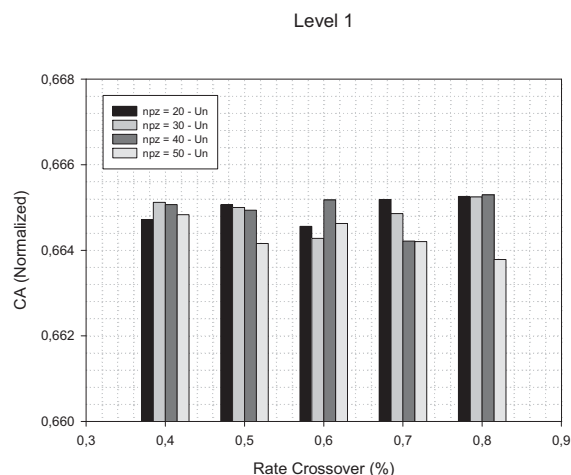
Figure 1. Analysis crossover rate and the population size and influence in the Cyclic Alcohol (CA) mass rate normalized - Uniform Crossover (Un).
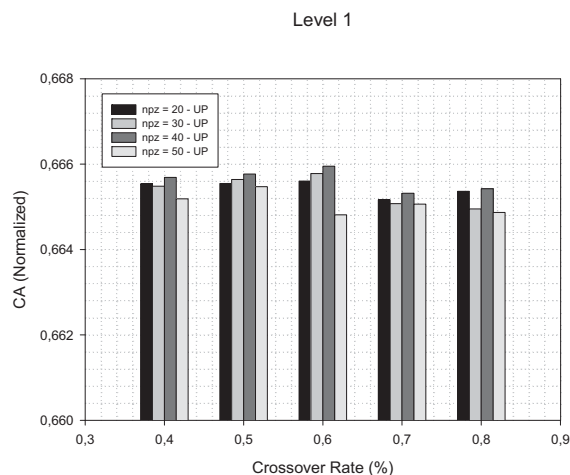
Figure 2. Analysis crossover rate and the population size and influence in the Cyclic Alcohol (CA) mass rate normalized – One-Point Crossover (UP).

Other analyses will be carried through considering the mutation form and rate, and its influence in the CA productivity.

References

1. Bäck, T., Fogel, D. B. and Michalewicz, T. (2000). editors. Evolutionary Computation 1: Basic Algorithms and Operators. Institute of Physics Publishing, 2000.
2. Carroll, D. L. (1996). "Chemical Laser Modeling with Genetic Algorithms". AIAA Journal, Vol. 34, No. 2, February.
3. Coussemant, F. and Jungers, J. C. (1950). "La Cinétique de L´Hydrogénation Catalytique des Phénols". Bull. Soc. Chim. Bel., vol. 59, pp. 295-326.
4. Deb, K. (1998). "Genetic algorithms in search and optimization: The technique and applications". Proceedings of International Workshop on Soft Computing and Intelligent Systems, Calcutta, India: Machine Intelligence Unit, Indian Statistical Institute, pp. 58 – 87.
5. Froment, G. F. and Bischoff, K. B. (1990). "Chemical Reactor Analysis and Design". John Wiley and Sons, 2ed., 664pp, New York.
6. Goldberg D. E. (1989). Genetic Algorithms in Search, Optimization, and Machine Learning. Addison-Wesley Publishing Company, INC.
7. Goldberg, D. E. and Deb, K. (1991). A Comparison of Selection Schemes Used in Genetic Algorithms, Foundation of Genetic Algorithms, edited by G. J. E. Rawlins, pp. 69-93.
8. Holland, J. H. (1992). Adaptation in Natural and Artificial Systems. University of Michigan Press, 2nd.
9. Hongqing C., Jingxian Y., Lishan K., Yuping C. and Yongyan C. (1999). The Kinetic Evolutionary Modeling of Complex Systems of Chemical Reactions. Computers e Chemistry, 23, pp. 143-151.
10. Moros, R., Kalies, H., Rex, H. G. and Schaffarczyk, St. (1996). A Genetic Algorithm for Generating Initial Parameter Estimations for Kinetic Models of Catalytic Processs. Computers Chem.Engineering, Vol. 20, No. 10, pp. 1257-1270.
11. Santana, P. L. (1995). Mathematical Modeling for three phase reactor: deterministic, neural and hybrid models, PhD Thesis, School of Chemical Engineering, Unicamp, São Paulo, Brazil (in Portuguese).
12. Simant R. U. and Kalyanmoy D. (1997). Optimal Design of an Ammonia Synthesis Reactor Using Genetic Algorithms. Computers Chem. Engineering, Vol. 21, No. 1, pp. 87-92.
13. Syswerda, G. (1989). Uniform Crossover in Genetic Algorithms. In J. D. Schaffer (Ed.), Proceedings of The Third International Conference on Genetic Algorithms, pp. 2-9.
14. Vasco de Toledo, E.C.., Santana, P.L., Wolf-Maciel, M.R., Maciel Filho, R. (2001). Dynamic modelling of a three-phase catalytic slurry reactor, Chem. Eng. Sci*., **56**, 6055-6061.
15. Wehrens, R and Buyders, M. C. (1998). Evolutionary Optimisation: A tutorial. Trends in Analytical Chemistry, Vol. 17, No. 4.

EVALUATION OF GENETIC ALGORITHM CODING TO OPTIMIZATION OF A CYCLIC ALCOHOL INDUSTRIAL REACTOR

Victorino, I.R.S. and Maciel Filho, R.

Laboratory of Optimization, Design and Advanced Control.

Department of Chemical Processes. School of Chemical Engineering.

State University of Campinas (UNICAMP)

P.O. Box 6066, 13081-970, Campinas, SP, Brazil,

Tel.:+55-19-37883971; Fax: +55-19-3788396

E-mails:igor_rsv@yahoo.com.br / maciel@feq.unicamp.br

Introduction

Evolutionary Algorithms as Genetic Algorithms (GAs) have gained great popularity since the last decade. The GAs have shown great potentiality and ability to decide complex problems of optimization in diverse fields, including Chemical Engineering. In this paper the main objective is to investigate the GAs performance for the optimization of an example related the industrial reactor of Cyclic Alcohol production. The intention is to find out optimal operating conditions so that the conversion might be optimized but at the same time constraints as temperatures inside the reactor does not be violated, the side products be minimized and a restrict range of reactant concentration at the reactor exit be guaranteed. This is important for environmental restriction and difficulties to the optimization problem.

As a case study is considered an industrial hydrogenation multiphase catalytic reactor to obtain a Cyclic Alcohol (CA). The system is analyzed for different level of operational requirements. The reactor consists of concentrical tubes, with the reactants flowing through the internal tubular part, while the coolant circulates through the inner anulles. The mathematical equations of the deterministic model are based on conservation principles (mass, energy and momentum) for the reactants and for the coolant and validated with real operational data. Industrial data of temperature are available and they will be used in the development and validation of the model. The model is written in steady-state regimen with the plug-flow assumption.

The main task is to develop and implement a GA code coupled in this reactor mathematical model, considering the analysis and comparison among two coding types inherent the Genetic Algorithms (binary and floating-point coding), in the optimization of reactor operational parameters. This analysis considers the use of specific genetic parameters of each coding type, and the respective influences in the reaction performance (CA productivity increase). The choice of an appropriate structure (representation or coding) for solutions (individuals) of a determined problem is a major determining factor to GAs success.

The intention is to show that this technique is suitable for cyclic alcohol production maximization obtaining good results with operational improvements (reduction catalyst rate, reduction main reactant rate – Benzylic Alcohol and undesired product rate – Cycloalkane), analyzing two coding types and the influence that these have in the reactor performance (CA productivity increase). The reduction main reactant rate must be considered, mainly when the emissions occur in high concentrations causing damages to the environment.

The results shown that, the method is very robust procedure which allows the reactor to be operated of high level of performance, restricting the emissions of toxic reactant and reducing the undesirable products.

The GA code coupled to the reactor model showed to be a very efficient technique for reactor optimization. Similar problems or other systems can be studied for verification of his efficiency.

At this point is welcome to remember the difficulties formal when conventional optimization as SQP are used. The results are dependent upon the initial values and a relatively high number of convergence difficulties are relatively common for large dimensional problem. This was not the case for the GA.

The process can be optimized in relation to other parameters that in future works will be considered, such as the kinetic parameters and the orders of reaction, besides others being studied.

OPTIMIZATION BASED ON GENETIC ALGORITHMS: APPLICATION TO INDUSTRIAL REACTOR PRODUCTION

Victorino, I.R.S. and Maciel Filho, R.

Laboratory of Optimization, Design and Advanced Control.

Department of Chemical Processes. School of Chemical Engineering.

State University of Campinas (UNICAMP)

P.O. Box 6066, 13081-970, Campinas, SP, Brazil,

Tel.:+55-19-37883971; Fax: +55-19-3788396

E-mails:igor_rsv@yahoo.com.br / maciel@feq.unicamp.br

Introduction

In the last decades, with the increase of the competitiveness of the world market (reduction of costs, prices increase of the productivity and efficiency of the productive processes) there was a great interest in to improve and to optimize the processes of chemical industries. Several optimization classic techniques have been used with this intention, but many of those techniques are not efficient, mainly when the problem is complex, and typically a high number of variables of the processes, non-linearity models that supply many possible solutions, and constraints that have to be considered lead the problem to be of difficult solution. As alternative a class of algorithms, denominated of Genetic Algorithms (an evolutionary algorithms category) present good potential to be used as a tool for complex and large scale systems.

Genetic Algorithms (GAs) are general-purpose search techniques for resolution of complex problems. They are based on the genetics and natural evolution principles of the species. The GAs work through repeated modifications in an artificial structures population denominated of individuals (chromosomes or set of solutions) applying the selection, crossover, and mutation operators. The evaluation of optimization happens with an objective function (fitness) that determines the performance of the genetic process. The fitness could be understood as the capacity of the individuals to survive in a natural environment.

This work has as objective the development of an optimization methodology, using Genetic Algorithms (GAs), as evolutionary procedure coupled with the concepts of

evolutionary operation to be applied in deterministic mathematical models. As case study an industrial multiphase catalytic reactor was considered. The reactor is tubular in shape and is built-up with concentric tubes using the same concept of the auto-thermal reactors, with coolant fluid flow in the external annular. The mathematical equations of the deterministic model are based on conservation principles (mass, energy and momentum) for the reactants and for the coolant fluid and validated with real operational data. Industrial data of temperature are available and they are used in the development and validation of the model. The model is written in steady-state with the plug-flow assumption.

The studied example was related to production of a specific cyclical alcohol (CA), optimizing some important operational parameters.

The interest of this work is to show that the Genetic Algorithms technique can be useful to CA production maximization, obtaining good results with operational improvements (reduction catalyst rate, reduction main reactant rate – benzilic alcohol (BA) and undesired product rate – cycloalkane (C)). Some cares must be considered, mainly with the reactants emissions (main reactant- benzilic alcohol) that occur in high concentrations causing damages to the environment.

This study observed the influence of some genetic parameters in the increase of the cyclic alcohol productivity. The parameters (genetic parameters) considered involved the population size, crossover types with variation of crossover rates. The used coding was the binary form.

The results are quit good, showing high performance in the CA productivity (considerable increase CA production) with changes in the operational parameters analyzed and showing that this optimization procedure is very robust and efficient. The results point out that this technique is very promising to deal with large scale system with complex behavior due to non-linearity and variable interactions.

Results

In the following figures, it is evaluated the application of the GAs in the optimization of the selected parameters, six coolant fluid outflows, (Q_{ri}'s), outflow of catalyst (Q_{cat}) and the reactant feed temperature (T_0). The results are represented in Figures 1, 2 and 3 respectively.

In the Figure 1 shows the optimization profile with the generations adopted in the simulation of Level 1 production. This level can to be understood as a specific operational

form. The reactor performance improvement is reached as verified in the in the same figure (Figure 1).

The Figures 2 and 3 present the molar fractions profiles of two main components. These are Cyclic Alcohol (CA) (desired product) and Benzylic Alcohol (BA) (main reactant BA). The values are normalized.
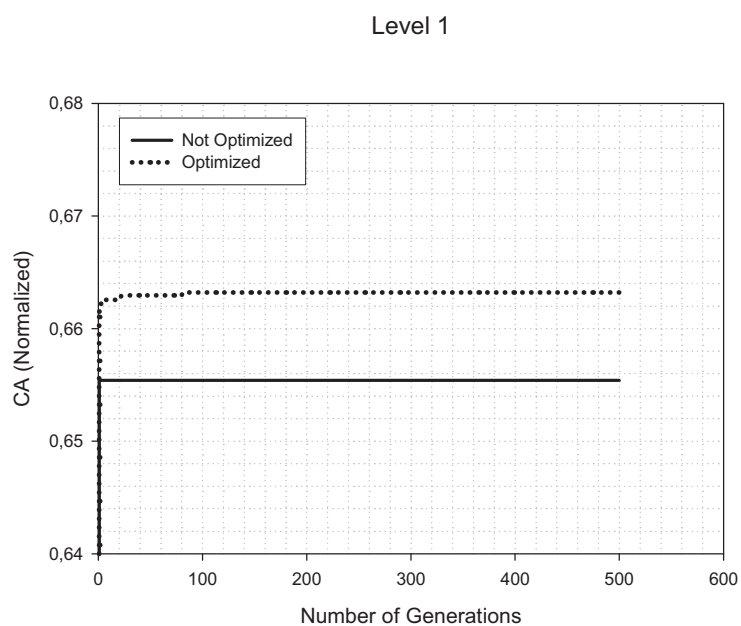
Level 1

Figure 1. Profile CA productivity (mass rate normalized) for production Level 1 with the optimization evolution.
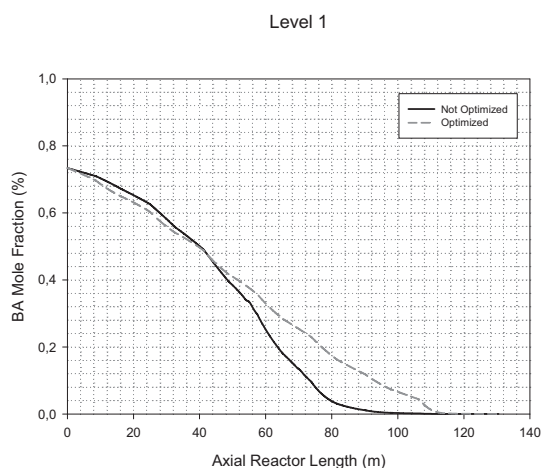
Figure 2. Main reactant (BA) mole fraction to the long the reactor length. Considering 500 generations.
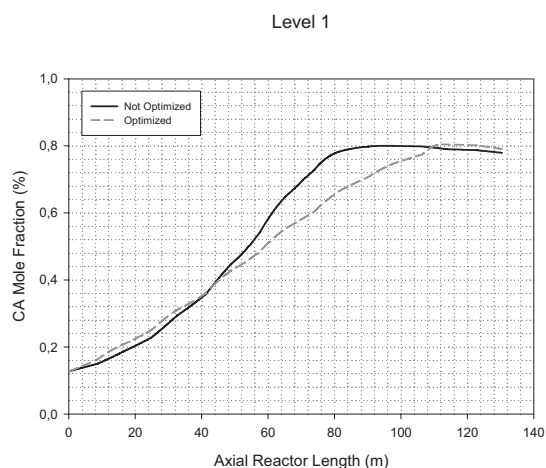
Figure 3. Product (CA) mole fraction to the long the reactor length. Considering 500 generations.

The GA code coupled to the reactor model showed to be a very efficient technique for reactor optimization. Similar problems or other systems can be studied for verification of his efficiency.

References

1. Bäck, T., Fogel, D. B. and Michalewicz, T. (2000). editors. Evolutionary Computation 1: Basic Algorithms and Operators. Institute of Physics Publishing, 2000.

2. Carroll, D. L. (1996). "Chemical Laser Modeling with Genetic Algorithms". AIAA Journal, Vol. 34, No. 2, February.

3. Coussemant, F. and Jungers, J. C. (1950). "La Cinétique de L´Hydrogénation Catalytique des Phénols". Bull. Soc. Chim. Bel., vol. 59, pp. 295-326.

4. Deb, K. (1998). "Genetic algorithms in search and optimization: The technique and applications". Proceedings of International Workshop on Soft Computing and Intelligent Systems, Calcutta, India: Machine Intelligence Unit, Indian Statistical Institute, pp. 58 – 87.

5. Froment, G. F. and Bischoff, K. B. (1990). "Chemical Reactor Analysis and Design". John Wiley and Sons, 2ed., 664pp, New York.

6. Goldberg D. E. (1989). Genetic Algorithms in Search, Optimization, and Machine Learning. Addison-Wesley Publishing Company, INC.

7. Goldberg, D. E. and Deb, K. (1991). A Comparison of Selection Schemes Used in Genetic Algorithms, Foundation of Genetic Algorithms, edited by G. J. E. Rawlins, pp. 69-93.

8. Holland, J. H. (1992). Adaptation in Natural and Artificial Systems. University of Michigan Press, 2nd.

9. Hongqing C., Jingxian Y., Lishan K., Yuping C. and Yongyan C. (1999). The Kinetic Evolutionary Modeling of Complex Systems of Chemical Reactions. Computers e Chemistry, 23, pp. 143-151.

10. Moros, R., Kalies, H., Rex, H. G. and Schaffarczyk, St. (1996). A Genetic Algorithm for Generating Initial Parameter Estimations for Kinetic Models of Catalytic Processs. Computers Chem.Engineering, Vol. 20, No. 10, pp. 1257-1270.

11. Santana, P. L. (1995). Mathematical Modeling for three phase reactor: deterministic, neural and hybrid models, PhD Thesis, School of Chemical Engineering, Unicamp, São Paulo, Brazil (in Portuguese).

12. Simant R. U. and Kalyanmoy D. (1997). Optimal Design of an Ammonia Synthesis Reactor Using Genetic Algorithms. Computers Chem. Engineering, Vol. 21, No. 1, pp. 87-92.

13. Syswerda, G. (1989). Uniform Crossover in Genetic Algorithms. In J. D. Schaffer (Ed.), Proceedings of The Third International Conference on Genetic Algorithms, pp. 2-9.

14. Vasco de Toledo, E.C.., Santana, P.L., Wolf-Maciel, M.R., Maciel Filho, R. (2001). Dynamic modelling of a three-phase catalytic slurry reactor, Chem. Eng. Sci., **56**, 6055-6061.

15. Wehrens, R and Buyders, M. C. (1998). Evolutionary Optimisation: A tutorial. Trends in Analytical Chemistry, Vol. 17, No. 4.

PP-127

EXPERIMENTAL STUDY OF THE HALIDE-FREE CARBONYLATION OF DIMETHYL ETHER

G.G. Volkova, <u>M.A. Shuvaeva</u>, A.A. Budneva, E.A. Paukshtis

Boreskov Institute of Catalysis SB RAS, Pr. Akademika Lavrentieva 5,

Novosibirsk, 630090, Russia

Acetic acid is an important industrial chemical which is manufactured on a large scale. The main route to acetic acid is through the carbonylation of methanol in the Monsanto process which uses a homogeneous rhodium catalyst and halide promoter [1]. Main disadvantages of this process are: a) halides are highly corrosive and are poisons for many types of catalysts b) it is difficult to separate the products and catalyst. These problems may be overcome by developing heterogeneous catalyst that can operate effectively without halide promoter.

Studies at Boreskov Institute of Catalysis have shown that acidic cesium salts of 12-tangstophosphoric acid promoted with rhodium revealed high activity in the iodide-free carbonylation of the dimethyl ether (DME) to methyl acetate (MA) [2-3] that is one order of magnitude higher than the activity of the rhodium salts of the same acid supported on silica [4]. DME is more favorable for carbonylation than methanol because it can be produced from syn-gas more effectively [5].

$$CH_3\text{-}O\text{-}CH_3 + CO \rightarrow CH_3\text{-}CO\text{-}O\text{-}CH_3$$
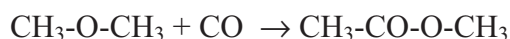
Investigations of the reaction over $1\%Rh/Cs_{1.5}H_{1.5}PW_{12}O_{40}$ catalyst were carried out at the excess CO, ratio DME : CO =1:19 and 1:10, temperature = 200, 220 and 250°C; space velocity = 2, 5, 10 liters hour^{-1}, pressure 10 atm.

It was observed that DME conversion increased with temperature and contact time raise. It was also shown that DME conversion was inversely proportional to initial DME concentration and it did not depend on CO concentration. The rate constants and activation energy for DME carbonylation at the excess CO were evaluate assuming that the reaction is first order in DME. E=12,3 Kcal mol^{-1}. It may be suggested that DME carbonylation reaction occurs through Eley-Rideal route where CO molecule from gas phase interacts with adsorbed molecule of DME: 1. DME+ [ ] = [DME]; 2. [DME] + CO → MA + [ ].

References

1. M.J. Howard, M.D. Jones, M.S. Roberts and S.A. Taylor, Catal.Today, 18 (1993) 325.
2. G.G. Volkova, L.M. Plyasova, A.N. Salanov, G.N. Kustova, T.M. Yurieva, V.A. Likholobov, Catal.Lett. 80 (2002) 175.
3. G.G. Volkova, L.M. Plyasova, L.N. Shkuratova, A.A. Budneva, E.A. Paukshtis, M.N. Timofeeva, V.A. Likholobov, Stud. Sur. Sci. Catal., 147 (2004) 403.
4. W.R.Wegman, European Patent 0353 722 (1989).
5. T. Shikada, Y. Ohno, T. Ogawa, M. Ono, M. Mizuguchi, K. Tomura, K. Fugimoto, Stud. Sur. Sci. Catal., 119 (1998) 515.

MATHEMATIC MODELING OF THE CONTINUOUS PROCESS FOR SYNTHESIS OF NANOFIBROUS CARBON IN THE REACTOR WITH A MOVING CATALYST BED AND GAS FLOW RECYCLING

Zavarukhin S.G., Kuvshinov G.G. and Ananyev I.V.[*]

Boreskov Institute of Catalysis SB RAS, Pr. Akademika Lavrentieva, 5, Novosibirsk 630090, Russia, Fax: 007 3833 308056, e-mail: zsg@catalysis.nsk.su

[*]*Novosibirsk State Technical University, K. Marx avenue, 20, Novosibirsk 630092, Russia*

Nanofibrous carbon (NFC) is a porous carbon material formed upon decomposition of gas carbons on the metal catalysts at the temperature 500-800°C. The uniqueness of this material is that it contains filaments 10-150 nm in diameter formed on the metal catalyst particles of the same dimensions. The present-day catalysts permit production of NFC as strong granules (3-6) mm in diameter, made by densely interlaced carbon filaments, in which the concentration of carbon is as high as 99.8%. The samples of such NFC materials have been obtained in the lab-scale and pilot reactors producing to 3 kg of carbon during an operation period [1]. Since the prospect of commercialization of the granular NFC production is very encouraging, a topical problem is the development of calculation methods of this process performance in different reactors, including the continuous reactors.

A moving catalyst bed reactor with intense gas flow recycling, which provides constant gas composition and temperature inside the reactor, is very promising for production of NFC. In this work we suggest a mathematical technique to calculate the process using the above mentioned reactor and 90 wt.% Ni-Al$_2$O$_3$ catalyst [2] and methane.

In stating the mathematical model, we made the following assumptions:

1. Recycling gas factor is sufficiently high, which provides the ideal mixing in the gas phase and isothermal process.

2. Particle sizes and the catalyst bed thickness are sufficiently low, which permits one to neglect inter and external diffusion resistance values and to assume that the process proceeds in the kinetic region.

3. The catalyst moves without mixing and its parameters are determined by longitudinal coordinate of the reactor.

4. The process is stationary and proceeds at temperature T and pressure P.

The reactor is schematically shown in Fig. 1, where a stirrer provides an ideal gas mixing.
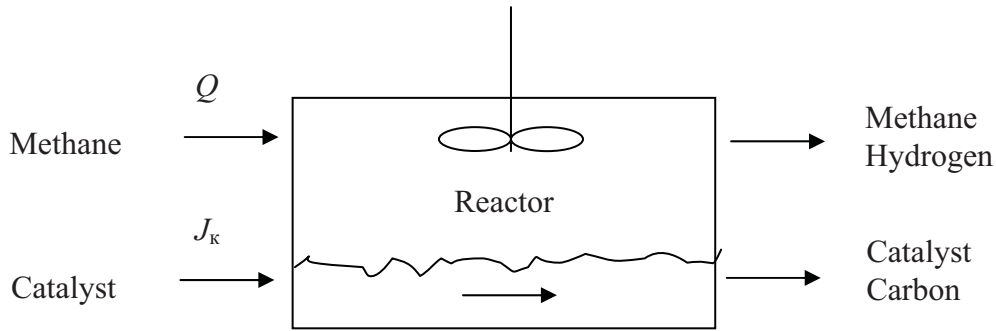
Fig. 1. Schematic of the reactor.

At the left of the schematic, a catalyst is fed at J_c (kg/h) and methane at Q (m³/h at standard conditions). The carbonized catalyst and a methane-hydrogen mixture are released on the right side. The reactor volume was chosen so that to provide a catalyst charge weight of m_0. It is required to determine characteristics of the catalyst and gas at the reactor outlet (specific carbon content c_1 and conversion of methane x).

In the calculations we used a kinetic model of NFC formation from CH_4-H_2 at atmospheric pressure in the presence of a high-loaded Ni catalyst to account for catalyst deactivation [3]. According to the model, the catalyst state is characterized at every instant by two parameters: weight of the formed carbon per catalyst weight unit c (kg/kg) (specific carbon content) and relative catalyst activity a, which obey the following equations:

$$\frac{dc}{dt} = r_m a \tag{1}$$

$$\frac{da}{dt} = -k_a r_m^2 c a \tag{2}$$

where t is time (h), r_m is the maximal specific rate of carbon formation depending on the gas mixture composition and temperature (kg/h kg).

$$r_m = k \frac{p_{CH4} - \dfrac{p_{H2}^2}{K_p}}{(1 + k_H \sqrt{p_{H2}})^2} \tag{3}$$

p_{CH4}, p_{H2} are partial pressures of methane and hydrogen (bar), respectively, K_p is the equilibrium constant of the methane decomposition into carbon and hydrogen, k_a, k, k_H are the coefficients whose dependence on temperature is given in ref. [3].

Since a moving catalyst is carbonized under the conditions of constant gas mixture composition, the specific carbon concentration at the reactor outlet c_1 can be determined by

integrating a system of equations (1)-(2) with the initial conditions such as $c = 0$ and $a = 1$ when $t = 0$.

$$c_1 = c_m th(\frac{r_m}{c_m}\tau) \tag{4}$$

where c_m is the maximal specific content of carbon on the catalyst, which equals:

$$c_m = \sqrt{\frac{2}{k_a r_m}} \tag{5}$$

where τ is the time of catalyst stay in the reactor, $\tau = m_0/J_k$.

Gas composition in the reactor, which can be characterized by partial pressure of hydrogen, was calculated from the equation of carbon balance between gas and catalyst (the carbon formed upon methane decomposition is released from the reactor along with the catalyst)

$$J_c x = J_k c_1 \tag{6}$$

where J_c (kg/h) is the flux of carbon in methane feedstock, $J_c = \frac{12 \cdot Q}{22.4}$.

When solving eq. (6) with respect to p_{H2}, one takes into account that $p_{CH4} = P - p_{H2}$ and the conversion of methane is associated with the value of partial hydrogen pressure by the following dependence:

$$x = \frac{p_{H2}}{2P - p_{H2}} \tag{7}$$

For computational convenience and analysis, we introduced specific parameters $j_k = J_k/m_0$, $j_c = J_c/m_0$ and $q = Q/m_0$, which permit to write equation (6) as

$$j_c x(p_{H2}) = j_k c_m(p_{H2}) th(\frac{r_m(p_{H2})}{c_m(p_{H2})j_k}) \tag{8}$$

As p_{H2} is determined from the numerical solution of eq. (8), the conversion of methane was calculated by eq. (7) and specific carbon content at the reactor outlet was obtained using the following dependence, which yields from eq. (6):

$$c_1 = \frac{j_c}{j_k} x \tag{9}$$

Fig. 2 shows the computational results of specific carbon content at the reactor outlet *versus* specific catalyst consumption at the following reaction conditions: $T = 823$ K, $P = 1$ bar, $q = 120$ m³/h·kg and j_k ranges from 0.02 to 0.1 kg/h·kg. The figure suggests that at the fixed consumption of methane, there exist an optimal consumption of the catalyst, which

allows a maximal specific yield of carbon that is typical of other continuous processes [4]. The maximal value of c_1 (156 kg/kg), achieved at $j_k = 0.053$ kg/h·kg, approximates the value of specific carbon yield in the batch reactor of ideal mixing of catalyst particles and gas obtained at similar temperature and specific methane consumption (159 kg/kg), which is characterized by maximal specific yield as compared to the other types of the reactors [3,5].
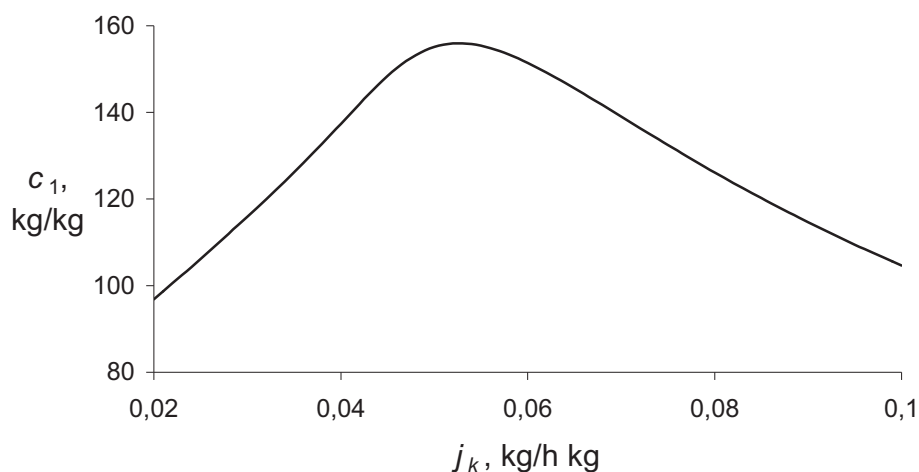
Fig. 2. Specific carbon content on the catalyst at the reactor outlet c_1 *versus* j_k at $T = 823$ K, $P = 1$ bar, $q = 120$ m^3/h·kg.

References

1. Kuvshinov G.G., Zavarukhin S.G., Mogilnykh Yu.I. et al //Khim. Prom–st (Moscow). 1998. № 5. P. 300.

2. Goncharova O.V., Avdeeva L.B., Fenelonov V.B. et al //Kinetics and Catalysis. 1995. V. 36. P. 268.

3. Zavarukhin S.G., Kuvshinov G.G. //Appl. Catal. A. 2004. V. 272. P. 219.

4. Zavarukhin S.G., Kuvshinov G.G. //Eurasian ChemTech Journal. 2004. V. 6. P. 201.

5. Zavarukhin S.G. and Kuvshinov G.G. //XV International Conference on Chemical Reactors "CHEMREACTOR-15", Helsinki, Finland, June 5-8, 2001. Novosibirsk, 2001. P. 185.

XVII International Conference on Chemical Reactors

Post-Symposium "Catalytic Processing of Renewable Sources: Fuel, Energy, Chemicals"

Plenary Lectures

Oral Presentations

Section 1. Kinetics of catalytic reactions

Section 2. Physico-chemical and mathematical bases of the processes in chemical reactors

Section 3. Catalytic processes and reactors development: modeling, optimization and catalyst design

Section 4. Catalytic technologies in fuel and energy production

– *hydrogen production*

– *production of environmentally safe fuel*

– *environmentally friendly energetics*

Post-Symposium
"Catalytic Processing of Renewable Sources: Fuel, Energy, Chemicals"

Plenary Lectures

Oral presentations

XVII International Conference on Chemical Reactors

Poster Presentations

734

XVII International Conference on Chemical Reactors
Post-Symposium "Catalytic Processing of Renewable Sources: Fuel, Energy, Chemicals"

List of participants

Svetlana V. **Ablizina**
Ministry of Education and Sciences RF
Tverskaya str., 11
103906 Moscow
Russia
Tel.: +7 495 629 0390

Ayse N. **Akin**
Kocaeli University
41040 Kocaeli
Turkey
Tel.: +90 262 335 0123
Fax: +90 262 335 5241
E-mail: akinn@kou.edu.tr

Dmitry G. **Aksenov**
Boreskov Institute of Catalysis SB RAS
pr. Akademika Lavrentieva, 5
630090 Novosibirsk
Russia
Tel.: +7 383 330 9827
Fax: +7 383 330 8056
E-mail: aksenov@catalysis.ru

Sulaiman **Al-Khattaf**
King Fahd University of Petroleum and
Minerals
P.O. Box 989
31261 Dhahran
Saudi Arabia
Tel.: 009 663 860 1429
Fax: 009 663 860 4234
E-mail: Skhattaf@kfupm.edu.sa

Tamara V. **Andrushkevich**
Boreskov Institute of Catalysis SB RAS
pr. Akademika Lavrentieva, 5
630090 Novosibirsk
Russia
Fax: +7 383 330 8056
E-mail: andrushk@catalysis.ru

A. **Antoniadis**
Aristotle University of Thessaloniki
54124 Thessaloniki
Greece
Tel.: +30 2310 997785
Fax: +30 2310 997709
E-mail: poulios@chem.auth.gr

Sergey N. **Antonyuk**
Lomonosov Moscow State Academy of Fine
Chemical Technology
pr. Vernadskogo, 86
119571 Moscow
Russia
Tel.: +7 495 246 4823
Fax: +7 495 246 4823
E-mail: antonyuk@mitht.ru

José **Aracil**
Complutense University
28040 Madrid
Spain
Tel.: 34 913 944 175
Fax: 34 913 944 167
E-mail: jam1@quim.ucm.es

Yury I. **Aristov**
Boreskov Institute of Catalysis SB RAS
pr. Akademika Lavrentieva, 5
630090 Novosibirsk
Russia
Tel.: +7 383 330 9573
Fax: +7 383 330 9573
E-mail: aristov@catalysis.ru

Gurutze **Arzamendi**
Public University of Navarre
Campus de Arrosadía. Edificio los Acebos
31006 Pamplona
Spain
E-mail: garzamendi@unavarra.es

Ayten **Ates**
Cumhuriyet University
58140 Sivas
Turkey
Tel.: +90 537 962 1742
Fax: +90 346 219 1179
E-mail: ates@cumhuriyet.edu.tr

George **Avgouropoulos**
Foundation for Research and Technology-
Hellas (FORTH), Institute of Chemical
Engineering and High Temperature Chemical
Processes (ICE/HT)
Stadiou street, Platani, P.O. Box 1414
GR-26504 Patras
Greece
Tel.: +30 2610 965268
Fax: +30 2610 965223
E-mail: geoavg@iceht.forth.gr

Viatcheslav S. **Babkin**
Institute of Chemical Kinetics and
Combustion SB RAS
Institutskaya avenue, 3
630090 Novosibirsk
Russia
Tel.: +7 383 333 0217
Fax: +7 383 330 7350
E-mail: babkin@kinetics.nsc.ru

Bair S. **Balzhinimaev**
Boreskov Institute of Catalysis SB RAS
630090 Novosibirsk
pr. Akademika Lavrentieva, 5
Russia
Tel.: +7 383 330 9770
Fax: +7 383 330 8056
E-mail: balzh@catalysis.ru

Viktor V. **Barelko**
Institute of Problems of Chemical Physics RAS
142432 Chernogolovka
Russia
Tel.: +7 096 522 1817
Fax: +7 096 522 1260
E-mail: barelko@icp.ac.ru

Sohbi **Bashir**
Petroleum Research Centre
123 Tripoli
Libya
Tel.: 00218 21 483 6821
Fax: 00218 21 483 6820
E-mail: mahdred@hotmail.com

Angelo **Basile**
Research Institute on Membrane and
Modelling of Chemical Reactors,
c/o University of Calabria
87030 RENDE (CS)
via P. BUCCI, cubo 17/C
Italy
Tel.: +39 0984 492013
Fax: +39 0984 402103
E-mail: a.basile@itm.cnr.it

Jamaleddin M. **Ben Saidan**
Industrial Research Department
3616638 Tripoli-Libya
Libya
Tel.: 002 182 148 30022
Fax: 002 182 148 0031
E-mail: jmsaidan@prclibya.org

Leonid A. **Bykov**
Institute of Problems of Chemical Physics RAS
142432 Chernogolovka
Russia
E-mail: barelko@icp.ac.ru

Jesús **Blanco**
Instituto de Catálisis y Petroleoquímica
Calle Marie Curie, 2
28049 Madrid
Spain
Tel.: + 34 91 585 4802
Fax: + 34 91 585 4789
E-mail: jblanco@icp.csic.es

Ludmilla N. **Bobrova**
Boreskov Institute of Catalysis SB RAS
pr. Akademika Lavrentieva, 5
630090 Novosibirsk
Russia
Tel.: +7 383 330 6278
Fax: +7 383 330 8056
E-mail: lbobrova@catalysis.ru

Daniel O. **Borio**
Universidad Nacional del Sur, UNS –
CONICET
Camino La Carrindanga Km. 7
8000 Bahía Blanca
Argentina
Tel.: 0054 291 486 1700 Ext:266
Fax: 54 291 486 1600
E-mail: julianap@plapiqui.edu.ar

Goran **Boskovic**
Faculty of Technology, University of Novi Sad
Bul. Cara Lazara 1
21000 Novi Sad
Serbia & Montenegro
E-mail: boskovic@uns.ns.ac.yu

Christophe **Bouvier**
Delft University of Technology
Julianalaan 136
2628 BL Delft
The Netherlands
Tel.: +31 15 27 85879
Fax: +31 15 278 5006
E-mail: C.P.Bouvier@tudelft.nl

Nezahat **Boz**
Kocaeli University
41040 Kocaeli/Izmit
Turkey
Tel.: +90 262 335 1148/1217
Fax: +90 262 335 5241
E-mail: nezahatboz@kou.edu.tr

Oleg F. **Brizitskiy**
Russian Federal Nuclear Center – All-Russian
Scientific Research Institute of Experimental
Physics
37, Mira ave.
607190 Sarov, Nizhegorodsky region
Russia
Tel.: +7 831 304 6537
Fax: +7 831 304 0032
E-mail: trn@gatestc.sarov.ru

Lev G. **Bruk**
Lomonosov Moscow State Academy of Fine
Chemical Technology
pr. Vernadskogo, 86
119571 Moscow
Russia
Tel.: +7 495 936 8904
Fax: +7 495 434 8711
E-mail: lbruk@rol.ru

Jie **Bu**
Institute of Chemical and Engineering
Sciences
No 1 Pesek Road
627833 Island
Singapore
Tel.: +65 679 63951
Fax: +65 631 66185
E-mail: bu_jie@ices.a-star.edu.sg

Wim **Buijs**
Delft University of Technology
Julianalaan 136
2628 BL Delft
The Netherlands
Tel.: +31 15 278 6133
Fax: +31 15 278 5006
E-mail: w.buijs@tudelft.nl

Valerii I. **Bykov**
Bauman Moscow State Technical University
105005 Moscow
Russia
E-mail: vibykov@mail.ru

Vincenza **Calabro'**
Departmento of Chemical Engineering -
University of Calabria
VIA P.BUCCI - Cubo 45/A
87030 Rende (CS)
Italy
Tel.: +39 0984 496703
Fax: +39 0984 496655
E-mail: vincenza.calabro@unical.it

Albert **Casanovas**
Universitat Politècnica de Catalunya
Avda. Diagonal, 647 Ed.Etseib
08028 Barcelona
Spain
E-mail: albert.casanovas.grau@upc.edu

Selim **Ceylan**
Marmara University
Göztepe
34722 Istanbul
Turkey
Tel.: +90 216 348 02 92728
E-mail: sceylan@eng.marmara.edu.tr

Supriya Kumar **Chakraborty**
Embassy of Russia in Bangladesh
1205 Dhaka
Bangladesh
Tel.: 0088 02 9118531
Fax: 0088 02 8125972
E-mail: supriya@accesstel.net

Subrahmanyam **Challapalli**
Ecole Polytechnique Fédéral de Lausanne
(LGRC-EPFL)
1015 Lausanne
Switzerland
Tel.: +41 21 693 3183
Fax: +41 21 693 3190
E-mail: subrahmanyam.challapalli@epfl.ch

Jean-Claude **Charpentier**
Department of Chemical Engineering/CNRS
BP 2077 Villeurbanne cedex
France
Tel.: +33 4 72 43 16 70
Fax: +33 4 72 43 17 02
E-mail: jean-claude.charpentier@ensic.inpl-nancy.fr

Victor N. **Chepelenko**
Moscow Special Alloys Processing Plant
Obrucheva str., 31
117246 Moscow
Russia
Tel.: +7 495 334 7362
Fax: +7 495 334 9277
E-mail: barelko@icp.ac.ru

Victor A. **Chumachenko**
Boreskov Institute of Catalysis SB RAS
pr. Akademika Lavrentieva, 5
630090 Novosibirsk
Russia
Fax: +7 383 330 8056
E-mail: vachum@catalysis.ru

Carlos Gregorio **Dallos**
Universidad Industrial De Santander
Calle 9, Carrera 27
678 Bucaramanga
Colombia
E-mail: cdallos@intercable.net.co

Sonia **Damyanova**
Institue of Catalysis.
Bulgarian Academy of Science
Acad. G. Bonchev str., block 11
1113 Sofia
Bulgaria
Tel.: +359 297 92588
Fax: +359 297 12967
E-mail: soniad@ic.bas.bg

Leonid B. **Datsevich**
University of Bayreuth
Universitaetsstr. 30
D95447 Bayreuth
Germany
Tel.: +49 921 55432
E-mail: datsevich@uni-bayreuth.de

Kusman D. **Dossumov**
D.V. Sokolsky Institute of Organic Catalysis
and Electrochemistry
D. Kunaev str.
050010 Almaty
Kazakhstan
Tel.: +7 3272 916632
Fax: +7 3272 915722
E-mail: tungatarova58@mail.ru

Pilar **De Frutos**
Repsol
Carretera de Extremadura A-5 Km 18
28931 Mostoles (Madrid)
España
Tel.: 349 134 87674
Fax: 349 134 88613
E-mail: pdefrutose@repsolypf.com

Nikolay M. **Dobrynkin**
Boreskov Institute of Catalysis SB RAS
pr. Akademika Lavrentieva, 5
630090 Novosibirsk
Russia
Tel.: +7 383 330 9491
Fax: +7 383 330 6878
E-mail: dbn@catalysis.ru

Valentin Yu. **Doluda**
Tver State Technical University
A. Nikitin str., 22
170000 Tver
Russia
Tel.: +7 4822 449348
Fax: +7 4822 449317
E-mail: sulman@online.tver.ru

Gennadii V. **Echevsky**
Boreskov Institute of Catalysis SB RAS
pr. Akademika Lavrentieva, 5
630090 Novosibirsk
Russia
Tel.: +7 383 330 9827
Fax: +7 383 330 9056
E-mail: egv@catalysis.ru

Elmahboub **Edreder**
Petroleum Research Centre
123 Tripoli
Libya
Tel.: 00218 21 483 6821
Fax: 00218 21 483 6820
E-mail: mahdred@hotmail.com

Ekaterina V. **Egorova**
Lomonosov Moscow State Academy of Fine
Chemical Technology
pr. Vernadskogo, 86
119571 Moscow
Russia
Tel.: +7 495 246 4823
Fax: +7 495 434 8711
E-mail: nhsigt@mitht.ru

Hamed Mohammed **El-Shora**
Mansoura University
050 Mansoura
Egypt
Tel.: 0101 109771
Fax: 0101 109771
E-mail: shora@mum.mans.edu.eg

Anna A. **Fedorova**
Lomonosov Moscow State University
123103 Moscow
Russia
Tel.: +7 495 042 1376
Fax: +7 495 939 0998
E-mail: fedorova@inorg.chem.msu.ru

Joana **Fernandes**
Instituto Superior Técnico
Avenida Rovisco Pais, 1
1049-001 Lisboa
Portugal
Tel.: +351 21 841 7887
Fax: +351 21 841 9198
E-mail: carla.pinheiro@ist.utl.pt

Sergey N. **Filimonov**
"Orenburggazprom"
Octyabrya str., 60
460000 Orenburg
Russia
Tel.: +7 353 273 0175
Fax: +7 353 273 0072
E-mail: S.Filimonov@ogp.gazprom.ru

Sabina **Fiorot**
Politecnico of Turin
C.so Duca degli Abruzzi 24
10129 Turin
Italy
Tel.: +39 011 564 4709
Fax: +39 011 564 4699
E-mail: sabina.fiorot@polito.it

Lucio **Forni**
University of Milan
via Golgi, 19
I-20133 Milano
Italy
Tel.: +39 02 503 14289
Fax: +39 02 503 14300
E-mail: lucio.forni@unimi.it

Sergey M. **Foshkin**
Russian Center of Science and Culture in
Athens
Travella, 7, Kato, Halandri
15232 Athens
Greece
Tel.: +30 210 677 85 67
Fax: +30 210 677 85 67
E-mail: foshkin@otenet.gr

Gilbert **Froment**
Texas A&M University, Department of
Chemical Engineering
USA
E-mail: gilbert.froment@skynet.be

Francesco **Frusteri**
Istituto di Tecnologie Avanzate per l'Energia
Via S. Lucia sopra Contesse 5
98126 Mesina
Italy
Tel.: +39 090 624233
Fax: +39 090 624247
E-mail: francesco.frusteri@itae.cnr.it

Camilla **Galletti**
Politecnico di Torino
corso Duce degli Abruzzi 24
10146 Torino
Italy
Fax: +39 011 564 4699
E-mail: camilla.galletti@polito.it

Fausto **Gallucci**
Research Institute on Membrane and
Modelling of Chemical Reactors, c/o University
of Calabria
via P. BUCCI, cubo 17/C
87030 Rende (CS)
Italy
Tel.: +39 0984 492011
Fax: +39 0984 402103
E-mail: f.gallucci@itm.cnr.it

Sergey A. **Galushin**
Tomsk Polytechnic University
Lenina str., 30
634050 Tomsk
Russia
Tel.: +7 382 2 563443
Fax: +7 382 2 563435
E-mail: bird@tpu.ru

Vladimir **Galvita**
Max-Plank-Institute for Dynamics of Complex
Technical Systems
Sandtorstr. 1
39104 Magdeburg
Germany
Tel.: +49 391 611 0391
E-mail: galvita@mpi-magdeburg.mpg.de

Luis **Gandía**
Public University of Navarre
Campus de Arrosadía. Edificio los Acebos
31006 Pamplona
Spain
Tel.: 34 948 169605
E-mail: lgandia@unavarra.es

Vasile **Georgescu**
Romanian Academy, Chemical Physics
Institute, Ilie Murgulescu
Independentei Splai str., 202
060041 Bucharest
Romania
Tel.: +40 213 167912
Fax: +40 213 121147
E-mail: vgeorgescu@icf.ro

Ali **Gharib**
Islamic Azad University
P.O. Box 91375-4193
Mashhad
Iran
Fax: 0098 212 053784
E-mail: aligharib5@yahoo.com

Irene **Glikina**
Vladimir Dal Eastern-Ukrainian National
University, Severodonetsk Technological
Institute
Sovetskiy av., 59-A
93400 Severodonetsk
Ukraine
Fax: +38 064 524 0342
E-mail: irene555@mail.ru

Egor V. **Golovnya**
JSC "Alvigo-M"
Shosse Entuziastov, 38
111123 Moscow
Russia
Tel.: +7 495 232 1465
Fax: +7 495 232 9906
E-mail: catalin@online.ru

Sergey N. **Gorodsky**
Moscow State Academy of Fine Chemical
Technology
119751 Moscow
Russia
Tel.: +7 495 936 8906
Fax: +7 495 434 8711
E-mail: Gorodsky@yandex.ru

Maria **Goula**
Technological Educational Institute of Western
Macedonia, Pollution Control Technologies
Department
Koila
50 100 Kozani
Greece
Tel.: +30 24610 40161 (int. 121)
Fax: +30 24610 39682
E-mail: mgoula@kozani.teikoz.gr

Milica **Hadnadjev**
Faculty of Technology, University of Novi Sad
Bul. Cara Lazara 1
21000 Novi Sad
Serbia & Montenegro
E-mail: boskovic@uns.ns.ac.yu

Yi-Fan **Han**
Institute of Chemical and Engineering
Sciences
1, Pesek Road, Jurong Island
627833 Singapore
Singapore
Tel.: +65 679 63806
Fax: +65 631 66182
E-mail: han_yi_fan@ices.a-star.edu.sg

Ahmad **Hanif**
PERTAMINA UPSTREAM
Jl. Merdeka Timur No.6
10110 Jakarta
Indonesia
Tel.: 62 21 352 1564
Fax: 62 21 350 8029
E-mail: ahanif@pertamina.com

Jiri **Hanika**
Institute of Chemical Process Fundamentals,
Czech Academy of Sciences
Rozvojova 135
165 02 Prague 6
Czech Republic
Tel.: +420 220 390 286
Fax: +420 220 920 661
E-mail: hanika@icpf.cas.cz

Vladimir L. **Hartmann**
JSC Novomoskovsk Institute of Nitrogen
Industry
Kirova str., 11
301650 Novomoskovsk
Russia
Tel.: +7 487 62 71661
Fax: +7 087 62 71661
E-mail: vhart@yandex.ru

Eleni **Heracleous**
Department of Chemical Engineering,
Aristotle University of Thessaloniki
54006 Thessaloniki
Greece
Tel.: +30 2310 996199
Fax: +30 2310 996184
E-mail: eheracle@cperi.certh.gr

Raimund **Horn**
University of Minnesota, Department of
Chemical Engineering & Materials Science
Washington Avenue 421 SE,
432 Amundson Hall
55455 MN Minneapolis
USA
Tel.: 001 612 625 8806
E-mail: horn@cems.umn.edu

Iraida **Ibadzadeh**
Institute of Chemical Problems, National
Academy of Sciences of Azerbaijan
29, Husein-Javid ave
370143 Baku
Azerbaijan
Tel.: +994 439 4159
E-mail: godsgivn@heart.baku.az

Eleni **Iliopoulou**
CPERI / CERTH
6th Charilaou-Thermi road
57001 Thessaloniki
Greece
Tel.: +30 2310 498312
Fax: +30 2310 498380
E-mail: eh@cperi.certh.gr

Arthur **Iordanidis**
ABB Switzerland Ltd
Segelhofstrasse 1 K / P.O. Box
CH-5405 Baden-Dattwil
Switzerland
Tel.: +41 58 586 7577
Fax: +41 58 586 7314
E-mail: arthouros.iordanidis@ch.abb.com

Angel **Irabien**
Departamento Ingenieria Quimica y QI.
Universidad de Cantabria
Avda de los Castros, s/n.
39005 Santander
Spain
Tel.: +34 9422 01597
Fax: +34 9422 01591
E-mail: irabienj@unican.es

Nikolay A. **Ishmaev**
Lomonosov Moscow State University
Lenynskie Gory
119992 Moscow
Russia
Tel.: +7 495 148 2408
Fax: +7 495 939 0998
E-mail: fedorova@inorg.chem.msu.ru

Zinfer R. **Ismagilov**
Boreskov Institute of Catalysis SB RAS
pr. Akademika Lavrentieva, 5
630090 Novosibirsk
Russia
Tel.: +7 383 330 6219
Fax: +7 383 339 7352
E-mail: zri@catalysis.ru

Lyubov A. **Isupova**
Boreskov Institute of Catalysis SB RAS
pr. Akademika Lavrentieva, 5
630090 Novosibirsk
Russia
Tel.: +7 383 330 8763
Fax: +7 383 330 8056
E-mail: isupova@catalysis.ru

Giuseppe **Italiano**
Chimica Industriale ed Ingegneria dei Materiali,
Università degli Studi di Messina,
Salita Sperone, 31
98166 Messina
Italy
E-mail: Giuseppe.Italiano@unime.it

Sholpan **Itkulova**
D.V. Sokolsky Institute of Organic Catalysis
and Electrochemistry
142, Kunaev str.
050100 Almaty
Kazakhstan
Tel.: +7 3272 916826
Fax: +7 3272 915722
E-mail: itkulova@nursat.kz

Polina G. **Itskova**
Al-Farabi Kazakh National University
Karasai Batyr str., 95 a
480078 Almaty
CIS, Kazakhstan
Tel.: +7 3272 926022
E-mail: Polina@kazsu.kz

Sergey S. **Ivanchev**
St. Petersburg Department of the Boreskov
Institute of Catalysis SB RAS
pr. Dobrolyubova, 14
197198 St. Petersburg
Russia
Tel.: +7 812 238 0890
Fax: +7 812 233 0002
E-mail: ivanchev@SM2270.spb.edu

Alexandra S. **Ivanova**
Boreskov Institute of Catalysis SB RAS
pr. Akademika Lavrentieva, 5
630090 Novosibirsk
Russia
Tel.: +7 383 330 8762
Fax: +7 383 330 8056
E-mail: iva@catalysis.ru

Viatcheslav **Kafarov**
Chemical Engineering School,
Industrial University of Santander
678 Bucaramanga
Colombia
Tel.: +57 7 634 4746
Fax: +57 7 634 4684
E-mail: kafarov@uis.edu.co

Aigana **Kagyrmanova**
Boreskov Institute of Catalysis SB RAS
pr. Akademika Lavrentieva, 5
630090 Novosibirsk
Russia
Tel.: +7 383 339 7558
Fax: +7 383 330 8056
E-mail: aigana@catalysis.ru

Mark L **Kaliya**
Ben-Gurion University of the Negev
P.O. Box 653
84105 Beer-Sheva
Israel
Tel.: 972 8 6461 449
Fax: 972 8 6479 427
E-mail: mkaliya@bgu.ac.il

Zoya S. **Kartasheva**
Semenov Institute of Chemical Physics RAS
Kosygin str., 4
119991 Moscow
Россия
Tel.: +7 495 939 7169
Fax: +7 495 651 2191
E-mail: kasaikina@chph.ras.ru

Olga T. **Kasaikina**
Semenov Institute of Chemical Physics RAS
Kosygin str., 4
119991 Moscow
Russia
Tel.: +7 495 939 7169
Fax: +7 495 651 2191
E-mail: kasaikina@chph.ras.ru

Rasim Mustafa **Kasimov**
Institute of Chemical Problems,
Azerbaijan National Academy of Sciences
29, Husein Javid pr.
AZ0143 Baku
Azerbaijan
Tel.: 99412 439 4159
E-mail: baku@bk.ru

Vadim V. **Kas'yanov**
Ben Gurion University of the Negev
Hashalom 1, POB 653
84105 Beer-Sheva
Israel
Tel.: 972 8 647 9317
Fax: 972 8 647 2960
E-mail: casianov@bgu.ac.il

Panagiotis **Kechagiopoulos**
Chemical Process Engineering Research
Institute, Centre for Research and Technology
Hellas
P.O. Box 361
GR-57001 Thermi-Thessaloniki
Greece
Tel.: +30 2310498318
E-mail: kechagio@cperi.certh.gr

Kharlampiy **Kharlampidi**
Kazan State Technological University
Kalr Marks str., 68
420015 Kazan
Russia
Tel.: +7 843 231 4352
Fax: +7 843 231 4162
E-mail: karalin@yandex.ru

Tatiana B. **Khlebnikova**
Boreskov Institute of Catalysis SB RAS
pr. Akademika Lavrentieva, 5
630090 Novosibirsk
Russia
Tel.: +7 383 333 1609
Fax: +7 383 330 8056
E-mail: khleb@catalysis.ru

Aleksandr P. **Khristolubov**
Russian Federal Nuclear Center – All-Russian
Scientific Research Institute of Experimental
Physics
37, Mira ave.
607190 Sarov, Nizhegorodsky region
Russia
E-mail: khap@gatestc.sarov.ru

Murat Efgan **Kibar**
Kocaeli University
41040 Kocaeli
Turkey
Tel.: +90 262 335 0123
Fax: +90 262 335 5241
E-mail: akinn@kou.edu.tr

Oleg V. **Kikhtyanin**
Boreskov Institute of Catalysis SB RAS
pr. Akademika Lavrentieva, 5
630090 Novosibirsk
Russia
Tel.: +7 383 330 9827
Fax: +7 383 330 8056
E-mail: kihtanin@catalysis.ru

Valery A. **Kirillov**
Boreskov Institute of Catalysis SB RAS
pr. Akademika Lavrentieva, 5
630090 Novosibirsk
Russia
Tel.: +7 383 330 6187
Fax: +7 383 330 8056
E-mail: vak@catalysis.ru

Oleg P. **Klenov**
Boreskov Institute of Catalysis SB RAS
pr. Akademika Lavrentieva, 5
630090 Novosibirsk
Russia
Tel.: +7 383 330 6278
Fax: +7 383 230 8056
E-mail: klen@catalysis.ru

Oleg V. **Klimov**
Boreskov Institute of Catalysis SB RAS
pr. Akademika Lavrentieva, 5
630090 Novosibirsk
Russia
Tel.: +7 383 330 9827
Fax: +7 383 330 8056
E-mail: klm@catalysis.ru

Gunther **Kolb**
Institut für Mikrotechnik Mainz GmbH (IMM)
Carl-Zeiss-Str.18-20
D-55129 Mainz
Germany
Tel.: +49 6131 990341
E-mail: Kolb@imm-mainz.de

Jury N. **Kondratjev**
Central R&D Institute for Complex Automation
8, Mozhaisky Val
Moscow
Russia
Tel.: +7 495 240 4871
Fax: +7 495 240 4206
E-mail: ukond@peterlink.ru

Gennadii S. **Kopachev**
Ministry of Education and Sciences RF
Tverskaya str., 11
103906 Moscow
Russia
Tel.: +7 495 629 65 57
Fax: +7 495 629 65 57

Ivan A. **Kozlovskii**
Mendeleev University of Chemical
Technology of Russia
9 Miusskaya Square
125047 Moscow
Russia
Tel.: +7 495 978 9554
Fax: +7 495 978 9554
E-mail: kra@muctr.edu.ru

Roman A. **Kozlovskiy**
Mendeleev University of Chemical
Technology of Russia
9 Miusskaya Square
125047 Moscow
Russia
Tel.: +7 495 978 9554
Fax: +7 495 978 9554
E-mail: kra@muctr.edu.ru

Ralph **Kraehnert**
Leibniz-Institut fur Katalyse e. V. an der
Universitat Rostock
Richard-Willstaetter-Str. 12
D-12489 Berlin
Germany
E-mail: kraehnert@aca-berlin.de

Duduku **Krishnaiah**
Chemical Engineering Programme, School of
Engineering and Information Technology,
University Malaysia Sabah
88999 Sabah
Malaysia
Tel.: +60 88 320000 Extn. 3059
Fax: +60 88 320348
E-mail: krishna@ums.edu.my

Vitalina V. **Kukueva**
Fire Safety Institute
Onoprienko str., 8
18034 Cherkassy
Ukraine
Tel.: 380472 438923
Fax: 380472 456157
E-mail: kukueva@yahoo.com

Narendra **Kumar**
Laboratory of Industrial Chemistry,
Åbo Akademi University
Biskopsgatan 8
20500 Turku
Finland
Tel.: +358 2 215 4555
Fax: +358 2 215 4555
E-mail: nkumar@abo.fi

Elena S. **Kurkina**
Lomonosov Moscow State University
Lenynskie Gory
119899 Moscow
Russia
Tel.: +7 095 939 4079
Fax: +7 095 939 2596
E-mail: elena.kurkina@cs.msu.su

Andrey V. **Kustov**
Mendeleev University of Chemical
Technology of Russia
9 Miusskaya Square
125047 Moscow
Russia
Tel.: +7 495 978 9554
Fax: +7 495 978 9554
E-mail: koustov@muctr.edu.ru

Alexey E. **Kuz'min**
Topchiev Institute of Petrochemical
Synthesis RAS
Leninsky pr., 29
119991 Moscow
Russia
Tel.: +7 495 955 4152
E-mail: kuzmin@ips.ac.ru

Boris N. **Kuznetsov**
Institute of Chemistry and Chemical
Technology SB RAS
K. Marx street, 42
660049 Krasnoyarsk
Russia
Tel.: +7 3912 494894
Fax: +7 3912 439342
E-mail: inm@icct.ru

Tatiana G. **Kuznetsova**
Boreskov Institute of Catalysis SB RAS
pr. Akademika Lavrentieva, 5
630090 Novosibirsk
Russia
Tel.: +7 383 330 8764
Fax: +7 383 330 8056
E-mail: tgkuzn@catalysis.ru

Armin **Lange de Oliveira**
hte Aktiengesellschaft
Kurpfalzring 104
D-69123 Heidelberg
Germany
Fax: +49.6221 749 7177
E-mail: armin.oliveira@hte-company.de

Oriana **Lanitou**
Institute of Physical Chemistry
15310 Athens
Greece
Tel.: +30 210 650 3634
Fax: +30 210 651 1766
E-mail: oriana@chem.demokritos.gr

Urszula **Laska**
University of Bath
Claverton Down
BA2 7AY Bath
United Kingdom
Tel.: +44 1225 385865
Fax: +44 1225 385713
E-mail: U.Laska@bath.ac.uk

Mark Z. **Lazman**
Aspen Technology Inc.
900–125-9th Avenue SE
T2P1H5 Calgary
Canada
Tel.: 403 303 1000
Fax: 403 303 0927
E-mail: Mark.Lazman@aspentech.com

Angeliki **Lemonidou**
Aristotle University of Thessaloniki,
Department of Chemical Engineering
P.O. Box 1517, University Campus
54124 Thessaloniki
Greece
Tel.: +30 2310 996273
Fax: +30 2310 996184
E-mail: alemonidou@cheng.auth.gr

Evgenii E. **Levchenko**
Russian Center of International Scientific and
Cultural Cooperation
Vozdvizhenka str., 14
101999 Moscow
Russia
Tel.: +7 495 290 15 50
E-mail: levchenko@rusintercenter.ru

Zhenyu **Liu**
State Key Laboratory of Coal Conversion,
Institute of Coal Chemistry,
Chinese Academy of Sciences
030001 Taiyuan
China
Fax: +86 351 404 8571
E-mail: zyliu@sxicc.ac.cn

Jordi **Llorca**
Institut de Tècniques Energètiques.
Universitat Politècnica de Catalunya
Diagonal 647, Ed. ETSEIB
08028 Barcelona
Spain
Tel.: +34 934 011708
Fax: +34 934 017149
E-mail: jordi.llorca@upc.edu

Tatiana **Luts**
Universität Leipzig, Fakultät für Chemie und
Mineralogie, Institut für Technische Chemie
Linnéstrasse 3
04103 Leipzig
Germany
Tel.: +49 341 973 6306
Fax: +49 341 973 6349
E-mail: luts@chemie.uni-leipzig.de

Anastasia **Macario**
University of Calabria
via P. Bucci
87036 Rende
Italy
Tel.: +39 0984 496667
Fax: +39 0984 496655
E-mail: macario@unical.it

F.H. **Mahfud**
Faculty of Matchematics and Natural Science,
University of Groningen
Nijenborgh 4
9747AG Groningen
The Netherlands
Tel.: +31 50 363 4497
Fax: +31 50 363 4479
E-mail: f.h.mahfud@rug.nl

Mikhail G. **Makarov**
Mendeleev University of Chemical Technology
of Russia
9 Miusskaya Square
125047 Moscow
Russia
Tel.: +7 495 978 9554
Fax: +7 495 978 9554
E-mail: kra@muctr.edu.ru

Lev L. **Makarshin**
Boreskov Institute of Catalysis SB RAS
pr. Akademika Lavrentieva, 5
630090 Novosibirsk
Russia
Tel.: +7 383 330 7831
Fax: +7 383 330 8056
E-mail: makarshin@catalysis.ru

Alexei G. **Makeev**
Lomonosov Moscow State University
Lenynskie Gory
119899 Moscow
Russia
Tel.: +7 495 939 4079
Fax: +7 495 939 2596
E-mail: amak@cs.msu.su

Päivi Elisa **Mäki-Arvela**
Åbo Akademi University
Biskopsgatan 8
20500 Turku
Finalnd
Tel.: +358 221 54424
Fax: +358 221 54479
E-mail: paivi.maki-arvela@abo.fi

Nataliya V. **Maksimchuk**
Boreskov Institute of Catalysis SB RAS
pr. Akademika Lavrentieva, 5
630090 Novosibirsk
Russia
Tel.: +7 383 330 6877
Fax: +7 383 330 8056
E-mail: nvmax@catalysis.ru

Taiana V. **Maksimova**
Semenov Institute of Chemical Physics RAS
Kosygin str., 4
119991 Moscow
Россия
Tel.: +7 495 939 7169
Fax: +7 495 651 2191
E-mail: kasaikina@chph.ras.ru

Heidi **Markus**
Laboratory of Industrial Chemistry,
Åbo Akademi University
Biskopsgatan 8
20500 Turku
Finland
E-mail: hmarkus@abo.fi

Masahiko **Matsukata**
Department of Applied Chemistry,
Waseda University
3-4-1 Okubo, Shinjuku-ku
169-8555 Tokyo
Japan
Tel.: +81 3 5286 3850
Fax: +81 3 5286 3850
E-mail: mmatsu@waseda.jp

Yury V. **Medvedev**
JSC "Tomskgazprom"
634050 Tomsk
Russia
E-mail: medvedevjv@vostokgazprom.ru

Valerie **Meille**
Laboratoire de Génie des Procédés
Catalytiques - CNRS/CPE Lyon
43, bd du 11 nov. 1918
69616 Villeurbanne
France
E-mail: vme@lgpc.cpe.fr

Natalia V. **Mezentseva**
Boreskov Institute of Catalysis SB RAS
pr. Akademika Lavrentieva, 5
630090 Novosibirsk
Russia
Tel.: +7 383 330 8763
Fax: +7 383 330 8056
E-mail: mnv@catalysis.ru

Tatyana P. **Minyukova**
Boreskov Institute of Catalysis SB RAS
pr. Akademika Lavrentieva, 5
630090 Novosibirsk
Russia
Tel.: +7 383 330 9109
Fax: +7 383 330 8056
E-mail: min@catalysis.ru

Olesya I. **Mnushkina**
PETON Company
Stroitelniy proezd 7A, k. 28
125424 Moscow
Russia
Tel.: +7 495 787 7824
Fax: +7 495 787 7824
E-mail: petonr@peton.com

Antonio **Monzón**
University of Zaragoza
Pedro cerbuna, 12. Ciudad Universitaria
50009 Zaragoza
Spain
Tel.: +34 976 761157
Fax: +34 976 762142
E-mail: amonzon@unizar.es

Sang-Jin **Moon**
Korea Research Institute of Chemical
Technology
100 Jang-Dong, Yuseong
305-343 Daejon
Republic of Korea
Tel.: +82 42 860 7517
Fax: +82 42 860 7590
E-mail: moonsj@krict.re.kr

Dmitry Yu. **Murzin**
Laboratory of Industrial Chemistry, Åbo
Akademi University
Biskopsgatan 8
20500 Turku
Finland
Tel.: +358 2 215 4985
Fax: +358 2 215 4479
E-mail: dmurzin@abo.fi

Victor. **Mushakov**
Ministry of Education and Sciences RF
Tverskaya str., 11
103906 Moscow
Russia
Tel.: +7 495 629 5293
Fax: +7 495 629 7188

Alexander V. **Myshlyavtsev**
Omsk Technical State University
Mira av., 11
644050 Omsk
Russia
Tel.: +7 3812 653407
Fax: +7 3812 653407
E-mail: myshl@omgtu.ru

Fizuli Akber oglu **Nasirov**
Institute of Petrochemical Processes of
Azerbaijan National Academy of Sciences
Khodjaly av., 30
AZ1027 Baku
Azerbaijan
Tel.: 99412 490 4204
Fax: 99412 490 4204
E-mail: fizulin52@rambler.ru

Manuel **Nau**
University of Dortmund
Dortmund
Germany
Tel.: +49 231 755 4316
Fax: +49 231 755 2698
E-mail: manuel.nau@bci.uni-dortmund.de

Stylianos **Neophytides**
Institute of Chemical Engineering and High
Temperature Chemical Processes
Greece
E-mail: neoph@terpsi.iceht.forth.gr

Patrick **Nguyen**
Laboratoire des Matériaux et Surfaces
Procédés pour la Catalyse (LMSPC)
25 rue Becquerel
67087 Strasbourg
France
Tel.: +33 3 90 242633
Fax: +33 3 90 242674
E-mail: pnguyen@chimie.u-strasbg.fr

Alexander S. **Noskov**
Boreskov Institute of Catalysis SB RAS
pr. Akademika Lavrentieva, 5
630090 Novosibirsk
Russia
Tel.: +7 383 330 6878
Fax: +7 383 330 6878
E-mail: noskov@catalysis.ru

751

Evgeniy **Nougmanov**
Lomonosov Moscow State Academy of Fine
Chemical Technology
pr. Vernadskogo, 86
119571 Moscow
Russia
Tel.: +7 495 246 4823
Fax: +7 495 246 4823
E-mail: jnugmanoff@mail.ru

Farida M. **Novruzova**
Institute of Petrochemical Processes of
Azerbaijan National Academy of Sciences
Khodjaly av., 30
AZ1027 Baku
Azerbaijan
Tel.: 994 12 490 4204
Fax: 994 12 490 4204
E-mail: fizulin52@rambler.ru

Cesare **Oliva**
University of Milan, Department of Physical
Chemistry and Electrochemistry
via Golgi 19
I-20133 Milan
Italy
Tel.: +39 02 50314270
Fax: +39 02 50314300
E-mail: cesare.oliva@unimi.it

Inmaculada **Ortiz**
Universidad de Cantabria
39005 Santander
Spain
Tel.: +34 942 201585
Fax: +34 942 201591
E-mail: ortizi@unican.es

Nickolay M. **Ostrovskii**
AD Hemijska Industrija HIPOL
Industrijska zona
25250 Odzaci
Serbia and Montenegro
Tel.: 381 25 743221
Fax: 381 25 743452
E-mail: ostrovski@hipol.com

Emel **Ozdemir**
Kocaeli University
41040 Kocaeli
Turkey
Tel.: +90 262 335 0123
Fax: +90 262 335 5241
E-mail: akinn@kou.edu.tr

Zinaida P. **Pai**
Boreskov Institute of Catalysis SB RAS
pr. Akademika Lavrentieva, 5
630090 Novosibirsk
Russia
Tel.: +7 383 3 397264
Fax: +7 383 3 308056
E-mail: zpai@catalysis.ru

Antonio Eduardo **Palomares**
Universidad Politecnica de Valencia
Micer Masco 12-5
46022 Valencia
Spain
Tel.: +34 963 879632
Fax: +34 963 877639
E-mail: apalomar@iqn.upv.es

Joan **Papavasiliou**
Foundation for Research and Technology
Hellas (FORTH), Institute of Chemical
Engineering and High Temperature Chemical
Processes (ICE/HT)
Stadiou Str., Rio
26504 Patras
Greece
Tel.: +30 2610 965268
Fax: +30 2610 965223
E-mail: jpapav@iceht.forth.gr

Adolfo **Parmaliana**
Chimica Industriale ed Ingegneria dei Materiali,
Università degli Studi di Messina,
Salita Sperone, 31
98166 Messina
Italy
Tel.: +39 090 676 5606
Fax: +39 090 391518
E-mail: Adolfo.Parmaliana@unime.it

Viorica Ion **Parvulescu**
Romanian Academy, Institute of Physical
Chemistry
Splaiul Independentei 202
060021 Bucharest
Romania
Tel.: +40 21 316 7912
Fax: +40 21 312 1147
E-mail: vpirvulescu@chimfiz.icf.ro

Edison **Patmar**
Chuvash State University
Moskovskii pr., 15
428015 Cheboksary
Russia
Tel.: +7 8352 498792
Fax: +7 8252 458278
E-mail: koltsov@chuvsu.ru

Svetlana N. **Pavlova**
Boreskov Institute of Catalysis SB RAS
pr. Akademika Lavrentieva, 5
630090 Novosibirsk
Russia
Tel.: +7 383 330 5672
Fax: +7 383 330 8056
E-mail: pavlova@catalysis.ru

Nicola **Pernicone**
Via Pansa 7
28100 Novara
Italy
Tel.: +39 348 601 9730
Fax: +39 0321 624241
E-mail: catcons@tin.it

Nikolai V. **Peskov**
Lomonosov Moscow State University
Lenynskie Gory
119992 Moscow
Russia
Tel.: +7 495 939 4079
Fax: +7 495 939 2596
E-mail: peskov@cs.msu.su

Elena V. **Pisarenko**
Mendeleev University of Chemical Technology
of Russia
9 Miusskaya Square
125047 Moscow
Russia
Tel.: +7 495 978 6589
Fax: +7 495 200 4204
E-mail: evpisarenko@mail.ru

Vitaliy N. **Pisarenko**
Mendeleev University of Chemical Technology
of Russia
9 Miusskaya Square
125047 Moscow
Russia
Tel.: +7 495 978 6589
Fax: +7 495 200 4204
E-mail: pvn@muctr.edu.ru

Irina V. **Pivovarova**
Boreskov Institute of Catalysis SB RAS
pr. Akademika Lavrentieva, 5
630090 Novosibirsk
Russia
Tel.: +7 383 330 6878
Fax: +7 383 330 6878
E-mail: pivo@catalysis.ru

Pawel Krzysztof **Plucinski**
University of Bath
Claverton Down
BA2 7AY Bath
United Kingdom
Tel.: +44 1225 386961
Fax: +44 1225 385713
E-mail: P.Plucinski@bath.ac.uk

Olga Yu. **Podyacheva**
Boreskov Institute of Catalysis SB RAS
pr. Akademika Lavrentieva, 5
630090 Novosibirsk
Russia
Tel.: +7 383 3 397357
Fax: +7 383 3 397352
E-mail: pod@catalysis.ru

Svetlana A. **Pokrovskaya**
Boreskov Institute of Catalysis SB RAS
pr. Akademika Lavrentieva, 5
630090 Novosibirsk
Russia
Tel.: +7 383 330 6278
Fax: +7 383 330 6278
E-mail: pokrov@catalysis.ru

Polad Firuz **Poladli**
Institut für Technishe Chemie
Linnestrasse 3
04103 Leipzig
Germany
Tel.: +49 341 36306
E-mail: poladli@chemie.uni-leipzig.de

Oleg S. **Popel**
Institute of High Temperatures RAS
Izhorskaya str., 13/19
125412 Moscow
Russia
Tel.: +7 495 484 2374
Fax: +7 495 484 2374
E-mail: O_Popel@oivtran.iitp.ru

Galina Ya. **Popova**
Boreskov Institute of Catalysis SB RAS
pr. Akademika Lavrentieva, 5
630090 Novosibirsk
Russia
Tel.: +7 383 339 7296
Fax: +7 383 330 8056
E-mail: gyap@catalysis.ru

Ademola Misbau **Rabiu**
University of Cape Town
7701 Cape Town
South Africa
Tel.: +27 73 192 1434
Fax: +27 21 650 4051
E-mail: amrabiu@chemeng.uct.ac.za

Riitta Hannele **Raudaskoski**
University of Oulu
P.O. Box 4300
90014 Oulu
Finland
Tel.: +358 8 553 2362
Fax: +358 8 553 2369
E-mail: riitta.raudaskoski@oulu.fi

Andreas **Reitzmann**
Institute of Chemical Process Engineering
(CVT), University of Karlsruhe
Kaiserstr. 12
76131 Karlsruhe
Germany
Tel.: +49 721 608 3848
Fax: +49 721 608 6118
E-mail: andreas.reitzmann@ciw.uni-
karlsruhe.de

Vladimir A. **Remnyev**
Boreskov Institute of Catalysis SB RAS
pr. Akademika Lavrentieva, 5
630090 Novosibirsk
Russia
Tel.: +7 383 330 8846
Fax: +7 383 330 8056
E-mail: remnyov@catalysis.ru

Sergey I. **Reshetnikov**
Boreskov Institute of Catalysis SB RAS
pr. Akademika Lavrentieva, 5
630090 Novosibirsk
Russia
Tel.: +7 383 333 1618
Fax: +7 383 330 8056
E-mail: reshet@catalysis.ru

Tatiana V. **Reshetnyak**
Boreskov Institute of Catalysis SB RAS
630090 Novosibirsk
Russia
Tel.: +7 383 339 7305
Fax: +7 383 330 8056
E-mail: tresh@catalysis.ru

Ilenia **Rossetti**
Dip. Chimica Fisica ed Elettrochimica -
Università degli Studi di Milano
v. C. Golgi 19
I-20133 Milano
Italy
Tel.: +39 02 50314308
Fax: +39 02 50314300
E-mail: ilenia.rossetti@unimi.it

Adel **Saadi**
Faculté de Chimie, USTHB
BP 32 El Alia, Bab-Ezzouar
16111 Algiers
Algeria
E-mail: adel_saadi@yahoo.fr

Mikhail A. **Salaev**
Tomsk State University
Lenina str., 36
634027 Tomsk
Russia
Tel.: +7 3822 775618
E-mail: mihan555@yandex.ru

Naum A. **Samoilov**
Ufa State Petroleum Technical University
Kosmonavtov str., 1
450062 Ufa
Russia
Tel.: +7 3472 420932
Fax: +7 3472 420932
E-mail: nhtukntu@bk.ru

Norio **Sato**
TOYOTA MOTOR EURTOPE NV/SA
Hoge Wei 33
1930 Zaventem
Belgium
Tel.: + 32 2 712 3145
Fax: + 32 2 712 3169
E-mail: karen.asselman@toyota-europe.com

Lanny D. **Schmidt**
University of Minnesota – Twin Cities,
Department of Chemical Engineering &
Materials Science
151 Amundson Hall,
421 Washington Avenue SE
MN 55455 Minneapolis
USA
Fax: +1 612 626 7246
E-mail: schmi001@umn.edu

Nataliya L. **Semendyaeva**
Lomonosov Moscow State University
Lenynskie Gory
119899 Moscow
Russia
Tel.: +7 495 939 4079
Fax: +7 495 939 2596
E-mail: NatalyS@cs.msu.ru

Maria **Shuvaeva**
Boreskov Institute of Catalysis SB RAS
pr. Akademika Lavrentieva, 5
630090 Novosibirsk
Russia
Tel.: +7 495 339 7289
Fax: +7 383 330 8056
E-mail: ggvolkova@catalysis.ru

Valeriy F. **Shvets**
Mendeleev University of Chemical
Technology of Russia
9 Miusskaya Square
125047 Moscow
Russia
Tel.: +7 495 978 9589
Fax: +7 495 973 3136
E-mail: shvets@muctr.edu.ru

Valentina I. **Simagina**
Boreskov Institute of Catalysis SB RAS
pr. Akademika Lavrentieva, 5
630090 Novosibirsk
Russia
Tel.: +7 383 3307336
Fax: +7 383 3307336
E-mail: simagina@catalysis.ru

Irina L. **Simakova**
Boreskov Institite of Catalysis SB RAS
pr. Akademika Lavrentieva, 5
630090 Novosibirsk
Russia
Tel.: +7 383 330 6222
Fax: +7 383 330 8056
E-mail: simakova@catalysis.ru

Evgeniy I. **Smirnov**
Boreskov Institute of Catalysis SB RAS
pr. Akademika Lavrentieva, 5
630090 Novosibirsk
Russia
Tel.: +7 383 330 9491
Fax: +7 383 330 6187
E-mail: esmirnov@catalysis.ru

Mathias Raoul Wilhelm **Snåre**
Laboratory of Industrial Chemistry, Åbo
Akademi University
Biskopsgatan 8
20500 Turku
Finland
Tel.: +358 2 215 4431
E-mail: msnare@abo.fi

Valery N. **Snytnikov**
Boreskov Institute of Catalysis SB RAS
pr. Akademika Lavrentieva, 5
630090 Novosibirsk
Russia
Tel.: +7 383 339 7308
Fax: +7 383 330 8056
E-mail: snyt@catalysis.ru

Frigyes **Solymosi**
Institute of Solid State and Radiochemistry,
University of Szeged
P.O.Box 168
H-6701 Szeged
Hungary
Tel.: +36 62 420 678
Fax: +36 62 420 678
E-mail: fsolym@chem.u-szeged.hu

Alexey A. **Spiridonov**
Boreskov Institute of Catalysis SB RAS
pr. Akademika Lavrentieva, 5
630090 Novosibirsk
Russia
Tel.: +7 383 339 7309
Fax: +7 383 330 8056
E-mail: pub@catalysis.ru

Dmitry V. **Staroverov**
Mendeleev University of Chemical Technology
of Russia
9 Miusskaya Square
125047 Moscow
Russia
Tel.: +7 495 978 95 54
Fax: +7 495 978 95 54
E-mail: stardv@muctr.edu.ru

Esfir M. **Sulman**
Tver State Technical University
A. Nikitin str., 22
170000 Tver
Russia
Tel.: +7 4822 449348
Fax: +7 4822 449317
E-mail: sulman@online.tver.ru

Yuhan **Sun**
State Key Laboratory of Coal Conversion,
Institute of Coal Chemistry,
Chinese Academy of Sciences
27, Taoyuan Nanlu Taiyuan
030001 Taiyuan
China
Tel.: +86 351 405 3801
Fax: +86 351 404 1153
E-mail: yhsun@sxicc.ac.cn

Vasileios **Takavakoglou**
Aristotle University of Thessaloniki
54124 Thessaloniki
Greece
Tel.: +30 2310 998769
Fax: +30 2310 998739
E-mail: takab@agro.auth.gr

Tsunehiro **Tanaka**
Department of Molecular Engineering,
Kyoto University
6158510 Kyoto
Japan
Tel.: +81 753 832558
Fax: +81 753 832561
E-mail: tanakat@moleng.kyoto-u.ac.jp

Yury Yu. **Tanashev**
Boreskov Institute of Catalysis SB RAS
pr. Akademika Lavrentieva, 5
630090 Novosibirsk
Russia
Tel.: +7 383 330 7831
Fax: +7 383 330 8056
E-mail: tanashev@catalysis.ru

Vadim **Tarasov**
Vladimir Dal Eastern-Ukrainian National
University, Severodonetsk Technological
Institute
Sovetskiy av., 59-A
93400 Severodonetsk
Ukraine
E-mail: vatarasov@rambler.ru

Valerii Ya. **Terentiev**
Russian Federal Nuclear Center – All-Russian
Scientific Research Institute of Experimental
Physics
37, Mira ave.
607190 Sarov, Nizhegorodsky region
Russia
Tel.: +7 831 304 2790
Fax: +7 831 304 0032
E-mail: trn@gatestc.sarov.ru

Fernand Charles **Thyrion**
Louvain-la-Neuve
1, voie Minckelers
1348 Louvain-la-Neuve
Belgium
Tel.: +32 10 472327
Fax: +32 10 472321
E-mail: Fernand.Thyrion@uclouvain.be

Anton V. **Tokarev**
Åbo Akademi University
Biskopsgatan 8
20500 Turku
Finland
Fax: +358 2 215 4479
E-mail: atokarev@abo.fi

Nikolay N. **Tolkachev**
Zelinsky Institute of Organic Chemistry RAS
47, Leninsky pr.
119991 Moscow
Russia
Tel.: +7 495 137 6277
E-mail: nick33@ioc.ac.ru

Gagik Hovhannes **Torosyan**
State Engineering University of Armenia
109 Teryan Street
375 009 Yerevan
Armenia
Tel.: +374 1 582327
Fax: +374 1 545843
E-mail: gtorosyan@seua.am

Valentin F. **Tretyakov**
Topchiev Institute of Petrochemical
Synthesis RAS
Leninskii pr., 29
119991 Moscow
Russia
Tel.: +7 495 955 4271
Fax: +7 495 230 2224
E-mail: tretjakov@ips.ac.ru

Svetlana A. **Tungatarova**
D.V. Sokolsky Institute of Organic Catalysis
and Electrochemistry
D. Kunaev str.
050010 Almaty
Kazakhstan
Tel.: +7 3272 916632
Fax: +7 3272 915722
E-mail: tungatarova58@mail.ru

Valery B. **Ukraintsev**
Technological Institute
Moskovsky pr., 26
190013 St. Petersburg
Russia
Tel.: +7 812 259 4787
Fax: +7 812 112 7781
E-mail: ukr4061@pochta.ru

Gleb A. **Urzhuntsev**
Boreskov Institute of Catalysis SB RAS
pr. Akademika Lavrentieva, 5
630090 Novosibirsk
Russia
Tel.: +7 383 330 9827
Fax: +7 383 330 8056
E-mail: urg@ngs.ru

Kevin M. **Van Geem**
University of Gent
Krijgslaan 281, S5
9000 Gent
Belgium
Tel.: +32 9 264 5678
Fax: +32 9 264 4999
E-mail: kevin.vangeem@ugent.be

Norbert N. **Vasen**
ETA - Renewable Energies
Piazza Savonarola, 10
50132 Florence
Italy
Tel.: +39 055 500 2174
Fax: +39 055 573425
E-mail: norbert.vasen@etaflorence.it

Constantinos G. **Vayenas**
University of Patras, Department
of Chemical Engineering
Caratheodory 1, St.
GR-26500 Patras
Greece
Tel.: +30 2610 997576
Fax: +30 2610 997269
E-mail: cat@chemeng.upatras.gr

Nadezhda V. **Vernikovskaya**
Boreskov Institute of Catalysis SB RAS
pr. Akademika Lavrentieva, 5
630090 Novosibirsk
Russia
Tel.: +7 383 339 7558
Fax: +7 383 330 6878
E-mail: vernik@catalysis.ru

Igor Ricardo de **Victorino**
State University of Campinas (UNICAMP)
Zeferino Vaz University City
13081-970 Campinas
Brasil
Tel.: +55 1937 883971
Fax: +55 1937 883965
E-mail: igor_rsv@yahoo.com.br

Hermenegildo **de A. L. Viana**
University of St. Andrews
KY16 9ST
Scotland
E-mail: jtsi@st-andrews.ac.uk

Alexander V. **Vosmerikov**
Institute of Petroleum Chemistry SB RAS
Akademichesky Avenue, 3
634021 Tomsk
Russia
Tel.: +7 3822 491021
Fax: +7 3822 491457
E-mail: pika@ipc.tsc.ru

Tatjana **Vulic**
University of Novi Sad, Faculty of Technology
Bul. Cara Lazara 1
21000 Novi Sad
Serbia & Montenegro
Fax: +381 21 450413
E-mail: tatjanavulic@yahoo.com

Krzysztof **Warmuzinski**
Institute of Chemical Engineering, Polish
Academy of Sciences
ul. Baltycka, 5
44-100 Gliwice
Poland
Tel.: +48 32 231 0318
Fax: +48 32 231 0318
E-mail: kwarmuz@iich.gliwice.pl

We **Wei**
State Key Laboratory of Coal Conversion,
Institute of Coal Chemistry, Chinese Academy
of Sciences
27, Taoyuan Nanlu Taiyuan
030001 Taiyuan
China
Tel.: +86 351 405 3801
Fax: +86 351 404 1153
E-mail: yhsun@sxicc.ac.cn

Vadim A. **Yakovlev**
Boreskov Institute of Catalysis SB RAS
pr. Akademika Lavrentieva, 5
630090 Novosibirsk
Russia
Tel.: +7 383 330 6254
Fax: +7 383 330 8056
E-mail: yakovlev@catalysis.ru

Fatima A. **Yandieva**
Topchiev Institute of Petrochemical
Synthesis RAS
Leninskii pr., 29
119991 Moscow
Russia
Tel.: +7 495 955 4239
Fax: +7 495 954 4798
E-mail: Yand@ips.ac.ru

Meltem **Yildiz**
Kocaeli University
Veziroglu Campus (VINSAN)
41040 Kocaeli/Izmit
Turkey
Tel.: +90 262 335 1148/1258
Fax: +90 262 335 5241
E-mail: myildiz@kou.edu.tr

Selahattin **Yilmaz**
Izmir Institute of Technology
35430 Izmir
Turkey
Tel.: +90 232 750 6659
Fax: +90 232 750 6645
E-mail: selahattinyilmaz@iyte.edu.tr

Tamara M. **Yurieva**
Boreskov Institute of Catalysis SB RAS
pr. Akademika Lavrentieva, 5
690090 Novosibirsk
Russia
Tel.: +7 383 330 9109
Fax: +7 383 330 8056
E-mail: yurieva@catalysis.ru

Andrey N. **Zagoruiko**
Boreskov Institute of Catalysis SB RAS
pr. Akademika Lavrentieva, 5
630090 Novosibirsk
Russia
Tel.: +7 383 3309491
Fax: +7 383 3306878
E-mail: zagor@catalysis.ru

Tatiana V. **Zamulina**
Boreskov Institute of Catalysis SB RAS
pr. Akademika Lavrentieva, 5
630090 Novosibirsk
Russia
Tel.: +7 383 330 6297
Fax: +7 383 330 8056
E-mail: zam@catalysis.ru

Aleksandra **Zarubica**
Faculty of Technology, University of Novi Sad
Bul. Cara Lazara 1
21000 Novi Sad
Serbia & Montenegro
E-mail: zarubica2000@yahoo.com

Ziyi **Zhong**
Institute of Chemical and Engineering
Sciences
1, Pesek Road, Jurong Island
627833 Singapore
Singapore
Tel.: +65 6796 3809
Fax: +65 6316 6182
E-mail: Zhong_ziyi@ices.a-star.edu.sg

Yurii N. **Zhukov**
FSUE "Biysk Oleum Plant"
659315 Biysk
Russia
Tel.: +7 385 4 234370
Fax: +7 385 4 234370
E-mail: root@boz.biysk.ru

Tatiana E. **Zhukova**
Ministry of Education and Sciences RF
Tverskaya str., 11
103906 Moscow
Russia
Tel.:+7 495 629 4212

XVII International Conference on Chemical Reactors
CHEMREACTOR-17

Editor: Professor Alexander S. Noskov

The abstracts are printed as presented, and all responsibilities we address to the authors. Some abstracts underwent a correction of misprints and rather mild editing procedure.

Compilers: Tatiana V. Zamulina

Elena L Mikhailenko

Computer processing of text: Natalia A. Tsygankova

Cover design and Disk maker: Alexey A. Spiridonov